

**INTERNATIONAL JOURNAL OF MODERN
ENGINEERING RESEARCH (IJMER)**

ISSN : 2249-6645



Volume 3 - Issue 6

Web : www.ijmer.com

Email : ijmer.editor@gmail.com

International Journal of Modern Engineering Research (IJMER)

Editorial Board

Executive Managing Editor

Prof. Shiv Kumar Sharma
India

Editorial Board Member

Dr. Jerry Van
Department of Mechanical, USA

Dr. George Dyrud
Research centre dy. Director of Civil Engineering, New Zealand

Dr. Masoud Esfal
R& D of Chemical Engineering, Australia

Dr. Nouby Mahdy Ghazaly
Minia University, Egypt

Dr. Stanley John
Department of Textile Engineering, United Kingdom

Dr. Valfitaf Rasoul
Professor and HOD of Electromechanical, Russian

Dr. Mohammed Ali Hussain
HOD, Sri Sai Madhavi Institute of Science & Technology, India

Dr. Manko dora
Associate professor of Computer Engineering, Poland

Dr. Ahmed Nabih Zaki Rashed
Menoufia University, Egypt

Ms. Amani Tahat
Ph.D physics Technical University of Catalonia-Spain

Associate Editor Member

Dr. Mohd Nazri Ismail
University of Kuala Lumpur (UniKL), Malaysia

Dr. Kamaljit I. Lakhtaria
Sir Padmapat Singhaniya University, Udaipur

Dr. Rajesh Shrivastava
Prof. & Head Mathematics & computer Deptt. Govt. Science & commerce College Benazir. M.P

Dr. Asoke Nath
Executive Director, St. Xavier's College, West Bengal, India

Prof. T. Venkat Narayana Rao
Head, CSE, HITAM Hyderabad

Dr. N. Balasubramanian
Ph. D (Chemical Engg), IIT Madras

Jasvinder Singh Sadana
M. TECH, USIT/GGSIPU, India

Dr. Bharat Raj Singh

Associate Director, SMS Institute of Technology, Lucknow

DR. RAVINDER RATHEE

C. R. P, Rohtak, Haryana

Dr. S. Rajendran

Research Supervisor, Corrosion Research Centre Department of Chemistry, GTN Arts College, Dindigul

Mohd Abdul Ahad

Department of Computer Science, Faculty of Management and Information Technology, Jamia Hamdad, New Delhi

Kunjai Mankad

Institute of Science & Technology for Advanced Studies & Research (ISTAR)

NILANJAN DEY

JIS College of Engineering, Kalyani, West Bengal

Dr. Hawz Nwayu

Victoria Global University, UK

Prof. Plewin Amin

Crewe and Alsager College of Higher Education, UK

Dr. (Mrs.) Annifer Zalic

London Guildhall University, London

Dr. (Mrs.) Malin Askiy

Victoria University of Manchester

Dr. ABSALOM

Sixth form College, England

Dr. Nimrod Nivek

London Guildhall University, London

Energy Losses And Turbulence Characteristics Through Hydraulic Structures Using Laser Doppler Velocimetry(LDV)

M. I. Attia

Assoc. Prof., Water & Water Structures Engg. Dept. Faculty of Engg., Zagazig University, Zagazig, Egypt,

ABSTRACT: This paper deals with the experimental investigation of energy losses and turbulence characteristics through hydraulic structures in a rectangular channel using Laser Doppler, measurements include turbulence intensity components and mean velocity components. Experiments were conducted with different contraction ratios at different expansion angles for different bed slopes. The results show that, the rate of variation of the energy loss increases till expansion angle about 30°. This rate of increase decreases above this value of angle of expansion. The energy loss is quite high at a contraction ratio of 0.7. Also, the results clearly show that, gradual expansion decrease the turbulence intensities in the wall and free surface regions compared to the sudden expansion. The maximum values of the turbulence intensities occur either close to the bed or at the free surface, with minimum values occurring within the core region. The turbulence intensities, however increases sharply at the free surface due to the free surface waves effect, and is the largest in sudden expansion.

KEY WORDS: Energy losses-Turbulence characteristics-Hydraulic structures-Laser Doppler velocimery-Contraction ratio-Free surface-Froude number-Expansion angle.

I. INTRODUCTION

The information regarding the turbulence characteristics in the transitional structures is somewhat scanty. Paradoxically enough, the problem of separation of the main stream of flow at open channel transitions or at an abrupt change of the boundary attracted the attention of investigators since the earliest time and yet it remains one of the least understood and the most critical problems of fluid dynamics today. Open channel transitions are commonly used in hydraulic structures in variety of situation to serve as link with minimum possible energy loss. Open channel transitions have been studied extensively because of their use in water resources engineering and their efficacy in reducing the energy loss in hydraulic structures. Transitions are provided, whenever the size or the shape of the cross section of an open channel changes. Such changes are often required in natural and artificial channels for water structures economically as well as for practical reasons. The transitions may be vertical or horizontal, contracting or expanding, sudden or gradually which are required for subcritical or supercritical flows. The change in the cross section disturbs the flow in the contracted reach and near it from both upstream and downstream. The change in the cross section, slope, and/or alignment over a specified reach is termed local transition, such channel transition is used mainly to avoid or minimize the excessive energy loss, to eliminate the cross waves, the resulting turbulence and to ensure safety of both the structure and the downstream channel reach. In the design of hydraulic structures, designers do their best to avoid sudden transition of the flow by sudden contractions to ensure smooth flow with minimum energy loss and to reduce turbulence pattern. As the flow passes through a bridge, a channel transition in the form of contraction and subsequent expansion is involved. Since these transitions are meant for continuous use, their role in minimization of the energy loss and attenuation of turbulence assumes significance. It is indispensable in hydraulic engineering to investigate structures of turbulence behind of multi vents water structures in the expansion zone in order to control turbulent flows and to design hydraulic structures properly. In designing of channel transitions, it is necessary to avoid excessive energy loss, to eliminate cross waves and the turbulence, to ensure smooth streamlined flow, to minimize standing waves, and to prevent the transition from acting as a choke influencing upstream flow. Free surface has a unique role in governing the turbulence in open channel flows. The phenomenon is usually so complicated that the resulting flow pattern is not readily subjected to any analytical solution. So, a practical solution is possible, however, through experimental investigation. The turbulent flow models in open channel flows were discussed by Garde [5,6], Rodi [12]; Nezu [10]. Measurements of turbulence characteristics in open channel flows using LDA have been pointed by several investigators [7, 9, 13, 14]. Experimental investigation of turbulent structure of back facing step have been reported by several investigators. [1, 8, 11, 3]. The main results of Formica were reported in Chow [2]. The present study of the how characteristics and turbulence structure behind of multi vents water structures, is a typical case of separation at an abrupt change of boundary. Thus, one of the purposes to study the turbulence behind of water structures in the expansion zone is to gain in sight into the properties and interactions of these turbulent structures. Much less information is available regarding the turbulence characteristics in the expansion zone of water structures.

Therefore, precise and accurate measurements of the energy loss are carried out to study the variation of the energy loss upstream, within and downstream of the multi vents water structures. Also, the present research involves measurements of mean and fluctuating flow characteristics such as streamwise and vertical turbulence intensities, and streamwise and vertical mean velocity components in the expansion zone behind the multi vents water structures. The measurements are carried out using a Laser Doppler Velocimetry(LDV) a non-intrusive Fiber Optic state of the art technique, in the expansion zones of water structures at different contraction ratio b/B of 0.9, 0.8, 0.7, 0.6, 0.5 and 0.4 at different expansion angles θ of 15°, 30°, 45°, 60°, 75°, and 90° for various bottom slope S_0 of 0.005, 0.01, 0.015, 0.02, and 0.025. Also, the objectives of the present research are: to use LDV, which includes the data acquisition system, data processing to measure mean and fluctuating flow characteristics at different locations in the expansion zones of the water structures; to conduct a comparative study of the depthwise variation of streamwise and vertical turbulence intensities at different cross sections in the expansion

zones of water structures, to make a comparative study of the depthwise variation of water structures, to make a comparative study of the depthwise variation of streamwise and vertical mean velocity components. Similarly, the measurements were made in the expansion zones along the centerline at relative depth ratio y/y_0 of 0.5 to study the variation of mean and fluctuating flow characteristics.

II. THEORETICAL STUDY

In the flow over the water structure through a channel, part of pressure head will lost partly due to dissipation of energy in separation zones, and partly due to friction between fluid and the channel wetted parameter. On the other hand, the constriction of flow by contraction will result in a corresponding backwater build up. Figure.3 shows a definition sketch of flow through contraction in sloping channel. The variables affecting the flow through the multi vents water structure are shown on the figure and explained at the notation section. The functional relationship of the energy loss through the water structure could be written as follows:

$$f_1(g, V_u, Y_u, b, B, Y_d, V_d, \Delta E, \Delta E_u, \Delta E_d, S_0, \theta) = 0 \quad (1)$$

Using the dimensional analysis, the following dimensionless relationship is obtained:

$$\frac{\Delta E}{Y_u} = f_2 \left[F_u, \frac{b}{Y_u}, \frac{B}{Y_u}, S_0, \theta \right] \quad (2)$$

Keeping in mind the properties on the non-dimensional quantities, the following expression could be obtained from Eq. (2)

$$\frac{\Delta E}{Y_u} = f_3 \left[F_u, \frac{b}{B}, S_0, \theta \right] \quad (3)$$

It may appear better to analyze the energy loss through the water structures as a ratio related to the upstream energy, E_u . Therefore, the E_u is used instead of Y_u in the left hand side of equation (3) which becomes:

$$\frac{\Delta E}{E_u} = f_4 \left[F_u, \frac{b}{B}, S_0, \theta \right] \quad (4)$$

The energy loss through the transition is equal to the difference in specific energies before and after the transition. From Fig.3, applying specific energy equation between sections (1-1) and (3-3)

$$\Delta E = E_u - E_d = \left(y_u + \frac{V_u^2}{2g} \right) - \left(y_d + \frac{V_d^2}{2g} \right) \quad (5)$$

And relative energy loss is expressed as

$$\frac{\Delta E}{E_u} = 1 - \frac{E_d}{E_u} \quad (6)$$

Similarly to equation (6), from Fig.3, applying the specific energy equation between sections (1-1) and (2-2) also between sections (2-2) and (3-3).

$$\frac{\Delta E_u}{E_u} = 1 - \frac{E_t}{E_u}, \text{ and} \quad (7)$$

$$\frac{\Delta E_d}{E_d} = \frac{E_t}{E_d} - 1 \quad (8)$$

Where;

E_u , E_t and E_d , specific energy upstream, within and downstream the water structure respectively, ΔE = total energy loss between sections (1-1) and (3-3), ΔE_u = upstream energy loss between sections (1-1) and (2-2), ΔE_d = downstream energy loss between sections (2-2) and (3-3).By knowing either the value of velocity or water depth upstream, within and downstream the multi water structure, the energy loss can be calculated by using equations (6), (7) and (8) for the known values of discharges and different contraction ratios b/B at different expansion angles θ .

III. EXPERIMENTAL SET UP AND PROCEDURE

The experiments were carried out in a rectangular open channel that is 8.0m long, 0.3m width and 0.5m height with glass wall 6 mm thick and a steel plate bed Fig.1 shows layout of the test facility. The water is supplied from a constant head overhead tank to the flume at a desired discharge that is continuously monitored with an on-line orifice meter. The discharges were measured using a pre-calibrated orifice meter in the feeding pipeline. And in-line discharge control valve that is fitted into the main supplying pipeline was used to regulate the flow rate. Depth measurements were taken using a needle point gauge with a reading accuracy of ± 0.10 mm. The flume side walls are made up of 6 mm glass sheets. A tail gate is provided at the downstream end of the flume to maintain a required water depth of the channel flow. The water is finally collected in a sump placed in the basement from where it is pumped back to the overhead tank by a 15 Hp pump. The experiments were carried out using six different lateral contraction ratios, b/B of 0.9, 0.8, 0.7, 0.6, 0.5, and 0.4 and five different expansion angles, θ of 15°, 30°, 45°, 60°, 75°, and 90°. Five different channel bottom positive slopes, S_0 of 0.005, 0.01, 0.015, 0.02, and 0.025 were used to illustrate the effect of bottom slope on the flow characteristics due to contraction. The slopes were selected based on the flume facilities. For each combination of lateral contraction ratio, b/B , expansion angles, θ , and bottom slope, five different flow rates ranging from about 15 Lit/sec to 40 Lit/sec were used. The upstream water depth was adjusted to produce a Froude number of approach ranging from 0.10 to 0.4. The flow through the transition was always subcritical but it may changed to supercritical state just at the end of the transition or away from it, depending upon the incoming flow rate, the applied flume bottom slope, the expansion angle and the contraction ratio. The effect of the expansion angle θ on the energy loss and turbulence intensities was also studied, for a different lateral contraction ratios b/B and a different bottom slope S_0 . Channel transitions were fabricated from transparent perspex sheets. One type of construction at the inlet was sudden and different expansions at the outlet were at expansion angles θ of 15°, 30°, 45°, 60°, 75°, and 90° downstream of two vents water structure.

IV. LASER DOPPLER TECHNIQUE

The experimental data were collected using the two color back scatter Laser Doppler Velocimetry (LDV) system. Fig.2 shows a block diagram of the two component LDV set up used for the measurements. A 5 Watt Argon-ion laser with two laser beams; one blue (488nm) and one green (514.5nm), were focused at a measuring point from one side of the channel through an optical lens. Two Burst Spectrum Analyzers (BSA) were used to evaluate the Doppler frequencies. Subsequent computer analysis consisted of velocity bias averaging and outlier rejection. The number of samples taken at every point was 5000 bursts. This correspond to a simple averaging time of about 100 seconds. The data rate was about (50-60) per second. Before acquiring the data, the LDV signal was checked for its quality on a 100 MHz Gold storage oscilloscope. The signal display as regular Doppler burst that correspond to a particle passing through the measuring volume. The measurements were taken at different cross sections in the expansion zones downstream of two vents water structure for different flow rate (Q). Fig.3 shows the location grid of the measuring stations.

With reference to the origin fixed at the channel bed and in the centre of lower vent as shown in Fig.3, transverse of measuring volume was run to obtain the profiles of both the RMS of the streamwise and vertical turbulence intensities, and streamwise and vertical mean velocity components. The measuring points were closely spaced in the region of high velocity gradient. All the measurements were made for a constant free steam water depth of 31cm irrespective of the flow rate. To obtain the vertical profiles of the mean and fluctuating flow quantities, the measurements were conducted in the vertical plane at $z/b= 0$ and 0.3 at different cross sections at different flow rates. In the vertical direction at every profile, 30 measurements at 5mm intervals up to 60 mm from the bed boundary and 15mm for the rest were taken. Similarly, the measurements were done in the expansion zones along the centerline at relative water depth $y/y_0= 0.5$ to study the variation of mean and fluctuating flow characteristics.

V. RESULTS AND DISCUSSION

The relative total energy loss with regard to the energy upstream of the multi water structure $\Delta E/E_u$ is plotted as a function of downstream expansion angles θ of 15°, 30°, 45°, 60°, 75°, and 90° at different contraction ratios b/B of 0.9, 0.8, 0.7, 0.6, 0.5 and 0.4 at various bottom slope S_0 of 0.005, 0.01, 0.015, 0.02 and 0.025, Fig.4. The total energy loss is the least value for channel contraction b/B of 0.9 and a maximum value for channel contraction b/B of 0.4. It is relatively small up to the contraction ratio b/B of 0.7. The rate of increase in energy loss, Fig.4, is almost the same between the contraction ratios b/B of 0.9 and 0.8; and 0.8 and 0.7. By taking the value of the rate of increase in energy loss between contraction ratios b/B of 0.9 and 0.8; and 0.8 and 0.7 as a reference. This rate of increase in energy loss has the double value between the contraction ratios b/B of 0.7 and 0.6. Similarly, this rate of increase in energy loss increases to about (5-6) times between b/B of 0.6 and 0.5 and almost about (10-12) times between contraction ratios b/B of 0.5 and 0.4 as compared to the increase in energy loss between the contraction ratios b/B of 0.9 and 0.8. This trend is almost the same for all other contraction. As the expansion angle θ increases up to 30°, the rate of increase in the head loss $\Delta E/E_u$ is relatively high for all the contraction ratios b/B , being very high for the contraction ratio b/B of 0.6. Above expansion angle θ of 30°, the increase in the energy loss is much slower. Particularly for expansion angle θ greater than 45° at which the energy loss is almost constant for all the practical purposes. Also, as shown in Fig.4, the energy loss $\Delta E/E_u$ increases with the increase of bottom slope S_0 .

Fig.5 depicts the variation of total relative energy loss $\Delta E/E_u$ with regard to the energy upstream with bottom slope S_0 at different contraction ratios b/B of 0.9, 0.8, 0.7, 0.6, 0.5 and 0.4 at different expansion angles θ of 15°, 30°, 45°, and 90°. From this figure, it can be observed that for a fixed expansion angle θ , the trend of variation between relative energy loss $\Delta E/E_u$ and bottom slope S_0 is increasing with a nonlinear trend. Also, at a particular bottom slope S_0 , relative energy loss $\Delta E/E_u$ as the channel contraction b/B increases.

Fig.6 shows the variation of relative total energy loss $\Delta E/E_u$ with upstream Froude number F_u for different contraction ratios b/B of 0.9, 0.8, 0.7, 0.6, 0.5 and 0.4 for the flow rates Q of 15 Lit/sec and 40 Lit/sec. Several Froude numbers respect to upstream depth were generated from these discharges by changing the depths for the given discharges. It can be noticed from the figure that the relationship between F_u and $\Delta E/E_u$ is a family of curves. The nature of the trend of variation of total energy loss $\Delta E/E_u$ is similar in all cases of flow. The curves are extended backward from $F_u=0.05$ and 0.1 for comparative purpose. With an increasing Froude number F_u , the energy loss $\Delta E/E_u$ increases with a slightly slower rate up to $F_u = 0.2$ say, for contraction ratio $b/B > 0.5$, the energy loss $\Delta E/E_u$ is small up to say $F_u=0.1$, after which energy loss increases rapidly as Froude number F_u increases above 0.1. The trend of variation of the relative energy loss $\Delta E/E_u$ for $b/B =0.6$ occupies an intermediate position between these two trends for contraction ratios b/B less than or equal to 0.7 or greater than or equal to 0.5. Again for the same Froude number, F_u , the relative energy loss increases rapidly as the channel contraction increases. Especially, this increase is quite significant for the channel contraction greater than 0.7. For higher Froude number above 0.2 (in the subcritical range of flow of the present investigation) this increase is several folds compared to the minimum channel contraction b/B of 0.9.

As shown in Fig.7, for each plot, the groups of curves representing the relationship between relative upstream energy loss $\Delta E_u/E_u$ and upstream Froude number, F_u , at various contraction ratios b/B of 0.9, 0.8, 0.7, 0.6, 0.5 and 0.4 at a fixed value of angle θ for different discharges Q of 15 Lit/sec and 40 Lit/sec. It clear that, the trend of variation $\Delta E_u/E_u$ is quite similar in its behavioral characteristics to the one described above for total energy loss $\Delta E/E_u$, but with reduced magnitude, as ΔE_u constitutes a part of the total energy loss ΔE . The study of each plot show that both $\Delta E_u/E_u$ and F_u increase with the increasing value of contraction ratio b/B . The value of $\Delta E_u/E_u$ was nonlinear function of F_u . Also, it is clear that, with the same value of contraction ratio b/B , the $\Delta E_u/E_u$ increases with the increasing upstream Froude number F_u . The decrease of the channel contraction, reduces separation zone, decreasing the upstream energy loss. It can be observed that by

extending the lower sides of curves through the point $F_u=0$, $\Delta E_u/E_u=0$, the hydrostatic condition prevails. An extension of the upper limbs of the earlier curves, till it reaches an optimum value of contraction ratio b/B .

Fig.8 demonstrates the relationship between relative downstream energy loss $\Delta E_d/E_d$ and upstream Froude number F_u for different contraction ratios b/B of 0.9, 0.8, 0.7, 0.6, 0.5, and 0.4 at a fixed value of expansion angle θ for discharges of 15 Lit/sec and 40 Lit/sec. Again the resulting curves indicated the same trend as discussed above for ΔE and ΔE_u . It is observed that, the downstream energy loss, ΔE_d (at water structure outlet) are more than the corresponding upstream energy losses (at water structure inlet), probably due to the creation of the larger recirculating fluid mass; separated flow at the outlet of the water structure in the expansion zones. Fig.9 shows the variation relative energy (efficiency) E_d/E_u with upstream Froude number F_u for different contraction ratios b/B of 0.9, 0.8, 0.7, 0.6, 0.5 and 0.4 for discharges of 15 Lit/sec and 40 Lit/sec at a fixed values of expansion angle and bottom slope. From this figure, it can be observed that for discharge, the trend of variation between E_d/E_u and F_u is decreasing with nonlinear trend. Also, at a particular F_u , E_d/E_u increases as channel contraction decreases. It is observed that the effect of F_u on E_d/E_u is significant. The E_d/E_u increases non-linearly with the decrease of F_u . Also, the E_d/E_u increases as the discharge decreases. Fig.10 shows the variation of relation water depth Y_d/Y_u as a function of upstream Froude number F_u at different contraction ratios b/B of 0.9, 0.8, 0.7, 0.6, 0.5 and 0.4 for discharges of 15Lit/sec and 40 Lit/sec at a fixed value of bottom slope and expansion angle. It is clear that, the trend of variation Y_d/Y_u is quite similar in its behavioral characteristics to the one described above for relative energy E_d/E_u . The study of each plot shows that Y_d/Y_u increases as F_u decreases with the decreasing of channel contraction. The value of Y_d/Y_u was nonlinear function of F_u . Fig.11 depicts the variation of relative heading up $\Delta Y/Y_u$ as a function of upstream Froude number F_u for different contraction ratios b/B of 0.9, 0.8, 0.7, 0.6, 0.5 and 0.4 for discharges of 15 Lit/sec and 40 Lit/sec at a fixed values of expansion angle θ and bottom slope S_o . From this figure, it is observed that the effect of F_u and Y_d/Y_u is significant. The Y_d/Y_u increases non-linearly with the increase of F_u . Also, at a fixed discharge Q , the trend of variation between Y_d/Y_u and F_u is increasing with a nonlinear trend. Also, at a particular F_u , Y_d/Y_u increases as the channel contraction increases.

Figs.12 and 13 depict the variation of streamwise and vertical components of turbulence intensities \bar{u}/U_o and \bar{v}/U_o as functions of channel depths y/y_o in the expansion zone of water structure at different expansion angles θ of 15° , 30° , 45° and 90° at different contraction ratios b/B of 0.7 and 0.5 for discharge of 40 Lit/sec along the depth at different cross sections. The trend of variation of \bar{u}/U_o and \bar{v}/U_o are similar in all the cases of expansion angles. The trend of \bar{u}/U_o and \bar{v}/U_o in the expansion zones in all the cases of expansion angles θ have higher values close to the bed, following a gradual fall in the wall region defined by $y/y_o < 0.2$, reaching minima in the core region defined by $0.2 < y/y_o < 0.6$. Turbulence intensities \bar{u}/U_o and \bar{v}/U_o rise gradually and then rapidly in the upper region (free surface region) defined $y/y_o > 0.6$, reaching the maximum at the free surface. The minimum turbulence intensities \bar{u}/U_o and \bar{v}/U_o always lie in the core region. The maximum turbulence intensities occur close to the bed or at the free surface depending on the location of the profile station. The nature of these variations is similar in all the cases of expansion angles, contraction ratios and discharges. Fig.13 shows the turbulence intensities \bar{u}/U_o and \bar{v}/U_o at $b/B = 0.5$ of the expansion angles θ of 15° , 30° , 45° , and 90° . The profiles of \bar{u}/U_o and \bar{v}/U_o in the expansion zones of the hydraulic structures, which depict the turbulence behavior more dearly, in expansion angle θ of 90° indicate large magnitude of turbulence in the wall and free surface regions, with fairly uniform turbulence in the core region. However, for expansion angle $\theta=15^\circ$, turbulence profile is fairly uniform with comparatively less increase of the turbulence in wall and free surface regions. In case of expansion angle $\theta=90^\circ$, as shown in Fig.13, the nature of variation in turbulence intensities \bar{u}/U_o and \bar{v}/U_o at the entry of expansion zones and subsequent sections downstream is somewhat distinct compared to the turbulence profiles in the case of gradual expansion $\theta=15^\circ$. Herein, in the core region of sudden expansion θ of 90° , turbulence intensity profiles \bar{u}/U_o and \bar{v}/U_o do not exhibit the tendency towards constancy unlike in the gradual expansion, $\theta=15^\circ$. Generally in sudden expansion $\theta=90^\circ$ after reaching the minimum turbulence intensities \bar{u}/U_o and \bar{v}/U_o as the flow distance increases from the wall, the turbulence tends to increase consistently till the free surface is reached. Turbulence intensities are particularly largest $\bar{u}/U_o = 45\%$, $\bar{v}/U_o = 29\%$ and $\bar{u}/U_o = 55\%$, $\bar{v}/U_o = 35\%$ at $x/b=2$, $z/b=0$ and $x/b=2$, $z/b=0.3$ closer to the wall region and free surface region respectively. Similarly, both the turbulence intensities \bar{u}/U_o and \bar{v}/U_o are large at all the sections investigated downstream of the inlet of expansion zone in 90° sudden expansion in the wall region and free surface region. The general trend in variation of depthwise turbulence is similar in the expansion zone up to $x/b=6$ observed in this work. Generally, the turbulence intensities \bar{u}/U_o and \bar{v}/U_o grows rapidly after the flow separation and spreads in vertical direction in all cases of expansion angle. Also, it can be seen that the gradual expansion θ of 15° , is more effective in minimizing the turbulence intensity in the expansion zones compared to the 90° expansion angle. Downstream of the inlet of the expansion zone along the centerline, it is noted that, farthest downstream at $x/b=6$, turbulence intensities \bar{u}/U_o and \bar{v}/U_o along the axis and $z/b=0.3$ are lowest for 15° expansion. However increase sharply at the free surface. Concluding, gradual expansion decreases the depthwise turbulence intensities \bar{u}/U_o and \bar{v}/U_o in wall and free surface regions compared to the sudden expansion. This dampening effect could be attributed to the reduced magnitude of surface waves observed in the gradual expansion compared to relatively larger surface waves in the 90° sudden expansion. Further, the results show the influence of the expansion angle (diversion angle) on the turbulence intensities \bar{u}/U_o and \bar{v}/U_o , which decrease with reduced diversion angle. Moreover with the increasing expansion and channel contraction, the vertical variation in turbulence intensities \bar{u}/U_o and \bar{v}/U_o become more pronounced. Changing rapidly in the wall, core and the free surface region.

Figs.14 and 15 depict the variation of streamwise and vertical components of turbulence intensity fluctuations \bar{u}/U_o and \bar{v}/U_o along the centerline at relative water depth $y/y_o = 0.5$ above the bed in the expansion zones for the flow of 40 Lit/sec, at different contraction ratios b/B of 0.5 and 0.7, at different expansion angles θ of 15° , 30° , and 90° . Clearly, the trend of turbulence intensities \bar{u}/U_o and \bar{v}/U_o variation are quite similar in all the cases of expansion angles θ and

contraction ratio b/B . Following a slight general fall, reaching minima, turbulence rises rapidly to reach maxima with subsequent monotonous decrease along the distance away from the outlet of hydraulic structure. Generally, maximum turbulence intensities \bar{u}/U_o and \bar{v}/U_o occur at the same location with slight shift noticed for gradual expansion $\theta=30^\circ$. The salient feature of the variation observed are as follow. For contraction ratios b/B of 0.7 and 0.5, the minimum values of \bar{u}/U_o and \bar{v}/U_o occurring at $0 < x/b < 1.5$ for all the expansion angles. The maximum values of \bar{u}/U_o and \bar{v}/U_o accruing at $2.2 < x/b < 4.5$. Similar trends are observed for turbulence intensities \bar{u}/U_o and \bar{v}/U_o for all contraction ratios b/B of 0.5 and 0.7 of the different expansion angles θ of 15° , 30° , and 90° . It may be concluded that downstream of the water structures beyond specific values of x/b for instance 3.8, turbulence intensities \bar{u}/U_o and \bar{v}/U_o are always higher in the case of 90° sudden expansion and lower for most gradual expansion of 15° , for all contraction ratios b/B of 0.7 and 0.5. The trend is exactly opposite as observed for $x/b < 2.7$. Also, it may concluded that turbulence intensity beyond $x/b = 4.1$ from the centre of the hydraulic structure decreases with angle of diversion decreases and is subsequently higher as for sudden expansion $\theta=90^\circ$, the lowest for gradual expansion θ of 15° and being the intermediate for gradual expansion $\theta=30^\circ$. The trend is reverse for $x/b < 2.7$ where the turbulence intensity is higher for gradual expansion $\theta=15^\circ$ and lower for 90° sudden expansion. At x/b of 2.7 up to 4.2, the maximum turbulence intensities \bar{u}/U_o and \bar{v}/U_o occur for all the expansion angles at different contraction ratios b/B and all different spanwise locations. Also, with increasing channel contraction, the turbulence intensities \bar{u}/U_o and \bar{v}/U_o increase for all the cases.

VI. CONCLUSIONS

The conclusions arising out from this study can be summarized as follows:

Form the evidence of the variation of the total energy loss $\Delta E/E_u$ with the expansion angle in the expansion zones downstream of the water structures, it appears that up to expansion angle of 30° and decreasing the expansion angle, the head loss decreases, but above this expansion angle of 30° , the effect of the boundary is insignificant. The energy loss is quite high if the contraction ratio $b/B > 0.7$. The energy loss increases rapidly up to expansion angle of 30° and tends to remain constant above expansion angle of 45° . Thus, expansion angle of 30° appears to be a critical angle defining a border value between the maximum energy loss and the value up to which total energy loss increases rapidly as expansion angle increases form 0° to 30° . The results indicate that, the most significant differences in energy loss occur with expansion angle in the range less than 45° . The total energy loss $\Delta E/E_u$, upstream energy loss $\Delta E_u/E_u$, and downstream energy loss $\Delta E_d/E_d$ of the multi vents water structures, increase with the increasing value of both upstream Froude number and channel contraction. The downstream energy loss (at hydraulic structure outlet) are more than the corresponding upstream energy loss (at hydraulic structure inlet), probably due to the creation of the large recirculating fluid mass, separated flow at outlet of the hydraulic structure in the expansion zones.

The streamwise turbulence intensities \bar{u}/U_o and \bar{v}/U_o are higher nearer the bed in the wall region defined by $y/y_o \leq 0.2$ due to wall effect and the free surface region defined by $y/y_o > 0.6$ due to free surface effect. In the intermediate core region defined by $0.2 < y/y_o \leq 0.6$, minimum turbulence intensities \bar{u}/U_o and \bar{v}/U_o occur, and consistently correspond to the maximum streamwise mean velocity \bar{u}/U_o , occurring in the same zone approximately at the same location with the local velocity gradient being zero. In the expansion zones, gradual expansion decrease the turbulence intensities \bar{u}/U_o and \bar{v}/U_o in wall and free surface regions compared to the sudden expansion. The maximum values of turbulence intensities \bar{u}/U_o and \bar{v}/U_o occur either close to the bed or at the free surface. As a comprehensive observation, it noted that the streamwise turbulence \bar{u}/U_o is always greater compared to the vertical turbulence \bar{v}/U_o . Also, it is concluded that with the decreasing of expansion angle and channel contraction in the expansion zone, turbulence intensities \bar{u}/U_o and \bar{v}/U_o decrease at all the cases. Along the depth, the trend of variation of turbulence intensities are similar in all the expansion angles in the expansion zone of hydraulic structures, and increase or decrease simultaneously of the all cases of expansion angles.

\bar{v} Vertical component of turbulence intensity in
y- direction (RMS),
x Longitudinal axis along channel length,
y Transverse axis along channel height,
z Transverse axis along channel width,
 S_o Bottom slope.
Q Flow discharge
 θ Expansion angle
RMS Root mean square

NOMECLATURE:

b Width of hydraulic structure(total width)
B Natural channel width
 \bar{u} Streamwise mean velocity in x-direction,
 U_o Streamwise mean free steam, velocity
averaged over the cross section.
 \bar{u} Streamwise component of turbulence intensity in x-
direction (RMS),
 \bar{v} Vertical mean velocity in y-direction,

REFERENCES

- [1.] Amino, R.S., and Goel, P.(1985) "Computations of Turbulent Flow Beyond Backward Facing Steps Using Reynolds Stress Closure", AIAA J., Vol. 23, No. 23, pp.1356-1361.
- [2.] Chow, V.T. (1959) "Open Channel Hydraulics", Mc Graw Hill Book Co., New York, pp. 461-468.
- [3.] Etheridge, D.W.,and Kemp, P.H.(1978)"Measurements of Turbulent Flow Downstream of a Rearward Facing Step", Fluid Mech. No.3.
- [4.] Formica, G. (1955) "Preliminary Test on Head loss in Channels due to Cross Sectional Changes", L.Energia Electrical, Milano, Vol. 32, No.7 pp. 554-568.
- [5.] Grade, H. (1993) "The Turbulent Flow Models in Open Channel Flows", Monograp, A.S. Balkema Puplichers, New Rood, V.T 08079, New Delhi, India.

- [6.] Garde, R.J. (1994) "Turbulent Flow", Published by H.S. Poplai for Willy Eastern Limited, New Age International Limited, 4835/24, Ansari Road Daryaganj, New Delhi-110002.
- [7.] Guoren, D., and Xiaonan, T. (1992) "Some Measurements of a Turbulent Structure in an Open Channel", Proceedings of the Conference of Flow Modelling and Turbulence Measurements, Ed., Zaiobao, Hemisphere Publishing Corporation, Washington.
- [8.] Nakagawa, H., and Nezu, I. (1995) "Experimental Investigation on Turbulent Structure of Backward Facing Step Flow in Open Channel" J. of Hydr. Research, Vol.25, No.1.
- [9.] Nezu, I., and Rodi, W., "Open Channel Flow Measurements with a Laser Doppler Velocimetry", J. Hydraulic Engg. ASCE, 112, pp. 335-355 (1986).
- [10.] Nezu, I., and Nakagawa, H. (1993) "Turbulence in Open Channel Flow", IAHA-Monograph, A.A. Balkma Publishers, Old post Road, Brookfield, VTO 5035, USA.
- [11.] Nakagawa, H., and Nezu, I. (1987) "Experimental Investigation on Turbulent Structure of Back Facing step Flow in an Open Channel" J. Hydraulic Research, IAHR, 25, pp. 67-88.
- [12.] Rodi, W. (1993) "Turbulence Models and their Application in Hydraulics", IAHR Monograph, A.A. Balkema Publishers, Old Post Roadfield, VTO 5036, USA.
- [13.] Song, T., and Chinew, Y. (2001) "Turbulence Measurement in Nonuniform Open Channel Flow Using Acoustic Doppler Velocimeter (ADV)," J. Engg. Mech., 127 (3), 219-231.
- [14.] Sukhodolov, A., and Thiele, M. (1998) "Turbulence Structure in a River Reach with Sand Beds", Water Resour., 34 (5), 1317-1334.

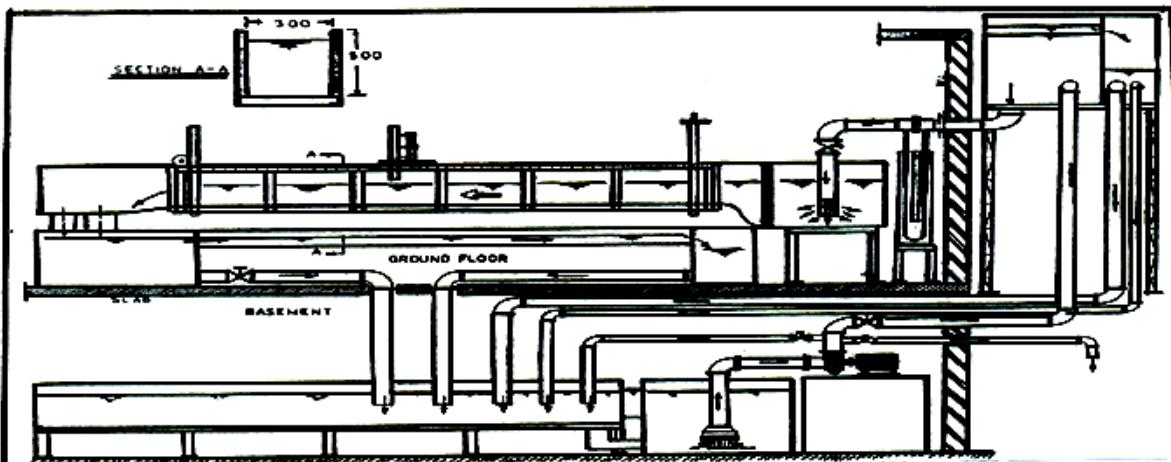


Fig. 1 Schematic sketch of test facility.

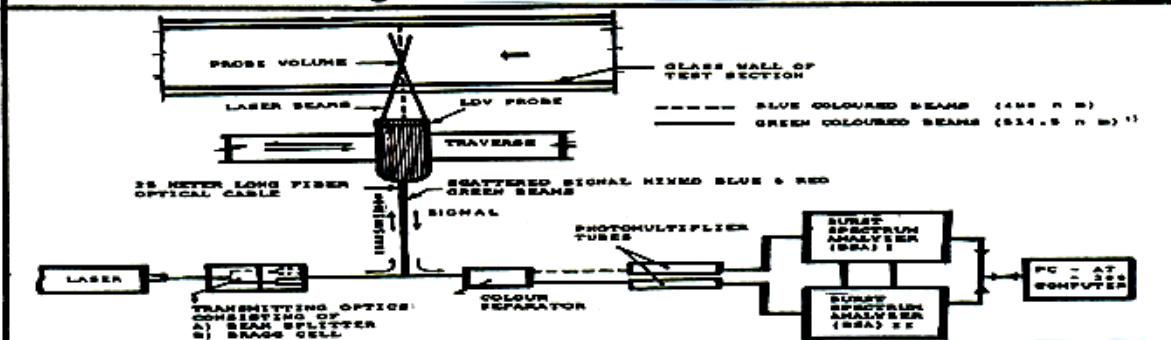


Fig. 2 Block diagram of the Laser Doppler Velocimetry.

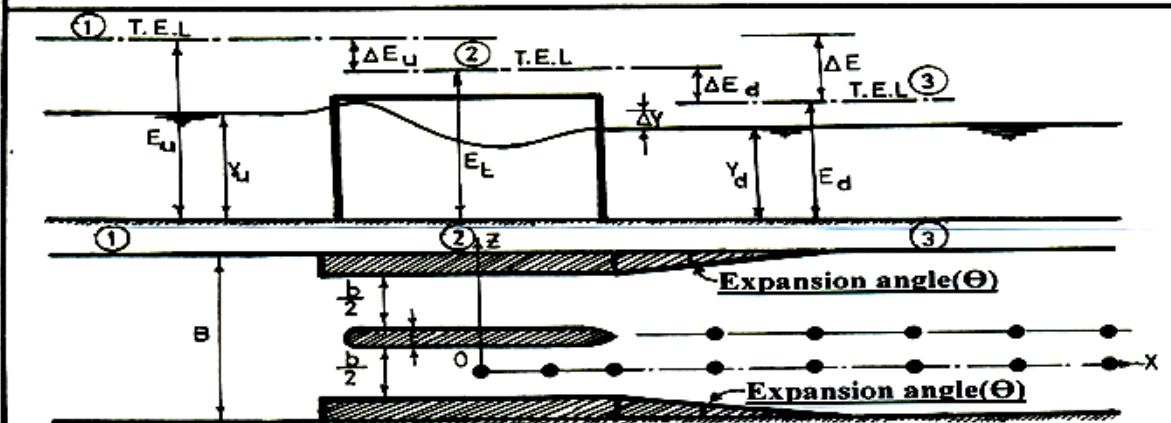


Fig. 3 Definition sketch showing the variables in the present study.

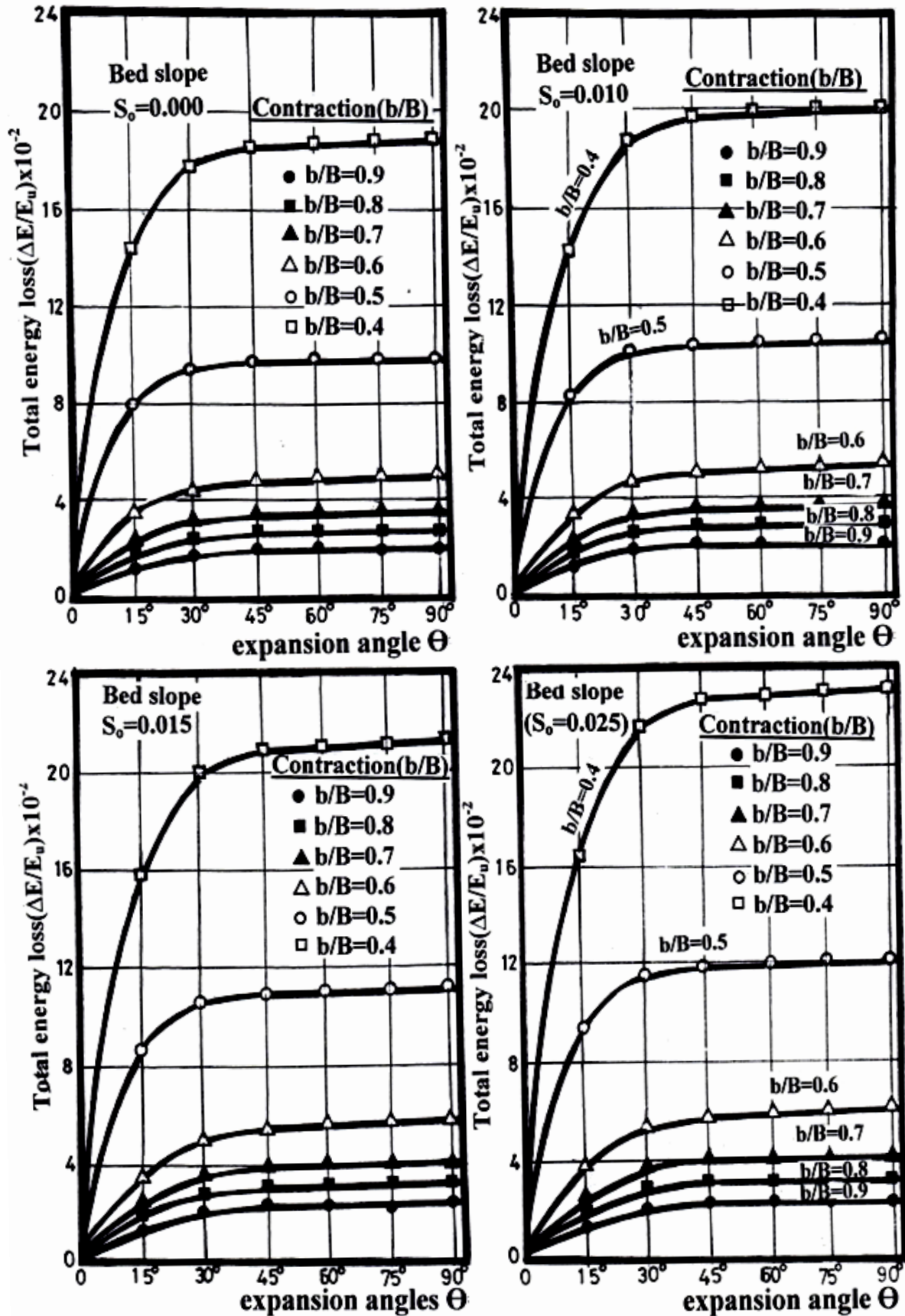


Fig.(4) Variation of total energy loss $\Delta E/E_u$ with expansion angle Θ for different contraction ratio b/B at different bottom slope S_o .

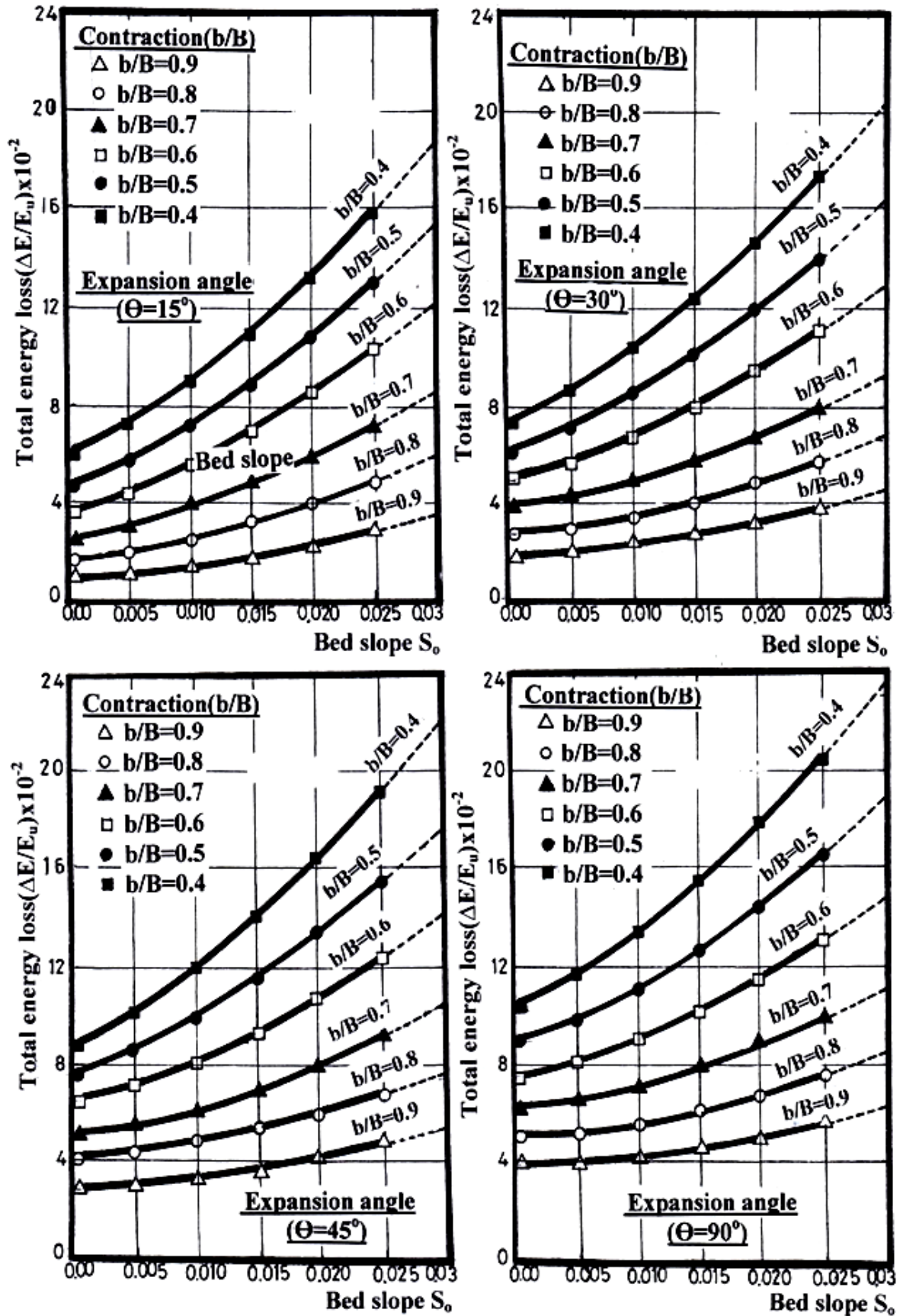
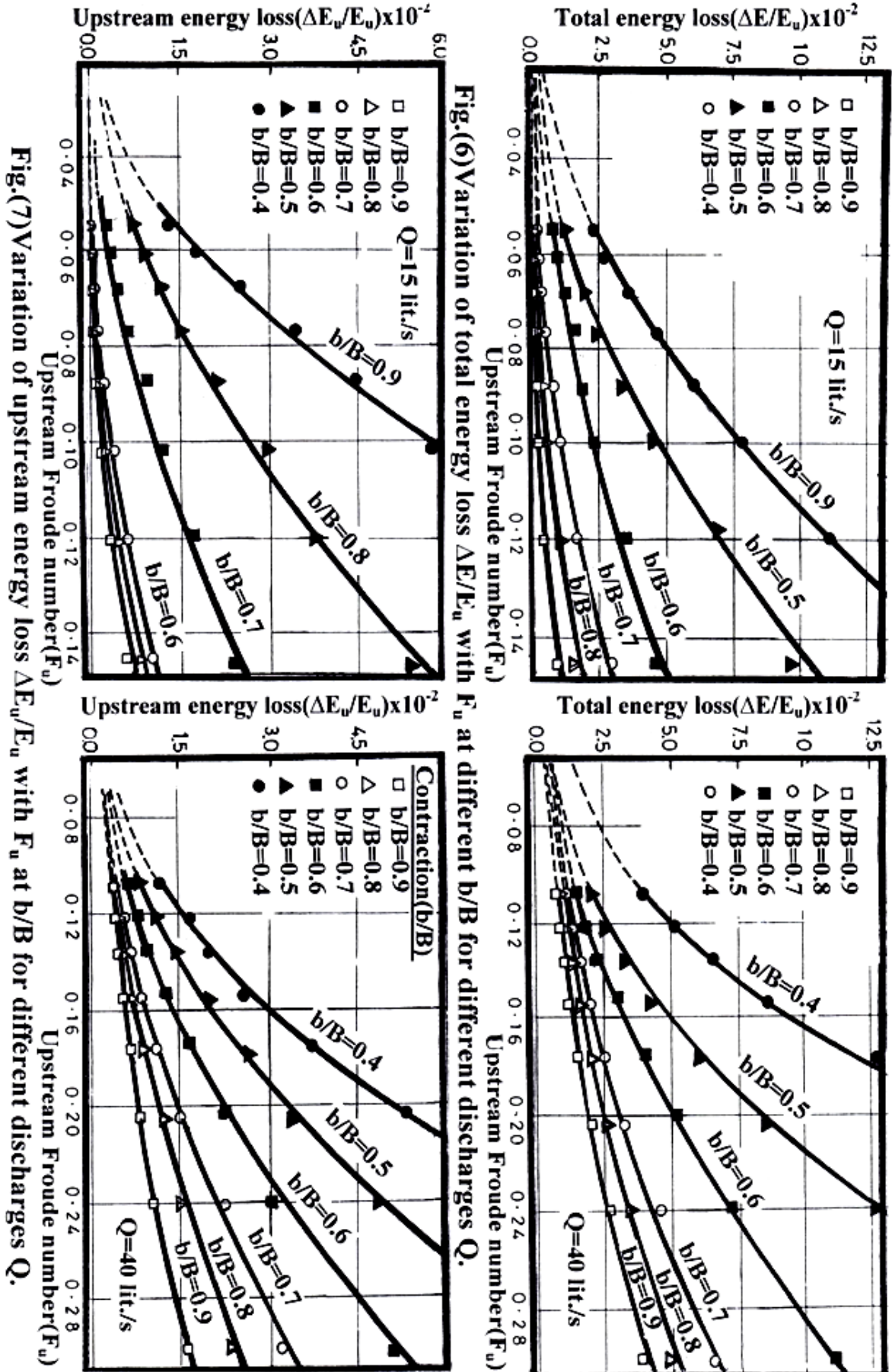


Fig.(5) Variation of total energy loss $\Delta E/E_u$ with bottom slope S_0 at different contraction ratio b/B for different expansion angle Θ .



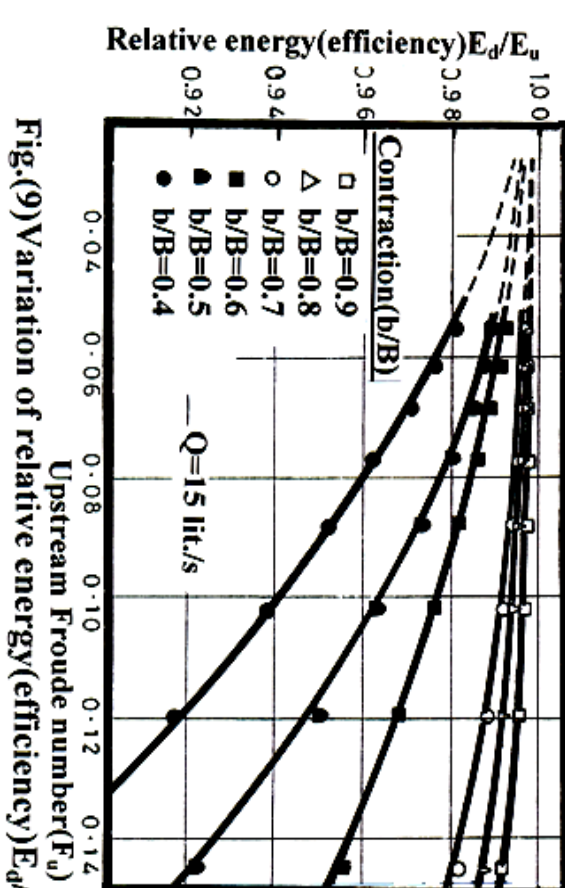


Fig.(9) Variation of relative energy (efficiency) E_d/E_u with F_u at different b/B at different discharges Q .

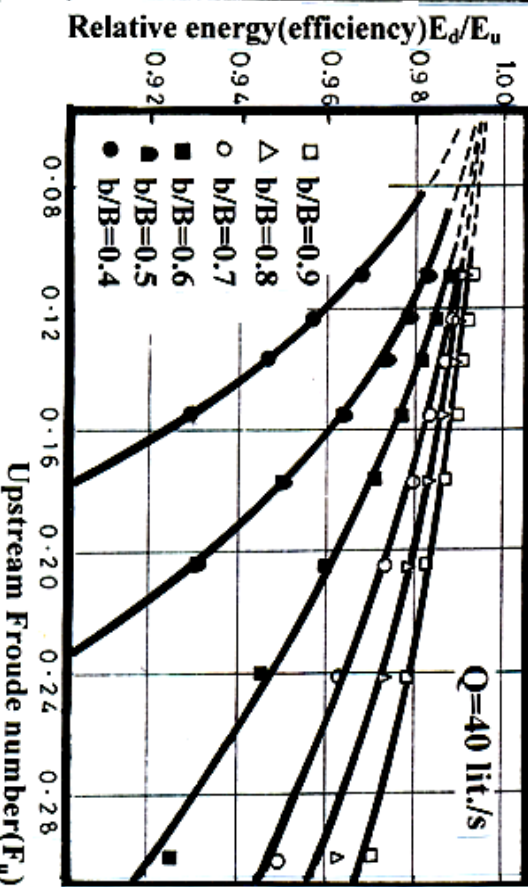
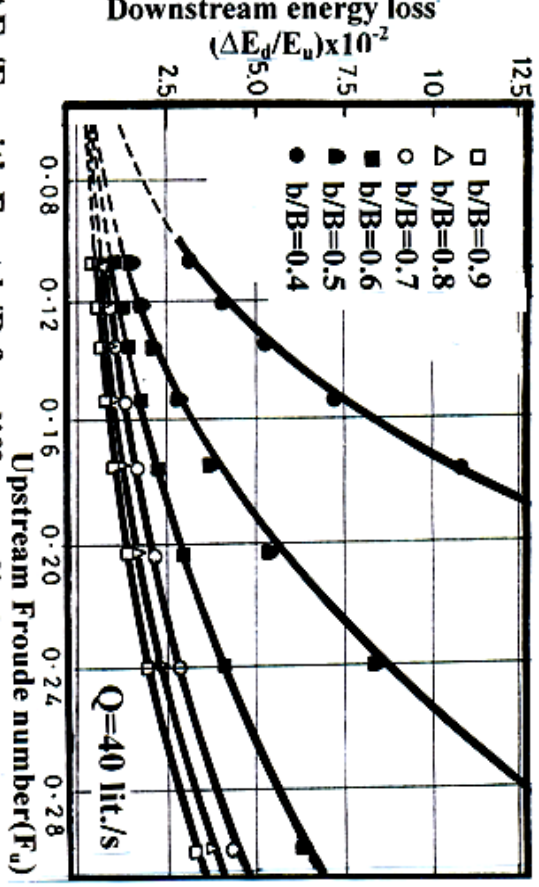
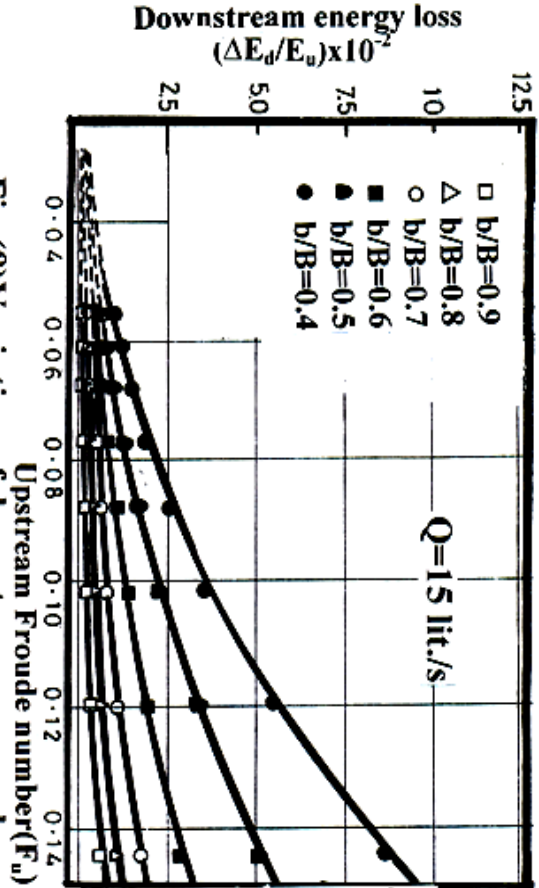


Fig.(8) Variation of downstream energy loss $\Delta E_d/E_u$ with F_u at b/B for different discharges Q .



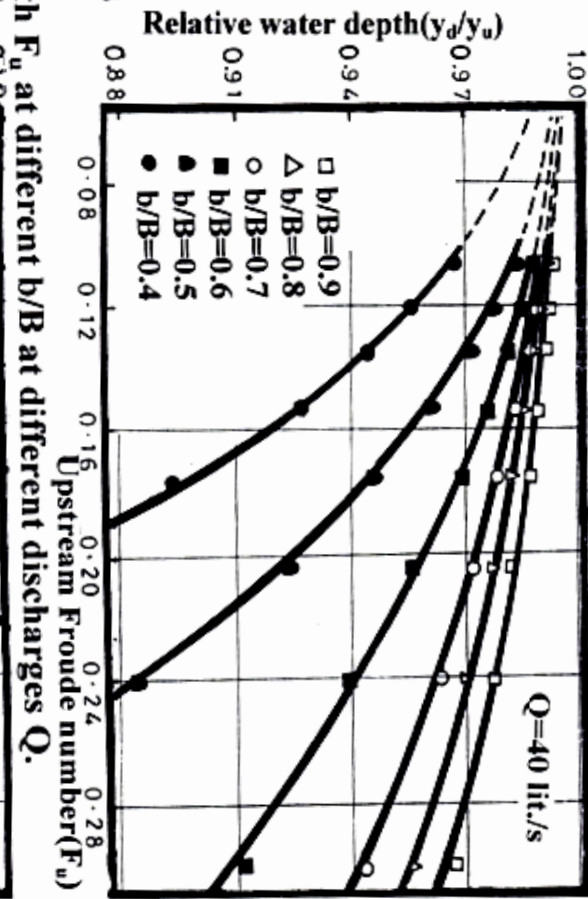
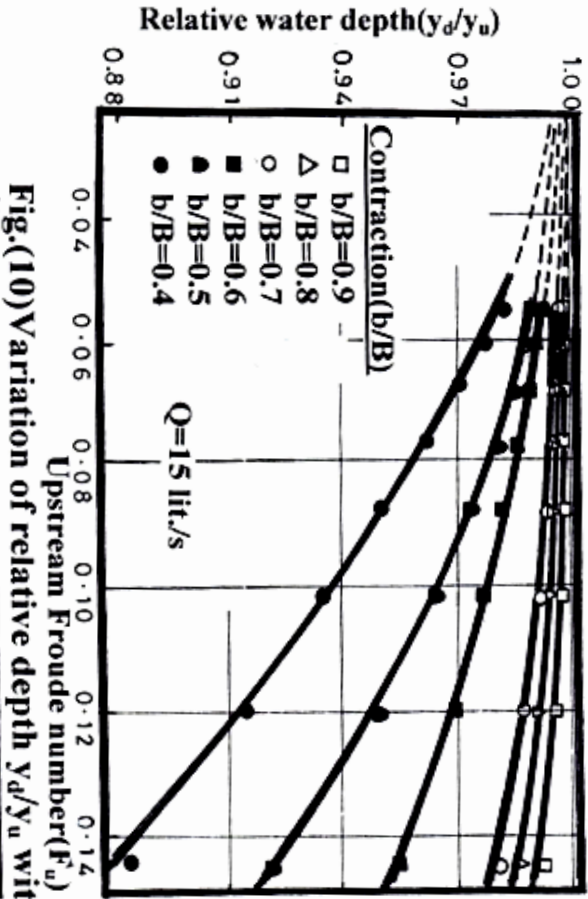
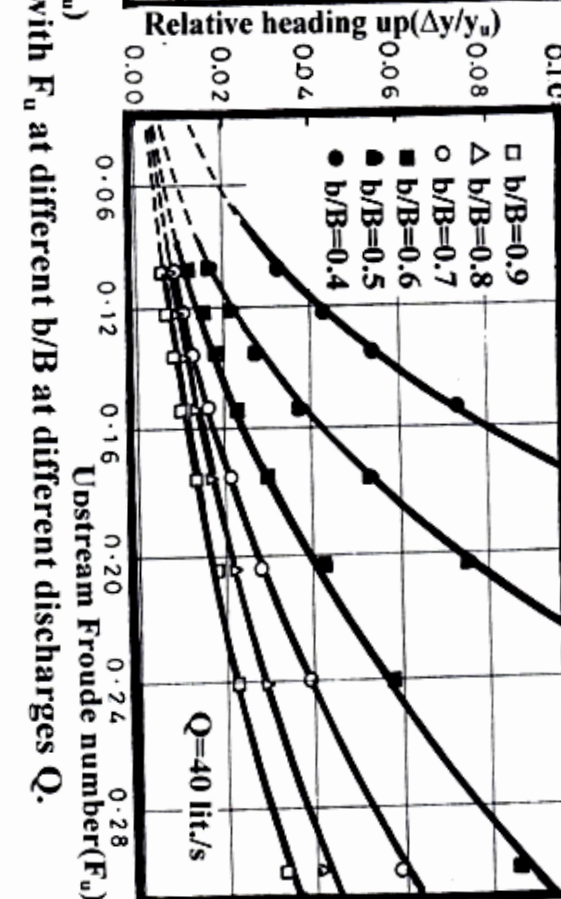
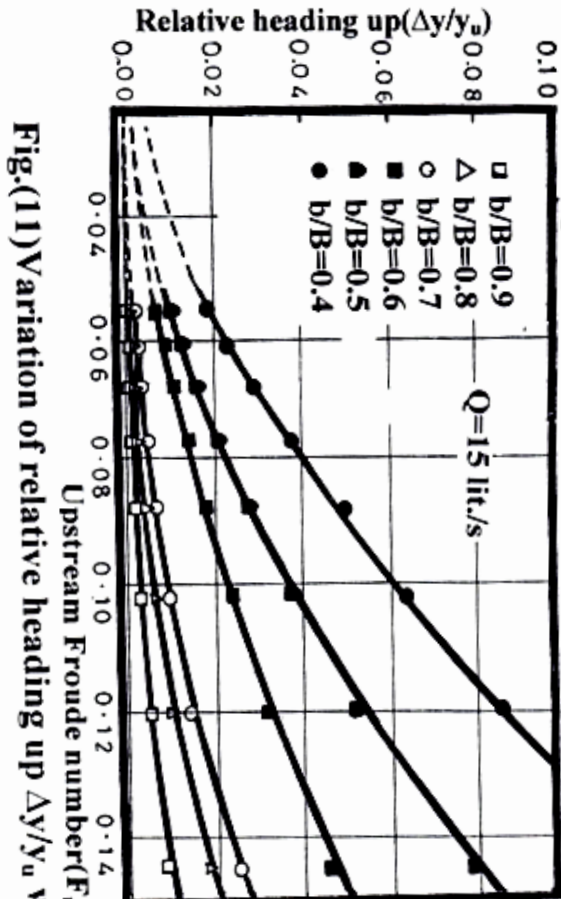


Fig.(11) Variation of relative heading up $\Delta y/y_a$ with F_u at different b/B at different discharges Q .

Fig.(10) Variation of relative depth y_d/y_a with F_u at different b/B at different discharges Q .

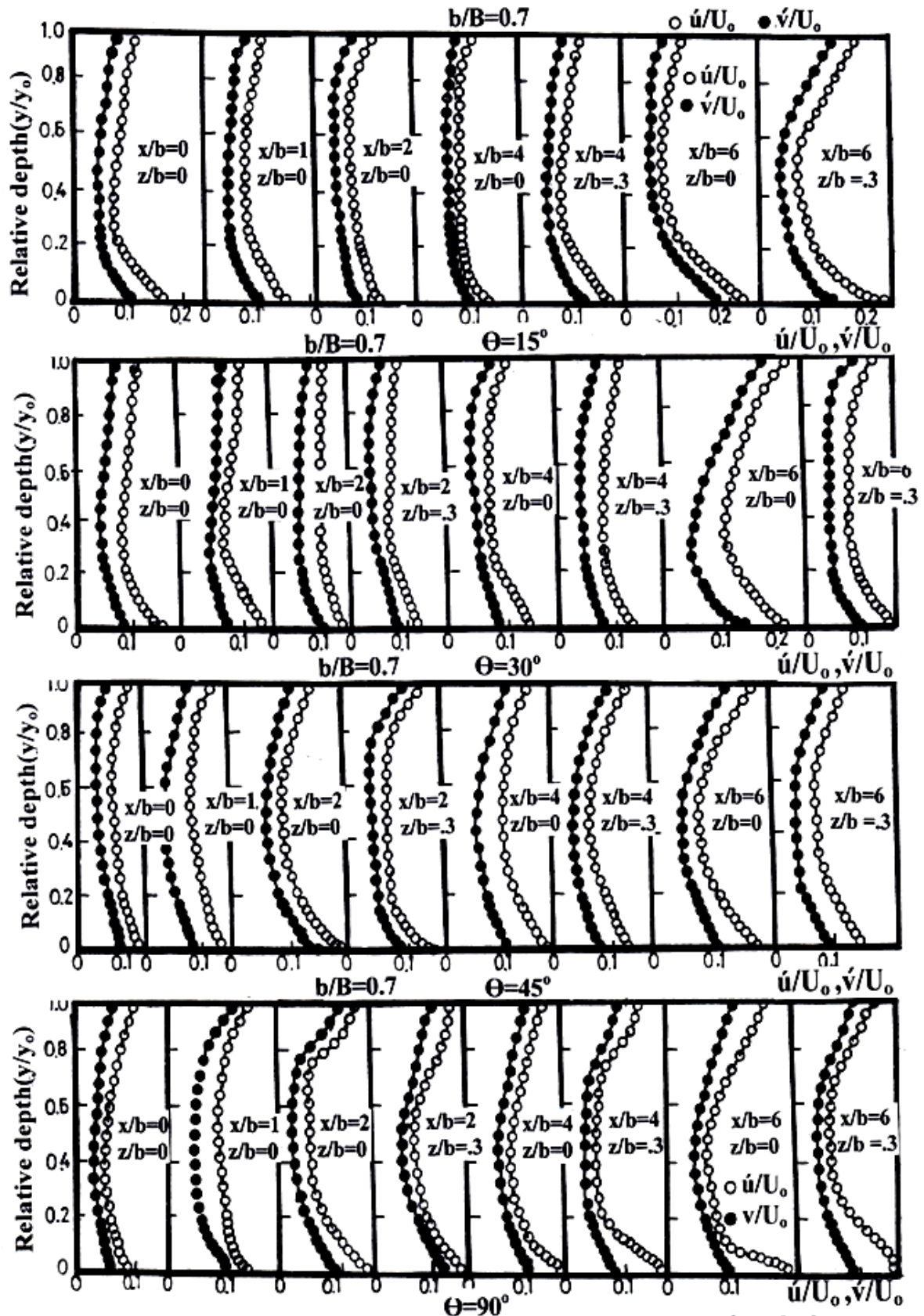


Fig.(12) Variation of streamwise and vertical components of turbulence intensities \bar{u}'/U_0 and \bar{v}'/U_0 with y/y_0 in the expansion zones at $b/B=0.7$ at expansion angles $\Theta=15^\circ, 30^\circ, 45^\circ$ and 90° for $Q=30$ lit./s .

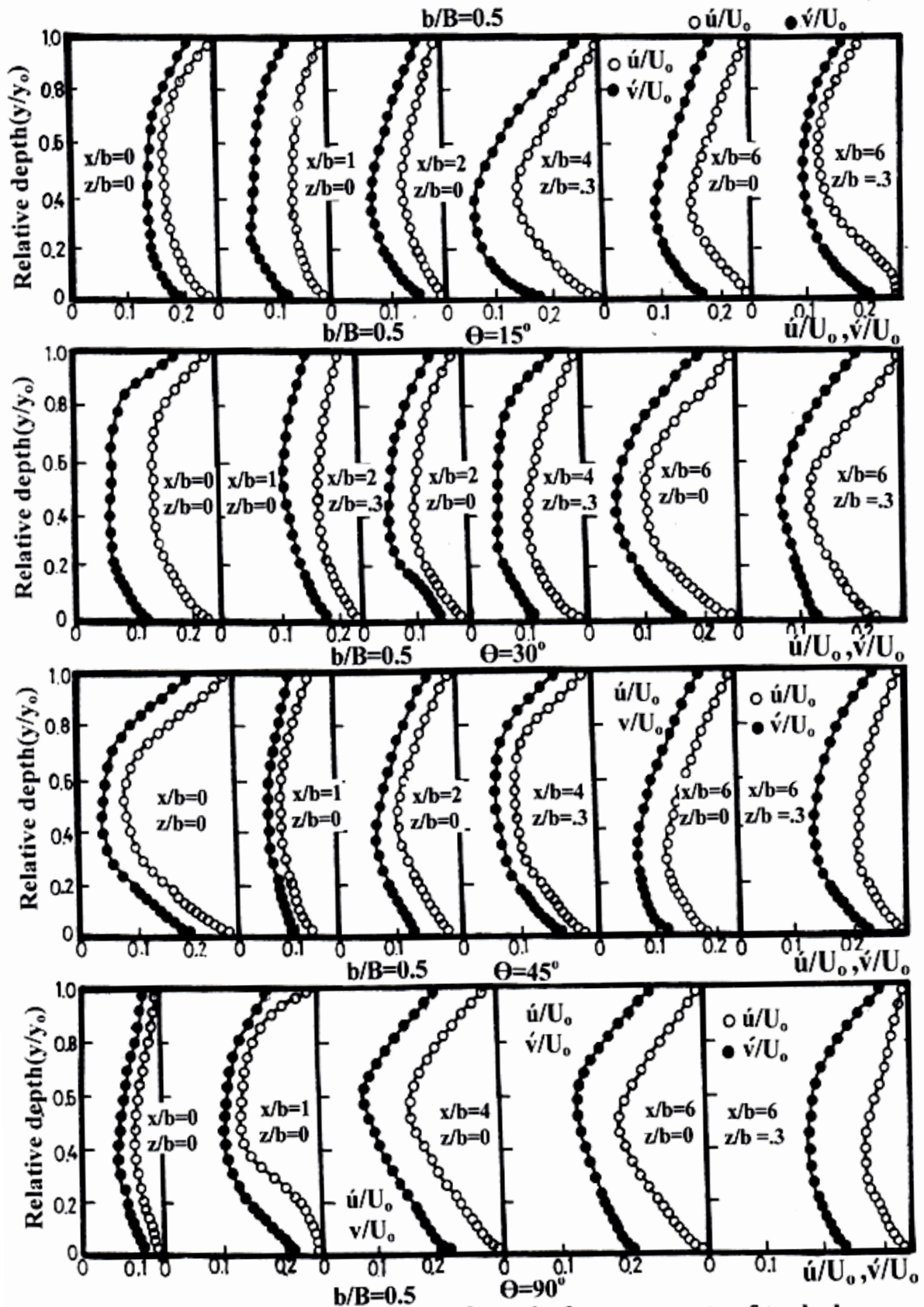


Fig.(13) Variation of streamwise and vertical components of turbulence intensities \dot{u}/U_0 and \dot{v}/U_0 with y/y_0 in the expansion zones at $b/B=0.5$ at expansion angles $\Theta=15^\circ, 30^\circ, 45^\circ$ and 90° for $Q=30$ lit./s .

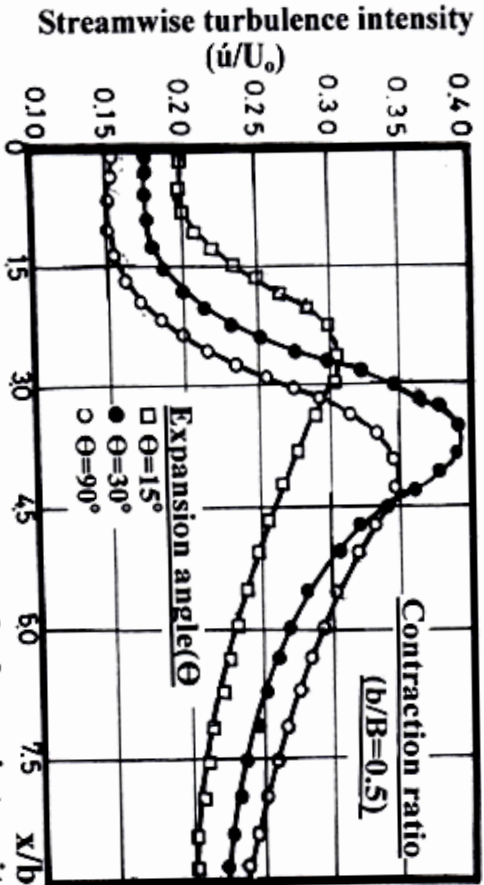


Fig.(14) Variation of streamwise turbulence intensity \bar{u}'/U_0 along the centerline at $y/y_0=0.5$ in the expansion zones at expansion angles $\Theta=15^\circ, 30^\circ$ and 90° at different contraction $b/B=0.7$ and 0.5 for $Q=40$ lit./s

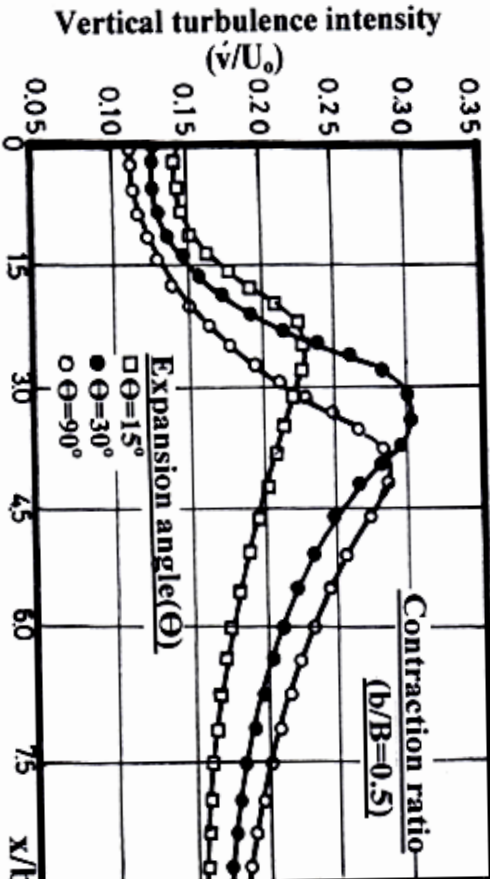
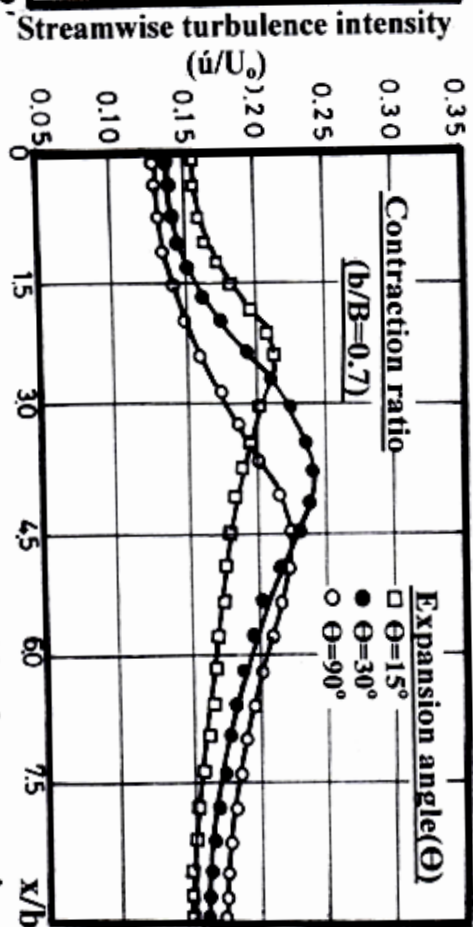
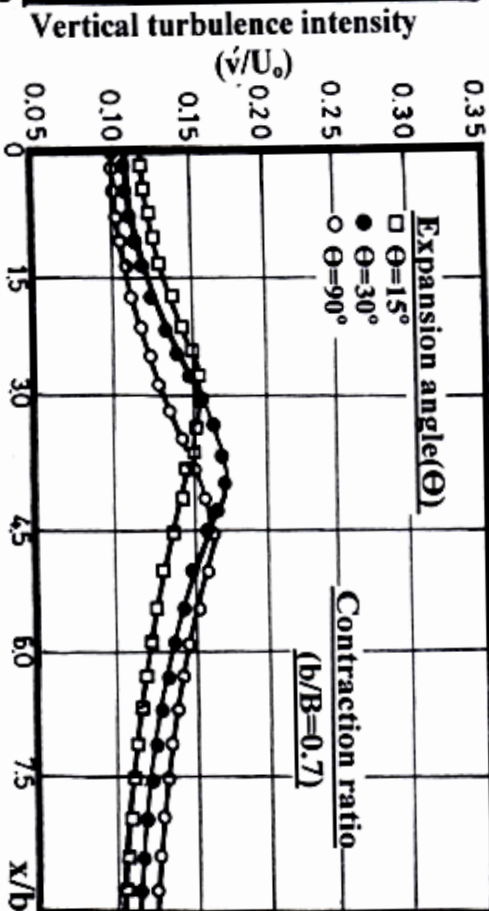


Fig.(15) Variation of vertical turbulence intensity v'/U_0 along the centerline at $y/y_0=0.5$ in the expansion zones at expansion angles $\Theta=15^\circ, 30^\circ$ and 90° at different contraction $b/B=0.7$ and 0.5 for $Q=40$ lit./s.



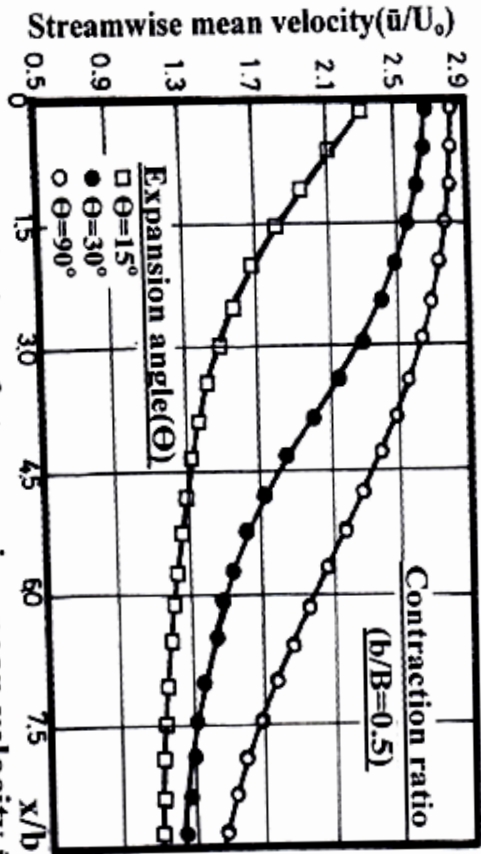


Fig.(16) Variation of streamwise mean velocity \bar{u}/U_0 along the centerline at $y/y_0=0.5$ in the expansion zones at different expansion angles $\Theta=15^\circ, 30^\circ$ and 90° at different contraction $b/B=0.7$ and 0.5 for $Q=40$ lit./s.

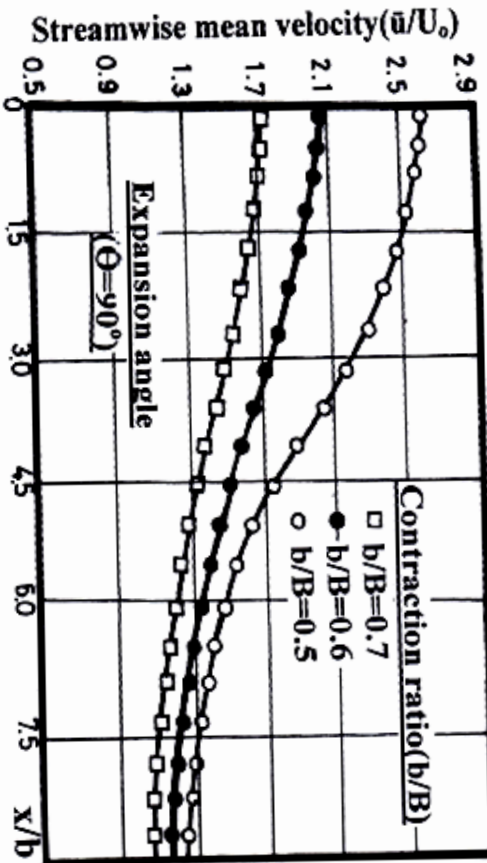
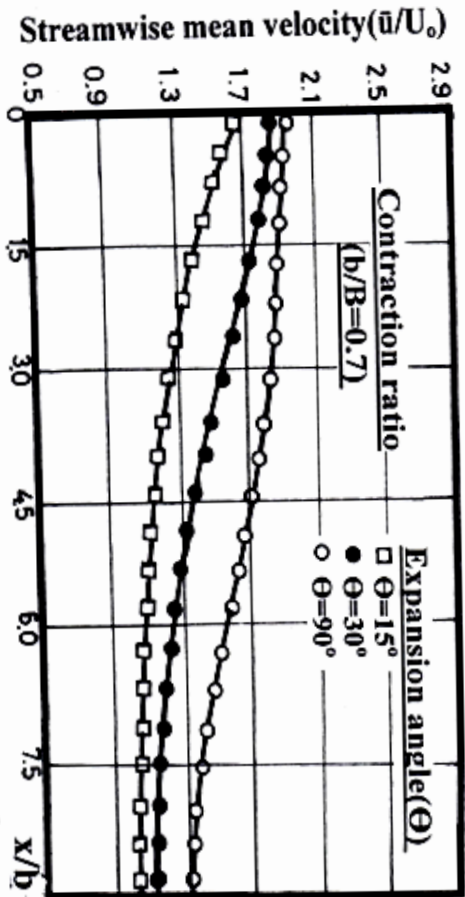
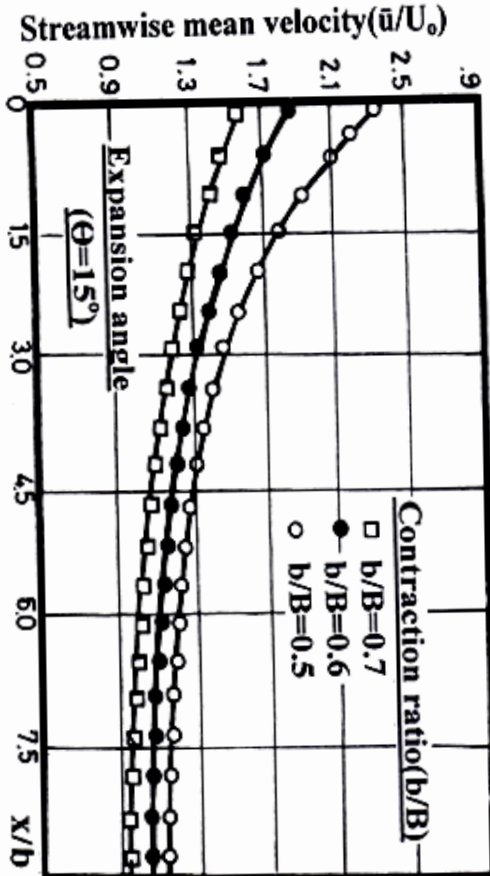


Fig.(17) Variation of Streamwise mean velocity \bar{u}/U_0 along the centerline at $y/y_0=0.5$ in the expansion zones at different contraction $b/B=0.5, 0.6$ and 0.7 at expansion angles $\Theta=15^\circ$ and 90° for $Q=40$ lit./s.



Analysis of Emergence of Cities

Ranjita Gaonkar¹, Varunakshi Bhojane²

¹(Department of Computer Engineering, Pillai Institute of Information Technology, Mumbai University, India)

²(Department of Computer Engineering, Pillai Institute of Information Technology, Mumbai University, India)

ABSTRACT : Emergence is the creation of systems of greater dimension than the elements that create it. Emergence is a phenomenon which is intrinsic to the way systems grow and evolve. Since the dawn of civilization, humans have made cities to support their societies. These cities, although they have been the source of progress, have never been fully understood, relying on traditions and trial-and-error processes for their growth. The reason for this is because they occur in the emergent dimension, and later attempts to plan them and bring them under the control of a central planner have resulted not in ordered cities, but disordered emergence. In this paper, we have discussed different aspects of emergence of cities and its analysis.

Keywords: City, population, urban planning, urbanization, optimization.

I. INTRODUCTION

At present, the population and economic activities in the metropolitan area is over-intensive, and this creates enormous pressure on urban operation. Developing a new city to expand urban space, optimize its structure, ease urban pressure coming from the population growth, and enhance the urban competitiveness, has become one of the key issues in the field of urban planning and management. In the context of this reality, the forecast and plan on urban spatial structure is very important to the development of urban economy. In the globalization environment, economic model changes substantially leading to population and industries to concentrate in the urban area where information, resources, capital, and human resources exchange rapidly among cities. This change leads to competition, originally among nations, gradually among cities [1]. One cannot predict the outcome of a city, but only try to determine the processes by which the city evolves. Studying the rules that enable emergence will allow us to build the systems to deal with the complexity of the universe.

II. CONTEXT

New cities are born at stochastically determined times when existing cities are larger than their optimal sizes and unstable. Emergence of cities is affected by several attributes within different facets ranging from geography to economics to environment. These variables have direct influences in the final characteristics of the emergent city [2]. In this work, primary aim is to determine idea behind optimal emergence of a new city in order to develop a new town. Determining optimal emergence from an initial setup is often a NP-class problem where solution cannot be expressed by formulae or algorithms. This work utilizes Genetic Algorithm (GA) in an attempt to discover an optimal emergence from a given arbitrary initial setup.

Genetic algorithms belong to the larger class of evolutionary algorithms (EA), which generate solutions to optimization problems using techniques inspired by natural evolution, such as inheritance, mutation, selection, and crossover. Genetic algorithms were developed by John Holland at the University of Michigan in the early 1970's [3]. They operate on a population (a group of individuals) of potential solutions applying the principle of survival of the fittest to generate improved estimations to a solution. At each generation, a new set of approximations is created by the process of selecting individuals according to their level of fitness and breeding them together using genetic operators inspired by natural genetics. This process leads to the evolution of better populations than the previous populations [4].

III. PURPOSE

There are some researches examine city formation in a country whose urban population is growing steadily over time, with new cities required to accommodate this growth [6]. There once was a time when designing new cities was one of the most ambitious and urgent tasks for any urban designer and planner. The purpose of studying city formation theory is to regulate the usage and construction of land. When a plan is drawn up it includes plans of where for example residential areas, workplaces, park and garden areas and traffic will be placed in the city. Town planning is divided into different planning levels. The more general plan directs how the more precise levels can be planned

IV. SIGNIFICANCE

Strategic urban planning is very important in ensuring sustainable utilization of land available in urban areas. A good urban planning plan can help to promote development in an area as well as solve some of the problems that face urban areas such as high population and sanitation problems. One of the importances of urban planning is to enable correction of mistakes that had earlier being made in the design of urban areas. Effective urban planning takes into consideration all the demographic factors in the area to ensure that the population has access to all the basic necessities of life.

V. MOTIVATION

Last few decades witness a dramatic increase in city population worldwide associated with excessive urbanization rates. This raises the necessity to understand the dynamics of urban growth process for sustainable distribution of available resources.

In India, with controversies on migration to cities and increasing infrastructure problems in metros like Mumbai and Delhi, the topic of urbanization is forcing itself on to the public sphere. There is a strong view worldwide, that cities that are planned and developed by private enterprises are the solution to these problems. India is going to experience rapid urbanization involving around 300 million people within the next two to three decades. This means that they will either drift to existing cities, thus congesting them further, or move into new cities. If it is new cities, then they will have to be either cities that are planned, or cities that evolve, more or less in an unplanned manner [5]. According to "A Vision of Smarter Cities" published by IBM, 500 new cities are to be developed in the next 20 years. This is equivalent to an increase of seven new cities at the size of city New York worldwide. And by 2050, 70% of the world population is expected to live in the cities. Although rapid urbanization is an indication of economic and social progresses for emerging countries especially, the global infrastructure is required to become smarter to cope with the environmental changes [1].

VI. LITERATURE SURVEY

In order to motivate this approach, it is useful to see how the extant literature has addressed them. The development of smart city can be categorized into two types, emerging city and redeveloped city [1].

- **Emerging Cities:** This is mostly found in emerging countries. A typical example is the Masdar Initiative, a future green city, of the United Arab Emirates, to be completed in 2015. Masdar is a city under construction with an area of 6.4 km² accentuating the world's very first city with zero waste, zero carbon emission, and zero radiation. The entire city is designed to be a gigantic recycling system for all resources. All energies employed in the city are from renewable energies, including solar, wind power, hydrogen, and green buildings implementing the concept of a sustainable city.
- **Redeveloped Cities:** This is found mostly in developed countries and often referred to as urban planning. A representative city is the Amsterdam Smart City Project in the Netherlands. Although exploiting existing infrastructure in the city, the energy efficiency is improved with additional sensors and control equipments. The landscape doesn't seem to change much after the redevelopment; however, through smart energy-saving technologies, carbon dioxide emission and energy consumption have been reduced substantially leading to an improved quality of life and environment. An urban plan can take a variety of forms including strategic plans, comprehensive plans, neighborhood plans, regulatory and incentive strategies, or historic preservation plans. Urban planning (urban, city, and town planning) is a technical and political process concerned with the control of the use of land and design of the urban environment, including transportation networks, to guide and ensure the orderly development of settlements and communities. It concerns itself with research and analysis, strategic thinking, architecture, urban design, public consultation, policy recommendations, implementation and management [7].

This research work focuses on the first type, Emerging city and will help in understanding the process of formation of a city on a particular land.

1.1 What is a city?

A city is a mesh of relationships between spaces. It begins once a space is built to provide a specialized function that is not fulfilled by another existing space, and the two spaces are linked together by a communication system.

1.2 Development Strategy

In this work, following important aspects are considered in order to ensure how an effective city can be formed in a particular place [1].

1.2.1 **Smart Environment:** The purpose is to establish a comfortable zoning guideline to make the best of land and to contemplate lifestyle and safety in designing architectures. Urban zoning concept is incorporated in planning disaster precaution system, against fire and typhoon especially. The area is further divided into regions, communities, and architecture and block model for management purposes accordingly.

1.2.2 **Smart Transportation:** The purpose is to minimize the impact from traffic by promoting the mobility and accessibility of public transportation in the city.

1.2.3 **Smart Lifestyle:** The purpose is to provide smart lifestyle in order to ensure Hazard prevention, health caring, power saving and sustainability, smart and convenient, comfortable and convenient, and leisure standard of living, also to ensure the success rate of services and products.

1.2.2 **Smart Economy:** Economy plays vital role in emerging city. Developing industries will boost job opportunities which will help to improve economy of the city.

In order to implement this development strategy, this work can use products and services to be provided in a particular land so as to analyze whether a city can be emerged in a particular area or not.

1.3 Urban Structure

Urban structure is the arrangement of land use in urban areas. Sociologists, economists, and geographers have developed several models, explaining where different types of people and businesses tend to exist within the urban setting. Urban structure can also refer to the urban spatial structure, which concerns the arrangement of public and private space in cities and the degree of connectivity and accessibility.

1.4 Urbanism

Since the dawn of civilization, humans have made cities to support their societies. These cities, although they have been the source of progress, have never been fully understood, relying on traditions and trial-and-error processes for their growth. The reason for this is because they occur in the emergent dimension, and later attempts to plan them and bring them under the control of a central planner have resulted not in ordered cities, but disordered emergence. Urbanity is the cooperation and mutual-support of large numbers of people in close proximity. It is inevitably emergent and to understand the science of emergence is the key to inventing the first fully emergent urbanism, capable of resolving all the complexities of a 21st century, sustainable city.

Designing cities is possible. The means of designing cities are, by the fact of the emergent nature of cities, completely different from modern architectural practice. Understanding those means is what will enable us to carry out the will of the billions of urbanites of the world: to live in more enjoyable, more beautiful environments, and be free to transform these environments. And hence it becomes important to understand and develop theory that gives the possibility to build a city.

1.5 Real World Scenarios

An evolution or an emergence of a city can be a slow or a sudden quick process. It can depend upon multiple factors, considering the resources, potentialities in different fields of the nation as a whole. Most of the times emergence of a city is occurred when basically the, main city has been over crowded or a city is actually needed when the scope of particular industries or educational institution is more.

The main factors for emergence/evolution of cities can be:

- The scope for an industry or educational institutions is given importance, i.e. the scale of activities like business trade, commerce etc.
- The scale of socio economic and cultural activities has dramatically grown and the co activities has been affected and thus the need of a new sister city is required.

Considering above mentioned factors, some real world scenarios can be considered as follows:

- Jamshedpur can be pointed out as the example for the first point of city evolved from industrial use. The city had evolved from the vision of Jamsetji Tata, when he conceptualized his dream city, was built on the ideology that it would comprise not merely Asia's first fully integrated steel plant, but also embody a step towards building a new Nation[9].
- Between 1951 and 1961, the population of Mumbai rose by 50% and in the next decade by 80.8%. This rapid growth was due to the increasing industrial and commercial importance of the city. It resulted in a deteriorated quality of life for many of the city's inhabitants. Expansion of the city was limited by the physical location of the city on a long, narrow peninsula with few mainland connections. The goal was to shift population and commercial activities from Mumbai to Navi Mumbai, which would be sustainable physically, economically and environmentally. The new city was projected to gain two million people and 750,000 jobs from the 1970s through the 1990s [8].

1.6 Optimization

Optimization is a process that finds a best or optimal solution for a problem. The process of city / town planning can be considered as optimization problem. In this work, primary aim is to determine idea behind optimal emergence of a new city in order to develop a new town. Determining optimal emergence from an initial setup is often a NP-class problem where solution cannot be expressed by formulae or algorithms. This work can further be implemented by using Genetic Algorithm (GA) and can be an attempt to discover an optimal emergence from a given arbitrary initial setup.

VII. CONCLUSION

From this study of analysis of emergence of cities, it can be concluded that planning of a new city or redeveloping an existing city is the area fall into optimization category of problem solving where computational techniques can be applied in order to study them more clearly. Further research can be carried out in different facets and an approach for solving this optimization problem of emergence of cities, Genetic Algorithm can be proposed in future.

REFERENCES

- [1] Hsieh, Hung Nien "A Study of Smart Town Development Strategies", 978-1-61284-774-0/11/\$26.00 ©2011 IEEE[2] S. E. Page, "On the Emergence of Cities", *Journal of Urban Economics*, vol. 45, pp. 184–8, 1999.
- [3] Holland, J. H., *Adaptation in natural and artificial systems*. Ann Arbor: The University of Michigan Press, 1975.
- [4] E. Eiben, R. Hinterding, and Z. Michalewicz, "Parameter Control in Evolutionary Algorithms", *IEEE Transactions on Evolutionary Computation*, IEEE, 3(2), 1999, pp. 124-141.
- [5] R N Bhaskar, "The New Cities Of India", Forbes, India, Nov 30, 2010
- [6] J. Vernon Henderson and Anthony Venables, "The Dynamics of City Formation", *NBER Working Paper No. 13769 February 2008 JEL No. O1,O18,R0,R1*
- [7] Allmendinger, Phil and Michael Gunder, 2005, "Applying Lacanian Insight and a Dash of Derridean Deconstruction to Planning's 'Dark Side'," *Planning Theory*, vol. 4, pp. 87–112.
- [8] CIDCO <http://cidconmia.com/website/about-cidco>
- [9] The Jamshedpur Story <http://www.tatasteelindia.com/corporate-citizen/corporate-sustainability/jamshedpur-story.asp>

Physical and Mechanical Properties of Fly Ash of Kosova B TPP for Utilization as Product for Partial Cement

Mevlan Qafleshi¹, Driton R. Kryeziu², Misin Misini³, Lulezime Aliko⁴

¹ Faculty of Mathematical Engineering and Physical Engineering, Polytechnic University of Tirana, Tirana, Albania

² University for Business and Technology, Prishtina, Republic of Kosovo

³ Faculty of Civil Engineering and Architecture, University of Prishtina, Prishtina, Republic of Kosovo

⁴ Faculty of Mathematical Engineering and Physical Engineering, Polytechnic University of Tirana, Tirana, Albania

ABSTRACT: In Kosovo the electricity generation from lignite-fired power plants produces around 1 Mt/annually of fly ash as combustion byproduct. The energy demand in Kosovo increases each year and the same with the lignite consumption that directly leads to the increase of fly ash production. Since the first operation of first thermal power plant till now there are around 27 Mt of unutilized fly ash, i.e. fly ash in Kosovo has not been treated or utilized at all. In the other hand, the concrete industry, respectively cement production process is associated with CO₂ emission, around 5% of world's CO₂, which is a greenhouse gas. The cement production is increasing due to high market needs and consequently more CO₂ emission in the atmosphere. The results of studies and researches show that each tonne of cement contributes with the emission of around 1 tonne of CO₂. In this paper, the studying of physical and mechanical properties of Kosovo B TPP Fly ash intends to boost efforts for utilization of fly ash of Kosovo as partial cement replacement or admixture through its standardization as construction product. The benefits of this utilization will be of great importance for saving the environment, the improvements of many properties of concrete built with a certain percentage of fly ash, and finally with the direct substitution of cement with fly ash which results with the decrease of CO₂ emissions from cement industry. The test results of this study are in favor of these benefits.

Keywords: Kosovo, fly ash, compressive strength, flexural strength, initial setting, standardization.

I. INTRODUCTION

The fly ash produced in Kosova A and Kosova B thermal power plants has high lime content, i.e. it is calcareous fly ash possessing cementitious and hydraulic properties [1]. As according to the ASTM C618 12a, the general classification of Fly ash is done conform to the percentage content of CaO, and since the Kosovo fly ash is produced from burning lignite, the test analyses showed that lime content in fly ash was 32.92 % [2]. The testing has been done in accordance with SIST EN 197-1, clause 3.1 and this percentage value classifies the Kosova B TPP Fly ash to Class C [3] [4]. Class C Fly ash in addition of pozzolanic properties has also cementitious properties enabling the use of this ash in cement, respectively concrete industry.

The chemical analyses regarding the composition of the fly ash from Kosova B TPP show no different or exceptional properties comparing to the fly ashes from other countries. This similarity in chemical composition would pave the way for utilization of Kosovo fly ash in the cement and concrete industry. As the chemical composition of fly ash generally allows its use, then the physical and mechanical properties should be in accordance with the standards that depict the use of fly ash in industry. This paper study aims to examine and test the basic physical and mechanical properties of the Kosovo fly ash and standardize it as an industrial construction product. This utilization may have a fundamental importance for producing green concrete: less CO₂ emissions and less surface land pollutions.

II. FLY ASH PRODUCTION FROM LIGNITE COMBUSTION

According to European standard for Fly ash in Concrete, fly ash is defined as "Fine powder of mainly spherical, glassy particles derived from burning of pulverized coal, with or without co-combustion materials, which has pozzolanic properties and consists essentially of SiO₂ and Al₂O₃ [5].

Kosovo with lignite reserves around 14 Bt [6] has oriented its energy strategy towards the Thermal Power plants with lignite as burning fuel. The total installed power capacity of TPP Kosova A and B is 1478 MW. The energy generation only from Kosovo Energy Corporation TPPs is over 97%. The rest is from hydro-power-plants [7]. The Kosovo Government has planned the construction of one other TPP unit "The New Kosovo", with anticipated installed capacity 1000 MW in the first phase, and with another 1000 MW in the second phase [8]. The increase of generating capacities implies increase of lignite consumption, more fly ash consequently.

Table I: Kosovo lignite quality and parameters [9]

Ash content	12-21%. The average values 14-17%		
Moisture content	35-50%		
Heating values	Bardh -Mirash	7800 KJ/kg	
	Sibovc	8100 KJ/kg	
	Total reserves	29%	> 8.4 MJ/kg
		43%	7.7-8.4 MJ/kg
25%		5.8-7.7 MJ/kg	
Sulfur content	1 %. In all deposits/mines. The average content of combustible sulfur is 0.35%		
Lime	The concentration of lime is sufficient to absorb the SO_x gas emitted during combustion- no need for desulfurization of flue gases		

From the analyses of Kosovo lignite, the content of ash in lignite is around 14-17% by mass [9]. This indicates that from burning of 1ton lignite the residue ash is around 160 kg, 80% of which is captured by ESP as Fly ash [10]. A calculation shows that up to 2012, in Kosovo there are around 27 Mt of unutilized fly ash. Only in 2012 the lignite combustion in Kosova A and B TPP produced around 1 Mt of fly ash [4]. Taking an average of 16% of ash content in Kosovo lignite, in the Table I it is shown the quantity of fly ash production during 2002-2012.

Table II: Fly ash production in TPP Kosova A and Kosova B [11] [12]

	Year	2002	2003	2004	2005	2006	2007	2008	2009	2010	2011	2012
Lignite consumption	Mt	5.23	5.64	5.59	6.27	6.35	7.11	7.46	8.41	9.34	9.11	9.35
Ash production	Mt	0.84	0.90	0.89	1.00	1.02	1.14	1.19	1.35	1.49	1.46	1.50
Fly ash production	Mt	0.67	0.72	0.72	0.80	0.81	0.91	0.95	1.08	1.20	1.17	1.20

As it is shown, the residues of burning lignite are millions of tonnes of fly ash that up to now in Kosovo have not been utilized at all. Explicitly said this ash is a waste. As many countries in the world utilize Fly ash either as direct cement replacement in concrete production and/or as mineral additive in concrete for improving specific properties of mortars and concrete, in Kosovo the Fly ash utilization is not taking place.

The use of fly ash in concrete industry has manifold advantages, apart from those environmental [13]. A brief description includes the improved workability and consistency of concrete made with fly ash, reduction of water demand [14], concrete pumping, compatibility, flow ability, reduced agglomeration, less risk of surface shrink holes [14], reduces water segregation [15].

The crucial part of this study focuses on the physical and mechanical properties of Kosovo Fly ash with the aim of standardizing this waste residue to a product conform to European Standard EN 450-1 for use in construction industry [5]. The results of this standardization would avoid all suspicions and concerns for the utilizations of Fly ash from KEK TPPs in concrete industry. If not to the world, but in Kosovo this would be a milestone of a great importance, economically and environmentally.

III. CHEMICAL AND MINERALOGICAL COMPOSITION OF KOSOVO B FLY ASH

The chemical composition favors to a great extent the utilization of fly ash in concrete industry as partial cement replacement. Based on its chemical composition, or better said due to high CaO content (in % by mass), Kosova B Fly ash belongs to calcareous fly ash, i.e. Class C fly ash [4].

Table III: Chemical composition of Kosovo B fly ash

constituent	formula	%/wght
Silica	SiO₂	29.7
Alumina	Al₂O₃	10.65
Iron Oxide	Fe₂O₃	6.18
Lime	CaO	32.92
Magnesium oxide	MgO	5.93
Sulfur	SO₃	9.98
Sodium oxide	Na₂O	0.74
Potassium oxide	K₂O	0.61
Loss on ignition		2.09

These chemical constituents influence the properties of concrete produced with a certain percentage of fly ash as cement replacement or admixture.

IV. PHYSICAL AND MECHANICAL PROPERTIES OF FLY ASH OF KOSOVO B TPP

The ash samples for analyses of physical and mechanical properties were taken from Kosovo B TPP and physical and mechanical analyses were conducted at laboratory **ZAG, Department of materials, Laboratory for cement, mortar and ceramics, Ljubljana, Slovenia**. The analyses were conducted in conformity with European Standards SIST EN 450-1:2005 5.2 and 5.3 [5].

Table IV: Physical properties of Fly ash

Component	Measured	Requirements SIST EN 450-1, cl. 5.3	Test method
Bulk density	2.56 g/cm ³	-	SIST EN 196-6
Fineness	35.9 %	□ 40%, N category	SIST EN 451-2
Soundness (expansion) CEM I +EF	1.1 mm	□ 10 mm	SIST EN 450-1, cl. 5.3.3
Water for standard consistency: CEM I CEMI+ EF	30.0% 31.8 %	- -	SIST EN 450-1, cl. 5.3.5
Initial setting CEM I CEM I + EF	185 min 260 min	□ 370 min	SIST EN 450-1, cl. 5.3.5
Final setting CEM I CEM I +EF	230 290	- -	SIST EN 450-1, cl. 5.3.5
Activity index in 28 days	79.5 %	□ 75%	SIST EN 450-, cl. 5.3.2
Activity index in 90 days	87.1 %	□ 85 %	SIST EN 450-, cl. 5.3.2

4.1. Soundness 1.1 mm

According to Brown et al. "Soundness is the ability of a cement paste, mortar or concrete to withstand internal stresses generated during cement hydration, without cracking [16]. During the process of hydration of cement blended with fly ash, the presence of expanding oxides as CaO and MgO reacting with water form respective hydroxides Ca(OH)₂, Mg(OH)₂ which have large molecular volume. This leads to internal stresses in concrete followed by cracks consequently [17]. In the case of Kosovo B TPP fly ash the expansion doesn't exceed 1.1 mm, which is in full compliance with the requirements of SIST EN 450-, cl. 5.3. [5]. The testing method according to SIST EN 196-3 [18], limits this soundness up to 10 mm, that our Fly ash, is very sound. The test designs a proportion of mixture of 30%/mass of calcareous fly ash and 70%/mass of cement CEM I.

4.2. Fineness 35.9 %

Fineness or particle size of fly ash is measured, commonly by sieve analysis and is expressed as the proportion of mass in percent of the ash retained when wet sieved on a 0.045 mm mesh sieve. This physical property is very important because the specific surface of fly ash directly influences the compressive and tensile splitting strength of concrete made with a certain percentage of fly ash [19]. The fineness is expressed as the mass proportion in percent of the ash retained when wet sieved on a 0.045 mm mesh sieve. The fineness is determined in accordance with the SIST EN 451-2, Method for testing fly ash-Part 2: Determination of fineness by wet sieving. This standard limits the fineness for category N not to exceed the value 40% by mass, and the Kosovo B fly ash with fineness 35.9% is compatible with the European standard.

4.3. Water for standard consistency 31.8%

This is determined in conformity with the method prescribed by European Standard **SIST EN 451-1, Cl. 5.3.5**. The test result for **CEM I+ Fly ash** is **31.8%**, whilst only for CEM I is **30%**. Even though the European Standard **SIST EN 451-1** does not have any requirement for water for standard consistency, this represents a fluctuation because the use of fly ash in concrete/cement generally should reduce the water demand for achieving the same consistency as cement alone [14].

4.4. Initial setting time 260 min

It represents the time when the cement paste, in our case cement + fly ash starts to stiffen. The test regarding the initial setting time of cement alone shall meet the requirements specified in **EN 197-1** [20], that in our case for CEM I (Portland cement CEM I 42, 5 R) is **185 min**. The determination of the initial setting time of **CEM + Fly ash** is done in accordance with **SIST EN 450-1: 2005+A1:2007 (E)**, respectively **EN 196-3** [18] and the setting time is **260 minutes**, which is smaller than the standards requirement ≤ 370 min, i.e. this is in compliance with the European standard requirement.

4.5. Activity index

Activity index is ratio of the compressive strength of cement paste, mortar or concrete with fly ash to that of compressive strength of control sample. As the compressive strength of the sample with or without fly ash is determined at the age of 28 days and 90 days, under the same curing conditions, here are presented the tests results for respective ages [20].

4.5.1. In 28 days 79.5 %

This is determined in accordance with SIST EN 450-1, cl.5.3, and the testing method conform SIST EN 450-1, cl. 5.3.2, which require the value/ratio not to be less than 75%. The activity index of Kosovo fly ash in 28 days is 79.5% that is in full compliance with the requirements of standard.

4.5.2. In 90 days 87.1 %

This is also determined in accordance with SIST EN 450-1, cl.5.3, and the testing method conform SIST EN 450-1, cl. 5.3.2, which require the value/ratio not to be less than 85%. The activity index of Kosovo fly ash in 90 days is 87.1 % that is in full compliance with the requirements of standard.

4.6 Flexural and Compressive strength of cement CEM I 42.5 R

In the Table V are shown the flexural strength and compressive strength of CEM I 42.5 R, which is considered to be the referent sample with which we will compare these two mechanical properties of cement mixed with fly ash. The analyses are done in accordance with SIST EN 197-1, which is the European Standard for cement [21], and SIST EN 196-1, which is the European standard for testing cement [22]. Both, flexural strength and compressive strength were tested at two ages, 28 and 90 days.

Regarding the flexural strength the SIST EN 197-1 does not set any requirements, but for compressive strength it does. The mean value of three measurements, at 28 days is 60.6 Pa. This is in compliance with the aforementioned standard.

Table V: Compressive strength and flexural strength of CEM I 42.5 R

Strength MPa	measurement							Requirement SIST EN 197-1	Test method
	1	2	3	Mean					
Flexural 28 d	9.1	8.1	9.1	8.7				-	SIST EN 196-1
Flexural 90 d	9.0	9.2	9.2	9.2				-	
Compressive 28 d	60.2	59.3	60.2	59.5	62.4	61.8	60.6	□ 42.5 □ 62.5	
Compressive 90 d	69.2	67.9	69.6	66.9	66.6	69.2	68.2	-	

4.7. Flexural and Compressive strength of mixture of CEM I + Fly Ash (SIST EN 450-1, cl. 5.3.2)

The flexural and compressive strength tests of the mixture of CEM I 42.5 R and Fly ash were also carried out in accordance with SIST EN 450-1, cl. 5.3.2. This in fact is the crucial part of this paper: The replacement of a certain part of cement by fly ash. The tests for determining flexural and compressive strength were performed at two ages: 28, respectively 90 days.

Table VI: Flexural and Compressive strength of mixture of CEM I 42.5 R + Fly Ash

Strength MPa	measurement							Requirement SIST EN 197-1	Test method
	1	2	3	Mean					
Flexural 28 d	6.9	7.6	6.7	7.1				-	SIST EN 196-1
Flexural 90 d	8.2	8.0	9.0	8.4				-	
Compressive 28 d	48.2	48.9	47.9	47.4	47.7	49.1	48.2	-	
Compressive 90 d	59.0	60.7	59.1	58.3	59.4	59.8	59.4	-	

The comparison of flexural and compressive strengths of mix CEM I + Fly ash with the one that is considered as referent, i.e. only cement paste, in fact justify the use of fly ash as cement replacement; the achieved values of these two strengths are very satisfying for utilizing of the fly ash. These tests that prove that Kosovo Fly ash meets the necessary requirements of standards, support the aim of this study for utilizing the fly ash of Kosovo as construction material by using as cement replacement in concrete production industry.

Table VII: Comparison of Flexural and Compressive strength

Strength (MPa)	Flexural		Compressive	
Age (days)	28	90	28	90
CEM I (Referent)	8.7	9.2	60.6	68.2
CEM I + Fly Ash	7.1	8.4	48.2	59.4

VI. CONCLUSIONS

The energy generation sector in the Republic of Kosovo is profoundly dependant from the energy production by thermal power plants. These plants use lignite as fuel for combustion. Apart from the emissions of greenhouse gases the process of lignite combustion produces around 1 Mt of fly ash annually. A simple calculation shows that since the first operation of first TPP Unit, in Kosovo there were produced more than 27 Mt of unutilized ash, and due to the increase of electricity generation this amount increases daily. Up to now, this ash has been considered as a waste and nothing was done for its utilization. Being so, it represents not only a waste that should be stockpiled, but it also represents an industrial pollutant of environment that must be considered very seriously.

This study aims to turn this industrial waste to an industrial construction product. The study of the chemical and mineralogical composition of Kosovo fly ash proved that many of its properties are in compliance with European Standard EN 450-1, which depicts the properties of the fly ash for use in concrete. The chemical analyses showed many advantages for utilization, but the content of CaO and MgO was higher and represented a fluctuation from the standard(s). This excessive content of these two oxides may lead to unsoundness of concrete made with a certain amount of fly ash. But, through this study of physical and mechanical properties, the test results prove brilliantly that Kosovo fly ash is very suitable for utilization in concrete industry, overcoming the concerns of unsoundness. The test regarding the soundness that was a concern from the chemical analyses showed that Kosovo fly ash is in full compliance with the SIST EN 450 requirements. The standard requires the value to be ≤ 10 mm, and the expansion (soundness) factor of Kosovo fly ash is much lower, ≤ 1.10 mm. Thus, concrete made with Kosovo fly ash will not undergo any undesired expansion that would cause cracks in the concrete. The fineness or particle size of fly ash which is a very important factor because directly affects the rate of hydration process of fly ash (cement) is very compatible with the requirements of standards. The setting time, both initial and final times meet the standard's requirements. These setting times are of importance because directly affect many properties of concrete such as strength, workability, placement, pumping etc. Regarding the water requirement for standard consistency, although the EN 450-1 does not apply any limit because Kosovo fly ash belongs to fineness class N, Kosovo fly ash show a discrepancy from the general properties of use of fly ash in concrete. Normally for achieving a specific consistency of cement (concrete) the presence of fly ash should reduce the water demand. This is an open issue to be considered for farther studies.

Two mechanical properties, compressive and flexural strength of cement paste made with an addition of Kosovo B fly ash showed very impressive results. These two achieved values of flexural and compressive strength definitely justify the use of Kosovo fly ash in concrete industry as partial cement replacement. The importance of this use is doubled: we will recycle the waste (fly ash) by use in concrete, and indirectly we reduce the CO₂ emissions resulting from the cement production industry.

ACKNOWLEDGEMENTS

The authors would like to thank IPE ProIng, Prishtina, R. of Kosovo for granting access to their data and premises.

REFERENCES

- [1] N. K. Koukouzas, C. Vassilatos, I. Glarakis, *Mixture of Lignite Fly ash in Concrete: Physical and Mineralogical characterization*, Case Study from Ptolemais, Northern Greece, *American Coal Association*, 2005.
- [2] ASTM, American Society for Testing and Materials, Standard Specification for Coal Fly Ash and Raw or Calcined Natural Pozzolan for Use in Concrete.
- [3] European Standard: Cement. Composition, specifications and conformity criteria for common cements.
- [4] M. Qafleshi, L. Aliko, Characterization, Classification and Standardization of Fly Ash of Kosovo Lignite-Fired Power Stations as Industrial Construction Product, *International Journal of Modern Engineering Research*, 3(5), 2013, 3063-3070.
- [5] European standard for fly ash in concrete 450-1, 2007.
- [6] Independent Commission for Mines and Minerals, R. of Kosovo, <http://www.kosovo-mining.org/kosovoweb/en/mining.html>.
- [7] Republic of Kosovo, Ministry of Economic Development, Annual Energy balance of R of Kosovo for the year 2013, 2013.
- [8] V. Sofiu, A. Pervizaj, B. Selimi, E. Erxhepi, The Strategy of energy as a good opportunity for protection of the environment in the republic of Kosovo, *International Journal of Modern Engineering Research*, 3(2), 2013, 604-610
- [9] Energy Strategy and Policy of Kosovo, EU Pillar, PISG Energy Office.
- [10] S. Isufi, *Emission Controls at Kosovo's Thermal Power Plants, Current and Future Capabilities*, AUK, Pristina, 2010
- [11] Kosovo Energy Corporation, KEK statistical data, Strategic development office.
- [12] Kosovo Agency of Statistics, Energy Balance in Kosovo Q4 2012, Kosovo, 2013.
- [13] W. von Berg, H. Hukko, *Fresh mortars and concrete with fly ash*, pp 24, Champan & Hall, London, 2005.
- [14] Berg, Vom, W. : *Kostenorientierter Betonentwurf fuer flugaschehaltige betone*. In: *BetonWerk und fertigteiltechnik* 47, S. 401-407, 1981.
- [15] W. von berg, H. Hukko, *Fresh mortar and concrete with fly ash*, Rilem Report, (Chapman & Hall, London, 2005).
- [16] Brown, P.W.; Berger, R.L.; J.R.; Frohnsdorf, G.; Limitations to fly ash use in blended cements. US. Department of commerce, National Bureau of Standards.
- [17] J.L. Alonso, K. Wesche, *Characterization of fly ash, Fly ash in concrete, properties and performance* (Champan & Hall, London, 2005).
- [18] EN 196-3, Methods of testing cement- Part 3: determination of setting time and soundness
- [19] S. Yazici, S. Arel, Effects of fly ash fineness on the mechanical properties of concrete, *Sadhana, Indian Academy of Sciences*, 37 (3), 2012, 389-403.
- [20] Activity related to strength, Rilem report, *Fly ash in concrete, properties and performance* (Chapman & Hall, London, 2005).
- [21] Cement-Part 1: Composition, specification and conformity criteria for common cements.
- [22] Methods of testing cements-Part 1: Determination of strength.

An Efficient Polynomial Pool-Based Scheme for Distributed Heterogeneous Wireless Sensor Networks

M. Senthil Kumar¹, M. Gopinath²

¹Assistant Professor, Department of ECE, Ranganathan Engineering College, Coimbatore, Tamil Nadu, India,

²PG Scholar, Department of ECE, Ranganathan Engineering College, Coimbatore, Tamil Nadu, India,

ABSTRACT: The Sinks are vivacious in many wireless sensor network (WSN) solicitations for competent data accumulation, confined sensor reprogramming, and for extricating and revoking conceded sensors. However, in sensor networks that make use of the temporal key dissemination schemes for pairwise key naissance and endorsement between sensor nodes and mobile sinks, the engross of mobile sinks for data assortment exalts a new reassurance challenge: in the basic probabilistic and q -composite key redistribution schemes, a mugger can easily procure a hefty number of keys by apprehending a small fraction of nodes, and hence, can gain control of the network by arraying a simulated mobile sink preloaded with some conceded keys. This critique designates a multifarious level general framework that authorities the use of any pair wise key redistribution scheme as its basic component. The new framework necessitates two separate key pools, one for the mobile sink to retrieve the network, and one for pair wise key disposition between the sensors. To auxiliary condense the reimbursements initiated by predetermined access node replication attacks; we have underwired the authentication mechanism between the sensor and the stationary access node in the propositioned framework. Through detailed analysis, we show that our security framework has sophisticated network resilience to a mobile sink replication attack as compared to the polynomial pool-based scheme.

Keywords: Distributed Security, Wireless Sensor Networks, Mobile Sinks

I. INTRODUCTION

The Recent advances in electronic technology have paved the way for the development of a new generation of wireless sensor networks (WSNs) consisting of a large number of low-power, low-cost sensor nodes that communicate wirelessly. Such sensor networks can be used in a wide range of applications, such as, military sensing and tracking, health monitoring, data acquisition in hazardous environments, and habitat monitoring. The sensed data often need to be sent back to the base station for analysis. However, when the sensing field is too far from the base station, transmitting the data over long distances using multichip may weaken the security strength (e.g., some intermediate may modify the data passing by, capturing sensor nodes, launching a wormhole attack, a sybil attack, selective forwarding sinkhole), and increasing the energy consumption at nodes near the base station, reducing the lifetime of the network. Therefore, mobile sinks (MSs) (or mobile soldiers, mobile sensor nodes) are essential components in the operation of many sensor network applications, including data collection in hazardous environments localized reprogramming, oceanographic data collection, and military navigation.

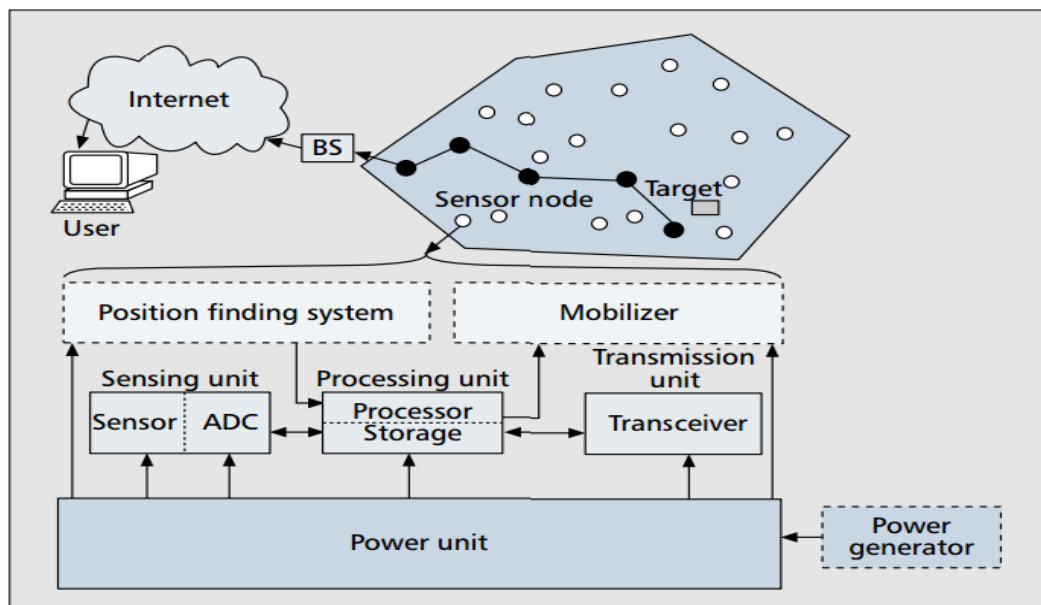


Fig. 1.1 Various Components in Sensor Nodes

In many of these applications, sensor nodes transmit critical information over the network; therefore, security services, such as, authentication and pairwise key establishment between sensor nodes and mobile sinks, are important. However, the resource constraints of the sensors and their nature of communication over a wireless medium make data confidentiality and integrity a nontrivial task. Traditional schemes in ad hoc networks using asymmetric keys are expensive due of their storage and computation cost.

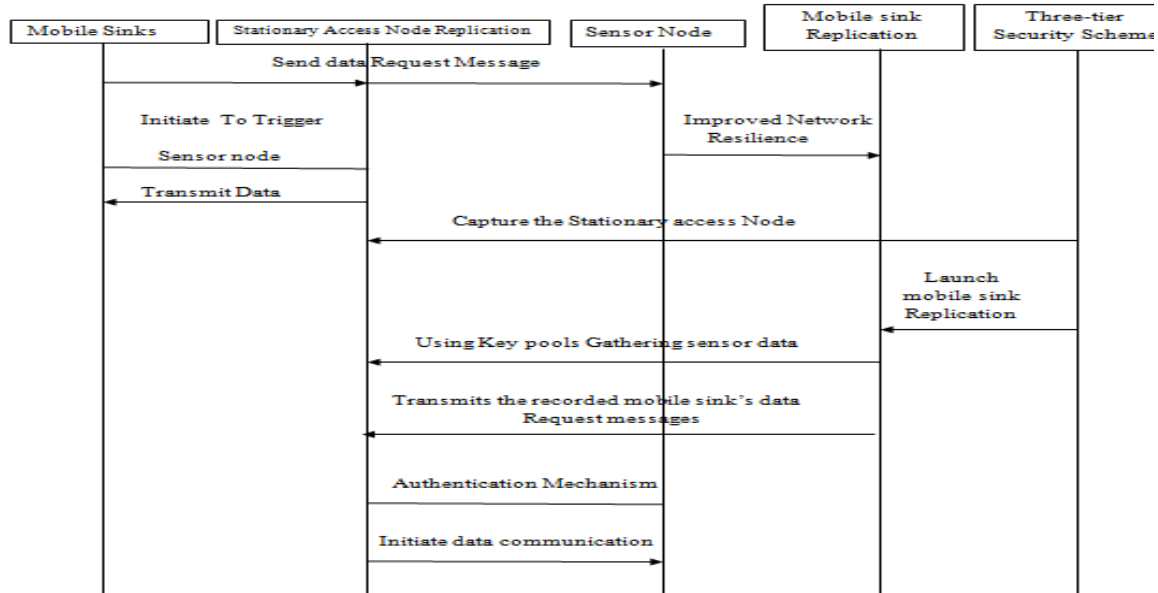


Fig. 1.2 Sequential Process of Mobile Sink Replication in Sensor Nodes

These limitations make key redistribution scheme tools of choice to provide low cost, secure communication between sensor nodes and mobile sinks. However, the problem of authentication and pairwise key establishment in sensor networks with MSs is still not solved in the face of mobile sink replication attacks. For the basic probabilistic and q-composite key redistribution schemes, an attacker can easily obtain a large number of keys by capturing a small fraction of the network sensor nodes, making it possible for the attacker to take control of the entire network by deploying a replicated mobile sink, preloaded with some compromised keys to authenticate and then initiate data communication with any sensor node. To address the above-mentioned problem, we have developed a general framework that permits the use of any pairwise key redistribution scheme as its basic component, to provide authentication and pairwise key establishment between sensor nodes and MSs. To facilitate the study of a new security technique, we first cultivated a general three-tier security framework for authentication and pairwise key establishment, based on the polynomial pool-based key redistribution scheme.

The proposed technique will substantially improve network resilience to mobile sink replication attacks compared to the single polynomial pool-based key redistribution approach, as an attacker would have to compromise many more sensor nodes to launch a successful mobile sink replication attack. In the new security framework, a small fraction of the preselected sensor nodes, called the stationary access nodes, act as authentication access points to the network, to trigger the sensor nodes to transmit their aggregated data to mobile sinks. A mobile sink sends data request messages to the sensor nodes via a stationary access node. These data request messages from the mobile sink will initiate the stationary access node to trigger sensor nodes, which transmit their data to the requested mobile sink. The scheme uses two separate polynomial pools: the mobile polynomial pool and the static polynomial pool. Using two separate key pools and having few sensor nodes that carry keys from the mobile key pool will make it more difficult for the attacker to launch a mobile sink replication attack on the sensor network by capturing only a few arbitrary sensor nodes. Rather, the attacker would also have to capture sensor nodes that carry keys from the mobile key pool. Keys from the mobile key pool are used mainly for mobile sink authentication, and thus, to gain access to the network for data gathering.

II. LITERATURE SURVEY

Classic routing strategies [12], [13] are usually based on a hierarchical organization of the nodes in the network. In fact, the simplest way to aggregate data flowing from the sources to the sink is to elect some special nodes which work as aggregation points and define a preferred direction to be followed when forwarding data. In addition, a node may be marked as special depending on many factors such as its position within the data gathering tree [4], its resources [35], the type of data stored in its queue [16], [7], or the processing cost due to aggregation procedures [8]. According to the tree-based approach [1], [3], [6] a spanning tree rooted at the sink is constructed first. Subsequently, such a structure is exploited in answering queries generated by the sink. This is done by performing in network aggregation along the aggregation tree by proceeding level by level from its leaves to its root. Thus, as two or more messages get to a given node, their aggregate can be computed exactly. However, this way of operating has some drawbacks as actual wireless sensor networks are not free from failures. More precisely, when a packet is lost at a given level of the tree, e.g., due to channel impairments, the data coming from the related sub tree are lost as well. In fact, a single message at a given level of the tree may aggregate the data coming from the whole related sub tree. In spite of the potentially high cost of maintaining a hierarchical structure in dynamic networks and the scarce robustness of the system in case of link/device failures, these approaches are particularly suitable to design optimal aggregation functions and perform efficient energy management.

In fact, there are some studies where the sink organizes routing paths to evenly and optimally distribute the energy consumption while favouring the aggregation of data at the intermediate nodes [6], [9], [10]. In [9] the authors compute aggregation topologies by taking into account the residual energy of each node through linear programming. Further

algorithms can be found in [4], [5], [11], [12]. In [11] the authors investigate which nodes in the network can be exploited as aggregation points for optimal performance. In [14], [12] the focus is on the nodes that should be entrusted with the transmission of the sensed values, whereas in [15] the emphasis is put on the proper scheduling of sleeping/active periods. Often, optimal paths are calculated in a centralized manner at the sink by exploiting different assumptions on the data correlation and selecting the best aggregation points by means of cost functions [13]. Recently, also tree-based schemes for real time or time-constrained applications have been proposed [14]–[16]. The pairwise key establishment problem, however, is still not solved. For the basic probabilistic [12] and the q composite [13] key pre-distribution schemes, as the number of compromised nodes increases, the fraction of affected pairwise keys also increases quickly. As a result, a small number of compromised nodes may affect a large fraction of pairwise keys. Although, the random pairwise key does not suffer from the above-mentioned problem, given a memory constraint, the network size is strictly limited by the desired probability that two sensor nodes share a pairwise key, as also by the number of neighbour nodes with which a sensor can communicate. An enhanced scheme using the t -degree bivariate key polynomial was proposed by Liu et al. [14]. They developed a general framework for pairwise key establishment using the polynomial-based key pre-distribution protocol [21] and the probabilistic key distribution in [12] and [13]. Their scheme could tolerate no more than compromised nodes, where the value of t was limited by the memory available in the sensor nodes.

III. METHODOLOGY

3.1 Existing Method

Three different routing metrics, that aims at an appropriate tradeoff between the detection performance and the energy expenditure. In particular, each metric relates the detection performance explicitly in terms of probabilities of detection and false alarm, with the energy consumed in sensing and routing. Prior to deployment, each mobile sink randomly picks a subset of polynomials from the mobile polynomial pool. In our scheme, to improve the network resilience to mobile sink replication attack as compared to the single polynomial pool based approach, we intend to minimize the probability of a mobile polynomial being compromised if R_c sensor nodes are captured. As an adversary can use the captured mobile polynomial to launch a mobile sink replication attack, the routing problems are formulated as combinatorial optimization programs, and we provide solutions drawing on operations research.

3.2 Disadvantages

The Neyman–Pearson criterion widely adopted for target detection and surveillance related applications. This formulation, as far as we are aware, is the first one which accounts for both the energy consumption in sensing and routing, and detection performance (in terms of detection probability and false alarm probability) at the same time. The detection performance and the energy expenditure are considered jointly in a different but interesting way by which an appropriate tradeoff between them is attained. Provide algorithms for solving those formulated integer programming problems, based on state-of-the-art operations research results.

3.3 Proposed Method

The study presented a general three-tier security framework for authentication and pairwise key establishment between mobile sinks and sensor nodes. The proposed scheme, based on the polynomial pool-based key redistribution scheme substantially improved network resilience to mobile sink replication attacks compared to the single polynomial pool-based key redistribution approach.

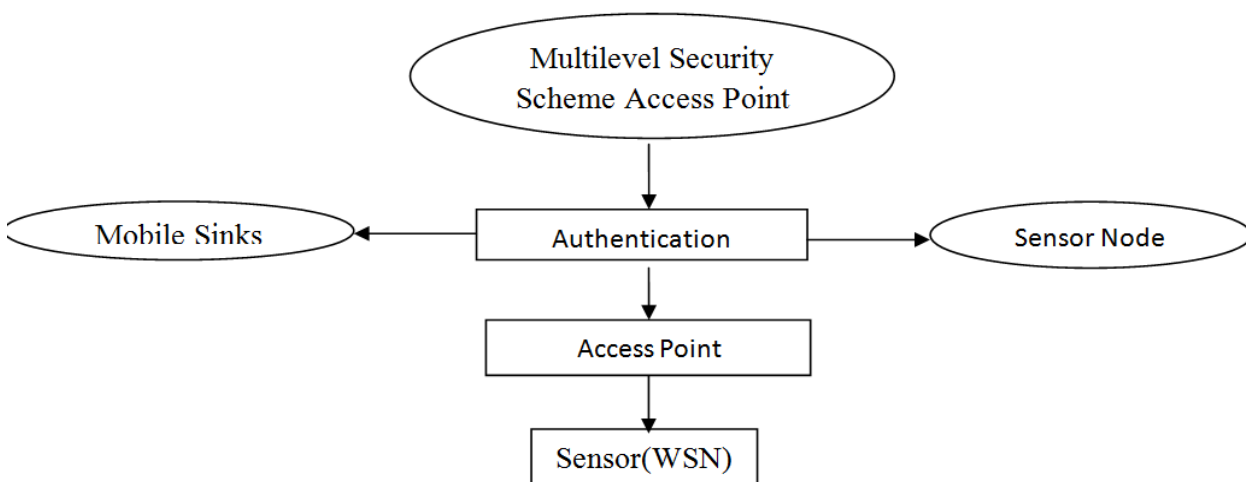


Fig 3.1 Data Flow Diagram

Using two separate key pools and having few stationary access nodes carrying polynomials from the mobile pool in the network may hinder an attacker from gathering sensor data, by deploying a replicated mobile sink. Analysis indicates that with 10 percent of the sensor nodes in the network carrying a polynomial from the mobile pool, for any mobile polynomial to be recovered, the attacker would have to capture. They act as authentication access points for the network and

trigger sensor nodes to transmit their aggregated data to the mobile sinks. A mobile sink sends data request messages to the sensor nodes via a stationary access node. The mobile sink's data request messages will initiate the stationary access node to trigger sensor nodes to transmit their aggregated data to the requested sink. Each stationary access node may share a mobile polynomial with a mobile sink. All sensor nodes, including the stationary access nodes, randomly select a subset of polynomials from the static polynomial pool. The advantage of using separate pools is that mobile sink authentication is independent of the key distribution scheme used to connect the sensor network. We divide our scheme into two stages: static and mobile polynomial pre-distribution and key discovery between a mobile sink and a sensor node.

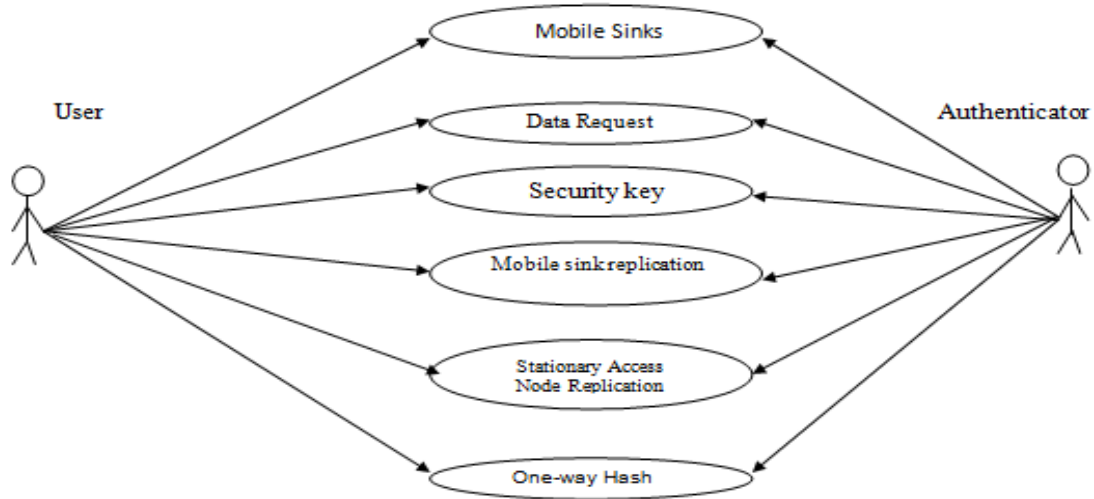


Fig 3.2 Use Case Diagram

3.4 Advantages

The three-tier security scheme is more robust against a stationary access node replication attack. The authentication mechanism between the stationary access nodes and sensor nodes using one-way hash chains algorithm in conjunction with the static polynomial pool-based scheme. The mobile polynomial pool are used to establish the authentication between mobile sinks and stationary access nodes, which will enable these mobile sinks to access the sensor network for data gathering. The random pairwise keys scheme randomly picked pairs of sensor nodes and assigned each pair a unique random key. Both schemes improved the security over the basic probabilistic key redistribution scheme. Using two separate key pools and having few sensor nodes that carry keys from the mobile key pool will make it more difficult for the attacker to launch a mobile sink replication attack on the sensor network by capturing only a few arbitrary sensor nodes.

IV. POLYNOMIAL POOL-BASED SCHEME

List of Modules

1. Mobile Sink
2. Q-Composite Key Scheme
3. Sensor Nodes
4. Mobile Sink Replication
5. Access Node Replication

Module Description

1. Mobile Sink

In this module, a mobile sink sends data request messages to the sensor nodes via a stationary access node. These data request messages from the mobile sink will initiate the stationary access node to trigger sensor nodes, which transmit their data to the requested mobile sink.

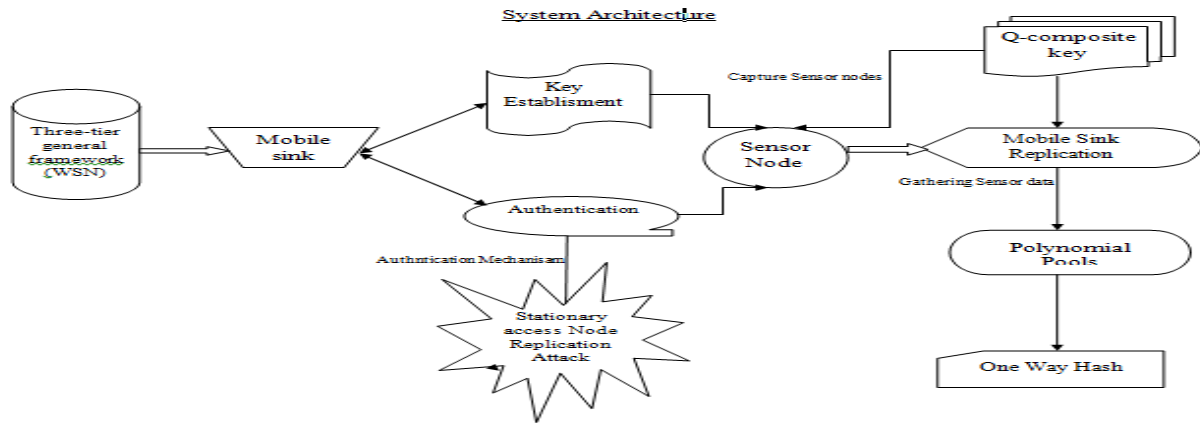


Fig. 4.1 Proposed Method Architecture

2. Q-Composite Key Scheme

Since this module is a three-tier security, we present the probability of a mobile polynomial being compromised; hence, an attacker can make use of the captured mobile polynomial to launch a mobile sink replication attack against the sensor network. For an attacker to launch a mobile sink replication attack on the network, the adversary has to compromise at least one polynomial from the mobile polynomial pool. The adversary must capture at least a specific number of stationary access nodes that hold the same mobile polynomial.

3. Sensor Nodes

This module is based on the polynomial pool-based key redistribution scheme substantially improved network resilience to mobile sink replication attacks compared to the single polynomial pool-based key redistribution approach. Using two separate key pools and having few stationary access nodes carrying polynomials from the mobile pool in the network may hinder an attacker from gathering sensor data, by deploying a replicated mobile sink.

4. Mobile Sink Replication

In this module, the attacker is able to launch a replication attack similar to the mobile sink replication attack. After a fraction of sensor nodes have been compromised by an adversary, captured static polynomials can be loaded into a replicated stationary access node that transmits the recorded mobile sink's data request messages to trigger sensor nodes to send their aggregated data.

5. Access Node Replication

In this module, we have strengthened the authentication mechanism between the stationary access nodes and sensor nodes using one-way hash chains algorithm in conjunction with the static polynomial pool-based scheme. They developed a general framework for pairwise key establishment using the polynomial-based key redistribution protocol and the probabilistic key distribution in the basic probabilistic and q-composite key redistribution schemes, an attacker can easily obtain a large number of keys by capturing a small fraction of the network sensor nodes, making it possible for the attacker to take control of the entire network by deploying a replicated mobile sink, preloaded with some compromised keys to authenticate and then initiate data communication with any sensor node.

V. EXPERIMENTAL RESULT

“.NET” is also the collective name given to various software components built upon the .NET platform. These will be both products (Visual Studio.NET and Windows.NET Server, for instance) and services (like Passport, .NET My Services, and so on). The code that target .NET, and which contains certain extra Information - “metadata” - to describe itself. Whilst both managed and unmanaged code can run in the runtime, only managed code contains the information that allows the CLR to guarantee, for instance, safe execution and interoperability. The multi-language capability of the .NET Framework and Visual Studio .NET enables developers to use their existing programming skills to build all types of applications and XML Web services. The .NET framework supports new versions of Microsoft's old favorites Visual Basic and C++ (as VB.NET and Managed C++), but there are also a number of new additions to the family. Visual Basic .NET has been updated to include many new and improved language features that make it a powerful object-oriented programming language. These features include inheritance, interfaces, and overloading, among others. Visual Basic also now supports structured exception handling, custom attributes and also supports multi-threading.. During system analysis the feasibility study of the proposed system is to be carried out. This is to ensure that the proposed system is not a burden to the company. For feasibility analysis, some understanding of the major requirements for the system is essential

SCREENSHOTS

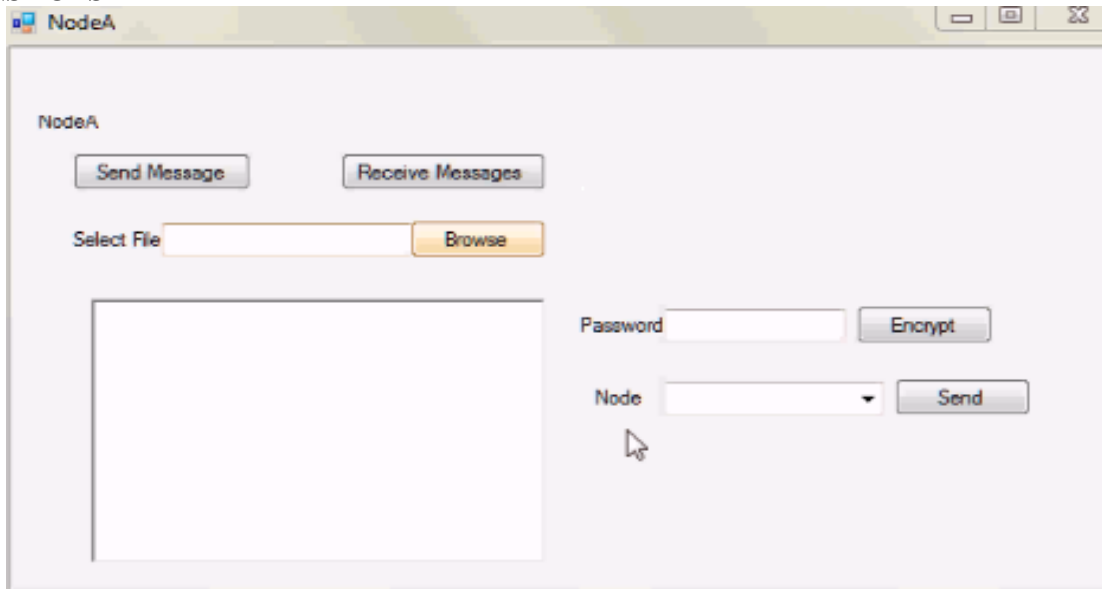


Fig. 5.1 Three Level Security in WSNs

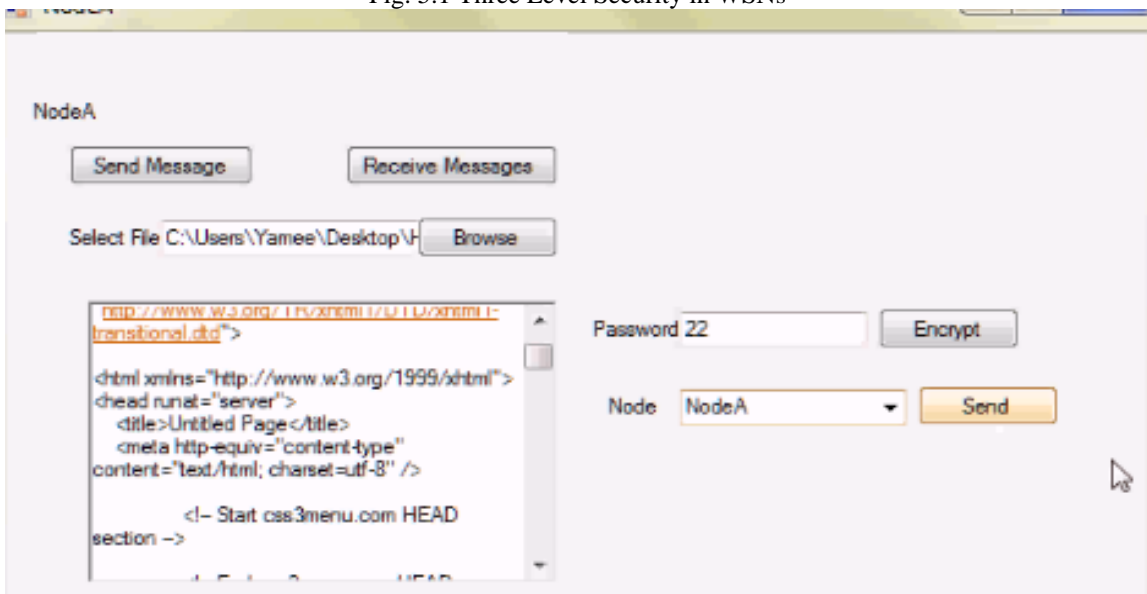


Fig. 5.2 Sending Data in WSNs

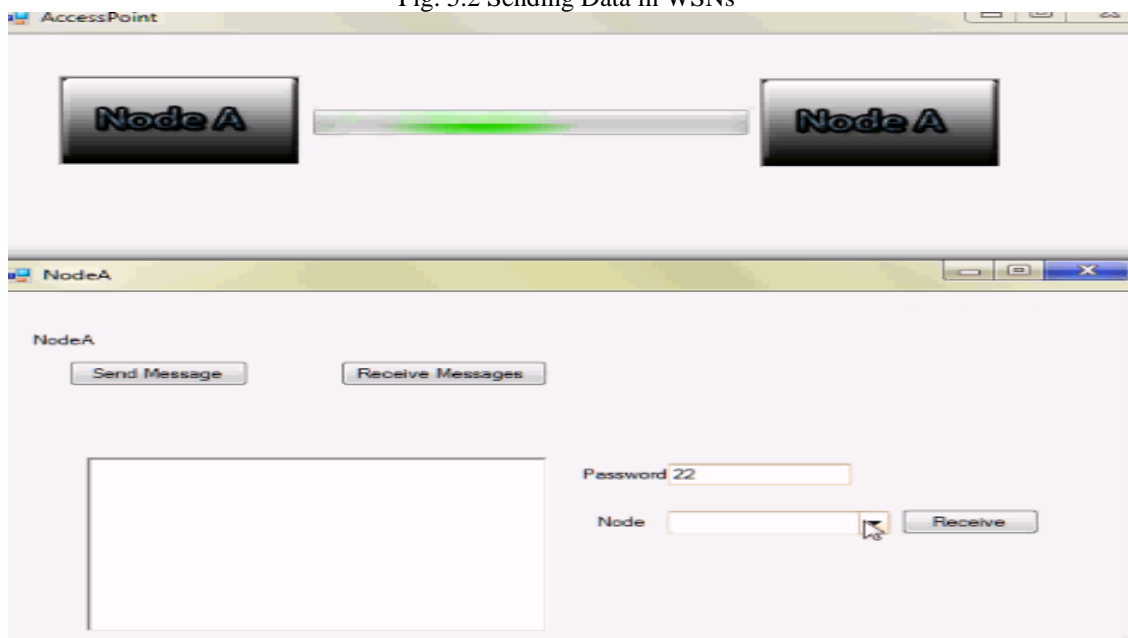


Fig. 5.3 Data Sending from Node 1 to Node 2 in WSNs

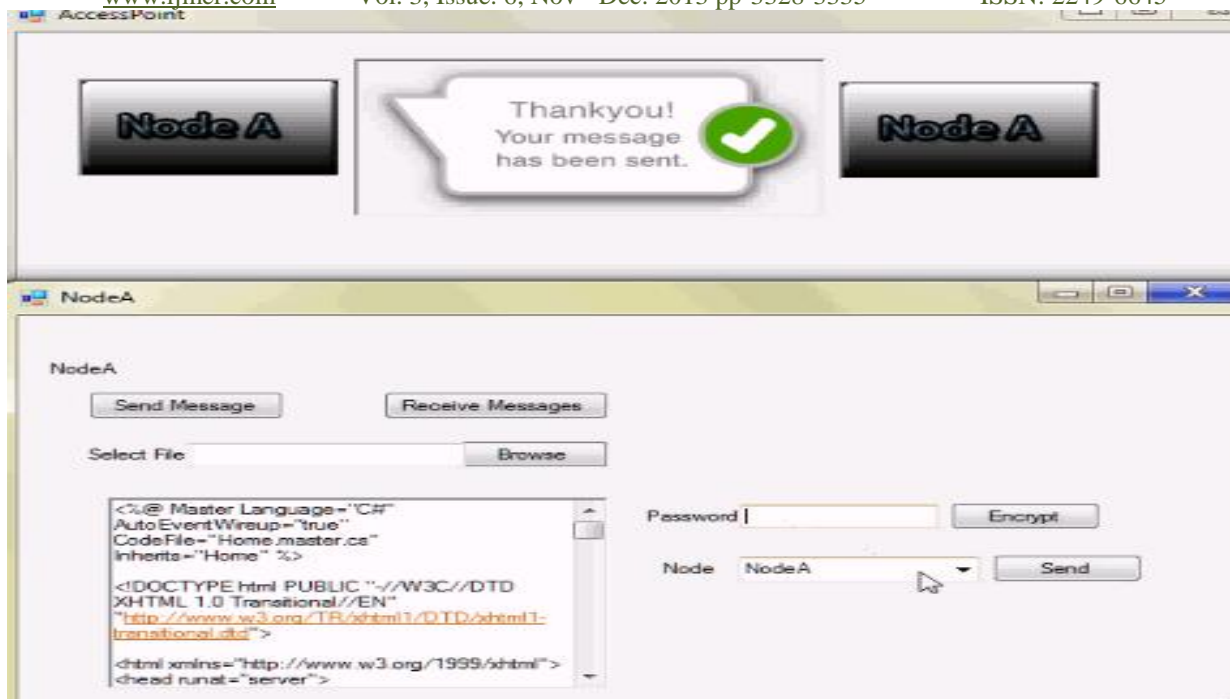


Fig. 5.4 Message Received with Authentication in WSNs

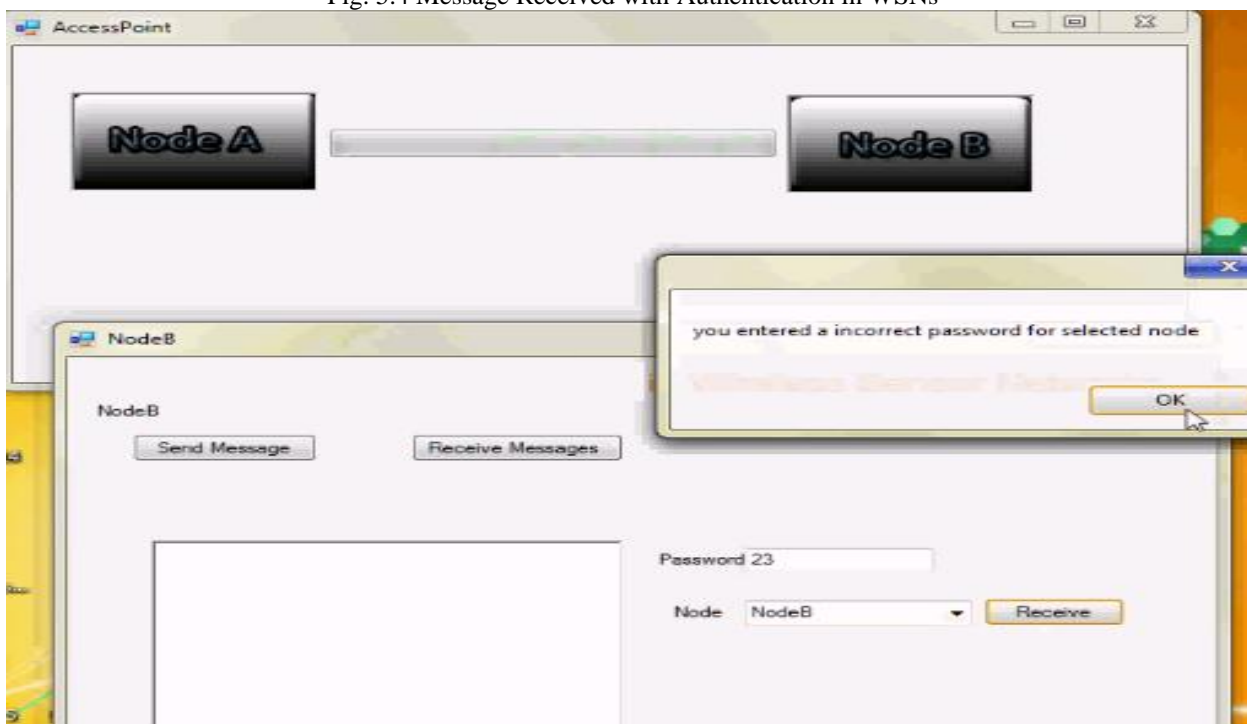


Fig. 5.5 Preventing the Message from Unauthorized User in WSNs

VI. CONCLUSION

In this paper, we have projected a general three-tier security framework for authentication and pairwise key establishment between mobile sinks and sensor nodes. The proposed scheme, based on the polynomial pool-based key redistribution scheme substantially improved network resilience to mobile sink replication attacks compared to the single polynomial pool-based key redistribution approach. Using two isolated key pools and having few stationary access nodes carrying polynomials from the mobile pool in the network may hinder an attacker from gathering sensor data, by deploying a replicated mobile sink. Analysis indicates that with 10 percent of the sensor nodes in the network carrying a polynomial from the mobile pool, for any mobile polynomial to be recovered, the attacker would have to capture multiple times more nodes as compared to the single polynomial pool approach.

6.1 Future Work

We have further improved the security performance of the proposed scheme against stationary access node replication attack by strengthening the authentication mechanism between stationary access nodes and sensor nodes. We used the one-way hash chains algorithm in conjunction with the static polynomial pool-based scheme.

REFERENCES

- [1] I.F. Akyildiz, W. Su, Y. Sankarasubramaniam and E. Cayirci, "Wireless Sensor Networks: A Survey", *Computer Networks*, vol. 38, no. 4, pp. 393-422, 2002.
- [2] T. Gao, D. Greenspan, M. Welsh, R.R. Juang, and A. Alm, "Vital Signs Monitoring and patient Tracking over a Wireless Network", *Proc. IEEE 27th Ann. Intl. Conf. Eng. Medicine and Biology Soc. (EMBS)*, Sept. 2005.
- [3] L. Hu and D. Evans, "Using Directional Antenna to Prevent Wormhole Attacks", *Proc. Network and Distributed System Security Symp.* 2004.
- [4] J.R. Douceur, "The Sybil Attack", *Proc. First Int'l Workshop Peer-to-Peer Systems (IPTPS '02)*, Mar. 2002.
- [5] B.J. Culpepper and H.C. Tseng, "Sinkhole Intrusion Indicators in DSR MANETs", *Proc. First Int'l Conf. Broadband Networks (Broad-Nets '04)*, pp. 681-688, Oct. 2004.
- [6] H. Deng, W. Li, and D.P. Agrawal, "Routing Security in Wireless Ad-Hoc Networks", *Proc. IEEE Comm. Magazine*, pp. 70-75, 2002.
- [7] C. Intanagonwiwat, R. Govindan, and D. Estrin, "Directed Diffusion: A Scalable and Robust Communication Paradigm for Sensor Networks", *Proc. MobiCom*, pp. 56-67, 2000.
- [8] A. Kansal, A. Somasundara, D. Jea, M. Srivastava, and D. Estrin, "Intelligent Fluid Infrastructure for Embedded Networks", *Proc. Second ACM Intl. Conf. Mobile Systems, Applications, and Services (MobiSys '04)*, June 2004.
- [9] Y. Tirta, Z. Li, Y. Lu, and S. Bagchi, "Efficient Collection of Sensor Data in Remote Fields Using Mobile Collectors", *Proc. 13th Int'l Conf. Computer Comm. and Networks (ICCCN '04)*, Oct. 2004.
- [10] A. Rasheed and R. Mahapatra, "An Energy-Efficient Hybrid Data Collection Scheme in Wireless Sensor Networks", *Proc. Third Intl. Conf. Intelligent Sensors, Sensor Networks and Information Processing*, 2007.
- [11] W. Zhang, G. Cao, and T. La Porta, "Data Dissemination with Ring-Based Index for Wireless Sensor Networks", *Proc. IEEE Intl. Conf. Network Protocols (ICNP)*, pp. 305-314, Nov. 2003.
- [12] H. Chan, A. Perrig, and D. Song "Random Key Pre-Distribution Schemes for Sensor Networks", *Proc. IEEE Symp. Research in Security and Privacy*, 2003.
- [13] D. Liu, P. Ning, and R. Li, "Establishing Pairwise Keys in Distributed Sensor Networks", *Proc. 10th ACM Conf. Computers and Comm. Security (CCS '03)*, pp. 52-61, Oct. 2003.
- [14] H. Chan, A. Perrig, and D. Song, "Key Distribution Techniques for Sensor Networks", *Wireless Sensor Networks*, pp. 277-303, *Kluwer Academic*, 2004.
- [15] L. Eschenauer and V.D. Gligor, "A Key-Management Scheme for Distributed Sensor Networks", *Proc. ACM Conf. Computer Comm. Security (CCS '02)*, pp. 41-47, 2002.

AUTHOR DETAILS



M. Senthil Kumar was born in Ramanathapuram District, Tamil Nadu, India in 1982. He obtained his B.Sc., M.Sc. and M.Tech. degrees in Electronics in the years 2002, 2004 and 2006 respectively. He has more than 7 years of teaching experience. He has presented more than 30 research papers in various national and international conferences. He has also published more than 5 research papers in reputed international journals. He has guided several UG and PG students for their project work. His area of interest is Energy Conservation and Optimization Techniques in Wireless Sensor Networks. Currently, he is with Ranganathan Engineering College, Coimbatore, India, as Assistant Professor in the Department of Electronics and Communication Engineering.

Effects of Crude Oil Spillage on Soil Physico-Chemical Properties in Ugorodo Community

¹oyem, Isama Lawrence Rank, ²oyem, Isama Lawrence

¹petroleum and Natural Gas Processing Department Petroleum Training Institute P.M.B. 20 Effurun Delta State Nigeria.

²Petroleum and Natural Gas Processing Department Petroleum Training Institute Effurun, Delta State, Nigeria

ABSTRACT: An oil prone community were identified as the study area, and this community has three quarters which are Orgonoko, Kana and Arunton. Soil samples were collected at the depths of 0-15 cm and 15-30cm at each sampling point. Four (4) samples each were collected from each quarters. These soil samples were analysed for physico-chemical properties that reflect soil nutrient content and fertility status in the laboratory using standard methods and the results from these three areas compared. Evidence of severe hydrocarbon contamination was established by high average extractable hydrocarbon content of 66,034mg/kg in Orgonoko and 31,328mg/kg in Kana and was compared to that of Arunton having total hydrocarbon content of 882mg/kg. High electrical conductivity as well as high moisture content all provided evidence of reduced metabolic activities on the affected sites (Orgonoko and Kana) explains the relatively high total organic carbon values obtained. Also, there were increase in the salinity levels of 24ppm and 13ppm for Orgonoko and Kana quarters respectively when compared to 6ppm in Arunton quarter. From the data obtained, the average pH value in samples analysed in Orgonoko area was 5.3 and that obtained in Kana was 5.7. Both values shows that the soils in these areas are acidic compared to the pH in Arunton which has the average value of 6.1. A pH value between 6.5 and 7.5 is considered optimum for the growth of many plants.

These high values means that Orgonoko and Kana soils (areas) are affected with oil spillage, therefore, it implies low soil fertility, which in turn implies low agricultural productivity and reduced source of livelihood in the affected areas.

Keywords: Oil spills, Contamination, Soil properties, Soil Fertility, Soil moisture,

I. INTRODUCTION

Oil production has continued to play a dominant role in the Nigerian economy, ranging from generation of foreign exchange to serving as a source of energy to run the nation's Economy. Industries cannot function effectively with the use of refined petroleum products Easy and faster means of transportation would have been impossible without pipelines. Production of other necessary needs of man derived from crude oil would not have been possible if crude oil was not discovered and exploited. The above-mentioned benefits and lots of others have shown that crude oil has been a blessing to man and the nation as a whole.

On the other hand, the process of employing modern technology in the exploration, production, processing and storage of this God-given resources has resulted in the abuse of man's environment directly or indirectly.

Bodies of water are polluted, leading to the destruction of useful aquatic lives. Cultivable lands are rendered uncultivable due to loss of soil fertility. Diseases due to polluted lands, water and air are on the increases. There are reports from the various communication media about community disturbances by youth in the host communities who feel cheated by these oil companies 'harvesting gold' in their land and leaving nothing in return. Large sums of money are lost daily due to shut down in oil production. Some of the oil company staffs have lost their lives to irate youths, who want to enjoy from the boom and not to be left in the doom. All these problems of pollution, fertility loss, rampant spread of diseases, loss of aquatic lives, killings, money loss, fire outbreaks, shut down in the oil production and community disturbances are traced to crude oil spillage.

Contamination of soil by oil spills is a wide spread environmental problem that often requires cleaning up of the contaminated sites. These petroleum hydrocarbons adversely affect the germination and growth of plants in soils (Samina and others, 2002). Oil spills affect plants by creating conditions which make essential nutrients like nitrogen and oxygen needed for plant growth unavailable to them (Adam and others, 2002). Phytoremediation is an alternative to more expensive remediation technologies because it is a feasible, effective and non-intrusive technology that utilizes natural plant processes to enhance degradation and removal of oil contaminants from the environment (Marmiroli and others, 2003). All stages of oil exploitation impact negatively on the environment, and the greatest single intractable environmental problem caused by crude oil exploration in the Niger Delta region is oil spillage. Over 6000 spills had been recorded in the 40 years of oil exploitation in Nigeria, with an average of 150 spills per annum. In the period 1976 –1996, 647 incidents occurred resulting in the spillage of 2,369,407.04 barrels of crude oil. With only 549,060.38 barrels recovered, 1,820,410.50 barrels of oil were lost to the ecosystem. The environmental consequences of oil pollution on the inhabitants of Delta State are enormous. Oil spills have degraded most agricultural lands in the State and have turned hitherto productive areas into wastelands. With increasing soil infertility due to the destruction of soil micro-organisms, and dwindling agricultural productivity, farmers have been forced to abandon their land, to seek non-existent alternative means of livelihood. Aquatic lives have also been destroyed with the pollution of traditional fishing grounds, exacerbating hunger and poverty in fishing communities. Many authors have reported a lower rate of germination in petroleum or its derivatives contaminated soil (Adam and others, 2002; Vavrek and Campbell, 2002; Méndez-Natera and others., 2004; Achuba, 2006; Smith and others, 2006, Sharifi and others,

2007; Korade and Fulekar, 2009; Ogbo, 2009). Petroleum hydrocarbons may form a film on the seed, preventing the entry of oxygen and water (Adam and others, 2002) and toxic hydrocarbon molecules could inhibit the activities of amylase and starch phosphorylase and thereby affecting the assimilation of starch (Achuba, 2006). Henner *and others.* (1999) reported that petroleum hydrocarbons consisting of small molecules and those that are water soluble are more phytotoxic for the germination.

The most common and important symptoms observed in the plants contaminated with oil and its by products include the degradation of chlorophyll (Malallah *and others.*, 1998).

Types of Oil Spillage

Oil spill is categorized into groups namely:

- Minor spill occurs when the volume of the spilled oil is less than 25 barrels in inland water or less than 250 barrels on land; offshore or coastal water that does not pose a threat to public health or welfare
- Medium spill takes place when the volume of the spill is 250 barrels or less in inland waters or 250 to 2500 barrels on offshore and coastal waters
- Major spill occur when the oil discharged to inland water is in excess of 250 barrels in offshore or coastal waters.
- Catastrophic spill refers to any uncontrolled well blowout, pipeline rupture or storage tank failure which poses an imminent threat to the public health or welfare. (Egbe, R.E and others,2010)

Oil lake types

Oil lakes vary in their type, area, volume, and depth of penetration. They differ in type due to the different formation condition. Studies categorized them into four types

- 1) *Wet oil lakes contamination* which is formed in areas of shallow depression and drainage channels. It's described as black, highly weathered and viscous liquid or semi-solid oil sludge over a thickness of oil contaminated soil that in turn overlies clean soil.
- 2) *Dry oil lakes contamination:* occurs in shallow depression and flat areas and it is comprised of a black, moderately hard, tar-like dry surface layer overlying dark brown oil contaminated soil that in turn overlies clean soil.
- 3) *Oil-Contaminated piles:* occurs when earthmoving equipment has been used to consolidate oil contaminated and/or liquid oil into mound. These piles were made to stop the flow of oil from wells, to clean areas of heavy oil contamination to facilitate fire fighting or subsequent KOC field operation.
- 4) *Oil trenches and associated oil spill* which consist primarily of oil-contaminated soil from back-filled trenches. Including in this category are oil contaminated soils associated with oil spills from Nigeria constructed pipelines.

Soil pH

The pH value determines to what degree the soil environment is acidic or alkaline. The pH of a solution is the logarithm of the reciprocal of the hydrogen ion concentration where $\text{pH} = \log 1/\text{H}^+$ and H_2O is ionized as an H^+ cation (acid) and an OH^- anion (base).

A pH value between 6.5 and 7.5 is considered optimum for the growth of many plants. Although many plants respond to an optimum pH, this value usually covers a range from 0.5 units below to 0.5 units above the optimum level. It should be noted one pH unit is a factor of 10. Therefore, plants have a fairly broad pH tolerance.

The pH of soil influences the absorption and availability of nutrients to plants. There are two general sources of soil nutrients. Some nutrients are absorbed on colloids and some are available to plants as ions in solution. In both cases the various nutrients are present as ions. In most cases the cations (positively charged ions) are absorbed on colloids and the anions (negatively charged ions) are in solution.

Soil is a highly buffered ecosystem. Hydrogen ions in the soil solution are in equilibrium with negative exchange sites on the soil particles. In cation exchange, hydrogen acts as a reserve pool which continuously supplies hydrogen ions to the soil.

In areas of high rainfall, soil tends to be acidic due to the leaching effect on the exchange sites. In arid and semi-arid regions, soils tend to be basic. Basic soils have higher concentrations of calcium, magnesium, and sodium carbonates. The pH of soil varies significantly in thin soil zones. These variations in pH are due to differences in both macro and micro ecosystems. The microbial population near root surfaces is an example of such an ecosystem. The rhizosphere bacteria population significantly impacts pH this microsystem and thus affects plant growth and the progress of soil remediation. Restoring the rhizosphere bacteria population and activity significantly increases available nutrients to the soil.

Since most soils in Niger Delta are basic, the addition of sulphur with fertilizer is an important part of the remediation. As pH approaches 8.7, the addition of sulphur can be justified. To lower the pH of an 8 inch deep loam soil 0.5 pH units, 1,000 lbs of sulphur per acre is required. Sulphur lowers the pH thus increases the solubility of gypsum.

Soil Moisture

The volume and movement of water in the soil is the single most important factor determining plant growth. Depending on the plant, water comprises 50% to 90% of the plant tissue.

Photosynthesis and nutrient availability depend on water. Water is the solvent in which all chemical reactions take place.

Similarly, water is the most important factor determining remediation of salt water and hydrocarbon spills. Approximately 12-14 inches of rain are required to remediate 10,000 $\mu\text{S}/\text{cm}$ of electrical conductivity per year, depending on soil type.

Gravitational force pulls water down through the soil matrix and is the predominant influence on water movement in soil.

Water can also move by capillary action due to hydrogen bonding and the subsequent magnetic attraction of water molecules to one another. Capillary forces can overcome gravitational forces and move water in a direction other than straight down into the soil. Both gravitational and capillary water movement is influenced by soil particle type and distribution in the soil. Water around soil particles is controlled by adhesive and cohesive forces. "Adhesion water" is held tightly and does not move. In contrast, "cohesion water" is held more loosely on soil particles and can be utilized by plants. Cohesive forces and capillary forces move water against gravitational forces in the root zone to increase water utilization by plants. The osmotic potential of water becomes important in a saline soil. At high salt concentrations, a higher osmotic potential decreases the movement of water into plants. Additionally, more energy is required to move water into the root at higher osmotic potentials.

Following a rain event, the soil is saturated as soil pores fill with water. Gravitational forces drain water from the root zone. Depending on the soil and amount of rain, the draining process is completed in 48 to 72 hours. As the soil drains, the soil reaches a "field capacity" state. At this point, air will fill the large pores and each soil particle will have a thick film of moisture (cohesion water). Plant uptake and evaporation will continue to deplete the cohesion water and shrink the soil-water film. As the film becomes thinner it is more difficult for the root to absorb water. As this process continues and capillary water and additional rain fall does not replenish the root zone, a "wilt point" will develop.

During this process of saturation and drainage, calcium ions can replace the sodium ions and remediation can occur. It is important that water move evenly through the soil as it drains out of the root zone. Therefore, pre-work of the soil to produce a "remediation seed bed" to facilitate water drainage out of the root zone is helpful to the total remediation process. Soil texture will determine the "water retention" capacity of a soil. A loamy soil will remediate at a faster rate than a sandy or heavy clay soil. (Gawel, 2003)

Soil Texture

The relative proportions of sand, silt and clay particles in a mass of soil (material less than 2mm in size). Soil characteristic is influenced by texture. Structure modifies the influence of texture in regard to moisture and air relationships, availability of plant nutrients, action of microorganisms and root growth.

Silt, the intermediate size, feels smooth when dry, and slippery but not sticky when moist. Because the smaller particle size promotes smaller pore spaces between particles, silty soils have a slower water intake rate but a higher water holding capacity than sandy soils. These are difficult for storage because they often lack aggregation. This results in high density and a pore size too small for suitable water percolation and aeration. Nevertheless, silt is an essential component of the medium textured, versatile soil called loam. Clay, the finest size fraction, gives the soils a sticky or plastic feel. Clay exhibits some unusual properties, unexpected if it were merely composed of smaller particles or the same minerals that make up sand and silt. Clay is largely composed of a different set of minerals, called secondary minerals. These are weathering products of the primary minerals -- quartz, feldspar, and mica -- of which sand and silt are largely composed.

Soil with large diameter particles (coarse texture) can contain less water than soil with small diameter particles. Loamy soil has about 30-50% silt and 20% less than clay particles. Sand contains rock particles with diameter in range 0.125-2.0mm. Clay has soil particles whose size is less than 2-4mm in diameter. Silt soil is composed of particles whose diameter ranges from 1/256-1/16mm. Soil texture relates primarily to particles smaller than 2 millimetres (.080 inches) in diameter - sand, silt, and clay - since these are the particles most active in soil processes which support plant growth. Coarser particles, gravel and stones, are either inert or detrimental to plant cultivation.

LOCATION

This study is limited to Ugborodo community situated between the Escravos River and the Atlantic Ocean of latitude 5°34'60N and longitude 5°10'0E, in Warri South-West Local Government Area of Delta State of Nigeria. The community of Ugborodo consists of three quarters namely Orgonoko, Kana and Arunton.

PURPOSE AND JUSTIFICATION

Oil spillage in the Niger-Delta area of Southern Nigeria has become a public concern as a result of its frequent occurrence which has been linked with Petroleum exploration and development activities. Crude oil spill affects plants negatively by creating conditions which makes essential nutrients like nitrogen, Oxygen etc needs for plant growth unavailable to them from the spilled affected soil. Therefore, the purpose of this study is to evaluate the effects of oil spillage on soil properties in these areas. The result will give an insight to the level of damage that oil spill has done to the fertility and nutrient status of the community farmland.

II. MATERIALS AND METHODS

2.1 MATERIALS/ PREPARATION

The Four (4) suspected soil samples were collected from each three different places (quarters) or locations (12 samples in all) -Orgonoko, Kana and Arunton about one kilometre apart by taking 5-10 auger boring at random. Soil samples from each sampling locations was put in a sterile polyethylene bag, flamed sealed, labelled and taken to the laboratory. The suspected soil samples were subjected to drying under atmospheric condition for several days and sieved with 2mm sieves before analysis of various parameters.

METHODOLOGY

A series of tests were performed to evaluate the physiochemical effect of crude oil spill on soil. Properties like C/N ratio, Electrical conductivity, bulk density, moisture content, pH, Salinity, THC and other physiochemical properties. All the tests were conducted in line with the API specification.

RESULTS.

Soil samples	Sample point	Depths (cm)	C/N ratio	Electrical conductivity ($\mu\text{s}/\text{cm}$)	Bulk Density (g/cm^3)	Carbonate (%)	Bicarbonate (%)	Moisture content (%)	pH	Nickek (mg/kg)	THC (mg/Kg)	Salinity (ppm)
Orgonoko	A1	0-15	8:1	101	1.00	2.27	0.11	0.78	5.28	0.90	86715	21
		15-30	4:1	89	1.00	1.94	0.11	0.54	5.24	1.45	50242	14
	A2	0-15	6:1	145	1.66	3.65	0.16	1.22	5.33	0.95	77413	33
		15-30	6:1	121	1.59	3.22	0.14	0.67	5.31	1.33	49766	28
Kana	B1	0-15	12:1	58.6	2.65	0.47	0.18	1.17	5.88	0.30	46408	12
		15-30	10:1	55.4	3.78	0.41	0.14	0.75	5.74	0.21	30266	12
	B2	0-15	10:1	66.4	4.55	0.64	0.25	1.77	5.67	0.15	28766	14
		15-30	8:1	59.8	5.67	0.60	0.21	0.73	5.66	0.09	19873	13
Arunton	C1	0-15	14:1	36.3	1.33	0.49	0.09	0.63	6.04	0.30	1200	8
		15-30	10:1	24.2	1.33	0.33	0.04	0.43	6.11	0.30	920	6
	C2	0-15	10:1	19.6	1.23	0.30	0.02	0.54	6.06	0.23	876	4
		15-30	10:1	20.4	1.20	0.30	0.02	0.46	6.11	0.15	532	5

Table 2.2 UGBORODO SOIL TEXTURE

Soil sample	Sample Point	Depths (cm)	Sand (%)	Clay (%)	Silt (%)
Orgonoko	A1	0-15	60	32	8
		15-30	58	34	8
	A2	0-15	56	28	16
		15-30	54	37	9
Kana	B1	0-15	77	21	2
		15-30	69	20	11
	B2	0-15	79	17	4
		15-30	70	22	8
Arunton	C1	0-15	51	43	6
		15-30	56	42	2
	C2	0-15	51	44	5
		15-30	57	41	2

III. DISCUSSION OF RESULTS**Total Hydrocarbon Content (THC)**

From the data obtained (table 2.1) shows a significant difference between the two impacted locations of Orgonoko and Kana and the area of Arunton. The total hydrocarbon content at the depth of 0-15cm was 86715 mg/kg and at the depth of 15-30 cm was 50242 mg/kg in one of the sample point, and then 77413 and 49766 mg/kg at the depths of 0-15cm and 15-30cm respectively in the second sampling point in Orgonoko quarters. This result shows that the total hydrocarbon content decreases with increases in depth. The average total hydrocarbon content in Orgonoko quarters was 66034 mg/kg.

The same trend was followed in the case of four samples collected at the depths of 0-15cm and 15-30cm respectively in Kana and Arunton quarters. The average total hydrocarbon content was 31,328 mg/kg in Kana and 882mg/kg in Arunton.

The hydrocarbon content of 66034 mg/kg and 31,328 mg/kg for Orgonoko and Kana respectively compared to total hydrocarbon content value of 882mg/kg in Arunton represents a high level of hydrocarbon contamination on the impacted sites. A review of such existing data on the Niger Delta Environment Survey-NDES (1999), Osuji and others, 2004, affirms that such high hydrocarbon levels affect both above-ground and subterranean flora and fauna, which are essential adjuncts in the biogeochemical cycle that affects availability of plant nutrients.

The intense infusion of degradable hydrocarbon likely stimulates aerobic and anaerobic microbial metabolism. As oxygen becomes limiting utilization of alternate electron acceptors produces an increasing reducing environment. In general, the essential elements required for plant growth, will be inherently low due to the high concentration of the degradable hydrocarbon.

The significant difference between Orgonoko sample and that of Kana sample may be attributed to the differences in volume of the spilled crude (hydrocarbon) on each location.

Electrical Conductivity (EC)

Electrical conductivity (EC) is a measure of ionic concentration in the soils and is therefore related to dissolve solutes. As salt content increases, so does Electrical conductivity. The significantly higher electrical conductivity values obtained for Orgonoko samples and Kana samples could be as a result of the high concentration of charged ions (cations and anions) in the oil impacted sites. Anions, metallic ions and carbonic acids contribute to electrical conductivity of tropical soils. However, the generally low electrical conductivity values of the soils of the study area is an indication of the high degree of leaching of nitrate salt taking place as a result of high rainfall in the Niger Delta. (Ekundayo, 1997).

Moisture Content

It was found from table 2.1 that the moisture content in the Arunton location (un-impacted by oil spill from the data obtained) was 0.63% at the depth of 0-15cm and 0.43% at the depth of 15-30cm. And on the second sampling point on Arunton quarter, was 0.54% and 0.46% at the depths of 0-15 and 15-30 cm respectively. Compared to the values obtained from Orgonoko and Kana quarters, which has the values of 0.78%, 0.54% and 1.22%, 0.67% at the depths of 0-15cm and 15-30cm at the two sampling points in Orgonoko quarters and 1.17%, 0.75% and 1.77% , 0.73% in Kana quarters. It can therefore be concluded that the spilled affected soils (Orgonoko and Kana) retained more water especially in Kana soil samples than the soil in Arunton. The higher moisture content of 0.78% for Orgonoko and 1.17% for Kana can be attributed to insufficient aeration of the soil that might have arisen from the displacement of air in the oil-spilled soils, this probably encouraged water logging and reduced rate of evaporation.

High moisture content may reduce microbial activities not as a result of the water itself but rather by the indirect hindrance to the movement of air which would reduce oxygen supply to plants

Salinity

From the data obtained (table 2.1) shows a significant difference in the salinity values between the value samples obtained at sampling points in Arunton and that of Orgonoko and Kana quarters. The average values for Orgonoko was 24ppm and that of Kana was 13ppm which were quite higher than that of Arunton with an average value of 6ppm.

Soil salinity is a soil condition when water soluble salts in the crop rooting zones impede crop growth. High salt content increases the osmotic potential of the soil solution and prevents crop uptake of water. Crops are generally most sensitive to salinity during germination and emergence. As soil salinity level increases, the stress on germinating seedlings also increases. This clearly shows that the crude oil spillage actually increased the soil salinity of the impacted locations- Orgonoko and Kana. Symptoms of salt damage include, brown stunted roots, dead and sections on the margins, burning and die-back of young growth and slow or no growth.

Carbon- Nitrogen Ratio

If the C/N ratio is affected by nitrogen-coating pollutants undesirable effects may occur. More so, very low C/N ratio values as in Orgonoko sample may lead to organic matter soil losses and to desertification problems. That is why a C/N ratio of around 25: 1 is considered optimal for soil fertility. As C/N ratio < 10:1 then problem arises.

If the organic material has a less amount of nitrogen in relation to the carbon then the micro organism will utilize the soil nitrogen for further decomposition and the soil nitrogen will be immobilized and will not be available for plant use.

Soil fertility in terms soil nitrogen content and total carbon showed apparent and significant increases for Orgonoko and Kana samples compared to Arunton (control). These increases confirmed the relationship between soil pH and soil nitrogen that the increase in pH with the oil spill contributed to the higher nitrogen value recorded in the crude oil contaminated soil (Orgonoko and Kana soil samples).

Soil pH

pH acts indirectly on plant growth by affecting availability of nutrients, the presence of toxins and the growth of soil microorganisms. . pH stands for "potential hydrogen" and measures the acidity of your soil using a scale from 0 to 14. A pH of 7 is neutral. If the pH is lower than 7, people refer to it as acidic, sour or low pH, while a pH over 7 is termed alkaline, basic, sweet or high pH.

From the data obtained, the average pH value in samples analysed in Orgonoko area was 5.3 and that obtained in Kana was 5.7. Both values showing that the soils in these areas are acidic compared to the pH in Arunton which has the average value

of 6.1. A pH value between 6.5 and 7.5 is considered optimum for the growth of many plants. Even though, Arunton's pH is little short of that.

pH affects plant growth primarily through its effects on nutrient availability. High or low pH cause deficiencies in essential nutrients that plants need to grow. According to the Clemson Cooperative Extension, acidic soils frequently experience deficiencies in calcium, phosphorus and magnesium. Alkaline soils demonstrate deficiencies in phosphorus and many micronutrients. The availability of aluminium and manganese can also approach toxic levels in acidic soils and impair plant growth. Furthermore, soil pH affects the behaviour of soil microbes, encouraging or inhibiting the growth of pathogens and affecting how well helpful microbes are able to break down organic material, freeing the nutrients it contains for plant use. (Thumma, 2000)

Acidic soil often causes the stunting and yellowing of leaves, resulting in the decrease in growth and yield of crops as the pH levels falls. Additionally, plants grown in adverse pH conditions may be more prone to disease and fungal attack. The availability of plant nutrients is considerably affected by soil pH. Calcium, potassium, magnesium and sodium are alkaline elements, which are lost with increasing acidity whereas phosphorous is more available in acidic soil conditions.

Soil Bulk Density

Bulk density is used to measure compaction. In general, the greater the bulk density the less the pore space for water movement, root growth, penetration and seedling germination. It reflects the soil ability to function for structural support, water and solute movement and soil aeration. Bulk densities above thresholds indicate impaired function.

From the table (2.1), the values of the average bulk density obtained from Orgonoko and Arunton (control) areas were 1.31g/cm³ and 1.27g/cm³ respectively shows that soil can actually support plant growth. But the oil impacted sample (Kana) has the value of 4.16g/cm³ shows that plant growth was severely restricted. Oil spillage really impacted significantly on the bulk density of Kana soil samples, and this adversely affected agricultural practice in this location. The average bulk density for Kana in particular, shows that the viscous crude oil settled into the pores to increase both the soils wet weight and the liquid content, this in turn cause increase in bulk density as compared to Arunton soil samples (control).

Soil Texture

The average soil texture at the first sampling point in Orgonoko quarters was 59% sand, 33% Clay, and 8.0% silt and at the second sampling point in Orgonoko, the average soil texture was 55% sand, 32.5% Clay and 12.5% silt at the depths of 0-30cm respectively. Therefore, the total average soil texture in Orgonoko at the depth of 0-30cm was **57%** sand, **32.75%** Clay and **10.25%** respectively.

At Kana quarter, the soil texture was 73% sand, 20.5 Clay, and 6.5% silt at site 1 and 74.5% sand, 19.5% Clay, and 6.0% silt at site 2. For Kana, the average soil textures at these locations were **73.75%** sand, **20%** and **6.25%** for Sand, Clay and Silt respectively.

In Arunton areas, sand content was 53.5%, clay was 42.5% and 4.0% silt at sampling site 1 and 54% sand, 42.5% clay and 3.5% silt at sampling point 2. For Arunton, which serves as control, has the following values as the average soil texture **53.75%**, **42.5%** and **3.75%** for sand, clay and silt respectively.(Table 2.2)

Kana quarter has the highest sand content, so, have the highest rapid water/ hydrocarbon infiltration and lowest water / hydrocarbon holding and very low nutrient storage capacity resulting in high C/N ratio .Arunton has almost balanced values of sand and clay soil with lowest amount of silt content.

Orgonoko has the highest amount of silt content which may result in slower hydrocarbon and water intake and higher water and holding capacity.

IV. CONCLUSION

It can be concluded that the test results obtained from the soil analysis of the oil-spilled impacted sites (Orgonoko and Kana) compared to the result of the un-impacted site (Arunton) shows that the total hydrocarbon levels observed from both the oil spilled locations have provided evidence of severe hydrocarbon contamination of the sites. These conditions generally imply low soil fertility, which in turns implies low agricultural productivity and reduce source of .livelihood in the affected areas. There was significant difference in electrical conductivity values between the impacted and un-impacted sites. More also, the salinity values for the oil spilled affected areas increased significantly when compares to Arunton (control). However, there was no significant change or difference in values for properties like nickel, carbonates and Bicarbonate content in both affected and un- affected sites or locations.

V. RECOMMENDATION

Having successfully analysed the soil samples from the three quarters involved in community, it has shown that the soil samples from Orgonoko and Kana are contaminated. Therefore, in order to minimize the rate of spills in these areas (community), the following recommendations are suggested.

The government of Nigeria should muster the political will to exact stricter respect for environmental laws and regulations by oil companies and a penalty plan established that require oil companies whose activities cause excessive pollution or are ill-equipped to forfeit their licenses.

Multinational and indigenous oil companies should ensure regular and constant inspection and maintenance of oil facilities to avoid accidental discharge or spillage of oil and other petroleum products.

The current compensation regime in Nigeria has to be reviewed for it to be fair and adequate to meet the emergency needs and concern of those affected by pollution.

Adequate security personnel should be provided to guard oil installation and such security arrangement should involve people from the host communities to work-in collaboration with government security forces to improve monitoring of oil facilities to avoid vandalisation.

Constant seminar, training workshop, public enlightenment campaign should be organized for host communities and other stakeholders in the oil industry to educate them on the negative impact of oil spillage on the soil properties.

Application of appropriate and sufficient inorganic NPK fertilizer to restore the Carbon to Nitrogen ratio to the optimum required to stimulate and sustain microbial activity.

Stimulating of the indigenous microbial growth by cultivating the soil to distribute the nutrient and lime and to aerate the treatment zone.

ACKNOWLEDGMENT

The author would like to express his profound gratitude to the staff of Petroleum and Natural Gas Processing Department, Petroleum Analysis Laboratory (PAL), Lighthouse Petroleum Engineering Company, Petroleum Training Institute, Effurun, Delta State, Nigeria, especially Mr Ikwoğu, G. O, Mrs. B. Oyem, for their assistance during the course of this research work.

REFERENCES

- [1] African Journal of Agricultural Research (July 2007) Vol2 (7)
- [2] Brandy, N.C and Weil, R.R. (2002); The Nature and Properties of Soil, 13th Edition, Prentice Hall, New York.
- [3] Department of Petroleum Resources, DPR (1997); Annual Report
- [4] Ekundayo, E .O and Obuekwe, C.O (1997); Effects of an Oil spill on Soil physico-chemical properties of a spill site in atypical Displacement of Midwestern Nigeria, Environmental Assessment Vol (45).
- [5] Jackson, M.L; (1962); Soil Chemical Analysis, Prentice Hall, New York
- [6] Oyem, A (2001) Christian Call for Action in Nigeria Oil Spill (Sage-Oxford's Christian Environment Group)
- [7] Effects of an oil spill on soil physico-chemical properties; <http://www.academicjournals.org/AJAR>; Retrieved 09 October, 2013.
- [8] pH Levels and Plant Growth; [http:// www.gardenguides.com](http://www.gardenguides.com); Retrieved 09 October,2013
- [9] Soil pH; <http://en.wikipedia.org/wiki/soilpH> ; Retrieved 09 October, 2013
- [10] Dawn Walls-Thumma, (2000); How does pH level affect the plant growth.
- [11] How does pH level affect plant growth; www.scienceproject.com; Retrieved 09 October, 2013
- [12] Oujı, L.C, Adesıyan, S.O, Obuıte, G.C (2004); Post Impact Assessment of Oil pollution in Agbada West plain of Niger Delta, Delta State.
- [13] Henner, P., Schiavon, M., Druelle, V. And Lichtfouse, E. (1999): Phytotoxicity of ancient gaswork soils. Effect of polycyclic aromatic hydrocarbons (PAHs) on plant germination. Organic Geochemistry-
- [14] Malallah, G., Afzal, M., Kurian, M., Gulshan, S. and Dhami, M.S.I. (1998): Impact of oil pollution on some desert plants.
- [15] Marmirolı, N. and McCutcheon S. C. (2003): phytoremediation a successful technology. Phytoremediation. Transformation and Control of Contaminants. John Wiley, Hoboken.
- [16] Achuba, F. I. (2006): The effect of sublethal concentrations of crude oil on the growth and metabolism of Cowpea (*Vigna unguiculata*) seedlings. African J.
- [17] Adam, G. and Duncan, H. J. (2002): Influence of Diesel Fuel on Seed Germination. Environ.Pollut.
- [18] Ogbo, E. M. (2009): Effects of diesel fuel contamination on seed germination of four crop plants - *Arachis hypogaea*, *Vigna unguiculata*, *Sorghum bicolor* and *Zea mays*. Biotechn.
- [19] Korade, D. L. and Fulekar, M. H. (2009): Effect of organic contaminants on seed germination of *Lolium multiflorum* soil. Biology and Medicine (Bio. Med.).
- [20] Smith, M. J., Flowers, T. H., Duncan, H. J. And Alder, J. (2006): Effects of polycyclic aromatic hydrocarbons on germination and subsequent growth of grasses and legumes in freshly contaminated soil and soil with aged PAHs residues.
- [21] Vavrek, M. C. and Campbell, W. J. (2002): Contribution of seed banks to freshwater wetland vegetation recovery. Louisiana Applied and Educational Oil Spill Research and Development Program, OSRADP.
- [22] Egbe, R.E. (2010); Environmental Challenges of Oil Spillage for Families in Oil Producing Communities of the Niger Delta Region.

Autonomous Order Processing System for Supply Chain Management-An Initiative to Match Demand and Supply for Processed Food Industries in Bangladesh

Mohd. Rifat Khan¹, Adnan Hasan², Shumon Kumar Ray², Anup Saha², A.B.M. Abdul Malek³

^{1,2} Dept. of Industrial and Production Engineering, Shahjalal University of Science and Technology, Bangladesh

³ Associate Professor, Dept. of Industrial and Production Engineering, Shahjalal University of Science and Technology, Bangladesh

Abstract: Sales order processing is accomplished in each business by its distribution channel consisting of distributors, wholesalers, retailers and customers. In a developing country like Bangladesh, the relationship between manufacturers and downstream intermediaries are not strong enough due to the infrastructure of the communication system of the country. As a result, a considerable amount of amplification of actual orders is seen throughout the supply chain for most of the manufacturers of Bangladesh. A business needs to create adaptive supply chain networks in which suppliers, manufacturers, distributors, and customers share information dynamically across the network. Supply chain performance solely depends upon the effective integration throughout the chain. Order processing is an important area for improvement to achieve efficiency in supply chain performance. Automation of sales order processing gives organizations more control and insight into what is happening on a daily basis. In most of the remote areas of Bangladesh, the only way to establish a strong relationship between customer and manufacturer is through mobile phone communication, where customers can place their orders through short message service (SMS). To achieve this, a research is done at a local company, Fiza and Co. to find the necessary requirements for building automated order processing software to help the manufacturer in keeping track with actual customer orders to satisfy customer needs and to gain competitive advantages. The waterfall model is used as a guide to develop the software. As a result the SMS based web integrated order processing software is developed. This software integrates the different divisions in the company and functions as a coordinator between the processes of handling customer orders through SMS. In addition to that, the software also generates reports for each division so that it could be analyzed by the management. The analysis done by the software would be able to help the management to make more informed and accurate business decisions in order to further enhance their competitiveness and overall performance.

Keyword: Automation, Order Processing, Short Message Service (SMS), Supply Chain Performance.

I. INTRODUCTION

Sales order processing is accomplished in each business by its distribution channel consisting of distributors, wholesalers, retailers and customers. It acts as a powerful tool for increasing productivity and enhancing customer service (IBSolution 2013). Orders from wholesalers, retailers and customers go to distributors, who in turn place a cumulative order for products to the manufacturer. The manufacturer generates a production plan comprising the total amount of products that include sales orders. In addition to amounts that are planned to sell based on sales forecasting. This plan necessitates a good coordination among different stakeholders in the supply chain of the company, such as different sections of the company, suppliers or other subsidiaries for raw materials. Lack of integration among different stakeholders in the supply chain causes fall in business performance and reduced profit and market share of the business (Whitepaper 2007). An efficient sales order processing helps to simplify the process of ordering, save time and reduce errors of order processing (Schubring 2009).

Order processing is an important area for improvement to achieve efficiency in supply chain performance. For high-performing organizations efficiency in the processing of customer orders is a distinguishing characteristic (Esker 2013).

Automation of sales order processing gives organizations more control and insight into what is happening on a daily basis (Mayank 2003). It helps organizations better manage customer and supplier relationships, manage inventory and production, comply with regulatory requirements, control finances and sales forecasting, bring visibility to business processes and improve overall profitability (Peoplesoft 2011).

Organizations today recognize that they must deliver outstanding customer service in order to acquire new customers and retain existing ones. The ability to process and ship orders accurately and on time, and to provide quick feedback to customers about the status of their orders is the key to success (USoPM 1997).

To achieve the ability to process customer orders effectively and efficiently web based software are being used in the developed countries. Some developing countries like Bangladesh, where the infrastructure of information technology is developing, the web based softwares are partially feasible (Howladar et al. 2012). Only 0.7% people are internet users. (Internet world stats 2012). In the most remote areas of Bangladesh, internet facilities are not available, but cellular telecommunication supported Short Messaging Service (SMS) is available to Retailers (Customers) (Ahmed et al. 2011). The distributors to these retailers usually reside in the urban areas where internet facilities are available. So to make an integrated communication between manufacturer, distributors and customers an SMS based web integrated order processing software is to be used to increase order processing accuracy, reduce time of collecting and organizing data, and to increase customer satisfaction to achieve their loyalty.

II. SOFTWARE DESIGN BASED ON THE STUDY

2.1 Introduction

This part will discuss and explain in detail about the organization under research. Information such as the organizational structure, functions, and core business activities are explained in detail.

Apart from that, the as-is processes, business processes are pictured in the data flow diagram (DFD) and the entity relationship diagram (ERD). With the help of these graphical depictions or diagrams, the flows of information that exist within Fiza and Co. can be better illustrated and understood.

Solicitation of user requirements is a fundamental step because it would ensure that the software to be developed is what the users want and is relevant to the user. This step is also very important because the users know the current system better and can provide better feedback regarding the hidden or visible drawbacks and flaws of the system. These flaws can later be solved by the newer software. This part will also discuss the user requirements that were solicited from the users. The overview of the newer improved software is illustrated through the use of DFD and ERD.

2.2 Organization under research

Fiza and Co. a well-known bakery food producer in Sylhet, Bangladesh. It is devoted to satisfy its customer by providing them scrumptious and tempting quality foods. Since 1985, and they have been serving people with various food items. They have six well known branches and more than 30 franchisees in Bangladesh. Their goal is to spread factory chain to whole Bangladesh. They are producing foods according to international standards and products are being exported in foreign countries especially in England and India. Major products that they export are biscuits, dry-cakes, sweets, spicy foods, traditional sweets and many other bakery foods (Fiza & Co. official website 2012).

Fiza and Co.'s head office is located at 51, Sagor Dighir Par, Sylhet. The objective of this company is to carry out the business as a manufacturer of quality foods for domestic and export market. To fulfill the needs of its customers, Fiza and Co. utilises sources for their raw materials from other subsidiaries within the local companies. These other companies thus act as the suppliers for Fiza and Co. The company sources the related packaging materials (tin cans, carton, tray, spoon and cap) from the suppliers.

The company currently operates one shift. Fiza's working hour starts from 8.00 a.m. to 6.00 p.m. for five working days. The plant is divided into three zones for good hygiene practice which is 1) GHP (Good Hygiene area), 2) Caring Area and 3) High Care Area. The employees need to look ahead to classify production areas into various zones for good manufacturing practices (GMP) purposes.

After the new set up of operations for good hygiene practice, Fiza and Co. has become a vehicle to enhance its status of competitiveness, and at the same time providing value added services. Thus the company is fully committed for serving quality foods to its consumers and continues to upgrade its operation in order to continue improving the industrial development.

2.2.1 Organizational structure of Fiza and Co.

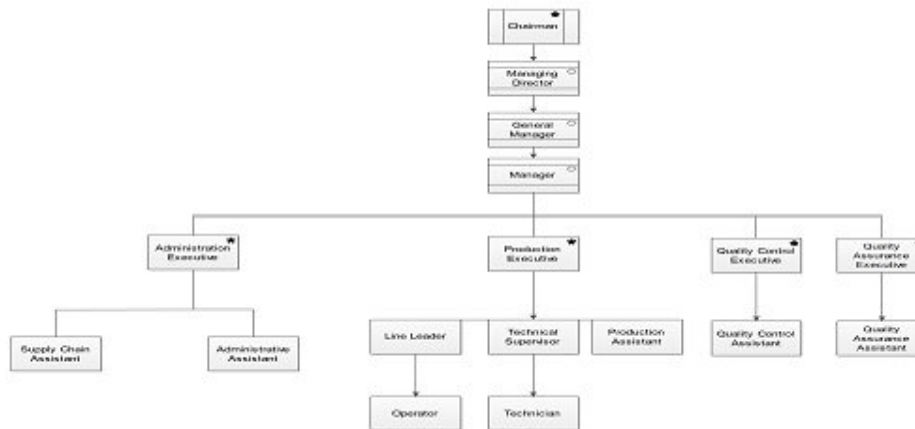


Figure 1: Organizational structure of Fiza and Co.

The chairman sits at the top of the management hierarchy. Next responsible persons in the management hierarchy is the managing director of Fiza and Co. The general manager is responsible for monitoring the responsibilities of all other managers of different departments. There are four departments: administration, production, and quality control and quality assurance departments. There are several staffs under these departments such as leader, supervisor, assistant, operator, technician etc.

2.3 Current business process and data model

Context diagram, data flow diagram (DFD) and entity relationship diagram (ERD) are used to give a clear picture of the as-is Process.

2.3.1 Context diagram and data flow diagram

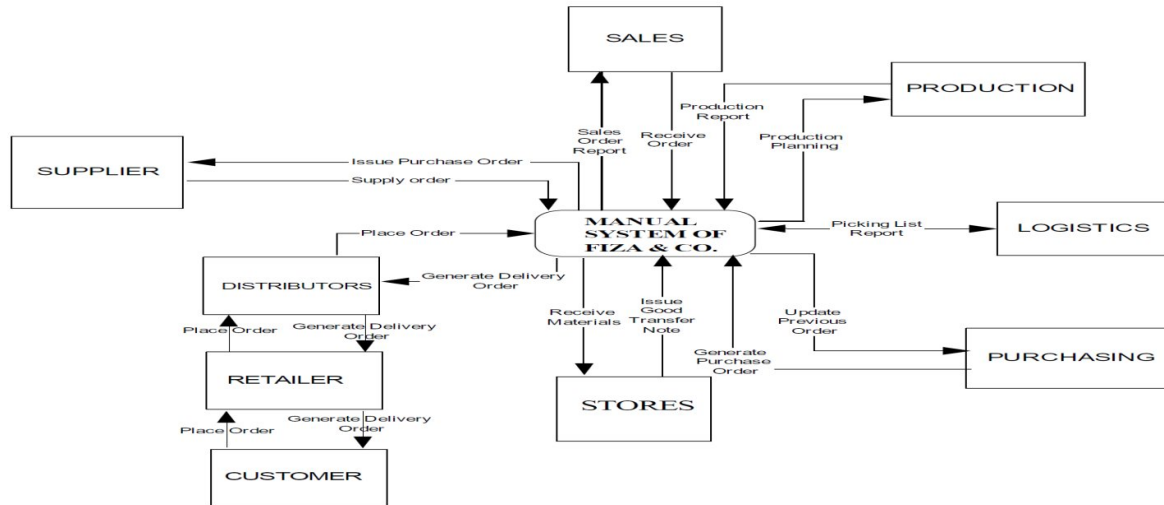


Figure 2: Context diagram for current processes.

Figure 2 describes the context diagram for the current process. The current manual system of Fiza and Co.'s functions as follows:

Sales: Customers place orders through Retailers. This process is discussed in the retailer section. Distributors place replenishment orders to sales department. Sales order consist of order information such as previous balance order, item ordered, quantity and delivery date. Sales order is a document that records all the information about customer order.

Production: Sales department gives sales order to production department to plan their production schedule and line. Production department will also check with the warehouse to ensure that all the materials are sufficient to produce the ordered items. If the raw material inventory is not adequate to produce the ordered items, production department will request to buy the insufficient materials to the purchasing department. When the ordered item is produced, production report will generate and store in filing software.

Purchasing: When the purchasing department receives material requisition from production department, purchase order will be issued to the supplier to supply the materials required. Besides that, purchasing department also will monitor the previous balance order.

Supplier: Suppliers will supply all the materials ordered. Delivery order document will be recorded in filing system upon receiving the materials.

Store: Store will receive the entire item from supplier and store all the items produced by production. Store will update all the incoming and outgoing items record. Store will ensure that all outgoing items will be delivered to the correct customer, in right quantity and at promised time.

Logistics: List record is a record that gives the information of items to be picked by the logistics to send all the finish good to the customer.

Customer: Customer can also place order to sales. When the order is fulfilled by production department, store will issue delivery order document to be sent with the finished good. Logistics will send the ordered items to the customer.

Distributor: Fiza and Co. has several distributors throughout Bangladesh and they pick orders from retailers. This company has been trying to coordinate its distribution system for efficiency, but due to several constraints, this aim is not completely fulfilled.

Retailers: Apart from direct selling from its several branches (six all over Bangladesh), there are a number of retailers who keep the products of Fiza and Co. These products are supplied from the designated distributors of Fiza and Co. These retailers make direct sell to the customers.

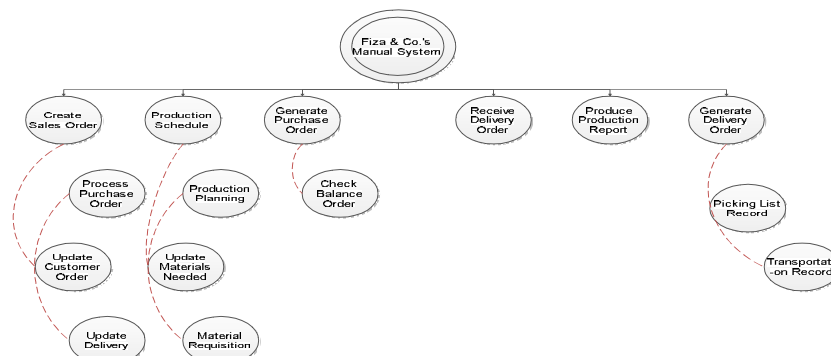


Figure 3: Decomposition diagram for current process

2.4.2 Distributor order module

- Allow to create bulk purchase order.
- Ability to produce documentation for delivery to customer.

2.4.3 Inventory module for distributors

- Ability to check for insufficient inventory level.
- Ability to check stock in warehouse
- Send SMS to customer about the available stock when order is greater than the available stock.
- Update stock in warehouse.

2.5 Conceptual design of the software

This section describes the models used to plan and build the software according to their requirements.

2.5.1 Business process and data Model

Figure 4.6 overviews how SMS based web integrated order processing software integrates all the databases into one central database. They share common data that are needed by all the departments involved in the supply chain. This information and data integration eases the flow of necessary information in the organization. In the SMS based web integrated order processing software, information that is needed can always be obtained in a much shorter time and more efficiently compared to other time-consuming systems.

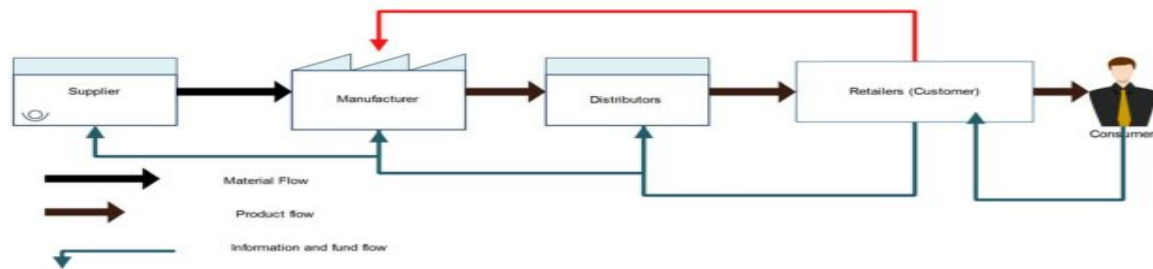


Figure 6: SMS based web integrated order processing software overview

In brief, the consumer or end customer gets the required product from the retailer. In the traditional system, the retailer places the orders to the distributor, the distributor places the accumulated orders to the manufacturer, which is illustrated by the dark blue lines in the figure 6. This traditional process leads to significant bullwhip effect. The new software attempts to accept orders directly from the retailers to the database installed in the manufacturer's side, illustrated by the red line in the above figure. The order is then redirected to the respective distributor for processing and delivery. This new software is expected to reduce the bullwhip effect in the supply chain.

The figure 7 below illustrates the context diagram for the SMS based web integrated order processing software:

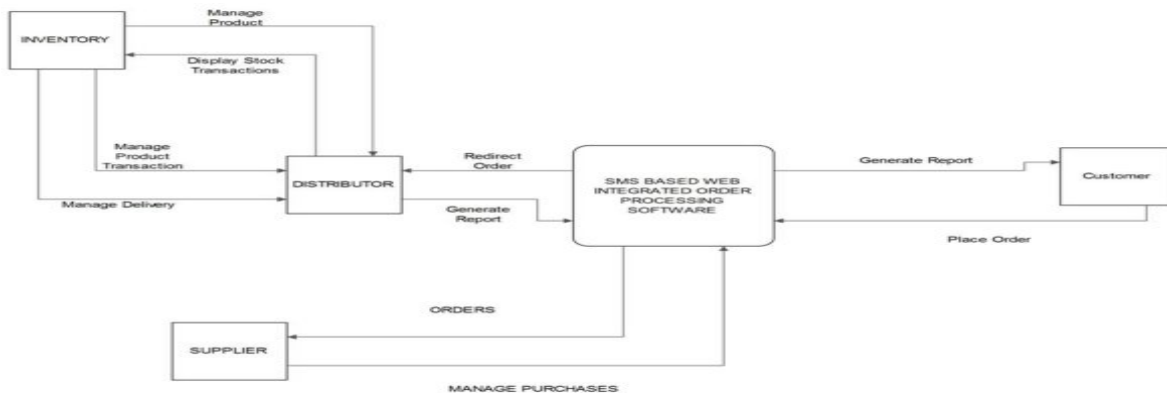


Figure 7: Context diagram for the SMS based web integrated order processing software

All customer orders arrive in the software's database first. Then they are sorted according to distributor code. The software automatically redirects the order to the respective distributor. The distributor then delivers the requested order to the respective customer (retailer). The distributors can also order in bulk amount to the manufacturer through this software for replenishing their inventory. The manufacturer can order to the suppliers for raw materials through this software.

The figure 8 describes DFD (data flow diagram) for SMS based web integrated order processing software from conceptual view:

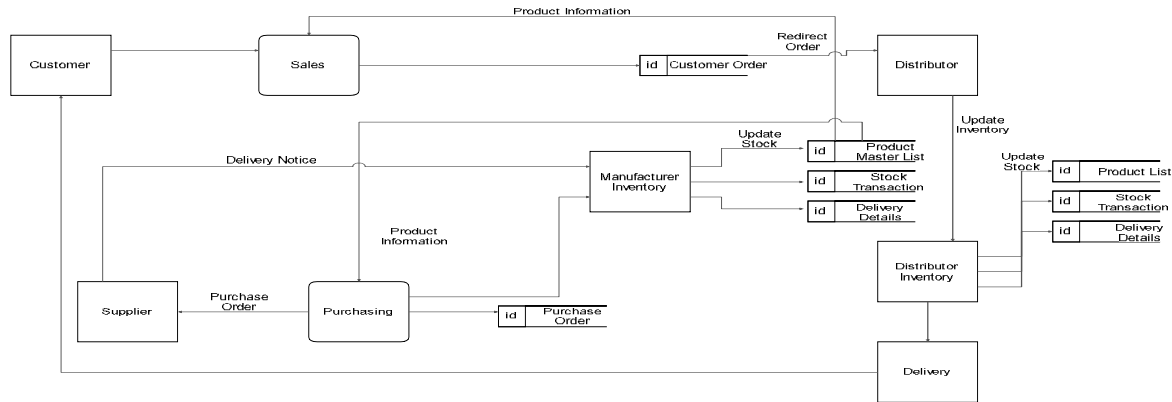
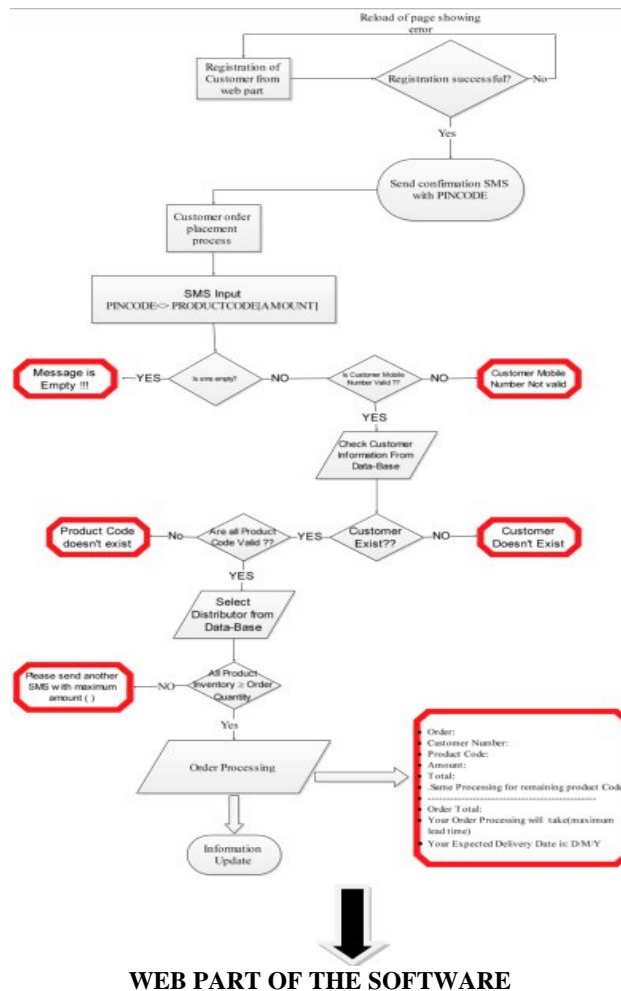


Figure 8: DFD (Conceptual view) for SMS based web integrated order processing software

When an order arrives, it is processed by the software and redirected to the distributor. First the software checks from the manufacturer’s product master list about the detailed information of the requested product. Then the system checks from the inventory data of that distributor whether the distributor is capable of processing the order or not. If the inventory balance is insufficient, then the system notifies the customer that inventory balance is insufficient. If the balance is sufficient, order request is accepted. The distributor then processes the order for delivery. The system virtually acts as sales department for coordinating the order processing activities. Similarly all other activities are coordinated by the software as depicted in DFD diagram. This figure illustrates the process of customer registration and the process of sending a SMS for placing an order.



WEB PART OF THE SOFTWARE

Figure 9: Decomposition diagram for SMS based web integrated order processing software

As shown in the figure 9, the customer is first registered from the web part of the software. Upon registration, the customer receives an SMS with pin code, which is to be used for placing an order to the system. When a customer sends an SMS with the proper format, the system first checks whether the customer's mobile number and pin code match or not. If the software finds a mismatch, it sends an SMS stating the user's information mismatch. If the mobile number and pin code is matched, then the software's logic proceed forward. Then the software checks the validity of the product code. If the amount requested is greater than the available inventory, then an SMS is sent stating the maximum available quantity. If all of these conditions are satisfied, the system accepts and processes the order request.

The following entity relationship diagram illustrates the software database structure:

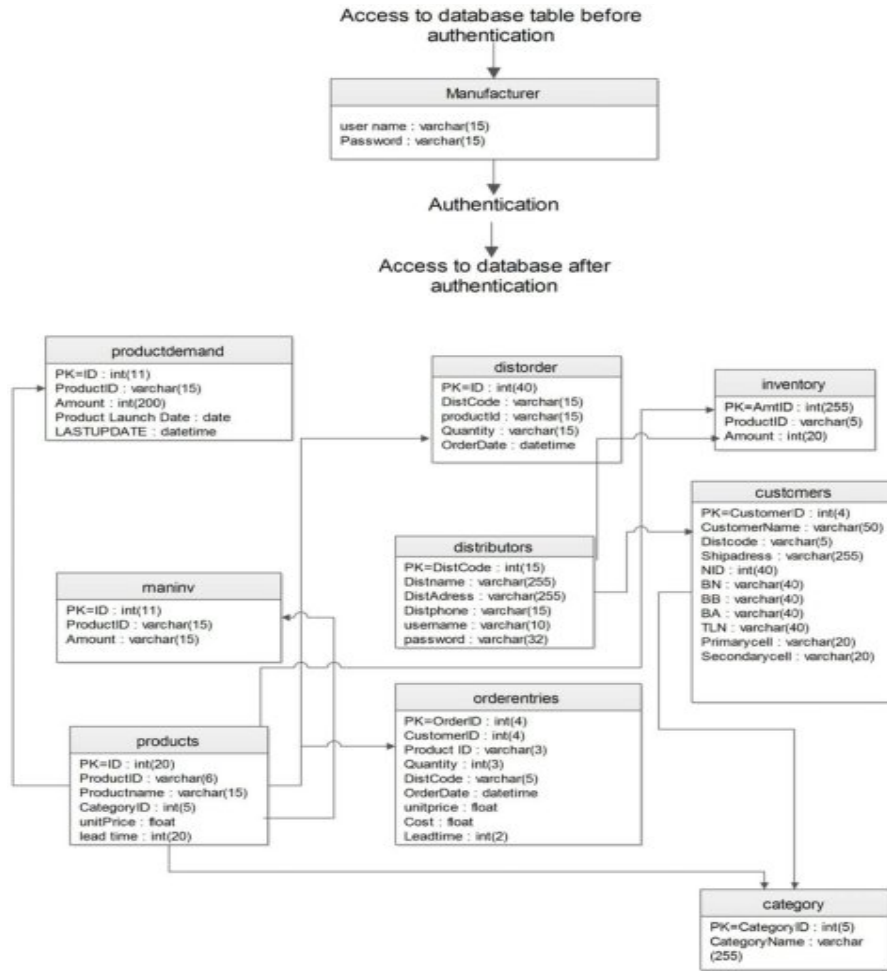


Figure 10: Entity relationship diagram (ERD) for conceptual design

Figure 10 above shows the ERD of the order processing software. ERD is used to model Fiza and Co.'s requirements. Each of the entity is assigned one Primary Key (PK) which uniquely identifies the entity. Each of the entities consists of attributes which represent the data that is required by the software. The relationship among all the entities exists between one or more entity. The 'Customer' and 'Orderentries' entities have one-to-many relationship. This explains that a customer may place many orders or many orders can be placed by only one customer. Similarly other such relationships are shown on the ERD of the new software.

2.5.2 Architecture of developed software

The SMS based web integrated order processing software is an application that is accessible from manufacturer and distributor's computers. The software is placed on an application server where all relevant clients can access it. By structuring the software accessibility this way, authentication and authorization of users can be centralized and managed more efficiently. A set of clients that call on service offered by the server will only be the set that has been granted the necessary permissions.

Communications between the clients and the server is done using internet connections. Since the software is to be used by different clients (Manufacturer and Distributors), it is therefore logical and practical to connect the users and the server through the internet connection. It is also possible to connect the clients and server through LAN and WAN

connectivity. The use of internet to this software has made it highly flexible. The customer (In our case, Retailer) does not need internet connectivity for placing an order. A mobile phone with the Short Messaging Service (SMS) feature is enough for this.

The software is designed in a way which supports user concurrency. This means that it allows the application to be opened by different users, now designed for 500 users, accessing multiple modules at the same time. This feature gives the Fiza and Co.'s users to access the software and complete their tasks without having to wait for their turn, unlike using log books in a manual system. The following figure shows the software architecture for SMS based web integrated order processing system.

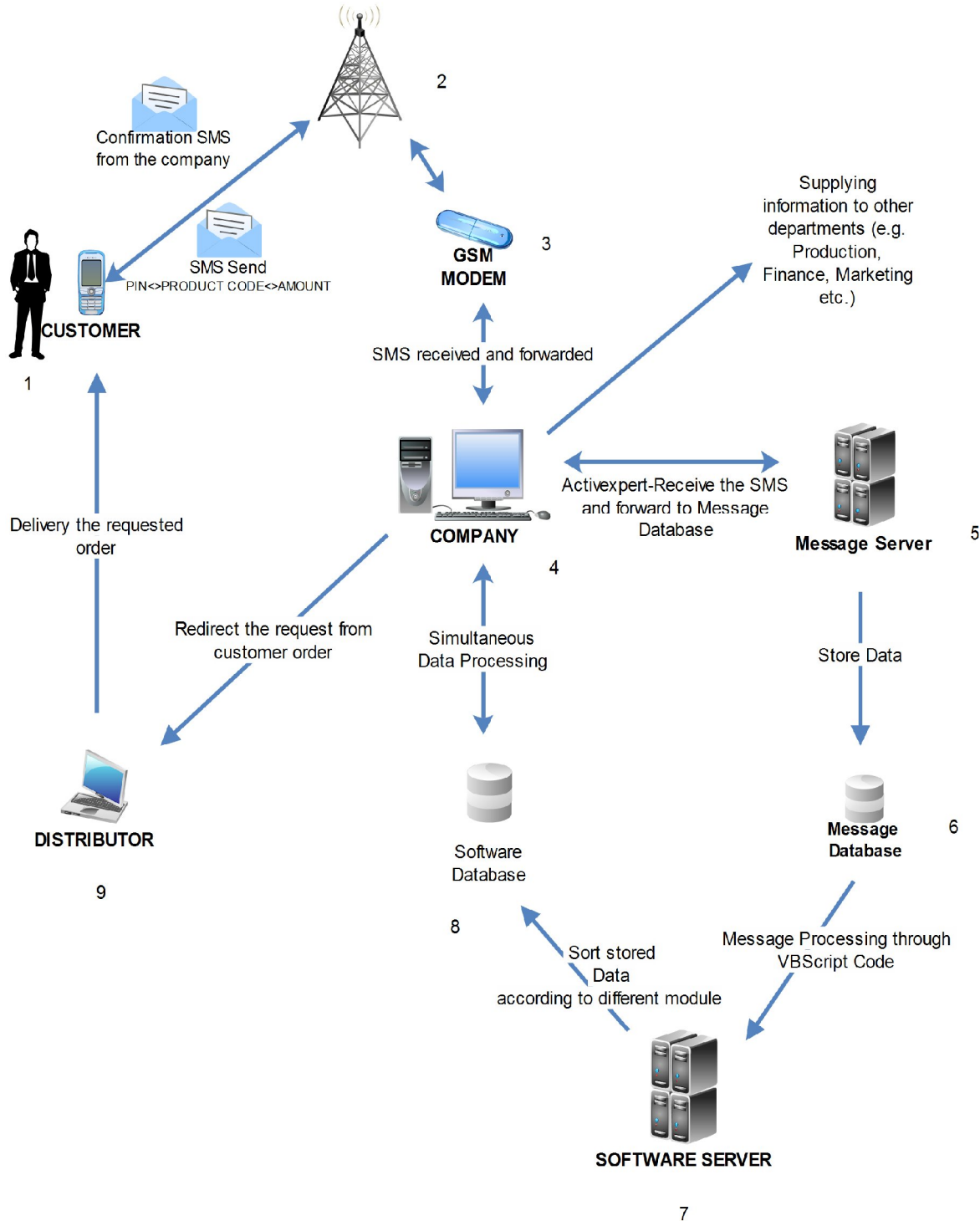


Figure 11: Software architecture for SMS based web integrated order processing software

2.5.3 Software capacity

A retailer can place 31 product orders in one SMS text (160 characters). [4 digit pincode+1 space+4 digit order code (2 digit product code+2 digit amount, the two digit amount is assumption, the software is capable of taking 3 digits)+1 space+30x{4 digit order code (2 digit product code+2 digit amount, the two digit amount is assumption, the software is capable of taking 3 digits)+ 1 space }=160 characters].

The product code database is made in a way that it supports 676 products. [AA+AB+AC+AD.....ZZ].

2.6 Physical design

In this section, the process flow of the software is detailed and explained. This section is composed of database design and software interface chart.

2.6.1 Database design

This database is made of the following tables:

1. Manufacturer (It stores the credentials for manufacturer login)
2. Distorder (It stores all orders from distributors to manufacturer)
3. Productdemand (This table accumulates the demand for various products from the time of product introduction)
4. Inventory (It contains the inventory status for various distributors)
5. Maninv (It contains records of manufacturer inventory)
6. Distributors (It contains login credentials and details about distributors)
7. Customers (This table contains the information about retailers, as this is the last end for the chain of this software)
8. Products (It contains all information about products the manufacturer has)
9. Orderentries (This table entries all the orders from customers)
10. Category (This table contains the information of different product categories)

2.6.2 Software interface chart

The SMS based web integrated order processing software consists of two level user login which describes as follows:

- Manufacturer login – administer the software and control the master file.
- Distributor login – Distributors use the software to do their own task.

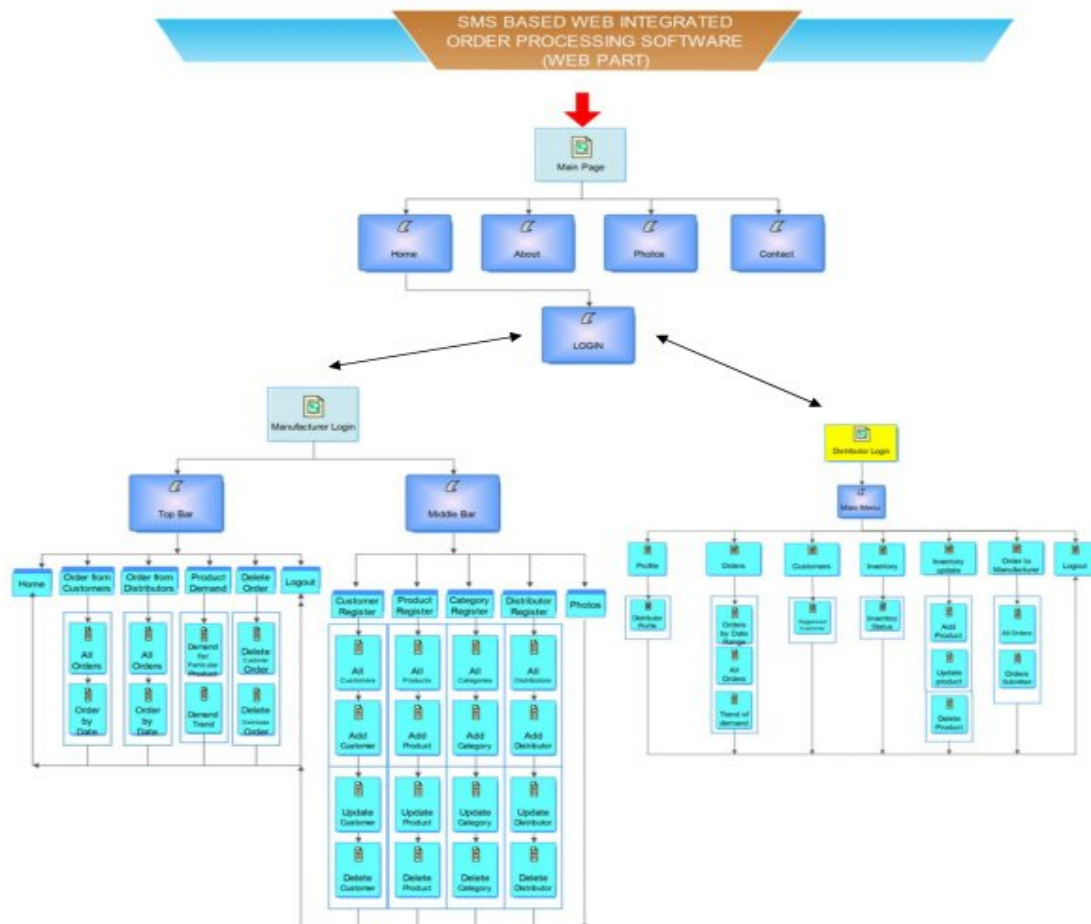


Figure 12: SMS based web integrated order processing software Interface chart.

2.7 **Hardware requirement for smooth running of the software**

In order to run the software, the minimum hardware requirements should be met so that the software can perform at its optimum level. The minimum hardware requirement designated for the software is as follows;

- PC with Core2 Quad 2.0 GHz processor
- Hard Disk: 250GB
- Memory: At least 2GB RAM
- Some backup solution for recovering data in case of an accident.

III. CONCLUSION

A software package was successfully developed, tested and used for the complete management of customer orders. It is a complete package for analyzing product demand with a focus on tracking actual demand. The accuracy of the results obtained is of publishable standard, and compares quite favorably to other available web based supply chain software packages.

A rather inconspicuous outcome of this study, albeit a very important one, is the level of automation of the software. Considering the large amount of order processing time reduced, this software brings real time automated order processing through SMS.

The drawback of the automation is that if too many SMS arrive at the same time, some messages are queued for processing, which takes a little bit time to send the confirmation message to the customer. But this software is able to reliably reduce more than 85% of the order processing time with great accuracy. This is quite a high percentage for software to achieve on its first release.

In the competitive business world, a company needs to get information flow faster and accurately. In a developing country like Bangladesh, SMS has been of great advantage in this area. Along with SMS, web is used to connect the all parties involved in fulfilling customers need. In the business world, most of the things are designed for improving effectiveness and reducing cost. In present competitive age, competition between business organizations shifts from company vs. company to supply chain vs. supply chain. To compete at the supply chain level, companies must adopt appropriate SCM strategies. Such strategies need integration and coordination throughout the supply chain to enhance the performance of supply chain members. An efficient supply chain strategy aims at cutting cost and eliminating non-value activities, which can be realized from the SMS based web integrated order processing software, as the supply chain activities begin with the customer order.

REFERENCES

- [1] Ahmed et al. (2011). Problems and prospects of mobile banking in Bangladesh. *Journal of Information Engineering and Applications*, 1(6), pp-16-17.
- [2] Alballaa H. and Al-Mudimigh A. S. (2011). Change Management Strategies for Effective Enterprise Resource Planning Softwares: A Case Study of a Saudi Company, *International Journal of Computer Applications*, 17(2), pp. 14-19.
- [3] Al-Mashari, M., Ghani, S.K. and Rashid, W. (2006). A Study of the Critical Success Factors of ERP Implementation in Developing Countries. *International Journal of Internet and Enterprise Management*, 4(1), pp. 68-95.
- [4] Aviv, Y. (2001). The effect of collaborative forecasting on supply chain performance, *Management Science*, 47(10), pp. 1326-1343.
- [5] Beamon, B.M., (1998). Supply chain design and analysis: Models and methods, *Int. Journal of Production Economics*, 55(3), pp. 281-294.
- [6] Bhatti, T. R. (2005). Critical Success Factors For The Implementation Of Enterprise Resource Planning (ERP): Empirical Validation. *Proceedings of the Second International Conference on Innovation in Information Technology (IIT'05)*. (pp. 1-10). Dubai, UAE
- [7] Biehl, M. (2007) Success Factors for Implementing Global Information Softwares, *Communications of the ACM*, 50(1), pp 53-58.
- [8] Bokhari R. H. (2001) User Participation and User Satisfaction in Information Software Development, Un-published Thesis, Department of Information Softwares and Computing, Brunel University, UK.
- [9] Buxmann , Anette von Ahsen, Luis Martín Díaz, Kristina Wolf (2004). Usage and evaluation of Supply Chain Management Software – results of an empirical study in the European automotive industry, *Information Systems Journal*, 14(3), pp. 295–309.
- [10] Cachon, G. P. & Fisher, M. (2000). Supply chain inventory management and the value of shared information. *Management Science*, 46(8), pp. 1032-1048.
- [11] Chen, F., Drezner, Z., Ryan, J. K. & Simchi-Levi, D. (2000). Quantifying the bullwhip effect in a simple supply chain: The impact of forecasting, lead times, and information. *Management Science*, 46(3), pp. 436-443.
- [12] Childerhouse, P., Disney, S. M. & Towill, D. R. (2008). On the impact of order volatility in the European automotive sector. *International Journal of Production Economics*, 114(1), pp. 2-13.
- [13] Claassen, M.J. T., van Weele, A. F. & van Raaij, E. M. (2008). Performance outcomes and success factors of vendor managed inventory (VMI). *Supply Chain Management-an International Journal*, 13(6), pp. 406-414.
- [14] Croson, R. & Donohue, K. (2003). Impact of POS data sharing on supply chain management: An experimental study. *Production and Operations Management*, 12(1), pp. 1-11.
- [15] Croson, R. & Donohue, K. (2006). Behavioral causes of the bullwhip effect and the observed value of inventory information. *Management Science*, 52(3), pp. 323-336.
- [16] Davenport T.H. (1998) Putting the Enterprise into the Enterprise Softwares. *Harvard Business Review*, 76(4), pp 121-131.
- [17] Eight Reasons for SMS Marketing. (n.d.). Retrieved from Mobile marketing ratings: (<http://www.mobilemarketingratings.com/eight-reasons-sms-marketing.html>), Access Date: March 25, 2012.
- [18] Esker. (2013). Automated Sales Order Processing for Order-to-Cash Performance (www.esker.com), Access Date: March 19, 2013.

- [19] Esteves, J. M., Pastor, M. J, and Casanovas, J. (2003) A Goal/Question/Metric Research to Monitor User Involvement and Participation in ERP Implementation Projects. Information Resource Management Association Conference (IRMA), Philadelphia (USA), pp. 325-327.
- [20] Finney, S. and Corbett, M. (2007) ERP Implementation: A Compilation and Analysis of Critical Success Factors, Business Process Management Journal, 13(3), pp. 329-347.
- [21] Fiza & Co. official website (www. fiza.com.bd/), Access Date: March 11, 2012
- [22] Francoise, O. Bourgault, M. and Pellerin R (2009) ERP Implementation Through Critical Success Factors' Management, Business Process Management Journal, 15(3), pp. 371-394.
- [23] Gordon A. (2006) ERP Applications: Myth and Misconceptions, EzineArticles (www.ezinearticles.com), Access Date: December 14, 2010.
- [24] Hartwick J., and Barki, H. (2001) Communication as a Dimension of User Participation, IEEE, 44(1), pp. 21-35.
- [25] Huang, Z. and Palvia, P. (2001) ERP Implementation Issues In Advanced And Developing Countries. Business Process Management Journal, 7(3), 276-284.
- [26] Howladar et al. (2012). Developing Online Shopping Intention among People: Bangladesh Perspective. 2(9), 2012, pp.69-71
- [27] Huang, Z. and Palvia, P. (2001) ERP Implementation Issues in Advanced and Developing Countries, Business Process Management Journal, 7(3), pp. 276-284.
- [28] Hwang, H. B.&Xie, N. (2008). Understanding supply chain dynamics: A chaos perspective. European Journal of Operational Research, 184(3), pp. 1163-1178.
- [29] IBSolution (www.ibsolutions.com), Access Date: February 14, 2013.
- [30] Jespersen, B. and Skjott-Larsen, T. (2005). Supply Chain Management: In theory and practice. 1st Ed. Copenhagen Business School Press, Denmark.
- [31] Kakumanu, P. and Mezzacca, M. (2005) Importance of Portal Standardization and Ensuring Adoption in Organizational Environments, Journal of American Academy of Business, 7(2), pp. 128-132.
- [32] Leon, A. (2008) Enterprise Resource Planning. 2nd Ed, MC-Graw-Hill, New Delhi, India.
- [33] Levi et al. (2008). Designing and Managing the Supply Chain. 3rd Ed. Tata McGraw-Hill, India.

Computer: - A Communication Device

*Anurag Rana, **Preeti Chib

*University Institute of Information Technology, Himachal Pradesh University.

**Arni University.

Abstract: Computer system is able to communicate more effectively than face-to-face. Computer programs are very important because they transcend mere "data"-they include procedures and processes for structuring and manipulating data. These are the main resources we can now concentrate and share with the aid of the tools and techniques of computers and communication, but they are only a part of the whole that we can learn to concentrate and share. The computer system was a significant aid in exploring the depth and breadth of the material.

Keywords: Computer, communication.

I. COMPUTER: A COMMUNICATION DEVICE

Now days, men will be able to communicate more effectively through a system than face to face.

Our significance on people is calculated. A communications engineer thinks of communicating as transferring information from one point to another in codes and signals. But to communicate is more than to send and to receive. Do two CD player recorder communicate when they play to each other and record from each other? Not really not in our sense. We believe that communicators have to do something non significant with the information they send and receive. And we believe that we are entering a technological age in which we will be able to interact with the richness of living information not merely in the inactive way that we have become commonly to using books and libraries, but as active participants in an ongoing process, bringing something to it through our interaction with it, and not simply receiving something from it by our connection to it.

To the people who telephone an airline flight operations information service, the CD player recorder that answers seems more than a passive depository. It is an often updated model of a changing situation - a synthesis of information collected, analyzed, evaluated, and assembled to represent a situation or process in an organized way. Still there is not much direct interaction with the airline information service; the CD recording is not changed by the customer's call. We want to significance something beyond its one-way transfer: the increasing significance of the jointly constructive, the mutually reinforcing aspect of communication -the part that exceeds "now we both know a fact that only one of us knew before." When minds interact, new ideas emerge. We want to talk about the creative aspect of communication.

Creative, interactive communication requires a moldable medium that can be modeled, a dynamic medium in which assumptions will flow into effects, and above all a common medium that can be contributed to and experimented with by all.

Such a medium is at hand -the programmed digital computer. Its presence can change the nature and value of communication even more deeply than did the printing press and the picture tube, for, as we shall show, a well-programmed computer can provide direct access both to informational resources and to the processes for making use of the resources,

II. COMMUNICATION: A COMPARISON OF MODELS

To understand how and why the computer can have such an effect on communication, we must examine the idea of modeling in a computer and with the aid of a computer. For modeling, we believe, is basic and central to communication. Any communication between people about the same thing is a common revelatory experience about informational models of that thing. Each model is a conceptual structure of abstractions formulated initially in the mind of one of the persons who would communicate, and if the concepts in the mind of one would be communicator are very different from those in the mind of another, there is no common model and no communication. The most numerous, most sophisticated, and most important models are those that reside in men's minds, In richness, plasticity, facility, and economy, the mental model has no peer, but, in other respects, it has short comings. It will not stand still for careful study. It cannot be made to repeat a run. No one knows just how it works. It serves its owner's hopes more faithfully than it serves reason. It has access only to the information stored in one man's head. It can be observed and manipulated only by one person.

Society rightly distrusts the modeling done by a single mind. Fundamentally, this amounts to the requirement that individual models be compared and brought into some degree of accord. The requirement is for communication, which we now define concisely as "cooperative modeling" cooperation in the construction, maintenance, and use of a model.

How can we be sure that we are modeling cooperatively, that we are communicating, unless we can compare models?

When people communicate face to face, they objectify their models so they can be sure they are talking about the same thing. Even such a simple objectify model as a flow diagram or an outline-because it can be seen by all the communicators serves as a focus for discussion. It changes the nature of communication:

When communicators have no such common framework, they merely make speeches at each other; but when they have a manipulable model before them, they express a few words, point, sketch or object.

The dynamics of such communication are so model centered as to suggest an important conclusion: Perhaps the reason present day two-way telecommunication falls so far short of face-to-face communication is simply that it fails to provide facilities for externalizing models. Is it really seeing the expression in the other's eye that makes the face-to-face conference so much more productive than the telephone conference call, or is it being able to create and modify external models?

III. THE PROJECT MEETING AS A MODEL

In a technical project meeting, one can see going on, in fairly clear relief, the modeling process that we contend constitutes communication. Nearly every reader can recall a meeting held during the develop phase of a project. Each member of the project brings to such a meeting a somewhat different mental model of the common undertaking -its purposes, its goals, its plans, its progress, and its status. Each of these models interrelates the past, present, and future states of affairs of (1) himself; (2) the group he represents; (3) his boss; (4) the project.

Many of the primary data the participants bring to the meeting are in undigested and uncorrelated form. To each participant, his own collections of data are interesting and important in and of themselves. And they are more than files of facts and recurring reports. They are strongly influenced by insight, subjective feelings, and educated guesses. Thus, each individual's data are reflected in his mental model. Getting his colleagues to incorporate his data into their models is the essence of the communications task.

Suppose you could see the models in the minds of two would be communicators at this meeting. You could tell, by observing their models, whether or not communication was taking place. If, at the outset, their two models were similar in structure but different simply in the values of certain parameters, then communication would cause convergence toward a common pattern. That is the easiest and most frequent kind of communication. When mental models are dissimilar, the achievement of communication might be signaled by changes in the structure of one of the models, or both of them.

If the two mental models were structurally dissimilar, then the achievement of communication would be signaled by structural changes in one of the models or in both of them. We might conclude that one of the communicating parties was having insights or trying out new hypotheses in order to begin to understand the other—or that both were restructuring their mental models to achieve commonality.

The meeting of many interacting minds is a more complicated process. Suggestions and recommendations may be elicited from all sides. The inter-play may produce, not just a solution to a problem, but a new set of rules for solving problems. That, of course, is the essence of creative interaction. The process of maintaining a current model has within it a set of changing or changeable rules for the processing and disposition of information.

The project meeting we have just described is representative of a broad class of human effort which may be described as creative informational activity. Let us differentiate this from another class which we will call informational housekeeping. The latter is what computers today are used for in the main; they process payroll checks, keep track of bank balances, calculate orbits of space vehicles, control repetitive machine processes, and maintain varieties of debit and credit lists. Mostly they have not been used to make coherent pictures of not well understood situations.

IV. FACE TO FACE THROUGH A COMPUTER

Tables were arranged to form a square work area with five on a side. The center of the area contained six television monitors which displayed the alphanumeric output of a computer located elsewhere in the building but remotely controlled from a keyboard and a set of electronic pointer controllers called "mice." Any participant in the meeting could move a near-by mouse, and thus control the movements of a tracking pointer on the TV screen for all other participants to see.

Each person working on the project had prepared a topical outline of his particular presentation for the meeting, and his outline appeared on the screens as he talked providing a broad view of his own model. Many of the outline statements contained the names of particular reference files which the speaker could recall from the computer to appear in detail on the screens, for, from the beginning of the project, its participants had put their work into the computer system's files.

So the meeting began much like any other meeting in the sense that there was an overall list of agenda and that each speaker had brought with him (figuratively in his briefcase but really within the computer) the material he would be talking about.

The computer system was a significant aid in exploring the depth and breadth of the material. More detailed information could be displayed when facts had to be pinpointed; more global information could be displayed to answer questions of relevance and interrelationship. A future version of this system will make it possible for each participant, on his own TV screen, to thumb through the speaker's files as the speaker talks—and thus check out incidental questions without interrupting the presentation for substantiation. A communication system should make a positive contribution to the discovery and arousal of interests.

Collections of primary data can get too large to digest. There comes a time when the complexity of a communications process exceeds the available resources and the capability to cope with it; and at that point one has to simplify and draw conclusions.

It is frightening to realize how early and drastically one does simplify, how prematurely one does conclude, even when the stakes are high and when the transmission facilities and information resources are extraordinary. Deep modeling to communicate to understand requires a huge investment. Perhaps even governments cannot afford it yet. But someday governments may not be able not to afford it. For, while we have been talking about the communication process as a cooperative modeling effort in a mutual environment, there is also an aspect of communication with or about an uncooperative opponent. As nearly as we can judge from reports of recent international crises, out of the hundreds of alternatives that confronted the decision makers at each decision point or ply in the "game," on the average only a few, and never more than a few dozen could be considered, and only a few branches of the game could be explored deeper than two or three such plies before action had to be taken. Each side was busy trying to model what the other side might be up to-but modeling takes time, and the pressure of events forces simplification even when it is dangerous.

Whether we attempt to communicate across a division of interests, or whether we engage in a cooperative effort, it is clear that we need to be able to model faster and to greater depth. The importance of improving decision-making processes not only in government, but throughout business and the professions is so great as to warrant every effort.

V. THE COMPUTER—SWITCH OR INTERACTOR?

As we see, group decision-making is simply the active, executive, effect-producing aspect of the kind of communication we are discussing. We have commented that one must oversimplify. We have tried to say why one must oversimplify. But we should not oversimplify the main point of this article. We can say with genuine and strong conviction that a particular form of digital computer organization, with its programs and its data, constitutes the dynamic, moldable medium that can revolutionize the art of modeling and that in so doing can improve the effectiveness of communication among people so much as perhaps to revolutionize that also. But we must associate with that statement at once the qualification that the computer alone can make no contribution that will help us, and that the computer with the programs and the data that it has today can do little more than suggest a direction and provide a few germinal examples. Emphatically we do not say: "Buy a computer and your communication problems will be solved."

What we do say is that we, together with many colleagues who have had the experience of working on-line and interactively with computers, have already sensed more responsiveness and facilitation and "power" than we had hoped for, considering the inappropriateness of present machines and the primitiveness of their software. Many of us are therefore confident (some of us to the point of religious zeal) that truly significant achievements, which will markedly improve our effectiveness in communication, now are on the horizon. Many communications engineers, too, are presently excited about the application of digital computers to communication. However, the function they want computers to implement is the switching function. Computers will either switch the communication lines, connecting them together in required configurations, or switch (the technical term is "store and forward") messages.

The switching function is important but it is not the one we have in mind when we say that the computer can revolutionize communication. We are stressing the modeling function, not the switching function. Until now, the communications engineer has not felt it within his province to facilitate the modeling function, to make an interactive, cooperative modeling facility. Information transmission and information processing have always been carried out separately and have become separately institutionalized. There are strong intellectual and social benefits to be realized by the melding of these two technologies. There are also, however, powerful legal and administrative obstacles in the way of any such melding.

VI. DISTRIBUTED INTELLECTUAL RESOURCES

We have seen the beginnings of communication through a computer communication among people at consoles located in the same room or on the same university campus or even at distantly separated laboratories of the same research and development organization. This kind of communication through a single multi-access computer with the aid of telephone lines is beginning to foster cooperation and promote coherence more effectively than do present arrangements for sharing computer programs by exchanging magnetic tapes by messenger or mail. Computer programs are very important because they transcend mere "data"—they include procedures and processes for structuring and manipulating data. These are the main resources we can now concentrate and share with the aid of the tools and techniques of computers and communication, but they are only a part of the whole that we can learn to concentrate and share. The whole includes raw data, digested data, data about the location of data and documents and most especially models.

To appreciate the importance the new computer-aided communication can have, one must consider the dynamics of "critical mass," as it applies to cooperation in creative endeavor. Take any problem worthy of the name, and you find only a few people who can contribute effectively to its solution. Those people must be brought into close intellectual partnership so that their ideas can come into contact with one another. But bring these people together physically in one place to form a team, and you have trouble, for the most creative people are often not the best team players, and there are not enough top positions in a single organization to keep them all happy. Let them go their separate ways, and each creates his own empire, large or small, and devotes more time to the role

of emperor than to the role of problem solver. The principals still get together at meetings. They still visit one another. But the time scale of their communication stretches out, and the correlations among mental models degenerate between meetings so that it may take a year to do a week's communicating. There has to be some way of facilitating communication among people without bringing them together in one place.

A single multi-access computer would fill the bill if expense were no object, but there is no way, with a single computer and individual communication lines to several geographically separated consoles, to avoid paying an unwarrantedly large bill for transmission. Part of the economic difficulty lies in our present communications system. When a computer is used interactively from a typewriter console, the signals transmitted between the console and the computer are intermittent and not very frequent. They do not require continuous access to a telephone channel; a good part of the time they do not even require the full information rate of such a channel. The difficulty is that the common carriers do not provide the kind of service one would like to have—a service that would let one have ad lib access to a channel for short intervals and not be charged when one is not using the channel.

It seems likely that a store-and-forward (i.e., store-for-just-a-moment-and-forward-right-away) message service would be best for this purpose, whereas the common carriers offer, instead, service that sets up a channel for one's individual use for a period not shorter than one minute.

The problem is further complicated because interaction with a computer via a fast and flexible graphic display, which is for most purposes far superior to interaction through a slow-printing typewriter, requires markedly higher information rates. Not necessarily more information, but the same amount in faster bursts—more difficult to handle efficiently with the conventional common-carrier facilities.

It is perhaps not surprising that there are incompatibilities between the requirements of computer systems and the services supplied by the common carriers, for most of the common-carrier services were developed in support of voice rather than digital communication. Nevertheless, the incompatibilities are frustrating. It appears that the best and quickest way to overcome them—and to move forward the development of interactive communities of geographically separated people—is to set up an experimental network of multi-access computers. Computers would concentrate and interleave the concurrent, intermittent messages of many users and their programs so as to utilize wide-band transmission channels continuously and efficiently, with marked reduction in overall cost.

COMPUTER AND INFORMATION NETWORKS

The concept of computers connected to computers is not new. Computer manufacturers have successfully installed and maintained interconnected computers for some years now. But the computers in most instances are from families of machines compatible in both software and hardware, and they are in the same location. More important, the interconnected computers are not interactive, general-purpose, multi-access machines of the type described by David [1] and Licklider [2]. Although more interactive multi-access computer systems are being delivered now, and although more groups plan to be using these systems within the next year, there are at present perhaps only as few as half a dozen interactive multi-access computer communities.

These communities are socio-technical pioneers, in several ways out ahead of the rest of the computer world: What makes them so? First, some of their members are computer scientists and engineers who understand the concept of man-computer interaction and the technology of interactive multi-access systems. Second, others of their members are creative people in other fields and disciplines who recognize the usefulness and who sense the impact of interactive multi-access computing upon their work. Third, the communities have large multi-access computers and have learned to use them. And, fourth, their efforts are regenerative.

In the half-dozen communities, the computer systems research and development and the development of substantive applications mutually support each other. They are producing large and growing resources of programs, data, and know-how. But we have seen only the beginning. There is much more programming and data collection—and much more learning how to cooperate—to be done before the full potential of the concept can be realized. Obviously, multi-access systems must be developed interactively. The systems being built must remain flexible and open-ended throughout the process of development, which is evolutionary.

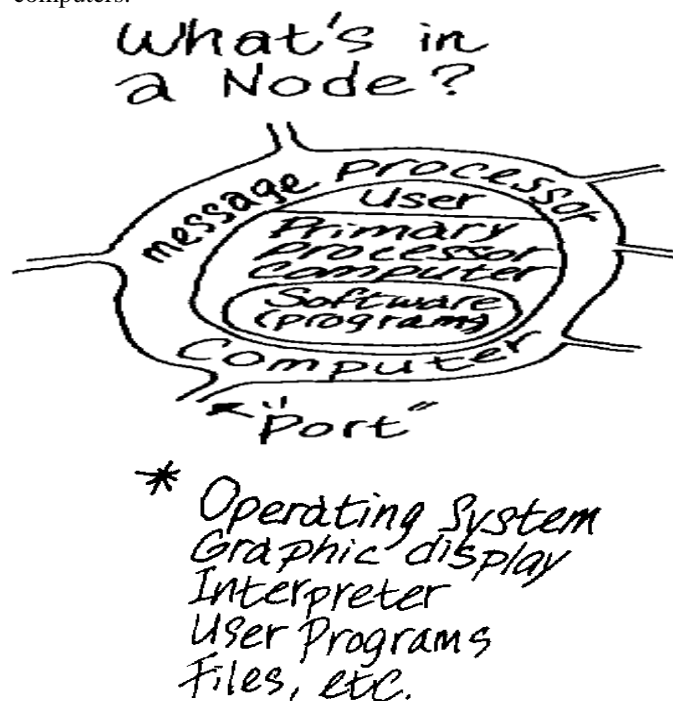
Such systems cannot be developed in small ways on small machines. They require large, multiaccess computers, which are necessarily complex. Indeed, the sonic barrier in the development of such systems is complexity.

These new computer systems we are describing differ from other computer systems advertised with the same labels: interactive, time-sharing, multi-access. They differ by having a greater degree of open-endedness, by rendering more services, and above all by providing facilities that foster a working sense of community among their users. The commercially available time-sharing services do not yet offer the power and flexibility of software resources the “general purposeless” of the interactive multi-access systems of which have been collectively serving about a thousand people for several years.

The thousand people include many of the leaders of the ongoing revolution in the computer world. For over a year they have been preparing for the transition to a radically new organization of hardware and software, designed to support many more simultaneous users than the current systems, and to offer them—through new languages, new file-handling systems, and new graphic displays—the fast, smooth interaction required for truly effective man-computer partnership.

Experience has shown the importance of making the response time short and the conversation free and easy. We think those attributes will be almost as important for a network of computers as for a single computer.

Today the on-line communities are separated from one another functionally as well as geographically. Each member can look only to the processing, storage and software capability of the facility upon which his community is centered. But now the move is on to interconnect the separate communities and thereby transform them into, let us call it, a super community. The hope is that interconnection will make available to all the members of all the communities the programs and data resources of the entire super community. First, let us indicate how these communities can be interconnected; then we shall describe one hypothetical person's interaction with this network, of interconnected computers.

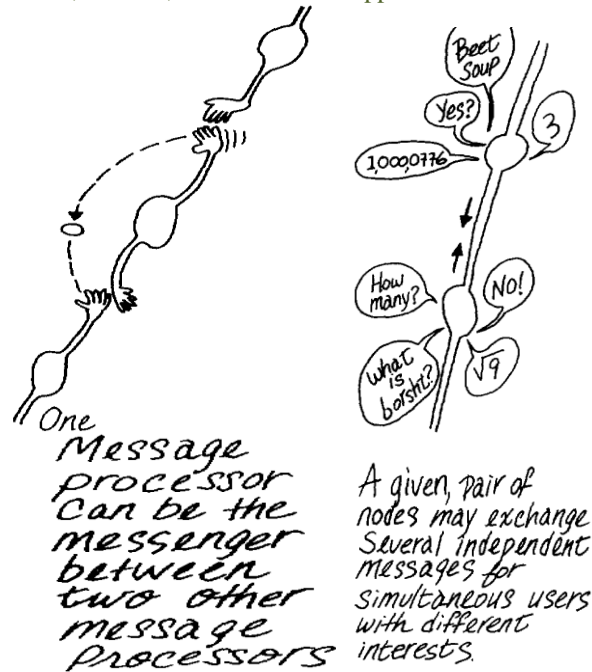


VII. MESSAGE PROCESSING

The hardware of a multi-access computer system includes one or more central processors, several kinds of memory disk and tapes—and many consoles for the simultaneous on-line users. Different users can work simultaneously on diverse tasks. The software of such a system includes supervisory programs (which control the whole operation), system programs for interpretation of the user's commands, the handling of his files, and graphical or alphanumeric display of information to him (which permit people not skilled in the machine's language to use the system effectively), and programs and data created by the users themselves. The collection of people, hardware, and software—the multi-access computer together with its local community of users—will become a node in a geographically distributed computer network. Let us assume for a moment that such a network has been formed.

For each node there is a small, general-purpose computer which we shall call a "message processor." The message processors of all the nodes are interconnected to form a fast store-and-forward network. The large multi-access computer at each node is connected directly to the message processor there. Through the network of message processors, therefore, all the large computers can communicate with one another. And through them, all the members of the super community can communicate—with other people, with programs, with data, or with selected combinations of those resources. The message processors, being all alike, introduce an element of uniformity into an otherwise grossly non-uniform situation, for they facilitate both hardware and software compatibility among diverse and poorly compatible computers. The links among the message processors are transmission and high-speed digital switching facilities provided by common carrier. This allows the linking of the message processors to be reconfigured in response to demand.

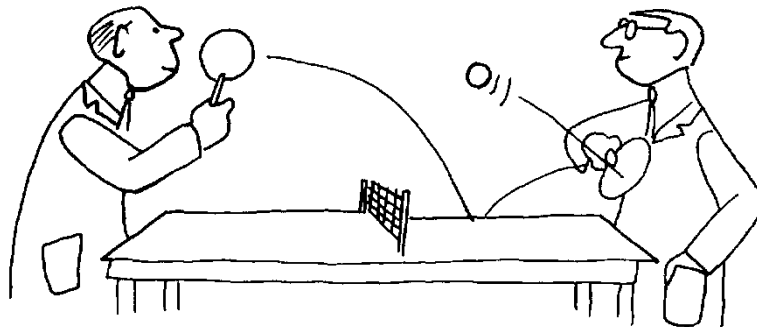
A message can be thought of as a short sequence of "bits" flowing through the network from one multiaccess computer to another. It consists of two types of information: control and data. Control information guides the transmission of data from source to destination. In present transmission systems, errors are too frequent for many computer applications. However, through the use of error detection and correction or retransmission procedures in the message processors, messages can be delivered to their destinations intact even though many of their "bits" were mutilated at one point or another along the way. In short, the message processors function in the system as traffic directors, controllers, and correctors.



Today, programs created at one installation on a given manufacturer's computer are generally not of much value to users of a different manufacturer's computer at another installation. After learning (with difficulty) of a distant program's existence, one has to get it, understand it, and recode it for his own computer. The cost is comparable to the cost of preparing a new program from scratch, which is, in fact, what most programmers usually do. On a national scale, the annual cost is enormous. Within a network of interactive, multi-access computer systems, on the other hand, a person at one node will have access to programs running at other nodes, even though those programs were written in different languages for different computers.

The feasibility of using programs at remote locations has been shown by the successfully.

The system's way of managing data is crucial to the user who works in interaction with many other people. It should put generally useful data, if not subject to control of access, into public files. Each user, however, should have complete control over his personal files. He should define and distribute the "keys" to each such file, exercising his option to exclude all others from any kind of access to it; or to permit anyone to "read" but not modify or execute it; or to permit selected individuals or groups to execute but not read it; and so on—with as much detailed specification or as much aggregation as he likes. The system should provide for group and organizational files within its overall information base.



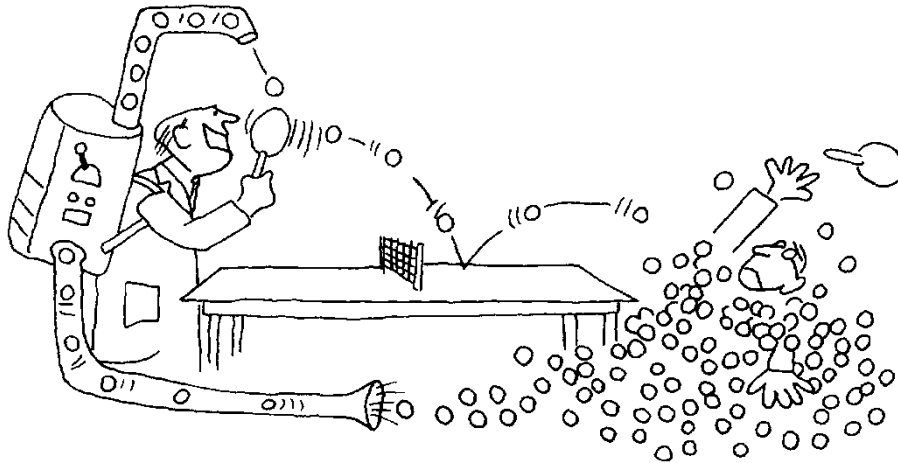
Interactive communication consists of short spurts of dialog.....

At least one of the new multi-access systems will exhibit such features. In several of the research centers we have mentioned, security and privacy of information are subjects of active concern; they are beginning to get the attention they deserve.

In a multi-access system, the number of consoles permitted to use the computer simultaneously depends upon the load placed on the computer by the users' jobs, and may be varied automatically as the load changes. Large general-purpose multi-access systems operating today can typically support 20 to 30 simultaneous users. Some of these users may work with low-level "assembly" languages while others use higher-level "compiler" or "interpreter" languages. Concurrently, others may use data management and graphical systems. And so on.

But back to our hypothetical user. He seats himself at his console, which may be a terminal keyboard plus a relatively slow printer, a sophisticated graphical console, or any one of several intermediate devices. He dials his local computer and "logs in" by presenting his name, problem number, and password to the monitor program. He calls

for either a public program, one of his own programs, or a colleague's program that he has permission to use. The monitor links him to it, and he then communicates with that program.



... obstructing destroys communication.

When the user (or the program) needs service from a program at another node in the network, he (or it) requests the service by specifying the location of the appropriate computer and the identity of the program required. If necessary, he uses computerized directories to determine those data. The request is translated by one or more of the message processors into the precise language required by the remote computer's monitor. Now the user (or his local program) and the remote program can interchange information. When the information transfer is complete, the user (or his local program) dismisses the remote computer, again with the aid of the message processors. In a commercial system, the remote processor would at this point record cost information for use in billing.

On-line interactive communities

But let us be optimistic. What will on-line interactive communities be like? In most fields they will consist of geographically separated members, some-times grouped in small clusters and sometimes working individually. They will be communities not of common location, but of common interest. In each field, the overall community of interest will be large enough to support a comprehensive system of field-oriented programs and data. In each geographical sector, the total number of users summed over all the fields of interest will be large enough to support extensive general-purpose information processing and storage facilities. All of these will be interconnected by telecommunications channels. The whole will constitute a labile network of networks ever-changing in both content and configuration.

What will go on inside? Eventually, every informational transaction of sufficient consequence to warrant the cost. Each secretary's typewriter, each data-gathering instrument, conceivably each dictation microphone, will feed into the network.

You will not send a letter or a telegram; you will simply identify the people whose files should be linked to yours and the parts to which they should be linked-and perhaps specify a coefficient of urgency. You will seldom make a telephone call; you will ask the network to link your consoles together, your computer will know who is prestigious in your eyes and buffer you from a demanding world.

With what priority, and who can have access to which of your personal files. It will know your organization's rules pertaining to proprietary information and the government's rules relating to security classification.

Available within the network will be functions and services to which you subscribe on a regular basis and others that you call for when you need them. In the former group will be investment guidance, tax counseling, selective dissemination of information in your field of specialization, announcement of cultural, sport, and entertainment events that fit your interests, etc. In the latter group will be dictionaries, encyclopedias, indexes, catalogues, editing programs, teaching programs, testing programs, programming systems, data bases, and—most important—communication, display, and modeling programs.

All these will be at some late date in the history of networking systematized and coherent; you will be able to get along in one basic language up to the point at which you choose a specialized language for its power or terseness.

When people do their informational work "at the console" and "through the network," telecommunication will be as natural an extension of individual work as face-to-face communication is now. The impact of that fact, and of the marked facilitation of the communicative process, will be very great both on the individual and on society.

First, life will be happier for the on-line individual because the people with whom one interacts most strongly will be selected more by commonality of interests and goals than by accidents of proximity. Second, communication will be more effective and productive, and therefore more enjoyable. Third, much communication and interaction will be with programs and programmed models, which will be (a) highly responsive, (b) supplementary to one's own capabilities, rather than competitive, and (c) capable of representing progressively more complex ideas without necessarily displaying all the levels of their structure at the same time-and which will therefore be both challenging and rewarding. And, fourth, there will be plenty of opportunity for everyone (who can afford a console) to find his calling, for the whole world of information, with all its fields and disciplines, will be open to him with programs ready to guide him or to help him explore.

For the society, the impact will be good or bad, depending mainly on the question: Will "to be on line" be a privilege or a right? If only a favored segment of the population gets a chance to enjoy the advantage of "intelligence amplification," the network may exaggerate the discontinuity in the spectrum of intellectual opportunity.

On the other hand, if the network idea should prove to do for education what a few have envisioned in hope, if not in concrete detailed plan, and if all minds should prove to be responsive, surely the boon to humankind would be beyond measure.

Unemployment would disappear from the face of the earth forever, for consider the magnitude of the task of adapting the network's software to all the new generations of computer, coming closer and closer upon the heels of their predecessors until the entire population of the world is caught up in an infinite crescendo of on-line interactive debugging.

REFERENCES

- [1] Edward E. David, Jr., "Sharing a Computer," International Science and Technology, June, 1966.
- [2] J. C. R. Licklider, "Man-Computer Partnership," International Science and Technology, May, 1965.

Aggrandize the Reliability by Bug Retrieval (ARBR)

Ms. J. Arthy

Assistant Professor, Dept. Of CSE, Rajiv Gandhi college of Engineering and Technology, Puducherry, India

Abstract: A complex software system has numerous defect prone tasks. There are many reasons for the defects in software. Many of these defects lead to failure of software. Software Reliability is the probability of failure-free software operation for a specified period of time in a specified environment. No good quantitative methods have been developed to represent Software Reliability without tedious manipulation. Therefore, we need a method to enhance the reliability without complexity. We proposed an approach named as ARBR reduces the complexity and manipulation of software metrics. ARBR collects the possible bugs from various applications and maintains an audit for the same. When the new application detects the bug as an audit then the system gets restarted automatically where the executed applications and operations saved so as to recover things easily then the system again try the applications by eliminating the bugs. This method is evaluated in some projects where the bugs are eliminated and gives desirable performance. ARBR satisfies the software reliability requirements with balancing the risk of failures and cost.

Keywords: Software reliability, Audit maintenance, Bug analysis, Recovery, KLOC.

I. INTRODUCTION

Nowadays, information processing systems and their software provide a good factor such as low cost, good control, compact processors, easy handling, etc.. This section discusses about the Software reliability, their parts and the various reasons.

1.1 SOFTWARE RELIABILITY

Software Reliability is defined as the probability of failure-free software operation for a specified period of time in a specified environment. Software reliability is different from hardware reliability because time is not a major constraint. It will not modify over time unless changed or upgraded happened frequently. There are many software quality features such as usability, maintainability etc.... Reliability is one of them and it is very hard to attain it because it leads to a high degree of complexity when the software application size is big and enormous. The complexity of an application is inversely related to reliability and directly related to quality. Good projects are emerging from good management such as time, cost and development.

Software reliability consists three parts: modeling, measurement and enhancement. Reliability modeling refers the optimized model which is ensured by a system testing. There are various estimation techniques to measure the reliability, enhancing the reliability is the process of increasing capability of software during testing and implementation.

There are various reasons behind software failures such as errors, interpretation faults, incompetence, testing and other problems. Design faults also affect the reliability of software. The measurement of software reliability completely depends on manipulation and calculation and so physical prediction is not possible. There are some worst situations where the error appears without any warning. For example, the inputs of a program also affect the software in the situations like redundancy, interference and overlapping. By analyzing the above issues the standard testing and large testing is examined to improve software reliability. But there are no standard methods other than some logic structures and calculations. There is not a simple method to measure software reliability. If the programmer or user doesn't understand the software system or application then it becomes very rigorous to measure it. Most of the software metrics not have a common definition or methods. There are many metrics taken into consideration such as product, process, fault and failure metrics. These metrics help the designer to measure reliability indirectly. There is no standard way of counting the application other than LOC (Lines Of Code) or LOC in thousands (KLOC). Software operating environments are different for every application and so it also affects the reliability. There are two issues which violate the software reliability. They are Control dependence and data independence. The hardware reliability is worn out but the software reliability is conceptual and document. To enhance software reliability first the measurement and improvement of the metrics are initialized. At the next step the cost, effort, time and other set of complexity metrics must be low. There are many real time examples of software failure such as accidental change of function when fault input to the system, encountered, misinterpretation of requirements etc., All the above discussed issues ensure that the reliability of a software is an unpredictable one. So there is a need for a good prediction method of software reliability. To enhance reliability the following steps to be done (i) standardizing data collecting methods (ii) documenting again and again (iii) inter-rater reliability. We propose a prediction reliability model in further sections.

II. RELATED WORK

Most reliability methods consider some assumptions and mathematical functions such as higher order exponential and logarithmic. There are numerous approaches can be used to increase the reliability. However, all of the methods are very tedious and rigorous to develop and implement by means of time and cost. In the literature, there are some works for attaining reliability models. Brown et al. introduced a cost model that determines the optimal number of software test cases based on a probabilistic model that incorporates the cost per test, the error cost, the number of software executions, and the estimated number of faults. The main disadvantage of this approach is that no distinction is made between different tests, and the fact that these different tests cover different possible faults. The main assumption used by these models in treating the fault correction process is that the rate of fault correction is proportional to the number of faults to be corrected, meaning that the expected cumulative number of corrected faults is proportional to the expected cumulative number of detected faults with constant delay. All the methods have some assumptions and calculations.

Eduardo Oliveria Costa et al. (2010) introduced a model by the method of Genetic Programming (GP) it gives the better reliability curve which is experimenting with time and coverage. Kapil Sharma et al. (2010) develop a deterministic quantitative model based on a distance based approach and then applied for evaluation, optimization and selection. Ahmed Patel et al. (2010) develop a technique for software application and reliability which is implemented with programming examples. Costa et al. (2010) follows a genetic programming approach for reliability modeling. J. Onishi et al. (2007) gives an improved surrogate method which solves redundancy and other problems which increases the reliability method. Yousif A. Bastaki (2012) developed an interactive method which gets the things from a user and increases the reliability modeling.

III. APPROACH

By analyzing the above models there is no single model which works in all environments efficiently. Some of them may be working well in a certain environment and not suited for other environments. To overcome the above drawbacks ARBR model is introduced where the manual calculation and complexity is very low and compatible with all environments. Many applications are examined by some tools and the errors and faults in the applications are experimented for ARBR-model. By analyzing and gathering these bugs it is possible to discover the errors in a new application. The main advantage of this work is to enhance reliability and redesign to another application. This method is generic considered until other methods. This method achieves high reliability through configuration and interactive and instantaneous development process. The below figure 1 give the overall description of ARBR model.

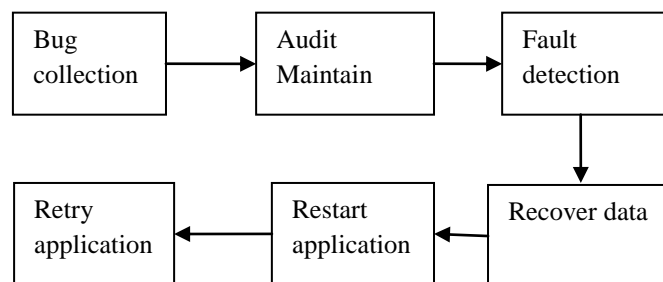


Fig 1 Overview of ARBR

The possible bugs are collected from various applications which help us to determine when the new software application faces the failure. The failures occurred in all types of system are gathered and maintain as a database. The collection is simple because the failures are collected during testing and some are reported by the users. The depth survey users are also given the needed details. Metrics determine the efficiency of the review collected from the user. For example, fault metrics used to measure reliability by means of failure density and Mean Time Between Failures (MTBF). Based on the above mentioned parameters there is a need to increase the reliability and quality. The database is maintained by any packages. So this method is compatible with all environments. When an application fails ARBR try to recover data and executed operations and then the system restarts automatically. The abrupt changes and disaster cannot affect this operation by the mode of recovery. During implementation when the application faces the collected defects in the database then the system is restarted automatically where the current operations and applications saved. In ARBR, It is very easy to retrieve the data from any defects. So the obtained and executed results are protected and we are able to retry the same application. This method has two phases (i) Prediction (ii) design. In the first phase the failure and other properties such as causes of failures are analyzed and in the second phase the application is accumulated. In the first phase some historical application is used and in the next phase predicts the reliability and estimate the same using any estimation techniques. The below diagram Fig 2 shows the method of collecting faults from various projects.

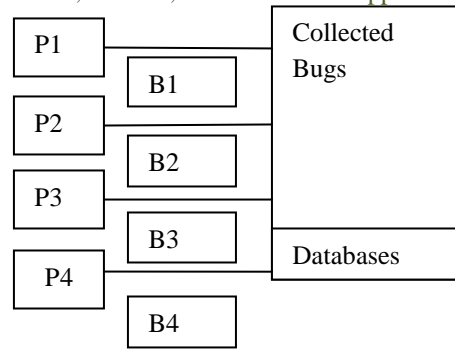


Fig 2 Bugs Collection

In the above figure 2 P1, P2, P3, P4 refers the various projects and B1, B2, B3 and B4 are the various bugs of corresponding projects. The faults are stored in any databases. These collected faults are implemented in the new application as follows. When these faults are stored we have to maintain these faults according to some predefined methods and hence it is easy to diagnose the fault in the new application. After storing, we have to check some conditions by deriving an expression. This step is very simple when using any high level languages. The expression and further operation are discussed in the following steps. (i) DETECT=FAIL COMPONENT then we confirm that the failure occurs in an application. After this step the data are recovered by means of any tool. This recovery happened instantly. When data is recovered the application is restarted. While restarting we have to ensure that the application released from failure. If failure remains establish a signal as RESTART FAILED. When the flag the application is retried and the application is running. There is a chance for new failures. For that purpose we use the signal RETRY FAILED. The retrieving of fault from the database and the remaining process are explained in the figure Fig 3. Below section gives the conducted and their results are discussed.

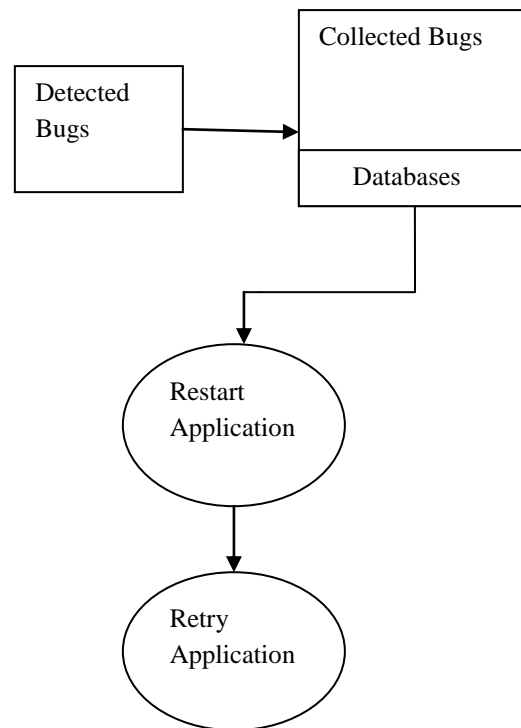


Fig 3 Retrieving bugs from database

When the detected faults and collected faults are same then restart the application after storing the results. When the data stored and the bugs are recovered then retry the same application.

IV. EXPERIMENT AND RESULTS

To evaluate the performance of this method at first we have to determine which portion of the application the measurement would be taken for reliability after that the input to the system is given. For this experiment a program in a .txt file is taken .To make the user interaction easier another .txt file is introduced where the proposed contents are stored. This work collects the bugs and hence the various .txt bugs are determined also the parameters such as KLOC and possible metrics are also collected. The bugs collected from a file which contains 10,000 LOC from various projects .The purpose of

the program is to collect a data from the user in a predetermined format and implement specific tasks. According to ARBR, more than 70 bugs are collected. The bugs are determined by various projects named as P1, P2, and P3. Based on the operational profile the bugs are injected into a database. The detected bugs are also numbered and sequenced for user compatibility and maintenance. When we maintain some sequential order then it is easy to categorize the method of bugs. This method will apply to any software application which gives meaningful results. This collection appears best in all situations. Most of the models leave the development process and the results alone for consideration. In this model bugs are taken into account and so the complexity is reduced and the abstraction is achieved. The below table summarize some bugs from the considered project. The table gives the line no where the bug appeared in the project. The determined bugs are categorized by some specifications such as hardware failures, redundancy etc. The summarization of bug retrieving and their properties are given in Table 1 and the bug profile of assigned projects is discussed in Table 2.

Table 1: Bug retrieving

Bug no	Line no	Category no
2	85	3
5	536	5
7	832	7

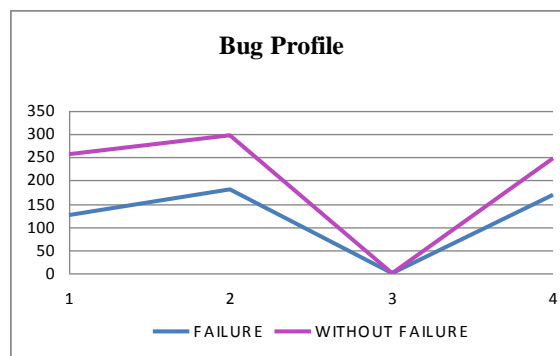
Table 2: Bug Profile

Project	Failure	Without Failure
3	124.87	130.47
5	180.39	117.17
7	170.11	78.83

Table 3: Bug detection and repairing

Project	Detection of bug	Repaired	Without failure
3	12.862	11.592	135.520
5	9.232	8.321	124.520
7	6.550	5.321	175.321

The bug detection profile is collected from randomly taken among various projects and an average of the profile is computed for the executed applications with and without failure. These results are given in table 3 and the corresponding graph for bug profile in the new application is given in below graph Fig 4.

**Fig 4 Bug profile analysis**

The above table 3 gives the average rate of fault detection and the recovery action and repairing rate on bug process when introducing the proposed ARBR process. The above table also gives the non failure process of new application. The corresponding graph is discussed in the graph below.

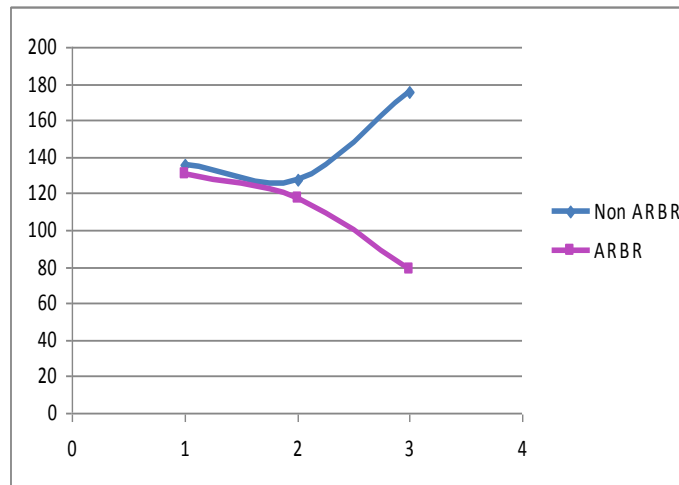


Fig 5 Reliability of new application

The above fig 5 gives that the reliability is enhanced by using ARBR. The average of bug rate is reduced considerably and hence the reliability is enhanced. By this method, 80 percent of the cases give the considerable enhancement in reliability.

This experiment shows that the proposed ARBR is implemented in the program is more efficient than existing works. The above given results indicate that the bug extraction and the retrieving are step-by-step process. But it is easier than other methods. If we complete all the steps start from extraction to retrieving successfully then ARBR is promising method to enhance reliability. This result fulfilling the objective of the work and it is a unique finding one. This method is capable to work in all environments automatically.

V. CONCLUSION

In order to achieve a required reliability, the ARBR is an optimized model. This model gives good development and it detects and repairs various failures in the application. Enhancement in reliability is hard but this model conquers the complexity. ARBR is an advanced approach but there are some limitations. When the required information's are lacking means this method is underway. The quality of ARBR depends upon the needs and quality requirements. Experiments showed that the reliability enhanced by means of ARBR and give the potential outputs without failures. It gives a promising progress to produce reliable software. Even though ARBR gives better integration between critical failure and application there is a side effect such as obtaining sensitive failures and their impact on their output. So, successive designs of ARBR for future versions will overcome these issues. This method is further enhanced as assuring defect free software and limiting of realistic constraints such as time and cost. Finally, it is concluded that the effective and the selection of a reliability model is not a simple task. The model which has low cost, time and effort is a good model. Therefore, ARBR is a good method to enhance reliability.

REFERENCES

- [1] Ahmed Patel, Liu Na, Rodziah Latih, Christopher Wills, Zarina Shukur and Rabia Mulla "A Study of Mashup as a Software Application Development Technique with Examples from an End-User Programming Perspective" Journal of Computer Science ,1406-1415, 2010.
- [2] Costa, E.O., A.T.R. Pozo and S.R. Vergilio, "A genetic programming approach for software reliability modeling", IEEE Trans. Reliability, pp .222-230, 2010
- [3] Eduardo Oliveira Costa, Aurora Trinidad Ramirez Pozo, and Silvia Regina Vergilio A Genetic Programming Approach for Software Reliability Modeling, IEEE Transactions On Reliability, Vol. 59, no. 1, March 2010,
- [4] Kapil Sharma , Rakesh Garg, Nagpal C. K, Garg R. K, " Selection of Optical software Reliability Growth Models Using a distance Based Approach" IEEE Transactions on Reliability , Vol 59, No. 2, June 2010.
- [5] J. Onishi, S. Kimura, R.J.W. James, and Y. Nakagawa, "Solving the Redundancy Allocation Problem with a Mix of Components Using the Improved Surrogate Constraint Method," IEEE Trans. Reliability, Vol. 56, no. 1, pp. 94-101, Mar. 2007.
- [6] Yousif A. Bastaki, "A Framework for Teaching Programming on the Internet: A Web-Based Simulation Approach" Journal of Computer Science,pp. 410-419. 2012.

Fuel Cell Converter Topology With and Without Filter.

Ritu K.R.¹,

Department of Electrical Engineering

¹Assistant Professor, SISTec-E,Bhopal

Abstract: Utilizing fuel cell for distributed power generation requires the development of an inexpensive converter topology which converts the variable d.c. of fuel cell into useful a.c. power converter topologies for fuel cell systems residential applications are presented in this paper for efficiency, cost, component count, input ripple current minimization technique, reliability for comparison analysis. The commercial feasibility of fuel cells rests on the cost of the fuel cell system and operating efficiency and fuel cost. The proposed power converter topology consists of DC-DC converters, and 180 degree mode of conduction with and without filter. Advantages of the proposed topology are reduced input ripple current, high efficiency, low maintenance cost, smaller size, modularity, redundancy.

Keywords: Fuel cell, Renewable Energy, Distributed Generation , DC-DC converter

I. INTRODUCTION

The Inverter is used to convert DC output Voltage to AC. which generate power as a direct current (DC), require power conversion units to convert the power from DC to AC. This power could be connected to the transmission and distribution network of a utility grid. There are other applications, where it is necessary to be able to control power flow in both directions between the AC and DC sides. For all these cases power conditioning units are used. Power conditioning unit are defined generally as electronic units that transform DC power to AC power, AC power to DC power, both bi-directional power electronic converters, or convert DC power at one voltage level to DC power at another voltage level. Using PCUs in Fuel Cell power systems, the input power of the system varies continuously with time. FC power systems can use the power conditioning units for this purpose and also to prevent the expensive electrochemical units such as fuel cell or electrolyser from damage, to step-up voltage for electrochemical units, to invert, to regulate, and to wave-shape the output voltage from all components.

An inverter is also needed to connect the system to the AC consumer loads. When all components of the system are directly connected, the two electrochemical components (fuel cell and electrolyser) have a relatively low output voltage. Therefore, the feasible system must enclose PCUs DC/AC inverter, and also to prevent the expensive electrochemical devices from damage. It seems reasonable that problems concerning efficiency are mainly caused by technical components of this system. Which can be attributed to operating the converters most of the time at very low power levels? Therefore, an accurate design of the components is very important. Most improvements in the circuit design of the PCU to increase the efficiency are in the use of modern power semiconductors with low conduction and driving losses, and in the use of recently developed designs of the integrated control circuits. The cost reduction of storing energy in hybrid systems can be achieved by increasing the efficiency and decreasing the cost of the PCU. The power conditioning sensitivity in systems has the greatest effect relative to other components in the system (Electrolyser, Fuel cell, Battery,). When an increase in the PCU efficiency by 1% is achieved, the cost of electric power generated is reduced by 0.94%.

II. SYSTEM DESCRIPTION

A. Operation and Topology

A fuel cell is an electrochemical cell that converts a source fuel into an electrical current. It generates electricity inside a cell through reactions between a fuel and an oxidant, triggered in the presence of an electrolyte. The reactants flow into the cell, and the reaction products flow out of it, while the electrolyte remains within it. Fuel cells can operate continuously as long as the necessary reactant and oxidant flows are maintained. Fuel cell has higher energy storage capability, thus enhancing the range of operation for automotive applications and is a cleaner source of energy. Fuel cell also has the further advantage of using hydrogen as fuel that could reduce world's dependence on nonrenewable hydrocarbon sources. In recent years different types of technologies have been developed , such as the: Alkaline Fuel Cell (AFC);Proton Exchange Membrane (PEM) Fuel Cell; Phosphoric Acid Fuel Cell (PAFC); Molten Carbonate Fuel Cell (MCFC);Solid Oxide Fuel Cell (SOFC) and Direct Methanol Fuel Cell(DMFC). One of the most diffused, the PEM fuel cell, has a high proton conductivity membrane as electrolyte. The Fuel Cell model used in this Proposed Work is realized in MATLABTM and Simulink.

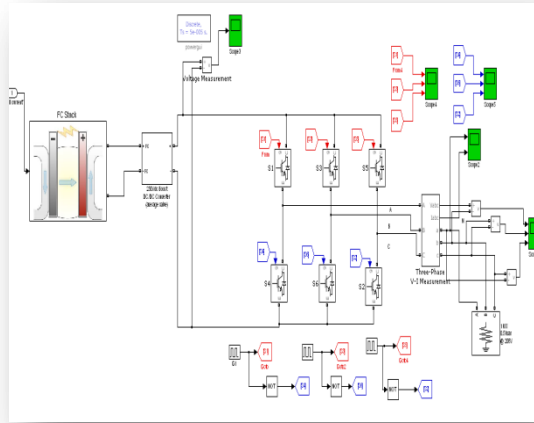


Fig1.1.simulink model of fuel cell inverter for 180 degree mode of conduction without filter.

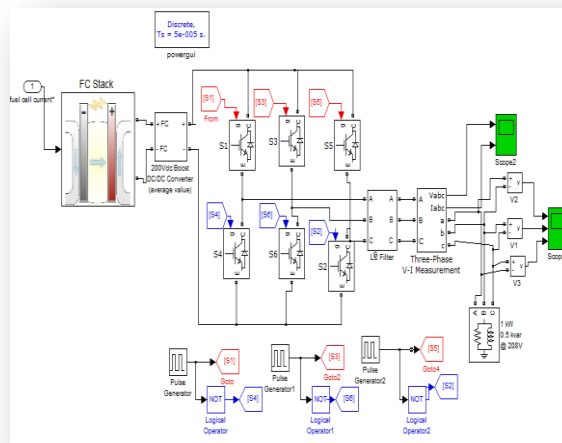


Fig1.2. simulink model of fuel cell inverter for 180 degree mode of conduction with filter.

1. Fuel Cell Stack Model

1.1. Model Assumptions

- The stack model will be based on the following assumptions.
- The gases are ideal.
- The stack is fed with hydrogen and air. If natural gas instead of hydrogen is used as fuel, the dynamics of the fuel processor must be included in the model, upstream of the hydrogen inlet; a first-order transfer function 6. The transfer function gain should reflect the changes in composition occurring during the process. The effect of the fuel processor in the model will be tested in the future. The channels that transport gases along the electrodes have a fixed volume, but their lengths are small, so that it is only necessary to define one single pressure value in their interior. The exhaust of each channel is via a single orifice. The ratio of pressures between the interior and exterior of the channel is large enough to consider that the orifice is choked. The temperature is stable at all times. The only source of losses is ohmic, as the working conditions of interest are not close to the upper and lower extremes of current. The Nernst equation can be applied.

1.2 Characterization of the Exhaust of the Channels:

According to Ref. 7, an orifice that can be considered choked, when fed with a mixture of gases of average molar mass $M_{kg/kmol}$ and similar specific heat ratios, at a constant temperature, meets the following characteristic:

$$\frac{W}{P_U} = K \sqrt{M} \quad (1.1)$$

Where W is the mass flow kg/s; K is the valve constant, mainly depending on the area of the orifice. P is the pressure up stream inside the channel. For the particular case of the anode, the concept of fuel utilization U can be introduced, as the ratio between the fuel flow that reacts and the fuel flow injected to the stack is also a way to express the water molar fraction at the exhaust. According to this definition, Eq. 4.1. can be written as:

$$\frac{W_{an}}{P_{an}} = W_{an} \sqrt{(1-U_f)M_{H_2} + U_f M_{H_2O}} \quad (1.2) \text{ where } W \text{ is the mass flow through the}$$

anode valve an kg/s; K_{an} is the anode valve constant ; M are the molecular masses of hydrogen H_2 , H_2O and water, respective kg/kmol; P is the pressure an inside the anode channel [atm]. If it could be considered that the molar flow of any through the valve is proportional to its partial pressure inside the channel, according to the expressions:

$$\frac{q_{H_2}}{p_{H_2}} = \frac{K_{an}}{\sqrt{M_{H_2}}} = K_{H_2} \quad (1.3) \quad \text{and}$$

$$\frac{q_{H_2O}}{p_{H_2O}} = \frac{K_{an}}{\sqrt{M_{H_2O}}} = K_{H_2O} \quad (1.4)$$

where q , q are the molar flows of hydrogen and $H_2 H_2O$ water, respectively, through the anode kmol/s; p , p are the partial pressures of hydrogen and water, $H_2 H_2O$ respectively (atm); K , K are the valve molar con- $H_2 H_2O$ stands for hydrogen and water, respectively kmol/(satm); the following expression would be deduced:

$$\frac{W}{P_{an}} = K_{an} \left[(1-U_f) \sqrt{M_{H_2}} + U_f \sqrt{M_{H_2O}} \right] \quad (1.5)$$

The comparison of Eqs. 4.2. and eqs4.5 Shows that for $U > 70\%$ the error is less than 7%. It is possible to f redefine slightly Eqs. 4.3and 4.4 so that the error is even lower. This error shows that it may be reasonable to use Eqs. 4.3 and eqs.4.4.. The same study for the cathode shows that the error in that valve is even lower, because of the similar molecular masses of oxygen and nitrogen.

$$p_{H_2} V_{an} = n_{H_2} RT \quad (1.6)$$

1.3 Calculation of The Partial Pressures:

Every individual gas will be considered separately, and the perfect gas equation will be applied to it. Hydrogen will be considered as an example.

$$\frac{d}{dt} p_{H_2} = \frac{RT}{V_{an}} q_{H_2} \quad (1.7)$$

where q is the time derivative of n , and represents the $H_2 H_2$ hydrogen molar flow kmol/s. There are three relevant contributions to the hydrogen molar flow: the input flow, the flow that takes part in the reaction and the output flow, thus:

$$\frac{d}{dt} p_{H_2} = \frac{RT}{V_{an}} (q_{H_2}^{in} - q_{H_2}^{out} - q_{H_2}^r) \quad (1.8)$$

where q_{in} is the input flow of kmol/s; q_{out} is the output $H_2 H_2$ flow of kmol/s; q_r is the hydrogen flow that reacts H_2 kmol/s. According to the basic electrochemical relationships, the molar flow of hydrogen that reacts can be calculated

$$\text{as: } q_{H_2}^r = \frac{N_0 I}{2F} = 2K_r I \quad (1.9)$$

where N is the number of cells associated in series in the 0 stack; F is the Faraday's constant/kmol; I is the stack current [A]; K is a constant defined for modeling pur- r poses kmol/(s a). Returning to the calculation of the hydrogen partial pressure, it is possible to write:

$$\frac{d}{dt} p_{H_2} = \frac{RT}{V_{an}} (q_{H_2}^{in} - q_{H_2}^{out} - 2K_r I_i) \quad (1.10)$$

Replacing the output flow by Eq. _3., taking the Laplace transform of both sides and isolating the hydrogen partial pressure, yields the following expression:

$$p_{H_2} = \frac{1/K_{H_2}}{1 + \tau_{H_2} s} (q_{H_2}^{in} - 2K_r I_j) \quad (1.11)$$

Where, $TH_2 = (van / KH_2 RT)$, expressed in seconds, is the H_2 an H_2 value of the system pole associated with the hydrogen flow.

1.4 Calculation of the stack Voltage

Applying Nernst's equation and Ohm's law to consider ohmic losses, the stack output voltage is represented by the following expression:

$$V = N_0 \left(E_0 + \frac{RT}{2F} \left[\ln \frac{P_{H_2} P_{O_2}^{0.5}}{P_{H_2O}} \right] \right) - rI \quad (1.12)$$

where E is the voltage associated

with the reaction free energy V ; R is the same gas constant as previous, but care should be taken with the system unit $J / kmolK$; r describes the ohmic losses of the stack Ω

1.5. Modeling of Power Conditioning Unit

The Power Conditioning unit is used to convert DC output Voltage to AC. which generate power as a direct current (DC), require power conversion units to convert the power from DC to AC. This power could be connected to the transmission and distribution network of a utility grid. There are other applications, where it is necessary to be able to control power flow in both directions between the AC and DC sides. For all these cases power conditioning units are used. Power conditioning unit are defined generally as electronic units that transform DC power to AC power.

1.6 DC-AC Converter (Inverter)

The main circuit is the part where the DC electric power is converted to AC [6]. This is virtually implemented with the one that is shown at the Fig. In this circuit we use a 3 leg inverter for 3-phase conversion which is composed of 6 IGBTs and the control unit. The last generates control pulses to drive the IGBTs. The pulse generation to gives a digital signal to the IGBTs. When the signal from the pulse generator is not zero then it reacts as a switch and opens. This consists the basic operation in order to convert the DC to AC, with the technique of the Pulse Width Modulation (PWM). The frequency of the IGBTs we use is 1 KHz. For the time interval the IGBTs are open, we get a pulse at power circuit, which has the same amplitude of source. The RMS time integral give us the output values. The on-off is determined by a control unit which is analyzed below. The modulation factor m_a can be used as a parameter for the dynamic control of the system.. The losses will be analogue to the change over the m_a . A useful reference for cascaded multilevel converters which discusses the control circuit of new topology. A three phase inverter has the basic advantage that generates power in 3-phase and is working without a hitch. At one node of the circuit, supposing we have an input voltage $V_{oi}(t)$ an LC filter ,L inductance and C capacitance and the r_L resistant Load ,if we apply the Kerchief's laws and if we consider that the IGBTs at an open state, we get:

$$r_L i_L + L di_L/dt + V_C = V_{oi}(t) \quad (1.13)$$

$$i_L - C(dV_C/dt) - V_C/R \quad (1.14)$$

The above problem is depending on the output of the PV array and in order to have a simple solution we consider only the switching part of the circuit that is in fig. one obtain the solution which is:

$$V_{SN} = \sum_{n=1,5,7,11}^{\infty} 4V/3n\pi(\cos n\pi/3+1)\text{Sinn}(\omega t 120) \quad (1.15)$$

$$V_{TN} = \sum_{n=1,5,7,11}^{\infty} 4V/3n\pi(\cos n\pi/3+1)\text{Sinn}(\omega t 240^\circ) \quad (1.16)$$

$$V_{RN} = \sum_{n=1,5,7,11}^{\infty} 4V/3n\pi(\cos n\pi/3+1)\text{Sinn}(\omega t) \quad (1.17)$$

Each one of the 3-phases to neutral voltage, the 1, 5, 7, 11 are the harmonics appearing and $\omega=2\pi f$ the basic frequency at 50Hz.

II.EXPERIMENTAL RESULT: A Comparative analysis of Simulation Result Of Fuel Cell Inverter For 180 Degree Mode Of Conduction with and without filter along with the its total harmonic distortion[TDH] is shown in the following figures.



Fig.1.3.Three phase Load Current and Load Voltage waveform for inverter 180⁰ mode of conduction without filter

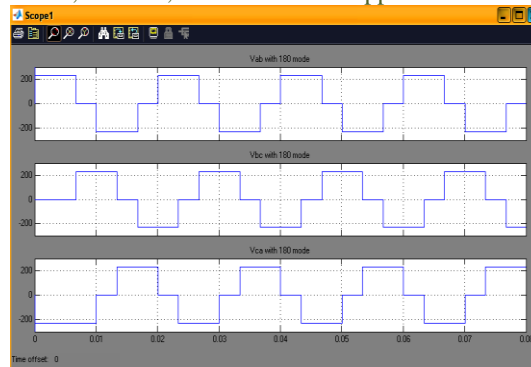


Fig.1.4.Vab, Vbc and Vca line to line Voltage waveform for inverter 180⁰ mode of conduction without filter

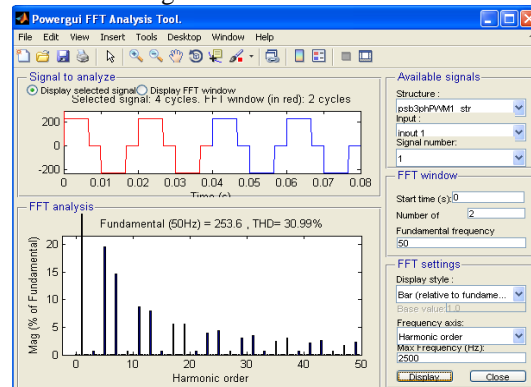


Fig.1.5.THD spectrums for Voltage waveform for inverter 180⁰ mode of conduction without filter .

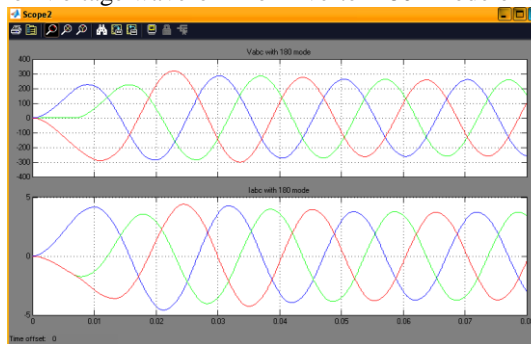


Fig.1.6.Three phase Load Current and Load Voltage waveform for inverter 120⁰ mode of conduction with filter .

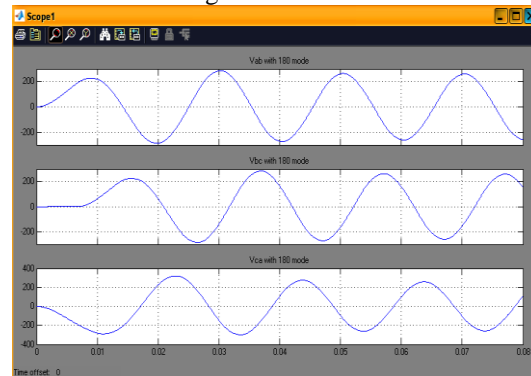


Fig.1.7.Vab, Vbc and Vca line to line Voltage waveform for inverter 180⁰ mode of conduction with filter

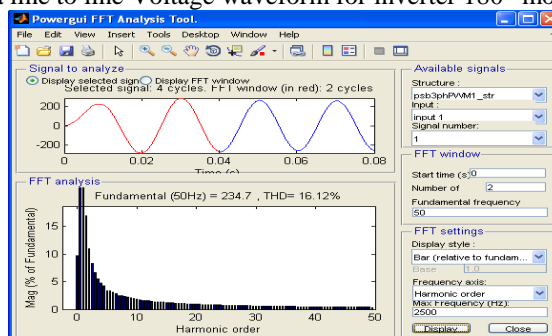


Fig.1.8.THD spectrums for Voltage waveform for inverter 180⁰ mode of conduction with filter .

III. CONCLUSIONS

Based on the literature review, simulations results and the performed experiments, Following points can be concluded:

1. Those Fuel Cells are preferred which have high voltage ratings and low current profile. This is because at higher current the losses within the fuel cell will be more and hence the efficiency of the system, for which it is known, will deteriorate. But the main drawback of higher voltage fuel cells is that voltage level can be increased only by adding series stacks. This adds to the system cost.
2. In low power rating fuel cells, low voltage is an issue. Boost converter provides solutions to raise the voltage level of the FC stack. Besides this bi-directional DC DC converters are also used for boosting and isolation. This increases the bulkiness of the whole application. For AC applications the inverter discussed in the above theory is a good candidate for single stage grid connected system. It is capable of boosting up the voltage level from a low level to a higher level, hence overcoming such systems where boost converter and other topologies are used. The output voltage of the capacitor is in good agreement with the reference grid voltage.
3. Simulation results show that the operation of the the inverter is such that it feed a nearly unity power factor current into the grid ($pf = 0.967$). Experimentally it is shown that the grid current is in phase with the voltage.

IV. FUTURE SCOPE

1. The operation of the converter, considered for the grid connection connection, can also be investigated for continuous conduction mode.
2. We have considered an application in which FC stack is integrated to the grid. FC can also be considered for stand alone power application systems or even backup systems.
3. FC stacks integration with various other DC/DC converters and study the behavior of a closed-loop controller for the same.

REFERENCES

- [1.] M. W. Breiter, *Electrochemical Processes in Fuel Cells*, New York, USA: Springer-Verlag, pp. 3-4, May 1969.
- [2.] J. Larminie, A. Dicks, *Fuel Cell Systems Explained, 2nd ed.*, Chichester, West Sussex, England: ohn Wiley & Sons Inc., pp. 48-56, 71-74, 2003.
- [3.] H.A. Liebhafsky, E.J. Cairns, *The Irreversible Fuel Cell, Fuel Cells and Fuel Batteries*, USA: John iley & Sons Inc., pp. 97-100, 1967.
- [4.] R. Parsons, J.O'M Bockeris, *Modern Aspects of Electrochemistry*, ed., Academic, New York,USA, pp. 246-248, 1954.
- [5.] T.E. Springer, T. Rockwood, T.A. Zawodzinski, S. Gottesfeld, "Model for Polymer ElectrolyteFuel Cell Operation on Reformate Feed," *Journal of Electrochemical Society*, vol. 148, no.1, pp.A11-A23, 2001.
- [6.] J.M. Correa, F.A. Farret, L.N. Canha, M.G. Simoes, "An Electrochemical-Based Fuel Cell ModelSuitable for Electrical Engineering Automation Approach," *IEEE Trans. Industrial Engineering*, vol. 51, no. 5, pp. 1103-1112, Oct. 2000.
- [7.] R.F. Mann, J.C. Amphlett, M.A.I. Hooper, H.M. Jensen, B.A. Peppley, P.R. Roberge, Development and Application of a generalized Steady-State Electrochemical Model for a PEM uel Cell," *J. of Power Sources*, vol. 86, pp. 173-180, 2000.
- [8.] E. Hernandez, B. Diong, "A Small-Signal Equivalent Circuit Model for PEM Fuel Cells," *IEEE,Applied Power Electronics Conference and Exposition*, vol. 1, no. 1, pp. 121-126, 6-10 March 2005.
- [9.] P. Famouri, R. S. Gemmen, "Electrochemical Model of a PEM Fuel Cell," *IEEE Power Engineering Society General Meeting*, vol. 3, pp. 1436-1440, Jul. 2003.
- [10.] R.F. Mann, J.C. Amphlett, T.J. Haris, B.A. Peppley, P.R. Roberge, R.M. Baumert, "Performance Modeling of the Ballard Mark IV Solid Polymer Electrolyte Fuel Cell," *J. of Electrochemical Society*, vol.142, no.1, pp. 9-15, Jan. 1995.
- [11.] M. Uzunoglu, M. S. Alam, "Dynamic Modeling, Design, and Simulation of a Combined PEM Fuel Cell and Ultracapacitor System for Stand-Alone Residential Applications," *IEEE Trans. Energy Conversion*, vol. 21, no. 3, pp. 767-775, Sept. 2006.
- [12.] J. Padulles, G. W. Ault, and J. R. McDonald, "An Integrated SOFC Plant Dynamic Model for Power System Simulation," *J. Power Sources*, vol. 86, no. 1-2, pp. 495-500, Mar. 2000.
- [13.] K. Xing, and A. M. Khambadkone, "Dynamic Modeling of Fuel Cell with Power Electronic Current and performance analysis," *IEEE International Conference on Power Electronics and Drive Systems*, vol. 1, pp. 607-612, 17-20, Nov. 2003.
- [14.] D. M. Mitchell, *DC-DC Switching Regulator Analysis*, USA: John Wiley & Sons Inc., 1988.
- [15.] P. T. Krein, S. Balog, Xin Geng, "High-Frequency Link Inverter for Fuel Cells Based on Multiple- Carrier PWM," *IEEE Trans. Power Electronics*, vol. 19, no. 5, pp. 1279-1288, Sept. 2005.
- [16.] H. Li, F. Z. Peng, "Modeling of a New ZVS Bi-directional DC-DC Converter," *IEEE Trans. Aerospace and Electronic Systems*, vol. 40, no. 1, pp. 272-283, Jan. 2004.
- [17.] H Matsuo, W. Lin, F. Kurokawa, T. Shigemizu, N. Watanabe, "Characteristics of the Multiple- Input DC-DC Converter," *IEEE Trans. Industrial Electronics*, vol. 51, no. 3, pp. 625-630, Jun. 2004.
- [18.] Z. Jiang, R. A. Dougal, "Control Strategies for Active Power Sharing in a Fuel-Cell-Powered Battery-Charging Station," *IEEE Trans. Industrial Electronics*, vol. 40, no. 3, pp. 917-924, May/June. 2004.
- [19.] N. D. Muhamad, M. R. Sahid, A. H. M. Yatim, N. R. N. Idris, and M. S. Ayub, "Design of Power stage and Controller for DC-DC Converter Systems Using PSPICE," *IEEE Power Electronics and Drives Systems*, vol. 2, pp. 999-1002, Nov. 2005.
- [20.] M. Y. El-Sharkh, A. Rahman, M. S. Alam, A. A. Sakla, P. C. Byrne, T. Thomas, "Analysis of Active and Reactive Power Control of a Stand-Alone PEM Fuel Cell Power Plant," *IEEE Trans. Power Systems*, vol. 19, no. 4, pp. 2022-2030, Nov. 2004.

Implementation of Multiple FTP Application using SCTP Multistreaming

Srikanth Porika¹, B.Rajani², T.Bharath Manohar³

¹ M.Tech, Dept of CSE, CMR COLLEGE OF ENGINEERING & TECHNOLOGY
(Affiliated to JNTU Hyderabad), Hyderabad, Andhra Pradesh, India.

² Asst. Prof., Dept of CSE, CMR COLLEGE, OF ENGINEERING & TECHNOLOGY
(Affiliated to JNTU Hyderabad), Hyderabad, Andhra Pradesh, India.

³ M.Tech, Dept of CSE, CMR COLLEGE OF ENGINEERING & TECHNOLOGY,
(Affiliated to JNTU Hyderabad), Hyderabad, Andhra Pradesh, India.

Abstract: We identify overheads associated with FTP, attributed to separate TCP connections for data and control, non-persistence of the data connections, and the sequential nature of command exchanges. We argue that solutions to avoid these overheads using TCP place an undue burden on the application. Instead we propose modifying FTP to use SCTP and its multistreaming service. FTP over SCTP avoids the identified overheads in the current FTP over TCP approach without introducing complexity at the application, and still remaining "TCP-friendly." We implemented FTP over SCTP in three ways: (1) simply replacing TCP calls with SCTP calls, thus using one SCTP association for control and one SCTP association for each data transfer, (2) using a single multistreamed SCTP association for control and all data transfers, and (3) enhancing (2) with command pipelining. Results comparing these 3 variations with the classic FTP over TCP indicate significant improvements in throughput for the transfer of multiple files by using multistreaming and command pipelining, with the largest benefit occurring for transferring multiple short files. More generally, this paper encourages the use of SCTP's innovative transport-layer services to improve existing and future application performance.

Keywords: SCTP, FTP Application, Multi-Streaming .

I. INTRODUCTION

The past decade has witnessed an exponential growth of Internet traffic, with a proportionate increase in Hyper Text Transfer Protocol (HTTP) [BFF96] and decline in File Transfer Protocol (FTP) [PR85], both in terms of use and the amount of traffic. The decline in FTP traffic is chiefly attributed to the inflexible nature of its interface.

Over the years, several FTP extensions have been proposed [AOM98, EH02, HL97], with a few efforts to improve performance by using parallel TCP connections [AO97, Kin00]. However, opening parallel TCP connections (whether for FTP or HTTP) is regarded as "TCP-unfriendly" [FF99] as it allows an application to gain an unfair share of bandwidth at the expense of other network flows, potentially sacrificing network stability. Our focus is to improve end-to-end FTP latency and throughput in a TCP-friendly manner.

Although FTP traffic has proportionately declined in the past decade, FTP still remains one of the most popular protocols for bulk data transfer on the Internet [MC00]. For example, Wuarchive [WUARCHIVE] serves as a file archive for a variety of files including mirrors of open source projects. Wuarchive statistics for the period of April 2002 to March 2003 indicate FTP accounting for 5207 Gigabytes of traffic, and HTTP accounting for 7285 Gigabytes of traffic. FTP is exclusively used in many of the Internet's software mirroring sites, for various source code repositories, for system backups, and for file sharing. All of these applications require transferring multiple files from one host to another.

In this paper we identify the overheads associated with the current FTP design mainly due to running over TCP, which constrains the FTP application. We present modifications to FTP to run over Stream Control Transmission Protocol (SCTP) RFC2960 [SXM⁺00] instead of TCP. SCTP is an IETF standards track transport layer protocol. Like TCP, SCTP provides an application with a full duplex, reliable transmission service. Unlike TCP, SCTP provides additional transport services, in particular, multistreaming. SCTP multistreaming logically divides an association into streams with each stream having its own delivery mechanism. All streams within a single association share the same congestion and flow control parameters. Multistreaming decouples data delivery and transmission, and in doing so prevents Head-of-Line (HOL) blocking.

This paper shows how command pipelining and SCTP multistreaming benefit FTP in reducing overhead, especially for multiple file transfers. We recommend two modifications to FTP that make more efficient use of the available bandwidth and system resources. We implemented these modifications in a FreeBSD environment, and carried out experiments to compare the current FTP over TCP design vs. our FTP over SCTP designs. Our results indicate dramatic improvements with lower transfer time and higher throughput for multiple file transfers particularly under lossy network conditions. Moreover, our modifications to FTP solve concerns current FTP protocol faces with NATs and firewalls in transferring IP addresses and port numbers in the payload data [AOM98, Bel94, Tou02].

This paper is organized as follows. Section 2 details and quantifies the overheads in the current FTP over TCP design. This section also discusses possible solutions to eliminate these overheads while still using TCP as the transport. Section 3 introduces SCTP multistreaming. Section 4 presents minor FTP changes needed to exploit SCTP multistreaming, and a description of how the new design reduces overhead. Section 5 presents the experimental results, and Section 6 concludes the paper.

II. MOTIVATION

2. Inefficiencies and possible solutions

2.1 Inefficiencies in FTP over TCP

FTP's current design includes a number of inefficiencies due to (1) separate control and data connection and (2) non-persistent data connection. Each is discussed in turn.

2.1.1 Distinct control and data connection

A. FTP's out-of-band control signaling approach has consequences in terms of end-to-end latency. In a multiple file transfer, traffic on the control connection tends to be send-and-wait, with no traffic transferred during the file transfer. This connection's congestion mechanism typically times out, and returns the connection to slow start for each new file to be transferred [APS99]. The control connection is particularly vulnerable to timeouts because too few packets are flowing to cause a TCP fast retransmit. An operation (involving a single control command) will be subject to a timeout in the event of loss of either a command or its reply. Attempts are needed to reduce the command exchange over the control connection.

B. With distinct connections, end hosts create and maintain on average two Transport Control Blocks (TCBs) for each FTP session. This factor is negligible for clients, but may significantly impact busy servers that are subject to reduced throughput due to memory block lookups [FTY99]. TCB overheads may be reduced by using ensemble sharing [BS01, Tou97].

C. Over the past years, considerable discussion has taken place on FTP's lack of security, often attributed to data connection information (IP address, port number) being transmitted in plain text in the PORT command on the control connection to assist the peer in establishing a data connection. Moreover, transferring IP addresses and port numbers in the protocol payload creates problem for NATs and firewalls that must monitor and translate addressing information [AOM98, Tou02].

2.1.2 Non-persistence of the data connection

A. The non-persistence of a data connection for multiple files causes connection setup overhead at least on the order of 1 RTT for each file transfer or directory listing. (Traffic overhead also exists for connection teardown, but this traffic overlaps the control commands for the next operation.)

B. Every new data connection must initially probe the available bandwidth (via a congestion window (cwnd)) during a slow start phase, before the connection reaches its steady state cwnd. A loss early in the slow start phase, before the cwnd contains enough packets to allow for fast retransmit, will result in a timeout at the server. Figure 1 graphically shows the nature of this re-probing overhead in the event of three consecutive file transfers (over three different TCP connections). The interval between the transfers indicates the time involved in terminating the previous connection, transferring control commands, and setting up a new connection. (Note: Figure 1 represents a generic example.)

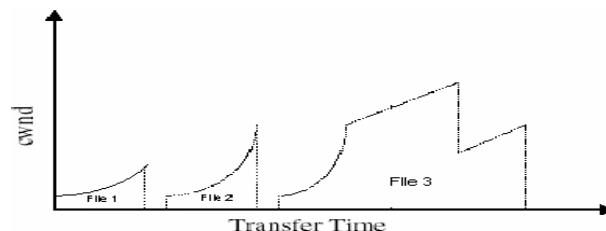


Figure 1: Expected cwnd evolution during a multiple file transfer in FTP over TCP

For each file transfer, at least one RTT overhead is incurred over the control connection for communicating the PORT command and its 200 reply.

D. In the event of multiple small file transfers, the server ends up having many connections in the TCP TIME-WAIT state and hence must maintain on average more than two TCBs per session. This per-connection memory load can adversely affect a server's connection rate and throughput [FTY99].

2.2. Possible solutions and drawbacks

We describe some of the possible solutions that try to avoid the above stated overheads while still using TCP as the underlying transport service. The drawbacks associated with each solution are presented.

A. Use one persistent TCP connection for control and data

Improvements: This approach avoids most overheads associated with FTP's current design listed in the previous section. The commands over the control connection can be pipelined (in the event of a multiple file transfer) to improve latency, and maintain the probed congestion window for subsequent transfers.

Drawbacks: TCP provides a byte-stream service and does not differentiate between the different types of data transmitted over the same connection. Using a single TCP connection requires the application to use markers to differentiate between control and data, and the beginning/end of each file. This marking burden increases application layer complexity. Control and file data in an FTP session are logically different types of data, and conceptually, are best kept logically if not physically, separate. Additionally, using a single connection risks Head-of-Line (HOL) blocking (discussed in Section 3).

B .Use two persistent TCP connections: one for control, one for data

Improvements: A persistent data connection eliminates the connection setup-teardown and command exchange overheads for every file transfer, thus reducing network traffic and the number of round trip delays.

Drawbacks: Due to the sequential nature of commands over the control connection, the data connection will remain idle in between transfers of a multiple files transfer. During this idle time, the data connection congestion window may reduce to as little as the initial default size, and later require TCP to re-probe for the available bandwidth [HPF00]. Moreover this approach still suffers from the overhead listed in Section 2.1.1.

C. Use two persistent TCP connections: one for control, one for data. Also use command pipelining on control connection.

Improvements: Command pipelining allows for the immediate request of multiple files over the control connection rather than requiring $file_i$ is completely retrieved before $file_{i+1}$ is requested. A persistent data connection with command pipelining will maintain a steadier flow of data (i.e., higher throughput) over the data connection by letting subsequent transfers utilize the already probed bandwidth.

Drawbacks: This approach still suffers from the overhead listed in Section 2.1.1.

D. Use one TCP connection for control, and 'n' parallel data connections

Improvements: Some FTP implementations do achieve better throughput using parallel TCP connections for a multiple file transfer.

Drawbacks: This approach is not TCP-friendly [FF99] as it may allow an application to gain an unfair share of bandwidth and adversely affect the network's equilibrium [BFF96, FF99]. Moreover past research has shown that parallel TCP connections may suffer from aggressive congestion control resulting in a reduced throughput [FF99]. As such, this solution should not be considered. This approach also suffers the overheads listed in Section 2.1.1.

Related Work: Apart from the above solutions, researchers in the past have suggested ways to overcome TCP's limitations and boost application performance [BS01, Tou97]. For example, T/TCP [Bra94] reduced the connection setup/teardown overhead by allowing data to be transferred in the TCP connection setup phase. But due to a fundamental security flaw, T/TCP could not succeed. Aggregating transfers has also been discussed for HTTP [PM94], but while HTTP semantics allowed for persistent data connections and command pipelining, FTP semantics do not allow similar solutions without introducing changes to the application (see A. above).

Having summarized ways for improving FTP performance while still using TCP, we now consider the main objective of this paper - improving FTP performance by using SCTP, an emerging IETF general-purpose transport protocol [SXM⁺00]. We note that the TCP alternatives that incorporate temporal and ensemble sharing [Bra94, BS01, Tou97] are not discussed further in this paper; future work should evaluate such alternatives.

III. LITERATURE SURVEY

3. SCTP multistreaming

One innovative transport layer service that promises to improve application layer performance is SCTP multistreaming. A stream in an SCTP association is "a uni-directional logical channel established from one to another associated SCTP endpoint, within which all user messages are delivered in sequence except for those submitted to the unordered delivery service" [SXM⁺00].

Multistreaming within an SCTP association separates flows of logically different data into independent streams. This separation enhances application flexibility by allowing it to identify semantically different flows of data, and have the transport layer "manage" these flows (as the authors argue should be the responsibility of the transport layer, not the application layer). No longer must an application open multiple end-to-end connections to the same host simply to signify different semantic flows.

Figure 2 shows Hosts A and B connected with a single multistreamed association. The number of streams in each direction is negotiated during SCTP's association establishment phase. In this example, three streams go from A to B, and one stream goes from B to A.

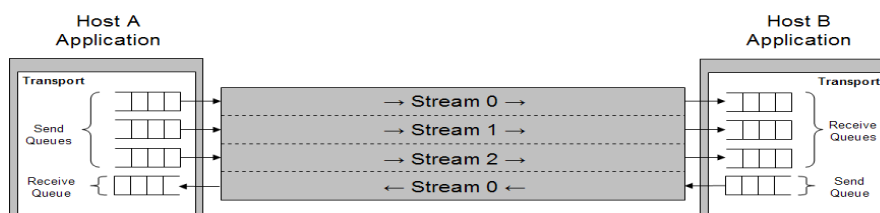


Figure 2: Use of streams within an SCTP association

Each stream has an independent delivery mechanism, thus allowing SCTP to differentiate between data delivery and reliable data transmission, and avoid HOL blocking. Similar to TCP, SCTP uses a sequence number to order information and achieve reliability. However, where TCP sequences bytes, SCTP sequences transport layer protocol data units (PDUs) or "chunks" using Transmission Sequence Numbers (TSN). The TSN number space is global over all streams. Each stream is uniquely identified by a Stream ID (SID) and has its own Stream Sequence Numbers (SSN). In TCP, when a sender transmits multiple TCP segments, and the first segment is lost, the later segments must wait in the receiver's queue until the

first segment is retransmitted and arrives correctly. This HOL blocking delays the delivery of data to the application, which in signaling and some multimedia applications is unacceptable. In SCTP, however, if data on *stream 1* is lost, only *stream 1* can be blocked at the receiver while awaiting retransmissions. The logically independent data flows on remaining streams can be deliverable to the application. SCTP's socket API extensions [SXY⁺03] provide data structures and socket calls through which an application can indicate or determine the stream number on which it sends or receives data.

IV. SYSTEM ANALYSIS & DESIGN

4. FTP over SCTP variants

We consider three variations of FTP over SCTP to help identify the various gains of different features. Each is described in turn.

4.1 FTP over SCTP (SCTP-Naïve)

Our first variation named "SCTP-naïve" maintains the semantics of FTP over TCP. We name this approach "naïve" because it naïvely uses one persistent SCTP association for control, and a new non-persistent SCTP association is opened, used, and closed for each file transfer, directory listing, or file namelist, as is done in the current FTP over TCP approach. SCTP-naïve does not exploit any of SCTP's advantages; it is evaluated to measure the inherent performance differences between our TCP and SCTP implementations. If the basic TCP and SCTP implementations were the same, then the performance should be similar. The SCTP-naïve approach is not recommended in practice.

To derive SCTP-naïve, all socket calls in both the client and server in the FTP over TCP version (herein "TCP") were changed from using IPPROTO_TCP to IPPROTO_SCTP. The timing is shown in Figure 3 with solid lines representing PDUs traveling over the control association, and dotted lines representing PDUs traveling over new associations. The large dashed box represents the sequence of PDUs that must be iteratively transmitted for each file of the multiple file transfer.

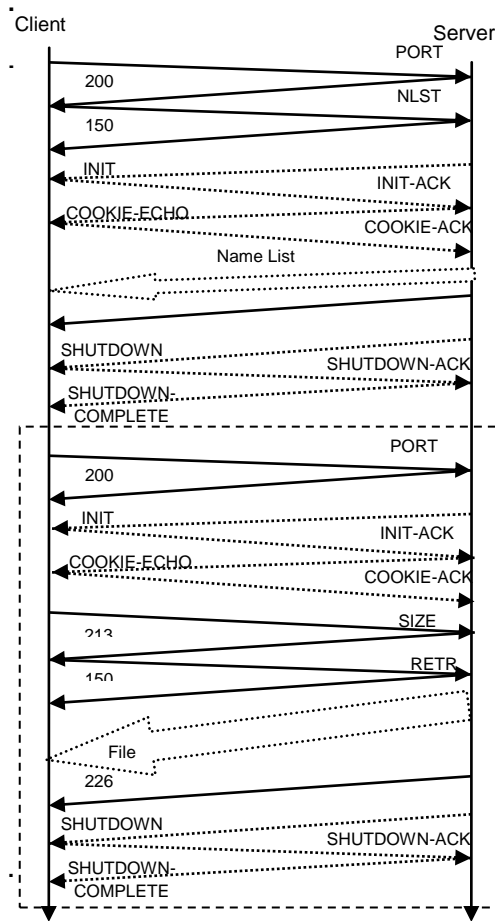


Figure 3: FTP over SCTP-Naïve

4.2 FTP over SCTP with multistreaming (SCTP-MS)

In "SCTP-MS", FTP control and data connections are combined over a single multistreamed SCTP association. That is, only one association exists for the entire multiple file FTP session. An FTP client establishes an SCTP association with the server with two streams opened in each direction. The client and the server send control information (commands and replies) on their respective *stream 0*. All data (files, directory listings, and file namelists) are transferred over their respective *stream 1*. This approach maintains semantics for streams analogous to control and data connections in FTP over TCP.

Recall that the data connection in FTP over TCP is non-persistent and the end of data transfer (EOF) is detected by the data connection's close. To detect EOF using one SCTP association, the SIZE command [EH02] is used. The SIZE command is already widely used in FTP for the purpose of detecting restart markers. For directory listings, the end of data transfer is detected by using the number of bytes read by *recvmsg* call provided by the SCTP socket API [SXY⁺03].

For a multiple file retrieval, the client sends out requests on outgoing *stream 0* and receives the files sequentially on incoming *stream 1* (see Figure 4). Data on *stream 1* is represented by dashed lines, and control messages on *stream 0* are represented by solid lines. The dashed box on the timeline in Figure 4 indicates the operations that are repeated sequentially for each file to be transferred.

This approach avoids most of the overheads described in Section 2.1. The number of round trips is reduced as: (1) a single connection (association in SCTP terminology) exists throughout the FTP session, hence repeated setup-teardown of each data connection is eliminated, and (2) exchanging PORT commands over the control connection for data connection information is unnecessary. The server load is reduced as the server maintains TCBs for at most half the connections required with FTP over TCP.

The drawback that this approach faces is similar to the drawbacks described in Section 2.1.2.B. For a multiple file transfer, each subsequent file transfer is unable to utilize the prior probed available bandwidth. Before transmitting new data chunks, the sender calculates the cwnd based on the SCTP protocol parameter *Max.Burst* [SOA⁺03] as follows:

$$\begin{aligned} \text{if } ((\text{flightsize} + \text{Max.Burst} * \text{MTU}) < \text{cwnd}) & \quad (1) \\ \text{cwnd} &= \text{flightsize} + \text{Max.Burst} * \text{MTU} \end{aligned}$$

Since the transfer of file_{i+1} cannot take place immediately (due to the exchange of control commands before each transfer (see Figure 4)), all data sent by the server for file_i gets acked, and the flightsize at the server reduces to zero. Thus in multiple file transfers, the server's cwnd reduces to *Max.Burst*MTU* before starting each subsequent file transfer ([SOA⁺03] recommends *Max.Burst* = 4).

4.3 FTP over SCTP with multistreaming and command pipelining (SCTP-MS-CP)

Finally, in "SCTP-MS-CP", SCTP-MS is extended with command pipelining (CP), similar to that defined in [PM94], to avoid unnecessary cwnd reduction between file transfers. In SCTP-MS, the cwnd reduction between file transfers occurs because the SIZE and RETR commands for each subsequent file are sent only after the previous file has been received completely by the client.

In Figure 5, we present a solution that allows each subsequent transfer to utilize the probed value of congestion window from the prior transfer. Command pipelining ensures a continuous flow of data from the server to client throughout the execution of a multiple file transfer. After parsing the name list of the files, the client sends SIZE commands for all files at once (which SCTP ends up bundling together in its SCTP-PDUs). As each reply for a SIZE command is received, the client immediately sends out the respective RETR command for that file. Since the control stream is ordered, SCTP guarantees the replies to the SIZE and RETR commands will arrive in proper sequence.

By using SCTP-MS-CP, FTP views multiple file transfers as a single data cycle. Command pipelining aggregates all of the file transfers resulting in better management of the cwnd. This solution overcomes all of the drawbacks listed in Section 2.1.

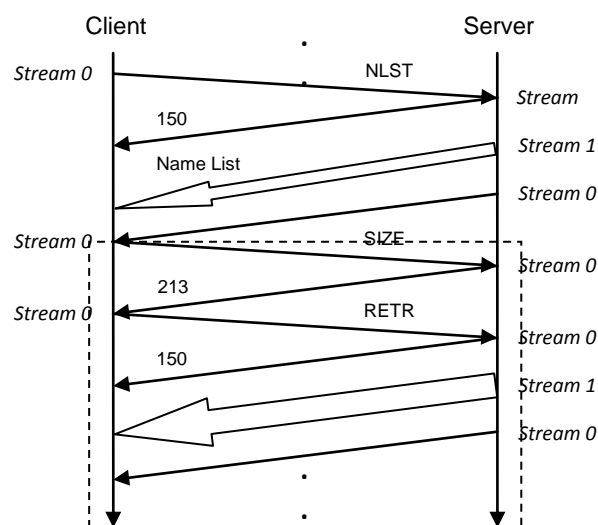


Figure 4: FTP over SCTP-MS

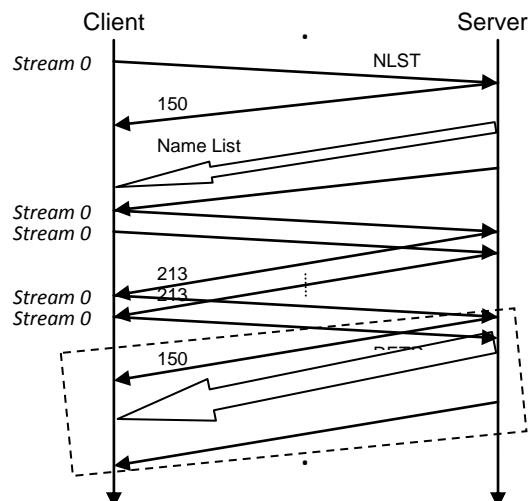


Figure 5: FTP over SCTP-MS-CP

V. RESULTS

To compare FTP over TCP vs. our three SCTP variations, we measured the total transfer time for a multiple file transfer for a varied set of parameters.

- *Bandwidth-Propagation Delay (B-D) configuration*: Three path configurations were evaluated: (3Mbps, 1ms), (1Mbps, 35ms), (256Kbps, 125ms). Both the client to server and server to client paths share the same characteristics. These configurations roughly represent an end-to-end connection on: a local network, U.S. coast-to-coast, and over a satellite, respectively.
- *Packet Loss Ratio (PLR)*: The PLRs studied were (0, .01, .03, .06, and .1). Loss was symmetric; each value represents the loss ratio for both the client to server and the server to client paths. We used a Bernoulli distribution to emulate packet loss. Certainly 10% loss represents an extreme case but we were interested in general trends as the loss rate increases. Moreover, higher loss rates are of serious interest in wireless and military networks.
- *File sizes*: We evaluated the potential overheads for a variety of file sizes: 10K, 50K, 200K, 500K, and 1M.

5.1 Experimental setup

Netbed [WLS⁺02] (an outgrowth of Emulab) was used to provide integrated access to experimental networks. Three nodes were used for each experiment: an FTP client, an FTP server, and an intermediate node running *DummyNet* [Riz97] to simulate a drop-tail router with a queue size of 500KB, and various bandwidths, propagation delays, and packet loss ratios. The router's queue was set large enough such that buffer overflow, i.e., loss due to congestion, did not occur. The client and server nodes were 850MHz Intel Pentium IIIs.

The client and the server nodes run FreeBSD-4.6. The dummyNet router node runs FreeBSD-4.10. The FreeBSD kernel implementation of SCTP available with the KAME Stack [KAME] was used on the client and server nodes. SCTP patchlevel 24 released October 11, 2004 from www.sctp.org was used for the SCTP-MS and SCTP-MS-CP runs. Because of the timing of the experiments, patchlevel 25 released February 21, 2005 was used for SCTP-naïve. KAME is an evolving and experimental stack targeted for IPv6/IPsec in BSD-based operating systems.

In our previous published results [Lad04], Netlab's control connection was inadvertently used by SCTP end-hosts for retransmissions. SCTP is inherently multihomed, and without knowing it, our SCTP associations used Netlab's essentially error-free, no-delay control channel, thus biasing results in favor of SCTP. When rerunning the experiments, only the path thru the dummyNet router was used.

We implemented protocol changes by modifying the FTP client and server source code available with the FreeBSD 4.6 distribution. Total transfer time was measured as follows. The starting time was when the "150 Opening" control reply from the server reached the client in response to the client's "NLST" request. The end time was when the server's "226 control reply" reached the client after the last file transfer.

Each combination of parameters (3 B-D configurations x 5 PLR x 5 file sizes) was run multiple times to achieve a 90% confidence level for the total transfer time. *Tcpdump* [TCPDUMP] (version 3.7.1) was used to perform packet level traces. SCTP decoding functionality in *tcpdump* was developed in collaboration of UD's Protocol Engineering Lab and Temple University's Netlab. Our results compare four FTP variants: "TCP" (the TCP variant used was New-Reno), "SCTP-naïve", "SCTP-MS", and "SCTP-MS-CP".

While we also performed experiments involving single (and multiple) file transfer, we only report the results of experiments involving multiple file transfers. Some minor improvement using SCTP multistreaming was witnessed in a single file transfer, but nothing significant. The major gains of multistreaming are more predominant when transferring multiple files. Additionally, comparing SCTP-naïve vs. TCP for multiple files provides insight on single file transfer.

5.2 Results

Figures 6, 7, and 8 (note: best viewed in color) show results obtained for our three bandwidth-delay configurations. Each graph displays the total time to transfer 100 same-size files for different loss probabilities using the four FTP variants.

5.2.1 TCP vs. Sctp-Naïve. Since Sctp-naïve is simply a straightforward substitution of TCP calls with Sctp calls, any performance difference must be attributed to the different ways our TCP and Sctp implementations handled connection/association establishment and/or data transfer (i.e., congestion control, loss recovery). Congestion control differences between Sctp and TCP can be found in [AAI02] where the authors note that the congestion control semantics and loss recovery mechanisms in Sctp are robust, and result in better steady state throughput at higher loss rates in a satellite environment.

For all three B-D configurations and file sizes, TCP and Sctp-naïve performed almost identically at 0% loss. In only one case (the long delay satellite configuration with smallest 10K file size) was there a noticeable difference of Sctp being ~10% slower.

As loss was introduced and increased, however, the performance of these two methods clearly diverged. Interestingly, for the smallest file size (10KB), Sctp-naïve performed consistently worse than TCP, and for all other file sizes 50KB – 1MB, Sctp-naïve transferred multiple files consistently faster than TCP. And as the file size increased, so did Sctp-naïve's relative performance improvement.

We investigated many of the tcpdumps and discovered several differences between the two studied implementations that help explain this behavior.

Why TCP does better for short files - First, each Sctp-naïve association establishment uses a 4-leg handshake while TCP connects using 3 legs. (This added leg provides Sctp associations with better defense against DoS attacks [SX01].) Sctp's extra $\frac{1}{2}$ RTT has significant impact; more so for short files. And as loss increases, Sctp incurs a greater chance (i.e., 4 to 3) that the establishment loses a leg, and requires a timeout before recover via retransmission. For newly established associations, this minimum timeout value is conservative (initially $\text{minRTO}=3\text{s}$; after the sender measures an RTT, $\text{minRTO}=1\text{s}$). Transferring a 10K file only involves ~7 PDUs, so for short transfers, a longer establishment time noticeably degrades Sctp-naïve performance. As file sizes increase, the establishment time becomes less a factor.

Second, an Sctp-naïve sender (and for that matter, all three Sctp variations) requires 4 missing reports before a fast retransmission, while a TCP sender fast retransmits on receipt of 3 dupacks. (Note: an Sctp missing report and a TCP dupack are analogous.) For short files, when the cwnd is often around size 3-4, TCP will be able to recover more often without a timeout via fast retransmit, while Sctp-naïve does not have sufficient PDUs in the pipe, and will require a timeout. As file sizes increase, this fast retransmit difference will not play as important a factor. (Note: in the latest Sctp design, only 3 missing reports will be required for a fast retransmit.) Sctp has Limited Transmit [ABF01], so this difference may not be significant.

Why Sctp-naïve does better for longer files - Sctp-naïve's significantly better performance for longer files (increasingly as loss rates increased) initially came as a surprise as it was widely understood that the congestion control mechanisms in TCP and Sctp are approximately the same. The largest improvement is demonstrated in Figure 6's LAN connection transferring 100 – 1MB files at the highest 10% loss rate: Sctp-naïve is four times faster than TCP.

On analysis, we realize that the currently prevalent FreeBSD version of TCP (New-Reno) does not have three congestion control mechanisms included in our Sctp model: Limited Transmit [ABF01], Appropriate Byte Counting [All03], and Selective Acks [MMF96]. One advantage of an experimental protocol such as Sctp is its ability to include newer mechanisms much sooner than for TCP. Once these extensions are included in TCP implementations, we expect (1) and (2) to perform similarly at different loss rates.

In any case, our primary goal is NOT to focus on whether FTP over Sctp-naïve is better or worse than FTP over TCP. Such a comparison would require equivalent FreeBSD implementations, which was beyond the scope of this study. We focus on the gains from multistreaming and command pipelining using Sctp-naïve as a baseline to see if and how much these mechanisms benefit file transfer.

5.2.2 Sctp-MS vs. Sctp-Naïve. We first consider the impact of FTP using a transport layer with multistreaming by comparing Sctp-MS vs Sctp-naïve. In Figures 6-8, we observe that in a lossy environment, significant gains from multistreaming are evident; more so for (1) smaller file sizes vs. larger file sizes, and (2) the highest bandwidth - shortest delay connection (LAN) vs the lowest bandwidth - longest delay connection (satellite). No significant performance difference was observed for (3) 0% loss in the LAN environment, and (4) for all B-D configurations and loss levels when transferring large (1MB) files.

Regarding (1), for all B-D configurations with loss present, multistreaming in Sctp-MS transfers 10KB files in roughly 1/2 the time than without multistreaming (Sctp-naïve) consistently across all loss probabilities. The relative gains decrease to roughly 30-40% faster for 50KB files. Sctp-MS avoids the overhead to set up an additional association for every file, an overhead that is relatively more significant for smaller files.

Evidence of (2) is seen, for example, by comparing the 50KB file transfers and seeing that Sctp-MS for the 3Mbps-1ms link (Figure 6) is ~40% faster than Sctp-naïve, and for the 256Kbps-125ms link (Figure 8), Sctp-MS improves on Sctp-naïve by only ~20%. Because Sctp-naïve has at least 7 extra PDUs (4 for association establishment; 3 for shutdown), Sctp-naïve will experience more timeouts per file transfer than Sctp-MS when there is loss. These additional timeouts degrade Sctp-naïve 'relatively' more when the RTT is shorter because the sender uses a fixed minimum RTO value. When the RTT = 2ms in the LAN scenario (Figure 6), a timeout with minRTO results in ~500 idle RTTs,

whereas for the satellite scenario (Figure 8), only 3 RTTs are idle. Further evidence of a fixed minRTO degrading shorter RTT paths relatively more than longer RTT paths can be found in [IAS05].

Regarding (3), in a LAN environment (see Figure 6), while SCTP-naïve does require an extra establishment association for each file, this overhead delay is minimal because the extra RTTs are short. Only as loss is introduced does the performance between these two versions diverge significantly, because loss in any of the extra 4 legs needed for SCTP-naïve association establishment requires a timeout before recovery via retransmission is possible, and timeouts are relatively 'expensive' in terms of relative delay.

Regarding (4), once files become very large (1MB), the amount of time transferring the file dominates any extra time spent having to establish an association.

One unexpected result appears in Figure 8's satellite link scenario. For large files (500KB - 1MB), SCTP-MS is slightly slower than SCTP-naïve at certain loss rates. We investigated tcpdumps for several runs in detail, and found no protocol behavior to explain this minor inconsistency. We noted that in redoing our experiments, the SCTP-MS version used a slightly older patch (#24) than SCTP-naïve (#25), which could explain the minimal 1-2% difference.

5.2.3 SCTP-MS-CP vs. SCTP-MS. As explained in Section 4.3, when transferring multiple files at once, command pipelining (a) reduces round trips for command exchanges, and (b) maintains the probed value of the congestion window for subsequent transfers in a multiple file transfer. We note that command pipelining is not exploiting a new transport layer mechanism as is the case of using multistreaming. Conceptually, FTP over TCP could also be designed to pipeline the file retrieval commands over the control channel.

We hypothesized the effect of (a) would remain fairly constant irrespective of file sizes being transferred and loss rate, and the effect of (b) would be more prevalent in transferring smaller files. For small files, more time (relatively) is spent by SCTP-MS in slow start probing for available bandwidth compared to the amount of time spent probing in large file transfers. By avoiding this reprobng for each file, and spending more time in steady state congestion avoidance phase, SCTP-MS-CP gains should be more evident for smaller files.

Figures 6-8 confirm these hypotheses. For all three B-D configurations, command pipelining introduces clear performance improvements, more so for the smaller files. The most pronounced improvement is seen in Figure 6, where for 10KB files, SCTP-MS-CP transfer files as much as 8 times faster than SCTP-MS as loss increases above 2%. Even for transferring one hundred 200KB files, SCTP-MS-CP does 30% better than SCTP-MS. When the file size increases to 1MB, some gain using command pipelining is noticeable, but the majority of time spent in congestion avoidance (as opposed to slow start, and doing command exchanges) dominates the transfer time, making the gain of SCTP-MS-CP over SCTP-MS only minimally significant.

VI. CONCLUSION

Our experimental results confirm that modifying FTP to use SCTP multistreaming and command pipelining can dramatically benefit mirroring (e.g., *fmirror*) and other applications which transfer a large number of files from host to host. These features:

- reduce the number of connections by aggregating the control and data connections,
- reduce the number of round trips required for connection setup/teardown, and command exchange, and
- use the bandwidth more efficiently by preserving the congestion window between file transfers.

Apart from transfer time improvements documented in our performance experiments, other advantages of FTP over SCTP-MS-CP vs. FTP over TCP are:

- The number of connections a server must maintain is reduced. Quantifying server load and its effects on throughput is beyond the scope of this paper. The interested reader is pointed to [FTY99]. We however expect that by using SCTP-MS-CP, servers could serve at least twice the number of clients compared to the current FTP over TCP design when the bottleneck for the number of simultaneous clients served is the TCBS reserved for the connections. This result should be of interest to busy servers that are constrained by the number of simultaneous clients.
- The number of PDUs exchanged between client and server is reduced (e.g., by reducing the command exchanges and connection establishments/teardowns) thus reducing the overall network load.
- Aggregating control and data connections into one SCTP multistreamed association solves concerns that FTP over TCP faces with Network Address Translators (NAT) and firewalls in transferring IP addresses and port numbers through the control connection [AOM98, Tou02].

ACKNOWLEDGMENT

I would like to express my sincere thanks to my Guide and my Co-Authors for their consistence support and valuable suggestions.

REFERENCES

- [1] R. Alamgir, M. Atiquzzaman, W. Ivancic, *Effect of Congestion Control on the Perf of TCP and SCTP over Satellite Nets*. Proc. NASA Earth Science Tech Conf, 6/02. Pasadena, CA.
- [2] M. Allman, H. Balakrishnan, S. Floyd, *Enhancing TCP's Loss Recovery Using Limited Transmit*, RFC 3042, 1/01.
- [3] M. Allman, A. Falk, *On the Effective Evaluation of TCP*. ACM CCR, 29(5), 10/99.
- [4] M. Allman, *TCP Congestion Control with Appropriate Byte Counting (ABC)*, RFC3465, 2/03.

[5] R. Elz, P. Hethmon, *Extensions to FTP*. draft-ietf-ftpext-mlst-16.txt, IETF Internet draft (work in progress), 3/03.

[6] S. Floyd, K. Fall, *Promoting the Use of End-to-End Congestion Control in the Internet*. IEEE/ACM Trans on Networking, 8/99.

[7] S. Floyd, T. Henderson, *The NewReno Modification to TCP's Fast Recovery Algorithm*. RFC2582, 4/99.

[8] T. Faber, J. Touch, W. Yue, *The TIME-WAIT State in TCP and Its Effect on Busy Servers*. Proc Infocom, 3/99, NYC.

[9] S. Ladha, P. Amer, *Improving multiple file transfers using SCTP multistreaming*, 23rd IEEE Int'l Perf, Computing, and Comm Conf (IPCCC), Phoenix, 4/04, 513-22

[10] S. McCreary, K. Clay, *Trends in WAN IP Traffic Patterns - Ames Internet Exchange..* ITC, 9/00. Monterey. [MMF96] M. Mathis, J. Mahdavi, S. Floyd, A. Romanow. *TCP Selective Acknowledgment Options*, RFC2018, 10/96.

[11] L. Rizzo, *Dumynet: a simple approach to the evaluation of network protocols*. ACM CCR, 27(1):3141, 1/97.

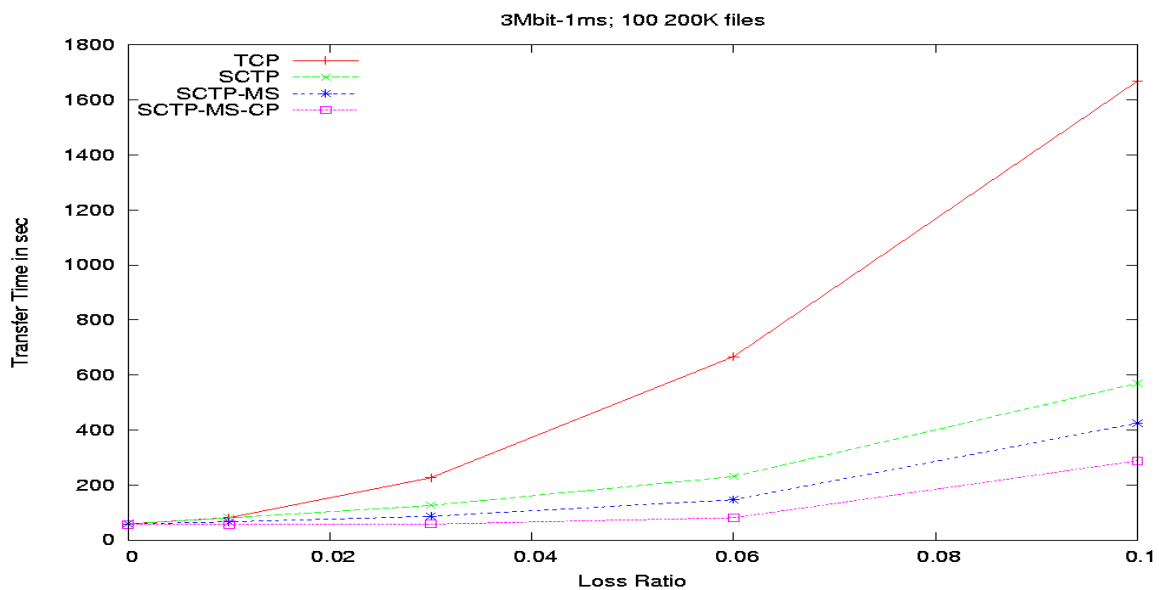
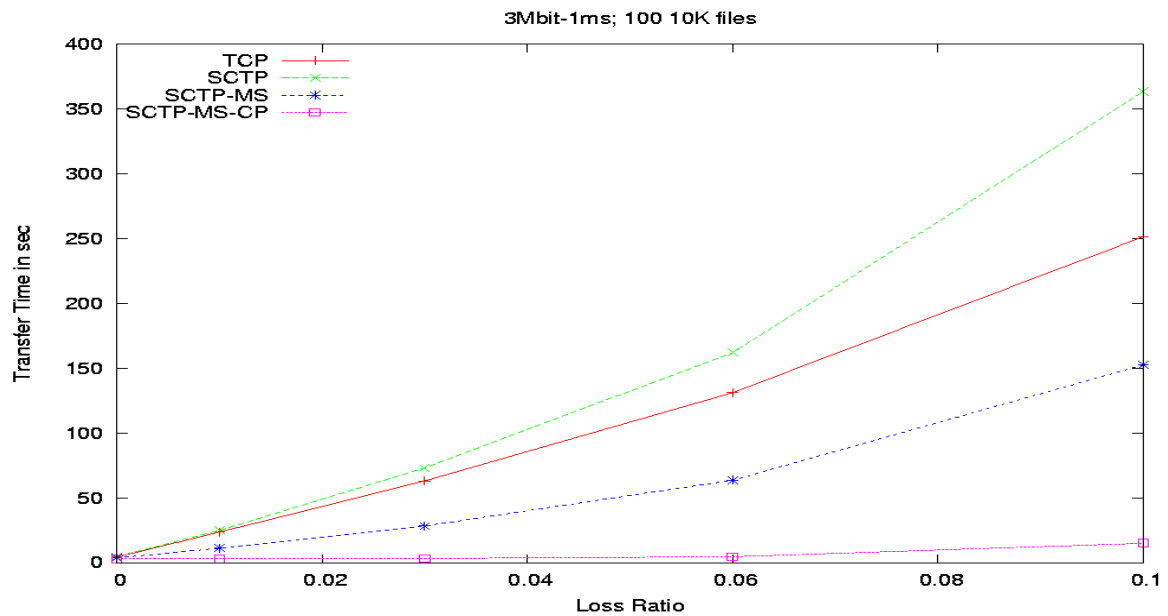
[12] R. Stewart, I. Arias-Rodriguez, K. Poon, A. Caro, M. Tuexen, *SCTP Implementers Guide*, draft-ietf-tsvwg-sctpimpguide-13.txt (work in progress), 2/05

[13] R. Stewart, Q. Xie, K. Morneault, C. Sharp, H. Schwarzbauer, T. Taylor, I. Rytina, M. Kalla, L. Zhang, V. Paxson, *SCTP*, RFC2960, 10/00.

[14] R. Stewart, Q. Xie, L. Yarroll, J. Wood, K. Poon., M. Tuexen, *Sockets API Extensions for SCTP*. draft-ietf-tsvwg-sctpsocket-10.txt, (work in progress), 2/05.

[15] B. White, et al. *An Integrated Experimental Environment for Dist'd Systems and Networks*. Proc. 5th Symp on OS Design and Implementation, 12/02. Boston.

[16] [WUARCHIVE] Usage Statistics for wuarchive, wuarchive.wustl.edu



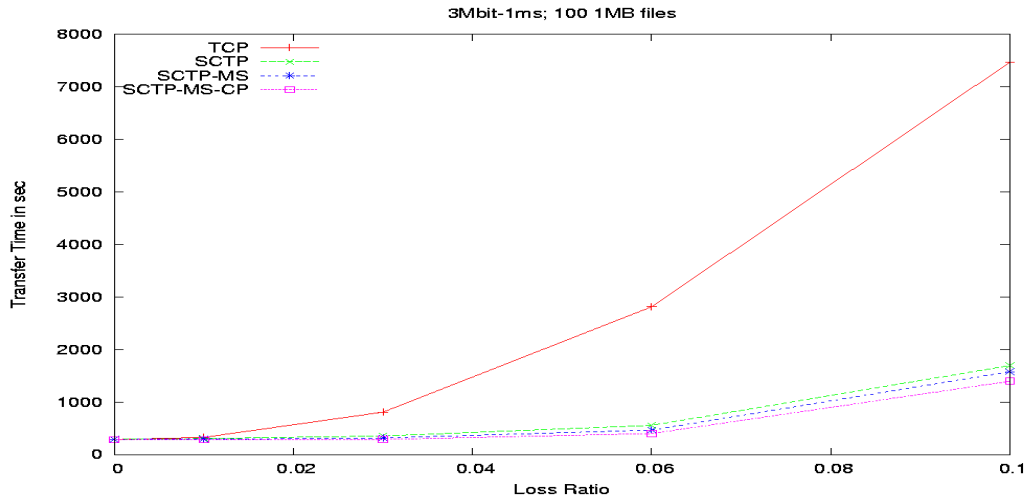
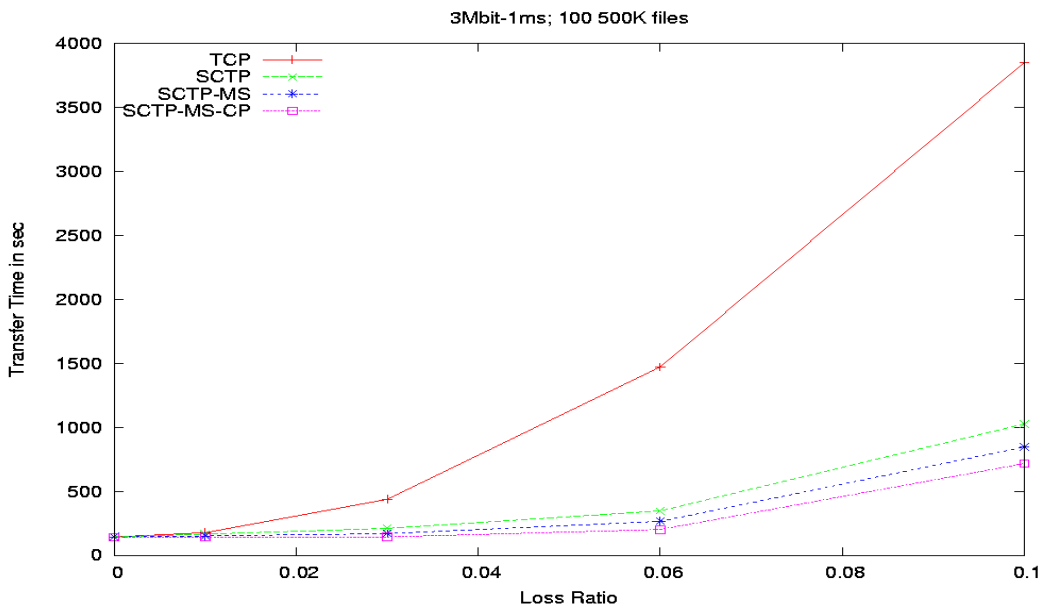
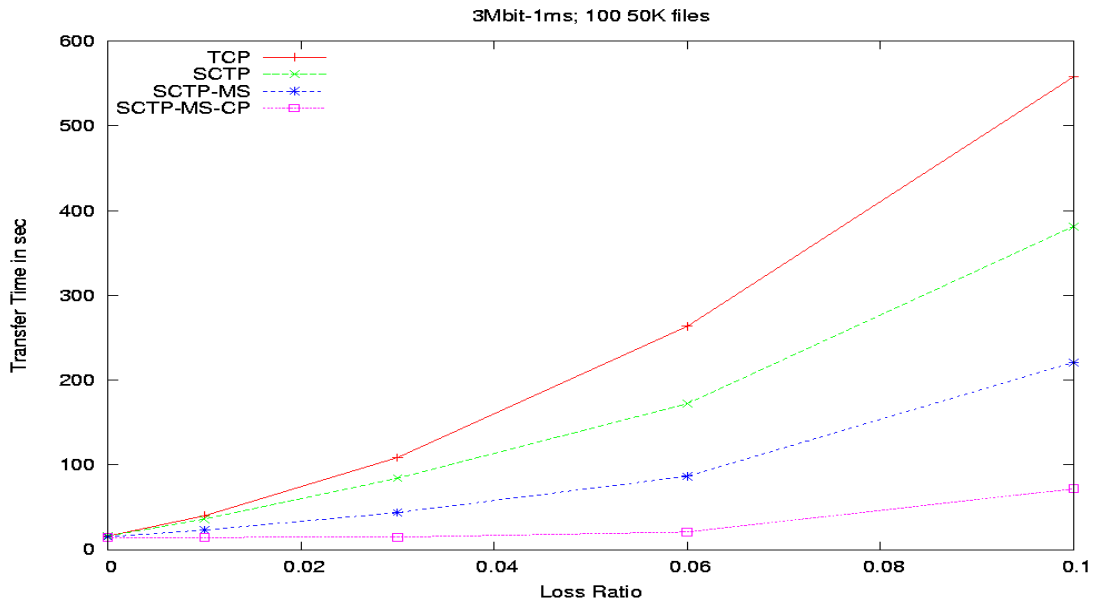
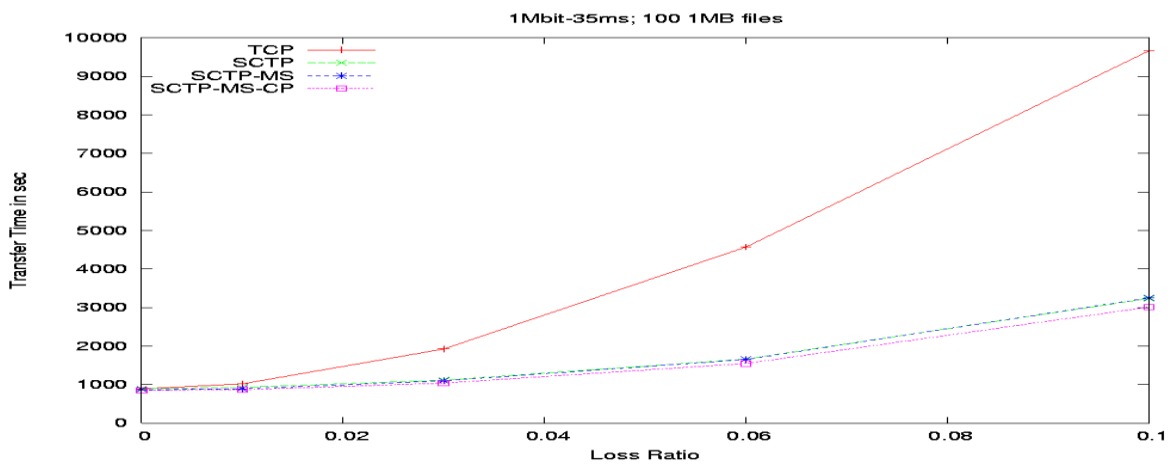
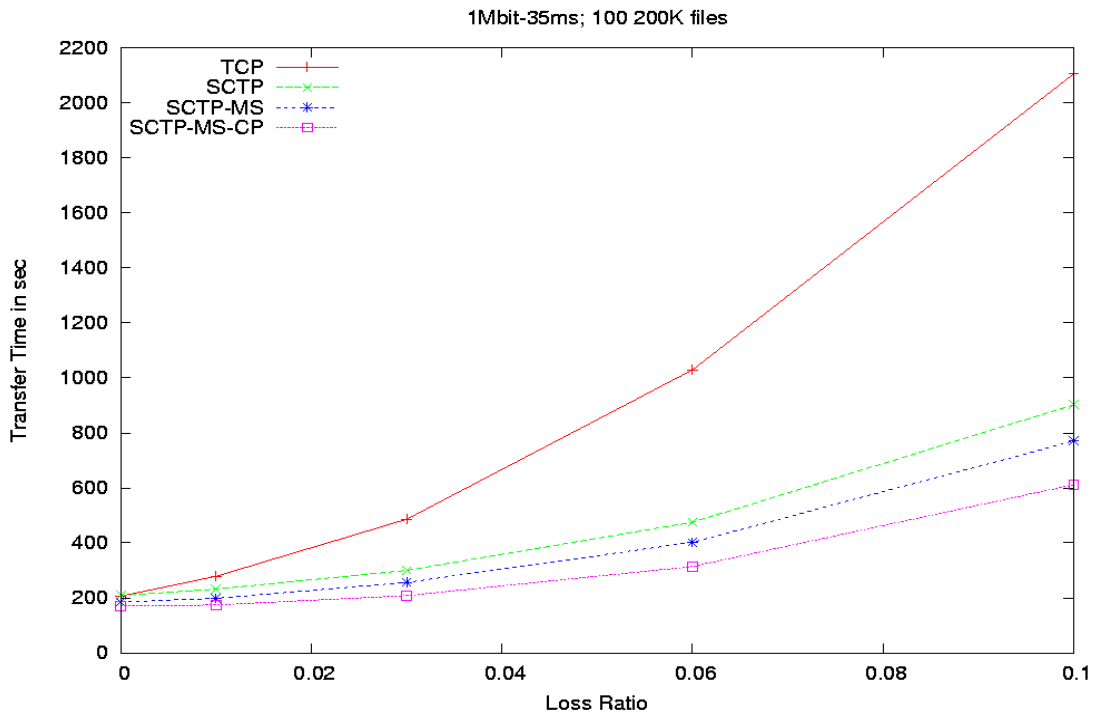
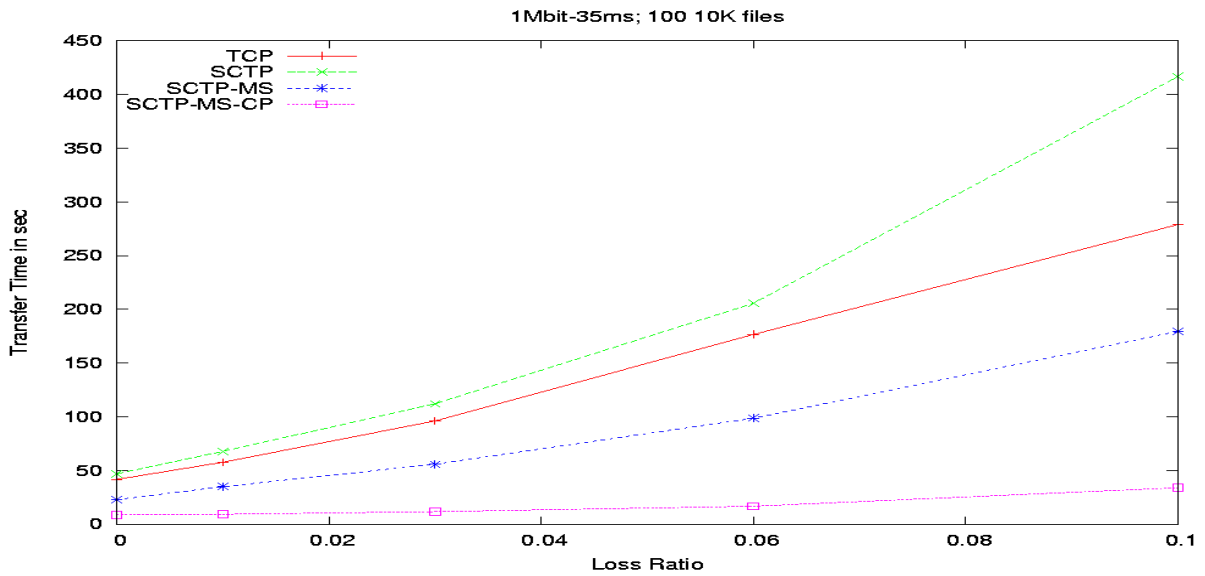


Figure 6: Transfer Time vs. Loss Ratio for a multiple transfer of 100 files on a LAN-like link (Bandwidth = 3Mbps, Propagation Delay = 1 ms)





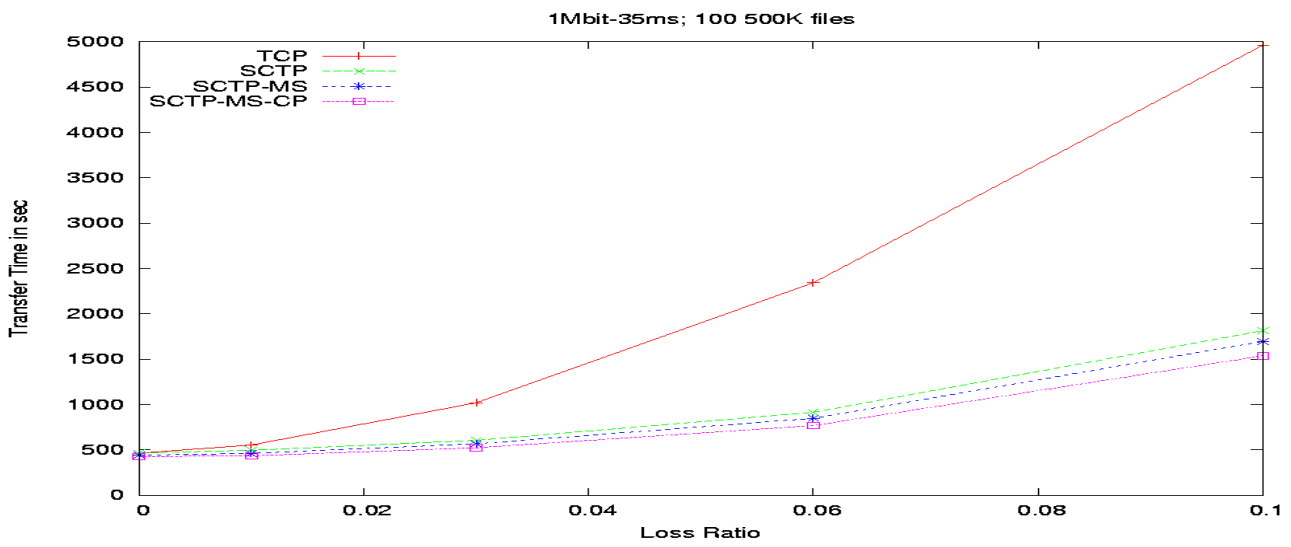
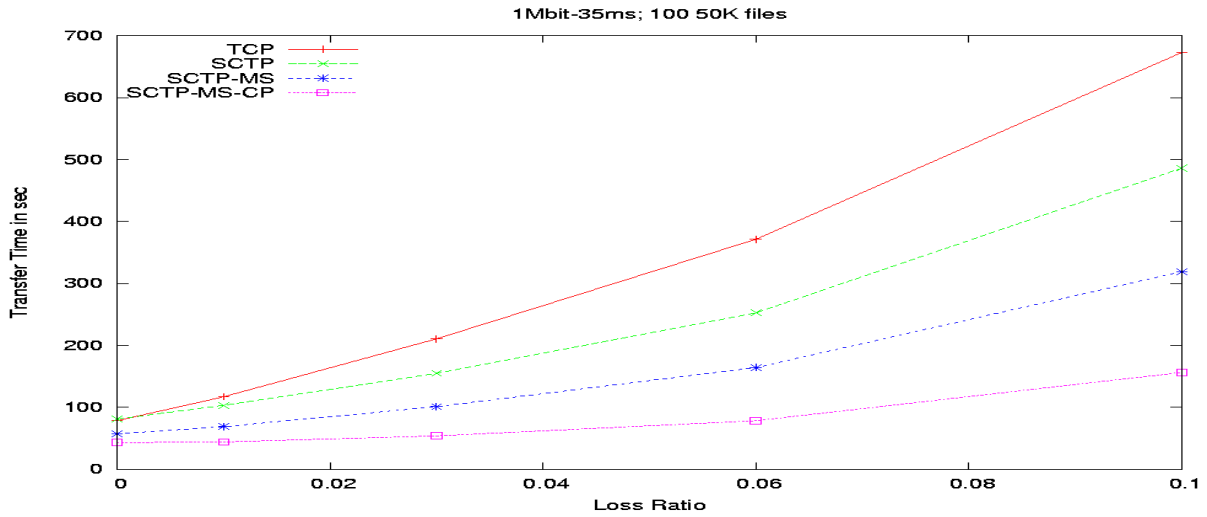
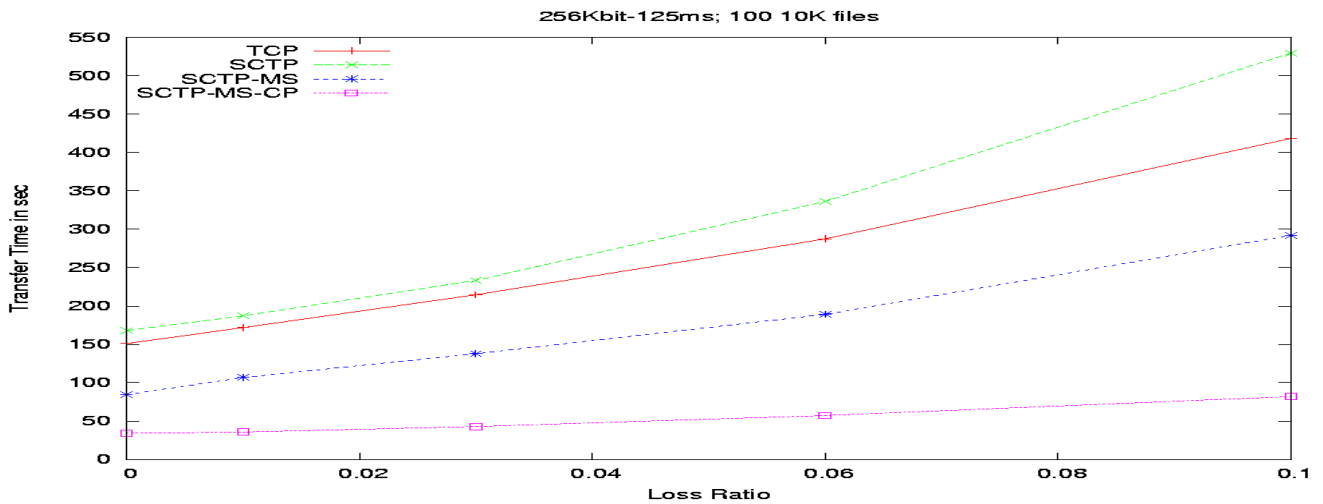


Figure 7: Transfer Time vs. Loss Ratio for a multiple transfer of 100 files on a US coast-to-coast-like link (Bandwidth = 1Mbps, Propagation Delay = 35 ms)



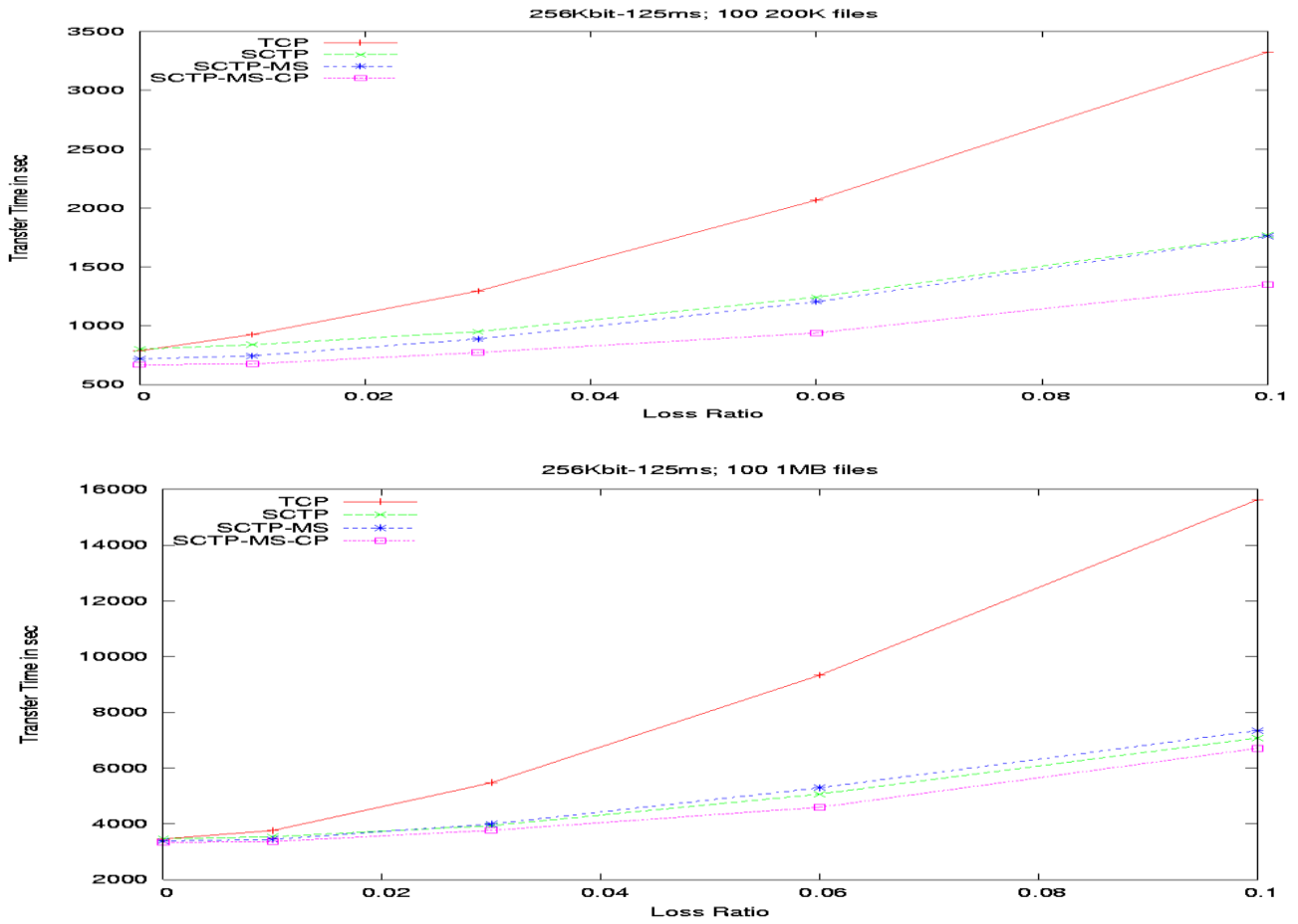


Figure 8: Transfer Time vs. Loss Ratio for a multiple transfer of 100 files on a satellite-like link
(Bandwidth = 256Kbps, Propagation Delay = 125 ms)

ns-2 Implementation of the OMA PoC Control Plane

Jong Min Lee

Dept. of Computer Software Engineering, Dong-Eui University, Busan, Republic of Korea

ABSTRACT : Recently technologies such as VoIP, VoLTE and VoWLAN have been widely used for the purpose of voice conversation since the proliferation of smart phones. A half-duplex group communication or the push-to-talk (PTT) has been standardized under the Open Mobile Alliance to replace the existing analog/digital TRS or a walkie-talkie service. In this paper, we design and implement the ns-2 module of the OMA PoC control plane which is a signaling protocol for the PTT service. Based on the SIP implementation of Rui Prior, we extend it to simulate the ad hoc PoC session establishment using on-demand session, which is a signaling protocol according to the rules and procedures of RFC 3261 with extended headers including PoC feature tags. Some simulation results have been shown for the verification purpose using the proposed implementation. With this implementation, we expect to perform the extensive simulation study of group communication in various network configuration.

Keywords: Control Plane, Group Communication, OMA PoC, Push-To-Talk, SIP

I. INTRODUCTION

Recently voice over IP (VoIP) has been used widely in lots of Internet applications. Among applications which support VoIP, there are several smart phone applications such as Voxer and TiKL which support the group communication as well as one-to-one communication, which is also known as the push-to-talk (PTT or P2T) [1, 2, 3]. Major communication and computer companies such as Nokia, Samsung Electronics, Qualcomm, Intel and Microsoft have standardized the Push-to-talk over Cellular (PoC) to support group communication under the Open Mobile Alliance (OMA) [4].

The OMA PoC standard is based on the SIP standard, which is an application-level network protocol to support call registration, session invitation and termination *etc.*[5] To study the performance of the OMA PoC standard, we need to develop the network simulator to satisfy its signaling protocol. Rui Prior [6] implemented the SIP signaling protocol based on ns-2.27 [7]. We extend the Rui Prior's work to support the ad-hoc PoC group session with unconfirmed indication which uses on-demand session. It is simpler than other session initiation methods defined in the OMA PoC standard and easy to understand intuitively, which provides a basic measure of the OMA PoC standard consequently. By using the implementation of this paper, we evaluate the network performance of the group session initiation of users in different networks and the same network.

In Section 2, we describe the basic architecture of the Rui Prior's work and the OMA PoC standard. The extended PoC architecture for the ns-2 network simulator will be presented in Section 3 and the performance study using the proposed scheme will be given in Section 4. Finally, we give a conclusion in Section 5.

II. RELATED WORKS

2.1 SIP Implementation of Rui Prior

Rui Prior implemented the SIP signaling protocol based on ns-2.27 [6]. Main functional components are the classes SIPUA and SIPProxy. SIPUA is a logical entity that makes a new SIP request for call setup and responds for the request. SIPProxy is a logical entity that manages the session information between SIPUA's. In the beginning, SIPUA sends a registration request to SIPProxy and then SIPProxy manages the registration information for later call setup.

Fig. 1 shows the class diagram of SIPUA. Both SIPUA and SIPProxy are subclasses of SIPTU, which performs the transaction user (TU) functionality in RFC 3261 [5]. Whenever a TU wants to send a request, it generates a client transaction instance (SIPTransaction), which is passed to the transaction layer, or SIPTransLayer. The class SIPTransLayer manages a list of SIPTransaction's, which are categorized into client non-invite transactions (CltNonINVITETrans) and client invite transactions (CltINVITETrans). Main functionalities of SIPUA is to register itself to SIPProxy and make an INVITE request for call setup according to the SIP call setup procedure.

Fig. 2 shows the class diagram of SIPProxy, which is also a subclass of SIPTU. SIPProxy handles a list of registered entry (RegEntry) as a registered DB for processing call setup requests between two SIPUA's. All SIPUA's should be registered into their own SIPProxy, which can be either only one in the network or all different, before session initiation. To initiate a session, one SIPUA sends an INVITE message to its SIPProxy and then the sender's SIPProxy forwards the INVITE message to the receiver's SIPProxy, which finally forwards the INVITE message to the receiving SIPUA. If the receiving SIPUA accepts the INVITE message, it sends 200 OK message to the sender following the reverse message path through both SIPProxy's. Upon receiving the 200 OK message, the sender generates an ACK message to the receiver to confirm the reception of the 200 OK message. This is called the INVITE/200/ACK three-way handshake. After this, end-point SIPUA's start a media session or a talk burst in the half-duplex mode.

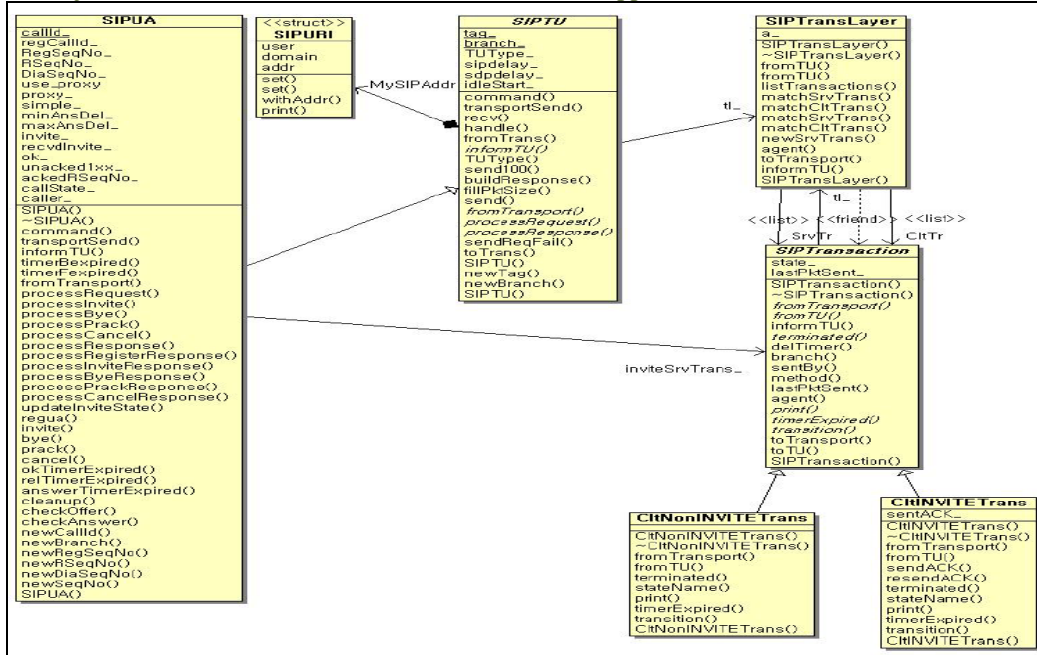


Figure 1. The class diagram of a SIP user agent

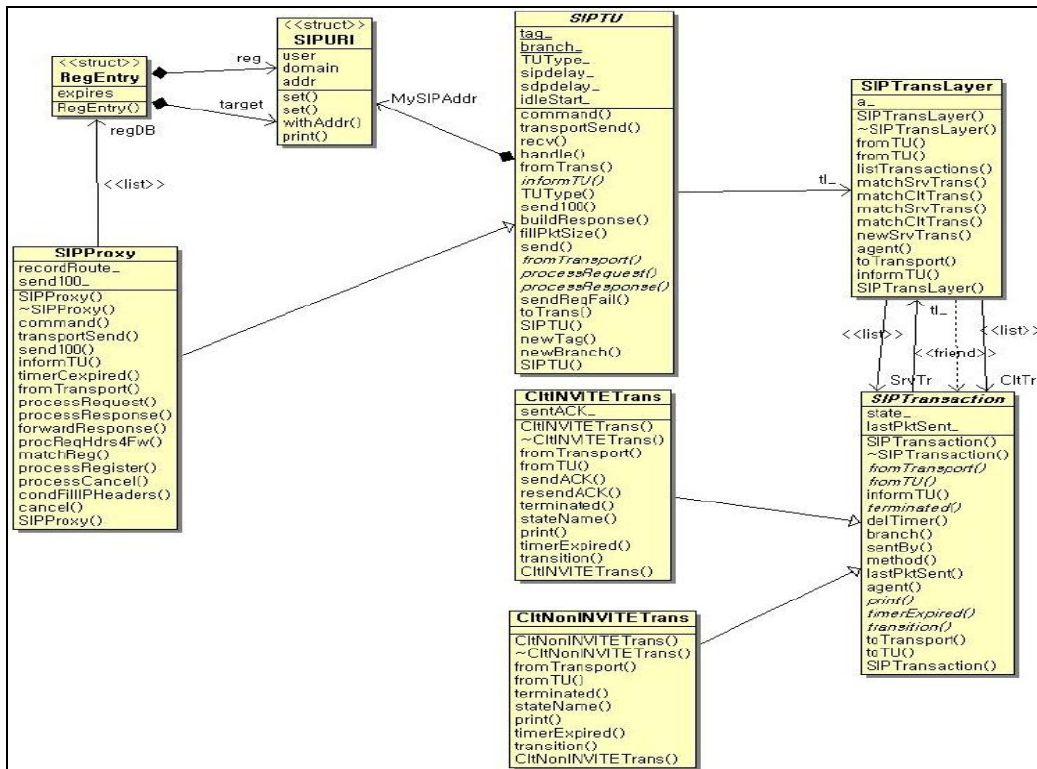


Figure 2. The class diagram of a SIP proxy

Fig. 3 shows the class diagram of SIP messages used in the Rui Prior's implementation. SIPMessage consists of lots of SIPHeader classes and at most one SIPBody. SIPMessage manages SIP header information as a linked list of several SIPHeader's, which defines a logical request recipient SIPHeaderTO, an identification information of a request sender SIPHeaderFrom, an address information of SIPUA SIPHeaderContact, a message grouping information SIPHeaderCallId, a transaction identification and ordering information SIPHeaderCSeq, a transport information for the transaction and location information for the response to be sent SIPHeaderVia and others.

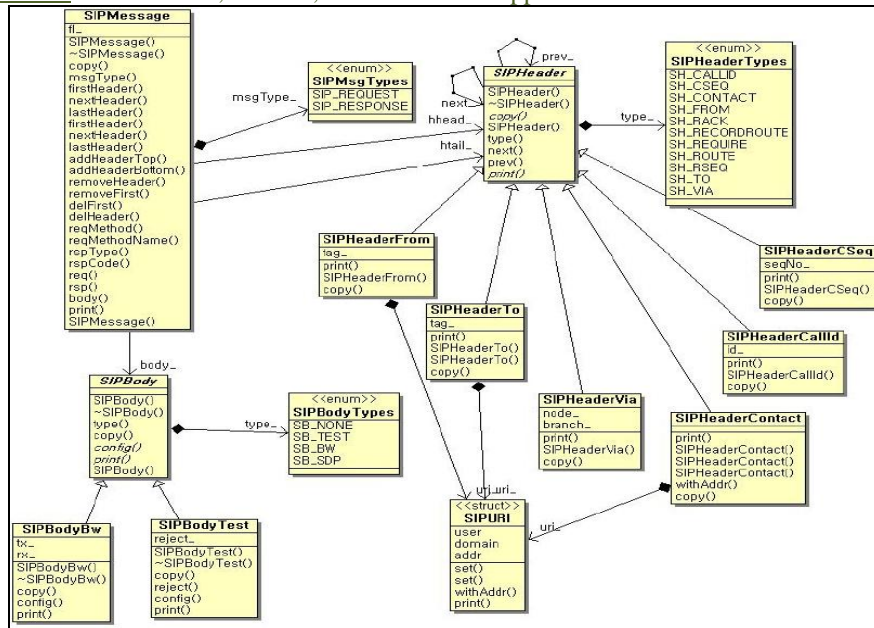


Figure 3. The class diagram of SIP messages

2.2 OMA PoC

The OMA PoC standard is mainly divided into the control plane protocol [8] which is a signaling protocol similar the SIP [5] and the user plane protocol [9] which carries user’s media traffic based on RTP [10]. Fig. 4 shows the brief OMA PoC architecture. The service logic for SIP sessions are implemented in the application server using SIP/UDP/IP. The application server functionality is implemented by the PoC server when the SIP/IP Core for the PoC service is according to 3GPP/3GPP2 IP Multimedia Subsystem (IMS) [11]. Thus the SIP/IP Core and PoC Server functionalities may be in one physical entity. Media packets carrying users’ voice data and the talk/media burst control for managing the talk right are transferred between PoC Clients and a PoC Server using RTP/UDP/IP [9].

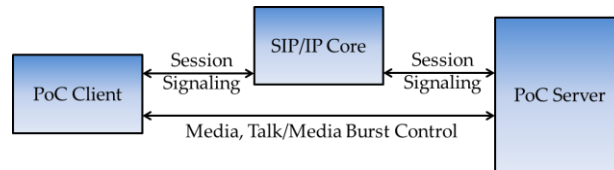


Figure 4. A brief OMA PoC architecture

The PoC Server performs either the Controlling PoC Function or the Participating PoC Function. In this paper, we call the PoC Server with the Controlling PoC Function and the Participating PoC Function as the Controlling PoC Server and the Participating PoC Server in short. The Controlling PoC Server mainly performs the management of PoC sessions such as the session establishment and the media burst control [8]. The Participating PoC Server performs relays the Talk Burst and Media Burst Control messages between the PoC Client and the Controlling PoC Server and may relay RTP media packets from the Controlling PoC Server.

Each PoC Client should register to their Participating PoC Server prior to participating in the PoC session according to rules and procedures of RFC 3261 [5] with extended headers including PoC feature tags [8]. Fig. 5 shows the registration procedure of the PoC Client. In the SIP REGISTER request of the PoC Client, information such as the SIP URI and IP address of the PoC Client can be found. This information is used in the proposed scheme to keep the location information of PoC Clients.

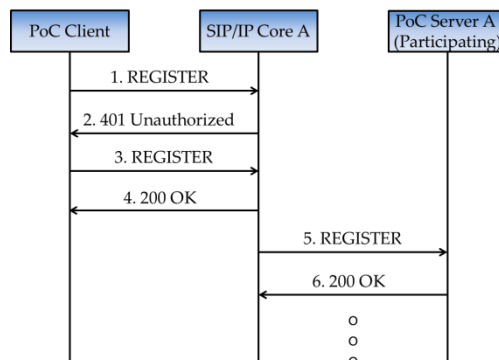


Figure 5. Registration procedure

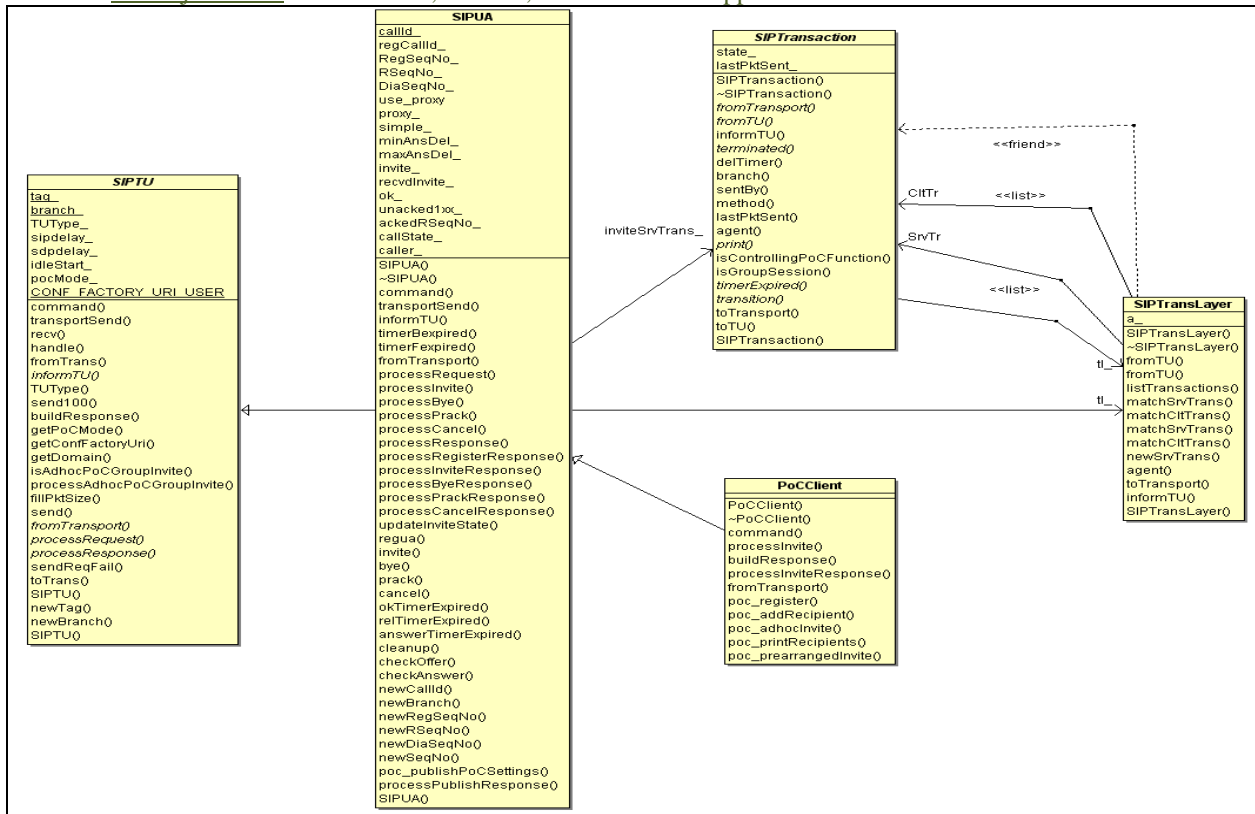


Figure 7. The class diagram related to PoCClient

A PoC server, which performs a Controlling PoC Function and/or a Participating PoC Function, deals with requests from a PoC client. Table 2 shows a brief description of the class PoCServer, of which the class diagram is shown in Fig. 8. PoCServer has main functionalities to process a PUBLISH message, a group session INVITE request, and other response messages and manage group session information. A Controlling PoC Server deals with request and/or response messages from a PoC client and one or more corresponding Participating PoC Servers according to the message exchange protocol as shown in Fig. 6. In a Controlling PoC Server, the information of an ad hoc PoC group session is maintained using the classes PoCGroupSession and PoCClientSession. PoCGroupSession has the information for the INVITE request to make a PoC group session. Whenever a Controlling PoC Server sends an INVITE request to each PoC client in the ad hoc PoC group, an instance of PoCClientSession is generated for that session. To support a PoC server, its base class SIPProxy should be modified to process an SIP PUBLISH request and an ad hoc PoC INVITE request. SIPTransaction deals with a transaction which consists of a request and responses relative to the request. SIPTransaction should be also modified to support the ad hoc PoC group session by adding functionalities to determine if a PoC server performs a Controlling PoC Function and if an INVITE request is a group session.

Table 3 shows a brief description of the class PoCSIPMessage, which extends the class SIPMessage to support messages defined in the OMC PoC standard. PoCSIPMessage, as shown in Fig. 9(a), allows multiple SIP bodies, which is useful to exchange media parameters between a PoC client and a PoC server for parameter negotiation. SIPMessage already allows multiple SIP headers, which is defined by the class SIPHeader, but it should be extended by adding subclasses PoCSIPHeaderContact, SIPHeaderAcceptContact, SIPHeaderAllow, SIPHeaderUserAgent etc. to support the OMA PoC standard. The added subclasses of the class SIPHeader are shown in Fig. 9(b).

Table 2. A brief description of PoCServer

Class	PoCServer
Base Class	SIPProxy
Functionalities	<ul style="list-style-type: none"> ● Processing of a PUBLISH request message ● Processing of an ad hoc PoC group session ● Processing of 183 session progress response from a participating PoC server ● Processing of a 200 OK message to an inviting user ● Management of session information
Added Classes	Description
PoCGroupSession	Deals with the information of PoC group sessions
PoCClientSession	Deals with the information of PoC client session for each PoC group session
Modified Classes	Added Functions
SIPProxy	Processes an SIP PUBLISH request and an ad hoc PoC INVITE request
SIPTransaction	Determines a PoC server's PoC function and a group session

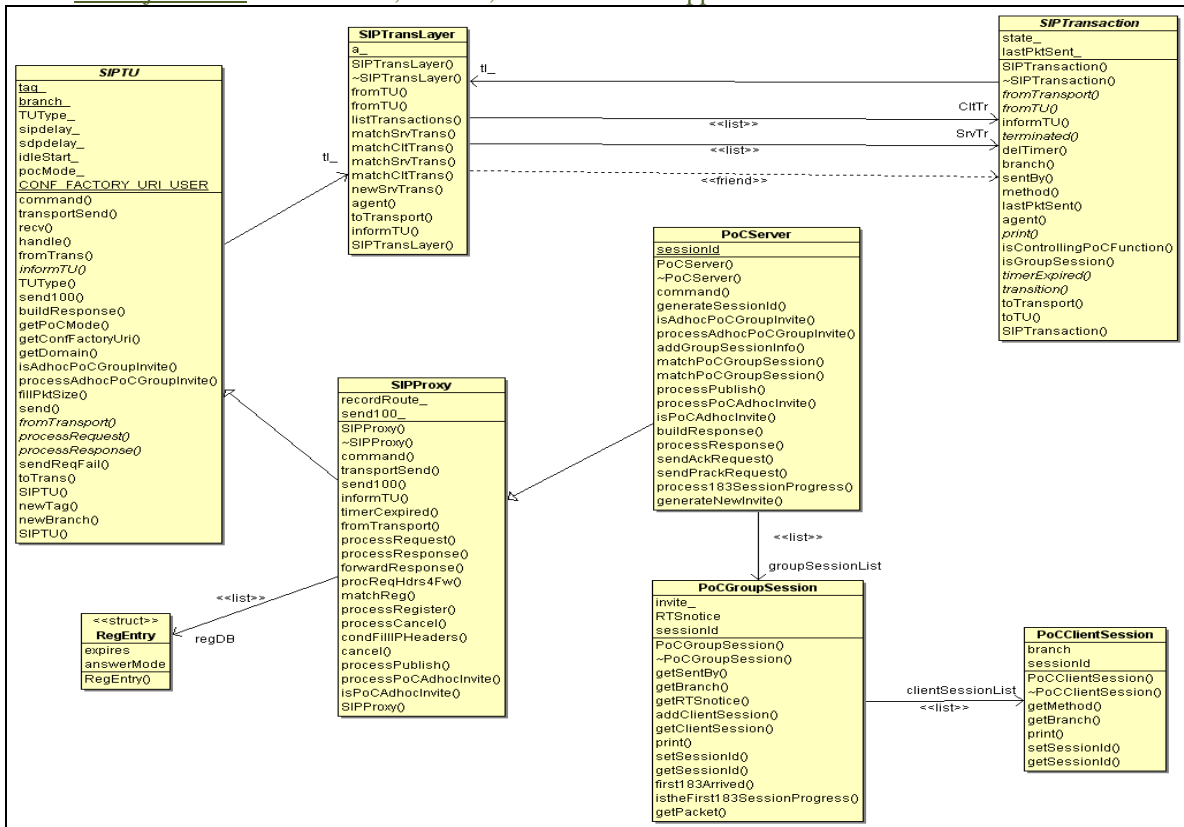


Figure 8. The class diagram related to PoCServer

Table 3. A brief description of PoCSIPMessage

Class	PoCSIPMessage
Base Class	SIPMessage
Functionalities	Defines the OMA PoC message to allow multiple SIP bodies
Added Classes	PoSIPHeaderContact, SIPHeaderAcceptContact, SIPHeaderAllow, SIPHeaderAnswerMode, SIPHeaderAnswerState, SIPHeaderSessionExpires, SIPHeaderSupported, SIPHeaderUserAgent
Modified Classes	SIPHeaderTypes

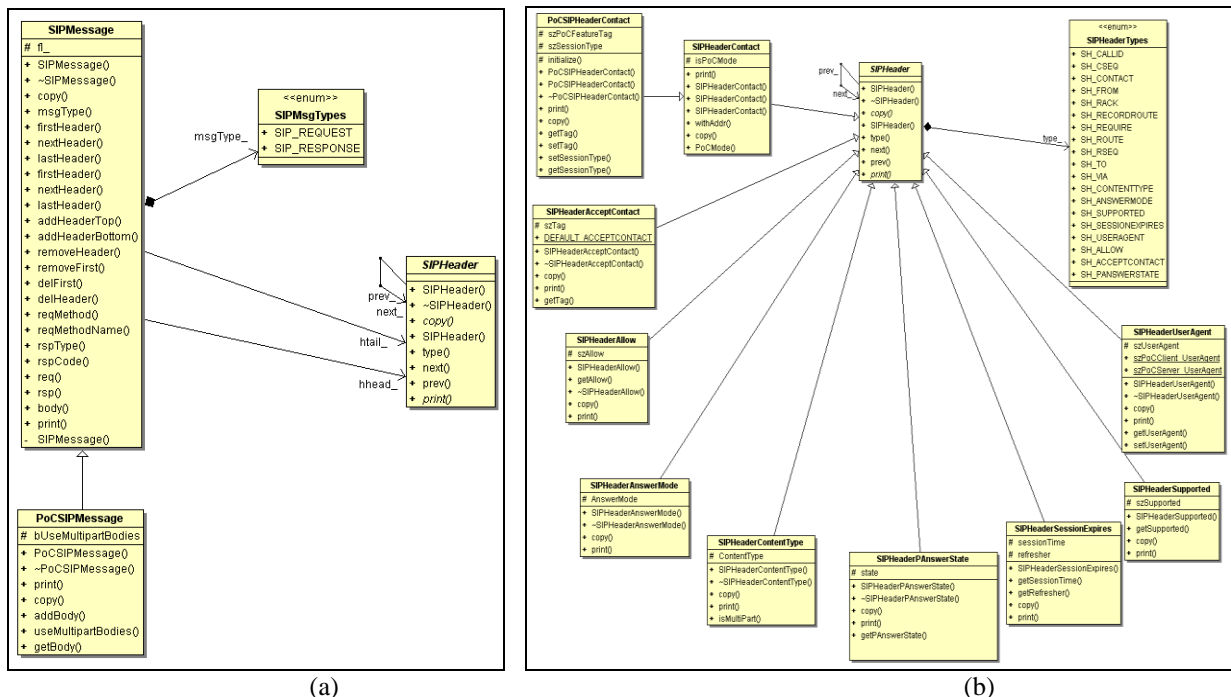


Figure 9. The class diagram related to PoCSIPMessage: (a) the representation of a PoC message; (b) SIP headers added for the OMA PoC.

IV. PERFORMANCE EVALUATION

In order to evaluate the network performance of the OMA PoC implementation proposed in this paper, we use ns-2.33 as a base network simulator, which is a discrete event simulator used for networking research widely since mid-90's [14]. Fig. 10 shows snapshots of simulation to compare the Rui Prior's implementation and the OMA PoC implementation. The call setup scenario used for the simulation is adopted from RFC 3261 [5]. Rui Prior's implementation, as shown in Fig. 10(a), can make only a 1-to-1 session for call setup. On the other hand, the OMA PoC implementation can make 1-to-many ad hoc group session. Fig. 10(b) shows the packet flow of the OMA PoC implementation for two recipients, from which we can find that the group session progresses successfully from one PoC client to two PoC clients.

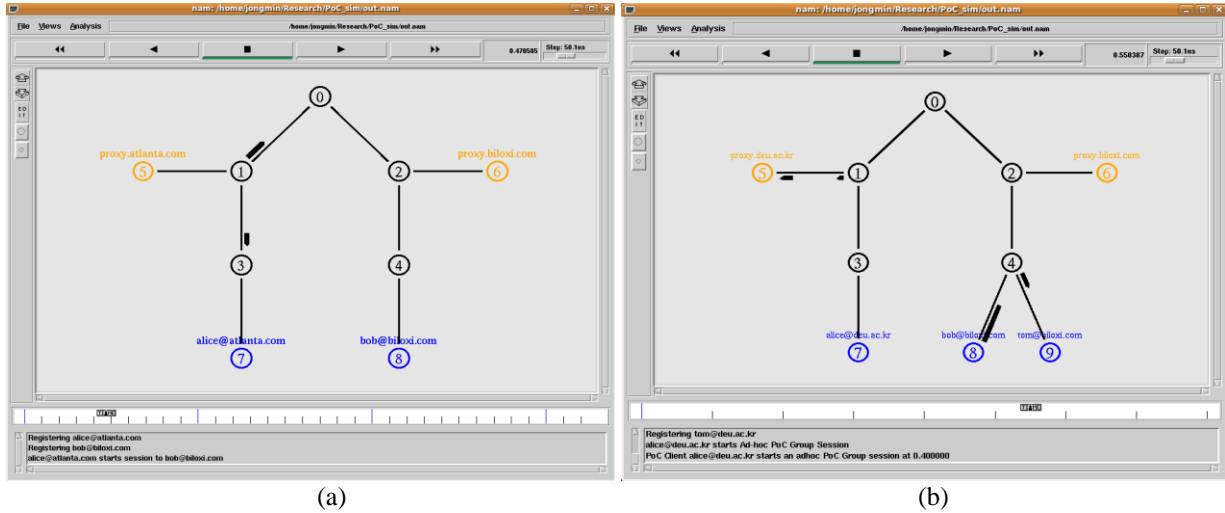


Figure 10. Snapshots of simulation to compare two implementations: (a) Rui Prior's implementation, (b) OMA PoC implementation.

To see the network performance in terms of a call setup time, we carry out two experiments for different wired network configuration as shown in Fig. 11. Fig. 11(a) is to simulate packet flows between two 1-to-2 group sessions, where senders and receivers are located in different networks. Two initiating PoC clients belong to the domain "deu.ac.kr" and all PoC recipients belong to the domain "biloxi.com." In the experiment, we evaluate the network performance as the link delay and the bandwidth vary between a PoC client and its neighbor node. Link parameters in Fig. 11(a) are as follows:

- Bandwidth between a PoC client and its neighbor node : 1~20Mbps
- Link delay between a PoC client and its neighbor node : 5~20msec
- Bandwidth of all other links : 100Mbps
- Link delay of all other links : 10msec

Fig. 11(b) is to simulate packet flows of many 1-to-2 group session where a sender and all other receivers are in the same network in order to see the network performance for the in-bound traffic congestion to a PoC server. All PoC clients belong to the same domain and are located in the same network. Link parameters Fig. 11(b) are fixed as follows: the bandwidth of all links is 100Mbps and the link delay of all links is 10msec. PoC clients are represented by $s(i)$, $r(2*i)$ and $r(2*i+1)$ for $i = 1\sim 12$. PoC clients in the bottom row are senders, $s(i)$. Recipients $r(2*i)$ and $r(2*i+1)$ for $s(i)$ are in the middle and the top rows respectively. Twelve one-to-two group sessions exist in Fig. 11(b).

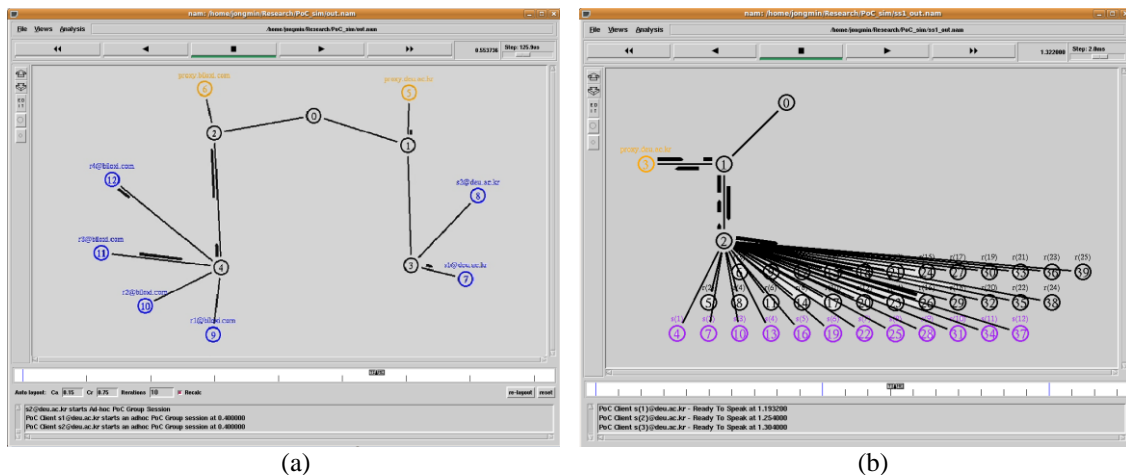


Figure 11. Snapshots of simulation for different network configuration: (a) group session initiation among PoC clients in different networks, (b) group session initiation among PoC clients in the same network.

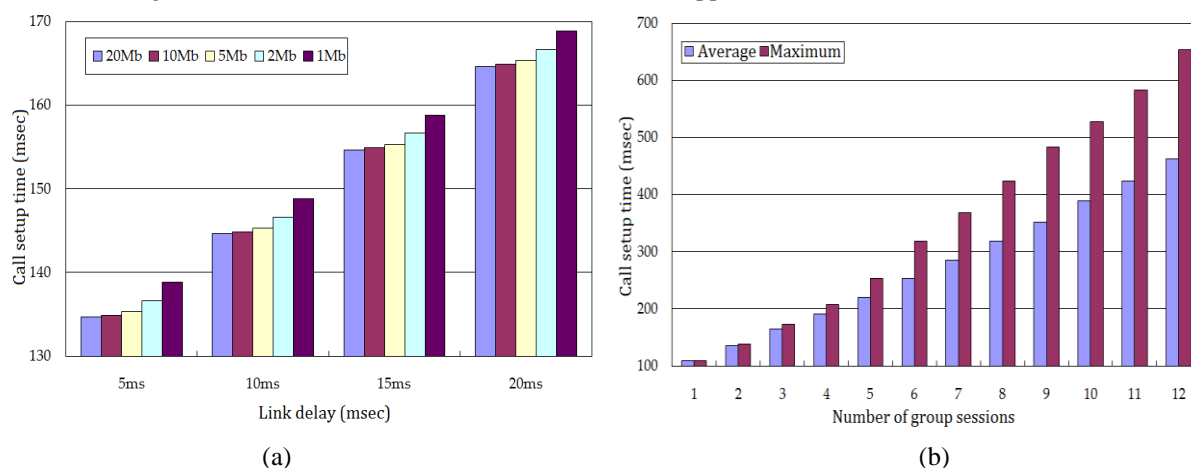


Figure 12. Call setup time: (a) group session initiation among PoC clients in different networks, (b) group session initiation among PoC clients in the same network.

Fig. 12(a) shows the simulation result of the experiment in Fig. 11(a). As the link delay increases, the average call setup time also increases linearly. We can find this result intuitively since signaling messages for call setup are exchanged among PoC clients and Controlling/Participating PoC Servers. The distribution of the call setup time is in the interval of 135~170msec, which is short enough to start media transfer after the connection of a group session. However, this result is derived from a situation that the signaling traffic is not enough to become overloaded. We try the experiment in Fig. 11(b) to make the network overloaded.

Fig. 12(b) shows the simulation result of the experiment in Fig. 11(b), which initiates many 1-to-2 group sessions in the same network. In this case, the traffic bottleneck is the PoC server, which performs both the Controlling PoC Function and the Participating PoC Function. Each group session consists of one initiating PoC clients and two recipient ones. As the number of group sessions increases, the traffic in the network also increases. The average call setup time increases linearly as the number of group sessions increases. But the maximum call setup time increases rapidly compared to the average call setup time, from which we can find that some PoC recipient clients cannot join its group session within a certain amount of time and thus media traffic such as voice cannot be delivered to those PoC clients for cooperation.

V. CONCLUSION

Recent wide-spread use of Internet technologies such as VoIP, VoLTE and VoWLAN results from the proliferation of smart phones. A half-duplex group communication mechanism or PTT has been standardized to replace the existing analog/digital walkie-talkie service. In this paper, we have designed and implemented the ns-2 module of the OMA PoC control plane to deal with the ad hoc PoC session establishment using on-demand signaling. We have used the SIP implementation of Rui Prior and extended it to deal with the signaling protocol for the ad hoc PoC session establishment using on-demand signaling. We have shown that the signaling protocol operates exactly for the purpose of verification and we have also performed the simulation study for various network configuration. We expect that the ns-2 implementation of the OMA PoC control plane can be used for the effective network simulation study of group communication.

ACKNOWLEDGEMENTS

This work was supported by Dong-Eui University Foundation Grant (2012).

REFERENCES

- [1] Open Mobile Alliance, *Push to talk over cellular (PoC) – architecture: approved version 2.0* (Aug. 2011).
- [2] R.S. Cruz, M. Serafim, G. Varatojo, and L. Reis, Push-to-talk in IMS mobile environment, *Proc. 2009 fifth Int'l Conf. on Networking and Services*, Valencia, Spain, 2009, 389-395.
- [3] L.-H. Chang, C.-H. Sung, H.-C. Chu, and J.-J. Liaw, Design and implementation of the push-to-talk service in ad hoc VoIP network, *IET Communications*, 3(5), 2009, 740-751.
- [4] Open Mobile Alliance Mobile Phone Standards and Specification, <http://openmobilealliance.org/>.
- [5] J. Rosenberg, H. Schulzrinne, G. Camarillo, A. Johnston, J. Peterson, R. Sparks, M. Handley and E. Schooler, SIP: Session Initiation Protocol, RFC 3261, June 2002.
- [6] Rui Prior's homepage – ns, <http://www.dcc.fc.up.pt/~rprior/ns/>.
- [7] ns-2 homepage, http://nsnam.isi.edu/nsnam/index.php/Main_Page.
- [8] Open Mobile Alliance, *OMA PoC control plane: approved version 2.0* (Aug. 2011).
- [9] Open Mobile Alliance, *PoC user plane: approved version 2.0* (Aug. 2011).
- [10] H. Schulzrinne, S. Casner, R. Frederick and V. Jacobson, RTP: A Transport Protocol for Real-Time Applications, RFC3550, July 2003.
- [11] G. Camarillo and M.A. Garcia-Martin, *The 3G IP Multimedia Subsystem (IMS): Merging the Internet and the Cellular Worlds*, 3rd ed. (West Sussex, UK: Prentice-Hall, 2008).
- [12] A. Niemi, Ed., Session Initiation Protocol (SIP) Extension for Event State Publication, RFC 3903, Oct. 2004.

- [13] M. Garcia-Martin, A Session Initiation Protocol (SIP) Event Package and Data Format for Various Settings in Support for the Push-to-Talk over Cellular (PoC) Service, RFC 4354, Jan. 2006.
- [14] ns-2 wiki homepage, http://nslam.isi.edu/nslam/index.php/Main_Page.



mobile computing, and parallel computing.

Jong Min Lee received the B.S. degree in computer engineering from Kyungpook National University, Korea, in 1992, and the M.S. and the Ph.D. degrees in Computer Science from Korea Advanced Institute of Science and Technology (KAIST) in 1994 and 2000, respectively. From Sept. 1999 to Feb. 2002, he worked for Samsung Electronics as a senior engineer. Since 2002, he has been a faculty member of the Department of Computer Software Engineering, Dong-Eui University, Busan, Korea. From Feb. 2005 to Feb. 2006, he visited the University of California, Santa Cruz as a research associate. From Feb. 2012 to Feb. 2013, he was a visiting scholar of the Department of Computer Science at The University of Alabama, Tuscaloosa, AL. His research interests include routing in ad hoc networks and sensor networks,

A New Intrusion detection system in data mining & fuzzy logic

Balaji.s.c.k¹, B.Kishore Kumar²

Assistant professor, SVIT, Hampapuram, Anantapuram (Dt), Andhra Pradesh

Abstract: The computers abnormal activities are identified by system defense. Traditional Intrusion detection relies on extensive knowledge of traditional expertise, in particular, on the familiarity with the systems to be protected. To reduce this dependence, various data-mining and machine learning techniques have been used in the literature. In the proposed system, we have designed fuzzy logic-based system for effectively identifying the intrusion activities within a network. Currently available intrusion detection systems focus mainly on determining uncharacteristic system events in distributed networks using signature based approach. Due to its limitation of finding novel attacks, we propose a hybrid model based on improved fuzzy and data mining techniques, which can detect both misuse and anomaly attacks. Our aim is to reduce the amount of data retained for processing i.e., attribute selection process and also to improve the detection rate of the existing IDS using data mining technique. We then use improved Kuok fuzzy data mining algorithm, which in turn a modified version of APRIORI algorithm, for implementing fuzzy rules, which allows us to construct if-then rules that reflect common ways of describing security attacks. We applied fuzzy inference engine using mamdani inference mechanism with three variable inputs for faster decision making

Keywords: Fuzzy logic, apriori, intrusion detection, hybrid system.

I. INTRODUCTION

In the current scenario, business does not have boundaries to carry out the task, as it is highly distributed across the globe. Securing these widely distributed data has become a hill-climbing task, as there are new types of threats arising from the people, especially in the current economic turmoil, who used to penetrate into the organization network, either for fun or for gaining some vital information which can fetch them monetary benefits. Network based defense systems normally combine network based IDS and packet filtering firewalls. The main drawbacks of these systems are its inability to identify and characterize new attacks and to respond them intelligently.

A significant challenge in providing an effective and efficient protective mechanism to a network is the ability to detect novel attacks at the initial phase and implement proper countermeasures. Information security process includes the risk assessment, which identifies the potential risk to the organizations networks, risk mitigation that suggests the methods to reduce the risks, and countermeasures. Intrusion Detection has become an integral part of the information security process. But, it is not technically feasible to build a system with no vulnerabilities; as such incursion detection continues to be an important area of research.

II. INTRUSION DETECTION SYSTEMS USING AI TECHNIQUES

Intrusion Detection Systems (IDS) is a powerful technology helping in protecting the precious data and networks from malicious and unauthorized access. An intruder is a hacker attempting to break into or misuse the resources of a computer system. Intruders come from outside an organizations network and may attempt to go around firewalls to attack machines on the internal network. Research and development of intrusion detection has been under way for nearly 27 years. The work that is most often cited is the technical report by James P.Anderson [1]. AI techniques like Fuzzy logic, Neural Networks, and recent development of Artificial Immune Systems (AIS) has played an important role in most misuse and anomaly detection. Few researchers [2] have applied the above mentioned techniques for the detection of malicious activities. Another direction of interest could be using ensemble approach [3], where by combining few approaches for detection individual classes.

A Intrusion detection using fuzzy logic and data mining

The method proposed by [4] extracts fuzzy classification rules from numerical data, applying a heuristic learning procedure. The learning procedure initially classifies the input space into non-overlapping activation rectangles corresponding to different output intervals. In this sense, our work is similar to that of [4,5]. There is no overlapping and inhibition areas. However, the disadvantage listed is, the high false positive rates which is the primary scaling of all the IDS. Researcher [6] describes the approaches to address three types of issues: accuracy, efficiency, and usability. This works is an enhanced version of the work by Lee [4]. First issues of improving accuracy is achieved by using data mining programs to analyze audit data and extract features that can distinguish normal activities from intrusions. Second issue, efficiency is improved by analyzing the computational costs of features and a multiple-model cost-based approach is used to produce detection models with low cost and high accuracy. Third issue, improved usability, is solved by using adaptive learning algorithms to facilitate model construction and incremental updates; unsupervised anomaly detection algorithms are used to reduce the reliance on labeled data. Researchers [7] developed the Fuzzy Intrusion Recognition Engine (FIRE) using fuzzy sets and fuzzy rules. FIRE uses simple data mining techniques to process the network input data and generate fuzzy sets for every observed feature. The fuzzy sets are then used to define fuzzy rules to detect individual attacks. FIRE does not establish any sort of model representing the current state of the system, but instead relies on attack specific rules for detection. Instead, FIRE creates and applies fuzzy logic rules to the audit data to classify it as normal or anomalous. Dickerson et al. found that the approach is particularly effective against port scans and probes. The primary disadvantage to

this approach is the labor intensive rule generation process. Our research work can be considered as an extension of the above work by automating the rule generation process.

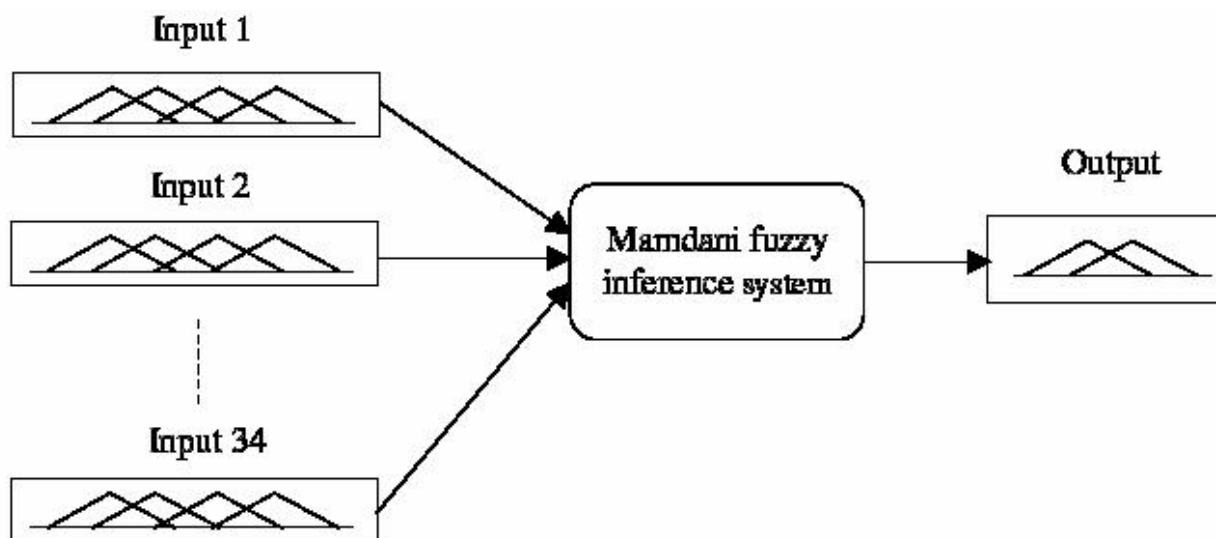


Figure 1. The designed Fuzzy system

The model proposed [8] combines neural networks and fuzzy logic. This system works by mapping a template graph and user action graph to determine patterns of misuse. The output of this mapping process will be used by the central strategic engine to determine whether an intrusion has taken place or not. The major drawback is that new type attacks rules need to be given by the external security officer i.e. it does not automate rule generation process and more number of components prevents it from working fast. Tombini used an approach wherein the anomaly detection technique is used to produce a list of suspicious items. The classifier module which uses a signature detection technique then classified the suspicious items into false alarms, attacks, and unknown attacks. This approach works on the premise that the anomaly detection component would have a high detection rate, since missed intrusions cannot be detected by the follow-up signature detection component. In addition, it also assumed that the signature detection component will be able to identify false alarms. While the hybrid system can still miss certain types of attacks, its reduced false alarm rate increases the likelihood of examining most of the alerts. Zhang and Zulkernine employed the method random forests algorithm in the signature detection module to detect known intrusions. Thereafter, the outlier detection provided by the random forests algorithm is utilized to detect unknown intrusions. Approaches that use signature detection and anomaly detection in parallel have also been proposed. In such systems, two sets of reports of possible intrusive activity are produced and a correlation component analyzes both sets to detect intrusions. Researchers use association based classification methods to classify normal and abnormal attacks based on the compatibility threshold.

III. PROPOSED IIDS FRAMEWORK

The proposed IIDS framework (Figure 2) has several components, and the following sections describe briefly about each.

A. Attributes

Prior to any data analysis, attributes representing relevant features of the input data (packets) must be established. The amount of data being sniffed from the network will be heavy. If only vital attributes are chosen then the overhead of fuzzy inference engine will be reduced to the maximum extent. There were 42 variables from DARPA training data. The set of attributes provided to the Data Analyzer is a subset of all possible attributes pertaining to the information contained in packets headers, packet payloads, as well as aggregate information such as statistics in the number and type of packets or established TCP connections. Attributes are represented by names that will be used as linguistic variables by the Data Miner and the Fuzzy Inference Engine. We use traditional attribute selection algorithm that utilizes information gain for selection each attributes based on the information gain obtained for that 2193 particular class of variables available.

B. Data Analyzer

Once attributes of relevance have been defined and the data source identified, Data Analyzer is employed to compute configuration parameters that regulate the operation of IDS. This module analyzes packets and computes aggregate information by grouping packets. Packets can be placed in fixed size groups (s-group) or in groups of packets captured in a fixed amount of time (t-group). Each s-group contains the same number of packets covering a variable time range and each t-group contains a variable number of packets captured over a fixed period of time.

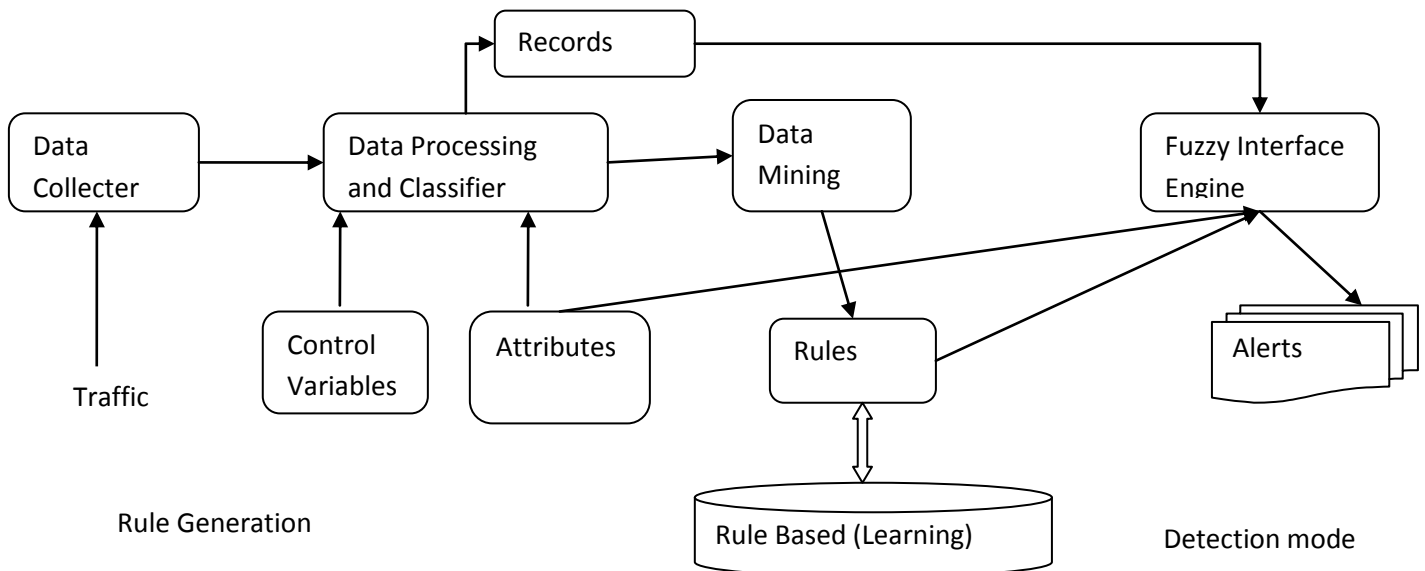


Figure 2. IIDS framework.

C. Data Miner

A variation of Kuok's algorithm is used to implement the Data Miner, which allows for efficient, single-pass, record processing by partitioning data into hierarchical files. From the data sample the algorithm reads the records and creates a file for each term of attribute. The algorithm carries over the same process for all the records in the data file. Once the entire data set is processed, the support value for every item set is calculated. The algorithm extracts all large item sets, and constructs rules from those large item sets. The rules with confidence value greater than or equal to min confidence moved to the rule base.

D. Inference Engine

An inference determines which rules are relevant to the given data. Our prototype utilizes FuzzyJess to check the rules. The engine uses three inputs as explained in the figure. We have configured the inference engine to use Mamdani inference mechanism. The shooting strength concludes whether the modeled behavior satisfies the fact. If the shooting strength is somewhere near to zero indicates a possibility of attack. F. Data set used for testing the prototype We used 1999 DARPA data which is an extension of 1998 data set available. The latest dataset was added with few more attacks that reflect more real-time data. A quick glance at the 1999 DARPA dataset shows it contains 3 weeks of training data and two weeks of testing data. First and third week data do not contain any attack and this was used as training data for anomaly intrusion detection. Second week contains all types of attacks so this was used for creating attack profiles. We used two weeks of test data for our testing. The record files were broken down into smaller files as there were few limitations like processing power of the hardware and the size of the main memory.

IV. CONCLUSIONS AND FUTURE WORK

A few contributions have been made by this research namely, improved apriori algorithm for faster rule generation and reduced querying frequency, reduced features for faster detection of attacks and reduced false positives. Even though the system was tested using off-22156 line data and in a small live environment, our next goal is to turn this system into a light weight system, by overcoming the existing limitations like bottle neck in packet processing, searching for known rules and very high false positive rates and improve the performance by means of faster detection and alert correlation and acceptable rate of false positives. As a token of appreciation to open-source community, our plan is to make this system an open source project once the system is complete and ready by all means to take the high level of real world challenge.

REFERENCES

- [1] Anderson, P. Computer security threat monitoring and surveillance. Fort Washington.1980.
- [2] Peyman Kabiri and Ali A. Ghorbani. "Research on Intrusion Detection and Response: A Survey". International Journal of Network Security, Vol.1, No.2, PP.84-102, Sep. 2005
- [3] Anazida Zainal, Mohd Aizaini Maarof and Siti Mariyam Shamsuddin "Ensemble Classifiers for Network Intrusion Detection System", Journal of Information Assurance and Security 4 (2009) 217-225
- [4] Lee, W. A "Data Mining framework for construction features and models for intrusion detection systems", Columbia University.2001.
- [5] Manganaris, S.. "A data mining analysis of RTID alarms." Computer Networks2000. 34(4): 571-577.
- [6] Stolfo, S. J.. "Data mining-based intrusion detectors: an overview of the columbia IDS project." ACM SIGMOD2001. 30(4): 5-14.
- [7] Dickerson, J. E. and J. A. Dickerson Fuzzy Network Profiling for Intrusion Detection. 19th International Conference of the North American Fuzzy Information Processing Society,2000,301-306.

- [8] Botha, M., Solms VR, Perry K, Loubser E, “The utilization of Artificial Intelligence in a Hybrid Intrusion Detection System”. Annual research conference of the South African institute of computer scientists and information technologists on Enablement through technology,2002, 149-155.

AUTHORS BIOGRAPHY

Balaji .s.c.k M.tech, Assistant Professor Dept of CSE, SVIT, Hampapuram, Anantapur. He has 3 years of teaching experience and 10 years of I.T experience .His areas of interest are Data mining and Data Warehousing .

B. Kishore Kumar M.tech, Assistant Professor Dept of CSE, SVIT, Hampapuram, Anantapur. He has 5 years of teaching experience .His areas of interest are Data mining and Data Warehousing

Study of the Internal Structure of Electronic Components RAM DDR-2 and Motherboard of Nokia-3120 by Using Neutron Radiography Technique

Shahajan Miah¹, Md. Hafijur Rahaman¹, Sudipta Saha², Md. Abu Taher Khan¹, Md. Aminul Islam¹, Md. Nurul Islam², Md. Khurshed Alam² and M. Habibul Ahsan¹

¹Department of Physics, Shahjalal University of Science & Technology, Sylhet, Bangladesh

²Institute of Nuclear Science and Technology, Atomic Energy Research Establishment, Dhaka, Bangladesh.

ABSTRACT: Neutron radiography technique has been applied in the present study to detect the internal structure of electronic components RAM DDR-2 and Motherboard of Nokia-3120. In present experiment, electronic RAM model: DDR-2 and motherboard of mobile phone, NOKIA-3120 was collected from shops. Thermal neutron radiography facility of 3MW TRIGA MARK-II research reactor at Atomic Energy Research Establishment, Savar, Dhaka has been adopted for present research. A series of neutron radiographic images were taken to find the optimum exposure time for the samples. The optimum exposure time is evaluated in this experiment is 2 minutes 45 seconds. Some spots have been identified from the radiographic images of the samples.

Key words: Neutron radiography, Homogeneity, Internal Structure and defect

I. INTRODUCTION

Neutron radiography is a powerful non-destructive imaging technique for the internal evaluation, such as voids/cavity, cracks, homogeneity etc. of materials or components. It involves attenuation of a neutron beam by an object to be radiographed and subsequently registration of the attenuation process (as an image) is done on film or video. A very well-known technique of non-destructive examination for characterizing the internal structure of an object is the use of penetrating radiation, such as x-ray radiography and neutron radiography. These two radiographic processes are often complementary. X-rays are stopped by dense materials and pass through light ones and in many instances neutrons have reverse properties. Neutron will penetrate the body of a large metal to give a good image of an internal structure. But for x-ray to record it, it would require long exposure, which would obliterate most of the details available by the radiography. These are the most important advantageous of the radiography method over other methods available for doing this experiment. Neutron radiography method has been used to detect internal defects/ water absorption behavior in different building industries; Jute reinforced polymer/ biopolcomposites (Islam *et al.* 2000, Alam *et al.* 2007, Alam *et al.* 2006). It is also used to investigate the quality of different rubber samples (Islam *et al.* 2000). Many ancient cultures have made useful and decorative items such as pottery, figurines, building tiles, and burial containers that become important parts of the archaeological record. The material aspects of clay and ceramic technology, the physical properties of clay and various constructions and firing methods can be investigated using archaeometric technique (Renfrew *et al.* 1996, Rice 1987) Ancient Technologies and Archaeological Materials (ATAM) researchers have employed standard techniques such as x-ray radiography, x-ray diffraction (XRD), scanning electron microscopy (SEM), and neutron activation analysis (NAA) to study structure and composition of the ceramic materials (Renfrew *et al.* 1996, Rice 1987). In this paper, we present very promising results by using neutron radiographic technique. We took radiographic image of RAM DDR-2 and Motherboard of Nokia-3120 for different exposure time and we found an optimum exposure time that is 2 minutes 45 seconds. From optimum radiographic images, we evaluated some spots in the samples. This result is remarkable for us because it is first time in Bangladesh both used of samples and experiment.

Neutron radiography facility

The neutron radiography facility installed at the Institute of Nuclear Science and Technology, Atomic Energy Research Establishment, Savar, Dhaka at 3 MW TRIGA MARK II research reactor of Bangladesh Atomic Energy Commission, is equipped to facilitate inspection of radioactive samples (mainly, fuel rods) as well as non-radioactive materials. The tangential beam port allows for selection of thermal neutron beam and is used for neutron radiography because the neutron beam coming out through this port contains less amount of gamma - radiation (Islam *et al.* 1995, Rahman *et al.* 1989) compared to other three beam ports. Moreover, a 15cm long bismuth filter is used inside the port to cut existing gamma - rays, because gamma - rays produce unwanted fogging in the radiography film. To control the beam of neutrons, a 120cm long conically shaped cylindrical divergent collimator having inner and outer diameter of 5 cm and 10 cm, respectively, has been installed inside the reactor biological shielding assembly. Barton (1967) has described the usefulness of a divergent collimator for neutron radiography. A beam stopper, having 4 wheels at the bottom capable of forward and backward movement on rail in front of the beam port has also been installed. The beam stopper is a wooden box, which contains neutron-shielding materials, like paraffin wax and boric acid inside. The NR facility includes a beam catcher having a hole in the middle of the front face. A lead block has been placed at the back of the hole for gamma shielding and the remaining part of the beam catcher has been filled with neutron shielding materials. In between the beam stopper and beam catcher there is a sample and NR camera/ cassette holder table. Finally, the NR facility has been housed to reduce neutron

and gamma background by using special concrete containing cement, heavy sand (mixture of ilmenite, magnetite and ordinary sand) and stone chips. Details of the NR facility can be found elsewhere (Rahman et al. 1989, Islam et al. 1995).

II. MATERIALS AND METHODS

2.1 Sample collection/preparation

We collected electronic components 1GB RAM model: DDR-2 and motherboard of mobile phone, model: NOKIA-3120 as samples from shop. We used the samples without change of shape.

2.2 Loading of the film and converter foil in the NR-cassette

Gadolinium (Gd) metal foil of 25 μ m thickness was used as converter in the NR cassette/ camera and Agfa structured D4_pDW industrial X-ray films were used as detector in our experiment. The films have emulsion in one side only. Initially the film was sized up by a cutter (Kaiser Hobby Cut) according to the geometry of the converter foil in the cassette. The cassette is a light-tight device for holding film and converter foil in close contact during exposure. During loading the film and the converter foil in the NR cassette, the emulsion surface of the film was kept in contact with converter foil. The cassette was then closed tightly. All these procedures have been done in the dark room. The cassette was, thus, made ready to take the neutron radiograph of the experimental samples.

2.3 Placing sample and the NR-cassette

The NR camera and the sample were placed on their respective tables across the neutron beam. In this position the camera was placed just after the sample. The sample holder table was set at the optimum sample position from the reactor biological shielding assembly. To obtain the high-resolution neutron radiograph the distance between the sample and the NR camera was made minimum. Light samples are attached in the surface of the neutron radiography camera by using aluminum tape. In our experiment we attached the samples in the surface of NR camera by using aluminum tape.

2.4 Exposure

Exposure means passing of neutron beam through a sample onto a special film (x-ray industrial film) in order to create a latent image of an object in the emulsion layers of that film. This discussion is confined to direct contact radiography (film in close contact with the Gd converter foil) of the film. The sample was irradiated for the optimum time, i.e., the time required to obtain good neutron radiograph of the sample. Exposure time differs for different samples, depending on the intensity of the neutron beam, density and thickness of the sample and neutron cross-section. The optimum exposure time of both the samples was determined through a series of experiments with different exposure time, while the reactor was operated at 2.4 MW. In this experiment the optimum exposure time is 2 minutes 45 seconds.

III. RESULT AND DISCUSSION

A series of neutron radiographs of the electronic components 1GB RAM model: DDR-2 and motherboard of mobile phone, model: NOKIA-3120 have been taken. The experiments were done at thermal neutron radiography facility of 3 MW TRIGA MARK-II Research Reactor of AERE, Savar, Dhaka. During the experiment the reactor was operated at 2.4 MW power level. 25 micro-meter thick gadolinium metal foil was used as the neutron converter in the experiment. Table 1.1 shows the optimum neutron exposure/irradiation time for the samples. The optimum neutron exposure/irradiation time is evaluated to be 2 minutes 45 seconds.

Table 1.1 Optimum irradiation/exposure time of the objects

Sample	Irradiation Time(min)	Optimum Irradiation Time(min)
RAM DDR-2	10	2.75
	6	
	3	
	2.50	
	2.75	

The Fig 1.1(a), 1.1(b) and Fig 1.2(a), 1.2(b) are showing the neutron radiographic images of electronic RAM DDR-2 and motherboard of NOKIA 3120 with the exposure time of 2 min 30 seconds and 2 min 45 seconds respectively. The neutron radiographic images of Fig 1.1(a) and Fig 1.2(a) are of same component electronic RAM DDR-2.

Sample	Irradiation Time(min)	Optimum Irradiation Time(min)
Motherboard of Nokia 3120	10	2.75
	6	
	3	
	2.50	
	2.75	

The later one is more clear but from the radiograph, some spots have been identified.

Similarly, neutron radiographic images in Fig.1.2(b) is more distinct than that of Fig 1.1(b). Due to some stainless steel material on the motherboard of NOKIA 3120, some extra highlighted portion of the image created problems to identify its neighboring area.

Radiographic Images

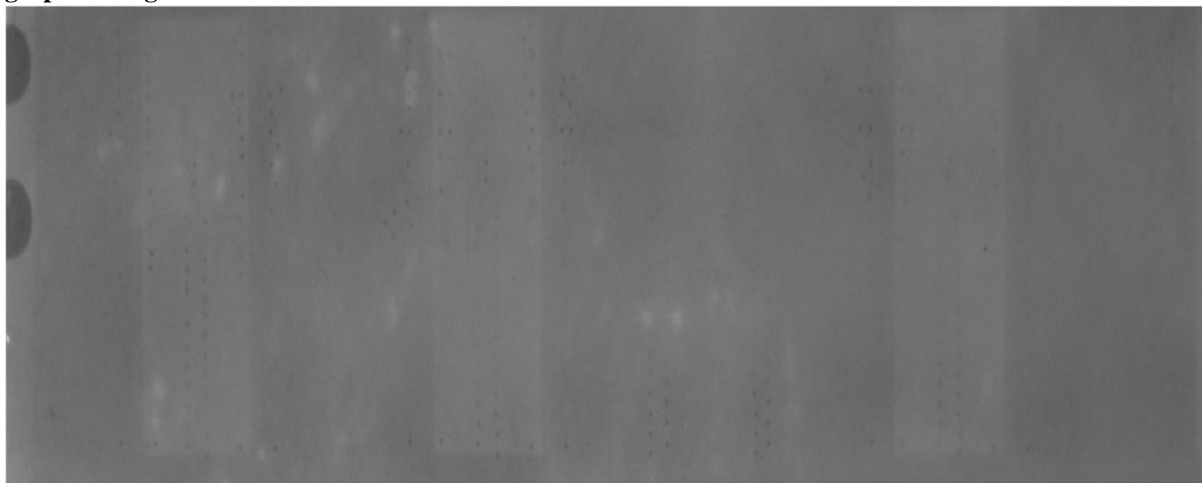


Fig 1.1(a): Neutron radiographic image of RAM DDR-2 (exposure time 2.50 min)

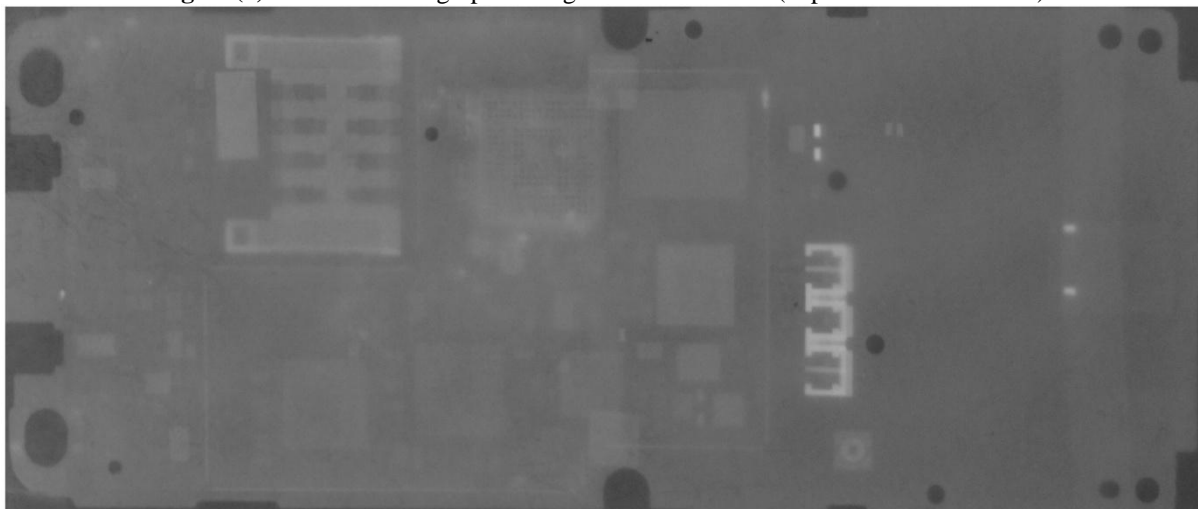


Fig 1.1(b): Neutron radiographic image of NOKIA-3120 (exposure time 2.50 min)

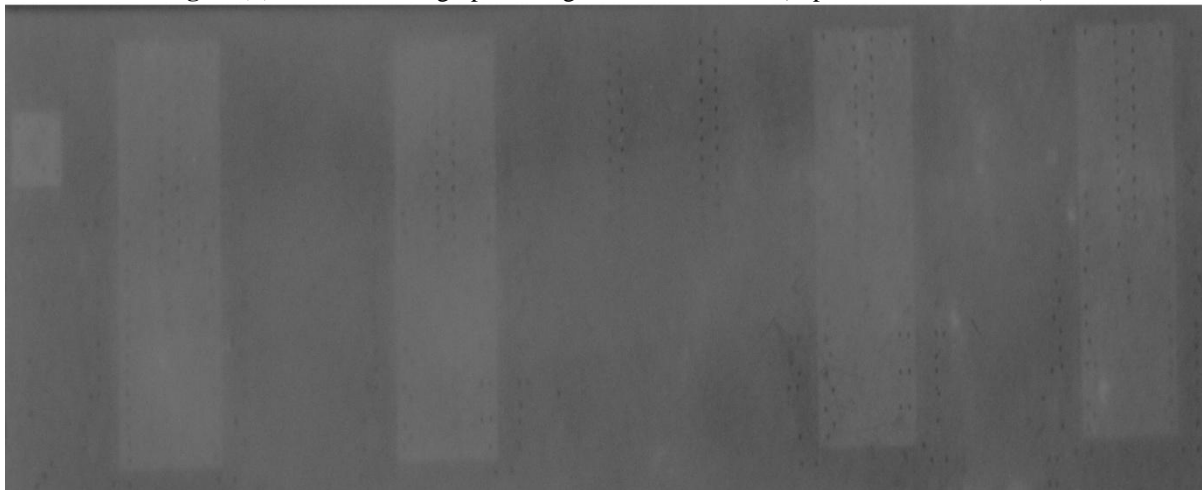


Fig 1.2(a): Neutron radiographic image of RAM DDR-2 (exposure time 2.75 min)

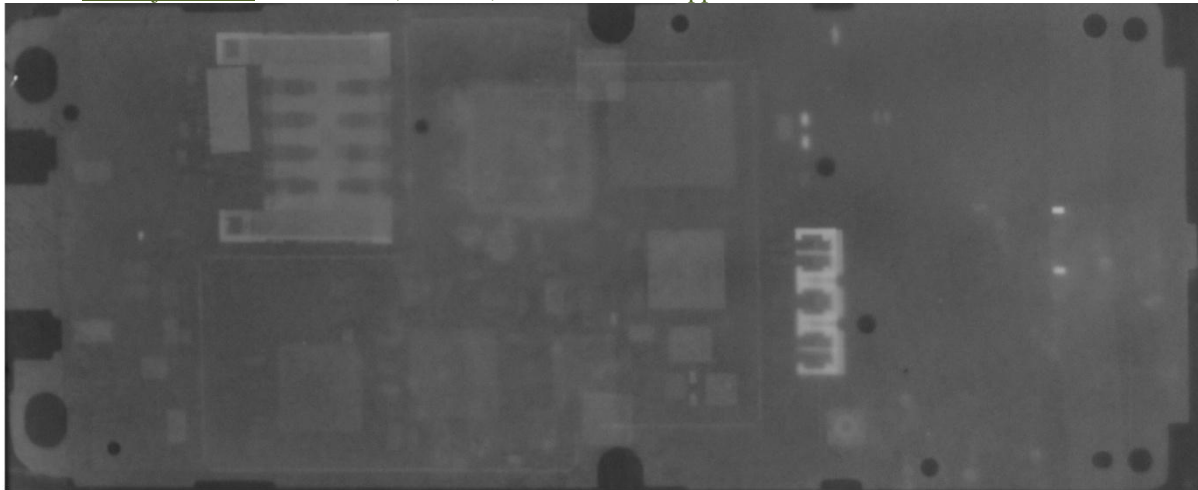


Fig 1.2(b): Neutron radiographic image of NOKIA-3120 (exposure time 2.75 min)

IV. CONCLUSIONS

We got some spots in the samples RAM DDR-2 and Motherboard of Nokia-3120 by using neutron radiography technique. Some spots indicated the discontinuity (Connection defect) in the samples. There are distinct from good one. This NR technique is a very useful technique to observe internal defects of different industrial products also.

REFERENCES

- [1] Alam M. K. and Islam M. N. (2007). Study of internal defects in different tiles using film neutron radiography technique. *Journal of Nuclear Science and Applications*. 16 (1): 17.
- [2] Alam M. K. and Khan M. A. (2006). Study of water absorption and internal defects in jute reinforced biopol composite using digital neutron radiography technique. *Journal of Bangladesh Academy of Sciences*. 30: 29.
- [3] Alam M. K., Khan M. A. and Lehmann E. H. (2006). Comparative study of water absorption behavior in Biopol and jute reinforced biopol composite using neutron radiography technique. *Journal of Reinforced Plastics & Composite*. 25: 1179.
- [4] Alam M. K., Khan M. A., Lehmann E. H. and Vontobel, P. (2007). Study of water uptake and internal defects of jute reinforced polymer composites using digital neutron radiography technique. *Journal of Applied Polymer Science*. 105 : 1958.
- [5] Arnold H. B. (1969). Methods for the study of sedimentary structures. A text book, Published by John Wiley and Sons and the author Arnold Bouma, New York, 1969, pp. 140.
- [6] Barton J. P. (1967). *Materials evaluation*, 45A: 259.
- [7] Harms A. A. and Wyman D. R. (1986) Mathematics and physics of neutron radiography, (D. Reidel Publishing Company, Holland), pp. 22.
- [8] Islam M. N., Alam M. K., Zaman M. A., Ahsan M. H. and Molla N. I. (2000). Application of neutron radiography to building industries. *Indian Journal of Pure & Applied Phys.* 38: 348.
- [9] Islam M. N., Rahman M. M., Zaman M. A. and Islam S. M. A. (2000). Neutron radiographic investigation of the quality of some rubber samples. *Indian Journal of Pure and Applied Phys.* 38: 675.
- [10] Islam M. N., Rahman M. M., Ahsan M. H., Mollah A. S., Ahsan M. M. and Zaman M. A. (1995). A study of neutron radiography parameters at the tangential beam port of the 3 MW TRIGA research reactor of AERE, Savar. *Jahangirnagar University Journal of Sciences*. 19: 181.
- [11] Norris P. M., Brenizer J. S., Raine D. A. and Bostain D. A. (1996). Measurements of water deposition in aerogel by neutron radiography. 5th World Conference on neutron radiography, 17-20 June, 1996 Berlin, Germany.
- [12] Rahman M. A., Podder J. and Kamal I. (1989). Neutron radiography facility in Bangladesh research reactor. Proceedings of 3rd World Conference on neutron radiography, NR 3, May 14-18, 1989, Osaka, Japan.
- [13] Renfrew C. and Bahn P. (1996). Archaeology: Theories, Methods, and Practice. *New York: Thames and Hudson*
- [14] Rice P. (1987). *Pottery Analysis: A Sourcebook*. Chicago: University of Chicago Press, New York.

Tracing and Transmission Cost Allocation of Active Power Flow Based On Extended Incidence Matrix

N.Prakash Reddy¹, Prof. P.Sangameswara Raju²

1-M.tech student Department Of E.E.E, Svuce, Tirupati, India

2-Professor Department Of E.E.E, Svuce, Tirupati, India

ABSTRACT: In the present open access restructured power system market, it is necessary to develop an appropriate pricing scheme that can provide the useful economic information to the market participants such as generation, transmission companies and customers. Because of the introduction of competition in the electricity supply industry, it has become much more important to be able to determine which generators are supplying a particular load, how much use each generator is making of a transmission line and what is each generator's contribution to the system losses. However, accurately estimating and allocating the transmission cost in the transmission pricing scheme is a challenging task although many methods have been proposed. The objective is to introduce a simple transmission pricing scheme using a power flow tracing method, in which transmission service cost is considered. The proposed method is an analytical method for tracing of power flow based on the concept of extended incidence matrix (EIM). The proposed method can handle any power system with or without loop flows and is flexible to start with an AC or DC power flow solution. After obtaining the load flow solution, the extended incidence matrix, distribution factor matrix and load extraction matrix are developed. Using the extended incidence matrix, the contribution of generator to each load and line are calculated. Then the Transmission service charge is allocated among the generators and loads according to the 50/50 split savings method. The effectiveness of the proposed method is illustrated using a 4-bus, IEEE 14-bus system, IEEE 30-bus system.

Keywords: Extended incidence matrix, loop flows, Power flow tracing.

I. INTRODUCTION

Tracing power flow (TPF) has been received more attention in recent years due to power industry restructuring. For power systems under the environment of deregulation and transmission open access, it is extremely important to calculate contributions of individual generators and loads to line flows, active power transfers between individual generators and loads, distributions of power losses and charges for the utilization of lines. Many methods have been presented to solve the TPF problem. The most popular approaches include topological generation distribution factors, nodal generation distribution factors and factors based on the generator domains. Presented an approach which is suitable for large-scale power systems. Based on the concept of extraction and contribution factor matrix, a method was suggested by using downstream and upstream tracing sequences. By using the concept of loop flow coefficient and series theory, proposed a TPF method based on graph theory which can be applied to networks with loop flows. Presented some models and algorithms for determining the contribution of individual generators and loads to power losses or energy losses. A main principle used to trace electricity flow in the published literatures so far is proportional sharing. The principle described in assumes that each outflow (a flow leaving a node) on a line is dependent only on the voltage gradient and impedance of the line, and that the contribution of each inflow (a line flow entering the node) to each outflow is in the same proportion as the inflow on each line divided by the total inflow of all lines at the node. The proportionality described in assumes that if the proportion of the inflow which can be traced to generator i is x_i , then the proportion of the outflow which can be traced to generator i is also x_i . The method proposed in is based on the assumption that the ratio of each bus load to the total system load is constant. All the principles can be easily utilized from an application point. This paper presents an analytical model for TPF based on the concept of extended incidence matrix (EIM). The proposed method does not need any assumption associated with the power sharing principle. It can handle any power system with or without loop flows and is flexible to start with an AC or DC power flow solution. The results of case studies indicate that the implicit distribution principle of the proposed method has the same effect as the explicit proportional principle in for cases without loop flow whereas it can also deal with cases with loop flow using the same formulation and procedure.

II. TRACING OF POWER FLOW USING EXTENDED INCIDENCE MATRIX

The proposed method is an analytical method for tracing of power flow based on the concept of extended incidence matrix (EIM). The proposed method does not need any assumption associated with the power sharing principle. It can handle any power system with or without loop flows and is flexible to start with an AC or DC power flow solution. The elements of the EIM will represent the power flow relationship between the buses.

2.1 Formation of EIM:

According to Kirchhoff's first law, the total inflow at a bus equals the total outflow from the same bus in any network. The inflow here is defined as the sum of powers injected by sources and powers imported to a bus from other buses. The outflow is defined as the sum of powers extracted from a bus by loads and powers exported to other buses. The elements of the EIM are formed based on the Eqn.(1) and it is denoted by matrix 'A'.

$$A_{ij} = \begin{cases} -P_{ij} & \text{for } i \neq j \text{ and } P_{ij} > 0 \\ 0 & \text{for } i \neq j \text{ and } P_{ji} > 0 \\ P_{Ti} & \text{for } i = j \end{cases} \dots (1)$$

where $P_{Ti} = \sum_{k=1, k \neq i}^n P_{ki} + P_{Gi}$ and $i, j = 1, 2, \dots, n$; $n = \text{no. of buses}$ (2)

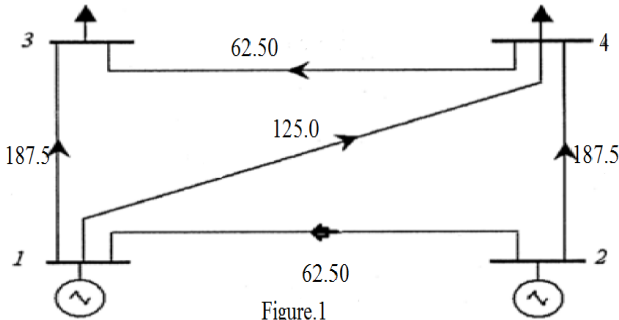


Figure.1

2.2 Properties of Extended incidence matrix:

Property 1. The sum of all elements in any row of an EIM equals the active load power at that bus and it is given in Eqn. 3

$$AE = P_L \dots(3)$$

For system in Fig 1 the sum of all elements in every column of the EIM is [250 250 0 0]. This is the row vector of generation outputs, i.e., (P_G^T) .

Property 2. The sum of all elements in any column of an EIM equals the total active power of generators at that bus k. i.e,

$$A^T E = P_G \dots (4)$$

Property 3. EIM is a diagonally dominant and full rank matrix. In other words, an EIM is an invertible matrix. The Inverse matrix B is

$$B = A^{-1} \dots (5)$$

From Eqns. (3) and (4)

$$E = A^{-1} P_L \dots (6)$$

and

$$E = (A^{-1})^T P_G \dots (7)$$

2.3 Tracing of power flow:

2.3.1 Contribution of each generator to the each load: The Generator capacity of the system can be represented in a matrix and the diagonal matrix is $P_{GG} = \text{diag}(P_{G1}, P_{G2}, \dots, P_{Gn})$. Then the individual generator capacity of the system is given in Eqn. (8)

$$P_G = P_{GG} E \dots (8)$$

By substituting the Eqn. (8) in the Eqn. (6), then

$$P_G = P_{GG} A^{-1} P_L \dots (9)$$

Eqn. (9) directly describes the relationship between P_G and P_L , which gives the contribution of each generator to each load. Rewriting the Eqn. (9)

$$P_G = K P_L \dots (10)$$

where, $K = P_{GG} A^{-1}$

And K is known as Distribution-Factor-Matrix (DFM).

In general, the individual generator capacity is

$$P_{Gi} = \sum_{j=1}^n K_{ij} P_{Lj} \dots(11)$$

where $K_{ij} P_{Lj}$ equals the active power contribution of generator output at bus i to the load at bus j. We denote:

$$P_{i \rightarrow j} = K_{ij} P_{Lj} \dots(12)$$

For the network shown in Fig 1, $P_{GG} = \text{diag} [250 \ 250 \ 0 \ 0]$ and the DFM is obtained by

$$K = \begin{bmatrix} 0.8 & 0 & 0.68 & 0.32 \\ 0.2 & 1.0 & 0.32 & 0.68 \\ 0 & 0 & 0 & 0 \\ 0 & 0 & 0 & 0 \end{bmatrix} \quad \dots(13)$$

It can be seen that the sum of all elements in every column of matrix K equals 1.

$$E^T K = E^T \quad \dots(14)$$

Eqs.(9),(10),(14) indicates the fact that the load at every bus equals the power extracted from all generators and the DFM gives the distribution relationship between loads and generators. Based on Eqs. (12),(13), the power transfers from generator 1 to load 3 and generator 2 to load 4 in LPN shown in Fig 1 are

$$P_{1 \rightarrow 3} = 0.6800 \times 250 = 170$$

$$P_{2 \rightarrow 4} = 0.3200 \times 250 = 80$$

2.3.2 Contribution of each generator to the each line flow:

From the distribution-factor-matrix, the each generator contribution to the each load through the different transmission lines in the network is obtained. So therefore, the each generator (i) contribution to power flow in each line flow($s-t$) is given by

$$P_{i \rightarrow s-t} = K_{is} * P_{s-t} \quad \dots (15)$$

where P_{s-t} = Power flow in each line($s-t$)

$P_{i \rightarrow s-t}$ = Power flow in line($s-t$) due to the generator (i)

The power transfer from generator 1 and 2 to line 4-3 in network is

$$P_{1 \rightarrow 4-3} = K_{14} P_{43} = 0.3200 \times 187.50 = 60$$

$$P_{2 \rightarrow 4-3} = K_{24} P_{43} = 0.200 \times 187.50 = 37.5$$

2.3.3 Power extracted by loads from generators:

The above description is based on the idea that each generator makes contribution to each load. We can also view the power flow tracing problem from another angle each load extracts power from each generator. Under this view, the EIM with loads extracting power from generators is the transformation matrix of the EIM with generators transferring power to loads.

The dual equation for Eqn. (9) is obtained as:

$$P_L = P_{LL} (A^{-1})^T * P_G \quad \dots (16)$$

Eqn. (16) directly describes the relationship between P_L and P_G , which gives the contribution of each generator to each load. Rewriting the Eqn.

$$P_L = L P_G \quad \dots (17)$$

where,

$$L = P_{LL} (A^{-1})^T$$

And L = Load extraction matrix.

$$L = \begin{bmatrix} 0 & 0 & 0 & 0 \\ 0 & 0 & 0 & 0 \\ 0.68 & 0.32 & 1.0 & 0.2 \\ 0.32 & 0.68 & 0 & 0.80 \end{bmatrix} \quad \dots\dots\dots(18)$$

For instance, the power extracted by load 3 from generator 1 is. $0.68 \times 250 = 170$, which is the same as the power contributed from generator 1 to load 3, as calculated in section 2.3

2.3.4 Power extracted by loads from each line flow:

From the extraction factor matrix, the each load extracts the power from the different transmission lines in the network. So therefore, power extraction by each load (i) from each line ($s-t$) is given in Eqn. 2.16.

$$P_{i \rightarrow s-t} = L_{si} * P_{s-t} \quad \dots (19)$$

where P_{s-t} = Power flow in each line($s-t$)

$P_{i \rightarrow s-t}$ = Power extracted by load (i) in flow line ($s-t$).

3.5 Allocation of Transmission service charge to generators and demands:

Generally, the transmission service cost is obtained as the sum of the costs of each transmission line. The cost of each line is directly obtained from its reactance value and the cost is given by $C = 1000 * x$ where reactance x is in p.u. and the total transmission service cost is considered as 50/50 split between generators and demands. Consider the usage cost of line $s-t$ is denoted as C_{s-t} (in Rs/h), then the charge allocated to a generator for this usage cost of line $s-t$ is given by

$$C_{i \rightarrow s-t} = \frac{C_{s-t}}{2} * \frac{P_{i \rightarrow s-t}}{P_{ij}} \quad \dots (20)$$

The total charge allocated to generators at any bus for the usage of all lines is

$$C_{i \rightarrow s-t} = \sum_{ij \in \emptyset} C_{i \rightarrow s-t} \quad \dots (21)$$

Where C_k is the total allocated charge for the generators at bus k , and \emptyset is the branch set. Similarly, the charge allocated to a load for the use of all lines is calculated by Eqn. (20) and the total charge allocated to loads at any bus for the usage of all lines is calculated by Eqn. (21)

III. ALGORITHM STEPS FOR THE TRACING OF ACTIVE POWER FLOW USING EIM:

- Step 1: Read the bus and line data (If phase shifting transformer is present Read the Phase shift Angle)
 Step 2: Form the Y-bus using the Singular Transformation method in AC power flow
 (Or) Form the susceptance matrix in the case of DC power flow.
 Step 3: Obtain the line flows and line losses from the NR method in case of AC power flow and DC power flow
 Step 4: Form the EIM using the Eqn.(1)
 Step 5: Obtain the B matrix using the Eqn. (5)
 Step 6: Obtain the Distribution Factor matrix (K) using the Eqn. (10)
 Step 7: Obtain the contribution of each generator to each load using the Eqn.(11)
 Step 8: Obtain the contribution of each generator to each line flow using the Eqn.(15)
 Step 9: Obtain the Load extraction matrix (L) using the Eqn. (17)
 Step10: Obtain the contribution of each line flow to the load using the Eqn. (19)
 Step 11: Allocate the transmission service charge to the each generator and the each load using Eqn.(20)
 Step 12: Print the results
 Step 13: STOP

IV. SIMULATION RESULTS AND DISCUSSION**IEEE 30-BUS SYSTEM(AC power flow)****Table 1 Generator contribution to each load (AC power flow)**

Bus	Load(MW)	Gen1(MW)	Gen 2(MW)	Gen5 (MW)	Gen8 (MW)	Gen 11(MW)	Gen 13 (MW)
1	0.0	0	0	0	0	0	0
2	21.7	13.1369	8.5631	0	0	0	0
3	2.4	2.400	11.7050	0	0	0	0
4	7.6	6.4815	0	0	0	0	0
5	94.2	43.9766	8.6694	24.1808	0.1591	0	0
6	0.0	0.0000	0	0	0	0	0
7	22.8	16.5430	5.9824	0	0.2746	0	0
8	30.0	0	0	0	30	0	0
9	0.0	0	0	0	0	0	0
10	5.8	2.5212	0.9117	0	0	2.3252	0
11	0.0	0	0	0	0.0418	0	0
12	11.2	5.9166	1.0210	0	0	0	4.2623
13	0.0	0	0	0	0	0	0
14	6.2	3.2753	0.5652	0	0	0	2.3595
15	8.2	4.3318	0.7475	0	0	0	3.1206
16	3.5	1.8490	0.3191	0	0	0	1.3320
17	9.0	4.0254	1.3349	0	0.0562	3.1233	0.4603
18	3.2	1.6905	0.2917	0	0	0	1.2178
19	9.5	4.4573	1.2621	0	0.0433	2.404	1.3328
20	2.2	0.9563	0.3458	0	0.0159	0.8820	0
21	17.5	7.6070	2.7509	0	0.1263	7.0158	0
22	0.0	0	0	0	0	0	0
23	3.2	1.6905	0.2917	0	0	0	1.2178
24	8.7	4.1360	1.1549	0	0.1080	2.0025	1.2985
25	0.0	0	0	0	0	0	0
26	3.5	1.9389	0.7011	0	0.8600	0	0
27	0.0	0	0	0	0	0	0
28	0.0	0	0	0	0	0	0
29	2.4	1.3295	0.4808	0	0.5897	0	0
30	10.6	5.8720	2.1235	0	2.6046	0	0

From the Table 1 for the load 2, the contribution of the generator 1 is 13.1369MW and the contribution of the generator 2 is 8.5631MW the remaining generators 8, 11, 13 do not contribute to the load 2. From the proposed method the cost allocation to the generator is calculated using Eqn. 2.17 and the results are tabulated in Table 2

Table 2 Allocation of transmission cost to the Generators (AC power flow)

Line (s-t)	Gen-1 cost(Rs/hr)	Gen-2 cost(Rs/hr)	Gen-5 cost(Rs/hr)	Gen-8 cost(Rs/hr)	Gen-11 cost(Rs/hr)	Gen-13cost(Rs/hr)	Transmission cost(C=x*1000)
1-2	28.7500	0	0	0	0	0	57.5000
1-3	82.6000	0	0	0	0	0	165.2000
2-4	52.5780	34.2720	0	0	0	0	173.7000
3-4	18.9500	0	0	0	0	0	37.9000
2-5	60.0243	39.1257	0	0	0	0	198.3000
6-2	53.3650	34.7850	0	0	0	0	176.3000
6-4	17.6536	3.0464	0	0	0	0	41.4000
5-7	42.0832	15.2184	0	0.6985	0	0	116.0000
6-7	29.7484	10.7578	0	0.4938	0	0	82.0000
6-8	0	0	0	21.0000	0	0	42.0000
6-9	108.1102	39.0954	0	1.7944	0	0	298.0000
6-10	201.7090	72.9431	0	3.3479	0	0	556.0000
9-11	0	0	0	0	104.0000	0	208.0000
9-10	17.8729	6.4633	0	0.2966	30.3672	0	110.0000
4-12	109.1621	18.8379	0	0	0	0	256.0000
12-13	0	0	0	0	0	70.0000	140.0000
12-14	67.5924	11.6643	0	0	0	48.6933	255.9000
12-15	34.4433	5.9438	0	0	0	24.8128	130.4000
12-16	52.4838	9.0570	0	0	0	37.8091	198.7000
14-15	52.7480	9.1026	0	0	0	37.9994	199.7000
16-17	50.7934	8.7653	0	0	0	36.5913	192.3000
15-18	57.7137	9.9595	0	0	0	41.5767	218.5000
18-19	34.1264	5.8891	0	0	0	24.5845	129.2000
19-20	14.7794	5.3446	0	0.2453	13.6307	0	68.0000
10-20	45.4248	16.4268	0	0.7539	41.8945	0	209.0000
10-17	18.3655	6.6414	0	0.3048	16.9382	0	84.5000
10-21	16.2790	5.8869	0	0.2702	15.0138	0	74.9000
22-10	32.5798	11.7817	0	0.5407	30.0477	0	149.9000
22-21	5.1293	1.8549	0	0.0851	4.7307	0	23.6000
15-23	53.3555	9.2075	0	0	0	38.4371	202.0000
22-24	38.9045	14.0689	0	0.6457	35.8809	0	179.0000
23-24	71.3167	12.3070	0	0	0	51.3763	270.0000
25-24	91.1818	32.9737	0	40.4445	0	0	329.2000
25-26	105.2524	38.0620	0	46.6856	0	0	380.0000
25-27	57.8057	20.9040	0	25.6402	0	0	208.7000
28-27	109.6841	39.6646	0	48.6513	0	0	396.0000
27-29	115.0298	41.5977	0	51.0224	0	0	415.3000
27-30	166.9359	60.3683	0	74.0458	0	0	602.7000
29-30	125.5551	45.4039	0	55.6910	0	0	453.3000
28-8	0	0	0	100.0000	0	0	200.0000
6-28	21.7309	7.8584	0	0.3607	0	0	59.9000
Total cost	2261.8	705.3	0	473	292.5	411.9	8289 Rs/hr

From the Table 2 It is observed that total cost allocated for generators is 4144.5 Rs/hr (2261.8+705.3+473+292.5+411.9) which is half of the total cost of the transmission service cost which is 8289 Rs/hr.

IEEE 30 bus system (DC POWER FLOW)

Table 3 Generator contribution to each load (DC power flow)

Bus	Load(MW)	Gen1(MW)	Gen2(MW)	Gen5(MW)	Gen8(MW)	Gen11(MW)	Gen13(MW)
1	0.0	0	0	0	0	0	0
2	21.7	12.8588	8.8412	0	0	0	0
3	2.4	2.4	0	0	0	0	0
4	7.6	6.429	1.1710	0	0	0	0
5	94.2	42.9855	26.4960	24.56	0.1584	0	0
6	0.0	0	0	0	0	0	0
7	22.8	16.3170	6.2243	0	0.2587	0	0
8	30.0	0	0	0	30.00	0	0
9	0.0	0	0	0	0	0	0
10	5.8	2.4693	0.9420	0	0.0391	2.3496	0
11	0.0	0	0	0	0	0	0
12	11.2	5.7578	1.0487	0	0	0	4.3935
13	0.0	0	0	0	0	0	0
14	6.2	3.1873	0.5805	0	0	0	2.4321
15	8.2	4.2155	0.7678	0	0	0	3.2167
16	3.5	1.7993	0.3277	0	0	0	1.3730
17	9.0	4.1212	1.2363	0	0.0386	2.3183	1.2856

18	3.2	1.6451	0.2996	0	0	0	1.2553
19	9.5	4.2727	1.3653	0	0.0467	2.8024	1.0129
20	2.2	0.9366	0.3573	0	0.0148	0.8912	0
21	17.5	7.4506	2.8421	0	0.1181	7.0892	0
22	0.0	0	0	0	0	0	0
23	3.2	1.6451	0.2996	0	0	0	1.2553
24	8.7	3.9575	1.3306	0	0.2469	2.4794	0.6856
25	0.0	0	0	0	0	0	0
26	3.5	1.9073	0.7276	0	0.8651	0	0
27	0.0	0	0	0	0	0	0
28	0.0	0	0	0	0	0	0
29	2.4	1.3079	0.4989	0	0.5932	0	0
30	10.6	5.7764	2.2035	0	2.6201	0	0

Table 4 Allocation of transmission cost to the Generators

Line (s-t)	Gen-1 cost(Rs/hr)	Gen-2 cost(Rs/hr)	Gen-5 cost(Rs/hr)	Gen-8 cost(Rs/hr)	Gen-11 cost(Rs/hr)	Gen-13 cost(Rs/hr)	Transmission cost(C=x*1000)
1-2	28.7500	0	0	0	0	0	57.5000
1-3	82.6000	0	0	0	0	0	165.2000
2-4	51.4650	35.3850	0	0	0	0	173.7000
3-4	18.9500	0	0	0	0	0	37.9000
2-5	58.7537	40.3963	0	0	0	0	198.3000
6-2	52.2353	35.9147	0	0	0	0	176.3000
6-4	17.5106	3.1894	0	0	0	0	41.4000
5-7	41.5082	15.8338	0	0.6581	0	0	116.0000
6-7	29.3420	11.1928	0	0.4652	0	0	82.0000
6-8	0	0	0	21.0000	0	0	42.0000
6-9	106.6331	40.6764	0	1.6906	0	0	298.0000
6-10	198.9530	75.8929	0	3.1542	0	0	556.0000
9-11	0	0	0	0	104.0000	0	208.0000
9-10	17.5950	6.7118	0	0.2790	30.4142	0	110.0000
4-12	108.2780	19.7220	0	0	0	0	256.0000
12-13	0	0	0	0	0	70.0000	140.0000
12-14	65.7772	11.9808	0	0	0	50.1920	255.9000
12-15	33.5184	6.1051	0	0	0	25.5765	130.4000
12-16	51.0744	9.3028	0	0	0	38.9728	198.7000
14-15	51.3314	9.3496	0	0	0	39.1690	199.7000
16-17	49.4293	9.0032	0	0	0	37.7175	192.3000
15-18	56.1638	10.2298	0	0	0	42.8564	218.5000
18-19	33.2099	6.0489	0	0	0	25.3412	129.2000
19-20	14.4754	5.5218	0	0.2295	13.7733	0	68.0000
10-20	44.4906	16.9715	0	0.7054	42.3326	0	209.0000
10-17	17.9878	6.8617	0	0.2852	17.1153	0	84.5000
10-21	15.9442	6.0821	0	0.2528	15.1709	0	74.9000
22-10	31.9098	12.1723	0	0.5059	30.3620	0	149.9000
22-21	5.0238	1.9164	0	0.0796	4.7801	0	23.6000
15-23	51.9226	9.4573	0	0	0	39.6201	202.0000
22-24	38.1044	14.5354	0	0.6041	36.2561	0	179.0000
23-24	69.4015	12.6409	0	0	0	52.9575	270.0000
25-24	89.6975	34.2161	0	40.6864	0	0	329.2000
25-26	103.5390	39.4961	0	46.9649	0	0	380.0000
25-27	56.8647	21.6917	0	25.7936	0	0	208.7000
28-27	107.8985	41.1591	0	48.9424	0	0	396.0000
27-29	113.1572	43.1651	0	51.3277	0	0	415.3000
27-30	164.2183	62.6429	0	74.4888	0	0	602.7000
29-30	123.5111	47.1147	0	56.0242	0	0	453.3000
28-8	0	0	0	100.0000	0	0	200.0000
6-28	21.4340	8.1762	0	0.3398	0	0	59.9000
Total cost	2222.7	730.7	0	474.5	294.2	422.4	8289 Rs/hr

From the Tables 1,2,3,4, it is observed that the power contributed by the generator to the loads are different in both AC and DC power flows, but the total cost allocated for generators is 4144.5 Rs/hr which is half of the total cost of the transmission service cost which is 8289 Rs/hr is same in case of both AC and DC power flows.

V. Conclusions

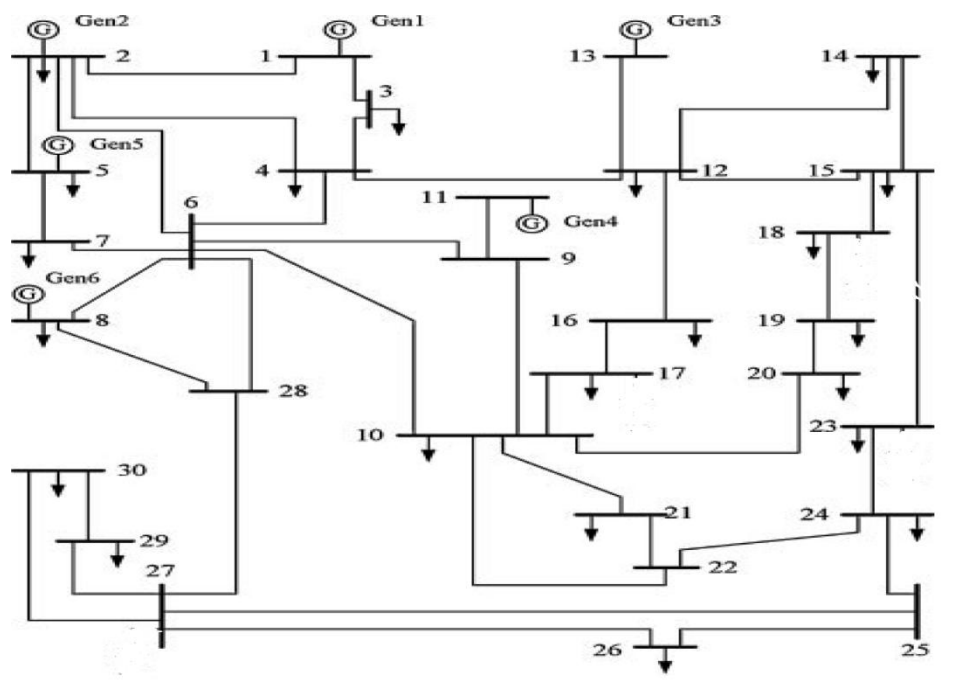
In the analysis of the IEEE 30 bus system, it was concluded that the each generator contribution to the load is different in AC and DC power flows, but the total cost allocated to generators are same in both AC and DC power flows. From the total analysis, it is concluded that the proposed method is used for any system like AC, DC, without loop and with loop power flow systems.

FUTURE SCOPE OF THE WORK

- In this project, the proposed method is developed without considering the type of the conductor. It can be further developed by considering the type of the conductor.
- The proposed method is applied for the single area interconnected system. It can be further developed for the multiple area interconnected systems.
- The proposed method is developed with considering the real power flow. It can be further developed by considering the reactive power flow.

REFERENCES

- [1] J. Bialek, "Tracing the flow of electricity", IEEE Proceedings on Generation, Transmission and Distribution, Vol. 143, No. 4, Apr. 1996, pp.313–320.
- [2] J. Bialek, "Topological generation and load distribution factors for supplement charge allocation in transmission open access", IEEE Transactions on Power System, Vol. 12, No. 3, Mar. 1997, pp.1185–1190.
- [3] J. Bialek, "Allocation of transmission supplementary charge to real and reactive loads", IEEE Transactions on Power Systems, Vol. 13, No. 3, Mar. 1998, pp. 749–754.
- [4] F.F.Wu, Y. Ni, "Power transfer allocation for open access using graph theory", IEEE Transactions on Power System, Vol. 15, No. 3, Mar. 2000, pp. 923–929.
- [5] F. Gubina, D. Grgic, I. Banic, "A method for determining the generators share in a consumer load", IEEE Transactions on Power System, Vol. 15, No. 4, Apr. 2000, pp.1376–1381.
- [6] A.R.Abhyankar, S.A. Soman, S.A. Khaparde, "Optimization approach to real power tracing: an application to transmission fixed cost allocation", IEEE Transactions on Power Systems, Vol. 21, No. 3, Mar. 2006, pp.1350–1361.
- [7] J.W. Bialek, P.A. Kattuman, "Proportional sharing assumption in tracing methodology", IEEE Proceedings on Generation, Transmission and Distribution, Vol. 151, No. 4, Apr. 2004, pp. 526–532.
- [8] Sanjoy Kumar Saha, "Sparse Matrix solution in Optimal D.C Load Flow by Crout Method", IJRTE, Vol. 2, No. 7, November 2009.

**Fig. 1 Single line Diagram of IEEE 30 bus system****Table 5 IEEE 30 bus system Line data**

Sending bus	Receiving bus	R(p.u)	X(p.u)	B(p.u)	Taps	Cost(Rs/hr)
1	2	0.0192	0.0575	0.0528	1.0000	57.5000
1	3	0.0452	0.1652	0.0408	1.0000	165.2000
2	4	0.057	0.1737	0.0368	1.0000	173.7000
3	4	0.0132	0.0379	0.0084	1.0000	37.9000
2	5	0.0472	0.1983	0.0418	1.0000	198.3000

6	2	0.0581	0.1763	0.0374	1.0000	176.3000
6	4	0.0119	0.0414	0.0090	1.0000	41.4000
5	7	0.0460	0.1160	0.0204	1.0000	116.0000
6	7	0.0267	0.082	0.0170	1.0000	82.0000
6	8	0.0120	0.0420	0.0090	1.0155	42.0000
6	9	0	0.2080	0	0.9629	298.0000
6	10	0	0.5560	0	1.0000	556.0000
9	11	0	0.2080	0	1.0000	208.0000
9	10	0	0.1100	0	1.0130	110.0000
4	12	0	0.2560	0	1.0000	256.0000
12	13	0	0.1400	0	1.0000	140.0000
12	14	0.1231	0.2559	0	1.0000	255.9000
12	15	0.0662	0.1304	0	1.0000	130.4000
12	16	0.9450	0.1987	0	1.0000	198.7000
14	15	0.2210	0.1997	0	1.0000	199.7000
16	17	0.0824	0.1923	0	1.0000	192.3000
15	18	0.1073	0.2185	0	1.0000	218.5000
18	19	0.0639	0.1292	0	1.0000	129.2000
19	20	0.034	0.0680	0	1.0000	68.0000
10	20	0.0936	0.2090	0	1.0000	209.0000
10	17	0.0324	0.0845	0	1.0000	84.5000
10	21	0.0348	0.0749	0	1.0000	74.9000
22	10	0.7270	0/1499	0	1.0000	149.9000
22	21	0.0116	0.0236	0	1.0000	23.6000
15	23	0.1000	0.2020	0	1.0000	202.0000
22	24	0.1150	0.1790	0	1.0000	179.0000
23	24	0.1320	0.2700	0	1.0000	270.0000
25	24	0.1885	0.3292	0	1.0000	329.2000
25	26	0.2544	0.3800	0	1.0000	380.0000
25	27	0.1093	0.2087	0	1.0000	208.7000
28	27	0	0.396	0	1.0000	396.0000
27	29	0.2198	0.4153	0	1.0000	415.3000
27	30	0.32020	0.6027	0	1.0000	602.7000
29	30	0.2399	0.4533	0	1.0000	453.3000
28	8	0.0636	0.2000	0.0428	1.0000	200.0000
6	28	0.0169	0.0590	0.1300	1.0000	59.9000

Characterisation of potential pollution sources in the quantitative assessment of risk to groundwater resources within the Birmingham aquifers, UK

O.S.Oladeji^{1†} and J. Elgy²

¹Dept of Civil Engineering, Ladole Akintola University of Technology, Ogbomoso Nigeria.

† Corresponding Author

²Sustainable Environment Research Group, School of Engineering and Applied Science, Aston University, Aston Triangle, Birmingham, B4 7ET, United Kingdom

ABSTRACT: This work presents a methodological approach where distribution of potential pollution sources and historical frequency of pollution incidents are included in the assessment of risk to groundwater resources. Calibrated flow and transport models were setup, and integrated with a FORTRAN coded risk model. The risk model was run to generate synthetic contaminant source terms that were subsequently transported by the coupled flow and transport models. The ranges of calibrated values obtained for horizontal and vertical hydraulic conductivities are 5.787×10^{-6} - 2.315×10^{-5} m/s and 5.787×10^{-8} - 1.157×10^{-7} m/s, respectively. Layering within the aquifer is thought to account for the large vertical anisotropy. The corresponding values for the specific yield and specific storage are 0.10 - 0.12, and 1×10^{-4} - 5×10^{-4} , respectively. The estimated historical frequency of pollution occurrence per stress period of 91 days is 35, while the probability of pollution occurring at any of the sources over a period of stress period is calculated as 0.0014. The generated risk maps provide anticipatory capability for risk quantification and show that approximately 55% of the monitoring boreholes have high (i.e. 70 – 100 %) likelihood of having contaminant concentration being less than 0.06 mg/l throughout the simulation.

KEYWORDS: Quantitative risk, Groundwater modelling, Probability, Vulnerability, Risk model

I. INTRODUCTION

The statistics of groundwater use (Zektste and Everett, 2004) has shown that groundwater has become one of the most important global natural resources. In Denmark, Malta and Saudi Arabia, groundwater constitutes the only major source of water supply, while in Tunisia and Belgium, approximately 95 and 83 % respectively of the country's water resources is sourced from groundwater. This importance is underpinned by the inherent valuable properties of the resource compared to the surface water. These properties include higher quality, better protection from anthropogenic activities, less seasonal variation, large storage, relatively inexpensive developmental cost and wide spread occurrence, among others. However, occurrences of global pollution is increasingly becoming one of the major environmental concerns that pose threats to groundwater resources and can potentially cause depletion of these values. Cases of pollution occurrences have been reported in Beijing in China (Marilyn, 2001), Taejon area in Korea (Jeong, 2001), as well as in the developing countries (Egbu, 2004). The scale of impacted groundwater bodies is becoming more widespread and the persistence of groundwater pollutants is increasing, making the cost of aquifer restoration to be excessive in many cases. Therefore, pollution prevention rather than pollution management appears to proffer the basis for a truly sustainable approach to groundwater protection.

Generally, the extent of protection of groundwater resources is assessed based on the risk posed by anthropogenic activities, or the measure of ease with which an infiltrating pollutant reaches the groundwater resource. The contemporary techniques for the assessment of risk and vulnerability to groundwater can be broadly be categorized into three groups namely: ranking index methods, process-based computer simulation, and post-pollution assessment methods (Al-Adamat *et al.*, 2003; Aller *et al.*, 1985; Connell and Dale, 2003; Foster, 1987; Gustafson, 1989; Van Stempvoort *et al.*, 1992; Khan and Liang, 1989; Rao *et al.*, 1985; and USEPA, 1989). According to Haines (2006), risk is defined as the result of a threat with adverse effects to a vulnerable system. Following from this definition, it implies that the most vulnerable groundwater is not at risk without the presence of threats. This concept of risk therefore comprises of two-dimensional components. From the point of view of the water resources, the first component is the probability of contaminant source terms being generated from potential pollution sources at the ground surface while the second component is the assessment of impact of such occurrence. The ranking index methods are essentially qualitative and subjective in approach, and generally lacking good scientific judgement. Also, none of the existing methods incorporates quantifications of the probability of occurrence of polluting source terms from the potential sources.

In this work, potential pollution source is defined as a single, identifiable and localized source with risk of discharging pollutants that may infiltrate into the aquifer. Hence, the fact that potential sources often constitute threats to groundwater resources necessitates the need to include their occurrence and distribution in quantifying any risk posed to the underlying groundwater resources. Quantifying the probability of occurrence of pollution is generally the most uncertain part of the assessment of risk posed to groundwater system. Therefore, this work is set to demonstrate the field application of a novel two-dimensional risk assessment methodological approach, where assessment of risk to groundwater resource incorporates both the quantification of the probability of occurrence of source terms, as well as the impact of such pollution event. A more detailed discussion on the concept and structure of the method has already been presented in Oladeji and Elgy (2012).

II. METHODOLOGY

The algorithm of the methodology implemented in this work is presented in Figure 1. The risk model components of the Risk Assessment Method (RAM) structure are implemented by a computer program written in a standard FORTRAN 90. The risk model is run over the same period of time as the flow and transport models. Contaminant source terms are generated for each stress period of the simulation, which are then transported within the subsurface environment using the coupled flow and transport models. The effects of the generated source terms are assessed by observing the spatial and temporal concentrations of the contaminant at pre-determined monitoring boreholes within the aquifer, as well as by counting the number of times the contaminant concentration exceeds user defined ranges of concentration magnitude. Two grid systems namely a local system and a global system are implemented in the risk model. This is to allow the risk model to be run independently of the flow and transport models, as well as to increase the efficiency in the implementation of the risk model in terms of the time and memory requirements. The local grid may be equal to or smaller than the global grid system used in groundwater flow and contaminant transport models.

The purpose of the Risk Model Parametization module (see Figure 1) is to prepare the input data for the risk model. This involves obtaining locations of the potential pollution sources at the ground surface. The geographical locations of the potential sources are initially obtained using global positioning equipment, and subsequently transformed into the appropriate layer, row and column numbers of the model grid using GIS utilities.

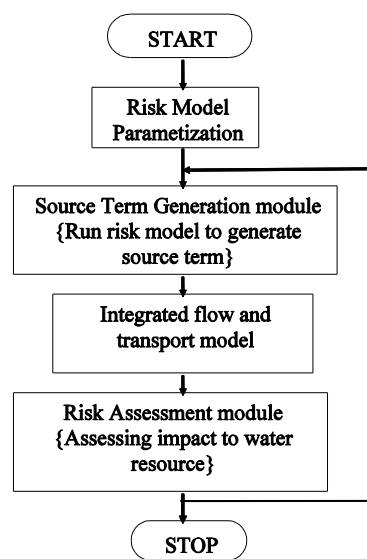


Figure 1: Conceptual algorithm of the risk assessment method

The process of the generation of synthetic source terms by the risk model involves determination of the condition for the generation of a synthetic source term, as well as the magnitude of the associated contaminant mass. In order to determine the condition for the generation of a synthetic source term in any stress period, the risk model computes a parameter called Probability of Pollution Occurrence (PPO) for each of the active model cells containing potential pollution source(s), using Equation 1:

$$PPO = \frac{\text{No of days of previously occurred pollution events} / \text{No of sources}}{\text{Total no. of days under consideration}} \quad (1)$$

Note that equation 1 is implemented when the PPO has to be evaluated during the execution of the risk model. If PPO is already known by priori knowledge, then the values can be entered appropriately.

Next, for each day in the current stress period and for each active node, the risk model generates a Random Number (RN) between 0.0 and 1.0, and compares the random generated number (RN) with the PPO value computed. If $PPO > RN$, then a pollution incident is assumed to occur. However, an array of integer values of between 0 and 5 is set for each model cell, and these dynamically control the actual proportion of infiltrating contaminant mass per each event. For example, a value of 0 indicates that all the synthetically generated probable mass loading rate of contaminant at a particular active node are transported from that source, while a value of 5 indicates that, although synthetic contaminant mass is generated at the source, no pollutant is assumed to be transported from that source. This utility is used to incorporate source control capability as mitigating measures based on the ground conditions. Also, in order to determine a contaminant mass associated with each of the synthetic pollution event, the risk model samples a random value from a range of the minimum and

maximum values of contaminant mass loading rates that have previously occurred based on historical records or other priori knowledge.

In this work, the probability distribution of the historical pollution events is represented by a Poisson distribution. A Poisson distribution expresses the probability of a number of events occurring in a fixed period of time if these events occur with a known average rate and independent of the time since the last event. If the expected number of occurrence in an interval of time is given as λ , then the probability that there are exactly k occurrences (where k being a non-negative integer) is given as:

$$f(k : \lambda) = \frac{\lambda^k e^{-\lambda}}{k!} \quad (2)$$

where e is the base of the natural logarithm, and $k!$ is the factorial of k .

Finally, the risk model extracts the spatial and temporal contaminant source terms generated for all the stress periods, and presents the source terms in a format that is compatible with the transport model input data file. In addition, the risk model transforms the row and column numbers from the local grid system into that of the global grid system used for flow/transport model.

The generated source terms serve as input into the transport model. After each run, the risk model counts the number of times at which the contaminant concentrations exceeds ranges of user defined concentration magnitudes, and express the result as a risk. These steps represents the first realisation of the risk assessment method, and subsequently iterated such that the frequency distribution of the observed contaminant concentration at points of interest in the aquifer is developed by observing the number of times that the user defined concentration magnitude is exceeded.

2.1 Description of the study area

The study area (Figure 2) extends 17 km from south to north, and 13 km from west to east, covering approximately 221 km², and forms part of the larger West Midlands conurbation. Birmingham has been a major manufacturing centre for over a century, and contains many industrial processes that may constitute risk to groundwater. According to Powell *et al.* (2000), the area is underlain by the Triassic sandstone, and consists of fluvioglacial thick successions of the sandstone deposit, commonly referred to as the Sherwood sandstone Group. The basal aquifer unit is the Kidderminster sandstone Formation, overlain by the Wildmoor and Bromsgrove sandstone Formations. These three sandstone aquifer horizons have distinct hydrogeological properties. The superficial geology consists of till, sand, gravel and alluvium, and overlies the Triassic geological successions. The soil types present within the study area are highly varied and complex, and their distribution and composition are influenced by factors such as climate, geology, geomorphology and hydrology. The landuse pattern is largely urban. The major rivers present within the study area are shown in Figure 2.

A major geological structure within the study area is the Birmingham Fault, which juxtaposes the Triassic mudstone to the east against the Triassic sandstone to the west. According to Allen *et al.*, (1997), transmissivity is generally reduced across the Birmingham Fault, and Knipe *et al.*, (1993) modelled the zone across the fault as a reduced aquifer thickness in order to represent the reduced transmissivity across the fault. The Triassic sandstone Group form the major aquifers in the study area, and their hydrogeological characteristics are dominantly controlled by lithological variations, vertical heterogeneity, anisotropy, fractures, scale of measurement, as well as uneven variations in the aquifer thickness (Allen *et al.*, 1997). The inorganic, organic contamination and the occurrence of pollution related acidification within the urban aquifer of Birmingham area have been respectively studied by Ford and Tellam, (1994), Rivett *et al.* (1990), and Ford *et al.* (1992).

2.2 Numerical groundwater flow and transport model

The U.S. Geological Survey numerical finite-difference groundwater flow model MODFLOW 2000 (Harbaugh *et al.* 2000) forms the basis for the model development and the subsequent calibration process. The initial conditions for the model setup are presented in Table 1. For the purpose of model calibration, the model was set up to run under transient conditions covering 20 years from January 1970 to December 1989, and validated using groundwater head data spanning from March 1985 to February 2015. The eastern and the southern boundaries of the aquifer geometry were defined using no flow cells because of the presence of Birmingham Fault which is assumed to inhibit flow across it. Also, the western boundary was defined as no flow because of the presence of the Westphalian Formations, which are older non permeable geological material. The northern boundary was delineated by the groundwater divide along an anticlinal axis on the base of Triassic sandstones (Knipe *et al.*, 1993), and therefore also represented as no flow boundary.

The initial groundwater heads within the aquifer horizons were interpolated from the available groundwater level observation data. Where the river path exists, the initial groundwater head was defined by the river stage. The rivers present within the model domain (see Figure 2) are contained within the first model layer. The Modflow head dependent river package allows the model to calculate the amount of streambed percolation and groundwater inflow to each river reach, using river bed conductance and the difference between the calculated model cell hydraulic head and the stage of the river.

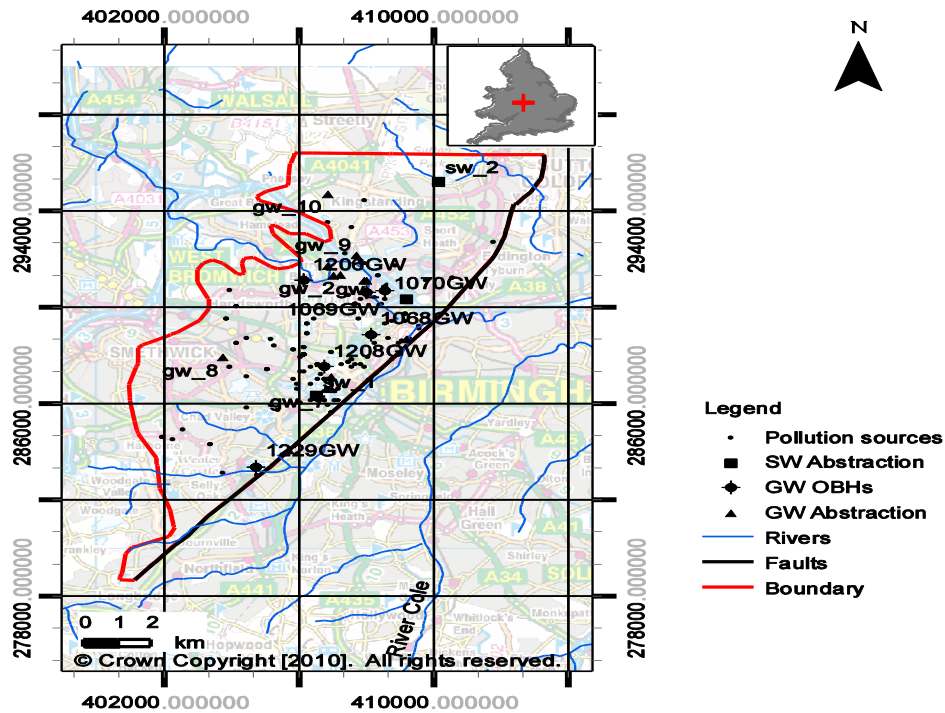


Figure 2: Location of the study area

Table 1: Summary of initial and final flow model data

Input parameter	Initial Conditions
Boundary Conditions	No flow conditions for the west, east, north and south boundaries.
Spatial discretization (m)	No of rows: 760; No of columns: 600; $\Delta x=25$; $\Delta y=25$
Horizontal hydraulic conductivity (m/s)	Bromsgrove Fm = 5.0×10^{-5} Wildmoor sst Fm = 2.0×10^{-4} Kidderminster Fm = 3.0×10^{-4}
Vertical hydraulic conductivity (m/s)	Bromsgrove Fm = 5.0×10^{-7} Wildmoor sst Fm = 1.0×10^{-6} Kidderminster Fm = 5.0×10^{-7}
Specific yield	Bromsgrove Fm = 0.10 Wildmoor sst Fm = 0.10 Kidderminster Fm = 0.10
Specific storage	Bromsgrove Fm = 1×10^{-3} Wildmoor sst Fm = 5×10^{-3} Kidderminster Fm = 1×10^{-3}
Effective Porosity (%)	Layer 1 = 26.8 %; Layer 2 = 23.8 %; Layer 3 = 26.4 %
α_L α_T ; α_{VT} / α_{VL} ; Mol. Diff. Coeff.	20 m ; 0.1 m; 0.01; $0.0 \text{ m}^2/\text{s}$

The river bed conductance controls the rate of flow to or from the river according to the difference between the river stage and the modelled groundwater head in the uppermost active cell. River bed conductance also defines the maximum leakage rate to the aquifer when heads fall below the bed of the river. The river paths contained within the model boundary were divided into reaches. The interaction with the underlying aquifer was simulated between each reach and the model cell that contains that reach. The river bed elevations were estimated from the digital elevation map (DEM), and the river stage was assumed to be 0.5 m above the estimated river bed.

The constant flux well package was used to simulate pumping from the 12 abstraction boreholes (gw_1 – gw_12) located within the model domain (Figure 2). The average abstraction rates used for each stress period are presented in

Figure 3a. The dearth of data for the abstraction rates restricts the use of the actual values of the historical abstraction rates in the transient model calibration. Also, the three locations (sw_1 - sw_3) where surface water abstraction is being abstracted within the study area (Figure 2) are lined and therefore no interaction with the underlying aquifer is assumed. The daily recharge values were estimated for the study area using a recharge calculator based on series of spreadsheet calculations underpinned by the Food and Agricultural Organisation (FAO) methodology. The average annual recharge values for the study area is 112 mm/yr, and represents the final recharge value distributed across each stress period (Figure 3b) in the flow model using the Modflow recharge package.

The model was calibrated with hydraulic head data spanning over 20 year period, from March 1970 and February 1989, by minimizing the residuals between the observed and the simulated groundwater head data. The convergence criterion for the hydraulic heads was set to 0.01 m within the Preconditioned Conjugate Gradient 2 (PCG2) solver package. The PCG2 solver package iteratively refines the initial estimates of the model until either an acceptable measure of residual is achieved or the difference between the results of successive iterations is less than a user specified convergence criteria.

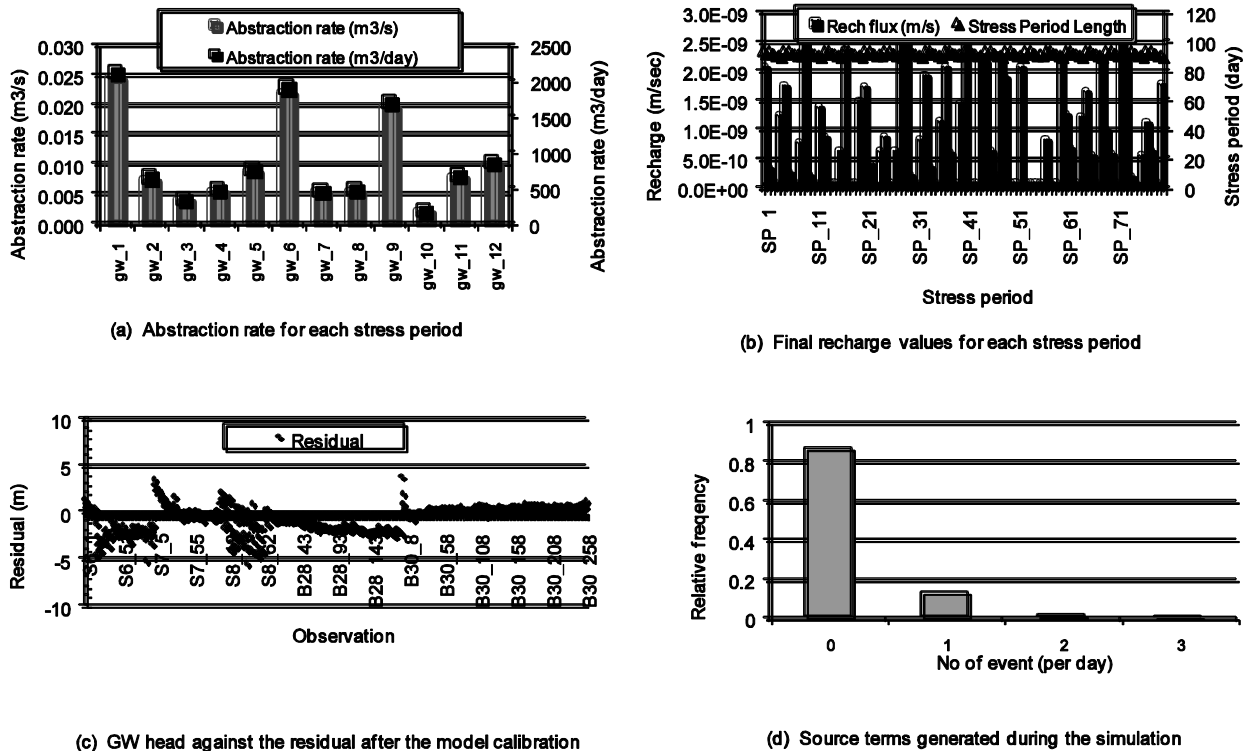


Figure 3: Abstraction and recharge as well as the residual and source terms

The groundwater level monitoring data obtained from the observation boreholes were used as targets for assessing the effectiveness of the calibration process. In order to make future predictions of the risk posed to the groundwater resource, the flow model was validated and further set up to run from March 1985 to February 2015. The corresponding groundwater head computed at the beginning of March 1985, which corresponds to the elapsed time of 15 years of the calibrated flow model, was set to be the initial groundwater heads for the model layers under the predictive transient simulation. Also, a predictive transport model (Zheng and Wang, 1999) was setup under transient conditions covering 30 years from March 1985 to February 2015.

2.3 Risk model

The records of the historical occurrence of chloride related pollution incidents within the study area spanning over January 2002 – December 2009 were used to determine the pattern of the historical occurrence of pollution incidents. This data is considered to be sufficient in the demonstration of the applicability of this risk assessment method, but thought that longer record length will be more representative for the study area. In order to keep the model simple, this work considered pollution sources from only five common industries within the Birmingham area, and these include food, chemical, garages, mining and mineral industries. The analysis of the historical pollution data shows that the average number of pollution incidents from the selected industries for the study area was 35 events per stress period of 91 days. These values were used to compute the PPO for the study area. The total number of pollution sources within the study area was 281. Using equation 1, the probability of pollution occurring at any of the sources over a given stress period of 91 days is computed as:

$$PPO = \frac{\text{No of days of previously occurred pollution events} / \text{No of sources}}{\text{Total no. of days under consideration}} = \frac{35 / 281}{91} = 0.0014$$

The calculated PPO was applied to each of the active cell of the risk model for each stress period. Although, the method as demonstrated in this work assumed that each type of the industry has the same probability of occurrence of pollution incidents in each of the stress period, this method can be adapted to assess the risk from the individual type of industry with varying probability of pollution occurrences per stress period for each of the industry.

III. PRESENTATION AND DISCUSSION OF THE RESULTS

The results of the applications of the risk assessment method are discussed under the following headings.

3.1 Flow model

The model was setup as a three-layer model, which represents (from top) the Bromsgrove, Wildmoor and the Kidderminster sandstone Formations. The respective final horizontal hydraulic conductivity values (K_h) are 5.787×10^{-6} , 2.315×10^{-5} , and 3.472×10^{-5} m/s. The corresponding values for vertical hydraulic conductivity (K_v) are 5.787×10^{-8} , 1.157×10^{-7} , and 5.787×10^{-8} m/s, respectively. Hydraulic layering within the Permo-Triassic sandstone aquifer is thought to account for the large vertical anisotropy in the final calibrated hydraulic conductivity values. The final horizontal conductivity values are within the same range compared to the values obtained by Allen *et al.* (1997) from field test data, for the respective aquifer horizons, as well as to those values obtained by Knipe *et al.* (1993). Furthermore, the final values for the specific yield are 0.12, 0.10 and 0.12, and for the specific storage are 1×10^{-4} , 5×10^{-4} , and 1×10^{-4} , respectively for Bromsgrove, Wildmoor and Kidderminster Formations. The value reported by Allen *et al.* (1997) for the specific yield of the undivided Sherwood sandstone Group is 0.12. Knipe *et al.* (1993) and Rushton and Salmon (1993) respectively reported specific yield value of 0.15, and 0.10 for the Bromsgrove sandstone Formation, and these values are similar to those obtained in this work.

The plot of the observations and the corresponding residual for the model calibration is presented in Figure 3c. The percentage numerical error associated with the volumetric balance is less than 0.1 % throughout the duration of the simulation, and this indicates that the model was converging without any significant numerical error. A sufficient degree of match was obtained between the measured head observations and the simulated equivalents (Figure 3c). The flow model was subsequently setup as a predictive model for a 30-year period spanning March 1985 – February 2015. The March 1985 groundwater head output of the calibrated model was used as the initial water level for the predictive model.

3.2 Risk model

The risk model was set up over the same period of 30 years, from March 1985 to February 2015. The global grid system for the risk model is the same as that of the flow and transport model. The number of potential sources of chloride pollution within the case study area was scoped for the food processing, garages, quarries, mineral and chemical industries, and 281 locations were identified as sources of chloride pollutant. The average occurrence of chloride pollution incidents over the eight-year period (2002 – 2009) was estimated as 35 incidents per stress period (91 days). Hence, the probability of pollution occurrence for each of the potential pollution source was computed to be 0.0014. The range of the contaminant mass loading rate of the historical pollution incidents within the study area is estimated based on the available information to be 250 – 5000 kg per incident. This represents the range of values within which the contaminant mass loading rate was sampled on each occasion when a synthetic pollution incident occurred.

The risk model was run to generate source terms for the transport model. The number of pollution events generated per each day is summarised in Figure 3d, and it indicates that zero incident occurred in 9,453 days out of the total 10,920 days. Single daily events occurred in 1363 days, two daily events in 98 days, while three daily events occurred in only 6 days. Given the generating mechanism used to create pollution events, the frequency of occurrence of 0, 1, 2... events per day should follow a Poisson distribution. The Chi (χ^2) test verifies this, as it showed that the probability that these are by chance from different distributions is very remote (1.02937×10^{-6}), and therefore confirms that the mechanism for generating random events is correct.

3.3 Transport model

The predictive transport model was setup over a 30-year period (March 1985 to February 2015). Chloride contaminant was used to demonstrate the applicability of this method because of its conservative and non reactive nature within the natural subsurface environment. The initial background chloride concentration was set to zero in order to prevent the background concentration from masking the effects of the generated source terms. The mass balance error is generally less than 0.1 %. The spatial distribution of the contaminant after 30 years of simulation is presented in Figure 4, and shows that the contaminant concentration within the study area varies between 0.0 – 0.1 mg/l. High correlation exists between the simulated contaminant concentration (see Figure 4) and the pattern of the distribution of the potential pollution sources (see Figure 2).

3.4 Risk assessment results

The risk to groundwater resources within the study area was determined as the number of times which chloride concentrations at the 12 observation boreholes exceeded the user defined concentration intervals. The two user defined

concentration intervals used are < 0.06 and > 0.06 mg/l. The risk of the contaminant concentration not exceeding 0.06 mg/l within the first model layer is presented in Figure 4. That is, Figure 4 shows that there is 70 – 100 % likelihood that the contaminant concentrations within 55 % of the monitoring boreholes will be less than 0.06 mg/l throughout the simulation period, while the confidence of this likelihood is less than 70 % at all other monitoring points. A major limitation in the application of this method is that it has not been possible to calibrate and validate the probabilistic component of the risk model. Also, it is very difficult to determine the probability of occurrence of extreme events because of lack of records. Furthermore, high pollution incidents usually have higher correlation compared to low pollution events, and the capability for assessing this type of correlation is not incorporated in the current level of the development of this risk assessment method.

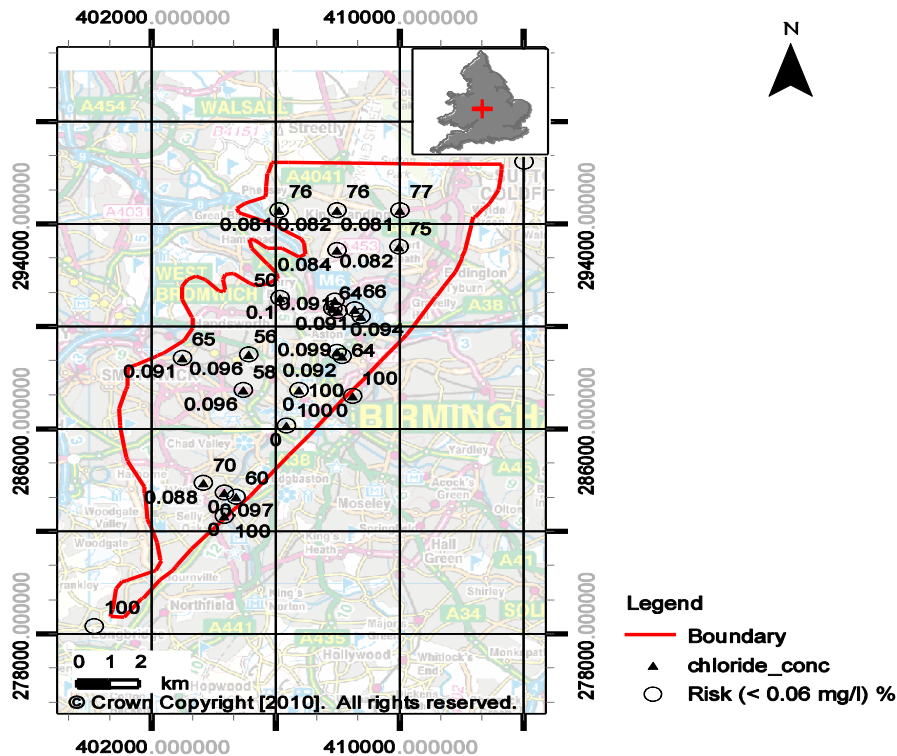


Figure 4: Final contaminant concentration and risk map for 0.06 mg/l

However, this approach of risk assessment presents a more resolved definition of risk distribution within the study area. The existing groundwater vulnerability maps classified the study area as high vulnerability area. Considering the potential pollution sources present within the study area, this work has further resolved this generic classification, with capability to delineate both spatially and temporally, the areas that are prone to quantified risk from the probable pollution. This involves isolating the specific risk to the individual water source as well as the relative trend of the risk distribution within the study area. The roles played by the incorporation of the occurrence and distribution of potential pollution sources at ground surface are not accounted for in the contemporary risk assessment methods.

Although, it is generally difficult to make definitive statements about the predictive accuracy of one risk assessment method compared to other, this method does offer a greater insight in the quantification of risks to a groundwater source, and will be preferred in circumstances where the anticipatory assessment of the risk to groundwater resources is required. Generally, any risk assessment approach requires continuous and dynamic reviewing and update, and this process may span over several years. Also, it is generally difficult to test regional risk assessment methods on a field scale in a similar way as site specific risk assessment methods will be tested or validated. Alternative validation approach is to apply more than one method to the same site and compare the results.

IV. CONCLUSIONS

This work presents the demonstration of the application of a two dimensional risk assessment method using a case study. The method assesses the effects of a probabilistic source terms, based on the historical frequency or externally determined probability distributions of pollution incidents, on groundwater source. Integrated flow, risk and transport models were setup and used as predictive tool to assess effects of synthetically generated source terms at the observation boreholes. Risk is calculated as the number of times at which a user defined contaminant concentration magnitudes are exceeded over a period of time. The risk of pollution from a number of sources all occurring by chance together was evaluated, and this capability to combine the risk to a groundwater feature from numerous potential sources of pollution proved to be a great asset to the method.

REFERENCES

- [1] Al-Adamat, R. A., Foster I. D., and Baban, S. M. 2003. Groundwater vulnerability and risk mapping for the Basaltic aquifer of the Azraq basin of Jordan using GIS, Remote sensing and DRASTIC. *Applied Geography*; 23 (4): 303-324.
- [2] Allen, D.J., Brewerton, L.J., Coleby, L.M., Gibbs, B.R., Lewis, M.A., MacDonald, A.M., Wagstaff, S.J., and Williams, A.T. 1997. The physical properties of major aquifers in England and Wales. *British Geological Survey Technical Report WD/97/34*. 312pp.
- [3] Aller, L., Bennett, T., Lehr, J. H., Petty, R.J., Hackett, G. 1985. Drastic: a standardised system for evaluating groundwater pollution potential using hydrographic settings. *US-EPA Report 600/287-035*.
- [4] Connell, L.D., Daele Gerd van den, 2003. A quantitative approach to aquifer vulnerability mapping. *Journal of Hydrology*; 276: 71 – 88.
- [5] Egbu, A.U., 2004. Constraints to effective pollution control and management in Nigeria. *The Environmentalist*; 20 (1): 13 – 17.
- [6] Ford, M. and Tellam, J.H., 1994. Source, type and extent of inorganic contamination within the Birmingham urban aquifer system, UK. *Journal of Hydrology*; 156: 101 – 135.
- [7] Ford, M., Tellam, J.H. and Hughes, M., 1992. Polluted – related acidification in the urban aquifer, Birmingham, UK. *Journal of Hydrology*; 140: 297 – 312.
- [8] Foster, S.S.D., 1987. Fundamental concepts in aquifer vulnerability, pollution risk and protection strategy. *TNO Committee for Hydrological Research. Proceedings and Information*, 38: 36 – 86.
- [9] Gustafson, D. I. 1989. Groundwater Uniquity Score: A simple method for assessing pesticide leachability. *Environmental Toxicology and Chemistry*; 8: 339 – 357.
- [10] Haines Y. Y., 2006. On the Definition of Vulnerabilities in Measuring Risks to Infrastructures. *Risk Analysis*, Vol. 26, Issue 2, Pp 293–296.
- [11] Harbaugh, A.W., Banta, E.R., Hill, M.C., and MacDonald, M.G., 2000. MODFLOW – 2000, The U.S. Geological Survey modular groundwater model: U.S. Geological Survey open – file report 00 – 92.
- [12] Jeong, C.H., 2001. Effect of land use and urbanization on hydrochemistry and contamination of groundwater from Taejon area, Korea. *Journal of Hydrology*. 253: 194-210
- [13] Khan, M.A., and Liang, T., 1989. Mapping pesticide contamination potential. *Environment Management*. 13: 233 – 242.
- [14] Knipe, C.V., Lloyd, J.W., Lerner, D.N., and Greswell, R. 1993. Rising groundwater levels in Birmingham and the engineering implications. *CIRIA Special Publication* 92, 116p.
- [15] Marilyn, B., 2001. *The Lancet*. 358.
- [16] Oladeji, O., and Elgy, J., 2012. Concepts and methods of quantitative assessment of risk to groundwater resources. *International Journal of Environmental Engineering and Management*. 3(3): 159 – 171.
- [17] Powell, J.H., Glover, B.W., and Waters, C.N., 2000. *Geology of the Birmingham area. Memoir of the British Geological Survey. Sheet 168 (England and Wales)*.
- [18] Rao, P.S.C., Hornsby, A.G., Jessup, R.E., 1985. Indices for ranking the potential for pesticide contamination of groundwater. *Soil & Crop Science Society of Florida Proceedings*;44: 1 – 4.
- [19] Rivett, M.O., Lerner, D.N., Lloyd, J.W. and Lewis C., 1990. Organic contamination of the Birmingham aquifer, UK. *Journal of Hydrology*. 113: 307 – 323.
- [20] Rushton, K.R., and Salmon, S. 1993. Significance of vertical flow through low conductivity zones in the Bromsgrove sandstone aquifer. *Journal of Hydrology*. 152, 131 – 152.
- [21] United State Environmental Protection Agency (USEPA), 1989. Risk assessment guidance for superfund. Volume I : Human Health Evaluation Manual (Part A). *Technical Report EPA/540/1-89/002*.
- [22] Van Stempvoort, D., Ewert, L., and Wassenaar, L. 1992. AVI: A method for groundwater protection mapping in the Praire Province of Canada. *PPWB Report, No.114, National Hydrology Research Institute, Saskatoon, Saskatchewan, Canada*.
- [23] Zheng, C. and Wang, P.P., 1999. MT3DMS: A Modular Three-Dimensional Multispecies Transport Model for Simulation of Advection, Dispersion and Chemical Reactions of Contaminants in Groundwater Systems; *Documentation and User's Guide, Contract Report SERDP-99-1, U.S. Army Engineer Research and Development Center, Vicksburg, MS*.
- [24] Zektster, I. S., and Everett, L. G., (Eds.). 2004. *Groundwater resources of the world and their use. IHP-VI, Series on Groundwater No. 6. United Nations Educational, Scientific and Cultural Organisation*. 342 pp

Analysis of Data Security Approach for Digital Computers

Aru Okereke Eze, Iroegbu Chibuisi, Enyenihi Henry Johnson

Department of Computer Engineering Michael Okpara University of Agriculture, Umudike, Umuahia, Abia State, Nigeria
Department of Electrical/Electronics Akwa Ibom State University, Akwa Ibom State, Nigeria

ABSTRACT: *This research is on the analysis of data security approach for digital computers. The three basic security factors to consider are Confidentiality, Integrity and Availability, while the concepts relating to the people who can access a particular data are authentication, authorization and non-repudiation. The method of cryptography helps in securing information on the internet. Private and public key encryption ensure that only the intended recipient can read confidential information or have access to data. This research analysis has aimed to act as a gadfly for future researchers to rely on.*

KEYWORDS: *Data, Security, Confidentiality, Integrity, Availability, Authentication, Authorization, Cryptography, Encryption*

I. INTRODUCTION

Security incidents are on the rise everywhere. Hackers frequently break into corporate organization and even military systems. Internet was originally conceived of and designed as a research and education network, usage pattern have radically changed.

Most disturbing, modern internet hackers have automated hacking programs that allow even unsophisticated hackers to wreck havoc with corporate network and computers. Also, internal corporate break-ins by employees and ex-employees are still the biggest security problems in organizations. As internet has expanded into areas of commerce, medicine, commercial communication and public service, increase reliance on it is expected over the next few years, along with increased attention to its security. Since the information and tools needed to penetrate the security of corporate networks are widely available, network security has become a major concern for companies throughout the world.

Data security approach for digital computers are the techniques use in securing data (information) on a private digital computer network when connecting a private network to a larger network such as the internet.

This research "Analysis of data security approach for digital computers" x-rayed data security issues that arise when connecting a private network to the internet.

Section II of this research examines the literature review and theory of data security approach; Section III surveyed the methodology, design and implementation of security measures; Section IV presents the result analysis and discussion, while section V summarizes and concludes the work.

II. BACKGROUND REVIEW

The internet began in 1969 as the ARPANET, a project funded by Advanced Research Project Agency (ARPA) of the U.S Department of Defense. When internet was born, little thought was given to security. One of the original goals of the project was to create a network that would continue to function even if major sections of the network failed or were attacked and to reroute network traffic automatically around problems in connecting systems.

As more locations with computer joined the ARPANET, the usefulness of the network grew. By 1971, the internet linked about two dozen research and government sites, and researchers had begun to use it to exchange information not directly related to the ARPANET itself. The network was becoming an important tool for collaborative research, but it was rare that a connection from a remote system was considered an attack, because ARPANET users comprised a small group of people who generally knew and trusted each other.

In 1986, the first well-publicized international security incident was identified by Cliff Stoll, then of Lawrence Berkeley National Laboratory in northern California. A simple accounting error in the computer records of systems connected to the ARPANET led Stoll to uncover an international effort, using the network to connect to computers in the United States and copy information from them. In 1988, the ARPANET has its first network security incident, usually referred to as "the Morris worm". In 1989, the ARPANET officially becomes the internet and moved from a government research project to an operational network. Security problems continued, with both aggressive and defensive technologies becoming more sophisticated.

Today, the use of the World Wide Web and Web-related programming languages creates new opportunities for network attacks. Intruders can steal or tamper with information without touching a piece of paper or a photocopier. They can create new electronic files, run their own programs, and hide evidence of their unauthorized activities.

III. THEORY

The three basic security concepts relevant to data (information) on the internet are confidentiality, integrity and availability. The concepts relating to the people who use that data (information) are authentication, authorization, and non-repudiation. It is easy to gain unauthorized access to data in an insecure networked environment, and it is hard to catch the intruders. Examples of important information are passwords, access control files and keys, personnel information and encryption algorithms.

When information is read or copied by some unauthorized person, the result is known as loss of confidentiality. Also when information is modified in unexpected ways, the result is known as loss of integrity, while when information is erased or become inaccessible, the result is loss of availability. To make information available to those who need it and who can be trusted with it, organizations use authentication and authorization. Authentication and authorization go hand in hand. Users must be authenticated before carrying out the activity they are authorized to perform. Security is strong when the means of authentication cannot later be refuted, the user cannot later deny that he or she performed the activity. This is known as non-repudiation.

IV. DESIGN METHODOLOGY AND IMPLEMENTATION OF SECURITY MEASURES

In the face of vulnerabilities and incident trends, a robust defense and protection measures becomes necessary and required flexible strategies that allows adaptation to the changing environment, well-defined policies and procedures, the use of robust tools, and constant vigilance.

4.1 Encryption

The most basic building block of security is encryption, which scrambles a message before transmission, so that an interceptor cannot read the message as it flows over the network. However, the receiver knows how to decrypt (descramble) the message, making it readable again. Encryption provides privacy, which is called confidentiality. Both terms means that message can be transmitted without fear of being read by adversaries.

Encryption methods falls into two categories (symmetric key encryption and public key encryption), with numerous specific encryption algorithms.

4.2 Symmetric key encryption

Symmetric key encryption has a single key that is used by both communication partners. Figure 1 shows a symmetric key encryption method.

- When party A sends to party B, party A encrypts with the single symmetric key and party b decrypts with the same key.
- When party B transmits to party A, in turn party B encrypts with the single symmetric key and also party A decrypts with the same key.



Figure 1: Symmetric key encryption

4.3 Public key encryption

In public key encryption, when one party sends to another, there are two keys; the receiver public key and the receiver private key. Both of the keys are those of the receiver, not of the sender.

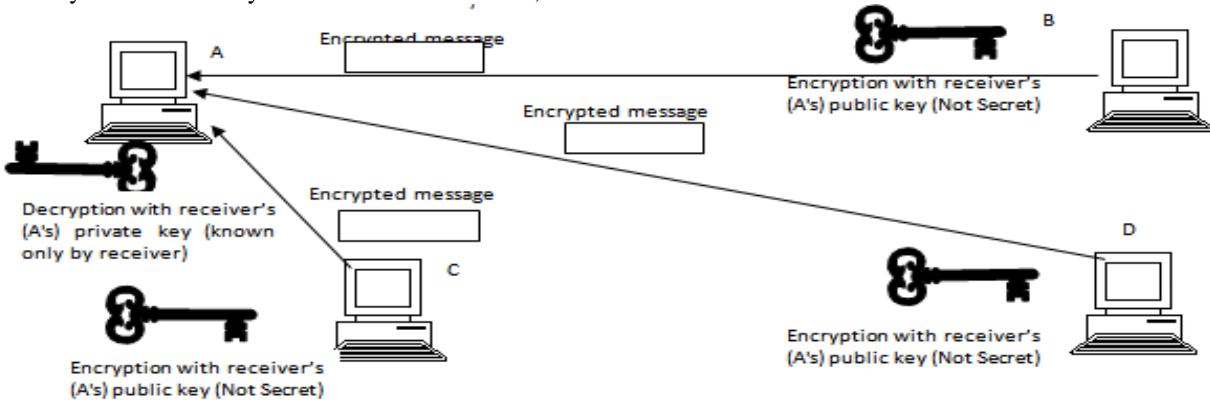


Figure 2: Shows a public key encryption method

4.4 Authentication

Authentication proves the sender's identity. If we get a message claiming to be from someone, we want to be certain that it is not really coming from someone else, we apply the concept of authentication. There are many forms of authentication; passwords authentication, authentication card, biometric authentication etc.

4.5 Hashing

Hashing takes a message of any length and computes a small bit string of fixed length. The two most popular hashing algorithms, MD5 and the Secure Hash Algorithm 1 (SHA-1), create hashes that are 128 bits and 160 bits long respectively, no matter how long the original message is. Hashing is different from encryption because, hashing is not reversible. It is a one-way function.

Other protective measures of safeguarding our network include; Integrated Security Systems (ISS), Multi Layer Security, Firewalling etc.

V. RESULT ANALYSIS AND DISCUSSION

From the design and implementation of security measures for digital computers emerge the following results.

5.1 Cryptography

One of the primary reasons why intruders are successful is that most of information they acquire from a system are in a form that can read and comprehend. Cryptography secures information by protecting its confidentiality. It can also be used to protect information about the integrity and authenticity of data. Also, cryptography checksums helps in preventing undetected modification by encrypting the checksum in a way that makes the checksum unique. To protect against the chance of intruders modifying or forging information in transit, digital signatures are formed, by encrypting a combination of a checksum of the information and the author's unique private key.

5.2 Operational technology

A variety of technologies have been developed to help organizations secure their systems and information against intruders. These technologies help protect systems and information against attacks, detect unusual or suspicious activities, and respond to events that affect security. No single technology addresses all the problems and threats. Nevertheless, organizations can significantly improve their resistance to attack by carefully preparing and strategically deploying personnel and operational technologies. Data resources and assets can be protected, suspicious activity can be detected and assessed, and appropriate responses can be made to security events as they occur.

5.3 Security analysis tools

Because of the increasing sophistication of intruder methods and the vulnerabilities present in commonly used applications, it is essential to assess periodically network susceptibility to compromise. A vulnerability identification tools are available, which have gained praises.

VI. CONCLUSION

This research work has analyzed data security approach for digital computers. It has attempted to present various attacks and vulnerabilities of data over the network, especially as the internet is a public network. Those affected by such attacks include banks, insurance companies, government agencies, network service providers, utility companies, universities etc. The consequences of a break- in cover a broad range of possibilities: decrease in productivities, loss of money or staff man hour, loss of market opportunity, legal liability etc.

In order to have a secured computer, both the network designer and IT security teams should work hand in hand to develop a security architecture that would be integrated into the existing enterprise network.

REFERENCES

- [1] Annabel Z. Dodd. The essential guide to telecommunication, second edition.
- [2] Caelli, W., Longley, D., and Shain, M., Information Security Handbook, Stockton Press, New York, 1991.
- [3] CERT coordination center, CERT advisories and other security information, CERT/CC, Pittsburgh, P.A. Available on line: <http://www.cert.org>.
- [4] Chapman, D.B. and Zwicky, E.D. Building Internet Firewall, O' Reilly & Associates, Sebastopol, C.A, 1995.
- [5] Denning, P.J. ed., Computers Under Attack Intruders, Worms and Viruses, ACM Press, Addison-Wesley, New York, 1990.
- [6] Garfinkel, S., and Spafford, G. Practical UNIX and Internet Security, 2nd ed, O'Reilly & Associates, Sebastopol, C.A. 1996.
- [7] Kaufman, C., Perlman, R., and Speciner, M., Network Security: Private Communication in a public world, Prentice-Hall, Eaglewood Cliffs, NJ, 1995.
- [8] National Research Council, computer at risk: Safe computing in the computer Age, National Academic Press, Washington D.C., 1991.
- [9] Randall K. Nicholas/ CSA Guide to cryptosystems McGraw-Hill 199, page 248

Aru, Okereke Eze is a lecturer in the Department of Computer Engineering, Michael Okpara University of Agriculture, Umuahia, Abia State, Nigeria. His research Interests include Computational Intelligence, Computer Hardware design and maintenance, Security system design, , Expert systems and Artificial Intelligence, Design of Microcontroller and Microprocessor based system, digital systems design using microcontrollers and other computer related subjects.

Iroegbu Chibuisi is a postgraduate student in the Department of Computer Engineering, Michael Okpara University of Agriculture, Umuahia, Abia State, Nigeria. Her research interests include Computer Hardware design and maintenance, Security system design, etc.

Enyenihi Henry Johnson is a lecturer in the Department of Electrical/Electronics Engineering, Akwa Ibom State University, Akwa Ibom State, Nigeria. His research interests include Computer Hardware design and maintenance, Electronic and Communication Systems, Data Communication system designs etc.

Finite Element Modeling of Magnetic Flux Leakage Technique in Plates with Defect and without Defect

Nagu.S¹

¹Mechanical Engineering, PSNACET, Kothandaraman Nagar, Dindigul, India, 632002,

ABSTRACT: In the area of non destructive testing ultrasonic testing using wave propagation is an emerging field. Ultrasonic testing uses transmission of high frequency sound waves into a material to object and reflections (echoes) are returned to a receiver from internal imperfections. The waves travel through a given medium at a specific speed, velocity, in a predictable direction and when they encounter a boundary with a different medium they will be reflected or transmitted. The aim of the simulation is to find out how different flaw geometries and orientations influence the measured signal. To find flaws near the surface, a magnetic flux leakage (MFL) inspection system can be applied. 3D FEM is used to analyze the MFL signals, a generalized potential formulation to the magneto static field, MFL problem is discussed. Typical 3D defects are accurately modeled and detailed comparison is done for model with defect. Finally, we want to infer the flaw geometry from the signals. In the pulse echo method, a piezoelectric transducer with its longitudinal axis located perpendicular to and mounted on or near the surface of the test material is used to transmit and receive ultrasonic energy. The characteristics of wave propagation problems are that the frequency content of the exciting force is very high.

Comsol Multiphysics was used as an analytical tool to model the wave propagation. This paper presents the three-dimensional FE modeling of leakage magnetic fields from surface and sub-surface defects of different dimensions in 12 mm thick carbon steel plate. The details of 3D model and results of FE study of the effects of depth location and depth on the detectability of sub-surface defects in the MFL technique are discussed in the paper.

Keywords: Non destructive testing, Magnetic flux Leakage, Finite element Method

I. INTRODUCTION

Magnetic flux leakage (MFL) technique is widely used for non-destructive detection and evaluation of surface and sub-surface defects in ferromagnetic objects such as long oil and gas pipelines, storage tank floors and wire ropes. The basic principle is that a powerful magnet is used to magnetize the steel. At areas where there is corrosion or missing metal, the magnetic field "leaks" from the steel. In an MFL tool, a magnetic detector is placed between the poles of the magnet to detect the leakage field. Analysts interpret the chart recording of the leakage field to identify damaged areas and hopefully to estimate the depth of metal loss. The magnetic interaction is described in terms of a vector field, where each point in space (and time) is associated with a vector that determines what force a moving charge would experience at that point. Ultrasonic wave propagation varies with change in the medium in which the wave propagates. In this technique, the test object is magnetized to near saturation flux density. The presence of a defect in the test object acts as localized magnetic dipole with effective magnetic moment opposite to the applied magnetic field. This results in a proportion of the magnetic field leak out of the object surface. This leakage flux is detected by magnetic sensors and used to estimate the shape and size of the defect.

$$\lambda = c/v$$

λ =wavelength=sound velocity, v =frequency

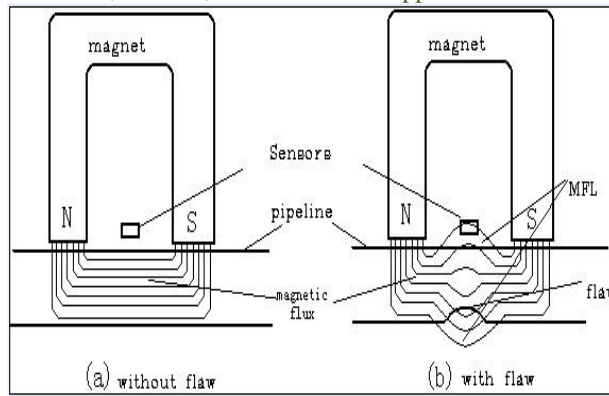
One advantage of MFL technique is its ability to model the leakage field from defect. The modeling enables the study of field/defect interactions and helps in better understanding and effective utilization of the MFL technique. In FE method, the leakage field is obtained by solving the relevant Maxwell's equations with appropriate boundary conditions. The FE method is capable of modeling of nonlinear problems and irregular geometries which are difficult to be modeled analytically.

1.1 Pulse echo method

An ultrasonic (NDT) method for the detection and characterization of defects in composites in which pulses are transmitted and received on the same side of the test panel after being reflected from the opposite face. Defects cause a decrease in the reflection amplitude.

1.1.1 MFL principle

As an MFL tool navigates the pipeline, a magnetic circuit is created between the pipe wall and the tool. Brushes typically act as a transmitter of magnetic flux from the tool into the pipe wall, and as the magnets are oriented in opposing directions, a flow of flux is created in an elliptical pattern. High Field MFL tools saturate the pipe wall with magnetic flux until the pipe wall can no longer hold any more flux. The remaining flux leaks out of the pipe wall and strategically placed tri-axial Hall effect sensor heads can accurately measure the three dimensional vector of the leakage field.



Typical axial components of MFL signals obtained for the geometry. These signals are a measure of the fields which leak out from under the defect and this makes the magnetic flux pass through the detected components, making a detour from the defects. The width of the signal is proportional to the defect length (axial dimension) and the amplitude of the signal is proportional to both the defect length and depth. The last step in an MFL inspection is analysis. Analysis is the process of estimating the geometry or severity of a defect (or imperfection) from the measured flux leakage field. The techniques and success of analyzing MFL data depend on the capabilities and limitations of the MFL tool, which are established by design and operational tradeoffs.

II. THREE-DIMENSIONAL FINITE ELEMENT MODELING

COMSOL 4.2 Multiphysics software package in magnetostatic mode has been used for 3D FE modeling. Figure 1 shows the mesh generated for the geometry which consists of a permanent magnet (length 90 mm, cross-sectional area 55 x 50 mm² and leg spacing 70 mm) and carbon steel plate (length 240 mm, breadth 150 mm and thickness 12 mm) with 15 mm long slot. The permanent magnet is used for magnetic induction to magnetize the plate to near saturation. An MFL tool consists of two or more bodies. One body is the magnetizer with the magnets and sensors and the other bodies contain the electronics and batteries. The magnetizer body houses the sensors that are located between powerful "rare-earth" magnets. The magnets are mounted between the brushes and tool body to create a magnetic circuit along with the pipe wall. As the tool travels along the pipe, the sensors detect interruptions in the magnetic circuit. Interruptions are typically caused by metal loss and which in most cases is corrosion. Mechanical damage such as shovel gouges can also be detected. The metal loss in a magnetic circuit is analogous to a rock in a stream.

Treating the MFL problem as magneto static, the following equations have been used with usual notations:

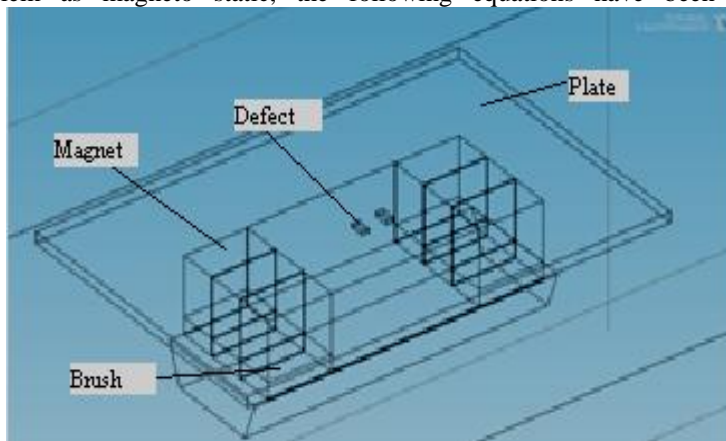


Figure 1.2. 3D Finite element modeling

$$\begin{aligned} \nabla \times \{ \mathbf{H} \} &= \{ \mathbf{J}_i \} & (1) \\ \nabla \cdot \{ \mathbf{B} \} &= 0 & (2) \\ \mathbf{B} &= \nabla \times \mathbf{A} & (3) \\ \mathbf{B} &= \mu_0 \mu_r \mathbf{H} = \mu_0 \mathbf{H} + \mu_r \mathbf{M} & (4) \end{aligned}$$

Where $\{ \mathbf{H} \}$ is the magnetic field intensity vector, $\{ \mathbf{J}_i \}$ is the applied source current density vector and $\{ \mathbf{B} \}$ is the magnetic flux density vector. The field equations are supplemented by the constitutive relation that describes the behavior of electromagnetic materials.

$$\{ \mathbf{B} \} = \{ \mu \} \{ \mathbf{H} \} + \mu_0 \{ \mathbf{M} \}$$

In other region

$$\{ \mathbf{B} \} = \{ \mu \} \{ \mathbf{H} \}$$

To describe the properties of the electromagnetic materials, the field equations are supplemented by the constitutive relationships.

III. 3D SIMULATION

Three-dimensional finite element (FE) modeling of magnetic flux leakage (MFL) technique has been performed using COMSOL 4.2.

3.1 Modeling Results and Discussion

The MFL method relies on calibration runs for correct interpretation of the leakage signals in terms of defect location, size and depth. The MFL signals obtained depend not only on the detector and the defect but also on running conditions, such as the tester's velocity and stress, life-off and so on.

Unlike analytical model finite elements simulation allows to consider actual defect shape features and also imperfections of magnetizing and measuring system. Still due to great amount of estimated parameters numerical diagnostic model built in such a way loses compactness property. In the MFL inspection tool, permanent or electromagnets are used to magnetize the pipe wall in an axial direction and an array of hall effect sensors is usually installed around the circumference of the pipe to sense the leakage flux caused by anomalies in the pipe wall.

3.2 Plotting

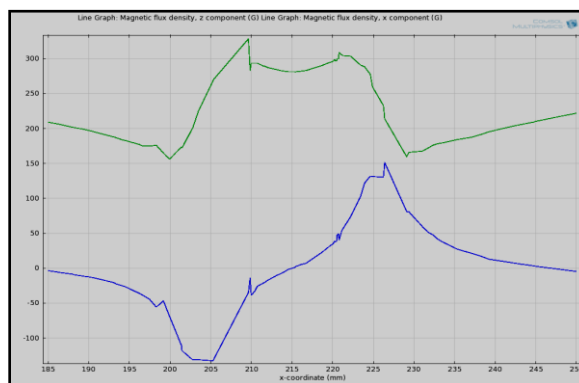
The axial component and radial component are plotted.

With the 2D simulation taking place in the x-z plane,

we use the following axis convention:

- X-axis: the horizontal direction (this is the direction in which the yoke moves)
- Y-axis: the height direction
- Z-axis: perpendicular to 2D simulation

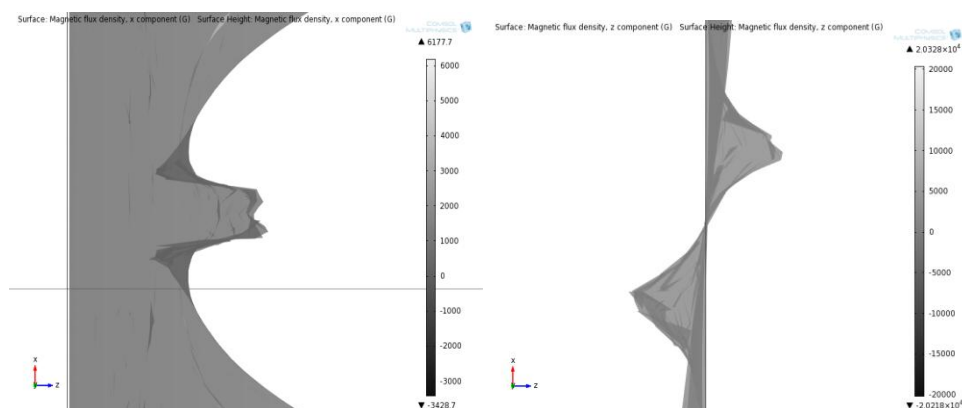
The 2D cross section shape (x-y-plane) of the yoke has been approximated by Beziér-curves. Concerning the coils, we waive to model single excitation windings. Instead, we define an external current on the cross section area. The steel object is a rectangular of 10 mm height and 115 mm width. The whole inspection scene is enclosed in a rectangular air region.



3D plotting Defect size - 4.25x20

3.3 Effect of defect location

Figure 1.2 shows the carbon steel plate with slots (length 15 mm, width 1 mm, depth 4 mm) located at 2 mm and 4 mm below the plate surface. Figures 3b and 3c show the model predicted contour plots of Bx and Bz components of leakage fields for the slots. The intensities of both the components of leakage fields for the slot are found to decrease with the increase in location below the surface while the lateral spread of signals are found to increase.



Graph indicating axial and radial component

IV. CONCLUSIONS

Three-dimensional FE modeling has been performed to study the effects of defect location and depth on the detectability of sub-surface defects in the MFL technique. The intensity of leakage fields is found to decrease with the increase in defect location below the surface while the intensity of leakage fields increases with the increase in defect depth. The effect of lift-off on MFL signals is also analyzed for enhancing the reliable detection of defects. Features such as peak amplitudes, full width at half maximum (FWHM), slope at half maximum. B_x - B_z loop area extracted from the model predicted signals may be useful for characterization of defects.

ACKNOWLEDGEMENTS

I like to thank everyone who has given extensive support for this work.

REFERENCES

- [1]. H. Zuoying, Q. Peiwen and C. Liang, “*3D FEM analysis in magnetic flux leakage method*”, NDT & E International, volume 39, pp. 61-66, 2006.
- [2]. M. Katoh, K. Nishio and T. Yamaguchi, “*FEM study on the influence of air gap and specimen thickness on the detectability of flaw in the yoke method*”, NDT & E International, volume 33, pp.333-339, 2000
- [3]. Yong Li, J Wilson and Gui Yun Tian, ‘*Experiment and simulation study of 3D magnetic field sensing for magnetic flux leakage defect characterization[J]*’, NDT&EInt, doi:10.1016/j.ndteint.2006.08.002, 2006.
- [4]. A. Groos, S. Nitsche, T. Schmitte, “*Modeling of Magnetic Flux Leakage Measurements of Steel Pipe’s*”, www.ndt.net, 2006

Analysis of Dual Resonant Solid State Tesla Transformer

Ali Abbasi¹, Mohammad Hosein Khanzade²

** (Faculty of FAVA Engineering, Imam Hosein University, Tehran, Iran)

ABSTRACT: In this paper, Analysis of dual resonant solid state tesla transformer (DRSSTS) is carried out. The fundamental difference between this types of tesla transformer and spark gap tesla transformer, is using of one or more power electronic switch instead of spark gap. Likewise DRSSTS is different from the solid state tesla transformer due to the addition of a primary tank capacitor. In this paper, tesla transformer is fed by full bridge inverter that generates square wave. For the sake of simplicity, tesla transformer is modeled only by lumped elements and resistive losses are neglected. Then, analytical equations for Tesla transformer's output voltage and primary side current, are calculated and conditions of increased tesla transformer's output voltage are also investigated. Using Euler numerical integration method and switching function concept, the effect of tesla transformer's operation, on inverter dc side voltage and current have been evaluated. The test system is simulated in MATLAB/Simulink software, and validity of calculated equations, is verified by simulation results.

Keywords: Tesla transformer, single phase inverter, square wave, switching function, numerical integration.

I. INTRODUCTION

A Tesla transformer is a resonant air core transformer invented by Nikola Tesla around 1891 that is used for producing high-voltage, low-current, high frequency alternating-current pulses. Tesla transformer increases the voltage in two steps: first by conventional step-up iron core transformer and second by an air core resonant transformer that increases voltage range up to several hundred kV. Usually a high voltage capacitor is connected to primary winding of air core transformer and comprises a resonant circuit after that the secondary winding of air core transformer with its self-capacitance form secondary resonant circuit. To achieve the best performance of the Tesla transformer resonance frequency of the primary and secondary windings must be equal [1,2]. In Fig.1 spark gap based Tesla transformer is shown. Spark gap (G), which is composed of two electrodes and an air gap, operates as voltage-controlled switch and when potential difference across it exceeds threshold of air breakdown then the arc will be produced and tesla transformer operates in dual resonant mode. To achieve this and improving tesla transformers performance, usually a conventional iron core is also used for increasing voltage in the first step which has a neon sign transformer (NST) because of its great leakage reactance. In Figure 1 the capacitor C_2 shows the distributed capacitance between ground and top load. In addition of need of step up transformer, tesla transformer of figure 1 has another major disadvantage, such as: High voltage capacitors are difficult to find, and you usually have to make. And if static spark gap is used, generated noise and light is extremely annoying, and rotary spark gap needs motor. Because of nonlinear nature of air ionization phenomena and practical limitations of spark gap, increasing in operating of frequency of system is not possible. Numerous articles and books have been published in dual tuned resonant transformer and analysis and implementation of spark gap based tesla transformer [1-8] and [11-13], For example, analysis of triple tuned resonant coils and tesla transformer based of iron core transformer instead of air core transformer are carried out in [9] and [10] respectively. Analysis of series resonant converter in order to producing high voltage is studied in [14]. According to spark gap based tesla transformers defects, use of Tesla transformer based on power electronic devices have been proposed [6]. The main idea is replacing of spark gap with one or more power electronic switches such as IGBT or MOSFET. In [15] measurement of resonance frequency and other parameters of single ended Tesla transformer in laboratory prototype system is performed. Investigation on occurrence of resonance phenomena in two coils with different structures when one of them is stimulated with square wave is carried out in [16] but theoretical details of inverter is not considered. A Dual Resonant Solid State Tesla Transformer is different from the Solid State Tesla Transformer due to the addition of a primary capacitor. In this paper, analysis of Tesla transformer fed by square wave that generated by full bridge inverter is studied and Tesla transformer is modeled by lumped elements and analytical equations are provided. Also switching frequency of inverter to generate maximum is determined. In this basis, first output voltage and primary current of Tesla transformer are calculated analytically, then dc link current and voltage of inverter are calculated by using switching function and Euler integration method. Obtained equations are compared with MATLAB/Simulink simulation results and are shown that they are in good agreement.

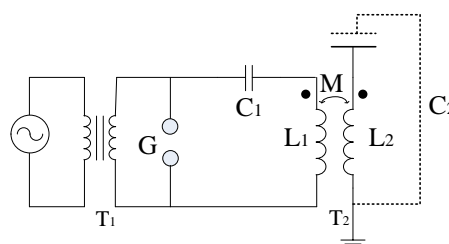


Fig.1 spark gap based tesla transformer

II. INVERTER BASED TESLA TRANSFORMER

Tesla transformer using lumped element is fed by full bridge inverter is shown in below.

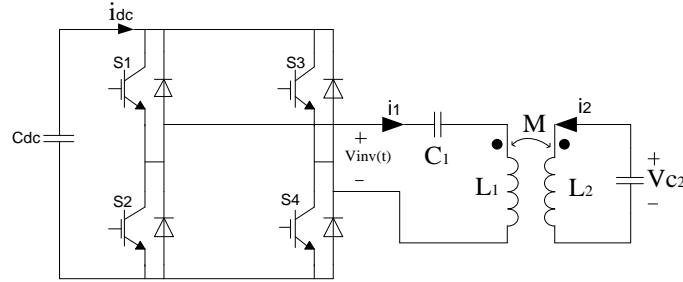


Fig.2 tesla transformer fed by full bridge inverter

In figure 2, inverter generates square wave with duty cycle $\frac{t_1}{T}$, that is shown in figure 3. Considering the Voltage Source $V_{inv}(t)$ as the voltage produced by the inverter and T equivalent circuit of coupled inductor, circuit of figure 2 converts to Figure 4.

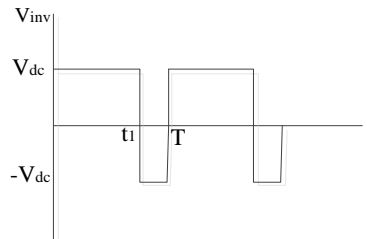


Fig.3 output voltage of full bridge inverter

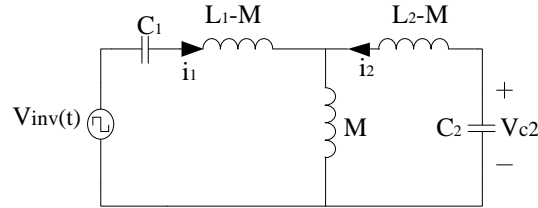


Fig.4 equivalent circuit of system

By neglecting resistive losses and using KVL:

$$\frac{1}{C_1} \int i_1 dt + L_1 \frac{di_1}{dt} + M \frac{di_2}{dt} = V_{inv}(t) \quad (1)$$

$$\frac{1}{C_2} \int i_2 dt + L_2 \frac{di_2}{dt} + M \frac{di_1}{dt} = 0$$

In figure 4, characteristic equation of system is equal to:

$$(1 - k^2)s^4 + (\omega_1^2 + \omega_2^2)s^2 + \frac{1}{C_1 C_2} = 0 \quad (2)$$

$$\omega_1 = \frac{1}{\sqrt{L_1 C_1}}, \quad \omega_2 = \frac{1}{\sqrt{L_2 C_2}}, \quad k = \frac{M}{\sqrt{L_1 L_2}}$$

In Eq.2 ω_1 and ω_2 are resonance frequency of primary and secondary coils respectively, and k is the coefficient of coupling. if inverter produces $V_{inv}(t)$, then fourier series of $V_{inv}(t)$ is equal to:

$$v_{inv}(t) = \sum_{n=0}^{\infty} a_n \cos(n\omega_0 t) + b_n \sin(n\omega_0 t) \quad (3)$$

In above equation, $\omega_0 = \frac{1}{T}$ is fundamental frequency of inverter and coefficients of fourier series are shown below:

$$a_0 = \left(\frac{2t_1}{T} - 1\right)V_{dc}$$

$$a_n = \frac{2V_{dc}}{\pi n} \sin\left(\frac{2\pi n t_1}{T}\right)$$

$$b_n = \frac{-2V_{dc}}{\pi n} \left[\cos\left(\frac{2\pi n t_1}{T}\right) - 1\right]$$

Differential equations of system in Laplace domain are equal to:

$$(L_1 s + \frac{1}{C_1 s})I_1 + M s I_2 = \sum_{n=0}^{\infty} a_n \frac{s}{s^2 + n^2 \omega_0^2} + b_n \frac{n \omega_0}{s^2 + n^2 \omega_0^2} \quad (4)$$

$$(L_2 s + \frac{1}{C_2 s})I_2 + M s I_1 = 0$$

Combining the above equations and after tedious calculations, finally output of tesla transformer in time domain is calculated as:

$$V_{c2} = \frac{-M \omega_0}{L_1 L_2 C_2 \sigma^2} \sum_{n=1}^{\infty} \left\{ n \frac{y_{1n}}{x_1} [a_n \cos(x_1 t) + b_n \sin(x_1 t)] + n \frac{y_{2n}}{x_2} [a_n \cos(x_2 t) + b_n \sin(x_2 t)] + \frac{y_{3n}}{\omega_0} [a_n \cos(n \omega_0 t) + b_n \sin(n \omega_0 t)] \right\} \quad (5)$$

That parameters of Eq.5 are given below:

$$\sigma^2 = 1 - \frac{M^2}{L_1 L_2}, \quad x_1^2 = \frac{\omega_1^2 + \omega_2^2}{2\sigma^2} + \sqrt{\left(\frac{\omega_1^2 + \omega_2^2}{2\sigma^2}\right)^2 - \frac{\omega_1^2 \omega_2^2}{\sigma^2}}, \quad x_2^2 = \frac{\omega_1^2 + \omega_2^2}{2\sigma^2} - \sqrt{\left(\frac{\omega_1^2 + \omega_2^2}{2\sigma^2}\right)^2 - \frac{\omega_1^2 \omega_2^2}{\sigma^2}}$$

$$y_{1n} = \frac{-x_1^2}{(x_1^2 - x_2^2)(x_1^2 - n^2 \omega_0^2)}, \quad y_{2n} = \frac{x_2^2}{(x_1^2 - x_2^2)(x_2^2 - n^2 \omega_0^2)}, \quad y_{3n} = \frac{n^2 \omega_0^2}{(x_1^2 - n^2 \omega_0^2)(n^2 \omega_0^2 - x_2^2)}$$

In case of equality of ω_1 and ω_2 , x_1^2 and x_2^2 are simplified as:

$$x_{1,2}^2 = \frac{\omega_1^2}{1 \pm k} \quad (6)$$

According to y_{1n} , y_{2n} and y_{3n} , it is obvious that with increasing n, y_{1n} , y_{2n} and y_{3n} will decrease with square reverse rate of n, and coefficients of Fourier series will decrease with reverse rate of n (Eq.3). Therefore, it is reasonable to approximate the output of Tesla transformer with low values of n. Considering n = 1 the output voltage Tesla transformer is equal to:

$$V_{c2} = \frac{-M \omega_0}{L_1 L_2 C_2 \sigma^2} \left\{ \frac{y_1}{x_1} [a_1 \cos(x_1 t) + b_1 \sin(x_1 t)] + \frac{y_2}{x_2} [a_1 \cos(x_2 t) + b_1 \sin(x_2 t)] + \frac{y_3}{\omega_0} [a_1 \cos(\omega_0 t) + b_1 \sin(\omega_0 t)] \right\} \quad (7)$$

If duty cycle of inverter is 50%, then a become zero and V_{c2} calculated as following equation:

$$V_{c2} = \frac{-M \omega_0}{L_1 L_2 C_2 \sigma^2} \left[\frac{y_1}{x_1} b_1 \sin(x_1 t) + \frac{y_2}{x_2} b_1 \sin(x_2 t) + \frac{y_3}{\omega_0} b_1 \sin(\omega_0 t) \right] \quad (8)$$

According to y_{1n} , y_{2n} , y_{3n} and Eq.6 it is ascertained that, when k is small, if ω_0 approaches to resonance frequency of each primary or secondary, output voltage will increase. But when k is almost unity, for generating higher voltage, ω_0 should approach to x_1 or x_2 . Theoretically maximum value of Eq.18 and primary current of Tesla transformer are calculated as Eq.9 and Eq.10.

$$V_{c2}^{\max} = \frac{M \omega_0 b_1}{L_1 L_2 C_2 \sigma^2} \left(\left| \frac{y_1}{x_1} \right| + \left| \frac{y_2}{x_2} \right| + \left| \frac{y_3}{\omega_0} \right| \right) \quad (9)$$

$$i_1 = \frac{\omega_0}{L_1 L_2 C_2 \sigma^2} \sum_{n=1}^{\infty} y_{1n} \left(L_2 C_2 - \frac{1}{x_1^2} \right) n [-a_n \sin(x_1 t) + b_n \cos(x_1 t)] +$$

$$y_{2n} \left(L_2 C_2 - \frac{1}{x_2^2} \right) n [-a_n \sin(x_2 t) + b_n \cos(x_2 t)] +$$

$$y_{3n} \left(L_2 C_2 - \frac{1}{n^2 \omega_0^2} \right) n [-a_n \sin(n \omega_0 t) + b_n \cos(n \omega_0 t)] \quad (10)$$

In general, dc link current of inverter, is calculated by convolution of primary current of tesla transformer (Eq.10) and in the frequency domain, or by multiplying of two mentioned functions in the time domain [17].

$$i_{dc}(t) = s(t)i_1(t) \tag{11}$$

Where $s(t)$ is switching function of inverter in time domain and is calculated as follows:

$$s(t) = \sum_{n=0}^{\infty} c_n \cos(n\omega_0 t) + d_n \sin(n\omega_0 t)$$

$$c_0 = \left(\frac{2t_1}{T} - 1\right)$$

$$c_n = \frac{2}{\pi n} \sin\left(\frac{2\pi n t_1}{T}\right)$$

$$d_n = \frac{-2}{\pi n} \left[\cos\left(\frac{2\pi n t_1}{T}\right) - 1\right]$$
(12)

And the dc link voltage can be calculated as follows:

$$V_{dc}(t) = V_0 - \frac{1}{C_{dc}} \int_0^t i_{dc}(t) dt \tag{13}$$

In above equation, V_0 is the initial voltage of capacitor. Because of nonexistence analytical equation for dc link current (Eq.11), Eq.13 is solved using Euler numerical integration method. Using Euler method, first order differential equation as a Eq.14 is written in discrete domain as a Eq.15:

$$\frac{d}{dt} y = f(y, t) \tag{14}$$

$$y(t_{k+1}) = y(t_k) + \Delta t \cdot f(y(t_k), t_k) \tag{15}$$

In Eq.15, $y(t_{k+1})$ is value of y in t_{k+1} and Δt is and the time step of integration that is equal to $t_{k+1} - t_k$.

III. SIMULATION RESULTS

To verify the obtained equations in the previous section, the test system in figure 2, is simulated with MATLAB/SIMULINK software and simulation results are compared with analytical and numerical results. It should be noted that in all of obtained equations to the 80th harmonic in the Fourier series is considered and other parameters of test system are given in table.1.

Table.1 simulation parameters

$L_1=10\mu\text{H}$	$L_2=1\text{mH}$	$K=0.6$	$f=50\text{kHz}$
$C_1=1\mu\text{F}$	$C_2=10\text{nF}$	$\frac{t_1}{T} = 0.5$	$V_{dc}=12\text{V}$

In this case x_1 and x_2 are approximately equal to 5×10^5 rad/s and 2.5×10^5 rad/s respectively and V_{c2}^{Max} (Eq.9) in terms of ω_0 is shown in figure 5.a. Both of simulation and analytical output voltage of tesla transformer (Eq.5) in the case of $\omega_0 = \omega_1$, $\omega_0 = 0.9x_2$ and $\omega_0 = 0.9x_1$ are shown in figure 5.b-d. According to figure 5.b-d it is obvious that maximum of tesla transformers output voltage, when ω_0 approaches to x_1 , is larger than when ω_0 approaches to x_2 . Comparison results Eq.8, primary current, dc link current and voltage in the case of $\omega_0 = \omega_1$, $C_{dc}=0.1\text{mF}$ and $\Delta t=0.1\mu\text{s}$ are shown in fig.6a-d. As shown in fig.6c with decreasing Δt , insignificant difference between the numerical results and simulation will decrease.

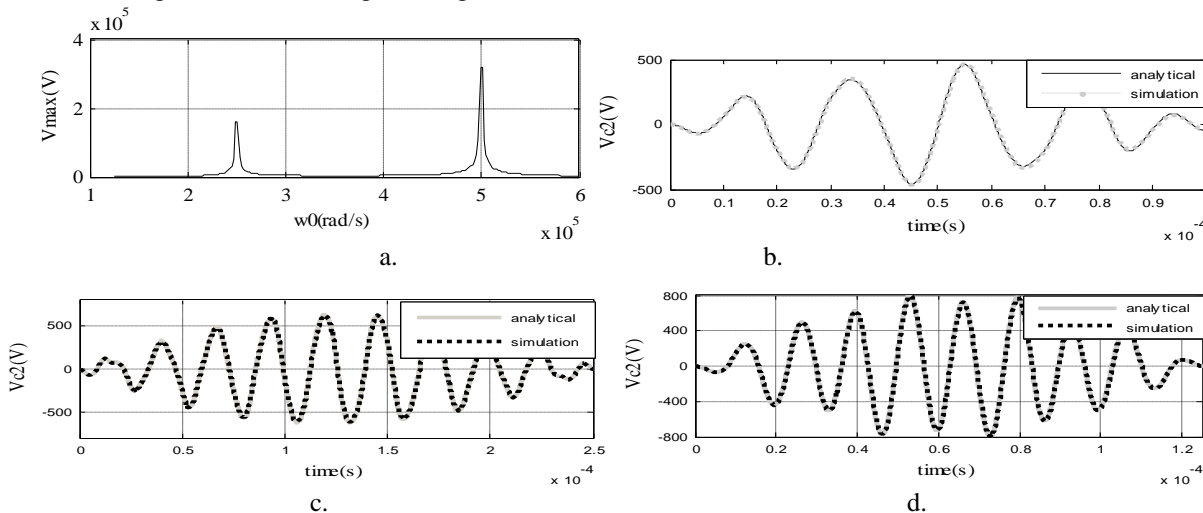


Fig.5 a: maximum output voltage of tesla transformer in terms of ω_0 .
 b: $\omega_0 = \omega_1$. c: $\omega_0 = 0.9x_2$. d: $\omega_0 = 0.9x_1$.

Comparison results Eq.8, primary current, dc link current and voltage in the case of $\omega_0 = \omega_1$, $C_{dc}=0.1\text{mF}$ and $\Delta t=0.1\mu\text{s}$ are shown in fig.6a-d. As shown in fig.6c with decreasing Δt , insignificant difference between the numerical results and simulation will decrease.

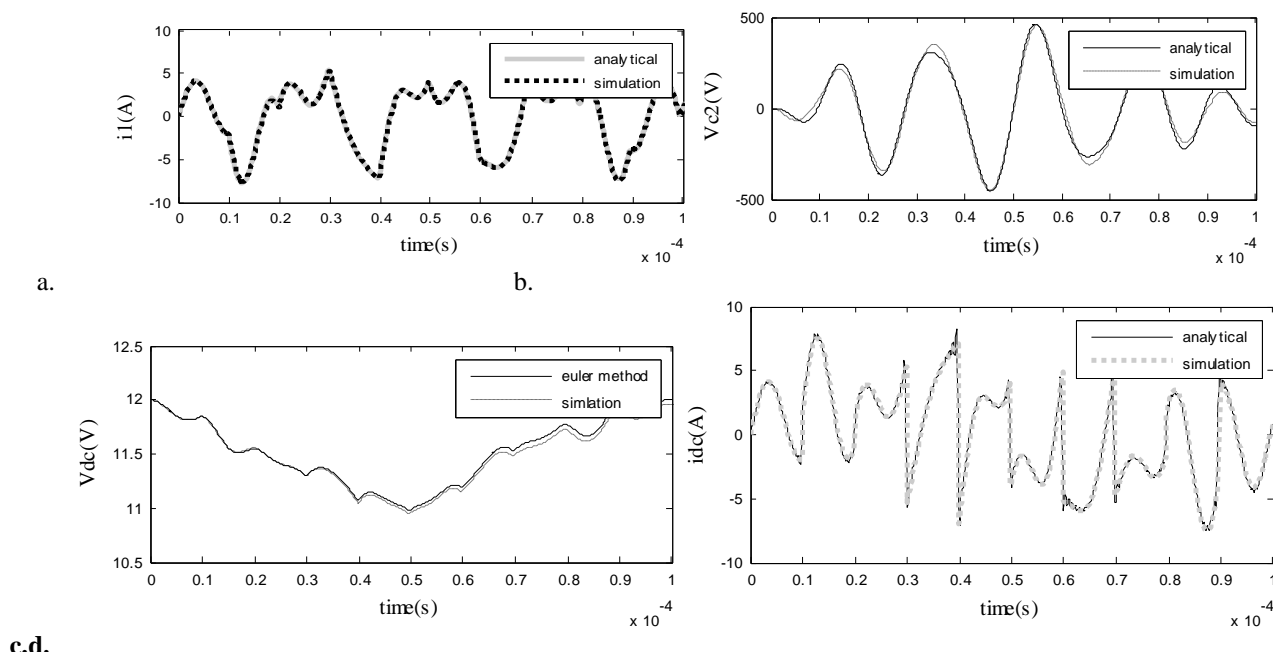


Fig.6 a: approximated output voltage of tesla transformer.

b: primary current. C: dc link current. D: dc link voltage

Figure.7 shows the results of numerical and simulation of the dc link voltage in the case of $C_{dc} = 50\mu\text{F}$.

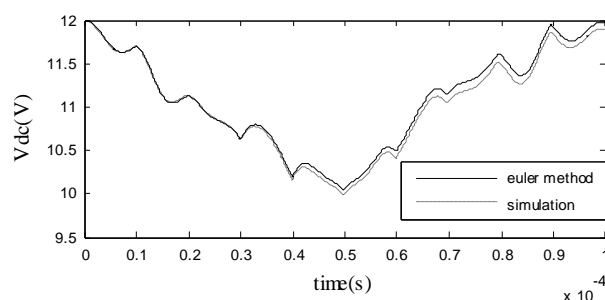


Fig.7 dc link voltage: $C_{dc}=50\mu\text{F}$

IV. CONCLUSION

According to the discussions, it was shown that the calculated equations are sufficiently accurate, And a closed equation for the maximum output voltage Tesla transformer is calculated and operating frequency of inverter that cause increment in output voltage of tesla is investigated. Also effect of tesla transformer operation on dc link voltage and current are studied in this paper and a method for sizing of dc link capacitor is proposed. For further works, impact of other parameters such as duty cycle of inverter and coupling coefficient and etc on output voltage of Tesla transformer and other variables of the system can be studied.

REFERENCES

- [1] R.E. Terman, "Radio Engineers Handbook (First Edition)" McGraw-Hill Book Company, 1943.
- [2] J. Corum, J. Daum, "Tesla Coil Research" US Army Armament Research, May 1992.
- [3] L. A. Kelley, "Direct Solution of Coupled Tuned Circuits" Electrical Engineering, vol.51, Issue.11, pp.789-794, Nov.1932.
- [4] Sanford, S. Richard, "Analysis Of A Tuned Coupled Circuit By Root-Locus Techniques" IEEE Trans, Educ, vol. 7, Issue: 2 & 3, pp. 82- 85, 1964.
- [5] N. de, N. Donaldson and T. A. Perkins, "Analysis of resonant coupled coils in the design of radio frequency transcutaneous links" Med.& Biol. Eng&Comput, vol.21, pp.612-627, 1983.
- [6] H. Suomalainen, "The Tesla Coil Theory and Applications", Sept.1993.
- [7] R. A. Martin, R. D. Teasdale, "Input Admittance Characteristics of a Tuned Coupled Circuit" Proc. IRE, Vol.40, Issue.1, pp.57-61, 1952.
- [8] J.J. Adams, "Under coupling in Tuned Coupled Circuits to Realize Optimum Gain and Selectivity" Proc. IRE, Vol.29, Issue.5, pp.277-279, 1941.
- [9] N.W. Mather, "An Analysis of Triple Tuned Coupled Circuits" Proc. IRE, Vol.38, Issue.7, pp.813-822, 1950.
- [10] V. A. Kolchanova, "On Calculation of the Tesla Coil with Iron Core" " Proc. SPCMTT, pp.40-41, 2003.
- [11] M. Paraliev, C. Gough, S. Ivkovic, "Tesla Coil Design for Electron Gun Application" PPC, pp.1085-1088, 2005.
- [12] M. Tilbury, *The Ultimate Tesla Coil Design and Construction Guide*, McGraw-Hill, Inc. 2008.

Optimization of a New Wedge Disc Brake Using Taguchi Approach

Mostafa M. Makrahy, Nouby M. Ghazaly, k. A. Abd El-Gwwad, K. R. Mahmoud and
Ali M. Abd-El-Tawwab

Automotive and Tractor Eng. Dept., College of Engineering, Minia University, El-Minia – 61111, Egypt

ABSTRACT: *In this study, a new wedge disc brake performance is assessed using brake dynamometer and Taguchi approach. The Taguchi method is widely used in the industry for optimizing the product and the process conditions. Taguchi orthogonal design method is used to gain better understanding about the factors that effect of wedge brake performance using L9 orthogonal array. Three control factors were considered as applied pressure, vehicle speed and wedge angle inclination, each at three levels is selected. The most affects parameters on brake performance were performed using the analysis of signal-to-noise (S/N) ratio and ANOVA analysis, respectively. It can be concluded that Taguchi method is reliable and reduce the time and experimental costs. In addition, the results indicated that the applied pressure and wedge angle are the most significant parameters for evaluation the wedge disc brake.*

Keywords: *Taguchi approach, wedge disc brake, applied pressure, sliding speed*

I. INTRODUCTION

In spite of the extensive research efforts that have been carried out to evaluate the brake systems during the last decades, still many challenges ahead and evaluation brake performance is still a complex phenomenon. This may be due to the fact that brake system is influenced by a large number of variables including materials of brake components, geometry of components, component interaction, many operating and environmental condition. Friction behavior is the most critical factor in brake system design and performance. For up-front design and system modeling it is desirable to describe the frictional behavior of a brake lining as a function of the local conditions such as contact pressure, temperature, and sliding speed. Typically, frictional performance is assessed using brake dynamometer testing of full-scale hardware, and the average friction value is then used for the remaining brake system development [1].

There are many research papers on investigation of the brake systems has been conducted using theoretical, numerical and experimental approaches. The experimental approaches have been used to measure the brake performance for the system during braking event. Experimental approaches using brake dynamometers have been widely used to study the brake performance at different design parameters and operating conditions. Moreover, Experimental approaches used to measure friction as a function of temperature, pressure, and temperature by external control of these variables [2, 3]. Many researchers used the brake dynamometer to examine the brake system during different design stages to optimize its performance. Iijima et al. [4] used a brake dynamometer to measure brake dust from three types of NAO pads. Pad or rotor temperature, brake pressure, rotational speed, and their associated ramp rates are all parameters that can be monitored precisely [5]. Actually, there are two basic designs for the brake dynamometer. The first design is an inertia dynamometer that has flywheel attached to it [6, 7]. The second design is a drag dynamometer that can only test the brake system at a constant speed [8-12].

Taguchi method is one of the most popular methods for optimizing the design parameters. This method improves product quality based on the concepts of statistics and engineering. The method is capable of establishing an optimal design configuration even when interactions exist among the control variables. Among several optimization techniques, the Taguchi method has been successfully applied for a systematic approach to optimize designs and to achieve manufacturing parameters [13]. The method can be used for improving the quality of existing products and processes and simultaneously reducing their costs very rapidly. Taguchi method is designed to minimize the number of experiments and to analyze the specific interactions between control factors and noise factors using an orthogonal array [14-15]. Lately, Taguchi method has become a well-recognized approach for analyzing the interaction effects while performing ranking and screening of various controllable factors. Moreover, this method is proven to be capable of solving a variety of problems involving continuous, discrete and qualitative design variables [16]. According to Taguchi method for optimization systems, all machines or set-up are classified as engineering systems (if it produces a set of responses for a given set of inputs). Those systems can be classified in to two categories. They are: i) Static system and ii) Dynamic system. Recently, Nouby et al. [17] used Taguchi method based design of experiment to evaluate the contributions of different materials of disc brake components and its interaction effects for effective reduction of disc brake noise and vibration. Their results concluded that the friction material of the brake system contributes approximately 56% to the total system instability.

In this study, the modeling and optimization of different parameters on wedge disc brake performance were investigated by using the Taguchi design method. This approach facilitated the study factors and their settings with a small number of experimental runs leading to considerable economy in time and cost for the process optimization. An L9 orthogonal array of the Taguchi method was implemented to investigate the effects of brake performance. The most affects parameters on brake performance were performed by using the analysis of signal-to-noise (S/N) ratio and ANOVA analysis, respectively. And also, the braking force results obtained as experimental and the results of the regression analysis obtained empirical equations are compared.

II. EXPERIMENTAL SETUP

The primary goal in the development of the current simplified dynamometer is to generate accurate braking forces data for use in evaluating the new wedge disc brake system. The dynamometer designed to study the effect of many operation and design parameters on the performance of the novel wedge disc brake. The operating parameters such as applied force, wedge inclination angle, sliding speed, and water spray as function of time. In addition, design parameters namely; friction material slots, different brake pad thickness and length, and different types of brake rotor. Moreover, the brake dynamometer can be used to study the noise and vibration of the brake systems.

In this study, the brake dynamometer is designed to provide the necessary disc rotation speed, applied pressure and wedge angle for investigating the new wedge brake mechanism. It can be divided into three main subsystems: the driving system, the braking system and the measurement facilities. Fig. 1 shows a photo of the test rig with its different systems. The driving system consists of an A.C. motor of 18.56 KW and 1500 rpm, that rotates the driving shaft at different rotating speeds. This is achieved with the help of a two manual gearboxes. The braking system contains the new wedge disc brake assembly which used in this study to increase the braking force, as shown in Fig. 2. Brake master cylinder is used to apply required pressure. The measurement facilities including suitable instruments to measure the following: Rotating speed (tachometer), Actuating pressure (a pressure gauge), temperature (thermocouple) and tangential force (load cell).

Brake performances are recorded at different vehicle speeds ranged from 6 to 36.3 km/hr., set from the gearboxes reduction ratio and measured by speed tachometer. Different brake pressure in the range of 2.5 to 10 bars is controlled and wedge angle is adjusted manually between 15° to 45° . Four-channel data acquisition system is used to monitor braking force. The acquired signals are transferred to a computer in digital form for storage and further analysis. For more details on experimental work details, see reference [18].



Fig. 1 Main components of the brake dynamometer.

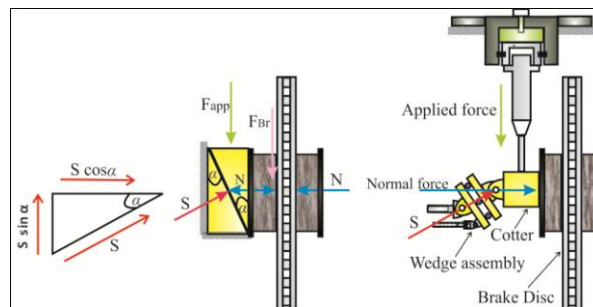


Fig. 2 Wedge disc brake.

III. TAGUCHI APPROACH

Despite of huge number of studies has been made on brake system; there is no general agreement about the effect of some parameters on the final product. In addition, the interrelationships between the effecting parameters involve complex processes. The study of factors influencing the final products phase is also a time consuming task. Hence, the analysis using conventional experimental methods is inefficient and expensive. Therefore for the present study, Taguchi orthogonal design method was used to gain better understanding and find out the significant contributions of the different operation variables with other design parameters. Taguchi method is a combination of mathematical and statistical techniques used in an empirical study, which is economical for optimization of complicated processes [19-20]. By application of this method, less experimental work is required in order to study multiple levels of all input parameters and some effects due to statistical variations are filtered out. The main steps of Taguchi method as follows:

1. Identify the quality characteristics and parameters to be evaluated.
2. Determine the number of levels for the parameters and possible interactions between the parameters.
3. Select the appropriate orthogonal array and assign the parameters to the orthogonal array.
4. Conduct the experiments based on the arrangement of the orthogonal array.
5. Analyse the experimental results using the signal-to-noise ratio and statistical analysis of variance.
6. Select the optimal levels of parameters.
7. Verify the optimal parameters through the confirmation experiment.

The wedge disc brake force as output response is tested through the dynamometer considering three factors namely; applied pressure, rotational speed and wedge angle. The levels of each factor are selected to further investigations using Taguchi approach. The factors and levels are shown in Table 1.

Table 1 Assignment of the levels to the factors

Symbol	Factors	Levels		
		1	2	3
A	Applied pressure (bar)	2.5	6.25	10
B	Rotational speed (rpm)	54	205	329
C	Wedge angle (degree)	15	30	45

3.1 Orthogonal Arrays

One of the major tools in the Taguchi method is called the orthogonal array. Orthogonal design is one of the most effective and time-saving methods for the studies involving multiple variables in order to find out which factors (or variables) influence to the most extent properties of the target product. An array is called orthogonal due to that each column indicates a value of a considered factor, and the factors listed in the orthogonal array can be evaluated independently. Every row in an orthogonal array represents a set of parameters for one run of the experiment. The L9 orthogonal array of the Taguchi method was chosen in our studies. The selection of the orthogonal array is based on the condition that the degrees of freedom for the orthogonal array should be greater than or at least equals sum of those of parameters. The factors (variables) and levels for L9 (3³) orthogonal array design are listed in Table 1. Three factors were considered namely; applied pressure (bar), rotational speed (rpm) and wedge angle (degree). For each factor, three levels were selected in order to eliminate the influence and validate the results. Nine experimental runs derived from the L9 orthogonal array design are shown in Table 2. The braking force was taken as measured responses. Applying the simple factorial design for study of the assigned three levels of each parameter, the numbers of permutations would be 27= (3³). However, the fractional factorial design reduced the number of experiments to 9 runs only. Experimental tests using brake dynamometer are conducted for each row of the orthogonal array and the output response is recorded, as shown in Table 2. The experimental observations are further transformed into Signal to noise ratio.

Table 2 Experimental design using L9 orthogonal array

Tests	pressure	Speed	Angle	Results
1	2.5	54	15	1850
2	2.5	205	30	956
3	2.5	329	45	721
4	6.25	54	30	2230
5	6.25	205	45	1543
6	6.25	329	15	2992
7	10	54	45	2861
8	10	205	15	4261
9	10	329	30	3217

3.2 Signal-to-Noise Ratio

Signal-to-noise (S/N) ratio is used to measure the quality characteristic deviating from the desired value. There are three types of quality characteristic in the analysis of the signal-to-noise ratio, (i.e. the lower-the-better, the higher-the-better, and nominal-the-better). Since, the requirement is to maximize the brake forces through selection a proper parameters; higher-the-better quality characteristic is employed for obtaining optimal computed to analyze the deviation between the experimental value and the desired value.

The S/N ratio η (the unit of S/N is dB) is given by:

$$\eta = -10 \log(MSD) \tag{1}$$

Where, MSD is the mean-square deviation for the output characteristic. MSD for the higher-the-better quality characteristic is calculated by the following equation,

$$MSD = \frac{1}{N} \left[\sum_{i=1}^n \frac{1}{Y_i^2} \right] \tag{2}$$

Where, Y_i is the brake force response for the i_{th} test, n denotes the number of tests and N is the total number of data points. The function ‘-log’ is a monotonically decreasing one, it means that we should maximize the S/N value. The S/N values are calculated using “equation 1” and “equation 2”. Table 3, shows the response table for S/N ratios using higher-the-better approach. The S/N analysis is based on the experimental data. It is suggested that quality characteristics are optimized when the S/N response is as larger as possible.

Table 3 Response for S/N ratio

Level	A	B	C
1	60.68	67.15	69.15
2	66.75	65.30	65.55
3	70.62	65.60	63.35
Delta	9.94	1.84	5.80
Rank	1	3	2

IV. RESULTS AND DISCUSSION

From Fig. 3 of S/N ratios plot and from Table3 of S/N ratio response,it is suggested that quality characteristics are optimized when the S/N response is as larger as possible. The response table for S/N ratios using higher-the-better approach is listed based on the experimental data. It is suggested that quality characteristics are optimized when the S/N response is as larger as possible. It is also observed that pressure value 2.5 bar combined with speed 54 rpm and 15 angle is the optimum combination for maximized the brake performance.

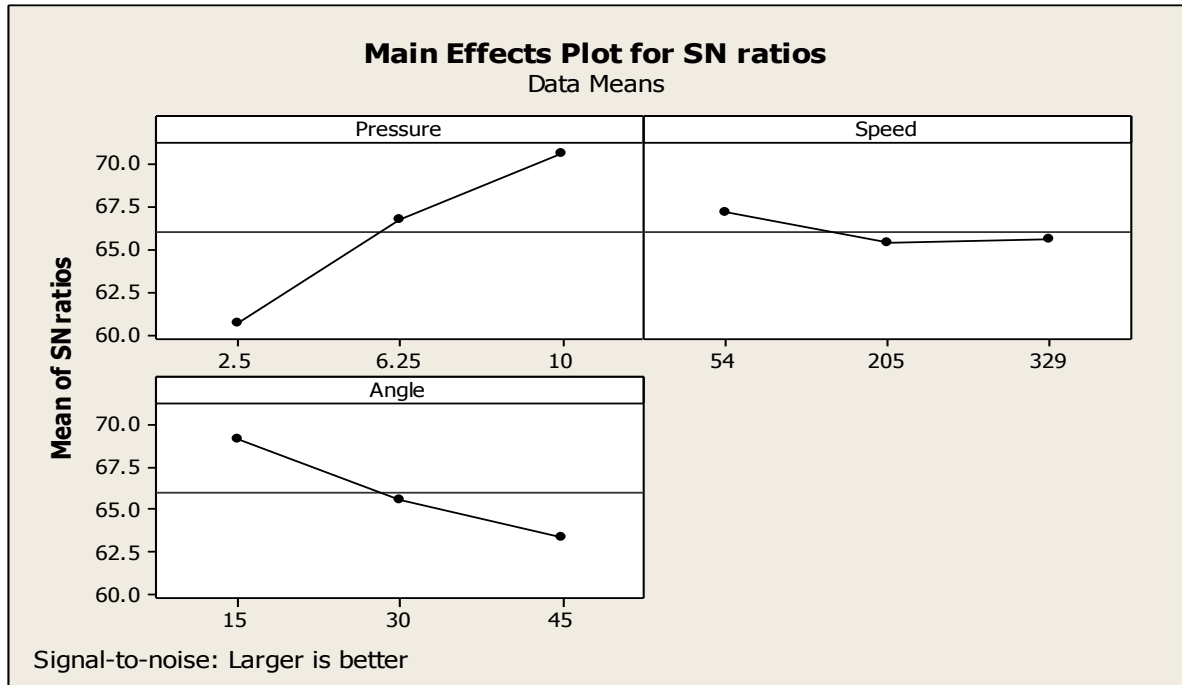


Fig.3 S/N ratios plot of the variables on the brake performance

V. ANALYSIS OF VARIANCE (ANOVA)

In general, Analysis of variance (ANOVA) can be used to understand the relative significance of the process effects on the experimental responses and to estimate the experimental error due to different associated factors. In this study, the ANOVA analysis is conducted to determine the effect of the parameters on wedge brake performance. ANOVA analysis is performed for a 5% (P < 0.05) significance level, i.e., for a 95% confidence level to identify the parameters that affect the wedge brake performance. Statistically, F-tests provided a decision at some confidence level that is the realized significance levels, for each source of variation as shown in Tables 4. The F test and P value illustrated that the variation of the process parameter made a big change on the performance characteristics. According to Table 4, applied pressure were found to be the major factor affecting the wedge brake performance whereas, wedge angle were found to be the second important factor. But, a vehicle speed shows a little effect on the brake performance.

Table 4 Analysis of Variance

Source	DF	Seq SS	Adj SS	Adj MS	F	P
Regression	3	10387620	10387620	3462540	90.489	0.00008
A	1	7747521	7747521	7747521	202.471	0.00003
B	1	33	33	33	0.001	0.97782
C	1	2640067	2640067	2640067	68.995	0.00041
Error	5	191324	191324	38265		
Total	8	10578944				

VI. CONTRIBUTIONS OF PARAMETERS

In this section, the effect of each parameter with different levels can be determined by averaging the S/N ratios in the experiments design. It can be seen that based on the Taguchi method and S/N ratio contributions of parameters are computed and plotted. Fig.4 shows the contribution of the three parameters on the brake performance. It is found that the applied pressure contributes 56.5 % of the total brake performance. It is followed by the wedge angle, which contributes 33 % of the system performance. And also, rotational speed in the selected range of experimental study is obtained a percentage contribution of 10.5 % only.

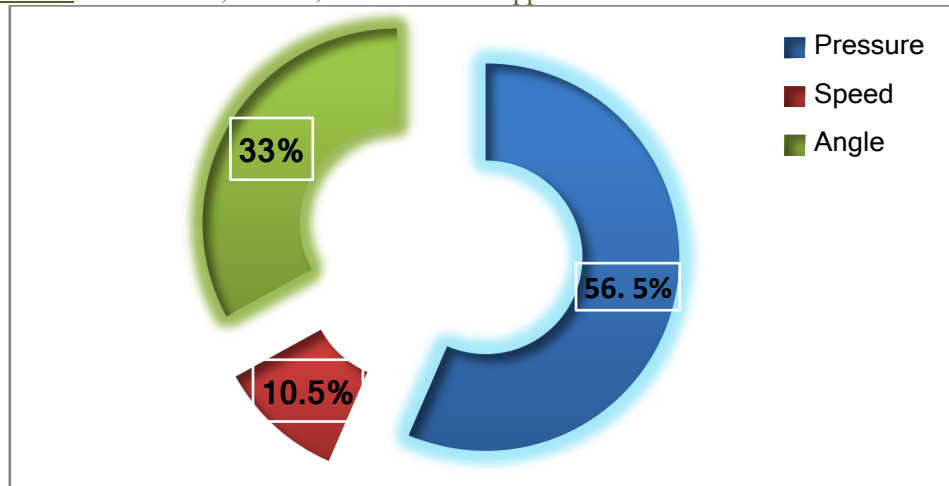


Fig.4 Contribution of parameter on the wedge brake performance

VII. CONCLUSIONS

In this study, Taguchi method is conducted to estimate the effects of the optimum parameters and their setting on the wedge brake performance. Taguchi method with L9 (33) orthogonal array is performed to investigate ranking of the effective parameters namely; the applied pressure, rotational speed and wedge angle on the performance of wedge disc brake. The ANOVA analysis is conducted to examine the significant of each factor. The results revealed that the applied pressure contributes 56.5 % of the total brake performance. It is followed by the angle, which contributes 33 % of the system performance. In addition, the rotational speed contributes a percentage of 10.5 % only. It can be concluded that Taguchi design method exhibit a good performance in the optimization of different parameters on measuring the braking force of the wedge disc brake.

REFERENCES

- [1] P.G. Sanders, T.M. Dalka, R.H. Basch, A reduced-scale brake dynamometer for friction characterization, *Tribology International* 34, 609–615, 2001.
- [2] Neuman RF, Urban JA, McNinch JH. ‘Performance characterization of dry friction materials’ In: *Braking of road vehicles*. London: Mechanical Engineering Publications Ltd, 1983:233–8, 1983.
- [3] Zimmer D. ATE friction test machine and other methods of lining screening. Society of Automotive Engineers paper 820163, 1982.
- [4] A. Iijima, K. Sato, K. Yano, M. Kato, K. Kozawa, N. Furuta, Emission factor for antimony in brake abrasion dusts as one of the major atmospheric antimony sources, *Environmental Science and Technology* 42 (8), 2937–2942, 2008.
- [5] V. Vadari, and M. Albright, An introduction to brake noise engineering, *J. sound and vibration*, Vol 35-7, Roush Industries Inc., Livonia, Michigan, 2001.
- [6] Trichés, M. J., Samir, N. Y. and Jordan, R. “Reduction of squeal noise from disc brake systems using constrained layer damping”, *J. of the Brazilian Society of Mechanical Science and Engineering*, Vol. 26, pp. 340-348, 2004.
- [7] Chen T. F., “Relationship between Formulation and Noise of Phenolic Resin Matrix Friction Lining Tested In Acoustic Chamber on Automotive Brake Dynamometer,” Master of Science Thesis, Southern Illinois University, 2005.
- [8] Amr M. M. Rabia, Nouby M. Ghazaly, M. M. M. Salem, Ali M. Abd-El-Tawwab. “An Experimental Study of Automotive Disc Brake Vibrations” *The International Journal of Engineering and Science (IJES)*, Vol.2, Issue 01, PP. 194-200, 2013.
- [9] Nouby, M. and Srinivasan, K. ‘Simulation of structural modifications of a disc brake system to reduce brake squeal, *Proc. IMechE, Part D: J. Automobile Engineering*, Vol. 225, No. 5, 653–672, 2011.
- [10] Cunefare, K. A. and Graf, A. J. “Experimental active control of automotive disc brake rotor squeal using dither”, *Journal of Sound and Vibration*, Vol. 250, No. 4, pp. 575-590, 2002.
- [11] Nouby M. Ghazaly “Study on Automotive Disc Brake Squeal Using Finite Element Analysis and Design of Experiments” PhD. Thesis, Department of Mechanical Engineering, Anna University, India, 2011.
- [12] Fieldhouse, J. D., Steel, W. P., Talbot, C. J. and Siddiqui, M. A. “Brake noise reduction using rotor asymmetric”, *Proc. of IMechE International Conference Braking 2004*, Professional Engineering Publishing Ltd, pp. 209-222, 2004.
- [13] D.C. Montgomery, *Design and Analysis of Experiments*, Wiley, New York, 1997.
- [14] G.S. Peace, *Taguchi Methods: A Hands-on Approach*, Addison-Wesley, Reading, MA, 1993.
- [15] S.J. Kim and H. Jang, Friction and wear of friction materials containing two different phenolic resins reinforced with aramid pulp. *Tribol. Int.* 33, pp. 477–484, 2000.
- [16] Hou, T.H., Su, C.H., Liu, W.L. ‘Parameters optimization of a nano-particle wet milling process using the Taguchi method, response surface method and Genetic algorithm. *Powder Technology*, 173, p.153-162, 2011.
- [17] Nouby, M. Abdo, J. Mathivanan D. and Srinivasan K. “Evaluation of Disc Brake Materials for Squeal Reduction’ *Tribology Transactions*, 54: 644-656, 2011.
- [18] Mostafa M. M., Nouby M. G., Abd El-Gwwad K. A., Mahmoud K. R. and Abd-El-Tawwab A. M., A Preliminary Experimental Investigation of a New Wedge Disc Brake, *Int. Journal of Engineering Research and Applications*, Vol. 3, Issue 6, pp.735-744, Nov-Dec 2013.

On the Exponential Diophantine Equations

$$x^x y^y = z^z \quad \text{and} \quad x^{x^n} y^{y^m} = z^{z^n}$$

M.A.Gopalan¹, G.Sumathi² and S.Vidhyalakshmi³

1. Department of Mathematics, Shrimathi Indira Gandhi College, Trichy-2, Tamilnadu,
2. Department of Mathematics, Shrimathi Indira Gandhi College, Trichy-2, Tamilnadu,
3. Department of Mathematics, Shrimathi Indira Gandhi College, Trichy-2, Tamilnadu,

ABSTRACT: In this paper, two different forms of exponential Diophantine equations namely $x^x y^y = z^z$ and $x^{x^n} y^{y^m} = z^{z^n}$ are considered and analysed for finding positive integer solutions on each of the above two equations. Some numerical examples are presented in each case.

Keywords: Exponential Diophantine Equation, integral solutions.
Mathematics subject classification number: 11D61

I. INTRODUCTION

The exponential diophantine equation $a^x + b^y = c^z$ in positive integers x, y, z has been studied by number of authors [1-5]. In [6-12] the existence and the processes of determining some positive integer solutions to a few special cases of an exponential diophantine equation are studied. In this paper, two different representations I and II of the exponential diophantine equations namely $x^x y^y = z^z$ and $x^{x^n} y^{y^m} = z^{z^n}$ are studied with some numerical examples.

II. METHOD OF ANALYSIS

Representation I

The exponential diophantine equation with three unknowns to be solved for its non-zero distinct integral solutions is

$$x^x y^y = z^z \tag{1}$$

where n is a natural number

Introducing the transformations

$$x = u z^n, y = v^{\frac{1}{n}} z \tag{2}$$

in (1), it becomes

$$z = u^{\frac{u}{1-nu-v}} v^{\frac{v}{1-nu-v}} \tag{3}$$

Taking

$$\frac{u}{1-nu-v} = -n_1, \quad \frac{v}{n(1-nu-v)} = -n_2 \tag{4}$$

and solving the above two equations, we have

$$u = \frac{n_1}{nn_1 + nn_2 - 1}, \quad v = \frac{nn_2}{nn_1 + nn_2 - 1} \tag{5}$$

Substituting (5) in (3) and (2), the corresponding solutions of (1) are

$$\left. \begin{aligned} x &= \left(\frac{nn_1 + nn_2 - 1}{n_1} \right)^{nn_1 - 1} \left(\frac{nn_1 + nn_2 - 1}{nn_2} \right)^{nn_2} \\ y &= \left(\frac{nn_1 + nn_2 - 1}{n_1} \right)^{n_1} \left(\frac{nn_1 + nn_2 - 1}{nn_2} \right)^{n_2 - \frac{1}{n}} \\ z &= \left(\frac{nn_1 + nn_2 - 1}{n_1} \right)^{n_1} \left(\frac{nn_1 + nn_2 - 1}{nn_2} \right)^{n_2} \end{aligned} \right\} \dots\dots\dots(6)$$

The numbers n_1 and n_2 can be chosen such that the solutions (6) be natural numbers.

Now taking

$$n_1 = n^{\alpha n - 1}, \quad \alpha > 0; \quad n_2 = \frac{1}{n}, \quad n > 0 \text{ in (5), the non-zero integral solutions of (2) are found}$$

to be

$$x = n^{n^{\alpha n}} n^{\alpha n - 1}$$

$$y = n^{n^{\alpha n - 1}}$$

$$z = n^{n^{\alpha n - 1}} n^{\alpha}$$

Numerical Examples

(α, n)	x	y	z
(1,2)	32	4	8
(2,3)	3^{734}	3^{243}	3^{245}
(1,3)	3^{29}	3^9	3^{10}
(2,2)	2^{19}	2^8	2^{10}

Representation II

The exponential Diophantine equation with three unknowns to be solved for its non-zero distinct integral solutions is

$$x^{x^n} y^{y^m} = z^{z^n} \tag{7}$$

where m,n are natural numbers

Considering the transformations

$$x = u^n z, \quad y = v^m z^m \tag{8}$$

in (7), it can be written as

$$z = u^{\frac{\frac{u}{n}}{1 - u - \frac{nv}{m}}} v^{\frac{\frac{v}{m}}{1 - u - \frac{nv}{m}}} \tag{9}$$

Assuming

$$\frac{\frac{u}{n}}{1 - u - \frac{nv}{m}} = -n_1, \quad \frac{\frac{v}{m}}{1 - u - \frac{nv}{m}} = -n_2 \tag{10}$$

and solving the above two equations, we have

$$u = \frac{nn_1}{nn_1 + nn_2 - 1}, \quad v = \frac{mn_2}{nn_1 + nn_2 - 1} \tag{11}$$

Substituting (11) in(9) and (8),the corresponding solutions of (6) are

$$\left. \begin{aligned} x &= \left(\frac{nn_1 + nn_2 - 1}{nn_1} \right)^{\frac{nn_1 - 1}{n}} \left(\frac{nn_1 + nn_2 - 1}{mn_2} \right)^{n_2} \\ y &= \left(\frac{nn_1 + nn_2 - 1}{n_1} \right)^{\frac{nn_1}{m}} \left(\frac{nn_1 + nn_2 - 1}{mn_2} \right)^{\frac{nn_2 - 1}{m}} \\ z &= \left(\frac{nn_1 + nn_2 - 1}{nn_1} \right)^{n_1} \left(\frac{nn_1 + nn_2 - 1}{mn_2} \right)^{n_2} \end{aligned} \right\} \dots\dots\dots(12)$$

The numbers n_1 and n_2 can be chosen such that the solutions (11) be natural numbers.

For illustration, Choosing

$$n = m\beta^m, n_2 = \alpha^{mn}n^{mn-1}, n_1 = \frac{1}{n}, n > 0 \text{ in (11), the non-zero integral solutions of (6)}$$

are represented by

$$\begin{aligned} x &= \beta^{m\alpha^{mn}n^{mn-1}} \\ y &= (\alpha n)^n \beta^{(\alpha n)^{mn} - 1} \\ z &= (\alpha n)^m \beta^{m\alpha^{mn}n^{mn-1}} \end{aligned}$$

Numerical examples:

(m,n)	(α, β)	x	y	z
(1,2)	(1,2)	2^2	2^5	2^3
(1,3)	(2,18)	$3^2 \cdot 18^{35}$	$18^{18} 3^{18^{36} - 1}$	$18^2 3^2 \cdot 18^{35}$

III. CONCLUSION

To conclude, one may search for other pattern of integer solutions to the above exponential diophantine equations.

REFERENCES

- [1] B.He and A.Togbe, The Diophantine equation $n^x + (n+1)^y = (n+2)^z$ revisited, Glasgow Math.J.51(2009),659-667
- [2] S.Cenberci and H.Senay, The Diophantine equation $x^2 + B^m = y^n$, International Journal of Algebra,3(13),2009,657-662
- [3] A.Suvarnamani, Solutions of the Diophantine equation $2^x + p^y = z^2$, International journal of Mathematical Sciences and Applications,6(3),2011,1415-1419
- [4] S.Cenberci, B.Pekar and S.Coskun, On solutions of the equation $x^2 \pm y^8 = \pm z^6$, International Journal of Contemp.Math.Sciences,7(14),2012,685-692
- [5] N.Terai, On the Exponential Diophantine Equation $(4m+1)^x + (5m^2-1)^y = (3m)^z$, International Journal of Algebra,1(23),2012,1135-1146
- [6] Tudor.GH.M.L, Diophantine Equation $x_1^{x_1} \cdot x_2^{x_2} \dots x_k^{x_k} = y_k^{y_k}$ (I), Bul.St.al Uni, Politehnica, din Timisoara, Seria Mat-Fiz.,2003, Nr.48(62),2,13-18
- [7] Tudor.GH.M.L, Diophantine Equation $(x_1^{x_1})^{m_1} \cdot (x_2^{x_2})^{m_2} \dots (x_k^{x_k})^{m_k} = y_k^{y_k}$ (II), Bul.St.al Uni, Politehnica, din Timisoara, Seria Mat-Fiz.,2004, Nr.49(63),1,13-19
- [8] Tudor.GH.M.L, Diophantine Equation $x_1^{x_1} \cdot x_2^{x_2} \dots x_k^{x_k} = y_1^{y_1} \cdot y_2^{y_2} \dots y_k^{y_k}$ (III), Bul.St.al Uni, Politehnica, din Timisoara, Seria Mat-Fiz.,2004, Nr.49(63),1,1-8
- [9] Tudor.GH.M.L, Diophantine equation $x_1^{x_1} \cdot x_2^{x_2} \dots x_k^{x_k} = w^{w^p}$ (IV), Bul.St.al Uni, Politehnica, din Timisoara, Seria Mat-Fiz.,2005, Nr.50(64),2,18-24
- [10] Tudor.GH.M.L, Diophantine Equation $x^x \cdot y^{y^q} = z^{z^p}$ (V), Bul.St.al Uni, Politehnica, din Timisoara, Seria Mat-Fiz.,2005, Nr.50(64),2,18-24
- [11] Gheorghe M.Tudor, Tudor Binzar, On the Diophantine equation $x^x y^{y^{k(y)}} = z^{z^p}$, Buletinul Academiei DE STINTE, A Repubuc11 Moldova, matematica, No.2(63),2010, pg 121-124
- [12] Tudor.GH.M.L, BINZAR.T, On the Diophantine Equation $x_1^{x_2^\alpha} \cdot x_2^{x_3^\alpha} \dots x_k^{x_1^\alpha} = w^{w^\alpha}$ (II), Bul.St.al Uni, Politehnica, din Timisoara, Seria Mat-Fiz.,2008, Nr.53(67),1,44-49

Design and Simulation of Dynamic voltage restorer (DVR) using SPWM and SVPWM Techniques for Voltage Sags & Voltage Swells Mitigation

G Mohan¹ (M.Tech), Prof. A Lakshmi Devi²

¹DEPARTMENT OF E.E.E, SVUCE, TIRUPATI, INDIA

²DEPARTMENT OF E.E.E, SVUCE, TIRUPATI, INDIA

ABSTRACT: This paper presents design and simulation of Dynamic voltage restorer(DVR) using sinusoidal pulse width modulation (SPWM) & space vector pulse width modulation(SVPWM). It describes the problems of voltage sags & swells and its severe impact on nonlinear loads (or) sensitive loads. DVR is a series connected device used for compensating the voltage sags & swells in distribution system. The detection of sags/swells is carried out with the help of dq0 theory, whereas the control of voltage source inverter is done with help of SPWM & SVPWM. This paper compares the total harmonic distortion(THD) of the DVR using SPWM & SVPWM. The simulation was carried out with the help of SIMULINK & MATLAB and the results were found to be in accordance with theoretical values.

Keywords: Dynamic voltage restorer (DVR), sinusoidal pulse width modulation (SPWM), space vector pulse width modulation (SVPWM),dq0 theory, voltage sag/swell.

I. INTRODUCTION

The term power quality is something that describes the quality of power, it is the quality of voltage rather than power (or)current. Power Quality problems encompass a wide range of disturbances such as voltage sags/swells, flicker, harmonics distortion, impulse transient, and interruptions .Because of the voltage deviation the electrical utility is not able to supply the pure sinusoidal voltage of required magnitude and frequency. Voltage sags can occur at any instant of time, with amplitudes ranging from 10 – 90% and a duration lasting for half a cycle to one minute .Voltage swell, on the other hand, is defined as a swell is defined as an increase in rms voltage or current at the power frequency for durations from 0.5 cycles to 1 min. typical magnitudes are between 1.1 and 1.8 up. These voltage problems can be solved using a series connected custom power device called dynamic voltage restorer(DVR). The emphasis has been given for switching control strategy i.e, pulse width modulation techniques and their results are presented.

II. DVR

The main function of a DVR[1] is the protection of sensitive loads from voltage sags/swells coming from the network The following steps are used to implement the DVR in injection mode.

Step 1: To find out whether there is any sag/swell in the source voltage. It is done by comparing the terminal source voltages with reference load voltages. The difference between the source voltages and reference load voltages is the required amount of voltage that has to be injected by the DVR.

Step 2: To generate switching commands to the VSI in order to track the reference voltages (generated in step 1) using a suitable switching scheme such as PWM.

Step 3: To filter out the harmonics that are present in the output of the voltage source inverter.

Step 4: To inject the filtered output through the three single phase series isolation transformers present between the source and the load.

Following above mentioned steps, the DVR should work only if there is any difference between the terminal source voltage and the load voltage. To implement above steps, the following building blocks are required to realize the DVR.

- i. Detection and control block
- ii. Voltage source inverter
- iii. Filter components
- iv. Isolation transformers

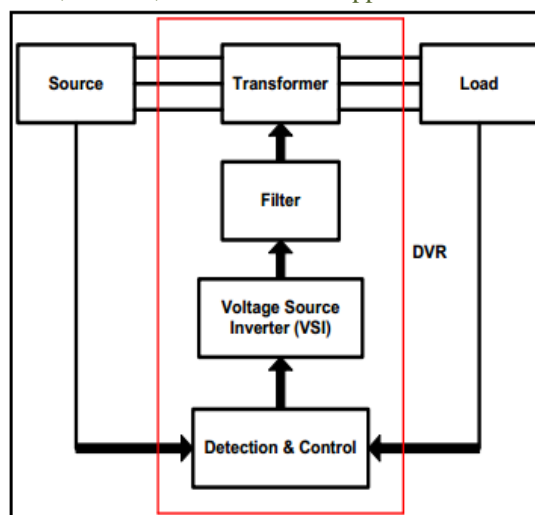


fig2.1: Block diagram of DVR

III. PWM TECHNIQUES

There are two types pulse width modulation (PWM) techniques used in this dynamic voltage restorer

3.1 Sinusoidal pulse width modulation (SPWM)

The most common PWM strategy for a two-level phase leg is a "sine-triangle" comparison of a (sinusoidal) low-frequency fundamental reference waveform against a high-frequency carrier waveform. The phase leg switches to the upper or the lower dc rail supply, depending on whether the reference waveform is greater or less than the carrier waveform. The carrier waveforms are classified as triangular, saw-tooth, trapezoidal. Triangular waveforms are most popular and used for PWM. The SPWM[2] technique has been widely used in conventional two-level inverter due to its simplicity and low distortion characteristics.

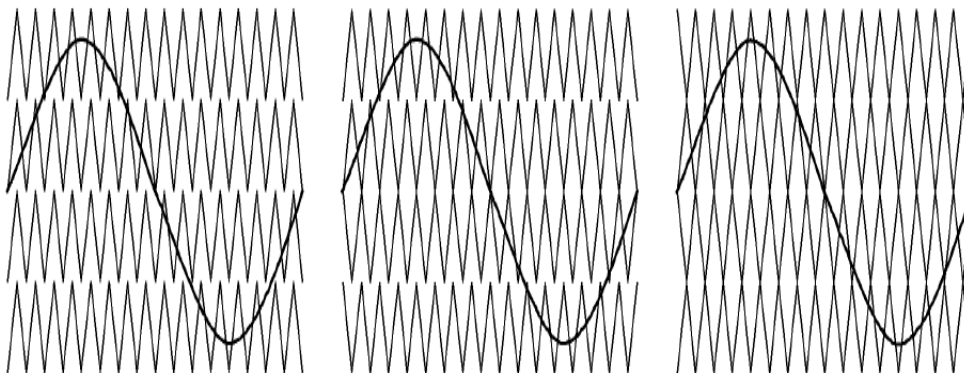


Fig3.1: Carrier (triangular) and reference (sinusoidal) waveform for five-level inverter.

3.2 space vector pulse width modulation (SVPWM)

Space vector PWM[3] refers to a switching scheme of the six power switches of a 3-phase VSI. It generates minimum harmonic distortion and also provides more efficient use of DC supply voltage in comparison with the sinusoidal modulation method. SVPWM treats the inverter as a single unit. Specifically the inverter can be driven to eight unique states. Modulation is accomplished by switching the state of inverter. Space vector pulse width modulation treats the sinusoidal voltage as a constant amplitude vector rotating at constant frequency.

In a two level three phase inverter total eight (2^3) vectors are possible among those six are non-zero vectors and two are zero vectors. Six non-zero vectors (V_1 - V_6) shape the axes of a hexagonal as depicted in Fig. 3.2, supplies power to the load. The angle between any adjacent two non-zero vectors is 60 degrees. Meanwhile, two zero vectors (V_0 and V_7) and are at the origin and apply zero voltage to the load. The eight vectors are called the basic **space vectors** and are denoted by ($V_0, V_1, V_2, V_3, V_4, V_5, V_6, V_7$). The same transformation can be applied to the desired output voltage to get the desired reference voltage vector, V_{ref} in the d-q plane. The objective of SVPWM technique is to approximate the reference voltage vector V_{ref} using the eight switching patterns. One simple method of approximation is to generate the average output of the inverter in a small period T_Z to be the same as that of V_{ref} in the same period.

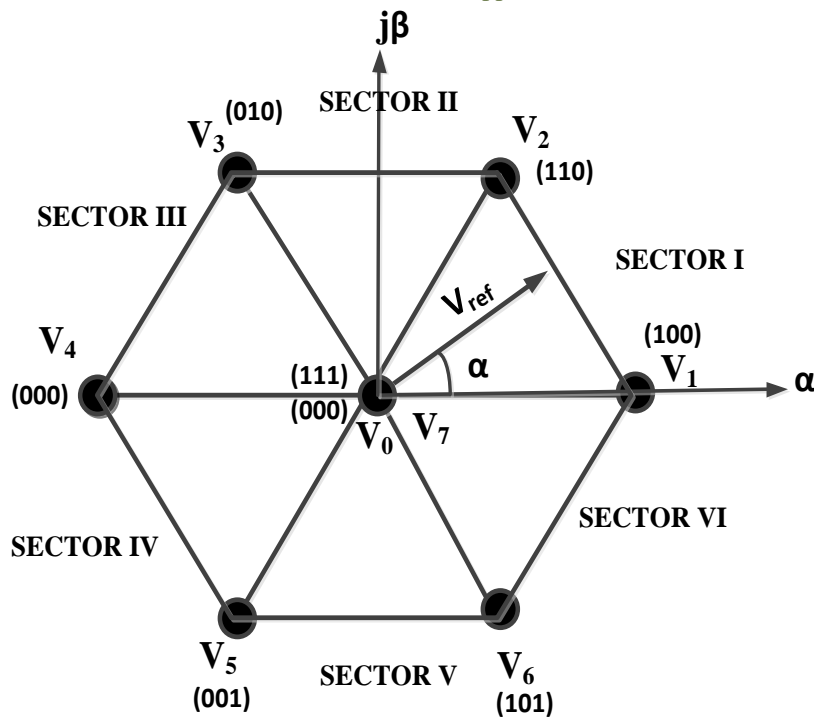


Fig. 3.2: Two-level space vector diagram

IV. SIMULATION RESULTS AND DISCUSSION

The designed DVR is used to compensate sags/swells of magnitude in the range (0.1p.u - 0.9 p.u). But in reality a DVR can compensate a maximum of 0.5p.u. For the purpose of demonstration sag of magnitude 0.2 p.u and a swell of magnitude 0.2 p.u are considered. The VSI is implemented using both SPWM as well as SVPWM and the results were compared

Table1:parameter values for simulation

Parameter	Value
RMS line-to-line voltage	400V
Resistance and Inductance of the line	0.1Ω,0.5mH
Transformer turns ratio	1: 1
Transformer no load losses	0.002p.u
Filter parameters	R=5Ω ; C=1μF; L=10mH
Active and Reactive power of load	1000W,200W
Line frequency	50HZ

4.1 voltage sags:

4.1.1:spwm waveforms

The first simulation shows of three phase voltage sag is simulated. The simulation started with the supply voltage 20% sagging as shown in Figure 3.1.1 (a).In Figure 3.1.1 (a) also shows a 20% voltage sag initiated at 0.2s and it is kept until 0.8s, with total voltage sag duration of 0.6s. Figures 3.1.1 (b) and (c) show the voltage injected by the DVR and the corresponding load voltage with compensation. As a result of DVR, the load voltage is kept at 1 p.u.

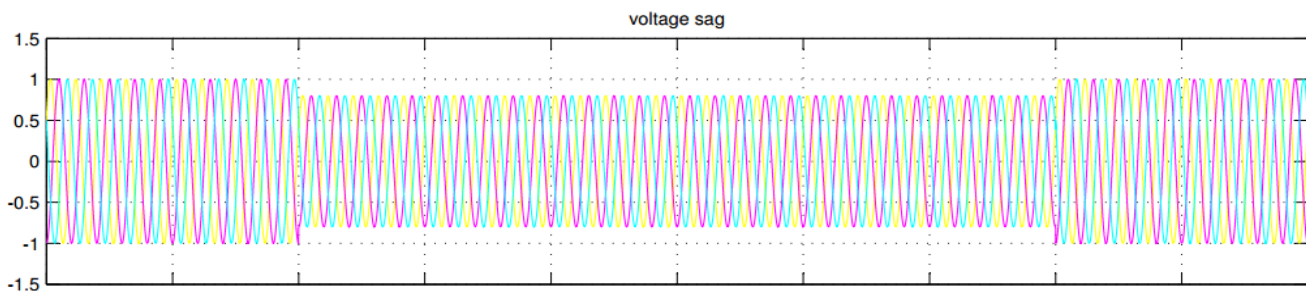


fig 4.1.1 (a):voltage sag of 0.2 p.u

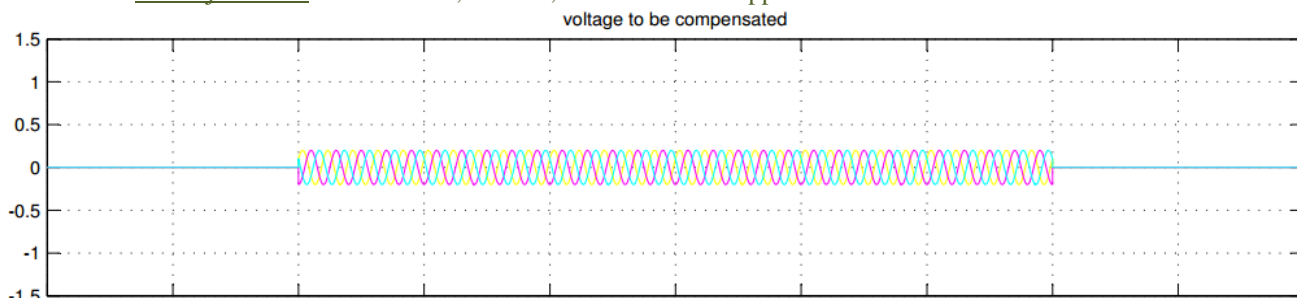


fig 4.1.1 (b): injected voltage

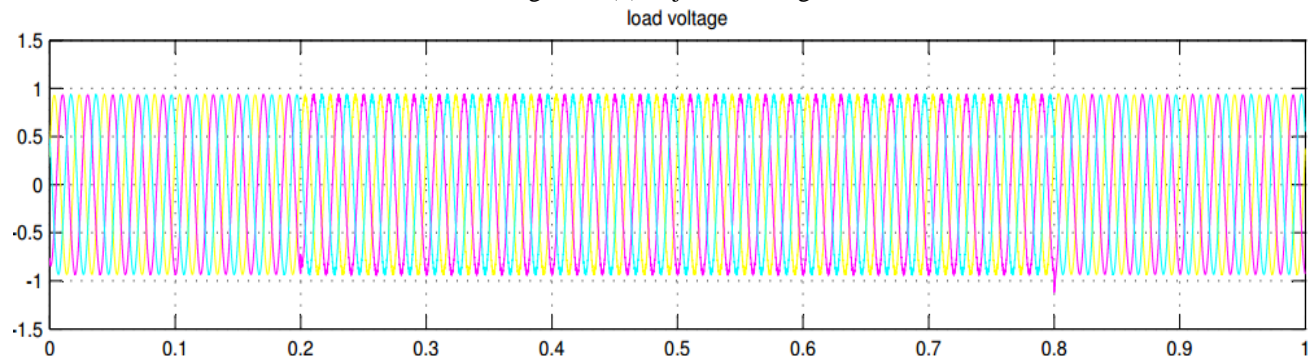


fig 4.1.1(c):load voltage

4.1.2:svpwm waveforms

The first simulation shows of three phase voltage sag is simulated. The simulation started with the supply voltage 20% sagging as shown in Figure 3.1.2 (a). In Figure 3.1.2 (a) also shows a 20% voltage sag initiated at 0.2s and it is kept until 0.8s, with total voltage sag duration of 0.6s. Figures 3.1.2 (b) and (c) show the voltage injected by the DVR and the corresponding load voltage with compensation. As a result of DVR, the load voltage is kept at 1 p.u.

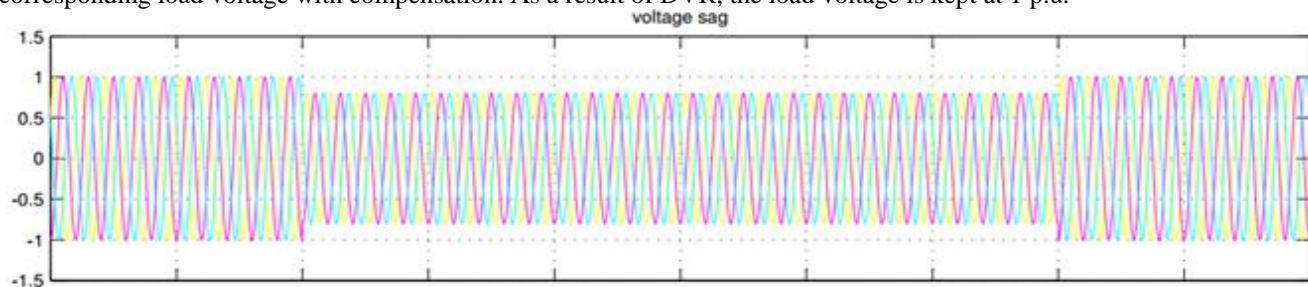


fig 4.1.2 (a):voltage sag of 0.2 p.u

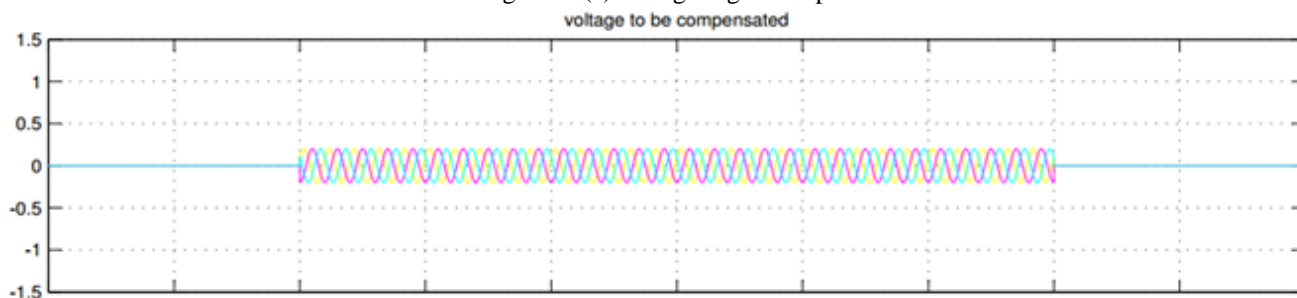


fig 4.1.2 (b): injected voltage

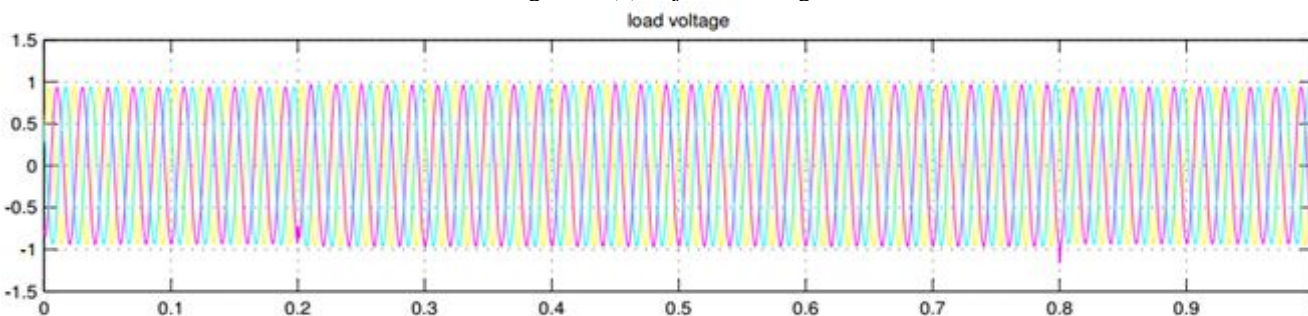


fig 4.1.2(c):load voltage

4.2 voltage swells:**4.2.1: spwm waveforms**

The first simulation shows of three phase voltage swell is simulated. The simulation started with the supply voltage 20% swell as shown in Figure 3.2.1 (a). In Figure 3.2.1 (a) also shows a 20% voltage swell initiated at 0.2s and it is kept until 0.8s, with total voltage sag duration of 0.6s. Figures 3.2.1 (b) and (c) show the voltage injected by the DVR and the corresponding load voltage with compensation. As a result of DVR, the load voltage is kept at 1 p.u.

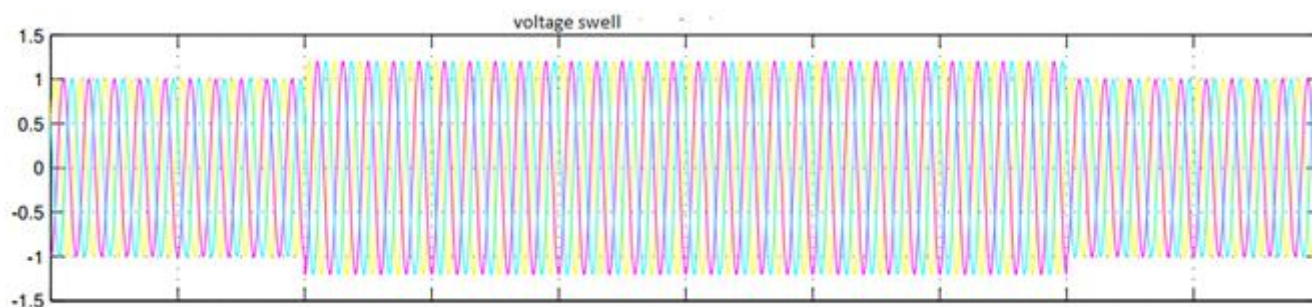


fig 4.2.1 (a):voltage swell of 0.2 p.u

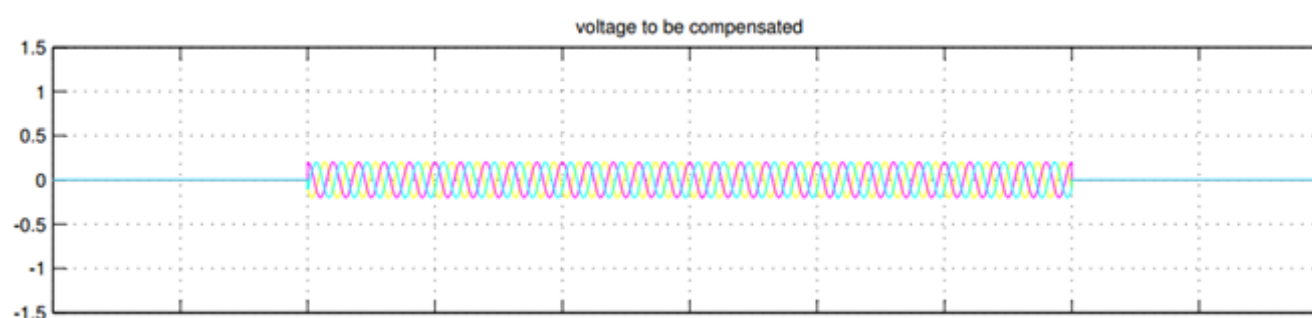


fig 4.2.1 (b): injected voltage

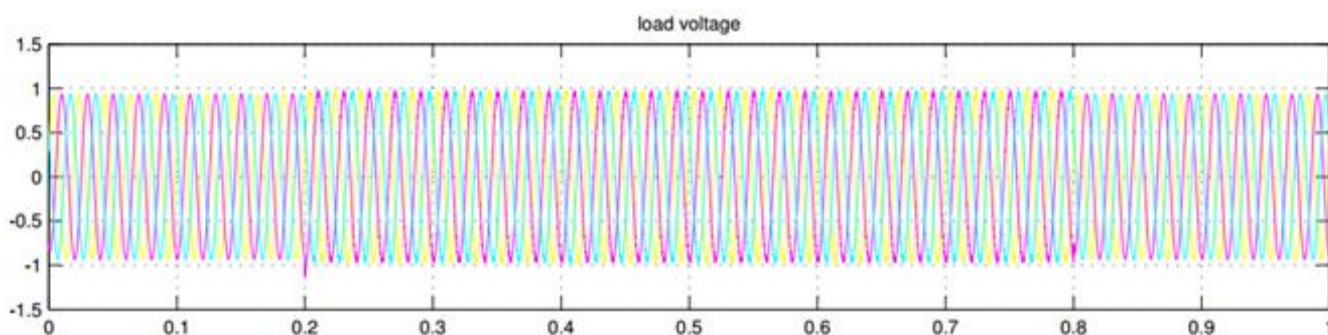


fig 4.2.1(c):load voltage

4.2.2:svpwm waveforms

The second simulation shows of three phase voltage swell is simulated. The simulation started with the supply voltage 20% swell as shown in Figure 3.2.2 (a). In Figure 3.2.2 (a) also shows a 20% voltage swell initiated at 0.2s and it is kept until 0.8s, with total voltage sag duration of 0.6s. Figures 3.2.2 (b) and (c) show the voltage injected by the DVR and the corresponding load voltage with compensation. As a result of DVR, the load voltage is kept at 1 p.u.

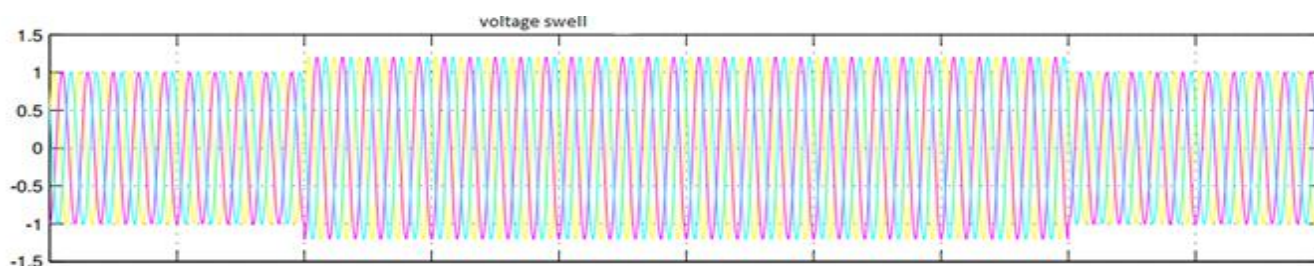


fig 4.2.2 (a):voltage swell of 0.2 p.u

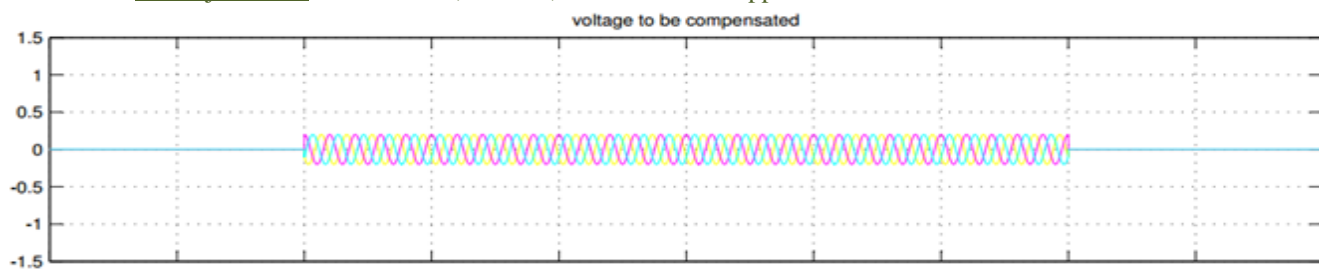


fig 4.2.2 (b): injected voltage

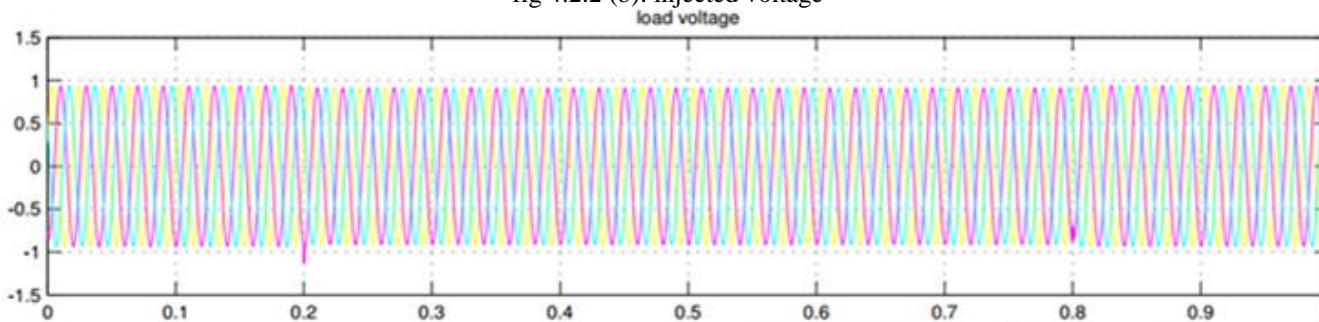


fig 4.2.2 (c): load voltage

4.3:FFT analysis of spwm & svpwm

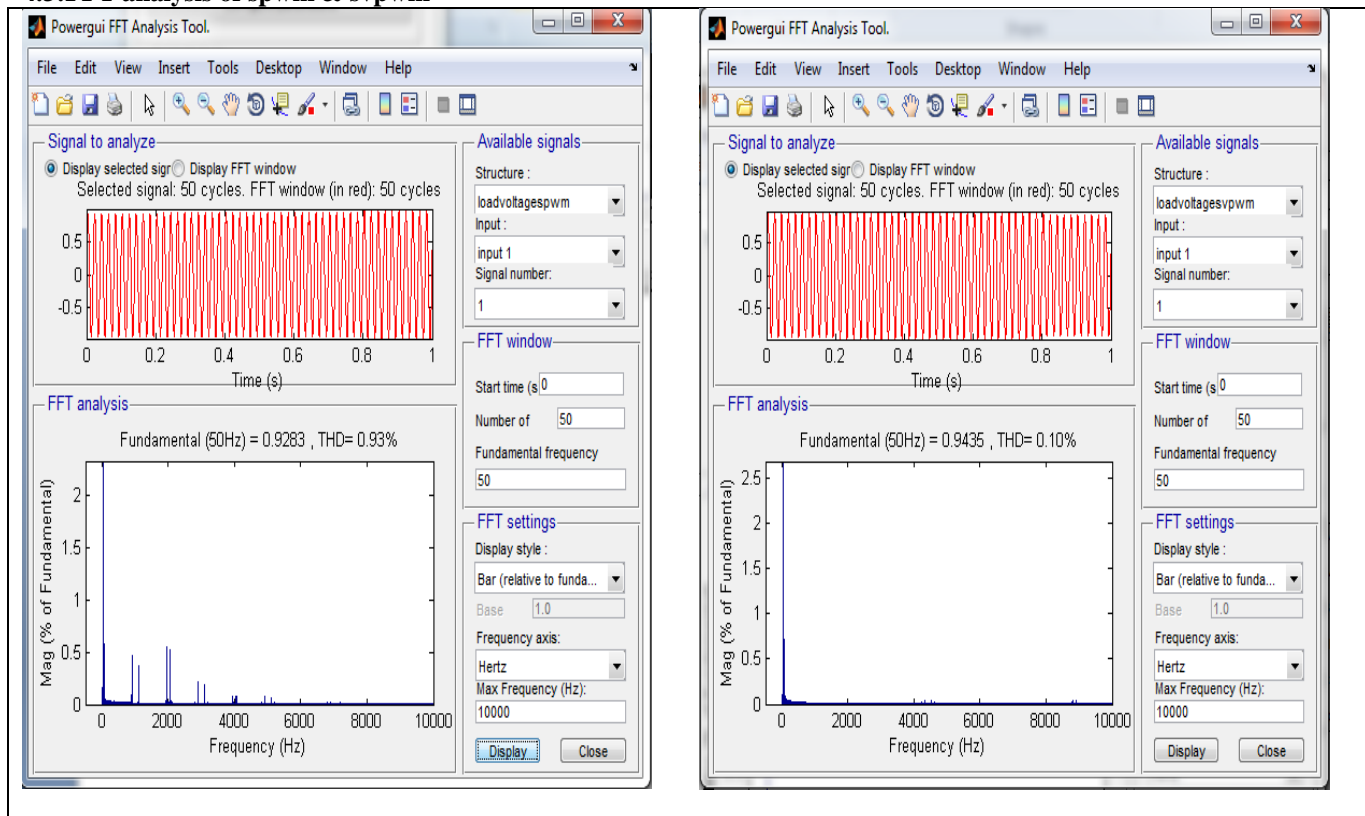


fig4.3.1: waveforms of showing the FFT analysis of load voltage of spwm & svpwm

Table 2: Comparison of THD values in SPWM & SVPWM

S.NO	Waveform	THD in SPWM(%)			THD in SVPWM(%)		
		Sag	Swell	Sag&Swell	Sag	Swell	Sag&Swell
1	inverter output voltage	163.74	163.56	223.96	89.56	89.54	125.76
2	filter output voltage	11.34	4.49	9.94	0.35	0.35	1.04
3	Source voltage	0.00	0.00	0.00	0.00	0.00	0.00
4	load voltage	1.10	1.08	0.93	0.09	0.09	0.1

From the FFT analysis it is clear that the harmonic presents in the inverter output voltage & filter output voltage are low in case of space vector pulse vector pulse width modulation (SVPWM) than the sinusoidal pulse width modulation

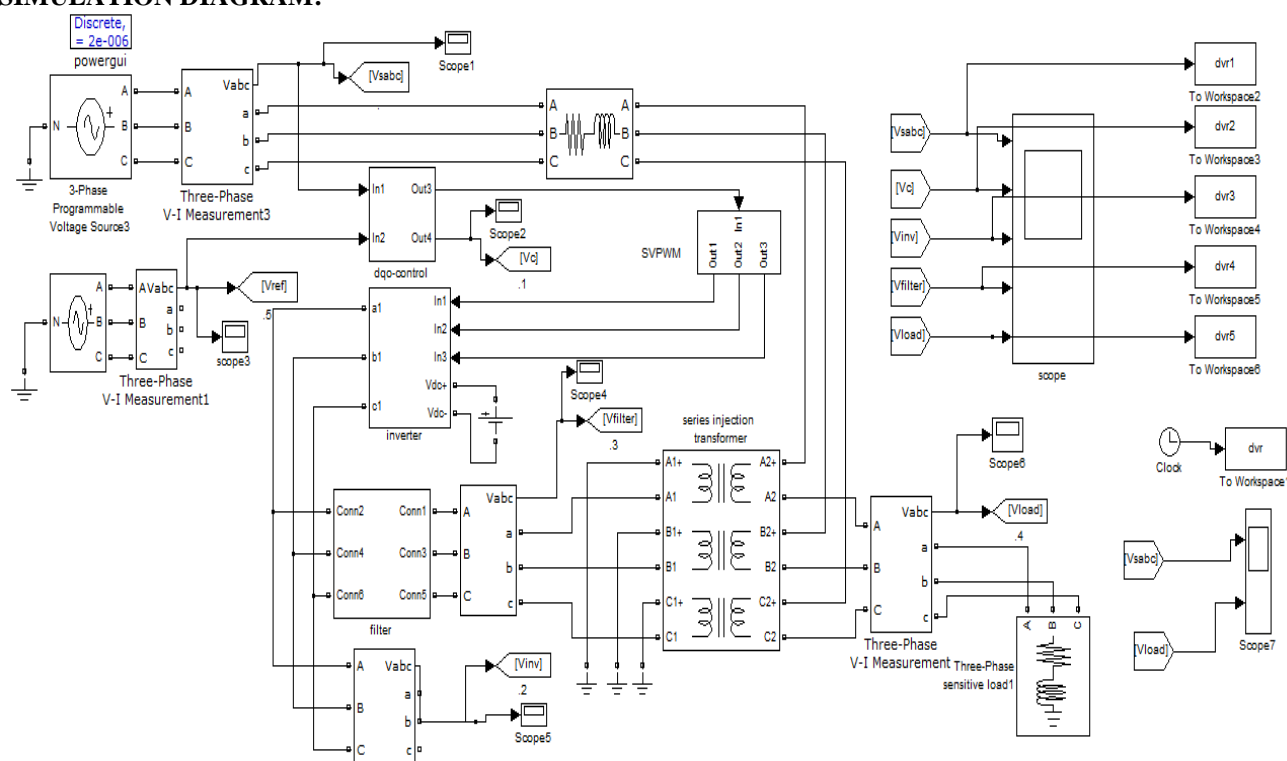
V. CONCLUSION

The modelling and simulation of DVR using MATLAB/SIMULINK has been presented. The performance of DVR is studied under voltage Sag & Swells by using SPWM and SVPWM Techniques. From the simulation results DVR compensates Sags & Swells quickly and provides better voltage regulation in both the cases. Space Vector PWM effectively restored the voltage of Sensitive load to normal and reduced the harmonic distortion in load voltage when compared with Sinusoidal PWM. The Simulation study reveals that SPWM requires 15% more dc voltage when compared to SVPWM for the same output. For the compensation of same amount of voltage Sags & voltage Swells SVPWM requires less amount of dc voltage when compared to SPWM. So by using SVPWM technique dc voltage required for inverter is less when compared to Sinusoidal PWM technique in order to generate same amount of output. The harmonics content in the output voltage is reduced by using Space Vector PWM technique as compared to SPWM technique.

REFERENCES

- [1] Design, Modelling and Simulation of Dynamic Voltage Restorer for Voltage Swell/Sag Mitigation. Journal of Engineering Science and Technology (IJEST). ISSN 0975-5462. Vol. 3 No. 6 June 2011
- [2] Design and Simulation of Dynamic Voltage Restorer (DVR) Using Sinusoidal Pulse Width Modulation (SPWM). Saripalli Rajesh, Mahesh K. Mishra, Senior Member IEEE and Sridhar. 16th national power systems conference, 15th-17th december, 2010.
- [3] Dynamic Voltage Restorer Based on Space Vector Pulse Width Modulation Technique. B.N S P Venkatesh* D.Prathap Hari Krishna, Gitam University. International Journal of Engineering Science and Technology (IJEST).ISSN : 0975-5462 Vol. 3 No. 7 July 2011.
- [4] Modelling And Simulation For Voltage Sags/Swells Mitigation Using Dynamic Voltage Restorer (DVR).Rosli Omar And Nasrudin Abd Rahim. 2008 Australasian Universities Power Engineering Conference (AUPEC'08).
- [5] Dynamic Voltage Restorer (DVR) for Voltage Sag Mitigation. Mahmoud A. El-Gammal¹, Amr Y. Abou-Ghazala², and Tarek I. El-Shennawy³.International Journal on Electrical Engineering and Informatics - Volume 3, Number 1, 2011.
- [6] New Control Technique Applied In Dynamic Voltage Restorer For Voltage Sag Mitigation 1Rosli Omar, 2Nasrudin Abd Rahim and 3Marizan Sulaiman. American J. of Engineering and Applied Sciences 3 (1): 42-48, 2010 ISSN 1941-7020 © 2010 Science Publications.
- [7] Matlab/Simulink Based Analysis Of Voltage Source Inverter With Space Vector Modulation. Auzanizidin, Tolesutikno. International Journal on Electrical Engineering and Informatics - Volume 3, Number 1, 2011.

SIMULATION DIAGRAM:



CFD analysis of double-chambered crematories using biomass producer gas as a fuel source

Yaowateera Achawangkul¹, Naoki Maruyama¹, Chatchawan Chaichana²
Masafumi Hirota¹, Akira Nishimura¹, Pimpawat Teeratitayangkul²

¹Graduate School of Engineering, Mie University, JAPAN

²Department of Mechanical Engineering, Faculty of Engineering, Chiang Mai University, THAILAND

ABSTRACT: This paper describes the simulation results of a biomass producer gas-based, double-chambered crematory using CFD analysis. The specific properties of biomass gas, such as thermal conductivity, specific heat capacity and viscosity, were determined by using the constituents of coffee bean pulp-derived gas obtained from the experiment. The criteria of simulation consist of coffins and human corpses contained in the primary combustion chamber, whereas the standard k -epsilon viscous model and SIMPLE algorithm were used. The simulation results show that the modified model, with a 25 degree downward angle in the primary chamber and an adjusted air nozzle, presents a good effectiveness in heat transfer and turbulent intensity. In addition, the results of the NO prediction present a high formation rate if there is only primary chamber ignition. However, the NO formation rate will increase when operating both primary and secondary chambers. Therefore, using the CFD assistant in the biomass gas-based double-chambered crematory can achieve various benefits, such as reducing apparatus construction costs and the experiment time, including the availability for pollution prediction.

Keywords: Biomass, Computational Fluid Dynamics, Crematory, Gasification, Producer Gas

I. INTRODUCTION

Petroleum fuels such as diesel oil and LPG have been utilized as main fuel sources for cremation, especially in modern crematories that contain a cremation chamber and a flue gas treatment chamber. However, operation costs per cremation become higher due to the increasing of global petroleum prices, which directly affects low income people. In addition, it is necessary to consider the environmental effects of using petroleum fuel. Hence, research and study for alternative energy application must be carried out.

Biomass is one alternative energy resource that presents high potential in Southeast Asian countries. At present, there are several biomass technologies that can be applied for thermal application. Biomass gasification is a thermo-chemical conversion that transforms solid biomasses into a gaseous form (called producer gas or syngas), which can be combusted efficiently. It, therefore, has been introduced for heat generation in many industries. According to the property of biomass producer gas that presents combustion characteristics close to those of liquid petroleum fuel, it is possible to utilize biomass producer gas for the cremation process.

In order to apply biomass producer gas as the main fuel for an actual double-chambered crematory, it is necessary to search for appropriate parameters that perform the highest efficiency in both combustion and emission control. Consequently, computational fluid dynamics (CFD) was used to analyze flow characteristics and significant parameters such as temperature, the turbulent scheme, and a pollution forecast.

Thavornun S. [1] studied and researched energy saving ideas for human crematories using diesel oil as the main fuel source. The primary burner should be located 25° at downward angle on the backside of the primary chamber wall in order to provide maximum impingement of the flame onto the corpse. Concerning fuel consumption, the incinerator uses 35 liters of diesel oil on average throughout the cremation process.

Doungsupa N. [2] studied the simulation of combustion in a ceramic fiber kiln using computational fluid dynamics (CFD). The ceramic fiber kiln contains eight LPG burners with a 1 m³ effective volume, whereas the CFD model solves conservation equations for mass, momentum and energy with the k - ϵ turbulent and non-static running model. The comparison between CFD simulation and actual experiments were that both results showed good agreement for temperatures below 800°C. In addition, the results also showed that the model with a slowly increasing pressure from 3 to 10 psi and 50% open damper the best condition.

Vorayos N. [3] studied computational fluid dynamics to determine the hot air (70°C) velocity flow field in a 2-dimensional model of tobacco curing barn by appointing the velocity of injected hot air as 2.8 m/s with a turbulent model. The solution showed that the low velocity contour usually took place at the middle of furnace, while the high velocity contour occurred between the low velocity contour and the furnace's wall. In addition, it was also found that if the tobacco furnace has a height and length ratio (H/L) less than 0.3, air distribution cannot reach the back of the furnace, which especially affects the quality of tobacco contained towards the back.

II. EQUATIONS

2.1 Governing equations

Fundamental governing equations used for simulation are Navier-Stokes Equations, which consist of mass conservation and momentum conservation.

$$\frac{\partial \rho}{\partial t} + \nabla \cdot (\rho \vec{V}) = 0 \quad (1)$$

$$\frac{\partial(\rho u)}{\partial t} + \nabla \cdot (\rho \vec{V} u) = \frac{\partial(-P + \tau_{xx})}{\partial x} + \frac{\partial \tau_{yx}}{\partial y} + \frac{\partial \tau_{zx}}{\partial z} + \rho f_x \quad (2)$$

$$\frac{\partial(\rho v)}{\partial t} + \nabla \cdot (\rho \vec{V} v) = \frac{\partial \tau_{xy}}{\partial x} + \frac{\partial(-P + \tau_{yy})}{\partial y} + \frac{\partial \tau_{zy}}{\partial z} + \rho f_y \quad (3)$$

$$\frac{\partial(\rho w)}{\partial t} + \nabla \cdot (\rho \vec{V} w) = \frac{\partial \tau_{xz}}{\partial x} + \frac{\partial \tau_{yz}}{\partial y} + \frac{\partial(-P + \tau_{zz})}{\partial z} + \rho f_z \quad (4)$$

2.2 Heat transfer model

An energy conservation equation is used for heat transfer inside a control volume prediction.

$$\begin{aligned} \frac{\partial(\rho h_0)}{\partial t} + \nabla \cdot (\rho \vec{V} h_0) = & \nabla \cdot (k \nabla T) + \frac{\partial p}{\partial t} + \left[\frac{\partial(u \tau_{xx})}{\partial x} + \frac{\partial(u \tau_{yx})}{\partial y} + \frac{\partial(u \tau_{zx})}{\partial z} \right] + \left[\frac{\partial(v \tau_{xy})}{\partial x} + \frac{\partial(v \tau_{yy})}{\partial y} + \frac{\partial(v \tau_{zy})}{\partial z} \right] \\ & + \left[\frac{\partial(w \tau_{xz})}{\partial x} + \frac{\partial(w \tau_{yz})}{\partial y} + \frac{\partial(w \tau_{zz})}{\partial z} \right] + S_h \end{aligned} \quad (5)$$

2.3 Standard $k - \varepsilon$ model

Standard $k - \varepsilon$ models are applied to the proper turbulent model in this research, which are represented in (6)-(7).

$$\frac{\partial}{\partial x_i} (\rho U_i k) = \frac{\partial}{\partial x_i} \left[\frac{\mu_t}{\sigma_k} \frac{\partial k}{\partial x_i} \right] + G - \rho \varepsilon \quad (6)$$

$$\text{and} \quad \frac{\partial}{\partial x_i} (\rho U_i \varepsilon) = \frac{\partial}{\partial x_i} \left[\frac{\mu_t}{\sigma_\varepsilon} \frac{\partial \varepsilon}{\partial x_i} \right] + C_1 \frac{\varepsilon}{k} G - \rho C_2 \frac{\varepsilon^2}{k} \quad (7)$$

where G and μ_t are the production rate of turbulence and the turbulence eddy viscosity, respectively.

$$G = \mu_e \left[\left(\frac{\partial u_i}{\partial x_i} + \frac{\partial u_j}{\partial x_j} \right) \frac{\partial u_i}{\partial x_j} \right] \quad (8)$$

$$\mu_t = \frac{\rho C_D k^2}{\varepsilon} \quad (9)$$

The Prandtl/Schmidt number (σ_ε) and model constants (C_1, C_2, C_D, σ_k) are shown in Table 1.

Table 1 Constants used for standard $k - \varepsilon$ model

C_1	C_2	C_D	σ_k	σ_ε
1.44	1.92	0.09	1.00	1.30

2.4 SIMPLE algorithm

The Semi-Implicit Method for the Pressure-Linked Equation (SIMPLE) algorithm is used to solve for the model's velocity flow field [4].

III. PRODUCER GAS PROPERTIES

The constituent of biomass producer gas was obtained from an experiment that used coffee bean pulp as fuel [5]. After that, the significant properties, such as thermal conductivity, viscosity and specific heat capacity, could be determined.

Table 2 Composition of coffee bean pulp producer gas

Constituent	H ₂	O ₂	N ₂	CO	CH ₄	CO ₂
Content (% by volume)	14.9	6.2	39.7	22.5	2.9	13.8

Table 3 Significant properties of coffee bean pulp producer gas

Specific heat capacity (J/kg-k)	1,467.70
Viscosity (N-s/m ²)	5.81 x 10 ⁻⁵
Thermal conductivity (W/m-k)	0.13745

IV. METHODOLOGIES

4.1 Crematory model implementation

SolidWorks 2012 is used for model implementation. The models of double-chambered crematories are separated into 4 types (A1-A4), as shown in Table 4. Five auxiliary air nozzles are arranged at both the left and right sides of the

chamber with different incline angles. On the chamber backside wall is the primary producer gas burner's position, with an incline angle of 0° for the commercial model (A1). Concerning the modified model (A3 and A4), the primary burner is located at a 25° downward angle in order to provide maximum impingement of the flame onto the coffin and corpse.

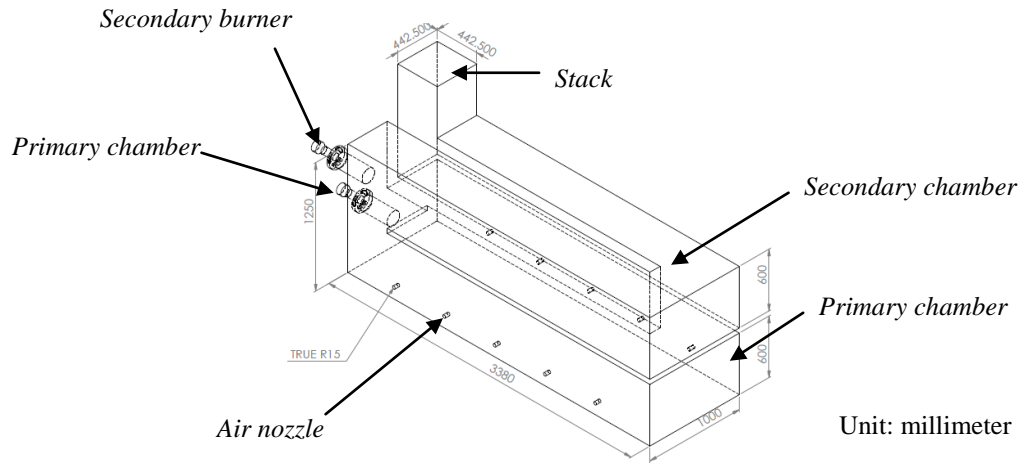


Fig.1 Schematic dimension of crematory

Table 4 Dimension of double-chambered crematory models

Conditions	A1 (Commercial type)	A2	A3	A4
	(Modified model)			
Chamber's dimensions (W x H x L) (mm.)	1,000 x 600 x 3,380			
Primary burner incline angle (deg)	0°	0°	25°	25°
Secondary burner incline angle (deg)	0°	0°	0°	0°
Auxiliary air incline angle	0°	$\phi = 30^\circ$ $\alpha = 30^\circ$	0°	$\phi = 30^\circ$ $\alpha = 30^\circ$

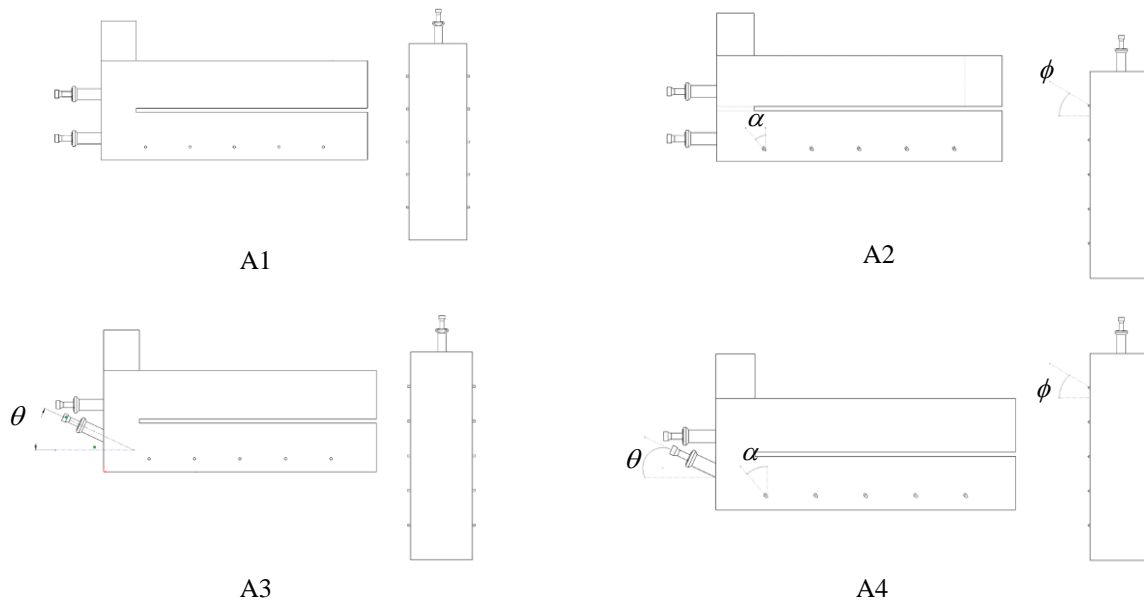


Fig.2 Crematory's model used for simulation

In order for the implemented model to be similar to actual cremation, the coffin model was also implemented. The coffin model was a replicate of the commercial coffin sold in Thailand, with the dimensions of 50 x 50 x 180 cm.

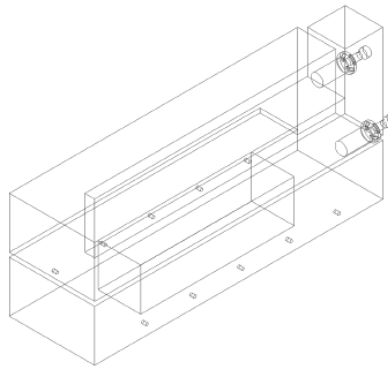


Fig.3 Coffin model implementation in the crematory

4.2 Simulation methodology and initial boundary conditions

ANSYS FLUENT was used to simulate flow characteristics inside the model. A pressure outlet boundary condition was applied to the outlet and the walls were treated at a constant wall temperature or adiabatic wall temperature. The wall was assumed to be stationary with no-slip conditions applied to the wall surface ($\vec{V}_x = \vec{V}_y = \vec{V}_z = 0$).

Velocity of producer gas at 1 st burner	5 m/s
Velocity of producer gas at 2 nd burner	5 m/s
Velocity of air injected to 1 st burner	5.6 m/s
Velocity of air injected to 2 nd burner	5.6 m/s
Velocity of auxiliary air injected to primary chamber	20 m/s
Temperature of producer gas	300 K
Temperature of combustion air	300 K

V. RESULTS AND DISCUSSION

5.1 Temperature

From the simulation results, as shown in Fig.4, the maximum temperature reached during the combustion reaction is approximately 1,700 K, which is close to the theoretical flame temperature of biomass producer gas combustion. If the crematory A1 (commercial model) was simulated using the coffin model, the temperature inside the primary chamber would be become highest at the exit of burner. However, the temperature at the front side of the crematory still had the lowest value, equal to that of the ambient temperature. This phenomenon occurred because some of the combustion heat from the burner was drafted into the secondary chamber by the influence of the exhaust fan, and the direction of the auxiliary air injected from the nozzle was dispersed perpendicularly onto the coffin’s surface, causing the air flow to counter the combustion heat. Hence, a majority of the heat was smoldered in the backside of the crematory.

When simulating the Model A2 crematory, where the incline angle of the air holds were modified, it was found that the temperature between the coffin and the crematory wall, including the front side, became higher compared to the A1 model simulation. When the airflow from the nozzles hits the coffin’s surface, a majority of the air is directed toward the crematory’s front, and also forces combustion heat from the back to the front.

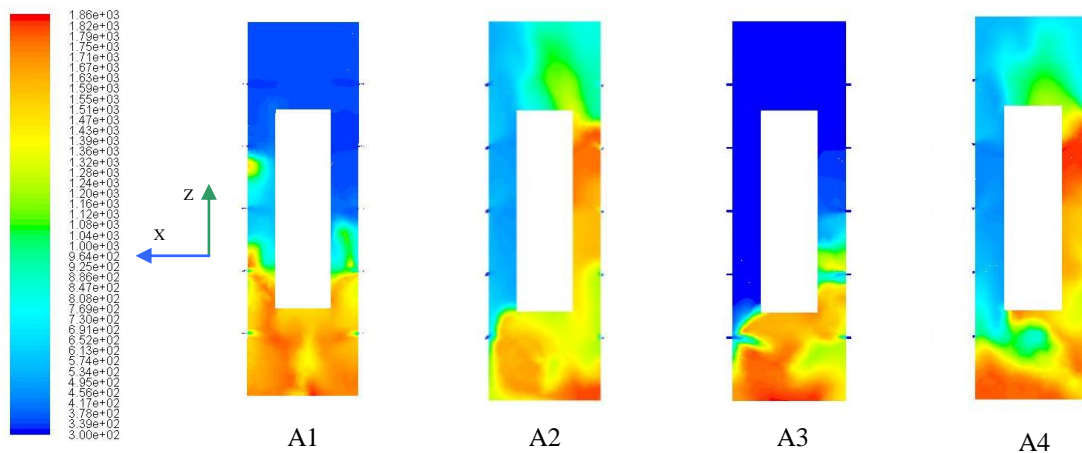


Fig.4 Top view of temperature contours inside the primary chamber with a coffin model

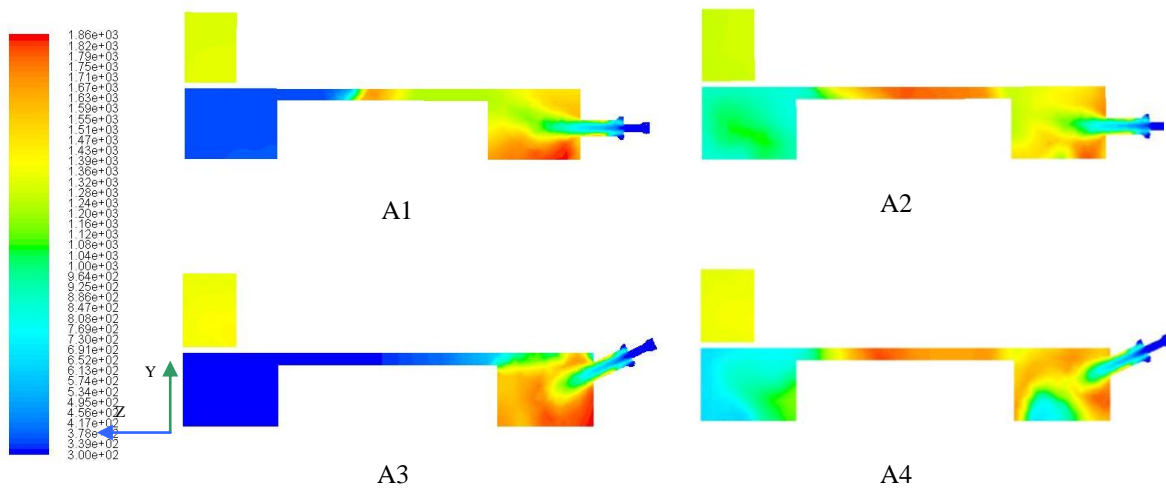


Fig.5 Side view of temperature contours inside the primary chamber with a coffin model

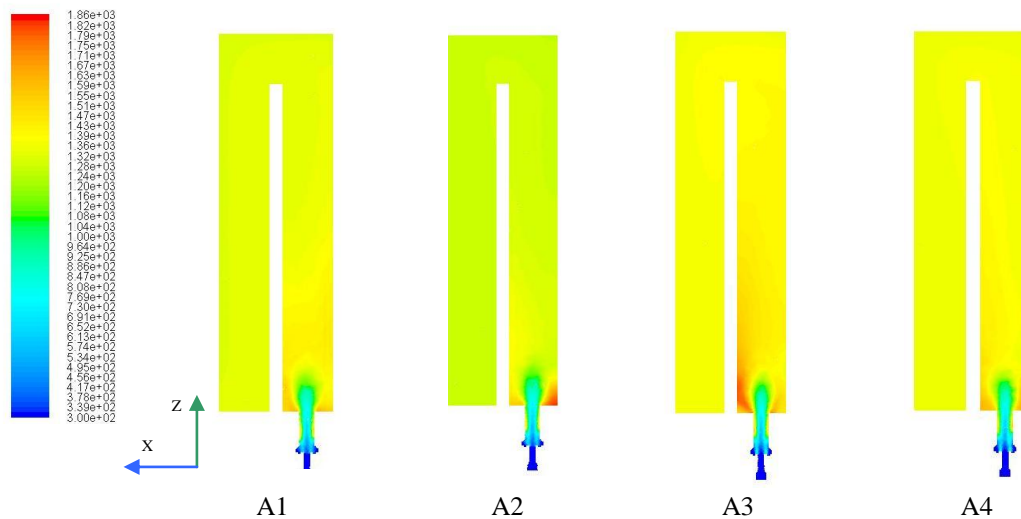


Fig.6 Top view of temperature contours inside the secondary chamber

When simulating the Model A2 crematory, where the incline angle of air holds were modified, it was found that the temperature between the coffin and the crematory wall, including the front side, became higher compared with the A1 model simulation. When the airflow from the nozzles hits the coffin's surface, a majority of the air is directed toward the front of the crematory, and also forces combustion heat from the back to the front.

The simulation of Model A3, in which the burner incline angle was 25° downward, also resulted in worse heat distribution, just as in Model A1. The position that had a high temperature was only in the back of the crematory, while the majority of the crematory model had an ambient temperature at the beginning. Consequently, this model was also deficient for the actual cremation in terms of a great deal of fuel consumption.

Finally, the simulation results of Model A4, in which both the burner and air hold incline angle were modified, presented a good heat distribution. The average temperature beside the coffin was approximately 1,500 K, while the temperature towards the crematory's front was 900 K on average. In addition, because of the little space between coffin's top and the crematory's upper wall, a main obstacle was created against heat transferring throughout the coffin's topside. From the simulations results, as shown in Fig.6, the distribution's contour of combustion heat between the coffin's top and the upper wall of models A2 and A4 was more efficient compared to models A1 and A3.

Accordingly, it can be concluded that the adjusted air hold's angle essentially influenced heat transferring to the front of the crematory. The models in which the burners and air hold angles were modified performed better heat transfers so that the coffin could reach the firing point and ignited faster, which can also reduce the overall cremation time.

5.2 Turbulent intensity

Turbulent intensity is used to investigate the effectiveness of the air flow inside the crematory, including the blending between producer gas and auxiliary air. Figure 7 shows the contour of turbulent intensity inside the primary chamber. It was found that the modified models (A2 and A4), in which the air nozzle angle was adjusted, presented better turbulent intensity compare to the commercial model (A1). This characteristic suggests that the modified models with

adjusted air nozzles result in a more effective air and fuel gas blending. At the same time, it can be implied that the combustion reaction in the modified crematory is efficient.

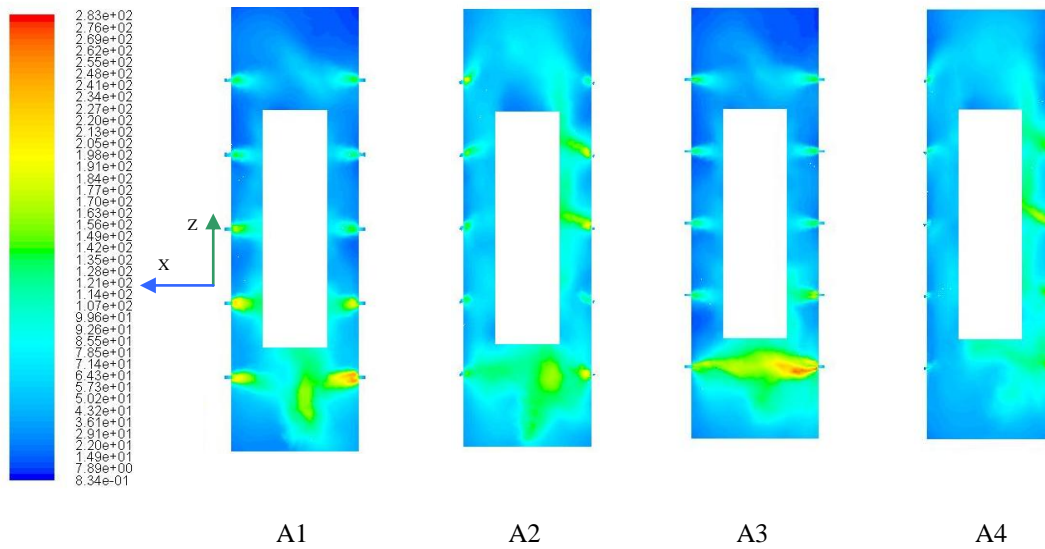


Fig.7 Turbulent intensity (%) contour of the crematory's primary chamber

5.3 NO formation

According to the composition of biomass producer gases that contain a Nitrogen constituent, the occurrence of pollution, such as a formation oxide of Nitrogen (NO_x), is also necessary to be considered. Hence, the prediction of NO formation is explained in this paper.

Figure 8 shows the contour of NO formation inside the crematory model when only the primary burner was operated. It was found that the formation of NO achieved a maximum in the back of the crematory, which was $245,000 \text{ mg/m}^3$. On the other hand, the average amount of NO formation throughout the primary chamber was $123,000 \text{ mg/m}^3$. However, the rate of NO formation decreased in the secondary chamber, and became zero in the crematory's stack. The reduction of NO in the secondary chamber can be explained by the low temperature in the secondary chamber, which then decreased the rate of NO formation, which is dependent on the temperature, until it was equal to zero.

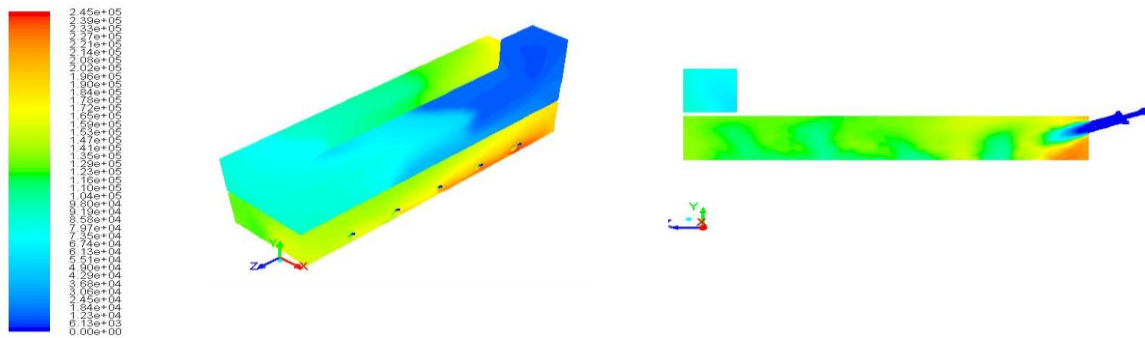


Fig.8 NO formation contour (mg/m^3) if operating only the primary burner

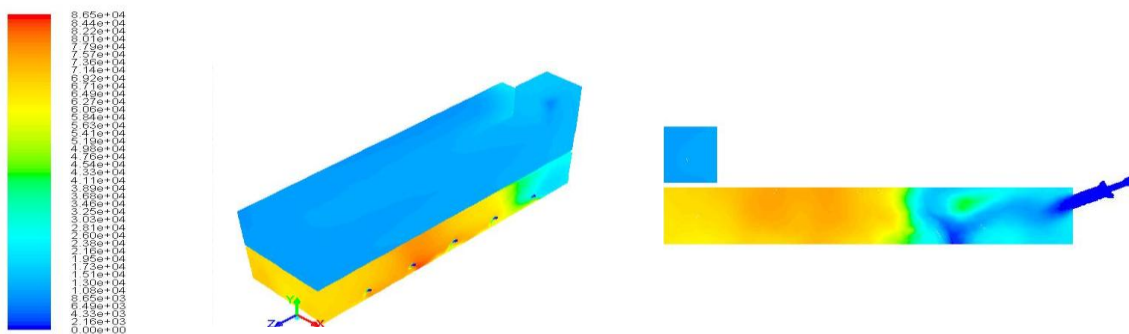


Fig.9 NO formation contour (mg/m^3) if operating both the primary and secondary burners

If both the primary and secondary burners are operated, as shown in Fig.9, the average NO formation inside the primary chamber was approximately $70,000 \text{ mg/m}^3$, and mainly reached its highest in the middle of the crematory. In addition, the NO concentration inside the secondary chamber and in the stack was approximately $20,000 \text{ mg/m}^3$, and then reduces gradually. Finally, the NO formation rate at the crematory's stack becomes $3,000 \text{ mg/m}^3$. Although it is found some NO formation at the stack for this case, compare to the operating only primary burner, however, the NO formation inside the primary chamber is lower than in the operation of only the primary burner. Consequently, NO formation inside the primary chamber can be reduced by operating the secondary burner.

VI. CONCLUSION

Owing to the property of biomass producer gas derived from a gasification process that is different from petroleum fuel, it is essential to pay attention to any application in which the producer gas is used. In particular, cremations that have high temperatures and efficient pollution control are needed. The CFD analysis, therefore, carries an advantage in reducing apparatus preparation costs and the time it takes to experiment. The analysis results show that the crematory's modified model, in which the primary burner angle is 25° downward and the air nozzle's angle is 30° and 30° along the z-axis and y-axis respectively, can reach an average temperature of around 1,500 K, which is enough to eliminate pollutants released after corpse combustion. Furthermore, the modified model could achieve the highest effectiveness for things such as gas flow and blending between fuel gas and air. For NO formation, it was found that the rate of NO formation decreases when both primary and secondary chambers are operated, compare to that in only primary chamber operation. Although these simulation results are different from an actual cremation due to the fact that a corpse's moisture evaporation and disintegration were not considered, nevertheless, the results exhibit several benefits to the design and construction of high-efficiency double-chambered crematories using biomass-derived gas as fuel.

ACKNOWLEDGEMENT

The authors would like to acknowledge the Dean of the Faculty of Engineering, Chiang Mai University, the faculty's lecturers and staff members for all their assistance, Associate Professor Kulachate Pienthong (Ubon Rajathani University) and Mr.Thanadej Kantachote, Manager of J.E.N. Construction CO. LTD, for all of their valuable comments and suggestions.

REFERENCES

- [1] S. Thavornnun, *Study and research on crematory for energy saving*, Research's report, Energy Policy and Planning Office, Ministry of Energy of Thailand, 2007.
- [2] N. Doungsupa et.al., Simulation of combustion in ceramic fiber kiln using computational fluid dynamics, *Proceeding of 11th Tri-University and Symposium Role of Asia in the World*, 2004, 192-195.
- [3] N. Vorayos, *Numerical modeling of air flow inside tobacco curing barn*, Research's report, Department of Mechanical Engineering, Faculty of Engineering, Chiang Mai University, 2002.
- [4] S.V. Patanka, *Numerical heat transfer and fluid flow* (Hemisphere Publishing Corporation, NY: Taylor & Francis, 1980).
- [5] Y. Achawangkul et.al., Biomass gasification utilization for double chambers crematory, *Proceeding of 2013 International Conference on Alternative Energy in Developing Countries and Emerging Economies (2013 AEDCEE)*, Bangkok, Thailand.

Thyristor Based Fault Current Limiter to Control Magnitudes of Fault Currents

L.Karunakar¹, G.Gantaiah swamy²

¹Assistant Professor, Department of Electrical and electronics Engineering, Andhra Loyola Institute of Engineering &Technology

²Assistant Professor, Department of Electrical and electronics Engineering ,Andhra Loyola Institute of Engineering &Technology

ABSTRACT: *The most common ways to limit fault currents are the costly replacement of substation equipments or imposition of changes in the configuration splitting power system that may lead to decreased operational flexibility and lower reliability. A novel idea is to use Fault Current Limiters (FCLs) to reduce the fault current to lower, acceptable level so that the existing switchgear can still be used to protect the power grid. This paper presents controlling the magnitude of fault current by using non super conducting fault current limiter with the help of controlled rectifier. Non superconducting fault current limiter consists of a rectifier and DC reactor. The diode rectifiers are uncontrollable, to make it as a controllable by replacing the thyristor in place of diode. By providing the suitable gate triggering to the thyristor circuit we can control the magnitude of current in DC reactor. By reduce the magnitude of fault current in a power system, which improve the voltage profile at faulted phase. The proposed NSFCL was simulated and studied with the help of MATLAB(Simulink).*

Key Words: fault current limiter, fault currents, non super conductor, and thyristor controlled rectifier

I. INTRODUCTION

Power quality problems are becoming more and more important for utilities due to growing number of sensitive loads. Short circuit results the large amount of current flow through the distribution network. The large fault currents flow may damage the series equipment, such as circuit breaker and other system components. The Fault current causes the voltage drop of a particular network. As a result, some industrial facilities experience production outage that results in economic losses. Therefore, utilities are currently exploring mitigation techniques that eliminate large fault current, increase the reliability of the power supply and improve the reliability and the system power quality. The most common ways to limit fault currents are the costly replacement of substation equipments or imposition of changes in the configuration splitting power system that may lead to decreased operational flexibility and lower reliability.

A novel idea is to use Fault Current Limiters to reduce the fault current to lower, acceptable level so that the existing switchgear can still be used to protect the power grid. An ideal FCL should have the following characteristics

- a) Zero resistance/impedance at normal operation;
- b) No power loss in normal operation and fault cases;
- c) Large impedance in fault conditions;
- d) Quick appearance of impedance when fault occurs;
- e) Fast recovery after fault removal;
- f) Reliable current limitation at defined fault current;
- g) Good reliability;
- h) Low cost.

Different configurations such as Is - limiters, solid state fault current limiters and superconducting fault current limiters were proposed in previous papers [6] [7] [8]. The SFCL structure offers a good way to control the fault current levels in distribution networks due to natural low losses in superconductors during the normal operation. Unfortunately, because of high technology and cost of superconductors, these devices are not commercially available. Therefore, replacing the superconducting coil with nonsuperconducting coil in FCL makes it simpler and much cheaper.

This paper proposes magnitude of fault current controlled by using thyristor circuit of a nonsuperconducting fault limiter. And also improves the voltage profile in a network. The circuit operation in normal and fault conditions are simulated and experienced.

II. CIRCUIT OPERATION

The circuit consists of a three phase transformer is connected to a thyristor circuit at source side. By providing the gate pulse to the thyristors to control the magnitude of fault current. And another three phase transformer is connected to a diode bridge rectifier at load side. The diode bridge rectifier is connected to a parallel connection of a discharging resistor and a thyristor switch and is connected in series with the D.C reactor is shown in figure.1.

In normal operation that is without fault condition semi-conductor switch is turn on. And resultant current flows through the diode rectifier and discharging resistor. And normal current flows to the thyristor circuit. By increasing the inductance value decreases the ripple of D.C current. During the fault condition, the switch is turn on that is when fault take place at load side then it results the D.C reactor current increases linearly. If the fault is present for long time the current through the D.C reactor will continue to increase. And results the source voltage drop take place. There is a control circuit

present by using that we can control the magnitude of fault current in case of diode rectifier circuit in previous paper[1]. That control circuit consists of a discharging resistor and a switch along with resistor. When a fault take place the switch can be turn on and fault current flows to the parallel resistor and it results the voltage drop take place at source side. In order to reduce the magnitude of fault current the switch can be turn-off and the fault current flows through the discharging resistor. It results there is a reduction of magnitude of fault current and improves the voltage profile at source side.

In this paper without using the control circuit we can control the fault current within prescribed below limits. That is in normal operation switch is turn on and normal current flows through the D.C reactor. In case of fault switch is turn on then the D.C reactor current increases. To control the magnitude of fault current by varying the duty cycle of thyristor circuit to reduce the magnitude of fault current in D.C reactor without using control circuit. Therefore it improves the voltage profile at source side. Due to controlling the D.C reactor current of proposed NSFCL, it is possible to reduce the current rating of inductance and cancelling out the super conducting cooling system. The compensating voltage provided by rectifier is

$$V_c = 2V_{DF} + V_{sw} + r_d L_d$$

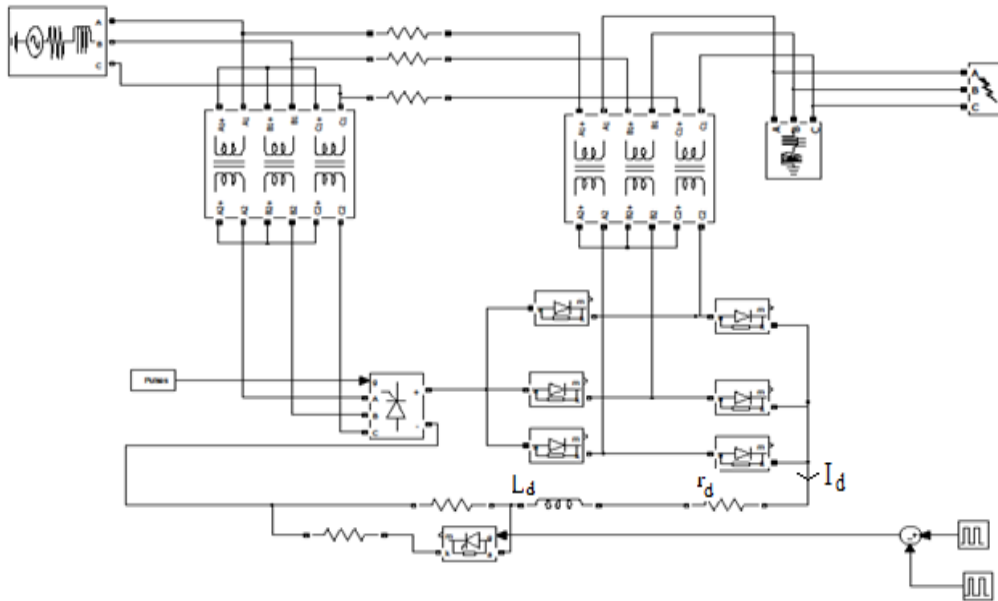


Figure.1 circuit diagram

III. SIMULATION RESULTS

The power circuit topology is shown in figure.1 is used to simulation. The simulation results are obtained NSFCL operation performance of a thyristor circuit at a fault condition, where a three phase to ground fault occurs at load side. The neutral of source grounded. The various operation performances are carried out as follows. The below, figure.2 shows the magnitude of fault line current, figure.3 shows the DC reactor current and figure.4 shows the source voltage drop of a distribution network. By using the thyristor circuit of applying the suitable duty cycle without turn off the switch then the reduced magnitude of fault line current is shown in figure.5, reduced magnitude of DC reactor current is shown in figure.6 and improved source voltage profile obtained shown in figure.7. The enlarged DC reactor current during the fault shown in figure.8 and DC reactor current during the transient fault were shown in figure.9.

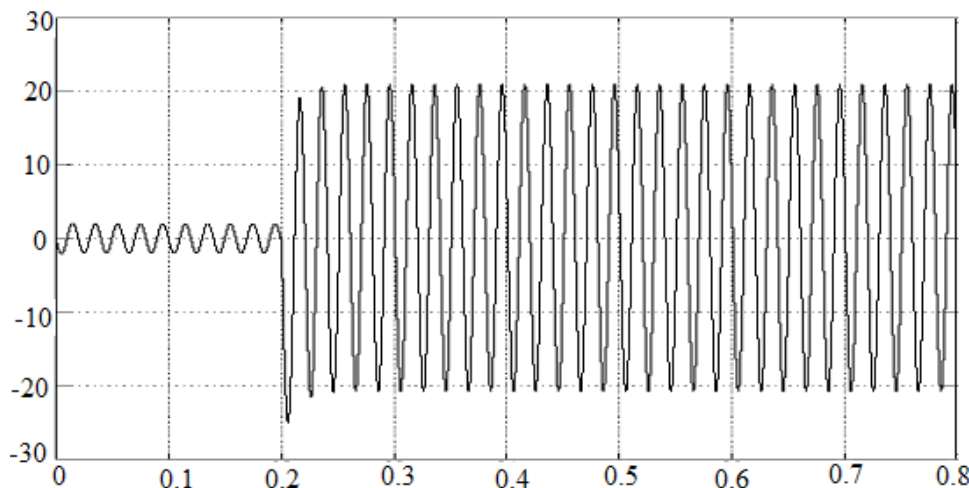


Figure.2 magnitude of fault current

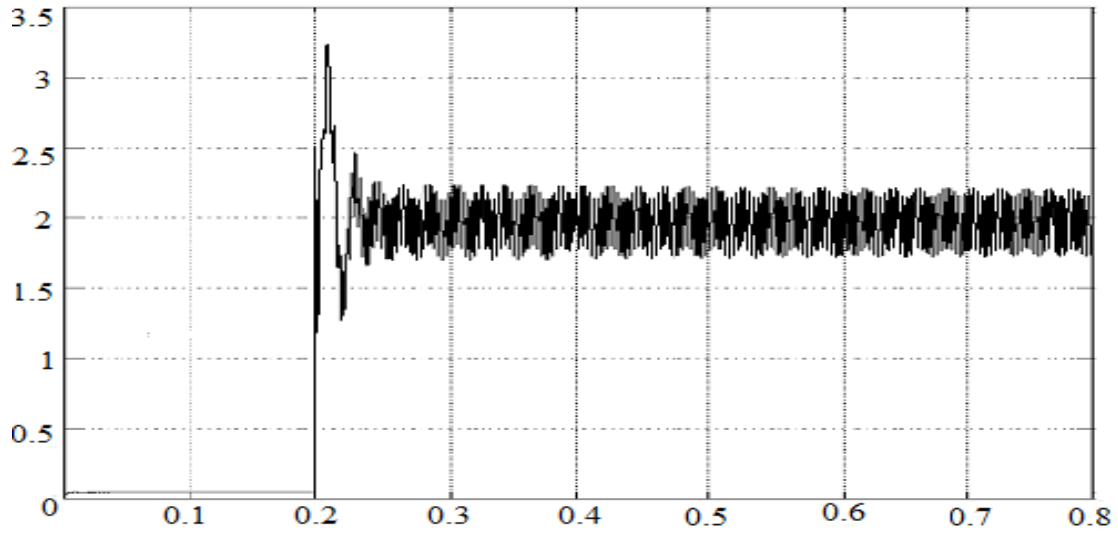


Figure.3 DC reactor current during the fault

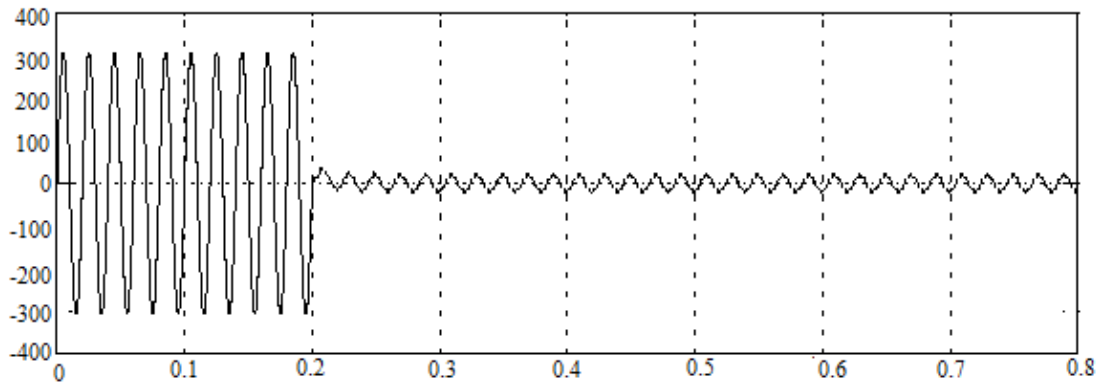


Figure.4 voltage drop during fault

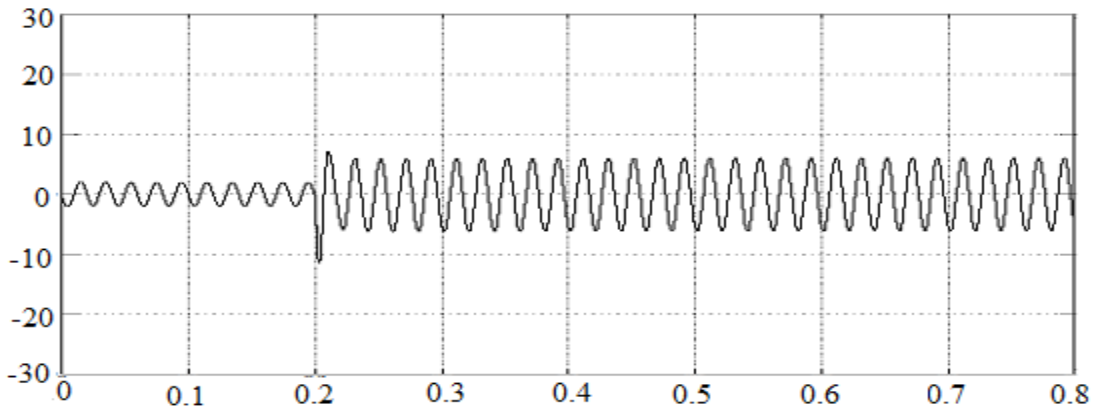


Figure.5 Reduced fault current

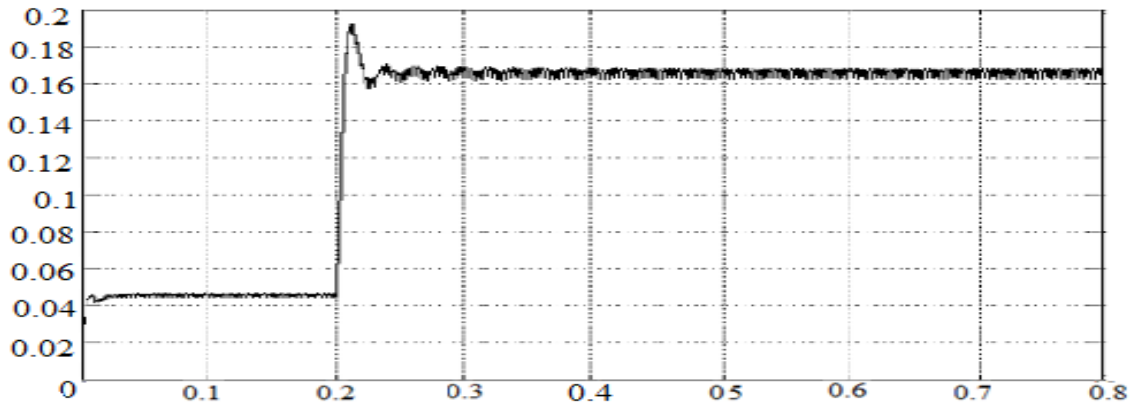


Figure.6 Reduced of dc reactor current

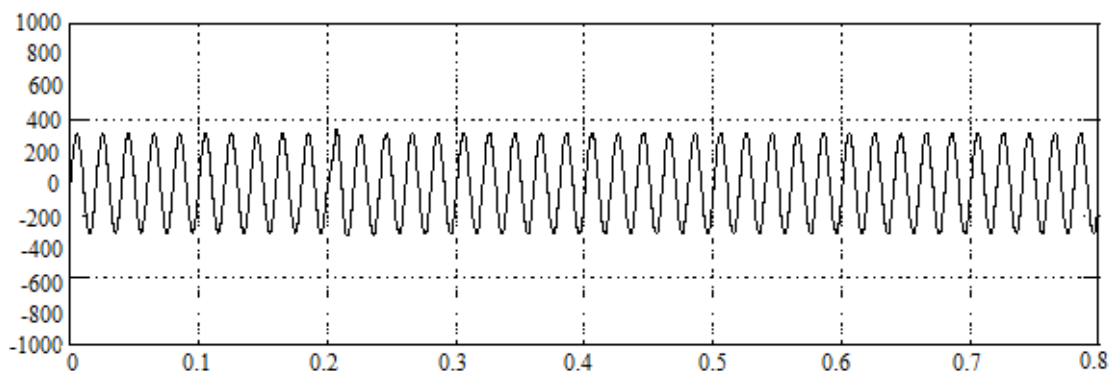


Figure.7 improvement of voltage profile

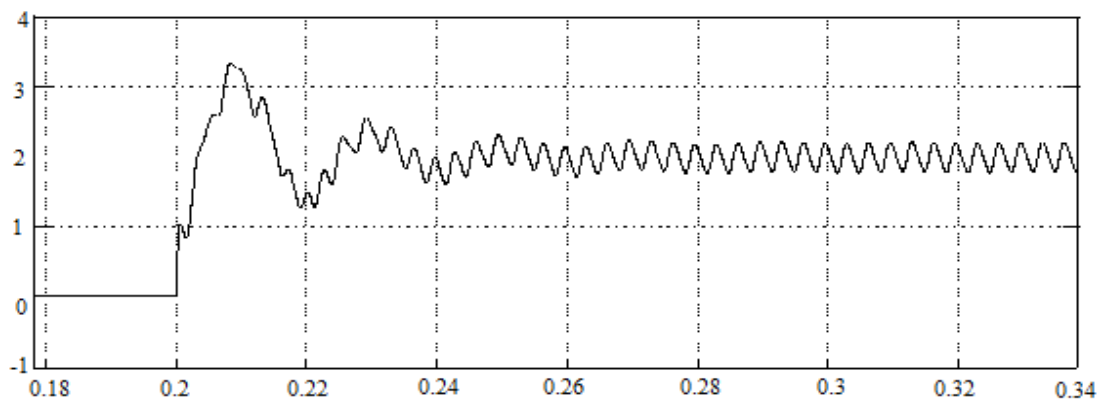


Figure.8 Enlarged DC reactor current during the fault

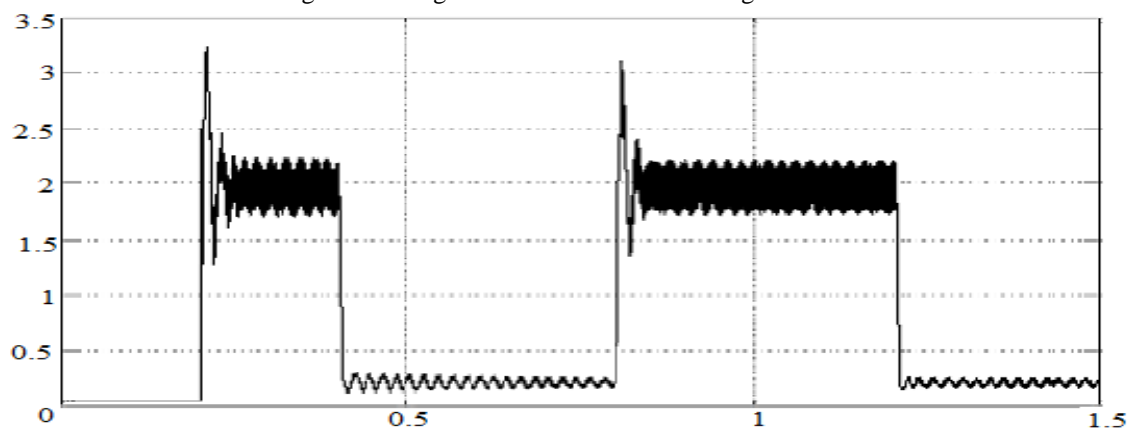


Figure.9 Dc reactor current during transient faults

PARAMETERS OF SIMULATION

Symbol	Content	Value
V_s	Source voltage	380V
r_s	Source resistance	1 Ω
r_d	DC reactor resistance	0.2 Ω
L_d	DC reactor inductance	0.2H
r_p	Discharging resistance	100 Ω
r_{Load}	Load resistance	50 Ω
L_{load}	Load inductance	100 Ω

IV. CONCLUSION

The three phase to ground fault is most severe fault in any power system. Whenever it happens to the system there is a severe dip in the voltage. This is one of the power quality problems. To mitigate the above problem we need to minimize the fault current. For which in this paper proposed fault current limiter minimizes the fault current and improves the voltage profile which is observed from the simulation result.

REFERENCES

- [1] M. THagh and M. adapour, "Nonsuperconducting fault limiter with controlling the magnitudes of fault currents," IEEE Trans. Power electronics, vol 24, pp.613-619, March 2009
- [2] E RO Lee, S. Lee, "Test of DC reactor type fault lim-iter," IEEETrans. Appl. Supercond., vol.12, no.2, march 2002
- [3] T.Hoshino, K.M.salim, "DC reactor effect on bridge type super conducting fault current limiter," IEEE Trans. Appl. Supercond., vol.11, no.1, pp.1944-1947, March 2001
- [4] M. Abapour and M. T. Hagh, "A noncontrol transformer inrush currentlimiter," in IEEE Inte. Conf. Ind. Technol., ICIT Sep. 15–17, 2006,pp. 2390–2395.
- [5] M. T.Hagh and M. Abapour, "DC reactor type transformer inrush currentlimiter," IET Elect. Power App., vol. 1, no. 5, pp. 808–814, Sep. 2007.
- [6] M. Tsuda, Y. Mitani, K. Tsuji, and K. Kakihana, "Application ofresistor based superconducting fault cur-rent limiter to enhancement ofpower system transient stability," IEEE Trans. Appl. Supercond., vol. 11,no. 1, pt. 2, pp. 2122–2125, Mar. 2001.
- [7] M. Yagami, T. Murata, and J. Tamura, "Stabilization of synchronous generators by superconducting fault current limiter," in IEEE Power Eng.Soc. Winter Meet., Jan. 23–27, 2000, vol. 2, pp. 1394–1398.
- [8] Y. Goto, K. Yukita, H. Yamada, K. Ichiyanagi, Y. Yokomizu, and T. Matsumura, "A study on power system transient stability due to introduction of superconducting fault current limiters," in Int. Conf.Power Syst. Technol., 2000, vol. 1, pp. 275–280.

L.Karunakar, received B.Tech from PVP Siddhartha college of engineering 2008. He has worked as a Lecturer in department of electrical and electronics in KL university between 2008 to 2010. He has received M.Tech from KL University in 2012.Present he is working at Andhra Loyola institute of Engineering & Technology.

G.Gantaiah Swamy received M.Tech from NIIT Calicut in EPS branch. Present he is working at Andhra Loyola institute of Engineering &Technology.

Cooling analysis of self Activating Bi-Metallic Valve using Thermo –Structural Coupled FEA

Swati G Paithankar 1a, Prof.P.T.Nitnaware 1, Vinay Patil2,

1 Mechanical Engg. Dept, D.Y.Patil College of Engineering,Akurdi,Pune,University of Pune,India

2 Vaftsy CAE, Pune-411028, India, University of Pune,India

ABSTRACT: To replace electronically actuated valves or to provide second layer of safety in case of electronic malfunction a totally mechanically actuated valve & warning system is designed. The process for which valve optimization is carried out is the process of nitrous oxide generation from ammonium nitrate. The main challenge in the process was maintaining temperatures below 200°C as above this temp ammonium nitrate becomes explosive & safety risks are involved. The secondary objective was to maintain this temperature above 170°C as below this temperature reaction does not proceed. All these objectives are fulfilled by employing a bimetallic valve. The primary purpose of the self actuation is achieved by selecting proper dimensions of the valve & designing warning system in which desirable deflection of the bimetallic strip is achieved. But main problem arises during cooling as there is the possibility of the bimetallic strip of may lead to high crushing stresses. The main requirement while carrying out cooling is that the bimetallic strip should again rest on the flow casing as previous i.e. it should close valve again while cooling & not crush on the flow casing or deflects beyond flow casing.

KEYWORDS: Thermo-Structural coupled FEA, Non linear FEA, Bi-metallic Valve, Warning system, Material Non linearity,Defining contact, Boundary Conditions, Meshing.

I. INTRODUCTION

The primary chemical reaction for which the valve is required is the commercial production of nitrous oxide by heating of ammonium nitrate. The heating is carried out using superheated steam

$$\text{NH}_4\text{NO}_3 (\text{solid}) \rightarrow 2 \text{H}_2\text{O} (\text{gas}) + \text{N}_2\text{O} (\text{gas}).$$

The chemical reaction is subjected to following thermal considerations.

- Below 170°C : No reaction
- 170°C to 200°C : Active reaction zone
- 200°C to 240°C : Warning zone
- Above 240°C : Possible explosion.

Based on above thermal considerations, the following design requirements are obtained for the system

- The system should remain closed below 200°C to maintain steam in the vessel
- 200°C should trigger opening of the valve (with a warning by a warning system)
- System should close back when temperature falls to 200°C.

When the valve opens, the super heated steam will escape, this will result in a pressure drop, which will translate into reduction of temperature of the steam.

Based on these requirements a bimetallic valve is designed in which purpose of self actuation above 200°C is achieved.

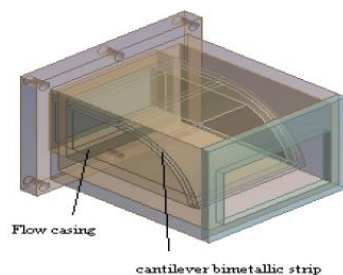


Fig 1: Thermal Bimetallic safety valve

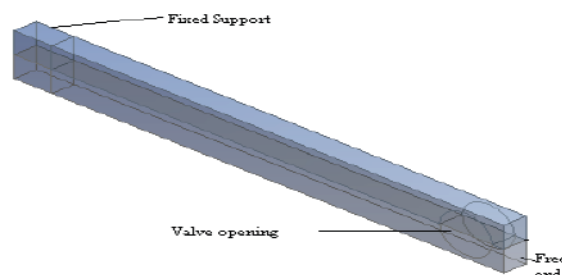


Figure2: Warning System

Figure 1 & figure 2 shows thermal bimetallic control valve & warning system in which purpose of self actuation is achieved, But cooling analysis is also foremost important as when no separation contact was defined between substrate & flow casing the flow casing constrained the free expansion of the strip which may lead to high crushing stresses. Hence further cooling analysis is required to be carried out to ensure satisfactory closing of the thermal flow control valve.

II. Background Theory

A self activating bimetallic valve design is proposed on basis of thermo structural coupled analysis during opening of the valve i.e. heating analysis. At that time inside temperature of the valve is high than the outside temperature. But once the valve is opened there is sudden reduction in pressure inside the valve & now inside temperature of the valve is reduced to atmospheric temperature & as superheated steam is escaped outside temperature gets increased. at this condition it is expected that the bimetallic strip which gets open during heating should close back during cooling, but there may be the possibility of high crushing stresses, which is not required at all as it may lead to war out of strip as well as flow casing. Hence we carry out thermo structural analysis again by changing temperature conditions for various described conditions. & comparing results we can conclude whether we can use self activating bimetallic valve or not. A finite element analysis is carried out to do the analysis.

III. FINITE ELEMENT ANALYSIS

Key characteristics of the finite element analysis (FEA) performed in ANSYS mechanical workbench are:

1. Type: Thermo – Structural coupled FEA (refer with: Fig. 5)
2. Elements: Tetra, Quad, 2nd Order hexahedron elements (refer with: Fig. 6, Fig. 7)
3. Non linearity: Material non linearity (refer with: Fig. 8, Fig. 9),
Contact non linearity (refer with: Fig. 10, Fig. 11),
Geometric non linearity (change in response due to large deformations)

Flow chart of the thermo structural coupled analysis is as shown in the figure. Firstly we have to give various inputs to carry out thermal analysis in that it include material input i.e. material conductivity, thermal coefficient of expansion of material etc as well as thermal boundary conditions in terms of temperature which results in temperature distribution. After temperature get distributed we have to apply thermal load which is going to act on bimetallic valve, at the same time we have to consider structural inputs like support or fixed face of valve various material inputs in case of structural analysis like Young's Modulus of elasticity etc.

After feeding all this input data meshing of the valve is carried out & by solving the analysis deformation, von mises stresses are observed

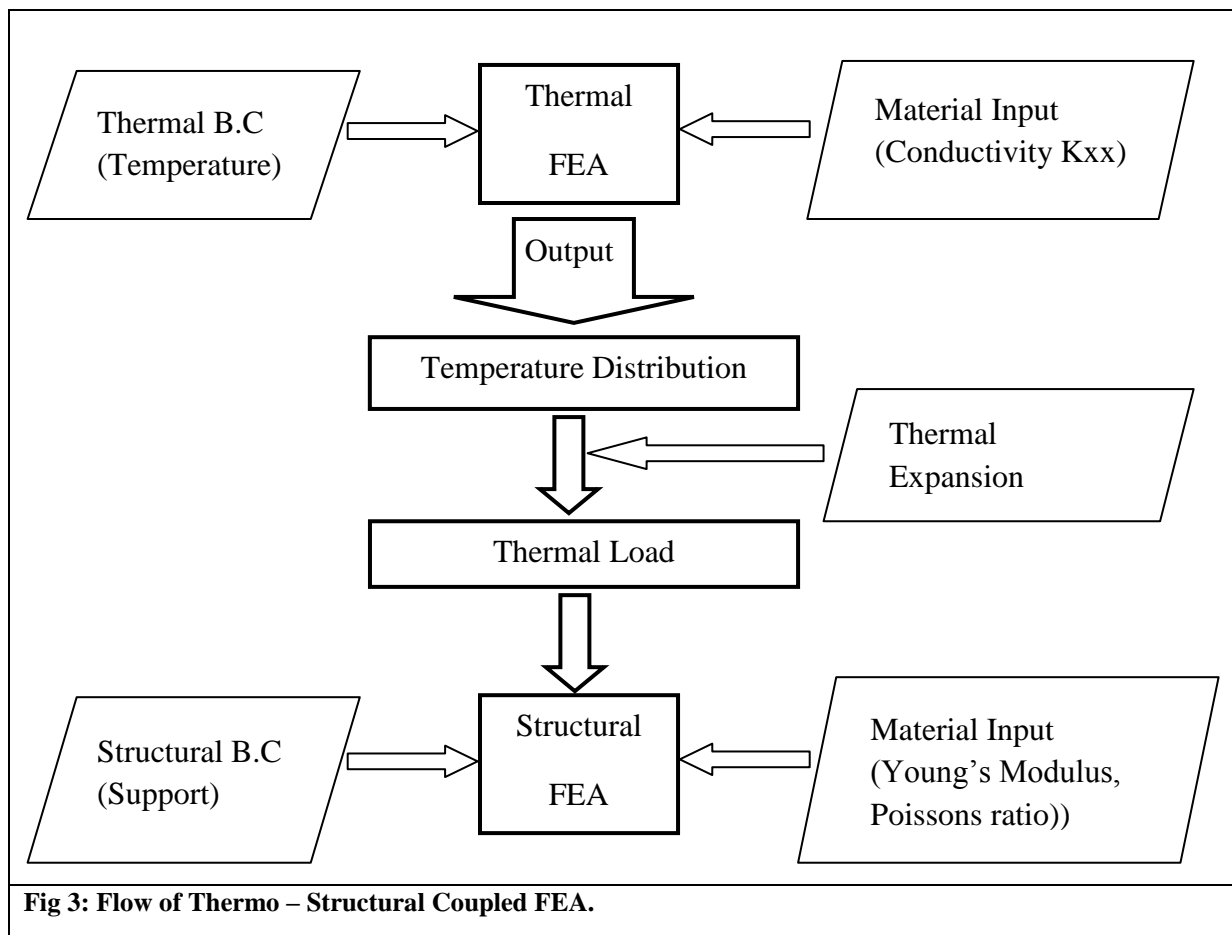
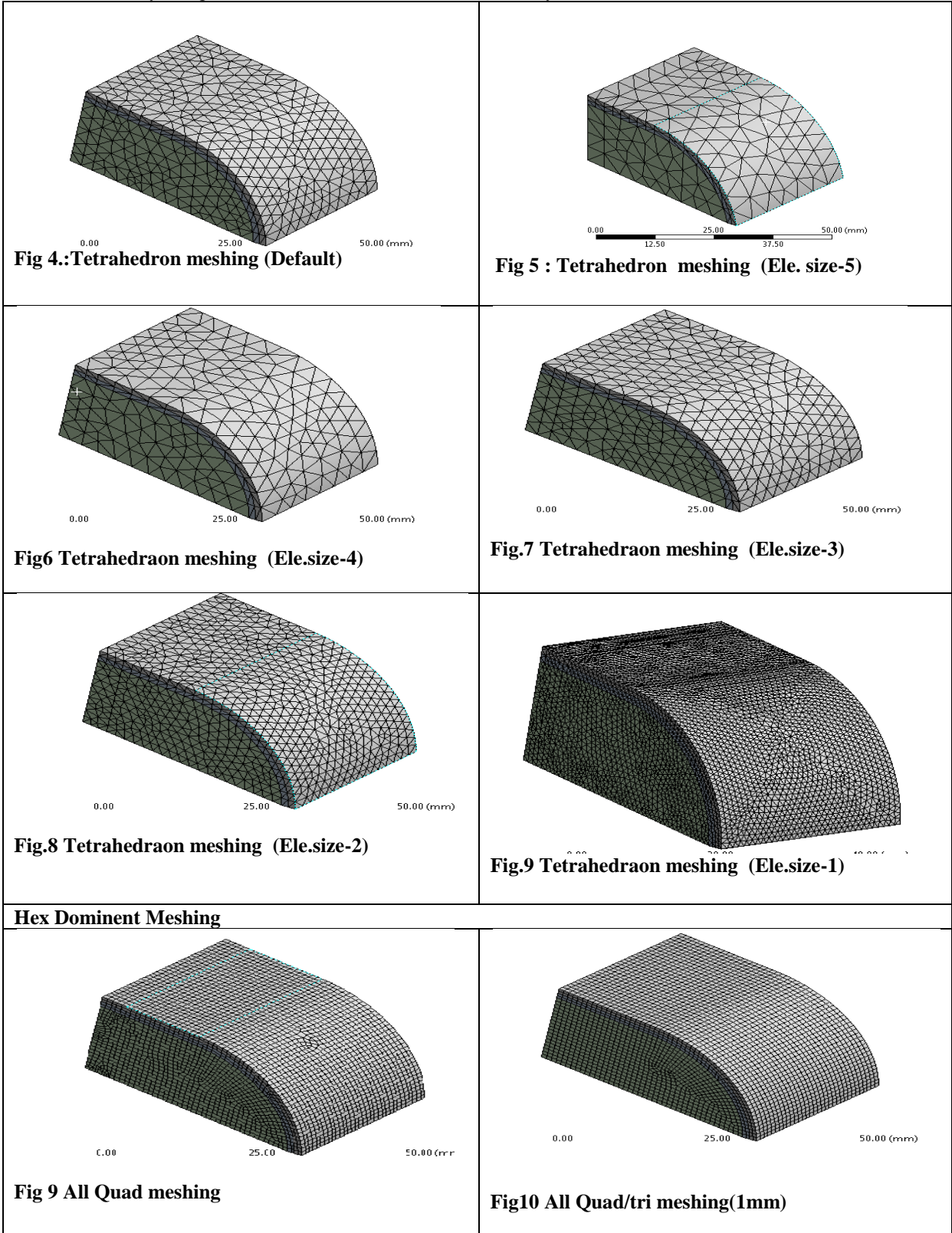
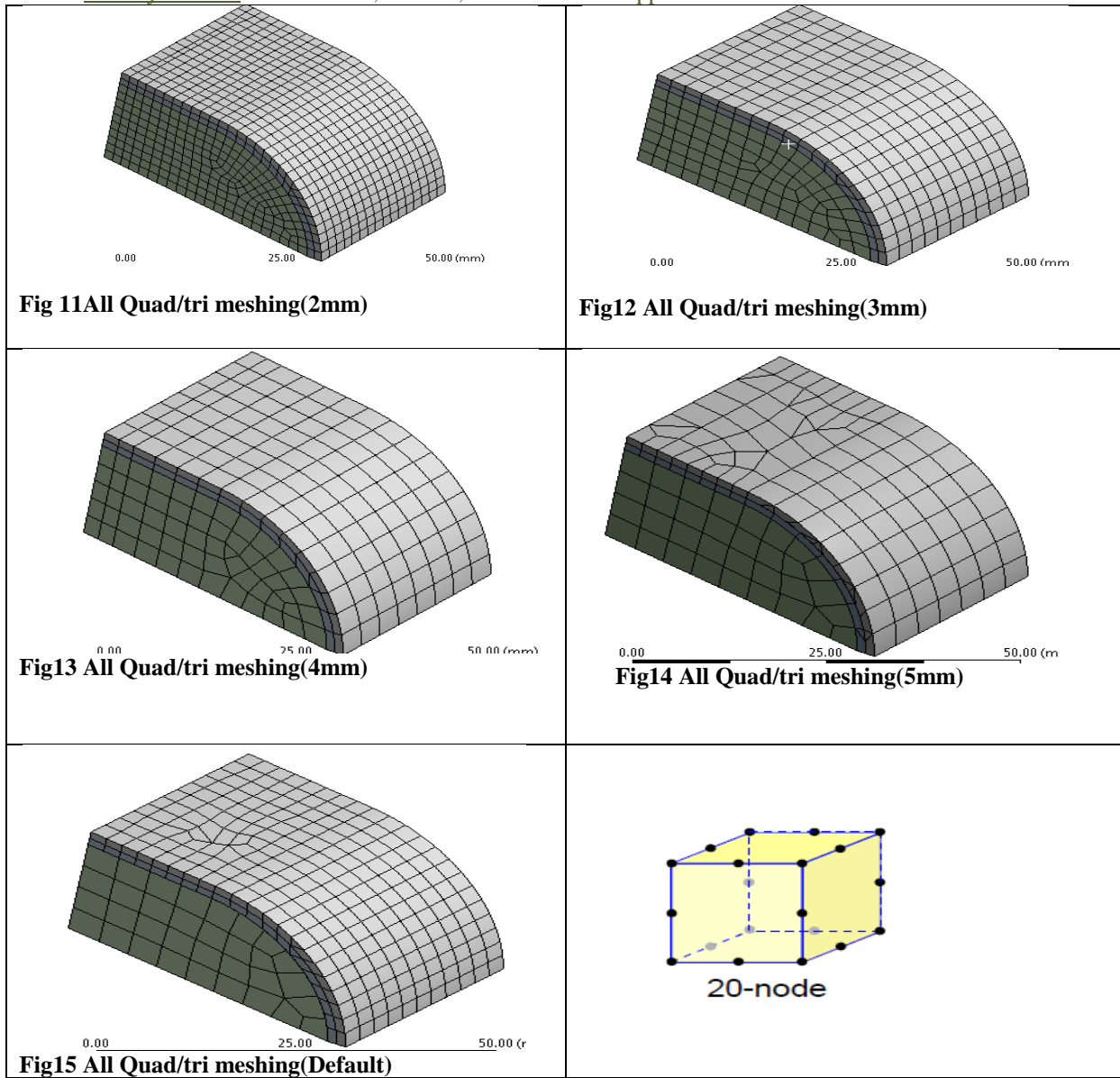


Fig 3: Flow of Thermo – Structural Coupled FEA.

3.1 Meshing : The system of interest is first discretized into elements; in this case ,the elements are tetrahedraon. The corner vertices of these tetrahedron are called nodes and are the arbitrarily point where the value of interest is solved. The system is discretized by using various elements sizes & results are analysed.





By meshing with various elements & element size & verifying results we come to conclusion that 2nd order hexahedron meshing give us accurate results. Hence we choose 2nd order hexahedron meshing.

3.2 Material Non linearity: - Non linear material properties such as conductivity K, Young’s modulus of elasticity E of the film meal (CZ-1400-E) and the substrate metal (IN-4082-SP) as shown in graphs are used in analysis.

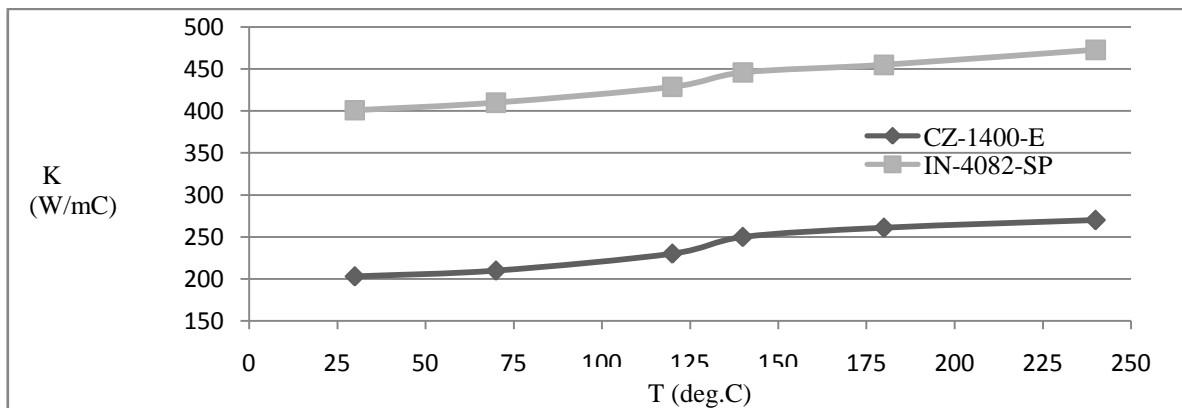


Fig 16 Conductivity as function of temperature T

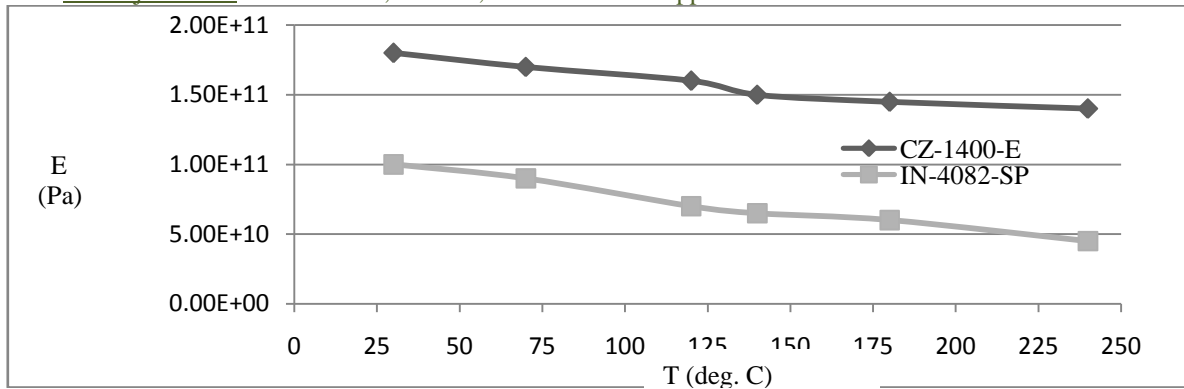


Fig 17 Modulus of Elasticity as function of T

Similarly Poisson's ratio and non linear thermal coefficient of expansion α of the film metal (CZ-1400-E) & the substrate metal (IN-4082-SP) as a function of temperature are used.

3.3 Defining contacts : Contact between film & substrate metal is defined as bonded contact. Accuracy achieved using multiple sub steps.

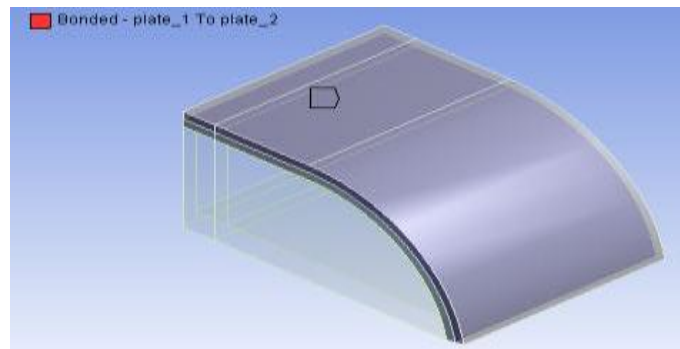


Fig 18 Bonded contact

While carrying out opening of the valve one of the contact region is no separation contact, which is required to be suppressed while carrying out cooling analysis.

3.4 Boundary Conditions: Thermal boundary condition for the analysis of the thermal safety valve and the warning system are applied as shown

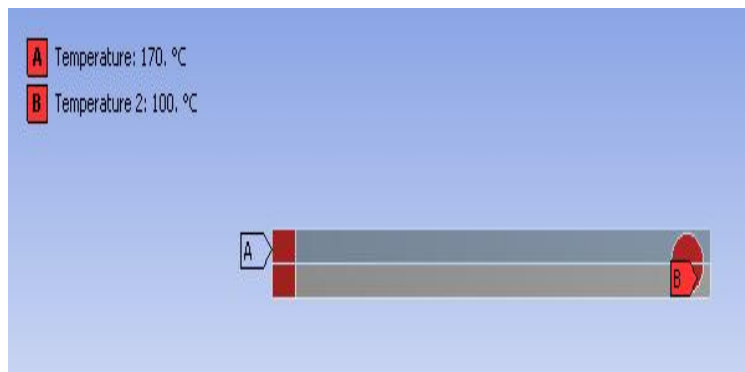


Fig 19 Boundary conditions of the warning system

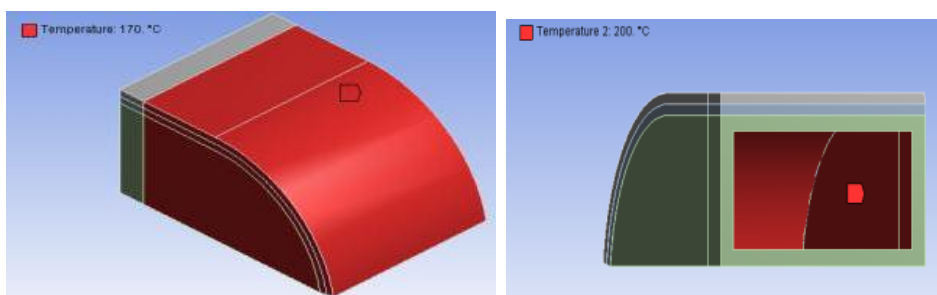


Fig 20 Boundary conditions for thermal safety valve

IV. RESULTS

Deformation and Von-Mises stresses were observed after performing the simulations. The main focus of analysis is on closing position of the bi-metallic valve with respect to change in temperature of superheated steam inside the process vessel.

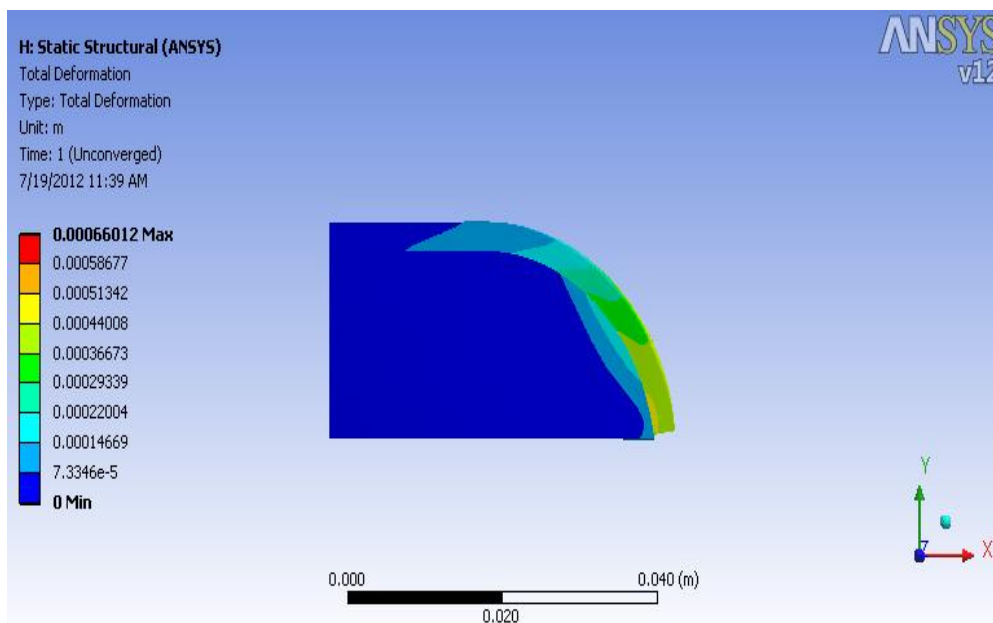


Figure 20.1: Deflection of Curved Bimetallic Strip in No Reaction Zone (No Separation).

Above results are of cooling analysis when no separation contact was defined between substrate and flow casing. The flow casing constrained the free expansion of the strip which will leads to high crushing stresses as shown in below figure

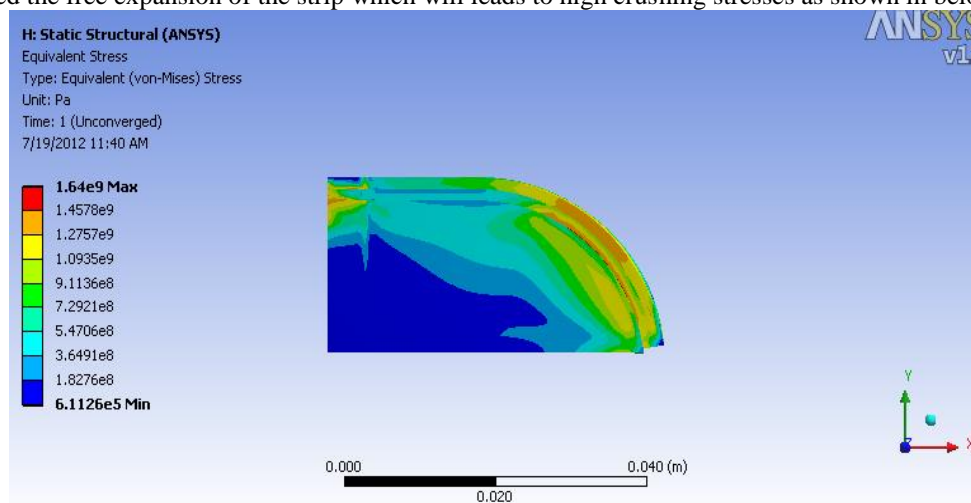


Figure 20.2 : Von Mises Stresses in Curved Bimetallic Strip in No Reaction Zone (No Separation).

The crushing stresses are coming high up to 1.49×10^9 Pa while doing cooling analysis The flow casing constrained the free expansion of the strip & closes the valve, which is our desired condition

V. CONCLUSION

Usage of non linear FEA alters the results significantly, hence for realistic determination of performance non linear FEA is recommended. Using a cantilever arrangement for a warning system, under which both the materials are exposed to the heat, is more effective in giving a range bound mechanism.

REFERENCES

- [1] Information on http://en.wikipedia.org/wiki/Nitrous_oxide.
- [2] S. Timoshenko, "Analysis of Bi-metal Thermostats," J. Opt. Soc. Am., 11(1925) 233.
- [3] J. W. Eischen and J. S. Everett, "Thermal Stress Analysis of a Bimaterial Strip Subject to an Axial Temperature Gradient," Vol. 111, Journals of Electronic Packaging (1989).
- [4] Moduluc Control Systems, USA: "Objective and outline document no 234221."

Harmonics Systems for Time Mining

Daniela López De Luise¹

*(CIIS Lab, Buenos Aires, Argentina)

ABSTRACT: Information management is currently one of the topics with most impact. Processes are studied in this paper in their temporality, mainly to be able to make predictions. Interesting information arises when what is being examined is not the complex information produced along the development of a process, but the temporality itself for the process. Such an alternative point of view enables the relation of this analysis to a real process, and its application in the very moment the events are taking place, knowing that there is a starting point of certain a priori knowledge.

This work shows this alternative stance, from the temporal perspective. There are applications of concepts and analogies brought from a different environment where time is handled in a more natural way. We shall call this approach "Harmonic Systems". We shall present the basis for harmonic systems, the focused approach we propose as a type of time mining, and its application.

Keywords: Data Mining, Information Systems, Process Mining, Process Modeling, Soft Computing

I. INTRODUCTION

Information management is currently one of the topics with most impact. It relates to a broad range of matters from those related to engineering processes to others such as speech processing and consumer profile generation. It is possible to obtain information with special types of mining. For example, there are mining techniques in the area of language that allow for a relatively efficient management of automated translation between different languages [1][2], detection of a writing style in an author, the study of the effects of bilingualism, etc. [3][4][5][6]

From the standpoint of mining, processes are studied in their temporality, mainly to be able to make predictions (of times, events and characteristics) and descriptions (of use, of information type, business profiles, user profiles, etc). [7] [8] [9]

Techniques are usually crucial for figuring out which information is concurrent or subsequent to a certain fact [10] [11]. But an interesting aspect arises when what is being examined is not the complex information produced along the development of a process, but the temporality itself for the process. Taking an opposite stance to the traditional one and eschewing the study of the characteristics of the process in favor of its rhythm, accelerations, static periods and any other aspect that can be related to the measurement of time features. Such an alternative view enables the relation of this analysis to a real process, and its application in the very moment the events are taking place, knowing that there is a starting point of certain a priori knowledge.

The main aim of this work is to show this alternative stance, from the temporal, through an application of concepts and analogies brought from a different environment where time is handled in a more natural way. We shall call this approach "Harmonic Systems". In this work we shall present the basis for harmonic systems (Section 2), the focused approach we propose as a type of time mining (Section 3) and a test application demo (Section 4).

II. HARMONIC SYSTEMS

2.1. Harmonic Systems Purpose

The production of meta-data from information generated in a sequence of data associated with a time evolution. These meta-data are subject to change with time (as opposed to those models created through mining) and comprise a model of dynamic approach with a certain behavior that typically evolves in time, while keeping its own identity pattern. Thus, a natural process could result in one of more patterns with the same or a different time variation. On the other hand, with the application of filters, a selection can be made of a certain time sub-sequence inside said temporal variation.

2.2. Harmonic Systems Application

Generating the model is just an intermediate step that defines whether a sequence resulting from a pattern is being produced. This way, it is possible to test the patterns of interest that could belong to software or hardware faults, concurrent processes, etc., while the information is being produced.

In these cases, the objective is to be able to act in the moment where the change is happening, with no regard to the temporal variations in its evolution, but focusing instead on the pattern. The search for accuracy is out of the question, as the aim is to detect the appearance of the pattern with a definite degree of certainty.

A comparison could be drawn to an analogous situation of a doctor evaluating a patient in given moment of the evolution of its illness: if he shows a certain sustained temperature, congestion and presence of nasal secretion, there could be further symptoms, but a decongestant is needed.

2.3. General Characteristics of Harmonic Systems

There are different types of harmonics. An harmonic is a combination of properties that are of interest, which in this context are referred to as "pattern". They represent one or more current subsets. Example pattern 1: ID-pattern=1, threshold $U=0.3$

T	Property-1	Property-2
t1= λ_1	PROC=A	USR=034
t2= λ_2	PROC=C	USR=035
t3= λ_3	PROC=A	USR=035

Table 1. Pattern 1

It can be observed that the pattern is a sequence of three moments t_1, t_2, t_3 , which must happen one after the other to be complete. We shall see below how a pattern can trigger actions in $1 < t < 3$ according to its associated triggering threshold. This concept will be explained further along.

An harmonic is in resonance when the sequences of changes in the values of the properties inside the pattern are in correspondence with those in the dataset that is being processed.

When an harmonic begins to resonate, a series of processes is triggered, being the monitoring and updating of the process the most important for the model. This is achieved simply by capturing the current sequence and adding it to the model.

2.4. Resonance

It comprises the event of detection of compatibility of an harmonic with certain data vectors. This comparison consists of two steps:

a) Pattern detection: patterns are evaluated according to the properties that describe them. When there is a matching with current data (in Example 1: Property-1=A, Property-2=034), the resonance must be checked, comparing the probability of the pattern against the threshold U (0.3 for the example).

b) Resonance: In case the resonance is verified, the model is updated in the following manner:

-Action P, which is associated to the patter, is triggered to produce meta-data and tracking data.

-The temporality of each step is captured (t_1, t_2 and t_3 in the example) as a difference between them.

-The size of n is compared against a certain cut-off threshold n_c (e.g., $n_c=80$). When $n < n_c$, $\text{small}(n)$ is true, otherwise it is false. When $\text{small}(n)$ gives true, the Binomial dispersion of harmonics is assumed, otherwise it is considered to be Poisson:

```

IF small(n) THEN
  IF  $B_i(t_i|\text{pattern}) > U$  THEN resonance
ELSE
  IF  $P_o(t_i|\text{pattern}) > U$  THEN resonance
  ELSE NOT (resonance)
    
```

Then U_i is updated and the new parameters with a Hebbian type learning [12], assuming the use of Poisson:

$$\begin{aligned}
 U &= U + \eta_u (U - P_o(t_1|\text{pattern}) \cdot P_o(t_2|\text{pattern}) \cdot P_o(t_3|\text{pattern})) \\
 \lambda_1 &= \lambda_1 + \eta (t_1 - \lambda_1) \\
 \lambda_2 &= \lambda_2 + \eta (t_2 - \lambda_2) \\
 \lambda_3 &= \lambda_3 + \eta (t_3 - \lambda_3)
 \end{aligned}$$

where h is a rate of learning for the parameters, a weighing factor for the relative importance of the pattern fulfillment. At the same time, the new threshold U will reflect variations with a sensitivity given by h_u . The values for h and h_u do not need to be the same.

2.5. Types of Harmonics

-Harmonics are data vectors with a threshold of tolerance to difference. Inside that threshold, data is considered to be resonating.

Characteristic 1: time data is used as a difference in respect to the previous time, $t=(t_i - t_{i-1})$, as opposed to the classic techniques [13] where the value of a certain property is compared in a time t in respect to t_{i-1} , and the measured magnitude or effect becomes a property associated to this time differential.

Consequently: there is no comparison of series length nor corrections in them due to a difference in length. There is also no normalization.

Characteristic 2: given that no component alignment is required between patterns, distance has no need for corrective techniques [13] such as Dynamic Time Warping, Longest Common Subsequence Similarity, local Scaling Functions, global scaling function, etc.

Characteristic 3: the temporal mining approach takes the properties being measured as a *pattern* which identifies the components in a time series, and models the time dispersion instead of the set of properties inside the pattern.

This calls for the development of a model of the pattern, one which could be analogous to Probabilistic similarity measure where methods are *model* based. They provide the ability to incorporate prior knowledge into the similarity measure. However, it is not clear whether other problems such as time-series indexing, retrieval and clustering can be

efficiently, general similarity approach involving a transformation rules language [4], and hundreds of algorithms from Data Mining to classify, cluster, segment and index time series.

-Data will have a degree of belonging to the harmonic it resonates with, which would decrease with the distance of the current t_i values in relation to those expected.

2.7. Filter Types

Data can previously go through some of the filters described below. The effect is focusing only in critical harmonics for the purposes of this study.

There are three filter types:

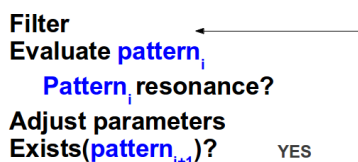
-High-pass filters: They leave the data that are beyond a certain distance (δ) that $t_i + \delta < t_{\text{actual}}|\text{pattern}$. Since the pattern's property $p_1..p_i$ is met, t_i exceeds the model value).

-Low-pass filters: They leave the data that are closer than a certain distance ($t_i - \delta > t_{\text{actual}}|\text{pattern}$). Since the pattern's property $p_1..p_i$ is met, t_i is lower than the model value).

-Band-pass filters: They leave the data that are within a certain distance range ($t_i + \delta > t_{\text{actual}}|\text{pattern} > t_i - \delta$). Since the pattern's property $p_1..p_i$ is met, t_i is within the model value with a certain distance).

2.8. Operating Mechanism

The data set is vectorized and then used based on a global distance. All filters will use this distance in their activities. Database vectors go through the following cycle:



Note that in each cycle the model of the pattern that feeds the subsequent cycle is optimized, therefore, if the model is stored, it is possible to start with a better description of the data –supposing fluctuation between starts is not wider.

III. TIME AS TEMPORALITY MINING

3.1. Temporality Mining Purpose

Performing mining based on merely temporal processes as a mechanism to assess and predict events that are concomitant with them. Among other things it is possible to obtain information regarding the typical evolution of these events, the importance of the event within the life of the system being studied.

3.2. Temporality Mining Characteristics

Data are considered if they meet the following requirements:

- They are captured from a process which is external to the system
- They have marked temporality: date, time, minutes, seconds, etc.
- They can be associated to a cyclic complex event or not, thus enabling generation of an approximate model starting from a measurable characteristic set and its temporality.
- They are produced by one or more identifiable and distinguishable source
- Events are defined and limited in time
- Their duration is variable or constant but they start and end at a defined time point
- They may undergo duration and frequency changes, but not changes in identifying characteristics –properties defined as behavior patterns.

3.3. Data Formats suitable for Temporality Mining

A temporality mining vector in this context

would be something like :
Header + characteristics + body

with Header= timestamp,

Characteristics= properties to be assessed taken to a numeric vector of numeric labels or not, which do not belong in a metric scale. E.g.: characteristics= process-ID+param₁+param₂+param₃, with param₁, param₂, param₃ =1 if these parameters are provided; otherwise, 0

Body= other dataset information not relevant to the current process

3.4. Applications of Temporality Mining

It is possible to apply this type of mining to different situations, mainly prediction of time variations, detection/removal of noise sources (data which do not fit in the time pattern expected), detection of mutations in temporal characteristics and detection of cycles and periodicities and their characteristics. There are many applications, including user profiling, intrusion detection, fault prediction, operation profile, product/buyer association profile, etc.

IV. HARMONICS AND TEMPORALITY MINING

The process explained in the temporality mining section is applied, adapting it to the special case of time mining with data format:

HEADER + CHARACTERISTICS + BODY + PROCESS

Where:

HEADER= timestamp

CHARACTERISTICS= numeric vectors with the values of properties to analyze.

E.g.:

characteristics= process-ID+param₁+param₂+param₃, (with param₁, param₂, param₃ =1 if these parameters are provided; otherwise, 0)

Body= other dataset information not relevant to the current process

PROCESS= the process triggered when current characteristics are met

4.1. Testing

The dataset was taken from [14]. Raw data is something as:

123.123.123.123 - - [26/Apr/2000:00:23:47-0400] "GET /asctorf/http/1.0" 200 8130
 "http://search.netscape.com/.../RTF" "Mozilla/4.05 (Macintosh; I; PPC)", which includes fields like IP, used ID, timestamp, result code, etc.

Data was processed and changed to the following format:

{head} + {characteristics} + {body}

For temporality mining purposes it is evident that the heading must be a time related field, such as the timestamp. Characteristics hold for properties of special interest during the current study:

{timestamp} + {ID-process, IP} + {rest of the information in the row}

From the given example the information entries result as:

20000426002347 +{GET, 123.123.123.123} + {/asctorf/http/1.0 200 8130 "http://search.netscape.com/.../RTF"
 "Mozilla/4.05 (Macintosh; I; PPC)}

4.2. Test 1: Temporality with harmonics

For demonstrative purposes, a test with 14 samples was performed. For all cases, the commands were replaced with numeric identifiers. E.g.: GET is replaced by 1.

The pattern to be studied was defined as:

pattern= 1,

U=0.03,

n₊ = 33,

n_T=70,

□=0.05,

□_u=0.3,

n_c=56

and IP=123.123.123.123, l₁=20.7, l₂=28.5, and l₃=67.5, n=14

Poisson is used to measure the pattern model against the patterns obtained from the data and confirm whether they resonate.

In the processing, no filter was applied, and for pattern detection the steps are as follows.

In ID =4 the first part of the following pattern is detected:

t2=* - 20000426002393,
t1=20000426002393- 20000426002372= 21

In ID=6 the second part of the pattern is detected:

t3=* - 20000426002423,
t2= 20000426002423 - 20000426002393= 30,
t1=20000426002393- 20000426002372= 21

In ID=9 the third part of the pattern is detected:

In ID=12, the pattern is completed –simplified for practical purposes, supposing the start of another activity finished the previous one:

$$t_3 = 20000426002483 - 20000426002423 = 60,$$

$$t_2 = 20000426002423 - 20000426002393 = 30,$$

$$t_1 = 20000426002393 - 20000426002372 = 21$$

For resonance verification: Resonance to the only pattern in process is verified, taking the Cumulative Poisson Distribution:

$$P_o(17.5, 21) \times P_o(22.5, 30) \times P_o(67.5, 60) :: U=0.03$$

$$0.585 \times 0.658 \times 0.198 :: 0.03$$

Since aggregated Poisson production was the pattern resonates and is considered compatible with the calculated model. the threshold U, $0.076 :: 0.03$

When the pattern is met, the model is updated, considering this case as favorable.

Since parameters are just an average of the number of tics, the average of tics is updated based on the new values found:

$$\lambda_1 = 20.7 + 0.05 \times (21 - 20.7) = 20.72$$

$$\lambda_2 = 28.5 + 0.05 \times (30 - 28.5) = 28.60$$

$$\lambda_3 = 67.5 + 0.05 \times (60 - 67) = 63.15$$

The pattern threshold is also updated:

$$U = U + \eta_u \times (U - P_o(17.5, 21) \times P_o(22.5, 30) \times P_o(67.5, 60))$$

$$U = 0.03 + 0.3 \times (0.03 - (0.585 \times 0.658 \times 0.198)) = 0.03 + 0.3 \times (0.076 - 0.03) = 0.04$$

Temporality mining with harmonics without threshold change:

$$t_1 = * - 20000426002372$$

It is possible to use the thresholds in a fixed way, in which case the information is collected precisely when the pattern is met as expected, and there are no attempts to model actual processes, but instead the purpose is to detect the patterns that fit into a given model (maybe to separate them).

4.3. Test 2: Using Filters

A high-pass filter was defined with a threshold of 60 time units and the process was previously performed with this filter. The system administrator intends to detect processes which take longer than usual.

The pattern to be studied was defined as: **pattern-ID= 2, U=0.053, n₊ = 34, n_T=71, n_c=80**, with initial parameters $l_1=20.72, l_2=28.60$, and $l_3=63.15$

Since n_T is not larger than n_c samples, Binomial distribution is used to measure the pattern model against the patterns obtained from the data and confirm whether they resonate. Due to space reasons, the dataset is not detailed here. For information purposes, the dataset comprises 996 samples selected with processes 1, 2 and 3 and enabled IPs were: 123.123.123.123, 123.123.123.120, 123.123.123.119 and 123.123.123.123.110

As preliminary step, the high-pass filter is applied, removing 58 of the 996 samples (5.8%) The remaining samples go through the process. During pattern detection 11 pattern occurrences were detected. It is worth noting that, if the above filter had not been applied, the patterns detected would have been 13. These 11 patterns correspond to 33 of a total of 354 inputs within the logs generated by the IP 123.123.123.123

Resonance was verified for each instance applying the formulas given in section I, item D (resonance). As instances were processed, the parameters were adjusted. U_f started to stabilize towards a higher value, represented the closeness of current processes to the model. At the same time, l_i values evolved from their initial values.

It is remarkable that almost all the patterns survived the high-pass filter, if n_c is the maximum delay, it could point to a problem of long times in the processes involved. From this point of view, it is confirmed by the parameter values obtained: $l_1=21.13, l_2=28.10, l_3=64.26$. Both process 1 and 3 should be revised since they are expected to be faster.

V. CONCLUSION AND FUTURE WORK

This work presented the *Harmonic Systems* model for mining in real time. The strategy is focused only in times and behavioral patterns. This approach may be a useful for studies related to certain automated processes and monitor hardware systems.

Other interesting alternatives should be analyzed and filter cadences need to be defined in a more sophisticated way (e.g., Gaussian). Also, alternative methods for the initial model should be specified and their efficacy compared. Reasonable alternatives to define the value of parameter δ should be analyzed.

REFERENCES

- [1] C. Faloutsos, M. Ranganathan, Y. Manolopoulos, Fast subsequence Matching in Time Series Databases. *Proc ACM SIGMOID*. 1994
- [2] R. Agrawal, K. Lin, H. Sawhney, K. Shim, Fast similarity search in the presence of noise, Scaling and translation in time series Databases. *Proc VLDB 95*. pp 490-501, 1995

- [3] D. López De Luise, A Morphosyntactical Complementary Structure for Searching and Browsing, *In Proc. of SCSS05*. Springer. 2005
- [4] D. López De Luise, MLW and bilingualism. *Adv. Research and Trends in New Technologies, Software, Human-Computer Interaction, and Communicability*. IGI Global. USA. 2013
- [5] K. Church, R. Mercer, Introduction to the Special Issue on Computational Linguistics Using Large Corpora. *Computational Linguistics*. MIT Press Cambridge, MA, USA . 1993
- [6] A. Kao, S. Poteet, Natural Language Processing and Text Mining (Springler. 1991)
- [7] F. Tak-chung, Engineering Applications of Artificial Intelligence. *Engineering Applications of Artificial Intelligence* 24, pp. 164–181. 2011
- [8] J. Han, M. Kamber, Mining Stream, Time-Series, and Sequence Data. *In Data Mining, Second Edition, Concepts and Techniques*. 2nd Edition. 2011
- [9] J. Shieh, E. Keogh, iSAX: Indexing and Mining Terabyte Sized Time Series. *Proceedings KDD'08*. pp 623-631. ACM. 2008
- [10] H. Jagadish, A. Mendelzon, Similarity based queries. *In Proc 14th PODS 95*. pp 36-45. 1995
- [11] B. Bollogás., G. Das, D. Gunopulos, H. Mannila, Time series similarity problems and well-separated geometric sets. *Nordic Journal of Computing*. Pp 409- 423. 2003
- [12] L. Clifford, Neural Networks. *Teoretical Foundations and Analysis (IEEE Press.1991)*
- [13] C.A. Ratanamahatana, J. Lin, D. Gunopulos, E. Keogh. Mining Time Series Data. *In Data Mining and Knowledge Discovery Handbook*, pp 1049-1077. 2010.
- [14] Apache logs: <http://www.herongyang.com/Windows/Web-Log-File-IIS-Apache-Sample.html>

Comparison of General Relativity and Brans-Dicke Theory using Gravitomagnetic clock effect

Md. Hafijur Rahaman¹, S.B. Faruque¹, Md. Abu Taher Khan¹, Shahajan Miah¹ and Md. Aminul Islam¹

¹Department of Physics, Shahjalal University of Science and Technology, Bangladesh

Abstract: We discuss the gravitomagnetic clock effect in the context of general relativity and Brans-Dicke theory. General relativity predicts that two freely counter revolving test particles in the exterior field of a central rotating mass take different periods of time to complete the same full orbit. This phenomenon was first put forward by Cohen and Mashhoon in 1993. The gravitomagnetic clock effect also arises in the orbit of a particle which is moving round a Brans-Dicke source of mass M on the equatorial plane, and this clock effect is the same as general relativity. So, the Brans-Dicke theory cannot be distinguished from GR using GCE.

Keywords: Brans-Dicke theory, general relativity, Gravitomagnetic clock effect

I. INTRODUCTION

The gravitomagnetic clock effect (GCE) consists in the loss of synchrony of identical clocks carried around a rotating body of mass M on the equatorial plane. This effect is a consequence of general relativity and its presence has been foreseen in connection with the so called gravitomagnetism, i.e. that part of the gravitational field which, in weak field approximation behaves as the magnetic part of the electromagnetic interaction[1]. The GCE has been considered as an interesting and promising means to test the general relativistic influence of the angular momentum of a mass on the structure of space time nearby and in particular on the pace of clocks orbiting around the body[2, 3].

Actually the GCE is strictly akin to the Sagnac effect, which is a special relativistic effect induced by pure rotations, first considered as a purely classical effect by G. Sagnac[4], further on recognized in its real nature and studied by several author (see for instance[5, 6]).

The real possibility that gravitomagnetic effects can be measured with the current technology of laser ranged satellites (LAGEOS and LAGEOS II) has aroused great interest in the subject[7]. It should be mentioned that the Relativity Gyroscope Experiment (Gravity Probe B) at Stanford University, in collaboration with NASA and Lockheed-Martin Corporation, has a program of developing a space mission to detect gravitomagnetism effects directly. Certainly, these experimental programs will open new possibilities of testing general relativity against other metric theories of gravity[8,9], in particular the scalar-tensor theory, one of the most popular alternatives to Einstein theory of gravitation.

GCE is a novel effect resulting from Einstein's theory of gravitation. According to general relativity, two freely counter revolving test particles in the exterior field of a central rotating mass take different periods of time to complete the same full orbit; this time difference leads to the gravitomagnetic clock effect; first indicated by Cohen and Mashhoon in 1993[1]. The general relativistic calculation of the gravitomagnetic clock effect for a general orbit is quite complicated. The first derivation in [1] was done for equatorial circular orbits; spherical orbits have been considered in[10]; arbitrary elliptical orbits have been considered in [11]. Various theoretical aspects of this effect have been investigated[12 – 17]. On the observational side, the possibility of its detection has been considered by a number of authors[18 – 23].

An addition to the scenario of GCE came in the orbit of a particle which is moving round a Brans–Dicke source of mass M on the equatorial plane in that it also contributes to the gravitomagnetic clock effect[24]; the magnitude of this contribution has been calculated in [24] and the result was confirmed and elaborated by Bini et al. [25].

This paper is organized as follows. In section II, we give gravitomagnetic clock effect in general relativity. This was first put forward by Cohen and Mashhoon in 1993[1]. In section III, we have examined gravitomagnetic clock effect in Brans-Dicke theory. Section IV is devoted to some remarks.

II. GRAVITOMAGNETIC CLOCK EFFECT IN GENERAL RELATIVITY

Imagine the motion of a free non-spinning test particle on a time-like circular geodesic orbit in the equatorial plane of a Kerr black hole. The space-time metric in the Boyer Lindquist coordinates is given by

$$ds^2 = -\left(1 - \frac{2Mr}{\Sigma}\right)dt^2 + \frac{\Sigma}{\Delta}dr^2 + \Sigma d\theta^2 + \frac{A}{\Sigma} \sin^2\theta d\varphi^2 - \frac{4Ma}{\Sigma} r \sin^2\theta dt d\varphi, \quad (1)$$

where

$$\Sigma = r^2 + a^2 \cos^2\theta, \quad \Delta = r^2 - 2Mr + a^2, \quad A = (r^2 + a^2)^2 - a^2 \Delta \sin^2\theta. \quad (2)$$

Units are chosen such that $G = c = 1$, unless specified otherwise. Here M is the mass and $a = J / M$ is the specific angular momentum of the black hole. The geodesic equation

$$\frac{d^2 x^\mu}{d\tau^2} + \tau_{\alpha\beta}^\mu \frac{dx^\alpha}{d\tau} \frac{dx^\beta}{d\tau} = 0, \quad (3)$$

for the radial coordinate r in the special case under consideration reduces to

$$\left(a^2 - \frac{r^3}{M}\right) d\varphi^2 - 2adtd\varphi + dt^2 = 0, \tag{4}$$

which can be written as

$$\frac{dt}{d\varphi} = a \pm \omega_K^{-1}. \tag{5}$$

Here, $\omega_K = \sqrt{M/r^3}$, is the Keplerian angular frequency. In Eq.(5) + (-) represent the motion of the test particle moving in the same (opposite) sense as the rotation of the black hole. To field the gravitomagnetic clock effect one integrates Eq.(5) over 2π for co-rotating and -2π for counter-rotating test particles. This results in $t_{\pm} = T_K \pm 2\pi a$, where $T_K = 2\pi/\omega_K$, the Keplerian period. Thus

$$t_+ - t_- = 4\pi a = \frac{4\pi J}{Mc^2}. \tag{6}$$

This is the gravitomagnetic clock effect for test particle orbit, where time period of the co-rotating orbits are measured by asymptotically static inertial observers.

III. GRAVITOMAGNETIC CLOCK EFFECT IN BRANS-DICKE THEORY

The gravitomagnetic clock effect arises in orbit of a particle which is moving around a Brans-Dicke source of mass M on the equatorial plane,

$$ds^2 = [1 - \varepsilon G_0] \left[-\left(1 - \frac{2G_0 M}{rc^2}\right) c^2 dt^2 + \left(1 + \frac{2G_0 M}{rc^2}\right) \{dr^2 + r^2(d\theta^2 + \sin^2 \theta d\varphi^2)\} - \frac{4G_0 J}{rc^3} \sin^2 \theta d\varphi c dt \right]. \tag{7}$$

The Brans-Dicke metric for the equatorial plane $\theta = \frac{\pi}{2}$, $d\theta = 0$ is given by

$$ds^2 = [1 - \varepsilon G_0] \left[-\left(1 - \frac{2G_0 M}{rc^2}\right) c^2 dt^2 + \left(1 + \frac{2G_0 M}{rc^2}\right) \{dr^2 + r^2(0 + d\varphi^2)\} - \frac{4G_0 J}{rc^3} d\varphi c dt \right], \tag{8}$$

where

$$G_0 = \phi_0^{-1} = \left(\frac{2\omega+3}{2\omega+4}\right) G \text{ and the function } \varepsilon(x) \text{ is a solution of the scalar field equation } \varepsilon = \frac{8\pi T}{c^4(2\omega+3)}, \text{ and units are such that } G=c=1.$$

Throughout the section III we shall use this convention unless otherwise specified.

Now from equation (8),

$$\begin{aligned} ds^2 &= [1 - \varepsilon G_0] \left[-\left(1 - \frac{2G_0 M}{r}\right) dt^2 + \left(1 + \frac{2G_0 M}{r}\right) (dr^2 + r^2 d\varphi^2) - \frac{4G_0 J}{r} d\varphi dt \right] \\ \text{Or, } ds^2 &= [1 - \varepsilon G_0] \left[-\left(1 - \frac{2G_0 M}{r}\right) dt^2 + dr^2 + r^2 d\varphi^2 + \frac{2G_0 M}{r} dr^2 + \frac{2G_0 M}{r} r^2 d\varphi^2 - \frac{4G_0 J}{r} d\varphi dt \right] \\ \text{Or, } ds^2 &= [1 - \varepsilon G_0] \left[-\left(1 - \frac{2G_0 M}{r}\right) dt^2 - \frac{4G_0 J}{r} d\varphi dt + (2G_0 M r + r^2) d\varphi^2 + \left(\frac{2G_0 M}{r} + 1\right) r^2 \right]. \end{aligned} \tag{9}$$

The motion of test particle of mass m in the Brans-Dicke field is governed by the geodesic equation:

$$\frac{d^2 x^\omega}{ds^2} + \Gamma_{\alpha\beta}^{\omega} \frac{dx^\alpha}{ds} \frac{dx^\beta}{ds} = 0. \tag{10}$$

To evaluate the gravitomagnetic clock effect, we need only the geodesic equation for the radial co-ordinate r :

$$\frac{d^2 r}{ds^2} + \Gamma_{tt}^r \left(\frac{dt}{ds}\right)^2 + \Gamma_{rr}^r \left(\frac{dr}{ds}\right)^2 + \Gamma_{\varphi\varphi}^r \left(\frac{d\varphi}{ds}\right)^2 + \Gamma_{r\varphi}^r \frac{dt}{ds} \frac{d\varphi}{ds} + \Gamma_{\varphi t}^r \frac{d\varphi}{ds} \frac{dt}{ds} = 0. \tag{11}$$

Now,

$$\begin{aligned} \Gamma_{tt}^r &= \frac{1}{2} g^{rm} \left(\frac{\partial g_{mt}}{\partial t} + \frac{\partial g_{mt}}{\partial t} - \frac{\partial g_{tt}}{\partial x^m} \right) \\ &= g^{rr} \frac{\partial g_{rt}}{\partial t} - \frac{1}{2} g^{rr} \frac{\partial g_{tt}}{\partial t} = -\frac{1}{2} g^{rr} g_{tt,r}, \end{aligned} \tag{12}$$

Since $g_{rt} = 0$.

Similarly,

$$\begin{aligned} \Gamma_{rr}^r &= \frac{1}{2} g^{rr} g_{rr,r}, \quad \Gamma_{\varphi\varphi}^r = -\frac{1}{2} g^{rr} g_{\varphi\varphi,r}, \\ \Gamma_{t\varphi}^r &= -\frac{1}{2} g^{rr} g_{t\varphi,r}, \quad \Gamma_{\varphi t}^r = -\frac{1}{2} g^{rr} g_{t\varphi,r}. \end{aligned} \tag{13}$$

Substituting these expressions in Eq.(11) and cancelling a common factor, we get

$$-\frac{2}{g^{rr}} \frac{d^2 r}{ds^2} + g_{tt,r} \left(\frac{dt}{ds}\right)^2 - g_{rr,r} \left(\frac{dr}{ds}\right)^2 + g_{\varphi\varphi,r} \left(\frac{d\varphi}{ds}\right)^2 + 2g_{t\varphi,r} \frac{dt}{ds} \frac{d\varphi}{ds} = 0. \tag{14}$$

Cancelling ds^2 in the denominators of the terms in Eq.(14) and dividing by $d\varphi^2$ all through in (14), we obtain

$$-\frac{2}{g^{rr}} \frac{d^2 r}{d\varphi^2} + g_{tt,r} \left(\frac{dt}{d\varphi}\right)^2 - g_{rr,r} \left(\frac{dr}{d\varphi}\right)^2 + 2g_{t\varphi,r} \frac{dt}{d\varphi} + g_{\varphi\varphi,r} = 0. \tag{15}$$

For circular orbit r is not a function of φ , and hence, we obtain from (15) the following radial geodesic equation in Brans-Dicke field:

$$g_{tt,r} \left(\frac{dt}{d\varphi}\right)^2 + 2g_{t\varphi,r} \frac{dt}{d\varphi} + g_{\varphi\varphi,r} = 0. \tag{16}$$

Solution to this equation

$$\frac{dt}{d\varphi} = \frac{-2g_{t\varphi,r} \pm \sqrt{(2g_{t\varphi,r})^2 - 4g_{tt,r} g_{\varphi\varphi,r}}}{2g_{tt,r}} = \frac{-g_{t\varphi,r}}{g_{tt,r}} \pm \sqrt{\left(\frac{g_{t\varphi,r}}{g_{tt,r}}\right)^2 - \frac{g_{\varphi\varphi,r}}{g_{tt,r}}}. \tag{17}$$

Now,

$$2g_{t\varphi,r} = \frac{d}{dr} \left\{ \left(-\frac{4G_0 J}{r} \right) [1 - \varepsilon G_0] \right\} = \left(\frac{4G_0 J}{r^2} \right) [1 - \varepsilon G_0]$$

$$g_{t\varphi,r} = \left(\frac{2G_0 J}{r^2} \right) [1 - \varepsilon G_0] , \tag{18}$$

$$g_{tt,r} = \frac{d}{dr} \left\{ \left(\frac{2G_0 M}{r} \right) [1 - \varepsilon G_0] \right\}$$

$$= - \left(\frac{2G_0 M}{r^2} \right) [1 - \varepsilon G_0] , \tag{19}$$

$$g_{\varphi\varphi,r} = \frac{d}{dr} \{ (2G_0 M r + r^2) [1 - \varepsilon G_0] \}$$

$$= (2G_0 M + 2r) [1 - \varepsilon G_0]$$

$$= 2(G_0 M + r) [1 - \varepsilon G_0] . \tag{20}$$

Substitution of these results into(17), we obtain

$$\frac{dt}{d\varphi} = \frac{-\left(\frac{2G_0 J}{r^2}\right) [1 - \varepsilon G_0]}{-\left(\frac{2G_0 M}{r^2}\right) [1 - \varepsilon G_0]} \pm \sqrt{\left(\frac{\left(\frac{2G_0 J}{r^2}\right) [1 - \varepsilon G_0]}{-\left(\frac{2G_0 M}{r^2}\right) [1 - \varepsilon G_0]}\right)^2 - \left(\frac{2(G_0 M + r)[1 - \varepsilon G_0]}{-\left(\frac{2G_0 M}{r^2}\right) [1 - \varepsilon G_0]}\right)} = \frac{J}{M} \pm \sqrt{\left(\frac{J}{M}\right)^2 + \left(\frac{G_0 M r^2 + r^3}{G_0 M}\right)}$$

$$= a \pm \sqrt{a^2 + \left(\frac{G_0 M r^2 + r^3}{G_0 M}\right)} = a \pm \sqrt{a^2 + r^2 + \frac{r^3}{G_0 M}} . \tag{21}$$

In true units this formula reduces to

$$\frac{dt}{d\varphi} = \frac{a}{c} \pm \sqrt{\frac{a^2}{c^2} + \frac{r^2}{c^2} + \frac{r^3}{G_0 M c^2}} . \tag{22}$$

The gravitomagnetic clock effect arises the difference in orbital period in prograde and retrograde orbits. Prograde orbit is one where the sense of orbital motion of the test body is same as the sense of rotation of the central body. In retrograde orbit the situation is opposite. Note that in Eq. (22) the +(-) sign refers to prograde (retrograde) motion. The orbital period in prograde motion can be found by integrating Eq. (22) with the plus sign from 0 to 2π . The orbital period in retrograde orbit can be found by integrating Eq.(22) with the minus sign from 0 to -2π .

We indicate by t_+ the prograde period which is

$$t_+ = \int_0^{2\pi} \left(\frac{a}{c} + \sqrt{\frac{a^2}{c^2} + \frac{r^2}{c^2} + \frac{r^3}{G_0 M c^2}} \right) d\varphi$$

$$= 2\pi \frac{a}{c} + 2\pi \sqrt{\frac{a^2}{c^2} + \frac{r^2}{c^2} + \frac{r^3}{G_0 M c^2}} . \tag{23}$$

Similarly ,

$$t_- = \int_0^{-2\pi} \left(\frac{a}{c} - \sqrt{\frac{a^2}{c^2} + \frac{r^2}{c^2} + \frac{r^3}{G_0 M c^2}} \right) d\varphi$$

$$= -2\pi \frac{a}{c} + 2\pi \sqrt{\frac{a^2}{c^2} + \frac{r^2}{c^2} + \frac{r^3}{G_0 M c^2}} , \tag{24}$$

which is the retrograde orbital period .The period difference is

$$t_+ - t_- = 2\pi \frac{a}{c} + 2\pi \sqrt{\frac{a^2}{c^2} + \frac{r^2}{c^2} + \frac{r^3}{G_0 M c^2}} + 2\pi \frac{a}{c} - 2\pi \sqrt{\frac{a^2}{c^2} + \frac{r^2}{c^2} + \frac{r^3}{G_0 M c^2}}$$

$$= 4\pi \frac{a}{c} . \tag{25}$$

This is the expression for gravitomagnetic clock effect. Clearly, the retrograde orbit is faster than the prograde orbit. Hence, the Brans-Dicke theory predicts the same GCE as the general relativity does. So, the Brans-Dicke theory cannot be distinguished from GR using the GCE.

IV. FINAL REMARKS

In this paper, we have examined gravitomagnetic clock effect in the context of general relativity and Brans-Dicke theory. In section II, the simplest case of gravitomagnetic clock effect has been shown in general relativity where we have followed the first derivation of the GCE by Cohen and Mashhon[1]. In section III, we have examined gravitomagnetic clock effect that arises in the orbit of a particle which is moving round a Brans-Dicke source of mass M on the equatorial plane, and hence this clock effect is the same as general relativity. So, the Brans–Dicke theory cannot be distinguished from GR using the GCE.

REFERENCES

- [1] J. M. Cohen, B. Mashhoon, Phys. Lett. A **181** (1993) 353.
- [2] A. Tartaglia, Class. Quantum Grav. **16** (1999) 1.
- [3] B. Mashhoon, F. Gronwald, D. S. Theiss, Ann. Phys. **8** (1999) 135.
- [4] G. Sagnac, Comptes rendus **157** (1913) 708.
- [5] J. Anandan, Phys. Rev. D **24** (1981) 338; G. E. Stedman, Rep. Prog. Phys. **60** (1997) 615.
- [6] G. Rizzi, A. Tartaglia, Found. Phys. **28** (1998) 1663.
- [7] I. Ciufolini, E. Pavlis, F. Chieppa, E. Fernandes-Vieira, J. P´erez-Mercader, Science, **279** (1998)2100.
- [8] A. Camacho, Gen. Rel. Grav. **34** (2002) 1403.
- [9] C. M. Will, Theory and experiment in gravitational physics, Cambridge University Press, Cambridge (1993). C. M. Will, Living Rev. Relativity **4** (2001) 4.
- [10] B.Mashhoon, F.Gronwald, D.S. Thesis, Ann. Phys. **8** (1999) 135.
- [11] B. Mashhoon, L.Iorio, H.Lichtenegger, Phys.Lett. A **292**(2001) 49.
- [12] O. Semerak, Class. Quantum Grav.**16**(1999) 3769.
- [13] B.Mashhon, N.O. Santos, Ann. Phys. **9**(2000) 49.
- [14] D.Bini, R.T.Jantzen, B.Mashhoon, Class. Quantum Grav.**18**(2001) 653.
- [15] W.B. Bonnor, B.R. Steadman, Class. Quantum Grav.**16**(1999) 1853.
- [16] A.Tartaglia, Gen. Rel. Grav.**32**(2000) 1745.
- [17] L.Iorio, H. Lichtenegger, B. Mashhoon, Class. Quantum Grav.**19**(2002) 39.
- [18] L. Iorio, Int.J. Mod.Phys. D **10**(2001) 465.
- [19] L. Iorio, Class. Quantum Grav.**18**(2001) 4303.
- [20] H. Lichtenegger, F. Gronwald, B. Mashhoon, Adv. Space Res. **25**(2000) 1255.
- [21] A. Tartaglia, Class. Quantum Grav.**17**(2000) 783.
- [22] A. Tartaglia, Class. Quantum Grav.**17**(2000) 2381.
- [23] H. Lichtenegger, L.Iorio, B. Mashhoon, Ann. Phys. **15**(2006) 868.
- [24] S.B. Faruque, Phys. Lett. A **327**(2004) 95.
- [25] D.Bini. F. de Felice, A. Geralico, Class. Quantum Grav.**21**(2004) 5441.

DSTATCOM with LCL Filter to Improve Voltage Sags and Current Harmonics in Power Distribution System

Firas Marwan Flaih¹, Jyoti Shrivastava²

*(Department of Electrical Engineering (Power System), SHIATS, Allahabad)

** (Department of Electrical Engineering, SHIATS, Allahabad)

ABSTRACT: An increasing demand for high quality, reliable electrical power and increasing number of distorting loads may leads to an increased awareness of power quality both by customers and utilities. The most common power quality problems today are voltage sags, harmonic distortion and low power factor. This paper presents the improvement of voltage sags, harmonic distortion and low power factor using Distribution Static Compensator (D-STATCOM) with LCL Passive Filter in power distribution network. The model is based on the Voltage Source Converter (VSC) principle. The D-STATCOM injects a current into the system to mitigate the voltage sags. a LCL(inductor-capacitor-inductor) Passive Filter with pulse width modulation (PWM) was then added to D-STATCOM to improve current harmonic distortion. The simulations were performed using MATLAB SIMULINK version R2009b.

Keywords: Distribution static compensator(D-STATCOM),(inductor-capacitor-inductor) LCL filter, Voltage Source Converter (VSC), Sine Pulse Width Modulation(SPWM), Voltage Sags, Total Harmonics Distortion (THD).

I. INTRODUCTION

DSTATCOM is one of the custom power devices, used for supplying reactive, harmonic currents of load demand in distribution system. DSTATCOM is connected in parallel to load at the point of common coupling (PCC) through interface filter. [1]

In other words, the switching frequency voltage at the leg of current controlled VSI is properly shaped by low pass L filter to inject the desired filter currents at PCC. Thus, the injected filter currents consist of switching frequency current ripple. These ripples are transferred to source currents, and also to the PCC voltages in presence of feeder impedance. Amplitude of this current ripple has inverse relation with respect to value of L filter. Thus, large value of L is required to have sufficient ripple attenuation, which increases cost, deteriorate compensation slew rate and consequently dynamic performance of system [2].

Higher order LCL filter has better switching ripple attenuation capability compared to L filter, and this can be achieved by using small values of overall inductance and capacitance [3].

An increasing demand for high quality, reliable electrical power and increasing number of distorting loads may leads to an increased awareness of power quality both by customers and utilities. The most common power quality problems today are voltage sags, harmonic distortion and low power factor Voltage sags is a short time (10 ms to 1 minute) event during which a reduction in r.m.s voltage magnitude occurs [4].

Voltage sags are one of the most occurring power quality problems. For an industry voltage sags occur more often and cause severe problems and economical losses. Utilities often focus on disturbances from end-user equipment as the main power quality problems [5].

Harmonic currents in distribution system can cause harmonic distortion, low power factor and additional losses as well as heating in the electrical equipment. It also can cause vibration and noise in machines and malfunction of the sensitive equipment [6].

power quality problems in transmission and distribution systems. Among these, the D-STATCOM is one of the most effective devices. A new PWM-based control scheme has been implemented to control the electronic valves in the DSTATCOM. The D-STATCOM has additional capability to sustain reactive current at low voltage, and can be developed as a voltage and frequency support by replacing capacitors with batteries as energy storage. [7, 8]

D-STATCOM is connected in shunt or parallel to the 11 kV test distribution system. It also is design to improve power quality such as voltage sags, harmonic distortion and low power factor in power distribution network.

II. DISTRIBUTION STATIC COMPENSATOR

A DSTATCOM is a controlled reactive source, which includes a Voltage Source Converter (VSC) and a DC link capacitor connected in shunt, capable of generating and/or absorbing reactive power. The operating principles of a DSTATCOM are based on the exact equivalence of the conventional rotating synchronous compensator.[9]

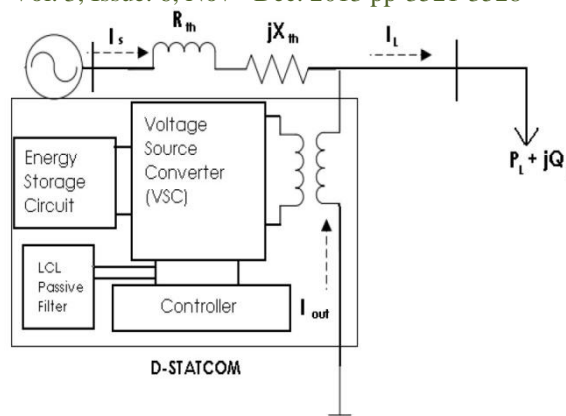


Figure 2.1. Schematic diagram of a D-STATCOM

A D-STATCOM consists of a two-level VSC, a dc energy storage device, controller and a coupling transformer connected in shunt to the distribution network. Figure 2.1 shows the schematic diagram of D-STATCOM.

$$I_{out} = I_L - I_S = I_L - \frac{V_{th} - V_L}{Z_{th}} \quad (2.1)$$

$$I_{out} < \gamma = I_L < (-\theta) - \frac{V_{th}}{Z_{th}} < (\gamma - \beta) + \frac{V_{th}}{Z_{th}} < (-\beta) \quad (2.2)$$

I_{out} = output current

I_S = source current

I_L = load current

V_L = load voltage

V_{th} = Thevenin voltage

Z_{th} = impedance

Referring to the equation 2.2, output current, I_{out} will correct the voltage sags by adjusting the voltage drop across the system impedance, ($Z_{th} = R + jX$). It may be mention that the effectiveness of D-STATCOM in correcting voltage sags depends on:

- The value of Impedance, $Z_{th} = R + jX$
- The fault level of the load bus.

2.2 Voltage source converter (VSC)

Two level Voltage Source Converter is a standard application widely used in industry as a rectifier, inverter and compensator system. This application is chosen as basic by leading world electrical companies for its efficiency and simplicity. Although it is regarded as a well known and established system, there are still some aspects worth analysing. Concurrently to multilevel converter systems development the high precision control and modulation systems of two level VSC are still considered [10]

A voltage-source converter is a power electronic device that connected in shunt or parallel to the system. It can generate a sinusoidal voltage with any required magnitude, frequency and phase angle. The VSC used to either completely replace the voltage or to inject the 'missing voltage'. The 'missing voltage' is the difference between the nominal voltage and the actual. It also converts the DC voltage across storage devices into a set of three phase AC output voltages [11].

Suitable adjustment of the phase and magnitude of the DSTATCOM output voltages allows effectives control of active and reactive power exchanges between D-STATCOM and AC system. In addition, the converter is normally based on some kind of energy storage, which will supply the converter with a DC voltage [12].

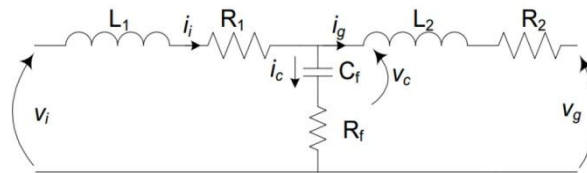
2.3 LCL Passive Filter

Commonly a high-order LCL filter has been used in place of the conventional L-filter for smoothing the output currents from a VSI [13].

The LCL filter achieves a higher attenuation along with cost savings, given the overall weight and size reduction of the components. LCL filters have been used in grid-connected inverters and pulse-width modulated active rectifiers [14].

because they minimize the amount of current distortion injected into the utility grid, Good performance can be obtained in the range of power levels up to hundreds of kW, with the use of small values of inductors and capacitors [15].

The following per-phase equivalent model has been fully described in an earlier paper written by the authors [16]. The LCL filter model is shown in Fig.2.2



where L1 is the inverter side inductor, L2 is the grid-side inductor, Cf is a capacitor with a series Rf damping resistor, R1 and R2 are inductors resistances, voltages Vi and Vg are the input and output (inverter voltage and output system voltage). A functional block diagram for the grid connected inverter using this LCL filter is shown in Fig 2.3

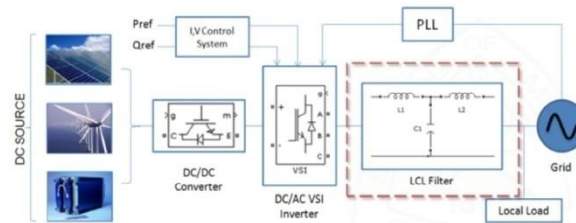


Fig. 2.3 General schematic for grid interconnected DC power source

To design it, equation (2.3), (2.4) and (2.5) are used [17].

$$L_g = \frac{E_n}{2\sqrt{6}i_{rpm}f_{sw}} \quad (2.3)$$

$$L_c = \frac{L_g}{2} \quad (2.4)$$

$$C_f = \frac{L + L_g}{LL_g (2\pi f_{res})^2} \quad (2.5)$$

Where $L_g = L1$, $L_c = L2$

To design an efficient LCL Passive filters make sure that,

$$10f_n \leq f_{res} \leq 0.5f_{sw}$$

2.4 Controller

Proportional-integral controller (PI Controller) is a feedback controller which drives the system to be controlled with a weighted sum of the error signal (difference between the output and desired set point) and the integral of that value. Figure 2.4 shows the block diagram of Controller system. The controller system is partially part of distribution system.

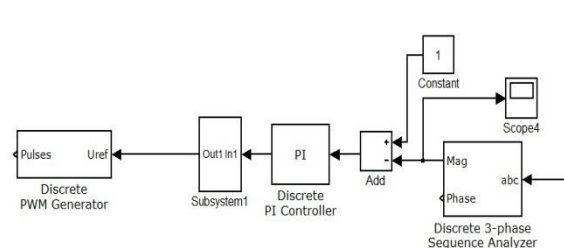


Figure 2.4. Block Diagram of Controller System

PWM generator is the device that generates the Sinusoidal PWM waveform or signal. To operate PWM generator, the angle is summed with the phase angle of the balance supply voltages equally at 120 degrees. Therefore, it can produce the desired synchronizing signal that required. PWM generator also received the error signal angle from PI controller. The modulated signal is compared against a triangle signal in order to generate the switching signals for VSC valves[18].

2.5 Energy Storage Circuit

DC source is connected in parallel with the DC capacitor. It carries the input ripple current of the converter and it is the main reactive energy storage element. This DC capacitor could be charged by a battery source or could be recharged by the converter itself as shown in figure 2.1 in energy storage circuit[18].

Symbol	Name	Quantity Value
E_n	RMS value of grid voltage	19kV (rms)
i_{ripm}	15% of peak value fundamental Harmonic current	793.1mA (rms)
L_g	Grid-side filter inductance	1630 mH
L_c	Converter-side filter inductance	815 mH
C_f	Filter capacitance	0.0017 uF
R_f	Resistance of converter-side filter	15 Ω
f_{sw}	Switching frequency	20kHz
f_{res}	Resonance frequency	5.25 kHz

TABLE 2.1. LIST AND VALUE OF PARAMETERS USE IN SIMULATION

Figure 2.5 shows the input current harmonic spectrum with respect to the IEEE STD 519-1992 harmonic limits.

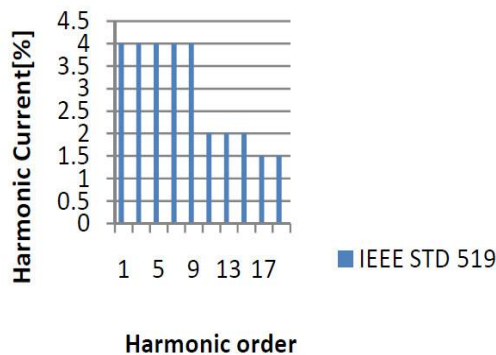


Figure 2.5.IEEE STD 519-1992 of current Harmonic spectrum

III. METHODOLOGY

To enhance the performance of distribution system, DSTATCOM was connected to the distribution system. DSTATCOM was designed using MATLAB simulink version R2009b.

3.2 Test System

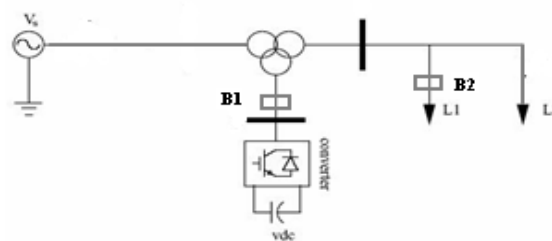


Figure3.1.Single line diagram of the test system

The test system shown in figure 3.1 comprises a 19kV, 50Hz transmission system, represented by a Thevenin equivalent, feeding into the primary side of a 3-winding transformer connected in Y/Y/Y, 19/11/11 kV. A varying load is connected to the 11 kV, secondary side of the transformer. A two-level D-STATCOM is connected to the 11 kV tertiary winding to provide instantaneous voltage support at the load point. A 750 μ F capacitor on the dc side provides the D-STATCOM energy storage capabilities. Breaker 1 is used to control the period of operation of the D-STATCOM and breaker 2 is used to control the connection of load 1 to the system.

3.3 Simulink Model for the test system

The test system was design using MATLAB simulink is shown in figure 3.2 below.

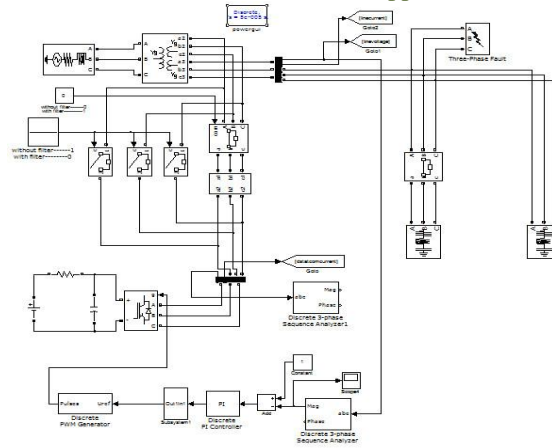


Figure3.2.Diagram of the test system

IV. RESULTS AND DISCUSSION

To create distortion in the distribution system, different types of fault such as Three Line to Ground (TLG), Double Line to Ground (DLG), Line to Line (LL), and Single Line to Ground (SLG) are injected.

4.2 Without insertion of D-STATCOM

TABLE4.1. RESULTS OF VOLTAGE SAGS FOR DIFFERENT TYPES OF FAULT.

Fault resistance R_f, Ω	Voltage sags for TLG fault (p.u)	Voltage sags for DLG fault (p.u)	Voltage sags for LL fault (p.u)	Voltage sags for SLG fault (p.u)
0.6	0.6296	0.6820	0.7388	0.8123
0.7	0.6803	0.7237	0.7719	0.8530
0.8	0.7270	0.7625	0.8035	0.8563
0.9	0.7678	0.7971	0.8327	0.8756

Table 4.1 shows the overall results of voltage sags in p.u for different types of fault. From the table, it can be observed that when the value of fault resistance is increase, the voltage will also increased for different types of fault.

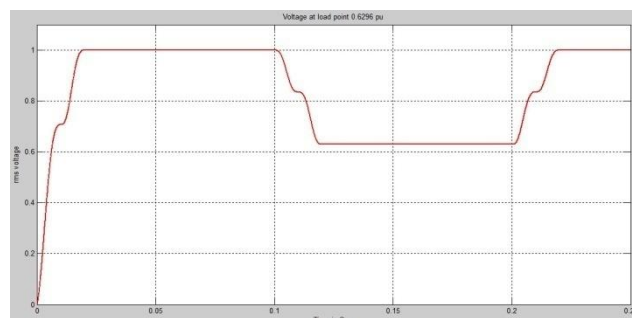


Figure4.1(a).voltage at load point is 0.6296 p.u TLG

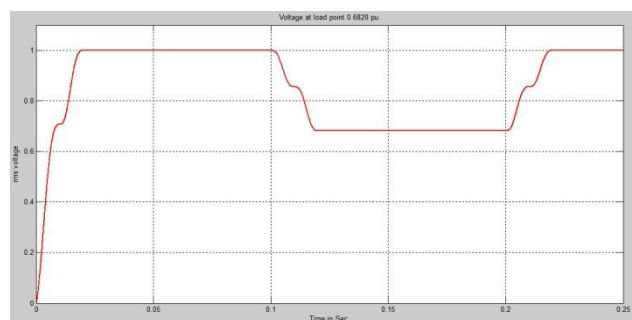


Figure4.1(b).voltage at load point is 0.6820 p.u DLG

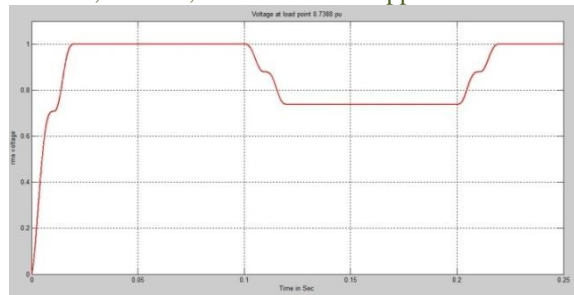


Figure4.1(c).voltage at load point is 0.7388 p.u LL

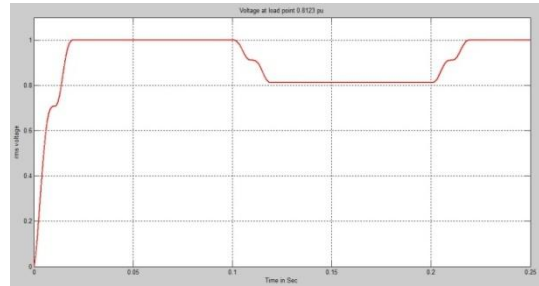


Figure4.1(d).voltage at load point is 0.8123 p.u SLG

Figure 4.1(a) to 4.1(d) show the simulation results of the test system for different types of fault. The fault occur during (100-200ms) when the fault resistance, $R_f=0.6 \Omega$.

4.3 With insertion of D-STATCOM

Fault resistance R_f, Ω	Voltage sags for TPG fault (p.u)	Voltage sags for DLG fault (p.u)	Voltage sags for LL fault (p.u)	Voltage sags for SLG fault (p.u)
0.6	0.9317	0.9796	1.0184	0.9849
0.7	0.9400	0.9802	1.0158	0.9829
0.8	0.9487	0.9827	1.0146	0.9835
0.9	0.9580	0.9879	1.0156	0.9881

TABLE4.2. RESULTS OF VOLTAGE SAGS FOR DIFFERENT TYPES OF FAULT

Table 4.2 shows the overall results of voltage sags in p.u with different types of fault. From the table, it can be observed that voltage sags improved with insertion of D-STATCOM. The value of voltage sags is between (0.9317 to 1.0184 p.u.).

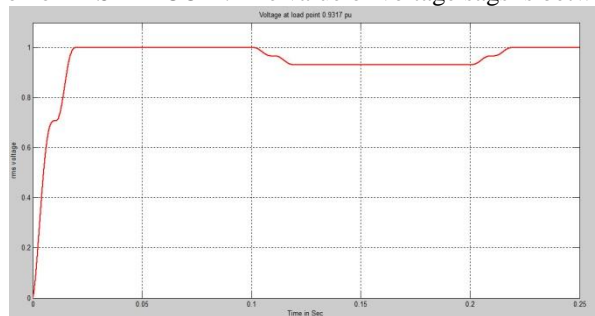


Figure4.2(a).voltage at load point is 0.9317 p.u TLG

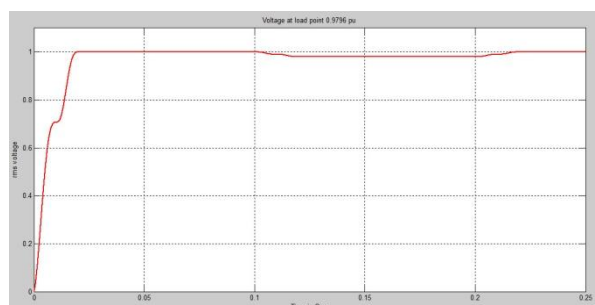


Figure4.2(b).voltage at load point is 0.9796 p.u DLG

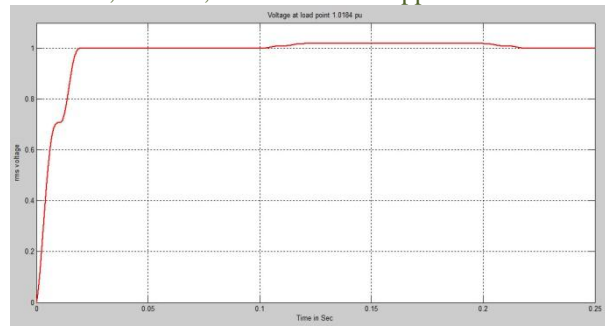


Figure4.2(c).voltage at load point is 1.0184 p.u LL

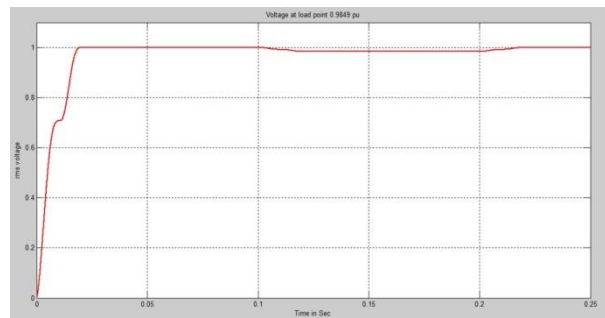


Figure4.2(d).voltage at load point is 0.9849 p.u SLG

Figure 4.2(a) to 4.2(d) show the simulation results of the test system for different types of fault. The fault occurs during (100-200ms) when the fault resistance is 0.6 Ω .

4.4 D-STATCOM without LCL Filter

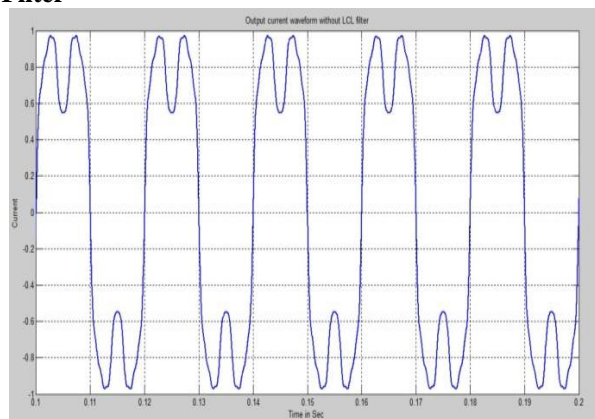


Figure4.3.waveform of distortion output current without LCL Filter

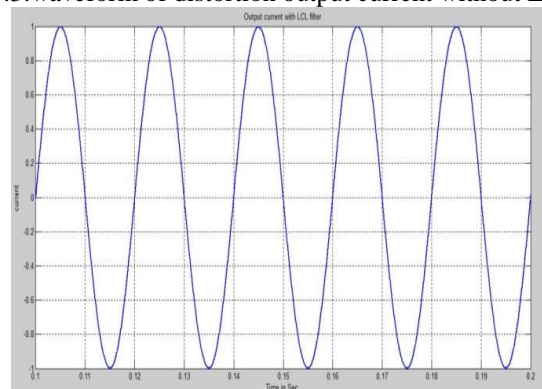


Figure4.4.waveform of output current with LCL Filter

Figure 4.3, shows the waveform of distortion output current without LCL Filter and Figure4.4.shows waveform of sinusoidal output current with LCL Filter.

V. CONCLUSION

The simulation results show that the voltage sags can be mitigate by inserting D-STATCOM to the distribution system. By adding LCL filter to D-STATCOM, The power factor also increase close to unity. Thus, it can be concluded that by adding D-STATCOM with LCL filter the voltage and current are improved.

REFERENCES

Journal Papers:

- [1] B. C. Parikshith, "Integrated approach to filter design for grid connected power converters", Master of Science Thesis, Indian Institute of Sciences, Bangalore, India, ,” 2009 .
- [2] W. Zhao and G. Chen, "Comparison of active and passive damping methods for application in high power active power filter with LCL filter," in International Conference on Sustainable Power Generation and Supply, pp 1-6, Apr. 2009.
- [3] M. Liserre, F. Blaabjerg, and S. Hansen, "Design and control of an LCL filter-based three-phase active rectifier," IEEE Trans. Ind. Appl., vol. 41, no. 5, pp. 1281–1291, Sept.-Oct.2008.
- [4] Anaya-Lara O, Acha E., "Modelling and Analysis Of Custom Power Systems by PSCAD/EMTDC", IEEE Transactions on Power Delivery, Volume 17, Issue: 2008, Pages: 266-272.
- [5] Bollen, M.H.J., "Voltage sags in Three Phase Systems", Power Engineering Review , IEEE, Volume 21, Issue :9, September 2011, PP: 11-15.
- [6] Noramin Ismail, Wan Norainin Wan Abdullah " Enhancement of Power Quality in Distribution System Using D-STATCOM" The 4th International Power Engineering and Optimization Conference (PEOCO2010), Shah Alam, Selangor, MALAYSIA. 23-24 June 2010,pp:418-224
- [7] M.Madriral, E.Acha., "Modelling OF Custom Power Equipment Using Harmonics Domain Twchniques",IEEE 2009
- [8] R.Meinski, R.Pawelek and I.Wasiak, "Shunt Compensation For Power Quality Improvement Using a STATCOM controller Modelling and Simulation", IEEE Proce, Volume 151, No. 2, March 2008.
- [9] Kolli Nageswar Rao, C. Hari Krishna, Kiran Kumar Kuthadi " Implementation of D-STACTOM for Improvement of Power Quality in Radial Distribution System", International Journal of Modern Engineering Research (IJMER), Vol. 2, Issue. 5, Sep.-Oct. 2012 pp-3548-3552.
- [10] G. Radomski, "Modelling and modulation of voltage source converter",13th Int. Power Electronics and Motion Control Conf. 1, 504–511 (2008).
- [11] J.Nastran , R. Cajhen, M. Seliger, and P.Jereb,"Active Power Filters for Nonlinear AC loads, IEEE Trans.on Power Electronics Volume 9, No.1, PP: 92-96, Jan 2009.
- [12] L.T. Moran ,P.D Ziogas, and G.Joos , Analysis and Design Of Three Phase Current source solid State Var Compensator, IEEE Trans. on Industry Applications. Volume 25, No.2, 2009, PP:356-365.
- [13] F. Bouchafaa, D. Beriber, and M. S. Boucherit, "Modeling and control of a grid connected PV generation system," in Control & Automation (MED), 18th Mediterranean Conference, 2010, pp. 315 – 320.
- [14] V. Blasko and V. Kaura, "A Novel Control to Actively Damp Resonance in Input LC Filter of a Three-Phase Voltage Source Converter," IEEE Transactions on Industry Applications, vol. 33, no. 2, pp. 542–550, 2007.
- [15] Y. Tang, S. Member, P. C. Loh, P. Wang, and F. H. Choo, "Generalized Design of High Performance Shunt Active Power Filter With Output LCL Filter," IEEE Transactions on Industrial Electronics, vol. 59, no. 3, pp. 1443–1452, 2012.
- [16] A. Reznik, M. G. Simões, A. Al-durra, and S. M. Mueyen, "LCL Filter Design and Performance Analysis for Small Wind Turbine Systems," in Power Electronics and Machines in Wind Applications (PEMWA), IEEE, 2012, pp. 1–7.
- [17] A. Reznik, M.Godoy Simões, Ahmed Al-Durra, S. M. Mueyen "LCL Filter Design and Performance Analysis for Grid Interconnected Systems", in The 7th International Conference on Power Electronics, 2012, pp. 1133–1138.

Books:

- [18] Narain G. Hingorani , Laszlo Gyugyi "Understanding FACTS" 2013 pp.171-177.

BIOGRAPHIES



Firas Marwan Fakhraldin has done his B.Tech degree in Electrical Engineering from University of Mosul , Mosul, Iraq, and his M.Tech degree in Electrical Power Systems from SHIATS, Allahabad, UP, India. He is working as Engineer in North Distribution Electricity , Ministry of Electricity, Iraq .



Dr. Jyoti Shrivastava has done her graduation in Electrical Engineering and her post graduation in Design of Heavy Electrical Equipments. At present she is serving as a Senior Assistant Professor in Electrical Engineering department at college of Engineering and Technology, SHIATS, Allahabad, India. She has several international and National papers to her credit. Her field of interest and research are Power system control and operation, power quality improvement and condition monitoring of heavy electrical equipments. Her research aims to increase Transmission & Distribution system capacity and enhancing system reliability.

Analysis of the effect of Modulation Techniques, Spreading Codes and Turbo Codes for HSDPA under Different Channel Conditions

*Dhruv Singh Thakur, **Krishnakant Nayak, ***Rohini Piplewar

*Assistant Prof. ECE Department BIST Bhopal (M.P.) India

**HOD. ECE Department BIST Bhopal (M.P.) India

***Mtech. Digital Communication BIST Bhopal (M.P.) India

ABSTRACT: HSDPA (High Speed Downlink Packet Access) is gaining popularity because of its capability of delivering higher data rate transmission with minimum latency than the GSM (global system for mobile communications) and 2.5G GPRS (general packet radio service) systems. The stated improvements are incorporated by the application of multi-codes and adaptive modulation and coding techniques combining the two in proper way gives the best data rate for the available channel conditions. The latest release of HSDPA (release 11) facilitates the selection of QPSK, 16-QAM and 64-QAM as modulation technique, orthogonal variable spreading factor (OVSF) as spreading codes and turbo codes with various code rates. Because of great impact of these factors on the selection of best data rate according to channel conditions in this paper we experimented with other available options for the modulation techniques, spreading codes and turbo codes for multipath fading channel conditions to achieve the most efficient combination for achieving the optimum data rate at particular channel conditions.

Keywords: W-CDMA (Wideband Code Division Multiple Access), HSDPA, Turbo Codes, Fading Channel.

I. INTRODUCTION

HSDPA enables the provision of a high bit data rate services with increased channel capacity and provided a suitable platform for the high speed networks, at lower investment. The efficient use of radio resources is realized by the shared channel concept of HSDPA. This supports high especially bursty non real time traffic such as variable rate and packet switched data.

The initial release of HSDPA (Release 5) allow maximum data throughput of approximately 14 Mbps, which is achieved by the introduction of 16-QAM and higher code rates. These physical layer Changes are almost achievable especially for line-of- Sight (LOS) conditions. The enhance data rate in different releases of HSDPA is achieved by employing adaptive modulation and coding technique (AMC) which provides flexibility to select best modulation technique and coding rate best suitable for the channel conditions hence makes the system more robust even under adverse multipath fading conditions.

Because of enormous demand for high speed data rates services the continuous research for the further improvement of the HSDPA is required in every aspect of the system from protocol to physical layer designing. In this paper we are mainly focusing on the physical layer modifications and analyzing the impact of the various modulation techniques, spreading techniques and coding rates which can provide the useful information about the optimum selection strategy for AMC.

II. LITERATURE REVIEW

This section presents a review on the some of the most relative work in the same field. Frank Brouwer et al [1] analyzed integration of HSDPA (High-Speed Downlink Packet Access) link-level simulation results into network-level simulations for Enhanced UMTS their link-level simulation model all physical layer features of the 3GPP standards from generation of transport blocks, turbo coding, rate matching, spreading, scrambling to modulation. Similarly at the receiver side, all complementary blocks were designed, with soft-decision demodulation, and a turbo decoder using the MAP (Maximum A Posteriori) algorithm with 8 iterations. They also using fading channel model with CQI (Channel Quality Indicator) selection technique. The overall model described is accurately approximates the practical performance of HSDPA. Hermann Buddendick et al [3] presented a dynamic W-CDMA system level simulator extended to enable the simulation of packet switched services with special focus on HSDPA. The complete simulation system contains traffic sources that create sequences of packets for each active User Equipment (UE), models the protocol stack and provides the possibility to collect performance indicators, e.g. sector packet data throughput, page throughput, and packet delays, in different scenarios for offline analysis. A cross-layer design is proposed by Xin Wang et al [4] for quality-of-service (QoS) guaranteed traffic. The proposed design jointly exploits the error-correcting capability of the truncated automatic repeat request (ARQ) protocol at the data link layer and the adaptation ability of the adaptive modulation and coding (AMC) scheme at the physical layer to optimize system performance for QoS guaranteed traffic. The queuing behavior induced by both the truncated ARQ protocol and the AMC scheme is analyzed with an embedded Markov chain. Analytical expressions for performance metrics such as packet loss rate, throughput, and average packet delay are derived. Using these expressions, a constrained optimization problem is solved numerically to maximize the overall system throughput under the specified QoS constraints. TNL Congestion Control Impact on the HSDPA Performance is presented by Thushara Weerawardane et al [5]. Their proposed work focuses to analyze the effect of congestion at the Iub interface on the HSDPA performance. The 3GPP (3rd Generation Partnership Project) Rel. 5 specifications highlight two congestion detection mechanisms which are based on the frame sequence number (FSN) and the Delay Reference Time (DRT) fields of HSDPA data frame. In

In addition to these, a third congestion detection mechanism based on Checksum of HSDPA data frame is considered. Vasileios M. Kapinas et al [8] proposed a generalized framework for handling Multiple-Input Multiple-Output (MIMO) schemes defined within the context of the Third Generation Partnership Project (3GPP) physical layer specifications. They introduce the Transmit Matrix (TRAM) concept that can include as special cases several MIMO systems (e.g. transmit diversity, spatial-multiplexing, etc.) regardless of the presence or not of a feedback channel their approach is based on the adoption of a novel measure called Necessary Transmit Information (NTI) and on its one-to-one correspondence with the TRAM. The last allows for a convenient alternative representation of a TRAM-based MIMO system model and serves the straight forward construction of NTI-codebooks for a wide range of transmission schemes.

III. THE PHYSICAL LAYER STRUCTURE OF HSDPA

The new HSDPA Physical channels are described as:

HS-PDSCH or High Speed Physical Downlink Shared Channel: This is a downlink channel which is both time and code multiplexed. The channelization codes have a fixed spreading factor, $SF = 16$. Multi-code transmissions are allowed that translates to UE being assigned multiple channelization codes in the same TTI, depending on the UE capability. The same scrambling code sequence is applied to all the channelization codes that form the single HS-DSCH CCTrCH. If there are multiple UE's then they may be assigned channelization codes in the same TTI (multiplexing of multiple UE's in the code domain).

HS-DPCCH or High Speed Dedicated Physical Control Channel: This is an uplink channel that carries the Acknowledgements of the packet received on HS-PDSCH and also the CQI (Channel Quality Indication). The CQI estimates have to be transmitted by the UE every 2.0 ms frame. This information is very important as it ensures reliability and impacts power capacity.

HS-SCCH or High Speed Shared Control Channel: The HS-SCCH is a fixed rate (60 kbps, $SF=128$) downlink physical channel used to carry downlink signaling related to HS-DSCH transmission. This provides timing and coding information thus allowing the UE to listen to the HS-DSCH at the correct time and using the correct codes to allow successful decoding of UE data.

Adaptive Modulation and Coding (AMC): HSPDA standard ensures that highest possible data rate is achieved for all users regardless of whether they are close to the base station or far off. This is done using ACM. For HS-DSCH, the transport format, including the modulation scheme and code rate, can be selected based on the downlink channel quality. The selection of transport format is done by the MAC-HS located in Node B and is based on channel quality feedback reported by the UE. The spreading factor cannot change but the coding rate can change between $1/4$ and $3/4$. The higher coding rate reduces the number of errors. Also the standards support multi-codes. This means that up to 15 codes can be allocated to a UE.

Hybrid Automatic Repeat Request (HARQ): In case of ARQ, the receiving system on receipt of data checks the CRC. If the CRC is the same as that received in the message ACK is sent back to the sender. In case if CRC does not match then NACK is sent back and the packet discarded. In case of HARQ, this method of CRC checking is improved based on the following two things.

Chase Combining: In this when an error is detected in CRC, NACK is sent back but the packet is not discarded. It is stored. In case the re-transmitted packet is again erroneous then the previous and current packet is combined in an attempt to recover from errors. Each time the packet is resent, the same scheme is applied. Eventually the error will be either resolved or maximum number of retries is reached. In that case higher layer protocols will deal with the error.

Incremental Redundancy (IR): IR is similar to Chase combining but the redundant information that was not transmitted earlier is also included to improve the chances of reception without errors or with enough errors removed so as to allow combining with the previously stored packet and resolve the errors.

Fast Cell Site Selection (FCSS): When the UE moves between the cells, it is possible that it would be served by different cells. Hence the UE will construct a list of Active Set (the term Active Set is incorrect and the term that will be used eventually is "Eligible Set") Cells that it can use at any one time. The mobile will indicate on HS-DPCCH as to which one is the best cell for DL transmission. The serving cell then decides the modulation and coding scheme to be used for the mobile and in addition may code multiplex multiple mobiles within that HSDPA frame. To simplify this procedure, it is further subdivided into Intra-Node B FCS and Inter-Node B FCS.

The complete structure of the physical layer for the HSDPA is shown in figure 1. This is a downlink channel which is both time and code multiplexed. The channelization codes have a fixed spreading factor, $SF = 16$. Multi-code transmissions are allowed that translates to UE being assigned multiple channelization codes in the same TTI, depending on the UE capability. The same scrambling code sequence is applied to all the channelization codes that form the single HS-DSCH. If there are multiple UE's then they may be assigned channelization codes in the same TTI (multiplexing of multiple UE's in the code domain).

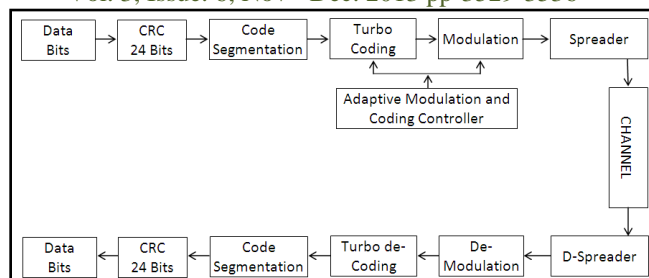


Figure 1: Block Diagram of HSDPA Physical Layer

In the first stage of the transmitter 24 bits CRC is appended to the input data after which the data is segmented into the proper block size for performing the turbo coding at the rate decided by the AMC based on the feedback which is then pass through the modulator, the modulation can be the QPSK, 16-QAM or 64-QAM which is also decided by AMC and depends upon feedback and at last the spreading is performed by using Orthogonal variable spreading factor (OVSF) with spreading factor (SF) of 16. After spreading the data is transmitted using radio waves which is then pass through the channel which produces abnormality (such as noise addition or fading, depending upon the environment conditions) on the signals pass through it. Now these signals are received at the receiver and at this end the inverse operations of transmitter side is performed to recover the data. The values used for the system are Fixed Spreading Factor of 16 for HS-DSCH, QPSK 16 QAM and 64 QAM Modulation, Static TTI Length of 3 Time Slots = 2ms, Fixed CRC of 24 bits, Error Correction using 1/3 to 3/4 Turbo Coding.

IV. TURBO CODES

The turbo codes are represents a class of high-performance forward error correction (FEC) codes initially proposed in 1993 which were the first practical implementable error control codes that achieve Shannon's bound to within 0.5 dB of signal-to-noise ratio. Because of such capability the turbo codes are used in 3G and (space) satellite communications and other applications where reliable information transfer with bandwidth or latency constrained are required.

A turbo coder is the parallel concatenation of a number of RSC (recursive systematic convolution) coders. The number of RSC coders depends upon the required performance, complexity and overhead. The working of the coder can be visualized by the figure 2 which shows the structure of turbo coder with two RSC coders. The input to the second decoder is an interleaved (Randomly Permuted) version of the input x , thus the outputs of coder 1 and coder 2 are time displaced codes generated from the same input sequence. The input sequence is only presented once at the output (y direct passing line). The outputs of the two coders may be multiplexed into the stream hence giving a rate $R=1/3$ code, or they may be punctured (sequentially selected by both coders) to give a rate $R=1/2$ code.

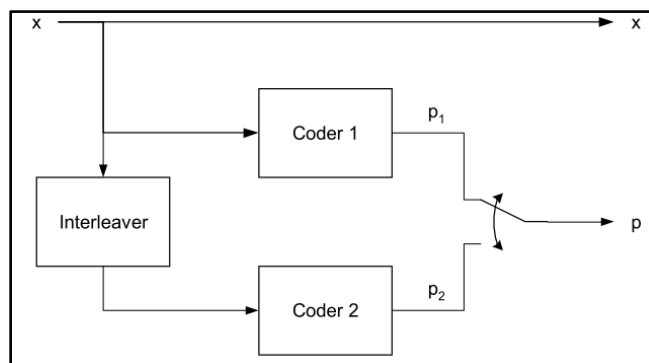


Figure 2: Structure of Turbo Encoder

Since the turbo coder is a complex combination of convolution encoder the decoding process also an extension of convolution decoder which generally utilizes two main concepts 1. Maximum A Posteriori (MAP) and 2. Soft Output Viterbi Algorithm (SOVA). MAP looks for the most likely symbol received; SOVA looks for the most likely sequence. Both MAP and SOVA perform similarly at high E_b/N_0 . At low E_b/N_0 MAP has a distinct advantage, gained at the cost of added complexity.

V. ORTHOGONAL VARIABLE SPREADING FACTOR (OVSF) CODES

These are the spreading codes required for the Code Division Multiple Access (CDMA) shown in figure 3, where in each transmitted signal is spread over a broad spectral range, using one of the codes from the codes set called users code. User's codes are to be carefully chosen so that they must have mutual orthogonally.

These codes are derived from an OVSF code tree, and each user given a different, unique code. An OVSF code tree is a complete binary tree, reflects the construction of Hadamard matrices.

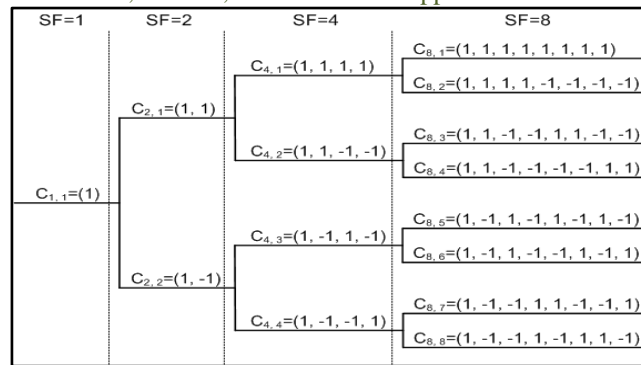


Figure 3: OVFSF code tree structure

VI. SIMULATION RESULTS

For the analysis of the system performance and scope the simulation of the HSDPA is performed for different channel conditions and with different system configurations and the simulated results are presented for each scenario.

Channel Conditions: Multipath Rayleigh Fading

Number of Paths = 4

Path Gains = 0,-1,-1,-3 dB

Path Delay = 0, 1e-7, 1.5e-7, 1.2e-6 seconds

Additive Wight Gaussian SNR: Varying from -10 to 10 dB

Spreading Codes: Orthogonal Codes Arranged and Numbered in Three Different Ways as shown in table 1, 2, and 3.

Finally the simulation is performed for the 20 Physical Layer Transport Blocks (TB) and the size of TB is calculated as follows:

$$Block\ Size\ (bits) = \frac{ChipRate}{SF * \left(\frac{1}{TTI}\right)} * BitsPerSymbol * ECR * NumOfCodes$$

Where:

ChipRate = 3.84 MHz

TTI = Transmission Time Interval = 2 ms

SF (Spreading Factor) = 16

Bits Per Symbol = Depends upon Modulation technique

ECR = Effective Coding Rate = Depends upon Turbo Coder

Num of Codes = Number of Multi-codes Allowed

TABLE 1: ORTHOGONAL CODES ARRANGEMENT 1

1	1	1	1	-1	-1	-1	-1	1	1	1	1	-1	-1	-1	-1
1	1	1	1	-1	-1	-1	-1	-1	-1	-1	-1	1	1	1	1
1	1	-1	-1	1	1	-1	-1	1	1	-1	-1	1	1	-1	-1
1	1	-1	-1	1	1	-1	-1	-1	-1	1	1	-1	-1	1	1
1	1	-1	-1	-1	-1	1	1	1	1	-1	-1	-1	-1	1	1
1	1	-1	-1	-1	-1	1	1	-1	-1	1	1	1	1	-1	-1
1	-1	1	-1	1	-1	1	-1	1	-1	1	-1	1	-1	1	-1
1	-1	1	-1	1	-1	1	-1	-1	-1	1	-1	1	-1	1	1

TABLE 2: ORTHOGONAL CODES ARRANGEMENT 2

1	1	1	1	-1	-1	-1	-1	-1	-1	-1	-1	1	1	1	1
1	1	1	1	-1	-1	-1	-1	1	1	1	1	-1	-1	-1	-1
1	1	-1	-1	-1	-1	1	1	1	1	-1	-1	-1	-1	1	1
1	1	-1	-1	-1	-1	1	1	-1	-1	1	1	1	1	-1	-1
1	1	-1	-1	1	1	-1	-1	-1	-1	1	1	-1	-1	1	1
1	1	-1	-1	1	1	-1	-1	1	1	-1	-1	1	1	-1	-1
1	-1	-1	1	1	-1	-1	1	1	-1	-1	1	1	-1	-1	1
1	-1	-1	1	1	-1	-1	1	-1	-1	1	1	-1	-1	1	-1

TABLE 3: ORTHOGONAL CODES ARRANGEMENT 3

1	1	-1	-1	1	1	-1	-1	1	1	-1	-1	1	1	-1	-1
1	-1	-1	1	1	-1	-1	1	1	-1	-1	1	1	-1	-1	1
1	1	1	1	-1	-1	-1	-1	1	1	1	1	-1	-1	-1	-1
1	-1	1	-1	-1	1	-1	1	1	-1	1	-1	-1	1	-1	1
1	1	-1	-1	-1	-1	1	1	1	1	-1	-1	-1	-1	1	1
1	-1	-1	1	-1	1	1	-1	1	-1	-1	1	-1	1	1	-1
1	1	1	1	1	1	1	1	-1	-1	-1	-1	-1	-1	-1	-1
1	-1	1	-1	1	-1	1	-1	-1	1	-1	1	-1	1	-1	1

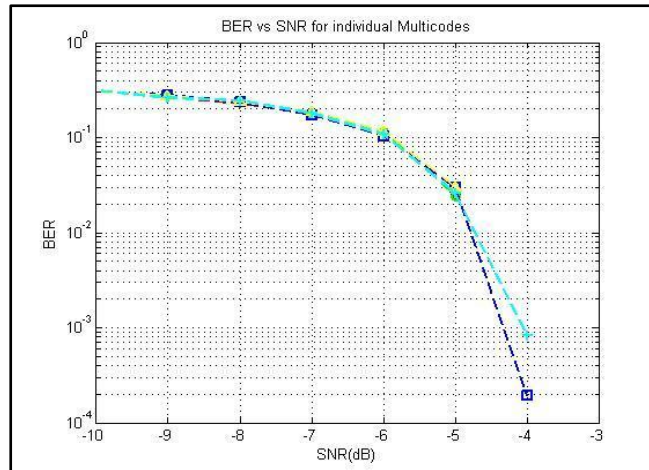


Figure 4(a): BER vs SNR plot for each user when Orthogonal Codes Arrangement 1 is used.

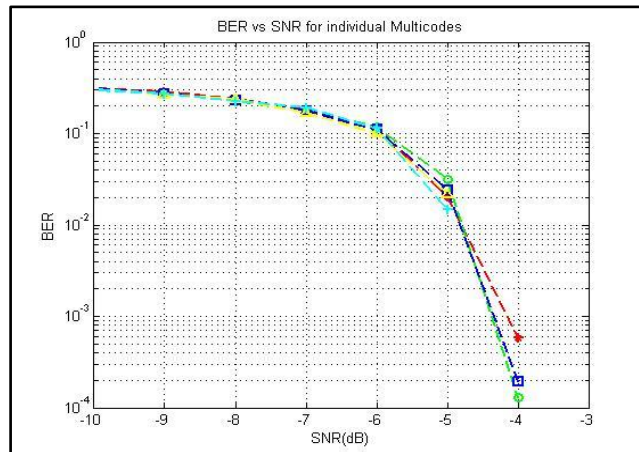


Figure 4(b): BER vs SNR plot for each user when Orthogonal Codes Arrangement 2 is used.

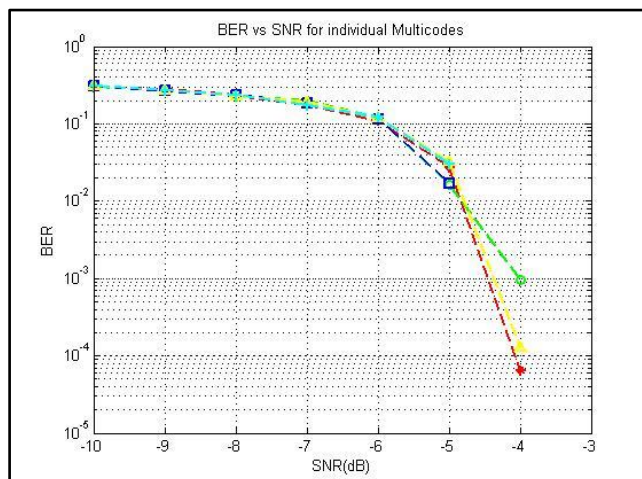


Figure 4(c): BER vs SNR plot for each user when Orthogonal Codes Arrangement 3 is used.

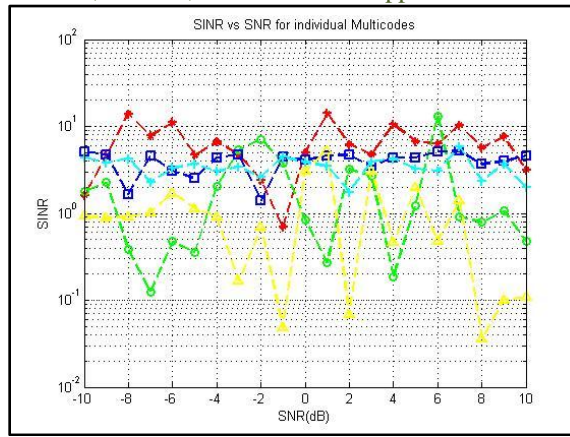


Figure 5(a): SINR vs SNR plot for each user when Orthogonal Codes Arrangement 1 is used.

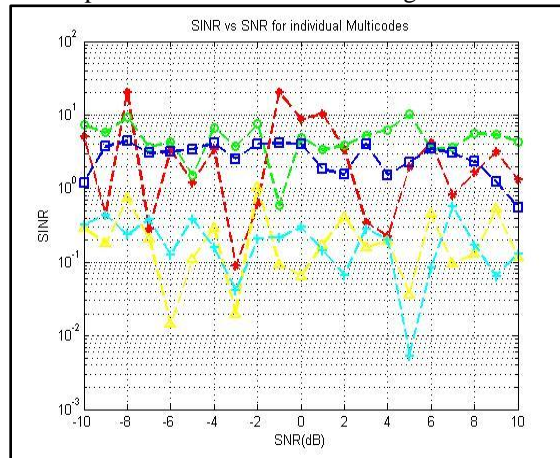


Figure 5(b): SINR vs SNR plot for each user when Orthogonal Codes Arrangement 2 is used.

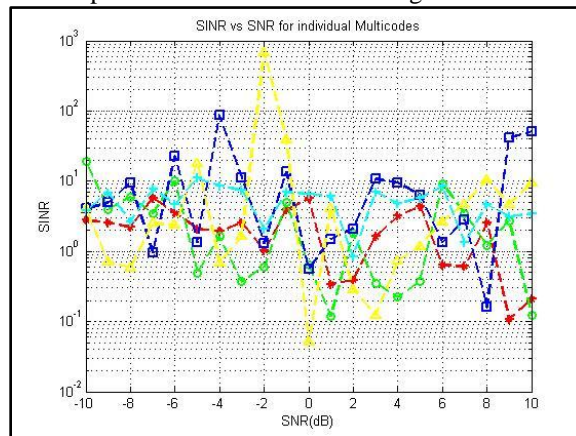


Figure 5(c): SINR vs SNR plot for each user when Orthogonal Codes Arrangement 3 is used.

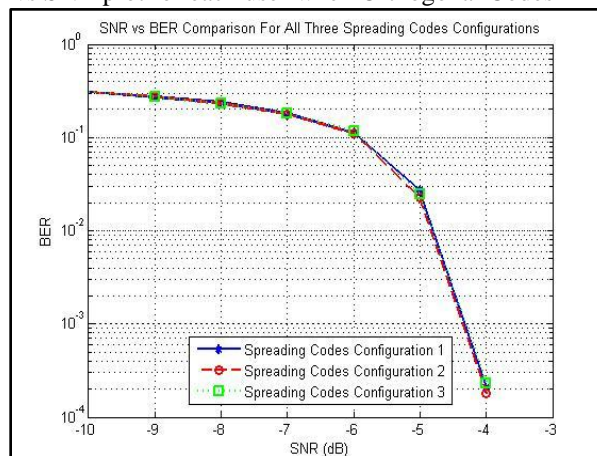


Figure 6: Average BER for all users for each configuration of orthogonal codes.

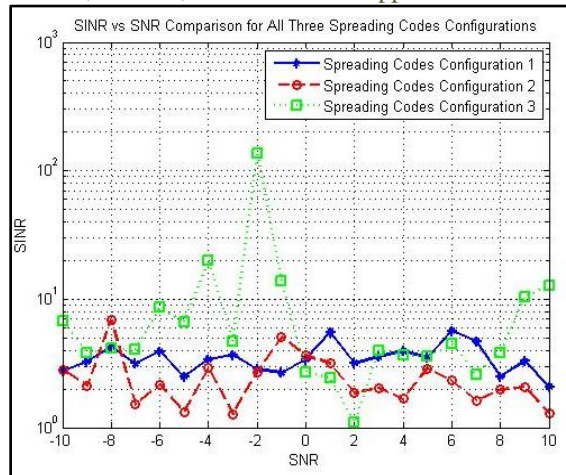


Figure 7: Average SINR for all users for each configuration of orthogonal codes.

The SNR vs BER and the SINR vs BER plot shown for each Orthogonal Codes Arrangement presents that each users BER is slightly different than others even in same operating condition this is because some combination of orthogonal codes produces less interference in fading channel conditions while others are not (as shown in figure 7 that the configuration 3 gives the best SINR then others) even though they are drawn from the same code set.

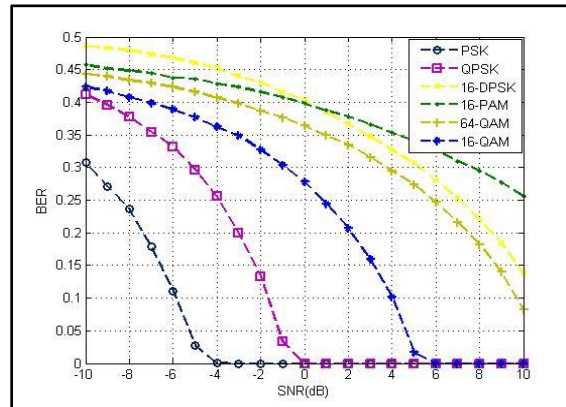


Figure 8: Comparison of the BER performance for different modulation techniques.

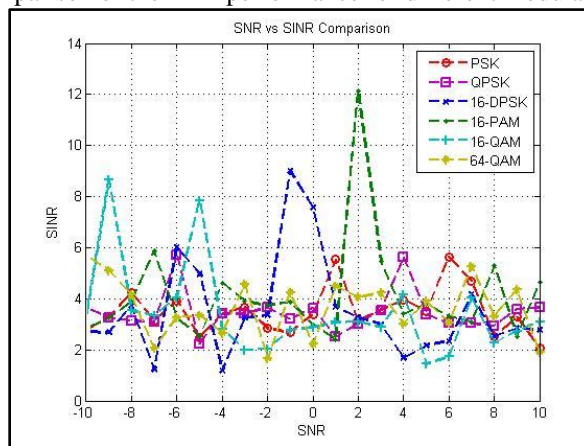


Figure 9: Comparison of the SINR performance for different modulation techniques.

From the figure 8 and 9 it can be concluded that the 16-QAM is an optimum solution for lower BER better data rate and SINR.

VII. CONCLUSION

In this paper a detailed analysis of the performance of different modulation technique is performed the main objective of the paper was to get the optimum configuration for HSDPA system which not only provide higher data rate but also work under the noisy environment conditions, we also wants to investigates the reduction in SINR (signal to interference ratio) because of improper functionality of orthogonal spreading codes caused by noise and fading effect of channel. After the analysis of simulation results we can say that the proper selection of orthogonal code set from all available codes can reduce the SINR and hence improve the BER performance during the study it is also found that some

modulation techniques also helps in improving SINR depending upon channel conditions. Considering all these scenarios finally we found that the 16-QAM provides an optimum solution for BER, SINR and Data Rate.

REFERENCES

- [1] Frank Brouwer, Irene de Bruin, Joao Carlos Silva, Nuno Souto, Francisco Cercas, Américo Correia "Usage of Link-Level Performance Indicators for HSDPA Network-Level Simulations in E-UMTS", ISSSTA2004, Sydney, Australia, 30 Aug. - 2 Sep. 2004 IEEE.
- [2] Claudio Cicconetti, Alessandro Erta, Luciano Lenzi, and Enzo Mingozzi "Performance Evaluation of the IEEE 802.16 MAC for QoS Support", IEEE TRANSACTIONS ON MOBILE COMPUTING, VOL. 6, NO. 1, JANUARY 2007.
- [3] Hermann Buddendick, Gerd Wölfle, Stefan Burger, Philipp Wertz "SIMULATOR FOR PERFORMANCE ANALYSIS IN UMTS FDD NETWORKS WITH HSDPA", Personal, Indoor and Mobile Radio Communications, 15th IEEE International Symposium on (Volume:3) 5-8 Sept. 2004.
- [4] Xin Wang, Qingwen Liu and Georgios B. Giannakis "Analyzing and Optimizing Adaptive Modulation Coding Jointly With ARQ for QoS-Guaranteed Traffic", IEEE TRANSACTIONS ON VEHICULAR TECHNOLOGY, VOL. 56, NO.2, MARCH 2007.
- [5] Thushara Weerawardane, Andreas Timm-Giel, Gennaro C. Malafra, Durastante Gianluca, Stephan Hauth, Carmelita Görg "Preventive and Reactive based TNL Congestion Control Impact on the HSDPA Performance", Vehicular Technology Conference, 2008. VTC Spring 2008. IEEE.
- [6] Y.-H. Lee, H.-W. Tseng, W.-C. Lee, J.-Y. Lin, Y.-G. Jan, and H.-W. Tsao "THE MEASUREMENT AND ANALYSIS OF WIMAX BASE STATION SIGNAL COVERAGE", Progress In Electromagnetics Research C, Vol. 25, 223-232, 2012.
- [7] Alan Barbieri, Aleksandar Damnjanovic, Tingfang Ji, Juan Montojo, Yongbin Wei, Durga Malladi, Osok Song, and Gavin Horn "LTE Femtocells: System Design and Performance Analysis", IEEE JOURNAL ON SELECTED AREAS IN COMMUNICATIONS, VOL. 30, NO. 3, APRIL 2012.
- [8] Vasileios M. Kapinas and George K. Karagiannidis "A Universal MIMO Approach for 3GPP Wireless Standards", IEEE Wireless Communications and Networking Conference Paris, France, April 1-4, 2012.
- [9] Sarabjot Singh, Ozgur Oyman, Apostolos Papathanassiou, Debdeep Chatterjee, and Jeffrey G. Andrews "Video Capacity and QoS Enhancements over LTE", Communications (ICC), IEEE International Conference on 10-15 June 2012.

Comparison of Conventional and "Satlevel" Collocation Model for Production of Contour Map of Yanbu Industrial City

K. F. Aleem^{1,2} H. Alghamdi¹ and M. M. Khayyat³

¹Department of Geomatics Engineering Technology, Yanbu Industrial College, Yanbu Industrial City, Saudi Arabia

²Surveying and Geoinformatics Programme, Abubakar Tafawa Balewa University, Bauchi Nigeria

³Urban Planning Department, Survey Section, Royal Commission for Jubail and Yanbu

ABSTRACT: Contour map is very useful as its portrays the three dimensional (3D) configuration of the area under study. Data acquisition by conventional method of production of such maps has been very tedious. There is need for simple and quick method of production like the use of "Satlevel" Collocation. This is a new method of geoid determination in which the ellipsoidal height is combined with orthometric height to model the geoid. Geoid determinations using integration of geodetic levelling and Global Navigation Satellite System (GNSS), which enables the geoid to be determined in patches, are taking over from the empirical geoid determination. Geoid so determined can be applied with ellipsoidal height to get orthometric height which height users always prefer. This can then be used for production of contour map. In this work, Conventional method was use to acquire data for orthometric height. Also, "Satlevel" Collocation model was used to generate orthometric heights in Yanbu Industrial city. The two data were used to produce the contour map of the study area using AutoCAD Civil 3D software. "Satlevel" Collocation model enables production of contour map without going through all the processes of data acquisition by levelling. The two results were compared and show that there is no significant difference between the new map and the other from the acquired data. This method can be extended to other parts of Saudi Arabia.

Keywords: Collocation, Contour, Geoid, Map, Model, "Satlevel"

تعد الخرائط الكنتورية الثلاثية الأبعاد من أهم أنواع الخرائط الواجب توفرها لدراسة أي منطقة على سطح الأرض. والحصول على هذه الخرائط يتطلب العديد من مراحل العمل وجمع البيانات وتطبيق نظريات مختلفة، الأمر الذي يدعو لإستكشاف نظريات مبسطة جديدة تمكن المختصين من التعامل معها بسهولة. "Satlevel" هي أحد النظريات التي يمكن تطبيقها للحصول على الجسم الأرضي أو الجيوييد "Geoid" وذلك بقياس منسوب الألبسويد "Ellipsoid" باستخدام أجهزة نظام تحديد المواقع العالمية GPS والمنسوب الأورثومتري "Orthometric" باستخدام أجهزة الميزان الدقيقة لنقاط محددة داخل منطقة ما، وتكوين علاقة بينهما ومن ثم الحصول على نموذج دقيق لشكل الجيوييد. الحصول على نموذج للجويييد باستخدام التكامل بين المنسوب الأورثومتري ومنسوب الألبسويد يساعد مستخدم أجهزة نظام تحديد المواقع العالمية من الحصول على المنسوب الأورثومتري لأي نقطة حيث أنه الارتفاع المفضل للمهندسين والعاملين في مجال الخرائط والتصاميم.

وفي هذا البحث تم استخدام نظرية "Satlevel" للحصول على المناسيب الأورثومتريّة باستخدام جهاز تحديد المواقع العالمية لعدد كبير ومنظم من النقاط داخل مدينة ينبع الصناعية وتكوين خرائط كنتورية للمنطقة باستخدام برنامج AutoCAD Civil 3D، وقد اتضح أن لهذه العملية دور كبير في تسهيل الحصول على المناسيب الأورثومتريّة باستخدام جهاز تحديد المواقع العالمية بدقة عالية دون الحاجة إلى عمليات قياسات للمناسيب باستخدام أجهزة الميزان، وقد تم اختبار هذه النتائج مع القياسات التي تم الحصول عليها باستخدام أجهزة الميزان، ووجد أن هذه النتائج دقيقة لدرجة تسمح لمستخدمي أجهزة نظام تحديد المواقع العالمية في عمليات الرفع الطبوغرافي وعمليات التوقيع بل وحتى عند إنشاء نقاط التحكم الرئيسية، كما يمكن تطبيق هذه الدراسة لتشمل جميع المناطق في المملكة العربية السعودية.

I. INTRODUCTION

1.1 Contour Map:

Maps are graphic representations of places that use point, line and area symbols, as well as colour, to show how selected human and physical features are located, arranged, distributed, and related to one another on the surface of the Earth. The complex nature of our environment and the unlimited demand for the uses of maps have made it difficult to have a single map that will satisfy all purposes. Therefore, different types of maps exist. Prominent among them is contour map. A contour map is made up of contour lines and depicts the shape of any portion of the earth surface. A contour line is an imaginary line drawn on the map to connect points with the same elevation or height on, above or below the earth surface to form a continuous line shown in brown colour on the map. Historically, Different types of maps were produced for the Kingdom by the foreign agencies, educational institutions and governments. The maps includes but not limited to the following:

Historical city maps of Mecca, Al-Madinah and Riyadh from Western Arabia and the Red Sea were produced by the Naval Intelligence Division of the Great Britain in 1946; while those of Dharan, Jeddah and Riyadh were produced by the United States of America (U.S) Department of State 1983 and 1986. Furthermore, the shaded relief map of Saudi Arabia was produced in 1974, reviewed in 1991 and 2003 by the United States Central Intelligence Agency (CIA). Thematic map from CIA Atlas of the Middle East was produced in 1993. Topographical maps which include contour were produced as part of Operation Navigational chart series by U.S. Defence Mapping Agency Aerospace Centre. In the recent time, U.S. National Imagery and Mapping Agency have produced the topographical maps of Saudi Arabia in a scale of 1:250,000 [PCL, 2012].

Presently, the Ministry of Municipal and Rural Affairs (MOMRA) is currently handling mapping and mapping related activities in the Kingdom.[Baris, 2012] Apart from production of maps in different scales, different maps are produced depending on the need and purposes by other agencies such as the General Commission for Survey (GCS). King Abdulaziz City for Science and Technology (KACST), Royal Commission for Jubail and Yanbu, Saudi Geological Survey, Companies

like the Saudi Aramco, Schlumpberger Consulting Engineers Inc., Educational Institutions such as King Saud University, King Abdulaziz University, Yanbu Industrial Colleges and others with Geomatics and GIS related disciplines.

In Yanbu Industrial City, the Urban Planning Department of the Royal Commission for Jubail and Yanbu, Royal Commission at Yanbu is currently handling all issues of Survey and Mapping under the Survey section that comprises of CAD and GIS sections. The Department produces different types of maps, which include topographical map that contained the contours either as a direct labour or contract to reputable mapping companies.

The contour maps, like most complex ones, are designed using index contours. Contour lines are shown in brown colour with the value of height written on it. The height is typical measured with reference to a known Datum. The datum usually adopted is the geoid [Aleem et al, 2011 and Williams, 2012].

The geoid is the surface which coincides with that surface to which the oceans would conform over the entire earth, if free to adjust to the combined effect of the earth's mass attraction (gravitation) and the centrifugal force of the Earth's rotation. Specifically, it is an equipotential surface, meaning that it is a surface on which the gravitational potential energy has the same value everywhere with respect to gravity. The geoid surface is irregular, but considerably smoother than earth's physical surface. Sea level, if undisturbed by tides, currents and weather, would assume a surface equal to the geoid when the observation is carried out for a numbers of years, usually 18.61years. [Aleem, 1996, Olaleye et al 2010; Aleem et al 2011, Aleem, 2013]

Determination of the geoid has been one of major challenges of geodesists. Gravity data have been used in the past with stokes integration and other approaches. These methods are time consuming, expensive and laborious. GNSS provide WGS84 ellipsoidal heights and when compared with orthometric height, from geodetic levelling, allows for the computation of the geoid, or the geoid-ellipsoid separation in the region of the survey [Aleem, 1996, Olaleye et al 2010; Aleem et al 2011, Aleem, 2013]. These height differences were used to derive the geoidal models called "satlevel" collocation model [Aleem, 2013]

The geoid model will give geoidal undulation at every point of observation. This can be substituted with the ellipsoidal height from GNSS observation to get the orthometric height has given in Equation 1.1 [Aleem, 1996, Olaleye et al 2010; Olaleye et al 2011 Aleem, 2013]:

$$H = h - N \quad (1)$$

Where:

H = Orthometric height

h = Ellipsoidal height

N = The Geoid-Ellipsoid separation Geoidal undulation

From the above Equation 1, orthometric height can be computed, which can be plotted on the map as spot heights. The spot heights can be interpolated to produce the contours.

1.2 Interpolation of Contour:

Traditionally, Interpolations of contours are often done by rough estimate. The procedure is to first plot all the available spot heights on the map and estimate the point for the contour. However, a more accurate but time consuming method used to be adopted is to use the formula [Aleem, 2011]:

$$PC = \frac{D}{Z} i \quad (2)$$

Where:

PC is distance to the point of contour

D is the distance between two spot heights

Z is the difference between the two spot heights

i is the difference between the contour and one of the Spot heights.

Distance PC will then be scaled and marked on the map, which are later connected to form the contour. The use of information Technology in surveying and geoinformatics has made software usage to be part of geomatics. Contour maps are nowadays prepared easily with software.

1.4 Contour Map Software:

There are different types of software in the market for production of contour, digital terrain and three dimensional surface model of any part of the world. This study used AutoCAD Civil 3D software.

1.4.1 AutoCAD Civil 3D.

A surface in Civil 3D is built on the basis of mathematical principles of planar geometry. Each face of a surface is based on three points within a circum-circle (a circle that passes through each of the vertices of a polygon) forming a triangle and defining a plane. Each of these triangular planes shares an edge with another, and a continuous surface is made. This methodology is typically referred to as a Triangulated Irregular Network (TIN). On the basis of Delaunay triangulation, this means that for any given (x,y) point, there can be only one unique z value within the surface [Golden Software, 2012]

1.4.2 3DField

3DField is a contouring surface plotting and 3D data program that runs under Microsoft Windows NT/XP/Vista/7. 3DField converts the data into contour maps and surface plots. It creates a 3D map or a contour chart from the scattered

points, numerical arrays or other data set. All aspects of 2D or 3D maps can be customized to produce the exact presentation desired [Galouchko, 2012].

1.4.3 Other Contour Map Software

Other Contour Map Software includes: Garmin Basemap, Mapviewer, Contour storyteller, Function Grapher, Auto plotter, Visual data, Filter test, AutoDEM Li Contour and several other software are available for production of contour map. Any of these Software can also be used for the production of Contour map of the study area.

1.5 Scope and Limitations of the Study:- The research covers the data acquisition, processing and presentation and comparison of the final product all were carried out in Yanbu Industrial City while the following are the limitations of this research:

1. The work is only carried out in Yanbu Industrial City.
2. Automatic level was used to obtain orthometric height as against the use of digital or geodetic level.

1.6 The study Area

The study was carried out in Yanbu Industrial City (popularly known as ‘Yanbu Al-Sina’iya’ in Arabic which literarily means Industrial Yanbu) in Madina Province of Saudi Arabia. The city was established around 1975, located on the Coast of Red Sea about 350km North of Jeddah. With Latitude $23^{\circ}59'57.840''N$ (23.9994) and longitude $38^{\circ}13'39.000''E$ (38.2275)



Figure 1: Map of Saudi Arabia and Location of Yanbu Industrial city

Yanbu Industrial City has a section called the Royal Commission (RC). Its residents are mostly expatriates mostly from Europe, America, and other Western Countries. RC Yanbu Existing Area is about 185 km² and the expansion Area is about 420 km². The industrial developed land is estimated to be 3240 Hectares [RCJY, 2012]. The presence of industries such as the oil refineries, plastics facility and several other petrochemical plants in the existing and expansion of Yanbu Industrial City will require detailed map and updating of the existing map of which contours have a prominent role to play. Contour maps will also enhance monitoring of the existing structures. Therefore, a quick and fast method such the use of "Satlevel" collocation model will minimise the rigour of data collection of the conventional method.

II. AIMS AND OBJECTIVES

The aim of this work is to produce contour map of the study area from data generated using conventional levelling and "Satlevel" Collocation Model for comparison.

The objectives are:

1. To acquire data for ellipsoidal and orthometric heights of the study area.
2. To compute geoidal coefficients of the "Satlevel" Collocation Model in the study area using Least squares adjustment.
3. To generate data for production of contour map.
4. To plot the contour map of the study area using AutoCAD Civil 3D software for the two methods
5. To compare the contour maps from the two methods.

III. METHODOLOGY

3.1 Materials and Data

The equipment needed for the exercise are:

GNSS receiver and its accessories to acquire data for ellipsoidal height

Digital Level and its accessories to acquire data for orthometric height

Computer and its accessories for computation and analysis.

AutoCAD Civil 3D software for plotting the contour

Any software or program that can implement least square adjustment.

In this exercise Microsoft Office excels was used for all computations, “Orthometric Height on Fly” developed by Aleem [2013] was used to validate the results.

3.2 “Satlevel” Collocation Model:

Detailed explanation of the derivation and assumption of “Satlevel” Collocation model can be seen in (Aleem, 2013). The model is of the form:

$$N_i = N_L + A_1 (\cos^3 \phi_i \cos \lambda_i + \sin^2 \phi_i \cos \phi_i \cos \lambda_i + \cos^3 \lambda_i \cos \phi_i + \sin^2 \lambda_i \cos \phi_i \cos \lambda) + \\ A_2 (\cos^3 \phi_i \sin \lambda_i + \sin^2 \phi_i \cos \phi_i \sin \lambda_i + \cos^2 \lambda_i \cos \phi_i \sin \lambda_i + \sin^3 \lambda_i \cos \phi_i) + \\ A_3 (\cos^2 \phi_i \sin \phi_i + \sin^3 \phi_i + \cos^2 \lambda_i \sin \phi_i + \sin^2 \lambda_i \sin \phi_i) + r_i \\ \text{[Aleem, 2013]}$$

Where:

N_L is the long wavelength part of the geoid undulation in the area.

A_1 , A_2 and A_3 are the geoidal coefficients which are unknown coefficients to be determined.

ϕ and λ are the WGS '84 geodetic coordinates (Latitudes and Longitudes)

r_i is residue at an observation point.

The “satlevel” collocation model geoidal coefficients of the area were computed using least squares adjustment observation equation method.

3.3 Data Acquisition: Levelling operation was carried out to obtain data for orthometric height. The study area is along the coast, therefore orthometric correction was neglected.

GNSS observation was carried out to acquire data for geodetic coordinates which includes the geodetic latitude, geodetic longitude and ellipsoidal height. Other relevant data such constant for the referenced ellipsoid were collected from various literature and INTERNET websites for data analysis and processing.

3.4 Data Processing:

Levelling reduction was done; the reduced levels were the orthometric height of each of the points. GNSS observation was processed to get the three dimensional coordinates. These are the geodetic latitude (ϕ), geodetic longitude (λ) and ellipsoidal height (h), which were used in “Satevel” collocation model.

The “Satlevel” collocation model geoidal coefficients were computed and used to obtain the geoidal undulation of each point in the area, which were connected to get the geoidal surface.

The geoidal undulations and Ellipsoidal heights obtained from the result of GPS observations were used in Equation 1 to get the orthometric height of each of the points in the study area.

The orthometric heights generated from “Satlevel” collocation and the geodetic coordinates of the area were plotted into contour map using AutoCAD Civil 3D software (Figure 5).

The orthometric heights acquired using geodetic levelling method and the geodetic coordinates of the area were also plotted into contour map using AutoCAD Civil 3D software (Figure 6).

The following procedure was used in producing contour maps in Auto CAD Civil 3D 2013:

- The data was imported as text file as CSV (Comma delimited) to create the points of the surface.
- The surface was created by a Triangulated Irregular Network (TIN) method with 1m interval.
- The major contours lines were labelled and brown coloured was applied for the contour to follow the convention.

IV. RESULTS AND DISCUSSIONS

4.1 Results

The some of the data used for this research acquired in Yanbu Industrial City were randomly selected and used to plot chart (Figure 2):

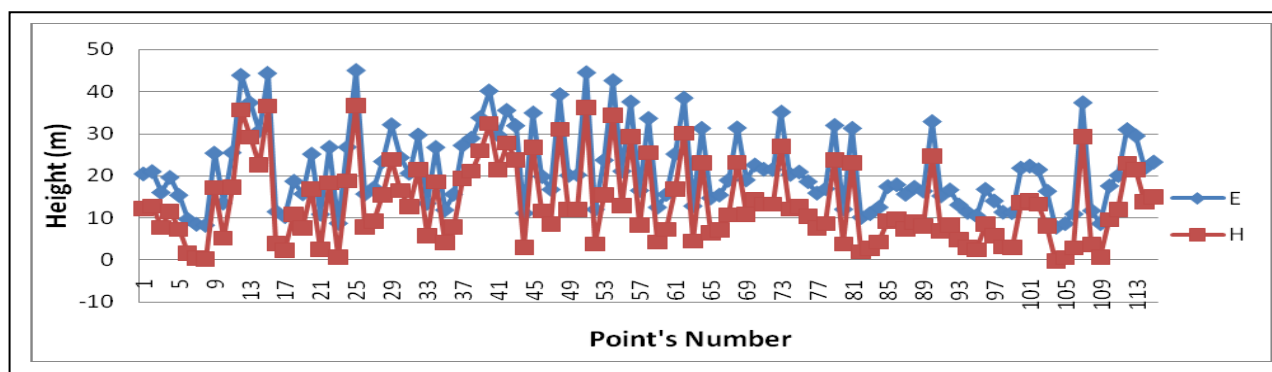


Figure 2: Orthometric and Ellipsoidal Heights of part of Yanbu Industrial City

The values of the geoidal coefficients computed using least square adjustment observation equation as:

$N_L=7.85995128$; $A_1=0.36447485$; $A_2=-0.5309024$; $A_3=0.15167311$

The results of the “Satlevel” collocation geoidal undulations were plotted into chart (Figure 3):

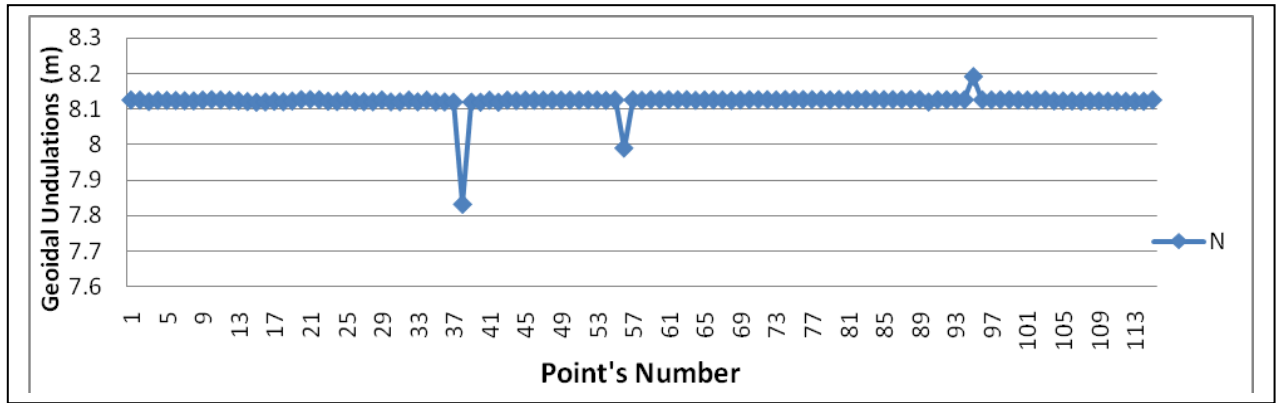


Figure 3: Geoidal Surface of parts of Yanbu Industrial City

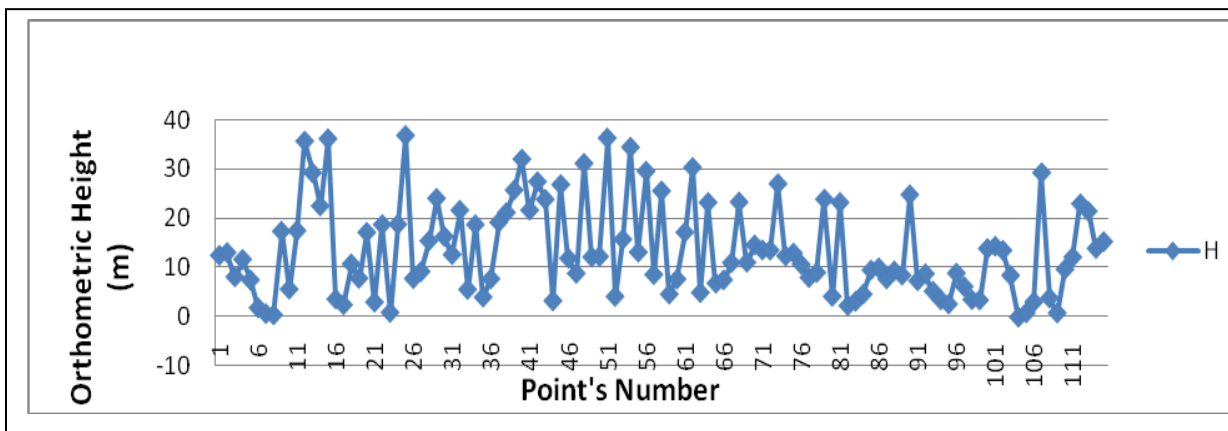


Figure 4: Orthometric Heights of parts of Yanbu Industrial City

The result of the “satlevel” collocation orthometric height were plotted into chart (Figure 5):

The results of the Orthometric from conventional levelling were plotted into chart (Figure 6)

The “Satlevel” collocation contour map (Figure 6):

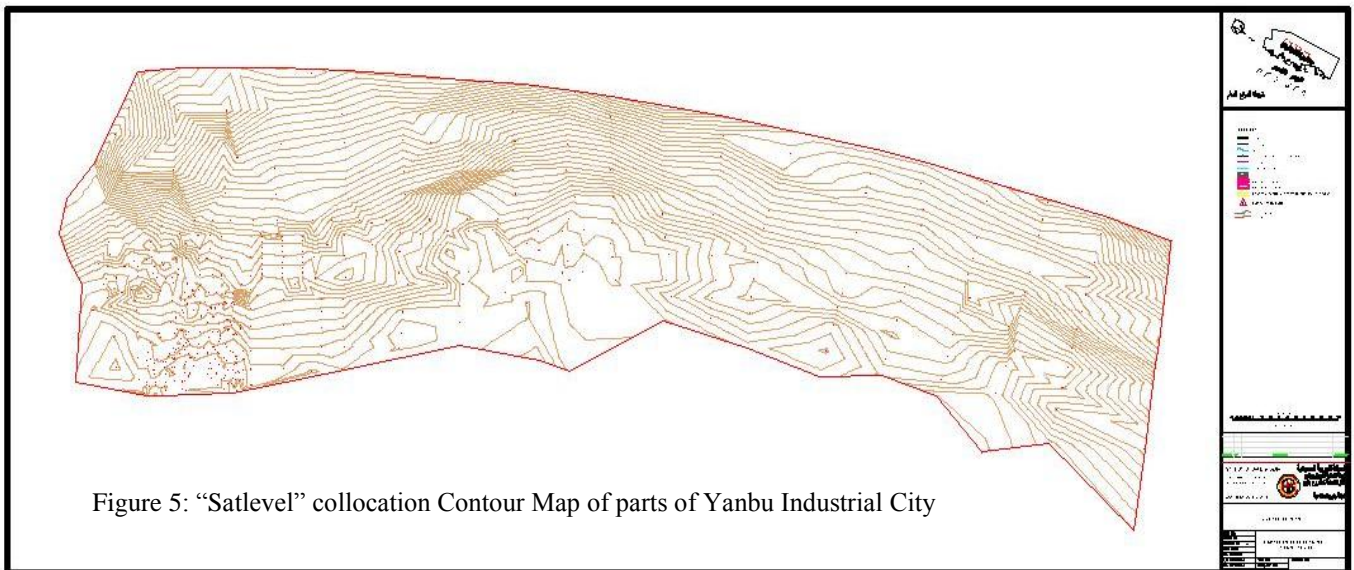


Figure 5: “Satlevel” collocation Contour Map of parts of Yanbu Industrial City

The contour map from levelling method (Figure 5)

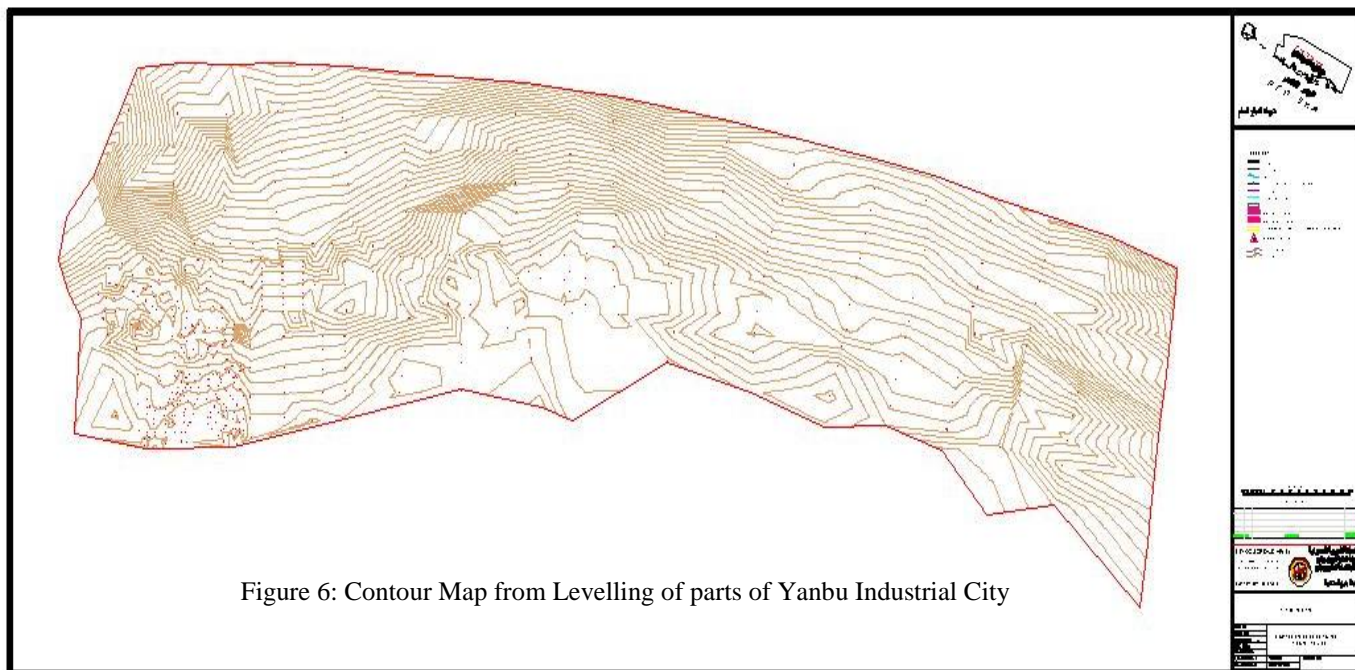


Figure 6: Contour Map from Levelling of parts of Yanbu Industrial City

4.2 Discussion

In this chart shown in Figure 2, ellipsoidal and orthometric height follows the same pattern is an indication that the two are true representation of the same terrain.

Figure 4 shows the geoidal surface of Yanbu Industrial City. In this chart, the geoidal Undulations of 3 of the points were outrageous, which is an indication that there was presence of outliers in the observations. These observations should have been removed because they are more than 3 standard deviations [Heliani et al, 2004]. This might have created impact on the map shown in Figure 6. When the outliers were removed, the chart produced a continuous and smooth surface. This is an indication that “Satlevel” Collocation like any other analyses required removal of outliers from the observation.

V. CONCLUSION AND RECOMMENDATION

5.1 Conclusion

In this study, levelled heights were established along with GPS observation in some parts of Yanbu Industrial city to model the geoid in the study area. We have coordinated some of the points collocated with both GNSS and levelling in the area. 'Satlevel' Collocation Model was used to get the geoidal coefficients, which were used to get the geoidal undulation for each of the points. Ellipsoidal heights from GNSS observation were used to get the orthometric heights, and used to plot the contour with AutoCAD Civil 3D software. Orthometric height information were also used to plot another map using the same AutoCAD Civil 3D software. The two maps were compared with the each other and shows that there is no significant difference between the “satlevel collocation and conventional methods of producing contour map.

5.2 Recommendations:

The area of coverage needs to be extended and more data should be acquired to improve the results. Contracts for the production of maps should be awarded to the Institutions of Higher learning in the Kingdom. This will enable the participating staff to acquire more experience, so as to improve the qualities of graduates for future challenges. A local geoid model for Saudi Arabia is hereby recommended to commence. The method can be applied in any other place.

REFERENCES

- [1] Aleem, K. F, GPS and Remote Sensing of Environment, The Graduate Surveyors, Journal of NISS University of Nigeria, Enugu Campus. 12(1) 24 – 29, 1996
- [2] Aleem, K. F., Drafting and Mapping (GET 102). Lecture Notes. Department of Geomatics Engineering Technologies, Yanbu Industrial College, Kingdom of Saudi Arabia. UNPUBLISHED. 2011.
- [3] Aleem, K. F. “Adaptation of a Global Orthometric to a Local Height Datum Using “Satlevel” Collocation Model”. A Ph.D Thesis. Department of Surveying and Geoinformatics, University of Lagos Nigeria,. UNPUBLISHED 2013.
- [4] Aleem, K. F. (2013) Satlevel Collocation Model for Production of Contour Map of Yanbu Industrial City, Saudi Arabia. Journal of Emerging Trends in Engineering and Applied Science. (JETEAS) 4(2): 156-161 April 2013. <http://jeteas.scholarlinkresearch.org/articles/Satlevel%20Collocation%20Model%20for%20Production.pdf>
- [5] Aleem, K. F., J. B. Olaleye, O. T. Badejo and J. O. Olusina, A Combination of Ellipsoidal Height from Satellite Method and Orthometric Height for Geoid Modelling, publication of the International Global Navigation Satellites Society IGNS website, . <http://ignss.org/Conferences/PastPapers/2011ConferencePastPapers/2011PeerReviewedPapers/tabid/108/Default.aspx> 2011

- [6] Baris Uz, MOMRA Mapping Reference Framework. Geo tech Briefly. GeoTech Quarterly Volume 1 Issue 1 <http://www.ags-group.com/gq/v1i1/?f=Z2VvdGVjaGJyaWVmbHhLnBocA==> 2012
- [7] Boehlke J., What Do Topographic Maps Show?, Online Article accessed on the 12th November, 2012
http://www.ehow.com/about_4614538_what-do-topographic-maps-show.html, 2012
- [8] Galouchko V., Contour Map Software 3DField, Accessed on 31st of December 2012. <http://field.hypermart.net/2012>.
- [10] Golden Software, Inc., “AutoCAD Civil 3D 11: Powerful Contouring, Gridding, and 3D Surface Mapping Software for Scientists and Engineers”. Online Article 12 November 2012 http://www.goldensoftware.com/products/AutoCAD_Civil_3D/AutoCAD_Civil_3D.shtml,2012.
- [11] Heliani, L. S., Y. Fukuda, and S. Takemoto. Simulation of the Indonesian land gravity data using a digital terrain model data. Earth Planets Space, 56(1): 15–24, 2004.
- [12] Olaleye, J. B., K. F. Aleem, J. O. Olusina and O. E. Abiodun, Establishment of an empirical geoid model for a small geographic area: A case study of Port Harcourt, Nigeria, Surveying and Land Information Science. 70(1): 39-48(10) <http://www.ingentaconnect.com/content/nsps/salis/2010/00000070/00000001/art00006>, 2010.
- [13] Perry-Castañeda Library (PCL), Map Collection. University of Texas. Available online. Accessed on 22nd of December, 2012 . http://www.lib.utexas.edu/maps/saudi_arabia.html
- [14] Royal Commission for Jubail and Yanbu (RCJY), Royal Commission at Yanbu, Annual Report of the Strategic Planning & Investment Development Division Economic Planning Department. Accessed on 20th January, 2012. <https://eservices.rcyanbu.gov.sa/Doc/YanbuIndustrialCityEconomicReview.pdf>, 2012.
- [15] Williams N. A.. What Does a Contour Map Show?, | eHow.com Online Article accessed on the 12th October, 2012 ,

Performance Analysis of Z-Source Cascaded H-Bridge Multilevel Inverter Based on Multi Carrier PWM Techniques

F.X.Edwin Deepak¹

1. Assistant Professor, EEE Department, PSNA CET, Dindigul, Tamil Nadu.

ABSTRACT : Multilevel inverter is one of the attractive topology for dc to ac conversion. Multilevel inverter synthesizes desired voltage wave shape from several levels of DC voltages. But the main drawback of MLI is its output voltage amplitude is limited to DC sources voltage summation. To overcome this limitation, a five-level Z-source cascaded H-bridge multilevel inverter has been proposed in this paper. In the proposed topology output voltage amplitude can be boosted with Z network shoot-through state control. It employs Z network between the DC source and inverter circuitry to achieve boost operation. The output voltage of proposed inverter can be controlled using modulation index and shoot through state. Performance parameters of Z -Source MLI have been analyzed for unipolar modulation and space vector modulation. Simulation model of Z-source cascaded multilevel inverter with unipolar ISCPWM, unipolar CDPWM and SVM Modulation technique has been built in MATLAB/SIMULINK and its performance has been analyzed.

Keywords: Multi Level Inverter, Total Harmonic Distortion, Pulse Width Modulation, Shoot-Through, Buck-Boost.

I. INTRODUCTION

Multilevel inverters are widely used in high power applications such as large induction motor drives, UPS systems and Flexible AC Transmission Systems (FACTS). Multilevel inverter obtains the desired output voltage from several levels of input DC voltage sources. By increasing the number of DC voltage sources, the inverter output voltage level increases. The multilevel inverters have advantages such as lower semiconductor voltage stress, better harmonic performance, low Electro Magnetic Interference (EMI) and lower switching losses. Despite these advantages, multilevel inverters output voltage amplitude is limited to the input DC sources voltage summation. It requires an intermediate DC to DC converter is for the buck or boost operation of MLI output voltage. Also occurring of short circuit can destroy multilevel inverters. In this paper multilevel inverter based Z-source is proposed which can solve above mentioned problems. The Z-source inverter utilizes Z impedance network between the DC source and the inverter circuit to achieve buck-boost operation. It utilizes shoot-through state control to boost the input dc voltage of inverter switches when both switches in the same phase leg are on. The Z-Source inverters have advantages such as lower costs, reliable, lower complexity and higher efficiency. The ac output voltage can be of fixed or variable frequency. This can be achieved either by controlled turn-on and turn-off devices (e.g., BJTs, MOSFETs, IGBTs, and GTOs) or by forced commutated thyristors, depending on applications. The output voltage waveforms of an ideal inverter must be sinusoidal. The voltage waveforms of practical inverters are non-sinusoidal and contain certain harmonics. The output frequency of an inverter is determined by the rate at which the semiconductor devices are switched on and off by the control circuit and can provide ac output of adjustable frequency. The dc input to the inverter may be a battery, fuel cell, solar cells or other dc sources. But in case industrial applications, it is fed by a rectifier.

In this paper, a single phase cascaded H-bridge five levels Z-Source inverter is proposed for renewable energy systems and it employs Z network between the DC source and inverter circuitry to achieve boost operation. The output voltage inverter can be controlled using modulation index and shoot through state control. Cascaded Z-Source Multilevel inverter is analyzed with unipolar inverse sine carrier, unipolar carrier disposition PWM, SVM techniques. Performance parameters have been analyzed for cascaded Z-Source MLI. The performances of the three techniques are compared for single phase 5-level Z-Source cascaded multilevel inverter. Simulation of the circuit configurations have been performed in

II. MATLAB/SIMULINK.

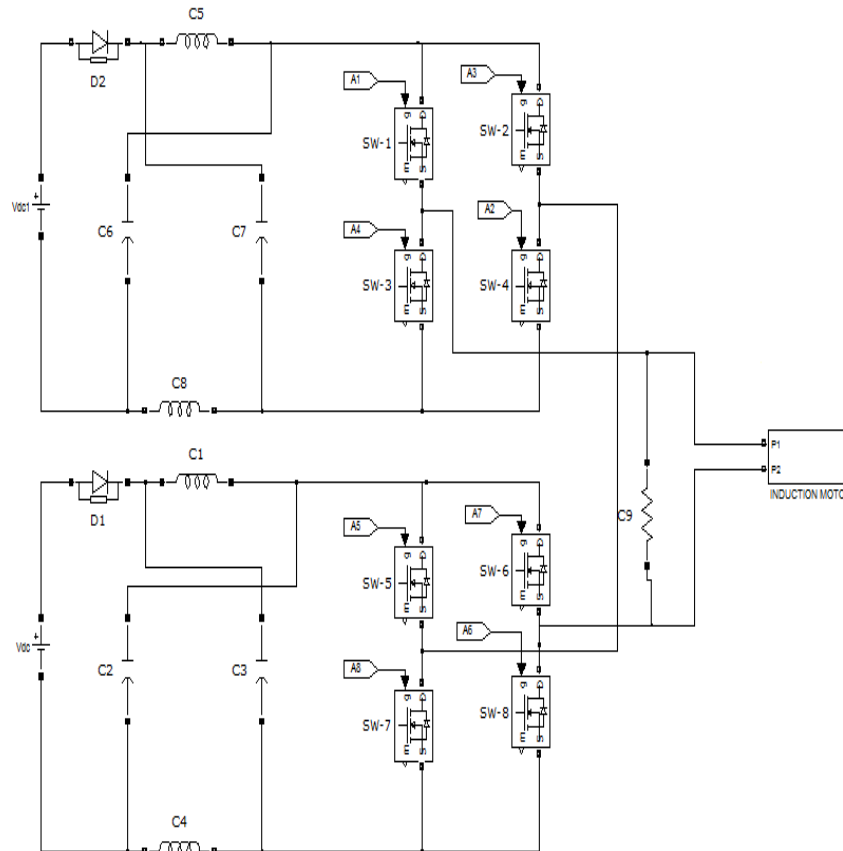


Fig.1 Single phase 5-level z-source cascaded multilevel inverter

III. Z-SOURCE CONVERTER

To overcome the problems of the traditional Voltage and current source converters, this paper presents an impedance source (or impedance-fed) power converter (abbreviated as Z-source converter) and its control method for implementing dc-to-ac power conversion [4]. It employs a unique impedance network (or circuit) to couple the inverter main circuit to the power source for providing unique features that cannot be observed in the traditional Voltage and current source converters where a capacitor and inductor are used, respectively. The Z-source converter overcomes the above-mentioned limitations of the traditional Voltage and current source converter and provides a novel power conversion concept [2]. In Fig. 2, a two-port network that consists of a split-inductor $L1$ and $L2$ and capacitors $C1$ and $C2$ connected in X shape is employed to provide an impedance source (Z-source) coupling the converter (or inverter) to the dc source. The dc source/or load can be either a voltage or a current source/or load. Therefore, the dc source can be a battery, diode rectifier, thyristor converter, fuel cell, an inductor, a capacitor, or a combination of those [3]. Switches used in the converter can be a combination of switching devices and diodes such as the antiparallel combination, the series combination etc.

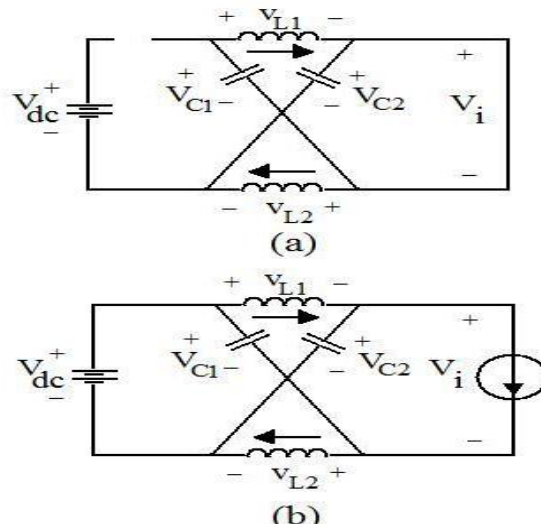


Fig.2 (a) Full shoot-through and (b) non-shoot-through equivalent circuits

The Z-source concept can be applied to all dc-to-ac, ac-to-dc, ac-to-ac, and dc-to-dc power conversion. To describe the operating principle and control, this paper focuses on an application example of the Z-source converter: a Z-source inverter for dc-ac power conversion needed for fuel-cell applications. The diode in series with the dc source is for preventing reverse current flow.

IV. CASCADED MULTILEVEL INVERTER TOPOLOGY

Cascaded multilevel inverters are made from series connected full bridge inverters, each with their own isolated dc bus. This multilevel inverter can generate almost sinusoidal waveform voltage from several separate dc sources. This type of converter does not need any transformer or clamping diodes or flying capacitors. Each level generates three different voltage outputs $+V_{dc}$, 0 and $-V_{dc}$ by connecting the dc sources to the ac output side by different combinations of the four switches. The output voltage of multilevel inverter is the sum of all the individual inverter outputs. Each of the H-bridge's active devices switches only at the fundamental frequency, and generates a quasi-square waveform by phase-shifting its positive and negative phase legs switching timings. Further, each switching device always conducts for 180° (or half cycle) regardless of the pulse width of the quasi-square wave. This switching method results in equalizing the current stress in each active device. This topology of inverter is suitable for high voltage and high power inversion because of its ability of synthesize waveforms with better harmonic spectrum and low switching frequency. Considering the simplicity of the circuit and advantages, Cascaded H-bridge topology is chosen for the presented work. A multilevel inverter has four main advantages firstly; the voltage stress on each switch is decreased due to series connection of the switches therefore, the rated voltage and consequently the total power of the inverter could be safely increased. Second, the rate of change of voltage (dV/dt) is decreased due to the lower voltage swing of each switching cycle. Third, harmonic distortion is reduced. Fourth, lower acoustic noise and electromagnetic interference (EMI) is obtained.

VOLTAGE LEVEL OUTPUT	VOLTAGE	ON SWITCHES
Level 2 (non shoot-through)	$2V_{in}$	S3,S4,S5,S6
Level 1 (non shoot-through)	V_{in}	S1,S3,S5,S6
Level 1 (shoot-through)	V_{in}	S1,S2,S3,S4,S5,S6
Level 1 (non shoot-through)	V_{in}	S3,S4,S5,S7
Level 1 (shoot-through)	V_{in}	S3,S4,S5,S6,S7,S8
Level 0 (zero state)	0V	S1,S3,S5,S7
Level 0 (shoot-through)	0V	S1,S2,S3,S4,S5,S7
Level 0 (shoot-through)	0V	S1,S3,S5,S6,S7,S8
Level -1 (non shoot-through)	$-V_{in}$	S1,S3,S7,S8
Level -1 (shoot-through)	$-V_{in}$	S1,S2,S3,S4,S7,S8
Level -1 (non shoot-through)	$-V_{in}$	S1,S2,S7,S8
Level -1 (shoot-through)	$-V_{in}$	S1,S2,S5,S6,S7,S8
Level -2 (non shoot-through)	$-2V_{in}$	S1,S2,S7,S8

Table 1 Conduction Table

V. MODELLING OF CASCADED H-BRIDGE INVERTER

For each full bridge inverter the output voltage is given by

$$V_{oi} = V_{di}(S1i - S2i) \quad (1)$$

and the input dc current is

$$I_{dci} = I_a(S1i - S2i) \quad (2)$$

where,

- (a) $i = 1, 2, \dots$ Number of full bridge inverters employed.
- (b) I_a is the output current of the cascaded inverter.
- (c) $S1i$ and $S2i$ is the upper switch of each full bridge inverter.

Now the output voltage of each phase of the multilevel cascaded inverter is given by:

$$V_{on} = \sum V_{oi}, \quad i = 1, 2, \dots, n \quad (3)$$

VI. CONTROL SCHEMES

The main aim of the modulation strategy of multilevel inverters is to synthesize the output voltage as close as possible to the sinusoidal waveform. Many modulation techniques have been developed for harmonic reduction and switching loss minimization. Multilevel inverter control techniques are based on fundamental and high switching frequency. Another widely used popular classification for the modulation methods developed to control the multilevel inverters is depend upon open loop and closed loop concepts.

A. UNIPOLAR-MCPWM technique

It is obtained by comparing the rectified sinusoidal reference or with two sine references (sine and 180 degree phase shifted sine), with multi carriers positioned above the zero level. This scheme has the advantage of effectively doubling the switching frequency as far as the output harmonics are concerned, where the lowest harmonics appears as side bands of twice switching frequency. Here only n carriers are required for obtaining $2n+1$ level, unlike in above methods $2n+1$ carriers are required.

1. UNIPOLAR-ISCPWM [inverted sine carrier PWM]:-

The control scheme uses an inverted (high frequency) sine carrier that helps to maximize the output voltage for a given modulation index. Enhanced fundamental component demands greater pulse area. The difference in pulse widths (hence area) resulting from triangle wave and inverted sine wave with the low (output) frequency reference sine wave can be easily understood.

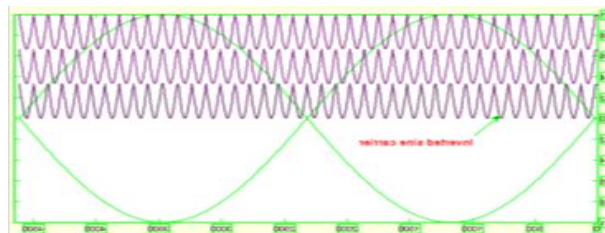


Fig.3 Unipolar-ISCPWM

2. UNIPOLAR-CDPWM: -

In this method four phase shifted carrier triangular signals are compared with the two modulating sinusoidal signals to produce switching PWM pulses. This method employs two straight lines that are greater than or less than the peak value of the reference sinusoidal signal to control the shoot-through duty ratio. Inverter operates in shoot-through whenever the triangular carrier signal is higher than the positive straight line or lower than the negative straight line. The frequency of the modulating signal is taken as 50Hz. The frequency of the triangular signal can be calculated by Frequency modulation index, mf which is given.

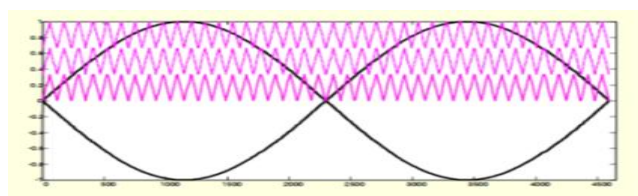


Fig.4 Unipolar CDPWM

For each full bridge inverter the output voltage is given by

$$"mf=" \quad fc/fo \quad (4)$$

where f_c is the frequency of the carrier signal and f_o is the frequency of sinusoidal and modulating signals. Output voltage depends on the boost factor

$$B = \frac{1}{1 - (2(V_{ca} - V_p)) / V_{ca}} = \frac{1}{1 - 2T_{sh} / T} \quad (5)$$

where,

V_{ca} - Peak value of the triangular waveform

V_p - Amplitude of the constant

T_{sh} - Total shoot-through state period

T - Period of switching

3. SPACE VECTOR MODULATION:-

The SVM technique can be easily extended to all multilevel inverters [13]–[19]. Fig. 5 shows space vectors for the traditional two-, three-, and five-level inverters. These vector diagrams are universal regardless of the type of multilevel inverter. In other words, Fig.5(c) is valid for five-level diode-clamped, capacitor-clamped, or cascaded inverter. The adjacent three vectors can synthesize a desired voltage vector by computing the duty cycle ($T_j, T_{j+1},$ and T_{j+2}) for each vector

$$V^* = \frac{(T_j V_j + T_{j+1} V_{j+1} + T_{j+2} V_{j+2})}{T} \quad (6)$$

Space-vector PWM methods generally have the following features: good utilization of dc-link voltage, low current ripple, and relatively easy hardware implementation by a digital signal processor (DSP). These features make it suitable for high-voltage high-power applications. As the number of levels increases, redundant switching states and the complexity of selecting switching states increase dramatically. Some authors have used decomposition of the five level space-vector diagram into two three-level space-vector diagrams with a phase shift to minimize ripples and simplify control [16]. Additionally, a simple space-vector selection method was introduced without duty cycle computation of the adjacent three vectors.

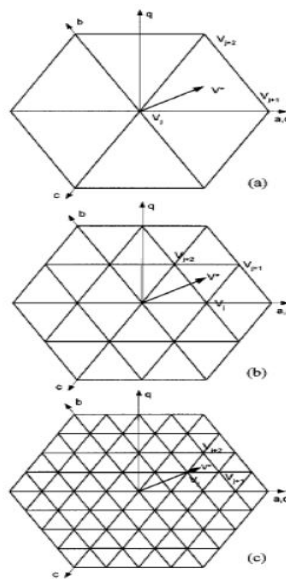


Fig.5. Space-vector diagram: (a) two-level, (b) three-level, and (c) five-level inverter.

VII. SIMULATION AND EXPERIMENTAL RESULTS

Fig.6 shows Matlab Simulink of Z-Source cascaded MLI using Unipolar PWM with Boost factor = 1.25, $m_a = 0.8$, R_{Load} where $R = 100\Omega$, Input voltage $V_{dc} = 100V$, Z impedances, $L = L_2 = L_3 = L_4 = L = 1000mH$ and $C = C_2 = C_3 = C_4 = 10mF$. Simulink circuit is shown with LC filter having. This LC filter can act as an electrical resonator, an electrical analogue of a tuning fork, storing electrical energy oscillating at the circuit's resonant frequency.

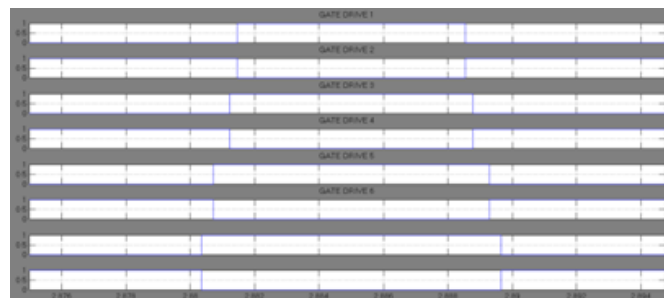


Fig.6 PWM pulse generation for unipolar PWM technique

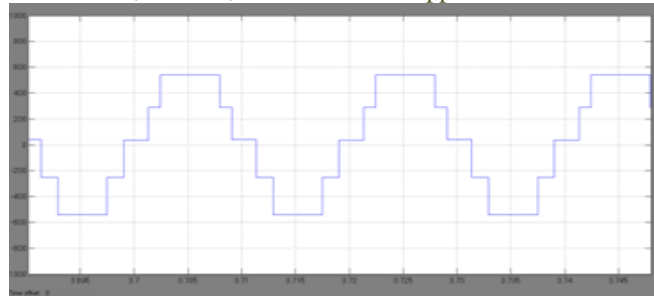


Fig.7 Output voltage of unipolar multicarrier techniques without filter

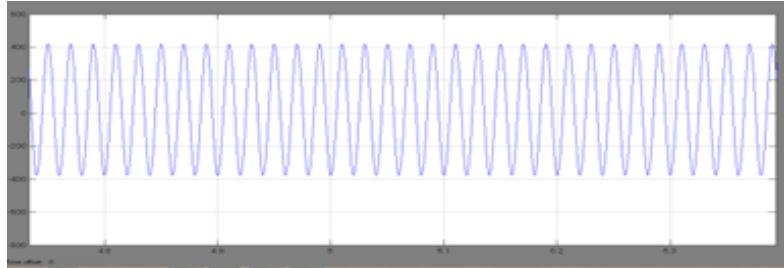


Fig.8 Output voltage with filter

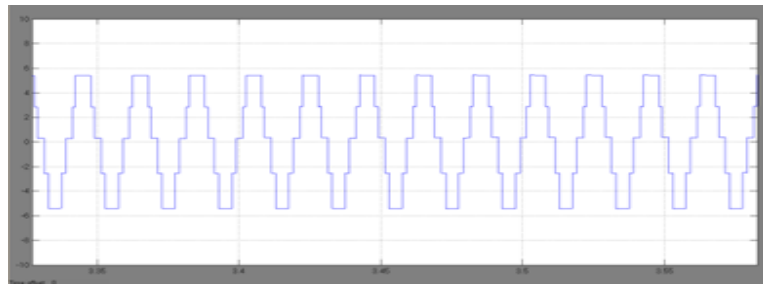


Fig.9 Output current without filter

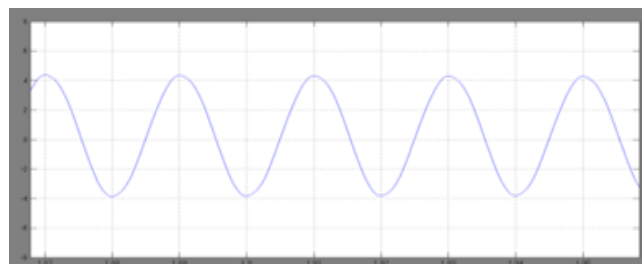


Fig.10 Output current with filter

Fig.7and Fig.8 shows the load voltage waveform without filter and its FFT spectrum. Figs.9 &10 show the load current waveform with filter and without filter. THD of a signal is a measurement of the harmonic distortion present and is defined as the ratio of the sum of the powers of all harmonic components to the power of the fundamental frequency. THD is calculated for various modulation index values and the comparison is shown in Fig 11. From the figure it is shown that THD is low for the chosen m_a of 0.8. Output voltage and other parameters are compared between Z-Source MLI. Compared with the latest sinusoidal PWM technique for cascaded multilevel Z-Source inverter, the proposed unipolar PWM technique does not produce the harmonics of carrier frequencies. The proposed modulation technique reduces the amplitude of significant harmonics and its sidebands for all modulation indexes thus making filtering easier, and with its size being significantly smaller.

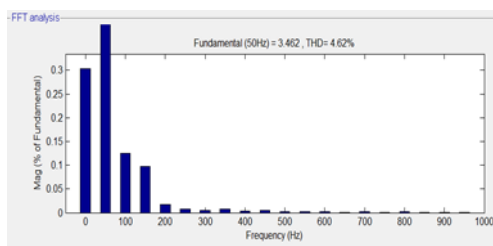


Fig.11 THD value of unipolar ISPWM

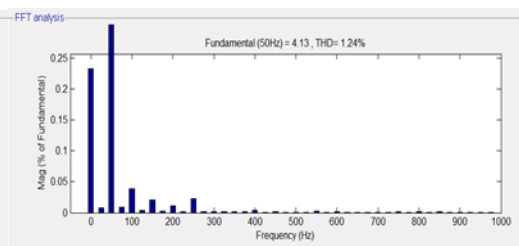


Fig.12 THD value of unipolar CDPWM

MEASURED QUANTITIES	UNIPOLAR ISCPWM	UNIPOLAR CDPWM	SVM
Input voltage	400V	400V	400V
Output voltage	450V	540 V	465V
THD	4.62%	1.24%	15.1%

TABLE 2COMPARISON

VIII. HARDWARE DETAILS

Power Circuit

230V, 50Hz ac supply is step down to 15V ac using a step down transformer. It is then converted to dc using a bridge rectifier. Capacitors placed immediately after the bridge rectifier filters the ripples in the rectified dc output and it linearly discharges during any power supply interruption. Output of the capacitor is fed to the L7805A voltage regulator that regulates the dc voltage value at 12V. This voltage is also fed to L7812A voltage regulator to obtain a 5V regulated dc. Hence two dc power supplies of 12V and 5V are obtained. The 5V dc output is fed to the control circuit and the 12V dc is fed to main circuit.

Control Circuit

As mentioned above, 5V dc is fed to PIC16F877 microcontroller and is programmed with space vector modulation technique to produce the PWM output. Crystal oscillator is provided in this circuit to give necessary clock input to the microcontroller. A reset switch and a potentiometer are also provided in this circuit.

Main Circuit

The main circuit consists of three parts

- Z-source circuit
- Isolation part
- Cascaded H-bridge

The 12V dc from the power circuit is fed to the z-source network and then the output of z-source network is connected to the cascaded H-Bridge inverter via optocoupler MCT2E. The PWM output of the control circuit is fed to the input terminal of the MCT2E optocoupler and the output is fed to the input of cascaded H-bridges which consist of eight IRF540 MOSFETs. The output of cascaded H-bridge is connected to a resistive load.



Fig 13 Hardware Unit

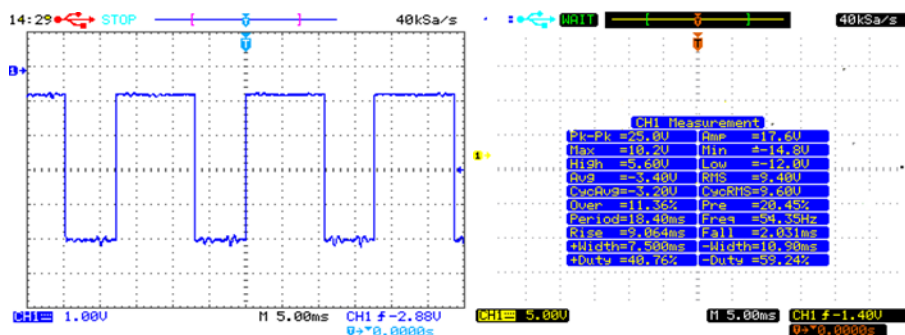


Fig 14 PWM output

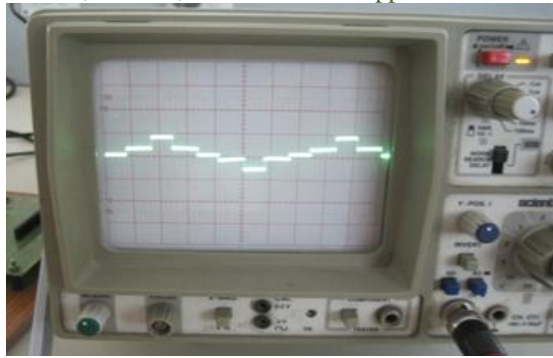


Fig 15 Five level output

IX. CONCLUSION

This paper has investigated a Z-source cascaded multilevel inverter. Z-Source cascaded multilevel inverter gives higher output voltage through its Z network. Unipolar PWM techniques have been employed for Z-MLI. The performance of the proposed Z-MLI has been compared. From the results, it is found that Z-MLI with unipolar PWM provides a higher RMS value of the output voltage, higher voltage gain, reduced voltage stress and avoids the intermediate boost DC-DC converter. Topology and modulation-method is selected based upon the application They are selected depending on their unique features and limitations like power or voltage level, dynamic performance, reliability, costs, and other technical specifications

ACKNOWLEDGEMENT

The author wish to thank the management of PSNA institution for providing the computational facilities to carry out this work.

REFERENCES

- [1] M. Reza Banaei and A.R. Dehghanzadeh, "A Z-Source novel based multilevel inverter for renewable sources fed DVR", IEEE International Conference, POIVer Quality Conference (PQC), pp.1-6, 2011.
- [2] M.R. Mohamad Reza Banaei and A.R. Ali Reza Dehghanzadeh, "DVR based cascaded multilevel Z-source inverter", IEEE International Conference, POIVer and Energy (PECon), pp.51-56, 2010.
- [3] Amitava Das, S. Chowdhury, S.P. Chowdhury and Prof. A. Domijan" Performance analysis of Z-source inverter based ASD System with reduced harmonics", POIVer and Energy Society General Meeting - Conversion and Delivery of Electrical Energy in the 21st Century, Pittsburgh, pp.145-151, 2010.
- [4] Y. Tang, S. Xie, C. Zhang and Z. Xu, "Improved Z-source inverter with reduced Z-source capacitor voltage stress and soft-start capability", IEEE Trans. Power Electron., vol. 24, pp. 409-415, Feb. 2009.
- [5] J. Holtz, "Pulse width modulation - a survey", IEEE Trans. Ind. Electron, vol. 39, pp. 410-420, 2009.
- [6] Miaosen Shen and FL Peng, "Modulation methods and characteristics of the Z-Source inverter with small inductance", Industry Applications Conference, Fortieth IAS Annual Meeting, Vol. 2, pp. 1253 - 1260, 2009.
- [7] P. C. Loh, F. Gao, F. Blaabjerg, and S. W. Lim, "Operational analysis and modulation control of three-level Z-source inverters with enhanced output waveform quality", IEEE Trans, Power Electron, vol. 24, no. pp. 1767-1775, Jul. 2009.
- [8] P. C. Loh, D. M. Vilathgamuwa, Y. S. Lai, G. T. Chua and Y. W. Li, "Pulse width modulation of Z-source inverters", IEEE Trans, Power Electronics, Vol. 19, NO. 3, pp.732-738, 2006.
- [9] P. C. Loh, D. M. Vilathgamuwa, C. I. Gajanayake, L. T. Wong and C. P. Ang, "Z-source current-type inverters: digital modulation and logic implementation", IEEE Trans. Power Electron, vol. 22, pp. 169- 177, 2007.
- [10] P. C. Loh, F. Gao, F. Blaabjerg and S. W. Lim, "Operational analysis and modulation control of three-level Z-source inverters with enhanced output waveform quality", in Proc, EPE'07, pp. 1-10, 2007
- [11] F. Z. Peng, M. Shen, and Z. Qian, "Maximum boost control of the Z source inverter," IEEE Trans, POIVer Electron, vol. 20, no. 4, pp. 833-838, 2006.
- [12] F. Gao, P. C. Loh, D. M. Vilathgamuwa, and F. Blaabjerg, "Performance analysis of random pulse-width modulated z-source inverter with reduced common mode switching," in Proc, IEEE PESC, pp. 1-7, 2006.

Modeling and Structural Analysis of A Pressure Hull under Dynamic Load

B. Mahendra¹, B. Ankanna², K. Tirupathi Reddy³, M. Ravichandra⁴,

*(PG student, School of Mechanical Engineering RGM College of Engg. & Technology, Nandyal-518501, India.)

** (School of Mechanical Engineering, RGM College of Engineering & Technology, Nandyal-518501, India)

*** (School of Mechanical Engineering, RGM College of Engineering & Technology, Nandyal-518501, India)

**** (School of Mechanical Engineering, RGM College of Engineering & Technology, Nandyal-518501, India)

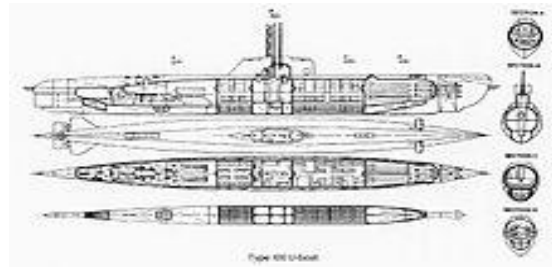
ABSTRACT: Pressure hulls are the main load bearing structures of naval submarines, and autonomous underwater vehicles (AUVs). A pressure hull is a structure that is designed to withstand the compressive forces associated with hydrostatic pressure. In this thesis, the assembly of the pressure hull including Navigation compartment shell, Battery compartment shell which are connected with bolts is designed which is used at present. Around 16 M12 bolts are used to connect the Navigation compartment shell and Battery compartment shell. These shells are to be disassembled very frequently for battery charging and other maintenance purpose. It is observed that the disassembling and assembling process is a very time consuming because it requires unbolting and bolting of all the 16 bolts every time. A new design of pressure hull is proposed where the bolts are removed and the navigation compartment and battery compartment are welded. In the present paper, design calculations are done as per ASME codes to withstand the pressure of 65 Bar. The design constraints considered for the analysis were stresses and deflections. The pressure hull have been modeled considering the elliptical cross section. The modeling of the pressure hull has been carried out by pro-5.0 and analysis soft ware is ansys 14.0 soft ware packages.

Keywords: Pressure hulls, steel, Static analysis, dynamic analysis.

I. INTRODUCTION

A light hull (casing in British usage) of a submarine is the outer non-watertight hull which provides a hydrodynamic ally efficient shape. The pressure hull is the inner hull of a submarine; this holds the difference between outside and inside pressure.

SUBMARINE HULL



Type XXI U-Boat, late WWII, with pressure hull almost fully enclosed inside the light hull Modern submarines are usually cigar-shaped. This design, already visible on very early submarines is called a "teardrop hull", and was patterned after the bodies of whales. It significantly reduces the hydrodynamic drag on the sub when submerged, but decreases the sea-keeping capabilities and increases the drag while surfaced.

TYPES

All small modern submarines and submersibles, as well as the oldest ones, have a single hull. However, for large submarines, the approaches have separated. All Soviet heavy submarines are built with a double hull structure, but American submarines usually are single-hulled. They still have light hull sections in bow and stern, which house main ballast tanks and provide hydro dynamically optimized shape, but the main, usually cylindrical, hull section has only a single plating layer.

LIGHT HULL

The double hull of a submarine is different from a ship's double hull. The external hull, which actually forms the shape of submarine, is called the outer hull, casing or light hull. This term is especially appropriate for Russian submarine construction, where the light hull is usually made of steel that is only 2 to 4 millimeters thick, as it has the same pressure on both sides. The light hull can be used to mount equipment, which if attached directly to the pressure hull could cause unnecessary stress.

PRESSURE HULL

Inside the outer hull there is a strong hull, or pressure hull, which actually withstands the outside pressure and has normal atmospheric pressure inside. The pressure hull is generally constructed of thick high-strength steel with a complex

structure and high strength reserve, and is separated with watertight bulkheads into several compartments. The pressure and light hulls aren't separated, and form a three-dimensional structure with increased strength. The interhull space is used for some of the equipment which doesn't require constant pressure to operate.

The list significantly differs between submarines, and generally includes different water/air tanks. In case of a single-hull submarine, the light hull and the pressure hull are the same except for the bow and stern.

II. SPECIFICATION OF THE PROBLEM

The objective of the present work is to design and analyse, of steel pressure hull including Navigation compartment shell, Battery compartment shell which are connected with bolts is designed. These shells are to be disassembled very frequently for battery charging and other maintenance purpose. It is observed that the disassembling and assembling process is a very time consuming because it requires unbolting and bolting of all the 16 bolts every time. A new design of pressure hull is proposed where the bolts are removed and the navigation compartment and battery compartment are welded. pressure hull is a created in Pro-E 5.0. Model is imported in ANSYS 14.0 for analysis by applying normal load and dynamic load conditions. After analysis a comparison is made between existing in terms of deflections and stresses, to choose the best one.

III. STRUCTURAL ANALYSIS OF PRESSURE HULL:

Dimensions of the structural and dynamic analysis the design of pressure hull without bolts and pressure hull with bolts. Pressure hull consists of 5 layers (thickness of each layer, 0.6mm). diameter of the pressure hull is 125mm. Since the properties of pressure hull vary with directions of a 3-D model of pressure hull is used for analysis in ANSYS 14.0. The loading conditions are assumed to be static and dynamic. The element chosen is SHELL LINEAR LAYER 99, which is a layered version of the 8-node structural shell model. The element has six degrees of freedom at each node : translations in the nodal x, y, and z directions and rotations about the nodal x, y, and z-axes. The finite element analysis is carried out on pressure hull with bolts as well as pressure hull with out bolts .From the analysis the equivalent stress (Von-mises stress) and displacements were determined and are shown in figure 2-15. Table 2 - 4 shows the Comparative structural and dynamic analysis of a pressure hull with bolts and without bolts.

IV. SPECIFICATIONS OF EXISTING PRESSURE HULL :

Table 1 shows the specifications of a steel pressure hull of alister 3000. The typical chemical composition of the material is 0.565C, 1.8% Si, 0.7%Mn, 0.045%P and 0.045% S.

Table: 1 Specifications of pressure hull

S.No	Parameters	Value
1	Total length of the pressure hull (Eye to Eye)	245mm
2	Diameter of the pressure hull	125 mm
3	Thickness of pressurehull	3 mm
4	applying the pressure	6.326N/mm ²
5	Young's Modulus of steel	2.1e5 N/mm ²
6	Density of steel pressure hull	7860 kg/m ³
7	Yield strength	500 N/mm ²
8	Tensile strength	620 N/mm ²
9	Passions ratio	0.3

V. STRUCTURAL AND DYNAMIC ANALYSIS OF PRESSURE HULL:

5.1 PRESSURE HULL WITH BOLTS

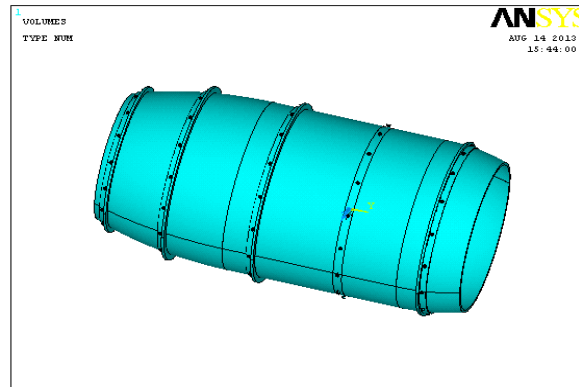


Fig2: Analysis of pressure hull with bolts

5.1.1 STRUCTURAL ANALYSIS:

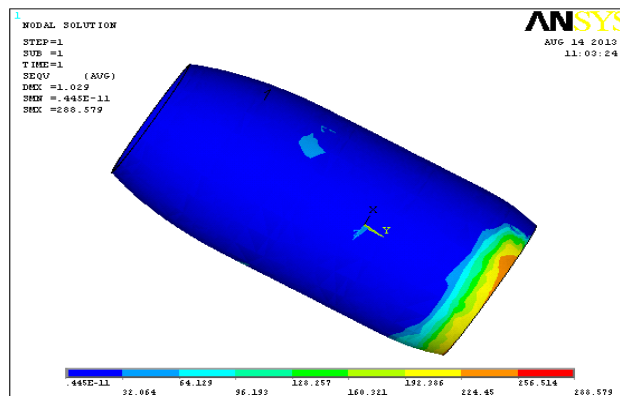


Fig3: Stress distribution for pressure hull

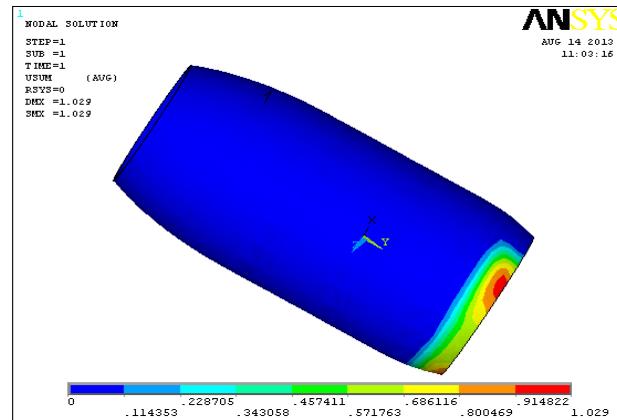


Fig 4: Displacement pattern for pressure hull

5.1.2 DYNAMIC ANALYSIS: 10SECS

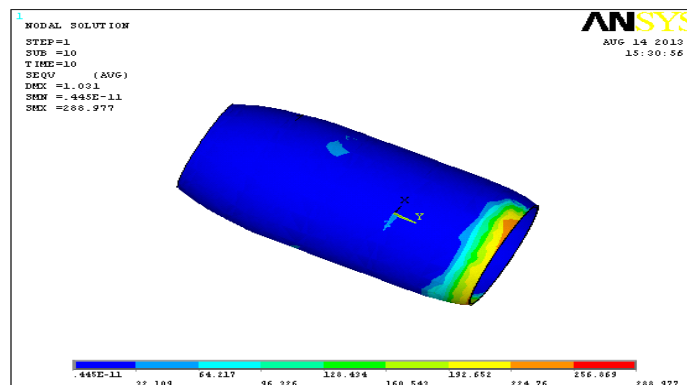


Fig5: Stress distribution for pressure hull

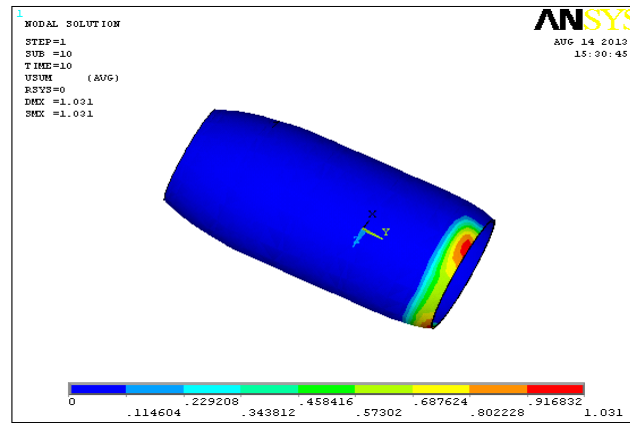


Fig 6: Displacement pattern for pressure hull

5.1.3 DYNAMIC ANALYSIS: 20 SECS

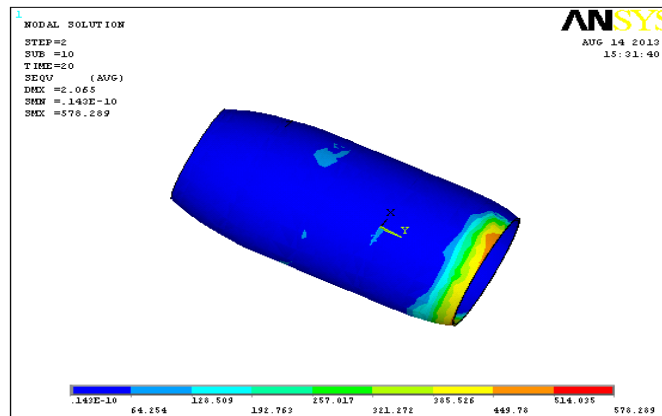


Fig7: Stress distribution for pressure hull

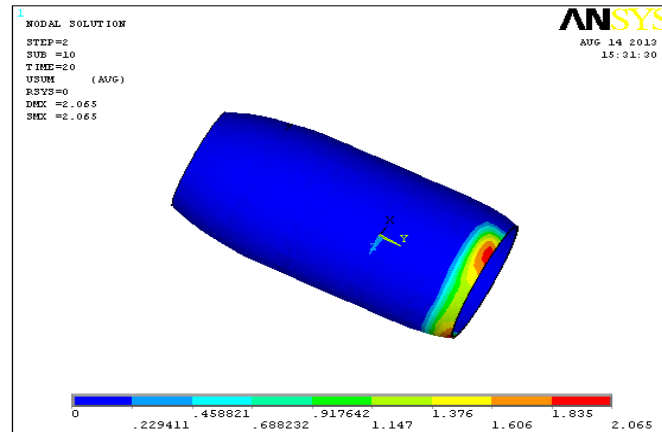


Fig 8: Displacement pattern for pressure hull

5.2 PRESSURE HULL WITH OUT BOLTS

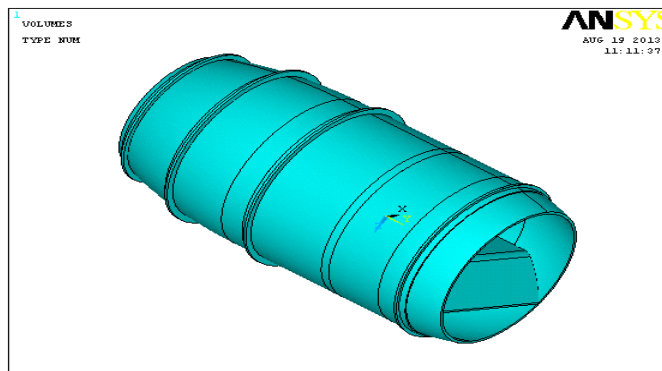


Fig9: Analysis of pressure hull without bolts

5.2.1 STRUCTURAL ANALYSIS:

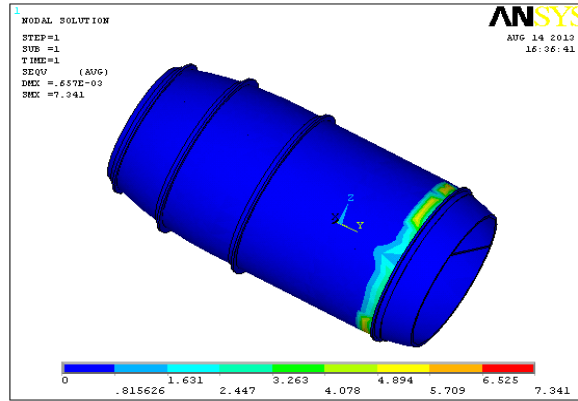


Fig10: Stress distribution for pressure hull

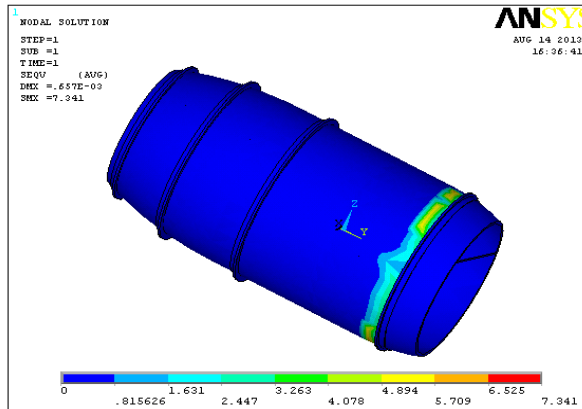


Fig 11: Displacement pattern for pressure hull

5.2.2 DYNAMIC ANALYSIS: 10SECS

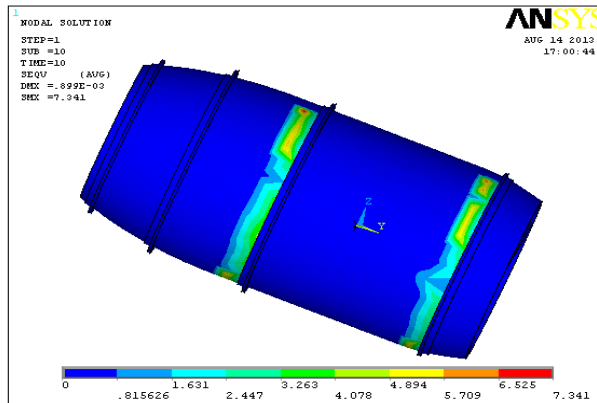


Fig12: Stress distribution for pressure hull

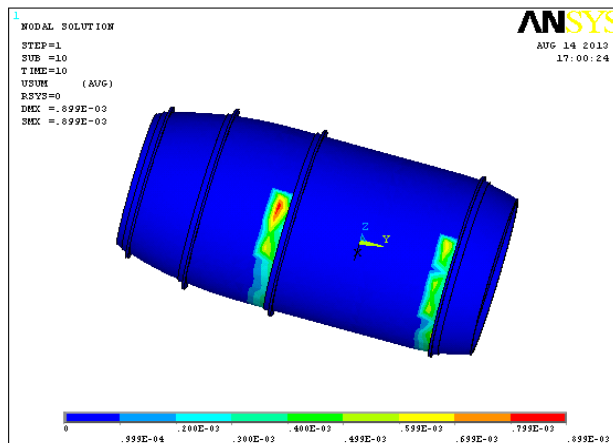


Fig 13: Displacement pattern for pressure hull

5.2.3 DYNAMIC ANALYSIS: 20SECS

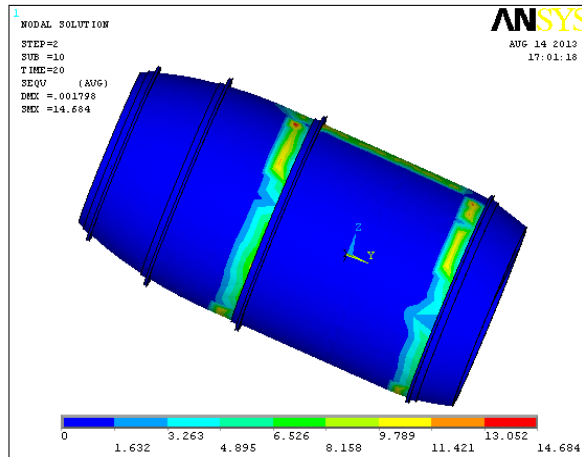


Fig14: Stress distribution for pressure hull

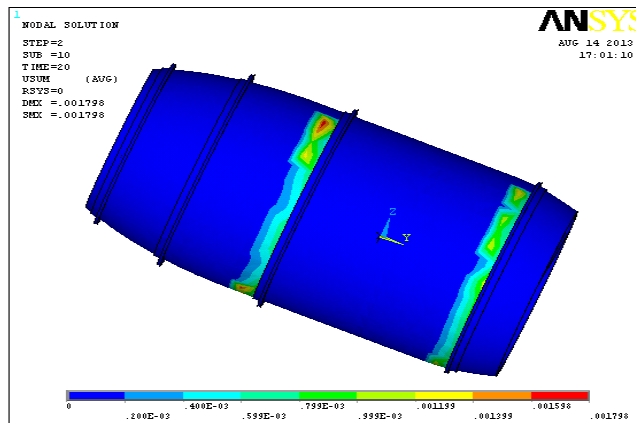


Fig 15: Displacement pattern for pressure hull

VI. RESULTS

6.1 STRUCTURAL ANALYSIS RESULTS:

Table2: Comparative structural analysis of a pressure hull with bolts and without bolts.

S. no	PH	Stress (N/mm ²)	Displacement (mm)	Strain
1	WB	288.579	1.029	0.001861
2	WOB	7.341	0.000657	0.000046

- Notes: 1. PH = pressure hull,
- 2. WB = With bolts,
- 3. WOB = Without bolts.

6.2 DYNAMIC ANALYSIS RESULTS:

Table3: Comparative dynamic analysis of a pressure hull with bolts and without bolts.

S. no	Parameter	Time	PH WB	PHWOB
1	Stress (N/mm ²)	10sec	288.977	7.341
2		20sec	578.289	14.684
3		30sec	867.749	22.06
4	Displacement(mm)	10sec	1.031	0.000899
5		20sec	2.065	0.001798
6		30sec	3.099	0.002697
7	Strain	10sec	0.001863	0.000046
8		20sec	0.003729	0.000094
9		30sec	0.005595	0.000141

- Notes: 1. PHWB = pressure hull with bolts,
 2. PHWOB = pressure hull Without bolts.

6.3 MODAL ANALYSIS RESULTS:

Table4: Comparative modal analysis of a pressure hull with bolts and without bolts.

S.no	PH with bolts		PH without bolts	
	Displacement(mm)	Frequency(Hz)	Displacement(mm)	Frequency(Hz)
1	1.0029	0	0.218416	0
2	0.32194	21.646	0.19668	0
3	0.23168	25.724	0.10598	0.000007
4	0.276541	26.2929	0.228769	0.0000081

- Notes: 1. PHWB = pressure hull with bolts,
 2. PHWOB = pressure hull Without bolts.

VII. GRAPHS:

7.1 Pressure Hull with bolts and without bolts for dynamic analysis:

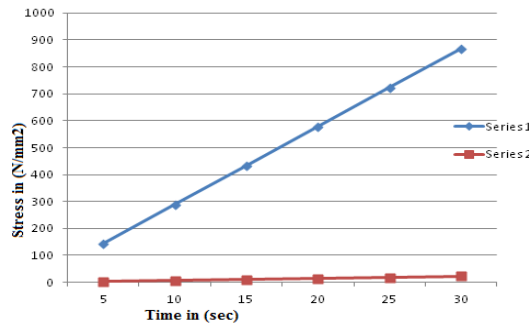


Fig 16: Time - Stress curves for PHWB and PHWOB.

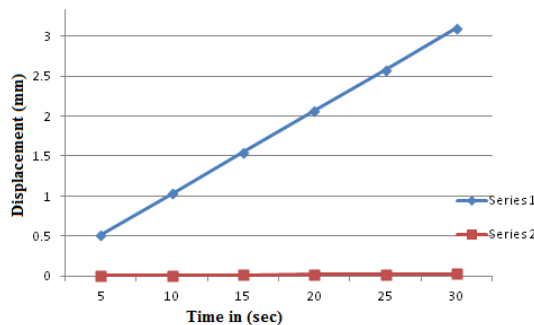


Fig 17: Time - Displacement curves for PHWB and PHWOB.

- Notes: 1. PHWB = pressure hull with bolts,
 2. PH WOB = pressure hull Without bolts,
 3. Series 1 = PHWB curve,
 4. Series 2 = PHWOB curve.

VIII. CONCLUSION:

To observe the all results and to compare the Pressurehull with bolts and pressurehull with out bolts with respect to weight, stiffness and strength.

By employing pressurehull without bolts for the same load carrying capacity, there is a reduction in are 32%~41% higher than pressurehull withbolts and 52~63% stiffer than the pressurehull with bolts.

Present used material for pressurehull with bolts is Stainlesssteel. I have considered pressurehull with bolts and pressurehull without bolts. Based on the results, it was inferred that pressurehull without bolts has superior strength and stiffness and lesser in weight compared to pressurehull with bolts.

From the results, it is observed that the pressurehull without bolts is lighter and more economical than the conventional pressurehull with bolts with similar design specifications.

REFERENCES

- [1.] Tsybenko A.S., Kuranov B.A., Chepurnoi A.D., Krishchuk N.G. & Shtefan E.V., State of Stress and Strain of Pressure Vessel during Pressurization, Plenum Publishing Corporation(1989).
- [2.] Liang C.C., Optimum Design of Filament-wound Multilayer- sandwich Submersible Pressure Hulls, Pergamon Ocean Engineering,30 (2003) 1941-1967.
- [3.] Ross C.T.F., A Conceptual Design of an Underwater Vehicle, Elsevier Ocean Engineering, 33 (2006) 2087-2104.
- [4.] Ross, C.T.F., A Conceptual Design of an Underwater Missile Launcher, Elsevier Ocean Engineering, 32 (2005) 85-99.
- [5.] Ross C.T.F. & Etheridge J., The Buckling and Vibration of Tube-stiffened Axisymmetric Shells under External Hydrostatic Pressure, Pergamon Ocean Engineering, 27 (2000) 1373-1390.
- [6.] Ross C.T.F., Little A.P.F. & Adeniyi K.A., Plastic Buckling of Ring-stiffened Conical Shell under External Hydrostatic Pressure, Elsevier Ocean Engineering, 32 (2003) 21-36.
- [7.] Ross C.T.F., Little A.P.F. & Leonidas Chasapides, Jeff banks, and Daniele Attanasio, Buckling of Ring Stiffened Domes under External Hydrostatic Pressure: Science Direct Ocean Engineering, 31 (2002) 239-252.
- [8.] Ross C.T.F. & Little A.P.F., The Buckling of a corrugated Carbon Fiber Cylinder under External Hydrostatic Pressure, Elsevier Ocean Engineering, 28 (2001) 1247-1264.
- [9.] Blachut J. & Smith P., Buckling of multi-segment underwater pressure hull, Elsevier Ocean Engineering, 35 (2007) 247-260.
- [10.] Derek Graham, Predicting the collapse of externally pressurized ring-stiffened cylinders using finite element analysis, Elsevier Marine Structures, 20 (2007) 202-217.

Synthesis of Third Order Active-R Multifunction Filter Using Feed Forward Input Signal

U. N. Chavan¹ and G. N. Shinde^{2*}

¹Department of Physics, Yeshwant Mahavidyalaya, Nanded, Maharashtra
²Indira Gandhi (SR) College, CIDCO, Nanded, Maharashtra, India

ABSTRACT: A realization of voltage-mode transfer functions with multiple feedback signal for third-order active-R filter using an operational amplifier has been presented. The single circuit gives three filter functions, low pass, high pass and band pass. This filter circuit can be used for different Q with high passband gain and ideal gain roll-off for higher Q values. The low pass and band pass performance of the circuit gives high passband gain and excellent GRPO for higher value of Q . For high pass filter, circuit shows gain stabilization at 0 dB for higher values of Q . Low pass, Band pass and High pass filter works excellent for higher values of Q .

Keywords: Filters; third-order; active-R; multiple feedback signal, passband.

I. INTRODUCTION

The operational amplifier (op. amp.) is now accepted as the basic active component for an inductor less filter. The circuit is realized using single pole (as “integrator”) behavior of an internally compensated operational amplifier [2,4,5,9]. The filter without the capacitor is called an active-R filter [1]. This filter has received much attention due to its potential advantages in terms of miniaturization, ease of design and high frequency performance [3,6,8]. This paper proposes realization and design method for third-order active-R filter with multiple feedback signals. This filter circuit gives three filter functions, low pass, high pass and band pass with ideal gain roll-off and high passband gain. The circuit is designed and studied for different values of circuit merit factor Q .

II. CIRCUIT CONFIGURATION

The proposed active-R third-order filter circuit diagram with multiple feedback is shown in figure-1. With the advent of the high frequency roll-off in the response of the op.amp, the circuit is constructed with multiple feedback.

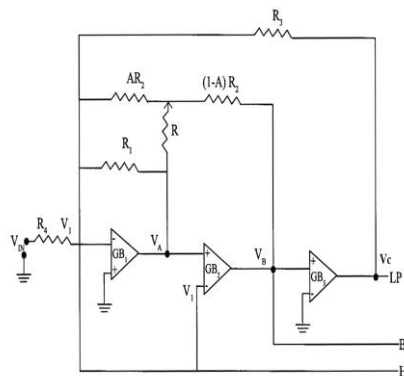


Figure 1. Circuit diagram for active-R third-order filter with multiple feedback signal.

There are three op.amplifiers (μ A741), with identical gain bandwidth product as an active element, and four resistances. This filter gives multiple outputs, which tend three filter functions, low pass, band pass and high pass. The negative feedback is introduced through resistances $R_1;R_2;R_3$ from the output of the three op.amplifiers to inverting input of the first op.amp.The resistance R_2 is tapped at different points for variation in feedback. The op-amps are coupled such that output of first op-amp is connected to non-inverting input of second op-amp and output of second op-amp is connected to non-inverting input of third op-amp. Non-inverting terminal of first op-amp, inverting terminal of third op-amp are grounded. The inverting terminal of second op-amp is connected to non-inverting terminal of first op-amp so that input V_1 appears at inverting terminal of second op-amp. The input is applied to inverting input of first op-amp through R_4 .

III. CIRCUIT ANALYSIS AND DESIGN EQUATIONS

The single-pole model of an op.amp. leads to complex gain and the transfer function is given by [8].

$$A(s) = A_0 \omega_0 / (S + \omega_0) \quad (1) \quad \text{Where,}$$

A_0 = open loop d.c. gain, ω_0 = open loop 3dB bandwidth, $GB = A_0 \omega_0$ = gain bandwidth product of op.amp.

$$A(s) = A_0 \omega_0 / S = GB / S, \quad (2)$$

Where, $S \gg \omega_0$

This shows that the op. amp. is an “integrator”, Thus the active-R third-order filter transfer function at three different terminals are given below. The voltage transfer function for low pass filter.

$$T_{LP}(S) = \frac{-(1/R_4)GB_1GB_2GB_3}{X_1S^3 + X_2S^2 + X_3S + X_4} \quad (3)$$

The voltage transfer function for band pass filter

$$T_{BP}(S) = \frac{-(1/R_4)GB_1GB_2S}{X_1S^3 + X_2S^2 + X_3S + X_4} \quad (4)$$

The voltage transfer function for high pass filter

$$T_{HP}(S) = \frac{(1/R_4)S^3}{X_1S^3 + X_2S^2 + X_3S + X_4} \quad (5)$$

Where,

$$X_1 = \left(\frac{1}{R_1} + \frac{1}{AR_2} + \frac{1}{R_3} + \frac{1}{R_4} - \frac{(1-A)MR}{A} \right)$$

$$X_2 = \left(\frac{1}{R_1} + (1-A)R_2M \right)$$

$$X_3 = (RM)$$

$$X_4 = \frac{GB_1GB_2GB_3}{R_3}$$

$$M = \frac{1}{A(1-A)R_2^2 + RR_2}$$

The circuit was designed using coefficient matching technique with general third-order filter transfer function [4,5]

$$T(S) = \frac{H_3S^3 + H_2S^2 + HS + H_0}{S^3 + S^2\omega_0[(1/Q)+1] + S\omega_0^2[(1/Q)+1] + \omega_0^3} \quad (6)$$

By comparing (3), (4), and (5) with (6), we get the design equation as

$$(1) R_1 = \frac{1}{\frac{P}{N} - [(1-A)R_2M]}$$

$$(2) R_2 = -X + \sqrt{X^2 + \frac{RN^2}{PA(1-A)}}$$

$$\text{Where } X = \frac{R}{2A(1-A)}$$

$$(3) R_3 = N^3$$

$$(4) R_4 = \frac{1}{1 - \frac{1}{R_1} - \frac{1}{AR_2} - \frac{1}{R_3} + \frac{(1-A)RM}{A}}$$

Values of R_1 ; R_2 ; R_3 , and R_4 can be calculated using these equations for different values Q (table 1).

For practical realization all values of resistances are scaled by 100.

TABLE 1
Resistance values for different Q

Q	R ₁ Ω	R ₂ Ω	R ₃ Ω	R ₄ Ω
0.2	9.41	232.6	175.6 k	1.12
0.5	18.9	426.1	175.6 k	1.06
1.2	28.6	595.4	175.6 k	1.04
2	38.4	747.8	175.6 k	1.03
5	48.3	887.6	175.6 k	1.02
10	52.8	947.7	175.6 k	1.02
15	54.5	969.8	175.6 k	1.02
20	55.4	981.2	175.6 k	1.02
25	55.9	988.2	175.6 k	1.02

IV. DISCUSSION FOR VARIATION IN Q

The circuit performance was studied with different values of Q ($Q = 0.2, 0.5, 1.2, 2, 5, 10, 15, 20, 25$). The table 1 shows resistance values of resistance for different Q value. The circuit was studied for different values of Q for centre frequency $f_0 = 10$ KHz. The observed frequency response shows good agreement with theoretical results. Following observations are noticed from experimental study at three different terminals; low pass, band pass and high pass filter function for different Q .

V. RESULT AND DISCUSSION

a) *Low pass response:*

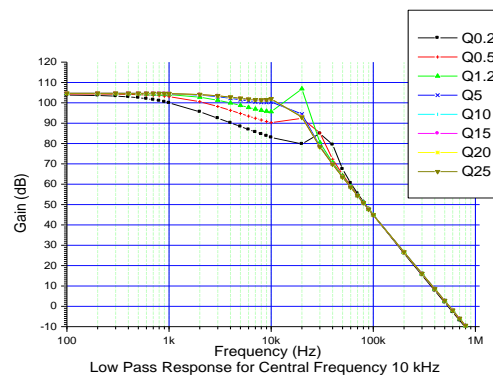


Figure 2 - Low pass (LP) responses for different values of Q

Low pass (LP) responses for different values of Q are shown in figure 2. The observed centre frequency is also in good agreement with the designed value. It is noticed that this circuit has high passband gain and it increases with increase in Q value and is constant for $Q > 10$. Gain roll off per octave is excellent for $Q > 1.2$. The % Change in F_{OL} decreases with Q value. Overshoot is observed and increases for $Q \geq 1.2$. The circuit shows excellent performance for $Q \geq 10$.

b) *Band pass response:*

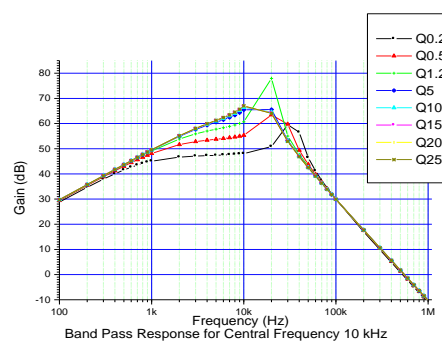


Figure -3 : The band pass (BP) response for different Q ,

The band pass (BP) response for different Q is shown in figure 3. The Maximum passband gain increases with Q value. The bandwidth is slightly deviated from central frequency value. It is observed that curves are symmetric on both sides. The circuit shows excellent performance for higher values of Q .

c) High pass response:

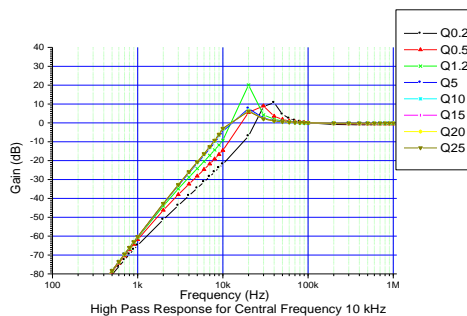


Figure -4 : High pass (HP) responses for different values of Q

High pass (HP) responses for different values of Q are shown in figure 4. The response shows that GRPO is excellent and close to ideal value for higher Q values. For $Q \geq 5$ gain stabilizes at 0 dB. The circuit shows ideal response for $Q \geq 10$.

VI. CONCLUSION

A realization of voltage mode transfer function for a third-order active-R filter using op.amp. with multiple feedback signal has been presented. This circuit is composed only of three op. amplifiers and four resistances. Also, this single filter circuit gives three filter functions; low pass, band pass and high pass. The low pass and band pass performance of the circuit gives high passband gain and excellent GRPO for higher value of Q . For high pass filter, circuit shows gain stabilization at 0 dB for higher values of Q . Low pass, Band pass and High pass filter works excellent for higher values of Q .

REFERENCES

- [1] Hioashimura M 1992 Active-R realization of current mode high pass filter. *Int. J. Electron.* 73: 1279–1283
- [2] Huelsman L P 1971 Equal-valued capacitor active-RC network realisation of a 3rd order low pass Butterworth characteristics. *Electron. Lett.* 7: 291–293
- [3] Kadam A B, Mahajan A M 1995 Effect of positive feedback on the response of active-R filter. *J. Instrum. Soc. India* 25: 48–55
- [4] Mohan N, Patil R L Ripple pass function and their active-R realization. *Indian J. Pure Appl. Phys.* 30: 749–750
- [5] Shinde G N, Patil P B 2002 Study of active-R second-order filter using feedback at non-inverting terminals. *Bull. Pure Appl. Sci.* D21: 23–31
- [6] Shinde G N, Mirkute P R, Achole P D 2003 Second order active-R filter with multiple feedback for different Q . *Indian J. Phys.* B77: 72–80
- [7] Soderstand M A, Mitra S K 1971 Sensitivity analysis of third-order filter. *Int. J. Electron.* 30: 265–273
- [8] Srinivasan S 1992 Synthesis of transfer function using the operation amplifier pole. *Int. J. Electron.* 73: 1279–1283
- [9] Sun Zhi-Xiao 1983 Active-R filter: a new biquadratic with four terminals. *Int. J. Electron.* 54: 523–530

An Extensive Review of Momentous Researches on Acoustic Emission and Vibration

A V Patil¹, Dr. Bimlesh Kumar²

*(Department of Mechanical Engineering, S.S.G.B.C.O.E & T, Bhusawal, India)

** (Department of Mechanical Engineering, J.T.M.C.O.E, Faizpur, India)

ABSTRACT: Nowadays, vibration is one of the major issues in the environment, which may cause some serious injuries to the human health. Vibration may occur due to mechanical oscillation from industrial machines, railway track nearby human reside, and many more reasons. There are two types of vibration: Free Vibration and Forced Vibration. Due to the interaction between humans and machines, vibration cause serious damage to the human health. Hence, it needs to be eradicated with proper controlling techniques. Before going to eradicate those faults we have to identify those fault localization. In this paper we have reviewed the acoustic emission and also the vibration, here author intend to find the fault localization and exploit it with acoustic emission and vibration.

Keywords: Acoustic emission, vibration, frequency.

I. INTRODUCTION

Modern society is characterized by an increasing attention for the environmental impact of newly developed machinery. One of the environmental criteria that are gaining importance is the noise emission level produced by a new machine since the legal regulations more and more restrict the allowable noise levels. [1] Acoustic emission monitoring refers to the detection of transient waves during the rapid release of energy from localized sources within a material. This in-service test technique explores the damage due to corrosion. [2]

Rolling element bearing condition monitoring has received considerable attention for many years because the majority of problems in rotating machines is caused by faulty bearings. [3] The acoustic emission (AE) method has attracted attention as a monitoring method for the friction and wear processes, as well as the lubricating conditions. [4] If the lubricating grease in a rolling bearing contains contaminants, this may indicate inadequate or damaged sealing of the bearing housing, or wear of the bearing. [5] As a consequence of their importance and widespread use bearing failure is also one of the foremost causes of breakdown in rotating machinery. [6]

Various strategies exist that aim to reduce the response of the structure to dynamic loads, typically falling into one of the categories of structural modification, passive control, active control, semi-active control or hybrid control (a combination of active and passive control). [7]

II. ACOUSTIC EMISSION

Over the last 20 last years the Acoustic Emission (AE) proved as a powerful method for the detection of incipient defects on rotating machines. The technology offers several significant advantages over conventional vibration analysis. [8] The traditional definition of acoustic emission (AE) is an elastic wave produced as a result of the swift discharge of energy from a source within a material that is compelled by an externally applied stimulus. [9] The first comprehensive investigation into the phenomenon of AE was undertaken by Kaiser in 1950. Kaiser was the first to digitally acquire AE signals produced in the crystal structure of materials during stress tests. The AE technology is continually developing into a complementary technology for condition monitoring of machines. [9]

Acoustic Emission (AE) is the phenomenon of transient elastic wave generation in materials under stress. When the material is subjected to stress at a certain level, a rapid release of strain energy takes place in the form of elastic waves that can be detected by transducers. Typical AE signal frequency range is between 20 kHz and 1 MHz. When surface traction occurs at asperity contacts, materials can exhibit two basic responses: elastic and plastic deformation of the surface and subsurface and fracture, which are potential AE sources. In metal to metal sliding contacts, the possible AE sources due to friction and wear include: (i) contact surface damage, (ii) subsurface cracking, nucleation and propagation, (iii) phase changes, (iv) chemical reactions, (v) impulsive shocks due to asperity collision and debris and (vi) micro-vibration excited by the stick-slip at the interface. [10]

The three most significant applications of AE techniques are as follows

- Source location - determine the locations where an event source occurred
- Material mechanical performance - estimate and characterizes materials/structures
- Health monitoring - monitor the safety operation of a structure

The detection of AE can be an effective non-destructive technique for investigating the conditions of gas pipes, welds and storage tanks, or for real-time monitoring of machining processes and the performance of structures under cyclic loading such as aircrafts. [11] Today's cars represent a complex compromise between contradictory requirement with regard to safety, exhaust emissions, noise, performance and price. However, since it's widely recognized that the quality of the life, particularly in the urban environment, is heavily influenced by air and noise pollution resulting from road traffic, one of the top priorities of car manufacturers is the reduction of noise and emissions from vehicles. [12]

III. RELATED WORK

In 2008, Tzu-Shien Chuang *et al.* [13] has described a stator flux oriented current vector control of a Sensorless three-phase 6/4 switched reluctance motor without position sensors was presented. Space current vector control technology based on torque angle estimation was used to reduce the acoustic noise and vibration of the motor drive system. The power converter for the 6/4 switched reluctance motor was a three-phase full bridge inverter. The experimental results show that the maximum level of acoustic noises and vibration are 73 dB and 8 dB; m/s/s, respectively, and the steady speed error of the drive system was less than 0.1% operated at the rated load when the drive system was operated below 1500 RPM. In addition, the transient speed performance was also satisfactory.

In 1999, Tandon *et al.* [14] have reviewed vibration and acoustic measurement methods for the detection of defects in rolling element bearings is presented in the proposed technique. Detection of both localized and distributed categories of defect has been considered. An explanation for the vibration and noise generation in the bearings was given. Vibration measurement in both time and frequency domains along with signal processing techniques such as the high-frequency resonance technique have been covered. Other acoustic measurement techniques such as sound pressure, sound intensity and acoustic emission have been reviewed. Recent trends in research on the detection of defects in bearings, such as the wavelet transform method and automated data processing, have also been included.

In 2011, T.H. Loutas *et al.* [15] The monitoring of progressive wear in gear using various non-destructive technologies as well as the use of advanced signal processing techniques upon the acquired recordings in the direction of more effective diagnostic schemes was the scope of the present work. For the proposed reason multi-hour tests were performed in healthy gears in a single-stage lab scale gearbox until they were seriously damaged. Three on-line monitoring techniques are implemented in the tests. Vibration and acoustic emission recordings in combination with data coming from oil debris monitoring (ODM) of the lubricating oil were utilized in order to assess the condition of the gears. A plethora of parameters/features were extracted from the acquired waveforms via conventional (in time and frequency domain) and non-conventional (wavelet-based) signal processing techniques. Final heuristic rules based on characteristic values of the resulted independent components were set, realizing thus a health monitoring scheme for gearboxes. The integration of vibration, AE and ODM data increases the diagnostic capacity and reliability of the condition monitoring scheme concluding to very interesting results. The present work summarizes the joint efforts of two research groups towards a more reliable condition monitoring of rotating machinery and gearboxes specifically.

In 2009, T.H. Loutas *et al.* [16] have discussed the condition monitoring of a lab-scale, single stage, gearbox using different non-destructive inspection methodologies and the processing of the acquired waveforms with advanced signal processing techniques is the aim of the present work. Acoustic emission (AE) and vibration measurements were utilized for this purpose. The experimental setup and the instrumentation of each monitoring methodology are presented in detail. Emphasis was given to the signal processing of the acquired vibration and acoustic emission signals in order to extract conventional as well as novel parameters–features of potential diagnostic value from the monitored waveforms. Innovative wavelet-based parameters–features are pro-posed utilizing the discrete wavelet transform. The evolution of selected parameters/features versus test time was provided, evaluated and the parameters with the most interesting diagnostic behavior are highlighted. The differences in the parameters evolution of each NDT technique are discussed and the superiority of AE over vibration recordings for the early diagnosis of natural wear in gear systems was concluded.

In 2009, Ziaur Rahman *et al.* [17] has described the acoustic emission (AE) technique was applied to rolling contact fatigue tests using a test-rig running under constant load and speed for detecting the incipient damage and damage location. The proposed technique incipiently-damaged roller was investigated in detail and monitored by further running to determine the damage severity and to understand the surface damage propagation process by applying the AE techniques. The conventional AE parameters and AE signal features were studied, and their relation to the AE source locator hit count rate were correlated. The results demonstrated the successful use of the AE measurement unit, which was principally, consists of the AE data analyzer and the AE source locator as a new system for detecting incipient damage produced by fatigue. Moreover, the system is able to forecast the position of the damage in the roller, capable of providing an indication of the severity of damage i.e. damage size, and thus it could allow the user to monitor the rate of further degradation of the rolling elements.

In 2009, Kean Chen *et al.* [18] have described the rolling element bearings are the most common cause of rotating machinery failure. Over the past 20 years, Acoustic Emission (AE) technology has evolved as a significant opportunity to monitor and diagnose the mechanical integrity of rolling element bearings. The proposed technique presents results of an investigation to assess the potential of the Acoustic Emission (AE) technology for detecting and locating natural defects in rolling element bearings. To undertake the proposed task a special purpose test-rig was built that allowed for accelerated natural degradation of a bearing race. It was concluded that the sub - surface initiation and subsequent crack propagation can be detected using a range of data analysis techniques on AE's generated from natural degrading bearings. The proposed technique also investigates the source characterization of AE signals associated with a defective bearing whilst in operation. The proposed also attempted to identify the size of a natural defect on bearings using AE technology.

In 2012, Zhang Zhi-qiang *et al.* [19] have proposed that the objective of the present study was investigating rolling contact fatigue (RCF) damage process of the sprayed coating by acoustic emission (AE) and vibration signals. Fe-based alloy coating was prepared on 1045 steel using the plasma spraying technology. The result shows that RCF damage process was composed of four stages. The AE with higher sensitivity can detect fatigue damage details, such as the material deformation, crack initiation and growth. The vibration could reflect the final failure, such as extensive and deeper pitting. The analysis of AE waveform and frequency are effective methods for studying RCF damage process.

Cyclostationarity was a relatively new technique that offers diagnostic advantages for analysis of vibrations from defective bearings. Similarly the Acoustic Emission (AE) technology has emerged as a viable tool for preventive maintenance of rotating machines. In 2011, Kilundu *et al.* [20] have presented an experimental study that characterizes the cyclo stationary aspect of Acoustic Emission signals recorded from a defective bearing. The cyclic spectral correlation, a tool dedicated to evidence the presence of cyclostationarity, was compared with a traditional technique, the envelope spectrum. The proposed technique comparison showed that the cyclic spectral correlation was most efficient for small defect identification on outer race defects though the success was not mirrored on inner race defects. An indicator, based on the proposed cyclostationary technique, has also been proposed. It was concluded that it offers better sensitivity to the continuous monitoring of defects compared to the use of traditional temporal indicators (RMS, Kurtosis, and Crest Factor).

The challenge in many production activities involving large mechanical devices like power transmissions consists in reducing the machine downtime, in managing repairs and in improving operating time. In 2010, Renaudin *et al.* [21] have proposed an alternative way of bearing condition monitoring based on the instantaneous angular speed measurement. By the help of a large experimental investigation on two different applications, they prove that localized faults like pitting in bearing generate small angular speed fluctuations which are measured with optical or magnetic encoders. They also emphasize the benefits of measuring instantaneous angular speed with the pulse timing method through an implicit angular sampling which ensures insensitivity to speed fluctuation. A wide range of operating conditions has been tested for the two applications with varying speed, load, external excitations, gear ratio, etc. The tests performed on an automotive gearbox or on actual operating vehicle wheels also establish the robustness of the proposed methodology. Sideband effects are evidently seen when the fault was located on rotating parts of the bearing due to load modulation.

In 2011, Eftekharijad *et al.* [22] has described the application of Acoustic Emission (AE) technology for machine health monitoring is gaining ground as a powerful tool for health diagnostic of rolling element bearing. The proposed technique provides an investigation that compares the applicability of AE and vibration technologies in monitoring a naturally degraded roller bearing. The proposed research was the first known attempt investigating the comparative effectiveness of applying the Kurtogram to both vibration and AE data from a defective bearing

Condition monitoring of induction motors was a fast emerging technology in the field of electrical equipment maintenance and has attracted more and more attention worldwide as the number of unexpected failures of a critical system could be avoided. Keeping this in mind a bearing fault detection scheme of three-phase induction motor has been attempted. In 2011, Konar *et al.* [23] study, Support Vector Machine (SVM) was used along with continuous wavelet transform (CWT), an advanced signal-processing tool, to analyze the frame vibrations during start-up. CWT has not been widely applied in the field of condition monitoring although much better results can be obtained compared to the widely used DWT based techniques. The encouraging results obtained from the present analysis was hoping to set up a base for the condition monitoring technique of induction motor which will be simple, fast and overcome the limitations of traditional data-based models/techniques

IV. PROPOSED RESEARCH SCOPE

In this review paper, I have analyzed acoustic emission and vibration to predict the fault localization. There are several aspects of the fault localization. In this work my ultimate aim is to predict the fault where it occurs for that, I intend to collect various acoustic emission and vibrating parameters in frequency under various faulty condition with various speed condition and also attain result for normal working condition. The frequency attainment under normal working condition is compared with the abnormal working condition, the difference between normal and abnormal working condition frequency range is unique to one another. This unique frequency range is classified into different sorts. The technique used to classify this process frequency is a multiple support vector machine (MSVM). This technique is implemented in the working platform MATLAB. The technique which I am going to propose gives better results for the classification process. This study may facilitate the researchers to further enhance the vibration and acoustic emission process and this review paper will be the enhanced background for the research on acoustic emission and vibration. In the future, we anticipate a large number of brainwaves will rise with the aid of our review.

V. CONCLUSION

In this review paper, an extensive technique work base on acoustic emission and vibration are reviewed thoroughly. The ultimate aim of the proposed technique is to predict the fault localization, for this process author intends to go with the multiclass support vector machine. This paves the path for the classifications which categorize the fault and predict the fault localization in the effective manner. The reviewed techniques were classified under various processes of acoustic emission and vibration. Thus, this review paves the path for the budding researchers to be acquainted with various techniques existing in this field.

REFERENCE

Journal Papers:

- [1] G. Pinte, S.Devos, B.Stallaert, W.Symens, J.Swevers and P.Sas, "A piezo-based bearing for the active structural acoustic control of rotating machinery", *Journal of Sound and Vibration*, Vol.329, pp.1235-1253, 2010
- [2] C. Jirarungsatian and A. Prateepasen, "Pitting and uniform corrosion source recognition using acoustic emission parameters", *Corrosion Science*, Vol.52, pp.187-197, 2010
- [3] James Li and Li, "Acoustic emission analysis for bearing condition monitoring", *Wear*, Vol.185, pp.67-74, 1995
- [4] Hisakado and Warashina, "Relationship between friction and wear properties and acoustic emission characteristics: iron pin on hardened bearing steel disk", *Wear*, Vol.216, pp.1-7, 1998

- [5] Juha Miettinen and Peter Andersson, "Acoustic emission of rolling bearings lubricated with contaminated grease", *Tribology International*, Vol.33, pp.777-787, 2000
- [6] shiroishi ,LI ,LIANG ,KURFESS and DANYLUK, "Bearing Condition Diagnostics Via Vibration And Acoustic Emission Measurements" ,*Mechanical Systems and Signal Processing*,Vol.11,No.5,pp.693-705,1997
- [7] M.J. Hudson and P. Reynolds, "Implementation considerations for active vibration control in the design of floor structures", *Engineering Structures*, Vol.44, pp.334-358, 2012
- [8] B. Kilundu, Chiementin, Duez and Mba, "Cyclostationarity of Acoustic Emissions (AE) for monitoring bearing defects", *Mechanical Systems and Signal Processing*, Vol.25, pp.2061-2072, 2011
- [9] Mirhadizadeh, Moncholi and Mba, "Influence of operational variables in a hydrodynamic bearing on the generation of acoustic emission", *Tribology International*, Vol.43, pp.1760-1767, 2010
- [10] Jun Sun , Wood ,Wang ,Care and Powrie, "Wear monitoring of bearing steel using electrostatic and acoustic emission techniques",*Wear*,Vol.259,pp.1482-1489,2005
- [11] Guo-Hua Feng and Ming-Yen Tsai, "Acoustic emission sensor with structure-enhanced sensing mechanism based on micro-embossed piezoelectric polymer", *Sensors and Actuators A*, Vol.162, pp.100-106, 2010
- [12] Diana Glaser, Richard D. Komistek , Harold E. Cates and Mohamed R. Mahfouz, "A non-invasive acoustic and vibration analysis technique for evaluation of hip joint conditions",*Journal of Biomechanics*,Vol.43,pp.426-432,2010
- [13] Tzu-Shien Chuang and Jin-Wei Liang, "A stator flux oriented current vector control of a Sensorless 6/4 SRM for reduction of acoustic noise and vibration", *Energy Conversion and Management*, Vol.49, pp.3075-3079, 2008
- [14] Tandon and Choudhury, "A review of vibration and acoustic measurement methods for the detection of defects in rolling element bearings", *Tribology International*, Vol.32, pp.469-480, 1999
- [15] T.H. Loutas, Roulias, Pauly and Kostopoulos, "The combined use of vibration, acoustic emission and oil debris on-line monitoring towards a more effective condition monitoring of rotating machinery",*Mechanical Systems and Signal Processing*,Vol.25,pp.1339-1352,2011
- [16] T.H. Loutas, Sotiriades, Kalaitzoglou and Kostopoulos, "Condition monitoring of a single-stage gearbox with artificially induced gear cracks utilizing on-line vibration and acoustic emission measurements", *Applied Acoustics*, Vol.70, pp.1148-1159, 2009
- [17] Ziaur Rahman, Hiroaki Ohba, Takeo Yoshioka and Takashi Yamamoto, "Incipient damage detection and its propagation monitoring of rolling contact fatigue by acoustic emission", *Tribology International*, Vol.42, pp.807-815, 2009
- [18] Elforjani and Mba, "Accelerated natural fault diagnosis in slow speed bearings with Acoustic Emission", *Engineering Fracture Mechanics*, Vol.77, pp.112-127, 2010
- [19] Zhang Zhi-qiang , Li Guo-lu , Wang Hai-dou , Xu Bin-shi , Piao Zhong-yu and Zhu Li-na, "Investigation of rolling contact fatigue damage process of the coating by acoustics emission and vibration signals" ,*Tribology International*,Vol.47,pp.25-31,2012
- [20] Kilundu, Chiementin, Duez and Mba, "Cyclostationarity of Acoustic Emissions (AE) for monitoring bearing defects", Vol.25, pp.2061-2072, 2011
- [21] Renaudin, Bonnard, Musy, Doray and Remond, "Natural roller bearing fault detection by angular measurement of true instantaneous angular speed", *Mechanical Systems and Signal Processing*, Vol.24, pp.1998-2011, 2010
- [22] Eftekharijad, Carrasco, Charnley and Mba, "The application of spectral kurtosis on Acoustic Emission and vibrations from a defective bearing", *Mechanical Systems and Signal Processing*, Vol.25, pp.266-284, 2011
- [23] Konar and Chattopadhyay, "Bearing fault detection of induction motor using wavelet and Support Vector Machines (SVMs)", *Applied Soft Computing*, Vol.11, pp. 4203-4211, 2011

Investigation of strain hardening effects in CNC milling and chemical etching of Al 7075: A comparative study

V.S.Rajashekhar¹, Pavithran Maris², K.Thiruppathi³, C. K. Dinakaraj⁴, R.Senthil⁵

¹PG student, Advanced Manufacturing, School of Mechanical Engineering, SASTRA University, India

²Student, Metallurgical and Materials Engineering, Department of Metallurgical and Materials Engineering, Indian Institute of Technology – Roorkee, India

³Senior Assistant Professor, School of Mechanical Engineering, SASTRA University, India

⁴Assistant Professor, Department of Mechanical Engineering, Adhiparasakthi Engineering College, India

⁵Professor, Department of Mechanical Engineering, Adhiparasakthi Engineering College, India

ABSTRACT: Data representation on the components can be done by engraving on the metal. This operation on the test specimen was done by two ways. CNC milling and chemical etching were done on aluminium 7075 to represent data on the test sample. Cuboid shaped aluminium 7075 was chosen as a test sample. The procedures for these 2 operations are explained. Then the merits, demerits and limitations for each of the chosen method were discussed. Strain hardening effects were detected by Vickers hardness profiling in the CNC milled and chemically etched samples. Thus data representation on aluminium 7075 components in the automobile and aerospace industries can be done by one of the suitable methods.

Keywords: Aluminium 7075, Chemical etching, CNC Milling, Engraving of metals, NaOH as etchant.

I. INTRODUCTION

1.1 A survey of CNC Milling

J. Sun, Y.B. Guo made a comprehensive experimental study on surface integrity by end milling Ti-6Al-4V [1]. J. Xie et al carried out dry micro-grooving on Si wafer using a coarse diamond grinding [2]. Justin S. Mecomber et al executed enhanced machining of micron-scale features in microchip molding masters by CNC milling [3]. Toshiyuki Obikawa et al performed high-speed grooving with applying MQL [4]. Mariana Dotcheva et al. explained about the application of tolerance analysis to the theoretical and experimental evaluation of a CNC corner-milling operation [5]. Min-Yang Yang et al performed hybrid adaptive control based on the characteristics of CNC end milling [6]. Aleksandra Bierla et al. performed mechanical and physico-chemical study of sulfur additives effect in milling of high strength steel [7]. Soichi Ibaraki published a paper on the removal of critical cutting regions by trochoidal grooving [8]. Yih-Fang Chang performed parametric curve machining of a CNC milling EDM [9]. Ali Lasemi et al. presented a recent development in CNC machining of freeform surfaces [10]. Lihui Wang et al. did a remote real-time CNC machining for web-based manufacturing [11]. Zezhong C. Chen et al. made an automated surface subdivision and tool path generation for 3 ½ ½ axis CNC machining of sculptured parts [12]. Therefore it is found that engraving data on the metals by using CNC machine is possible.

1.2 A survey of Chemical etching

Fadaei Tehrani et al. found a new etchant for the chemical machining of St304 [13]. T.K.K.R. Mediliyegedara et al. made a preliminary study on an intelligent pulse classification system for electro-chemical discharge machining [14]. S. Ho, T. Nakahara et al. did chemical machining of nano crystalline Ni [15]. J.P. Choi et al. performed chemical-assisted ultrasonic machining of glass [16]. K.L. Bhondwe presented finite element prediction of material removal rate due to electro-chemical spark machining [17]. Ching-Chuan Mai, Jehnming Lin performed supersonic flow characteristics in laser grooving [18]. F. Klocke et al. performed technological and economical comparison of roughing strategies via milling, EDM and ECM for Titanium- and Nickel-based Blinks [19]. Sanjay K. Chak, P. Venkateswara Rao performed trepanning of Al₂O₃ by electro-chemical discharge machining (ECDM) process using abrasive electrode with pulsed DC supply [20]. Hereby it is found that etching can be done in order to create pattern on the metal by using chemicals.

1.3 Our main focus

In order to perform CNC milling operations on the test specimen, perfect jig and fixtures are needed. More than that, electrical energy is needed to run the CNC machine. In a CNC, additional electrical equipment like motor, driller and tools are needed. It requires skilled labor to carry out the milling operation to form patterns.

But in the case of chemical etching we need no electric power, and other electrical equipment. Only chemicals are used to carry out the milling operation. Therefore it requires only chemical agents to carry out the etching process.

Finally the hardness values with respect to depth from the milled and etched surfaces are plotted. Standard deviation and variance were calculated for the values obtained.

II. PREPARATION OF TEST SAMPLE

2.1 CNC Milling

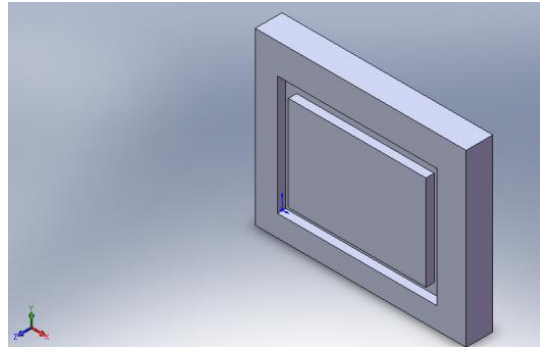


Fig 1 Isometric view of the test specimen that is to be used for CNC machining

The test specimen which is cuboidal in shape is 102x82x13mm in dimension. The shape to be milled is as shown in the Fig 1. It was created using SOLIDWORKS™ modeling software. The G code for the milling process was generated using EDGECAM™ software. Many patterns were created using the 3 axis CNC milling machine. One of them is chosen for the study of hardness variation.

2.2 Chemical etching

The test specimen which has to be chemically milled was modeled using SOLIDWORKS™ with the alphabet “T” was written on it.

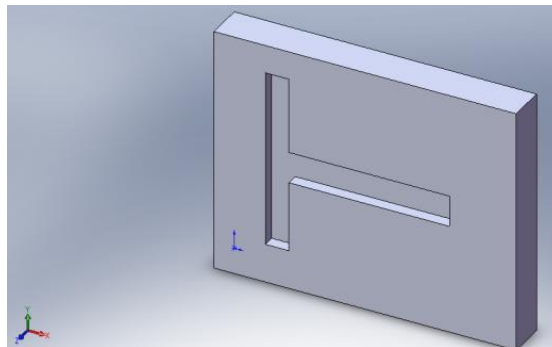


Fig 2 Trimetric view of the test specimen that is to be used for chemical machining

III. EXPERIMENTATION OF THE MILLING PROCESS

3.1 CNC Milling

A 3 axis CNC milling machine as shown in Fig 3 was used. The G codes were fed. The aluminium 7075 workpiece was fed to the jig and fixtures of the machine in order to hold the test sample firmly. The different patterns were obtained after machining.



Fig 3 The CNC Milling machine

3.2 Concept

The test specimen was fixed to the CNC milling machine using the jig and fixtures. Then the tool traversed on the global XY plane. It also has a driller type of projection and hence it has 3 degrees of freedom (3DOF).

3.3 Results of CNC milling

The 3DOF CNC milling was done on different Aluminium 7075 pieces. Drawing curves, straight lines, arcs were possible. It is as shown in Fig 4.



Fig 4 Various lines and curves done using the 3 DOF CNC milling

IV. COMPOSITION OF Al 7075 ALLOY

The chemical composition of the aluminium 7075 is as shown in the Table 1.

Table 1: Composition of Al 7075 alloy

Element (%)	Alloy
	7075
Zn	5.10 - 6.10
Mg	2.10 - 2.90
Cu	1.20 - 2.00
Cr	0.18 - 0.28
Fe	0.50 (Max.)
Si	0.40 (Max.)
Mn	0.30 (Max.)
Ti	0.20 (Max.)
Others	0.05 (Max.) each 0.15 (Max.) total
Remainder	Aluminium

V. CHEMICAL ETCHING

5.1 Concept

The workpiece was covered with a maskant. Then the area exposed to the atmosphere was fully covered with NaOH pellets. The pellets were changed once in every 120 minutes and the sequence was repeated 5 times. The schematic of the chemical etching is as shown in the Fig 5.

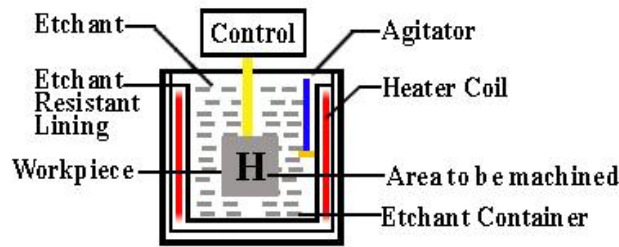


Fig 5 Schematic of chemical etching/machining [21]

5.2 Preparation of the test specimen

The test specimen was exposed to the atmosphere and the maskant was applied to it. The cross sectional view of the masked test specimen is as shown Fig 6.

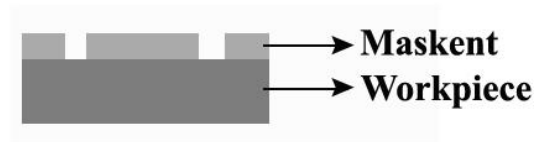


Fig 6 The workpiece and the maskant

5.3 Preparation of the maskant

A paper was taken and the alphabet "T" was drawn on it as shown in Fig 7. Then the shape was cut out as shown in Fig 7. Then the shape was placed on the test specimen.

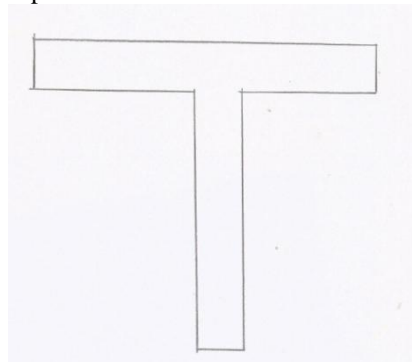


Fig 7 The alphabet "T" to be chemically etched

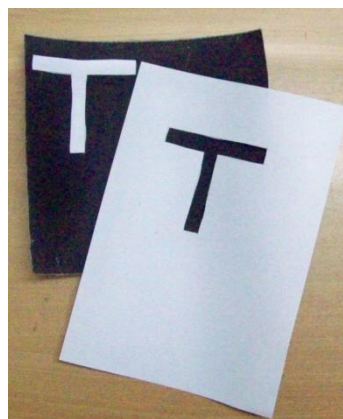


Fig 8 The "T" shape cut out as a maskant for the chemical etching

5.4 Testing the Aluminium 7075 with chemicals

The test specimen was exposed to HNO_3 and NaOH for 30 minutes. We found that NaOH was able to etch the Aluminium 7075 metal. Hence NaOH was chosen as the etchant. It is as shown in Fig 9.



Fig 9 Red box denotes the area where reaction of NaOH on the Al metal has happened

5.5 Masking the Aluminium 7075 metal

A white paper was held close to the Aluminium 7075 metal. The molten wax was poured on to the region except the region that had a “T” shaped paper. Then the “T” shaped paper was removed. Then the region was as shown in Fig 10.

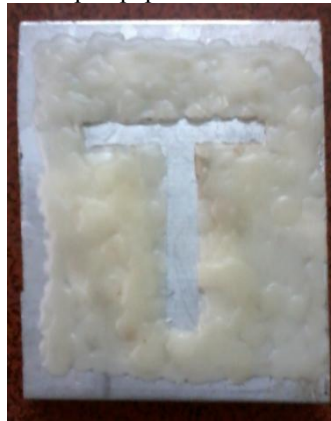


Fig 10 Wax applied as a maskant on the Al test specimen

5.6 Result of chemical etching

The region exposed to the atmosphere was filled with NaOH pellets. The NaOH was exposed to the masked Aluminium 7075 for about 600 minutes. The “T” shape was formed on the test sample. It is as shown in the Fig 11. The chemical reaction is as follows.



Fig 11 The chemically etched test specimen (the formation of the T structure)

VI. INTRODUCTION TO DEFORMATION AND ITS DEPENDENCE ON GRAINS OF A MATERIAL

Hardness of a material is a measure of its resistance to deformation. Deformation occurs by the movement of dislocation lines through the crystal lattice of materials. So, a material having higher hardness resists the movement of dislocations in its crystal. Single crystal (or single grain) materials that are homogeneous in nature with a uniform arrangement of atoms throughout the body of the material offer the least resistance to dislocation movement. The unit cell arrangement of the material is followed throughout the material allowing for easy displacement of atoms from their original lattice sites. However, materials we use in everyday life are not all single crystals. They are made up of a huge number of tiny single crystals called grains inside which a uniform orientation of the unit cells is followed, but the material as a whole

does not have a common orientation. These materials are called polycrystalline materials, since they are composed of many single crystalline grains. The common area of contact between two adjacent grains is called the grain boundary. At any grain boundary, there is a mis-match in the orientation of the crystal between the two grains that form the grain boundary. As a result, a dislocation line trying to move from one grain to another has to make some extra effort to move into the next grain. If both the grains have the same orientation, they would be just one grain by theory. The bigger the difference in orientation between two adjacent grains, the harder it is for a dislocation line to move from one to the other. This concept of grain boundaries impeding dislocation movement is used to make materials stronger. It is called grain boundary strengthening or Hall-Petch strengthening. Since dislocation movement is impeded by the presence of a grain boundary, increasing the total grain boundary area would make deformation more difficult. So, the average grain size is minimized, thus increasing the net grain boundary area.

This concept is quantified by the Hall-Petch relationship which relates the yield strength of a material to its average grain diameter.

$$\sigma_y = \sigma_0 + \frac{k}{d^{0.5}}$$

where

σ_y is the yield stress

σ_0 is a materials constant for the starting stress for dislocation movement (or the resistance of the lattice to dislocation motion)

k is the strengthening coefficient (a constant unique to each material)

d is the average grain diameter.

Mechanical strength of a material is also increased by strain hardening. Mechanical processes like machining, forging, rolling, etc. have been studied and are proven to increase the residual strain in the material. This also contributes to higher hardness values, but it also increases the brittleness along with it. The increase in hardness is attributed to the deformation of grains, breaking them down to smaller grains, thus increasing the net grain boundary area.

VII. VICKERS HARDNESS

The effects of mechanical strain hardening by CNC milling has been investigated by measuring hardness values in the direction perpendicular to the milling direction. An attempt has been made to generate a hardness value profile with respect to depth as a result of the milling. Vickers hardness measurement was done using a VM-50 model Vickers hardness tester manufactured by Fuel Instruments and Engineers Pvt. Ltd.

The metal samples whose hardness profile was to be measured was cut and the surface at which the polishing is to be done was subject to emery paper polishing ranging from size 320 (coarsest) to 1500 (finest)(changing the direction of polishing by 90 degrees for consecutive papers). After this, the sample surface was polished on a cloth using Magnesium Oxide powder of particle size ~ 1 micron, to obtain a scratch free surface for hardness measurement.

The hardness values were measured with a load of 1kgf(kilogram force) along a slanted line approximately 30° to the direction of milling in order to avoid strain hardening effects of nearby prior indentations. It was taken care that the points where readings were taken always fell within the region below the CNC milled region so that the hardness value vs depth could be plotted.



Fig 12 (Left) The cross section area where indentation was made to measure the hardness. (Right) Vickers Hardness tester

To get the reading at the surface of the milled region (i.e. at height=0), the top plane was subjected to a less intense polishing in order to leave the strain hardened region unaffected, and the hardness measured.

The Vickers Hardness is calculated as $HV = \frac{1.854 \times F}{D^2}$

Where

F is the load applied in kgf

D is the average length of the diagonals of the square indentation

VIII. RESULTS AND DISCUSSION

Three sets of data were collected for both the chemical etching and mechanically milled samples.

8.1 Hardness in Chemically etched samples

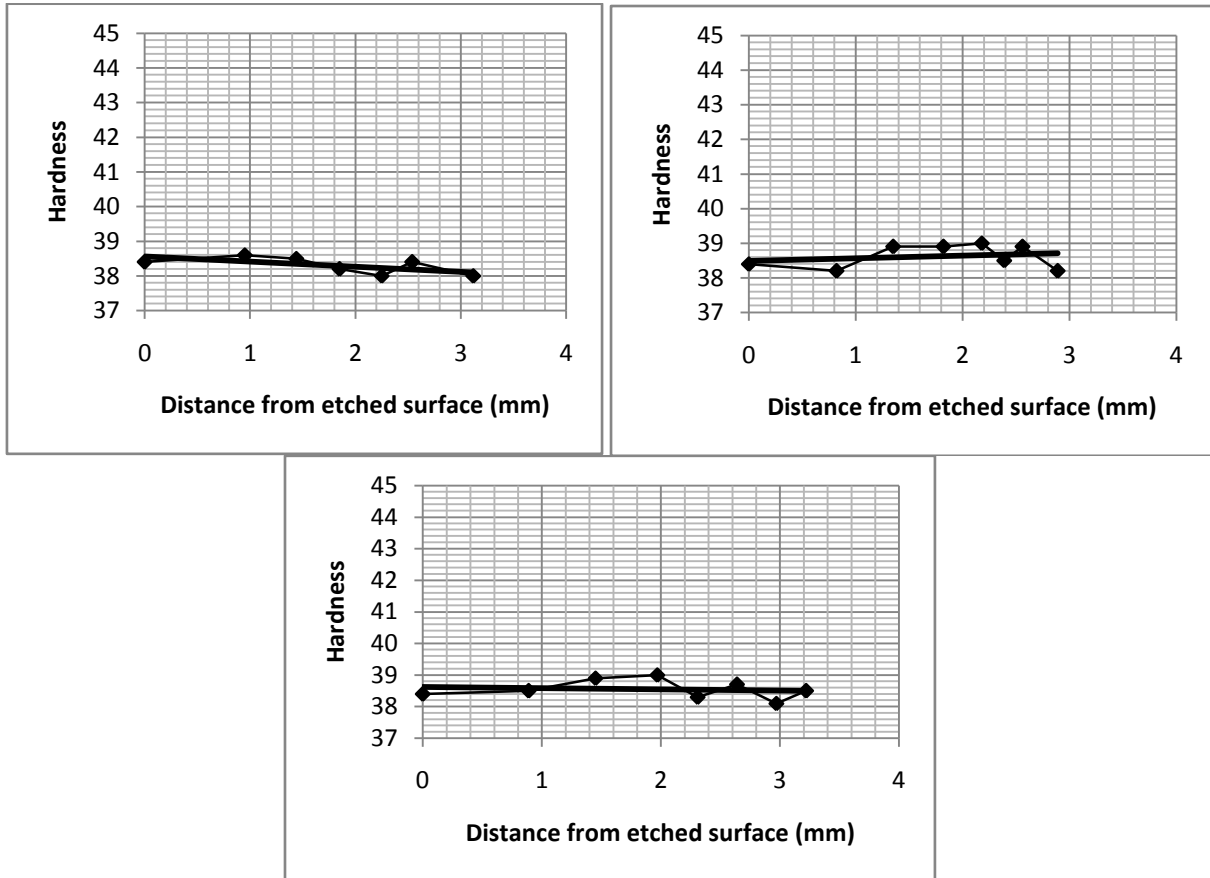


Fig 13. A plot between Hardness and Distance from etched surface

8.2 Hardness in CNC milled samples

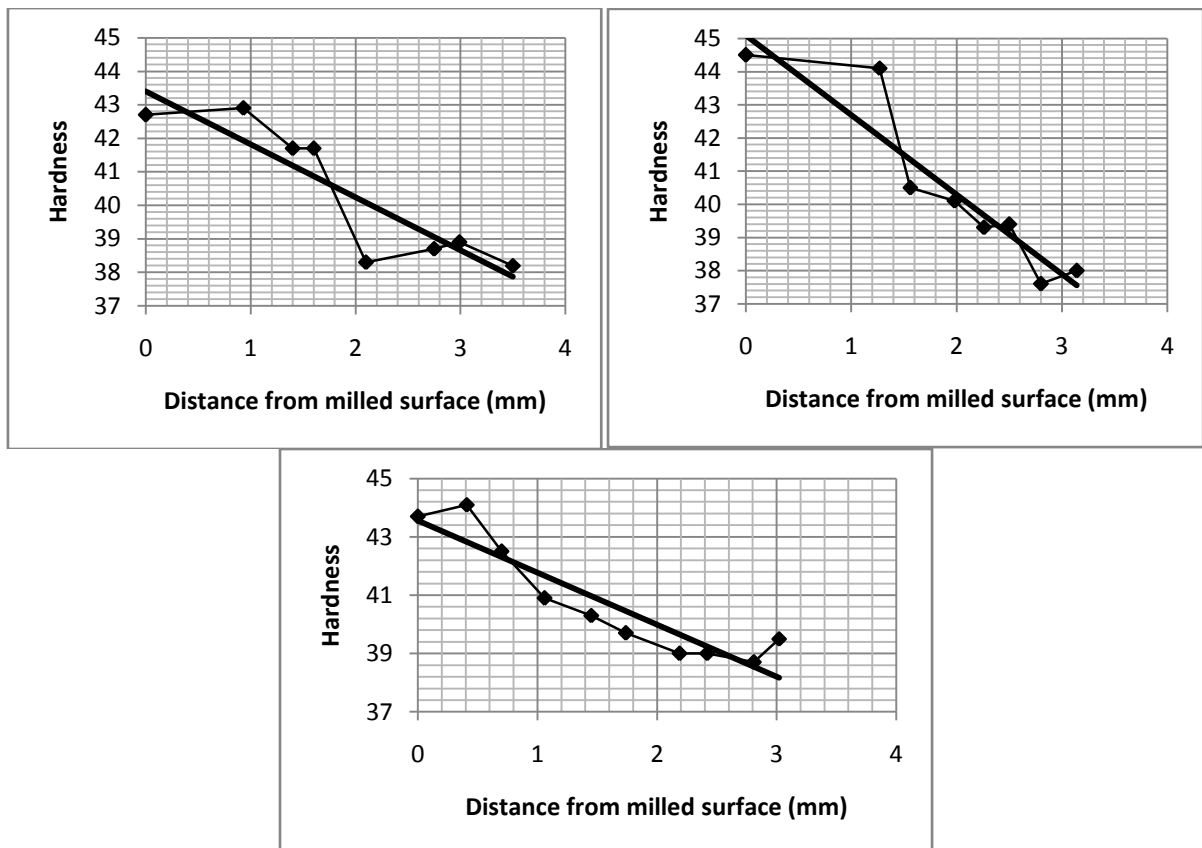


Fig 14. A plot between Hardness and Distance from milled surface

To plot the hardness data, identical scales are taken so as to see the difference in effect visually. Apart from the scatter plot of hardness value vs. depth, the trend line feature on Microsoft Excel has been used to see the pattern of the data points. Considering that the scale of the ordinate axis is taken equal in all plots, it is quite apparent that there is a good variation in the hardness values in the mechanically milled sample. To make a more quantitative analysis of this, the standard deviation and variance of the hardness values of all datasets has been calculated.

Table 2: Standard Deviation and Variance of the hardness values

Chemical		Mechanical	
Std. Deviation	Variance	Std. Deviation	Variance
0.238047614	0.056666667	2.046207293	4.18696429
0.337003603	0.113571429	2.574566538	6.62839286
0.302371578	0.091428571	2.005658662	4.02266667

Average variance of chemically etched sample hardness = 0.0872

Average variance of mechanically milled sample hardness = 4.946

It is evident from the difference of average variances that the CNC milling has in fact contributed to an increase in the hardness by producing strain hardening. The reason for this is that the chemical etching process is purely a non-mechanical process that involves no external pressure or stress on the sample.

IX. CONCLUSION

Milling and etching of metals is not so easy and involves a formation of new surfaces. Strong mechanical forces are involved in the process. This requires energy to break the bonds in the material. As mentioned previously, the chemical etching process took about 600 minutes, whereas the CNC milling is a much faster process. So, higher power is required to accomplish CNC milling and more energy is transferred to the material over a very short period of time, thus resulting in enormous forces acting on the milling surface. We would expect that the grains near the surface have been subjected to strong shear forces in the direction of milling as well as compressive forces perpendicular to the direction of milling. These forces are responsible for the deformation of the grains, leading to the accumulation of strain in them. Thus, when the region close to the CNC milled area is subjected to indentation during the Vickers hardness testing, the already strain hardened grains and higher grain boundary area offer better resistance to deformation, thus resulting in higher hardness values near the milled surface. Strain hardening effects contribute to increase in the brittleness of the material and thus make crack formation more probable at the surface. Chemical etching has not affected the properties of the material in any way, making it a safer method of engraving on metals. So, it is advisable to keep the material's properties in mind while doing CNC milling.

ACKNOWLEDGEMENTS

The authors would like to thank the management of Adhiparasakthi Engineering College for providing with necessary CAD/CAM software. They would also like to thank the management of Department of Metallurgical and Materials Engineering, Indian Institute of Technology – Roorkee and SASTRA University for providing us with instruments to measure the hardness of the metal.

REFERENCES

Journal Papers:

- [1] J. Sun, Y.B. GuoA, "Comprehensive experimental study on surface integrity by end milling Ti-6Al-4V", *Journal of Materials Processing Technology* 209, (2009), 4036-4042.
- [2] J. Xie n, H.F.Xie, X.R.Liu, T.W.Tan, "Dry micro-grooving on Si wafer using a coarse diamond grinding", *International Journal of Machine Tools & Manufacture* 61,(2012),1-8.
- [3] Justin S. Mecomber, Douglas Hurd, Patrick A. Limbach, "Enhanced machining of micron-scale features in microchip molding masters by CNC milling", *International Journal of Machine Tools & Manufacture* 45, (2005) ,1542-1550.
- [4] Toshiyuki Obikawaa, Yasuhiro Kamataa, Jun Shinozuka, "High-speed grooving with applying MQL", *International Journal of Machine Tools & Manufacture* 46, (2006), 1854-1861.
- [5] Mariana Dotcheva, Huw Millward, "The application of tolerance analysis to the theoretical and experimental evaluation of a CNC corner-milling operation", *Journal of Materials Processing Technology* 170, (2005), 284-297.
- [6] Min-Yang Yang, Taik-Min Lee, "Hybrid adaptive control based on the characteristics of CNC end milling", *International Journal of Machine Tools & Manufacture* 42, (2002) ,489-499.
- [7] Aleksandra Bierla, Guillaume Fromentin, Clotilde Minfray, Jean-Michel Martin, Thierry Le Mogne, Nicole Genet, "Mechanical and physico-chemical study of sulfur additives effect in milling of high strength steel", *Wear* 286- 287 (2012), 116- 123.
- [8] Soichi Ibaraki, Iwao Yamaji, Atsushi Matsubara, "On the removal of critical cutting regions by trochoidal grooving", *Precision Engineering* 34, (2010), 467-473.
- [9] Yih-Fang Chang, Rong-Chi Hong, "Parametric curve machining of a CNC milling EDM", *International Journal of Machine Tools & Manufacture* 45, (2005), 941-948.
- [10] Ali Lasemi, Deyi Xue, Peihua Gu, "Recent development in CNC machining of freeform surfaces: A state-of-the-art review", *Computer-Aided Design* 42, (2010), 641-654.

- [11] Lihui Wang, Peter Orban, Andrew Cunningham, Sherman Lang, "Remote real-time CNC machining for web-based manufacturing", *Robotics and Computer-Integrated Manufacturing* 20, (2004), 563–571.
- [12] Zezhong C. Chena, Zuomin Dongb, Geoffrey W. Vickers, "Automated surface subdivision and tool path generation for 3 ½ ½ -axis CNC machining of sculptured parts", *Computers in Industry* 50, (2003), 319–331.
- [13] Fadaei Tehrani, E. Imanian, "A new etchant for the chemical machining of St304", *Journal of Materials Processing Technology* 149, (2004), 404–408.
- [14] T.K.K.R. Mediliyegedara, A.K.M. De Silva, D.K. Harrison, J.A. McGeough, "An intelligent pulse classification system for electro-chemical discharge machining (ECDM)—a preliminary study", *Journal of Materials Processing Technology* 149 ,(2004) ,499–503.
- [15] S. Ho, T. Nakahara, G.D. Hibbard, "Chemical machining of nanocrystalline Ni", *Journal of materials processing technology* 208, (2008), 507–513.
- [16] J.P. Choi a, B.H. Jeon b, B.H. Kimc, "Chemical-assisted ultrasonic machining of glass", *Journal of Materials Processing Technology* 191, (2007), 153–156.
- [17] K.L. Bhondwe, Vinod Yadava, G. Kathiresan, "Finite element prediction of material removal rate due to electro-chemical spark machining", *International Journal of Machine Tools & Manufacture* 46,(2006) ,1699–1706.
- [18] Ching-Chuan Mai, Jehnming Lin, "Supersonic flow characteristics in laser grooving", *Optics & Laser Technology* 35, (2003), 597 – 604.
- [19] F. Klockea, M. Zeisa, A. Klinka, D. Veselovaca, "Technological and Economical Comparison of Roughing Strategies via Milling, EDM and ECM for Titanium- and Nickel-based Blisks", *Procedia CIRP* 2 ,(2012), 98 – 101.
- [20] Sanjay K. Chak, P. Venkateswara Rao, "Trepanning of Al₂O₃ by electro-chemical discharge machining (ECDM) process using abrasive electrode with pulsed DC supply", *International Journal of Machine Tools & Manufacture* 47 ,(2007) ,2061–2070.

Books:

- [21] Vijay K. Jain, *Advanced Machining processes* (Allied Publishers Private Limited, 2011).

Controlling Of Chaos in Modified Nicholson-Bailey Model

Debasish Bhattacharjee¹, Tarini Kumar Dutta²

¹B. Borooah College; Guwahati 781007; INDIA

²Gauhati University; Guwahati 781014; INDIA

Abstract: In this paper, a non-linear ecological map may be called as modified Nicholson-Bailey map is considered, which becomes chaotic in nature with the increase of the control parameter. As in most of the cases chaos is an unwanted phenomenon, so controlling of chaos becomes a necessary part of study. First of all Chau's method is applied on this map and the chaotic region is controlled forming periodic trajectories. Again OGY method is applied on the map to have chaos controlled. Lastly, the model has been modified to Chau's form which generates a set of fixed points which have been stabilized by OGY method.

Key Words: Chaos/Periodic orbits/Accumulation point/Control of chaos 2010 AMS Classification: 37G15, 37G35, 37C45

I. Introduction

The Nicholson-Bailey model describes the population dynamics of host-parasite (predator-prey) system and is described as follows:

$$y_{n+1} = x_n(1 - e^{-a y_n}) \dots \dots \dots x_{n+1} = L x_n e^{-a y_n} \dots \dots \dots (1.1.1)$$

Where x_{n+1} represents the number of hosts (or prey) at stage n and y_{n+1} represents number of parasites (or predator) at n^{th} stage. It has been observed [21] that the model fulfils the fact that equilibrium state never occurs for predator system in nature. Hence a modified version has been introduced by Dutta, T.K., et al [6] to restrict the unlimited growth of host (or prey), which arises in Nicholson Bailey model. The modified model is as follows:

$$y_{n+1} = x_n(1 - e^{-a y_n}) \dots \dots \dots x_{n+1} = L x_n e^{-a y_n - x_n^2} \dots \dots \dots (1.1.2)$$

In fact various modified forms have been discussed in the literature [3,6,11,14].

It has been shown that with the increase of the control parameter, the model (1.1.2) follows a period doubling bifurcation route to chaos [6]. As chaos is observed as undesirable part in engineering control. So, a desirable task is to control the chaotic region. Since 1990 after the discovery of OGY method [22], chaos control problem attracts various researchers.

We use the periodic pulse method to control chaos which was discussed by N.P. Chau, which restricts the way of choosing initial point resulting periodic orbit. Further, OGY method is applied such that the known unstable periodic point is made stable with a small disturbance in the control parameter.

II. Controlling of chaos in the map by Chau's method

Chau's theory [2] applied to the map is as follows:

The model can be written as follows:

$X_{n+1} = F(X_n)$, where X_n is a vector in R^2 . Let $G = KF^p$, where K is a diagonal matrix having the diagonal elements say k_1, k_2 , and F^p is the composition map of F up to p times. If X is a fixed point of G i.e. $KF^p(X) = X$, then the fixed point will be stable if the absolute value of the largest eigen value of the Jacobian matrix of G is less than 1. The next step is to get the value of k_1, k_2 , such that chaos is controlled.

For p=1,

The Jacobian matrix of G is as follows:

$$\begin{pmatrix} k_1 & 0 \\ 0 & k_2 \end{pmatrix} \begin{pmatrix} e^{-x^2-ay}(1-2x^2)L & -aLxe^{-x^2-ay} \\ 1 - e^{-ay} & axe^{-ay} \end{pmatrix}$$

i.e.

$$\begin{pmatrix} k_1 e^{-x^2-ay}(1-2x^2)L & -aLxe^{-x^2-ay} \\ 1 - e^{-ay} & k_2 axe^{-ay} \end{pmatrix} \quad (1.2.1)$$

The fixed points will be stable if $|\lambda| < 1$, where λ is the eigen value of the Jacobian matrix.

If $X=(x,y)$ is the fixed point of G, then

$$k_1 L x e^{-a y - x^2} = x, \text{ considering } x \neq 0, \text{ we have } k_1 = \frac{1}{L e^{-a y - x^2}} \quad \text{Similarly} \quad k_2 = \frac{y}{x(1 - e^{-a y})}$$

(1.2.2) We choose (x,y) such that absolute value of λ is less than 1.

The basin of (x,y) chosen such that it satisfies both (1.2.1) and (1.2.2) is shown graphically as follows:

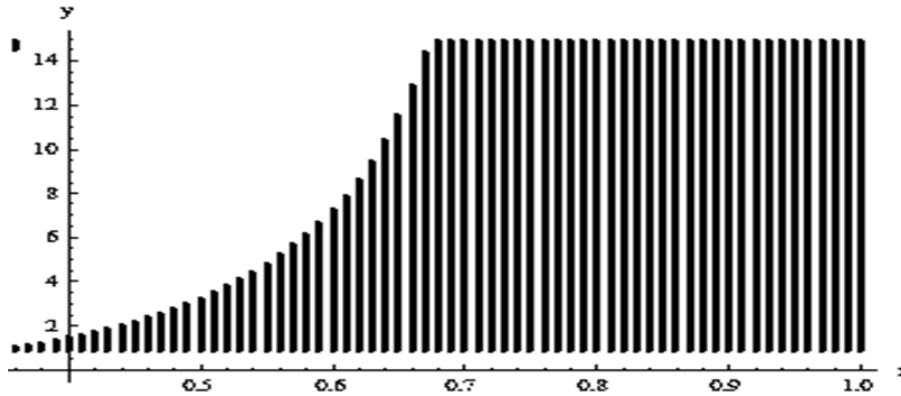


Fig: 1.2.1 Above picture shows the the value of x,y which for particular value of k_1, k_2 and $p=1$ becomes a stable fixed point for $L=3.85$ and $a=0.1$;

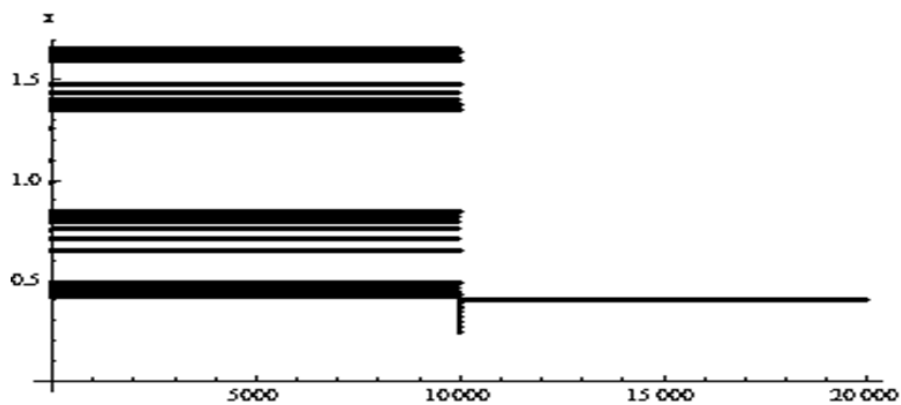


Fig: 1.2.2: Above figure shows the chaotic region up to 10000 iterations after which chaos control key k_1, k_2 is activated to make x fixed.

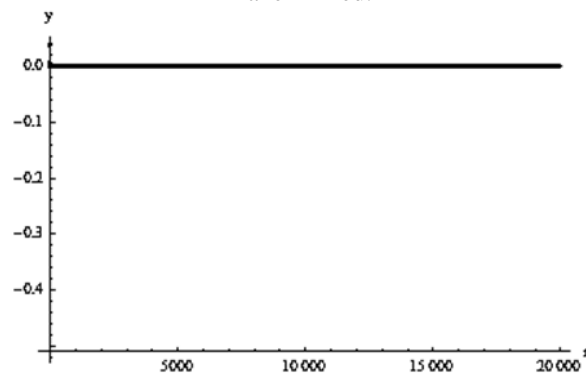


Fig: 1.2.3: In the above figure it is clear that y co-ordinate already achieves the fixed value as iteration proceeds.

Thus as a whole it is clear that once the chaos controlling switch is turned on, the trajectory points (x,y) achieves stability to form a fixed point as iteration proceeds.

If it is desired to obtain a periodic trajectory of period p, we have,

$$k_1 = \frac{x}{x_{p-1} e^{r \left(1 - \frac{x_{p-1}}{k}\right) - b y_{p-1}}}, k_2 = \frac{x}{1 - e^{-a y_{p-1}}}$$

Where x_{p-1} =first component of f^{p-1} and y_{p-1} is the second component of f^{p-1} . And the Jacobian matrix is given as

$$\begin{pmatrix} k_1 & 0 \\ 0 & k_2 \end{pmatrix} \begin{pmatrix} \frac{\partial x_p}{\partial x} & \frac{\partial x_p}{\partial y} \\ \frac{\partial y_p}{\partial x} & \frac{\partial y_p}{\partial y} \end{pmatrix}$$

For $p=2$;

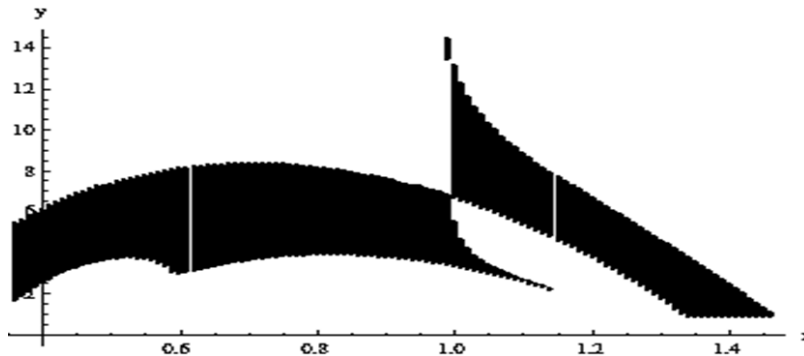


Fig: 1.2.3 Above picture shows the value of x, y which for particular value of k_1, k_2 and $p=2$ becomes a stable fixed point for $L=3.85$ and $a=0.1$;

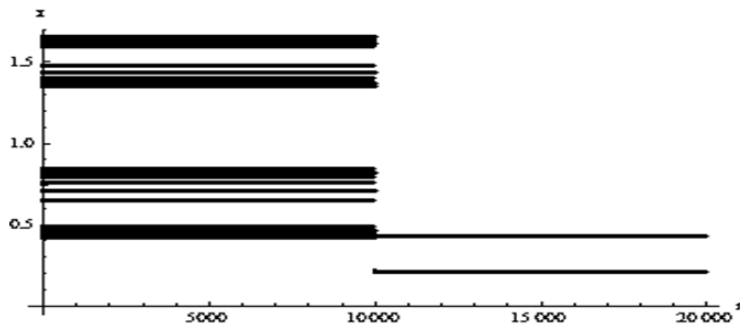


Fig: 1.2.4: Above figure shows the chaotic region up to 10000 iterations after which chaos control key k_1, k_2 is activated to make x fixed.

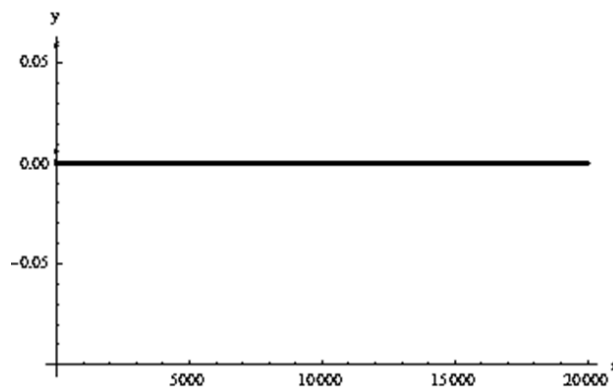


Fig: 1.2.5: In the above figure it is clear that y co-ordinate already achieves the fixed value as iteration proceeds.

For $p=4$, we have

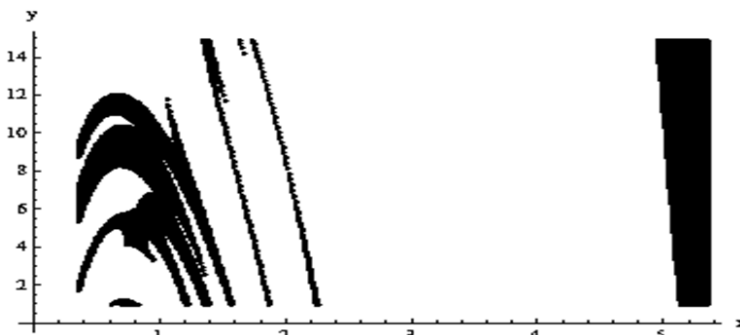


Fig: 1.2.6: Above picture shows the the value of x, y which for particular value of k_1, k_2 and $p=2$ becomes a stable fixed point for $L=3.85$ and $a=0.1$;

It has been observed that the pool of data as shown in the figure above although serve the purpose of a stable periodic point of period two, they are not always able to attract the trajectory towards them as the radius of the basin of attraction is small enough. Thus although stable periodic points are created by the kicking method, chaos may not be controlled unless the starting point lies in the basin of attraction.

Similarly the basin of periodic points of period 8 is created which are stable with the help of a suitable computer program.

For p=8;

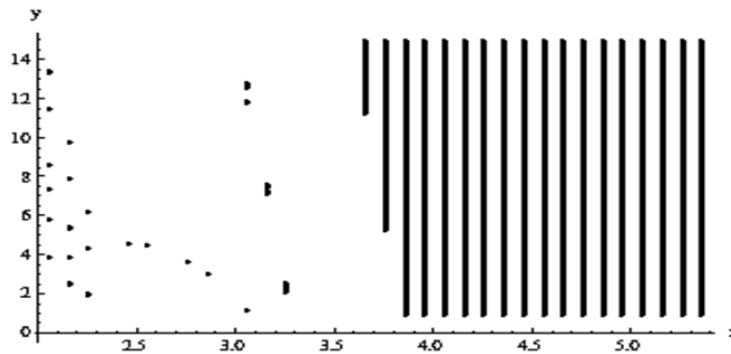


Fig:1.2.7: Above picture shows the the value of x,y which for particular value of k_1, k_2 and $p=2$ becomes a stable fixed point for $L=3.85$ and $a=0.1$;

III. Controlling of chaos in the map by OGY method

The OGY method [16,22] applied is as follows:

Let the two dimensional map (1.1.2) be written as :

$Z_{n+1} = f(Z_n, L)$. Let $Z_s(L)$ be an unstable fixed point of equation (1.1.2). For values of L near L_0 (say) in a small neighborhood of $Z_s(L_0)$. The map can be approximated by a linear map given by

$$Z_{n+1} - Z_s(L_0) = J(Z_n - Z_s(L_0)) + C(L - L_0) \dots \dots \dots (1.3.1)$$

Where J is the Jacobian and C is $\frac{\partial f}{\partial L}$, at the point $Z_s(L_0)$. Assuming that in a small neighbourhood around the fixed point

$L - L_0 = -K(Z_n - Z_s(L_0))$, where K is a constant vector of dimension 2 to be determined. Then the equation (1.3.1) becomes

$$Z_{n+1} - Z_s(L_0) = (J - CK)(Z_n - Z_s(L_0)) \dots \dots \dots (1.3.2)$$

Using equation (1.3.2) at the parameter value $L=3.85$, a time series plot is shown below, where after 300 iterations, chaos is switched on.

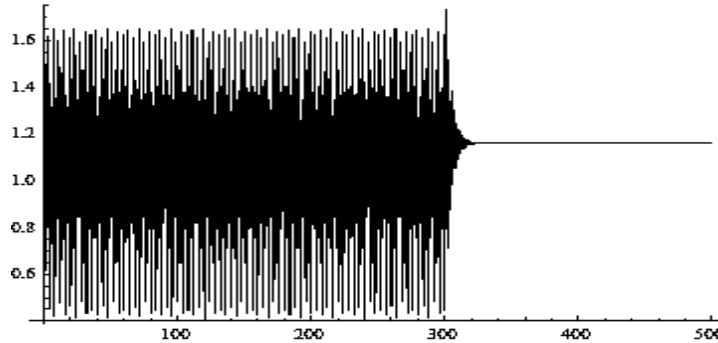


Fig: 1.3.a: Time series graph showing chaos control.

IV. Applying OGY method on Chau's method

Let (x^*, y^*) be a point and let the modified equation of (1.1.2) be

$$x_{n+1} = \frac{x_n e^{-a y_n - x_n^2}}{e^{-a y^* - x^{*2}}}$$

$$y_{n+1} = \frac{x_n (1 - e^{-a y_n}) y^*}{x^* (1 - e^{-a y^*})} \dots \dots \dots (1.4.1)$$

Which may be written as $h(x, y) = (f(x, y), g(x, y))$, where $f(x, y) = \frac{x e^{-a y - x^2}}{e^{-a y^* - x^{*2}}}$, $g(x, y) = \frac{x (1 - e^{-a y}) y^*}{x^* (1 - e^{-a y^*})}$, clearly $h(x^*, y^*) = (x^*, y^*)$. We

consider $x^* = f_1(L), y^* = f_2(L)$, which helps to calculate $C = \begin{pmatrix} \frac{\partial f}{\partial L} \\ \frac{\partial g}{\partial L} \end{pmatrix}$. Now applying equation (1.3.2) we have

$$\begin{pmatrix} x_{n+1} \\ y_{n+1} \end{pmatrix} = \begin{pmatrix} x^* \\ y^* \end{pmatrix} + (J - CK) \begin{pmatrix} x_n - x^* \\ y_n - y^* \end{pmatrix} \dots \dots \dots (1.4.2)$$

Equation (1.4.2) says that $\begin{pmatrix} x^* \\ y^* \end{pmatrix}$ is a fixed point whose stability will be determined the eigen values of $J-CK$, where $K = \begin{pmatrix} k_1 & 0 \\ 0 & k_2 \end{pmatrix}$. If λ_1, λ_2 be two eigenvalues then k_1, k_2 are to be determined in such a way that $-1 < |\lambda_1|, |\lambda_2| < 1$. Calculating $J-CK$, we have

$$J-CK = \begin{pmatrix} A_1 & B_1 \\ C_1 & D_1 \end{pmatrix}, \text{ where}$$

$$A_1 = 1 - 2f(L)^2 - k_1f(L)(2f(L)f'(L) + ag'(L))$$

$$B_1 = -af(L) - k_2f(L)(2f(L)f'(L) + ag'(L))$$

$$C_1 = \frac{g[L]}{f[L]} - k_1 \left\{ -\frac{g(L)f'(L)}{f(L)} + g'(L) - \frac{ae^{-ag(L)}g(L)g'(L)}{(1-e^{-ag(L)})} \right\}$$

$$D_1 = \frac{ae^{-ag(L)}g(L)}{(1-E^{-ag(L)})} - k_2 \left\{ -\frac{g(L)f'(L)}{f(L)} + g'(L) - \frac{ae^{-ag(L)}g(L)g'(L)}{(1-e^{-ag(L)})} \right\}$$

Let $a_1 = 1 - 2f(L)^2, a_2 = f(L)(2f(L)f'(L) + ag'(L))$,

$b_1 = -af(L), b_2 = f(L)(2f(L)f'(L) + ag'(L))$,

$c_1 = \frac{g[L]}{f[L]}, c_2 = -\frac{g(L)f'(L)}{f(L)} + g'(L) - \frac{ae^{-ag(L)}g(L)g'(L)}{(1-e^{-ag(L)})}$

$d_1 = \frac{ae^{-ag(L)}g(L)}{(1-E^{-ag(L)})}, d_2 = -\frac{g(L)f'(L)}{f(L)} + g'(L) - \frac{ae^{-ag(L)}g(L)g'(L)}{(1-e^{-ag(L)})}$

Then the matrix J-CK = $\begin{pmatrix} a_1 - k_1 a_2 & b_1 - k_2 b_2 \\ c_1 - k_1 c_2 & d_1 - k_2 d_2 \end{pmatrix}$

Whose eigen values are

$\lambda_{1,2}$

$= \frac{1}{2} (a_1 + d_1 - a_2 k_1 - d_2 k_2$

$\pm \sqrt{(a_1 + d_1 - a_2 k_1 - d_2 k_2)^2 + 4(-a_1 d_1 + b_1(c_1 - c_2 k_1) + (-b_2 c_1 + a_1 d_2 + b_2 c_2 k_1)k_2 + a_2 k_1(d_1 - d_2 k_2))}$

Taking $x^*=y^*=L/3$, and following the above theory, we have controlled chaos at $L=3.85, a=0.1$.

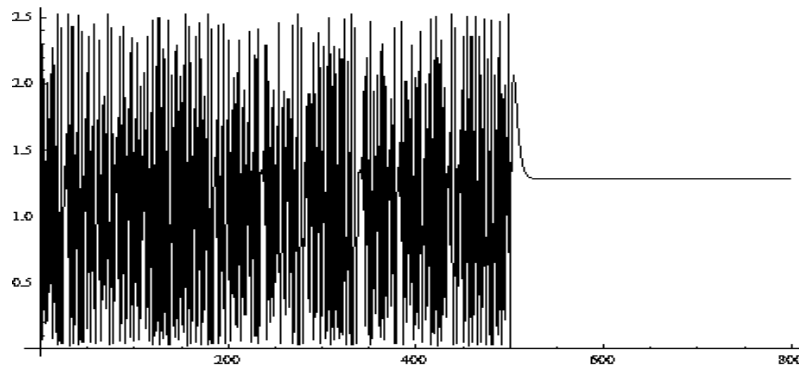


Fig: 1.4.a representing chaos upto iteration 500 and then control switch is turned on till 800 iteration converging to the stable x-coordinate $L/3$.

References

- [1] Beddington, J.R., Free, C.A., Lawton, J.H., "Dynamic Complexity in predator-prey models framed in difference equations", Nature, 225(1975),58-60.
- [2] Chau, N.L., "Controlling Chaos by periodic proportional pulses", physics Letters A, 234 (1997), 193-197.
- [3] Comins, H.N., Hassel, M.P., May, R., "The spatial dynamics of host-parasitoid systems", Journal of Animal Ecology, vol-61(1992), pp-735-748.
- [4] Dutta, T.K., Bhattacharjee, D., "Stability and Feigenbaum's Universality in a two dimensional non-linear map", International Journal of Mathematics and Analysis, in press.
- [5] Dutta, T.K., Bhattacharjee, D., "Bifurcation Points, Lyapunov Exponent and Fractal Dimensions in a Non Linear Map", Advances in Theoretical and Applied Mathematics, Vol-7, No-3(2012), LL. 223-235.
- [6] Dutta, T.K., Bhattacharjee, D., Bhuyan, B.R., "Some Dynamical Behaviours of a Two Dimensional Non Linear Map", IJMER, Vol-2, No-6, 2012.
- [7] Falconer, K.J., "Fractal Geometry: Mathematical Foundations and Applications", John Wiley publication.
- [8] Feigenbaum, M.J., "Qualitative Universality for a class of non-linear transformations", J.Statist.Phys, 19:1(1978), 25-52.
- [9] Feigenbaum, M.J., "Universality Behavior in non-linear systems", Los Alamos Science, 1.(1980), 4-27.
- [10] Gottlieb, H.L.W., "Properties of Some Generalised Logistic Maps With Fractional Exponents", Complexity International, vol.2, 1995
- [11] Hassel, M.P., Comins, H.N., May, R., "Spatial structure of chaos in insect population dynamics", Nature, Vol-353(1991), pp-255-258.
- [12] Henon, M., "A two dimensional mapping with a strange attractor", Comm. Math. phys. Lett.A 300(2002), 182-188
- [13] Hilborn, R.C., "Chaos and Non-linear dynamics", Oxford Univ. Press. 1994.
- [14] Hone, A.N.W., Irlé, M.V., Thurera, G.W., "On the Neimark-Sacker bifurcation in a discrete Predator-Prey system", 2009.
- [15] Kuznetsov, Y., "Elements of Applied Bifurcation Theory", Springer(1998).
- [16] Lynch, S., "Dynamical Systems with Applications Using Mathematica", Birkhäuser
- [17] Matias, M.A., Guemez, J., "Stabilization of Chaos by Proportional Pulses in the System Variables", Vol.72, No.10(1994)1455-1460.
- [18] May, R.M., "Simple Mathematical Models With Very Complicated Dynamics", Nature, Vol.261(1976), 459.
- [19] Murray, J.D., "Mathematical Biology I: An Introduction", Third Edition, Springer.
- [20] Murray, J.D., "Mathematical Biology II: Spatial Models and Biomedical Applications", Springer.
- [21] Nicholson, A.J., Bailey V.A., "The Balance of Animal Populations-Part-1", Proceedings of the Zoological Society of London, Vol-105, issue-3(1935), pp-551-598
- [22] Ott, E., Grebogi, C., and Yorke, J. A., "Controlling chaos," Phys. Rev.Lett., vol. 64, no. 11, LL. 1196-1199, 1990.

Hiding Data Transmission with High Security in Cloud Computing with Cloud Server

Fahmida Begum¹, K. Bhargavi², Venkateswarlu Maninti³

¹Asso.Professor, Dept. of MCA, Dr. K.V Subba Reddy college of MCA, Kurnool. (Dt), A.P,

²Asst. Professor in MCA Dept. Palamuru University,

³Asst. Professor, Dept. of IT, Fishermen Training Institute, Salalah, Sultante of Oman,

ABSTRACT : Cloud computing economically enables the paradigm of data service outsourcing. However, to protect data privacy, sensitive cloud data has to be encrypted before outsourced to the commercial public cloud, which makes effective data utilization service a very challenging task. Focusing on engineering computing and optimization tasks, this paper investigates secure outsourcing of widely applicable linear programming computations. In order to achieve practical efficiency, our mechanism design explicitly decomposes the LP computation outsourcing into public LP solvers running on the cloud and private LP parameters owned by the customer. The resulting flexibility allows us to explore appropriate security/ efficiency tradeoff via higher-level abstraction of LP computations than the general circuit representation. The result verification mechanism is extremely efficient and incurs close-to-zero additional cost on both cloud server and customers. Extensive security analysis and experiment results show the immediate practicability of our mechanism design.

Keywords: Confidential data, Computation Outsourcing, Optimization, Cloud Computing.

I. INTRODUCTION

Cloud Computing provides convenient on-demand network access to a shared pool of configurable computing resources that can be rapidly deployed with great efficiency and minimal management overhead. The fundamental advantage of the cloud paradigm is computation outsourcing, where the computational power of cloud customers is no longer limited by their resource-constraint devices. By outsourcing the workloads into the cloud, customers could enjoy the literally unlimited computing resources in a pay-per-use manner without committing any large capital outlays in the purchase of both hardware and software and/or the operational overhead therein. On the one hand, the outsourced computation workloads often contain sensitive information, such as the business financial records, proprietary research data, or personally identifiable health information etc. To combat against unauthorized information leakage, sensitive data have to be encrypted before outsourcing so as to provide end to- end data confidentiality assurance in the cloud and beyond. On the other hand, the operational details inside the cloud are not transparent enough to customers .For example, for the computations that require a large amount of computing resources, there are huge financial incentives for the cloud to be “lazy” if the customers cannot tell the correctness of the output. Besides, possible software bugs, hardware failures, or even outsider attacks might also affect the quality of the computed results. Thus, we argue that the cloud is intrinsically not secure from the viewpoint of customers. Without providing a mechanism for secure computation outsourcing, i.e., to protect the sensitive input and output information of the workloads and to validate the integrity of the computation result, it would be hard to expect cloud customers to turn over control of their workloads from local machines to cloud solely based on its economic savings and resource flexibility. For practical consideration, such a design should further ensure that customers perform less amount of operations following the mechanism than completing the computations by themselves directly.

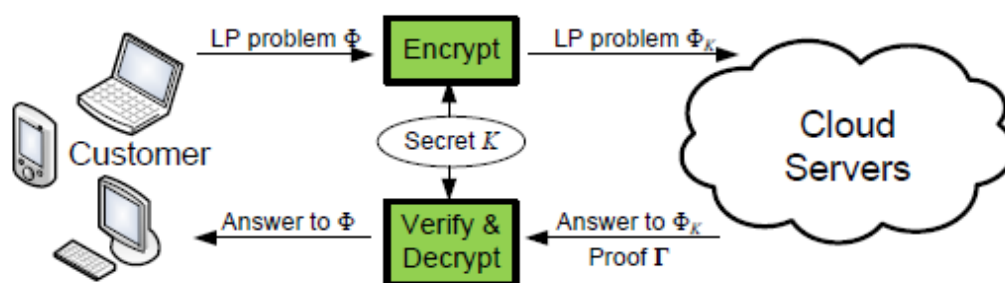


Fig1. Architecture of secure outsourcing linear programming problems in Cloud Computing

In this paper, we study practically efficient mechanisms for secure outsourcing of linear programming (LP) computations. Linear programming is an algorithmic and computational tool which captures the first order effects of various system parameters that should be optimized, and is essential to engineering optimization. It has been widely used in various engineering disciplines that analyze and optimize real-world systems, such as packet routing, flow control, power management of data centers, etc. Because LP computations require a substantial amount of computational power and usually involve confidential data, we propose to explicitly decompose the LP computation outsourcing into public LP solvers running on the cloud and private LP parameters owned by the customer. The flexibility of such a decomposition allows us to explore higher-level abstraction of LP computations than the general circuit representation for the practical efficiency.

II. PROBLEM DEFINITION

On the one hand, the outsourced computation workloads often contain sensitive information, such as the business financial records, proprietary research data, or personally identifiable health information etc. To combat against unauthorized information leakage, sensitive data have to be encrypted before outsourcing so as to provide end-to-end data confidentiality assurance in the cloud and beyond. However, ordinary data encryption techniques in essence prevent cloud from performing any meaningful operation of the underlying plaintext data, making the computation over encrypted data a very hard problem. On the other hand, the operational details inside the cloud are not transparent enough to customers. As a result, there do exist various motivations for cloud server to behave unfaithfully and to return incorrect results, i.e., they may behave beyond the classical semi honest model.

Fully homomorphic encryption (FHE) scheme, a general result of secure computation outsourcing has been shown viable in theory, where the computation is represented by an encrypted combinational Boolean circuit that allows to be evaluated with encrypted private inputs.

III. EXISTING SYSTEM:

Despite the tremendous benefits, outsourcing computation to the commercial public cloud is also depriving customers direct control over the systems that consume and produce their data during the computation, which inevitably brings in new security concerns and challenges towards this promising computing model. On the one hand, the outsourced computation workloads often contain sensitive information, such as the business financial records, proprietary research data, or personally identifiable health information etc.

To combat against unauthorized information leakage, sensitive data have to be encrypted before outsourcing, so as to provide end-to-end data confidentiality assurance in the cloud and beyond. However, ordinary data encryption techniques in essence prevent cloud from performing any meaningful operation of the underlying plaintext data, making the computation over encrypted data a very hard problem. On the other hand, the operational details inside the cloud are not transparent enough to customers. As a result, there do exist various motivations for cloud server to behave unfaithfully and to return incorrect results, i.e., they may behave beyond the classical semi honest model. Thus, we argue that the cloud is intrinsically not secure from the viewpoint of customers.

Disadvantages of Existing System:

- 1) Fully homomorphic encryption (FHE) scheme, a general result of secure computation outsourcing has been shown viable in theory.
- 2) The cryptography and the theoretical computer science communities have made steady advances in “secure outsourcing expensive computations”.
- 3) It is Semi-Honest Model.

IV. PROPOSED SYSTEM

Cloud computing economically enables the paradigm of data service outsourcing. However, to protect data privacy, sensitive cloud data has to be encrypted before outsourced to the commercial public cloud, which makes effective data utilization service a very challenging task. Focusing on engineering computing and optimization tasks, this paper investigates secure outsourcing of widely applicable linear programming computations. In order to achieve practical efficiency, our mechanism design explicitly decomposes the LP computation outsourcing into public LP solvers running on the cloud and private LP parameters owned by the customer. The resulting flexibility allows us to explore appropriate security/ efficiency tradeoff via higher-level abstraction of LP computations than the general circuit representation. The result verification mechanism is extremely efficient and incurs close-to-zero additional cost on both cloud server and customers. Extensive security analysis and experiment results show the immediate practicability of our mechanism design.

ADVANTAGES:

- 1) To combat against unauthorized information leakage, sensitive data have to be encrypted before outsourcing.
- 2) To provide end-to-end data confidentiality assurance in the cloud and beyond.
- 3) The operational details inside the cloud are not transparent enough to customers.

V. MODULE DESCRIPTION

A) Mechanism Design Framework:

We propose to apply problem transformation for mechanism design. The general framework is adopted from a generic approach, while our instantiation is completely different and novel. In this framework, the process on cloud server can be represented by algorithm ProofGen and the process on customer can be organized into three algorithms (KeyGen, ProbEnc, ResultDec). These four algorithms are summarized below and will be instantiated later.

- KeyGen($1k$) \rightarrow $\{K\}$. This is a randomized key generation algorithm which takes a system security parameter k , and returns a secret key K that is used later by customer to encrypt the target LP problem.
- ProbEnc(K, \emptyset) \rightarrow $\{\emptyset k\}$. This algorithm encrypts the input tuple \emptyset into $\emptyset k$ with the secret key K . According to problem transformation, the encrypted input $\emptyset k$ has the same form as \emptyset , and thus defines the problem to be solved in the cloud.
- ProofGen($\emptyset k$) \rightarrow $\{(y, \Gamma)\}$. This algorithm augments a generic solver that solves the problem K to produce both the output y and a proof Γ . The output y later decrypts to x , and is used later by the customer to verify the correctness of y or x .

• ResultDec(K, \emptyset, y, Γ) $\rightarrow \{x, \perp\}$. This algorithm may choose to verify either y or x via the proof Γ . In any case, a correct output x is produced by decrypting y using the secret K . The algorithm outputs \perp when the validation fails, indicating the cloud server was not performing the computation faithfully.

B) Basic Techniques:

Before presenting the details of our proposed mechanism, we study in this subsection a few basic techniques and show that the input encryption based on these techniques along may result in an unsatisfactory mechanism. However, the analysis will give insights on how a stronger mechanism should be designed. Note that to simplify the presentation, we assume that the cloud server honestly performs the computation, and defer the discussion on soundness to a later section.

1) Hiding equality constraints (A, b): First of all, a randomly generated $m \times m$ non-singular matrix Q can be part of the secret key K . The customer can apply the matrix to Eq.

(2) for the following constraints transformation, $Ax = b \rightarrow A'x = b'$

where $A' = QA$ and $b' = Qb$.

C) Enhanced Techniques via Affine Mapping:

To enhance the security strength of LP outsourcing, we must be able to change the feasible region of original LP and at the same time hide output vector x during the problem input encryption. We propose to encrypt the feasible region of \emptyset by applying an affine mapping on the decision variables x . This design principle is based on the following observation: ideally, if we can arbitrarily transform the feasible area of problem \emptyset from one vector space to another and keep the mapping function as the secret key, there is no way for cloud server to learn the original feasible area information. Further, such a linear mapping also serves the important purpose of output hiding.

D) RESULT VERIFICATION:

Till now, we have been assuming the server is honestly performing the computation, while being interested learning information of original LP problem.

However, such semi honest model is not strong enough to capture the adversary behaviors in the real world. In many cases, especially when the computation on the cloud requires a huge amount of computing resources, there exists strong financial incentives for the cloud server to be "lazy". They might either be not willing to commit service-level-agreed computing resources to save cost, or even be malicious just to sabotage any following up computation at the customers. Since the cloud server promises to solve the LP problem $\emptyset_k = (A', B', b', c')$, we propose to solve the result verification problem by designing a method to verify the correctness of the solution y of \emptyset_k . The soundness condition would be a corollary thereafter when we present the whole mechanism in the next section. Note that in our design, the workload required for customers on the result verification is substantially cheaper than solving the LP problem on their own, which ensures the great computation savings for secure LP outsourcing.

The LP problem does not necessarily have an optimal solution. There are three cases as follows.

- Normal: There is an optimal solution with finite objective value.
- Infeasible: The constraints cannot be all satisfied at the same time.
- Unbounded: For the standard form, the objective function can be arbitrarily small while the constraints are all satisfied.

VI. PERFORMANCE ANALYSIS

A) THEORETIC ANALYSIS:

1) CUSTOMER SIDE OVERHEAD:

According to our mechanism, customer side computation overhead consists of key generation, problem encryption operation, and result verification, which corresponds to the three algorithms KeyGen, ProbEnc, and ResultDec, respectively. Because KeyGen and Result-Dec only require a set of random matrix generation as well as vector-vector and matrix-vector multiplication, the computation complexity of these two algorithms are upper bounded via $O(n^2)$. Thus, it is straight-forward that the most time consuming operations are the matrix-matrix multiplications in problem encryption algorithm ProbEnc. Since $m \leq n$, the time complexity for the customer local computation is thus asymptotically the same as matrix-matrix multiplication, i.e., $O(n\rho)$ for some $2 < \rho \leq 3$. In our experiment, the matrix multiplication is implemented via standard cubic-time method, thus the overall computation overhead is $O(n^3)$. However, other more efficient matrix multiplication algorithms can also be adopted, such as the Strassen's algorithm with time complexity $O(n^{2.81})$. In either case, the over all customer side efficiency can be further improved.

2) SERVER SIDE OVERHEAD:

For cloud server, its only computation overhead is to solve the encrypted LP problem \emptyset_k as well as generating the result proof Γ , both of which correspond to the algorithm ProofGen. If the encrypted LP problem \emptyset belongs to normal case, cloud server just solves it with the dual optimal solution as the result proof Γ , which is usually readily available in the current LP solving algorithms and incurs no additional cost for cloud. If the encrypted problem \emptyset_k does not have an optimal solution, additional auxiliary LP problems can be solved to provide a proof. Because for general LP solvers, executed at first to determine the initial feasible solution, proving the auxiliary LP with optimal solutions also introduces little additional overhead. Thus, in all the cases, the computation complexity of the cloud server is asymptotically the same as to solve a normal LP problem, which usually requires more than $O(n^3)$ time. Obviously, the customer will not spend more time to

encrypt the problem and solve the problem in the cloud than to solve the problem on his own. Therefore, in theory, the proposed mechanism would allow the customer to outsource their LP problems to the cloud and gain great computation savings.

3) EXPERIMENT RESULTS:

We now assess the practical efficiency of the proposed secure and verifiable LP outsourcing scheme with experiments. We implement the proposed mechanism including both the customer and the cloud side processes in Matlab and utilize the MOSEK optimization through its MATLAB interface to solve the original LP problem and encrypted LP problem ϕ_k . Both customer and cloud server computations in our experiment are conducted on the same workstation with an Intel Core 2 Duo processor running at 1.86 GHz with 4 GB RAM. In this way, the practical efficiency of the proposed mechanism can be assessed without a real cloud environment. We also ignore the communication latency between the customers and the cloud for this application since the computation dominates the running time as evidenced by our experiments.

VII. CONCLUSIONS

We formalize the problem of securely outsourcing LP Computations in cloud computing, and provide such a practical mechanism design which fulfills input/output privacy, cheating resilience, and efficiency. By explicitly decomposing LP computation outsourcing into public LP solvers and private data, our mechanism design is able to explore appropriate security/efficiency tradeoffs via higher level LP computation than the general circuit representation. We develop problem transformation techniques that enable customers to secretly transform the original LP into some arbitrary one while protecting sensitive input/output information. We also investigate duality theorem and derive a set of necessary and sufficient condition for result verification. Such a cheating resilience design can be bundled in the overall mechanism with close-to-zero additional overhead. Both security analysis and experiment results demonstrates the immediate practicality of the proposed mechanism.

LITERATURE REFERENCES

- [1] P. Mell and T. Grance, "Draft nist working definition of cloud computing," Referenced on Jan. 23rd, 2010 Online at <http://src.nist.gov/groups/SNS/cloud-computing/index.html>, 2010.
- [2] Cloud Security Alliance, "Security guidance for critical areas of focus in cloud computing," 2009, online at <http://www.cloudsecurityalliance.org>.
- [3] C. Gentry, "Computing arbitrary functions of encrypted data," *Commun. ACM*, vol. 53, no. 3, pp. 97–105, 2010.
- [4] Sun Microsystems, Inc., "Building customer trust in cloud computing with transparent security," 2009, online at https://www.sun.com/offers/details/sun_transparency.xml.
- [5] M. J. Atallah, K. N. Pantazopoulos, J. R. Rice, and E. H. Spafford, "Secure outsourcing of scientific computations," *Advances in Computers*, vol. 54, pp. 216–272, 2001.
- [6] S. Hohenberger and A. Lysyanskaya, "How to securely outsource cryptographic computations," in *Proc. of TCC*, 2005, pp. 264–282.
- [7] M. J. Atallah and J. Li, "Secure outsourcing of sequence comparisons," *Int. J. Inf. Sec.*, vol. 4, no. 4, pp. 277–287, 2005.
- [8] D. Benjamin and M. J. Atallah, "Private and cheating-free outsourcing of algebraic computations," in *Proc. of 6th Conf. on Privacy, Security, and Trust (PST)*, 2008, pp. 240–245.
- [9] R. Gennaro, C. Gentry, and B. Parno, "Non-interactive verifiable computing: Outsourcing computation to untrusted workers," in *Proc. Of CRYPTO'10*, Aug. 2010.
- [10] M. Atallah and K. Frikken, "Securely outsourcing linear algebra computations," in *Proc. of ASIACCS*, 2010, pp. 48–59.
- [11] A. C.-C. Yao, "Protocols for secure computations (extended abstract)," in *Proc. of FOCS'82*, 1982, pp. 160–164.
- [12] C. Gentry, "Fully homomorphic encryption using ideal lattices," in *Proc of STOC*, 2009, pp. 169–178.
- [13] D. Luenberger and Y. Ye, *Linear and Nonlinear Programming*, 3rd ed. Springer, 2008.
- [14] C. Wang, N. Cao, J. Li, K. Ren, and W. Lou, "Secure ranked keyword search over encrypted cloud data," in *Proc. of ICDCS'10*, 2010.
- [15] S. Yu, C. Wang, K. Ren, and W. Lou, "Achieving secure, scalable, and fine-grained access control in cloud computing," in *Proc. of IEEE INFOCOM'10*, San Diego, CA, USA, March 2010.
- [16] S. Boyd and L. Vandenberghe, *Convex Optimization*. Cambridge University Press, 2004.
- [17] D. Coppersmith and S. Winograd, "Matrix multiplication via arithmetic progressions," in *Proc. of STOC'87*, 1987, pp. 1–6.
- [18] P. Paillier, "Public-key cryptosystems based on composite degree residuosity classes," in *Proc. Of EUROCRYPT'99*, 1999, pp. 223–238.
- [19] J. Li and M. J. Atallah, "Secure and private collaborative linear programming," in *Proc. of CollaborateCom*, Nov. 2006.
- [20] S. Goldwasser, Y. T. Kalai, and G. N. Rothblum, "Delegating computation: interactive proofs for muggles," in *Proc. of STOC*, 2008.

AUTHOR PROFILES

1). **Fahmida Begum** did his MCA from Osmania University, and pursuing Ph.D from MJPRU , U. P. Her interested areas are mobile computing and cloud computing . I have 9 years experience of Teaching in various colleges. At present she is working as an Associate Professor in Dr. K.V Subba Reddy college of MCA, Kurnool.(Dt).



2). **K.Bhargavi** working as Asst.prof in MCA Dept. Palamuru University, she Completed M.Tech from NU. Her Research interests in security Issues in cloud Computing.



3). **Mr.Venkateswarlu Maninti** has received Master" s Degree from Jawaharlal Nehru Technological University,Anantapur, AP (India). He is currently Lecturer in Information Technology, Fishermen Training Institute, Salalah, Sultante of Oman. He served different levels as a Lecturer at SGPR Govt. Polytechnic, Kurnool, AP (India), Asst. Professor, Associate Professor and Head of the Department of Computer Science and Engineering of Dr.K.V.Subba Reddy College of Engineering for Women, Kurnool, AP (India). His research interest includes Denial of Services in Cloud Computing and Cloud Storage, Grid Computing Network and Wireless Networks & Database applications. He has published 5 peer reviewed national journal papers, 2 International journal papers. Published IEEE publications and organized national conferences/workshops and also having Microsoft Certification and IBM certification etc.

An Adaptive Hello Messaging and Multipath Route Maintenance in On-Demand MANET Routing Protocol

P. Divya¹, S. Hemalatha²

¹II MECSE, Sri Shakthi Institute of Engineering and Technology, Coimbatore, India

²Assistant Professor-CSE, Sri Shakthi Institute of Engineering and Technology, Coimbatore, India

ABSTRACT: In mobile ad-hoc networks, local link connectivity information is extremely important for route establishment and maintenance. Periodic Hello messaging is a widely-used scheme to obtain local link connectivity information. However, unnecessary Hello messaging can drain batteries more quickly. In this paper an adaptive Hello messaging scheme to reduce unnecessary Hello messages has been proposed. Simulation results show that the proposed scheme reduces energy consumption and network overhead without any explicit difference in throughput.

Keywords: Hello messaging, ad hoc routing, network overhead, local connectivity, energy saving.

I. INTRODUCTION

MANET [1] is a wireless infrastructure less network having mobile nodes. Communication between these nodes can be achieved using multi hop wireless links. Each node will act as a router and forward data packets to other nodes. Mobile adhoc networks are operating without any centralized base station. It uses multi hop relaying. Since the nodes are independent to move in any direction, there may be frequent link breakage. The advantage of MANET is its instant deployment.

MANET routing protocol(e.g., Ad hoc On-Demand Distance Vector (AODV) [2], is used, where a new path is discovered through Route Request (RREQ) and Route Response (RREP) packet exchanges. Route maintenance of active routes in AODV is done by continuous monitoring of link status of next hops. HELLO messages as sent periodically to the neighbor node to check whether the link exists. A RERR message is sent upstream to source node when a link failure is noticed. Source finds an alternate route to the unreachable nodes by reinitiating the route discovery [2].

AOMDV is a multi path routing protocol based on AODV. It extends AODV by computing multiple paths to destination during route discovery itself. New route discovery is required only when all the existing alternate paths fail. This improves the delay and data loss incurred by AODV during link failure [3].AOMDV ensures loop freedom in multiple paths. Instead of rejecting each copy of RREQ like AODV, in AOMDV a duplicate RREQ is accepted as an alternate route if it is coming from a different neighbor.

AOMDV uses the notion 'advertised hops' which means maximum hop count to a destination to avoid loops [3].Each intermediate node in an active route stores list of next hops. AOMDV provides link disjoint paths. Destination will reply to multiple RREQs only if they are coming from unique nodes [3].AOMDV has to keep multiple paths in the routing table instead of a single route as in AODV. But selection of alternate route on link failure should not initiate a new route discovery. An alternate path can be selected quickly from the next hop list without much data loss. HELLO messages are flown to use to check the liveability of other routes. When there is no path available from source to destination then route discovery process again start.

In this paper, we propose an adaptive Hello messaging scheme for neighbor discovery by effectively reduce unnecessary Hello messages. Simulation results show that our proposed scheme suppresses unnecessary Hello messaging and reduces the energy consumption up to 20% without any additional delay.

II. DESIGN OF AN ADAPTIVE HELLO MESSAGING INTERVAL SCHEME

The source node send Hello Packets is responsible for establishing and maintaining neighbor relationships.[4] It also ensures that communication between neighbors is bidirectional. Hello packets are sent periodically to out all the network router interfaces. Bidirectional communication is indicated when the router sees itself listed in the neighbor's Hello packet.

The Hello packets are sent out each functioning router interface. They are used to discover and maintain neighbor relationships. But due to this periodic HELLO messages, the node's battery drains more quickly, In this paper an adaptive HELLO messaging scheme for neighbor discovery that avoids the unnecessary energy utilization. In this scheme, the unwanted broadcasting of HELLO packets are reduced. The method estimates an average time gap between two consecutive events (sending or receiving a data packet) on a node.

Interval between two events = previous event end time-current event start time

By monitoring the event intervals, the scheme estimate how actively a node is involved in sending or forwarding. Initially the source node send Hello Packets, If the link is available then Calculates the interval between two events and Broadcast hello packet within the interval. Otherwise the node broadcast hello packet to check the link availability.

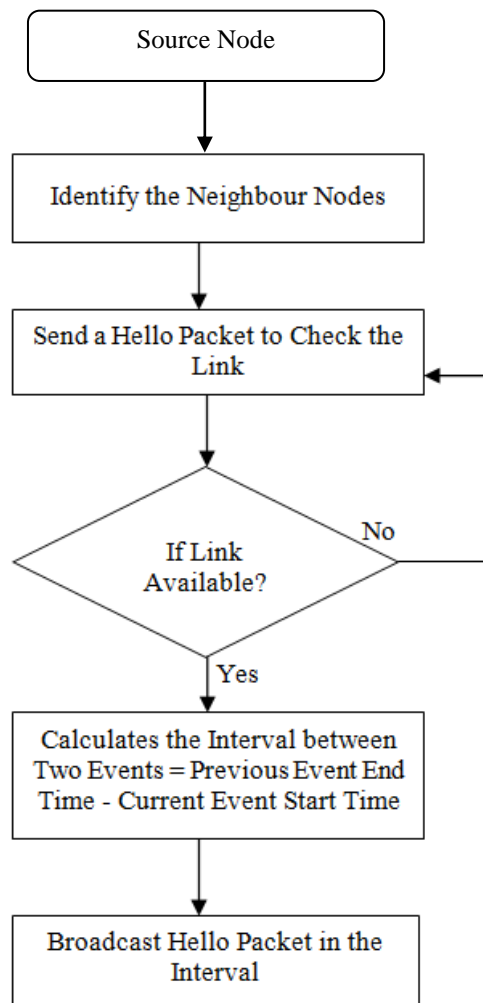


Fig1. Flow diagram for adaptive hello messaging scheme

III. RESULTS AND DISCUSSION

The Simulation is carried out in NS2 under LINUX platform. The aim of these simulations is to analyze the AODV protocol by comparing it with AODV-AH for its efficiency in terms of energy consumption, delay, and throughput. A new protocol is designed based on AODV-AH so that the new protocol had better performance than AODV in all the above parameters. The following table shows that the important parameters chosen for the NS2 simulation:

Table 1 Simulation Parameters

PARAMETER	VALUE
Simulation Time	100s
Channel type	Wireless channel
MAC Type	MAC 802.11
Radio propagation Model	Two Ray Ground
Antenna	Omni Antenna
Topology Size	1000m x 1500m
Routing protocol	AODV, AODV-AH
Number of nodes	50 , 100, 150, 200
Traffic type	CBR

3.1. Simulation parameters

- 1. Energy consumption:** This is the ratio of the average energy consumed in each node to total energy.
- 2. End to end delay:** This is the ratio of the interval between the first and second packet to total packet delivery.
- 3. Throughput:** The throughput metric measures how well the network can constantly provide data to the sink. Throughput is the number of packet arriving at the sink per ms.

3.2. Simulation Results

The following two tables show the performance result of simulation of AODV and AODV-AH for various parameters. The tables show AOMV-AH has better throughput, energy consumption, average end to end delay for number of nodes. For all other cases AODV-AH has better result for the above parameters.

Table 2. Simulation results for AODV

NUMBER OF NODES	THROUGHPUT	AVERAGE END TO END DELAY	ENERGY
50	19789	1.8608	60
100	21789	1.2434	56
150	23111	1.5092	43
200	26026	1.8919	30

Table 3. Simulation results for AODV-AH

NUMBER OF NODES	THROUGHPUT	AVERAGE END TO END DELAY	ENERGY
50	24387	0.5517	75
100	25688	1.1467	63
150	26561	1.4742	52
200	33702	1.5132	47



Fig 1. Comparison Of Throughput Versus No Of Nodes For AODV,AODV-AH

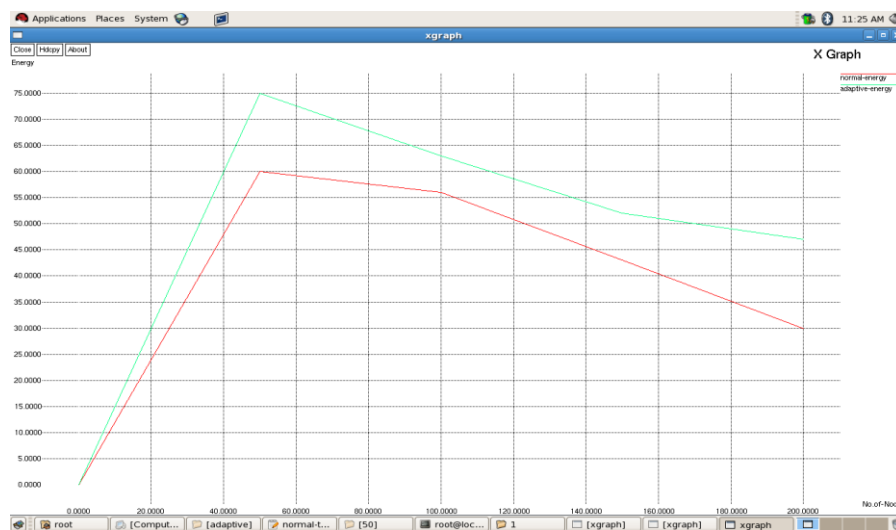


Fig 2. Comparison of Energy Consumption Versus Number Of Nodes For AODV, AODV-AH

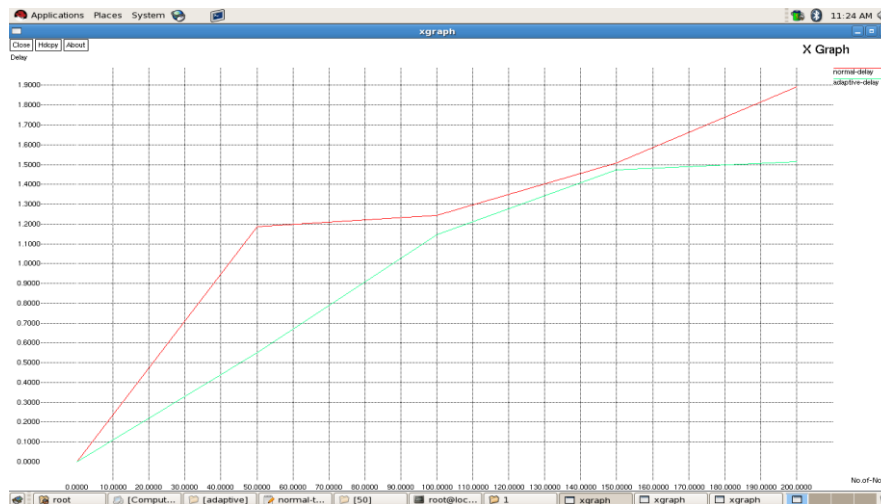


Fig 3 Comparison Of Delay Versus Number Of Nodes For AODV,AODV-AH

IV. Conclusion And Future Enhancement

In this paper, we proposed an adaptive Hello interval to reduce battery drain through practical suppression of unnecessary Hello messaging. Based on the event interval of a node, the Hello interval can be enlarged without reduced detectability of a broken link, which hidden energy consumption. In future we enhancement Multipath routing use AOMDV protocol with adaptive Hello messaging scheme needs the link availability information and establishment of multiple paths between a single source and single destination node. Energy efficient Multipath routing algorithms use route selection criterion to choose the best path from available multiple paths.

References

- [1] Jeroen Hoebeke, Ingrid Moerman, Bart Dhoedt and Piet Demeester, "An Overview of Mobile Ad Hoc Networks: Applications and Challenges," 2001.
- [2] E. Belding-Royer and S. D. C. Perkins, "Ad hoc on-demand distance vector (AODV) routing," July 2003.
- [3] M. Marina and S. Das, "On-demand Multipath Distance Vector Routing in Ad Hoc Networks", in Proceedings of the International Conference for Network Procotols (ICNP), Riverside, Nov. 2001.
- [4] T. Clausen, C. Dearlove, and J. Dean, "Mobile ad hoc network (MANET) neighborhood discovery protocol (NHDP)," 2010.

Experimental Study of Full Authority Digital Engine Control (FADEC) System on Lycoming Engine

Md. Akhtar khan¹, Md. Muqthar ghor², Syed Abdul Khaliq³, Md. Mohsin Ali⁴

ABSTRACT: Full authority digital engine control (FADEC) is a system consisting of digital computer, called an electronic engine controller (EEC) or engine control unit (ECU), and its related accessories that control all aspects of aircraft engine performance. FADECs have been produced for both piston engines and jet engines. FADEC consist of HMU, Sensor and EEC. The proposed single chip SOC ASIC device integrates many diverse and improved functions required for interfacing with most types of FADEC Control sensors and actuators. FADEC or to expand the capabilities of a legacy FADEC system by adding a sensor or actuator. The same Smart Nodes can be applied without hardware change for controlling actuators, interfacing with sensors or a combination providing an affordable, scalable and reusable solution for Commercial and military engines, small or large, missiles and UAVs. True full authority digital engine controls have no form of manual override available, placing full authority over the operating parameters of the engine in the hands of the computer. If a total FADEC failure occurs, the engine fails. If the engine is controlled digitally and electronically but allows for manual override, it is considered solely an EEC or ECU. An EEC, though a component of a FADEC, is not by itself FADEC. When standing alone, the EEC makes all of the decisions until the pilot wishes to intervene.

Keywords: FADEC, UAVs, Lycoming engine, sensor, Ignition system, BPMS, Electrical system

I. INTRODUCTION

The UAV is an acronym for Unmanned Aerial Vehicle, which is an aircraft with no pilot on board. UAVs can be remote controlled aircraft (e.g. flown by a pilot at a ground control station) or can fly autonomously based on pre-programmed flight plans or more complex dynamic automation systems. UAVs are currently used for a number of missions, including reconnaissance and attack roles.

UAV is defined as being capable of controlled, sustained level flight and powered by a jet or reciprocating engine. In addition, a cruise missile can be considered to be a UAV, but is treated separately on the basis that the vehicle is the weapon. The acronym UAV has been expanded in some cases to UAVS (Unmanned Aircraft Vehicle System). The FAA has adopted the acronym UAS (Unmanned Aircraft System) to reflect the fact that these complex systems include ground stations and other elements besides the actual air vehicles. Officially, the term 'Unmanned Aerial Vehicle' was changed to 'Unmanned Aircraft System' to reflect the fact that these complex systems include ground stations and other elements besides the actual air vehicles. UAV no longer only perform intelligence, surveillance, and reconnaissance (ISR) missions, although this still remains their predominant type. Their roles have expanded to areas including electronic attack (EA), strike missions, suppression and/or destruction of enemy air defence (SEAD/DEAD), network node or communications relay, combat search and rescue (CSAR), and derivations of these themes. [1]



II. DEGREE OF AUTONOMY

Some early UAVs are called drones because they are no more sophisticated than a simple radio controlled aircraft being controlled by a human pilot (sometimes called the operator) at all times. From this perspective, most early UAVs are not autonomous at all. In fact, the field of air vehicle autonomy is a recently emerging field, whose economics is largely driven by the military to develop battle ready technology for the war fighter.

Autonomy technology that will become important to future UAV development falls under the following categories:

Sensor fusion: Combining information from different sensors for use on board the vehicle

Communications: Handling communication and coordination between multiple agents in the presence of incomplete and imperfect information

Motion planning (also called Path planning): Determining an optimal path for vehicle to go while meeting certain objectives and constraints, such as obstacles.

Trajectory Generation: Determining an optimal control manoeuvre to take to follow a given path or to go from one location to another.

Task Allocation and Scheduling: Determining the optimal distribution of tasks amongst a group of agents, with time and equipment constraints.

Cooperative Tactics: Formulating an optimal sequence and spatial distribution of activities between agents in order to maximize chance of success in any given mission scenario.



Fig. 1: Schiebel S-100 fitted with a Lightweight Multirole Missile



Fig. 2: Aeron Scout in flight

III. CURRENT DAY UAVS

PREDATOR

It is a MALE armed surveillance UAV. It was first designated as RQ-1A in 1997. In May 1998, a more powerful turbo charged engine and wing de-icing system was installed. In the February of 2001, it became the first UAV to be weaponized destroying a ground target with live Hellfire missile during flight tests.

Description:

The airframe is a low wing monoplane with slender fuselage, high aspect ratio wing and inverted V- tail. It has an advanced low speed aerodynamic configuration and computer designed low Reynolds number aerofoils which provide high aerodynamic efficiency. Inverted V- tail is a unique feature providing propeller protection and keeping the tail control surfaces clear of wing turbulence. Advanced graphite/ epoxy construction resulted in very sturdy airframe and light structure. It has a tri-cycle landing gear.[5]

Guidance and control:

Predator missions are conducted from the GA-ASI mobile GCS. Predator system comprises of several air vehicles, their payloads, one GCS, communications and support equipment, spare parts and support.

Powerplant:

The predator is equipped with one 78.3kw(105hp) Rotax 914 four cylinder four stroke turbo charged engine with two blade variable pitch propeller.



Fig. 3: UAV Predator

GLOBAL HAWK

The Northrop Grumman RQ-4 is high altitude long endurance surveillance UAV.

Description:

The airframe is of high aspect ratio, low mounted CFRI (Carbon Fibre Reinforced Plastics), and quarter chord swept back fitted with inboard and outboard ailerons plus spoilers. It has a V- Tail surface made up of composites (dihedral angle 50degrees), with inboard and outboard ruddervators, plus rear fuselage, nacelle and fairings. It has a retractable tri cycle landing gear.

Powerplant:

It has one 33.8KN FADEC equipped Rolls Royce F137-AD-100 turbofan engine.



Fig.4: UAV Global hawk

T-HAWK

The Honeywell T-Hawk is a VTOL (Vertical Takeoff and Landing) Micro UAV (MAV). It was selected as winner of U.S Army's future combat system.

Description:

It has a barrel-shaped ducted fan with control vanes in fan slipstream with four curved landing legs.

Guidance and control:

Pre programmed control with dynamic retasking and manual intervention, using Honeywell micro-electrical mechanical systems (MEMS) technology. It has INS/GPS navigation with upto 100 waypoints storage. Mission computer activates control vanes to tilt vehicles in transition to forward flight, this being achieved by combination of fan thrust and wing lift from fan duct.

Power plant:

The T-MAV has one 3.0KW (4hp) 3W model motoren flat twin piston engine driving a fixed pitch ducted fan. Production versions have electronic flat injection rather than carburettor. The D-MAV is equipped with a diesel engine.



Fig. 5: UAV T-Hawk

RUSTOM 1

The project deals with automation of the engine installed on UAV Rustom-1, which is under development at Aeronautical Development Establishment (ADE). **Rustom** is a Medium Altitude Long Endurance (MALE) Unmanned Combat Aerial Vehicle (UCAV) being developed by Defence Research and Development Organisation (DRDO) for the three services; Indian Army, Indian Navy and the Indian Air Force of the Indian Armed Forces.[6]

Variants of Rustom UAV:

There will be three variants of the Rustom UAV.

- **Rustom-I:** Tactical UAV with endurance of 12 hours (based on NAL's LCRA which was inspired by Burt Rutan's Long-EZ)
- **Rustom-H:** Larger UAV with flight endurance of over 24 hours (wholly different design from Rustom-1), higher range and service ceiling than Rustom-1.
- **Rustom-II:** An unmanned combat air vehicle based on *Rustom-H* model. It's often compared with Predator drones by Indian Media as well as Indian Scientist.



Fig 6: Rustom 1 UAV during its 5th successful flight

IV. ADVANCED GROUND CONTROL STATION (AGCS)

Equivalent of a cockpit is the Advanced Ground Control Station (AGCS). All controls and displays to check out and fly the UAV are provided to the IP. Navigation display on a map and plot of the UAV trajectory is also available.

Functionalities:

- Mission planning
- Air vehicle control by IP & EP
- Internal Pilot control Console & Display
- External Pilot Control Console
- Payload Control
- Data recording, Display & Playback
-



Fig.7: Ground Control Station for UAV

V. POWERPLANT: LYCOMING O-320-B ENGINE

The Lycoming O-320 series engines are four-cylinder, direct-drive, horizontally opposed, and air-cooled models. The cylinders are of conventional air-cooled construction with heads made from an aluminium-alloy casting and a fully machined combustion chamber. The cylinder barrels are machined from chrome nickel molybdenum steel forgings with deep integral cooling fins, ground and honed to a final specified finish. The O-320 series engines are equipped with a float-type carburetor. Particularly good distribution of the fuel-air mixture to each cylinder is obtained through the center-zone induction system, which is integral with the oil sump and is submerged in oil, ensuring a more uniform vaporization of fuel and aiding in cooling the oil in the sump. In addition, the IO-320 has a fuel injector. The fuel-injection system schedules fuel flow in proportion to airflow. Fuel vaporization takes place at the intake ports. [2]

The orientation and the direction of rotation for the engine are as referenced below:

1. The power take-off is considered the front.
2. Accessory drive end is considered the rear.
3. Sump section is in the bottom.
4. Direction of rotation of crankshaft viewed from rear is clock-wise.

5.1 PARTS OF ENGINE

The major parts of the Lycoming O-320-B engine are as listed below:[3]

Cylinders: The cylinders are convectional air-cooled construction with two major parts: head and barrel, screwed and shrunk together made of aluminium alloy. The cylinder barrel has deep integral cooling fins.

Valve Operating Mechanism: A convectional type camshaft is located above and parallel to camshaft which actuates hydraulic tappets which operate valves through push rods and valve rockers.

Crank-Case: Crank-case assembly consists of two reinforced Aluminium alloy castings, fastened together by means of studs, bolts and nuts.

Crank-Shaft: It is made of chrome nickel-molybdenum steel forging.

Connecting-Rod: They are made in the form of H sections from alloy steel forgings. They have replaceable bearing inserts in the crankshaft ends and bronze bushings in the piston ends.

Pistons: They are made of Aluminium alloy, and are full floating type with a plug located in each end of piston pin. Depending on cylinder assembly, pistons may employ either half wedge or full wedge rings.

Accessory-Housing: It is fastened to rear of crank-case and top rear of the sump. It forms housing for oil pump and various accessory drives.

Oil Sump: It incorporates oil drain plug, oil suction screen, mounting pad for carburetor, the intake riser and intake pipe connections.



Fig. 8: Lycoming O-320-B Engine on Test Bed

VI. SYSTEMS OF ENGINE

Cooling Systems: These engines are designed to be cooled by air pressure. Baffles are provided to build up a pressure and force the air through cylinder fins.

Induction System: Lycoming engines are equipped with a float type carburetor. Good distribution of fuel air mixture is obtained through center zone ignition system. From the riser the fuel-air mixture is distributed to each cylinder by intake pipes.

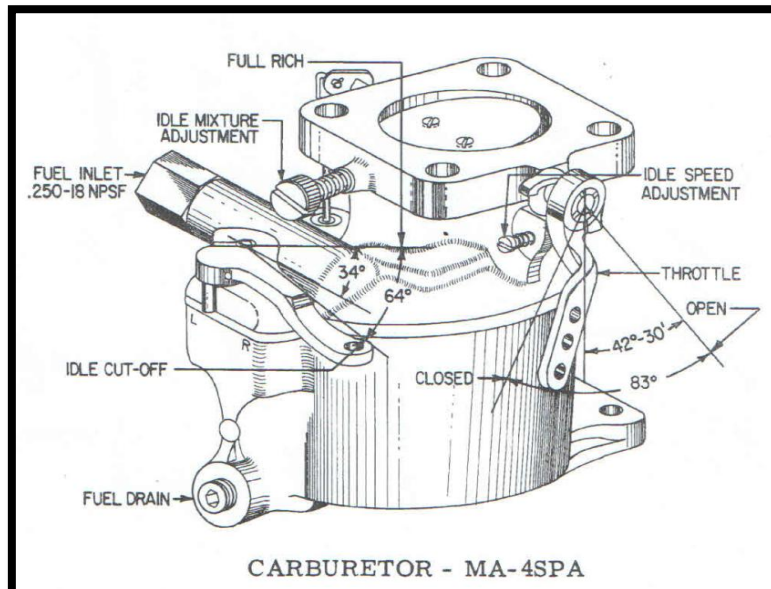


Fig. 9: Fuel Metering System, Carburetor

Lubrication Systems: It is pressure-wet sump type. The main bearings, connecting rod bearings, camshaft bearings, push-rods and crankshaft idler gears are lubricated by means of oil collectors and spray.

Priming System: The provision for the primer system is provided for all engines.

Ignition System: Dual ignition is furnished by two magnetos. Bendix magnetos are designed to permit periodic internal maintenance; slick electro magnetos are designed to operate for 900 hours without internal maintenance.

ENGINE SPECIFICATIONS

Rated Horsepower	160
Rated Speed (RPM)	2700
Bore (Inches)	5.125
Stroke (Inches)	3.875
Displacement (Cubic Inches)	319.8
Compressor Ratio	8.5:1
Firing Order	1-3-2-4
Spark occurs (Degrees BTC)	25
Valve Rocker Clearance	0.028-0.080
Propeller Drive Ratio	1:1
Propeller Drive Rotation	Clockwise

VII. PERFORMANCE CURVE

Performance data for correction of BHP from Altitude, RPM, Manifold Pressure & Air Inlet Temperature.

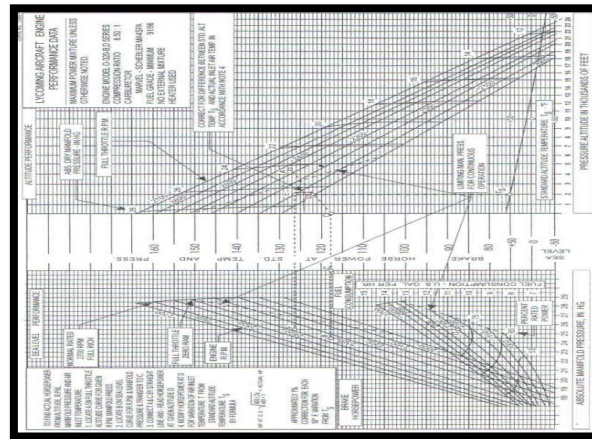


Fig.10 Graph for Sea Level & Altitude Performance for Lycoming O-320-B Engine

AUTOMATION OF ENGINE

The existing Internal Combustion engine is the Lycoming O-320-B which is four-cylinder air-cooled horizontally opposed engine with fixed pitch propeller. It has certain drawbacks that have to be considered and solved for the better performance and safety of the system. The two basic areas where the problem arises are the Fuel Injection system and the Ignition system.

With the automation of engine, these problems are ciphered and the system is improved. The automation of engine deals with the installation of an Electronic Controlling unit for handling the inputs and outputs of the system and control the function of Ignition and Fuel Injection.

The automation is achieved with the installation of FADEC system. **FADEC** stands for **Full Authority Digital Engine Control**. The ECU (Engine Control Unit - digital computer) controls all aspects of the engine performance and decides on the amount of fuel it injects into the inlet ports as well as the exact timing of the spark advance.

This deals with the major drawbacks of the Internal Combustion engine and how the installation of FADEC system deals with these problems. Following are the disadvantages of the I.C. engines that are dealt by FADEC system:

- **Ignition system:** Magneto Ignition system replaced with Electronic Ignition system
- **Fuel Injection system:** Carburetor replaced with Electronic Fuel Injection system

VIII. FADEC (FULL AUTHORITY DIGITAL ENGINE CONTROL) SYSTEM

The FADEC (Full Authority Digital Engine Control) is a total system for the control of an engine. It controls all aspects of aircraft engine performance. In simpler words, FADEC is a computer that controls the engine of the aircraft, just like Fly-by-wire but in an engine's aspect.

FADEC's main purpose is to provide optimum engine efficiency for a given flight condition. FADEC controls the aircraft's engine and propeller in order to perform at a maximum efficiency. It does this by controlling the power of the reciprocating engine and by adjusting the amount of fuel injection during the combustion process.

It controls and regulates the fuel pump, providing to the engine the necessary amount of fuel for safe and controlled operation. The FADEC system also continuously monitors and controls ignition timing, fuel injection timing, and fuel-to-air ratio mixture.

Certain input variables necessary for the flight such as air density, engine temperature and engine pressure are fed into the system.

Since FADEC is more or less a computer that has no manual override, it operates with certain limits provided by the manufacturer of each engine aircraft. During aircraft starting, the FADEC primes the cylinders, adjusts the fuel to air mixture, and positions the throttle based on engine temperature and ambient pressure. During cruise flight, the FADEC constantly monitors the engine and adjusts fuel flow, and ignition timing individually in each cylinder.[4]

The FADEC also allows the manufacturer to program engine limitations and receive engine health and maintenance reports. For safety, FADEC is housed with a separate generator with two channels (A and B) to prevent a total failure. The two channels are housed in one assembly but physically separated. If one channel fails completely, the other channel will take over and it is unlikely that both channels would fail. Aircraft input power of 12V (or 24V) DC is necessary for back-up power.

OPERATIONS

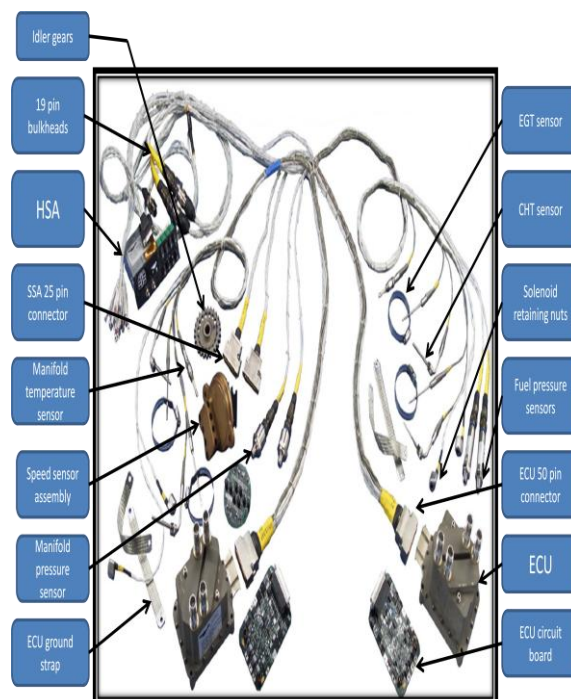
The various operations of FADEC are:

- Controls the ignition spark
- Controls the air-fuel mixture of the engine
- Engine acceleration to idle speed during start
- Acceleration and deceleration limiting
- Minimum approach idle speeds during descents
- Selection of alternative power modes
- Monitors cylinder head, manifold and exhaust gas temperatures and pressures.

8.1 PARTS OF FADEC SYSTEM

The FADEC system is a redundant system which includes the following components that will be installed on the engine or the airframe:[8]

- Two Master Power Control Units("MPC-1" And "MPC-2")
- Sensors For Manifold Temperature And Pressure
- Cylinder Head Temperature (CHT) Sensor
- Exhaust Gas Temperature (EGT) Sensor
- Speed Sensors
- Speed Sensor Assembly
- Fuel Pressure Sensors
- Low Voltage Harness
- High Voltage Harness
- Throttle Body Assembly
- Health Status Annunciator(HSA)
- Fuel Injection System



FADEC SYSTEM DESCRIPTION

Each MPC unit has a lower portion and an upper portion. The lower portion contains an electronic circuit board; the upper portion houses the ignition coils. The Electronic circuit board contains two, independent microprocessor controllers called "control channels".

Each control channel is assigned to a single engine cylinder. Since there are two control channels in each MPC, a single MPC unit can operate two engine cylinders. (There are no shared electronic components between the two control channels.)

For redundancy, each control channel is capable of operating its assigned cylinder and a cylinder assigned to the second control channel within the same MPC unit.

Each control channel monitors the current operating conditions and manages its cylinder in a manner that will yield maximum operating performance and efficiency within specified operating parameters. If operating conditions change, the control channel adjusts both the fuel mixture and ignition timing to return the cylinder to normal operating parameters.

The control channels also receive input from the pilot via the throttle control thereby eliminating manual mixture control. Primary/Secondary power is supplied by the Cabin Harness through the Bulkhead Connectors.

Information from the MPC units is conveyed to the HSA and the cockpit-mounted data port through the same Cabin Harness/Bulkhead Connector Assembly.

The FADEC system continuously monitors fuel and ignition conditions. The MPC units receive information from sensors via the Low Voltage Harness which interfaces with the MPC units via 50-pin connectors. The Low Voltage Harness connects to the Cabin Harness via firewall-mounted Bulkhead Connectors.

The status of the FADEC system is conveyed to the pilot by the HSA. Discrete lamps in the HSA will illuminate upon detection of system faults and during some normal control actions.

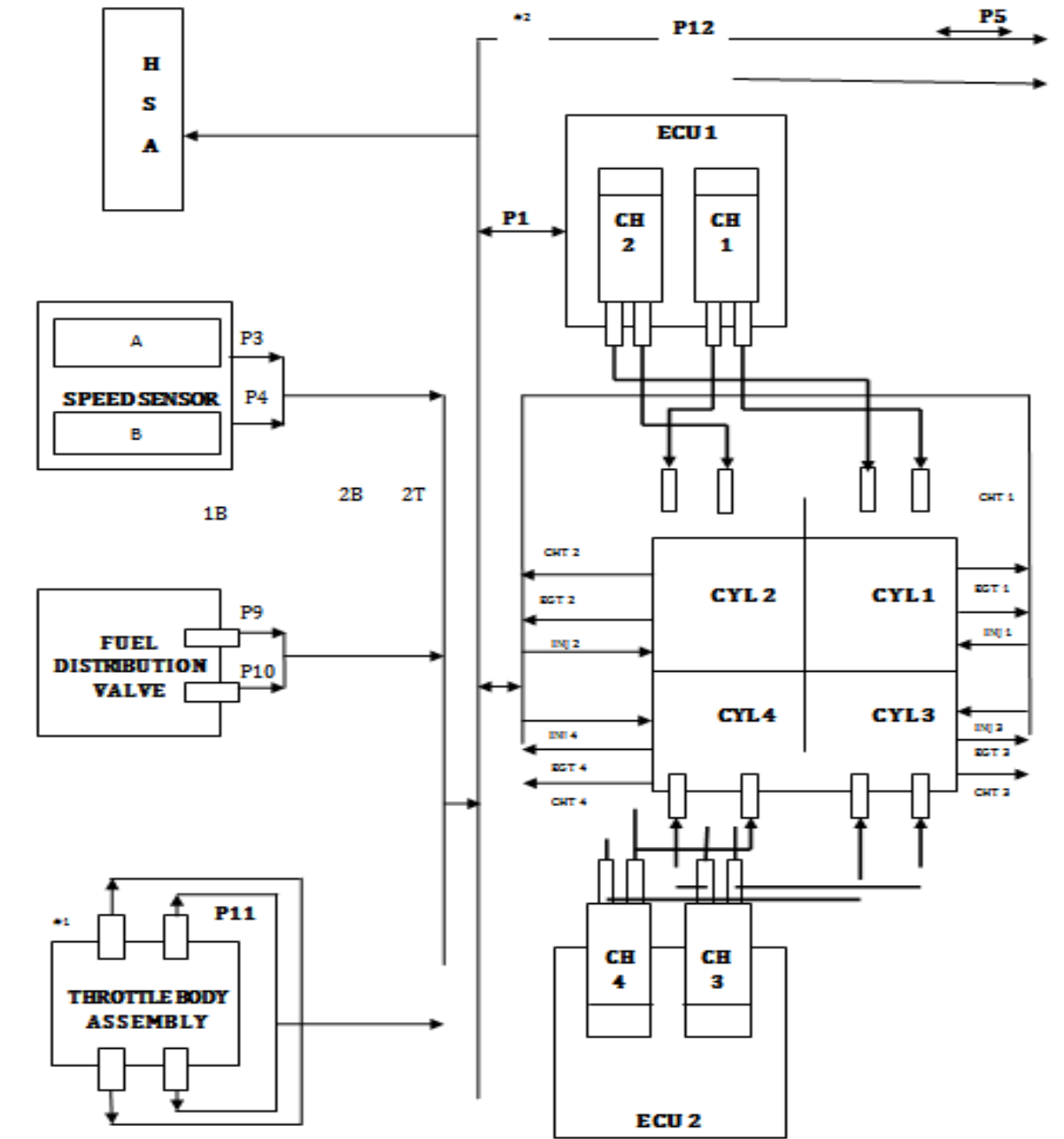
Sensor input to each control channel includes engine speed, crank position, fuel pressure, intake manifold air pressure, intake manifold air temperature and Wide Open Throttle (WOT) position. In addition, each control channel also receives exclusive signals for measuring its cylinder's head temperature and exhaust gas temperature.

The control channels in the MPC units use the signals from sensors to determine the required fuel mixture and ignition timing for its cylinder's next combustion event. The required fuel quantity is injected into each cylinder intake port at the appropriate time, with respect to crank position, by a solenoid style fuel injector. The injector's control coil is driven directly by the associated control channel.

All critical sensors are redundant with one sensor from each pair connected to channels in different MPC units. Synthetic software default values are also used if both sensors of a redundant pair should fail. This arrangement supports the functional redundancy of the FADEC system. [6]

The FADEC system is electrically powered and not self-excited. As such, the system requires two, independent power supply sources. Typically one source will be the aircraft's primary electrical bus, referred to as Primary Power. The second source, referred to as Secondary Power, may be a second aircraft bus, an engine driven generating device, or a battery. Electrical power to the FADEC system is controlled from the cockpit by two switches used to interrupt the Primary Power and Secondary Power.

Using a conventional aircraft-style Ignition Switch, the pilot controls the enabling, starting, and disabling of the FADEC system. The Fuel System must be pressurized at start-up to suppress vapour. The mechanical engine driven fuel pump provides pressure for normal operation. For this reason, an Electric Boost Pump is required for starting. efficiency will be reduced. **BLOCK DIAG. OF FADEC SYSTEM**



IX. IGNITION SYSTEM

System Description:

The ignition system is a waste-spark type. Each cylinder's spark plugs are fired twice per engine cycle, once on the compression stroke and again on the exhaust stroke.

The FADEC system schedules the spark timing and the intensity using two Master Power Control (MPC) units. The system includes spark plug wires and the low voltage harness. The timing of the spark is variable and is set according to a predetermined map of ignition advance settings.

Each microprocessor drives a single spark transformer. There are two high voltage terminals on each spark transformer. One terminal is connected to the top spark of the cylinder designated as primary for the control channel. The second terminal is connected to the bottom spark plug of the opposing cylinder, which allows each control computer to ignite two cylinders establishing redundancy of ignition.[10]

MPC-1 fires the top and bottom spark plugs for cylinders 1 & 2 and MPC-2 fires the spark plugs for cylinders 3 & 4.

For both spark plugs in a given cylinder to fire on the compression stroke, both control channels within an MPC unit fire their coil pack.

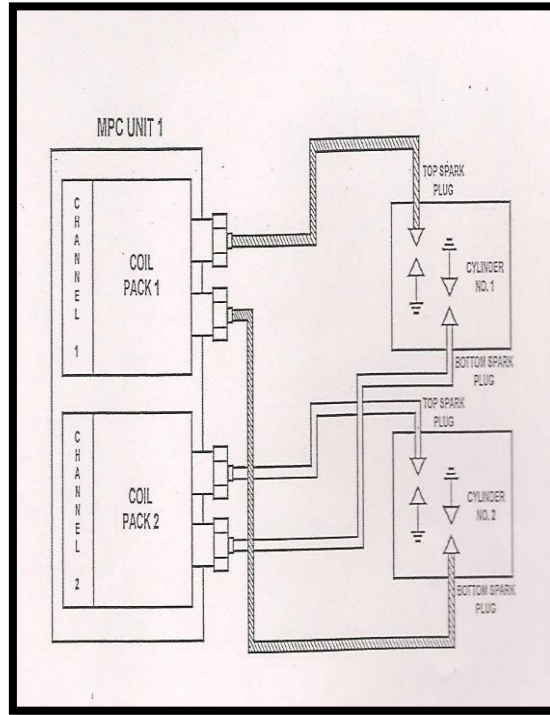


Fig.10: Ignition system

X. FUEL INJECTION SYSTEM

System Description:

The FADEC system schedules the amount of fuel and the injection timing for the multi-port fuel injectors, thereby eliminating the mixture control. The FADEC system compensates for changes in altitude by monitoring the intake manifold pressure. [6]

The FADEC system controls the fuel supplied to each cylinder using solenoid-actuated sequential port Fuel injectors. The Fuel Injection System is composed of:

- An engine-driven Fuel Pump
- Fuel Distribution Block and fuel lines
- Solenoid-controlled Fuel Injection Nozzles

Each computer channel in the MPC unit obtains data from its own sensors and computes the amount of fuel to inject. The electronic fuel injector injects fuel into the intake port upstream of the intake valve. The fuel injection timing is based on engine speed and position. The flow is therefore intermittent, and not a continuous flow.

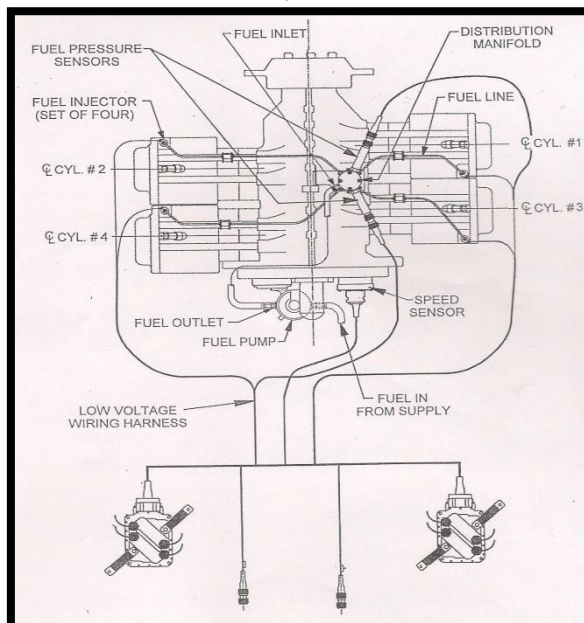


Fig11: FADEC Fuel Distribution System

ELECTRICAL SYSTEM

System Description

The engine electrical interfaces are the starter, the alternator, battery terminals, the FADEC system main power supply and the FADEC system auxiliary power supply. The FADEC connections also supply operating data to the Health Status Annunciator (HSA) panel and the optional Engine Performance Display (EPD). The FADEC system has a data port for engine diagnostics using a compatible computer. [8]

The FADEC system requires two independent power sources. The primary source of FADEC electrical power is provided from the aircraft power bus. The redundant source of FADEC electrical power can be provided from either of the below three modes:

- A dedicated backup battery
- A dedicated alternator
- An essential aircraft electrical bus

In the FADEC system being installed on the converted Lycoming engine, the auxiliary power is provided by a dedicated backup battery. The circuit diagram for it is depicted here.[7]

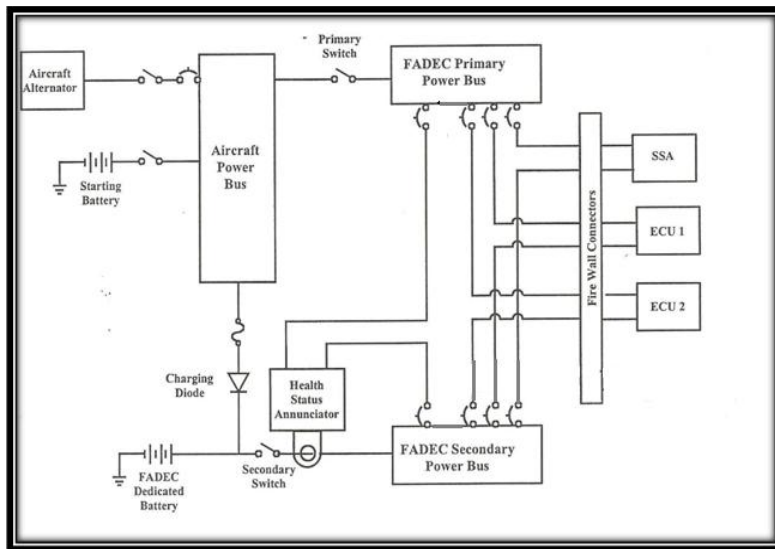
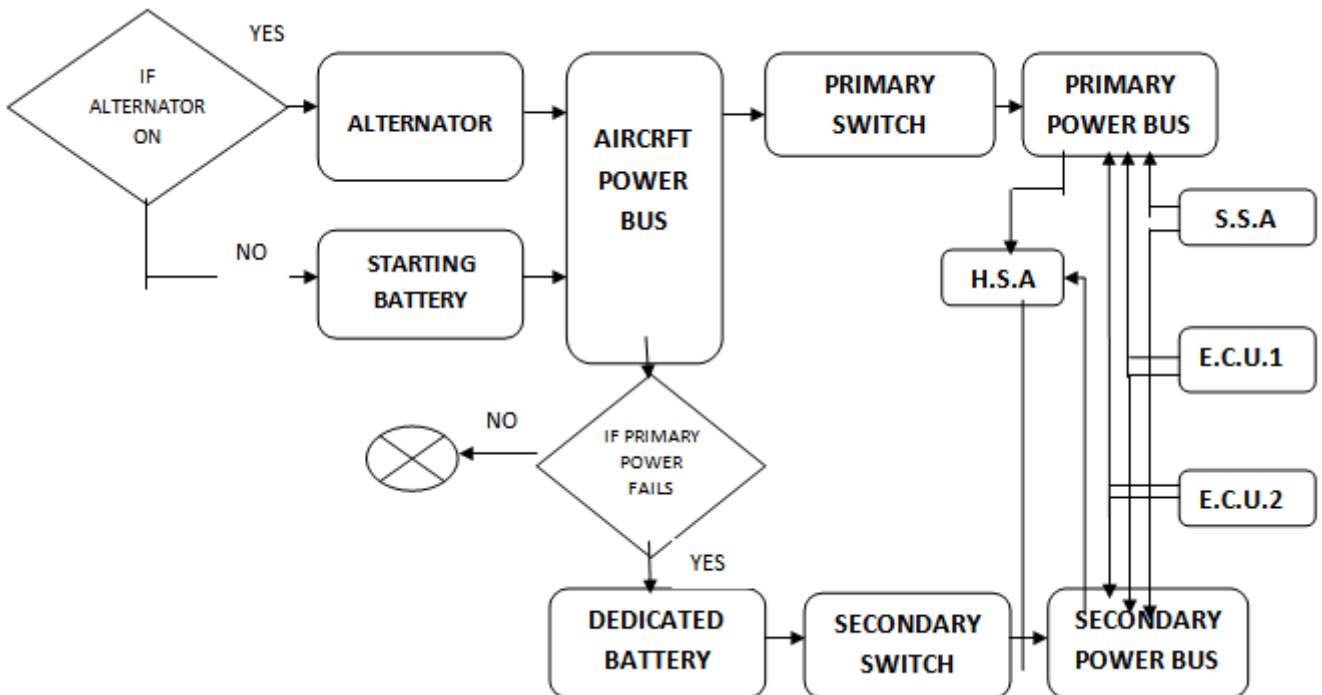


Fig12: Dedicated Battery Electrical Supply for FADEC system Auxiliary Power

ELECTRICAL SYSTEM FADEC BLOCK DIAGRAM:

A block diagram depicting the basic connection of the Electrical system is as follows:[8]



XI. TESTING AND VALIDATION

The Powerplant of Rustom-1: Lycoming O-320-B engine is integrated with the Full Authority Digital Engine Control (FADEC) system following the procedure explained in the previous chapter. This chapter deals with the testing and validation of the FADEC integrated Lycoming Engine. The procedure and test run data are included here.

APPARATUS USED:

- FADEC Integrated Lycoming Engine
- Engine Test Bed
- Alternator/ Starter Motor
- Fuel Sump
- Oil Sump
- Control Panel
- Engine Performance Monitor: VM-1000 software

PROCEDURE:

ENGINE STARTING

1. The FADEC System is energized by Switching ON the FADEC Master Switch.
2. Primary Power Switch is switched ON.
3. Secondary Power Switch is switched ON.
4. Throttle Position Switch is opened to 1/4- inch.
5. Boost Pump Mode Switch (BPMS) is switched to either ON or AUTO.
6. Engine Starter is engaged.
7. Engine is primed with initial charge of fuel.
8. Camshaft signal is monitored for the timing pulse.
9. Position of Crankshaft is ascertained.
10. First Spark is commanded.
11. Camshaft timing pulse is received from the timing sensor.
12. Commencement of Fuel Injection and Ignition Control by FADEC system.
13. The engine Starts.
14. Starter is disengaged.

TESTING

15. Engine start time, Fuel quantity at start and Oil level at start are noted.
16. The RPM is slowly increased using the throttle actuators.
17. Fuel Consumption and Thrust values are recorded for various RPMs along with Manifold Pressure and Fuel Pressure.
18. The Engine is switched off.
19. Engine stop time, Fuel quantity at stop and Oil level at stop are noted. Quantity of Fuel and Oil consumed is also recorded.

OBSERVED VALUES:

DAT E	20/9/2013	Fuel Qty. At START	18	Oil Level at START	7.5 ltr	Ignition Drop Check
ENGINE TYPE	Lycoming O-320	Fuel Qty. At STOP	15	Oil Level at STOP	7.3 ltr	BOTH
ENGINE NO.	B-2B	Fuel Consumed	3	Oil Consumed	0.2 ltr	LEFT
START TIME	1625	Propeller	Catto 2 bladed	Alternator No.		RIGHT
STOP TIME	1640	TEST DURATION	00:15			

Following tables gives the readings for Engine run test data:

Sl. No.	RPM (N)	MANIF OLD PR. (inch of Hg) P_m	FUE L PR. (psi) P_f	FUEL CONSUMPTION (Lt/Hr) V_f	THRUST (kgF) F
1.	730	11	6	1.4	13
2.	1200	14.7	6	4.2	45
3.	1500	17.4	6	6.6	65
4.	1700	20	5	9	85
5.	1900	22	5	10.8	100
6.	1950	23.1	5	12.8	107
7.	2000	23.4	5	13.2	116
8.	2100	24.5	5	14	120
9.	2200	25.1	5	15	130
10.	2285	25.9	5	15.8	138

XII. CONCLUSION

The FADEC Integrated Lycoming Engine is run successfully at various RPMs and the values of Fuel Consumption and Thrust are recorded. The fuel efficiency is increased and performance of engine is improved too. The study of "Integration of FADEC system on Lycoming Engine" on Unmanned Aerial Vehicles (UAV) is carried out. Its working, classification and applications are discussed along with current day UAVs. Rustom-1 is a Medium Altitude Long Endurance (MALE) UAV being developed by DRDO for the Indian Armed Forces. The basics of Internal Combustion engine are discussed. The Powerplant of Rustom-1 is the subject of study in the project. Lycoming O-320-B is a 160 BHP @2700 RPM four cylinder, horizontally opposed, air cooled engine with fixed pitch propeller. The efficiency and performance of the engine is studied. The need for the automation of engine is mentioned by listing the shortcomings of conventional systems and the advantages of Electronic Fuel injection and ignition systems. An extensive study of Full Authority Digital Engine Control (FADEC) system is carried out. Its major parts, system description and working are studied.

FUTURE SCOPE

Full Authority Digital Engine Control (FADEC) system finds practical application in various domains like Aviation Industry and Automobile Industry. The automation of engine has multitudinous advantages over conventional systems of engine. By projecting the supremacy of the FADEC system, the need for conversion of conventional engines is emphasized. But the system is not completely void of any drawbacks. It doesn't provide any manual override since it takes over the engine completely. In case of emergency, the system becomes highly unreliable. Also due to the complexity of the system, a lot of efforts have to be put for its development and validation.

It deals with the integration of FADEC system in Lycoming O-320-B engine. It improves the engine performance and fuel efficiency. The integrated engine is tested for various throttle settings. The fuel consumption and thrust are recorded for different engine RPMs.

The test should be carried out for various altitudes too so that the actual engine BHP can be recorded as opposed to theoretical values.

REFERENCES

- [1] Gunston (1990) Avionics: The story and technology of aviation electronics Patrick Stephens Ltd, Wellingborough UK. 254pp, ISBN 1-85260-133-7
- [2] Moren, Chuck. Interview with student. FADEC. Embry-Riddle Aeronautical University, Daytona Beach. 2007-03-13.
- [3] Title 14 CFR: Federal Aviation Regulations. FAA. 2007-03-10.
- [4] Jane's Journals: Jane's UAV and Targets (Issues 30-37).
- [5] Aircraft Powerplants, 4th edition by Ralph D. Bent & James L. McKinley
- [6] Fundamentals of I.C engines by Paul W. Gill & James H. Smith
- [7] Manual: Lycoming O-320-B engine by Teledyne Motors
- [8] Manual: Integration of Full Authority Digital Engine Control (FADEC) System in Textron Lycoming O-360 engine .
- [9] "Safran Electronics Canada: FADEC and EEC". Retrieved 2010-04-30.
- [10] "Hispano-Suiza: Digital Engine Control". Retrieved 2007-03-09.

A Novel Multi Copy Routing Scheme for Delay Tolerant Networks

Ch. S. Vasudeva Sastry¹, Syed Sadat Ali²

¹M. Tech, Nimra College of Engineering & Technology, Vijayawada, A.P., India.

²Assoc.Professor & Head, Dept.of CSE, Nimra College of Engineering & Technology, Vijayawada, A.P., India.

ABSTRACT: A delay tolerant network (DTN) is a network designed to operate effectively over extreme distances such as those encountered in space communications or on an interplanetary scale. In such an environment, long latency -- sometimes measured in minutes, hours or days -- is inevitable. However, similar problems can also occur over more modest distances when interference is extreme or the network resources are severely overburdened. DTNs involves some of the same technologies as are used in a disruption-tolerant network but there are important distinctions. A DTN requires hardware that can store large amounts of data. Such media must be able to survive extended system restarts and power loss. This paper presents a multi- copy routing method for DTNs. For this we introduce a novel DTN routing protocol, called Self Adaptive Utility-based Routing Protocol (SAURP) that aims to overcome the shortcomings of the previously reported multi-copy schemes. Our main goal is to achieve a superb applicability to the DTN scenario with densely distributed hand-held devices. The main feature of SAURP method is the strong capability in adaptation to the fluctuation of network status, traffic patterns/characteristics, user encounter behaviors, and user resource availability, so as to improve network performance in terms of message delivery delay, message delivery ratio, and number of transmissions.

Keywords: Delay tolerant network, Multi copy, SAURP, Routing.

I. INTRODUCTION

The widespread adaptation and employment of the wireless technologies means that a wide range of devices can be interconnected over vast distances through wireless links. As successful as these networks have been, they nonetheless cannot reach everywhere, and for some applications, the high cost of the associated scenarios is mainly prohibitive. One of the most serious challenges arises in cases in which the network connectivity cannot be guaranteed. For such challenged networking environments, the current networking technology relies on the set of fundamental assumptions that are not true in all practical environments. The first and most of the important fundamental assumption is the existence of a direct end-to-end path from a source to a destination. This assumption can easily be violated due to power-saving policies, nodal mobility, or unreliable packet delivery strategies. As a result, the mechanism of the TCP/IP-based network model that provides end-to-end communication is not valid, so any synchronous communication paradigm is likely perform very poorly. For these challenged networking environments, such as those found in mobile in motion networks and the dynamic wireless networks, network connectivity is rather opportunistic.

Techniques for producing applications that can tolerate high delays and disruptions in network connectivity are essential for these opportunistic networks. Networks that include such applications are often collectively called as Intermittently Connected Mobile Networks (ICMNs) or Delay Tolerant Networks (DTNs) [1]. Many real ICMNs fall into this category, such as Military Networks [2], Inter-Planetary Networks (IPN)[3], Pocket Switched Networks (PSN)[4], wildlife tracking and habitat-monitoring sensor networks [5], and networks that provide low-cost Internet service to remote communities [6]. These networks belong to the general category of delay networks, in which delays incurred are unpredictable and can be very long. This situation arises because of the sparse network topologies, node heterogeneity, and volatile link conditions that are possibly due to wireless propagation phenomena and node mobility. As a result, network links may be mostly disconnected or highly susceptible to a variety of disruptions that cause them to perform a set of disconnected clusters of the nodes. To achieve eventual delivery, some nodes must store the messages and wait for the opportunity to forward the interrupted messages.

Routing is one of the most fundamental problems in dealing with the intermittently connected networking. In contrast to the routing schemes in Mobile Ad-hoc Networks (MANETs) such as Dynamic Source Routing (DSR), Optimized Link State Routing Protocol (OLSR), Ad hoc On-demand Distance Vector (AODV)[7], a DTN may lack an end-to-end path for a given node pair for most of the time. Protocols developed for adhoc networks are therefore unable to address the intrinsic characteristics of a DTN. This paper presents a multi- copy routing method for DTNs.

II. RELATED WORK

Intermittently connected wireless systems represent a challenging environment for networking research, due to the problems of ensuring the messages delivery in spite of frequent disconnections and random meeting patterns. Due to the mobility of the nodes, protocols such as Adhoc On-demand Distance Vector routing (AODV), Optimized Link State Routing (OLSR), Dynamic Source Routing (DSR), continuously update routes when users require them (AODV and DSR) or in a proactive way (OLSR). These routes commonly time out after a few number of seconds. When a path between two nodes does not exist through the network, then no route can be created. Needless to say that these protocols can hardly run over Delay Tolerant Networks (DTNs) and will fail to deliver the data most of the time, because the assumption on the existence at a given time of a complete path between a source and a destination is simply not met. Many solutions have been proposed for use in such tolerant environments over the last few years. In [8], the authors proposed a new family of routing protocols. This family, called as Spray routing, can be viewed as a tradeoff between single and multiple copies techniques. Spray

routing consists of two steps: the first is called spray, and the second is either wait (spray-and-wait protocol) or focus (spray-and-focus protocol). In the spray step, a carefully chosen number of copies of the message are generated and disseminated in the network to the same number of relay nodes. In the wait step, relays simply wait to meet the destination in order to deliver the message. In the focus step, each copy of the message is routed according to a utility-based single copy routing algorithm. The authors showed that, if carefully designed, spray routing incurs significantly fewer transmissions per message than epidemic routing, and achieves a trade-off between efficient message delivery and low overhead.

Another related work with a routing scheme called as Binary Spray and Wait routing algorithm [9] works as, the source of a message initially starts with L copies; any node A that has $n > 1$ message copies, encounters another node called B with no copies, hands over to B , $n/2$ and keeps $n/2$ for itself; when it is left with only one copy, it switches to direct transmission. This algorithm performs well in both the message delivery and transmissions rate. The next scheme is similar to the single copy routing scheme, which scheme uses only one copy per the message. In [10], the authors used Seek and Focus (hybrid) routing algorithm. In this method each node maintains a timer for every other node. Nodes emit beacon signal, which then advertise their presence. Other nodes which sense this beacon signal and establish the relationship by exchange id, called encounter. A node holding the single message- copy, will handover to another node it encounters. The above algorithm has bad transmission rate when a single copy get lost.

III. PROPOSED WORK

The main feature of self adaptive utility based routing protocol (SAURP) is its ability in adaptation to the fluctuation of network status, traffic patterns/characteristics, and user behaviors, so as to reduce the number of transmissions, message delivery time, and increase delivery ratio. This is achieved by jointly considering the node mobility statistics, congestion, and buffer occupancy, which are subsequently fused in a novel quality-metric function. In specific, the link availability and the buffer occupancy statistics are obtained by sampling the channels and buffer space during each contact with another node. We use time-window based update strategy because it is simple in implementation and rather robust against the parameter fluctuation. Note that the network conditions could change very fast and make a completely event-driven model that is unstable. The developed quality-metric function targets to facilitating the decision making for each active data message, resulting in optimized network performance. Figure 1 illustrates the functional modules of the SAURP architecture along with their relations.

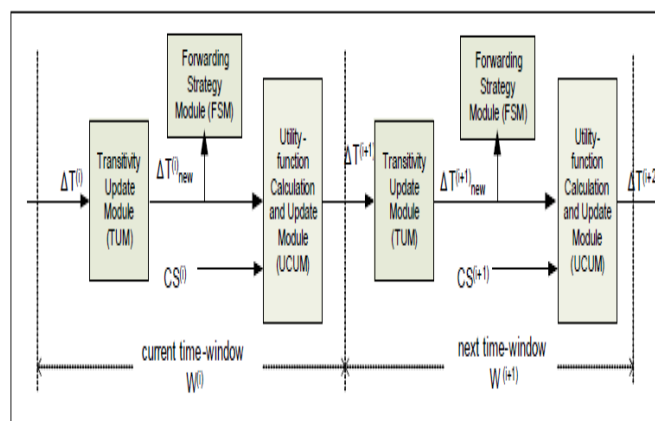


Figure 1: The SAURP Architecture

A. Contact Statistics

To compromise between the network state adaptability and the computation complexity, each node continuously updates the network status over a fixed time window. The maintained network states are called as Contact Statistics (CS), which include nodal contact durations, channel conditions, and buffer occupancy state, and are fed into UCUM at the end of each time window. The statistics collection process is described as follows. Let two nodes A and B be in the transmission range of each other, and each node broadcasts a pilot signal per k time units in order to look for its neighbors within its transmission range. Let $T(A,B)$, T_{free} , and T_{busy} represent the total contact time, the amount of time the channel is free and the buffer is not full, and the amount of time that the channel is busy or the buffer is full, respectively, at node A or B during time window $W(i)$. Thus, the total duration of the time in which node A and B can exchange information is calculated as:

$$T_{free} = T(A,B) - T_{busy}$$

B. Utility-function Calculation and Update Module (UCUM)

This module is applied at the end of each time window and is used to calculate the currently observed utility that will be further used in the next time window. The two inputs to this module in time window $W^{(i)}$ are:

1. The predicted inter-contact time $\Delta T^{(i)}$, which is calculated according to the previous time window utility and
2. The observed interencounter time obtained from the current $CS^{(i)}$ (denoted as $\Delta T_{CS}^{(i)}$).

An eligible contact of the two nodes occurs if the duration of the contact can support a complete transfer of at least a single message between the two nodes. Thus, in the event that node A encounters node B for a total time duration T_{free} during time window $W^{(i)}$, the number of eligible contacts in the time window is determined by:

$$n_c^{(i)} = \left\lfloor \frac{T_{free}}{T_p} \right\rfloor$$

where T_p is the least time duration required to transmit a single message. Let $\Delta T_{CS(A,B)}^{(i)}$ denotes the average inter-encounter time duration of node A and B in time $W^{(i)}$ and is given by:

$$\Delta T_{CS(A,B)}^{(i)} = \frac{W^{(i)}}{n_c^{(i)}}$$

C. The Transitivity Update Module (TUM)

When the two nodes are within transmission range of each other, they exchange utility vectors with respect to the message destination, based on which the custodian node decides whether or not each message should be forwarded to the encountered node. With a newly received utility vector, the transitivity update is initiated and we propose a novel adaptive transitivity update rule as follows. The transitivity property is based on the observation that if the node A frequently encounters node B and B frequently encounters node D, then node A has a good chance to forward messages to D through B. Such a relation is implemented in the proposed work using the following update strategy:

$$\Delta T_{(A,D)_{new}}^{(i)} = \alpha \Delta T_{(A,D)}^{(i)} + (1 - \alpha)(\Delta T_{(A,B)}^{(i)} + \Delta T_{(B,D)}^{(i)})$$

where α is a weighting factor that must be less than 1.

D. The Forwarding Strategy Module (FSM)

The decision of message forwarding in proposed work is mainly based on the utility function value of the encountered node regarding the destination, and the number of message copy tokens. If more than one message copy is currently carried, the weighted copy rule is applied; otherwise the forwarding rule is applied. The forwarding rule is as follows: If the destination node is one hop away from the encountered node, the custodian node hands over the message to the encountered node and completes the message delivery. If the inter-encounter time value of the encountered node relative to that of the destination node is less than that value of the custodian node by a threshold value, a custodian node hands over the message to the encountered node. The complete mechanism of the forwarding strategy in SAURP protocol is summarized in the following algorithm.

Algorithm:

Step 1: On contact between node A and B, exchange summary vectors

Step 2: for every message M at buffer of custodian node A do

Step 3: if destination node D in transmission range of B

Step 4: then A forwards message copy to B

Step 5: end if

Step 6: else if $\Delta T_{(A,D)}^{(i)} > \Delta T_{(B,D)}^{(i)}$ do

Step 7: if message tokens > 1 then

Step 8: apply weighted copy rule

Step 9: end if

Step 10: else if $\Delta T_{(A,D)}^{(i)} > \Delta T_{(B,D)}^{(i)} + \Delta T_{th}$ then

Step 11: A forwards message to B

Step 12: end else if

Step 13: end else if

Step 14: end for

IV. CONCLUSION

The objective of this work is to achieve end-to-end data delivery over intermittently connected mobile networks. Regular adhoc network protocols fail to provide successful communications due to user's frequent disconnections and long disconnection periods. This research work has presented our studies and has provided a suit of solutions to problems of routing in DTNs. Based on this proposed work, the research has been expanded to cover the routing problem for highly

congested DTNs. In this paper, self adaptive utility-based routing Protocol (SAURP) is proposed. SAURP is characterized by the ability of identifying potential opportunities for forwarding the messages to their destinations via a novel utility function based mechanism, in which a suite of environment parameters, such as the wireless channel condition, nodal buffer occupancy, and encounter statistics, are jointly considered. Thus, SAURP can reroute the messages around nodes experiencing high buffer occupancy, wireless interference, and/or congestion, while taking a considerably small number of transmissions.

REFERENCES

- [1] Delay Tolerant Networking. <http://www.dtnrg.org>.
- [2] Disruption tolerant networking. <http://www.darpa.mil/ato/solicit/DTN/>.
- [3] S. Burleigh, A. Hooke, L. Torgerson, K. Fall, V. Cerf, B. Durst, and K.Scott. Delay-tolerant networking: an approach to interplanetary Internet. IEEE Communications Magazine, 2003
- [4] A. Chaintreau, P. Hui, J. Crowcroft, C. Diot, R. Gass, and J. Scott. Pocket switched networks: Real-world mobility and its consequences for opportunistic forwarding. Technical Report UCAM-CL-TR-617, University of Cambridge, 2005
- [5] P. Juang, H. Oki, Y. Wang, M. Martonosi, L. S. Peh, and D. Rubenstein. Energy- efficient computing for wildlife tracking: design trade of early experiences with zebnet. In Proceedings of ASPLOS, 2002.
- [6] A. Seth, D. Kroeker, M. Zaharia, S. Guo, and S. Keshav. Low-cost communication for rural internet kiosks using mechanical backhaul. In Proceedings MobiCom, 2006
- [7] J. Broch, D. A. Maltz, D. B. Johnson, Y.-C. Hu, and J. Jetcheva. A performance comparison of multi-hop wireless ad hoc network routing protocols. In Mobile Computing and Networking, pages 85_97, 1998.
- [8] Autonomic Information Diffusion in Intermittently Connected Networks ,Sara Alouf, Iacopo Carreras, Álvaro Fialho, Daniele Miorandi and Giovanni Neglia 2010.
- [9] T. Spyropoulos, K. Psounis, and C. S. Raghavendra, "Spray and wait: Efficient routing in intermittently connected mobile networks," in Proc. ACM SIGCOMM Workshop on Delay Tolerant Networking (WDTN), 2005.
- [10] T. Spyropoulos, K. Psounis, and C. S. Raghavendra, "Efficient routing in intermittently connected mobile networks: The Single copy case," IEEE Trans. Networking, vol. 16, no. 1, Feb. 2008.

Comparative Studies on Exhaust Emissions from Two Stroke Copper Coated Spark Ignition Engine with Alcohol Blended Gasoline with Catalytic Converter

K. Kishor¹, M. V. S. Murali Krishna¹, P. V. K. Murthy²

¹Mechanical Engineering Department, Chaitanya Bharathi Institute of Technology, Gandipet, Hyderabad- 500 075, Andhra Pradesh, India

²Jaya Prakash Narayan Educational Society Group of Institutions, Mahabubnagar-509001, Andhra Pradesh, India

ABSTRACT: Experiments were conducted to control the exhaust emissions from four stroke, variable speed, variable compression ratio, single cylinder, spark ignition (SI) engine, with alcohol blended gasoline (80% gasoline, 10% methanol, 10% ethanol by volume) having copper coated combustion chamber [CCCC, copper-(thickness, 300 μ) coated on piston crown, inner side of cylinder head] provided with catalytic converter with sponge iron as catalyst and compared with conventional SI engine (CE) with pure gasoline operation. Aldehydes were measured by wet chemical method. Exhaust emissions of CO and UBHC were evaluated at different values of brake effective pressure, while aldehydes were measured at full load operation of the engine. A microprocessor-based analyzer was used for the measurement of CO/UBHC in the exhaust of the engine. Copper coated combustion chamber with alcohol blended gasoline considerably reduced pollutants in comparison with CE with pure gasoline operation. Catalytic converter with air injection significantly reduced pollutants with test fuels on both configurations of the engine. The catalyst, sponge reduced the pollutants effectively with both test fuels in both versions of the engine.

Keywords: S.I. Engine, CE, copper coated combustion chamber, Exhaust Emissions, CO, UBHC, aldehydes, Catalytic converter, Sponge iron, Air injection

I. INTRODUCTION

The paper is divided into i) Introduction, ii) Materials and Methods, iii) Results and Discussions, iv) Conclusions, Research Findings, Future scope of work followed by References.

This section deals with exhaust emissions from SI engine, their formation, effect of pollutants on human health, their impact on environment, change of fuel composition to reduce pollutants, engine modification to improve the performance and reduce pollutants, methods of reducing pollutants, catalytic converter, research gaps, objective of the experimentation.

Carbon monoxide (CO) and un-burnt hydrocarbons (UBHC), major exhaust pollutants formed due to incomplete combustion of fuel, cause many human health disorders [1-2]. These pollutants cause asthma, bronchitis, emphysema, slowing down of reflexes, vomiting sensation, dizziness, drowsiness, etc. Such pollutants also cause detrimental effects [3] on animal and plant life, besides environmental disorders. Age and maintenance of the vehicle are some of the reasons [4-5] for the formation of pollutants. Aldehydes which are intermediate compounds [6] formed in combustion, are carcinogenic in nature and cause detrimental effects on human health and hence control of these pollutants is an immediate task. Engine modification [7-9] with copper coating on piston crown and inner side of cylinder head improves engine performance as copper is a good conductor of heat and combustion is improved with copper coating. The use of catalysts to promote combustion is an old concept. More recently copper is coated over piston crown and inside of cylinder head wall and it is reported that the catalyst improved the fuel economy and increased combustion stabilization.

Catalytic converter is one of the effective [10-14] methods to reduce pollutants in SI engine. Reduction of pollutants depended on mass of the catalyst, void ratio, temperature of the catalyst, amount of air injected in the catalytic chamber. A reduction of 40% was reported with use of sponge iron catalyst while with air injection in the catalytic chamber reduced pollutants by 60%.

Alcohol was blended [15-17] with gasoline to reduce pollutants. CO and UBHC emissions reduced with blends of alcohol with gasoline.

The present paper reported the control of exhaust emissions of CO, UBHC and aldehydes (formaldehydes and acetaldehydes) from two stroke SI engine with alcohol blended gasoline in different configurations of the combustion chamber with catalytic converter with sponge iron as catalyst and compared with gasoline operation on CE.

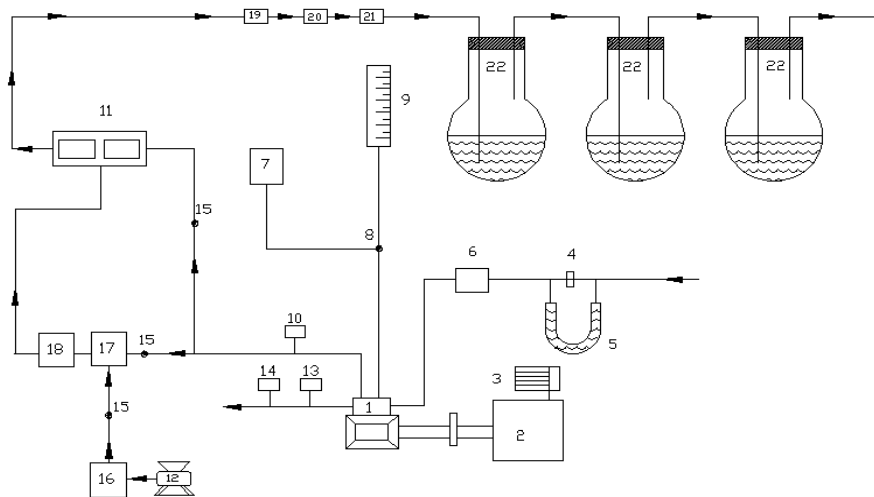
II. MATERIALS AND METHODS

This section deals with fabrication of copper coated combustion chamber, description of experimental set up, operating conditions of catalytic converter and method of measuring aldehydes and definition of used values

In catalytic coated combustion chamber, crown of the piston and inner surface of cylinder head are coated with copper by flame spray gun. The surface of the components to be coated are cleaned and subjected to sand blasting. A bond coating of nickel- cobalt- chromium of thickness 100 microns is sprayed over which copper (89.5%), aluminium (9.5%) and iron (1%) alloy of thickness 300 microns is coated with METCO flame spray gun. The coating has very high bond strength and does not wear off even after 50 h of operation [7].

Figure.1. shows schematic diagram for experimental set-up used for investigations. A four-stroke, single-cylinder, water-cooled, SI engine (brake power 2.2 kW, rated speed 3000 A rpm) was coupled to an eddy current dynamometer for measuring brake power. Compression ratio of engine was varied (3 -9) with change of clearance volume by adjustment of cylinder head, threaded to cylinder of the engine. Engine speeds are varied from 2400 to 3000 rpm. Exhaust gas temperature is measured with iron- constantan thermocouples. Fuel consumption of engine was measured with burette method, while air consumption was measured with air-box method. The bore of the cylinder was 70 mm while stroke of the piston was 66 mm. The engine oil was provided with a pressure feed system. No temperature control was incorporated, for measuring the lube oil temperature. Recommended spark ignition timing was 25°aTDC. CO and UBHC emissions in engine exhaust were measured with Netel Chromatograph analyzer.

CO and UBHC emissions in engine exhaust were measured with Netel Chromatograph analyzer.

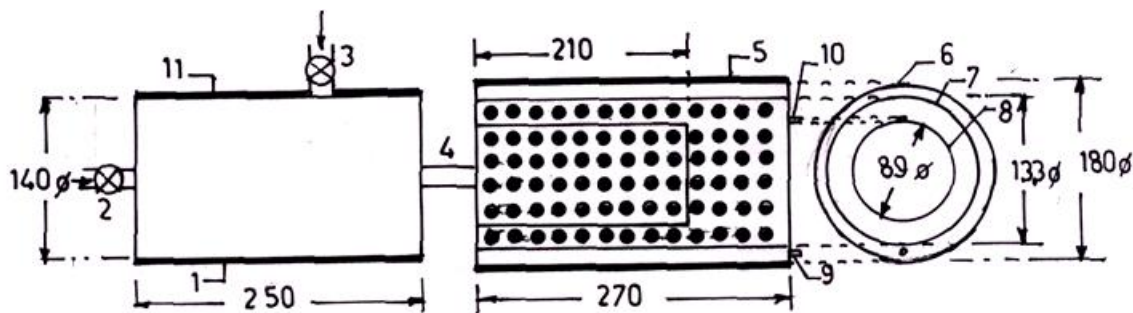


1. Engine, 2. Eddy current dynamometer, 3. Loading arrangement, 4. Orifice meter, 5. U-tube water monometer, 6. Air box, 7. Fuel tank, 8. Three-way valve, 9. Burette, 10. Exhaust gas temperature indicator, 11. CO analyzer, 12. Air compressor, 13. Outlet jacket water temperature indicator, 14. Outlet jacket water flow meter, 15. Directional valve, 16. Rotometer, 17. Air chamber and 18. Catalyst chamber 19. Filter, 20. Rotometer, 21. Heater, 22. Round bottom flasks containing DNPH solution

Figure1: Schematic Diagram of Experimental set up

A catalytic converter [11] (Figure.2) is fitted to exhaust pipe of engine. Provision is also made to inject a definite quantity of air into catalytic converter. Air quantity drawn from compressor and injected into converter is kept constant so that backpressure does not increase. Experiments are carried out on CE and copper coated combustion chamber with different test fuels [pure gasoline and alcohol blended gasoline (20% by vol)] under different operating conditions of catalytic converter like set-A, without catalytic converter and without air injection; set-B, with catalytic converter and without air injection; and set-C, with catalytic converter and with air injection. Air fuel ratio is varied so as to obtain different equivalence ratios.

For measuring aldehydes in the exhaust of the engine, a wet chemical method [6] is employed. The exhaust of the engine is bubbled through 2,4-dinitrophenyl hydrazine (DNPH) in hydrochloric acid solution and the hydrazones formed from aldehydes are extracted into chloroform and are analyzed by high performance liquid chromatography (HPLC) to find the percentage concentration of formaldehyde and acetaldehyde in the exhaust of the engine.



Note: All dimensions are in mm.

1. Air chamber, 2. Inlet for air chamber from the engine, 3. Inlet for air chamber from compressor, 4. Outlet for air chamber, 5. Catalyst chamber, 6. Outer cylinder, 7. Intermediate cylinder, 8. Inner cylinder, 9. Outlet for exhaust gases, 10. Provision to deposit the catalyst and 11. Insulation

Figure 2: Details of Catalytic converter

Definitions of used values:

Brake mean effective pressure: It is defined as specific torque of the engine. Its unit is bar.

$$BP = \frac{BMEP \times 10^5 \times L \times A \times n \times k}{60000}$$

BP = Brake power of the engine in kW;

BMEP= Brake mean effective pressure of the engine in bar

L= Stroke of the piston in m

A= Area of the piston = $\frac{\pi \times D^2}{4}$, Where D= Bore of the cylinder in m

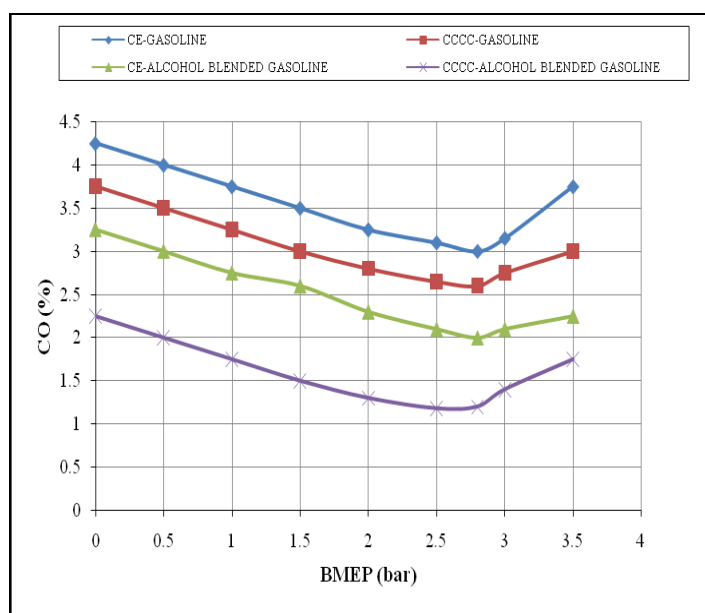
n= Effective number of power cycles = $\frac{N}{2}$, where N=Speed of the engine = 3000 rpm

III. Results and Discussion

This section deals with variation of CO emissions and UBHC emissions with brake mean effective pressure (BMEP) of the engine, variation of CO emissions and UBHC emissions with equivalence ratio and control of these pollutions along with aldehydes with different operating conditions of the catalytic converter.

Figure.3 shows the variation of CO emissions with BMEP in different versions of the engine with both pure gasoline and alcohol blended gasoline. CO emissions decreased with alcohol blended gasoline at all loads when compared to pure gasoline operation on copper coated combustion chamber and CE, as fuel-cracking reactions [13] were eliminated with alcohol.. The combustion of methanol or ethanol produces more water vapor than free carbon atoms as methanol has lower C/H ratio of 0.25, while with ethanol 0.33, against 0.50 of gasoline. Methanol or ethanol has oxygen in its structure and hence its blends have lower stoichiometric air requirements compared to gasoline. Therefore more oxygen that is available for combustion with the blends of methanol and gasoline, leads to reduction of CO emissions. Methanol or ethanol dissociates in the combustion chamber of the engine forming hydrogen, which helps the fuel-air mixture to burn quickly and thus increases combustion velocity, which brings about complete combustion of carbon present in the fuel to CO₂ and also CO to CO₂ thus makes leaner mixture more combustible, causing reduction of CO emissions.

Copper coated combustion chamber reduced CO emissions in comparison with CE. Copper or its alloys acts as catalyst in combustion chamber, whereby facilitates effective combustion of fuel leading to formation of CO₂ instead of CO. Similar trends were observed with Reference [7] with pure gasoline operation on copper coated combustion chamber.

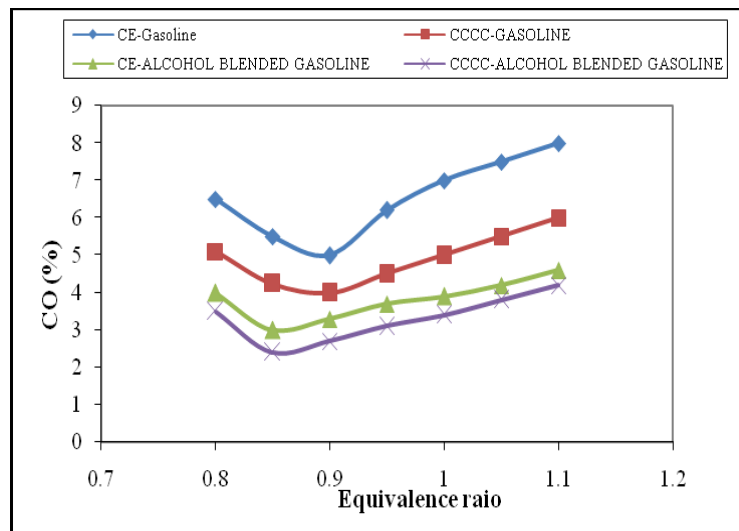


CE- conventional engine: CCCC-Copper coated combustion chamber, CO- Carbon monoxide emissions: BMEP-Brake mean effective pressure

Figure 3: Variation of CO emissions with BMEP in different versions of the combustion chamber with pure gasoline and alcohol blended gasoline at a compression ratio of 7.5:1 and speed of 3000 rpm

Figure.4 shows the variation of CO emissions with equivalence ratio, ϕ in both configurations of the engine with pure gasoline and alcohol blended gasoline. At leaner mixtures marginal increased CO emissions, and rich mixtures drastically increased CO emissions with both test fuels in different configurations of the combustion chamber. With alcohol

blended gasoline operation, minimum CO emissions were observed at $\phi = 0.85$, and with pure gasoline operations, minimum CO emissions are observed at $\phi = 0.9$ with both configurations of the engine. This was due to lower value of stoichiometric air requirement of alcohol blended gasoline when compared with gasoline. Very rich mixtures have incomplete combustion. Some carbon only burns to CO and not to CO_2 .



CE- conventional engine; CCCC-Copper coated combustion chamber, CO- Carbon monoxide emissions:

Figure 4: Variation of CO emissions with Equivalence ratio in both versions of the combustion chamber with different test fuels with a compression ratio of 7.5:1 at a speed of 3000 rpm

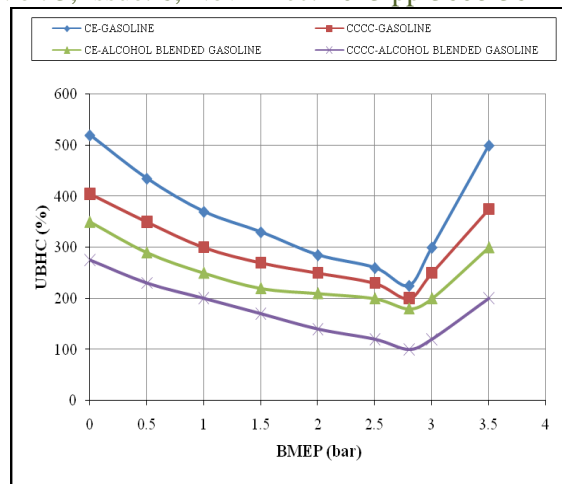
Table-1 shows the data of CO emissions with different test fuels with different configurations of the combustion chamber at different operating conditions of the catalytic converter with different catalysts. From the table, it can be observed that CO emissions decreased considerably with catalytic operation in set-B with alcohol blended gasoline and further decrease in CO is pronounced with air injection with the same fuel. The effective combustion of the alcohol blended gasoline itself decreased CO emissions in both configurations of the combustion chamber. CO emissions were observed to be higher with alcohol blended gasoline operation in comparison with pure gasoline operation in both versions of the combustion chamber at different operating conditions of the catalytic converter. This is due to the reason that C/H ratio of alcohol blended gasoline is lower in comparison with that of pure gasoline operation.

Table I: Data of 'Co' Emissions (%) with Different Test Fuels with Different Configurations of the Combustion Chamber at Different Operating Conditions of the Catalytic Converter at a Compression Ratio of 9:1 and Speed of 3000 Rpm

Set	Conventional Engine (CE)		Copper Coated Combustion Chamber (CCCC)	
	Pure Gasoline	Alcohol blended gasoline	Pure Gasoline	Alcohol blended gasoline
Set-A	5	3.2	4	2.6
Set-B	3	2.0	2.4	1.6
Set-C	2.0	1.3	1.6	1.1

Set-A- Without catalytic converter and without air injection, Set-B: With catalyst and without air injection, Set-C: With catalyst and with air injection

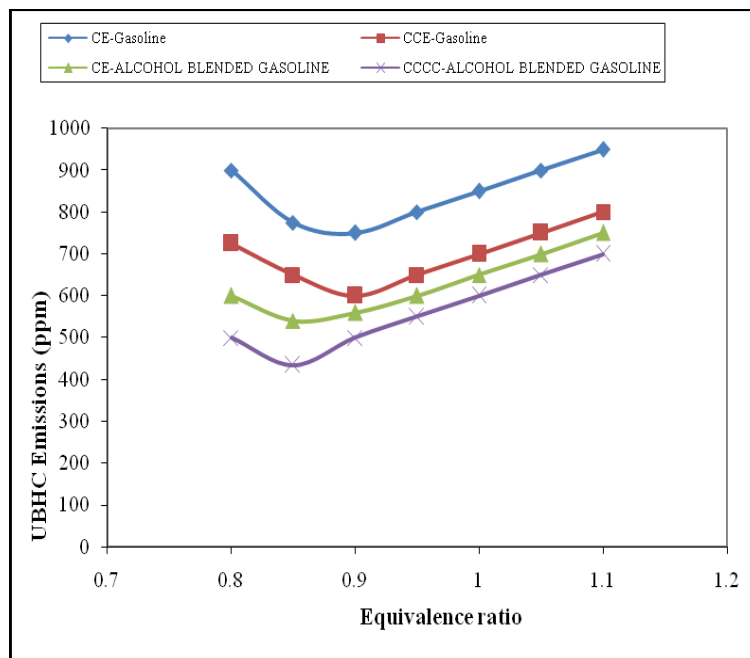
Figure.5 shows the variation of un-burnt hydro carbon emissions (UBHC) with BMEP in different versions of the combustion chamber with both test fuels. UBHC emissions followed the similar trends as CO emissions in copper coated combustion chamber and CE with both test fuels, due to increase of flame speed with catalytic activity and reduction of quenching effect with copper coated combustion chamber.



CE- conventional engine: CCCC-Copper coated combustion chamber, UBHC- Un-burnt hydro carbons: BMEP-Brake mean effective pressure

Figure 5: Variation of UBHC emissions with BMEP in different versions of the combustion chamber with pure gasoline and alcohol blended gasoline at a compression ratio of 7.5:1 and speed of 3000 rpm

Figure.6 shows the variation of UBHC emissions with equivalence ratio, ϕ with pure gasoline and alcohol blended gasoline with both configurations of the combustion chamber. The trends followed by UBHC emissions are similar to those of CO emissions. Drastic increase of UBHC emissions was observed at rich mixtures with both test duels in different configurations of the combustion chamber. In the rich mixture some of the fuel will not get oxygen and will not burn. During starting from the cold, rich mixture was supplied to the engine, hence marginal increase of UBHC emissions was observed at lower value of equivalence ratio.



CE- conventional engine: CCCC-Copper coated combustion chamber, UBHC-Un-burnt hydro carbons

Figure. 6 Variation of UBHC emissions with Equivalence ratio in both versions of the combustion chamber with different test fuels with a compression ratio of 7.5:1 at a speed of 3000 rpm

Table-2 shows the data of UBHC emissions with different test fuels with different configurations of the combustion chamber at different operating conditions of the catalytic converter with sponge iron. The trends observed with UBHC emissions were similar to those of CO emissions in both versions of the combustion chamber with both test fuels. From Table, it is observed that catalytic converter reduced UBHC emissions considerably with both versions of the combustion chamber and air injection into catalytic converter further reduced pollutants. In presence of catalyst, pollutants further oxidised to give less harmful emissions like CO₂. Similar trends are observed with Reference [7] with pure gasoline operation on copper coated combustion chamber.

Table II: Data Of 'UBHC' Emissions (ppm) with Different Test Fuels with Different Configurations Of The Combustion Chamber at Different Operating Conditions of The Catalytic Converter at a Compression Ratio of 9:1 And Speed of 3000 Rpm

Set	Conventional Engine (CE)		Copper Coated Combustion Chamber (CCCC)	
	Pure Gasoline	Alcohol blended gasoline	Pure Gasoline	Alcohol blended gasoline
Set-A	500	300	375	200
Set-B	300	140	205	105
Set-C	200	95	105	60

Set-A- Without catalytic converter and without air injection, Set-B: With catalyst and without air injection, Set-C: With catalyst and with air injection

The data of formaldehyde and acetaldehyde emissions is listed in Table-3 and Table-4 respectively at full load with different versions of the engine at different operating conditions of the catalytic converter with different test fuels of pure gasoline and alcohol blended gasoline repetitively. The formaldehyde emissions in the exhaust decreased considerably with the use of catalytic converter, which was more pronounced with an air injection into the converter. Alcohol blended gasoline increased formaldehyde emissions considerably due to partial oxidation compared with pure gasoline. The low combustion temperature lead to produce partially oxidized carbonyl (aldehydes) compounds with alcohol blended gasoline. Copper coated combustion chamber decrease formaldehyde emissions when compared with CE.

The trend exhibited by acetaldehyde emissions is same as that of formaldehyde emissions. The partial oxidation of alcohol blended specifically ethanol during combustion predominantly leads to formation of acetaldehyde. Copper (catalyst) coated engine decreased aldehydes emissions considerably by effective oxidation when compared to CE. Catalytic converter with air injection drastically decreased aldehyde emissions in both versions of the combustion chamber due to oxidation of residual aldehydes in the exhaust.

TABLE III: Data of Formaldehyde Emissions (% Concentration) with Different Test Fuels with Different Configurations of the Combustion Chamber at Different Operating Conditions of the Catalytic Converter at a Compression Ratio of 9:1 And Speed of 3000 Rpm.

Set	Conventional Engine (CE)		Copper Coated Combustion Chamber (CCCC)	
	Pure Gasoline	Alcohol blended gasoline	Pure Gasoline	Alcohol blended gasoline
Set-A	6.5	15	4.5	12
Set-B	4.5	6.0	2.5	5.5
Set-C	2.5	5.2	1.5	3.8

Set-A- Without catalytic converter and without air injection, Set-B: With catalyst and without air injection, Set-C: With catalyst and with air injection

TABLE IV: Data of Acetaldehyde Emissions (% Concentration) with Different Test Fuels with Different Configurations of the Combustion Chamber at Different Operating Conditions of the Catalytic Converter at a Compression Ratio Of 9:1 and Speed of 3000 Rpm.

Set	Conventional Engine (CE)		Copper Coated Combustion Chamber (CCCC)	
	Pure Gasoline	Alcohol blended gasoline	Pure Gasoline	Alcohol blended gasoline
Set-A	5.5	11.0	3.5	7.0
Set-B	3.5	5.0	2.5	4.0
Set-C	1.5	4.0	1.0	2.8

Set-A- Without catalytic converter and without air injection, Set-B: With catalyst and without air injection, Set-C: With catalyst and with air injection

IV. Conclusions

1. CO and UBHC emissions at full load operation decreased by 20% with CCE when compared with CE with both test fuels.
2. With copper coated combustion chamber, formaldehyde emissions decreased by 25% in comparison with pure gasoline operation on CE

3. With copper coated combustion chamber, formaldehyde emissions decreased by 39% in comparison with alcohol blended gasoline operation on CE
4. With copper coated combustion chamber, acetaldehyde emissions decreased by 36% in comparison with pure gasoline operation on CE
5. With copper coated combustion chamber, acetaldehyde emissions decreased by 21% in comparison with alcohol blended gasoline operation on CE
6. Set-B operation decreased CO, UBHC and aldehyde emissions by 40%, while Set-C operation decreased these emissions by 60% with test fuels when compared with Set-A operation.
7. Sponge iron is proved to be more effective in reducing the pollutants.

4.1 Research Findings and Future Scope of Work

Investigations on control of exhaust emissions in two-stroke SI engine were systematically carried out. However, performance of the copper coated combustion chamber is to be studied.

Acknowledgements

Authors thank authorities of Chaitanya Bharathi Institute of Technology, Hyderabad for facilities provided. The financial assistance from Andhra Pradesh Council of Science and Technology (APCOST), Hyderabad, is greatly acknowledged.

References

- [1] M.H.Fulekar, Chemical pollution – a threat to human life, Indian J Env Prot, 1, 2004 353-359.
- [2] B.K.Sharma, Engineering Chemistry (Pragathi Prakashan (P) Ltd, Meerut 2004, 150-160).
- [3] S.M Khopkar , Environmental Pollution Analysis,(New Age International (P) Ltd, Publishers, New Delhi 2005, 180-190).
- [4] M.K.Ghose, R.Paul R and S.K.Benerjee, Assessment of the impact of vehicle pollution on urban air quality, J. Environ Sci & Engg, 46, 2004, 33-40.
- [5] T. Usha Madhuri, T.Srinivas and K.Ramakrishna, A study on automobile exhaust pollution with regard to carbon monoxide emissions, Nature, Environ & Poll Tech, 2, 2003, 473-474.
- [6] P.V.K.Murthy, S.Narasimha Kumar, M.V.S.Murali Krishna, V.V.R.Seshagiri Rao, and D.N.Reddy, **Aldehyde emissions from two-stroke and four-stroke spark ignition engines with methanol blended gasoline with catalytic converter, International Journal of Engineering Research and Technology, (3)3, 2010, 793—802.**
- [7] N.Nedunchezian N & S.Dhandapani, Experimental investigation of cyclic variation of combustion parameters in a catalytically activated two-stroke SI engine combustion chamber, Engg Today, 2,2000, 11-18.
- [8] M.V.S.Murali Krishna, K.Kishor, P.V.K.Murthy, A.V.S.S.K.S. Gupta, and S.Narasimha Kumar, Performance evaluation of copper coated four stroke spark ignition engine with gasohol with catalytic converter, International Journal of Engineering Studies, 2(4), 2010, 465-473.
- [9] S.Narasimha Kumar, M.V.S.Murali Krishna, P.V.K.Murthy, V.V.R.Seshagiri Rao, and D.N.Reddy, Performance of copper coated two stroke spark ignition engine with gasohol with catalytic converter , International Journal on Mechanical & Automobile Engineering (IJMAE), 12(1), 2011, 36-43.
- [10] Murali Krishna, M.V.S and Kishor, K., “Control of pollutants from copper coated spark ignition engine with methanol blended gasoline”, Indian Journal of Environmental Protection. 25(8), 732-738, 2005
- [11] M.V.S.Murali Krishna, K.Kishor, P.R.K.Prasad, and G.V.V.Swathy, Parametric studies of pollutants from copper coated spark ignition engine with catalytic converter with gasoline blended methanol, Journal of Current Sciences, 9(2), 2006, 529-534.
- [12] M.V.S.Murali Krishna, K.Kishor, and Ch.V.Ramana Reddy, Control of carbon monoxide emission in spark ignition engine with methanol blended gasoline and sponge iron catalyst, Ecology, Environment & Conservation. 13(4), 2008, 13-17.
- [13] M.V.S.Murali Krishna, and K.Kishor, Investigations on catalytic coated spark ignition engine with methanol blended gasoline with catalytic converter, Indian Journal (CSIR) of Scientific and Industrial Research, 67, 2008, 543-548..
- [14] K.Kishor, M.V.S.Murali Krishna, A.V.S.S.K.S.Gupta, S.Narasimha Kumar, and D.N.Reddy, Emissions from copper coated spark ignition engine with methanol blended gasoline with catalytic converter, Indian Journal of Environmental Protection, 30(3), 2010, 177-18.
- [15] M.A.Ceviz, and F.Yu`ksel, Effects of ethanol–unleaded gasoline blends on cyclic variability and emissions in a spark ignition engine, Applied Thermal Engineering, 25, 2005, 917–925.
- [16] M.Bahattin Celik, Experimental determination of suitable ethanol–gasoline blend rate at high compression ratio for gasoline engine, **Applied Thermal Engineering**, 28, 2008, 396–404.
- [17] Al-Baghdadi, Measurement and prediction study of the effect of ethanol blending on the performance and pollutants emission of a four-stroke spark ignition engine, Proceedings of the Institution of Mechanical Engineers, 222(5), 2008, 859-873.

Spectroscopic Investigations of Mn (II) Doped Ni L-Histidine Hydrochloride Monohydrate Crystals

P. N. V. V. L. Prameela Rani¹, J. Sai Chandra¹,
V. Parvathi¹, Y. Sunandamma²

¹Dept. of Chemistry, Acharya Nagarjuna University, Nagarjuna Nagar- 522 510

²Dept. of Chemistry, Vikrama Simhapuri University, Nellore-524 001.

ABSTRACT: The main focus of this work had been to grow good quality crystals from amino acids and amino acid based materials for spectroscopic applications. Growth of crystals from aqueous solution is one of the methods of crystal growth which is extremely popular in the production of technologically important crystals. For the first time, Mn(II) doped Ni L-Histidine Hydrochloride monohydrate, Mn-NiLHICL crystals were grown from aqueous solution at room temperature by slow evaporation technique. The Mn(II) doped crystals were characterized by spectroscopic techniques such as X-Ray diffraction studies, Electron Paramagnetic Resonance(EPR), Optical absorption and FTIR studies. From the powder diffraction patterns of the grown crystals, lattice cell parameters were evaluated, $a = 1.5186$ nm, $b = 0.8917$ nm and $c = 0.6889$ nm. Values calculated from EPR studies for 'g' and Hyperfine Splitting factor for Mn(II) ion in the host crystal, $g = 2.071$, $A = 103 \times 10^{-4} \text{ cm}^{-1}$ indicated octahedral symmetry. Optical absorption studies confirmed the octahedral symmetry of Mn(II) ions in the host crystal. Crystal field and inter electronic parameters were evaluated for Mn^{2+} ion as $Dq = 855 \text{ cm}^{-1}$, $B = 810 \text{ cm}^{-1}$ and $C = 2480 \text{ cm}^{-1}$. Characteristic vibrations of the structure in the crystal confirmed the nature of bonding between the doped metal ion and the amino acid complex.

Keywords: Crystal growth, XRD, EPR, Optical, FTIR studies.

I. INTRODUCTION

Amino acid crystals doped with transition metal ions are suitable model systems to understand the basic aspects of role of metal ions in proteins. The critical role that dopants play in semiconductor devices stimulated the research on the potential applications of doped crystals. Doping is a well-chosen and widely accepted technique for incorporating the required physical properties in a bulk material for technological applications [1-4]. The technique has been extensively explored to modify the properties like electro optical (photoluminescence), conductivity and crystal growth [5,6]. It has also been demonstrated that metal ions, specially the transition metal ions are the most versatile in modifying the properties of a compounds dopant ions[7-9]. It is also well known that doping of a paramagnetic ion in a paramagnetic or diamagnetic host lattice of known symmetry helps one to understand the symmetry and covalency around the embedded ion. Doped amino acids and amino acid complexes were reported to exhibit NLO properties as they combine the advantages of organic and inorganic materials [[10,11]. L-Histidine is a protein forming amino acid, playing a fundamental role in several biological mechanisms including the formation of haemoglobin and is being used in the treatment of allergic diseases and anaemia [12]. Multi-dentate complexes of amino acids with metal ion dopants are at present considered as novel materials for second harmonic generation (SHG) properties [13]. Mn(II) is a well-known paramagnetic probe for both NMR and EPR investigations of metal ion binding sites and ligand interactions in enzymes and other proteins [14]. Studies were reported on Cu(II), Ni(II), Cr(III) and Zn(II) ion doped crystalline structures of pure L-Histidine hydrochloride monohydrate. In all these cases, dopant ions occupied interstitial positions in the crystal lattice of L-Histidine hydrochloride monohydrate and exhibited very good NLO properties. [4,15,16].

As far as our literature search goes, little attention has been paid to doped amino acid complexes and few investigations have been carried out on this class of compounds[16]. Thus there is a great need to explore their full potential by undertaking studies on these materials and the present study is one in this direction. Various transition metal ion doped amino acid complexes were grown in our laboratory in crystalline form and were characterized initially to understand the structure, site symmetry and nature of bonding. Mn(II) ion doped NiLHICL complex was one such system whose growth aspects were studied by slow evaporation technique. The grown crystals were characterized by X-Ray Diffraction, EPR, FTIR and Optical absorption studies to understand the site symmetry and the nature of bonding.

II. Experimental Section

Nickel L-Histidine Hydrochloride Monohydrate (here after called as Ni-LHICL) crystals were grown by slow evaporation technique at room temperature from aqueous, equimolar and equivolume solutions of Nickel Chloride Hexahydrate ($\text{NiCl}_2 \cdot 6\text{H}_2\text{O}$) and L-Histidine Hydrochloride Monohydrate ($\text{C}_6\text{H}_{10}\text{N}_3\text{O}_2\text{Cl} \cdot \text{H}_2\text{O}$). For the preparation of Mn(II) doped crystals, an amount of 0.01 mol% of Manganese Chloride was added to the growth solution and yields Mn(II) doped Ni-LHICL crystals about fifteen days during the slow evaporation process. Powder X-Ray diffraction patterns of the prepared Mn(II) doped Ni-LHICL crystals are recorded on PHILLIPS PW1830 X-ray diffractometer. A suitable crystal was selected for optical absorption spectrum and taken from JASCO V-670 Spectrophotometer. Electron Paramagnetic Resonance spectrum was recorded on JEOL- JES-FA 200 Spectrophotometer. Fourier Transformed-Infra Red (FT-IR) spectrum was recorded using KBr pellets on Thermo Nicolet 6700 FT-IR spectrophotometer in the region $400\text{-}4000 \text{ cm}^{-1}$.

III. Results and Discussion**3.1 Crystal Structure:**

Mn(II) doped Nickel L-histidine Hydrochloride monohydrate single crystals are Orthorhombic with space group $P2_12_12_1$. The unit cell dimensions are $a = 1.5186$, $b = 0.8917$ and $c = 0.6889$ nm. L-Histidine molecule consists of two groups of very nearly co-planar atoms. In the unit cell, these two groups are turned towards each other and the molecule is said to exist in the closed form [17].

3.2. Powder X-ray diffraction data:

Powder X-ray diffraction pattern of Mn(II) doped Ni-LHICL crystals is shown in the Fig. 1 and it contains sharp, clean patterns which indicates the highly crystalline phases. The prepared crystal system belongs to orthorhombic system and the corresponding lattice cell parameters are evaluated by using POWD programme. The obtained lattice cell parameters are, $a = 1.5186$, $b = 0.8917$ and $c = 0.6889$ nm. These values agreed well with the reported values of pure LHICL crystal cell parameters, $a = 1.5317$, $b = 0.8929$, $c = 0.6851$ nm [23]. The powder X-ray diffraction data for Mn(II) doped Ni-LHICL crystals are given in the Table 1.

3.3. EPR spectrum of Mn(II) doped NiLHICL crystals:

EPR Spectra of Mn(II) at room temperature are well resolved due to long spin lattice relaxation times in its ground state [18-20]. The EPR spectrum of Mn(II) ions in general can be analyzed using the spin Hamiltonian.

$$H = g \beta BS + SAI + SDS$$

Where 'g' is the isotropic factor, ' β ' the Bohr magneton, 'B' is External magnetic field, 'S' is the vector operator of the electron spin momentum and 'A' is the hyperfine interaction parameter, 'I' is the vector operator of nuclear spin momentum and 'D' is the zero field splitting parameter. The isotropic signal at $g = 2.071$ is due to Mn(II) in an environment close to octahedral symmetry. The value of 'A' in the range of $103.84 \times 10^{-4} \text{cm}^{-1}$ is consistent with Mn(II) in octahedral co-ordination [21]. It has been shown by Van Wieringen[22] that there is a regular variation of hyperfine coupling constant with covalency.

3.4. Optical absorption studies of Mn(II) doped NiLHICL crystals:

The five d-electrons of Mn(II) ions are distributed in the t_{2g} and e_g orbitals, with three in the former and two in the later. Thus the ground state configuration is $t_{2g}e_g$. This configuration gives rise to the ${}^6A_{1g}$, ${}^4A_{1g}$, 4E_g , ${}^4T_{1g}$, ${}^4T_{1g}$ and a number of doublets states of which ${}^6A_{1g}$ lies lowest according to Hund's rule. The free ion level for of Mn(II) in the order of an energy increasing are 6S , 4G , 4P , 4D and 4F etc. The energy levels of Mn(II) ion in octahedral environment i.e. coordination number 6 are ${}^6A_{1g}(S)$, ${}^4T_{1g}(G)$, ${}^4T_{2g}(G)$, 4E_g , ${}^4A_{1g}(G)$, ${}^4T_{2g}(D)$ and ${}^4E_g(D)$. The ${}^4E_g + {}^4A_{1g}(G)$ and ${}^4E_g(D)$ levels have relatively less influence compared to the other levels by crystal field. It means that the relative sharp lines can be expected in the absorption or excitation spectrum, which is the criterion for assignments of levels for Mn(II) ion [23,24]. Manganese free ion ground term is ${}^6S_{5/2}$ therefore no spin-allowed absorptions are possible. The electronic d-d transitions from a high spin d^5 configuration must necessarily involve the pairing of some electron spins. Such transitions are both spin-forbidden and orbitally forbidden therefore the bands are weak these transitions are assigned using Tanabe-Sugano diagram[25].

The spectrum recorded in the optical absorption region is shown in Fig.3. The observed bands at 685 nm corresponds to ${}^6A_{1g}(S) \rightarrow {}^4T_{1g}(G)$, the band at 405 nm is assigned to ${}^6A_{1g}(S) \rightarrow {}^4T_{2g}(D)$ for Mn(II) ions in the Mn(II) doped NiLHICL crystals [26-29]. The optical absorption spectrum also exhibited three characteristic bands at 1185, 720 and 422 nm for Ni(II) ion in the host lattice. These three intense bands observed are 6 assigned to the three spin allowed transitions ${}^3A_{2g}(F) \rightarrow {}^3T_{2g}(F)$, ${}^3A_{2g}(F) \rightarrow {}^3T_{1g}(F)$ and ${}^3A_{2g}(F) \rightarrow {}^3T_{1g}(P)$ will be intense. Based on these assignments energy matrices (d^5 and d^8) are solved for different values of inter-electronic repulsion parameters B, C and Crystal field parameter Dq. The following values are for Mn(II) ion $Dq = 855$, $B = 810$ and $C = 2480 \text{ cm}^{-1}$. For Ni(II) ion $Dq = 840$, $B = 820$ and $C = 2950 \text{ cm}^{-1}$. The observed and calculated band head positions of Mn(II) doped NiLHICL crystals are shown in Table 2.

3.5. FT-IR spectra of Mn(II) doped NiLHICL crystals:

FT-IR spectroscopy was effectively used to identify the functional groups in the grown crystal. FT-IR spectrum of the Mn(II) doped NiLHICL crystals is shown in Fig. 4. The NH_3^+ stretching and characteristic of hydrogen bonding region shows broad bands in the range $3500\text{-}2500 \text{ cm}^{-1}$. The N-H stretching vibration of the amino group in L-Histidine gives rise to an amide band between 3310 and 3270 cm^{-1} . The amide band is usually part of a Fermi resonance doublet with the second component absorbing weakly between 3100 and 3030 cm^{-1} [30]. The CH_2 group of Histidine produces peaks at 2602 and 3035 cm^{-1} due to its symmetric and asymmetric stretching modes. The peak at 1574 cm^{-1} is attributed to the skeletal vibrations of Histidine ring. The values are shown in Table 3. The FT-IR spectral study reveals the presence of various functional groups and confirms the slight distortion of the structure of the crystal due to doping. These values are compared with the values of pure L-Histidine [31] and doping of L-Histidine hydrochloride monohydrate crystal [32].

IV. Conclusion

Mn (II) NiLHICL Crystals are grown at room temperature and are characterized using Powder XRD, EPR, Optical absorption and FT-IR studies. The following conclusions are drawn

Powders XRD pattern confirms the pure LHICL crystal structure. The deviation of evaluated cell parameter with the pure crystals may confirm the incorporation of transition metal ions in the host lattice. The analysis of the optical absorption spectra confirms the coordination of Ni(II) and Mn(II) ions is octahedral site symmetry in the host lattices. The crystal field and Racah parameters are determined. From the EPR spectral studies, spin-Hamiltonian and hyperfine splitting parameters also suggests the octahedral sites for Mn(II) ions in the host lattice. By correlating EPR and optical results, the evaluated parameters indicate the partial covalence between Mn(II) ions and its ligands. From FT-IR studies, the prepared Mn(II)-NiLHICL crystals shows different vibrational bands related to stretching modes of NH_3^+ , COO^- groups, and in plane C-H deformation imidazole ring which confirms the presence of amino acid. A five membered ring is formed with the metal, amine nitrogen and the carboxylic oxygen.

Acknowledgments

The author PNVVL Prameela Rani is very thankful to R.V.S.S.N Ravikumar for his valuable suggestions regarding spectral data calculations and also Y.Sunandamma is thankful to the UGC, Government of India New Delhi, for sanctioning Major Research project to carry out the present research work.

References

- [1] S.J. Lippard, J. M. Berg, Principles of Bioinorganic Chemistry, University Science Books: Mill Valley, CA, 1994.
- [2] L. Pickart, W.H Goodwin, W. Burgua, TB. Murphy, D K. Johnson, Journal of Biochemical Pharmacology 32 (1983) 3868.
- [3] P.Zanello, S.Tamburini, P.A.Vigato, G.A.Mazzocchine, Coordination Chemical Reviews. 77 (1987) 165
- [4] G.D.Whitener, JR Hagardorn, J Arnold, Journal of Chemical Society & Dalton Transactions (1999) 1249.
- [5] T.Arumanayagam, P.Murugakoothan, Material Letters 65 (2011) 2748.
- [6] V. G. Dmitriev, G. G. Gurzadyan, D. N. Nikgosyan, Hand book of nonlinear optical crystals, 2nd ed., Springer, New York, 1997.
- [7] X Lai, K J Roberts, L H Avanci, L P Cardoso, J M Sasaki Journal of Applied Crystallography 36 (2003) 1230.
- [8] D A H Cunningham, R B Hammond, X Lai, K J Robert Chemical Materials 7 (1995) 1690.
- [9] X Lai, K J Robert, J M Bedzyk, P F Lyman, L P Cardoso, J M Sasaki Chemical Materials 17 (2005) 4058.
- [10] S. Tamilselvan, X. Helan Flora, A. Cyrac Peter, M. Gulam Mohamed, C.K. Mahadevan, M. Vimalan, J. Madhavan, Scholars Research Library Archives of Applied Science Research, 2011, 3 (1) 235.
- [11] AlosiousGonsago, Helen Merina Albert, R. Umamaheswari, A.Joseph Arul Pragasam, Indian Journal of Science & Technology 5 (3) (2012) 2369.
- [12] Wen-Chen Zheng, Physics Status Solidi B 205 (1998) 627.
- [13] C.M.R. Remedios, W. Paraguassu, P.T.C. Freire, J.Mendes-Filho, J.M. Sasaki, F.E.A. Melo, Physics Review B 72 (2005) 014121.1.
- [14] George H Reed, George D Markham, B.D.Nageswara Rao, Journal of Magnetic Resonance, 33 (3) (1979) 595.
- [15] C.Prema Thomas, S.Arun, J.Madhavan, ReenaIitya Chan, Joseph AculPrasasam, Joe G.M. Jesudurai, K.Prapa, P.Sagayaraj, Indian Journal of Pure Applied Physics 45 (2007) 591.
- [16] P. Praveen Kumar, V. Manivannan, P.Sagayaraj, J.Madhavan, Bulletin of Material Science 32 (2009) 431.
- [17] Ram Kripal, Sangita Pandey, Journal of Physics and Chemistry of Solids, 72 (2011) 67–72.
- [18] A. Abragam, B.Bleaney, Electron Paramagnetic Resonance of Transition Ions, Clarendon Press, Oxford, (1970).
- [19] J.R. Pilbrow, Transition Ion electron Paramagnetic Resonance, Clarendon Press, Oxford, UK, (1990).
- [20] B.R.Mc. Garvey, in: R.L. Carlin (Ed.), Transition Metal Chemistry. 3rd Ed, (1966) P.89.
- [21] D.L. Griscom, R.E. Griscom, Journal of Chemistry and Physics 47 (1967) 2711.
- [22] J. S. Van Wieringen, Faraday Society Disc 19 (1955) 118.
- [23] R.P. SreekanthChakradhar, K.P.RameshJ.L.Rao, J.RamaKrishna, Journal of Physics and Chemistry of Solids 64 (2003) 641.
- [24] J.Wang, S.Wang, Q.Su, Journal of Solid-State Chemistry 177 (2004) 895.
- [25] Y.Tanabe, S.Sugano, Journal of Physical Society of Japan. 9 (1954) 753.
- [26] A. B. P. Lever, Inorganic electronic spectroscopy, Elsevier, Amsterdam, (1968) p.296.
- [27] R.V.S.S.N. RaviKumar, K.Ikeda, A.V.Chandrasekhar, Y.P.Reddy, P.S.Rao, Jun Yamauchi, Journal of Physics and Chemistry Solids 64 (2003) 2433.
- [28] G. Lakshminarayana, S.Buddhudu, Spectro Chimica Acta. A 63 (2006) 295.
- [29] S. Boobalan, P.Sambasiva Rao, Journal of Organo Metallic Chemistry 695 (2010) 963..
- [30] R.Silverstein, G.C.Bassler, T.C.Morrill, Spectroscopic Identification of Organic Compounds, John Wiley & Sons Singapore. (1981).
- [31] J.Madhavan, S.Aruna, P.C.Thomas, M.Vimalan, S.A.Rajasekar, P.Sagayaraj, Crystal Research Technology 42 (2007) 59.
- [32] D.Syamala, V.Rajendran, R.K.Natarajan and S.MoorthyBabu, Journal of Crystal Growth and Design 7 (2007) 1695.

Figures

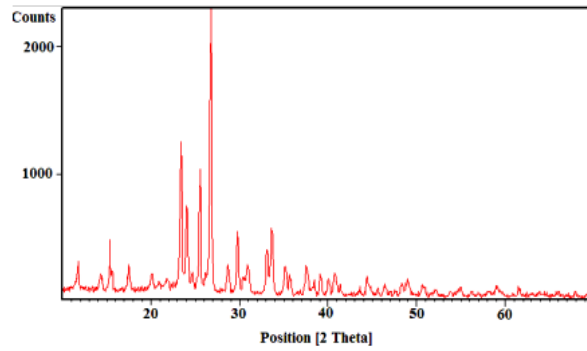


Fig.1 XRD spectrum of Mn (II) doped Ni L-HCl crystal.

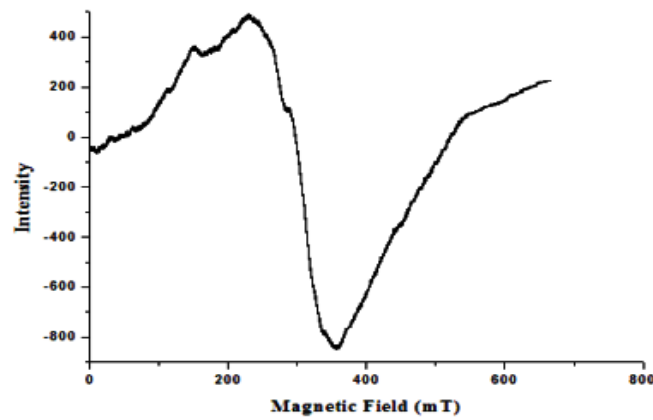


Fig.2 EPR spectrum of Mn(II) doped Ni L-HCl.

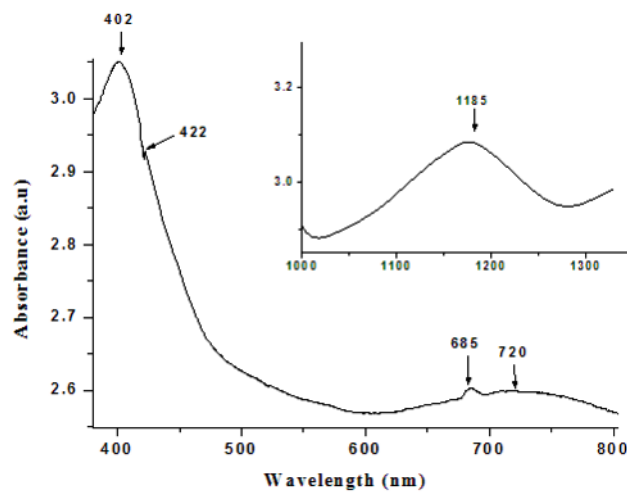


Fig.3 Optical spectrum of Mn (II) doped Ni L-HCl

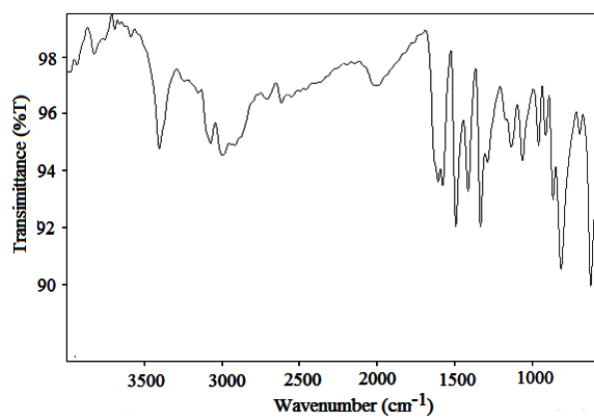


Fig.4 FTIR of Mn(II) doped Ni L-HCl

Table :1 d-spacing and h k l values obtained for of Mn(II) doped NiLHICL Crystal.

Sys: Orthorhombic P Lambda= 1.540600 F30= 2.0(.032,464) X30= 0

Lo30/ Lc464 M20= 2.8 A= 21.36 B= 104.63 C= 159.43 D= 41.10 E= 1.80 F= 30.

a=1.5186 nm , b= 0.8917nm, c= 0.6889 nm

d-spacing A		Indices			2 θ	
obs.	calc.	h	k	l	obs.	calc
7.5306	7.5306	0	1	0	11.74	11.74
6.1630	6.1630	1	1	0	14.36	14.36
5.7576	5.7576	1	0	1	15.38	15.38
5.1587	5.1587	0	1	1	17.17	17.17
4.4096	4.4096	0	1	1	20.12	20.12
4.0681	4.0681	1	1	1	21.83	21.83
3.8002	3.7653	0	2	0	23.39	23.61
3.6983	3.7174	3	2	0	24.04	23.92
3.4875	3.4890	5	1	0	25.52	25.51
3.3306	3.3336	5	0	0	26.75	26.72
3.1086	3.1068	5	1	1	28.69	28.71
2.9970	2.9980	0	1	2	29.79	29.78
2.8894	2.8947	1	1	2	30.92	30.87
2.7039	2.7031	1	1	2	33.10	33.11
2.6621	2.6566	3	0	2	33.64	33.71
2.5496	2.5498	6	2	1	35.17	35.17
2.5139	2.5136	6	0	1	35.69	35.69
2.3933	2.3896	3	2	1	37.55	37.61
2.3005	2.3035	3	1	2	39.13	39.07
2.2118	2.2114	6	3	1	40.76	40.77
2.0731	2.0698	6	0	2	43.63	43.70
2.0368	2.0361	5	3	2	44.44	44.46

Table : 2 Optical transitions for the Mn(II) doped NiLHICL crystals

Transitions From ${}^6A_{1g}(S)$	Observed		Calculated
	Wavelength (nm)	Wavenumber (cm^{-1})	Wavenumber (cm^{-1})
For Mn(II) ${}^6A_{1g}(S) \rightarrow {}^4T_{1g}(G)$	405	24685	24881
${}^6A_{1g}(S) \rightarrow {}^4T_{2g}(D)$	685	14594	14558
For Ni(II)			
${}^3A_{2g}(F) \rightarrow {}^3T_{1g}(F)$	422	23690	23696
${}^3A_{2g}(F) \rightarrow {}^3T_{1g}(P)$	720	13885	13803
${}^3A_{2g}(F) \rightarrow {}^3T_{2g}(F)$	1185	8436	8400

Table : 3 Observed Vibrational modes of Mn(II) doped Ni L-Histidine Hydrochloride Monohydrate Crystals

Wavenumber (cm^{-1})	Assignments
3403	O-H stretching of water
2997	N-H Symmetrical stretching
2616	C-H Symmetrical stretching
1635	C=O stretching
1605	Asymmetric bend of NH_3^+ and C=N stretching
1575	Asymmetric mode of $-COO^-$ and C=C stretching
1491	Symmetric bend of NH_3^+
1416	Symmetric mode of $-COO^-$ and C-N stretching
1070	C-O stretching of carboxylic group
863	C-H out of plane bending

Simulation of Explosive Welding with Reasonable Gap Based on ALE Method

Wei Deng¹, Ming Lu², Xiaojie Tian³

¹(College of Field Engineering, PLA University of Science and Technology, China)

²(College of Field Engineering, PLA University of Science and Technology, China)

³(College of Mechanical and Electronic Engineering, China University of Petroleum, China)

ABSTRACT: In order to study the range of reasonable gap of explosive welding composite pipe, using Arbitrary Lagrange Euler (ALE) method to carry out Finite Element Analysis of explosive welding composite pipe, and simulating the dynamic process of explosive welding composite pipe in different gaps. The results showed that the influence of the gap to the collision speed, collision pressure, and effective plastic strain were obvious. While the collision speed increases with the increase of the gap, the collision pressure decreases with the gap increases, and the effective plastic strain was increased with the increase of the gap. The lower limit of the gap should meet that the composite tube collision velocity greater than the minimum impact speed. Combined with empirical formulas and experiment, a reasonable gap that was given by the simulation results is 0.5mm-0.8mm for such composite pipe.

Keywords: Explosive welding; Al/Ti composite pipe; ALE method; gap

I. INTRODUCTION

Explosive welding is a welding process that using high temperature, high pressure instantly generate from explosive detonation in a very short period of time to achieve a combination metal. Gap is an important parameter of explosive welding process. Chemical energy of explosives can not be directly supplied to the welding metal; the energy must be passing through the absorption, conversion, and distribution. Therefore, there is no gap, where can not be achieved between the explosive welding metals [1]. Many scholars demonstrated the importance of the gap from the test and theory, and given the empirical formula of gap [2, 3]. Since the explosive welding process with instantaneous and dangerous, there are some technical problems directly to test the process. But using computer simulation, not only can visually reflect the impact circumstances of explosive welding between the base pipe and flyer pipe, but also can reduce the number of tests, and reduce costs. So, it is an effective method to study the explosive welding process.

Currently, numerical simulation study on explosive welding have been reported, such as Akbari et al. simulated the explosion of a composite plate welding process by finite element software AUTODYN, used Willamsburg equation of state simulated different states of explosives in the reference [4,5]. In the reference [6], Grignon et al. simulated the different welding parameters aluminum welding using two-dimensional finite element method, and got the parameters law of the explosive direct combination interface. Ma bei established a three pipe explosive welding model using three-dimensional finite element and study the process of forming and welding quality problems under different gap in the reference [7].Huang Qin et al. described the use of LS-DYNA software to simulate the influence space and charge volume of the pipe explosive welding process in the reference [8]. However, the above references were limited to qualitative analysis, did not give a reasonable method to determine the size of the gap.

In this paper, on the basis of the establishment of the explosive welding composite pipe dimensional finite element model, the relationship between the different size of the gap and the dynamic composite pipe explosion welding process parameters were studied, and a range of composite pipe explosive welding gap was given. This provided an effective method to determine a reasonable composite pipe explosive welding gap.

II. THEORETICAL RANGE OF GAP

The material of base tube is titanium (TA2), and flyer tube is commercial purity aluminum (1060). And the basic performance parameters of Al tube and Ti tube are list in Table 1.

Table 1 Basic performance parameters of Al tube and Ti tube

Material	$\rho(\text{g}\cdot\text{cm}^{-3})$	$H_V(\text{kg}/\text{mm}^2)$	$\sigma_b(\text{MPa})$	melting point($^{\circ}\text{C}$)	Thickness (mm)
1060	2.71	72	143	660	1
TA2	4.51	160	560	1668	2

In explosive welding composite pipe, neither the theoretical formula method, nor test calculation method to determined the size of the gap between the base pipe and flyer pipe. Based on this situation, people in determining the size of the gap between the composite pipe, commonly used Ezra empirical formula to determine the gap of the explosive welding composite plate [2]:

$$d < 5, h/3 < S < 2h/3 \quad (1)$$

Where: d is the density of flyer material, h is the thickness of the flyer material, S is the gap between the base pipe and flyer pipe.

Table 1 showed gravity and thickness of aluminum flyer tube is 2.71 and 1mm, therefore, the range of gap between the stainless steel base pipe and the aluminum flyer pipe is 0.33mm~0.67mm by the equation (1).

III. ALE SIMULATION IN DIFFERENT GAP AND RESULTS ANALYSIS

3.1 ALE simulation

Arbitrary Lagrange Euler method (ALE) was used to simulate the explosive welding. ALE is neither Euler with a fixed mesh nor Lagrange with the volume mesh, but a suitable mesh that every step of the construction material according to the boundary region and the next step can be calculated facilitate[9]. So this method has a strong advantage calculating the large deformation, while beneficial of observation and analysis the latter results.

A physical model was created using AUTODYN software. In order to save computer resources, to reduce the calculation time, the analysis of the object is 1/4 simplify model when modeling, taking into account the symmetry axis of the tube model. Fig. 1a is a model of the material, the outer layer titanium tube, which has 20mm diameter and 2mm thickness, the middle layer is an aluminum tube, which wall thickness has 1mm. Using the Johnson-Cook equation of state (JC-EOS)described the metal materials instantaneous strain process. Inner layer is emulsion explosive, and using Jones-Wilkins-Lee equation of state (JWL-EOS) described detonation process of explosive [10]. To facilitate the observation of simulation results, the interface combined position of tube were sampling, locations shown in Fig. 1b.

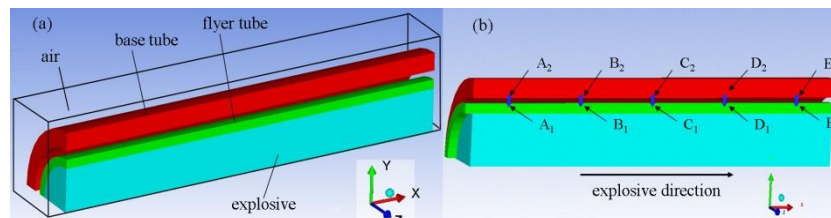


Figure 1 Simulation model (a) and sampling node location (b) combined position of tube

3.2 Numerical simulation

According to the empirical formula obtained from the first section, Gap ranges from 0.33mm~0.67mm. Given the convenience of numerical simulation, the value of gap expanded appropriately when using numerical simulation. And the value of gaps were 0.3mm, 0.4mm, 0.5mm, 0.6mm, 0.7mm, 0.8mm, 0.9mm, 1.0mm.

When the gap was 0.5mm, the traveled distance result of the composite pipe was shown in Fig. 2. It could visually be found the nodes A_1 and A_2 , B_1 and B_2 , C_1 and C_2 , D_1 and D_2 , E_1 and E_2 , corresponding to the titanium tube and the aluminum tube, were moved by the radial explosive effect in Fig. 2a. And the movement distance difference of titanium tube and the aluminum tube was more than 0.5mm. It indicates that the aluminum layer and the titanium layer has been welded together, that is the bonding interface of composite pipe welded successful and effective. It was confirmed that this model was reliable model.

It could be found plastic deformation effective occurred in the bonding interface of the aluminum layer with the titanium layer and explosive layer with aluminum layer, compared to the elastic deformation of the rest in Fig. 2b. This was further evidence of successful and effective bonding interface welding.

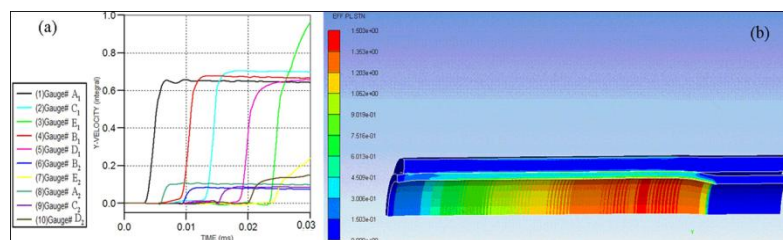


Figure 2 Simulation results of the value gap of 0.5mm (a) Movement distance of interface node (b) effective plastic strain of composite pipe

3.3. Results and Analysis

3.3.1 The impact of gap on the collision velocity

It was gotten the collision flight speed of aluminum flyer tube under different gap by numerical simulation, and shown in Fig. 3. It could be found intuitively in graphics that, with the increase of gap distance, meaning that increase of flyer pipe distance to accelerate, collision velocity tube obtained also increase. Gap of 0.3mm, the speed of the aluminum node obtained about 300m/s; gap of 1mm, the speed of the aluminum flyer pipe nodes obtained about 500m/s. Meanwhile it could be found that collision velocity of the flyer pipe in the one same gap also increases along the direction of detonation.

According to calculated the material properties of the metal "weld-ability window", minimum collision speed (v_{pmin}) could be represented by the formula in [11]:

$$v_{pmin} = K\sqrt{H_V / \rho_f} \tag{2}$$

Where: K is a constant value between 0.6~1.2; H_V is the material Vickers Hardness of the flyer pipe; ρ_f is material density of the flyer pipe. The H_V and ρ_f of aluminum were substituted into the equation (2) and K take 0.7. It could be calculated that the v_{pmin} was 360m/s, which reliably welded required.

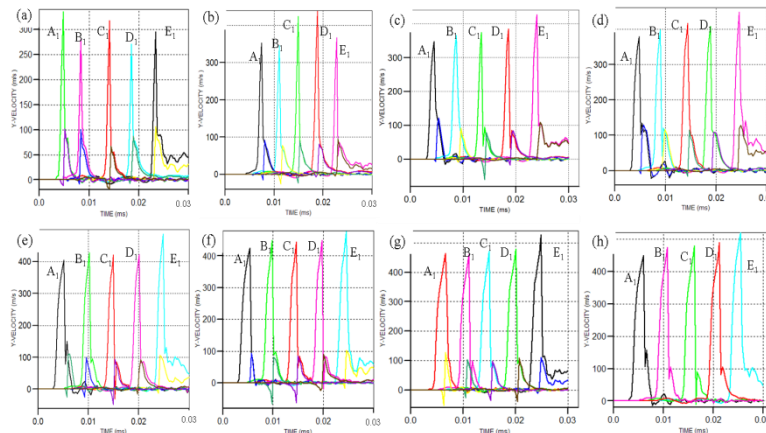


Figure 3 Collision speed of composite pipe under different gap (a)0.3mm gap (b)0.4mm gap (c)0.5mm gap (c)0.6mm gap (e)0.7mm gap (f)0.8mm gap (g)0.9mm gap (h)1mm gap

According to the shown of Fig. 3(a), the flight speed of flyer tube was less than the minimum impact speed 360m/s, when the value gap is the 0.3m, did not meet the speed requirements of explosive welding, and would be lead to weld failure. The speed of the nodes A1 and B1 of flyer tube was less than 360m/s, when the value gap is the 0.4m, was shown in Fig. 3(b), and also would be lead to weld failure. Therefore, the value of gap should be greater than 0.4mm.

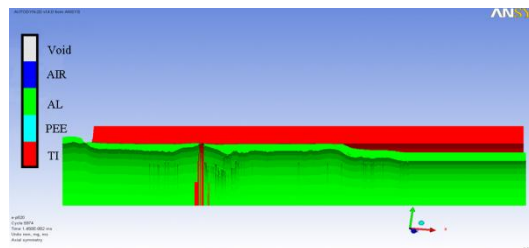


Figure 4 Situation of rupture of flyer tube

According to the shown of Fig. 3(g) and 3(h), the flight speed of flyer tube was greatly exceeded the minimum impact speed 360m/s when the value gap were the 0.9mm and 1mm. Fig. 4 showed that the rupture of flyer tube was occurred in the process of explosive welding when the value gap was the 0.9mm. This is because under the powerful force of explosive detonation, the distance of the outward expansion of aluminum was increased when the gap became large; wall thickness of the tubes was getting thinner, more than its limit; and aluminum pipe would be brook down.

In summary, according to the requirements of critical flight speed of flyer layer and of rupture limit of aluminum material, it could be inferred the range of the gap should be between 0.5~0.8mm.

3.3.2 The impact of gap on the collision pressure

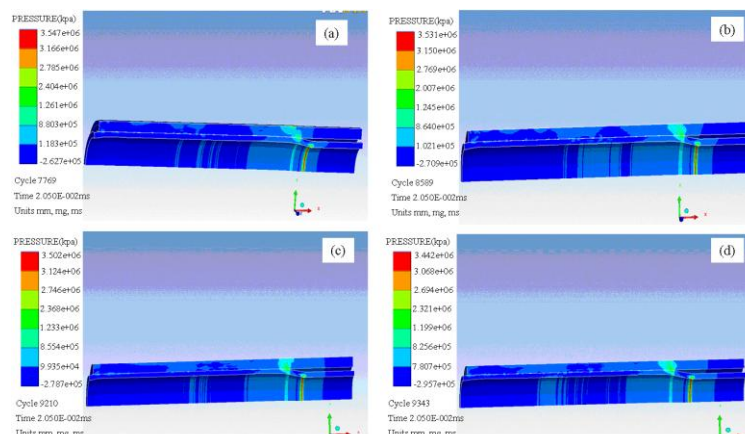


Figure 5 Pressure of composite pipe under different gap (a) 0.5 mm gap (b) 0.6 mm gap (c) 0.7 mm gap (d) 0.8mm gap

It was gotten the collision pressure of pipe under different gap that 0.5mm, 0.6mm, 0.7mm, 0.8mm by numerical simulation in 20.5 μ s, and shown in Fig. 5.

It could be found that maximum pressure occurred in the position of collision interface of the composite pipe, while the gap increased, the peak pressure was gradually reduced, but the reduction amount was less. It was analyzed that substantially pressure pulse of flyer tube obtained from the explosive detonation was the same instant in the difference distance of gap, and then decreased with increasing time. The time to drive the flyer tube was required accordingly increasing with the increase of gap distance. When the base tube and flyer tube were collided, the pressure was reduced accordingly. Simultaneously, due to the time that accelerated flyer pipe was very short, reduce the amount of collision pressure was little.

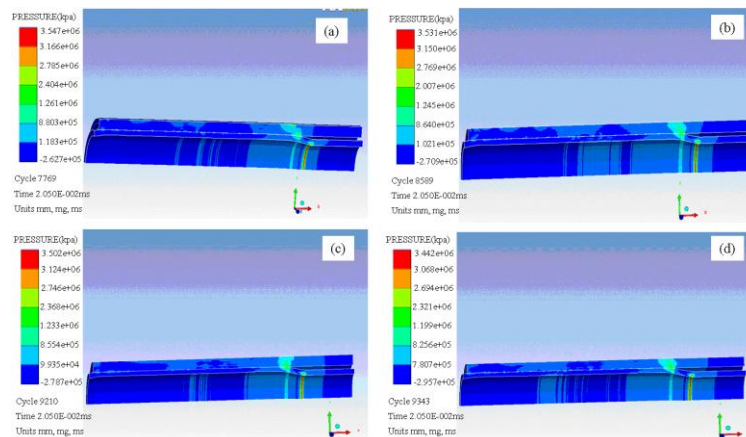


Figure 5 Pressure of composite pipe under different gap (a) 0.5 mm gap (b) 0.6 mm gap (c) 0.7 mm gap (d) 0.8mm gap

3.3.3 The impact of gap on the effective plastic strain

In the explosive welding process, the bonding interface metal plastic strain is the reason and the necessary conditions to achieve succeed welding[1]. It was gotten the effective plastic strain of composite pipe under different gap that 0.5mm, 0.6mm, 0.7mm, 0.8mm by numerical simulation in 20.5 μ s, and shown in Fig. 6.

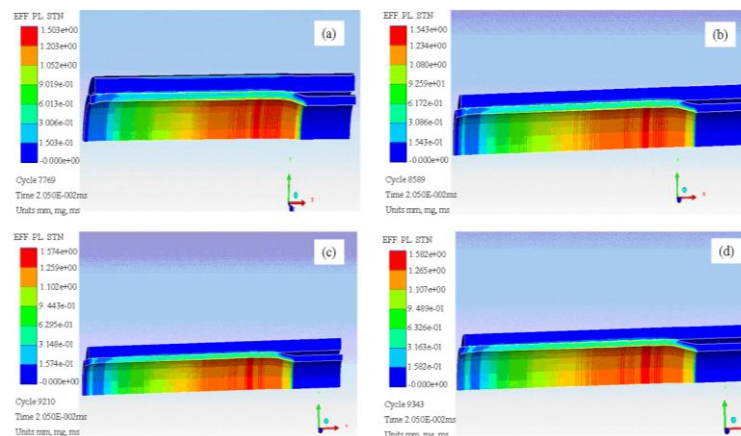


Figure 6 Effective plastic strain of composite pipe under different gap(a) 0.5 mm gap (b) 0.6 mm gap (c) 0.7 mm gap (d)0.8mm gap

It could be found that the areas of large plastic deformation were mainly concentrated in the interface of flyer tube in contact with the base tube and interface with explosives in contact with flyer tube. As the detonation process, the plastic strain at the interface had an increasing trend along the detonation direction. The gap larger, the effective plastic strain at the interface was greater. It was analyzed that the gap larger, the distance that accelerated the flyer tube by the explosive detonation would be greater. The speed and the collision energy of the flyer pipe would be greater. That would be lead to an increased effective plastic strain inevitably.

IV. EXPERIMENT

According to simulation results of a gap in the range 0.5~0.8mm, it was carried out 5 group experiments for each gap using the experiment method was used in [12], as shown in Fig. 7.



Figure 7 Composite tube of Al/Ti

Any composite tube sample was taken from each group carried out analysis. After intercepting the middle of the sample, the scanning electron microscope (SEM) was conducted. According to the SEM image of the sample was found as Fig. 8, combined bonding interface was wavy, and there were no gaps and voids of the bonding interface microscopic defects. It was suggested that those were good composite pipe welding following those gaps.

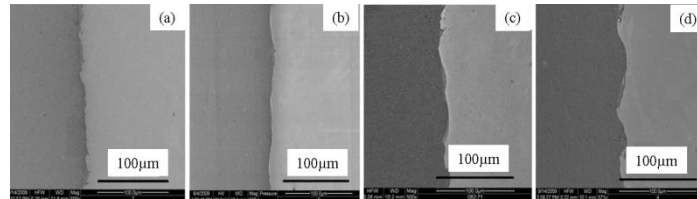


Figure 8 SEM Morphology of Al/Ti composite pipe under different gap (a) 0.5 mm gap (b) 0.6 mm gap (c) 0.7 mm gap (d) 0.8mm gap

To demonstrate the rationality of 0.5~0.8mm gap more, from the view of the mechanical properties of the composite pipe, the quality of the combines of the extracted samples was studied. Fig. 9 was the picture of the mechanical properties test of the sample. It was carried out compression test, flattening test and bending test. Any division phenomenon of composite pipe joint surface did not occur. From the above tests shown that composite pipe in range gap of 0.5~0.8mm can achieve good quality welding.



Figure 9 Mechanical properties test and result of the sample (a) flattening test and result (b) compression test and result (c) bending test and result

V. CONCLUSION

Numerical simulation can accurately simulate the whole dynamics process of composite pipe explosive welding. The value of the gap has an important influence on collision speed, collision pressure and effective plastic deformation of composite pipe. The reasonable range of the gap should be between 0.5~0.8mm when the density of flyer material was less than 5g/cm³.

REFERENCES

- [1] Z. Yuan-mou. *explosive welding and metallic composite and their engineering application*, (Changsha: central south university press, 2002)
- [2] A. A. Ezra *Metal Explosive Processing Principles and Practice*, (Beijing: China Machine Press, 1981)
- [3] T. Z. Blazy. *Welding, Forming and Pressing*, (Beijing: China Machine Press, 1988)
- [4] A.A. Akbari Mousavi, S.T.S. Al-Hassani. Numerical and experimental studies of the mechanism of the wavy interface formations in explosive/impact welding, *Journal of the Mechanics and Physics of Solids*, 53, 2005, 2501–2528.
- [5] A.A. Akbari Mousavi, S.J. Burley, S.T.S. Al-Hassani. Simulation of Explosive Welding with ANFO Mixtures, *Propellants, Explosives, Pyrotechnics*, 29, 2004, 188-196.
- [6] F. Grignon, D. Benson, K. S. Vecchio. Explosive welding of aluminum to aluminum: Analysis, computations and experiments, *Int J Impact Eng*, 30, 2004, 1333–1351.
- [7] M. Bei, L. Hongwei, C. Hui, H. Rui. Simulation of effects of stand off distance on explosive welding of three layer tubes, *Transactions of the China Welding Institution*. 16, 2009, 33-36.
- [8] H. Qin, L. Ming, L. Peng, P. Jingjun, D Ruxun, S. Xianjun. Numerical simulation and experimental study of stand-off distance on explosive welding of composite tube, *Ordnance Material Science and Engineering*, 34, 2011, 69-71.
- [9] N. Jianguo, W. Cheng, M. Tianbao. *Explosion and Shock Dynamics*, (Beijing: National Defense Industry Press, 2012)
- [10] W. Jianmin, Z. Xi, L. Ranquan. Three dimensional numerical simulation for explosive welding, *Transactions of the China Welding Institution*, 28, 2007, 109-112.
- [11] O. Drennov, O. Burtseva, A. Kitin. Explosive welding of pipes. *Journal de Physique IV*, 134, 2006, 1239-1243.
- [12] D. Wei, L. Ming, T. Xiaojie, D. Ruxun. Experimental and Interfacial Waveform Investigation on Aluminum/Stainless Steel Composite Tube by Explosive Welding, *Advances in Mechanical Engineering and its Applications*. 3(2). 2013, 304-307.

A solution of one-dimensional dispersion phenomenon by Homotopy Analysis Method

Kajal Patel¹, M. N. Mehta², Twinkle R. Singh³

¹(Research scholar, Department of Applied Mathematics and Humanities, S. V. National Institute of Technology Surat-395007, Gujarat, India)

²(Department of Applied Mathematics and Humanities, S. V. National Institute of Technology Surat-395007, Gujarat, India)

ABSTRACT: The present paper discusses solution of dispersion phenomenon by using Homotopy analysis method. Solution represents concentrations of any contaminated or salt water disperse in homogenous porous media saturated with fresh water. The solution of non-linear partial differential equation has been obtained in term of series solution of exponential function of X and time T under assumption of guess value of concentration of contaminated or salt water. Here solution converges for parameter $\varepsilon = 1$ for embedded parameter $h = 0.1$. The graphical presentation is given by using Maple coding. It is concluded that concentration of contaminated or salt water dispersion is decreasing when distance X as well as time T increasing and convergence of the solution has been discussed.

Keywords: Advection, Diffusion, Homotopy analysis Method

I. INTRODUCTION

The present paper discusses the solution of longitudinal dispersion phenomenon, which arising in the miscible fluid flow through homogenous porous media. The problem of solute dispersion during underground water movement has attracted interest from the early days of this century [1], but it was only since 1905 in general topic of hydrodynamic dispersion or miscible displacement becomes one of the more systematic studies. The phenomenon of the dispersion has been receiving good attention from hydrologist, agriculture, environmental, mathematicians, chemical engineering and soil scientists. The specific problem of fluid mixing in fixed bed reactors has been investigated by Bernard and Wilhelm [2]. Kovo [3] has worked with the parameter to be modeled in the longitudinal or axial dispersion coefficient D in chemical reactors model.

The fundamental interest of this paper is to find concentration of contaminated or salt water. The term concentration expresses a measure of the amount of a substance within a mixture. The dispersion process is associated with molecular diffusion and mechanical dispersion. Molecular diffusion is the spreading caused by the random molecular motion and collisions of the particles themselves and mechanical dispersion is the spreading of a dissolved component in the water phase by variations in the water velocity (i.e. flow of a fluid). These two basic mechanisms molecular diffusion and mechanical dispersion cause a concentration front of fluid particles to spread as it advances through the porous media. These two combine processes of molecular diffusion and mechanical dispersion are known as hydrodynamic dispersion or dispersion.

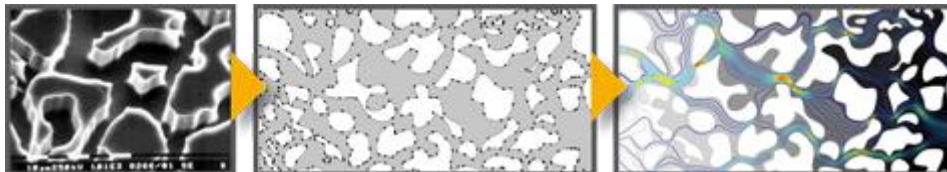


Fig 1: The geometry of microscopic pores, where velocity distributions in different pore size.

When groundwater flows, the actual microscopic velocity in the pores varies widely in space even when the Darcy macroscopic velocity is constant. The result is more intense mixing, which is called hydrodynamic dispersion. Figure 1 gives a schematic view of the trace movement on macroscopic level. This phenomenon can be observed in coastal areas, where the fresh waterbeds are gradually displaced by seawater. This phenomenon plays an important role in the seawater intrusion into reservoir at river mouths and in the underground recharge of groundwater.

Most of the works reveal common assumption of homogenous porous media with constant porosity, steady seepage flow velocity and constant dispersion coefficient. For such assumption Ebach and White [4] studied the longitudinal dispersion problem for an input concentration that varies periodically with time. Hunt [5] applied the perturbation method to longitudinal and lateral dispersion in no uniform seepage flow through heterogeneous aquifers. Mehta and Patel [6] applied Hope-Cole transformation to unsteady flow against dispersion of miscible fluid flow through porous media. Marino [7] considered the input concentration varying exponentially with time. Eneman et al.[8] provided analysis for the systems where fresh water is overlain by water with a higher density in coastal delta areas. Experimental evidence of such lenses was given by Lebbe et al. [9], and Vandenbohede et al. [10]. Meher and Mehta [11, 12] studied the Dispersion of Miscible fluid in semi infinite porous media with unsteady velocity distribution using Adomain decomposing method.

The present paper discusses the approximate analytical solution of the nonlinear differential equation for longitudinal dispersion phenomenon which takes places when miscible fluids (contaminated or salt water) mix in the

direction of flow. The mathematical formulation of the problem yields a non linear partial differential equation. The analytical solution has been obtained by using homotopy analysis method.

II. STATEMENT OF THE PROBLEM

Considering dispersion of contaminated or salt water with concentration $C(x,t)$ flowing in x-direction, dispersion taking place in porous media saturated with fresh water. Hence it will be miscible fluid flow through homogenous porous media. Therefore, it will obey the Darcy's law, which dates back to 1856 [13]. The following assumptions have been made for present analysis (Schidegger 1954, Day 1956, deJony 1958) [14,15, 16]:

- The medium is homogenous.
- There is no mass transfer happen between the solid and liquid phases.
- The solute transport across any fixed plane, due to microscopic velocity variation in the flow tube, may be quantitatively expressed as the product of a dispersion coefficient and the concentration gradient.

To find concentration of the dispersing contaminated or salt water as a function of time t and distance x , as the two miscible fluids flow through homogenous porous media. Since the mixing (contaminated or salt water and fresh water) takes place both longitudinally and transversely. Dispersion adds a spreading effect to the diffusion effects. Science dispersion is driven by the mean flow of the water, the dispersion coefficients related to the characteristic length or pore length L . In three dimensions, the spreading caused by dispersion is greater in the direction of the flow than in the transverse direction. One dimensional treatment of these systems avoids treatment of a radial or transverse component of dispersion. We only consider the dispersion phenomenon in the direction of flow (i.e. longitudinal dispersion), which takes places when miscible fluids flow in homogenous porous media.

III. MATHEMATICAL STRUCTURE

According to Darcy's law, the equation of continuity for the mixture, in the case of incompressible fluids is given by Bear [1].

$$\frac{\partial \rho}{\partial t} + \nabla \cdot (\rho \vec{V}) = 0 \tag{1}$$

Where, ρ is the density for mixture [ML^{-3}], t is time [T] and \vec{V} is the pore seepage velocity vector [LT^{-1}].

The equation of diffusion for a fluid flow through a homogeneous porous medium, without increasing or decreasing the dispersion of contaminated or salt water is given by

$$\frac{\partial C}{\partial t} = -\nabla \cdot (C\vec{V}) + \nabla \cdot \left[\rho \bar{D} \cdot \left(\frac{C}{\rho} \right) \right] \tag{2}$$

Where C is the concentration of dispersing contaminated or salt water per unit volume [ML^{-3}] and \bar{D} is the tensor coefficient of dispersion with nine components D_{ij} [L^2T^{-1}].

Since contaminated or salt water is flowing through a homogeneous porous medium at constant temperature, ρ may be considered as constant. Then

$$\nabla \cdot \vec{V} = 0 \tag{3}$$

where \vec{V} is velocity of contaminated /salt water dispersion.

Hence Eq. (2) may be written as

$$\frac{\partial C}{\partial t} = -\vec{V} \cdot \nabla C + \nabla \cdot [\bar{D} \nabla C] \tag{4}$$

When the seepage velocity \vec{V} of contaminated or salt water is dispersing along the x-axis, then the non-zero components will be $D_{11} = D_L = \frac{L}{C_0}$, (coefficient of longitudinal dispersion and L is length of dispersion in flow direction) and

$D_{22} = D_t$ (coefficient of transverse dispersion) and other D_{ij} are zero. From this assumption the equation (4) becomes,

$$\frac{\partial C}{\partial t} = -u \frac{\partial C}{\partial x} + D_L \frac{\partial^2 C}{\partial x^2} \tag{5}$$

where u is the component of seepage velocity of contaminated or salt water in x direction which is function of x and t and $D_L > 0$. It has been observed that seepage velocity u is related with concentration of contaminated or salt water dispersion. We assume that seepage velocity u is directly proportional to $C(x,t)$ [11]

$$u = \frac{C(x,t)}{C_0} \tag{6}$$

where $1/C_0$ is constant of proportionality and the guess approximation of the concentration of contaminated or salt water dispersion. To get dimensionless form of equation (5) using the dimensionless variables

$$X = \frac{C_0 x}{L}, \text{ and } T = \frac{1}{L} t$$

then equation (5) can be written as,

$$\frac{\partial C}{\partial T} = -C \frac{\partial C}{\partial X} + \varepsilon \frac{\partial^2 C}{\partial X^2}, \text{ where } \varepsilon = \frac{D_L C_0^2}{L} \text{ and } \varepsilon \in [0,1], 0 \leq X \leq 1, 0 \leq T \leq 1 \quad (7)$$

Since concentration C is decreasing as distance X increase for T > 0. It appropriate to choose guess value of concentration solution as, [12]

$$\square (X, T; \varepsilon) = \left(1 - \frac{1}{2}XT\right) e^{-X} + \varepsilon^m \quad (8)$$

Hence, the equation (7) together with boundary condition (8) represents the governing non-linear partial differential equation for concentration of the longitudinal dispersing material of miscible fluids flowing through a homogenous porous medium.

IV. THE SOLUTION WITH HOMOTOPY ANALYSIS METHOD

For one dimensional non-linear partial differential equation for longitudinal dispersion phenomenon, we assumed that the concentration C(X,T) of the dispersing contaminated or salt water, at time T=0 is expressed as,

$$\square (X, T, \varepsilon = 0) = \left(1 - \frac{1}{2}TX\right) e^{-X} + \varepsilon^m, \text{ where } \varepsilon = 0 \text{ for the concentration of contaminated or salt water} \quad (9)$$

Now we apply the homotopy analysis method into the longitudinal dispersion phenomenon during miscible fluid flow through homogenous porous media. We consider the equation (7) as nonlinear partial differential equation as

$$\square [\square (X, T; \varepsilon)] = 0 \quad (10)$$

Where \square is a non-linear operator, $\square (X, T; \varepsilon)$ is considered as unknown function which represent the concentration C of the dispersing contaminated or salt water at any distance X for given time T > 0, for $0 \leq \varepsilon \leq 1$. We use auxiliary linear operator $\Im[\square (X, T; \varepsilon)] = \frac{\partial \square (X, T; \varepsilon)}{\partial T}$ and initial approximation of concentration of dispersing contaminated or salt

water $C_0(X, T) = \left(1 - \frac{1}{2}TX\right) e^{-X}$ to construct the corresponding zeroth order deformation equation. As the auxiliary linear operator \Im which satisfies $\Im[C_4] = 0$, where C_4 is arbitrary constant. This provides a fundamental rule to direct the choice of the auxiliary function $H(X, T) \neq 0$, the initial approximation $C_0(X, T)$, and the auxiliary linear operator \Im , called the rule of solution expression. Establish the zero-order deformation equation of longitudinal dispersion phenomenon as [20],

$$(1 - \varepsilon) \Im[\square (X, T; \varepsilon) - C_0(X, T)] = \varepsilon h H(X, T) \square [\square (X, T; \varepsilon)] \quad (11)$$

where $C_0(X, T)$ denote an initial guess value of concentration of dispersing contaminated or salt water of the exact solution C(X,T) which is our purpose to find it. Since $h \neq 0$ an auxiliary parameter and $H(X, T) \neq 0$ an auxiliary function such that $\varepsilon \in [0,1]$ an embedding parameter. The auxiliary parameter h is providing a simple way to ensure the convergence of series. Thus it renamed h as convergence control parameter [20]. Let \Im an auxiliary linear operator with the property that,

$$\Im[\square (X, T; \varepsilon)] = 0 \text{ when } C(X, T; \varepsilon) = 0$$

When $\varepsilon = 0$, the zero-order deformation equation (11) becomes

$$\Im[\square (X, T; \varepsilon) - C_0(X, T)] = 0 \quad (12)$$

Which gives the first rule of solution expression and according to the initial guess $C_0(X, T) = \left(1 - \frac{1}{2}TX\right) e^{-X}$, it is straightforward to choose

$$\square (X, T; 0) = C_0(X, T) \quad (13)$$

When $\varepsilon = 1$, since $h \neq 0$, $H(X, T) \neq 0$ the zero-order deformation equation (7) is equivalent to

$$\square [\square (X, T; \varepsilon)] = 0 \quad (14)$$

which is exactly the same as the original equation (10) provided

$$\square (X, T; 1) = C(X, T) \quad (15)$$

According to (13) and (15) as the embedding parameter ε increases from 0 to 1, solution $\square (X, T; \varepsilon)$ varies continuously from the initial guess value of the concentration $C_0(X, T)$ of dispersing contaminated or salt water to the solution C(X,T) and its solution is assumed by expanding $\square (X, T; \varepsilon)$ in Taylor series with respect to ε as,

$$\square (X, T; \varepsilon) = \square (X, T; 0) + \sum_{m=1}^{\infty} C_m(X, T) \varepsilon^m \quad (16)$$

$$\text{Where, } C_m(X, T) = \frac{1}{m!} \left. \frac{\partial^m \square (X, T; \varepsilon)}{\partial \varepsilon^m} \right|_{\varepsilon=0} \quad (17)$$

i.e. the concentration of dispersing contaminated or salt water is function of distance X and time T for any parametric value ε is expressed as, the concentration of dispersing contaminated or salt water at time $T=0$, $C_0(X,T)$ and sum of concentration of dispersing contaminated or salt water $C_1(X,T), C_2(X,T), \dots$ at different time T for different value of parameter ε . Here, the series (16) is called homotopy-series; the series (16) is called homotopy series solution of $\square[\square(X,T;\varepsilon)]=0$ and $C_m(X,T)$ is called the m th-order derivative of \square . Auxiliary parameter h in homotopy-series (16) can be regard as iteration factor and is widely used in numerical computations. It is well known that the properly chosen iteration factor can ensure the convergence of homotopy series (16) is depending upon the value of h , one can ensure that convergent of homotopy series, solution simply by means of choosing a proper value of h as shown by Liao [20]. If the auxiliary linear operator, the initial guess, the auxiliary parameter h , the auxiliary function $H(X,T)$ are so properly chosen, the series (16) converges at $\varepsilon = 1$.

Hence the concentration of dispersing water can be expressed as,

$$C(X,T) = C_0(X,T) + \sum_{m=1}^{\infty} C_m(X,T) \tag{18}$$

And $C_m(X,T)$ can be calculated by equation (23). This must be one of solution of original non-linear partial differential equation (7) of the concentration of dispersing contaminated or salt water problem in homogenous porous medium.

According to the definition (17), the governing equation can be deduced from the zero-order deformation equation (11), define the vector

$$\vec{C}_m = \{C_0(X,T), C_1(X,T), \dots, C_n(X,T)\}$$

Differentiating equation (11) m -times with respect to the embedding parameter ε and then setting $\varepsilon = 0$ and finally dividing them by $m!$, we have the so-called m th order deformation equation of the concentration $C(X,T)$ will be as, [20]

$$\Im[C_m(X,T) - \chi_m C_{m-1}(X,T)] = \varepsilon h H(X,T) R_m(\vec{C}_{m-1}, X, T) \tag{19}$$

$$\text{Where } R_m(\vec{C}_{m-1}, X, T) = \frac{1}{(m-1)!} \left. \frac{\partial^{m-1} \square[\square(X,T;\varepsilon)]}{\partial \varepsilon^{m-1}} \right|_{\varepsilon=0} \tag{20}$$

$$\text{And } \chi_m = \begin{cases} 0, & m \leq 1 \\ 1, & m > 1 \end{cases} \tag{21}$$

It should be emphasized that $C_m(X,T)$ for $m \geq 1$, is governed by the linear equation (20) with the linear boundary condition that came from original problem, which can solved by symbolic computation software Maple as bellow. The rule of solution expression as given by equation (8) and equation (11), the auxiliary function independent of ε can be chosen as $H(X,T) = 1$, [20]

According to (15) and taking inverse of equation (19) the equation (20) becomes,

$$C_m(X,T) = \chi_m C_{m-1}(X,T) + h \Im^{-1} [R_m(\vec{C}_{m-1}, X, T)] \tag{22}$$

$$R_m(\vec{C}_{m-1}, X, T) = \frac{1}{(m-1)!} \left. \frac{\partial^{m-1} N[\square(X,T;\varepsilon)]}{\partial \varepsilon^m} \right|_{\varepsilon=0} \tag{23}$$

In this way, we get $C_m(X,T)$ for $m=1, 2, 3, \dots$ successively by using Maple software as,

$$C_1(X,T) = \frac{1}{12} hT (-T^2 X^2 + T^2 X + 3TXe^X - 6Te^X + 6TX - 3T - 6Xe^X - 12 - 12e^X) e^{-2X} \tag{24}$$

$$C_2(X,T) = Th \left[\begin{array}{l} -0.5hXe^{2X} - 0.25TXe^{2X} + 0.052hT^3 + 0.146hT^3 X^2 e^X + 0.58hT^2 - 0.92hT^2 Xe^X + hTXe^X \\ + 1.58hT^2 e^X + 2.5hTe^X - he^{2X} - 0.5Te^{2X} - 0.5Xe^{2X} - he^X - 0.5hTe^{2X} + 0.19hT^3 e^X \\ - 0.083T^2 X^2 e^X + 0.5TXe^X + 0.083T^2 Xe^X - e^{2X} - 0.083hT^2 Xe^{2X} - 0.25hT^2 X^2 e^X + 1.5hT \\ - hT^2 X + 0.25hT^3 X^2 - 0.32hT^3 X + 0.05hT^4 X^2 - 0.017hT^4 X - 0.025hT^4 X^3 \\ - 0.438hT^3 Xe^X - e^X + 0.5hTXe^{2X} - 0.25Te^X + 0.33hT^2 e^{2X} \end{array} \right] e^{-3X} \tag{25}$$

Using initial guess value of concentration from equation (8) and successive

$$C(X,T) = \left\{ \begin{array}{l} \left(1 - \frac{1}{2} XT \right) e^{-X} + \frac{1}{12} hT \left(-T^2 X^2 + T^2 X + 3TXe^X - 6Te^X \right) e^{-2X} \\ + Th \left[\begin{array}{l} -0.5hXe^{2X} - 0.25TXe^{2X} + 0.052hT^3 + 0.146hT^3 X^2 e^X + 0.58hT^2 \\ - 0.92hT^2 Xe^X + hTXe^X + 1.58hT^2 e^X + 2.5hTe^X - he^{2X} - 0.5Te^{2X} \\ - 0.5Xe^{2X} - he^X - 0.5hTe^{2X} + 0.19hT^3 e^X - 0.083T^2 X^2 e^X + 0.5TXe^X \\ + 0.083T^2 Xe^X - e^{2X} - 0.083hT^2 Xe^{2X} - 0.25hT^2 X^2 e^X + 1.5hT \\ - hT^2 X + 0.25hT^3 X^2 - 0.32hT^3 X + 0.05hT^4 X^2 - 0.017hT^4 X \\ - 0.025hT^4 X^3 - 0.438hT^3 Xe^X - e^X + 0.5hTXe^{2X} - 0.25Te^X + 0.33hT^2 e^{2X} \end{array} \right] e^{-3X} + \dots \end{array} \right\} \tag{26}$$

V. NUMERICAL AND GRAPHICAL SOLUTION

Numerical and graphical presentations of equation (26) have been obtained by using Maple coding. Fig 2 represents the graphs of concentration $C(X,T)$ vs. distance X, for $T = 0.1, 0.2, 0.3, 0.4, 0.5, 0.6, 0.7, 0.8, 0.9, 1.0$ is fixed, and Table I indicates the numerical values. The fig 2 and the table 1, indicate the graphical representations of the longitudinal dispersion phenomenon of the concentration. The convergence of the homotopy series (16) is dependent upon the value of convergence-parameter h [17, 18, 19, 20]. Therefore we choose proper value of the convergence-parameter $h = 0.1$ to obtain convergent homotopy-series solution [20].

Table I: Concentration of the Contaminated or Salt Water $C(X,T)$ For Different Distance X For Fixed Time T = 0.1, 0.2, 0.3, 0.4, 0.5, 0.6, 0.7, 0.8, 0.9, 1.0.

Distance X	$C(X,T)$ T= 0.1	$C(X,T)$ T= 0.2	$C(X,T)$ T= 0.3	$C(X,T)$ T= 0.4	$C(X,T)$ T= 0.5	$C(X,T)$ T= 0.6	$C(X,T)$ T= 0.7	$C(X,T)$ T= 0.8	$C(X,T)$ T= 0.9	$C(X,T)$ T=1.0
0.1	0.8674	0.8287	0.7887	0.7476	0.7054	0.6623	0.6183	0.5736	0.5282	0.4822
0.2	0.7814	0.743	0.7037	0.6635	0.6225	0.5807	0.5383	0.4953	0.4517	0.4077
0.3	0.7038	0.666	0.6274	0.5881	0.5482	0.5077	0.4667	0.4253	0.3834	0.3412
0.4	0.6338	0.5966	0.5589	0.5206	0.4818	0.4426	0.403	0.3631	0.3228	0.2822
0.5	0.5707	0.5343	0.4974	0.4602	0.4226	0.3847	0.3465	0.308	0.2692	0.2302
0.6	0.5137	0.4782	0.4424	0.4063	0.3699	0.3333	0.2964	0.2594	0.2221	0.1846
0.7	0.4624	0.4279	0.3932	0.3583	0.3231	0.2878	0.2523	0.2167	0.1809	0.1449
0.8	0.4162	0.3828	0.3492	0.3155	0.2816	0.2476	0.2135	0.1793	0.1449	0.1105
0.9	0.3745	0.3423	0.3099	0.2775	0.2449	0.2123	0.1795	0.1467	0.1138	0.0808
1.0	0.3369	0.3059	0.2748	0.2437	0.2124	0.1812	0.1498	0.1184	0.0869	0.0554

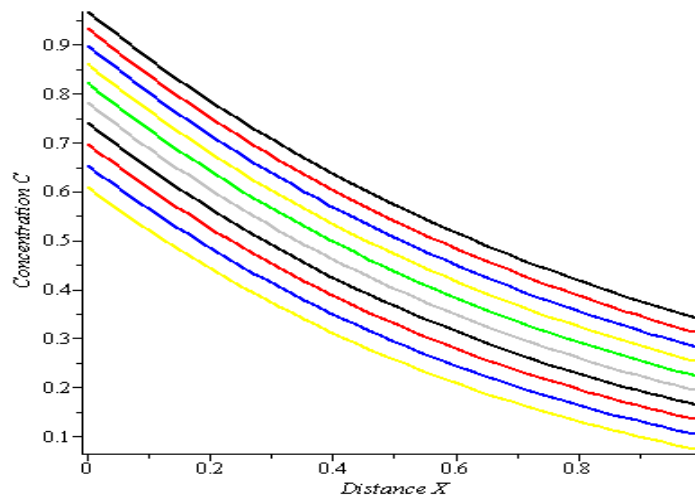


Fig 2: Represents concentration of contaminated or salt water $C(X,T)$ vs. distance X for auxiliary parameter $h = 0.1$ and auxiliary function $H(Z,T)=1$ [20] when T =0.1, 0.2, 0.3, 0.4, 0.5, 0.6, 0.7, 0.8, 0.9 and 1.0 is fixed.

VI. CONCLUSION AND DISCUSSION

The equation (26) represents concentration of the contaminated or salt water for any distance X and time $T > 0$. It is converges for embedding parameter $\epsilon = 1$ and for auxiliary parameter $h = 0.1$ which is expressed in term of negative exponential term of X and time $T > 0$. Concentration C will be one from guess value of the exact solution for $X = 0, T = 0.1, 0.2, 0.3, 0.4, 0.5, 0.6, 0.7, 0.8, 0.9, 1.0$. Fig 2 represents the solution for concentration C vs. distance X shows that concentration of the contaminated or salt water is decreasing as distance X increasing for $T > 0$. From fig. 2 it can conclude that for $T = 0.1$ concentration of contaminated or salt water is decreasing as distance X increasing and when time is increasing and due to different deformation added to C, the concentration of contaminated or salt water is successively decreasing exponentially. Since the equation (7) is diffusion type Burger's equation for longitudinal dispersion phenomenon. Hence solution is graphically as well as physically consistent with phenomenon. This is physically fact with phenomenon of the longitudinal dispersion of contaminated or salt water in homogenous porous medium.

REFERENCES

- [1] J. Bear, Dynamics of Fluids in Porous Media, Dover Publications, New York, 1972.
- [2] R. A. Bernard, and R. H. Wilhelm, Chem. Eng. Progr., 46, 233, 1950.
- [3] S. A. Kovo, Mathematical modelling And simulation of dispersion in a nonideal plug flow reactor, Taylor & Francis Group, ISSN: 0193-2691, 29: 2008, 1129-1134.
- [4] E. H. Ebach, and R. White, Mixing of fluids flowing through beds of packed solids, A. J. Ch. E., Vol. 4, 1958, 161.
- [5] Hunt, Dispersion calculations in nonuniform seepage, J. Hydrol., Vol. 36, 1978, 261-277.
- [6] M. N. Mehta, & T. A. Patel, A Solution of Burger's Equation for Longitudinal Dispersion of Miscible Fluid Flow through Porous Media, Indian Journal of Petroleum Geology, 14(2),2005, 49-54.
- [7] M. A. Marino, Flow Against Dispersion in Non Adsorbing Porous Media, J. Hydrology, 37, 1978, 149-158.
- [8] S. Eeman, Van Der Zee, S. E. A. T. M., A. Leijnse , De Louw, P. G. B and Maas C., Response to recharge variation of thin lenses and their mixing zone with underlying saline groundwater, Hydrol. Earth Syst. Sci. Discuss., 16, 2012, 355-349.
- [9] L. Lebbe , N. Van Meir and P. Viaene, Potential implications of sea-level rise for Belgium, J. Coast Res, 24(2), 2008, 358-366.
- [10] A. Vandenbohede , K. Luyten and L. Lebbe, Effects of global change on heterogeneous coastal aquifers: a case study in Belgium. Jcoast Res, 24, 2008, 160-170.
- [11] M. N. Mehta, A solution of Burger's equation type one dimensional Ground water Recharge by spreading in Porous Media, Journal of Indian Acad.Math.Vol.28, No.1, 1977, 25-32.
- [12] R. K. Meher, Dispersion of Miscible fluid in semi infinite porous media with unsteady velocity distribution, International Journal of mathematical Sciences and Engineering applications, Vol.3, No.IV, 2009.
- [13] H. Darcy, Les Fontaines publiques de lo ville de Dijon, Dalmont, Paris, 1856.
- [14] A. E. Scheidegger, Statistical hydrodynamics in porous media: Appl. Phys. Jour., Vol.25, 1945, 994-1001.
- [15] P. R. Day, Dispersion of a moving salt-water boundary advancing through saturated sand: Am. Geophys. Union Trans., Vol. 37, 1956, 595-601.
- [16] G. de J. deJong, Longitudinal and transverse diffusion in granular deposits: Am. Geophys. Union Trans., Vol. 39, 1958, 67-74.
- [17] S. J. Liao, A kind of approximate solution technique which does not depend upon small parameters (II): an application in fluid mechanics, Int. J. Nonlinear. Mech, 1997, 32-815.
- [18] S. J. Liao, An explicit, totally analytic approximation of Blasius viscous flow problems, Int. J. Nonlinear. Mech. Vol. 34, 1999, 759-778.
- [19] S. J. Liao, Magyari E., Exponentially decaying boundary layers as limiting cases of families of algebraically decaying ones, ZAMP, 57(5), 2006, 777-92.

Book:

- [20] S. J. Liao, Beyond perturbation: introduction to Homotopy analysis method. CRC Press: Chapman & Hall; 2003.

Variable Threshold MOS Circuits

Dr. Ragini K.¹, Dr. Satyam M.², Dr. Jinaga B. C.³

¹G. Narayanamma Institute of Technology & Science,

Department of Electronics and Communication Engineering, Hyderabad, India

²International Institute of Information Technology, Hyderabad, India

³Jawaharlal Nehru Technology University, Hyderabad, India

ABSTRACT: Dynamic threshold MOS (DTMOS) circuits provide low leakage and high current drive, compared to CMOS circuits, operated at low voltages. This paper proposes a modified DTMOS approach, called Variable threshold MOS (VTMOS) approach. The VTMOS is based on operating the MOS devices with an appropriate substrate bias which varies with gate voltage, by connecting a positive bias voltage between gate and substrate for NMOS and negative bias voltage between gate and substrate for PMOS. With VTMOS, there is a considerable reduction in operating current and power dissipation, while the remaining characteristics are almost the same as those of DTMOS. Results of our investigations show that VTMOS circuits improves the power up to 50% when compared to CMOS and DTMOS circuits, in sub threshold-region. The performance characteristics of VTMOS circuits - The Power dissipation, Propagation delay and Power delay product with the substrate bias have been evaluated through simulation using H spice. The dependency of these parameters on frequency of operation has also been investigated.

Keywords: Sub- threshold, Dynamic threshold MOS Inverter, Propagation delay, Noise-margin, Variable threshold MOS Inverter, Power dissipation.

I. INTRODUCTION

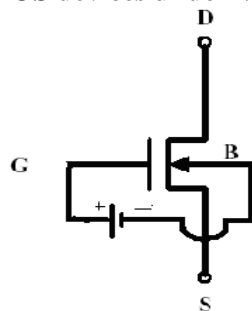
Over the past twenty years, semi conductor industry emerged considerably and demand for VLSI has grown all over the world. During the recent years, there is a great demand for portable devices like cellular phone, palm top computers, GPRS receivers, pocket calculator, and pacemakers, they all demand for low power. Hence low power design has emerged as a very attractive and fast development field. The limited battery life time demands for the reduction of power consumption of portable devices. High performance digital systems such as DSP, microprocessor's, and other applications insists for low power design. Besides this, the environment also demands for low power design. As the electronic equipment usage increases, the power consumption and the cost for excessive cooling system increases.

In view of this it is essential to minimize the power dissipation. The various techniques that are employed to reduce the power dissipation are recycling the energy that might be stored in nodal capacitances, reduction in transitions (0 to 1 or 1 to 0), reduction in voltages and currents, and so on. The techniques based on operation at very low currents usually below the normal conduction region, especially in FET based circuits is known as sub threshold operation. This has attracted several investigators, as it has flexibility to choose their own logic levels and power dissipation. This paper is only an attempt to modify the normal sub threshold operating condition to reduce the power dissipation without affecting the performance. The modified operation that is suggested is based on biasing the substrate of FET dynamically in tune with the gate voltage. This we termed as variable threshold MOS operation. It has been shown that VTMOS operation can result in power saving of up to 50% compared to CMOS operation and can be used in cascaded circuits like CMOS circuits.

1.1 Current voltage characteristics of NMOS and PMOS Transistors under VTMOS operating conditions

in sub-threshold region: To evaluate the behavior of NMOS and PMOS devices under VTMOS operating conditions, the current voltage characteristics are measured and plotted using H spice simulation tool. The transistor's are chosen from 65nm technology. The threshold voltage for NMOS and PMOS devices are 0.22v and -0.22v respectively. The width of NMOS (W_n) and PMOS (W_p) is chosen as 200nm and 400nm respectively. The supply voltage is taken as 0.2v which is below the threshold of both the devices.

1.1.1 Current voltage characteristics of NMOS devices under VTMOS operating conditions:



(a) n-MOSFET

Figure 1

As shown in Figure (1), the NMOS transistor is connected to gate through V_{AN} , which bias the substrate negative with respect to gate. For different values of V_{AN} starting from 0 to 0.2v, the current voltage characteristics of NMOS, i.e Id versus V_{gs} are plotted and given in Figure(2).

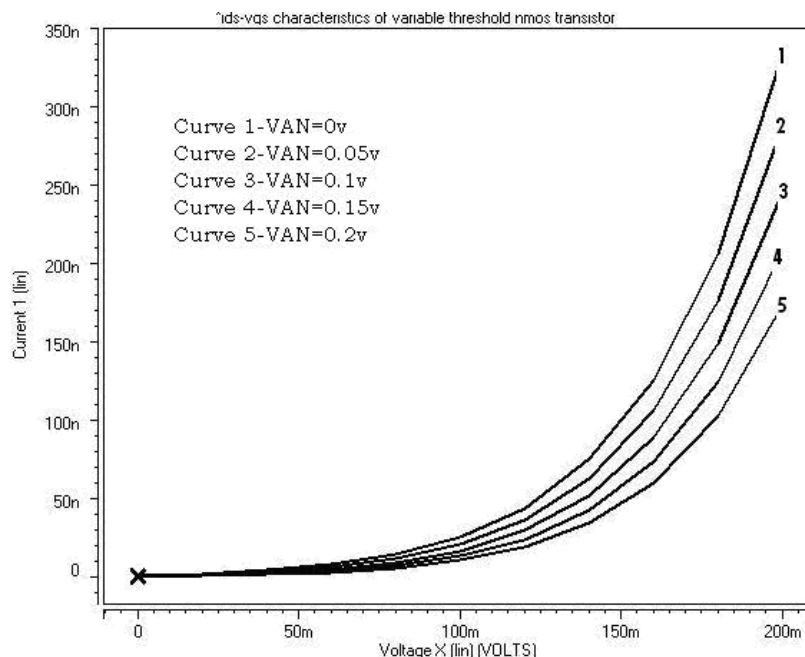


Figure: 2 Ids-Vgs curves of Variable Threshold NMOS Transistor (V_{AN} varying from 0(top)to 0.2v(bottom))

When V_{AN} is varied from 0 to 0.2v, the transistor substrate bias is dynamically adjusted, depending on the gate voltage, causing the threshold voltage of the device to adjust dynamically. The variation in threshold voltage causes variation in leakage currents and power dissipation.

The VTNMOS transistor is operated in two modes i.e ON mode and OFF mode .As the entire operation is limited to sub threshold region , for a given V_{AN} , the 'ON' condition is defined for NMOS transistor when $V_{gs}=0.2v$. Similarly for a given V_{AN} , 'OFF' condition is defined for NMOS transistor when $V_{gs} = 0v$. In the 'ON' mode, when $V_{AN}=0.2v$ and $V_{gs}=0.2v$, then the substrate bias of NMOSFET transistor is switched to 0v. In this condition, the VTNMOS transistor is similar to NMOS ON transistor operation. Hence the drain current of VTNMOS is same as NMOS transistor under normal conditions and is found to be 171nA.

For the condition, that $V_{AN}=0v$ and $V_{gs}=0.2v$ (DTNMOS condition), the source and substrate of MOSFET is forward biased, which implies that the effective threshold voltage of the device is reduced. hence one expects much higher current than the current that flows under normal NMOS operation ($V_{gs}=0.2v$). This current has been found to be 334nA from the Figure (2).

The OFF condition of the transistor in this article is defined as the condition in which $V_{gs} = 0$ and V_{AN} is varied from 0 to 0.2v. when $V_{gs}=0v$ and $V_{AN}=0V$, the condition corresponds to normal NMOS transistor .when $V_{AN}=0.2v$, the substrate is biased negative w.r.t source by -0.2v and hence ,the threshold voltage increases and the current decreases further .From the Figure(2), the value of current for $V_{gs}=V_{AN}=0$ is measured as 1.4nA and for $V_{gs}=0v$ and $V_{AN}=0.2v$ it is 550pA, which is about one-third of the leakage current ,when the substrate is biased at 0v.

1.1.2 The current voltage characteristics of PMOS under VT MOS operating conditions:

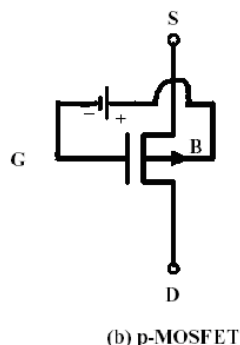


Figure 3

The PMOS device under VT MOS operating condition is shown in Figure (3). It may be seen that the substrate is positively biased w.r.t gate.

Figure 4(a) shows the I_{ds} versus V_{gs} curves of PMOS device under VT MOS operating conditions, for different values of V_{AP} , starting from 0 to -0.2v. The V_{ds} is considered as -0.2v and V_{gs} is varied from 0 to -0.2v.

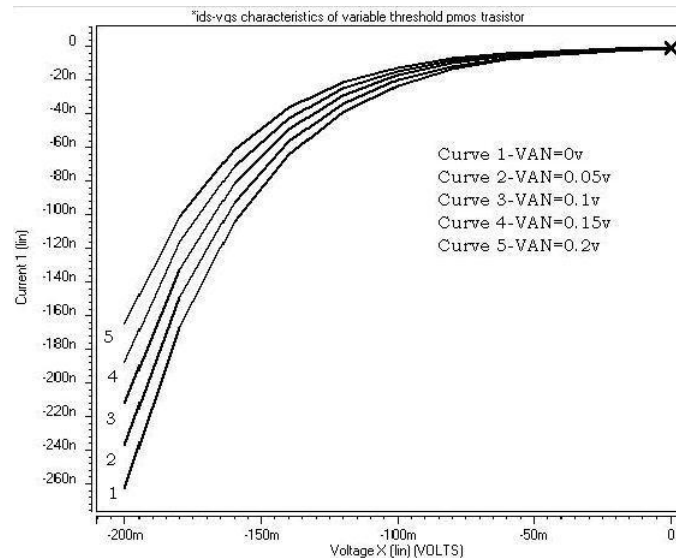


Figure: 4 (a) I_{ds} - V_{gs} curves of Variable Threshold PMOS Transistor (V_{AP} varying from 0(bottom)to 0.2v(top))

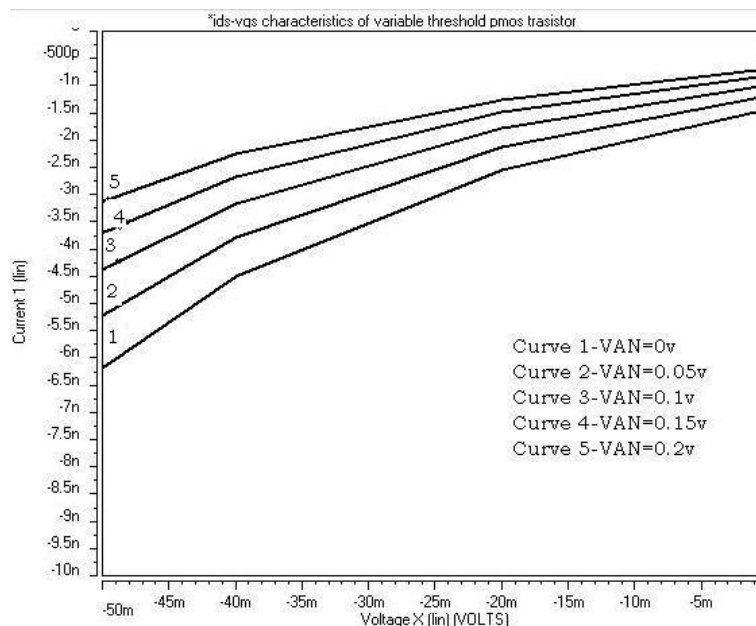


Figure: 4(b) I_{ds} - V_{gs} curves of Variable Threshold PMOS Transistor (V_{AP} varying from 0(bottom)to 0.2v(top))-zoomed version to Measure I_{off} current

For different values of V_{AP} starting from 0 to -0.2v, the current voltage characteristics of PMOS is plotted.

When V_{AP} is varied from 0 to -0.2v, the PMOS transistor's threshold voltage is varied dynamically as in the case of NMOS device. The ON and OFF conditions for PMOS device are similar to that of NMOS device. Considering the ON condition of VT PMOS transistor, for $V_{AP}=0v$ and $V_{gs}=-0.2v$ (DTP MOS condition) it is observed that there is highest drain current of $I_{on}=-262nA$. When $V_{AP}=-0.2v$ and $V_{gs}=-0.2v$, lowest I_{on} drain current $I_{on}=-164nA$ is recorded for VT PMOS and is observed from Figure 4(a).

Considering the PMOS off condition, it is observed from the Figure 4(b), that for $V_{AP} = 0 v$, the I_{off} current is 1.4nA and for $V_{AP} = 0.2v$, the I_{off} current is less and is measured as 695pA. thus the current levels (I_{on} & I_{off}) get reduced with increase in bias voltage when VT PMOS substrate is positively biased with respect to gate.

II. VT MOS SEQUENTIAL CIRCUITS

Sequential circuits are those in which the output depends on the present inputs and previously applied inputs. As mentioned earlier this sequential circuits are generally realized by making use of combinational circuits with appropriate positive feedback. VT MOS based sequential circuits are realized using VT MOS combinational circuits. The transistor's for

sequential circuits are chosen from 65nm technology. The width of PMOSFETS and NMOSFETS are chosen as 400nm and 200nm respectively. The supply voltage is taken as 0.2v which is below the threshold of the devices.

For different values of V_{AN} starting from 0 to 0.2v and corresponding V_{AP} of same magnitude from 0 to -0.2v, the performance parameters of VT MOS sequential circuits– average power dissipation, propagation delays, rise and fall time delay, power-delay –product and frequency response have been obtained through simulation .The VT MOS JK master slave flip flop is designed and performance analysis is done in the following sections . The performance results of the VT MOS JK master slave flip flop are compared with the CMOS JK master slave flip flop circuits.

2.1 VT MOS JK master slave flip flop:

The VT MOS JK master slave can be constructed with a pair of JK flip flops using VT MOS NAND gates. The circuit diagram, Truth table and operation of the circuit is given in Figure 5 and Table (1)below. The first flip flop serves as master and second flip-flop serves as slave. There is a feedback connection from the output of second to the input of first. The master is enabled for clock=1 and slave is enable for clock = 0.

Circuit Diagram:

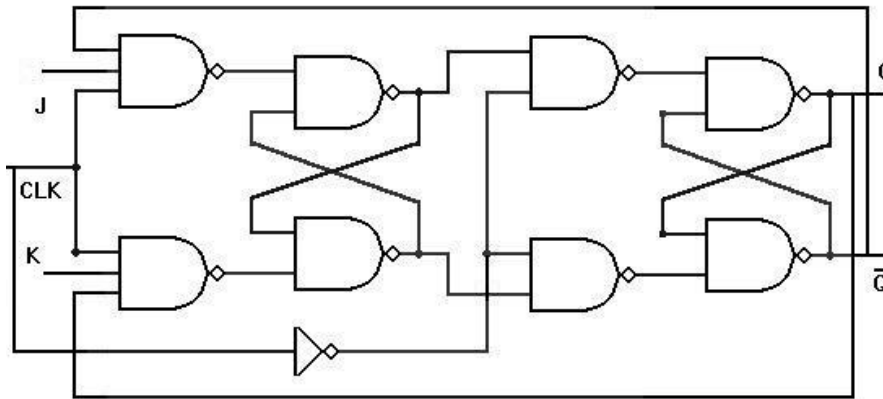


Figure 5

Truth table:

Inputs			Outputs	
Clock	J	K	Q	\bar{Q}
×	×	×	0	1
↑	0	0	No change	
↑	0	1	0	1
↑	1	0	1	0
↑	1	1	Toggle	

Table 1

When clock = 1, the master is enabled, and output of master responds to the input J and K according to the truth table. When clock = 0, the master is disabled and slave is enabled. The state of master output is now transferred to slave output. the master slave flip flop functions properly only when the clock width is larger than the propagation delay time through the master flip flop. The performance of this latch in terms of power dissipation , logic levels ,propagation delay ,rise and fall time delays ,frequency response have been analyzed and described below.

2.2 Input output wave forms for VT MOS JK master slave flip flop circuit:

Function of the VT MOS JK master slave flip flop circuit has been compared with conventional JK master slave flip flop circuit and verified with inputs taken in the form of pulses varying from 0 to 0.2v, with a rise and fall time of 25ns. As in the case of combinational circuits, the supply voltage is 0.2v and load capacitance is 10fF. The input pattern chosen for analysis of performance parameters is J=111001101 and K=010110010 and clock=0101010101 at a sample time of 10 microseconds (100kHz) frequency. The output wave forms are plotted for all Flip-flops where v (3),v(4) represents the output corresponding to Master flip-flop and v(8),v(9)represents Slave output.. From the figures 6(a), 6(b) and 6(c), it may be seen that the output logic levels are almost the same as input logic levels and the output is as for expected for the given input .Thus the VT MOS JK master slave flip flop circuit is found to be working properly as that of conventional CMOS JK master slave flip flop circuit.

Circuits (VTMOS JK master slave flip flop for $V_{AN}=V_{AP}=0v$, VTMOS JK master slave flip flop for $V_{AN}=V_{AP}=0.2v$, and CMOS JK master slave flip flop.) for a period of 200 microseconds is shown in Figure 6(a), Figure 6(b) and Figure 6(c).

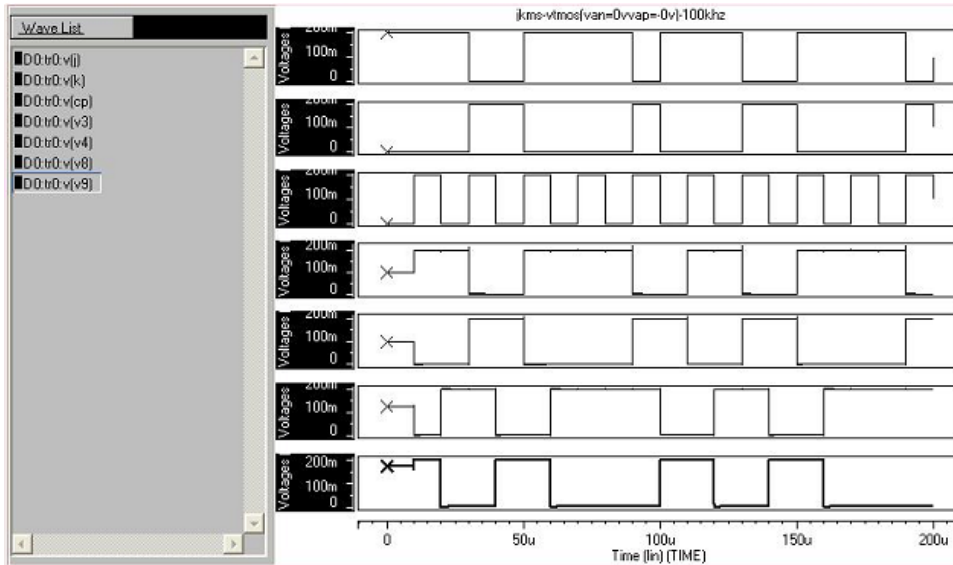


Figure 6(a): INPUT-OUTPUT WAVEFORMS OF VTMOS JKMS Flip flop($V_{AN}=0V, V_{AP}=0V$) -100KHZ

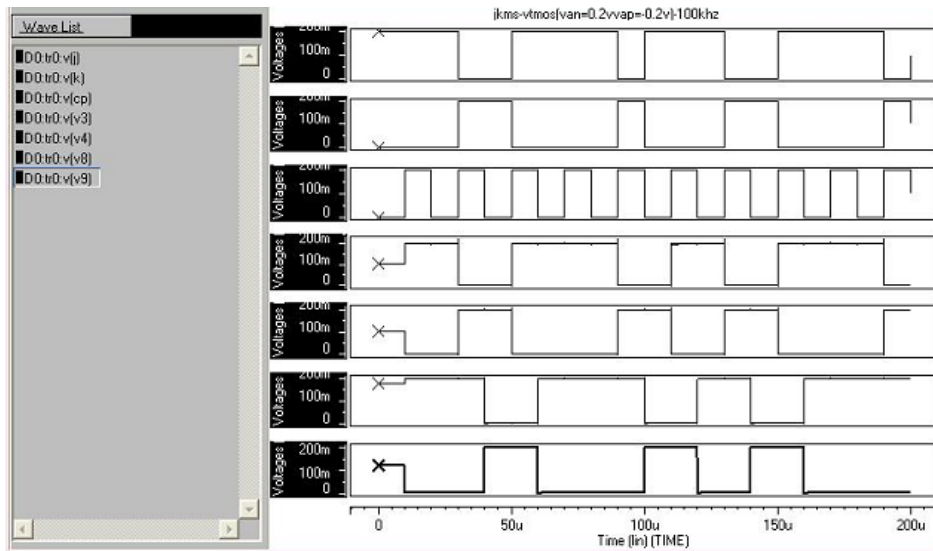


Figure 6(b): INPUT-OUTPUT WAVEFORMS OF VTMOS JKMS Flip flop($V_{AN}=0.2V, V_{AP}=0.2V$) -100KHZ

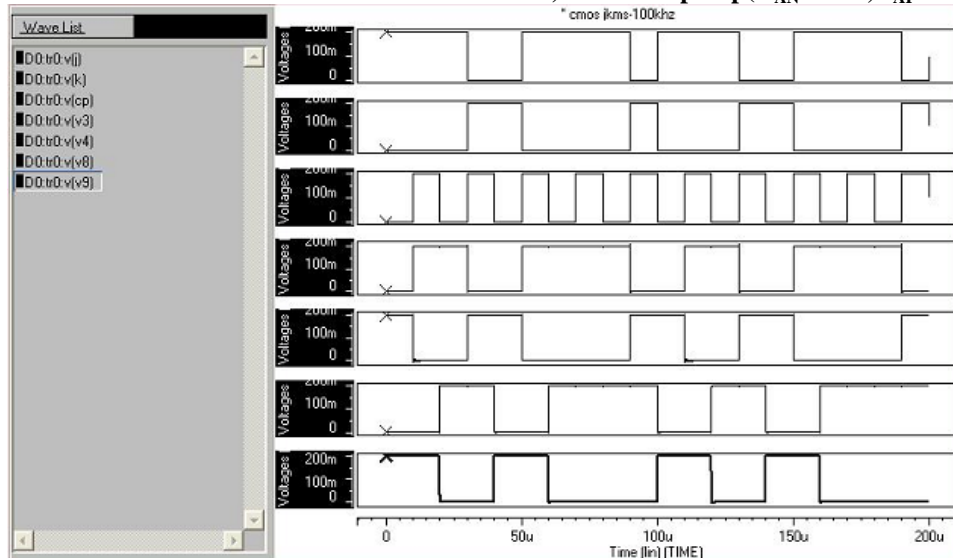


Figure 6(c): INPUT-OUTPUT WAVEFORMS OF CMOS JKMS Flip flop-100KHZ

From the figures 6(a), 6(b) and 6(c), it may be seen that the output logic levels are almost the same as input logic levels and the output is as for expected for the given input. Thus the VT MOS JK master slave flip flop circuit is found to be working properly as that of conventional CMOS clocked SR latch circuit.

The performance of VT MOS JK master slave flip flop circuit with $|V_{AN}|=|V_{AP}|$ varying from 0 to 0.2V is compared with CMOS JK master slave flip flop. The performance analysis is done in following section and result discussion is made in the next section. At last the frequency analysis is done.

III. PERFORMANCE ANALYSIS OF VT MOS JK MASTER SLAVE FLIP FLOP CIRCUIT

The propagation delay, the rise and fall time delay, average power dissipation and power delay product are measured for VT MOS JK master slave flip flop circuit (for $|V_{AN}|=|V_{AP}|$ varying from 0 to 0.2v) at a particular input signal frequency of 100 kHz for performance evaluation. The performance results of VT MOS JK master slave flip flop are also compared with the conventional CMOS JK master slave flip flop in this section.

The variation of performance parameters (propagation delay, average power dissipation and power delay product) for different JK master slave flip flop circuits (Sub threshold VT MOS JK master slave flip flop circuit with $|V_{AN}|=|V_{AP}|$ varying from 0 to 0.2v and CMOS JK master slave flip flop Circuit), are tabulated in Table 2(a) for a frequency of 100 khz, and at supply voltage of 0.2v. The input pattern is repeated for a period of 5000 microseconds. The variation of rise and fall time delays of all JK master slave flip flop circuits is shown in Table 2(b). Along with this, the variation of propagation delay, power dissipation and power delay product for $|V_{AN}|=|V_{AP}|$ varying from 0 to 0.2 v at 100 khz. is also shown in the Figure. 7(a), 7(b), 7(c)

The discussion on the performance analysis is done in the next following section.

S.no	Circuit	T_{PLH} (seconds)	T_{PHL} (seconds)	T_P (seconds)	Average power dissipation (watts)	Power delay product (joules)
1	VTOMS (0V)	4.058E-08	2.280E-08	3.169E-08	4.287E-10	1.358E-18
2	VTMOS(0.05V)	4.607E-08	2.533E-08	3.570E-08	2.566E-10	0.916E-18
3	VTMOS(0.1V)	5.062E-08	2.739E-08	3.901E-08	2.133E-10	0.832E-18
4	VTMOS(0.15V)	5.811E-08	3.238E-08	4.524E-08	1.729E-10	0.782E-18
5	VTMOS(0.2V)	6.724E-08	3.575E-08	5.149E-08	1.464E-10	0.754E-18
6	CMOS	5.177E-08	2.702E-08	3.940E-08	3.121E-10	1.229E-18

Table 2(a) – Variation of propagation delay, power dissipation and power delay product for different JKMS Flip flop circuits

S.no	Circuit	Rise time delay (seconds)	Fall time delay (seconds)
1	VTMOS(0V)	1.167E-08	9.287E-08
2	VTMOS(0.05V)	1.784E-08	2.993E-08
3	VTOMS(0.1V)	2.208E-08	3.105E-08
4	VTMOS(0.15V)	2.418E-08	3.453E-08
5	VTMOS(0.2V)	2.837E-08	5.451E-08
6	CMOS	2.529E-08	4.098E-08

Table 2(b) -Variation of rise and fall time delay for different JKMS Flip flop circuits

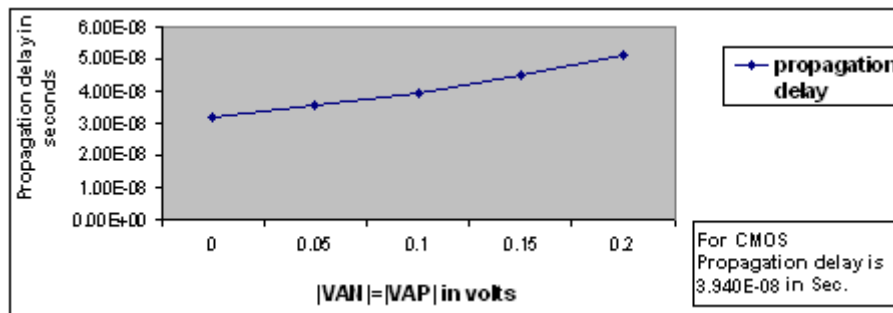


Figure 7(a): Variation of propagation delay for VT MOS JK master slave Flip flop ($|V_{AN}|=|V_{AP}|$ varying from 0 to 0.2v)

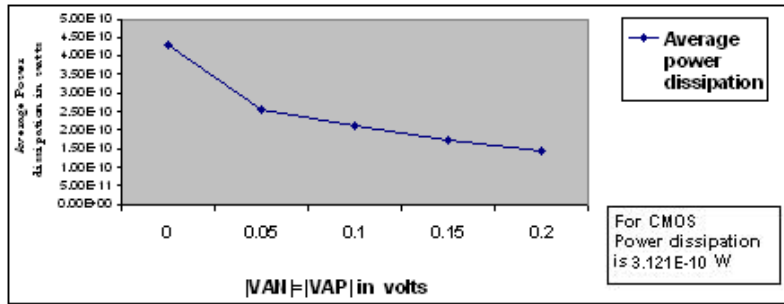


Figure 7(b): Variation of Power dissipation for VT MOS JK master slave Flip flop ($|V_{AN}|=|V_{AP}|$ v varying from 0 to 0.2v)

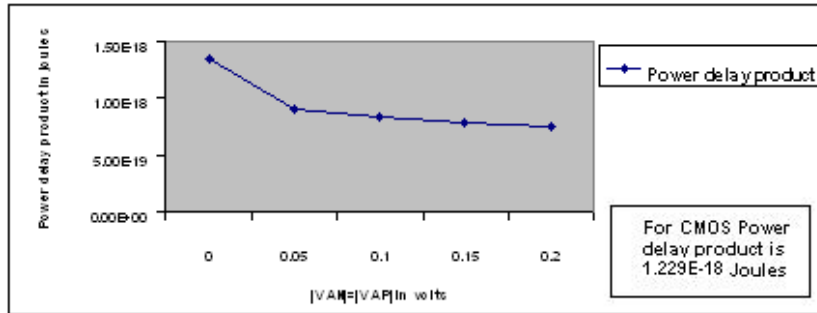


Figure 7(c) : Variation of Power delay product for VT MOS JK master slave Flip flop($|V_{AN}|=|V_{AP}|$ varying from 0 to 0.2v)

3.1 Result Discussion:

Results are obtained from HSPICE simulations using 65nm technology . The variation of propagation delay of VT MOS JKMS Flip flop with $|V_{AN}|=|V_{AP}|$ varying from 0 to 0.2v is plotted in figure 7(a). It is observed that propagation delay of VT MOS JKMS Flip flop, increases with increase in $|V_{AN}|=|V_{AP}|$. The propagation delay is lowest for VT MOS JKMS Flip flop with $|V_{AN}|=|V_{AP}|=0v$ and the propagation delay of VT MOS JKMS Flip flop with $|V_{AN}|=|V_{AP}|=0.2v$, almost approaches the CMOS JKMS Flip flop circuit.

Figure 7(b) gives the variation of power dissipation of VT MOS JKMS Flip flop with $|V_{AN}|=|V_{AP}|$ varying from 0 to 0.2v. It is observed that power dissipation is highest for VT MOS JKMS Flip flop at $|V_{AN}|=|V_{AP}|=0V$. Over all 53% reduction in power dissipation is observed for VT MOS JKMS Flip flop at $|V_{AN}|=|V_{AP}|=0.2v$ when compared to CMOS JK master slave flip flop.

The variation of power delay product of VT MOS JKMS Flip flop with increase in $|V_{AN}|=|V_{AP}|$ is observed in Figure 7(c). The power delay product also reduces with increase in $|V_{AN}|=|V_{AP}|$ which is invited feature of VT MOS JK master flip flop.

3.2 Effect of frequency:

The effect of frequency on performance characteristics is noted by varying the frequency from 100 khz to 8 Mhz. The input and output wave forms of VT MOS JK master slave flip flop at $|V_{AN}|=|V_{AP}|=0v$, VT MOS JK master slave flip flop at $|V_{AN}|=|V_{AP}|=0.2v$ and CMOS JK master slave flip flop are given in Figure 8(a), 8(b) and 8(c) for 2 MHZ(sample time of 500 microseconds) frequency for the same input pattern of J=111001101 and K=010110010 and clock=0101010101.

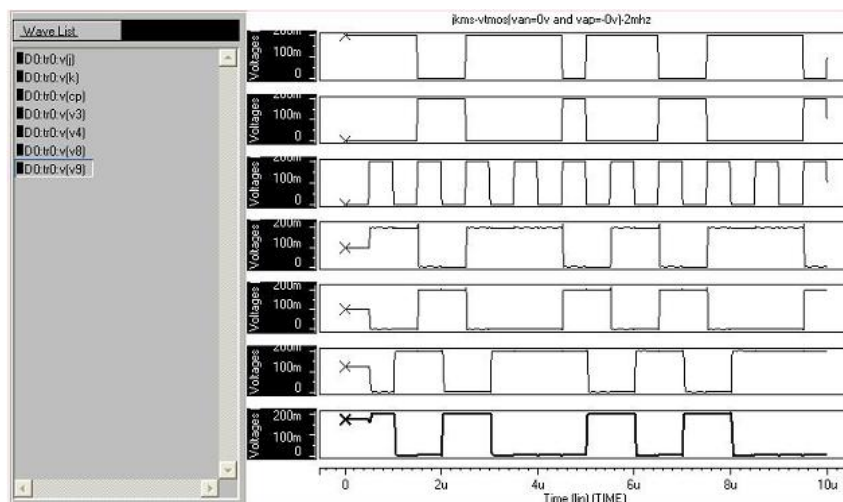


Figure 8(a): INPUT-OUTPUT WAVEFORMS OF VT MOS JKMS Flip flop($V_{AN}=V_{AP}=0V$) -2MHZ

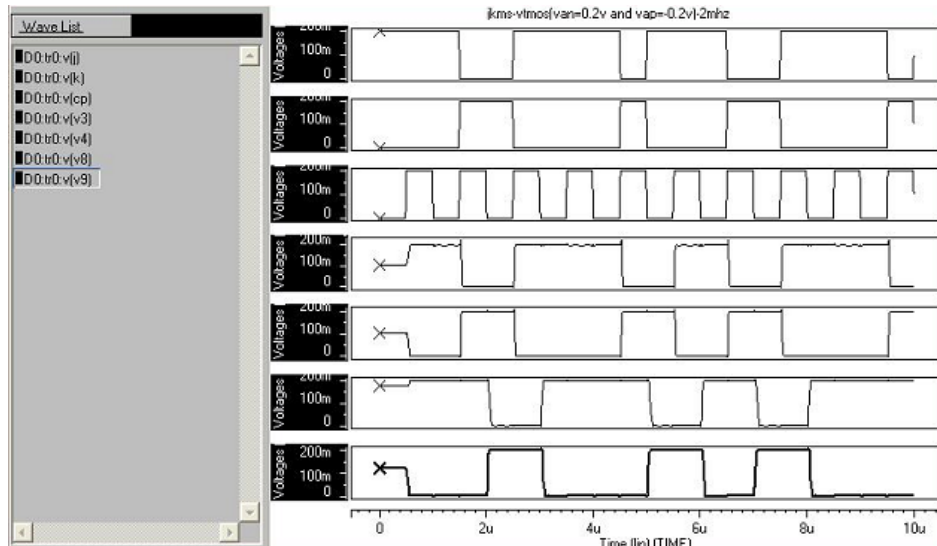


Figure 8(b): INPUT-OUTPUT WAVEFORMS OF VT MOS JKMS Flip flop($V_{AN}=V_{AP}=0.2V$) -2MHZ

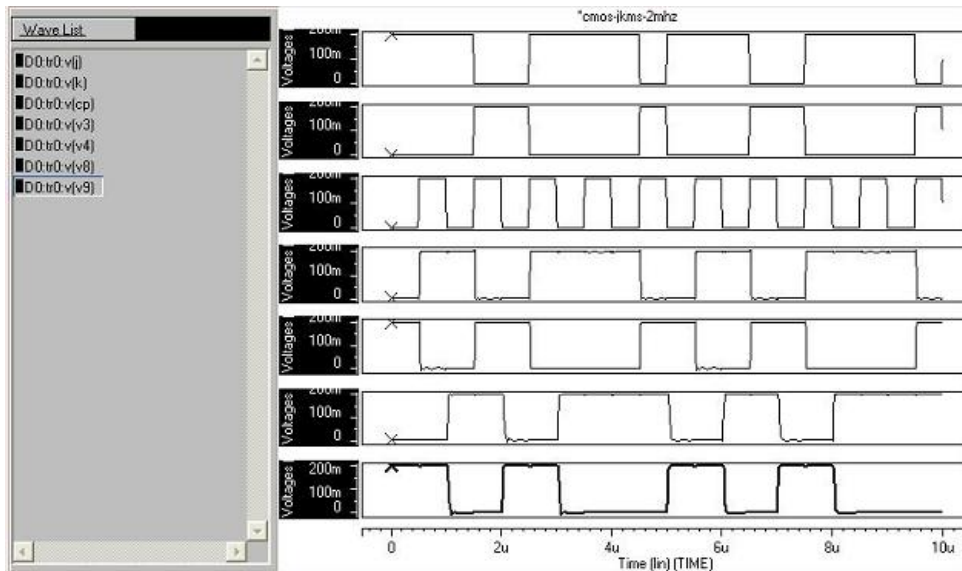


FIGURE 8(c): INPUT-OUTPUT WAVEFORMS OF CMOS JKMS -2MHZ

From the figures it may be seen that the output waveforms resembles the input waveforms at 2Mhz frequency .Hence it can be said that VT MOS JK Master slave circuit is working properly at higher frequencies. With increase in frequency the general trend of variation of power dissipation and propagation delay are maintained as those reported at 100Khz. The variation of power dissipation with frequency for sub threshold VT MOS JK Master slave circuit (0 TO 0.2V) and sub threshold CMOS JK Master slave circuit is shown in Figure 9.It is observed that average power dissipation increases with frequency, but propagation delay and power delay product remains almost constant with frequency. As in the case of VT MOS combinational circuits the power dissipation of VT MOS JK master slave flip flop increases much more faster than in the case of CMOS JK master slave flip flop as frequency is increased. The reasons for this rapid increase in power dissipation in the case of VT MOS JK master slave flip flop are similar to that explained for VT MOS inverter circuits.

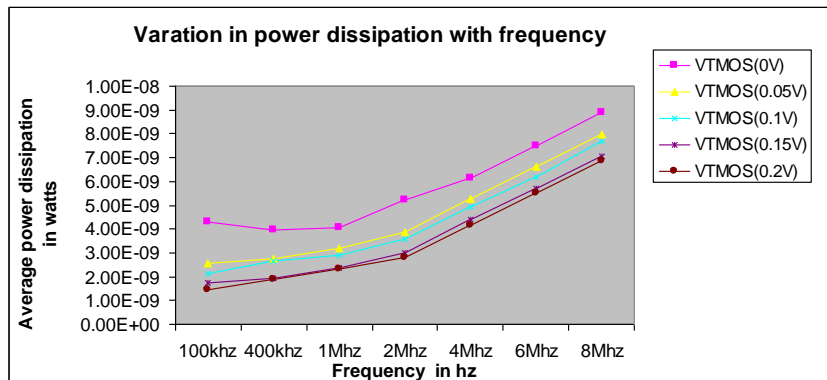


Figure 9: variation of average power dissipation with frequency for JK master slave

IV. CONCLUSIONS

This paper reports a modified DTMOS approach which is called VT MOS approach. In these circuits the substrate is operated with a fixed bias (V_{AN}/V_{AP}) which results in further reduction in the operating currents compared to DTMOS circuits. The Proposed scheme shows improved power efficiency compared to CMOS and DTMOS circuits, up to a frequency of 8 MHz (for the specific devices used in this Investigation).

Using these concepts one may be able to build low power digital circuits like [19, 20] which consume lower power than the conventional CMOS and DTMOS circuits.

REFERENCES

- [1] H.Soeleman, K.Roy, and B.C.Paul. : "Robust Sub threshold Logic for Ultra Low Power Operation", IEEE trans VLSI system, Feb 2001, Vol. 9, PP. 90-99.
- [2] Jabulani: Nyathi and Brent Bero: "Logic Circuits Operating in Sub Threshold Voltages", ISLPED 06, October 4-6, 2006, Tegernsee, Germany.
- [3] C.Hyung, - 11 Kim, H.Soeleman, and K.Roy: "Ultra-Low Power DLMS Adaptive Filter for Hearing Aid Applications", IEEE transactions on very large scale integration (VLSI) system, vol. 11, No.6, December, 2003. PP 1058-1067.
- [4] H. Soeleman and K. Roy, "Ultra-low power digital subthreshold logic circuits", in Int. Symp. Low Power Electron. Design, 1999, pp. 94-96.
- [5] Fariborz Assaderaghi, Stephen Parke, Dennis Simitsky, Jeffrey Bokor, Ping K. KO. Chenming Hu: "A Dynamic Threshold Voltage MOSFET (DTMOS) for Very Low Voltage Operation", IEEE Electron device letters, vol. 13, No.12, December 1994.
- [6] Tae-Hyoung Kim, Hanyang Eom, John. Keane and Chris Kim: "Utilizing Reverse Short Channel Effect for Optimal Sub Threshold Circuit Design", ISLPED 06, October 4-6, 2006. Tegern see, Germany.
- [7] H. Soeleman, K. Roy, B. Paul : "Robust ultra-low power sub-threshold DTMOS logic", in Int. Symp. Low Power Electron. Design, 2000 ,pp.25 - 30.
- [8] J. Gil, M. Je, J. Lee and H. Shin: "A High Speed and Low Power SOI Inverter using Active Body-Bias", in Int. Symp. Low Power Electron.Design , 1998 , pp.59-63.
- [9] F. Assaderaghi, D. Sinitsky, S. Parke, J. Bokor, P. K. Ko, and C. Hu: "A dynamic threshold voltage MOSFET (DTMOS) for ultra-low voltage operation", in IEDM Tech. Dig., 1994, pp. 809-812.
- [10] I.Chung, Y.Park, and H. Min: "A new SOI inverter for low power applications", in Proc. 1996 IEEE Int. SOI Conf., 1996, pp. 20-21.
- [11] A.Drake, K. Nowka, R. Brown: " Evaluation of Dynamic-Threshold Logic for Low-Power VLSI Design in 0.13um PD-SOI", VLSI-SOC 2003,pp. 263-266.
- [12] M.R. Casu, G. Masera, G. Piccinini, M. Ruo Roch, M. Zamboni: "Comparative Analysis of PD-SOI Active Body-Biasing Circuits," Proc. IEEE International SOI Conference, pp. 94-95, Oct. 2000.
- [13] S.Soleimani, A.Sammak, B.Forouzandeh "A Novel Ultra-Low-Energy Bulk Dynamic Threshold Inverter Scheme", Proceedings of the International Multi Conference Of Engineers and Computer Scientists 2009 Vol 1 IMECS 2009, March 18-20, 2009, Hong Kong
- [14] Assaderaghi et al, F.: "Dynamic Threshold - Voltage Mosfet (DTMOS) for Ultra - Low Voltage VLSI", IEEE trans Electron Devices, Vol. 44, PP 414-422, Mar 1997.
- [15] T.Kobayashi, and T.Sakurai : "Self-adjusting Threshold Voltage Scheme (SATS) for Low-Voltage High - Speed Operation", in Custom Integrated Circuits Conf., May 1994, pp.271-274.
- [16] J.M Rabaey: "Digital Integrated circuits: A Design Perspective 1st ed Upper Saddle River" New Jersey: Prentice Hall, 1996.
- [17] H.Soeleman., K.Roy.: "Digital CMOS Logic Operation in the Sub-threshold Region," in Tenth Great Lakes Symp.VLSI, Mar.2000, pp.107-112.
- [18] Wet Jin and Philip Chan, CH.: "A Comparative Study of SOI Inverter Circuits for Low Voltage and Low Power Applications", Proceedings 1997 IEEE International SOI conference, Oct. 1997.
- [19] Jaydeep P.Kulkarni, Keejong Kim, and Kaushik Roy.: "A 160 mV Robust Schmitt Trigger Based Subthreshold SRAM", IEEE Journal Of Solid-State Circuits, VOL 42, NO.10, Oct 2007.
- [20] V.Moalemi, Afjali A.Koosha: "Subthreshold 1-Bit Full Adder Cells in sub-100nm Technologies", Proc.of the IEEE Computer Society Annual Symposium on VLSI, pp.514-515, 2007.

BIO-DATA OF AUTHORS

Dr.K.RAGINI-Received B.Tech degree from Sri Venkateswara University, Tirupathi in 1990 and M.Tech and Ph.D degree in Electronics and Communication Engineering from JNTU, Hyderabad in 2000 and 2013 respectively. Worked as Assistant Professor in ECE Department at Chaitanya Bharathi Institute of Technology and Science, Gandipet, Hyderabad from 2000-2005. Then joined as Associate Professor in ECE Department at G.Narayanamma Institute of Technology and Science and presently working in the same institute. She is guiding number of M.Tech students and recently guiding Ph.D Students. she has 10 publications to her credit.

DR.M.SATYAM-Received B.E.(Electronics) from Madras University in 1958. Obtained M.E. and Ph.D from Indian Institute of Sciences in 1960 and 1963 respectively. He worked in various capacities at IISc, Bangalore till his retirement. Presently he is working as visiting professor, IIIT, Hyderabad. He guided 33 Ph.D students and 11 M.S. students. He has 139 publications in various National and International Journals. He has 10 patents to his credit. He is actively engaged in Research and Teaching.

DR.B.C.JINAGA- Born on June, 1950, graduation from Karnataka University, Dharwad, Post Graduation from Regional Engineering, Warangal and Ph.D. from Indian Institute of Technology, Delhi. He has been with JNT University since 21 years. Prof.B.C. Jinaga was occupied various key positions at JNT University and presently Rector at JNT University. He guided several students for Ph.D. He has published quite number of papers in reputed international and National journals. His research interest includes signal Processing and Coding Techniques. He received Best Teacher Award for the year 2002 - Awarded by Government of Andhra Pradesh.

An Integrated Inventory Optimization for Deteriorating Products under Multi - Echelon Just In Time (JIT)

Raj Mohan R.¹, Krishnaveni K.²

¹(Department of Mechanical Engineering, TRP Engineering College, India)

²(Department of Mechanical Engineering, TRP Engineering College, India)

ABSTRACT: This paper deals with the deterioration inventory model which focuses on optimally coordinating Just In Time (JIT) policy among all the partners with various issues in the supply chain in order to minimize the joint total cost. The total cost for an integrated inventory model includes all costs from multiple suppliers, one producer and multiple buyers and the individual's total cost consist of ordering cost, holding cost, order receiving cost setup cost and deterioration cost. A multiple buyers –multiple suppliers coordination model is developed to facilitate the frequent deliveries in a small lot sizes in a manufacturing supply chain for the deteriorating item. The model based on the integrated total relevant costs for the multiple buyers, a single producer and the multiple suppliers, determines optimal order quantity and number of deliveries over a finite planning horizon in a relatively simple Just In Time scenario.

Keywords: Deteriorating Item, Inventory, Just in Time, Multi Echelon, Supply Chain, Traditional Production, Total Cost..

I. INTRODUCTION

The ultimate goal of JIT from the production / inventory management standpoint is to produce small – lot sizes with high – quality products. Investing capital in shortening lead time and improving quality are regarded as the most effective means of achieving this goal. With such characteristics, researchers have modified traditional inventory models to incorporate the implementation of JIT concepts. Just – in – time (JIT) is a philosophy of manufacturing based on planned elimination of all wastes and on continuous improvement of productivity.

Deterioration is applicable to many inventory items in practice, like volatile liquids, agricultural products, radioactive substances, drugs, blood, fashion goods, electronic components, and high-tech products. The deteriorating items are subject to a continuous loss in their masses or utilities throughout their lifetime due to decay, damage, spoilage, and plenty of other reasons.

This paper develops a multiple buyer – multiple supplier coordination model to facilitate frequent deliveries in small lot sizes in a manufacturing supply chain. This based on the integrated total relevant costs of both multiple buyer and supplier, determines optimal order quantity, the number of deliveries over a finite planning horizon in a relatively simple JIT multiple buyer – multiple supplier scenario.

II. LITERATURE REVIEW

Liang-Yuh Ouyang et. al, discussed that an integrated inventory model with a price sensitive demand rate, determining jointly economic lot size of the buyer's ordering and the supplier's production batch, are developed to maximize the total profit per unit time. [1]

Monique Bakker et. al to give a comprehensive literature review of models for inventory control with deteriorating items and mentioned that Multi-echelon inventory control is gaining importance due to the need for supply chain integration in today's competitive environment. [2]

Kung-Jeng Wang et. al investigates how different deterioration rates in each echelon affect performances of individuals and integrated inventory policies. Sensitivity analysis is given to justify that the impact of changes in deterioration rates of each echelon is significant and the joint cost of the proposed integrated inventory policy is found to be much less than the individual policies. [3]

Ali Arkan, and Seyed Reza Hejazi extended inventory model for two-level supply chain which contains single buyer and single supplier, under the credit option. The uncertain demand faced by buyer is adapted with normal distribution. The lead time for receiving his order, can be reduced at an added crashing cost; in other words, it is controllable. On the other hand, ordering cost can also be controlled and reduced through various efforts. [4]

P.C Yang et. al discussed about a closed-loop supply chain inventory system with multi- manufacturing cycles and multi-remanufacturing cycles is analyzed using sequential and global optimization. In the case of sequential optimization, the decision is made initially by the down-stream player, then by the up-stream player. [5]

Hsin Rau et. al developed a multi-echelon inventory model for a deteriorating item and to derive an optimal joint total cost from an integrated perspective among the supplier, the producer, and the buyer. A computer code is developed to derive the optimal solution. the integrated approach strategy results in the lowest joint total cost as compared with the independent decision approaches. [6]

Changyuan Yan et. al developed an integrated production–distribution model for a deteriorating item in a two-echelon supply chain and determined the optimal supply chain decisions with the objective of minimizing the total system cost .[7]

Chao-Kuei Huang et.al dealt with the order-processing cost reduction and permissible delay in payments problem in the single-vendor single-buyer integrated inventory model and to minimize the annual integrated total cost by optimizing simultaneously the delivery interval, the number of deliveries per order and the investment cost in order-processing time. An

integrated total cost function is derived, and an algorithm procedure is proposed for determining the optimal decision variables. [8]

Jonas C. P. Yu et. al proposed a supply chain network system with two producers, a single distributor and two retailers. Each retailer has a deterministic demand rate. A mathematical model of deteriorating item is developed to consider a vertical integration of the producer, the distributor and the retailer and a horizontal integration of the producers. [9]

Jin-Shan Yang and Jason Chao-Hsien Pan presented an integrated inventory model to minimize the sum of the ordering/setup cost, holding cost, quality improvement investment and crashing cost by simultaneously optimizing the order quantity, lead time, process quality and number of deliveries while the probability distribution of the lead time demand is normal. This integrated inventory model is useful particularly for JIT inventory systems where the vendor and the purchaser form a strategic alliance for profit sharing. [10]

III. PROBLEM DEFINITION

Based on the research studies, it was observed that small lot sizing as a means of implementing successful JIT purchasing, with the buyer – supplier coordination focusing on material flows with an objective of minimizing supply chain costs. The total cost for an integrated inventory model includes all costs from both buyer and supplier. An integrated approach allows the buyer and the supplier to reduce their total costs as compared to non – integrated approach.

IV. INTEGRATED MODEL

Small lot sizing improves the system's productivity by obtaining lower levels of inventory and scrap, lower inspection costs for incoming parts, and earlier detection of defects, etc., even though possible higher delivery costs and loss of discount rates may be incurred. In general, implementation of frequent deliveries in small lots requires firms to reduce the number of suppliers (even to a single supplier). Otherwise, the potential strength of relationship between buyer and supplier would be weakened. Here, the supplier is viewed as part of a team, providing certified quality material at lower costs, rather than as an opponent who is consistently seeking short – term price breaks in an adversarial bargaining process. The supplier and buyer work in a cooperative manner to synchronize supply with actual customer demand. In this scenario, it could be more reasonable to determine the order quantity and the delivery schedule based on their integrated total cost function, rather than using the buyer's or the supplier's individual cost functions.

V. MODEL DEVELOPMENT

The model developed in based on the concepts of deterioration inventory system, the JIT production environment, and the supply chain system & multi stage multi echelon model. To consider a deteriorating item and to develop an optimal joint total cost from the perspectives of a multiple supplier, a manufacturer and a multiple buyer under a JIT production environment.

1. Assumptions

To derive optimal number of deliveries production and order cycle with multiple suppliers, manufacturer and multiple buyers when the integrated joint total cost is minimized globally.

- Demand rate and production rate is deterministic and constant.
- Production rate is greater than demand rate.
- Negligible lead time.
- Shortage is not allowed.
- Multiple supplier – One producer – Multiple buyer.
- Deterioration rate is deterministic and constant.
- Single item.
- Multiple lot size deliveries per order.
- Supplier delivers same lot size of same size of raw materials each time to the producer.
- Producer delivers same lot size of finished item each time to the buyer.

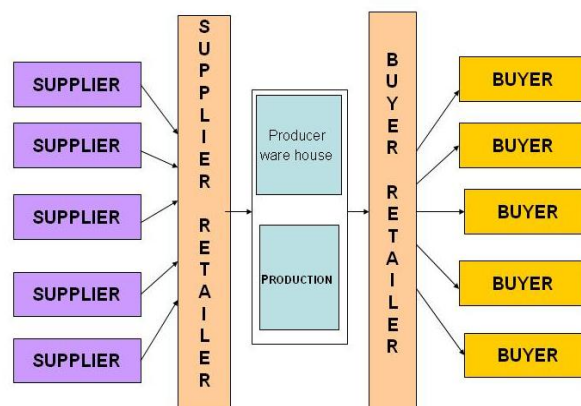


Fig. 1 Integrated Supply Chain Model

This integrated supply chain system model illustrates the supplier – retailer procures raw materials from outside suppliers and delivers them in fixed quantities to the producer’s warehouse at a fixed time interval. The producer withdraws raw materials from the warehouse and processes them into finished goods. The producer then delivers the finished goods in fixed quantities to the buyer. Retailer at a fixed time interval and delivers to various buyers also at fixed time interval. The demand of the supplier retailer will be equal to the demand of the producer which will be procured from the outside suppliers and the buyer retailer will have the demand equal to the demand given by the outside suppliers

2. Buyer –Retailer’s finished Good Inventory Model

The total cost of finished goods for the buyer retailer per period ‘T’ can be expressed as the sum of the order cost, receiving cost, holding cost and the deteriorating cost

$$TC_{BR} = A + n.F_{BR} + n.\Sigma. \left(\frac{H_{BR}}{\theta_{BR}} (e^{\theta_{BR} t} - 1 - \theta_{BR} t) + P_{BR} (e^{\theta_{BR} t} - 1 - \theta_{BR} t) \right) \quad (1)$$

Where, TC_{BR} is Buyer – Retailer’s total Cost, H_{BR} is the holding cost per unit per unit time by Buyer-retailers, θ is Deterioration rate for Buyer - Retailer, P_{BR} is deterioration cost per unit per unit time by retailers, A is ordering cost per time, n is Number of deliveries of finished goods from the producer to buyer per order cycle T , F_{BR} is Receiving cost of finished goods per receiving for the buyer, t is replenishment cycle time for buyer - retailer.

3. The Producer’s Warehouse Raw Materials Inventory Model

Total cost for the producer’s ware house raw material can be expressed as the sum of the receiving cost, holding cost and the deteriorating cost.

$$TC_{PW} = n.(F_{PW} + A_{PW} + H_{PW} + P_{PW}(q_{PW} - p_t)) \quad (2)$$

Where , TC_{PW} is Producer warehouse total cost , n is number of deliveries , F_{pw} is Receiving cost of raw materials per receive for the producer , A_{pw} is ordering cost per time from producer’s warehouse, H_{pw} is holding cost per unit per unit time by producer’s warehouse , P_{pw} is deterioration cost per unit per unit time by producer’s warehouse , q_{pw} is Lot size raw materials per delivery from the supplier of the producer’s warehouse , t_p is replenishment cycle time for producer.

4. The Producer’s Finished Good Inventory Model

The total finished goods cost for the producer can be expressed as the sum of the setup cost, delivery cost, holding cost and deteriorating cost

$$TC_P = n. \left[S_P + F_P + (P t_P - q_{BR}) \left[\frac{H_P}{\theta_P} + P_P \right] \right] \quad (3)$$

Where TC_P is Producer’s Total Cost , q_{BR} is Lot size raw materials per delivery from the supplier of the buyer-retailer , H_p is holding cost per unit per unit time by producer , θ_p is Deterioration rate at producer , P_p is deterioration cost per unit per unit time for producer , S_p is Setup cost of per setup for the producer , F_p is Delivery cost of finished goods per deliver for the producer.

5. The Supplier –Retailer’s Inventory Model

Total raw material cost for the supplier retailer can be expressed as the sum of the order cost, delivery cost, holding cost and the deteriorating cost

$$TC_{SR} = S + n. \left\{ F_{SR} + H_{SR} \left[\frac{Q_{PW} [(1 - \theta_{SR})^t - Q_{PW}]}{\ln(1 - \theta_{SR})} \right] \right\} \quad (4)$$

Where , TC_{SR} is Supplier –Retailer’s total cost , H_{SR} is holding cost per unit per unit time by supplier – retailer , θ_{SR} is Deterioration rate at Supplier – Retailer , Q_{PW} is Lot- size of raw materials from the outside supplier to the supplier , t is replenishment cycle time at supplier retailer , S is Setup cost of per setup .

6. Integrated Joint Total Cost

The integrated total cost for the buyer – retailer, the manufacturer and the supplier – retailer TC_I is

$$TC_I = TC_{BR} + TC_{PW} + TC_P + TC_{SR} \quad (5)$$

VI. NUMERICAL EXAMPLE

1. Buyer - Retailer's Parameter Data

Demand rate of finished goods is 9500 units per week. The ordering cost of finished goods is Rs.280 per order; the receiving cost of finished goods is Rs.23 per receiving; the holding cost of finished goods per unit is Rs.14; the deteriorating cost of finished goods per unit is Rs.105; the deterioration rate is 0.07.

2. Producer's Parameter Data

Production rate of finished goods is 19500 units per week. The setup cost of finished goods is Rs.475 per setup; the delivery cost of finished goods is Rs.140 per delivery the holding cost of finished goods per unit is Rs.11.50; the deteriorating cost of finished goods per unit is Rs.85; the deterioration rate is 0.09. The receiving cost of materials is Rs.17 per receiving; the holding cost of raw materials per unit is Rs.10; the deteriorating cost of raw materials per unit is Rs.80, the deterioration rate is 0.095.

3. Supplier - Retailer 'S Parameter Data

The ordering cost of raw materials is Rs.240 per order; the delivery cost of raw materials is Rs.120 per delivery; the holding cost of raw materials per unit is Rs.7; the deteriorated cost of raw materials per unit is Rs.70, the deterioration rate is 0.1.

The above parameters data is substituted into the derived supply chain inventory model for deteriorating items in the JIT environment. The problem is to determine the optimal value of N that minimizes TC. A computer code using the software Mat lab is develop to derive the optimal solution; namely the optimal delivery times N and total cost.

VII. RESULTS AND DISCUSSION

The comparison between integrated view of JIT and traditional view is made. In JIT, the optimal number of delivery is 23 and for the traditional is 48. Optimal joint total cost in traditional view is Rs.88288 and Rs.37611 for JIT respectively showing that JIT implementation is more cost effective than the traditional view.

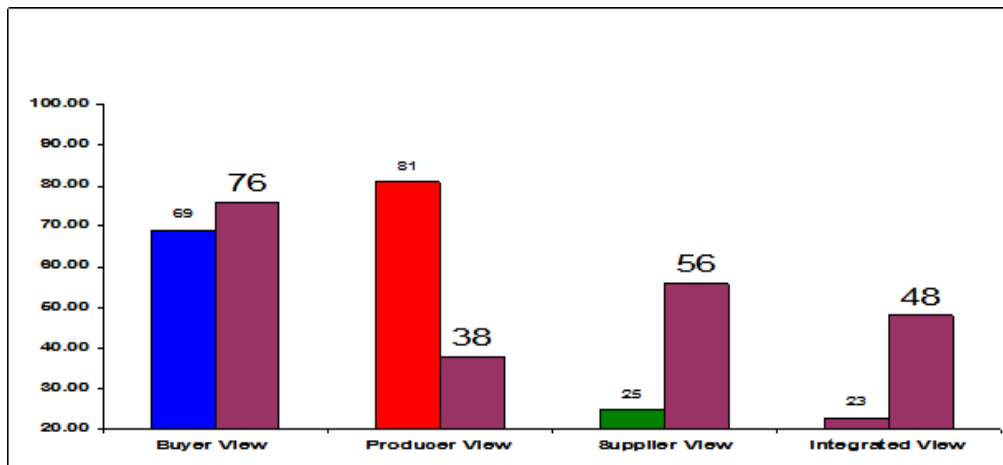


Fig.2 JIT Vs Traditional Number of deliveries for the different views

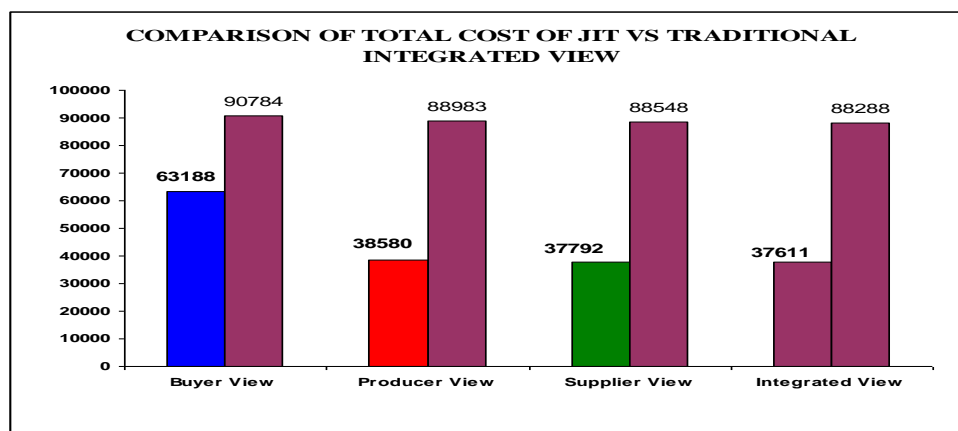


Fig.3 Comparison of Total Cost of JIT Vs Traditional Integrated View

VIII. CONCLUSION

The JIT production was adopted to achieve lower inventory costs. From model development, we determined how to minimize the total cost in each view. It was also shown that the integrated approach has the lowest joint total cost among all views. The JIT integrated view is compared with traditional inventory system show the JIT production environment is more cost effective than the traditional production environment for deteriorating item.

References

- [1] Liang-Yuh Ouyang et. al, An optimization approach for joint pricing and ordering problem in an integrated inventory system with order-size dependent trade credit, *Computers & Industrial Engineering*, 57, 2009, 920–930.
- [2] Monique Bakker et. al, Review of inventory systems with deterioration since 2001, *European Journal of Operational Research*, 221, 2012, 275–284.
- [3] Kung-Jeng Wang et. al, Using Optimizing inventory policy for products with time-sensitive deteriorating rates in a multi-echelon supply chain, *Int. J. Production Economics*, 130, 2011, 66–76.
- [4] Ali Arkan, and Seyed Reza Hejazi , Coordinating orders in a two echelon supply chain with controllable lead time and ordering cost using the credit period, *Computers & Industrial Engineering*, 62, 2011, 56–69.
- [5] P.C. Yang et. al, Sequential and global optimization for a closed-loop deteriorating inventory supply chain, *Mathematical and Computer Modelling*, 52, 2010, 161-176.
- [6] Hsin Rau et. al, Integrated inventory model for deteriorating items under a multi-echelon supply chain environment ,*Int. J. Production Economics*, 86 , 2003, 155–168.
- [7] Changyuan Yan et. al, An integrated production–distribution model for a deteriorating inventory item, *Int. J. Production Economics*, 133, 2011, 228–232.
- [8] Chao-Kuei Huang et.al , An optimal integrated vendor–buyer inventory policy under conditions of order-processing time reduction and permissible delay in payments, *Int. J. Production Economics* ,128, 2010 ,445–451.
- [9] Jonas C. P. Yu et. al, Supply chain partnership for three-echelon deteriorating inventory model, *Journal Of Industrial And Management Optimization*, 4(4) ,2008,827-842.
- [10] Jin-Shan Yang and Jason Chao-Hsien Pan, Just-in-time purchasing: an integrated inventory model involving deterministic variable lead time and quality improvement investment, *Int. J. Prod. Res.*, 42(5), 2004, 853–863.

Application of CNTFET as Logic Gates and its implementation using HSPICE

Sameer Prabhu¹, Dr. Nisha Sarwade²

¹(Department of Electronics and Telecommunication Engineering SVKM's NMIMS MPSTME Mumbai, INDIA)

²(Department of Electronics Engineering V.J.T.I Mumbai, INDIA)

Abstract: The steady reduction in the dimension of transistors, according to Moore's law has been the main force behind the regular leaps in the level of performance of the silicon ICs. Due to the effects like the short channel effects, tunnelling effect, additional heat dissipation, interconnect problems etc problems arise. So it is not possible to reduce the size further. Hence now it is necessary to adopt new material or technology. Carbon Nano Tube Field Effect Transistors (CNTFETs) are being widely studied as possible successors to silicon MOSFETs. This paper focuses on simulation of CNTFET based digital circuits using HSPICE and parameters like delay, power and PDP are calculated.

Keywords: Avanwaes, Carbon Nanotube, Carbon Nanotube Field Effect Transistor, Logic gates, Top gated transistor.

I. Introduction

For many years MOSFET has been used as a basic element of circuit designing [1]. As the miniaturization of silicon based circuits reaches its physical limitations scientists are trying to adopt new material or technology which preserve a lot of what's good about existing silicon technology and also cope up with the problem associated with physical limits. CNTFET is a novel device that is projected to outperform scaled CMOS technologies. CNTFET-based devices offer high mobility for near-ballistic transport, high carrier velocity for fast switching. HSPICE compatible CNT model is used to design digital circuits and simulation is done on Avanwaves. In this paper, section II Introduces the Carbon nanotubes, section III delves into the CNTFET and model which is used. Simulation results and parameter calculation of digital circuits are in section IV. Finally, Sections V discuss the conclusion and future scope.

II. Carbon Nanotube (CNT)

The first person to see carbon nanotubes was Sumio Iijima of NEC Crop in Tokyo, who discovered them in 1991 while studying electron microscope images of the soot produced by electrical discharges between carbon electrodes. Carbon nanotubes are basically hollow cylinders with diameters ranging from 1 nm to 50 nm and length, over 10 μ m [2]. The carbon atoms are arranged into hexagons that form a honeycomb pattern. A nanotube can be viewed as a single layer or multilayer of graphite rolled into a seamless cylinder, as shown in Fig. 1. There are two types of nanotubes; one is a single-wall nanotube (SWCNT) that is made up of a single layer of graphite ("graphene" sheet), and the other is a multiwall nanotube (MWCNT) that consists of multiple shells [3].

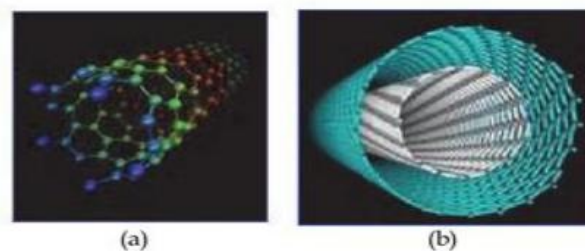


Figure 1: Structure models of nanotubes (a) SWCNT (b) MWCNT

The way that graphene is rolled is described by a pair of indices (n, m), which are called "chiral vector". According to the chiral vector of a CNT, it can be determined whether it's a metallic or semiconducting CNT.

III. Carbon Nanotube Field Effect Transistor (CNTFET)

A single carbon nanotube is positioned as a bridge between two electrodes. The electrodes became the source and drain of the transistor, and the nanotube played the role of the channel, as shown in the schematic Fig. 2.

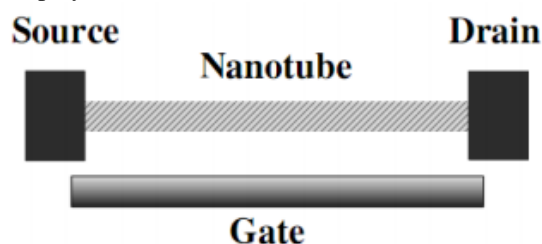


Figure 2: Schematic of CNTFET

Applying the appropriate voltage to gate the nanotube is on or off. The first carbon nanotube field-effect transistors (CNTFETs) were reported in 1998. In the nanotube device, the transistor action occurs at the contact points between the metal electrodes and the carbon nanotube. Semiconducting CNTs have been used to fabricate CNTFETs, which show promise due to their superior electrical characteristics over silicon based MOSFETs [4]. In terms of the device operation mechanism, CNFET can be categorized as either Schottky Barrier (SB) controlled FET or MOSFET-like FET. The ambipolar behaviour of SB-controlled CNFET makes it undesirable for complementary logic design. Considering both the fabrication feasibility and superior device performance of the MOSFET-like CNFET as compared to the SB-controlled FET, **we choose to focus on MOSFET-like CNFETs in this work.** The complete CNFET device model [5, 6] which is used is implemented hierarchically in three levels. Device nonidealities are included hierarchically at each level. The summary of model which is used is given in the table below.

Device Types	n-type/p-type CNFET
Device Dimensions:	
Channel Length (Minimum)	~10nm
Channel Length (Maximum)	Unlimited
Channel Width (Minimum)	4nm
Channel Width (Maximum)	Unlimited
Number of CNTs / device (Minimum)	1
Number of CNTs / device (Maximum)	Unlimited

Table 1: Summary of the CNFET Model

32nm technology with (19, 0) semiconducting with 1.5nm diameter CNT is used. The supply given is 0.9V and gate and drain voltage can be varied upto supply voltage i.e. 0.9V.

IV. SIMULATION RESULT

The logic gates like AND gate, OR gate, EXOR gates are simulated. Their output characteristics are plotted. All the following circuits are simulated at room temperature and the supply voltage is 0.9V. For all circuits a 10 femto Farad load capacitor has been used. Delay, Power and PDP calculations are also done for these logic gates. The AND gate performs logical multiplication, the AND gate shown in Fig. 3 If A and B are two inputs, then output Y can be represented mathematically as $F = A.B$, here dot (.) denotes the AND operation. Fig. 4 shows the behaviour of output of AND gate is HIGH only when all its inputs are AND gate. Table 2 shows variations in delay and average power for AND gate on varying the supply voltages.



Figure 3: symbol of AND gate

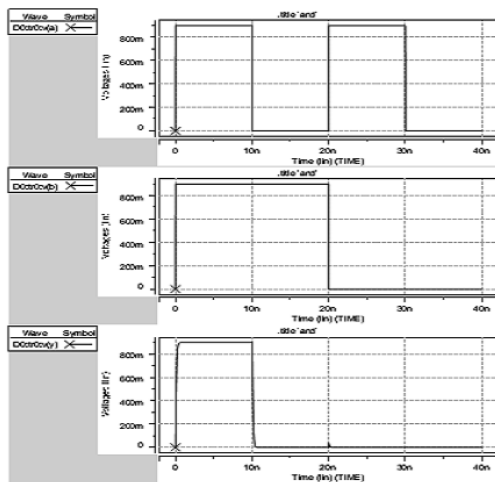


Figure 4: characteristics of CNTFET-AND gate

SUPPLY (V)	AND GATE		
	DELAY (sec)	POWER (W)	PDP (J)
0.9	8.639e-11	1.840e-06	1.589e-16
0.8	7.711e-11	1.500e-06	1.156e-16
0.65	6.319e-11	1.065e-06	6.729e-17

Table 2: AND gate simulation results

The OR gate performs logical addition, the OR gate shown in Fig. 5. The output of OR gate is HIGH only when any one of its inputs are high. If A and B are two inputs, then output Y can be represented mathematically as $Y = A+B$. Fig. 6 shows the behaviour of output of OR gate is HIGH when any or both of its inputs are high. Table 3 shows variations in delay and average power for OR gate on varying the supply voltages.



Figure 5: symbol of OR gate

SUPPLY (V)	OR GATE		
	DELAY (sec)	POWER (W)	PDP (J)
0.9	8.451e-11	1.830e-06	1.546e-16
0.8	7.349e-11	1.490e-06	1.095e-16
0.65	6.022e-11	1.055e-06	6.353e-17

Table 3: OR gate simulation results

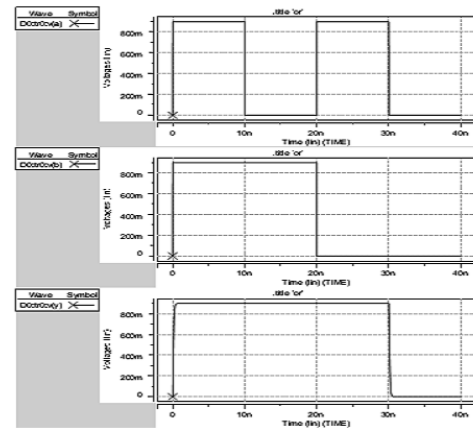


Figure 6: characteristics of CNTFET-OR gate

An Exclusive-OR (XOR) gate is gate shown in Fig. 7 with two inputs and one output. The output of a two-input XOR gate assumes a HIGH state if one and only one input assumes a HIGH state. If A and B are two inputs, then output Y can be represented mathematically as $Y = A'B + AB'$. Fig. 8 shows the behaviour of output of XOR gate is HIGH when only one of its inputs is high. Table 4 shows variations in delay and average power for EXOR gate on varying the supply voltages.



Figure 7: symbol of EXOR gate

SUPPLY (V)	EXOR GATE		
	DELAY (sec)	POWER (W)	PDP (J)
0.9	1.019e-08	1.839e-06	1.873e-14
0.8	1.017e-08	1.499e-06	1.524e-14
0.65	1.014e-08	1.064e-06	1.078e-14

Table 4: EXOR gate simulation results

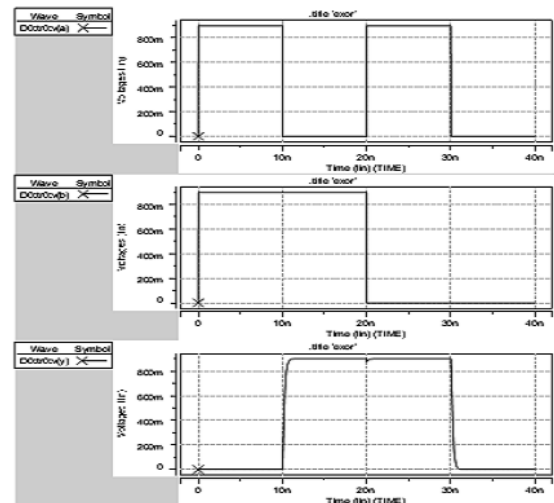


Figure 8: characteristics of EXOR gate

V. Conclusion And Future Scope

Unipolar, MOSFET like CNTFET model is used to implement various digital circuits like AND,OR, EXOR gates. This model is used for designing digital circuits whose coding has been done in HSPICE, the output waveform is displayed on AvanWaves and delay, average power calculations have been done for these digital circuits for various value of supply i.e. 0.9, 0.8, 0.65 V.

Complex digital circuits based on CNTFET technology can be designed using these basic gates and a comparative study can be done with that of Silicon technology.

REFERENCE

- [1] P. Avouris, "Super tubes." IEEE Spectrum, pp. 41-45, Aug 2004.
- [2] Y.M. Lin et al., "High-Performance Carbon Nanotube Field-Effect Transistor With Tunable Polarities", IEEE Trans. on Nanotech, Vol. 4, No. 5, pp. 481-489, 2005.
- [3] Y. Saito, "Preparation and Properties of CNT," International Symposium on micromechatronics and human science, pp.43-49,1999.
- [4] Ali Keshavarzi, Arijit Raychowdhury, Juanita Kurtin, Kaushik Roy, and Vivek De, "Carbon Nanotube Field-Effect Transistors for HighPerformance Digital Circuits—Transient Analysis, Parasitic, and Scalability", IEEE Transactions On Electron Devices, Vol. 53, NO. 11, Nov-2006.
- [5] C. Dwyer, M. Cheung and D. J. Sorin, "Semi empirical SPICE models for carbon nanotube FET logic," in Proc. Conf. Nanotechnology, Aug. 2004, pp. 386–388.
- [6] Fabien Pregaldiny et.al.,—Compact Modelling and Applications of CNTFETs for Analog and Digital Circuit Design, IEEE Trans. Elec.dev., pp. 1030–1033, 2006.

Vibration mitigation using passive damper in machining

Pranali Khatake¹, P. T. Nitnaware²

¹Department of Mechanical Engineering, DYPIET, Pimpri

²Department of Mechanical Engineering, DYPCOE, Akurdi

ABSTRACT: This paper introduces a vibration mitigation for boring bar with enhanced damping capability. The principle followed in this paper was to enhance the damping capability, minimizing the loss in static stiffness through implementation of passive damper. The newly designed tool has been compared to a conventional tool. The evaluation criteria were the dynamic characteristics, frequency and damping ratio, of the machining system, as well as the surface roughness of the machined work pieces.

Keywords: boring bar, passive damper, static stiffness, surface roughness, vibration mitigation

I. INTRODUCTION

Vibrations are undesirable for structures, due to the need for structural stability, position control, durability (particularly durability against fatigue), performance, and noise reduction. Vibrations are of concern to large structures such as aircraft, as well as small structures such as electronics.

Vibration reduction can be attained by increasing the damping capacity and/or increasing the stiffness (which is expressed by the storage modulus). The loss modulus is the product of these two quantities and thus can be considered a figure of merit for the vibration reduction ability.

Damping of a structure can be attained by passive or active methods. Passive methods make use of the inherent ability of certain materials (whether structural or non-structural materials) to absorb the vibration energy (for example, through mechanical deformation), thereby providing passive energy dissipation. Active methods make use of sensors and actuators to attain vibration sensing and activation to suppress the vibration in real time.

The attenuation of machine tool vibration is a field of research that has been the concern of many engineers over the past few decades. The driving force behind the ongoing research can be related to the fact that the level of vibration at the tool tip, limits the tool life as well as tolerances and the surface finish obtained by the machining process. Traditionally, the rate of material removal is reduced to obtain the required tolerances and surface finish. The reduction in rate of material removal reduces the efficiency of the machine, since the component manufacturing time is increased and lower production is obtained from the machine over a period of time. The objective of the vibration attenuation is to improve the dynamic stiffness of the machine tool structure, to increase the rate of material removal and thereby prolonging the life of the tool tip.

Acoustic noise emission during the machining process results from the relative motion between the tool tip and work piece. High levels of acoustic noise can cause discomfort in the working environment. The problem is related to the dynamic stiffness of the machine tool structure. By improving the dynamic stiffness of the structure, the level of noise emission from the machining process can be reduced.

II. EFFECTS OF VIBRATION ON MACHINING

Tool or work-piece vibration in machining processes is the main limiting factor for metal removal rate and machining efficiency. In boring process due to the slenderness of boring bar, its flexibility is much more than the work-piece.

Accordingly, the tool is more susceptible to vibrations. On the other hand, boring is a process that is used in finishing of precise components.

Tool vibrations result in poor surface finish, reduced tool life, dimensional errors and may also introduce chatter, which is highly unfavorable. Therefore, the machining parameters should be set in a way to avoid any kind of unstable vibration during the machining process.

Tool vibrations- The machine, cutting tool and work-piece form a structural system with complex dynamic characteristics. Under certain conditions this system may undergo excessive vibrations.

Types of vibrations- In machine tool structures can be generally categorized into three main groups: Free or transient vibrations: Free vibrations in machine tools occur almost in every machining operation. The vibrations due to the initial engagement of the tool and work-piece or the vibrations caused by the rapid reciprocal motion of the machine tool table are some sorts of transient vibrations. The machine tool vibrates in its natural modes until the vibration is damped.

Forced vibration: Forced vibrations occur when a periodic force is applied to the machine tool structure. The engagement of multi- insert tools in the cut and the run-out of the tooltip are the two main sources of forced vibrations. Also, there exist other sources like the vibrations transmitted to the machine tool by its foundation from the nearby machinery. The system vibrates in the actuating frequency and if this frequency coincides one of the system's natural frequencies the resonance occurs.

Self-excited vibration: The most important type of vibration in machining processes is self-excited vibration. When the tool initially engages the cut, it undergoes transient vibrations. If machining parameters like depth of cut, feedrate and cutting speed are not set properly, transient vibration may lead to self excited or chatter operations.

III. TOOLS AND TECHNIQUES FOR VIBRATION MITIGATION

3.1 Active vibration control

There is different method for the introduction of secondary vibration in boring bars. Here the actuator is mounted in a milled space in a longitudinal direction below the centerline of the boring bar. When the actuator applies a load on the boring bar in its longitudinal direction due to the expansion of the actuator, the boring bar will bend and stretch. By introducing secondary anti-vibrations via the actuator applied bending moment on the boring bar, the original vibrations from the cutting process can be reduced

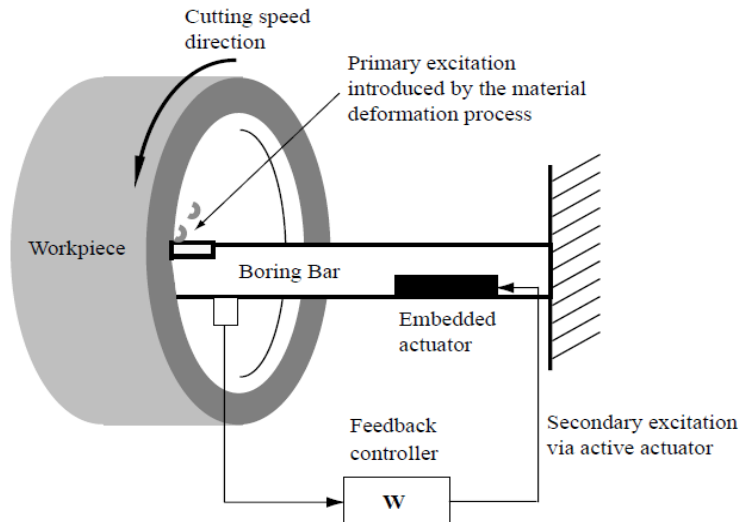


Fig 3.1 Active Boring bar control system

3.2 Passive vibration control

Particle damping is a passive damping concept to use metal or ceramic particles or powders of small size that are placed inside cavities within or attached to the vibrating structures shown in fig . Metal particles of high density such as lead or tungsten steel are the most common materials for better damping performance. In contrast to viscoelastic materials which dissipate the stored elastic energy particle damping treatment focuses on energy dissipation in a combination of collision, friction and shear damping. It involves the potential of energy absorption and dissipation through Momentum exchange between moving particles and vibrating walls, friction, impact restitution, and shear deformations. It is an attractive alternative in passive damping due to its conceptual simplicity, potential effectiveness over broad frequency range, temperature and degradation

Insensitivity and very low cost

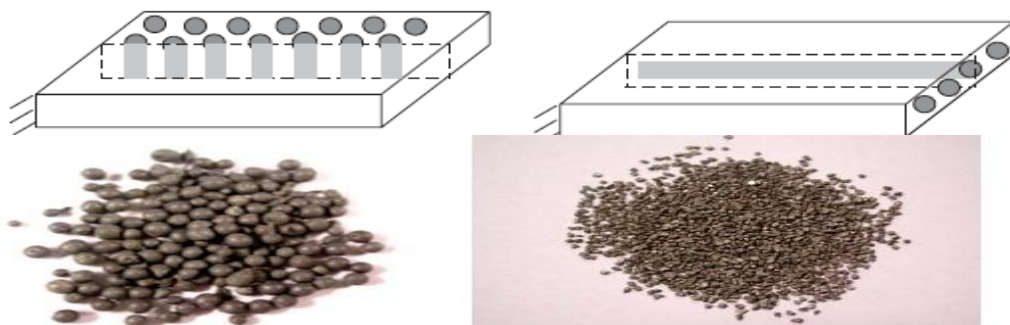


Fig 3.2 Particle Damping

IV. EXPERIMENTAL PROCEDURE

Number of experiments was conducted to analyze the effect of vibration on surface finish. Boring bar of 20 mm × 20 mm cross-section and 200 mm long of WIDAX make is used. The work piece material used for study is EN9. The boring operations were carried out on CNC turning centre

The work piece was mounted using a pneumatic chuck in CNC turning centre. The machining parameters like feed (feed rate s-0.9mm/min), depth of cut (t=0.6 mm), clamping pressure (10 bar), etc. were selected based on the manufacturers recommendations and were kept constant for all the samples used. Only the cutting speed, passive damper position on boring bar and overhang length was changed. The recommended parameters are shown in table 4.1. Boring was carried out for 110 mm internal diameter



Fig 4.1 boring bar



Fig 4.2 installation of boring bar



Fig 4. Sample work piece

Table 4.1

Boring Tool	BT1	BT2	
Overhang length L (mm)	30	60	90
Position of passive damper	Vertical	Horizontal	
Cutting speed (rpm)	70	140	210



Fig 4.4 CNC Turning Centre

RESULT

Speed-210 rpm, Depth of cut-0.6 mm, Feed-0.09 mm/min

Sr. No	Overhang length of Boring bar (mm)	Surface finish (μm) without passive damper	Surface finish (μm) With passive damper	
			Vertical	Horizontal
1	30	2.63	2.41	2.63
2	60	2.59	2.51	1.46
3	90	2.80	3.19	3.25

V. CONCLUSION

An innovative method is proposed to reduce tool chatter and enhance surface finish in boring operation. The results prove the passive damping technique has vast potential in the reduction of tool chatter. Passive dampers are also relatively cheaper than other damped boring bars. It is therefore concluded that passive damping has a good effect in improving surface finish in boring operation

Significant improvement is observed between the results of surface finish obtained using boring bar without passive damper and boring bar with passive damper.

REFERENCES

Journal Papers:

- [1] Lorenzo Daghini, Andreas Archenti, and Cornel Mihai Nicolescu "Design, Implementation and Analysis of Composite Material Dampers for Turning Operations" World Academy of Science, Engineering and Technology vol 53(2009).
- [2] B. Moetakef-Imani, N.Z.Yussefian "Dynamic simulation of boring process" International Journal of Machine Tools & Manufacture vol 49 (2009) pp 1096–1103
- [3] L. Andr en and L. H akansson Active "Vibration Control of Boring Bar" Vibrations Department of Signal Processing School of Engineering Blekinge Institute of Technology August, 2004
- [4] Zhiwei Xua, Michael Yu Wangb, Tianning Chen "Particle damping for passive vibration suppression: numerical modeling and experimental investigation" Journal of Sound and Vibration vol 279 (2005) pp 1097–1120

- [5] Lonnie Houck, Tony L. Schmitz, K. Scott Smith “A tuned holder for increased boring bar dynamic stiffness” Journal of Manufacturing Processes Vol.13 (2011) pp 24–29
- [6] Dai Gil Lee, Hui Yun Hwang, Jin Kook Kim “Design and manufacture of a carbon fiber epoxy rotating boring bar” Composite Structures Vol 60 (2003) pp 115–124
- [7] Norikazu Suzukia, Kohei Nishimurab, Ryo Watanabea, Takashi Katoa and Eiji Shamotoa “Development of novel anisotropic boring tool for chatter suppression” vol 1 (2012) pp 56 – 595th CIRP Conference on High Performance Cutting 2012
- [8] M. H. Migue, L.Rubio, J.A.Loya, J.Fernandez-Saez “Improvement of chatter stability in boring operations with passive vibration absorbers” International Journal of Mechanical Sciences vol 52 (2010) pp 1376–1384.

Measurement of the Thickness of Thin Foam Films by Laser Interferometry

Reza CheraghiKootiani, Ariffin Bin Samsuri

(Department of Petroleum Engineering, Faculty of Petroleum and Renewable Engineering, University Technology Malaysia)

ABSTRACT: Foams are involved in many industrial processes, including foods and beverages, firefighting, subsoil environmental remediation and enhanced oil recovery. In these applications, foam stability and dynamics depend on the permeability of the thin liquid films to gases. An important parameter in the description of the foam permeability is the thickness of the thin liquid films. The foam film permeability is can be measured using (laser) light interferometry. In this paper, we survey the principles of this technique and compute the expressions for the thickness for a free standing foam film. The foam film is consists of five layers: a core aqueous layer with two surfactant monolayers, each consisting of consisting of hydrocarbon tails and polar head-groups sub-layers. From its reflection intensity coefficient for perpendicularly incident light.

Keywords: foam film, thickness, interferometry, intensity

I. INTRODUCTION

Foam is a dispersion of a gas phase in a continuous liquid phase, stabilized by a surfactant. Applications involving foams in modern industrial processes have grown considerably in the last few decades. Hence, foam is matter of interest in many physical, biological and technological researches, including food and beverage technology, medical research (breathing), environmental remediation and petroleum engineering and research [1-3]. Use of foams in petroleum engineering includes enhanced oil recovery, well treatments and drilling operations [4]. The efficiency of the foam depends strongly on the stability and dynamics of foam films. As depicted in fig. 1, we can represent a foam film by a thin aqueous layer bound by monolayers of adsorbed surfactant molecules; the main function of the surfactant molecules is to stabilize the foam film [5]. The adsorption of surfactants onto the gas liquid interfaces can inhibit the flux of gas through the foam film [6-9]. The permeability of the foam films to gases limits the stability of the foam [10,11]. One of the key parameters in determining the film permeability to gases is the thickness of the foam film which results from the equilibrium between the film surfaces. Therefore, knowing the thickness of the foam films helps the better understanding of the physical properties of the foam. In this paper, first the formulas to calculate the thickness of a uniform homogenous liquid film by interferometry will be presented in details. Next, considering the structure of the foam films, these formulas will simplified. These formulas can be used both for horizontal and vertical (free standing) films.

II. MODEL DESCRIPTION

Below we present the equations for computing the fraction of a light wave reflected by a flat interface between two dielectric media, with different refractive indices; these are the Fresnel equations. It proceeds by considering the boundary conditions at the interface for the electric and magnetic fields of the light waves. In fig 2, the xy plane in the interface plane. The x axis is the projection of the rays on the plane boundary and the y axis is perpendicular to the plane of drawing. According to the electromagnetic theory of the light the incident, reflected and transmitted waves of light can be written as [12,13]:

$$E_0^d = A_0 \exp(i\tau_0^d), E_0^r = R_0 \exp(i\tau_0^r), E_1^d = A_1 \exp(i\tau_1^d) \dots \dots \dots (1)$$

Where,

$$\tau_0^d = \omega \left(t - \frac{x \sin \theta_0 + z \cos \theta_0}{v_0} \right), \tau_0^r = \omega \left(t - \frac{x \sin \theta_0 - z \cos \theta_0}{v_0} \right),$$

$$\tau_1^d = \omega \left(t - \frac{x \sin \theta_0 + z \cos \theta_0}{v_1} \right) \dots \dots \dots (2)$$

In these equations t is the time, ω is the circular frequency of the light wave, θ_0 is the angle of incident light and v_0 and v_1 are the velocity of the ray in the first and second media respectively. The vector of the amplitude of the incident, reflected and transmitted light waves (electric field strength), A_0, R_0 and A_1 , have two components: (a) a component lying in the plane of reflection (or incident, i.e., plane xz) and (b) a component perpendicular to the plane of reflection i.e., plane xy. For the reflected wave these two components are given by [12,13]:

$$R_{0,P} = \frac{n_1 \cos \theta_0 - n_0 \cos \theta_1}{n_1 \cos \theta_0 + n_0 \cos \theta_1} A_{0,P}, R_{0,S} = \frac{\tan(\theta_0 - \theta_1)}{\tan(\theta_0 + \theta_1)} A_{0,P} \dots \dots \dots (3)$$

$$R_{0,P} = \frac{n_0 \cos \theta_0 - n_1 \cos \theta_1}{n_0 \cos \theta_0 + n_1 \cos \theta_1} A_{0,S} = -\frac{\sin(\theta_0 - \theta_1)}{\sin(\theta_0 + \theta_1)} A_{0,S} \dots\dots\dots (4)$$

n_0 and n_1 are the refractive indices of two media. For the ratio of reflected and incident amplitudes:

$$r_P = \frac{R_{0,P}}{A_{0,P}} = \frac{n_1 \cos \theta_0 - n_0 \cos \theta_1}{n_1 \cos \theta_0 + n_0 \cos \theta_1} = \frac{\tan(\theta_0 - \theta_1)}{\tan(\theta_0 + \theta_1)} \dots\dots\dots (5)$$

$$r_S = \frac{R_{0,S}}{A_{0,S}} = \frac{n_0 \cos \theta_0 - n_1 \cos \theta_1}{n_0 \cos \theta_0 + n_1 \cos \theta_1} = -\frac{\sin(\theta_0 - \theta_1)}{\sin(\theta_0 + \theta_1)} \dots\dots\dots (6)$$

The intensity of reflected light is given for both components by:

$$I_P^r = r_P^2 \dots\dots\dots (7)$$

$$I_S^r = r_S^2 \dots\dots\dots (8)$$

III. RESULTS AND DISCUSSION

We assume a homogenous film in which the refractive index n_f is constant in the whole thickness ϵ_{eq} (Fig. 3). For a thin film for two components of the reflected light we obtain the following equations [12]:

$$r_P \exp(i\delta_P) = \frac{r_P' + r_P'' \exp(-i\Delta\phi)}{1 + r_P' r_P'' \exp(-i\Delta\phi)} = \frac{r_P' \exp(i\Delta\phi) + r_P'' \exp(-i\Delta\phi)}{\exp(i\Delta\phi) + r_P' r_P'' \exp(-i\Delta\phi)} \dots\dots\dots (9)$$

$$r_S \exp(i\delta_S) = \frac{r_S' + r_S'' \exp(-i\Delta\phi)}{1 + r_S' r_S'' \exp(-i\Delta\phi)} = \frac{r_S' \exp(i\Delta\phi) + r_S'' \exp(-i\Delta\phi)}{\exp(i\Delta\phi) + r_S' r_S'' \exp(-i\Delta\phi)} \dots\dots\dots (10)$$

$$\Delta\phi' = \frac{2\pi\epsilon_{eq}}{\lambda_0} 2n_f \cos \theta \dots\dots\dots (11)$$

$$\Delta\phi = \frac{\Delta\phi'}{2} = \frac{2\pi n_f \epsilon_{eq}}{\lambda_0} \cos \theta \dots\dots\dots (12)$$

Multiplication of equations (9) and (10) by the complex conjugate expression $r_P \exp(-i\delta_P)$ and $r_S \exp(-i\delta_S)$ respectively gives:

$$I_P^r = r_P^2 = \frac{r_P'^2 + r_P''^2 + 2r_P' r_P'' \cos \Delta\phi'}{1 + r_P'^2 r_P''^2 + 2r_P' r_P'' \cos \Delta\phi'} \dots\dots\dots (13)$$

$$I_S^r = r_S^2 = \frac{r_S'^2 + r_S''^2 + 2r_S' r_S'' \cos \Delta\phi'}{1 + r_S'^2 r_S''^2 + 2r_S' r_S'' \cos \Delta\phi'} \dots\dots\dots (14)$$

Where r_P' is calculated from equation (9) and,

$$r_P'' = \frac{n_2 \cos \theta_1 - n_1 \cos \theta_2}{n_2 \cos \theta_1 + n_1 \cos \theta_2} = \frac{\tan(\theta_1 - \theta_2)}{\tan(\theta_1 + \theta_2)}$$

$$r_S'' = \frac{n_1 \cos \theta_1 - n_2 \cos \theta_2}{n_1 \cos \theta_1 + n_2 \cos \theta_2} = -\frac{\sin(\theta_1 - \theta_2)}{\sin(\theta_1 + \theta_2)}$$

The intensity of the incident light is assumed to be one and the amplitudes r_P and r_S are taken with positive signs.

$$(I_P)_{max} = \frac{r_P'^2 + r_P''^2 + 2r_P' r_P''}{1 + r_P'^2 r_P''^2 + 2r_P' r_P''} = \left(\frac{r_P' + r_P''}{1 + r_P' r_P''} \right)^2 \dots\dots\dots (15)$$

$$(I_P)_{min} = \frac{r_P'^2 + r_P''^2 - 2r_P' r_P''}{1 + r_P'^2 r_P''^2 - 2r_P' r_P''} = \left(\frac{r_P' - r_P''}{1 - r_P' r_P''} \right)^2 \dots\dots\dots (16)$$

$$(I'_s)_{max} = \frac{r_s'^2 + r_s''^2 + 2r_s' r_s''}{1 + r_s' r_s''} = \left(\frac{r_s' + r_s''}{1 + r_s' r_s''} \right)^2 \dots\dots\dots (17)$$

$$(I'_s)_{min} = \frac{r_s'^2 + r_s''^2 - 2r_s' r_s''}{1 + r_s' r_s''} = \left(\frac{r_s' - r_s''}{1 - r_s' r_s''} \right)^2 \dots\dots\dots (18)$$

Since $\cos 2x = 1 - 2\sin^2 x$ then equation (13) and (14) can be rearranged to:

$$I'_p = r_p^2 = \frac{(r_p' + r_p'')^2 - 4r_p' r_p'' \sin^2 \Delta\phi}{(1 + r_p' r_p'')^2 - 4r_p' r_p'' \sin^2 \Delta\phi} \dots\dots\dots (19)$$

$$I'_s = r_s^2 = \frac{(r_s' + r_s'')^2 - 4r_s' r_s'' \sin^2 \Delta\phi}{(1 + r_s' r_s'')^2 - 4r_s' r_s'' \sin^2 \Delta\phi} \dots\dots\dots (20)$$

When light is normally incident on the film ($\theta_0 = 0$, as in Fig. 4), Fresnel's formula can be rewritten in a simplified form:

$$r'_p = \frac{n_1 - n_0}{n_1 + n_0} = -r''_p \dots\dots\dots (22)$$

$$r'_s = \frac{n_1 - n_0}{n_1 + n_0} = -r''_s \dots\dots\dots (23)$$

Both components of the amplitude of the reflected light have the same magnitude but different signs; this means that one component is shifted by π with respect to the other.

Therefore in this section we confine ourselves to one component and drop the subscripts, s and p.

$$I_r = r^2 = \frac{(r' + r'')^2 - 4r' r'' \sin^2 \Delta\phi}{(1 + r' r'')^2 - 4r' r'' \sin^2 \Delta\phi} \dots\dots\dots (24)$$

Now if we put $r' = r'' = r_f$ which means that the film is placed between two optical media having a high reflectivity at the boundaries of the optical medium and film (Figure4). Thus, considering film as a homogenous layer with the refractive index of n_f and assuming no light absorption into the film, the following formula will be obtained:

$$\frac{I_r}{I_0} = \frac{4r_f^2 \sin^2 \Delta\phi}{1 - 2r_f^2 \cos 2\Delta\phi + r_f^4} \dots\dots\dots (25)$$

Where,

I_r : Intensity of light reflected by the film

I_0 : Intensity of the incident light (which is normally is assumed to be one)

r : Reflection coefficient for the amplitude for a single interface between the film with refractive index n_f and the surrounding medium with refractive index n_0 .

For perpendicularly incident light:

$$r_f = \frac{n_f - n_0}{n_f + n_0} \dots\dots\dots (26)$$

$\Delta\phi$ is the phase difference between light at the front face and back face of the film which in the case of normal beam is equal to:

$$\Delta\phi = \frac{2\pi n_f \epsilon_{eq}}{\lambda_0} \dots\dots\dots (27)$$

Where λ_0 is the wavelength in vacuum.

Replacing $\cos 2\Delta\phi = 1 - 2\sin^2 \Delta\phi$ and $R = r_f^2$ in equation (25) we lead to:

$$I_r = I_0 \frac{4R \sin^2 \Delta\phi}{(1 - R)^2 + 4R \sin^2 \Delta\phi} \dots\dots\dots (28)$$

I_r Has the minimum value when $\sin \Delta\phi = 0$. Therefore, $I_{min} = 0$ when:

$$\Delta\phi = \frac{2\pi n_f \epsilon_{eq}}{\lambda_0} = p\pi, \text{ where } p \in Z. \text{ Then in this case the thickness of the film is equal to:}$$

$$\varepsilon_{eq} = \frac{p}{2n_f} \lambda_0 \dots\dots\dots (29)$$

I_r has the maximum value when $\sin \Delta\varphi = 1$. Therefore, $I_{max} = \frac{4R}{(1+R)^2}$ when:

$$\Delta\varphi = \frac{2\pi n_f \varepsilon_{eq}}{\lambda_0} = (4p + 1) \frac{\pi}{2} \text{ Where } p \in Z. \text{ Then in this case the thickness of the film is equal to:}$$

$$\varepsilon_{eq} = \left(\frac{4p+1}{2n_f} \right) \lambda_0 \dots\dots\dots (30)$$

I we define $\Delta = \frac{I_r - I_{min}}{I_{max} - I_{min}}$ and substitute the parameters in this formula we will get:

$$\Delta = \frac{\frac{4R \sin^2 \Delta\varphi}{(1-R)^2}}{\left(1 + \frac{4R \sin^2 \Delta\varphi}{(1-R)^2} \right) \left(\frac{4R}{(1+R)^2} \right)}$$

$$\Delta = \frac{(1+R)^2 \sin^2 \Delta\varphi}{(1-R)^2 + 4R \sin^2 \Delta\varphi} \dots\dots\dots (31)$$

$$\Delta(1-R)^2 + 4R \Delta \sin^2 \Delta\varphi = (1+R)^2 \sin^2 \Delta\varphi$$

$$\sin^2 \Delta\varphi \left(\frac{(1+R)^2}{(1-R)^2} - \frac{4R\Delta}{(1-R)^2} \right) = \Delta$$

$$\sin^2 \Delta\varphi \left(\frac{(1+R)^2 + 4R(1-\Delta)}{(1-R)^2} \right) = \Delta$$

$$\sin^2 \Delta\varphi (1 + (4R(1-\Delta)/(1-R)^2)) = \Delta$$

$$\sin^2 \Delta\varphi = \frac{\Delta}{1 + (4R(1-\Delta)/(1-R)^2)}$$

$$\sin \Delta\varphi = \sqrt{\frac{\Delta}{1 + (4R(1-\Delta)/(1-R)^2)}}$$

$$\Delta\varphi = \sin^{-1} \sqrt{\frac{\Delta}{1 + (4R(1-\Delta)/(1-R)^2)}}$$

$$\varepsilon_{eq} = \frac{\lambda_0}{2\pi n_f} \sin^{-1} \sqrt{\frac{\Delta}{1 + (4R(1-\Delta)/(1-R)^2)}} \dots\dots\dots (32)$$

The thickness calculated by equation (32) is the equivalent thickness of the film which is slightly thicker than the actual film thickness. Moreover, a foam film consists of three homogenous layers, a core aqueous layer with the thickness of ε_w sandwiched by two surfactant monolayers with the thickness of ε_w . We assume a uniform thickness for the foam film and neglect the curvature in the corners (Figure 5). These three layers have different refractive indices (refractive index of surfactant monolayer is larger than that of solution). A surfactant monolayer itself consists of a head group with the refractive index of n_{pg} and a hydrocarbon chain with the refractive index of n_{hc} which in fact indicates that the film can be considered to have five layers. Therefore, equation (32) should be corrected to calculate the thickness of core aqueous layer. The following correction derived by Duyvis [14]:

$$\varepsilon = \varepsilon_{eq} - 2\varepsilon_{hc} \left(\frac{n_{hc}^2 - n_w^2}{n_w^2 - 1} \right) - 2\varepsilon_{pg} \left(\frac{n_{pg}^2 - n_w^2}{n_w^2 - 1} \right) \dots\dots\dots (33)$$

ϵ_{eq} is the equivalent thickness calculated by equation (32), ϵ_{hc} is the thickness of the hydrocarbon chain of the surfactant molecule and ϵ_{pg} is the thickness of head group of the surfactant molecule. Thus the thickness of the aqueous layer is calculated by:

$$\epsilon_w = \epsilon - 2\epsilon_m \dots\dots\dots (34)$$

Where $\epsilon_m = \epsilon_{hg} + \epsilon_{hc}$ is the thickness of a surfactant monolayer.

Equation (33) can be used to measure the thickness of very thin foam films in the range of few nanometers. The accuracy of these equations is reported to be less than $\pm 0.1\text{nm}$ [5,15].

IV. FIGURES

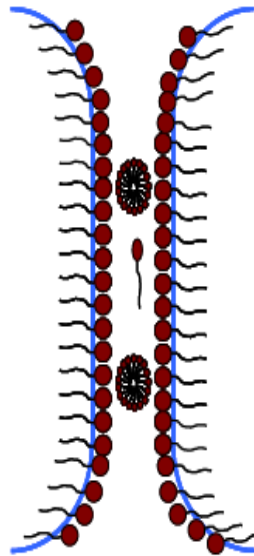


Figure 1 Schematic of a foam film (lamellae), sandwich model, an aqueous layer with adsorbed surfactant monolayers.

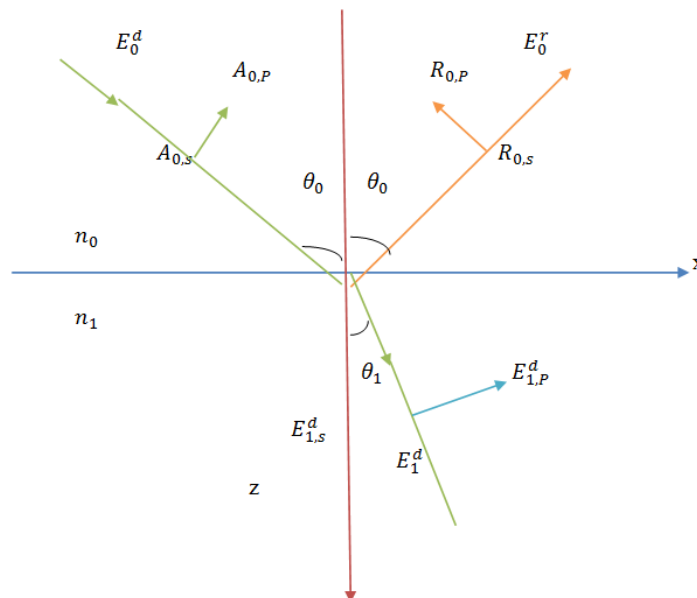


Figure 2 Reflection and refractive of light at plane boundary between two media.

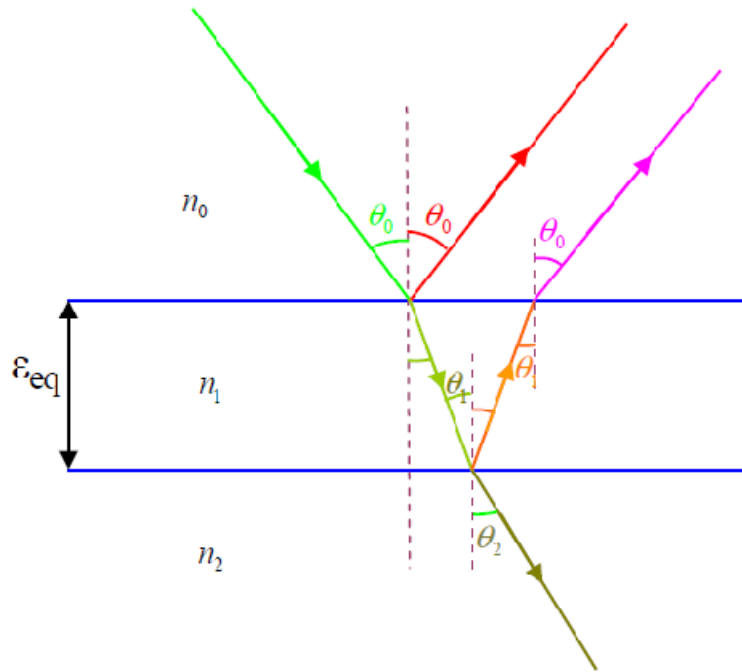


Figure 3 Reflection and refractive of light by one thin film.

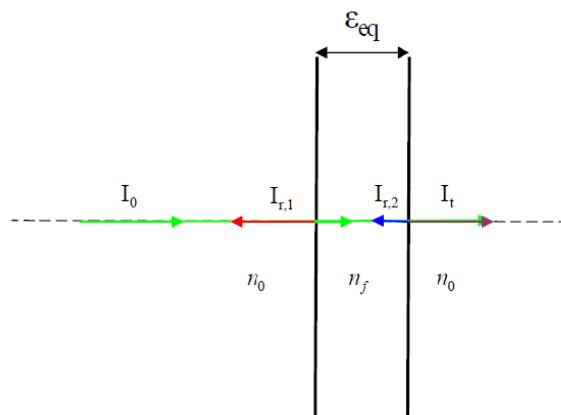


Figure 4 Schematic of a uniform liquid film.

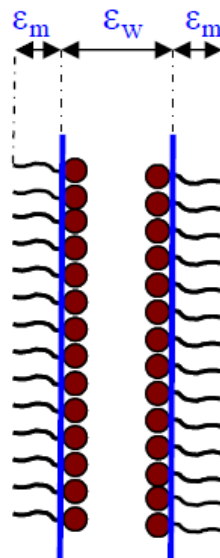


Figure 5 Schematic of foam without considering the Plateau border.

V. CONCLUSION

In this paper a method to measure the thickness of the thin foam films was reviewed and considering the structure of the film the related formulas were presented in some detail. First a formula was derived for the thin homogenous liquid film and then the derived equation was corrected for surfactant monolayers. The calculated thickness is very useful in investigating the stability of foam films and the study of interaction between adsorbed surfactant molecules.

Acknowledgements

I would like to appreciate Universiti Teknologi Malaysia for their continual support during the course of this paper. Special thanks go to my supervisor Prof. Dr. Ariffin Bin Samsuri for his support in the publication of this paper.

REFERENCES

- [1] Fendler, J. H. J. *Mater.* 1987, *Sci.*, 30, 323.
- [2] Moriizumi, T. *Thin Solid Films.* 1988, 160, 413.
- [3] Tieke, B. *Adv. Mater. (Weinheim, Ger.)* 1991, 3, 532.
- [4] Quoc P. Nguyen. *Dynamics of foam in porous media*, PhD dissertation, Delft University of Technology, The Netherlands. 2004.
- [5] A. Sheludko, J. *Adv. Coll. Inter.* 1967, *Sci*, Vol. 1, issue 4.
- [6] Princen, H.M., Overbeek J. Th. G., Mason, S.G., *J. Colloid Int. Sci.* 1967, 24, 125-130.
- [7] Quoc P. Nguyen, P.L.J. Zitha and P.K. Currie, *J. Colloid Int. Sci.* 2002, 248, 467-476.
- [8] R. Krustev, D. Platikanov and M. Nedyalkov. *Colloid Surf.* 1993, A., 79, 129.
- [9] R. Krustev, D. Platikanov and M. Nedyalkov. *Colloid Surf.* 1996, A., 123-124, 383.
- [10] R. Prud'homme and S. Kahn. *Foams*, 1996., New York: Marcel Dekker.
- [11] Stanely P. Frankel and Karol J. Mysels, *J. Applied Phys.* 1996, vol 37, 10.
- [12] A. Vasicek. *Optics of thin films*, Amsterdam : NHPC. 1960.
- [13] Lord Rayleigh. *Proc. Roy. Soc. London*, 1936, Ser. A, 156, 343.
- [14] E.M. Duyvis. *The equilibrium thickness of free liquid films*, PhD thesis, Utrecht University. 1962.
- [15] D. Exerowa and P.M. Kruglyakov. *Foams and Foam Films*, 1998. Elsevier, New York.

Investigation of Storage Potential of Different Biodiesel and Their Blends

Muhammad Amir Khan¹, Nitin Shrivastava²

^{1,2} Department of Mechanical Engineering, University Institute of Technology – RGPV, Bhopal

Abstract: As we know that biodiesel is easily influenced by oxidative attack and acidity is always a prime concern for their long term usage. To look over these difficulties we have to investigate their potential for storage purpose. For which we have to study the changes occurred in Acid number during a given set of time under thermal cyclic condition. We use diesel fuel and three biodiesel fuel blends (B100, B40, and B20) for this study. Amongst base fuel of three biodiesel, COME and JOME shows the major increase in Acid Number while the third biodiesel namely NOME shows least increase in Acid number. The Acid numbers of diesel and fuel blends are between (0.1-0.4) mg KOH.g⁻¹ under thermal cyclic condition throughout the period.

Keywords: Biodiesel, Storage potential, blends, Renewable energy, Acid number (AN).

I. INTRODUCTION

Worldwide the countries have been facing a power defect; the crisis is more critical among the developing nations. The world fuel reserves are decreasing rapidly day by day, due to which the demand of alternate source is arising from all parts of the world. Solution of long term energy problem will come only through research in the field of renewable energy resources [1]. The uses of renewable energy sources (vegetable oils, animal fats) instead of conventional energy sources have received much attention in recent past [2, 3]. The increased power demand, depleting fossil fuel resources and environmental pollution have led the world to think seriously for the alternate source of energy. The main reason behind to switch over these alternative resources are sustainability, renewability and pollution reduction. In India the energy generation is around 70% from fossil fuels i.e. coal, crude oil, natural gas etc in which oil is imported around of 80% of domestic consumption [4, 5, 6,].

To fulfill the gap between supply and demand renewable energy is a better alternative. Due to limited oil reserves in India we depend on substantial imports for fulfilling our present and future needs. The bulk demand of oil is from commercial transport sectors and in order to reduce the load from this section it is necessary to explore possibilities of developing substitute fuels like biomass (biodiesel). This led new employments and self dependency because fuel can be managed from local sources and thus provides rural development opportunities. The renewable energy resources are available worldwide, this encourages finding other possibilities in non conventional energy [7]. Also the environment has suffered a lot much destruction due to the haphazard use of these fossil reserves. In the path of this chase the innovation of using vegetable oil emerged in the last part of the 19th century. According to many researches vegetable oils can be used as an alternative fuel for diesel engines without any modification [8, 9].

Vegetable oil having common physical and chemical properties with diesel fuel but there are certain problem associated with this, namely higher viscosity, low volatility, high density and this will cause problem such as sticking of piston, carbon deposition and gumming. To protect engine from these difficulties direct usage of vegetable oil is avoided thus reduction in viscosity and improving fuel properties is our major concern. This could be happen by several ways such as emulsification, dilution of vegetable oil, transesterification and pyrolysis [10, 11].

From the above process transesterification is mostly preferred; in this process the vegetable oil is reacted with alcohol to form ester [17]. By this process biodiesel is formed which contains about 8-10% of oxygen, which led to the reduction in carbon monoxide, hydrocarbon and other emissions. Thus the oxygen content is main factor behind the emission control. Biodiesel having so many advantages over diesel fuel such as low sulphur content, fuel lubricity, environmental friendly, non toxic, higher biodegradability. Apart from this there are certain disadvantages also associated with it i.e. up to some extent oxides of nitrogen is increased, secondary slight decrease in brake power, torque while increment in fuel consumption as compared with petro diesel. Biodiesel can be prepared from different feedstock generally soyabean oil, cottonseed oil, rapeseed oil, jatropha oil, neem oil etc and they all show same result in performance parameters [12, 13].

Instead of that it is difficult to use B100 i.e. 100 percent biodiesel directly to the diesel engine because still viscosity, density and volatility are a matter of concern when compared with petro diesel. To overcome from this difficulty we use [14]. In this study we have to concentrate over the storage stability of biodiesel because biodiesel is very much prone to oxidation than diesel fuel. The storage stability is based on the changes occurred in acid number of the biodiesel over 6 months of period under thermal cyclic condition [15].

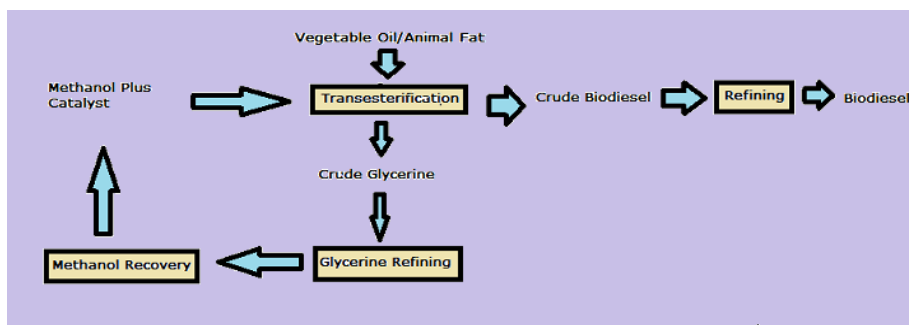


Figure 1: Biodiesel production via transesterification process.

II. EXPERIMENTAL METHODOLOGY

2.1 Production of fatty acid methyl ester

Production of biodiesel via transesterification process was carried out in a biodiesel reactor of 10 liters capacity, in which raw vegetable oil is heated to about 75°C. After this a mixture of methanol 35% and 0.75% of potassium hydroxide is added to the heated vegetable oil (10L) in the biodiesel reactor. After this mixture at a constant temperature was stirred for around 50 minutes, then we leave it for cooling following which separation of glycerol and ester takes place. The glycerol and fatty oil methyl ester were separated and taken in another vessel for further process. After separation by using heated distilled water washing process takes place which removes unreacted methanol and catalyst about three washing process is required, though some loss of ester takes place. After distillation process which was carried out at 65°C for removal of water content, then esterifies oil i.e. FAME (fatty acid meth ester) left to cool down.



Figure 2 Biodiesel Reactor

2.2 Fuel and Blends

Conventional diesel fuels was obtained from Indian oil and blended with biodiesel derived from cottonseed oil, jatropha oil, neem oil. The crude oil was obtained from local market and biodiesel is prepared by esterification process. The properties of diesel, biodiesels and its blend are carried at laboratory. Biodiesel and its blends with petro diesel were stored in a 500 ml bottles.

III. STORAGE CONDITION

The biodiesels and its blends were obtained in a partial oxidative surrounding in tightly kept bottles. Set of fuels were stored in room temperature over the time in thermal cyclic conditions (15°C to 40°C) over a period of six months from January to June. Test of samples was performed once per month at second week of every month.



Figure 3 B100 Test samples of COME, JOME and NOME biodiesel

3.1 Acid Number

For determination of AN of all fuels and their blends and to indicate relative change that occurred during storage a procedure (titration) is adopted. In this procedure a known amount of sample dissolved in organic solvent, is titrated with a solution of potassium hydroxide with known concentration and phenolphthalein as a color indicator. The acid number is used to quantify the amount of acid present, for biodiesel, It is the quantity of base, expressed in milligrams of potassium

hydroxide that is required to neutralize the acidic constituents in 1g of sample. For each AN determination approximately 25g of base fuel or blend was used.

IV. RESULT AND DISCUSSION

4.1 Properties of Fuel

The chemical properties of diesel, biodiesel and its blends were carried out in laboratory. The properties of diesel and biodiesel base fuel B100 shown in table:

Table 1 Fuel Properties of Diesel and COME, NOME, JOME.

Properties	Test method	Diesel	COME	NOME	JOME
Kinematic Viscosity@40°C,cst	D455	2.64	5.561	4.5	5.8
Density @15°C,kg/m ³	D128	835	880	873	893.2
Flash Point, °C	D94	56	190	165	167
Net Calorific Value, MJ/kg	D240	43.8	40.83	38.8	38.92
Water and Sediment % volume	D2709	0.01	0.015	0.018	0.02
Sulfur, % wt	D4294	0.30	0.003	0.004	0.01
Specific Gravity @ 15°C	D5355	0.85	0.889	0.83	0.92

The test fuel during this study are neat COME, JOME, Neem biodiesel (NOME) and its blends of 20% and 40% by volume with diesel fuel is used. Experiment was carried out over six months under thermal cyclic condition (15°C - 40°C).

4.2 Storage Stability

The test sample of COME, JOME, and Neem biodiesel (NOME) base fuels and its blends (B20) and (B40) were stored in 500 ml glass bottle under thermal cyclic condition for a period of about six months. After the close inspection of sample, we have obtained subsequent results as shown in figures.

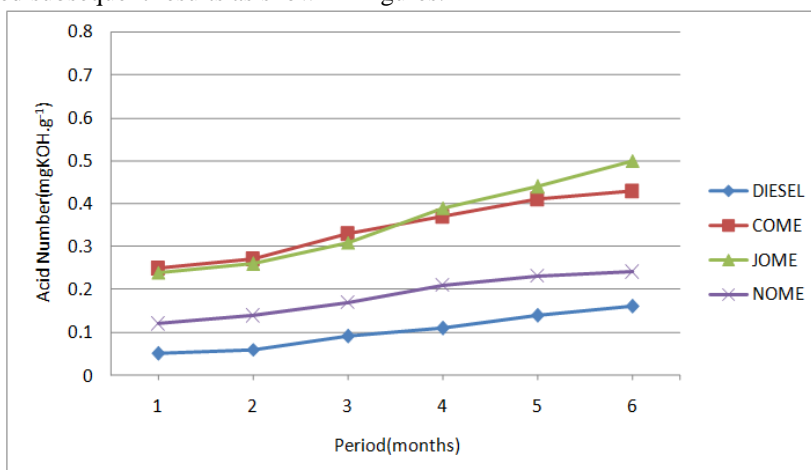


Figure 4 Acid number of all three biodiesel base fuels B100 of COME, JOME, NOME and Diesel as a function of storage duration (6 months) under thermal cyclic condition(15° to 40°C).

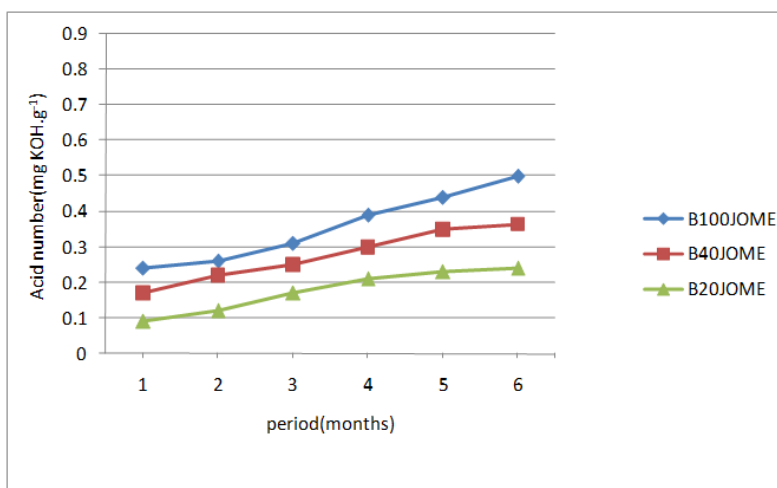


Figure 5 Acid number of JOME biodiesel base fuel B100 and its blends B40 and B20 with diesel as a function of storage duration (6 months) under thermal cyclic conditions (15° to 40°C).

In Fig. 4, the acid number is plotted over time (storage periods in months) for diesel and base fuel (B100) of all three biodiesel under thermal cyclic condition. The result presents that the acid number of JOME and COME shows larger increase in AN. While the third one NOME shows little increment i.e. below ($0.3 \text{ mg.KOH.g}^{-1}$). All fuels shows steady increment in AN. The acid number of diesel fuel was within the limit of the ASTM Standard. Among the three Biodiesel JOME debase more and touching the ASTM standard of $0.5 \text{ mg.KOH.g}^{-1}$. NOME biodiesel evidently a superior base fuel with lesser AN and remain stable for months. Initially, the acid number of COME and JOME is below 0.3 mgKOH.g^{-1} but as time proceeds we have observed that, there is an increase in acid number away from the limit because of elevated amount of free water and sediments, sulphated ash.

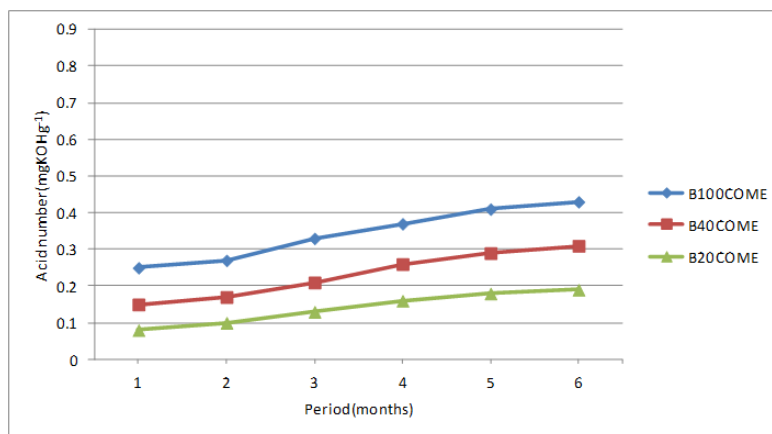


Figure 6 Acid number of COME biodiesel base fuel B100 and its blends B40 and B20 with diesel as a function of storage duration (6 months) under thermal cyclic conditions (15° to 40°C).

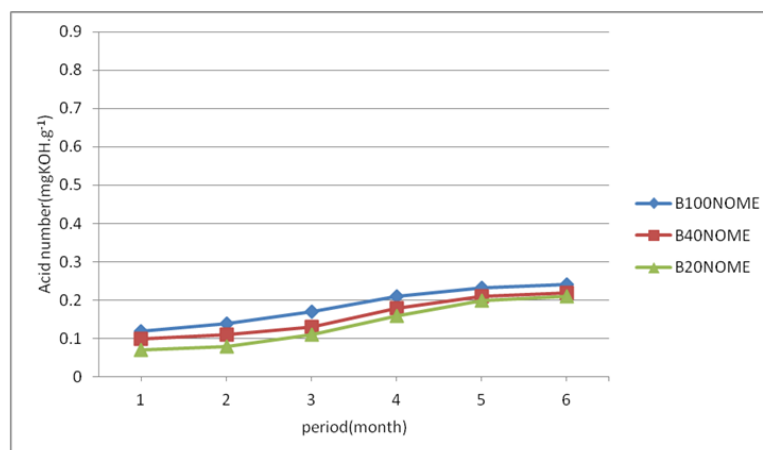


Figure 7 Acid number of NOME biodiesel base fuel B100 and its blends B40 and B20 with diesel as a function of storage duration (6 months) under thermal cyclic conditions (15° to 40°C).

This elucidates the larger increase in acid number over couple of months. In Fig 5-7 shows the graph between AN as a function of period (in months) under thermal cyclic condition of all the biodiesel blends (B40, B20) of JOME, COME, NOME respectively. Fascinatingly, the acid number of all fuel blends increased at a rate in contrast to diesel. While, that of base fuel has increased at a faster pace than the blends [16]. We have observed that there is an increase in acid number of (B40) blend within limits prescribed by ASTM as shown in the figure.

Acid number values started to go up steadily over the storage period. It is clear from the figure, that the acidity of any blend was decided by the acidity of (B100) base fuel mixed with diesel. The acid numbers of (B40) blend of JOME and COME biodiesel are less than or near to 0.4 mgKOH.g^{-1} during the storage period. While that of NOME biodiesel it is less than 0.3 mgKOH.g^{-1} . The acid number of (B20) blend of JOME, COME and NOME is below 0.2 mgKOH.g^{-1} or approaching to 0.2 mgKOH.g^{-1} . Consequently the outcome show that even (B100) with acid number close to $0.5\text{-}0.6 \text{ mgKOH.g}^{-1}$ can produce blend approaching to standard for storage all along time under deliberate situation.

V. CONCLUSION

Amongst all three biodiesel base fuel i.e. JOME, COME and NOME (B100) and its blends, the JOME and COME biodiesel showed the major increase in acid number during 6 months of storage at thermal cyclic situation while the third one i.e. NOME shows least increment of AN. The acid number for diesel fuel and all blends i.e. (B20) and (B40) stay in the range of 0.1mgKOH.g^{-1} to 0.4mgKOH.g^{-1} under thermal cyclic condition all through the storage period which is adequately lower than the ASTM standard 6751 limit i.e. 0.5mgKOH.g^{-1} . All blends illustrate a lesser raise in acid number than of base

fuel. Consequently, the larger stability of blends over biodiesel base fuel was shown. Among all three biodiesel the NOME shows greater stability.

REFERENCES

- [1] Ekrem Buyukkaya. Effect of biodiesel on a DI diesel engine performance, emission and combustion characteristics. *Fuel*.2010,89(10), 3099-3105.
- [2] Chen X, Du W and Liu D. Response surface optimization of biocatalytic biodiesel production with acid oil. *Biochemical Engineering*.2008, 40(3), 423-429.
- [3] A.S. Ramadhas, C. Muraleedharan, S. Jayaraj. Performance and emission evaluation of a diesel engine fueled with methyl esters of rubber seed oil, 2005, 30(12), 1789-1800.
- [4] Altin R, Cetinkaya S and Yucesu H S. The potential of using vegetable oil fuels as fuels for diesel engines. *Energy Conversion Management*, 2001, 42, 529-538.
- [5] M Martin, D Prithviraj. Performance of pre-heated cottonseed oil and diesel fuel blends in a compression ignition engine. *Jordon Journal of Mechanical and Industrial Engineering*, 2011, 5(3), 235-240.
- [6] Agarwal A, Rajamanoharan k. Performance and emission of karanja oil and its blends in a single cylinder agricultural diesel engine. *Applied Energy*.2009,86, 106-112.
- [7] F. Karaosmanoglu. Vegetable oil fuels: a review, *Energy source* 21.1999, 221-231.
- [8] A S Ramadhas, S. Jayaraj, C. Murleedharan. Use of vegetable oil as I.C engine fuels: a review. *Renewable Energy*. 2004, 29(5),727-742.
- [9] Nitin Shrivastava, S. N. Varma & Mukesh Pandey, Experimental investigation of diesel engine using EGR and fuelled with Karanja oil methyl ester, *International Journal of Sustainable Engineering*, 2012, DOI:10.1080/19397038.2012.749310.
- [10] Kalligeros S., Zannikos F., Stournas S., Lois E., Anastopoulos G., Teas Ch., et al. An investigation of using biodiesel/marine diesel blends on the performance of a stationary diesel engine. *Biomass Bioenergy*. 2003,24,41-49.
- [11] Y.D. Wang, An experimental investigation of the performance and gaseous exhaust emissions of a diesel engine using blends of a vegetable oil. *Applied Thermal Engineering*.2006, 26(14-15), 1684-1691.
- [12] D Agarwal, S.K. Singh, A.K. Agarwal. Effect of Exhaust Gas Recirculation (EGR) on performance, emission, deposits and durability of a constant speed compression ignition engine. *Applied Energy*.2011, 88, 2900-2907.
- [13] M. Nurannabi, M.S. Akhter, M.M.Z Shahadat, Improvement of engine emission with conventional diesel fuel and diesel-biodiesel blends. *Bioresource Technology*.2006, 97(3), 372-378.
- [14] Nabi N, Rehman M and Akhter S, Biodiesel from cotton seed oil and its effect on engine performance and exhaust emissions.2009, 29, 2265-2270.
- [15] Leenus Jesu Martin.M, Edwin Geo. V, Prithviraj.D. Effect of diesel addition on the performance of cottonseed oil fuelled DI diesel engine.2011, 2(2), 321-330.
- [16] M Farhani, M.P.Turingia, B.D.Tucker and D.J.Y.S.Page. Storage stability of biodiesel and ultralow sulfur diesel fuel blends. *Journal of Energy Resource Technology*.2009,131(4), 041801-6.
- [17] Murat Karabektas, Gokhan Egen, Murat Hosoz. The effect of preheated cottonseed oil methyl ester on the performance and exhaust emissions of a diesel engine. *Applied Thermal Engineering*.2008, 28, 2136-2143.

An Application of Pareto Analysis and Cause-Effect Diagram for Minimizing Defect Percentage in Sewing Section of a Garment Factory in Bangladesh

Tanvir Ahmed¹, Raj Narayan Acharjee¹, MD.Abdur Rahim², Noman Sikder³,
Taslima Akther³, Mohd. Rifat Khan³, MD.Fazle Rabbi³, Anup Saha³

^{1,3} Dept. of Industrial and Production Engineering, Shahjalal University of Science and Technology, Bangladesh

²Dept. of Industrial and Production Engineering, Bangladesh University of Engineering and Technology, Bangladesh

Abstract: As Readymade Garments sector is a large industrial sector in Bangladesh, quality improvement can play a vital role for improving productivity as well as economic development for the country. This paper represents a detail investigation on quality improvement of a garment factory by applying Pareto Analysis and Cause-Effect Diagram. The aim of this study is to minimize defects that will reduce rework and rejection rate. Our studied organization is "Rainbow Apparel Limited". In this organization we worked in a particular section (i.e. sewing section) for a particular product (i.e. woven pants). Four months defect data has been collected from the management and Pareto Analysis is performed on them. From this analysis 6 top defect positions are identified where 78.56% defects occur. On those top positions further Pareto Analysis is performed to identify the top defect types. That resulted in total 115 concerning areas where 71.40% defects occur, which should be the major concerning areas to reduce defect percentage. So hierarchies of causes for individual defect types are organized and Cause-Effect Diagrams are constructed for those defect types. Then relative suggestions to those causes are also provided. In the end necessary clues and recommendations have been added for the advancement of the study.

Keywords: Defects, Parito Analysis, Root Cause, Parito Analysis, Quality

I. Introduction

The garment industry has played a pioneering role in the development of industrial sector of Bangladesh. Though it started in late 1970s but it soon established its reputation in the world market within a short span of time. Resultantly garment is now one of the main export items of the country. It accounts for 78% of country's export earnings and contributes more than 10% to Gross Domestic Product (GDP). Besides enriching the country's economy it has played a very important role in alleviating unemployment. With 5,000 factories employing about 3.6 million workers (80% of them women), Bangladesh is clearly ahead of other Southeast Asian suppliers in terms of capacity of the Readymade Garments industry. Around 20 million people are directly and indirectly depending on this sector for their immediate livelihoods.

The export-quota system and the availability of cheap labor are the two main reasons behind the success of the industry. In the 1980s, the Readymade Garments industry of Bangladesh was concentrated mainly in manufacturing and exporting woven products. Since the early 1990s, the knit section of the industry has started to expand. Shirts, T-shirts, trousers, sweaters and jackets are the main products manufactured and exported by the industry. The phase-out of the export-quota system from the beginning of 2005 has raised the competitiveness issue of the Bangladesh Readymade Garments industry as a top priority topic.

As the global economic condition changing in a rapid motion, generally in an industry more focus is given on profit margin, customer demand for high quality product and improved productivity. In garment manufacturing, it is usual to see a lot of rejected garments after shipment. These non-repairable defects may occur due to low quality raw materials or faulty process or employee casual behavior. In the contemporary world of manufacturing, due to high competitive nature of the market, different companies have started to look for different approaches and practices to reduce the defect percentage. Pareto Analysis helps to identify different defects and classify them according to their significance. These defects often lead to the rejection of raw materials. To determine possible root causes of rejection, Cause-Effect Diagram is also a very useful tool. It helps to identify, sort, and display causes of a specific problem or quality characteristic. It graphically illustrates the relationship between a given outcome and all the factors that influence the outcome and hence to identify the possible root causes.

In this paper, sewing section of a garment factory is studied where pants are produced in five production lines. In this study Pareto chart and Cause-Effect Diagram have been used with an objective to identify and classify the reasons that are responsible for various defects in the production lines.

II. Background Of The Study

At present the success of the Readymade Garments sector highly depends on several factors such as manufacturing lead time, quality of product, production cost etc. These factors are hampered due to various defects in the products. These defects can be repairable that leads to rework or non-repairable that leads to rejection. Rework in the garments industry is a common work that hampers the smooth production rate and focus poor quality products having an impact on overall factory economy. Minimization of reworks is a must in quality and productivity improvement. Rework is a vital issue for poor quality product and low production rate. Reworks are the non-productive activities focusing on any activity that customer are not willing to pay for. Non-productive activities describe that the customer does not consider as adding value to his product.

By reacting quicker in minimization of reworks to make a product as per customer demand with expected quality, the company can invest less money and more costs savings. Whereas rejection causes waste and decreases resource efficiency.

In this context Readymade Garments sector is selected for research work. The selected garment factory consists of several departments such as cutting, sewing, finishing, packing etc. Among these departments the sewing section is selected. This study tried to extract the common scenario of Readymade Garments sector of Bangladesh by depicting the existing condition of sewing section.

III. Methodology

This study contains use of quality tools to minimize defects and rework on garment industry. It includes the theoretical ideas about various defects, various quality tools specially Pareto Analysis and Cause-Effect diagram. The case study research conducted on the selected garment factory "Rainbow Apparel Limited". This segment includes the understanding about the quality control system of the selected factory and how this could be improved. The conceptual development includes the generation of ideas for minimizing defects by identifying major concerning areas and by providing respective suggestions. Finally, the last segment contains the comparative theoretical and mathematical evaluation about the quality control system. Steps involved in the study

Step 1: Factory Selection

After gathering information we made contact with some garment factories and tried to select a newly established factory where we can place or utilize our knowledge to make some contribution for the development of the factory. Thus we have selected a particular garment factory in Haliashahar, Chittagong.

Step 2: Conducting of Case Study

Finally we conduct our research work in a particular garment factory named "Rainbow Apparel Limited" established in 2006 which situates in Haliashahar, Chittagong. The demography of the situated organization is presented in Table 1.

Table 1. Demography of "Rainbow Apparel Limited"

Company Name	Rainbow Apparel Limited
Location	Haliashahar college road, Chittagong
Established	2006
Product type	Woven shirt, Woven pant
Number of production line	5
Total worker	250
Production capacity per day	3000 PCS
Working hour per day	10 Hours (maximum)
Buyers	Long Street (USA), Target (USA)

Step 3: Gather Information

In this step we have gathered information on the Quality Control system of the sewing section of the selected garment factory. Here we have collected data of various defects from the sewing section provided by the management which is used for the Analysis purpose of the study.

Step 5: Identify the Problem

Identification of the major concerning areas to minimize the defects was next step. According to the observation and using management data we have seen some repetitive defects occur in the sewing section. So we tried to do our research work on this section which is our major concern.

Step 6: Analysis and Suggestions

In this step Pareto Analysis is performed which is required to identify major concerning areas. After that Cause-Effect Diagrams have been constructed for top defect types. Then we have provided some respective suggestions to minimize the frequency of those defects.

IV. Findings And Data Analysis

In the previous section we have discussed about the research work of some repetitive defects exist in the sewing section of a particular product i.e. woven pant. From our own observation and data given by the management level we saw that there are different types of defects occurred in the production lines. These defects cause reworks and rejection which leads to time waste and decrease in productivity. By concentrating on those few repetitive defects in particular positions, most of the defects can be minimized. So with this respect, we have tried to identify those particular defects and positions using Pareto Analysis. Then we have analyzed the causes of those defects and constructed Cause-Effect diagrams. And finally we have provided some suggestions in relation to those causes that will ultimately reduce those defects.

4.1 Overview of Production Line

We performed our research work in a particular garment factory named “Rainbow Apparel Limited” established in 2006 and situated in Haliashahar, Chittagong. There we conduct our research in a particular section (i.e. sewing section) for the woven pant. There are 5 production lines in this section. Here we have seen three types of quality checkpoints in each production line. These are called (1) In-line or process QC table, (2) End line QC table and (3) Finishing QC table. These checkpoints check the products for defects and if found then the defect type and defect position are identified and listed in the check sheet. An overview of the existing layout of a single production line is shown in figure 1.

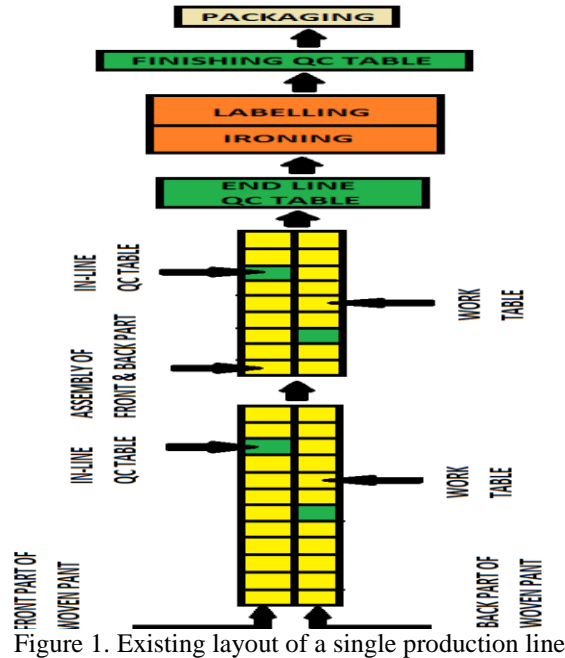


Figure 1. Existing layout of a single production line

4.2 Data Collection

For our research work we have collected four months defect data from management months starting from October 2012 to January 2013. The data has been taken from five production lines of sewing section during the production of woven pant. In the case of woven pant production 50 defect positions are identified where 25 types of defects occur. Among the defect types Uncut Thread for all positions are counted together for 50 positions. Similarly two other defect types, Spot and Oil Mark are also counted together. Number of defects of all the production lines are listed on the Check Sheet by QC supervisors if found any. In our visited factory various defect types of sewing section are expressed by some specific defect codes. The defect types with their corresponding codes are presented in table 2. and sample of a check Sheet is shown in figure 2. Then four months combined defect data is presented in table 3.

Quality Inspection-100% (Sewing)

Style No.	Order No.		QC Name:				Line No.		Date:	
	8.00-9.00	9.00-10.00	10.00-11.00	11.00-12.00	12.00-1.00	2.00-3.00	3.00-4.00	4.00-5.00	5.00-6.00	6.00-7.00
No. of Pieces Checked										
Total Defects										
Hourly DHU										
Supervisor										
Line Quality Head										
Operations ↓	Defect Codes									
TOTAL										

Figure 2. Sample of a Check Sheet

Table 2. Defect types with their corresponding codes

SL No.	DEFECT TYPE	DEFECT CODES
1	Skipped Stitch	A
2	Broken Stitch	B
3	Loose Tension	C
4	Uneven Stitch	D
5	Run Off Stitch	E
6	Slanted	F
7	High/Low	G
8	Puckering	H
9	Crooked	I
10	Out of Shape	J

11	Raw Edge	K
12	Position	L
13	Pullness	M
14	Uncut Thread	N
15	Overlap	O
16	Incomplete	P
17	Visible Joint	Q
18	Wrong SPI	R
19	Spot	S
20	Oil Mark	T
21	Twisting	U
22	Label Mistake	V
23	Visible Top Stitch	W
24	Color Shading	X
25	Needle Mark	Y

Table 3. Four months combined defect data for woven pant

Defect Types →	A	B	C	D	E	F	G	H	I	J	K	L	M	N	O	P	Q	R	S	T	U	V	W	X	Y	Total	
Defect Position ↓																											
Uncut Thread for All Position	0	0	0	0	0	0	0	0	0	0	0	0	0	0	0	0	0	0	0	0	0	0	0	0	0	0	8988
Spot for All Position	0	0	0	0	0	0	0	0	0	0	0	0	0	0	0	0	0	0	0	0	0	0	0	0	0	0	7845
Waist Belt	231	976	46	538	154	4	7	134	161	88	765	5	30	0	72	40	14	5	0	0	123	42	987	0	0	4422	
Bottom Hem	942	980	95	1043	76	93	72	45	86	18	58	8	12	0	6	66	87	31	0	0	80	1	5	1	0	3805	
Side Seam	783	537	26	62	59	22	43	62	72	18	596	6	12	0	2	31	0	4	0	0	4	0	35	0	12	2386	
Waist Belt Top Stitch	313	798	36	245	77	7	5	96	22	36	65	13	26	0	61	11	11	2	0	0	12	1	490	0	0	2327	
Loop	38	15	2	30	0	389	2	0	56	0	3	11	189	0	0	76	0	0	0	0	0	0	0	0	0	811	
Front / Back Rise	211	134	32	23	58	16	15	10	31	16	43	3	31	0	2	21	4	32	0	0	1	0	0	0	0	683	
In Seam	126	112	8	26	9	2	0	45	31	5	173	2	4	0	4	23	0	8	0	0	2	6	0	0	0	586	
Back Pocket	66	198	13	53	23	2	4	10	108	0	55	0	1	0	31	6	1	1	0	0	0	0	0	0	0	572	
Mouth Close	3	29	1	25	14	132	321	6	7	3	3	4	4	0	0	9	0	7	0	0	0	0	2	0	0	570	
Front Pocket	93	136	13	26	15	1	57	3	114	0	43	5	29	0	1	14	0	0	0	0	3	0	0	4	0	557	
Oil Mark for All Position	0	0	0	0	0	0	0	0	0	0	0	0	0	0	0	0	0	0	0	0	0	0	0	0	0	432	
Loop Joint	2	10	0	2	0	342	19	0	2	0	0	12	0	0	10	0	0	0	0	0	0	1	0	0	0	400	
Bartack	6	5	2	0	0	23	10	0	51	0	2	0	144	0	3	132	0	0	0	0	2	3	0	0	0	383	
Label Joint	11	50	0	1	6	50	0	2	45	0	11	1	15	0	8	22	0	2	0	0	0	124	0	0	5	353	
Front Part	81	127	4	10	8	0	14	2	20	3	33	0	4	0	16	8	0	0	0	0	2	0	0	7	0	339	
Loop Tack	2	35	0	0	3	214	2	4	1	0	33	5	4	0	4	2	0	3	0	0	0	0	0	0	0	312	
Back Part	101	102	2	10	12	0	2	3	11	0	31	0	6	0	19	0	1	0	0	0	0	0	0	0	0	300	
Label	2	42	0	6	3	5	4	0	14	0	1	5	2	0	0	31	0	0	0	0	0	97	0	0	0	212	
Loop Bartack	0	2	0	0	0	123	32	0	0	3	0	0	2	0	0	11	0	0	0	0	0	0	0	0	0	173	
Front Pocket Bartack	4	8	0	0	0	40	45	3	4	0	2	2	24	0	0	0	0	0	0	0	0	0	0	0	0	132	
JStitch	7	41	1	0	0	0	0	0	2	0	0	0	0	0	4	3	0	0	0	0	0	0	0	72	0	130	
Back Dart	35	28	0	6	1	1	1	0	13	2	12	10	0	0	0	8	0	0	0	0	0	1	1	1	0	120	
Zipper joint	0	15	0	0	1	0	0	74	3	0	0	0	0	0	0	0	0	0	0	0	0	0	0	0	0	93	
Mouth Tack	1	1	0	4	0	57	26	0	0	0	0	0	0	0	1	2	0	0	0	0	0	0	0	0	0	92	
Zipper Fly	3	32	0	21	0	0	0	0	28	0	0	0	0	0	0	7	0	0	0	0	0	0	0	0	0	91	

Table 3(continued). Four months combined defect data for woven pant

Defect Types →	A	B	C	D	E	F	G	H	I	J	K	L	M	N	O	P	Q	R	S	T	U	V	W	X	Y	Total	
Defect Position ↓																											
Fly Top Stitch	27	15	3	13	0	0	0	10	0	0	0	0	0	0	2	0	0	0	0	0	0	0	0	4	0	74	
Loop Sadel Stitch	69	0	0	0	0	0	0	0	0	0	0	0	0	0	0	0	0	0	0	0	0	0	0	0	0	69	
Front Dart	57	4	0	0	0	0	0	0	0	0	0	0	0	0	0	1	0	0	0	0	0	0	0	0	0	62	
Pocket Bartack	0	0	0	0	0	20	0	0	0	0	0	0	9	0	33	0	0	0	0	0	0	0	0	0	0	62	
Side Slit	9	21	0	2	0	0	23	0	0	0	2	0	0	0	0	0	0	0	0	0	0	0	0	0	0	57	
WaistBelt Tack	0	0	0	0	0	0	0	1	0	0	0	29	0	0	0	0	0	0	0	0	0	0	18	0	0	48	
Sadel Stitch	19	17	0	0	0	0	0	0	8	0	0	0	0	0	0	0	0	0	0	0	0	0	0	0	0	44	
Back Pocket Sadel Stitch	15	9	0	0	0	3	0	0	1	0	0	13	0	0	0	0	0	0	0	0	0	0	0	0	0	41	
Waist Belt Joint	0	16	1	3	1	0	3	5	0	0	0	0	0	0	0	0	0	0	0	0	2	0	9	0	0	40	
Front Panel	32	1	0	0	0	0	2	0	0	0	0	0	0	0	2	0	0	0	0	0	0	0	0	0	0	37	
Slit at Back Bottom	0	4	0	0	0	0	0	4	12	0	0	12	0	0	1	0	0	0	0	0	0	0	0	0	0	33	
Front / Back Pocket	1	10	0	1	3	3	3	1	0	0	4	0	2	0	0	0	0	0	0	0	0	0	0	0	0	28	
Back Yoke	10	10	0	0	0	0	0	0	2	0	0	0	0	0	0	0	0	0	0	0	0	0	0	0	0	22	
Mouth	0	0	0	0	0	3	13	0	6	0	0	0	0	0	0	0	0	0	0	0	0	0	0	0	0	22	
Pocket	2	7	0	2	0	1	0	0	5	0	1	0	0	0	3	0	0	0	0	0	0	0	0	0	0	21	
Dart Sadel Stitch	9	11	0	0	0	0	0	0	0	0	0	0	0	0	0	0	0	0	0	0	0	0	0	0	0	20	
Button	0	0	0	0	0	0	0	1	0	0	2	4	0	5	6	0	0	0	0	0	0	0	0	0	0	18	
Front Pocket Sadel Stitch	15	2	0	0	0	0	0	0	0	0	0	0	0	0	0	0	0	0	0	0	0	0	0	0	0	17	
Back Pocket Flap	0	0	0	0	0	8	0	0	0	7	0	0	0	0	0	0	0	0	0	0	0	0	0	0	0	15	
Reject	0	0	0	0	0	0	0	0	0	0	0	0	0	0	0	0	0	0	0	0	0	0	2	12	14	14	
Mending	0	0	0	0	0	0	0	0	0	0	0	0	0	0	0	0	0	0	0	0	0	0	0	0	9	9	
Blind Stitch	1	7	0	1	0	0	0	0	0	0	0	0	0	0	0	0	0	0	0	0	0	0	0	0	0	9	
Back Pocket Overlock	0	4	0	0	0	0	0	0	0	0	4	0	0	0	0	0	0	0	0	0	0	0	0	0	0	8	
Hook & Bar	0	0	0	0	0	7	0	0	0	0	0	0	0	0	0	0	0	0	0	0	0	0	0	0	0	7	
Front Part Overlock	0	4	0	0	0	0	0	0	0	0	0	0	0	0	0	0	0	0	0	0	0	0	0	0	0	4	
WaistBelt Shape	0	0	0	0	0	0	0	0	0	2	0	0	0	0	0	0	0	0	0	0	0	0	0	0	0	2	
Total	3327	4555	285	2153	523	1560	733	519	918	194	1947	94	608	8988	274	545	119	95	7845	432	231	278	1621	15	38	37897	

Table 3. Shows four months combined defect data where green cells represent defect types and red cells represent defect positions. Here total amount of defects for Uncut Thread are counted together for 50 positions and put in a single cell marked by yellow color. For Spot and Oil Mark similar work have been done.

4.3 Pareto Analysis

We have performed our Pareto Analysis based on four months combined defect data of 5 production lines from the sewing section for woven pants. From this analysis we can identify the “Vital few” areas where maximum defects occur. The analysis is shown in figure 3. Here horizontal axis represents defect positions, vertical axis at left side represents defect amount and vertical axis at right side represents defect percentage. The defect positions with their respective defect amounts have been represented by the blue colored bars. The cumulative percentage and 80% line are represented respectively by red and green color. After the analysis top defect position bars are replaced with yellow color.

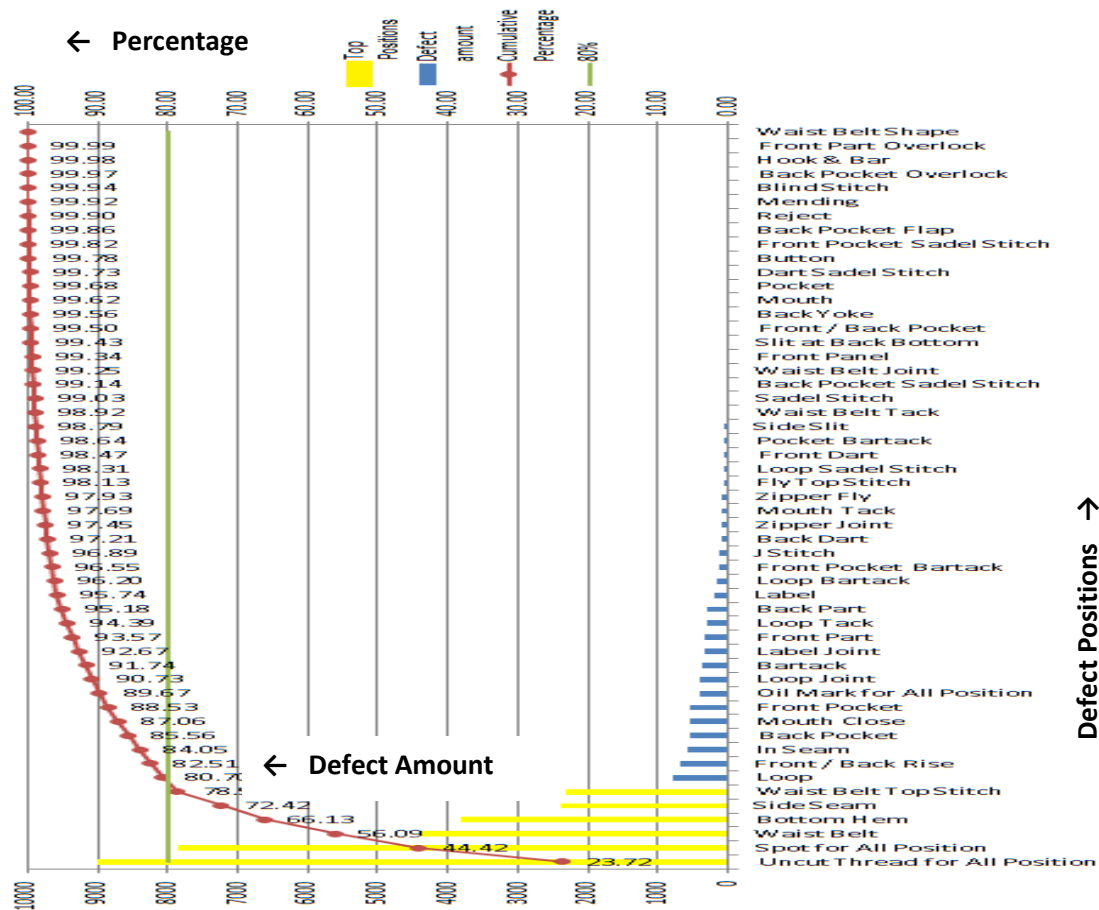


Figure 3. Pareto Analysis for top defect positions

4.3.1 Observations from Pareto Analysis for Top Defect Positions

1. Uncut Thread is the most frequent defect with as much as 23.72% of the total.
2. Spot is the second most frequent defect with 20.70% of the total.
3. Among other defects contribution of Waist Belt is 11.67%, Bottom Hem is 10.04%, Side Seam is 6.30% and Waist Belt Top Stitch is 6.14%.
4. These six top defect positions are the “vital few” where 78.56% of total defects occur.
5. We need to perform further Pareto Analysis on those top defect positions to identify the vital few defect types that are responsible for maximum amount of defect.

4.3.2 Further Pareto Analysis for Top Defect Types

As Uncut Thread and Spot are individually defect types as well as defect positions, there is no need of further analysis for identifying top defect types in those two positions. So we have performed further Pareto Analysis for Waist Belt, Bottom Hem, Side Seam and Waist Belt Top Stitch. From these analysis we have identified “vital few” defect types for each positions.

Pareto Analysis for Waist Belt: Pareto Analysis for Waist Belt for is shown in figure 4.

Table 4. Waist Belt defect data

Waist Belt		
Defect Types	Defect Codes	Defect Amount
Visible Top Stitch	W	987
Broken Stitch	B	976
Raw Edge	K	765
Uneven Stitch	D	538
Skipped Stitch	A	231
Crooked	I	161
Run Off Stitch	E	154
Puckering	H	134
Twisting	U	123
Out of Shape	J	88
Overlap	O	72
Loose Tension	C	46
Label mistake	V	42
Incomplete	P	40
Pullness	M	30
Visible Joint	Q	14
High/Low	G	7
Position	L	5
Wrong SPI	R	5
Slanted	F	4
TOTAL		4422

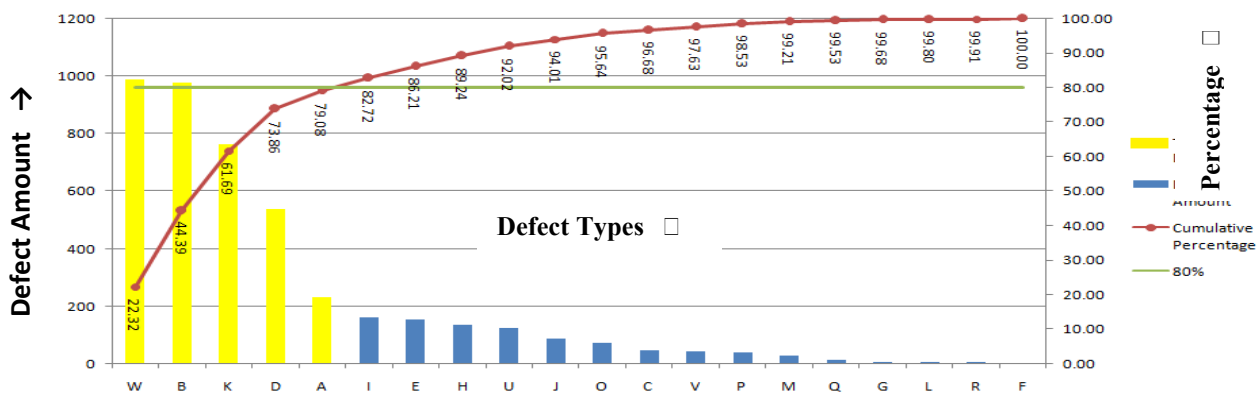


Figure 4. Pareto Analysis for Waist Belt

Observations from the Analysis:

- Visible Top Stitch (W) is the most frequent defect type with 22.32% of total Waist Belt defect.
- Among other defect types contribution of Broken Stitch (B) is 22.07%, Raw Edge (K) is 17.30%, Uneven Stitch (D) is 12.17% and Skipped Stitch (A) is 5.22%.
- So these five defect types are responsible for 79.08% of total Waist Belt defects.
- Pareto Analysis for Bottom Hem: Pareto Analysis for Bottom Hem for is shown in figure 5.

Table 5. Bottom Hem defect data

Bottom Hem		
Defect Types	Defect Codes	Defect Amount
Uneven Stitch	D	1043
Broken Stitch	B	980
Skipped Stitch	A	942
Loose Tension	C	95
Slanted	F	93
Visible joint	Q	87
Crooked	I	86
Twisting	U	80

Run Off Stitch	E	76
High/Low	G	72
Incomplete	P	66
Raw Edge	K	58
Puckering	H	45
Wrong SPI	R	31
Out of Shape	J	18
Pullness	M	12
Position	L	8
Overlap	O	6
Visible Top stitch	W	5
Label Mistake	V	1
Color Shading	X	1
TOTAL		3805

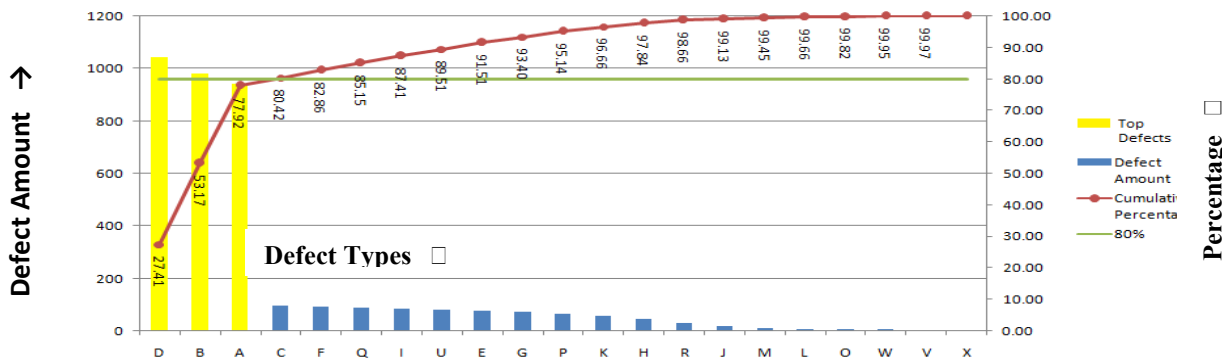


Figure 5. Pareto Analysis for Bottom Hem

Observations from the Analysis:

- Uneven Stitch (D) is the most frequent defect type with 27.41% of total Bottom Hem defect.
- Among other defect types contribution of Broken Stitch (B) is 25.76% and Skipped Stitch (A) is 24.76%.
- So these three defect types are responsible for 77.92% of total Bottom Hem defects.
- **Pareto Analysis for Side Seam:** Pareto Analysis for Side Seam for is shown in figure 6.

Table 6. Side Seam defect data

Side Seam		
Defect Types	Defect Codes	Defect Amount
Skipped Stitch	A	783
Raw Edge	K	596
Broken Stitch	B	537
Crooked	I	72
Uneven Stitch	D	62
Puckering	H	62
Run Off Stitch	E	59
High/Low	G	43
Visible Top Stitch	W	35
Incomplete	P	31
Loose Tension	C	26
Slanted	F	22
Out of Shape	J	18
Pullness	M	12
Needle Mark	Y	12
Position	L	6

Wrong SPI	R	4
Twisting	U	4
Overlap	O	2
TOTAL		2386

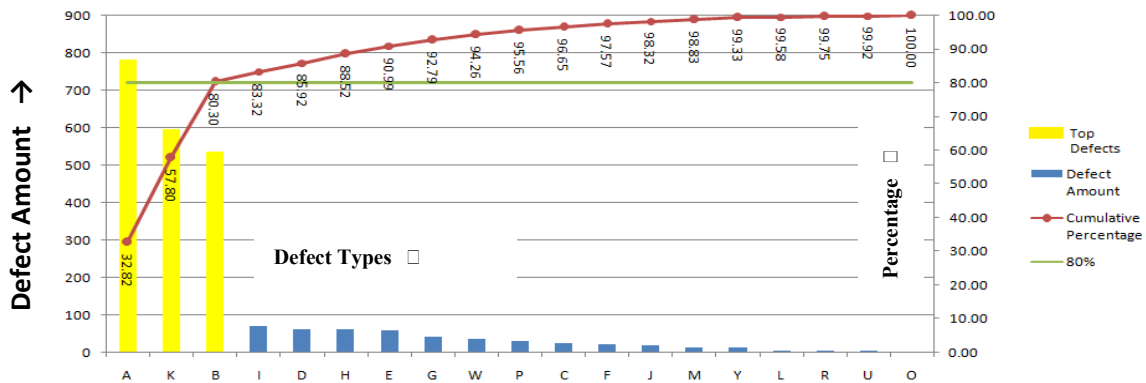


Figure 6. Pareto Analysis for Side Seam

Observations from the Analysis:

- Skipped Stitch (A) is the most frequent defect type with 32.82% of total Side Seam defect.
- Among other defect types contribution of Raw Edge (K) is 24.98%, Broken Stitch (B) is 22.51%
- So these three defect types are responsible for 80.30% of total Side Seam defects.
- **Pareto Analysis for Waist Belt Top Stitch:** Pareto Analysis for Waist Belt Top Stitch for is shown in figure 7.

Table 7. Waist Belt Top Stitch defect data

Waist Belt Top Stitch		
Defect Types	Defect Codes	Defect Amount
Broken Stitch	B	798
Visible Top Stitch	W	490
Skipped Stitch	A	313
Uneven Stitch	D	245
Puckering	H	96
Run Off Stitch	E	77
Raw Edge	K	65
Overlap	O	61
Loose Tension	C	36
Out of shape	J	36
Pullness	M	26
Crooked	I	22
Position	L	13
Twisting	U	12
Incomplete	P	11
Visible Joint	Q	11
Slanted	F	7
High/Low	G	5
Wrong SPI	R	2
Label Mistake	V	1
TOTAL		2327

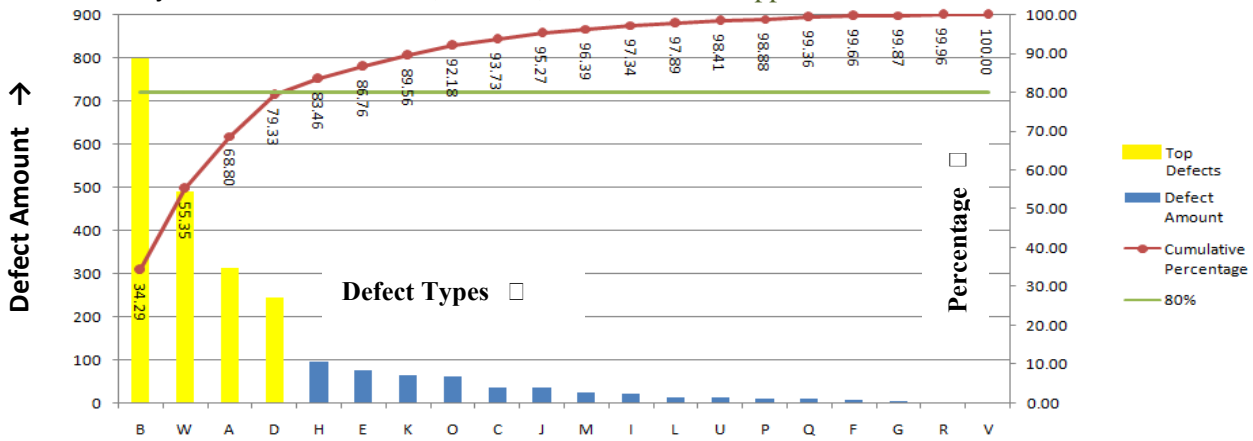


Figure 7. Pareto Analysis for Waist Belt Top Stitch

Observations from the Analysis:

Broken Stitch (B) is the most frequent defect type with 34.29% of total Waist Belt Top Stitch defect. Among other defect types contribution of Visible Top Stitch (W) is 21.06%, Skipped Stitch (A) is 13.45% and Uneven Stitch (D) is 10.53%. So these four defect types are responsible for 79.33% of total Waist Belt Top Stitch defects.

Major Concerning Areas at a Glance:

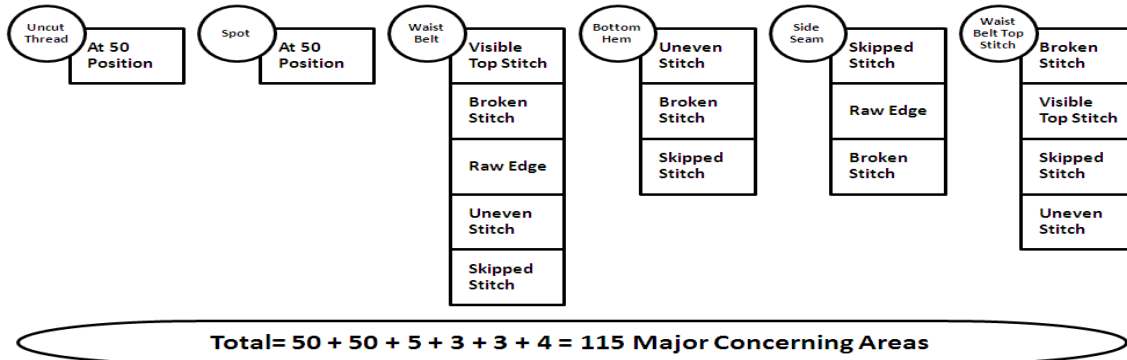


Figure 8. Major Concerning Areas at a Glance

4.4 Result of the Pareto Analysis

After Pareto Analysis it is found that total seven types of defect in the identified top defect positions are responsible for maximum amount of defects. The defect types and the corresponding positions with their respective defect amount are shown in table 8.

Table 8. Total Amount of Defects in Major Concerning Areas

MAJOR CONCERNING AREAS		Defect amount
Defect Types	Defect Positions	
Uncut Thread (N)	At 50 positions	8988
Spot (S)	At 50 positions	7845
Skipped Stitch (A)	Waist Belt	231
	Bottom Hem	942
	Waist Belt Top Stitch	313
	Side Seam	783
Broken Stitch (B)	Waist Belt	976
	Bottom Hem	980
	Waist Belt Top Stitch	798
	Side Seam	537
Uneven Stitch (D)	Waist Belt	538
	Bottom Hem	1043
	Waist Belt Top Stitch	245

Raw Edge (K)	Waist Belt	765
	Side Seam	596
Visible Top Stitch (W)	Waist Belt	987
	Waist Belt Top Stitch	490
Total amount		27057

Total number of defects = **37897**
 Total number of defects in major concerning area = **27057**
 Percentage of defects in major concerning area = $\frac{27057 \times 100}{37897} \% \approx 71.40\%$

There are 25 defects types of which Uncut Thread, Spot and Oil Mark are individually counted together for 50 positions. Rest of the 22 defect types can occur in 50 different positions of the woven pants. So the number of total concerning area is $[22 \times 50 + 50 \text{ (Uncut Thread)} + 50 \text{ (Spot)} + 50 \text{ (Oil Mark)}] = 1250$ which is responsible for total amount of defects. But we have identified total 115 concerning areas by Pareto Analysis which is responsible for 71.40% defects.

Total number of concerning area = **1250**
 Total number of major concerning area = **115**
 Percentage of major concerning area = $\frac{115 \times 100}{1250} \% \approx 9.20\%$

So by concentrating only on 9.20% areas most of the defects can be reduced.

4.5 Hierarchy of Causes and Cause-Effect Diagram

From Pareto Analysis we have identified top defect positions and by further analyzing we have also identified top seven defect types in those positions. Those defect types are Skipped Stitch, Broken Stitch, Uneven Stitch, Raw Edge, Uncut Thread, Spot and Visible Top Stitch. These types of defect occur due to some specific causes. By our own observation and data provided by 20 QC supervisors from five production lines through questionnaires we have identified the causes for each specific defect types. Then these causes are ordered in a hierarchy according to the frequency of the feedback provided by QC supervisors. These hierarchies are shown in table 9, 10, 11, 12, 13, 14 and 15. After that we have constructed Cause-Effect Diagram for each of the defect types using 4M (Man, Machines, Materials and Methods) bones. These Cause-Effect Diagrams are shown in figure 9, 10, 11, 12, 13, 14 and 15.

Table 9. Hierarchy of Causes for Uncut Thread

SL. NO.	CAUSES	FREQUENCY (OUT OF 20)
1	Operator inefficiency	20
2	Improper trimming	16
3	Improper finishing	11

Table 10. Hierarchy of Causes for Spot

SL. NO.	CAUSES	FREQUENCY (OUT OF 20)
1	Operator carelessness	20
2	Mishandling	17
3	Defective machine	13
4	Dirty work area	06

Table 11. Hierarchy of Causes for Visible Top Stitch

SL. NO.	CAUSES	FREQUENCY (OUT OF 20)
1	Operator inefficiency	20
2	Improper trimming	15

Table 12. Hierarchy of Causes for Broken Stitch

SL. NO.	CAUSES	FREQUENCY (OUT OF 20)
1	Inappropriate thread tension	17
2	Wrong needle size and thread size	15
3	Needle plate, pressure foot, needle holes may have sharp edges	12
4	Excessive abrasion or chemical degradation of the thread during washing	07
5	Weak thread	06

Table 13. Hierarchy of Causes for Raw Edge

SL. NO.	CAUSES	FREQUENCY (OUT OF 20)
---------	--------	-----------------------

1	Improper seaming	20
2	Improper folding	20

Table 14. Hierarchy of Causes for Uneven Stitch

SL. NO.	CAUSES	FREQUENCY (OUT OF 20)
1	Operator speeding up machine too rapidly	17
2	Operator holding back or pulling fabric through in variance with correct machine feed	13

Table 15. Hierarchy of Causes for Skipped Stitch

SL. NO.	CAUSES	FREQUENCY (OUT OF 20)
1	Needle deflection or bending	17
2	Loop size or needle is small	13
3	Tension variation in lopper and needle thread	11
4	Hook, lopper or needle is not able to hold the thread loop in proper time	11
5	Improper handling of cut pieces	07
6	Operator inefficiency	02

Cause-Effect Diagram for Uncut Thread

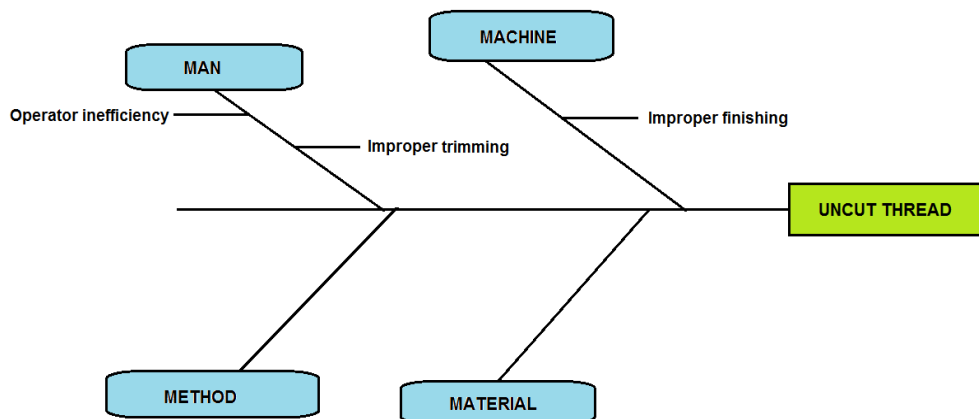


Figure 9. Cause-Effect diagram for Uncut Thread

Cause-Effect Diagram for Spot

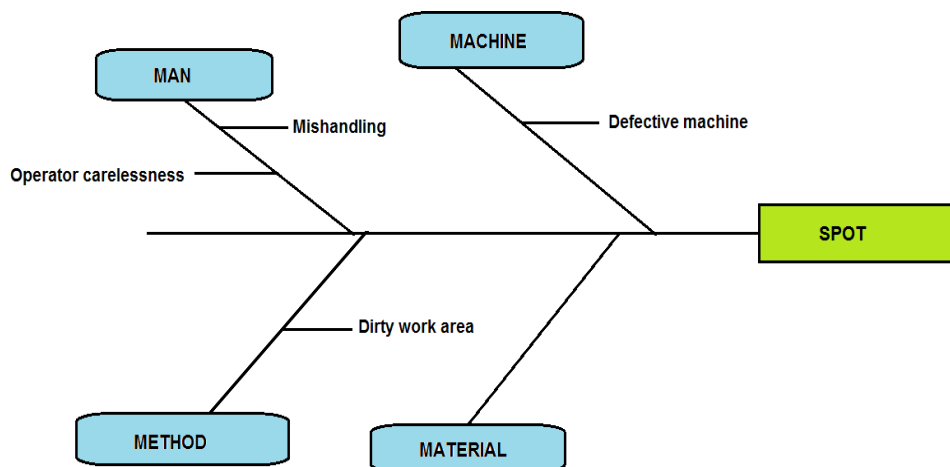


Figure 10. Cause-Effect diagram for Spot

Cause-Effect Diagram for Visible Top Stitch

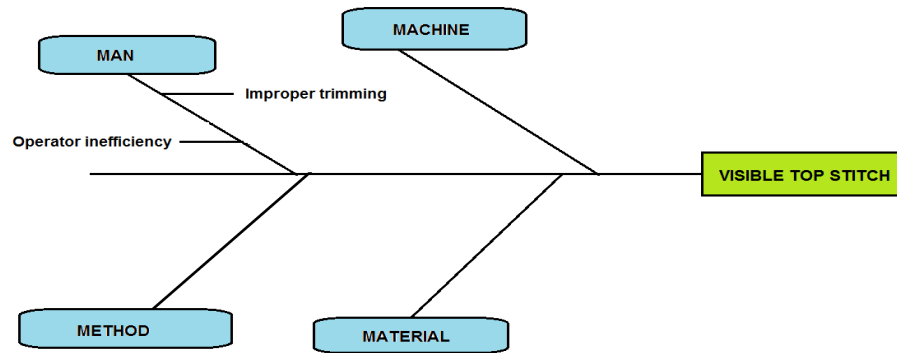


Figure 11. Cause-Effect diagram for Visible Top Stitch

Cause-Effect Diagram for Broken Stitch

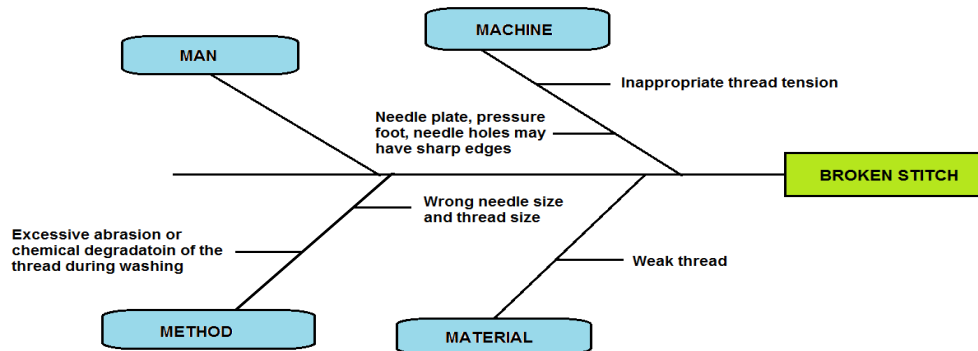


Figure 12. Cause-Effect diagram for Broken Stitch

Cause-Effect Diagram for Raw Edge

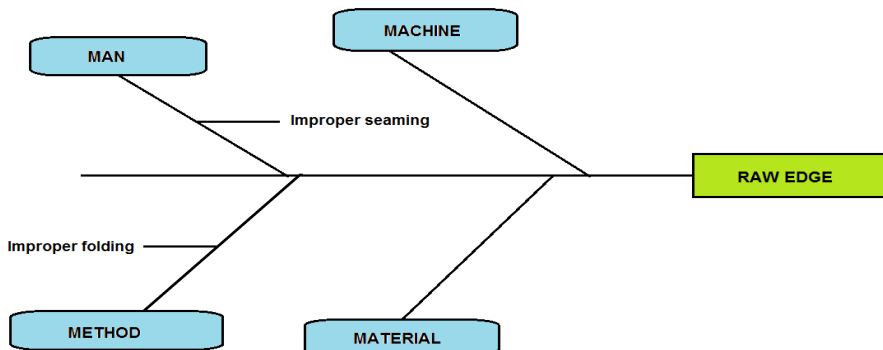


Figure 13. Cause-Effect diagram for Raw Edge

Cause-Effect Diagram for Uneven Stitch

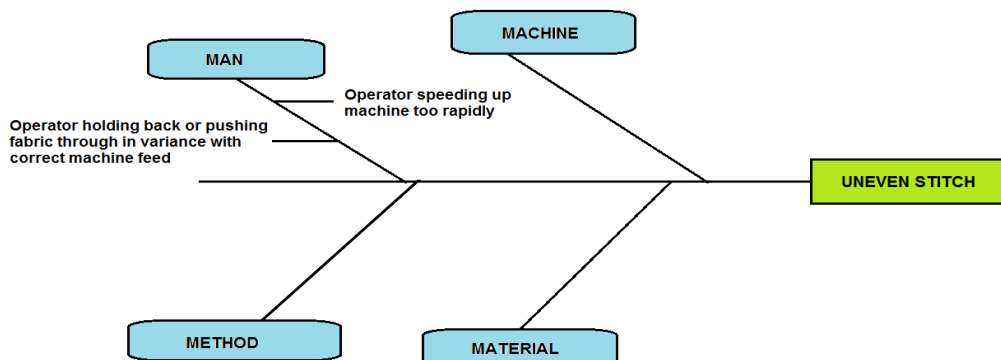


Figure 14. Cause-Effect diagram for Uneven Stitch

Cause-Effect Diagram for Skipped Stitch

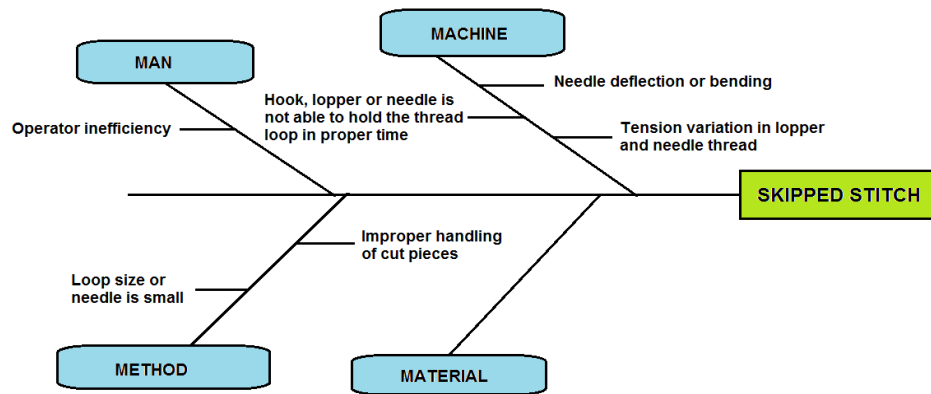


Figure 15. Cause-Effect diagram for Skipped Stitch

4.6 Suggestions to Reduce Top Defects Percentage

From our own observation, literature review and consultation with management some suggestions with their corresponding causes are provided below to reduce defect percentage:

Table 16. Suggested Solutions for Uncut Thread

Cause Types	Causes	Suggested Solutions
Man	Operator inefficiency	Provide adequate training to the operators.
	Improper trimming	Provide thread cutter to every operator and make used to.
Machine	Improper finishing	To cut thread properly, start regularly checking system to check the auto trimming machine is properly functioning or not.
		Improve quality inspection system.

Table 17. Suggested Solutions for Spot

Cause Types	Causes	Suggested Solutions
Man	Mishandling	Wash hands of operator before starting work and after lunch, establish preventive maintenance.
	Operator carelessness	Improve supervision.
Machine	Defective machine	Clean machine properly twice in a day.
Method	Dirty work area	Keep workplace neat and clean.

Table 18. Suggested Solutions for Visible Top Stitch

Cause Types	Causes	Suggested Solutions
Man	Operator inefficiency	Provide adequate training to the operators.
	Improper trimming	Teach operators.

Table 19. Suggested Solutions for Broken Stitch

Cause Types	Causes	Suggested Solutions
Machine	Inappropriate thread tension	Tension of the thread properly adjusted.
	Needle plate, pressure foot, needle holes may have sharp edges	Inspect the needle point at regular intervals and check for sharp or burred points. Sharp edges should be removed.
Method	Wrong needle size and thread size	Needle size and thread size should be synchronized.
	Excessive abrasion or chemical degradation of the thread during washing	Special care should be taken during washing.
Material	Weak thread	Select good quality thread which is free from flaws.

Table 20. Suggested Solutions for Raw Edge

Cause Types	Causes	Suggested Solutions
Man	Improper seaming	Teach operator
Method	Improper folding	Improve or change folding system

Table 21. Suggested Solutions for Uneven Stitch

Cause	Causes	Suggested Solutions
-------	--------	---------------------

Types		
Man	Operator speeding up machine too rapidly	Control the speed of machine, use right needle and correct feed control.
	Operator holding back or pulling fabric through in variance with correct machine feed	Improve the skill of operator, use good quality sewing thread, and provide standard quality specification.
		Never pull on the fabric while sewing, let it be taken up by the machine.

Table 22. Suggested Solutions for Skipped Stitch

Cause Types	Causes	Suggested Solutions
Man	Operator inefficiency	Provide adequate training to the operators.
Machine	Hook, lopper or needle is not able to hold the thread loop in proper time	Timing of hook or lopper with needle should be adjusted properly.
		Use needle which design to facilitate loop formation.
		Repair damage machine parts.
	Needle deflection or bending	Adjust the needle height and testing before bulk sewing.
		Check needle is properly mounted on the sewing machines with right eye position.
	Tension variation in lopper and needle thread	Adjust tension properly.
Select good quality thread which is free from flaws.		
		Choice of sewing thread in accordance with the needle size.
Cause Types	Causes	Suggested Solutions
Method	Loop size or needle is small	Adjust needle and thread size.
	Improper handling of cut pieces	Reduce gap between presser foot and the hole of needle plate

4.7 Suggested Additional Features for Existing Production Lines

- There are four in-line QC tables in each production line. These are currently placed in such a way that when defects occur in first few work tables, it takes too much time to identify the defects. Before reaching the QC table many operations are performed on those defected pieces and it results in more reworks than necessary. That is why more In-line QC tables should be included which will identify defects earlier, thus reduce rework percentage.
- After performing operation in each work table garments are kept mostly in the floor and sometimes in paper boxes which is one of the major reason for spot. To avoid the occurrence we have suggested providing a trolley between every two workers and that will also result in easy and smooth transportation
- Finally we have suggested to provide paper manual in every work table containing important issues for workers, such as:
 - Clean table and machines before starting day's work.
 - Wash hands properly before starting work and after lunch.
 - Never pull on the fabric while sewing, let it be taken up by the machine.
 - Adjust needle height, thread type and thread tension before bulk sewing.
 - Use right size of needle for specific type of fabrics.
- Keeping all these features in mind an improved version of existing layout of a single production line is shown in figure 16.

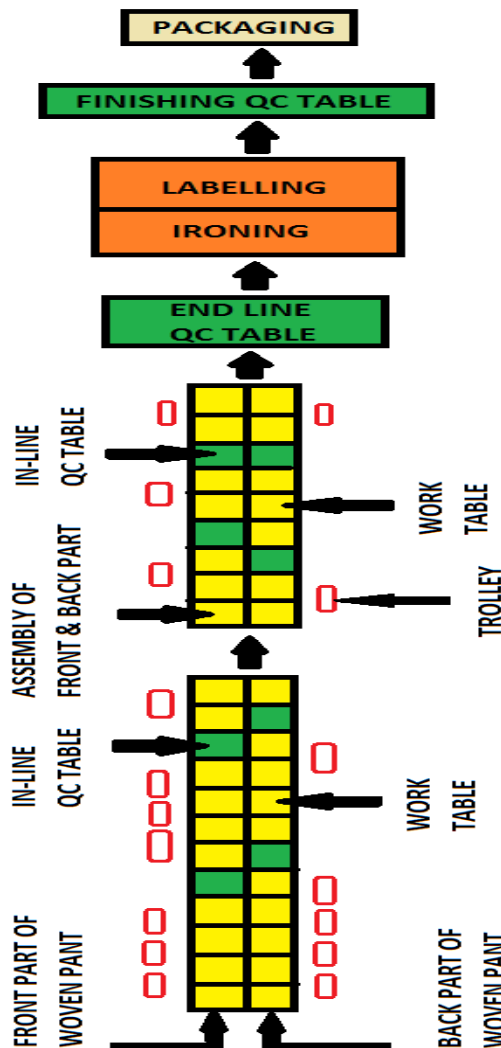


Figure 16. Proposed layout of a single production line

4.8 Result

We have found that up to 71.40% defect can be reduced by concentrating only on 9.20% areas. We have provided some suggestions related to those defect types. It is almost impossible to achieve zero defect. But by taking effective measure it is possible to reach near zero defect. So the more successfully those suggestions can be applied, the more the defects can be minimized.

V. Conclusion

Minimizing defect is very important for ensuring the quality of products. The importance of the garment industry in the economy of Bangladesh is very high. The perceived quality of a garment is the result of a number of aspects, which together help achieve the desired level of satisfaction for the customer. However, we should bear in mind that 1% defective product for an organization is 100% defective for the customer who buys that defective product. So manufacturing the quality product is mandatory to sustain in this global competitive market. Our first objective is to identify the top positions where maximum defects occur and second is to identify the top defect types in those positions. Keeping this in mind we have performed Pareto Analysis and identified top 6 positions out of 50 positions where 78.56% of total defects occur. Then we have performed further Pareto Analysis individually in those top positions to identify the top defect types. Thus we have identified just 115 major concerning areas which are responsible for 71.40% defects in total. Then the hierarchy of causes for each defect types are organized and the causes of those defect types are shown individually using Cause-Effect Diagram. Finally we have provided some suggestions so that the management can apply them to minimize the frequency of those defects. Thus we can effectively minimize reworks, rejection rate and waste of time that will ultimately increase productivity.

References

- [1] BGMEA B2B Web Portal, <http://www.bgmea.com.bd/home/pages/Strengths> (date of retrieval: May 15, 2012)
- [2] Production Process of RMG – Essays, <http://www.studymode.com/essays/Production-Process-Of-Rmg-580425.html> (date of retrieval: May 15, 2012)
- [3] Md. Mazedul Islam, Adnan Maroof Khan and Md. Mashiur Rahman Khan, “Minimization of Reworks in Quality and Productivity Improvement in The Apparel Industry”, International Journal of Engineering and Applied Sciences, January 2013. Vol. 1, No.4,
- [4] Mohiuddin Ahmed and Nafis Ahmad, “An Application of Pareto Analysis and Cause-and-Effect Diagram (CED) for Minimizing Rejection of Raw Materials in Lamp Production Process”, Management Science and Engineering, Vol. 5, No. 3, 2011, pp.87-95,
- [5] Learn About Sewing Problems/Problems Of Sewing/Different Type Of Sewing Problems, <http://textileeducationtips.blogspot.com/2013/03/learn-about-sewing-problemsproblems-of.html> (date of retrieval: July 19, 2012)
- [6] Common Defects In Denim Jeans Sewing, <http://www.denimsandjeans.com/denim/manufacturing-process/common-defects-in-denim-jeans-sewing/> (date of retrieval: July 19, 2012)
- [7] Defects of Sewing, http://www.jukiindia.com/item-list/defcts_of_sewing.pdf (date of retrieval: July 19, 2012)
- [8] Abhishek Kumar, “Apparel Standards Specifications and Quality Control, Cutting, Sewing & Finishing Defects”, National Institute of Fashion technology, <http://share.pdfonline.com/7926bbe6d71d4dcbb81ec5c1a603df26/Abhishek.htm> (date of retrieval: July 19, 2012)
- [9] Glossary of Defect Terminology Used in the Garment Industry, http://www.garmento.org/quality/Glossary_of_Defect_Terminology.pdf (date of retrieval: July 19, 2012)
- [10] Garment defects, <http://www.slideshare.net/2008000400034/garment-defects> (date of retrieval: July 19, 2012)
- [11] William J. Kolarik, Creating Quality, International Editions 1995, McGraw-Hill Inc., page: 173-192
- [12] Ahsan Akhtar Hasin, Quality Control and Management, First Edition 2007, Bangladesh Business Solutions, page: 30-50
- [13] Dung, Nguyen Hoang Phuong, “Improving the quality of service, Case: International SOS Viet Nam”, Bachelor’s Thesis of Degree Programme in International Business, Lahti University of Applied Sciences, Winter 2010,
- [14] Perzyk, M. (2007), “Statistical and Visualization Data Mining Tools for Foundry Production”, Foundry Commission of the Polish Academy of Sciences, 7 (3), page: 111 – 116.
- [15] Chandna, P., & Chandra, A. (2009), “Quality Tools to Reduce Crankshaft Forging Defects: An Industrial Case Study”, Journal of Industrial and Systems Engineering, 3 (1), page: 27-37.
- [16] Mahto, D., & Kumar, A. (2008), “Application of Root Cause Analysis in Improvement of Product Quality and Productivity”, Journal of Industrial Engineering and Management, 01 (02), page: 16-53.
- [17] Khekalei, S. N., Chatpalliwar, A. S., & Thaku, N. (2010), “Minimization of Cord Wastages in Belt Industry Using DMAIC”, International Journal of Engineering Science and Technology, 2 (8), page: 3687-3694.
- [18] Tips for Better Topstitching, <http://www.threadsmagazine.com> (date of retrieval: July 25, 2012)
- [19] A&E Visual Examples of Stitch & Seam Defects - Garmento.org <http://www.garmento.org/quality/a&estitchseamdefects.pdf> (date of retrieval: July 25, 2012)
- [20] Alterations | Sew for dough <http://sewfordough.wordpress.com/category/alterations> (date of retrieval: July 25, 2012)
- [21] Major/Minor/Critical defects: what are they? <http://www.asiaqualityfocus.com/blog/major-minor-critical-defects> (date of retrieval: July 25, 2012)

Design and Analysis Special Shaped Milling Cutter Using Finite Element Analysis

K. Chaitanya¹, M. Kaladhar²

¹M.Tech student, Department of Mechanical Engineering, Raghu Engineering College, Visakhapatnam, Andhra Pradesh, India

²Associate Professor, Department of Mechanical Engineering, Raghu Engineering College, Visakhapatnam, Andhra Pradesh, India

ABSTRACT: Milling is a production process which is based on material removal using multipoint cutting tools, as a result higher material removal rates can be achieved along with high surface finish. The common operations performed on milling machine are: facing, shaping, slot cutting, drilling, T-slot cutting etc. This paper presents an indiscriminate model of Special Shaped milling cutter made of high speed steel material for the purpose of predicting stress and deformation on it. At sudden torque applied by machine, harmonic motion, natural frequency and also loads acting on the cutter at varying speed and cutter thickness. The results obtained with the aid of FEM software for stresses are compared with theoretical values of stresses.

Keyword: catia, milling, FEM, Ansys

I. Introduction

Increasing the productivity and the eminence of the machined parts are the main challenges of metal-based industry. There has been increased interest in monitoring all aspects of the machining process. These machines assisted man in maintaining accuracy and uniformity while duplicating parts that could not be manufactured with the use of a file. Development and improvements of the milling machine and components continued, which resulted in the manufacturing of heavier arbors and high speed steel and carbide cutters. These components allowed the operator to remove metal faster, and with more accuracy, than previous machines. Variations of milling machines were also developed to perform special milling operations, Milling is the process of machining flat, curved, or Milling machines are basically classified as vertical or irregular surfaces by feeding the work piece against a rotating horizontal. These machines are also classified as knee-type, cutter containing a number of cutting edges. The milling ram-type, manufacturing or bed type, and planer-type, Most machine consists basically of a motor driven spindle, which milling machines have self-contained electric drive motors, mounts and revolves the milling cutter, and a reciprocating coolant systems, variable spindle speeds, and power-operated adjustable worktable, which mounts and feeds the work piece, table feeds [1,2]. This paper aims to develop an optimum geometric model of a plain cutter based on the application. To overcome the difficulties associated with modeling a complex cutter, an interface in the form of a customized tool design modeler is developed. This design tool can render the three-dimensional geometry of the cutter in any commercial CAD environment for validation and design improvements. In this work, the proposed 3D model of the special shaped milling cutter is used for finite element analysis to optimize its design. The results of stress distribution and deformation are presented.

II. Literature Review

Mohammed and Tandon (2000) developed geometric design model of a brazed insert-based CEFM cutter in terms of three-dimensional (3D) parameters. The model defined the CEFM cutter in terms of 3D rotational angles and also developed a provision of interface of 3D CEFM cutter directly for the purpose of methodology validation. Finite element analysis (FEA) was used to determine the effects on cutting insert under transient dynamic load conditions. [3] Mohammed and Tandon (2000) proposed a shape design methodology in order to develop the geometry of a generic special shaped milling cutter. The proposed three-dimensional parametric definition of the cutter with varying the rake angle of the insert and insert seat was analyzed using FEM. Though there is a good amount of work is done by the researcher to study and develop the various models for the conventional single point and multipoint cutting tools, but a few works have been recorded on the development of special shaped milling cutter model. [4]

III. Kinds of Milling Cutters

3.1 Plain Milling Cutter: The most common type of milling cutter is known as a plain milling cutter. It is merely a metal cylinder having teeth cut on its periphery for producing a flat horizontal surface.

3.2 Metal Slitting Saw Milling Cutter: The metal slitting saw milling cutter is essentially a very thin, it is ground slightly thinner toward the center to provide side clearance. It is used for metal sawing and for cutting narrow slots in metal.

3.3 End Milling Cutters: End milling cutters, also called end mills, have teeth on the end as well as the periphery. The smaller end milling cutters have shanks for chuck mounting or direct spindle mounting. Larger end milling cutters are called shell end milling cutters and are mounted on arbors like plain milling cutters. End milling cutters are employed in the

production of slots, keyways, recesses, and tangs. They are also used for milling angles, shoulders, and the edges of work pieces.

3.4 Concave and Convex Milling Cutters: Concave and convex milling cutters are formed tooth cutters shaped to produce concave and convex contours of one-half circle or less. The size of the cutter is specified by the diameter of the circular form the cutter produces.

3.5 Corner-rounding Milling Cutter: The corner-rounding milling cutter is a formed tooth cutter used for milling rounded corners on work pieces up to and including one-quarter of a circle. The size of a cutter is specified by the radius of the circular form the cutter produces, as with concave and convex cutters.

3.6 Special Shaped-formed Filing Cutter: Formed milling cutters have the advantage of being adaptable to any specific shape for special operations. The cutter is made for each specific job. In the field, a fly cutter is made to machine a specific shape.

3.7 T-Slot Milling Cutter: The T-slot milling cutter is used to machine T-slot grooves in worktables, fixtures, and other holding devices. The cutter has a plain or side milling cutter mounted to the end of a narrow shank. The throat of the T-slot is first milled with a side or end milling cutter and the headspace is then milled with the T-slot milling cutter [5]

IV. Design Implementation

In this work, a customized tool design modeler has been developed. This design tool helps in rendering the proposed three-dimensional model, defined with the help of parametric equations, in any CAD environment by suitable translation of the geometric data of the cutter. Developing an interface is advantageous in comparison to using the APIs of existing CAD packages, as it does not limit the convenience of the proposed modeling paradigm, primarily the conversion of free-form parametric surfaces. This also helps in validating the mathematical models,

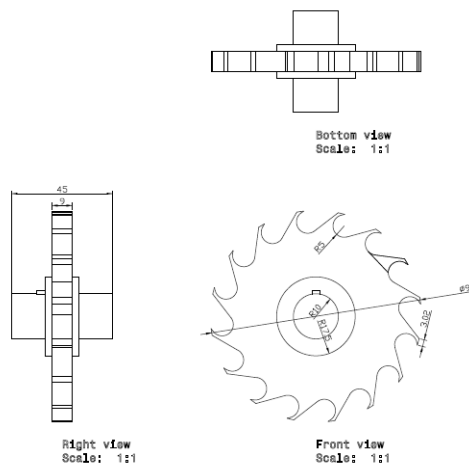


Figure-1

High Speed steel is the material chosen for the milling cutter and the properties are tabulated in Table 1

Table 1
MECHANICAL AND THERMAL PROPERTIES OF TOOL INSERT (HSS)

Materials	High Speed Steel
Density (kg/m ³)	7980
Young's modulus, E (GPa)	210
Poisson's ratio, n	0.30
Tensile strength (MPa)	970
Thermal conductivity (W/m°C)	20.9

V. Finite Element Analysis of Plain Milling Cutter

In order to perform a finite element analysis, it is necessary to determine the forces acting on the cutter. From the given conditions the force acting on the cutter (W) may be calculated as:

$$W = \frac{60 \times H}{\pi d n} \quad \text{- Equation (1)}$$

Where H is the power, in kW, n is the speed, in rpm, and D is the diameter of the cutter.

The stress calculation at the tip of the tooth of the cutter is estimated based on the concept of gear tooth stresses. The stress at each speed is determined by [6]

$$\sigma = \frac{6Wl}{Ft^2} \quad \text{-Equation (2)}$$

VI. Analysis of Single Tooth Using Ansys

The Cutting Forces on the cutter for different speeds are calculated and the same are applied on the tip of the cutter modal. The variation in stresses and deformation on cutter from ANSYS are Shown in following Figures. The results are tabulated

Stress at speed 100 rpm thickness 9mm

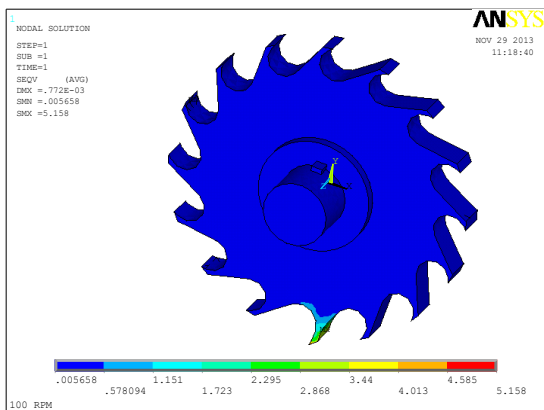


Figure-2

Deformation at speed 100 rpm thickness 9mm

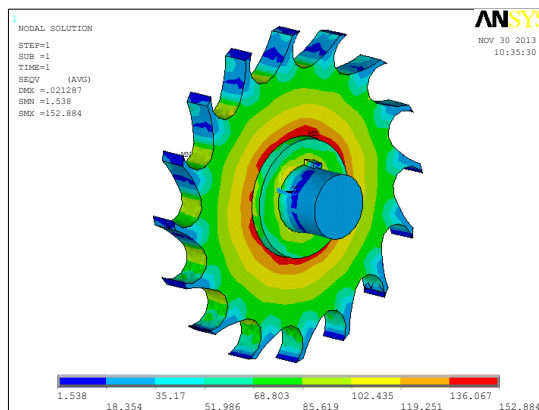


Figure-3

Stress at speed 1600 rpm thickness 9mm

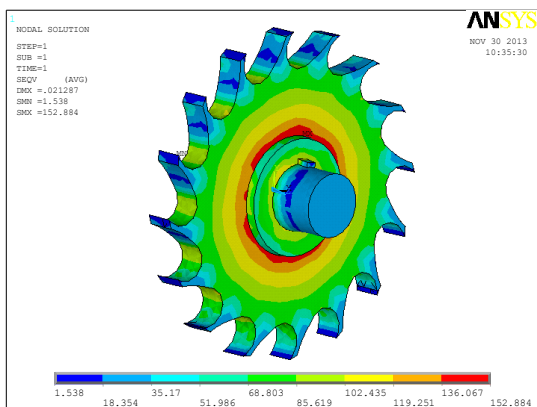


Figure-4

Deformation at speed 1600 rpm thickness 9mm

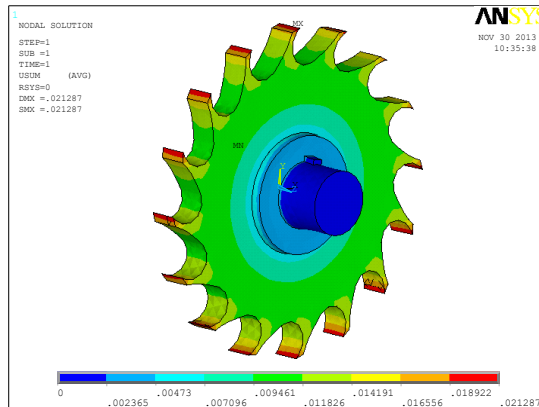


Figure-5

Stress at speed 100 rpm thickness 12mm

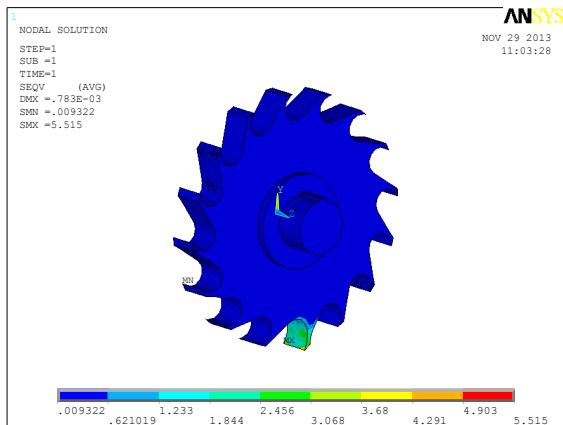


Figure-6

Deformation at speed 100rpm thickness 12mm

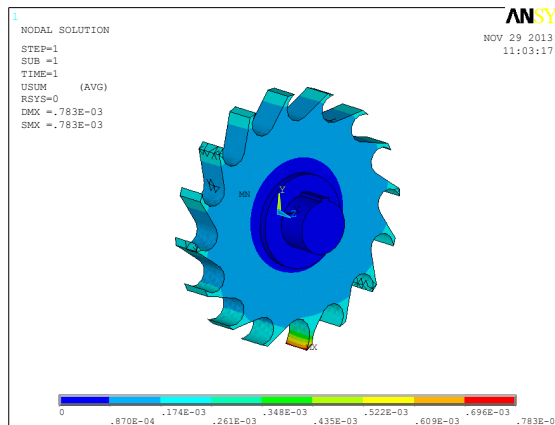


Figure-7

Stress at speed 1600 rpm thickness 12mm

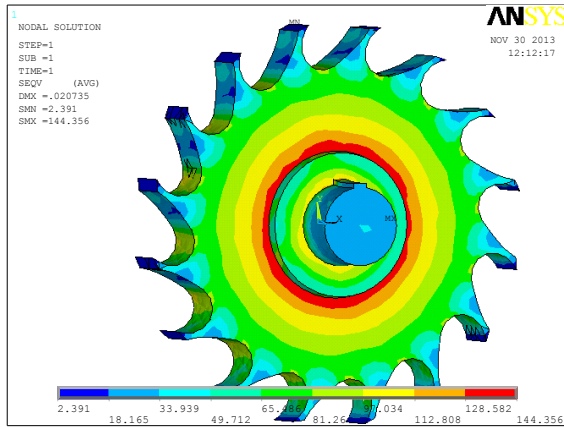


Figure-8

Deformation at speed 1600rpm thickness 12mm

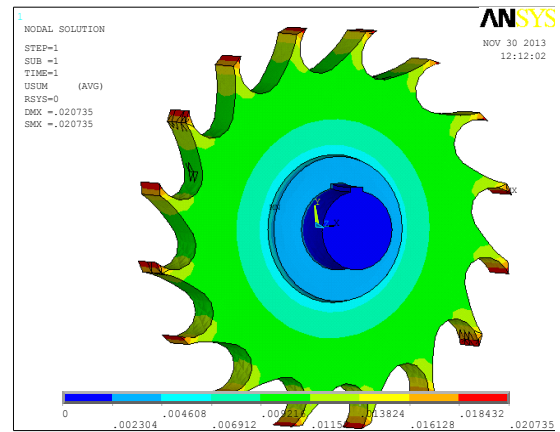


Figure-9

Stress at speed 100 rpm thickness 15mm

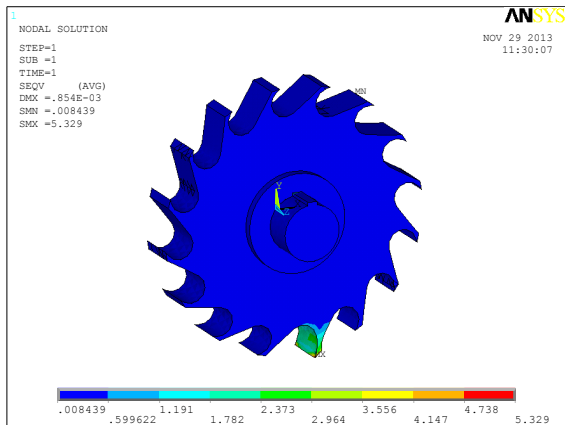


Figure-10

Deformation at speed 100rpm thickness 15mm

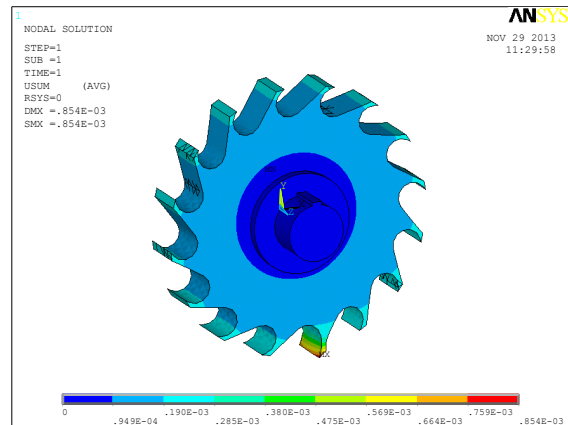


Figure-11

Stress at speed 1600 rpm thickness 12mm

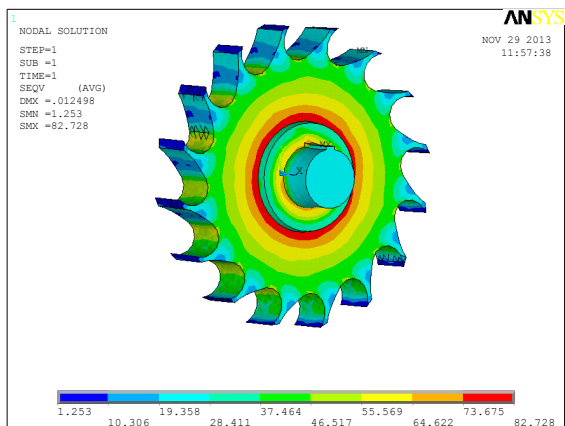


Figure-12

Deformation at speed 1600rpm thickness 12mm

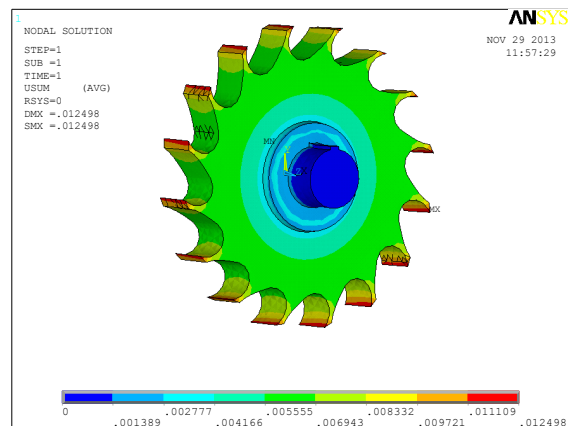


Figure-13

VII. Results Obtained

Table.2

The following results tabulates milling cutter with thickeness if 9mm

S.NO	DIA	SPEED	LOAD	STRESS Ansys, Results	STRESS (Theoretical)
1.	94	100	3.0477	5.158	6.528
2.	94	200	1.5238	2.162	3.465

3.	94	300	1.0158	5.054	7.268
4.	94	400	0.7465	8.986	9.458
5.	94	500	0.6095	14.08	15.248
6.	94	600	0.5079	20.218	22.167
7.	94	700	0.4353	27.218	25.748
8.	94	800	0.3809	35.493	38.745
9.	94	900	0.3362	45.49	49.751
10.	94	1000	0.3047	61.916	65.214
11.	94	1100	0.2770	67.913	68.215
12.	94	1200	0.2534	80.875	76.458
13.	94	1300	0.2108	94.912	90.154
14.	94	1400	0.2170	110.74	115.154
15.	94	1500	0.2031	126.359	124.251
16.	94	1600	0.1906	152.884	155.547

Table.3
The following
milling cutter
12mm

S.NO	DIA	SPEED	LOAD	STRESS Ansys, Results	STRESS (Theoretical)
1.	94	100	3.0477	5.515	6.268
2.	94	200	1.5238	3.528	4.258
3.	94	300	1.0158	5.076	8.456
4.	94	400	0.7465	9.021	11.254
5.	94	500	0.6095	14.859	17.987
6.	94	600	0.5079	20.294	24.875
7.	94	700	0.4353	27.622	30.687
8.	94	800	0.3809	36.077	34.567
9.	94	900	0.3362	45.66	49.874
10.	94	1000	0.3047	56.453	54.846
11.	94	1100	0.2770	68.207	65.784
12.	94	1200	0.2534	81.176	79.814
13.	94	1300	0.2108	95.293	97.147
14.	94	1400	0.2170	112.985	116.876
15.	94	1500	0.2031	126.834	120.574
16.	94	1600	0.1906	144.356	150.745

results tabulates
with thickens if

Table.4
The following results tabulates milling cutter with thickens if 15mm

S.NO	DIA	SPEED	LOAD	STRESS Ansys, Results	STRESS (Theoretical)
1.	94	100	3.0477	5.329	6.574
2.	94	200	1.5238	2.808	3.852
3.	94	300	1.0158	5.021	7.154
4.	94	400	0.7465	8.924	10.254
5.	94	500	0.6095	13.924	15.247
6.	94	600	0.5079	20.075	22.946
7.	94	700	0.4353	27.325	30.246
8.	94	800	0.3809	35.689	38.654
9.	94	900	0.3362	45.169	49.854
10.	94	1000	0.3047	55.769	59.624
11.	94	1100	0.2770	67.473	70.487
12.	94	1200	0.2534	80.394	85.124
13.	94	1300	0.2108	94.488	100.523
14.	94	1400	0.2170	108.295	105.781
15.	94	1500	0.2031	125.466	130.847
16.	94	1600	0.1906	82.729	90.657

Graph Represents variation in stress with respect to variation in load for both FEA model and theoretical results for Table.2

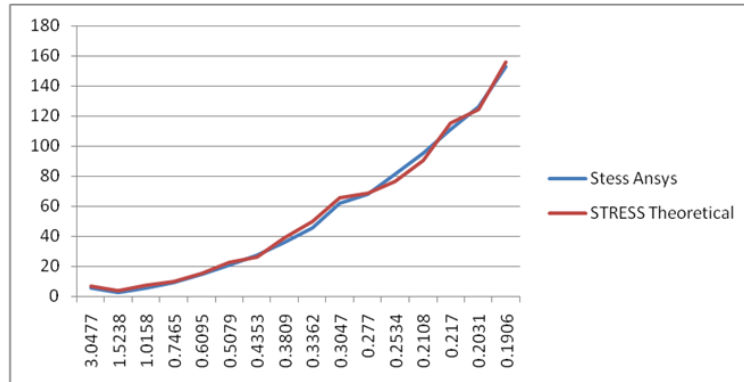


Figure-14

Graph Represents variation in stress with respect to variation in load for both FEA model and theoretical results for Table.3

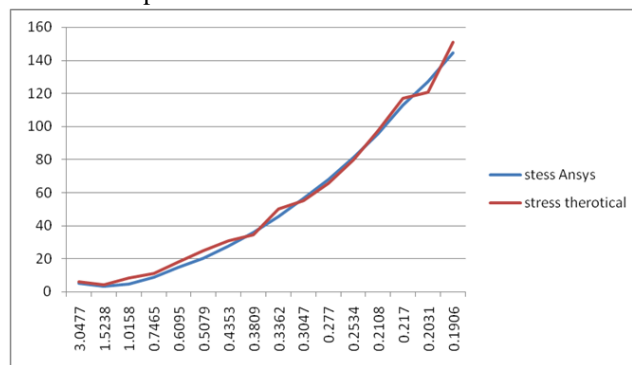


Figure-15

Graph Represents variation in stress with respect to variation in load for both FEA model and theoretical results for Table.4

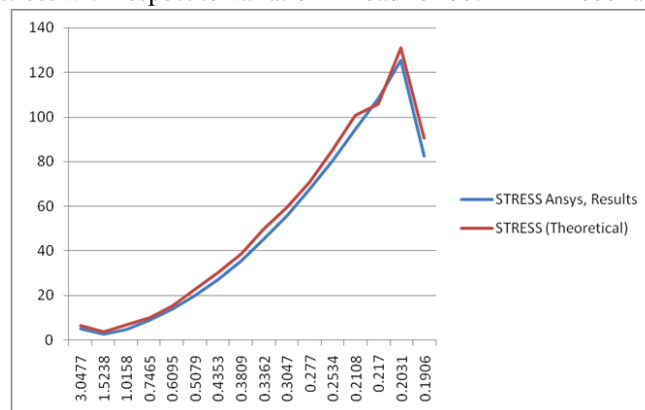


Figure-16

VIII. Findings

- From the Figurers 14 and 15, it is observed that the low values of stresses and deformation are recorded at the combination of 200 rpm and thickness of 9 mm and 12 mm.
- Figurer 16 indicates the lowest value of stresses and deformation at the combination of 1600 rpm and 15 mm thickness.

IX. Conclusions and Discussion

This work illustrates an advanced modeling paradigm that can be used to accurately model a special shaped milling cutter and thus, opens up paths to define conveniently various customized cutters. Here, different design activities, such as geometric modeling, finite element analysis and design improvements have been integrated. As is evident, the approach illustrated in this paper is flexible and easy to use. This approach can also be used to design any complex mechanical component, specifically for the cutter design, it produced the cutting variables that yield the minimum cost of manufacturing. The different design activities, such as design solid modeling, and finite element analysis, have been integrated. The values

obtained are compared with the model and theoretical stress values of the special shaped milling cutter. It was observed from the results, both stresses and deformation values were drastically reduced at the combination of 1600 rpm and 15 mm thickness.

REFERENCES

- [1] K. Lalitha Babu¹, M. Kumara Swamy² *International Journal of Modern Engineering Research (IJMER) www.ijmer.com Vol. 2, Issue. 6, Nov-Dec. 2012 pp-4480-4483 ISSN: 2249-6645*
- [2] Prof. BHARAT S PATEL¹, Mr. Hiren Pal² *International Journal of Applied Engineering Research, ISSN 0973-4562 Vol.7 No.11 (2012)*
- [3] Mohammed Rajik Khan, and Puneet Tandon, *Member, IAENG Proceedings of the World Congress on Engineering 2013 Vol I, WCE 2013, July 3 - 5, 2013, London, U.K.*
- [4] Mohammed Rajik Khan and Puneet Tandon *PDPM-Indian Institute of Information Technology, Computer-Aided Design & Applications, 7(2), 2010, 213-219*
- [5] <http://www.enggpedia.com/mechanical-engineering-encyclopedia/dictionary/machine-design/1643-milling-operation-milling-process-a-types-of-milling>
- [6] Integrated computer-aided optimal design and finite element analysis of a plain milling cutter Nand K. Jha and Kathryn Hornik

Preparation and Characterization of B₄C Particulate Reinforced Al-Mg Alloy Matrix Composites

M. Marimuthu¹, L. John Berchmans²

¹Department of Mechanical Engineering, Thiagarajar College of Engineering, Madurai

²Electropyrometallurgy Division, CSIR – Central Electrochemical Research Institute, Karaikudi

ABSTRACT: This paper describes the fabrication and mechanical testing of Al-Mg-boron carbide particulate composites using stir casting technique. The size of the boron carbide particulates is ranging between 30 to 100 μm . The boron carbide contents are varied from 3 and 7% by weight and are dispersed in the alloy matrix. The mechanical properties of the castings, particularly their tensile properties and hardness are measured. The micro structural features of the fabricated composite materials are evaluated using a Scanning Electron Microscope (SEM).

Key words: Aluminum-Magnesium alloy, Particulate reinforcement, Composites, B₄C, UTS, Microstructure.

I. INTRODUCTION

Particulate-reinforced metal matrix composites are attractive materials for various light weight structural applications. Many materials have been tried on particulate materials in Al SiC particulate has been extensively utilized as reinforcement in various Al, Al-Mg, Mg-SiC alloy matrices [1-6]. Composites of SiC particulates in aluminum alloys have been successfully produced by powder metallurgy processing and casting techniques [7-11]. It has been demonstrated that significant improvements in stiffness, strength, fatigue crack propagation, creep strength, and wear resistance were achieved as compared with the unreinforced aluminum alloys. Besides, they can also be shaped by conventional metal working processes such as extrusion, forging, rolling or super plastic forming into complex structural parts. Hence, they are inexpensive to produce compared with other metal matrix composite systems. Potential applications of these composites include advanced aerospace structures, automobile engine components, electronic packaging, etc.

Boron carbide (B₄C) particulates are promising candidates as reinforcement for light weight metal matrix composites. B₄C has a lower specific gravity than either Al or SiC (2.52 g/cm³ compared with 2.7 for Al and 3.2 for SiC). It has a similar thermal expansion coefficient, higher specific stiffness and strength as compared to SiC. Increased application of chills in Al alloy B₄C composites and their mechanical properties have been studied [12-24]. In the present investigation, we have prepared B₄C particulate-reinforced Al-Mg matrix composites using stir casting technique. The purpose of this paper is to fabricate and characterize the microstructure and mechanical properties of the resulting composites, and to identify the failure mechanisms under various loading conditions.

A composite can be said to be a multifunctional system that provides characteristics not obtainable from any discrete material [2-5]. Aluminum and its alloys probably form the most widely used matrix materials for metal matrix composites [6]. Although reinforcements in the form of continuous and discontinuous fibers have already been investigated in depth [7], discontinuous reinforcement such as that of dispersoid is becoming more and more popular. Subsequent working of such dispersoid-reinforcement metal matrix composites can also enhance their mechanical properties. Al matrix composites have demonstrated improved mechanical properties compared to properties of un-reinforced Al alloys.

Metal matrix composites (MMCs) are emerging as advanced engineering materials for application in aerospace, defense, automotive and consumer industries (sports goods, etc.). Aluminum or its alloy is favored as metallic matrix material because of its low density, easy fabricability and good engineering properties. In general, the benefits of aluminum metal matrix composites (AMCs) over unreinforced aluminum alloy include increased specific stiffness, improved wear resistance and decreased coefficient of thermal expansion. The reinforcement materials for AMCs are SiC and Al₂O₃. In the present work, boron carbide (B₄C) powder was chosen as reinforcement because of its higher hardness (very close to diamond) than the conventional and routinely used reinforcement such as SiC, Al₂O₃, etc. further its density (2.52 g cm⁻³) is very close to Al alloy matrix. Al-5% Mg alloy was chosen as matrix alloy in order to utilize the beneficial effect of Mg in improving wettability between B₄C particles and the alloy melt.

B₄C particulates are other promising candidates as reinforcement for light weight metal matrix composites. B₄C has a lower specific gravity than either Al or SiC (2.52 g/cm³ compared with 2.7 for Al and 3.2 for SiC). It has a similar thermal expansion coefficient, higher specific stiffness and strength as compared to SiC [5]. In this study, a B₄C particulate – reinforcement 7091 Al matrix composite has been developed.

The Mg-9 wt% Li matrix alloy was prepared by vacuum casting and consisted of two phases, α (hexagonal-close-packed structure) and β (body-centered-cubic structure). The α phase, making up about 30 vol% of the material, is elongated and dispersed within the β matrix. The as-cast material was cut into plates, and these were given a repeated sequence of cold-rolling and annealing treatments until foils of about 0.20 mm thick were obtained. The total reduction of the individual foils was 200 to 1. The B₄C particles (less than 20 μm in size) were suspended in an ethanol solution and then painted on one side of the foils.

II. EXPERIMENTAL PROCEDURE

2.1 Preparation of test specimens

Al-Mg alloy matrix-B₄C particulate reinforced composites were fabricated by stir casting method. In this method Al-Mg alloy was first melted as per their weight proportions and super heated to 800°C in closed type electrical resistance furnace. The melt was degassed with argon gas and then stirred at a rate of 300–400 rpm by using a mechanical impeller. The blades were made of inconel plate. Argon gas was purged in to the melting chamber to reduce the oxidation of the melt. B₄C powder was preheated to 600°C for 1 h, in a separate furnace and it was added slowly to the Al-Mg molten melt. Complete mixing of powder and melt was done by uniform stirring. This ensure the dispersion of the B₄C particles uniformly in to the melt. The process was continued for 15min to obtain a homogeneous composite of alloy and particulates. During the entire process argon atmosphere was maintained. The homogeneous molten alloy composite was then poured into a graphite mold, which was preheated to 200° C. Cylindrical rods of 10mm diameter and 100mm height were machined and extruded in the form of rod. Composites with 3 and 7wt % of B₄C particulates were fabricated. The fabricated composite materials were characterized using various analytical techniques such as XRD, EDAX and SEM. The mechanical behavior of the composite materials was assessed an Instron tensile testing machine. The hardness of the composites was determined using a standard Micro hardness test machine.

2.2 Microstructure characterization

For the micro structural studies, specimens were cut from extruded rods and mounted in Bakelite, ground with grit paper, using copious amounts of water as lubricant. The mounted samples were then mechanically polished using a 1µm alumina-powder suspended in distilled water. Fine polishing to near mirror like finish was achieved using 0.5 µm diamond paste and etched with Keller's reagent. Reinforcement morphology and its distribution in the metal matrix along with other intrinsic micro structural features were identified by examining the samples in a JEOL JSM 3.5 CF Japan make Scanning Electron Microscope (SEM).

2.3 Mechanical testing

Tensile tests were performed using an instron tensile testing machine on ASTM standard tensometer specimens. Each test result reported in this paper, is the average obtained from at least three test specimens taken from the same location in the mould and cast under identical conditions.

Bulk hardness measurements were performed using a standard Micro hardness test machine. The measurements were carried out in order to investigate the influence of particulate volume fraction on the matrix hardness.

III. RESULTS AND DISCUSSION

3.1 MICROSTRUCTURE OF CAST COMPOSITES

The microstructures of the composites were evaluated by scanning electron microscope (SEM). The micrographs revealed a relatively uniform distribution of B₄C particles and good interfacial integrity between matrix and B₄C particles. The microstructures of Al-Mg- B₄C composites containing 3 and 7 wt. % boron are shown in Figs. 4.1, 4.2 and 4.3 respectively. These photo micro graphs show that the boron particles are of nearly uniform size and are uniformly dispersed in the aluminum matrix. However, micro structural studies reveal that, Mg migrated to the grain boundaries. This migration of alloying elements into the grain boundaries leaving behind the dispersoids in the grains result in a higher concentration of boron within the grains, which may be one of the main reasons for the increase in strength and soundness of the composite developed, as will be described below.

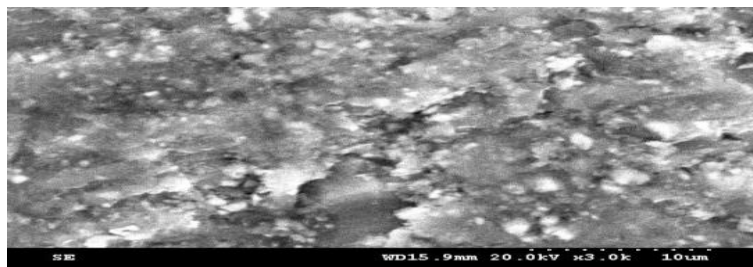


Fig 3.1: Micro structure of unreinforced Al-Mg alloy

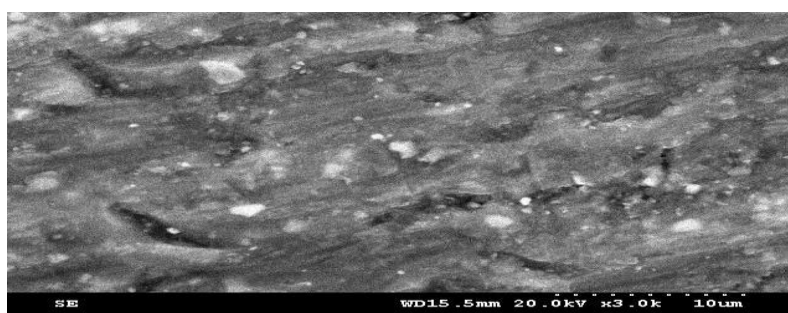


Fig 3.2: Micro structure of Al-Mg-B₄C MMC (3wt. % B₄C)

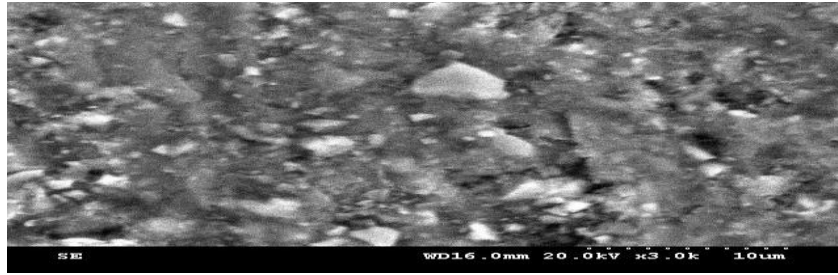


Fig 3.3: Micro structure of Al-Mg-B₄C MMC MMC (7 wt. % B₄C

3.2 EDAX

The element composition of Al-Mg alloy was assessed by EDAX spectral analysis. The EDAX spectrum exhibits presents of Al and Mg in appropriate weight ratio. The EDAX values are shown below figure 4.4, 4.5 and 4.6.

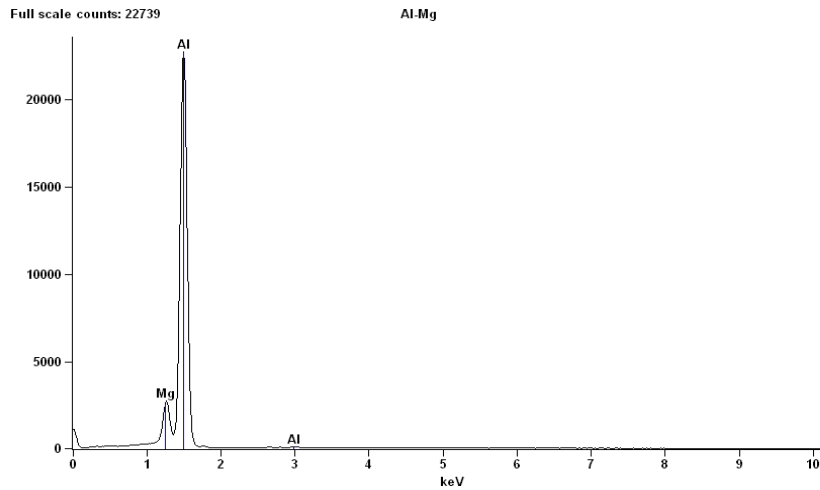


Fig 3.4: EDAX analysis of 92.5% Al -7.5% Mg

Table 3.1: Quantitative Results 92.5% Al-7.5%Mg

<i>Element</i>	<i>Net Counts</i>	<i>Weight %</i>	<i>Atom %</i>
<i>Mg</i>	25180	7.67	8.44
<i>Al</i>	243589	92.33	91.56
<i>Total</i>		100.00	100.00

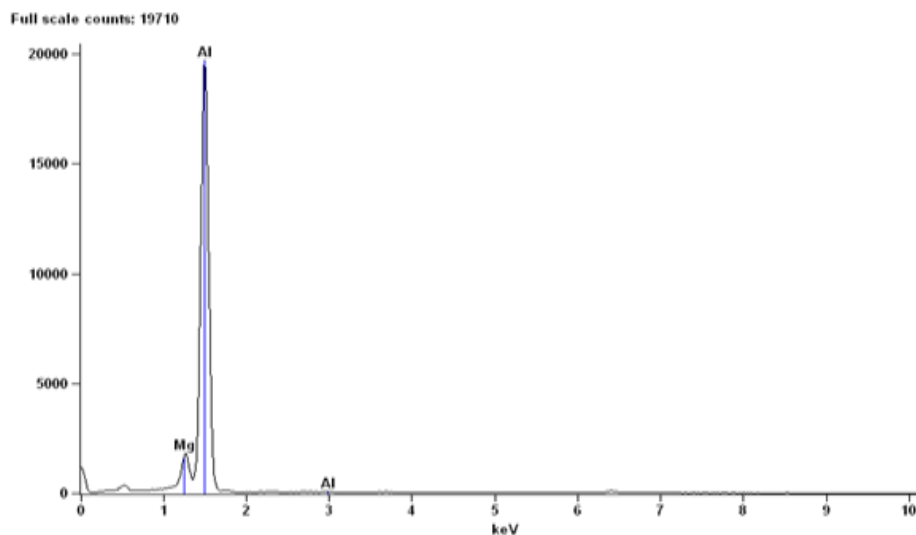


Fig 3.5: EDAX analysis of 92.5% Al - 7.5% Mg - 3% B₄C

Table 3.2: Quantitative Results 92.5%Al-7.5%Mg-3%B₄C

Element	Net Counts	Weight %	Atom %
Mg	15793	7.51	7.75
Al	213346	92.49	92.25
Total		100.00	100.00

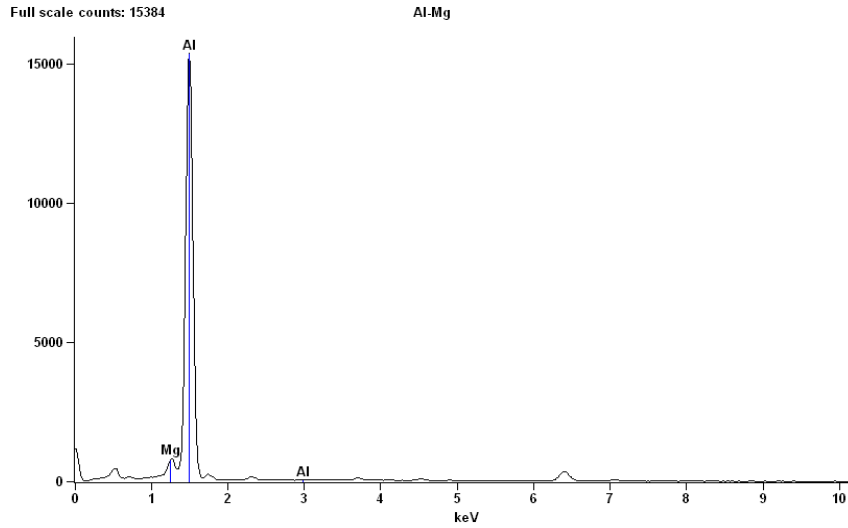


Fig 3.6: EDAX analysis of 92.5% Al – 7.5% Mg - 7% B₄C

Table 3.3: Quantitative Results 92.5%Al-7.5%Mg-7%B₄C

Element	Net Counts	Weight %	Atom %
Mg	5833	7.42	7.32
Al	164862	92.58	92.68
Total		100.00	100.00

3.3 XRD

The synthesized Al-Mg alloys were analyzed by XRD spectral analysis. 100% peak shows that the compound is in pure form. The XRD measurement shown in figure: 4.7,4.8 and 4.9.

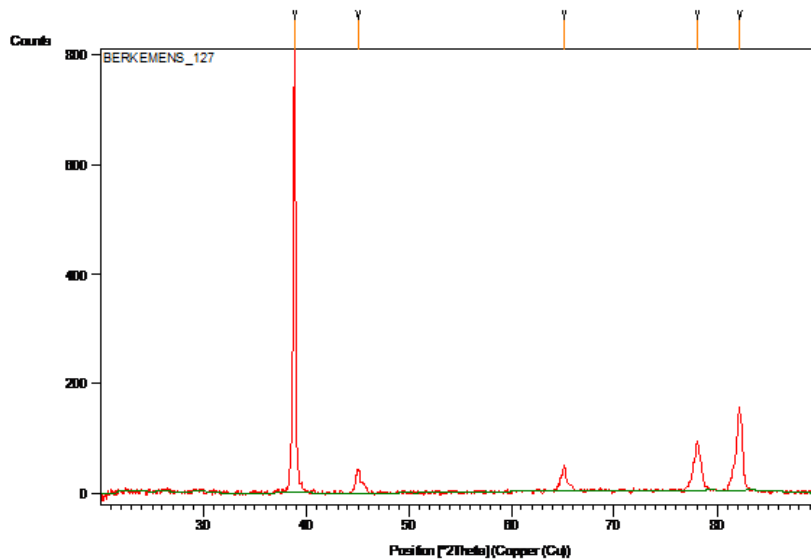


Fig 3.7: XRD measurement –Al- Mg

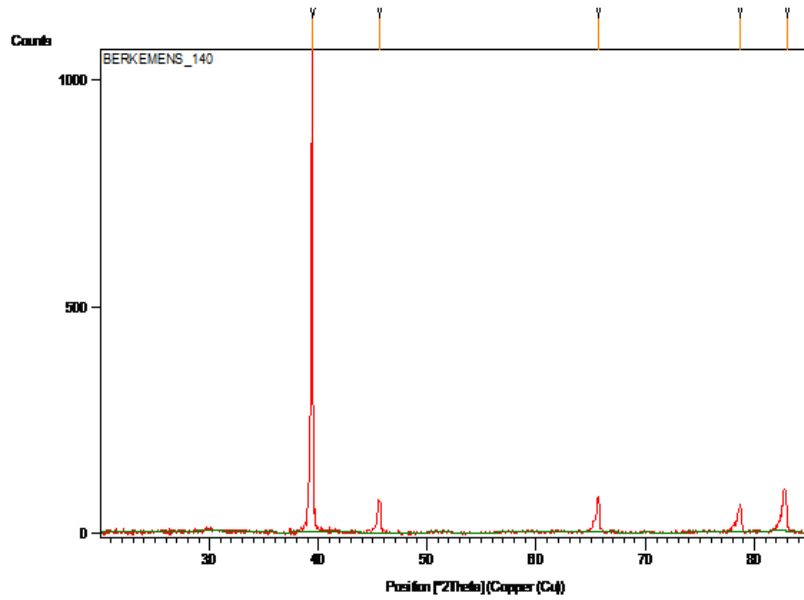


Fig 3.8: XRD measurement –Al- Mg - 3% B₄C

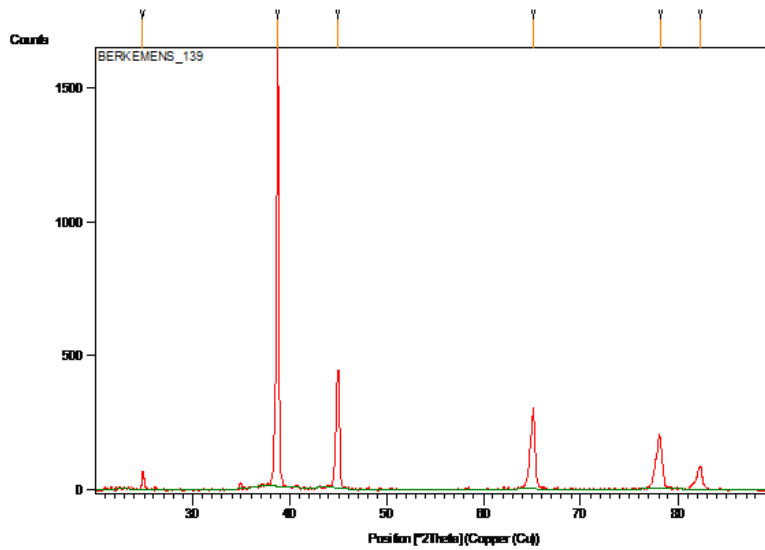


Fig 3.9: XRD measurement –Al- Mg- 7% B₄C

3.4 MECHANICAL PROPERTIES

Table 3.4: Tensile properties and Micro hardness test of composites

SPECIMAN	UTS (MPa)	%Elongation	%Area Reduction	Hardness (Rockwell)
92.5%Al-7.5%Mg	108.85	6.66	7.7	79
92.5%Al-7.5%Mg-3%B ₄ C	113.39	6.25	6.8	82
92.5%Al-7.5%Mg-B ₄ C	127.63	6.18	6.4	85

From the above table it is clear that addition of B₄C leads to improvement in the ultimate tensile strength of the aluminium alloy and increase in hardness value is more in case of 92.5% Al-7.5% Mg -7%B₄C as compared with others. The addition of Magnesium improves the strength of the composites significantly.

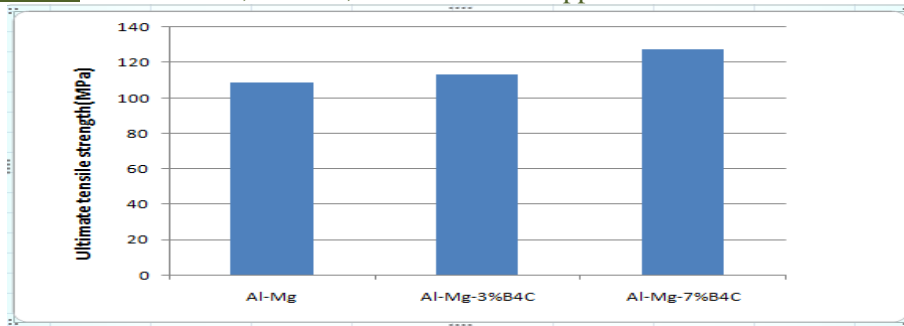


Fig 3.10 Ultimate Tensile Strength

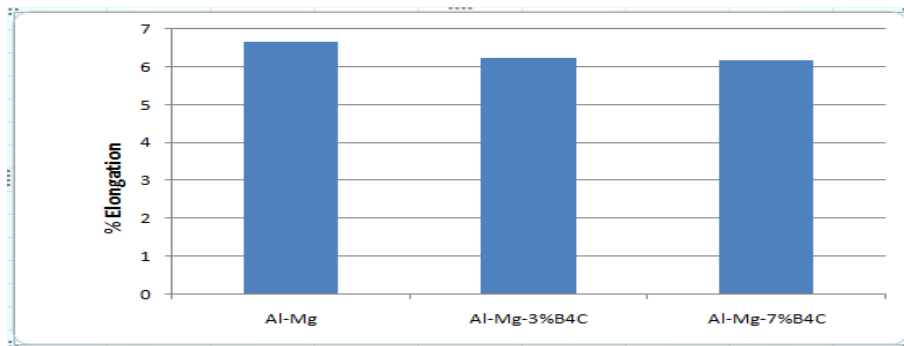


Fig 3.11 % Elongation

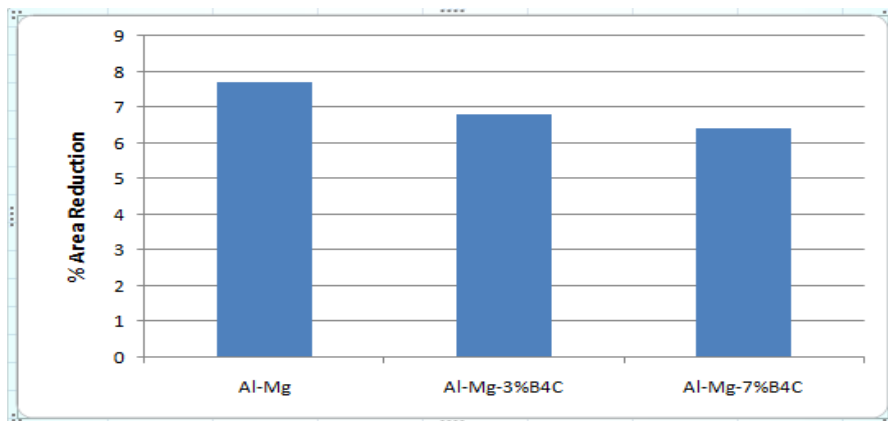


Fig 3.12 % Area Reduction

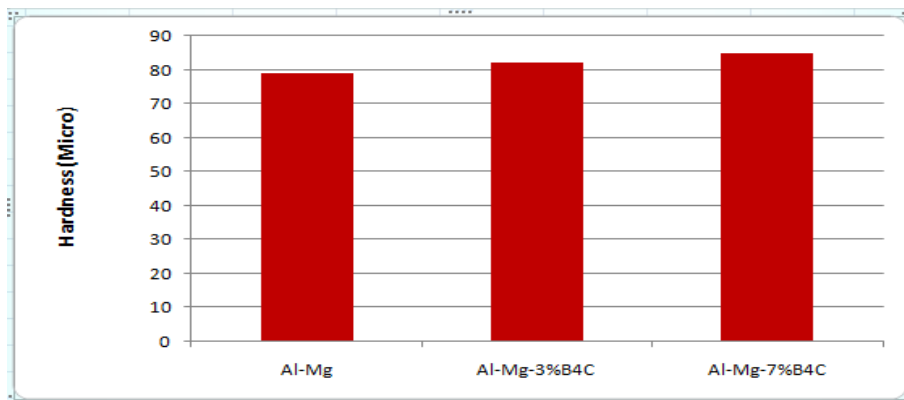


Fig.3.13 Graph showing variation in hardness with composition of MMCs

IV. Conclusion

- In the Al-Mg-B₄C composites both tensile and hardness properties of the composites are found to increase as the content of B₄C particulates is increased up to 6% by weight.
- From the micro structural studies, it has been concluded that the B₄C dispersoids are uniformly distributed in the alloy matrix, by influences the mechanical properties to achieve better hardness.
- There is a greater scope for the development of Al-Mg- B₄C composites for the application in the field of nuclear industries.

References

- [1]. Biswas PK, Dev SC, Krishnan CSS. *Mg alloys and composites as the future challenging materials for automobile applications*. Ind Foundry J 1999; 45(3):17-26.
- [2]. Luo A, Perquelyuz MO. *Review cast Mg alloy for elevated temperature applications*. J Mater Sci 1994; 29:5259-71.
- [3]. Lewandowski JJ. In: Clyne TW, editor. *Metal matrix composites*, vol.3. Amsterdam: Elsevier; 2000. p. 151–87.
- [4]. Divecha AP, Fishman SG, Karmarkar SD. *Synthesis of metal-matrix composites*. J Metals 1981;33:12–15.
- [5]. Stephens JR. *High temperature metal matrix composites for future aerospace systems*. NASA TM 1987;100–212.
- [6]. Nair SV, Tien JK, Bates RC. *Int Metals Rev* 1985;30(6):285–97.
- [7]. Rozak GA, Lewandowski JJ, Wallace JF, Altmy sog̃ lu A. *Effect of casting conditions and deformation processing on A356 Al and A356 - 20 vol.% SiC composites*. J Compos Mater 1992;26:2079–106.
- [8]. Shi N, Arsenault RJ. *Plastic flow in SiC/Al composites-strengthening and ductility*. Annu Rev Mater Sci 1994;24:321–57.
- [9]. Co cen U, O nel K, O zdemir I *Microstructures and age hardenability of Al–5% Si–0.2% Mg based composites reinforced with particulate SiC*. Compos Sci Technol 1997;57:801–8
- [10]. O zdemir I, Co cen U , O nel K. *The effect of forging on the properties of particulate SiC reinforced aluminium alloy-composites*. Compos Sci Technol 2000;60:411–9.
- [11]. Umit Cocen, KazimoneI. *Ductility and strength of extruded SiC/ Aluminium-alloy composites*.
- [12]. W.D. Waither, *techniques of improving strength and ductility of Al alloy castings*, trans. AFS 62(1954) 219-227.
- [13]. R.W. Ruddle , *solidification of castings*. J .inst met, 77(1950)37-69.
- [14]. R.A. Flinn, *copper base casting alloys-physical properties and void volume correlation with solidification*, Trans AFS 67(1959)385-398.
- [15]. A. Couture, *solidification behavior and mechanical properties of Al-12% Si plate castings*, Trans AFS 74(1966)164-178.
- [16]. M.V. Chamberlin, *Effect of chilling on strength and hardness of Al-Cu alloy plate castings*, Trans AFS 34(1946)648-658
- [17]. S. Seshan, M.R. Seshadir, *Action of chills on soundness of Al-45% Cu alloy castings* , Br. Foundryman, 61(1968)339-347.
- [18]. J.T. Berry, *solidification behavior of Al-12% Si end chilled plate casting on dendrite arm spacing and microstructure*, Trans AFS 78(1970) 421-432.
- [19]. K.V. Prabhakar, G.P. Reddy , *influence of chills on soundness of Al-12%Si alloy castings*, Trans AFS 87(1979) 377-385.
- [20]. D.J. Towle, C.M. Friend, *the effect of alumina fiber array on the age hardening characteristics of an Al-Mg-Si alloy*, Scr. Metall, 26(1992) 437-442.
- [21]. Joel Hemanth, *tribological behavior of cryogenically treated B₄C/Al-12%Si composites*.
- [22]. K.M. Shorowordi, A.S.M.A. Haseeb, J.P Celis. *Trio-surface characteristics of Al-B₄C and Al-SiC composites worn under different contact pressures*.
- [23]. Kirity Bhusan Khan, T.R.G. Kutty, M.K. Surappa. *Hot hardness and indentation creep study on Al-5% Mg alloy matrix-B₄C particle reinforced composites*.
- [24]. Ozkan Sarikaya, Selahaddin Anik, Salim Aslanlar, S. Cem Okumus, Erdal Celik. *Al-Si/4C. Composite coatings on Al-Si substrate by plasma spray technique*.

On A Group with a Faithful Ordinary Representation

Chun P. B., Gau P. D., Babangida B. G., Tiya P. A.

Abstract: This communication provides an Improvement on an established result which has been proven earlier by Brauer in [1]. Brauer proved that, for a solvable (soluble) group G with a faithful ordinary representation of degree $m < P-1$ for a Prime p , G has a normal, abelian sylow p -subgroup say Q .

In this paper, the assumption that G is solvable is dropped and the existence of such an abelian, normal sylow- p subgroup is established with the provision that the degree of such a faithful ordinary representation is reduced from $m < (p-1)$ to $m < \frac{1}{2}(p-1)$. The prove of our claim is obtained by a series of lemmas using the method of contradiction.

Key Words: A solvable group, sylow- P -group, faithful representation, irreducible representation, group character.

I. INTRODUCTION

Brauer had early in 1943 [1] proved that for a solvable group G , which has a faithful ordinary representation of degree say “ m ” less than $P-1$, G has a normal abelian sylow p -subgroup. We observe that if G is a faithful KG -module V of dimension $m \leq P-1$, then its sylow- P -subgroups are always abelian. Indeed, if Q is a sylow p -subgroup then the restriction irreducible constituents of V_Q divides $|Q|$. since $m < P$, this means that the irreducible constituents of V_Q all have dimension 1. Moreover, since V is faithful, this shows that Q is abelian. Obviously Q is also normal.

LEMMA 1.1

Let H be a normal subgroup of the group G . let χ be an irreducible ordinary character of G such that $H \subseteq \text{Ker } \chi$ and suppose that some $x \in G$ satisfy $C_H(x) = 1$ then $\chi(x) = 0$

Proof: We enumerate the irreducible ordinary characters of G so that $\chi_1, \chi_2, \dots, \chi_r$ has H in their kernels and $\chi_{r+1}, \dots, \chi_s$ does not contain H in their kernels. The condition that $C_H(x) = 1$ shows that $|C_G(x)| = |C_{G/H}^{(Hx)}|$. Indeed each H_x centralizing Hx in G/H contains exactly one element of $C_G(x)$. The characters χ_1, \dots, χ_r correspond to a complete set G of irreducible characters for G/H . So the usual orthogonality relations give

$$\sum_{i=1}^r |\chi_i(x)|^2 = |C_{G/H}(Hx)| = |C_G(x)| = \sum_{i=1}^s |\chi_i(x)|^2$$

Hence $\chi_{r+1}(x) = \dots = \chi_s(x) = 0$.

MAIN RESULT

Our main result which does not assume that G is solvable is given in the theorem 1.2 below.

THEOREM 1.2:

Let G be a group with a faithful ordinary representation of degree $m < \frac{1}{2}(P-1)$, then G has a normal abelian sylow P - subgroup say Q .

Proof: To prove the theorem, we shall suppose that the theorem is false and then obtain a contradiction. To achieve this, we now assume that G is a minimal counter example. Thus G has a faithful ordinary character χ of degree $m < \frac{1}{2}(P-1)$ and clearly G is not abelian so $m > 1$

Let Q be a sylow P -subgroup of G , it implies that Q is abelian. We now proceed on the proof in a series of lemmas;

LEMMA 1.3

For each normal subgroup H of G with $H \neq G$, $H \cap Q \leq Z(G)$

Proof: Since G is a minimal counter example, $Q_P(H)$ is the sylow P -subgroup of H .

Put $L = C_G(O_P(H)) \Delta G$. Since Q is abelian, $Q \leq L$. if $L = G$, then $Q = O_P(L)$ by minimalism of G and so $Q \Delta G$ since $L \Delta G$. this is contrary to the hypothesis, so $L = G$, hence $H \cap Q \leq O_P(H) \leq Z(G)$ and this implies that $H \cap Q \leq Z(G)$. \diamond

LEMMA 1.4

Let G^1 be the derived group of G , then $G = G^1$

Proof: Since $Q \leq Z(G)$, it follows from Lemma 1.3 that $QG^1 = G$. Suppose that $G^1 \neq G$, then $G^1 \cap Q = 1$. Since Q is not normal in G , we can choose a prime q so that q divides $|G:N_G(Q)|$

Let T be a sylow q -subgroup of G for each $x \in G$, $x^{-1}Tx$ is also a sylow q -subgroup of G^1 so $x^{-1}Tx = y^{-1}Ty$ for some $y \in G^1$.

This shows that $x \in N_G(T) \leq N_G(T)G^1$, this holds for all $x \in G$

So $G = N_G(T)G^1$. Hence $N_G(T)$ contains a sylow P -subgroup T_1 , say of G . consider now the subgroup TT_1 , then $T \Delta TT_1$, so TT_1 is solvable on the other hand, since T_1 is conjugate to Q , the choice of Q shows that $T \leq N_G(T_1)$. So T_1 is not normal in TT_1 , which contradicts Brauer's theorem.

Thus $G = G^1$ as claimed.

LEMMA 1.5

χ is irreducible.

Proof: Suppose χ is not irreducible, then we can write $\chi = \chi_1 + \chi_2$ as a sum of characters. By this choice χ, χ_1, χ_2 are not faithful and so by the choice of $G, O_Q(G/\text{Ker}\chi_i)$ is the sylow P-subgroup of $G/\text{ker}\chi_i$ ($i=1,2,3,\dots$)

Then $O_Q(G/\text{Ker}\chi_1 \times G/\text{Ker}\chi_2)$ is the sylow P-subgroup of $(G/\text{Ker}\chi_1 \times G/\text{Ker}\chi_2)$ since $\text{Ker}\chi_1 \cap \text{Ker}\chi_2 = \text{Ker}\chi = 1$. There is an injection homeomorphism of G into this latter group given by $\chi \rightarrow (\chi/\text{Ker}\chi_1, \chi/\text{Ker}\chi_2)$. But that implies that $O_Q(G)$ is the sylow P-subgroup of G contrary to the hypothesis i.e G is minimal. Thus χ is irreducible. \diamond

LEMMA 1.6

$Z(G)$ is the unique maximal normal subgroup of G . It is a P-group and $G/Z(G)$ is simple and non-cyclic.

Proof: Let H be a maximal normal subgroup of G , then the subgroup $QH \neq G$; for otherwise $G/H \cong Q/Q \cap H$ is abelian and so $H = G$ by lemma 1.4. But by Lemma 1.3, $Q \cap H \leq Z(G) = Z(G) \cap G^1$; so we have that $Q \cap H = 1$, since QH is a proper subgroup of G .

The minimalism of G shows that $Q \triangleleft QH$. But $H \triangleleft QH$, so $QH = QXH$. This shows that $Q \leq C_G(H) \triangleleft G$. Since $Q \not\leq Z(G)$, Lemma 1.3 now shows that $C_G(H) = G$, so $H \leq Z(G)$. Since G is non-abelian and H is maximal subgroup, $H = Z(G)$. Since $H \cap Q = 1$, we have that $Z(G)$ is a P-group. Since H is a maximal normal subgroup, $G/Z(G)$ is simple. Finally $G/Z(G)$ is non-cyclic since otherwise G would be abelian \diamond

LEMMA 1.7

Let $N = N_G(Q)$ and $N_0 := \{x \in N / C_Q(x) \neq 1\}$ then

(a) $x^{-1}Qx \cap Q = 1$ for all $x \in G/N$

(b) $x^{-1}N_0x \cap N_0 = \begin{matrix} N_0 & \text{if } x \in N \\ Z(G) & \text{if } x \in G/N \end{matrix}$

REMARK: Before we continue, we introduce the following notations. Let $|G| = P^e$, $|Z(G)| = P^e$ and $|N| = P^e h$.

Let $\chi_i = \chi_{i1}, \dots, \chi_{i2}, \dots, \chi_{is}$ be the irreducible ordinary characters of G and write

$(\chi_i)_N = \alpha_i + \beta_i$, ($i=1,2,3,\dots$) where α_i is the sum of the remaining irreducible constituents of $(\chi_i)_N$, none of which contain Q in their kernels and β_i is the sum of the remaining irreducible constituents. Since the representation affording χ_i is scalar on $Z(G)$, then $|\beta_i(x)| = \beta_i(1)$ for all $x \in QZ(G)$.

LEMMA 1.8

For each $i > 1$ we have that, $\beta_i(1)^2 P^e < \chi_i(1)^2$.

Proof: It follows from (b) of lemma 1.7 that $N_0/Z(G)$ has $|G:N|$ distinct conjugates that are mutually disjoint. Therefore for $i > 1$,

$$\langle \chi_i, \chi_i \rangle = \frac{1}{g} \sum_{x \in G} |\chi_i(x)|^2 \geq \frac{|G:N|}{g} \left| \sum_{x \in N_0/Z(G)} |\chi_i(x)|^2 + \frac{1}{g} \chi_i(1)^2 \right|$$

For each irreducible character χ_i , $|\chi_i(x)| = \chi_i(1)$

whenever $x \in Z(G)$

therefore $1 > \frac{1}{|N|} \left\{ \sum_{x \in N_0} |\chi_i(x)|^2 - |Z(G)| \chi_i(1)^2 \right\}$

$$\frac{1}{|N|} \sum_{x \in N_0} \left\{ |\alpha_i(x)|^2 + \alpha_i(x)\beta_i(x) + \alpha_i(x)\beta_i(x) + |\beta_i(x)|^2 \right\} - \frac{1}{hp1/2^e} \chi_i(1)^2$$

$$\geq \langle \alpha_i, \alpha_i \rangle + 2 \langle \alpha_i, \beta_i \rangle + \frac{1}{h} \beta_i(1)^2 - \frac{1}{hp1/2^e} \chi_i(1)^2$$

Since $\alpha_i = 0$ on N/N_0 by lemma 1.1 and $|\beta_i(x)| = \beta_i(1)$

On $QZ(G)$ by the definition of β_i . However, the definition of α_i and β_i shows that

$\langle \alpha_i, \beta_i \rangle = 0$. Moreover since $\chi_i \neq \chi_1 = I_G$, lemma 1.6 shows that $Q \leq \text{ker}\chi_i$. So $\alpha_i \neq 0$.

Therefore we conclude that;

$$\chi_i(1)^2 = P^e \{ \beta_i(1)^2 + h \langle \alpha_i, \alpha_i \rangle - h \}$$

$$\geq P^e \{ \beta_i(1)^2 \}$$

LEMMA 1.9 $(I_Q)^G = \sum_{i=1}^e \beta_i(1)^2 \chi_i$

Proof: By Frobenius reciprocity,

$$\langle I_Q^G, \chi_i \rangle = \langle I_Q, (\chi_i)_Q \rangle = \langle I_Q, (\alpha_i)_Q + (\beta_i)_Q \rangle$$

By the definition of α_i and β_i ,

we have that; $\langle I_Q, (\alpha_i)_Q \rangle = 0$ and $\langle I_Q, (\beta_i)_Q \rangle = \beta_i(1)$ and so the result follows.

PROOF OF MAIN RESULT (THEOREM 1.2)

We first show that $m \leq 1 + \sum_{i=2}^s \langle \chi_i, \chi\chi \rangle (\beta_i)(1)$. Now by lemma 1.9 we have that;

$$\sum_{i=2}^s \langle \chi_i, \chi\chi \rangle (\beta_i)(1) = \langle (I_Q)^G, \chi\chi \rangle$$

$$= \langle I_Q, (\chi\chi)_Q \rangle$$

$$= \langle \chi_Q, \chi_Q \rangle = \chi(1) = m$$

Since χ_Q is a sum of $\chi(1)$ characters of degree 1. Since $\langle \chi_i, \chi\chi \rangle (\beta_i)(1) = \langle \chi, \chi \rangle = 1$. The assertion follows. Therefore from lemma 1.8, it follows that;

$$m \leq 1 + \frac{1}{p^{1/2^s}} \sum_{i=2}^s \langle \chi_i, \chi\chi \rangle (\chi_i)(1)$$

$$= 1 + \frac{1}{p^{1/2^s}} \{ \langle I^G, \chi\chi \rangle - 1 \}$$

$$\text{Because } I^G = \sum_{i=2}^s \chi_i(1) \chi_i$$

$$\text{Since } \langle I^G, \chi\chi \rangle = \chi(1)^2 = m^2. \text{ This shows that } p^{1/2^s} \leq \frac{m^2 - 1}{m - 1} = m + 1.$$

But $m + 1 < \frac{1}{2}(p + 1)$ by hypothesis and so $m = 1$.

However by Lemma 1.4 this means that the hypothesis of Brauer's theorem is satisfied, and that shows our counter example is impossible. This completes the proof of our main results (Theorem 1.2).

II. CONCLUSION

We have been able to establish through a series of Lemmas that if the condition on Brauer's theorem that the group G be soluble is dropped, then the condition that G be of degree say $m < (p - 1)$ for a prime P, would now be that G is of degree $m < \frac{1}{2}(p - 1)$ and the result would still hold i.e there would exist a normal abelian Sylow P-subgroup say Q for G provided G has an ordinary faithful representation.

REFERENCES

- [1]. Brauer, R (1943) On Permutation groups of prime degree and related classes of groups. Annals of mathematics, 44,57-59
- [2]. Momoh, S.U (2003) on faithful ordinary representation of groups. Abacus Vol 30 No 2B PP 269-274
- [3]. Bentse, P.C (2008) Existence of a normal abelian Sylow P-subgroup of a group with a faithful ordinary representation.
- [4]. Isaac, L.M (1976) Character theory of finite groups Academic Press new-York PP 29-35
- [5]. Puttaswamaiah, B.M (1977) Modula representation of groups
- [6]. Walter, L (1972) A handbook of applicable mathematics Volume 1 Wiley-Inter-Science Publication Chichester – New York
PP 262-282

Environmental Issues of the Ajaokuta Steel Complex in Nigeria

Mohammed A. Al-Amin

(Department of Geography, Nigerian Defence Academy, Kaduna)

ABSTRACT: The aim of this article is to analyse the various industrial processes in the Ajaokuta and the waste products each produces, with the view to highlighting some conservation measures that will enhance the environmental management plan of the Ajaokuta steel complex. A background information was provided on the general production system of steel, was provided, before a detailed description of major plants in the complex that produce environmental wastes, these included Sintering Plant, Cake Oven, Blast Furnace, Iron and steel making plants, Rolling Mills and the Thermal Power Plant. Pollution inventory of these were made and its highlights revealed that the Cake oven and Sinter plants are highly polluting, while the Electric Arc Furnace (EAF) and Electric Induction Furnace (EIF) plants that use scrap and DRI are relatively less polluting due to lower scales of operation and the nature of the feedstock being used in the Ajaokuta complex. Generally the air pollutants most visible are those of particulate matter, oxides of sulphur and nitrogen. Some corrective measures were proposed including the introduction of emission control technologies like scrubbers, bag filters and electro static precipitators. Water quantity and quality measures were also recommended in order to reduce water use from the existing $15\text{m}^3/\text{tcs}$ to less than $5\text{m}^3/\text{tcs}$. Similarly the existing volume of solid waste being generated by the processes inventoried at 600 to 800kg per ton of steel and adequate measures were recommended in order to reduce it to the global average of 400 to 500 kg per ton of steel.

Keywords: Environment, Steel, Ajaokuta, Pollutants, Emission, Sludge

I. INTRODUCTION

Steel as a finished product may be one of the most environment friendly products used in our daily life, owing to its excellent mechanical properties, versatility and its recyclability. Today steel usage also ranges from the ordinary household items to the complex construction and defence equipments. However, the process of steel making itself is highly energy and fossil fuel intensive and therefore the cause of environmental concerns across the world. In fact, the manufacturing process involves a myriad operations which may contribute to three basic sources of pollution i.e., of Air via volumes of emissions by the plants, of water via liquid effluents discharged and of soil via disposal of solid wastes.

Steel can be defined as an alloy of iron and carbon. The carbon in steel varies from 0.04 – 1.7%. By nature of the raw materials and method of producing steel, all steels contain varying amounts of sulphur, manganese, phosphorus and traces of other elements. When other elements are added to the steel, such as chromium, cobalt, or nickel, the steel becomes an alloy steel (Agba 2006; DCM 2012; AISi 2005). Steel making may therefore be defined as the production of an extensive series of complex alloys of iron, carbon and other elements. There are many processes for making steel which had developed over time with the production of iron bloom or sponge iron, to wrought iron and to higher quality steel produced in through the crucible technique (Oyebanji and Oluwale, 1988; Banergee 2002). The crucible technique is a system that allowed broken ingots of bloom to be heated in crucibles for long period of time.

There are basically two methods of steel production which are the Basic Oxygen Furnace/Blast Furnace (BOF/BF) and the Electric Arc Furnace/Direct Reduction (EAF/DR). For the purpose of this article, the process of steel making using the Basic Oxygen Furnace/Blast Furnace (BOF/BF) method will be discussed because that is the method that was designed for the Ajaokuta Steel Plant. The work therefore focuses on the process of making steel, the structure and operation of the Ajaokuta Complex, It went further to discuss the various units of the plant and the impact of the industry on Air and water quality as well as on solid waste generation and the impacts on the immediate environment and the carbon foot print in general.

II. OVERVIEW OF STEEL PRODUCTION SYSTEMS

Steelmaking in integrated plants is a complex of at least five industrial units related vertically to each other which are referred to as the primary plants. There are also a number of supportive facilities not directly involved in the production of steel but which are essential to the plant's operations. These supportive facilities are referred to as the secondary plants. A typical steel plant makes use of four basic raw materials, namely: coal, iron ore, fluxes and scrap. It also makes use of a number of other essential inputs like refractories, water and electric power. (Sato, 2009; AGM 2012; Deshpande 2008)

The first stage in steel production begins with good quality coal or coking coal being fed into the coke ovens, which is the first major unit of a steel plant. In addition to the coke produced from the coke ovens, important by-products such as coal tar and coke oven gas are also produced which may be sold or used as fuel by the plant itself. The second stage is the preparation of iron ore concentrates, limestone combined with the processed coke and fed into the Blast Furnace which is the second major unit of a steel plant. The blast furnace produces molten iron either by smelting lump ore or artificial iron bearing materials such as sinter and pellets. The Coke serves as a reducing agent, its carbon forms a chemical union with the oxygen in ore. Fluxes are a third essential input of the blast furnace. It facilitates the separation of metal from impurities in iron ore. The most commonly used fluxes are limestone and dolomite. The desired combination of iron bearing materials, coke and fluxes is known as the *charge*.

The third stage is the transfer of the principal product of the blast furnace which is hot metal to the iron making shop which is the third major unit. The hot metal will then be cast into pig iron and sold. It could also be formed and molded into several shapes of iron depending on the future use of such iron. Some steel making plants by passes this stage with the recent technology and transports the hot metal directly to the steel melt shop which is the fourth major unit of a steel plant.

The steel melt shop as earlier stated is the fourth stage of a steel plant. It receives hot metal or pig iron and adjusts the composition of carbon and other impurities to form steel. A most important part of any steel plant that uses the blast furnace method of production is the converter. This is usually a pear-like shaped vessel with a spherical bottom, cylindrical middle portion and a conical top. It is lined in the interior with basic refractories usually tar-bonded unburnt dolomite, magnesite, and magnesite - chromite bricks. The converter is solely used to effect the conversion of molten pig iron into steel without the use of fuel for heating the metal. This is achieved by blowing a current of air (oxygen or other gaseous matter capable of evolving oxygen) to the molten pig iron contained in the converter.

The fifth stage is the movement of the steel produced in the steel melt shop to the fifth major unit of an integrated steel plant which are the rolling mills. Only a relatively small amount of additional rolling is necessary to produce bars, structurals, rails and plates. To produce sheets, slabs may first be rolled into strips, then, finished in a cold rolling mill, and in some plants, galvanized, tinned, or corrugated. It is germane to note that steelmaking has had a long history that included constant improvements in the techniques of making and using steel products.

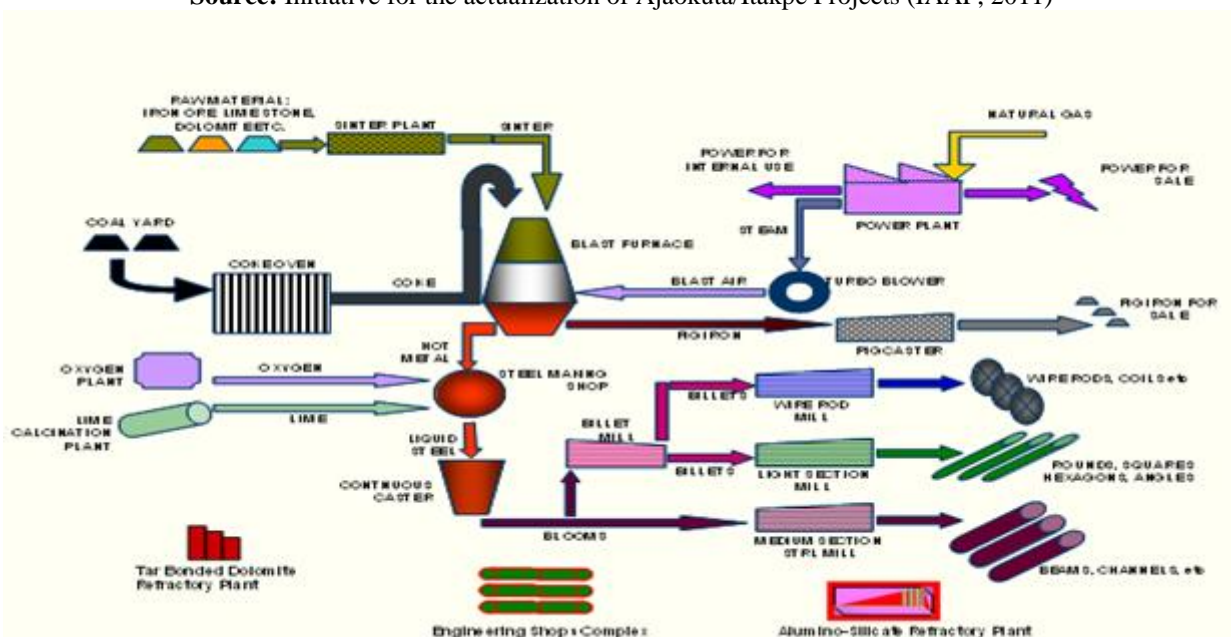
III. THE AJAOKUTA STEEL PLANT

The Ajaokuta Steel Project was designed to produce long products like iron bars, wire rods, angles, squares, channels, beams, and structures in its first phase. Most of the products were expected to be used in the civil engineering and construction industry. The structure and operation of the Ajaokuta steel plant has no spectacular difference with other steel plants around the world using the blast furnace method of steel production. The primary and secondary plants of Ajaokuta steel plant have reached about 98% stage of completion.

The Ajaokuta Integrated Iron and Steel plant is based on the Blast Furnace /Basic Oxygen Furnace (BF-BOF) process of iron making. This process, often referred to as the conventional method has been acknowledged by steel experts to be the most versatile means of producing crude steel. The method accounted for over 70% of steel production in the world. The Ajaokuta Steel Plant has a raw materials preparation unit, a sintering plant, Coke-oven unit, the iron making plant, steel making plant and the rolling mills known as the primary plants. The Ajaokuta steel was built in its conception with four rolling mills. These are 150mm Wire Rod Mill, 320mm Light Section and Bar Mill, 700mm Medium Section and Structural Mill and 900/630 semi-continuous Billet Mill.²⁰ Two of these mills, the light section and Wire Rod mills were originally supposed to be the priority rolling mills. This meant that these priority rolling mills was accorded accelerated speed in their construction so as to produce steel with imported billets and scraps while the blast furnace and other components of the steel plant were on going. These priority mills were actually completed and commissioned between 1983 and early 1994 and production started with imported billets (Agbu, 2006, Audu 1992; Easter et al 2009)

FIG 1: AJAOKUTA STEEL PLANT PROCESS CHART

Source: Initiative for the actualization of Ajaokuta/Itakpe Projects (IAAP, 2011)



3.1 RAW MATERIALS PREPARATION UNIT:

This is the unit of the Steel Project that is responsible for the handling of unprocessed or partially processed material used as inputs for processing operation. This unit receives about 2.135 million tons of iron ore in concentrated form annually. Other raw inputs handled by this unit includes coking coal which is about 1.32 million tons in a year, limestone whose supply is about 669 million tons in a year. The unit also receives 250 million tons of dolomite and 85 million tons of manganese ore annually. This unit over time especially in the early 1980's received some of these raw materials but not up to half of the expected capacity due to the non completion of the blast furnace and other infrastructural facilities like the warri – Portharcourt- Onne railroad.

3.2 SINTERING PLANT AND COKE OVEN UNIT:

The Sintering Plant comprises of a sinter machine with a sintering area of 360m² & one straight cooler having cooling area of 420m². The capacity of the plant is 600 t/h of sinter. The sintering plant removes some of the impurities of artificial iron bearing materials such as sinter and pellets.

The coke oven unit is a rectangular shaped room of about 10-15 meters long, 3-7 meters in height and a volume of 30.3 cubic meters. It is closed at each end by a removable cast iron or steel door. This unit primarily handles the blending of coking coals. The unit is built in such a flexible manner that it is able to blend coking coals from different local and external sources. (Ajasteel, 1981, Audu 1992; Halliday et al 2009)

3.3 BLAST FURNACE AND IRON MAKING PLANT:

The blast furnace has been regarded as the heart of the steel plant. Ajaokuta has a proposal for two blast furnaces in the first phase. The construction of the blast furnaces began in 1982 and by 1987, one of the furnaces was 100% completed, the other is about 15% complete as at 1994 when the Soviet company, TPE's contract was determined. A single blast furnace has a capacity of 2000 cubic meters capable of producing 1.35 million tons of hot metal annually. This furnace is designed to function under high pressure. About 1.2 million tons of molted iron are expected to be produced in a year and passed to the steel making shop for further processing while about 150,000 tons of molted iron remaining in the iron making plant are cast in the pig casting machine for the provision of pig iron used in local foundries. It should be noted that the blast furnace has never been put to use since its construction because according to the Assistant General Manager, Blast Furnace, if the blast furnace is lit, it cannot be put off until after ten years. The implication is that, the blast furnace will be working twenty four hours producing hot metals which Ajaokuta steel plant has not made adequate preparation for. But with the completion of the steel project, and all units working, the availability of raw material that can sustain the blast furnace, the blast furnace will be put to maximum use.

The iron making plant is one of the principal units of the Ajaokuta Steel Project. It is essentially a vertical cylindrical steel shell. It has an average height of 33 meters and a diameter of 8.4 meters. The shell acts as a container through which iron ore descends and 90% of these iron ore is reduced to pig iron through the blast furnace process of iron making.

3.4 Steel Making Unit And Rolling Mills:

This is often called the steel making shop. It is the place where various processes for steel making from pig iron take place. The unit is of two top blown oxygen converters of 135 tons each. The converters require rich oxygen injection for the refinement of hot metal to steel. The major products of this unit are blooms which are sent to the rolling mills within the plant.

Rolling mills is the unit in which the iron product is fed past spring loaded rollers that apply force against the side of a revolving bowl. It is actually a grinding mill. This unit consists of the wire rod mill (WRM), the billet mill (BM), the medium section and structural mill (MSSM) and the light section mill (LSM). The wire rod mill has the capacity of producing 130,000 tons of wire rod coils with 5,000 tons of scrap sent to the scrap processing unit annually.()

The billet mill has the capacity of producing 295 million tons of saleable billets. 150,000 tons of billets used in the medium section and structural mill and 40,000 tons of scrap for the scrap processing unit. The medium section and structural mill has the capacity of producing about 560,000 tons of medium section and structural steel and 65,000 tons of scrap for use in the scrap processing unit. The light section mill has the capacity of producing about 400,000 tons of scrap that is sent to the scrap processing unit.

3.5 The Thermal Power Plant

The Thermal Power Plant (TPP) which is a Captive Power Plant has two turbo-generators of 55MW each with a full capacity of 110MW. It supplies electricity to the steel plant and the steel township. The Steel plant cannot do without constant power supply due to the equipments which needs cooling to maintain its lifespan. The blast furnace uses electricity and as earlier discussed, if lit, it will remain on for about ten years and it needs this power to keep it on. The Ajaokuta Steel Plant cannot exhaust the 110 MW produced. It actually consumes about 65MW. At a time, the excess was sold to the national grid but due to non maintenance and lack of gas, the plants do not supply to the national grid any longer. (Sato, 2009, Ajasteel 1983; IAAP,2011)

IV. Environmental Issues And Solution In The Ajoakuta Plant

As already mentioned the manufacture of steel from ore involves a large number of operations covering large scale usage of mineral resources and high levels of energy consumption. While the large integrated steel plants based

on the BF-BOF route (with associated coke ovens & sinter plants) are highly polluting, the EAF and EIF route using scrap and DRI are relatively less polluting due to lower scales of operations. The coal based DRI of the Ajaokuta complex units also are often criticized for not adopting/operating pollution control facilities. The environmental issues associated with the Ajaokuta complex can be treated under the following topics;

4.1 Air Environment:

The environmental concern with respect to air pollution by the industry arises mainly due to particulate emissions (dust) from process and non process operations. The emissions of volatile matter associated with coke oven and dioxins from sinter plant operations also have serious health implications. Other gaseous pollutants like oxides of sulphur and nitrogen are another cause of worry wherever the Integrated Steel plants are large and are located in the vicinity of large thermal power plants as the in the case of Ajaokuta complex.

The specific emissions of air pollutants like dust, oxides of sulphur and nitrogen in the steel plants are still above 1.0 kg per ton of steel as compared to less than 0.5 kg per ton of steel in developed countries. A substantial reduction in specific air emissions may be possible with introduction of larger capacity units like sinter plants, blast furnaces, taller coke ovens, increased size of steel converter etc, by reducing the number of process operations. But given the very high operational costs linked to air pollution control, the introduction of state of the art pollution control facilities in smaller units, though technically feasible, may not be economically viable to the Ajaokuta Industry. There is a need to limit the capacity of the processing units to a threshold level.

As regards high dust emissions from the sponge iron units based on coal, this has attracted adverse opinion leading to suspension of operations of some of the units. The high emissions are mainly due to inadequate design of pollution control systems to handle widely varying type of raw materials in the kilns. Since this route is the main supplier of raw material for secondary steel production, there is an urgent need to share the best practices for environment control by developing a Best Available Technology (BAT) document for the secondary steel sector.

Over the years, there has been substantial improvement in particulate control technologies like scrubbers, bag filters and electrostatic precipitators. Bag houses (bag filters) have now emerged as the main technology for dust control in steel plants with capabilities to meet extremely stringent emission standards at marginally high cost. The efficiency of installed dust control equipment in some of the steel plants however continues to be poor, due to improper design of hoods and mismatch of estimated and installed ventilation volumes. Considering the very high energy cost of operation, there is an urgency to introduce improved practices for design of control equipment for effective capture and control at lower cost. The use of mathematical models like Computational Fluid Dynamics (CFD) can be very useful in this respect.

The control of fugitive dust emissions from non process operations is another major concern in the Ajaokuta steel plants and some of the available technologies for their control are as given below:

Table 1: Suggested Technologies to Control Dust Emissions

Area	Control systems
1. Raw material handling	Bag filters, Dust suppression, Enclosures
2. Raw material storage	Wind nets, Covering by tarpaulins, Chemical spray, Green belt
3. Raw material movement	Tyre washing, Covering of material, Speed control
4. Sinter/pellet plant	Large capacity ESP or bag filter
5. Coke ovens	
Coal charging emissions in coke ovens	Efficient aspiration of COG in top charge batteries. Dedusting car or charge gas transfer car in stamp charged batteries.
Coal carbonization	Good oven doors, Water sealed AP caps, good operational practices
Coke pushing emissions	Stationary bag filters
6. Blast furnace	Bag filters for stock house and Cast house dedusting.
7. Hot metal pretreatment	Bag filters for secondary emissions
8. Secondary dust emissions from BOF, EAF, Furnaces	Large capacity Bag filters

As may be noted, the major contributory factors to air pollution by the industry are on account of the quality of raw materials, operational practices, process controls etc.

All these factors may separately or else jointly be responsible for fugitive emissions and need to be addressed accordingly. (Jones et al 1988)

In integrated steel plants, sinter plant and thermal power plants are the major sources of emission of SO_x and NO_x. Several technologies for control of sulphur dioxide and nitric oxides from waste gases have been developed in

other countries, though at very high costs. The use of low sulphur coal in coke ovens and desulphurization of coke oven gas can lead to reduction of more than 80% of SO₂ emissions from the steel plants and is recommended for SO₂ control. Further reductions can be made by introducing desulphurisation of waste gases from sinter plants, though at extremely high capital and operating costs. Similarly NO_x emissions in the plants can be controlled by use of staged burners, suitable selection of fuels etc. Further reductions can be made by introducing denitrification of waste gases from sinter plants, though at extremely high capital and operating costs.

The state of the art technologies available for emissions control in various areas of the steel plant are given below:

Table 2: New Available Technologies for Control of Emissions

Area	Technology
Coke Ovens	Induced aspiration of leaking gases by HPAL or steam. Forced aspiration by ID fans Individual oven pressure control during coal charging Coke pushing emission control with stationary bag filters
Sinter Plant	Dust :Air fine system(VAI) ESP: Pulse energisation (Coromax); Movable electrode (Mitsubishi) Gas & dust conditioning DeSO _x & DeNO _x : Lime injection ; wet scrubbing after ESP ; Activated carbon Dioxin removal by high efficiency particulate control
Blast furnaces	Secondary emission control during charging. Dry gas cleaning using bag filters. Cast house fume extraction systems,
Steel melting	BOF: Dry type ESP for gas cleaning

4.2 WATER ENVIRONMENT:

The steel making process involving high temperature operations also uses a large volume of water in cooling and cleaning operations. Over the years, the fresh water consumption for steel production has been brought down from 12-15m³/tcs to less than 5 m³/tcs, with some integrated steel plants operating at volumes less than 3.0 m³/tcs, against a norm of 5m³/tcs for flat and 8 m³/tcs for long products.

Total water management audits will help in identification of potential areas for improvement and ensuring transition to zero discharge. Some of the techniques/technologies considered necessary to ensure zero discharge by the steel industry may include the following:

Table 3: Recommended Techniques/ Technologies for Water Management

Area of water usage	Measures
Water storage	Use of chemicals to reduce evaporation from large ponds
Fresh Water treatment	Use of slurry dewatering equipment; Control of TDS in fresh water by suitable mixing
Water usage in cooling Towers	Continuous Blow down control; use of chemicals; Fin-Fan heat exchangers; Improved COC; leakage control; High recycle rates aiming at >98% recycling
Water cascading	Blow down from one unit to be used as make up of another unit, after assessing water chemistry
Water reuse	In less critical applications like ore washing, slag and coke quenching; gardening, spray on raw material yards and roads etc
Reverse osmosis	Recovery of good water from blow down water
Evaporation of RO rejects	In evaporators using steam/electricity.

The existing technology for water treatment systems in Ajaokuta steel plants are at par with the best available for the industry and the performance of steel plants in terms of meeting compliance to wastewater discharges has also been satisfactory except for coke ovens, with respect to presence of cyanides. Further, several modifications and upgrades of the coke oven wastewater treatment are also necessary in the steel plants to improve the performance. Another area of concern is the usage of treated wastewater from coke ovens after the introduction of coke dry quenching technology in coke ovens and this aspect needs to be taken into account while planning installation of CDQ facilities.

4.3 SOLID WASTES

During the iron and steel making process, the impurities present in the raw materials like iron ore, lime stone and coal are normally removed as slag. Further, the operations of air and water pollution control equipment generate dusts and sludge. Currently this volume of solid wastes generated in the Ajaokuta plants is relatively high at 600-800 kg per ton of steel as compared to 400-500 kg in developed countries. This is mainly due to higher impurity

levels in the raw materials. The steel industry has been successfully converting these wastes into useful byproducts for recycling or else for use as a raw material in other industries, but that is not the case in the Ajaokuta Plants

The limited use of steel slag from BOF and EAF in Indian steel plants (less than 30%, mainly used in sinter plant as lime substitute, and use of recovered metallic in steel making) remains a matter of concern. In contrast in developed countries, the steel making slag is used as construction material ensuring 100% utilization. The main reason for the lower domestic slag utilization may be attributed to the presence of free lime, which makes it unfit for construction industry due to its hydration and expansion after aging. Reportedly steel slag (with less than 5% free lime and a maximum 5% expansion during steam testing) can be effectively used as a construction material. This can be achieved by weathering of slag; granulation by air or water. JSW Steel has introduced a BOF slag granulation facility using water (BSSF technology) which is reported to reduce free lime content in the slag to less than 5%.

Steel slag can be effectively used as a material for construction, substituting other natural resources like aggregates and sand, first by developing a product standard for steel slag by the steel plants and later mandating its use in construction as has been done in case of fly ash. Steel slag after removal of metallic's can also be used as soil conditioner for conditioning acidic soils and also to some extent in cement making. The use of slag generated in hot metal pretreatment and secondary metallurgy is another potential area of use to be studied by the industry. (Oribe 1978; Rai 2006)

Dusts and sludge collected from air and water pollution control equipment is extremely fine and is currently recycled through sinter making. However, in case of larger units, the recycling of large volumes of micro fine dusts is problematic, as it hinders the productivity of sinter plant. Many of our integrated steel plants elsewhere in the world have evolved innovative means of recycling dust and sludge and this need to be adopted by the Ajaokuta steel plant. Some of the practices followed are as given below;

Table 4: Global Best Practices in handling Sludge and Dust

Process dusts/sludge	Interim usage	Preferred usage
ESP dust from sinter/pellet plants	Recycle in sinter plant	Micro pellets
Flue dust from Blast furnaces	Sinter plant depending on alkali loading	Micro pellets
Dust from bag filters of coke ovens	Power plants	Micro pellets
Sludge from gas cleaning plant of blast furnaces	Disposed	Micro pellets after dewatering
Dust from secondary fume extraction system (ESP or bag filter)	Sinter plant/ BOF Converters	Micro pellets for use in sinter plant/briquetting for use in
Sludge from gas cleaning plant	Sinter plant/BOF Converters	Micro pellets for use in sinter plant/briquetting for use in converters after dewatering
Mill scales from caster and Mills	Sinter plant, depending on oil content	Briquetting for use in BOF Converters.

Steel plant operations also generate hazardous wastes and the relevant global best practices in effective management of this hazardous waste cover the following:

Table 5: Global Best Practice in the Management of Hazardous Wastes

Area	Hazardous waste	Usage/Disposal
Coke ovens	Decanter sludge, BOD plant sludge, Tar sludge	Used in coke ovens
	Still bottoms	Incineration / Cement plant
Blast furnace	High zinc containing flue dust	Hazardous waste disposal or sale
Others	Acidic, alkaline sludge, sludge from water treatment,	Hazardous waste disposal
	Waste and used oils, electric wastes.	Sale to authorized agencies for recycling

It is to be noted that the management of dusts and sludge depends on the steel plant configuration and requires innovative solutions (Singhal 2009; Shah 2003 and Skrotzki 2002). There is therefore a need for the Ajaokuta Plant to obtain the experience of successful recycling schemes from other steel plants.

V. CONCLUSION

The Ajaokuta integrated Steel Plant and its thermal power plant were a product of an efficient design this then latest technological and environmental considerations in place. However, Forty years since that design several things have change in the steel making technology and the environmental/waste control and management. These changes were haven not incorporated in the Ajaokuta Complex.

Similarly, the various challenges encountered by the project in the construction and assemblage of the plants, which culminated into the change of Contractors and Engineers for five times have also confused the configuration process and is certainly affecting the environmental quality of the ecosystem.

It is therefore imperative for the Ajaokuta Steel Complex to be overhauled with the suggested environmentally friendly technologies that are recommended in this article. Further, a comprehensive environmental audit of the steel complex and the township is urgently necessary in order to determine the toxicity states of the various media, so that the ecosystem integrity and sustainability of the entire Ajaokuta region is assured.

REFERENCES

- [1] Agbu O. (2006): The Iron and Steel Industry and Nigeria's Industrialization: Exploring Cooperation with Japan. Institute of Developing Economy, Japan.
- [2] AGM Blast Furnace (2012): Interview with Technical Staff of the Ajaokuta Steel Company
- [3] Ajasteel (1981): General M. Ajaokuta Steel Project, Ajasteel News letter Ajaokuta press
- [4] Ajasteel (1983): Ajaokuta Steel Complex: The path to true IndustrilizationAjasteel News letter Ajaokuta press
- [5] Audu M.S. (1992): Transformation of Ajaokuta 1900-1990, unpublished M.A. Thesis Bayero University Kano
- [6] AISI American Iron and Steel Institute (2005) Saving One Barrel of Oil per Ton: A New Roadmap for Transformation of Steelmaking Process. <http://tinyurl.com>
- [7] Banerjee S. (2002), Process for making steel, "US Patent 6424671.
- [8] DCM Production (2012): Interview with Technical Staff of the Ajaokuta Steel Company
- [9] Dethloff F.H. (1979): "Process and apparatus for treatment of waste gases," US patent 4176019.
- [10] Deshpande M.V. (2008): Elements of Electric Power Station Design. Wheeler Publishing Company
- [11] Easter H. and SiemagSMS (2009): "Energy recovery technology for EAFs," presented at the International Convention on Clean, Green, and Sustainable Technologies in Iron and Steelmaking, Bhubaneswar, India.
- [12] Halliday D., Resnick R, Walker J., Fundamentals of Physics. Wiley.
- [13] IAAP (2011): Initiative for the Actualization of Ajaokuta/Itakpe Projects: The Ajaokuta Steel plant (PAST, PRESENT & FUTURE). A paper presented at the maiden conference on steel production in Ajaokuta.
- [14] Jones J.A.T., Bowman B., and Lefrank P.A. (1988): Electric Furnace Steelmaking, in the Making, Shaping and Treating of Steel, 525-660. Fruehan R.J., TheAISE Steel Foundation: Pittsburgh.
- [15] Oyebanjo O. and Oluwole A, (1988): Technological Change and Projection Execution IDRC Canada.
- [16] Oribe K.H., Watanabe, and Machida T. (1978): "Electric furnace waste heat recovery method and apparatus," US Patent 4099019.
- [17] Rai G.D (2006): Non Conventional Energy Sources, 17th Edition, Khanna Publishers: New Dehl.
- [18] Sato H. (2009): The Iron and Steel Industry in Asia: Developing and Restructuring. Institute of Developing Economy, Japan.
- [19] Singhal K.K. (2009): "Energy efficiency in steel industry & Clean Development Mechanism," presented at the International Convention on Clean, Green, and Sustainable Technologies in Iron and Steelmaking, Bhubaneswar, India.
- [20] Shah R.K. (2003): Fundamentals of Heat Exchanger Design. John Wiley and Sons Skrotzki B.G.A. & Vopat W.A. (2002): Power Station Engineering and Economy, 22nd Edition. Tata McGraw Hill.

Dynamic Voltage Stability Enhancement of a Microgrid with Static and Dynamic Loads Using Microgrid Voltage Stabilizer

Kenan Hatipoglu¹, Ismail Fidan², Ghadir Radman³

¹ Electrical and Computer Engineering Department, West Virginia University Institute of Technology, USA

² Manufacturing and Engineering Technology Department, Tennessee Tech University, USA

³ Electrical and Computer Engineering Department, Tennessee Tech University, USA

Abstract: Voltage stability is a dynamic phenomenon and in order to tackle the voltage stability problem more realistically, dynamic representation of all power system components is necessary. The influence of load on dynamic stability is significant. In most studies, load representation of power systems are considered as constant power type but in real life there are different types of loads as industrial, agricultural and residential etc. Loads in a power system have to be represented realistically by adding static and dynamic types of loads to the system. It is known that a major portion of load is induction motors. In this paper, microgrid test system will be expended to a point that various combinations of static and dynamic loads can be considered as loads. After modeling part, effectiveness of the microgrid voltage stabilizer (MGVS) developed for microgrids that have only constant power type of loads will be studied under various combinations of static and dynamic loads.

Keywords: Load modeling, Power grids, Voltage control, Voltage stability.

I. NOMENCLATURE

Subscript m – imaginary axis;

Subscript r – real axis;

V_0, P_0, Q_0 – initial conditions of the system, (Voltage, active power, reactive power respectively);

a_1 to a_6 – Parameters of ZIP load model;

K_{pf}, K_{qf} – Frequency sensitivity parameters;

e – First cage voltage;

Ω_b – Base radian electrical frequency;

σ – Slip;

x_R – Cage rotor reactance;

r_R – Cage rotor resistance;

T_M – Mechanical torque applied at the shaft;

T_e – Electrical torque;

x_m – Magnetization reactance;

x_s – Stator reactance;

r_s – Stator resistance;

H – Shaft inertia constant;

$V_{i\ des}$ – Desired voltage

$V_{i\ dyn}$ – Dynamic voltage

$\Delta V_{i\ err}$ – Per unit (pu) difference between the desired voltage and the dynamic voltage

ΔV_{err} – Total voltage deficiency

K – Gain constant

T_1, T_2 – Time constants

V_{MGVS} – Output of the controller

$\alpha_1, \alpha_2, \dots, \alpha_l$ – The weighting factors for load buses

II. INTRODUCTION

Load representation is a critical issue on approaching power system modeling realistically. Loads are still considered as one of the most uncertain components of a power system to model because of their randomness, different timescale properties and their statistical nature. The results of the stability studies of power systems depend on how the load models represent the real load types. Several studies have shown the crucial effect of load representation in voltage stability studies [1] - [2]. Induction motors (IM) are used for representing the dynamic part of the load models. Depending on the type of the user profile, between 50% and 70% of the entire load consists of three phase IMs [3]. Static Polynomial (ZIP) load types are also commonly used and can be classified into constant impedance (Z), constant current (I) and constant power (P) load. The power has a quadratic dependence on voltage for Z load. For an I load, this dependency is linear, and power is independent of voltage changes for P type of load.

In addition to load representation and modeling, increasing power demand is another leading issue exists for utility companies. More demand on power is stressing the generation system capabilities and transmission lines. Low efficiency of central plants and transmission and generation losses plus frequent power outages cost the United States hundreds of billion dollars per year [4]. Researchers are looking for alternatives that can fix those pricey problems without adding new

transmission lines. Integration of the distributed energy sources to main grid can be a possible answer for these questions but this concept has its own shortcomings. Therefore, researchers and scientists proposed a network called “Microgrid”. Several blackouts have been associated with voltage stability problems in a power system [5]-[6]. A fast voltage collapse can be avoided by using available dynamic reactive power capabilities sufficiently. Transferring the reactive power within long distances causes massive voltage drop for typical power systems. But this is not the case for microgrid systems. Sustaining the dynamic voltage stability for microgrids can be possible with coordinated compensation of reactive power sources because electrical distance between the loads and the sources of the reactive power are relatively short. This concept has been used for designing Microgrid Voltage Stabilizer (MGVS) [7].

In this study, a 21-bus microgrid system, as shown in Fig. 1, run by diesel engine generators (DEG) will be used and load types will be considered as IM and ZIP loads to make the microgrid environment as realistic as possible to investigate voltage stability issues. After adding the IM and ZIP loads to microgrid model, effectiveness of the MGVS will be investigated for all load types.

III. MICROGRID

A microgrid is a distributed energy system which is a part of a large power system and it is supported by one or more distributed generation (DG) units. Microgrids are almost 85% efficient and have combine heat and energy applications and lesser transmission losses [8]. Its capability of operating in parallel with the grid or being able to operate in islanding mode during power outages and disturbances provides higher flexibility and reliability of operation. In islanding mode, microgrids retain power availability, avoid lost productivity and blackouts.

The aim of a microgrid is to provide a value to both customer and utility by supplying to local loads [9]. Higher power quality, reduction in environmental pollutants, higher reliability of power distribution, and decreasing power line congestion can be listed as some of the benefits of the integration of microgrids into utility grid.

IV. MODELING OF LOADS

Previous studies on modeling of the microgrid itself [10] is extended to a point that all of its loads at the microgrid are converted to static and dynamic type of loads from constant power loads. In this section, modeling of dynamic and static loads will be presented.

1. STATIC POLYNOMIAL (ZIP) LOAD

ZIP Load Model is one of the oldest load representations. It is called ZIP because it is a combination of Z, I and P type of loads. Following equations represent the static polynomial load model [11]

$$P = P_0 \left[a_1 \left[\frac{V}{V_0} \right]^2 + a_2 \left[\frac{V}{V_0} \right] + a_3 \right] (1 + K_{pf} \Delta f) \quad (1)$$

$$Q = Q_0 \left[a_4 \left[\frac{V}{V_0} \right]^2 + a_5 \left[\frac{V}{V_0} \right] + a_6 \right] (1 + K_{qf} \Delta f) \quad (2)$$

2. INDUCTION MOTOR

In this study, third order single cage induction motor has been used [12]. The single-cage induction motor’s simplified electrical circuit can be seen in Fig. 2. The equations are formulated in terms of real and imaginary axes, with respect to the network reference angle.

The network and stator machine voltage is:

$$v_r = -V \sin \theta \quad (3)$$

$$v_m = V \cos \theta \quad (4)$$

The power absorptions are:

$$P = v_r i_r + v_m i_m \quad (5)$$

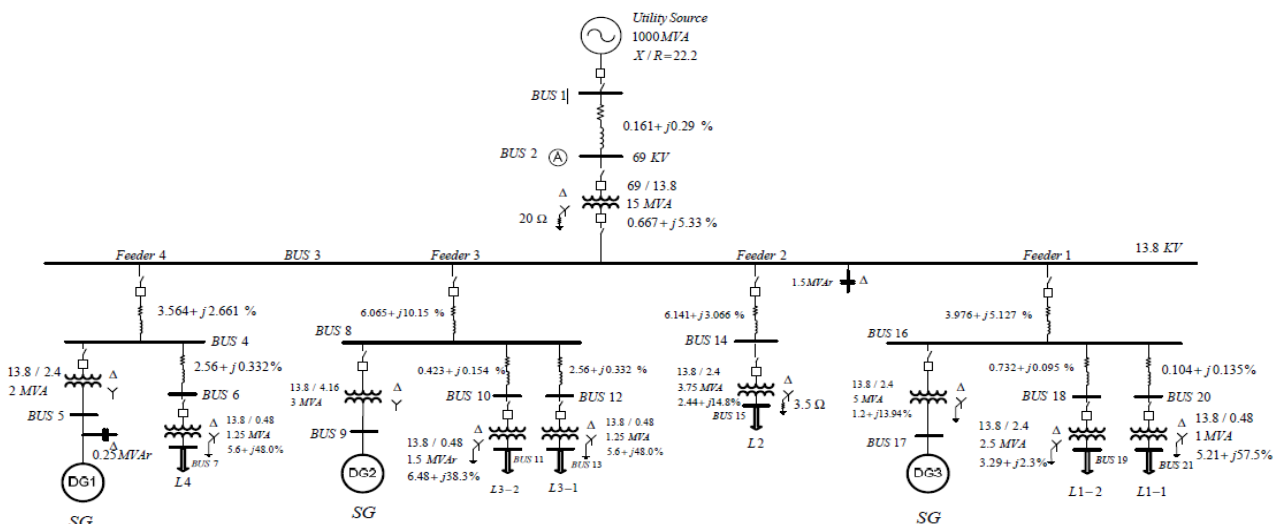


Figure 1. 21- Bus Microgrid System.

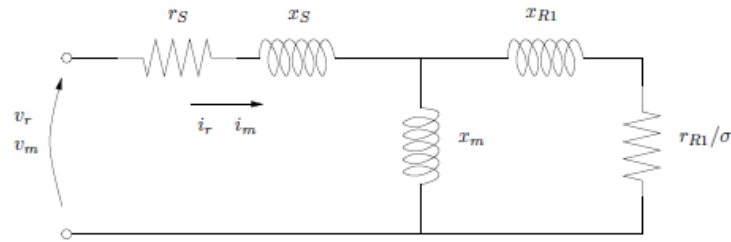


Figure 2. Simplified electrical circuit for single cage IM.

$$Q = v_m i_r + v_r i_m \quad (6)$$

In terms of the voltage behind the stator resistance r_s , the differential equations are [12]:

$$\frac{d}{dt} e_r' = \Omega_b \sigma e_m' - \frac{e_r' + (x_0 - x') i_m}{T_0'} \quad (7)$$

$$\frac{d}{dt} e_m' = -\Omega_b \sigma e_r' - \frac{e_m' + (x_0 - x') i_r}{T_0'} \quad (8)$$

The link between state variables, currents and voltages is:

$$v_r - \frac{d}{dt} e_r' = r_s i_r + x' i_m \quad (9)$$

$$v_m - \frac{d}{dt} e_m' = r_s i_m + x' i_r \quad (10)$$

where x_0 , x' and T_0' can be obtain from the motor parameters.

$$x_0 = x_s + x_m \quad (11)$$

$$x' = x_s + \frac{x_{R1} x_m}{x_{R1} + x_m} \quad (12)$$

$$T_0' = \frac{x_{R1} + x_m}{\Omega_b r_{R1}} \quad (13)$$

At last, the mechanical equation is:

$$\frac{d}{dt} \sigma = \frac{T_m(\sigma) - T_e}{2H_m} \quad (14)$$

where the electrical torque is:

$$T_e = e_r' i_r + e_m' i_m \quad (15)$$

V. MICROGRID VOLTAGE STABILIZER

The MGVS has a similar functionality compared to a power system stabilizer (PSS) in terms of approaching voltage stability problem of a power system. The PSS gives an input to the excitation system of a generator to bring voltage stability to a power system. In order to prevent any voltage collapse, The MGVS gives an input to reactive power loops of DGs or the excitation systems, which lets DGs to kick in more reactive power into the microgrid. By implementing this method, using of costly dynamic reactive sources like capacitor banks, SVC or STATCOM can be avoided. The MGVS model and its simplified version can be seen in Fig. 3 and Fig. 4 respectively.

The MGVS input is a measurement of the per unit (pu) difference ($\Delta V_{i\text{err}}$) between the desired voltage ($V_{i\text{des}}$) and the dynamic voltage ($V_{i\text{dyn}}$). This voltage deficiency is calculated for all the load buses [7].

$$\Delta V_{i\text{err}} = \frac{V_{i\text{des}} - V_{i\text{dyn}}}{V_{i\text{des}}} \quad i = 1, 2, \dots, l \quad (16)$$

Based on the importance of the bus, weighting factors for all buses are defined. In order to get a total voltage deficiency (ΔV_{err}) of the system, a weighted average of $\Delta V_{i\text{err}}$ is taken. A lead/lag block consisting of gain constant (K) and time constant T_1 and T_2 takes the ΔV_{err} as an input. As shown in Fig. 3, V_{MGVS} is the output of this MGVS controller [7].

$$\Delta V_{\text{err}} = \frac{\alpha_1 \Delta V_{1\text{err}} + \alpha_2 \Delta V_{2\text{err}} + \dots + \alpha_l \Delta V_{l\text{err}}}{\alpha_1 + \alpha_2 + \dots + \alpha_l} \quad (17)$$

The weighting factors for load buses are $\alpha_1, \alpha_2, \dots, \alpha_l$. For this study, all α values are equal to each other because loads at all buses are considered equally important.

The block diagram in Fig. 4 can be implemented in MATLAB. The corresponding differential equations representing the MGVS are given below.

$$\dot{x}(t) = -\frac{1}{T_1} x(t) + \frac{K(T_1 - T_2)}{T_1^2} \Delta V_{\text{err}} \quad (18)$$

$$V_{\text{MGVS}}(t) = x(t) + K \frac{T_2}{T_1} \Delta V_{\text{err}} \quad (19)$$

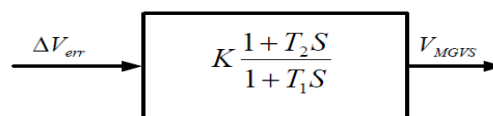


Figure 3. Microgrid Voltage Stabilizer

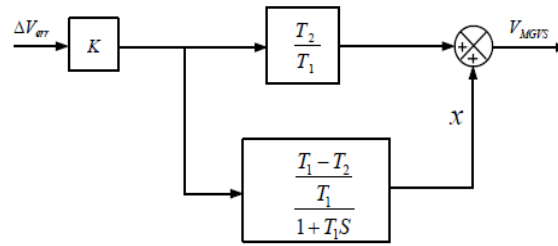


Figure 4. Simplified Microgrid Voltage Stabilizer Model

VI. SIMULATION AND RESULTS

After modeling of the microgrid system and its components, voltage stability of the system will be studied by implementing a three phase short circuit fault to a selected bus. In this paper, MATLAB programming environment is used to model the 21-bus microgrid system that has three diesel engine generators and 6 loads and to implement the fault conditions [13]. Fig. 1 shows the details of the microgrid system used for this study. There will be two case studies. In first case study, load types will be considered as either 100% ZIP or 100% IM type and response of the system after disturbances will be evaluated. For the second case study, load types will be considered as 50% ZIP and 50% IM type. The results will be used to compare the cases of with and without presence of the MGVS. This will help us to understand the behavior of MGVS with ZIP and IM type of loads and its effectiveness.

Case study 1: Three phase short circuit fault at Bus 7 with 100% ZIP and 100% IM Loads

In this case study, a three phase short circuit fault is applied to Bus 7 for 1.5 sec. The disturbance starts at 0.5 sec. and overall simulation time is 7 sec. Bus Voltages, Active Power and Reactive Power for Bus 15 have been plotted separately for various load types with and without presence of MGVS as listed below.

- | | |
|-------------------------------|-----------------------------|
| 1) 100% I M | 4) 100% P with MGVS control |
| 2) 100% I M with MGVS control | 5) 100% Z |
| 3) 100% P | 6) 100% Z with MGVS control |

In each case, only one type of load is considered and all results are shown in one plot for comparison. Aim for having only one type of load is for observing the system behavior for those loads individually. Depending on load types, the voltage at Bus 15 drops at the time of fault to a point that is all different for each case. As it can be seen from the Fig. 5, the biggest drop took place with 100% P load and least drop was observed with 100% Z load. Without presence of MGVS voltage drops around 0.92 pu and stay around that point. The MGVS works effectively for all load types to compensate the voltage drop. Voltage turns back to nominal point in 1.5 s. The results show that when the MGVS is active, the response of system after the fault for covering the voltage is alike for all load types. But when we look at Fig. 6 for active power and Fig. 7 for reactive power response of the system, they are all different for each case.

Z and P loads are the upper and lower limit for voltage dependency of active and reactive power of ZIP load respectively. Any other percentage of these Z-I-P load types will be in that range. Active and reactive power at all load buses for 100% P load is constant because they are independent from voltage changes. Largest decrease on producing active and reactive power happened for 100% Z load because its dependence of voltage is quadratic. At the times of fault and the fault clearing, 100% IM load has instant pick values for reactive power as in Fig 7. With presence of the MGVS, there is a significant increase for reactive power and active power for all load types. It is normal to observe this behavior because MGVS is improving the voltage profile of the system by using the reactive power compensation.

Case study 2: Three phase short circuit fault at Bus 7 with 50% ZIP and 50% IM Loads

Depending on the type of the user profile, between 50% and 70% of the entire load consists of three phase IMs. For this case study, 50% ZIP and 50% IM Loads is considered in order to make the load profile more realistic and suitable for real life applications. A Three phase short circuit fault is applied to Bus 7 for 1.5 s. Total simulation time is 7 s. Bus Voltages, Active Power and Reactive Power for Bus 15 have been plotted for various load types for the case of with and without presence of MGVS as listed below. Results are shown in one plot for comparison for each case.

- | | |
|-------------------------------------|-------------------------------------|
| 1) 50% P + 50% IM with MGVS control | 3) 50% Z + 50% IM with MGVS control |
| 2) 50% P + 50% IM | 4) 50% Z + 50% IM |

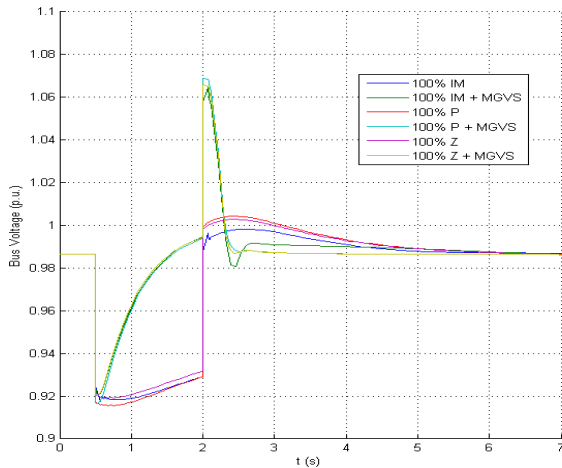


Figure 5. Comparison of Bus Voltage at Bus 15 for Case Study 1.

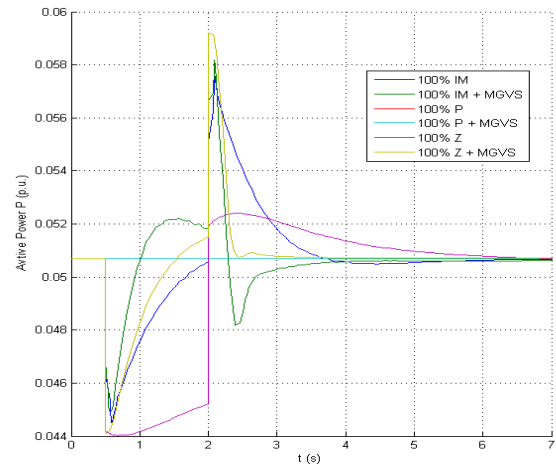


Figure 6. Comparison of Active Power at Bus 15 for Case Study 1.

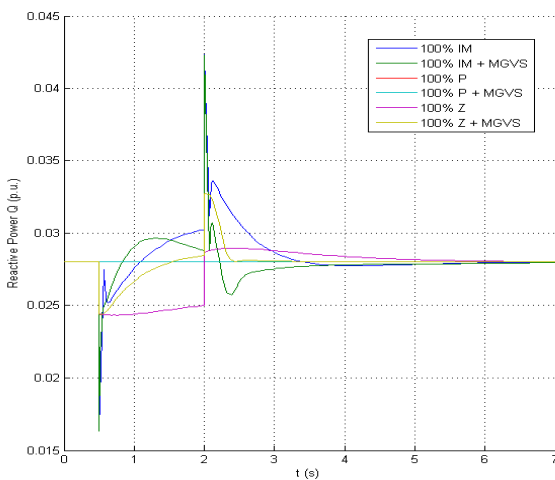


Figure 7. Comparison of Reactive Power at Bus 15 for Case Study 1.

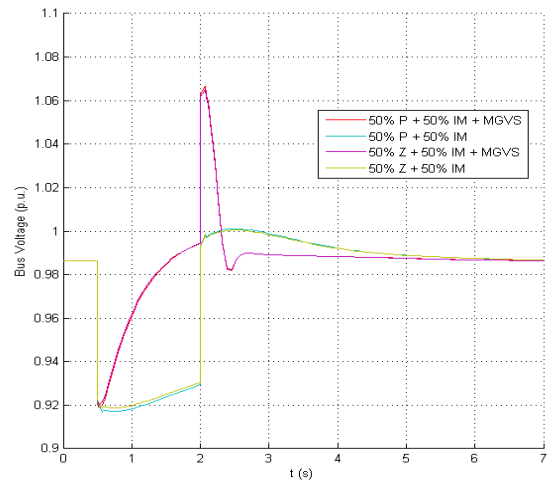


Figure 8. Comparison of Bus Voltage at Bus 15 for Case Study 2.

In this case study, we have 50% fixed IM load. 50% ZIP load considered as 50% Z and 50% P type of load in order to see the range of possible variations. Depending on Z and P loads, the voltage at Bus 15 drops to a point that is slightly different for each case. As it can be seen from Fig. 8, voltage drop is more for the case having P load compared to the case having Z load. Without presence of MGVS voltage drops around 0.92 pu and stay around that point. When the MGVS is active, voltage turns back to nominal point in 1.5 s. and there is an 8% improvement in bus voltages. But when we look at Fig. 9 for active power and Fig. 10 for reactive power response of the system, they are all different. As it was observed at the case study 1, largest drop for active and reactive power occurred at the case having Z load because its dependence to voltage is quadratic. At the times of fault and fault clearing, instant pick values for reactive power can be seen because of IM load for all cases. With presence of the MGVS, there is a significant increase for reactive power and active power for all load types. MGVS is using the available reactive power capabilities to improve the voltage profile of the system.

VII. CONCLUSION

Modeling of static and dynamic loads of a 21-bus microgrid test system and successful implementation of three phase short circuit fault with variable ZIP load and dynamic IM load has been presented using MATLAB. By using this simulation study, it was observed that the static ZIP and IM load models can have different load power characteristics depending on the relation with the voltage. Most of the real load types that are being tried to model have all variety of load types like industrial, residential and agricultural. Combining ZIP and IM loads made microgrid system more realistic because this is the common practice in real life. By changing the percentage of the ZIP load parameters and overall percentage of IM load, desired load characteristics can be accomplished. By using this test system, effectiveness of MGVS on voltage stability enhancement has been investigated. After testing MGVS with pure ZIP, pure IM and combination of ZIP+IM loads, results showed that MGVS is kicking enough reactive power to the system to prevent voltage collapse and it is enhancing the voltage profile of load buses for each type of loads successfully.

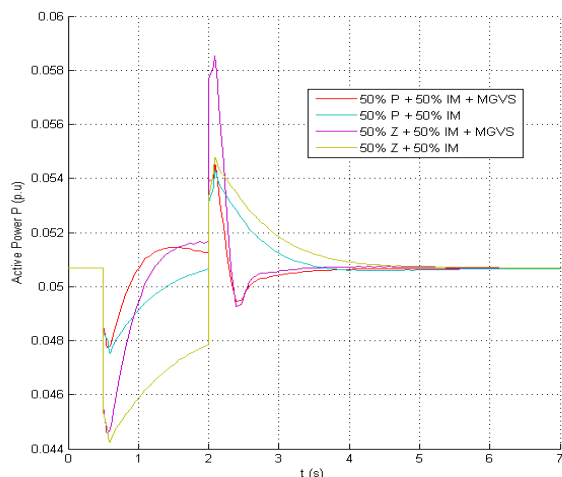


Figure 9. Comparison of Active Power at Bus 15 for Case Study 2.

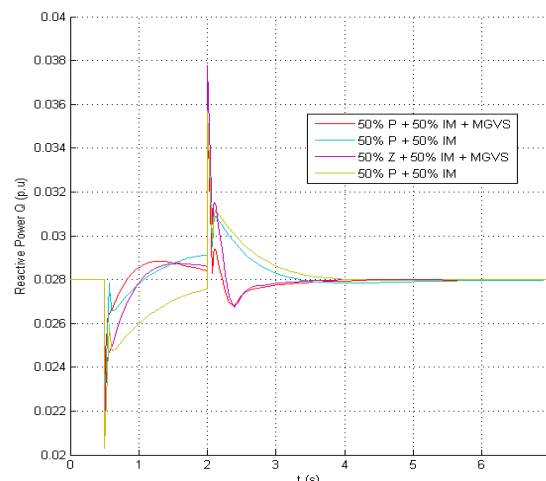


Figure 10. Comparison of Reactive Power at Bus 15 for Case Study 2.

REFERENCES

- [1] IEEE Stability Special: Voltage Stability of Power Systems: Concepts, Analytical Tools and Industry Experience, *IEEE Special Publication*, 90TH0358-2-PWR, 1990.
- [2] C.W. Taylor, *Power System Voltage Stability*, pp 17-135. (Electric Power Research Institute, McGraw-Hill, USA, 1994).
- [3] M. A. Merkle and A. M. Miri, Modelling of industrial loads for voltage stability studies in power systems, *Proc. Can. Conf. Electr. Comput. Eng.*, vol. 2, pp.881 -886 2001
- [4] Hodge N., Power trip - Expert risk articles, Allianz. Available: <http://www.agcs.allianz.com/insights/expert-risk-articles/energy-risks/> Dec. 2012
- [5] A. Kurita and T. Sakurai, The power system failure on July 23, 1987 in Tokyo, *Proceedings of the 27th IEEE Conference on Decision and Control*, Austin, 1988, pp. 2093 - 2097.
- [6] US-Canada power system outage task force, Final report on the August 14, 2003 Blackout in the United States and Canada: Causes and Recommendations, *Department of Energy*, 18 Pages.
- [7] A. Tamersi, G. Radman, M. Aghazadeh, Enhancement of microgrid dynamic voltage stability using Microgrid Voltage Stabilizer *Southeastcon, 2011 Proceedings of IEEE*, P. 368 - 373
- [8] M.U. Zahnd, *Control Strategies for Load-Following Unbalanced MicroGrids Islanded Operation*, Faculté Sciences et Techniques de l'Ingénieur, Lausanne, MS Thesis 2007.
- [9] R. H. Lasseter, A. Akhil, C. Marnay, J. Stevens, J. Dagle, R. Guttromson, A. S. Meliopoulos, R. Yinger, and J. Eto. White paper on integration of distributed energy resources. The CERTS microgrid concept. *In Consortium for Electric Reliability Technology Solutions*, Apr 2002.
- [10] K. Hatipoglu, I. Fidan, G. Radman, Investigating Effect of Voltage Changes on Static ZIP Load Model in a Microgrid Environment *North American Power Symposium (NAPS) 2012. Proceedings of IEEE*, Page(s): 111- 117.
- [11] A. Maitra, A. Gaikwad, P. Pourbeik, D. Brooks, Load Model Parameter Derivation Using an Automated Algorithm and Measured Data, *IEEE*, 2008
- [12] F. Milano, *Power System Analysis Toolbox documentation for PSAT version 1.3.4*, July 14, 2005, pp. 135-149
- [13] F. Katiraei and M. R. Iravani. Transients of a microgrid system with multiple distributed generation resources. *In International Conference on Power Systems Transients (IPST'05)*, pages 1–6, 2005.

Transitioning Cities: Choices and Agenda to Address Growth and Management: The Case of Bangalore

S. Gopi Prasad¹, Dr. B. Shankar²

¹ Director, IDES Consulting Private Limited, Bangalore, Karnataka, India.

² Associate Professor of Urban and Regional Planning, Institute of Development Studies, University of Mysore, Mysore

Abstract: The growing urban problems such as population expansion, urban sprawl, disparities between city core and its periphery, urban decay in city centres, increasing traffic volume and congestion, and inadequate fiscal resources and budget provisions for infrastructure pose fresh challenges as well as opportunities for rethinking the city development and management. The cities are attempting to seize both local and global opportunities and they must address the dilemmas of planning for safeguarding the environment, provisioning of basic services, inclusive development, understanding the changing pattern of the city for institutional setup in both regional and local contexts. This may be possible through active participation of citizens and all the stakeholders along with the adoption and deployment of interventions. The authors trace the important patterns concerning the population, urban structure and social-economic (income) structure between the census periods. These patterns are significant for formulating balanced spatial plans to address growth and sustainable management.

Key words: Transition, Densities, Urban Sprawl, Land use, Environment, Spatial Planning, Governance.

I. Introduction

Cities are in constant change. The older parts of Indian cities are witnessing greater land use transformations, while new areas are opened up for urban expansion. India has 5161 cities and towns. About 37.87 percent of the total urban population are living in 35 metropolitan cities as per the census 2001. The city structure comprises of central business districts including old city and cantonments, planned developments such as residential neighbourhoods with the efforts of organisations such as Urban Development Authorities, Cantonment Boards, etc; unauthorised colonies, revenue layouts, slums and squatter settlements and urban villages in the urban-scape of metropolitan cities in India. These are often locked within the city landscape with poor infrastructure provision. According to a 2002 NSS report on 'Housing Conditions in India', 22 cities with more than a million people, have slum population ranging from 10% to 54% of their total population. In metropolitan cities (million plus), a feeble formation of central business district with predominantly trade and service activities and often, aspiring to be a part of global economy; and a larger hinterland region comprising of two or more towns and villages, linked with road networks. The remaining hinterlands are agricultural area and vacant undeveloped land. According to Census 2001, there are spatial growth differentials in mega cities and there is no exception in case of Bangalore. Bangalore Urban Agglomeration is experiencing a very high spatial growth followed by the high density, high rise and growing infrastructure stress on parking, road space, open spaces, amenities and services; whereas, in case of Delhi, the periphery is also witnessing a very high growth¹. The activity of spatial planning revolves around organising the territories and complexities associated with it for sustainable development.

Metropolitan cities for the long time have been subjected to planning concepts, where as the periphery has been encouraged to receive the population, while dispersing the activities from the city centres to periphery. The understanding of the existing pattern and dynamics through population, area and social economic aspects will enable the planners and urban managers to formulate effective goals and objectives. The paper is attempted to make comparative studies on secondary data sources.

II. Bangalore: A Changing City

Bangalore, the capital of Karnataka State is one of India's fast developing city with an average annual exponential growth rate of 4.06% and population of 8.50 Million (Provisional Census of India, 2011). Bangalore is located at 12° 50' North Latitude and 77° 57' East longitude, over the ridges delineating four watersheds, viz. Hebbal, Koramangala, Challaghatta and Vrishabhavathi and is situated at an altitude of 920 m above mean sea level. The mean annual total rain fall is about 970 mm. Today, it is India's one of the largest cities, the momentum of its industrial, commercial and information technology growth unequalled in the country. The salubrious climate all around the year has enabled in attracting the investment in technology and other sectors.

III. Demography Profile of The City

The population of Bangalore Urban Agglomeration has risen from 4.13 million in 1991 to 5.68 million in 2001 and an increase of 1.55 million in 10 years and with an average of 155,000 Persons/year. During the inter-censal period of 1991-2001, the city had the highest growth rate among the Indian cities (i.e. of more than 5 million inhabitants) next to Delhi. The city's population has tripled within a period of about 30 years and is now the fifth biggest city in India. The

¹ Census of India, Paper -2, Rural- Urban Distribution, Census of India, 2001 and Handbook of Urbanization in India (Spatial growth During 1991-2001).

population growth trends in 2001 was 3.25 per cent and has increased to about 7 per cent in 2011, it is expected to reach the 10 million mark by 2015.

IV. Changing Spatial Growth Trends

The changing population growth trends has been traced three significant periods and are:

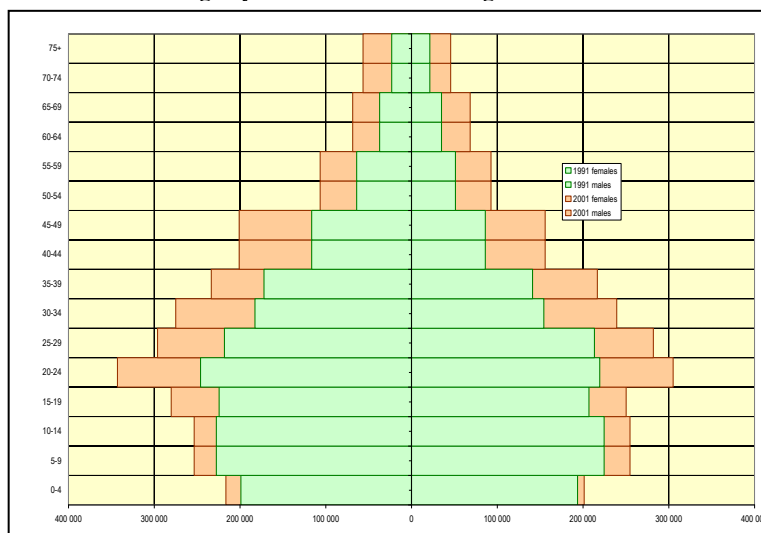
- The colonial time with the presence of British rulers and they established the army base, and the cantonment area in the city from 1870 onwards.
- The years 1940 to 1960, with the National Independence and the second world war, industrialization period of the city and the creation of the big public sector undertakings (Hindustan Aeronautics Limited, Bharat Electronics Limited, Indian Telephone Industries)
- The decade 1970-81 was a demographic boom followed by textile and silk industries development, and from the beginning of the 1990s, Information Technology (IT) and IT enabled services etc.

At present the city's population growth rate, which remains predictably high enough and it is moving towards a period of demographic stabilisation.

V. ERA of Demographic Maturity

The age-wise structure in urban agglomeration of Bangalore² brings to light a very steep drop in the percentage of the children, (the adult age bracket is maintained between 20 and 29 years). This particular structure reflects the marked domination of a population in the age-bracket of gainful employment; emphasising the strong appeal that Bangalore exerts on this chunk of the population. In structural terms, this modification of the age pyramid of the city is sustained by the migrations favoured by job offers and training, rising life-expectancy, slump in the natural growth. The age pyramid structure reveals an era of demographic maturity of the population of Bangalore. The increase in the number of households with respect to the population is also an important fact to be considered regarding urban projections, especially housing.

Chart 1: Age Pyramid Structure for Bangalore



Source : Bangalore Development Authority

VI. Changing Urban Spatial Pattern

A: A Radial System

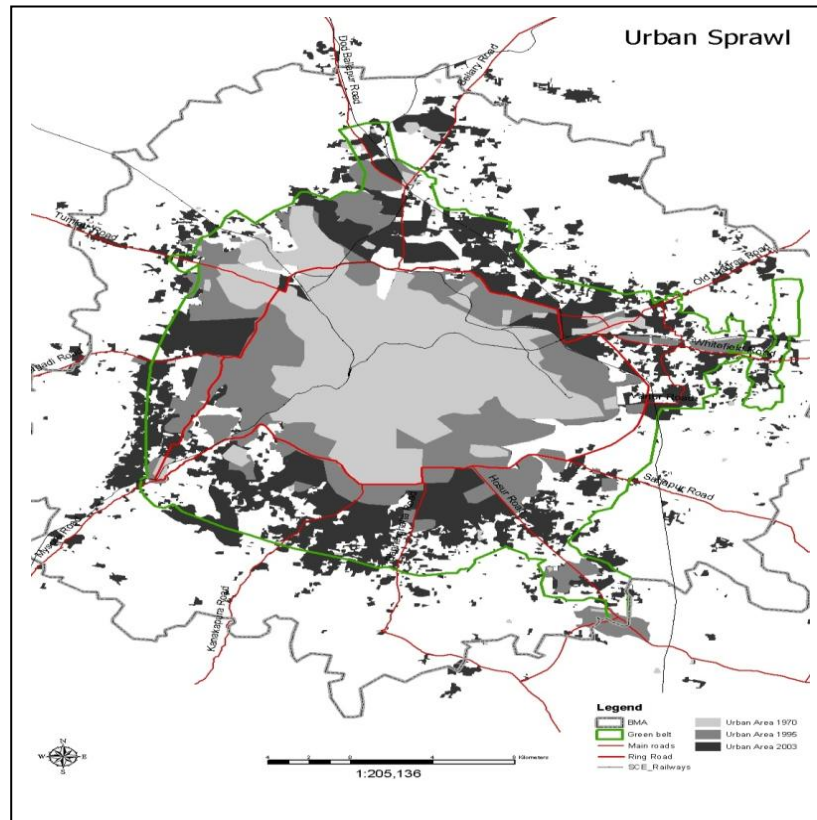
Bangalore is characterized by a radial system formed by five big axes, which converge towards the centre of the city. Among these five main major roads, five other secondary major roads are situated between the main corridors making the structure with a ten-pointed star and systems of ring roads viz. inner, intermediate and outer ring roads. These constitute the organisation system of the city and service the bulk of the industrial, commercial and residential activity.

B: A Multi-Directional Extension

The urbanized area of the agglomeration increased from 202 to 288 sq.kms from 1983 to 1990 and it increased to 464 sq.kms in 2003. An average of 1350 hectares /year of land has being utilised for the urbanisation process and thus, expansion of extensions are very significant and it gives the extent of the efforts to be deployed to satisfy the demand, develop the lands and provide sufficient housing, potable water, energy, civic amenities etc. In the absence of the natural limit pronounced, the city today stretches in all the directions and along the major corridors. The growth of urbanization along these axes generally seems to be determined by the industry, the inhabitants occupying the intermediary spaces. Corridor type urbanisation is observed along the National Highway and State highways. The Devanahalli-Yelahanka

² Estimated, on one hand, from the 1991 pyramid population and the proportion of 0-6 in 1991 and 2001 in Bangalore (censuses) and, on the other hand, from the age pyramids in 1991 and 1999 in urban Karnataka (SRS).

corridor which is the major connector to the International Airport has seen growth and rapid development since 2000. The sprawl impacts the service provision and agricultural land adversely.



Source: Bangalore Development Authority

For the planning purposes and overall governance, the Bangalore Metropolitan Area³ comprises of:

- The Bruhat Bangalore Mahanagara Palike (BBMP) or Greater Bangalore, it includes Bangalore City Corporation area, the erstwhile seven City Municipal Councils and one Town Municipal Council and 111 villages an extent of 696.17 sq km, with 84.74 lakhs as per census 2011.
- Bangalore Development Authority: the local planning authority prepares the master plan for the Bangalore Metropolitan area with an area of 1294 sq.km.
- The Bangalore Metropolitan Area (BMA) covers an area of 1307 sq.km and comprises the Bruhat Bangalore Mahanagara Palike, surrounding villages and the Bangalore-Mysore Infrastructure Corridor Project Area (BMICPA)⁴.

The expansion of the boundaries of the BMP to form the BBMP is significant, as the area for the corporation has been enhanced to 800 sq.km of area. The enhanced area has contributed to the complexities of development and management.

VII. Diversity Of Densities Inside The Agglomeration

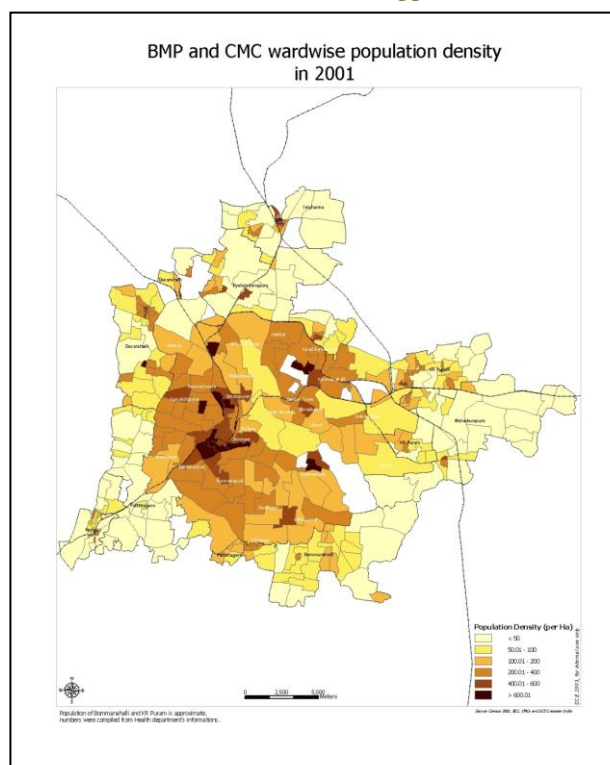
The overall density of the population in agglomeration⁵ is 130 persons/hectare, which is a relatively a low figure when compared with the surface area available for the residential purposes⁶ and it is close to 300 inhabitants/hectare, a high density. The occupancy rate is very high, while there are large vacant spaces in the city under Public and semi Public uses. Inside the erstwhile Bangalore City Corporation, the overall density is about 214 inhabitants/hectare. The density of population in the city corporation does not however seem to have progressed between 1991 and 2001, which can be explained by the reduction in size of households, competition between the trade and commerce, and housing in the core area and the transfer of the population growth on the CMC territory. The population density map of Bangalore brings out two historical parts of the city (Old Petta to the West and Cantonment area in the East) separated between them by a North-West/South-East arc of very low density occupied by the administrative sector, park and open spaces (Cubbon Park) and military grounds.

³ The Bangalore Metropolitan Area (BMA): BMA comprising of a Bangalore Mahanagara Palike, seven City Municipal Council and one Town Municipal Council and 111 villages.

⁴ Bangalore Development Authority, Master Plan: Vision Document – 2015, Bangalore

⁵ With respect to the urbanized surface in 2003

⁶ The semi net residential space occupies close to 40 % of the overall surface (CDP 95 data)



The distribution of the economic activities reflects the history of the city, its different stages of development as well as the underlying socio-spatial contexts. Several distinct combinations therefore emerge from the geography of the activities of Bangalore. Within these two parts, the highest densities are seen in Chickpet, Cottonpet, Binnypet and along the Mysore road link (Padarayanapura, Jagajeevanramnagar, Bapujinagar) between the railway track and the SH 17 and the North- East sector of the city (Hebbal, Kaval Byrasandra, Shivajinagar). Within these areas, very high concentrations of population are sometimes seen as in Cottonpet (620 inhabitants/hectare), Chickpet (560 inhabitants/hectare), Rajajinagar (440 inhabitants/hectare) and Kaval Byrasandra in the North-East (400 inhabitants/hectare). Higher densities more than 800 inhabitants/hectare are seen along the Tumkur Road in the Bhashyamnagar and Prakashnagar wards which indicate the socio-economic conditions and overcrowding of housing and its conditions. Tendencies towards higher density of population are observed along the main corridors (Mysore Road, Magadi Road, Tumkur Road).

VIII. Distribution Of Incomes

The work carried out by the Bangalore Local Urban Observatory and UNCHS⁷ and “Information-Based Strategies for Urban Management” published in the Bangalore City Indicators Program indicate some important trends. Though, this work is based on a specific survey concerning 3000 households of the Bangalore Municipality of limited statistical base, interpretation is to be carried out with caution. The study reveals the trends. The survey data show that the income of the households has increased on an average by close to 10% per year, which is considerable. The analysis was carried out by dividing the entire population into five quintiles and comparison of the same reveals that the annual growth rate change is from 2.7 percent for the first and 13.7 percent for the fifth. The disparity ratio of the incomes between the first and the last quintile has changed in ten years from 4.9 to 13.6, which is a real qualitative jump that implies a profound change in the equilibrium of the city and a transformation phase. In order to factor the inflation, the incomes in 2001 were calculated on the currency constant of 1991 by deflating the rupee on the dollar⁸. This data indicates the important changes of the Bangalore’s social economic structure whose consequences should be considered for the urban planning in terms of transport, housing etc. While the traditional inequality was till today moderate, we are now about to witness emergence of a new society, marked by a strong inequalities and disparities. Broadly, three categories could be identified as a pattern:

- Category- 1: that is rapidly expanding and reflects patterns similar to the income /consumption pattern of those international standards of comfort (about 25 percent)
- Category -2: that is stagnating and remains confronted with the difficulties of daily life.(About 50 percent)
- Category -3: areas of poverty in the slums and the under-developed housing. (About 25 percent).

Though the variations and sub variations in the ranges are possible, in terms of physical development and planning, it will be important to consider the categories discussed.

⁷ Bangalore City Indicators Programme. Society for Development Studies. UNCHS Regional Institution for Asia Pacific and Arab Regions, November 2000.

⁸ 1\$ = INR 18.2 of 1991 = INR 48.69 of 2001

IX. Pattern Of Use Of Resources

In the past decade, various authorities and parastatals have drawn up plans for the management of resources. Notable ones include the City Development Plan (CDP), Revised Master Plan 2015 and the Greater Bangalore Water and Sanitation Plan, the Metro Rail project plan. The CDP has enabled Bangalore city and BBMP to access central funding and mobilise resources for the city development. The JnNURM mission has emphasised on the “reforms” to be taken up. The Master plan (RMP 2015) has given regulatory and land use controls for the protection of the lakes and valleys. The other areas include the recycling of water, solid waste management and use of technology for creating citizen interfaces and information platforms. The use of resources and the changing pattern will need to be addressed with respect to the changes in the population, social and economic structure.

X. Conclusions

Bangalore as city in transition requires multiple interventions at different scales and levels. This is to preserve the continuity of the urban dynamics related to population, social and economic structure as well as development. While predicting the future trends and patterns, the ongoing initiatives and the plans will have to be reviewed and analysed for its impact on the pattern. The resources base will have to be worked out for strengthening the effective working of the city. The impact of the investments and undertaking of the large infrastructure projects such as the Greater Bangalore Water Supply project, the implementation of metro transportation project, the development by various public authorities in the last inter-censal period which needs to be addressed.

References

- [1]. 3i Network (2006), “Indian Infrastructure Report 2006- Urban Infrastructure”, *Oxford University Press*.
- [2]. 3i Network (2009), “Indian Infrastructure Report 2009, Land—A Critical Resource for Infrastructure”, *Oxford University Press*.
- [3]. Bangalore Development Authority (BDA) (2007), *Revised Master Plan – 2015, Vision Document, Volume 1*, Bangalore
- [4]. Bangalore Development Authority (BDA) (2007). ‘*Revised Master Plan - 2015, Vision Document, Volume 3*’, Bangalore.
- [5]. Bangalore Development Authority(BDA) (1995), *Comprehensive Development Plan-2011, Report and Land Use Zonal Regulations*, Government of Karnataka, Bangalore
- [6]. BCIP, UNCHS, 2000, “Information-Based Strategies for Urban Management”, unpublished report
- [7]. Bertaud, A.(2004), *The Spatial Organization of Cities: Deliberate Outcome or Unforeseen Consequence?*, Institute of Urban and Regional Development University of California at Berkeley, USA.
- [8]. Jawaharlal Nehru National Urban Renewal Mission (JNNURM) (2006) *City Development Plan for Bangalore*, available at <http://jnnurm.nic.in/toolkit/Bangalore.htm>
- [9]. Millennium Development goals, UNDP, <http://www.beta.undp.org/india/en/home/mdgoverview.html> accessed on 20 November 2011, 16:55 hrs
- [10]. UNECE (2000). *UNECE Strategy for Sustainable Quality of Life in Human Settlements in the Twenty-first Century (HBP/1999/4/Rev.1)*. UNECE, Geneva.

BIOGRAPHIES



S. Gopi Prasad received B.Arch degree in 1995 from MNIT, Jaipur and Master of Urban Design in 1999 from School of Architecture and Planning, New Delhi. He is currently heading the urban practice in Ides Consulting Private Limited. His research interests include decision support, infrastructure development, spatial/land use planning and legislation.



B. Shankar received the B.E. degree in Civil Engineering in 1984, M.U.R.P degree in Urban and Regional Planning in 1989 and Ph.D. degree in Urban and Regional Planning in 1997 from the University of Mysore, Mysore. He is working as Associate Professor in Urban and Regional Planning at the Institute of Development Studies, University of Mysore, Mysore. His research interests include Urban Planning, Spatial and Land Use Planning, Community Development, Heritage Conservation, and Planning Legislation.

Variable Floor for Swimming Pool Using an Expert System

Prof. Dr. Samy Abu Naser¹, Dr. Aeman M. Aead²

¹Department of Information Technology, Faculty of Engineering & Information Technology, Al-Azhar University, Palestine

²Department of Engineering, Faculty of Engineering & Information Technology, Al-Azhar University, Palestine

ABSTRACT : The indoor variable floor for swimming pool gives many possibilities of usages in the area where exists, for example, swimming pool, welcoming room, and sport hall. Therefore, we came to the idea of using the indoor variable floor for swimming pool due the shortages of open areas in Gaza Strip. The heating of the water in this pool when it is closed saves a lot of energy and time. During the winter season, people do not go the sea; but the can go to indoor swimming pools. The indoor variable floor for swimming pools can be built in schools for teaching the swimming courses for all ages of students. Since the depth of the water can be controlled, all students with different ages and classes can use the pool with high safety. To insure that, we designed an expert system to determine the height of the water in the pool according to some factors like: age, type usage, and time of the day. In the outdoor variable floor for swimming pool, it can be closed easily when it is not used to keep it clean and avoid falling kids in it.

Keywords: Expert system, movable floor, pool, variable pool, swimming pool.

I. INTRODUCTION

The variable floor for swimming pool is categorized by the addition of an additional floor board on top of the existing floor, which can go up and down like a lift. This additional floor board permits adapting the depth of the pool for diverse usages. Therefore, depending on the selected elevation of the additional floor, your pool can be transformed into a paddling pool for children or a suitable space for sports hall [1,2].

In the uppermost position the variable floor becomes not only powerful security system for your pool, but also a part of the original courtyard that surrounds it. This is owed to the region of pool becoming entirely covered and inaccessible.

The variable floor is usually built by a structure of tubes and/or beams of stainless steel which are bolted or welded together into the shape of the pool opening. This structure is then covered by a finishing surface like: exotic wood, stone, tiles, PVC or mosaic [2, 3].

Variable floor is well equipped with a trap door to permit access to the bottom of the pool in order to perform maintenance or for regular pool cleaning.

The device works through an electronic control accessible only by keypad. You can visualize and operate the position of the variable floor inside the pool through a touch screen [4].

The open areas in Gaza Strip where we live is limited so, the variable floor for swimming pool is an ideal solution. That means when we need a swimming pool we uncover it and determine its depth according to the group of users and we need to use its space we cover it and use it for other non water activities and events.

We use an expert system that determine the depth of the variable pool according to may factors such as : time of day, age of users, school swimming, processional swimming, private Lessons, Swimming for Seniors, Synchronised Swimming, Diving, Hydro Spinning, and Mothers with Babies.

1.1 History of variable floor for swimming pools

The variable floor for swimming pool idea began in Germany about 40 years ago. The first variable floor in North America was built in the Olean, New York YMCA in 1975 [1, 4]. Variable floor pools were mainly used in rehabilitation centres, hospitals, colleges, universities, schools and private homes.

1.2 Benefits of variable floor for swimming pool

A good facility is essential to the proper development of sporting opportunities for everyone from young toddlers just beginning to top level professional athletes. Variable floor for swimming pool provides the opportunity to easily increase the capacity of a pool by providing the tools to run an efficient and well organized facility. By increasing the flexibility of the pool you will be able to increase your program options maximizing the appeal to your customers.

Variable floor for swimming pool is the solution to the impact of winter for pool. One can maintain the pools water temperature, thus rapidly paying off with a reduction in heating and water bills [4].

The surface of the variable floor of the swimming pool is a very important element. We have the choice of wooden decking, stone, tiles, PVC or mosaic surface. In order to correctly make the pool completely hidden, an identical surface to match the area surrounding pool should be selected. Small areas are able to accommodate a pool while still keeping a space for relaxation or guests.

II. METHODS OF MECHANISMS FOR VARIABLE FLOOR OF SWIMMING POOLS

There are a few methods of mechanisms for constructing variable floor swimming pools such as motorized variable floor of swimming pools and hydraulic variable floor of Swimming Pools.

2.1 Motorized System for Variable Floor of Swimming Pools

The innovative and economical motorization system makes use of water hydraulic principles to move the floor and is an integral part of the floor configuration itself. When pulled back, the profile of the Spiralift is included into the moving floor structure (low height) with no extra excavation necessary. All the equipment is intended to work in water, getting rid of the need for a dried up room to home additional machinery/cables. In fact, the whole drive system can be fixed into the floor structure proceeding to arrival on site [2]. Safe openings in the floor permit easy access to the drive for examination and maintenance as in fig. 1.



Figure 1. Motorized variable floor of Swimming Pool

Spiralift units can be optimally located precisely where essential for an perfect sharing of the load between the actuators. This keeps the structure as light and reasonable as possible with a least number of Spiralift units necessary per platform. All components are intended to ensure the firmness and constancy of the platforms without any “bounciness” and to hold up rated floor masses. Running the platform is simply done by means of a simple control [3].

2.2. Hydraulic System for Variable Floor of Swimming Pools

A hydraulic cylinder system with variable floor consists of: moving floor, supported by four hydraulic cylinders as seen in fig. 2. To adjust the depth of the water which are controlled by a control unit [2]. A hydraulic cylinder system with variable floor is very reliable, very strong, requires little maintenance, and appropriate for large pools.

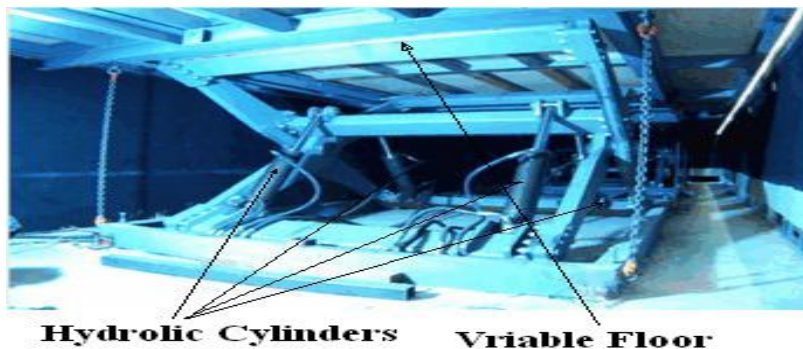


Figure 2. Hydraulic variable floor of Swimming Pool

2.3. Mechanical System for Variable Floor of Swimming Pools

The four lift arms connecting with two leading screws when closing the pool, moving up as shown in the fig. 3. The lead screw is driven by an electrical motor which located outside the pool. The depth of the water can be controlled by the number of revolutions of the lead screws [1].



Figure 3. Mechanical System for Variable Floor of Swimming Pools

III. EXPERT SYSTEMS

Artificial Intelligence (AI) was introduced in the 70s, the aim of AI scientists has always been to build up computer programs that can think and solve problems at the point compatible to human experts. An expert system is usually a computer program which performs tasks similar to the one performed by an intelligence human expert[8,9,10].

The term "expert system" could be applied to any computer program which is able to portray conclusions and make decisions, based on knowledge, represented as a database, it has. Expert systems usually consists of three core parts: User Interface, a knowledge base in certain domain and an inference engine which is a set of algorithms, which perform judgment and reasoning [11,12].

There are two stages during creating expert systems: data acquisition and reasoning. Data acquisition provides a way "to teach" a system, this results in a knowledge base, while reasoning is the major mode an expert system works in. The performance of expert systems depends on their knowledge bases mostly [10]. It was expressed: "more knowledge less search", the more knowledge you have the faster you find an appropriate solution. So the main problem is to create a suitable knowledge base [10,11].

The expert system developed in this work consists of the user interface, the knowledge base, and the inference engine. The structure of the expert system is shown in Fig. 4.

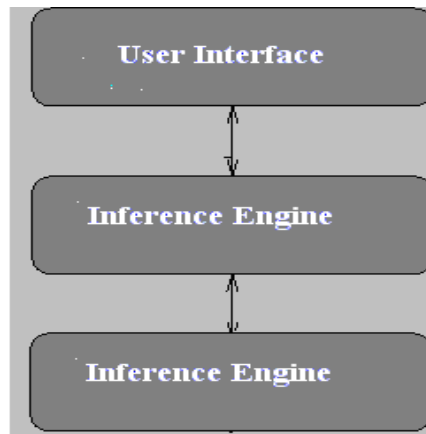


Figure 4. Structure of Expert Systems

The methodologies constitute the second generation of expert systems and they have the tendency to be developed to the direction of on one side directed also dedicated knowledge (expertise orientation) and on the other hand in the development of applications in specialized problems (problem - oriented). In the present research paper the problem of the variable floor for swimming pool are implemented by methodology of rule based expert systems. One of the well-know methods of representation of knowledge in the expert systems is the productive representation as the CLIPS (C Language Integrated Production System)[11].

CLIPS keep in memory a fact list, a rule list, and an agenda with activations of rules. Facts in CLIPS are simple expressions consisting of fields in parentheses. Groups of facts in CLIPS, usually follow a fact-template, so that to be easy to organize them and thus design simple rules that apply to them. Our expert system contains 37 CLIPS rules. An example of a rule in the expert system is shown in fig. 5.

```
(defrule sw-pool-cont-to-yes-branch
  ?nod <- (current-nod ?name)
  (nod (name ?name)
    (type decision)
    (yes-node ?yes-branch))
  ?answer <- (answer yes)
  =>
  (retract ?nod ?answer)
  (assert (current-nod ?yes-branch))
```

Figure 5. An example of a rule in the expert system

The goal of our expert system is to determine the proper height or the depth of the water in the swimming pool according to the following factors:

1. Time of the day: 8 am – 10 pm.
2. Usage of the pool :
 - Regular swimming
 - Teaching swimming
 - Professional swimming
 - Therapy swimming
 - Diving
 - aqua dance
3. Age of users
 - babies with mothers

- kids from 8-11 years
- teen age from 11-16 years
- Grownup 17 and up years

IV. USAGE OF VARIABLE FLOOR OF SWIMMING POOL

The variable floor allows the use of one swimming pool for a number of activities: water sport activities, none water sport activities, Social events, and reception hall.

4.1 Water Sport Activities

The variable floor of swimming pool can be used for many water sport activities like swimming competitions, baby swimming with their parents, aqua dance, disabled/remedial activity, swimming instruction, diving, activities that require different levels of water depth, water therapy, and school trips (See fig. 6).

For example: variable floor of swimming pool recognizes the value of a therapy pool for physical rehabilitation. Hydrotherapy pools require varying depths depending on the patients' disability, age and training activity. Because these treatments often take place in private, semi-private or small groups, variable floors can help achieve maximum results. They allow flexibility in size and depth but also support in operating the range of pool temperatures for specific kinds of therapy.



Figure 6: Swimming pool for water sport activities

4.2 None water sport activities

The pool can be converted to a large sport hall when making the height of the water to be zero and covering it by a finishing surface like: exotic wood, stone, tiles, PVC or mosaic. This large sport hall can be used for a number of different sports activities: including football, badminton, basketball and netball, and Ping pong (See Fig. 7).



Figure 7: Can be adapted to be used none water sport events

4.3 Social events

The pool and surrounding areas can be transformed into a stylish indoor exhibition area - making it perfect for social events, parties, weddings, concerts, meetings, Reception Hall, and presentations. Fig. 8 is suitable for all social events mentioned after little adjustment.



Figure 8: Can be adapted to be used as for social events

V. CONCLUSION

In this research paper, we have studied the benefits, usages and the mechanisms of indoor variable floor for swimming pool. This type of pools is very suitable for Gaza Strip. The area where the pool exists can be used for many purposes such as: water sport activities, none water sport activities, and social events. This type of pool gives the opportune to be used by all age groups all year round. In order to be suitable for all age groups, we designed an expert system to take into account all factors affecting indoor variable floor for swimming pool to determine the proper water depth of the pool.

REFERENCES

- [1] AGOR Engineering Enterprises, Movable floors for swimming pools <http://www.agor-eng.com/>. 11-11-2013.
- [2] Materialicious , Hydrofloors' Swimming Pool With Movable Floors, www.enpundit.com, Accessed on: 10-11-2013.
- [3] Barr and Wray , Variopool Moveable Floors, <http://www.variopool.nl/>, Accessed on: 13-11-2013.
- [4] AFW Movable Floors, Movable swimming pool floor systems, Aquatic Development Group, Inc, <http://www.aquaticgroup.com>, Accessed on: 15-11-2013.
- [5] BRS Pools, Swimming Pools , Lanark, Scotland, <http://www.brspools.co.uk>, Accessed on: 17-11-2013.
- [6] S. Simin, M. Fatemeh., A. Fatemeh, T. Marjan, And A. Afsaneh, Investigate the effect of expert systems application on management performance, *Interdisciplinary Journal of Contemporary Research in Business*, 4(12), 2013.
- [7] Riely, G., 2013 CLIPS: A tool for building expert system, available www.lipsrules.sourceforge.net, Accessed on: 20-11-2013.
- [8] Joseph C. Giarratano, Gary D. Riley, Expert Systems: Principles and Programming, (Fourth Edition, Course Technology), 2004.
- [9] Elaine Rich & Kevin Knight. 1991. Artificial Intelligence. Second Edition. (Tata McGraw Hill Edition), 1991.
- [10] Leonard Bolc, M.J. Coombs, Expert System Applications (Symbolic Computation / Artificial Intelligence), (Springer-Verlag Berlin and Heidelberg GmbH & Co. K), 2011.
- [11] Peter Jackson ,1998, Introduction To Expert Systems, 3rd edition (Addison-Wesley),;1998.
- [12] Ali.Adeli, Mehdi. Neshat. 2010. "A Fuzzy Expert System for Heart Disease Diagnosis", Proceedings of the International Multi Conference of Engineers and Computer Scientists 2010 Vol I, IMECS 2010, March 17 - 19, 2010, Hong Kong.

A Novel Control Strategy for Direct Power Control with MC-Based UPFC

K. Raju¹, B. Sampath Kumar²

¹PG scholar, Dept. of EEE, Teegala Krishna Reddy Egg College, Meerpet, Hyd, A.P., India.

²Associate Professor of EEE, Teegala Krishna Reddy Egg College, Meerpet, Hyd, A.P., India

Abstract: This paper presents a novel control strategy for direct power control with MC-based UPFC. In general power control techniques are two methods; first one is a well-known method of indirect active and reactive power control is based on current vector orientation with respect to the line voltage vector [voltage-oriented control (VOC)]. Another less known method based on instantaneous direct active and reactive power control is called direct power control (DPC). A new simple method of line voltage sensor less DPC with constant switching frequency using space-vector modulation (DPC-SVM) is presented. DPC is based on the instantaneous active and reactive power control loops. Therefore, the key point of the DPC implementation is a correct and fast estimation of the active and reactive line power. A direct power control (DPC) for three-phase matrix converters operating as unified power flow controllers (UPFCs). Matrix converters (MCs) allow the direct ac/ac power conversion without dc energy storage links; therefore, the MC-based UPFC (MC-UPFC) has reduced volume and cost, reduced capacitor power losses, together with higher reliability. Theoretical principles of direct power control (DPC) based on sliding mode control techniques are established for an MC-UPFC dynamic model including the input filter. The simulation result of MC-based UPFC line active and reactive power, together with ac supply reactive power can be directly controlled by selecting an appropriate matrix converter switching state guaranteeing good steady-state and dynamic responses. Finally proposed Fuzzy controller forces the amplitude of the output current space vector to be constant so that the output current is free of harmonic.

Keywords: Direct power control (DPC), matrix converter (MC), unified power-flow controller (UPFC), space vector modulation (SVM).

I. INTRODUCTION

The AC-AC power converters known as matrix converters contain an array of bi-directional semiconductor switches that allow the connection of all the input voltage lines to all the output voltages. These bi-directional switches result from the association of power semiconductors consisting of a pair of devices with turn-off capability, usually insulated gate bipolar transistors (IGBTs), in either a common collector or a common emitter back-to-back arrangement. Usually, Each IGBT has an anti-parallel diode that may be avoided if reverse blocking IGBTs are used. Matrix converters, also known as all silicon converters, present the advantage of not needing an intermediate energy storage link. However, its absence implies input/output coupling, thus increasing the difficulty to define adequate control strategies. Nevertheless, over the years some pulse width modulation (PWM) techniques have been developed, although the first were mainly concerned with the output voltage control, neglecting the waveform quality of the input currents. In the 1980s, Alesina and Venturini introduced the matrix converter high frequency PWM approach enabling low harmonic contents for both output voltages and input currents and an output/input Voltage ratio of 0.86. Since then, other control approaches such as space vector modulation (SVM) [7] have been studied. The SVM technique, used for most three-phase converters, is based on the representation of output voltages or input currents resulting from all allowable matrix converter switching combinations, as vectors in the complex plane. It has the advantage of allowing a better selection of the required voltage and current vectors, simplifying control algorithms and providing maximum voltage transfer ratio without the need to add third harmonic modulator components.

The matrix converter direct control is achieved using the Sliding mode control technique [7], based on the space vector representation, to allow on-line the control of output voltages and input power factor. Sliding mode is designed to guarantee the on-line compensation of the displacement factor introduced by the input filter, a subject not addressed in previous publications. Unified power-flow controllers (UPFC) enable the operation of power transmission networks near their maximum ratings, by enforcing power flow through well-defined lines. These days, UPFCs are one of the most versatile and powerful flexible ac transmission systems (FACTS) devices [1]. L.Gyugyi [2, 3] proposed concept of The UPFC results from the combination of a static synchronous compensator (STATCOM) and a static synchronous series compensator (SSSC) that shares a common dc capacitor link.

The existence of a dc capacitor bank originates additional losses, decreases the converter lifetime, and increases its weight, cost, and volume. . The existence of a dc capacitor bank originates additional losses, decreases the converter lifetime, and increases its weight, cost, and volume. In the last few decades, an increasing interest in new converter types, capable of performing the same functions but with reduced storage needs, has arisen. These converters are capable of performing the same ac/ac conversion, allowing bidirectional power flow, guaranteeing near sinusoidal input and output currents, voltages with variable amplitude, and adjustable power factor[6]. Conventional UPFC controllers do not guarantee robustness and. In, the dependence of the matrix converter output voltage on the modulation coefficient was investigated, concluding that MC-UPFC is able to control the full range of power flow. In the last few years, direct power control techniques have been used in many power applications, due to their simplicity and good performance. A matrix converter- based UPFC [5] power transmission network using matrix converter is proposed in section II. In order to design UPFCs, presenting robust behavior to parameter variations and to disturbances, the proposed DPC-MC control method, in section III, is sliding mode-control techniques based on space vector modulation, allowing the real-time selection of adequate matrix vectors to control input

and output electrical power. The Fuzzy controller for matrix converter system is proposed in section III to improve its quality of output. Fuzzy controller forces the amplitude of the output current space vector to be constant so that the output current is free of harmonic. The steady-state behavior of the proposed DPC-MC P, Q control method is evaluated and discussed using detailed simulations implementation (section IV). Simulation results obtained with the DPC for matrix converter-based UPFC technology show decoupled series active and shunt/series reactive power control, zero steady-state error tracking, and fast response times, presenting faultless steady-state responses.

II. MODELING OF THE UPFC POWER SYSTEM

1. General Architecture

A simplified power transmission network using the proposed matrix converter UPFC is presented in Fig.1, where V_s and V_r are, respectively, the sending-end and receiving-end sinusoidal voltages of the and generators feeding load. The matrix converter is connected to transmission line 2, represented as a series inductance with series resistance (L_2 and R_2), through coupling transformers T_1 and T_2 . Fig.2 shows the simplified three-phase equivalent circuit of the matrix UPFC transmission system model in [4]. For system modeling, the power sources and the coupling transformers are all considered ideal. Also, the matrix converter is considered ideal and represented as a controllable voltage source, with amplitude and phase. In the equivalent circuit, is the load bus voltage. The DPC-MC controller will treat the simplified elements as disturbances. Considering a symmetrical and balanced three-phase system and applying Kirchhoff laws to the three-phase equivalent circuit (Fig.2), the ac line currents are obtained in coordinates

$$\frac{dI_d}{dt} = \omega I_q - \frac{R_2}{L_2} I_d + \frac{1}{L_2} (V_{Ld} - V_{R0d}) \tag{1}$$

$$\frac{dI_q}{dt} = -\omega I_d - \frac{R_2}{L_2} I_q + \frac{1}{L_2} (V_{Lq} - V_{R0q}). \tag{2}$$

The active and reactive power of sending end generator are given in coordinates by

$$\begin{bmatrix} P \\ Q \end{bmatrix} = \begin{bmatrix} V_d & V_q \\ V_q & -V_d \end{bmatrix} \begin{bmatrix} I_d \\ I_q \end{bmatrix}. \tag{3}$$

Assuming ω and θ as constants and a rotating reference frame synchronized to the source so that 0, active and reactive power and are given by (4) and (5), respectively

$$P = V_d I_d \tag{4}$$

$$Q = -V_d I_q. \tag{5}$$

Based on the desired active and reactive power, reference currents can be calculated from (4) and (5) for current controllers. However, allowing actual powers are sensitive to errors in the values.

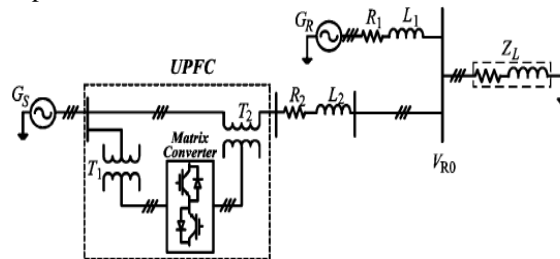


Fig 1: Transmission network with matrix converter UPFC.

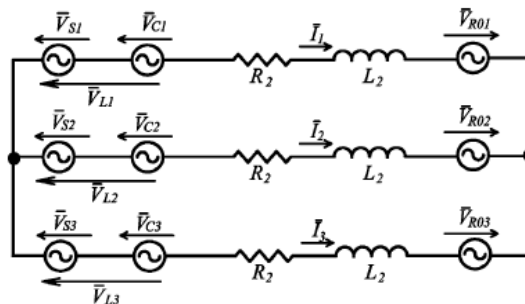


Fig 2: Three-phase equivalent circuit of the matrix UPFC and transmission line

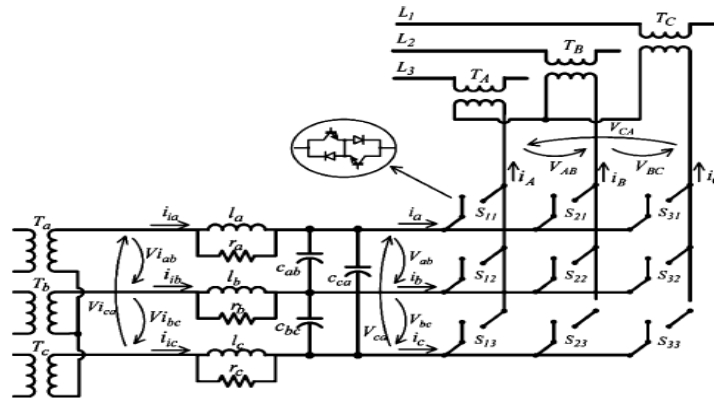


Fig 3: Transmission network with matrix converter UPFC.

2. Matrix Converter Output Voltage and Input Current Vectors

A diagram of the UPFC system (Fig.3) includes the three-phase shunt input transformer (with windings), the three-phase series output transformer (with windings) and the three-phase matrix converter, represented as an array of nine bidirectional switches with turn-on and turn-off capability, allowing the connection of each one of three output phases directly to any one of the three input phases. The three-phase input filter is required to re-establish a voltage-source boundary to the matrix converter, enabling smooth input currents. Applying coordinates to the input filter state variables presented in Fig.3 and neglecting the effects of the damping resistors, the following equations are obtained

$$\begin{cases} \frac{di_{id}}{dt} = \omega i_{iq} - \frac{1}{2l} V_d - \frac{1}{2\sqrt{3}l} V_q + \frac{1}{l} V_{id} \\ \frac{di_{iq}}{dt} = -\omega i_{id} + \frac{1}{2\sqrt{3}l} V_d - \frac{1}{2l} V_q + \frac{1}{l} V_{iq} \\ \frac{dV_d}{dt} = \omega V_q - \frac{1}{2\sqrt{3}C} i_{iq} + \frac{1}{2C} i_{id} - \frac{1}{2C} i_d + \frac{1}{2\sqrt{3}C} i_q \\ \frac{dV_q}{dt} = -\omega V_d + \frac{1}{2\sqrt{3}C} i_{id} + \frac{1}{2C} i_{iq} - \frac{1}{2\sqrt{3}C} i_d - \frac{1}{2C} i_q \end{cases} \quad \mathbf{S} = \begin{bmatrix} S_{11} & S_{12} & S_{13} \\ S_{21} & S_{22} & S_{23} \\ S_{31} & S_{32} & S_{33} \end{bmatrix} \quad (6)$$

Where $V_{id}, V_{iq}, i_{id}, i_{iq}$ represent, respectively, input voltages and input currents in dq components (at the shunt transformer secondary) and are the matrix converter voltages and input currents in components, respectively. Assuming ideal semiconductors, each matrix converter bidirectional switch can assume two possible states: “ $S_{kj} = 1$ ” if the switch is closed or “ $S_{kj} = 0$ ” if the switch is open. The nine matrix converter switches can be represented as a 3x3 matrix (7). The matrix converter topological constraint implies. Based on (7), the relationship between load and input voltages can be expressed as (8) The input phase currents can be related to the output phase currents (9), using the transpose of matrix S From the 27 possible switching patterns, time-variant vectors can be obtained (Table I) representing the matrix output voltages and input currents in $\alpha\beta$ coordinates, and plotted in the $\alpha\beta$ frame [Fig.4 (b)].

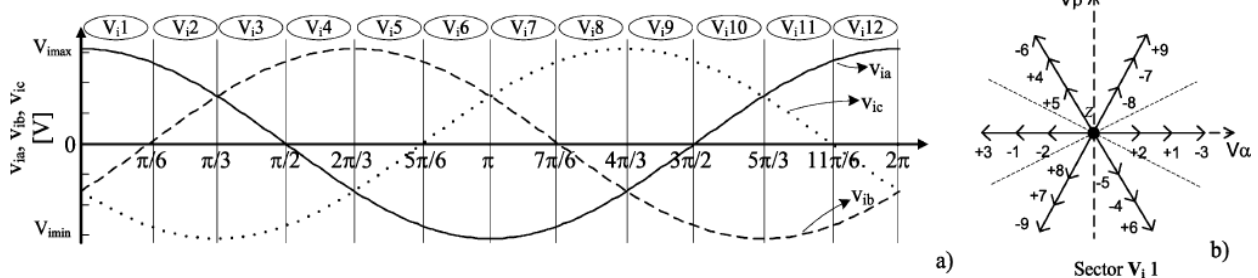


Fig 4: (a) Input voltages and their corresponding sector. (b) Output voltage state-space vectors when the input voltages are located at sector vi1.

The matrix converter topological constraints implies $\sum_{j=1}^3 S_{kj} = 1$.

$$[u_A \ u_B \ u_C]^T = \mathbf{S}[u_a \ u_b \ u_c]^T \quad (8)$$

$$[i_a \ i_b \ i_c]^T = \mathbf{S}^T[i_A \ i_B \ i_C]^T \quad (9)$$

The active and reactive power DPC-MC will select one of these 27 vectors at any given time instant.

TABLE I SWITCHING COMBINATIONS AND OUTPUT VOLTAGE/INPUT CURRENT STATE-SPACE VECTORS

Group	Name	A	B	C	v_{AB}	v_{BC}	v_{CA}	i_a	i_b	i_c	V_o	δ_o	I_j	μ_i
I	1g	a	b	c	v_{ab}	v_{bc}	v_{ca}	i_A	i_B	i_C	v_i	δ_i	$\sqrt{3}i_o$	μ_o
	2g	a	c	b	$-v_{ca}$	$-v_{bc}$	$-v_{ab}$	i_A	i_C	i_B	$-v_i$	$-\delta_i + 4\pi/3$	$\sqrt{3}i_o$	$-\mu_o$
	3g	b	a	c	$-v_{ab}$	$-v_{ca}$	$-v_{bc}$	i_B	i_A	i_C	$-v_i$	δ_i	$\sqrt{3}i_o$	$-\mu_o + 2\pi/3$
	4g	b	c	a	v_{bc}	v_{ca}	v_{ab}	i_C	i_A	i_B	v_i	$\delta_i + 4\pi/3$	$\sqrt{3}i_o$	$\mu_o + 2\pi/3$
	5g	c	a	b	v_{ca}	v_{ab}	v_{bc}	i_C	i_C	i_A	v_i	$\delta_i + 2\pi/3$	$\sqrt{3}i_o$	$\mu_o + 4\pi/3$
	6g	c	b	a	$-v_{bc}$	$-v_{ab}$	$-v_{ca}$	i_C	i_B	i_A	$-v_i$	$-\delta_i + 2\pi/3$	$\sqrt{3}i_o$	$-\mu_o + 4\pi/3$
II	+1	a	b	b	v_{ab}	0	$-v_{ab}$	i_A	$-i_A$	0	$\sqrt{2/3}v_{ab}$	0	$\sqrt{2}i_A$	$-\pi/6$
	-1	b	a	a	$-v_{ab}$	0	v_{ab}	$-i_A$	i_A	0	$-\sqrt{2/3}v_{ab}$	0	$-\sqrt{2}i_A$	$-\pi/6$
	+2	b	c	c	v_{bc}	0	$-v_{bc}$	0	i_A	$-i_A$	$\sqrt{2/3}v_{bc}$	0	$\sqrt{2}i_A$	$\pi/2$
	-2	c	b	b	$-v_{bc}$	0	v_{bc}	0	$-i_A$	i_A	$-\sqrt{2/3}v_{bc}$	0	$-\sqrt{2}i_A$	$\pi/2$
	+3	c	a	a	v_{ca}	0	$-v_{ca}$	$-i_A$	0	i_A	$\sqrt{2/3}v_{ca}$	0	$\sqrt{2}i_A$	$7\pi/6$
	-3	a	c	c	$-v_{ca}$	0	v_{ca}	i_A	0	$-i_A$	$-\sqrt{2/3}v_{ca}$	0	$-\sqrt{2}i_A$	$7\pi/6$
	+4	b	a	a	$-v_{ab}$	v_{ab}	0	i_B	$-i_B$	0	$\sqrt{2/3}v_{ab}$	$2\pi/3$	$\sqrt{2}i_B$	$-\pi/6$
	-4	a	b	b	v_{ab}	$-v_{ab}$	0	$-i_B$	i_B	0	$-\sqrt{2/3}v_{ab}$	$2\pi/3$	$-\sqrt{2}i_B$	$-\pi/6$
	+5	c	b	c	$-v_{bc}$	v_{bc}	0	0	i_B	$-i_B$	$\sqrt{2/3}v_{bc}$	$2\pi/3$	$\sqrt{2}i_B$	$\pi/2$
	-5	b	c	b	v_{bc}	$-v_{bc}$	0	0	$-i_B$	i_B	$-\sqrt{2/3}v_{bc}$	$2\pi/3$	$-\sqrt{2}i_B$	$\pi/2$
	+6	a	c	a	$-v_{ca}$	v_{ca}	0	$-i_B$	0	i_B	$\sqrt{2/3}v_{ca}$	$2\pi/3$	$\sqrt{2}i_B$	$7\pi/6$
	-6	c	a	c	v_{ca}	$-v_{ca}$	0	i_B	0	$-i_B$	$-\sqrt{2/3}v_{ca}$	$2\pi/3$	$-\sqrt{2}i_B$	$7\pi/6$
+7	b	b	a	0	$-v_{ab}$	v_{ab}	i_C	$-i_C$	0	$\sqrt{2/3}v_{ab}$	$4\pi/3$	$\sqrt{2}i_C$	$-\pi/6$	
-7	a	a	b	0	v_{ab}	$-v_{ab}$	$-i_C$	i_C	0	$-\sqrt{2/3}v_{ab}$	$4\pi/3$	$-\sqrt{2}i_C$	$-\pi/6$	
+8	c	c	b	0	$-v_{bc}$	v_{bc}	0	i_C	$-i_C$	$\sqrt{2/3}v_{bc}$	$4\pi/3$	$\sqrt{2}i_C$	$\pi/2$	
-8	b	b	c	0	v_{bc}	$-v_{bc}$	0	$-i_C$	i_C	$-\sqrt{2/3}v_{bc}$	$4\pi/3$	$-\sqrt{2}i_C$	$\pi/2$	
+9	a	a	c	0	$-v_{ca}$	v_{ca}	$-i_C$	0	i_C	$\sqrt{2/3}v_{ca}$	$4\pi/3$	$\sqrt{2}i_C$	$7\pi/6$	
-9	c	c	a	0	v_{ca}	$-v_{ca}$	i_C	0	$-i_C$	$-\sqrt{2/3}v_{ca}$	$4\pi/3$	$-\sqrt{2}i_C$	$7\pi/6$	
III	x_a	a	a	a	0	0	0	0	0	0	0	0	-	
	x_b	b	b	b	0	0	0	0	0	0	0	0	-	
	x_c	c	c	c	0	0	0	0	0	0	0	0	-	

3. General Structure of Fuzzy System

Fuzzy logic has two different meanings. In a narrow sense, fuzzy logic is a logical system, which is an extension of multi valued logic. However, in a wider sense fuzzy logic (FL) is almost synonymous with the theory of fuzzy sets, a theory which relates to classes of objects with UN sharp boundaries in which membership is a matter of degree. Every fuzzy system is composed of four principal blocks (Fig 5):

1. Knowledge base (rules and parameters for membership functions)
2. Decision unit (inference operations on the rules)
3. Fuzzification interface (transformation of the crisp inputs into degrees of match with linguistic variables)
4. Defuzzification interface (transformation of the fuzzy result of the inference into a crisp output)

In this simulation, we partitioned a space of input and output variables into 7 fuzzy subsets. They are presented by 7 membership functions as in the Table.V these functions are:

- Negative Big (NB)
- Negative Medium (NM)
- Negative Small (NS)
- Close to Zero (ZE)
- Positive Small (PS)
- Positive Medium (PM)
- Positive Big (PB)

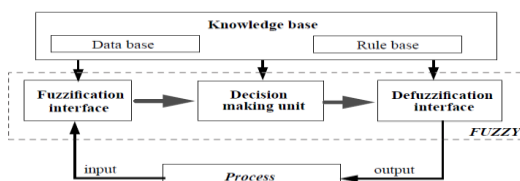


Fig 5: General structure of fuzzy inference system

The rule base that we can take the rule base proposed by Mamdani for the simulation of Fuzzy based DPC controller in [8]. These rules are shown in the Table V. The table is read in the following way, If the error is negative small (NS) **and** the change in error positive big (PB), **than** the control action is positive medium (PS). The inference method of Mamdani is max-min composition is chosen in the work to simplify the programming algorithm. After several trials has been made to select membership function. And finally it is decided to select triangular membership function. The fuzzy based DPC controller is used for ac-ac Matrix converter. The fuzzy controller forces the amplitude of the output current space vector to be constant so that the output current is free of harmonic.

TABLE V. Fuzzy controller rule base

		Rule base for Fuzzy controller Change in error(e)						
		NB	NM	NS	ZE	PS	PM	PB
E	NB	NB	NM	NS	ZE	PS	PM	PB
	R	NM	NB	NM	NS	NS	ZE	PS
O	NS	NS	NM	NM	NS	NS	ZE	PS
	R	ZE	NM	NS	NS	ZE	PS	PM
(e)	PS	PS	NS	NS	ZE	PS	PM	PM
	PB	PM	NS	ZE	PS	PS	PM	PB
		PB	ZE	PS	PS	PM	PM	PB

III. Direct Power Control of MC-UPFC

The matrix converter direct power control is achieved using the sliding mode control technique [7], based on the space vector representation, to allow on-line the control of output voltages and input power factor. DPC is based on the instantaneous active and reactive power control loops. This approach allows the design of the controller considering the converter and the dynamics of its associated LC filter. Together with the space vector representation technique, sliding mode allows the precise determination of switching times between the bi-directional switches, thus being appropriate to the nonlinear ON/OFF behavior of the matrix converter power semiconductors. As the switching occurs just in time, this technique guarantees fast response times and precise control actions, ensuring that the output voltages and the input currents track their references and making input power factor regulation independent of the input filter parameters. This feature has special interest in applications requiring unity input power factor, when feeding AC drives, or applications needing variable and accurate input power factor regulation, usually related to power quality enhancement. In DPC there are no internal current control loops and no PWM modulator block, because the converter switching states are selected by a switching table based on the instantaneous errors between the commanded and estimated values of active and reactive power. Therefore, the key point of the DPC implementation is a correct and fast estimation of the active and reactive line power.

1. Line Active and Reactive Power Sliding Surfaces

The DPC controllers for line power flow are here derived based on the sliding mode control theory. The Sliding mode control techniques present special interest for variable structure systems as they can use this property to successfully solve the control problem, guaranteeing the choice of the most appropriate control actions. Matrix converters are variable structure systems, as a result of the ON/OFF switching of their power semiconductors, but the design of sliding mode controllers and the choice of the most appropriate space vectors represent a tough challenge, since the input and output variables are interdependent. In fact, according to Table 1, the output voltage vectors depend on the input (mains) voltages and the input current vectors depend on the output currents, assumed nearly sinusoidal, but dependent on the matrix converter output voltages. To overcome these problems, it will be necessary

1. To guarantee the adequate control of the output variables in order to use the current space vectors as defined in Table 1;
2. To consider the input/output power constraint.

From Fig.4, in steady state, V_d is imposed by source V_s from (1) and (2), the transmission-line currents can be considered as state variables with first-order dynamics dependent on the sources and time constant of impedance. Therefore, transmission-line active and reactive powers present first-order dynamics and have a strong relative degree of one, since from the control viewpoint; its first time derivative already contains the control variable. From the sliding mode control theory [7], robust sliding surfaces to control the P and Q variables with a relatively strong degree of one can be obtained considering proportionality to a linear combination of the errors of the state variables. Therefore, define the active power error e_p and the reactive power error e_Q as the difference between the power references P_{ref} , Q_{ref} and the actual transmitted powers P, Q respectively

$$e_P = P_{ref} - P \quad (10) \quad S_P(e_P, t) = k_P(P_{ref} - P) = 0 \quad (12)$$

$$e_Q = Q_{ref} - Q. \quad (11) \quad S_Q(e_Q, t) = k_Q(Q_{ref} - Q) = 0. \quad (13)$$

Then, the robust sliding surfaces $S_p(e_p, t)$ and $S_Q(e_Q, t)$ must be proportional to these errors, being zero after reaching sliding mode are shown above in Eq. (12&13). The proportional gains K_P and K_Q are chosen to impose appropriate switching frequencies.

2. Line Active and Reactive Power Direct Switching Laws

The DPC uses a nonlinear law, based on the errors e_p and e_Q to select in real time the matrix converter switching states (vectors). Since there are no modulators and/or pole zero-based approaches, high control speed is possible. To guarantee stability for active power and reactive power controllers, the sliding-mode stability conditions (14) and (15) must be verified

$$S_P(e_P, t) \dot{S}_P(e_P, t) < 0 \quad (14)$$

$$S_Q(e_Q, t) \dot{S}_Q(e_Q, t) < 0. \quad (15)$$

These conditions mean that if $S_p(e_p, t) > 0$, then the $S_p(e_p, t)$ value must be decreased, meaning that its time derivative should be negative $\dot{S}_p(e_p, t)$. Similarly, if $S_p(e_p, t) < 0$, then $\dot{S}_p(e_p, t) > 0$. According to (12) and (14), the criteria to choose the matrix vector should be

1. If $S_P(e_P, t) > 0 \Rightarrow \dot{S}_P(e_P, t) < 0 \Rightarrow P < P_{ref}$, then choose a vector suitable to increase P .
2. If $S_P(e_P, t) < 0 \Rightarrow \dot{S}_P(e_P, t) > 0 \Rightarrow P > P_{ref}$, then choose a vector suitable to decrease P .
3. If $S_P(e_P, t) = 0$, then choose a vector which does not significantly change the active power. (16)

The same procedure should be applied to the reactive power error. To choose a vector, from (4) and (12), and considering Pref and V_d in steady state, the following can be written:

$$\begin{aligned} \dot{S}_P(e_P, t) &= k_P \left(\frac{dP_{ref}}{dt} - \frac{dP}{dt} \right) = -k_P \frac{dP}{dt} \\ &= -k_P \frac{d(V_d I_d)}{dt} = -k_P V_d \frac{dI_d}{dt}. \end{aligned} \quad (17)$$

From (16), considering V_d and Pref constant, if $S_P(e_P, t) > 0$, then it must be $\dot{S}_P(e_P, t) < 0$. From (17), if $k_P V_d$ is positive, then $dI_d/dt > 0$, meaning that P must increase. From the equivalent model in dq coordinates presented in (1), if the chosen vector has $V_{Ld} > V_{R0d} - \omega L2Id + R2I_d$, then $dI_d/dt > 0$, the selected vector being suitable to increase the active power (reaching condition). Similarly, from (5) and (13), with reactive power Qref and V_d in steady state

$$\begin{aligned} \dot{S}_Q(e_Q, t) &= k_Q \left(\frac{dQ_{ref}}{dt} - \frac{dQ}{dt} \right) = -k_Q \frac{dQ}{dt} \\ &= -k_Q \frac{d(-V_d I_q)}{dt} = k_Q V_d \frac{dI_q}{dt}. \end{aligned} \quad (18)$$

Considering the I_q current dynamics written in dq coordinates (2) then, to ensure the reaching condition, the chosen vector must have $V_{Lq} < V_{R0q} + \omega L2Id + R2I_q$, to guarantee then $dI_q/dt < 0$, meaning the voltage vector has a q component suitable to increase the reactive power. To ease vector selection (Table I), sliding surfaces and should be transformed to coordinates. To design the DPC control system, the six vectors of group I will not be used, since they require extra algorithms to calculate their time-varying phase. From group II, the variable amplitude vectors, only the 12 highest amplitude voltage vectors are certain to be able to guarantee the previously discussed required levels of V_{Ld} and V_{Lq} needed to fulfill the reaching conditions. The lowest amplitude voltages vectors, or the three null vectors of group III, could be used for near zero errors. If the control errors e_p and e_Q are quantized using two hysteresis comparators, each with three levels (-1, 0 and +1), nine output voltage error combinations are obtained. If a two-level comparator is used to control the shunt reactive power, as discussed in next subsection, 18 error combinations will be defined, enabling the selection of 18 vectors.

Since the three zero vectors have a minor influence on the shunt reactive power control, selecting one out 18 vectors is adequate. As an example, consider the case of $C_\alpha = S_\alpha(e_p, t) > 0$ and $C_\beta = S_\beta(e_p, t) > 0$. Then $dp/dt > 0$ and $dQ/dt < 0$, $dI_q/dt > 0$ imply that $dI_\beta/dt > 0$ and. According to Table I, output voltage vectors depend on the input voltages (sending voltage), so to choose the adequate output voltage vector, it is necessary to know the input voltages location [Fig.4(a)]. Suppose now that the input voltages are in sector [Fig. 4.(b)], then the vector to be applied should be +9 or -7. The final choice between these two depends on the matrix reactive power controller result C_{Qi} . Using the same reasoning for the remaining eight active and reactive power error combinations and generalizing it for all other input voltage sectors, Table II is obtained. These P, Q controllers were designed based on control laws not dependent on system parameters, but only on the errors of the controlled output to ensure robustness to parameter variations or operating conditions and allow system order reduction, minimizing response times.

TABLE II
STATE-SPACE VECTORS SELECTION FOR DIFFERENT ERROR COMBINATIONS

C_α	C_β	Sector					
		$V_i 12; 1$	$V_i 2; 3$	$V_i 4; 5$	$V_i 6; 7$	$V_i 8; 9$	$V_i 10; 11$
-1	+1	-9; +7	-9; +8	+8; -7	-7; +9	+9; -8	-8; +7
-1	0	+3; -1	+3; -2	-2; +1	+1; -3	-3; +2	+2; -1
-1	-1	-6; +4	-6; +5	+5; -4	-4; +6	+6; -5	-5; +4
0	+1	-9; +7; +6; -4	-9; +8; +6; -5	+8; -7; -5; +4	-7; +9; +4; -6	+9; -8; -6; +5	-8; +7; +5; -4
0	0	Za; Zb; Zc; -8;+2;-5;+8;-2;+5	Za; Zb; Zc; -7;+1;-4; +7;-1;+4	Za; Zb; Zc; +9;-3;+6;-9;+3;-6	Za; Zb; Zc; -8;+2;-5;+8;-2;+5	Za; Zb; Zc; -7;+1;-4; +7;-1;+4	Za; Zb; Zc; -9;+3;-6; +9;-3;+6
0	-1	-6; +4; +9; -7	+5; -6; -8; +9	+5; -4; -8; +7	-4; +6; +7; -9	+6; -5; -9; +8	-5; +4; +8; -7
+1	+1	+6; -4	+6; -5	-5; +4	+4; -6	-6; +5	+5; -4
+1	0	-3; +1	+2; -3	-1; +2	+3; -1	-2; +3	+1; -2
+1	-1	+9; -7	+9; -8	+7; -8	+7; -9	-9; +8	+8; -7

3. Direct Power Control Using Space Vector Modulation of Mc

The SVM technique, used for most three-phase converters, is based on the representation of output voltages or input currents resulting from all allowable matrix converter switching combinations, as vectors in the complex plane. It has the advantage of allowing a better selection of the required voltage and current vectors, simplifying control algorithms and providing maximum voltage transfer ratio without the need to add third harmonic modulator components [7]. Based on

sliding surfaces, the state-space vectors have to be chosen in order to verify the stability conditions. Accordingly, the sliding mode is reached only when the vectors applied to the converter have the necessary amplitude and direction. The matrix converter output voltage and input current vectors (Table 1) have the following characteristics. The vectors of group I have high fixed amplitude and should be able to guarantee the stability condition. However, as they rotate in the $\alpha\beta$ -plane, they may not have the correct direction when necessary (there are only six vectors). Besides, they are not easy to locate, as it will be necessary to consider at least 12 sectors for the mains voltages (Fig. 4), in order to know their approximate location. The 18 vectors of group II have variable amplitude and may not always guarantee the stability condition for this reason, at each time instant, only the 12 highest amplitude voltage vectors, which must be able to guarantee the stability condition, should be chosen to control the output variables.

The null vectors of group III guarantee the stability condition when both sliding surface values are nearly zero. As a result in order to simplify the control system, the six vectors of group I will not be used. The choice of the remaining 15 voltage vectors, the 12 highest amplitude vectors of group II and the three null vectors of group III, will guarantee the matrix converter maximum input/output voltage transfer ratio of 0.866 like in SVM [7].

The MC adopts a Space Vector Modulation (SVM) switching strategy [6] which can be used for any MC applications. The SVM switching approach enables the MC to:

- Achieve the maximum voltage transfer ratio without utilizing the third harmonic component injection method;
- Accommodate any input power factor independent of the output power factor;
- Reduce the effective switching frequency in each cycle, and thus the switching losses;
- Minimize harmonics.

In an SVM strategy only the switching states of Group II and III are utilized. The switching states in Group I are not used since the corresponding SSVs are rotating with time. Output voltage SSVs and input current SSVs of each switching state in Group II are illustrated in Fig.6. and Fig.7. The output voltage (input current) SSVs are expressed in the output (input) $\alpha\beta$ plane. Sector numbers 1 to 6 are assigned for the vector spaces between two adjacent SSVs in both the input and the output $\alpha\beta$ planes as shown below Fig 6. and Fig 7. And corresponding selection of switching states shown in Table IV Therefore, each switching state specifies one output voltage and one input current space vector, which are called as voltage and current switching space vectors (SSVs), respectively.

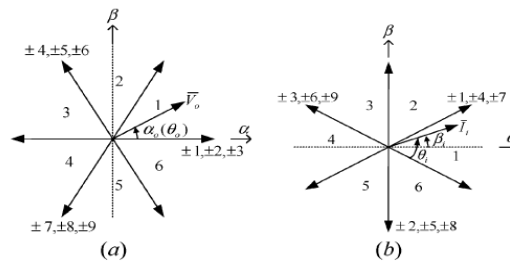


Fig. 6: (a) Output voltage SSVs. (b) Input current SSVs.

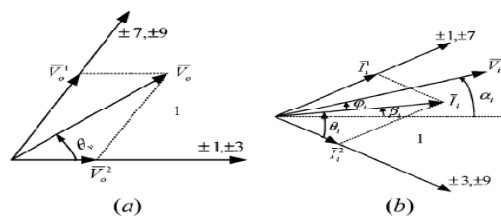


Fig. 7: (a) Output voltage vector synthesis. (b) Input current vector synthesis

TABLE IV
SELECTION OF SWITCHING STATES

Sector # of \bar{I}_i	Sector # of V_o											
	1 or 4				2 or 5				3 or 6			
1 or 4	7	9	1	3	4	6	7	9	1	3	4	6
2 or 5	8	7	2	1	5	4	8	7	2	1	5	4
3 or 6	9	8	3	2	6	5	9	8	3	2	6	5
Symbol	I	II	III	IV	I	II	III	IV	I	II	III	IV

4. Direct Control of Matrix Converters Input Reactive Power

In addition, the matrix converter UPFC can be controlled to ensure a minimum or a certain desired reactive power at the matrix converter input. Similar to the previous considerations, since the voltage source input filter (Fig. 4.3) dynamics (6) has a strong relative degree of two, and then a suitable sliding surface (19) will be a linear combination of the desired reactive power error and its first-order time derivative

$$\dot{S}_{Q_i}(e_{Q_i}, t) = (Q_{i_{ref}} - Q_i) + K_{Q_i} \frac{d}{dt} (Q_{i_{ref}} - Q_i). \quad (19)$$

The time derivative can be approximated by a discrete time difference, as has been chosen to obtain a suitable switching frequency, since as stated before, this sliding surface needs to be quantized only in two levels (-1 and +1) using one hysteresis comparator. To fulfill a stability condition similar to (15), considering the input filter dynamics (6), (20) is obtained

$$\begin{aligned} \dot{S}_{Q_i}(e_{Q_i}, t) = \\ V_{id} \left(\frac{di_{iq}}{dt} + K_{Q_i} \frac{d^2 i_{iq}}{dt^2} \right) = V_{id} \left(-\omega i_{id} + \frac{1}{2\sqrt{3}l} V_d - \frac{1}{2l} V_q \right) + \\ V_{id} K_{Q_i} \left(-\omega^2 i_{iq} + \frac{\omega}{l} V_d + \frac{\omega}{\sqrt{3}l} V_q - \frac{\omega}{l} V_{id} - \frac{i_{iq}}{3lC} + \frac{i_q}{3lC} \right). \end{aligned} \quad (20)$$

From (20), it is seen that the control input, the iq matrix input current, must have enough amplitude to impose the sign of $\dot{S}_{Q_i}(e_{Q_i}, t)$. Supposing that there is enough iq amplitude, (19) and (20) are used to establish the criteria (21) to choose the adequate matrix input current vector that imposes the needed sign of the matrix input-phase current iq related to the output-phase currents by (9).

1. If $S_{Q_i}(e_{Q_i}, t) > 0 \Rightarrow \dot{S}_{Q_i}(e_{Q_i}, t) < 0$, then select vector with current $i_q < 0$ to increase Q_i
2. If $S_{Q_i}(e_{Q_i}, t) < 0 \Rightarrow \dot{S}_{Q_i}(e_{Q_i}, t) > 0$, then select vector with current $i_q > 0$ to decrease Q_i . (21)

If then select vector with current to increase If then select vector with current to decrease (21) The sliding mode is reached when vectors applied to the converter have the necessary current amplitude to satisfy stability conditions, such as (15). Therefore, to choose the most adequate vector in the chosen dq reference frame, it is necessary to know the output currents location since the input current depends on the output currents (Table I). Considering that the dq -axis location is synchronous with the input voltage (i.e. dq reference frame depends on the input voltage location), the sign of the matrix reactive power can be determined by knowing the location of the input voltages and the location of the output currents. Considering the previous example, with the input voltage at sector V_{i1} and sliding surfaces signals $S_\alpha(e_p, t) > 0$ and $S_\beta(e_Q, t) < 0$ both vectors +9 or -7 would be suitable to control the line active and reactive powers errors (Fig. 4.4). However, these vectors have a different effect on the $\dot{S}_{Q_i}(e_Q, t)$ value: if iq has a suitable amplitude, vector +9 leads to $\dot{S}_{Q_i}(e_Q, t) > 0$ while vector -7 originates $\dot{S}_{Q_i}(e_Q, t) < 0$. So, vector should be chosen if the input reactive power sliding surface is quantized as $C_{Q_i} = -1$, while vector -7 should be chosen when is quantized as $C_{Q_i} = +1$. When the active and reactive power errors are quantized as zero, $S_\alpha(e_p, t) = 0$ and $S_\beta(e_Q, t) = 0$, the null vectors of group III, or the lowest amplitude voltages vectors at sector V_{i1} (-8,+2,-5,+8,-2,+5) at Fig. 4.(b) could be used. These vectors do not produce significant effects on the line active and reactive power values, but the lowest amplitude voltage vectors have a high influence on the control of matrix reactive power. Using the same reasoning for the remaining eight combinations at sector V_{i1} and applying it for the other output current sectors, Table III is obtained.

IV. IMPLEMENTATION OF THE DPC-MC AS UPFC

Control scheme of direct power control of the three-phase matrix converter operating as a UPFC. As shown in the block diagrams [Fig. 8] the control of the instantaneous active and reactive powers requires the measurement of voltages and output currents necessary to calculate and sliding surfaces. The output currents measurement is also used to determine the location of the input currents q component. The control of the matrix converter input reactive power requires the input currents measurement to calculate $S_{Q_i}(e_{Q_i}, t)$. At each time instant, the most suitable matrix vector is chosen upon the discrete values of the sliding surfaces, using tables derived from Tables II and III for all voltage sectors.

TABLE III
STATE-SPACE VECTORS SELECTION, FOR INPUT VOLTAGES LOCATED AT SECTOR V_{i1}

C_α C_β		Sector											
		$I_{012}; I_{01}$		$I_{02}; I_{03}$		$I_{04}; I_{05}$		$I_{06}; I_{07}$		$I_{08}; I_{09}$		$I_{010}; I_{011}$	
		C_{Q_i}	C_{Q_i}	C_{Q_i}	C_{Q_i}	C_{Q_i}	C_{Q_i}	C_{Q_i}	C_{Q_i}	C_{Q_i}	C_{Q_i}	C_{Q_i}	C_{Q_i}
-1	+1	-9	+7	-9	+7	-9	+7	-9	+7	-9	+7	-9	+7
-1	0	+3	-1	+3	-1	+3	-1	+3	-1	+3	-1	+3	-1
-1	-1	-6	+4	-6	+4	-6	+4	-6	+4	-6	+4	-6	+4
0	+1	-9	+7	-9	+7	-9	+7	-9	+7	-9	+7	-9	+7
0	0	-2	+2	-2	+2	-2	+2	-2	+2	-2	+2	-2	+2
0	-1	-7	+9	-7	+9	-7	+9	-7	+9	-7	+9	-7	+9
+1	+1	-4	+6	-4	+6	-4	+6	-4	+6	-4	+6	-4	+6
+1	0	+1	-3	+1	-3	+1	-3	+1	-3	+1	-3	+1	-3
+1	-1	-7	+9	-7	+9	-7	+9	-7	+9	-7	+9	-7	+9

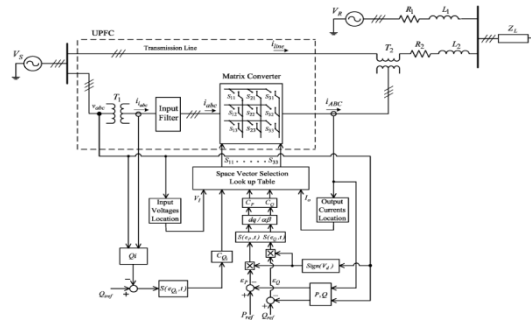


Fig 8: Control scheme of direct power control of the Three-phase matrix converter operating as a UPFC

V. SIMULATION RESULTS

The performance of the proposed direct control system was evaluated with a detailed simulation model in Fig.9, and matrix converter in Fig.10 using the MATLAB/Simulink SimPowerSystems to represent the matrix converter transformers, sources and transmission lines, and Simulink blocks to simulate the control system. Ideal switches were considered to simulate matrix converter semiconductors minimizing simulation times. In order to evaluate the performance of the direct controlled system, some tests were done, under different operating conditions, and the simulation results in Fig.11-Fig.14, obtained using the proposed method, were compared with the well-known Venturing and SVM strategies. The Matrix converter output currents (iA, iB, iC) THD for DPC and FUZZY shown in Fig.15. The controlled matrix converter should be able to guarantee that the output variables follow their references and, at the same time, that the input currents have the desired power factor: unity power factor if the matrix converter is used to control AC drives; and unity or leading/lagging power factor if the converter is used in applications related to power quality enhancement.

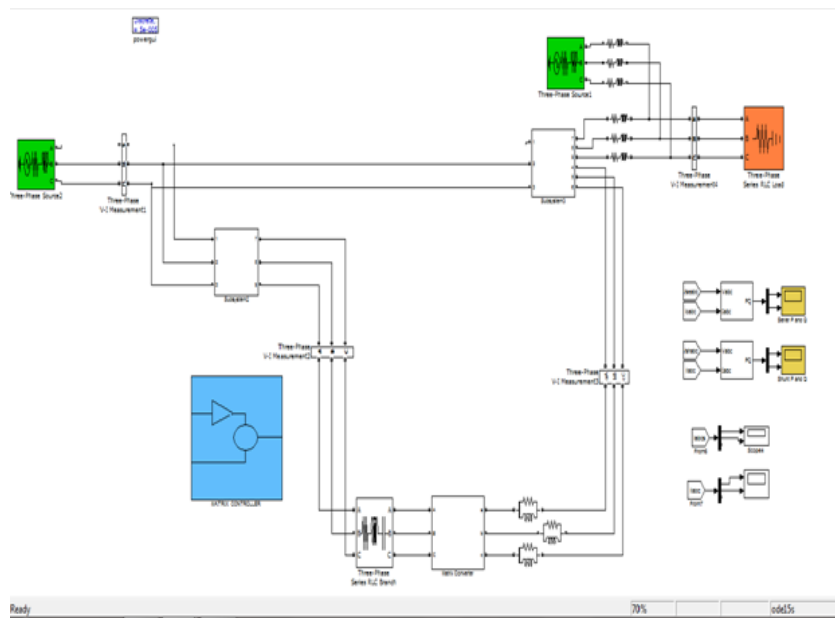


Fig 9: Simulation Model of UPFC with Matrix Converter

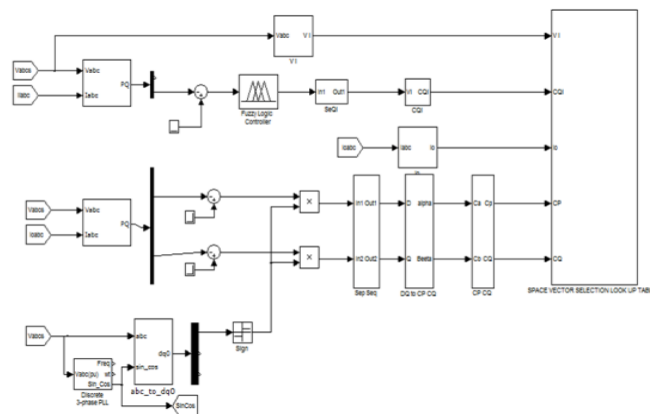


Fig 10: Fuzzy based DPC matrix converter control scheme.

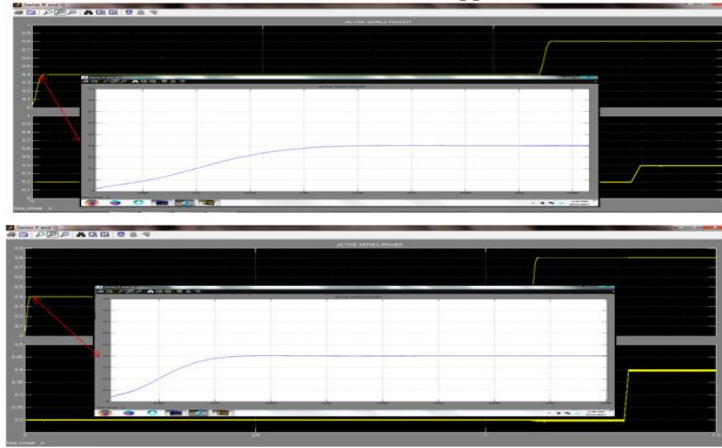


Fig 11: Simulation Result of Active and Reactive Series Power Responses with DPC and Fuzzy

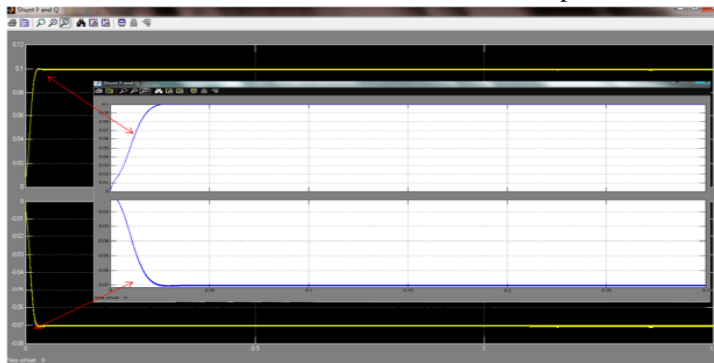


Fig 12: Simulation result of Active and Reactive shunt power with DPC

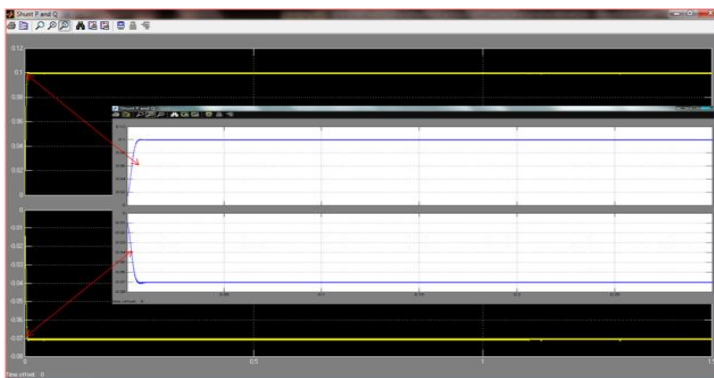


Fig 13: Simulation results of Active and Reactive shunt power with fuzzy

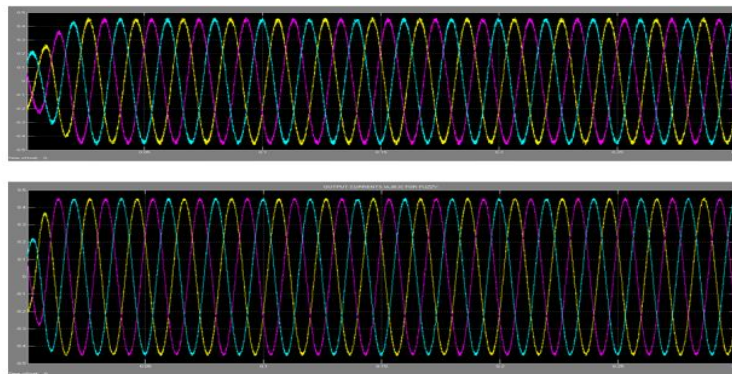


Fig 14 : Matrix converter output currents (iA, iB, iC) for DPC and FUZZY

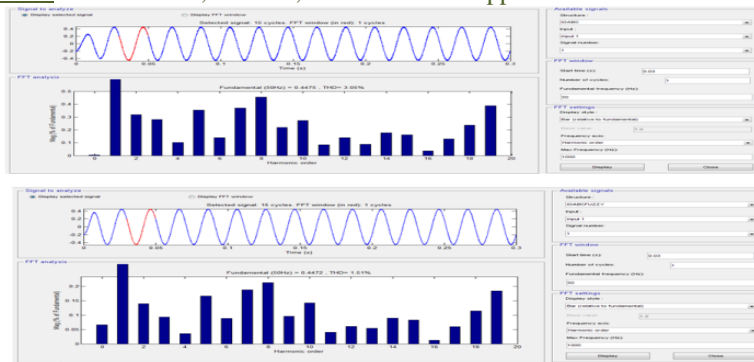


Fig. 15 : Matrix converter output currents (iA, iB, iC) THD for DPC and FUZZY

VI. CONCLUSION

The use of sliding mode controllers in variable structure systems such as matrix converters may present advantages such as easy on-line implementation and a quick and efficient choice of the correct switching combinations, ensuring that the system tracks their references. The active and reactive power flow can be advantageously controlled by using the proposed Fuzzy based DPC. The Fuzzy based DPC give Fast response times. It ensures transmission-line power control as well as sending end reactive power or power factor control. The dynamic and steady-state behavior of the proposed fuzzy based DPC-MC P, Q control method is evaluated and discussed using detailed simulations implementation. Obtained simulation results show that active and reactive power flow can be advantageously controlled by using the proposed fuzzy based DPC. The results of line and input matrix converter Currents are almost sinusoidal with small ripple content. From result, line active and reactive power, together with ac supply reactive power, can be directly controlled by selecting an appropriate matrix converter switching state guaranteeing good steady-state responses. The fuzzy controller forces the amplitude of the output current space vector to be constant so that the output current is free of harmonic.

Acknowledgements

The authors wish to acknowledge the support provided by Teegala Krishna Reddy Engineering College and Jawaharlal Nehru Technological University, Hyderabad to complete the work successfully.

REFERENCE

- [1] N. Hingorani and L. Gyugyi, Understanding FACTS—Concepts and Technology of Flexible AC Transmission Systems. Piscataway, NJ: IEEE Press/Wiley, 2000.
- [2] L. Gyugyi, “Unified power flow control concept for flexible AC transmission systems,” Proc. Inst. Elect. Eng. C, vol. 139, no. 4, Jul. 1992.
- [3] L. Gyugyi, C. Schauder, S. Williams, T. Rietman, D. Torgerson, and A. Edris, “The unified power flow controller: A new approach to power transmission control,” IEEE Trans. Power Del., vol. 10, no. 2, pp. 1085–1097, Apr. 1995.
- [4] J. Menteiro, Student Member, IEEE, J. Fernando Silver, Senior Member, IEEE, S. F. Pointo, Member, IEEE, and J. Palma “Matrix Converter–Based Unified Power- Flw Contoller: Advanced Direct Power Control Method” IEEE Transactions on power delivery, vol. 26, no. 1, January 2011.
- [5] R. Strzelecki, A. Noculak, H. Tunia, and K. Sozanski, “UPFC with matrix converter,” presented at the EPE Conf., Graz, Austria, and Sep. 2001.
- [6] P. Wheeler, J. Rodriguez, J. Clare, L. Empringham, and A. Weinstein, “Matrix converters: A technology review,” IEEE Trans. Ind. Electron., Vol. 49, no. 2, pp. 276–288, Apr. 2002.
- [7] S. Pinto and J. Silva, “Sliding mode direct control of matrix converters,” Inst. Eng. Technol. Elect. Power Appl., vol. 1, no. 3, pp. 439–448, 2007.
- [8] N. Mahendran, Dr. G. Gurusamy Research Scholar, Department of Electrical Engineering, Bannari Amman Institute of Technology, “Fuzzy controller for matrix converter system to improve its quality of output ” International Journal of Artificial Intelligence & Applications (IJAIA), Vol.1, No.4, October 2010.

Displacement in Load Bearing Straw Bale Walls Due To Concentric Compressive Loading

Gihan L. K. Garas, Mostafa E. Allam, Ahmad K. Abdel Gawad,
Mohamed Abdel Moneim

Civil Engineering Department, National Research Center, Cairo, Egypt

Abstract: The objective of this research was to provide structural performance data and information for straw bale home builders, building inspectors and engineers. Structural testing of 2 full-scale straw bale walls was undertaken. The tested walls were instrumented and subjected to compressive vertical loading. The results were interpreted in the light of the expected loads that must be withstood in single storey domestic applications. Two specimens of straw baled walls were tested using two techniques for measuring displacement under a maximum load of 2 ton. Pre-compression improved initial stiffness of the straw bale walls. The displacements recorded ranged between 7- 10 mm. It was concluded that placement of a wooden cap plate on top of the straw bale wall is important to insure uniform transfer of the loads along the whole length of the wall. Also this technique of building would confine the connection between the wire mesh, the straw and the plaster to insure the sandwich panel behavior in the section.

Keywords: Rice straw bales- compression test- sandwich panel hybrid sections- plastered straw-bale walls

I INTRODUCTION

1.1 General background

In order to test the performance of plastered straw-bale walls, it is essential to understand that, once plaster is applied directly to either one or both bale surfaces, the structure is now a hybrid of straw and plaster. Effectively, any further loading will go mostly or entirely into the plaster skins. This is because of the relative stiffness, or in other words the various moduli of elasticity of the two adjacent materials. Any kind of plaster is far stiffer than the straw, and will therefore “attract” any subsequent loading. When any load is applied on a plastered straw-bale structure, the soft, flexible straw yields, and the brittle plaster skin attracts all the stresses. Unlike in a pure concrete structure, however, where such a failure of a bearing (or shear) concrete wall or column could be both sudden and catastrophic, the failure of the plaster skin would throw any loads back on the straw-bale assembly. The capacity of the bales to pick up the load yielded by cracked plaster is fairly substantial. [1]

1.2 Sandwich Panel Behavior

Tests conducted in various laboratories over the past 10 years have proven that an un-plastered straw bale wall can carry an appreciable amount of vertical load, as well as some in-plane and out-of-plane shear, and would therefore provide a backup against failure of the plaster skins. Furthermore, recent tests in Washington and California have revealed the surprising strength, ductility and toughness of plastered walls, even when cracked and subjected to cyclic loading. We are finding that the bale walls, when plastered on both sides, behave much more like an integral sandwich panel structure than might be expected [2]. The structural model is complex: Rigid inside and outside skins are attached to the comparatively soft straw-bale “masonry” assembly. Most important to the whole package, there is both some shear capacity in the bales and some shear transfer capacity between the bale surfaces and the skins. Though it is essential to see the plaster skins as the primary load-carrying elements, it is nevertheless also important to recognize that the straw bales are still crucial elements of the package. This is analogous to the relationship of web to flanges in a steel I-beam: The flanges (skins) carry bending loads, but rely on the shear capacity of, and connection to, the web (in this case, the straw-bale assembly). So the assembly consists of strong, brittle, thin “concrete walls” braced by, and somewhat elastically connected by, the straw-bale core. [3]

II. METHODOLOGY

2.1 Materials

Two batches of rice straw bales were purchased from 2 different farms located in Kafr El-Sheikh Governorate North of Cairo. The bales were harvested during the autumn months of 2012 (October- November) then compacted and stored. The bales in the first and second batches had approximate dimensions of 100 ± 2.5 cm length, 35 ± 2.5 cm height and 50 cm width and 150 ± 2.5 cm length, 35 ± 2.5 cm height and 50 cm width. The average weights of samples of three bales chosen randomly were 22- 25 kg for the batch of length 100 cm and 30-32 for the bales of length 150 cm. The bales had an average bulk density of 125 kg/m³. The average moisture content of bales recorded 18.3 % which meets the California Straw Bale Codes recommendation for a maximum of 20% of total bale weight.

2.2 Specimens

2.2.1 Walls Construction

Two wall specimens (designated A and B) each measuring approximately 360cm length x 200cm height x 50cm width were made up on plain concrete base footing of dimensions 390 cm length x 30cm height x 65cm width. The walls were constructed by stacking of bales from the two batches mentioned earlier. A 16 mm diameter steel bar was embedded in the

walls with a distance of 50 cm between each bar along the full walls' length to tighten the bales. The steel bars were an in the plain concrete footing for a distance of 25cm.

2.2.2. Walls Plastering

Plastering of walls was applied after the pre-compression tests. A galvanized chicken wire mesh 1mm diameter was first stapled to the top plate and bottom plain concrete footing. It was then pulled close to the bales by stitching the mesh with baling twine pulled through the bales. The final step in the construction was the application of the plaster referred to as the "skin". This was done by hand, or by trowel. The skin material is mortar of a combination between cement, sand and lime with proportions 1:6:1 respectively, but the thickness of this skin varied appreciably as it fills in the gaps and notches. The initial layer was worked into the straw. Subsequent layers were built up until the plaster was visually judged to extend beyond the edge of the top plate, sides, and bottom till reaching the concrete footing. The plaster was then allowed to stand and cure in the open air to resemble reality. As for wall A the top layer of the bales were directly subjected to the wire mesh and the plastering layer. While, on top of the bales of wall B, a wooden cap plate was inserted firmly on the bales surface over which the wire mesh and the plaster were provided.

2.3 Testing procedures

Two testing procedures were applied on the specimen walls A and B. The first was the "Leveling procedure" during which the settlement of some fixed points on wall A was observed using the leveling surveying technique. This method is usually used in practice for establishing fixed or temporary bench mark heights above the adopted datum Fig.1 by using a leveling instrument and a rod. In this case, the height difference in each level setup is determined by simultaneously using two rods and taking back sight and fore sight rod readings. According to the pre-specified standard specifications of leveling, the expected accuracy of rod readings is usually in the order of 1 millimeter. The second testing procedure was by using the "Linear Voltage Displacement Transducers" (LVDTs) to measure the settlement in wall B.

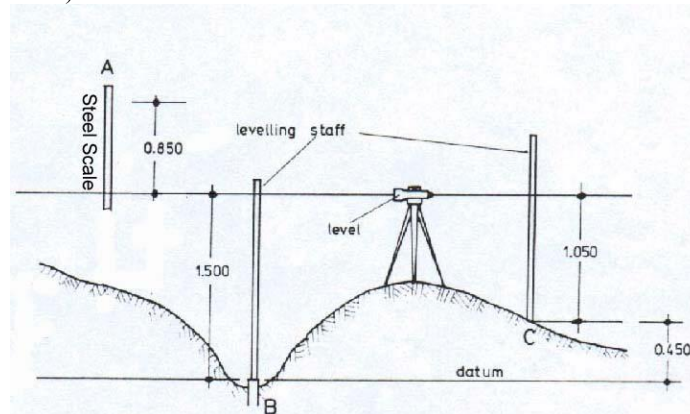


Figure 1: Leveling method with steel scale

2.4 Pre-compression Tests

A pre-compression test Fig. 2 was undertaken on wall A by applying one ton of cement bags on top of the bales of the tested wall directly and left for 5 days before plastering. The observed settlement just after loading is shown in Table 1 measured by the Leveling procedure.

Table 1: The settlement of the observed points at wall A in cm

point	Settlement in cm
1	7.3
2	9.7
3	9.0
4	9.9
5	6.7

Five points were fixed at the tested rice straw wall using steel bars fixed through the wall width. Also, one control point was fixed at a nearby building out of the loading area. From the control point, the levels of the five points were computed. The vertical movement (deflection) of point (T), between any two vertical positions (I and J), came from two loading cases, and were computed by subtracting the two levels of point (T) as indicated in equation (1).

$$D_T = L_j - L_I \quad (1)$$

Where:

L_I Is the initial difference in level between the target and control point (before loading of point).

L_j Is the difference in level between the target and control point (after loading of point).

D_T Is the vertical movement of point (T).



Figure 2: Pre-compression Test of full scale wall A

Five points are fixed at the tested rice straw wall using steel bars fixed through the wall width. Also, one control point is fixed at a nearby building out of the loading area. From the control point, the levels of the five points can be computed. The vertical movement (deflection) of point (T), between any two vertical positions (I and J), comes from two loading cases, can be computed by subtracting the two levels of point (T) as indicated in equation (1).

$$D_T = L_j - L_I \quad (1)$$

Where:

L_I Is the initial difference in level between the target and control point (before loading of point).

L_j Is the difference in level between the target and control point (after loading of point).

D_T Is the vertical movement of point (T).

As for wall B and due to the non uniformity of the settlement results throughout the whole length shown in wall A, a wooden U shaped cap was constructed to cover the top of the wall. On top of this plate all the loads were applied to insure uniform settlement of the bales prior plastering but no records were taken.

2.5 After Plastering tests

2.5.1 Wall A

After releasing the pre-compression load, a steel wire mesh was used to cover wall A from top and both sides before the plastering application. Cement plastering then took place for the wall and left for curing and drying for a period of 28 days before testing. On top of the bales in wall A another set of cement bags for loading were applied regularly. These cement bags were laid on a wooden platform along the length of the wall. The leveling technique was used to measure the settlement in the wall. The used surveying instruments in the experiment were calibrated and adjusted before using them. The control and target points were observed using the level, and the scale readings were recorded before loading, then after applying 1 ton of loads and finally after applying 2 tons of loads. Fig. (3) & (4) show the position of the monitored points as well as the dimensions of the wall.

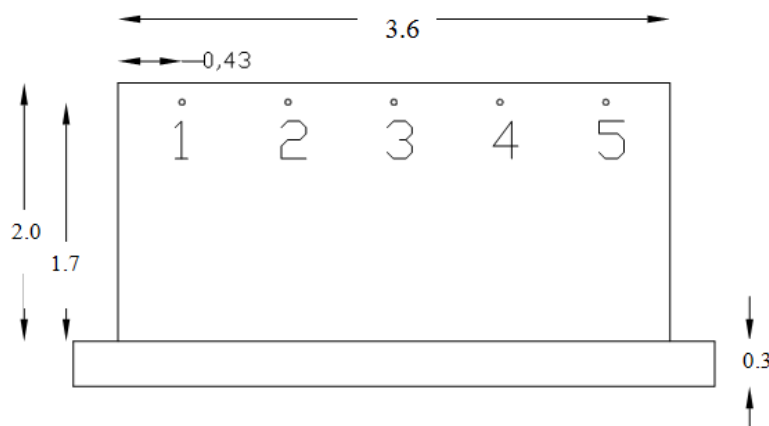


Figure 3: The position of the monitored points and the dimensions of the wall



Figure 4: The 2nd loading case after plastering the wall

The following results in Table 2 were recorded after applying 2 tons of cement bags on top of the wall.

Table 2: The settlement of the observed points at the wall in mm

point	after loading 1 ton	after loading 2 ton
1	1.0	3.5
2	1.0	5.0
3	2.0	3.5
4	1.5	4.0
5	2.0	3.0
Mean	1.5	3.8

The test never ended up till this point of loading as the plan was to keep loading the wall until we reach the failure point as shown in Fig. 5. The failure point was reached after applying over 2.5 tons of cement bags on top of the wall.



Figure 5: Failure point of loading

2.5.2 Wall B

This wall was plastered in a slightly different way from wall A where the top wooden cap plate was inserted on top of the bales then the wire mesh and plaster were applied. This procedure was undertaken to insure more load uniformity over the wall and to avoid the catastrophic failure seen of wall A. The loads were distributed on a wooden platform erected 35cm above the top wooden plate of the wall as shown in Fig. 6. Then 2 hydraulic jacks were set between the wooden platform carrying the load and the top wooden plate of the wall to transfer the loads gradually to the wall. Also 2 LVDTs were connected to the hydraulic jacks to record the settlement in the wall as shown in Fig. 7.



Figure 6: The loading technique on Wall B



Figure 7: The connection between the Hydraulic Jacks and the LVDTs on Wall B

III OBSERVATIONS AND DISCUSSION

As Walls A and B were 2 specimens of relatively similar local rice straw material, which was cultivated and baled in the same circumstances, it was rational to compare between the accuracy of settlement results for the 2 walls of similar length, width and height despite the difference between them in techniques of loading and instrumentation.

3.1 Wall A

The displacements of wall A (vertical movement) were recorded and the settlement was calculated using equation (1). The average settlement was plotted in Fig. 8. The deflection of the wall showed that the response under loading was fairly linear up to 2 tons of distributed load indicating a uniform loading condition. The average recorded settlement in the wall was about 3.8 mm at a load 2 tons with a maximum settlement of 5mm and a minimum of 3 mm at some points. After this point and as loads were increased some cracks initiated to appear in the upper segment along the wall width especially at the tips. In applying more loads and due to difficulty in applying them in a uniform manner, a sudden failure took place in the top tip of the wall. Unfortunately, the researchers were not able to record the readings of deflection of the wall between loading 2 and 2.5 tons of cement. It should be noted that in no instance did the wall fail in a catastrophic manner. Failure was typically preceded by widespread cracking of the plaster.

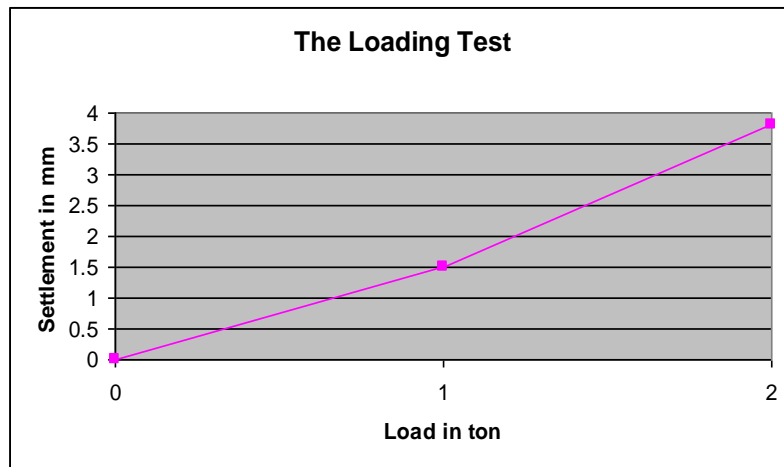


Figure 8: Average settlement of the wall

3.2 Wall B

Fig. 9, 10, 11 and 12 showed typical load versus vertical deflection plot. The vertical deflections were measured by 2 linear voltage displacement transducers (LVDTs) on the edges of the wall at a distance of 0.75m from each end. The recorded readings are expressed on the charts as right and left displacement according to the deflection under each LVDT in place. Each chart begins with the initial reading under zero loading for each LVDT. The loads were increased regularly by a value of 0.4 ton distributed uniformly on the full width of the wall, till reaching the max loading value after which all loads are released and displacement recorded.

Fig. 9 showed some variance in the displacement values of both right and left LVDTs with a maximum value of 3 mm under a concentric compressive load 1.6 ton and 6mm after release of loads. This initial non-linear response can be attributed to the elasticity of the straw at the top of the wall which was not compressed enough before the top plate begins to bear on the plaster skins.

The response of the wall in the 2nd, 3rd and 4th loading phases was fairly linear up to an applied load of 2 ton and also after releasing the loads. It can be seen that in general, the load-deflection response of the wall before reaching the 2 ton load consists of an initial non-linear response, followed by linear behavior up to the maximum load. This indicates that the loading of the wall was uniform. Up till this stage of loading (2 ton) no cracks appeared on both faces of the wall.

The maximum displacement recorded in the wall was 10 mm at the 1st loading phase. After this phase the displacement in the wall decreased from a maximum of 9mm in phase 2 of loading till a constant value of 7mm in phases 3 and 4 of loading. These results showed that the wall gave the same displacement after repetition of loading and unloading indicating that the plaster skin and the bales (supporting system) acted as a composite section or a sandwich panel behavior.

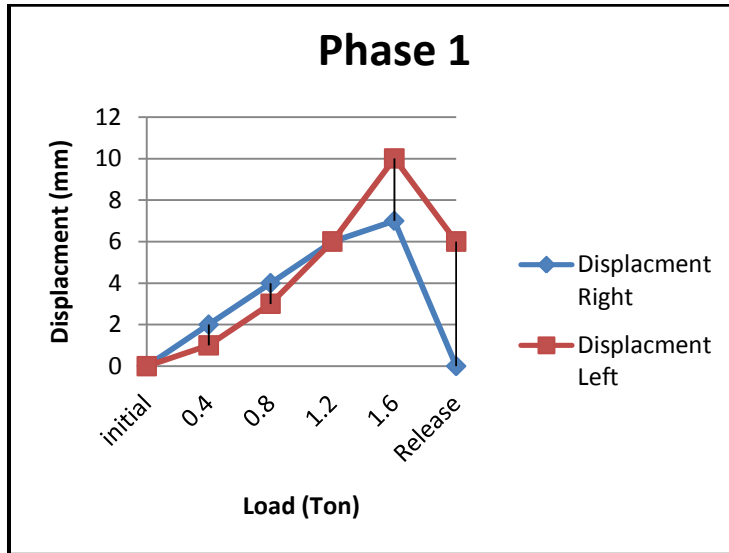


Fig 9: 1st phase of loading

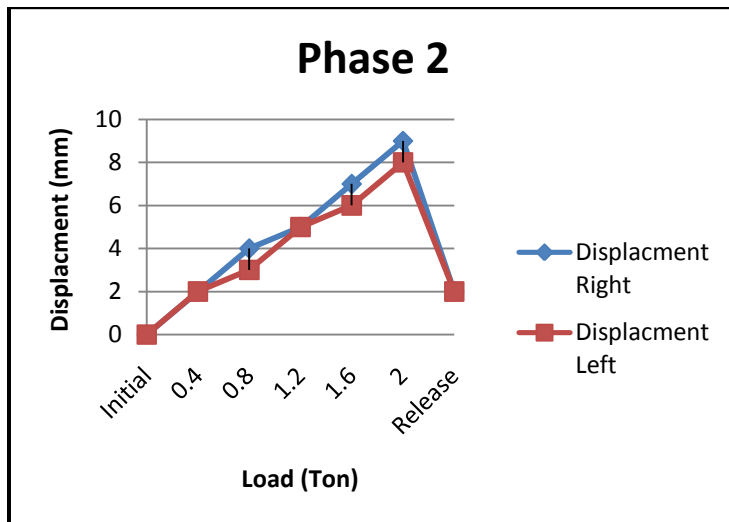


Fig 10: 2nd phase of loading

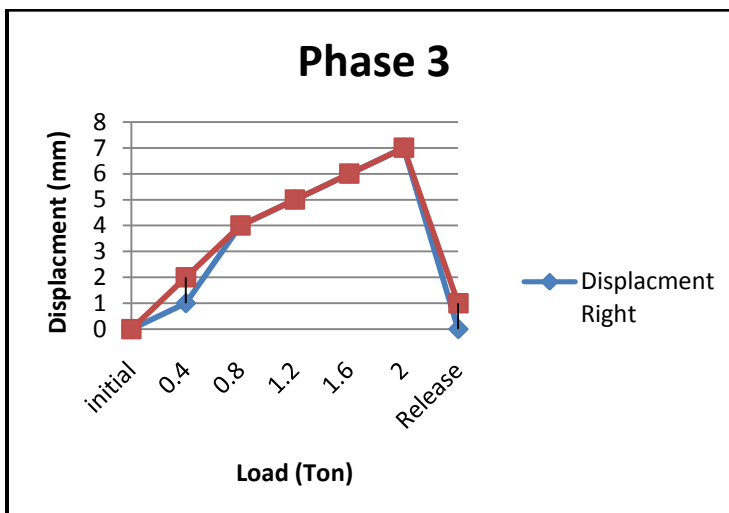


Fig 11: 3rd phase of loading

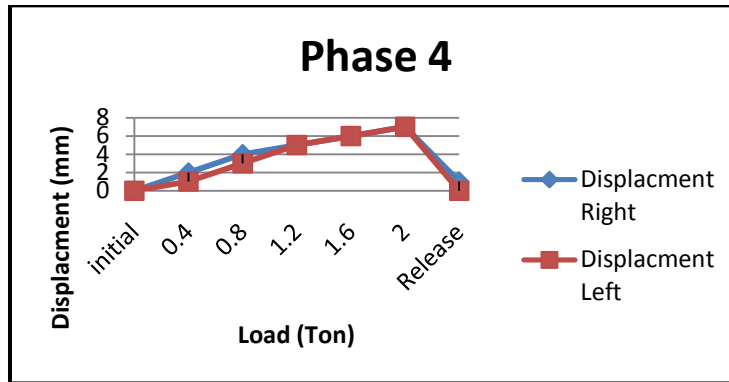


Fig 12: 4th phase of loading

These results does not coincide with the results recorded for Wall A conducted using the leveling technique which presented an average maximum settlement (displacement) of 3.8 mm at a maximum load 2.0 ton. This diversion in the results reinforces the idea that the leveling technique was inaccurate and the loose top wooden plate over which the loads were laid in the 1st experiment failed to give the effect of a cohesive composite section with the plastered wall. As a result it is highly recommended that during the construction of any load bearing straw bale wall, a wooden cap plate should be inserted on top of the wall to insure uniform transfer of the loads along the whole length of the wall. Also this technique of building would confine the connection between the wire mesh, the straw and the plaster to insure the sandwich panel behavior in the section.

Despite the variance in specimens' materials, dimensions, construction techniques, as well as loading and displacement measurements procedures' undertaken by scientists interested in straw bale construction, the authors found it valuable to make an absolute comparison between local and previously reported experimental values of compressive testing results.

In accordance to the Egyptian case of study the un-plastered rice straw wall recorded displacements ranging between 67 and 99 mm. This result falls within the range of displacements of un-plastered walls reported by Bhattarai P. et al, 2012 [4] that varied between 72 and 198 mm. Similarly, Carrick J. et al [5] reported vertical displacement of un-plastered straw bale walls of 66m.

This behavior was attributed to the walls creep with time under load following an initial instantaneous deformation, immediately recovering some deformation on load removal, followed by further time dependent recovery but exhibiting a final permanent deformation. Researchers agreed that pre-compression improved initial stiffness of the straw bale wall. In case of plastered walls, the maximum loads applied in the Egyptian case of study was 2 ton with a displacement ranging between 7-10 mm. This result contradicts with the Indian case conducted by Bhattarai P. et al, 2012 showing a displacement of 55 mm under a load of 4.1 ton while Carrick J. et al [5] reported an average displacement of 5.1mm under an average vertical load of 7.5 ton.

IV. Conclusion

This testing was undertaken with a view to determining the structural properties of the rice straw plastered walls for applications in domestic construction. The load applied for testing the specimens complied with the California Straw bale Codes [6] that recommended an allowable vertical load of not more than 2.15 ton/m² (400 pounds per square foot) on load bearing walls. Two specimens of straw baled walls of dimensions 360cm length x 200cm height x 50cm width were tested using two techniques for displacement measurement under a maximum load of 2 ton. Pre-compression improved initial stiffness of the straw bale walls. It was concluded that placement of a wooden cap plate on top of the straw bale wall is important to insure uniform transfer of the loads along the whole length of the wall. Also this technique of building would confine the connection between the wire mesh, the straw and the plaster to insure the sandwich panel behavior in the section. The displacements recorded ranged between 7- 10 mm. No hair cracks appeared on both surfaces of plastering during repetitive loading till reaching the maximum load.

References

- [1]. King, B. (2006) "Design of straw bale buildings." Green Building Press, San Rafael California. 259 pp.
- [2]. King, B. (2001) "Straw-Bale Construction A Review of Testing & Lessons Learned To Date" Ecomaterials Conference.
- [3]. King, B. (1998) "Straw Bale Construction" Building Standards/ September- October
- [4]. Bhattarai, P., Raj Dhakal, D., Neupane, K. and Chamberlin, K., " Straw Bale in Construction of Building and its Future in India", International Journal of Modern Engineering Research (IJMR), Vol. 2, Issue 2, Mar-Apr 2012 pp-422-426.
- [5]. Carrick, J., and Glassford, J. (1998), "Compressive, Transverse and Racking Tests of Load-Bearing Walls," *Research Report*, Building Research Centre, University of New South Wales, Australia.
- [6]. California Straw Bale Code, Bill Number: Ab 1314 Chaptered (10/16/1995) ,Chapter 941 Introduced By Assembly Members Sher, Richter, and Woods (Coauthor: Senator Johannessen)

Modeling and Transient Analysis of Wind Generator during Grid Voltage Drop

Patturu Chinnaiah¹, Prof. M.L.S. Deva kumar²

Energy systems, Jawaharlal Nehru Technological university Anantapur, India

ABSTRACT: In recent years, wind energy has become one of the most important and promising sources of renewable energy, which demands maintaining better means of system stability. The performance of a grid-connected wind energy conversion system (WECS), based on a doubly fed induction generator (DFIG) fed by an AC-DC-AC converter, is presented. The stator winding of the DFIG is connected directly to the grid and the rotor of the DFIG is connected to the grid through a AC/DC/AC converter.

The main power is transferred through the stator windings of generator that are directly connected to the grid. Around 65-75% of total power is transmitted through the stator windings and the remaining 25% of total power is transmitted using rotor windings (i.e.) through the converters. The major advantage of speed control of variable speed wind turbine generators is usually optimized which gives the maximum power in the system. This project focuses towards an efficient control strategy to improve the overall efficiency and stability in Doubly Fed Induction Generator (DFIG) using converters.

Keywords: DFIG, Back to Back converter, wind turbine.

I. INTRODUCTION

Due to increasing demand on electrical energy and environmental concerns, a considerable amount of effort is being made to generate electricity from renewable sources of energy. The major advantages of using renewable sources are abundance. Wind is the one of the most abundant renewable sources of energy in nature. The wind energy can be harvested by using a wind energy conversion system, composed of a wind turbine, an electrical generator, a power electronic converter and a control system. With increased penetration of wind power into electrical grids, DFIG wind turbines are largely deployed due to their variable speed generation and they are the most important generators for wind energy applications.

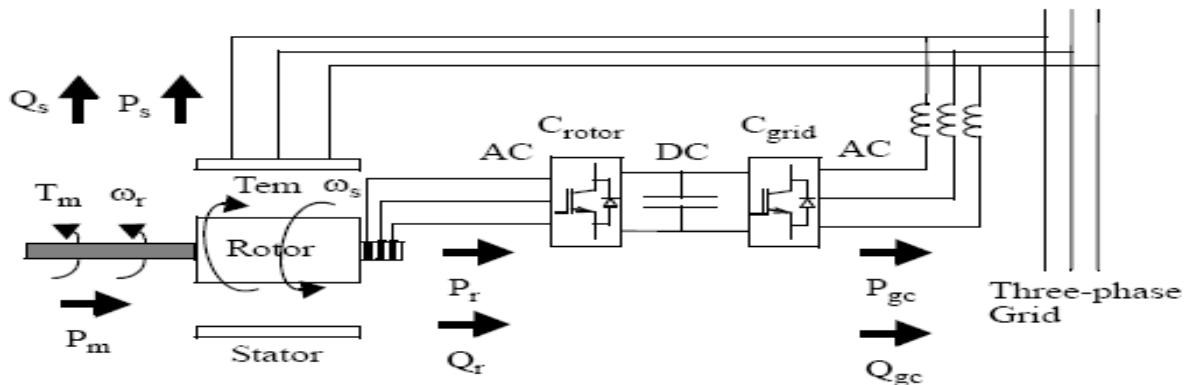


Fig 1.1 DFIG connected to Back to Back converter

In conventional implementation of a grid connected DFIG, back-to-back converters are used to connect the DFIG rotor to the utility. The rotor side converter controls the magnetizing and torque rotor currents. The grid side converter regulates the voltage in the dc bus of the back-to-back converters. It should be recognized here that thyristors are commonly used as switching devices in the shaft generator system because of their higher reliability, efficiency and easy acquisition of large ratings. Since the output frequency and voltage of the DFIG driven by the wind turbine are changed due to unexpected fluctuation in the wind, ac power generated by the DFIG is converted once into dc power with the thyristor rectifier, and then the dc power is converted again into ac power with constant frequency and constant voltage with the inverter, which is supplied to the loads (or electric power utility).

REASONS FOR USING DFIG

DFIG-based WECS are highly controllable, allowing maximum power extraction over a large range of wind speeds. Furthermore, the active and reactive power control is fully decoupled by independently controlling the rotor currents. Finally, the DFIG-based WECS can either inject or absorb power from the grid, hence actively participating at voltage control. The synchronous nature of PMSG may cause problems during startup, synchronization and voltage regulation and they need a cooling system, since the magnetic materials are sensitive to temperature and they can lose their magnetic properties if exposed to high temperature. Hence DFIG is dominantly used when compared to PMSG.

A three-phase wound-rotor induction machine can be set up as a doubly-fed induction motor. In this case, the machine operates like asynchronous motor whose synchronous speed (i.e., the speed at which the motor shaft rotates) can be varied by adjusting the frequency of the ac currents fed into the rotor windings. The same wound-rotor induction machine setup can also serve as a doubly-fed induction generator. In this case, mechanical power at the machine shaft is

converted into electrical power supplied to the ac power network via both the stator and rotor windings. Furthermore, the machine operates like a synchronous generator whose synchronous speed (i.e., the speed at which the generator shaft must rotate to generate power at the ac power network frequency ($f_{network}$) can be varied by adjusting the frequency of the ac currents fed into the rotor windings.

In a conventional three-phase synchronous generator, when an external source of mechanical power (i.e., a prime mover) makes the rotor of the generator rotate, the static magnetic field created by the dc current fed into the generator rotor winding rotates at the same speed (n_{rotor}) as the rotor. As a result, a continually changing magnetic flux passes through the stator windings as the rotor magnetic field rotates, inducing an alternating voltage across the stator windings. Mechanical power applied to the generator shaft by the prime mover is thus converted to electrical power that is available at the stator windings.

MODES OF OPERATION IN DFIG

Depending on the rotor speed, there are two modes of operation in a DFIG WECS. (1) Super-synchronous mode, in which the generator operates above the synchronous speed, (2) sub synchronous mode, in which the generator operates below the synchronous speed. The slip is negative in the super-synchronous mode and becomes positive in the sub-synchronous mode. Depending on whether the slip is positive or negative, the rotor circuit can receive or deliver power from or to the grid. In the super synchronous operation mode, the mechanical power $|P_m|$ from the shaft is delivered to the grid through both stator and rotor circuits. The rotor power $|P_r|$ is transferred to the grid by power converters in the rotor circuit, whereas the stator power is delivered to the grid directly. Neglecting the losses in the generator and converters, the power delivered to the grid $|P_g|$ is the mechanical power $|P_m|$ of the generator. For the sub synchronous operation the rotor receives the power from the grid. Both mechanical power $|P_m|$ and rotor power $|P_r|$ are delivered to the grid through the stator. Although the stator power is the sum of $|P_m|$ and $|P_r|$, it will not exceed its power rating since in the sub-synchronous mode the mechanical power $|P_m|$ from the generator shaft is lower than that in the super-synchronous mode. As in the previous case, neglecting the losses, the total power delivered to the grid $|P_g|$ is the input mechanical power $|P_m|$.

II. MODELING OF WIND TURBINE

The modeling of wind turbine consists of three important parameters. They are a) Transmission system b) Wind turbine system c) Distribution system.

TRANSMISSION SYSTEM

The electrical energy produced at various power stations are transferred to the consumers through conductor lines. It consists of a voltage source, step-up transformer, transmission line, a bus bar, step down transformer, V-I measurement block, scope and a resistive load.

1) AC Power Supply Scheme

The large network of conductors between the power station and the consumers can be broadly divided into two parts namely transmission and distribution systems. Each part is subdivided into primary and secondary transmission.

2) Generating Station

The generating station where electric power is produced by 3-phase alternator is operated in parallel. The usual generating voltage is 11kv. For economy in the transmission of electric power, the generated voltage is stepped up to 132kv at the generating station with the help of 3-phase transformers.

3) Primary Transmission

The electric power at 132kv is transmitted by 3-phase, 3-wire overhead system. This forms the primary transmission.

4) Secondary Transmission

The primary transmission line terminates at the receiving station. At the receiving station the voltage is reduced to 33kv by step-down transformers. From this station, electric power is transmitted at 33kv by 3-phase 3-wire over head System to various sub-stations. This forms the secondary transmission.

5) Primary Distribution

The secondary transmission line terminates at the sub-station where voltage is reduced from 33kv to 11kv 3-phase, 3-wire. This forms the primary distribution. From this the large consumers which are using 11kv are distributed from here.

6) Secondary Distribution

The electric power from primary distribution line (11kv) is delivered to distribution sub-stations. These sub-stations step down the voltage to 400V, 3-phase and 4-wire for secondary distribution. The voltage between any two phases is 400V and between any phase and neutral is 230V. From this the voltage is supplied to the feeders and to the consumers.

Wind turbines convert the kinetic energy present in the wind into mechanical energy by means of producing torque. Since the energy contained by the wind is in the form of kinetic energy, its magnitude depends on the air density and the wind velocity. The wind power developed by the turbine is given by the equation (1.1):

$$P = \frac{1}{2} C_p \rho A V^3 \dots (1.1)$$

Where C_p is the power co-efficient, ρ is the air density in kg/m^3 , A is the area of the turbine blades in m^2 and V is the wind velocity in m/sec . The power coefficient C_p gives the fraction of the kinetic energy that is converted into

mechanical energy by the wind turbine. It is a function of the tip speed ratio λ and depends on the blade pitch angle for pitch-controlled turbines. The tip speed ratio may be defined as the ratio of turbine blade linear speed and the wind speed.

$$\lambda = R\omega/V \dots (1.2)$$

Substituting (1.2) in (1.1), we have:

$$P = \frac{1}{2} C_p(\lambda) \rho A(R/\lambda) \omega^3 \dots (1.3)$$

The output torque of the wind turbine Turbines calculated by the following equation (1.4)

$$\text{Turbine} = \frac{1}{2} \rho A C_p V / \lambda \dots (1.4)$$

where R is the radius of the wind turbine rotor(m). There is a value of the tip speed ratio at which the power coefficient is maximum. Variable speed turbines can be made to capture this maximum energy in the wind by operating them at a blade speed that gives the optimum tip speed ratio. This may be done by changing the speed of the turbine in proportion to the change in wind speed.

III. Converter Methodology

Wind turbines use a doubly-fed induction generator (DFIG) consisting of a wound rotor induction generator and an AC/DC/AC IGBT based PWM converter. The stator winding is connected directly to the 50 Hz grid while the rotor is fed at variable frequency through the AC/DC/AC converter. The DFIG technology allows extracting maximum energy from the wind for low wind speeds by optimizing the turbine speed, while minimizing mechanical stresses on the turbine during gusts of wind. The optimum turbine speed producing maximum mechanical energy for a given wind speed is proportional to the wind speed. Another advantage of the DFIG technology is the ability for power electronic converters to generate or absorb reactive power, thus eliminating the need for installing capacitor banks as in the case of squirrel-cage induction generator. Where V_r is the rotor voltage and V_{gc} is grid side voltage. The AC/DC/AC converter is basically a PWM converter which uses sinusoidal PWM technique to reduce the harmonics present in the wind turbine driven DFIG system. Here C_{rotor} is rotor side converter and C_{grid} is grid side converter. To control the speed of wind turbine gear boxes or electronic control can be used.

IV. Control Parameters

The block diagram for control parameters shows different modes of operation in which we can select the voltage regulation mode and Var regulation mode. Also we can set the external reactive current I_q ref for grid side to zero which gives flexibility to simulate various fault conditions. Here we input the required values of voltage regulator gains (both proportional and integral), power regulator gains, current regulator gains and their respective rate of change.

V. Induction Machine Model

The model of the IG is an instantaneous values full order one, i.e. fifth order with the derivative of the stator fluxes included. This is the best choice to accurately simulate transients in the power systems when the electrical dynamics of the IG is of primary interest. The values of the IG parameters have been chosen as per the requirements. The DFIG wind farm is composed of 6 aggregated units of 1.5MW each.

VI. Grid Side Converter

The GSC is modeled using a universal bridge model with IGBTs connected to the IG terminals through a series RL filter. The control of the GSC aims at keeping the DC-link capacitor voltage constant at nominal value. It does not contribute to grid voltage regulation or reactive power injection ($I_q = 0$). The converter maximum power is half the IG rated power.

VII. Rotor Side Converter

The RSC controls the active power delivered by the DFIG, by determining a torque reference (following a power-speed curve). This torque reference is used along with a flux estimate to determine the reference rotor current I_{dr} . The RSC model has been modified so as to support the grid voltage with reactive power injection. The reference for the reactive power is determined through a PI controlled by measuring the grid voltage and comparing it with a reference.

VIII. Network Model

A 9-MW wind farm consisting of six 1.5 MW wind turbines connected to a 25-kV distribution system exports power to a 120-kV grid through a 30-km, 25-kV feeder. A 2300V, 2-MVA plant consisting of a motor load (1.68 MW induction motor at 0.93 PF) and of a 200-kW resistive load is connected on the same feeder at bus B25.

MATLAB/SIMULINK MODEL

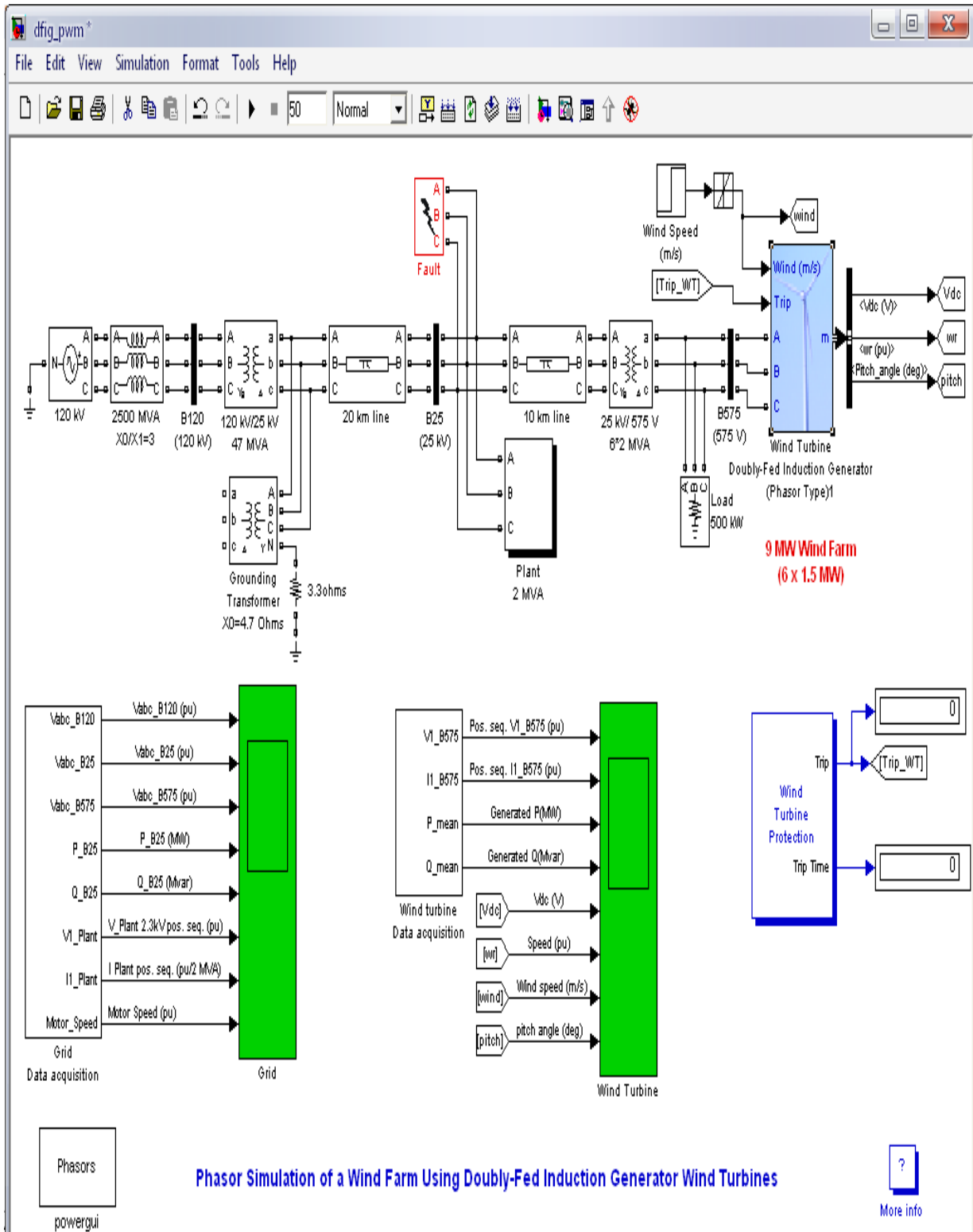


Fig 1.2 DFIG Matlab/Simulink Model

IX. Results and Discussions

In the "Wind Speed" step block specifying the wind speed. Initially, wind speed is set at 8 m/s, then at t = 5s, wind speed increases suddenly at 14 m/s.

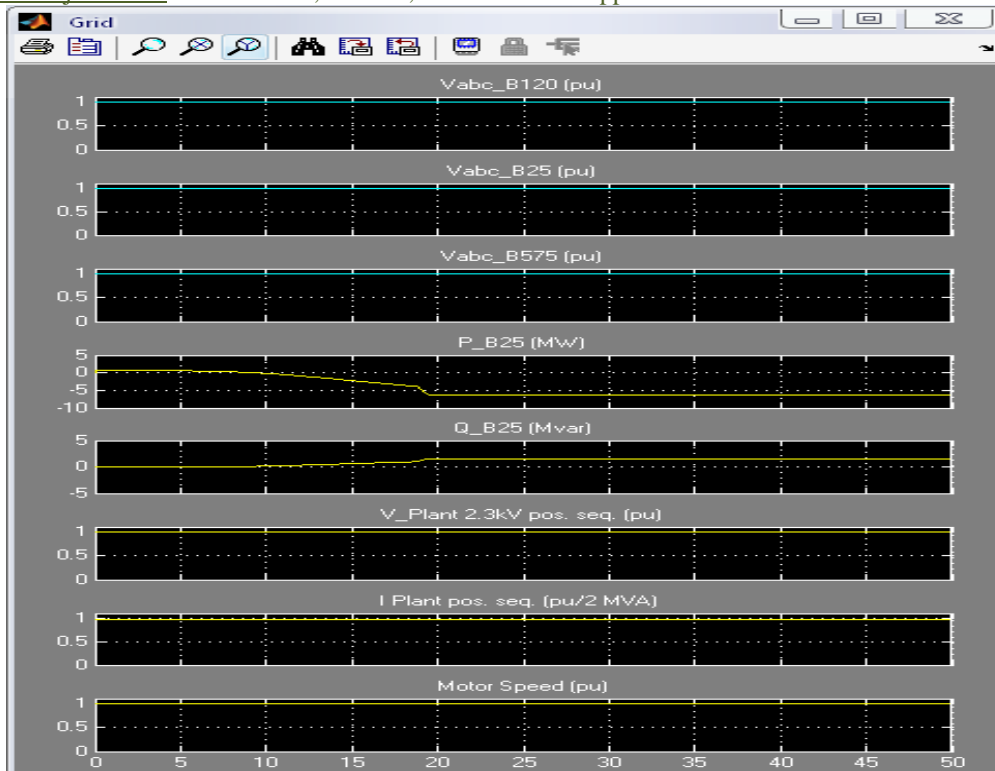


Fig 1.3 Outputs of Grid

Start simulation and observe the signals on the "Wind Turbine" scope monitoring the wind turbine voltage, current, generated active and Reactive powers, DC bus voltage and turbine speed. At $t = 5$ s, the generated active power starts increasing smoothly (together with the turbine speed) to reach its rated value of 9 MW in approximately 20 s. Over that time frame the turbine speed will have increased from 0.8 PU to 1.21 PU. Initially, the pitch angle of the turbine blades is zero degree and the turbine operating point follows the red curve of the turbine power characteristics up to point D. Then the pitch angle is increased from 0 deg to 0.76 deg in order to limit the mechanical power. We also observed the voltage and the generated reactive power. The reactive power is controlled to maintain a 1 PU voltage. At nominal power, the wind turbine absorbs 0.68 Mvar (generated $Q = -0.68$ Mvar) to control voltage at 1PU.

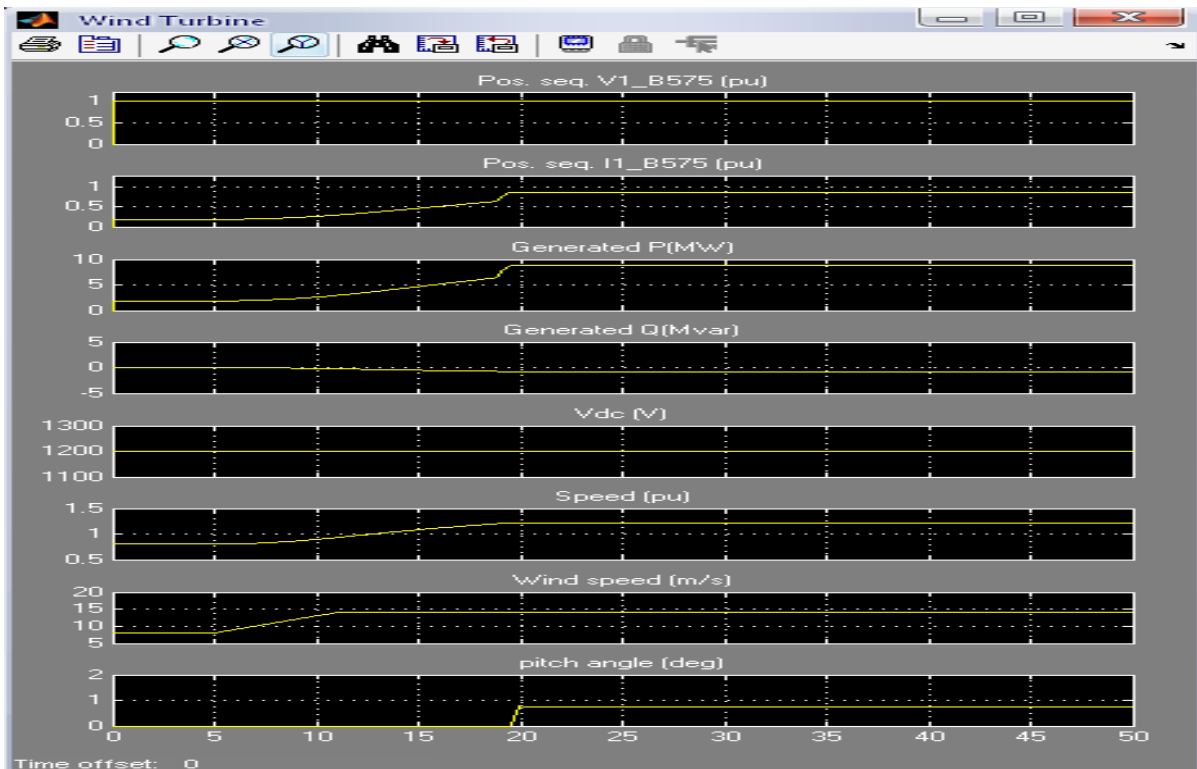


Fig 1.4 Outputs of Wind turbine

X. Conclusion

The wind farm is built with the rectifiers and the inverters. The features are low cost, low commutation power losses and high reliability. The rotor side converter (RSC) usually provides active and reactive power control of the machine while the grid-side converter (GSC) keeps the voltage of the DC-link constant. So finally we simulated grid side and wind turbine side parameters and the corresponding results have been displayed.

The model is a discrete-time version of the Wind Turbine Doubly-Fed Induction Generator (Phasor Type) of MATLAB/SimPowerSystems. Here we also took the protection system in consideration which gives a trip signal to the system when there is a fault (single phase to ground fault) on the system. The faults can occur when wind speed decreases to a low value or it has persistent fluctuations. The DFIG is able to provide a considerable contribution to grid voltage support during short circuit periods. Considering the results it can be said that doubly fed induction generator proved to be more reliable and stable system when connected to grid side with the proper converter control systems.

References

- [1]. Akhmatov V., Analysis of dynamic behavior of electric power systems with large amount of wind power, PhD thesis, 2003, Ørsted DTU.
- [2]. Heier S. Grid Integration of Wind Energy Conversion Systems, John Wiley & Sons, Ltd. Chichester UK, 1998.
- [3]. Hansen A.D., Michalke G., Fault ride-through capability of DFIG wind turbines, *Renewable Energy*, vol 32, 2007, pp 1594-1610.
- [4]. Akhmatov V., Variable-speed wind turbines with doubly fed induction generators. Part II: Power System Stability. *Wind Engineering*, Vol. 26, No. 3, 2002, pp 171-188.
- [5]. Akhmatov V., Variable-speed wind turbines with doubly fed induction generators. Part IV: Uninterrupted operation features at grid faults with converter control coordination. *Wind Engineering*, Vol. 27, No. 6, 2003, pp 519-529.
- [6]. Sørensen P., Bak-Jensen B., Kristiansen J., Hansen A.D., Janosi L., & Bech J. Power plant characteristics of wind farms. *Wind Power for the 21st Century. Proceedings of the International Conference, Kassel, 2000*, 6pp.
- [7]. Eping C., Stenzel J., Poeller M., Mueller H., Impact of Large Scale Wind Power on Power System Stability, Fifth International Workshop on Large-Scale Integration of Wind Power and Transmission Networks, Glasgow, 2005, 9pp.
- [8]. Kayikci M., Anaya-Lara O., Milanovic J.V., Jenkins N., Strategies for DFIG voltage control during transient operation, CIGRE, 18th Int. Conference on Electricity Distribution, Turin, 2005, 5pp.
- [9]. Akhmatov V., A small test model for the transmission grid with a large offshore wind farm for education and research at Technical University of Denmark., *Wind Engineering*, vol.30, No. 3, 2006, pp. 255-263.

Final open pit design for Monte Raso phosphate mine

Adilson Curi¹, Marcos Antônio Pereira², Wilson Trigueiro de Sousa³, Valdir Costa Silva⁴
^{1,2,3,4}(Department of Mining Eng., Graduate Program, School of Mines, Federal University of Ouro Preto, UFOP, Brazil)

ABSTRACT: A fundamental aspect in the development of any open-pit mining project is the determination of the mineable reserves and the respective design of the ultimate pit limits. The design of the ultimate pit is of prime importance for practical open pit mining as is evident from the worldwide attention it has been receiving in the past decades. All major mining software offer some version of pit limits design packages among their services. The Monte Raso property (MR mine) is a phosphate prospect located in the central state of Goiás, in Brazil. The drillhole information and the topographic map have been kindly provided by a Brazilian phosphate mining company. As the true location of the prospect is not important in this case study authors have modified it to the vicinity of a real phosphate mine in order to provide a realistic geological information from published sources. In this fictitious account, the names of the structural features have been retained. In this paper, at first, the Vulcan software, applied over the data of MR phosphate deposit, will be introduced. The modeling of the ore deposit was done using a geological database of 41 diamond core samples. Finally, the ultimate pit limits of the deposit were determined and the design of the ultimate pit presented.

Keywords: Design, Mining, open pit, phosphate

I. INTRODUCTION

The mineral resources are nonrenewable in the human scale of time and their exploitation should be made thoughtfully objectifying the maximal recovery of the mineral reserves. The mining of an open pit is a complex operation that extends for many years and involves a huge capital and risks. Before *start up* is fundamental to classify the ores of the mineral deposit (ore types, ore grades, ore amount and ore spatial distribution) and establish as these ores should be mined to get profit. A fundamental aspect in the development of any open pit mining project is the determination of the mineral reserves to be exploited through the design of the called ultimate pit limits [1], [2], [3], [4]. Currently, the different types of algorithms used to optimize the mine open pit can be divided in two categories [5]:

Heuristics: the experience demonstrates that their results in terms of mine open pit optimization are satisfactory although without a mathematical demonstration to assure their validity. This is the case of the methods of the Flotation Cone, Korobov, and Function of parameterization of François-Bongarçon.

Rigorous: When the optimization has a complete mathematical demonstration. The most characteristic and famous is the method of Lerchs & Grossmann [6].

II. The Monte RASO Phosphate Deposit

The Monte Raso phosphate deposit exploration was made by the Mineração Boa Esperança S.A - MBESA [7]. The phosphate reserves, for which a basic project for definition of the final open pit limits was developed in this paper, is a unreal reserve, but it is not impossible. The structure of this reserve was based on a real reserve and the grades are resulting of the multiplication of the grades of the original deposit by a certain unknown factor. The justification for this procedure is based on confidentiality needs and in the convenience of joining, in a same ore reserve, most of the problems that generally happen in a mine project. The phosphate reserves of Monte Raso are located in the state of Goiás, approximately at 200 km (NW) of Brasília and 250 km of Goiânia. (Fig.1).

The older geologic formations of this region have a correlation with the Precambrian era. The geology of the deposit of Monte Raso is stratigraphically positioned in Paraobepa formation of Bambuí geological Group. The phosphate rocks are located in the top of the Paraobepa formation in conformity with a layer of weathered slate with high grade of magnesium (WM). On the other hand, the phosphate mineralization is covered by a layer of calcium-chlorite-schists. The phosphate layers were submitted to a light geological weathering characteristic of the Bambuí group and Paraopeba formation. In the determination of the typology of the phosphate ores of the reserve of Monte Raso the grades of P_2O_5 , CaO and $Al_2O_3 + Fe_2O_3$ were considered and were included samples off all of the 41 survey holes. The method used for ore characterization is denominated Cluster Analysis. In this methodology the objective is the formation of homogeneous groups of ores based in chemical and/or mineralogical composition of the samples. As conclusion of this studies three elementary types of ore were established: the weathered slate superior (WSS), weathered slate medium (WSM) and the weathered slate inferior (deep) (WSI). The wavellitic crust (WC), the black slate (BS) and the horizon slate with magnesium (WM), although they constitute different groups, were not classified as ore. The conclusion is that the primary ore of the deposit is a weathered slate (WS) with an average grade of 10% of P_2O_5 [8].



Figure 1 - Location map of the Monte Raso Phosphate Reserve (MR mine).

Source: CPRM - Brazilian Geological Service

III. THE VULCAN PROGRAM

The Vulcan program is a dynamic graphic system with the most modern three-dimensional technique (3D) to accomplish the exploration and to model the geology, project of mines, production of mines, topography, extraction of resources, geostatistics, surfaces in general, environmental rehabilitation, planning of open pit and underground mines [9] [10]. This program uses the algorithm of Lerchs & Grossmann as optimization method for open pit mines. The program VULCAN allows the construction, visualization and manipulation of models of blocks, providing an optimization of the space representation of the geometry of the ore body starting from the definition of the size of the initial block or root (or secondary blocks, if it is necessary) and the variables of the model. The number of variables that can be inserted in the model is satisfactory including those that store the revenue generated in each block, the number of samples used to estimate the grades, the average distance of the samples to the block, the number of holes used in the estimate and the variance of the estimate of each block. The program VULCAN facilitates the estimate of referred grades of the blocks, the definition of the geologic reserves and the drawing of the final limits of the pit. Several geologic scenarios can be modeled (as metallic deposits of good stratigraphic conformity, deposits of coal and complex disseminated deposits or veins). The program incorporate geostatistical tools and of analysis of data and estimate of the reserves. One of the modules of the program allows the interface with programs and algorithms of optimization as Lerchs&Grossmann and the program Whittle 3D.

IV. OPEN PIT MINE DESIGN METHODOLOGY

The open pit mine design methodology starts by construction of databases containing the general data of the mine exploration, visualization of the surveys, geologic modeling and, based in the topographic map of the Monte Raso region (Figure 2), generation of the topographical surface (Fig.3). The next steps are implementation of the model of blocks, evaluation of reserves and project of the final limits of the pit [11] [12]. For modeling the ore body are used, frequently, regular blocks and a great collection of regular blocks to represent the overall mineral body.

According to Hustrulid, W. and Kuchta, M. [11] the steps that were generally used to create a block model for a mine to evaluate the mineral reserves are listed below :

- a) Create a file containing the collar coordinates of the exploration drill holes, the hole directions and the assay values along the hole lengths.
- b) Create a surface topography and plot the locations of the drill holes.
- c) Plot vertical sections through lines of drill holes in order to examine probable pit location.
- d) Choose the size and position of the blocks and the model grid. The thickness (B_z) of the blocks is usually set to planned bench height. The block width (B_x) and (B_y) height dimensions are chosen arbitrarily (normally equal to one another) but a rule of thumb is that the block size (in plan) should not be less than one-fourth the average drill hole spacing. The location of the grid can be decided upon by examining the plan and section maps and locating the block grid such the potential pit area (including a provision for pit slopes) is covered. Create a composite file from the drill hole file. In order to estimate block values, the assay samples must be regularized to form composites defined over core sections of equal length. It is common in open pit mining to choose the composite lengths to be equal to the bench height, or a submultiple of the bench height, and to calculate the composites such that their centers fall at the midpoints of the blocks.

- e) Assign the block grades. After preparing the necessary data files and deciding on the size and location of the block model, a grade must be assigned to each block. In this simulation, the geostatistical methods was used for assigning block values.
- f) Create horizontal plan maps and vertical section maps through the block model to be used for planning purposes.

Assign economic values to the blocks. From the block grades and estimated mining costs, an economic value for each block is assigned. In the specific case of a mine after mineral grades for each block have been calculated, the economic block values were assigned using a benefit function (BF) presented in equation 1.

$$BF = \gamma \times v \times x (\% \text{ mineral}) \times (\text{mineral recovery}) \times (\text{price of mineral product}) - \text{costs of (refine + milling + processing + administration + mining + haulage)} \quad (\text{Eq.1})$$

being γ the density of “*in situ*” material, v the block volume and x the block grade. The equation 1 is a general mathematical expression to determine the net value of each block of a block model according to economic parameters. This function determines the net value of each block of the block model by calculating the difference between the revenue based on the mineral contained and the costs for mineral production. The economic parameters for the benefit function used in the simulations are presented in Table 1 and were evaluated taking in to account data of the Brazilian production of phosphate rock. This figures were calculated based in information of the references [13] and [14].

Table 1 – Mine economic parameters of the exploitation in US \$ per ton

General mineral recovery (mining and processing)	0.7
Cost of mining & processing	- 54
Price of mineral product	+ 62.0

- g) Calculate the final pit limits. From the economic block values, the pit limit shell may be calculated using one of the several available optimization techniques. It was used a slope bench angle of 60°. In this simulation a L&G algorithm included in the Vulcan software was used.
- h) Locate in the ultimate pit the blocks of waste and the blocks of ore by restricting the entire block model using the surface topography (Fig.3) and the ultimate pit limits calculated in the item g). A select tridimensional vision of the resulted open pit restricted by topography and ultimate pit limits is presented in the Fig.6.

Usually a pattern of ore dissimilarity is reached subdividing the mineral deposit in areas that are geologically homogeneous. The attribution of the blocks grades (Table 2) usually is made by a procedure of deterministic interpolation as, for example, the methods of the inverse of the distance or kriging. Besides, the experience demonstrates that, frequently, about 95% of the elementary blocks of the block model don't have any value and not even contains any sample value. The estimate of the blocks of the pit and consequently, the geologic reserves of phosphate of Monte Raso were made using a geostatistical method. The block model built for evaluation of the geologic reserves of Monte Raso presented a total of 403.117 blocks with tridimensional dimensions established for each block of 10 x10 x 10 meters.

It is important to reminder that the task to attribute or to esteem values of costs for the blocks in an open mine is not easy. This fact has a huge influence on costs and time in terms of evaluation of the model.

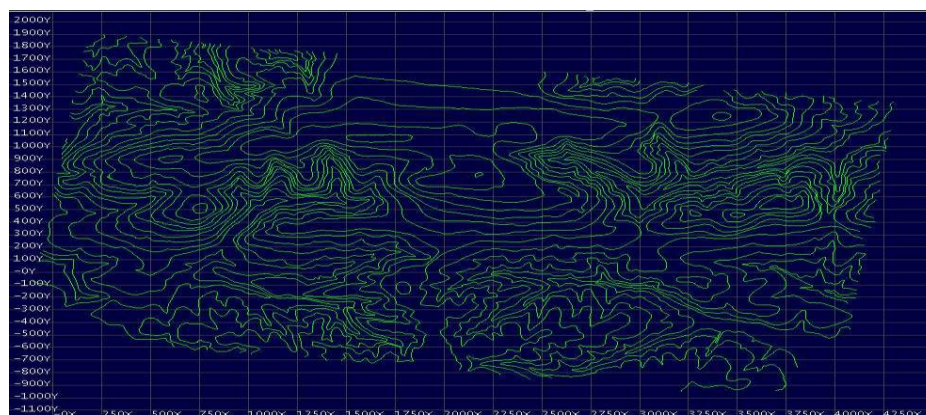


Figure 2 - General aspect of the topographic map of Monte Raso region (without scale).

Source: Pereira, 2000

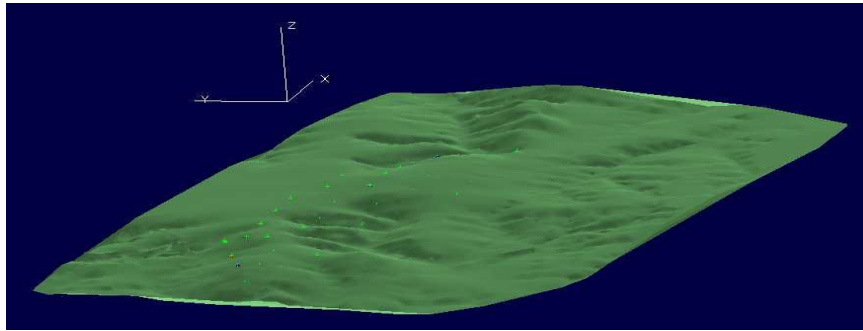


Figure 3 - General aspect of the surface map of Monte Raso region including drill holes (green dots) (without scale)

Source: Pereira, 2000

Table 2 - Statistical analysis of the data for Monte Raso reserve

Products	%P ₂ O ₅	%CaO	%Fe&Al
Arithmetic average	6,5	8,7	5,3
Standard variation	3,6	4,8	2,8
Variance	12,8	22,8	7,7
Median	6,0	8,3	4,6

In the definition of geologic reserves any limitation or restriction of cutoff was applied. It results in a subtotal of 41.082 blocks (in a total collection of 403.117 blocks of the whole block model). The table 3 presents the grades and mass calculated for each lithology as mentioned in the section II . It is important to highlight that the average grades for P₂O₅ and CaO were pondered by mass. The general average grade of phosphate is 7,3 % of P₂O₅ for a total geologic reserve of 50 million tons and a volume of 31 million of cubic meters, considering a average density of 1,60 ton/m³. The weathered slate lithology (WSS, WSM) and the deep weathered slate (WSI) are the ones that presented higher grades of P₂O₅, being, therefore, the lithologies that represent the ore body to be mined.

Table 3 - Results of the geologic reserves of MR.

Lithology	%P ₂ O ₅	%CaO	Mass (ton)	Volume (m ³)
WSS	3,3	3,2	1.323.400	827.125
WSM	8,2	10,6	35.804.601	22.377.875
WSI	5,3	7,9	10.924.400	6.827.750
BS	3,4	7,0	972.750	486.375
WCc	1,5	0,7	620.500	310.250
Total	7,3	9,6	49.645.651	30.829.375

The options to define the final pit limits of the MR mine were done by a specific module of the Vulcan program. Several simulations bearing in mind the obtainment of better pit were made considering economic factors and mainly the profit; the key objective of a mining industry. The resultant final pit was which one that presented the higher profit considering the whole ore body to be mined. Taking into account the economic aspects the ore body to be mined was divided in several horizontal layers (levels) or mine benches. Starting from the bottom of the ore body the first level or mine bench where the profit was positive (profit > 0) was determined. The open pit was so built taking this level as a level of reference. The other mine levels or benches were so projected and designed in the surface (Fig. 3) direction (down / top) using the geometrical parameters of the pit listed in the Table 4 (See below). It results in a subtotal of 36.026 blocks (in a total collection of 403.117 blocks of the whole block model). The first level or mine bench is in the elevation of 805m in relation off the sea level. Starting from the level 805 m, foot of the first bench, the other levels of the open pit were built. The values of the geometrical parameters of the open pit are shown in the table 4 [15]:

Table 4 - Geometrical parameters of the MR mine

Parameters	Value
Width of the berms (m)	5
Height of the bench (m)	10
Angle of the face of the slope (degree)	60°
Width of the road (m)	12
Maximal inclination of the road	10

V. RESULTS

The pit to be selected must be the one that provides the maximal recovery of the reserve to be mined, that is, the reserve that if exploited will generate maximal profit. The benefit function used to select the pit should consider the objectives of long term, taking in to account the value of the money, submitted to an interest rate along the time [16]. The final pit selected for the reserve of MR was the one that provided the highest profit and it has (13) mine benches with height of ten (10) meters, that is, benches 805 m, 815 m, 825 m, 835 m, 845 m, 855 m, 865 m, 875 m, 885 m, 895 m, 900 m, 905 m, 915 m and 925 m. (Figure 6). Were made simulations for cutoffs of 6%, 7%, 8% and 9% of P_2O_5 being obtained evaluations of the amount of ore and waste, waste/ore ratio and profit. The Fig.4 presents the variation of the ore tonnage in function of the cutoff off % P_2O_5 [14].

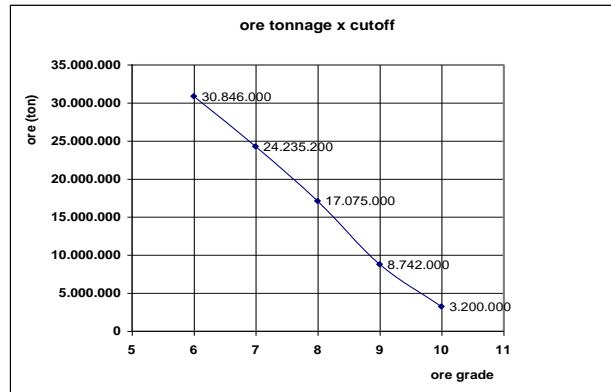


Fig.4 - Analysis of sensibility (ore grade x cutoff of P_2O_5)

The determination of the general waste/ore ratio, and also waste/ore ratio along the years, is of fundamental importance for the mining planning. The waste/ore ratio for the MR mine is not different of the reality that is found in an usual open pit mine. By analysis of the results could be concluded that the best pit is the one designed with a cutoff of 6,0% of P_2O_5 resulting in a mineable reserve of 30.846.000 tons of ore, an average ore grade of 8,5% of P_2O_5 , a general waste/ore ratio of 0,39 and a gross profit (not discounted cash flow) of US\$ 5.023.909.166. It is important to point out that this value didn't take into account the interest rates or the investments that will be applied during the life of the mine.

VI. Conclusions

The main conclusions of the case study are [15]:

- The estimate of the ores by sections (Fig.5) and of the parameters of the blocks for the geostatistic method using the ordinary kriging of blocks was quite reliable, facilitating the construction of a concise block model for the MR pit.
- The general average grade was estimated in 7,3% of P_2O_5 and 9,6% of CaO for a total geologic reserve of 50 million tons and 31 million of cubic meters of P_2O_5 , considering an average density of 1,60 ton/m³.
- The lithology of medium weathered slate (WSM) and deep weathered slate (WSI) presented higher grades of P_2O_5 , being, therefore, the lithologies that represent the ore body to be mined.
- The basics geometrical parameters of the MR are:
 - angle of final slope of the face of the benches of 60 degrees;
 - height of the mine benches of 10 meters;
 - minimum width of the berms of 5 meters;
 - width of the ramps and main roads of transport of 12 meters;
 - ramp or road gradient of 10%.
- The final pit selected for MR was the one that presented higher profit. This pit has thirteen (13) mine benches with height of ten (10) meters (Fig. 6).
- By analysis of the results could be concluded that the best pit is the one that took in consideration the cutoff of 6,0% of P_2O_5 with a mineable reserve of 30.846.000 tons of ore with average ore grade of 8,5% of P_2O_5 , for a waste/ore ratio of 0,39 and a gross profit (not discounted) of US\$ 5.023.909.166. It is important to point out that this value doesn't take into account the interest rates or the investments that will be applied during the life of the mine.

In an earlier investigation made by Costa[8], for the same case study, the ore reserve was evaluated in 109 million tons, with a average grade of 8,5% in P_2O_5 , corresponding to a cutoff of 6%. This great difference can be explained, partially, by the overestimate of the reserves due of the non-use, at that time, of a tool as the computers, that allowed more reliability in the evaluation of the mineable reserves.

Acknowledgements

Special thanks to Maptek Informática do Brasil and Brazilian Council of Research (CNPq) for their support in this academic research. It is important to inform that the Department of Mining Engineering of the Federal University of Ouro Preto in Brazil acquired an educational license of the Maptek Informática do Brasil Ltda. to use the Vulcan Software in this research.

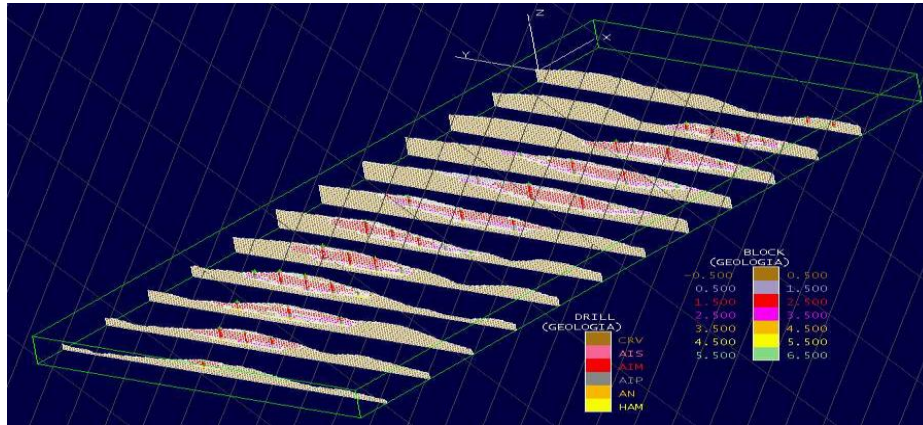


Fig. 5 - Estimate of the ore body by vertical sections for the of the Monte Raso region considering the topography of the region and the data of the mining exploration (drill holes). (Without scale)

Source: Pereira, 2000

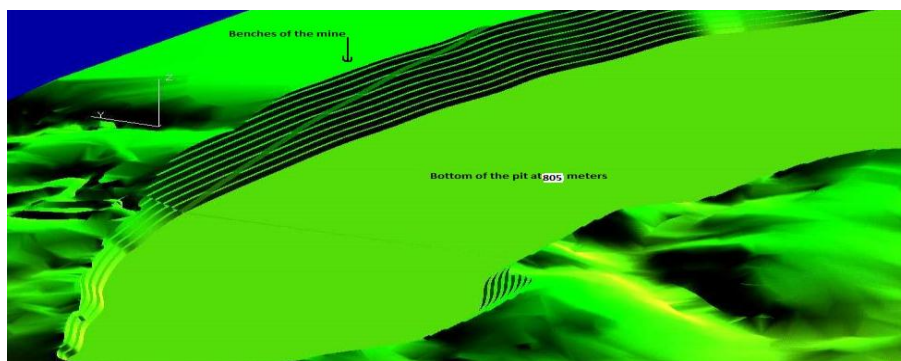


Fig. 6 - Partial view of the MR final open pit including the bottom of the pit at the level 805 m (without scale).

Source: Pereira, 2000

References

- [1]. Whittle. J, Open pit optimization., Surface Mining, Society of Mining Engineers (AIME), 1990, p. 470-475, New York.
- [2]. Whittle, J. Whittle open pit optimization software. Whittle Programming Proprietary Limited, 1992, 117p, Melbourne.
- [3]. Dowd. P.A, Optimal open pit design; sensitivity to estimate block values.. Public. Mineral Resource Evaluation II, methods and case histories, vol. 79. p. 87-94, Geological Society Sp Editor's: M.K.G. Whateley and P.K. Harvey. 1994 New York.
- [4]. Dowd. P.A, Onur. A.H, Open-pit optimization - part1: optimal open-pit design. Trans. Institution of Mining and Metallurgy, section A: Mining Industry, vol. 102, 1993, p. A95-104, New York.
- [5]. Carlos López Jimeno and Manuel Bustillo Revuelta, Manual de evaluación y diseño de explotaciones mineras. Gráficas Arias Montano S.A., 706p., Madrid, 1997.
- [6]. Lerchs. Helmut, Grossmann Ingo F. Optimum design of open-pit mines, Canadian Mining and Metallurgical Bulletin, vol. 58. p., 1965, 47-54, Montreal.
- [7]. Roberto Rodrigues Costa . Mining project. Textbook in Portuguese . Federal University of Ouro Preto. UFOP. Brazil. Vol.1. p. 1-155, Ouro Preto (MG), Brazil, 1979 .
- [8]. Roberto Rodrigues Costa. Mining project. Textbook in Portuguese. Federal University of Ouro Preto. UFOP. Brazil. Vol.2. p. 186, Ouro Preto (MG), Brazil .
- [9]. Tutorial básico do Vulcan. Software em 3D para a ciência e indústria. Maptek Informática do Brasil Ltda., 2ª ed. 112p. Belo Horizonte, 1998.
- [10]. Maptek site: <http://www.maptek.com/products/vulcan/index.html> eletronic acces in 29th november 2013
- [11]. Willian Hustrulid and Mark Kuchta, Open pit mine planning & design;, Colorado School of Mines, vol. 1 Fundamentals. 636 p., Colorado, 2006.
- [12]. Neme M. B, CURI A, SILVA, J. M and CARNEIRO A. C. B, Underground mine design using specific softwares. Rem: Rev. Esc. Minas [online]. 2011, vol.64, n.4, pp. 519-524. ISSN 0370-4467. <http://dx.doi.org/10.1590/S0370-44672011000500019>.
- [13]. Gildo de Araújo Sá Cavalcanti de Albuquerque. A produção de fosfato no Brasil: uma apreciação histórica das condicionantes envolvidas.CETEM/CNPq, Rio de Janeiro, Brazil, 1996.
- [14]. José Aloísio Paione. Jazida mineral: Como calcular seu valor. CPRM, Rio de Janeiro, Brazil, 1998
- [15]. Pereira, Marcos Antônio, Estudo dos parâmetros envolvidos na determinação dos limites finais da cava a céu aberto, Master degree dissertation, Department of Mining Eng., Graduate Program, School of Mines, Federal University of Ouro Preto, UFOP, Brazil, 2000
- [16]. Carmo F. A. R. and CURI, A. and SOUSA, W. T. Otimização econômica de explorações a céu aberto. Rem: Rev. Esc. Minas [online]. 2006, vol.59, n.3, pp. 317-321. ISSN 0370-4467. <http://dx.doi.org/10.1590/S0370-44672006000300011>.

Implement Public Audit ability and Data Dynamics with Security in Cloud Computing

¹P. Srinivasa Rao, ²K. Prasada Rao

¹(M. Tech), Dept. of CSE, AITAM (Tekkali), Srikakulam, A.P, India
²Sr. asst. Prof., Dept. of CSE, AITAM (Tekkali), Srikakulam, A.P, India

Abstract: Cloud Computing has been visualized as the next-generation architecture of IT Enterprise. It moves the application software and databases to the centralized large data centers, where the management of the data and services may not be fully trustworthy. This unique paradigm brings about many new security challenges, which have not been well understood. This work studies the problem of ensuring the integrity of data storage in Cloud Computing. In particular, we consider the task of allowing a third party auditor (TPA), on behalf of the cloud client, to verify the integrity of the dynamic data stored in the cloud. The introduction of TPA eliminates the involvement of the client through the auditing of whether his data stored in the cloud are naturally **intact**, which can be important in achieving economies of scale for Cloud Computing. The support for data dynamics via the most general forms of data operation, such as block modification, insertion, and deletion, is also a significant step toward practicality, since services in Cloud Computing are not limited to archive or backup data only. While prior works on ensuring remote data integrity often lacks the support of either **public Auditability** or dynamic data operations, this paper achieves both. We first identify the difficulties and potential security problems of direct extensions with fully dynamic data updates from prior works and then show how to construct a dignified verification scheme for the **seamless -integration** of these two salient features in our protocol design. In particular, to achieve efficient data dynamics, we improve the existing proof of storage models by manipulating the **classic Merkle Hash Tree** construction for block tag authentication. To support efficient handling of multiple auditing tasks, we further explore the technique of **bilinear aggregate signature** to extend our main result into a multi-user setting, where TPA can perform multiple auditing tasks simultaneously. Extensive security and performance analysis show that the proposed schemes are highly efficient and provably secure.

Index terms: seamless-integration, intact, classic merkle hash tree, bilinear aggregate

I. INTRODUCTION

SEVERAL trends are opening up the era of Cloud Computing, which is an Internet-based development and use of computer technology. The ever cheaper and more powerful processors, together with the “software as a service” (SaaS) computing architecture, are transforming data centers into pools of computing service on a huge scale. Meanwhile, the increasing network bandwidth and reliable yet flexible network connections make it even possible that clients can now subscribe high-quality.

Services from data and software that reside solely on remote data centers. Although envisioned as a promising service platform for the Internet, this new data storage paradigm in “Cloud” brings about many challenging design issues which have profound influence on the security and performance of the overall system. One of the biggest concerns with cloud data storage is that of data integrity verification at un trusted servers. For example, the storage service provider, which experiences Byzantine failures occasionally, may decide to hide the data errors from the clients for the benefit of their own. What is more serious is that for saving money and storage space the service provider might neglect to keep or deliberately delete rarely accessed data files which belong to an ordinary client. Consider the large size of the outsourced electronic data and the client’s constrained resource capability, the core of the problem can be generalized as how can the client find an efficient way to perform periodical integrity verifications without the local copy of data files.

In order to solve the problem of data integrity checking, many schemes are proposed under different systems and security models. In all these works, great efforts are made to design solutions that meet various requirements: high scheme efficiency, stateless verification, unbounded use of queries and retrievability of data, etc. Considering the role of the verifier in the model, all the schemes presented before fall into two categories: private auditability and public auditability. Although schemes with private audit ability can achieve higher scheme efficiency, public audit ability allows anyone, not just the client (data owner), to challenge the cloud server for correctness of data storage while keeping no private information. Then, clients are able to delegate the evaluation of the service performance to an independent third party auditor (TPA), without devotion of their computation resources. In the cloud, the clients themselves are unreliable or may not be able to afford the overhead of performing frequent integrity checks. Moreover, for efficiency consideration, the outsourced data themselves should not be required by the verifier for the verification purpose. Another major concern among previous designs is that of supporting dynamic data operation for cloud data storage applications. In Cloud Computing, the remotely stored electronic data might not only be accessed but also updated by the clients, e.g., through block modification, deletion, insertion, etc. Unfortunately, the state of the art in the context of remote data storage mainly focus on static data files and the importance of this dynamic data updates has received limited attention so far . Moreover, as will be shown later, the direct extension of the current provable data possession (PDP) or proof of retrievability (PoR) schemes to support data dynamics may lead to security loopholes. Although there are many difficulties faced by researchers, it is well believed that supporting dynamic data operation can be of vital importance to the practical application of storage outsourcing services. In view of the key role of public auditability and data dynamics for cloud data storage, we propose an efficient construction for the seamless integration of these two components in the protocol design. Our contribution can be summarized as follows: 1. We motivate

the public auditing system of data storage security in Cloud Computing, and propose a protocol supporting for fully dynamic data operations, especially to support block insertion, which is missing in most existing schemes. 2. We extend our scheme to support scalable and efficient public auditing in Cloud Computing. In particular, our scheme achieves batch auditing where multiple delegated auditing tasks from different users can be performed simultaneously by the TPA. 3. We prove the security of our proposed construction and justify the performance of our scheme through concrete implementation and comparisons with the state of the art.

1.1 Existing System:

The perspective of data security, which has always been an important aspect in quality of service, Cloud Computing inevitably poses new challenging security threats for number of reasons. Firstly, traditional cryptographic primitives for the purpose of data security protection cannot be directly adopted due to the users' loss control of data under Cloud Computing. Therefore, verification of correct data storage in the cloud must be conducted without explicit knowledge of the whole data. Considering various kinds of data for each user stored in the cloud and the demand of long term continuous assurance of their data safety, the problem of verifying correctness of data storage in the cloud becomes even more challenging simply called as a integrity of data Secondly, Cloud Computing is not just a third party data warehouse. The data stored in the cloud may be frequently updated by the users, including data dynamics like insertion, deletion, modification, appending, reordering, etc. To ensure storage correctness under dynamic data update is hence of paramount importance.

II. PROBLEM STATEMENTS

2.1 System Model

A representative network architecture for cloud data storage is illustrated in Fig. 1. Three different network entities can be identified as follows:

Client: an entity, which has large data files to be stored in the cloud and relies on the cloud for data maintenance and computation, can be either individual consumers or organizations;

Cloud Storage Server (CSS): an entity, which is managed by Cloud Service Provider (CSP), has significant storage space and computation resource to maintain the clients' data;

Third Party Auditor(TPA): an entity, which has expertise and capabilities that clients do not have, is trusted to assess and expose risk of cloud storage services on behalf of the clients upon request. In the cloud paradigm, by putting the large data files on the remote servers, the clients can be relieved of the burden of storage and computation. As clients no longer possess their data locally, it is of critical importance for the clients to ensure that their data are being correctly stored and maintained. That is, clients should be equipped with certain security means so that they can periodically verify the correctness of the remote data even without the existence of local copies. In case that clients do not necessarily have the time, feasibility or resources to monitor their data, they can delegate the monitoring task to a trusted TPA. In this paper, we only consider verification schemes with public auditability: any TPA in possession of the public key can act as a verifier. We assume that TPA is unbiased while the server is untrusted. For application purposes, the clients may interact with the cloud servers via CSP to access or retrieve their prestored data. More importantly, in practical scenarios, the client may frequently perform block-level operations on the data files. The most general forms of these operations we consider in this paper are modification, insertion, and deletion. Note that we don't address the issue of data privacy in this paper, as the topic of data privacy in Cloud Computing is orthogonal to the problem we study here.

2.2 Design Goals:

Our design goals can be summarized as the following:

1. Public verification for storage perfectness assurance
2. Real time operations on information like modify, insert, update, delete etc...

2.3 Proposed System:

In this paper, we propose an effective and flexible distributed scheme with explicit dynamic data support to find the correctness of users' data in the cloud. We rely on erasure correcting code in the file distribution preparation to provide redundancies and guarantee the data dependability. This construction drastically reduces the communication and storage overhead as compared to the traditional replication-based file distribution techniques. By utilizing the homomorphic token with distributed verification of erasure-coded data, our scheme achieves the storage correctness insurance as well as data error localization: whenever data corruption has been detected during the storage correctness verification, our scheme can almost guarantee the simultaneous localization of data errors, i.e., the identification of the misbehaving server(s).

Bilinear map: A bilinear map is a map $e : G \times G \rightarrow GT$, where G is a Gap Diffie-Hellman (GDH) group and GT is another multiplicative cyclic group of prime order p with the following properties :

- 1) Computable: there exists an efficiently computable algorithm for computing e ;
- 2) Bilinear: for all $h_1, h_2 \in G$ and $a, b \in \mathbb{Z}_p$; $e(a h_1, b h_2) = e(h_1, h_2)^{ab}$;
- 3) Non degenerate: $e(g, g) \neq 1$, where g is a generator of G .

Merkle hash tree: A Merkle Hash Tree (MHT) is a well studied authentication structure [17], which is intended to efficiently and securely prove that a set of elements are undamaged and unaltered. It is constructed as a binary tree where the leaves in the MHT are the hashes of authentic data values. Fig. 2 depicts an example of authentication. The verifier with the authentic hr requests for $fx_2; x_7g$ and requires the authentication of the received blocks. The prover provides the verifier

with the auxiliary authentication information (AAI) $_2 \frac{1}{4} < h\delta x1P; hd >$ and $_7 \frac{1}{4} < h\delta x8P; he >$. The verifier can then verify x_2 and x_7 by first computing $h\delta x2P; h\delta x7P; hc \frac{1}{4} h\delta h\delta x1Pkh\delta x2P\delta P\delta P; hf \frac{1}{4} h\delta h\delta x7Pkh\delta x8P\delta P\delta P; ha \frac{1}{4} h\delta hckhdP; hb \frac{1}{4} h\delta hekhdP$ and then checking if the calculated hr is the same as the authentic one. MHT is commonly used to authenticate the values of data blocks. However, in this paper, we further employ MHT to authenticate both the values and the positions of data blocks. We treat the leaf nodes as the left-to-right sequence, so any leaf node can be uniquely determined by following this sequence and the way of computing the root in MHT.

III. MODELING THE SYSTEM

In this section, we present our security protocols for cloud data storage service with the aforementioned research goals in mind. We start with some basic solutions aiming to provide integrity assurance of the cloud data and discuss their demerits. Then, we present our protocol which supports public auditability and data dynamics. We also show how to extend our main scheme to support batch auditing for TPA upon delegations from multiusers.

3.1 Definition

$(pk, sk) \leftarrow \text{KeyGen}(1^k)$. This probabilistic algorithm is run by the client. It takes as input security parameter 1^k , and returns public key pk and private key sk . $(\Phi, \text{sig}_{sk}(H(R))) \leftarrow \text{SigGen}(sk; F)$ This algorithm is run by the client. It takes as input private key sk and a file F which is an ordered collection of blocks $\{m_i\}$ and outputs the signature set Φ , which is an ordered collection of signatures $\{\sigma_i\}$ on $\{m_i\}$. It also outputs metadata—the signature $\text{sig}_{sk}(H(R))$ of the root R of a Merkle hash tree. In our construction, the leaf nodes of the Merkle hash tree are hashes of $H(m_i)$ straightforwardly as the verification covers all the data blocks. However, the number of verifications allowed to be performed in this solution is limited by the number of secret keys. Once the keys are exhausted, the data owner has to retrieve the entire file of F from the server in order to compute new MACs, which is usually impractical due to the huge communication overhead. Moreover, public auditability is not supported as the private keys are required for verification. Another basic solution is to use signatures instead of MACs to obtain public auditability. The data owner precomputes the signature of each block $m^i (i \in [1, n])$ and sends both F and the signatures to the cloud server for storage. To verify the correctness of F , the data owner can adopt a spot-checking approach, i.e., requesting a number of randomly selected blocks and their corresponding signatures to be returned. This basic solution can provide probabilistic assurance of the data correctness and support public auditability. However, it also severely suffers from the fact that a considerable number of original data blocks should be retrieved to ensure a reasonable detection probability, which again could result in a large communication overhead and greatly affects system efficiency. Notice that the above solutions can only support the case of static data, and none of them can deal with dynamic data updates.

3.2 Construction

To effectively support public auditability without having to retrieve the data blocks themselves, we resort to the homomorphic authenticator technique. Homomorphic authenticators are unforgeable metadata generated from individual data blocks, which can be securely aggregated in such a way to assure a verifier that a linear combination of data blocks is correctly computed by verifying only the aggregated authenticator. In our design, we propose to use PKC-based homomorphic authenticator (e.g., BLS signature or RSA signature-based authenticator) to equip the verification protocol with public auditability. In the following description, we present the BLS-based scheme to illustrate our design with data dynamics support. As will be shown, the schemes designed under BLS construction can also be implemented in RSA construction. In the discussion of Section 3.4, we show that direct extensions of previous work have security problems, and we believe that protocol design for supporting dynamic data operation is a major challenging task for cloud storage systems. Now we start to present the main idea behind our scheme. We assume that file F (potentially encoded using Reed-Solomon codes) is divided into n blocks m_1, m_2, \dots, m_n where $m^i \in \mathbb{Z}_p$ and p is a large prime. Let $e : G * G \rightarrow G_T$ be a bilinear map, with a hash function $H : \{0,1\}^* \rightarrow G$, viewed as a random oracle. Let g be the generator of G . h is a cryptographic hash function. The procedure of our protocol execution is as follows:

3.3 Setup

The client's public key and private key are generated by Invoking key gen (.). By running sig gen (.), the data file F is preprocessed, and the homomorphic authenticators together with metadata are produced. $\text{keyGen}(1^k)$ The client generates a random signing key pair (spk, ssk) . Choose a random $\alpha \rightarrow \mathbb{Z}_p$ and compute $v \leftarrow g^\alpha$. The secret key is $sk = (\alpha, \text{ssk})$ and the public key is $pk = (v, \text{spk})$. $\text{SigGen}(sk, f; \text{FP})$. Given $F = (m_1, m_2, \dots, m_n)$, the client chooses a random element $u \leftarrow G$. Let $t = \text{name} \parallel n \parallel u \parallel \text{ssig}_{\text{ssk}}(\text{name} \parallel n \parallel u)$ be the file tag for F . Then, the client computes signature σ_i for each block $m_i (i = 1, 2, \dots, n)$ as $\sigma_i \leftarrow (H(m_i) \cdot u^{m_i})^\alpha$. Denote the set of signatures by $\Phi = \{\sigma_i\}, 1 \leq i \leq n$. The client then generates a root R based on the construction of the MHT, where the leaf nodes of the tree are an ordered set of hashes of "file tags". $H(m_i) (i = 1, 2, \dots, n)$ Next, the client signs the root R under the private key

$\alpha : sig_{sk}(H(R)) \leftarrow (H(R))^\alpha$. The client sends $\{F, t, \phi, sig_{sk}(H(R))\}$ to the server and deletes $\{F, t, \phi, sig_{sk}(H(R))\}$ from its local storage.

3.4 Default Integrity Verification

The client or TPA can verify the integrity of the outsourced data by challenging the server. Before challenging, the TPA first use sk to verify the signature on t . If the verification fails, reject by emitting FALSE; otherwise, recover u . To generate the message "chal," the TPA (verifier) picks a random c -element subset $I = \{s_1, s_2, \dots, s_c\}$ of set $[1, n]$, where we assume $s_1 \leq \dots \leq s_c$. For each $i \in I$ the TPA chooses a random element $v_i \leftarrow B \subseteq \mathbb{Z}_p$. The message "chal" specifies the positions of the blocks to be checked in this challenge phase. The verifier sends the to $chal = \{(i, v_i)\}_{s_1 \leq i \leq s_c}$ the prover (server). Gen proof $(f, \phi, chal)$ Upon receiving the challenge $chal = \{(i, v_i)\}_{s_1 \leq i \leq s_c}$, the server computes

$$\mu = \sum_{i=s_1}^{s_c} v_i m_i \in \mathbb{Z}_p \text{ and } \sigma = \prod_{i=s_1}^{s_c} \sigma_i^{v_i} \in G$$

where both the data blocks and the corresponding signature blocks are aggregated into a single block, respectively. In addition, the prover will also provide the verifier with a small amount of auxiliary information $\{\Omega_i\}_{s_1 \leq i \leq s_c}$, which are the node siblings on the path from the leaves $\{h(H(m_i))\}_{s_1 \leq i \leq s_c}$ to the root R of the MHT. The prover responds the verifier with proof $P = \{\mu, \sigma, \{H(m_i), \Omega_i\}_{s_1 \leq i \leq s_c}, sig_{sk}(H(R))\}$. Verify Proof $(pk, chal, P)$. Upon receiving the responses from the prover, the verifier generates root R using $\{H(m_i), \Omega_i\}_{s_1 \leq i \leq s_c}$ and authenticates it by checking $e(sig_{sk}(H(R)), g) = e(H(R), g^\alpha)$. If the authentication fails, the verifier rejects by emitting FALSE. Otherwise, the verifier checks

$$e(\sigma, g) = e(\prod_{i=s_1}^{s_c} H(m_i)^{v_i} \cdot u^\mu, v)$$

If so, output TRUE; otherwise FALSE. The protocol is illustrated in Table 1.

PROTOCOLS FOR DEFAULT INTEGRITY VERIFICATION

1. Generate a random set $\{(i, v_i)\}_{i \in I}$
2. Compute $\mu = \sum_i v_i m_i$
3. Compute $\sigma = \prod_i \sigma_i^{v_i}$
4. Compute R using $\{H(m_i), \Omega_i\}_{i \in I}$
5. Verify $sig_{sk}(H(R))$ and output False if fail
6. Verify $\{m_i\}_{i \in I}$

PROTOCOL FOR PROVABLE DATA UPDATE

1. Generate $\sigma_i^1 = (H(m_i^1) \mu^{m_i^1})^\alpha$
2. Update F and compute R^1
3. Compute R using $\{H(m_i), \Omega_i\}$
4. Verify $sig_{sk}(H(R))$ and output False if fail
5. compute R_{new}^1 using $\{\Omega_i, H(m_i^1)\}$ verify update by checking $R_{new}^1 = R^1 \cdot \text{sign } R^1$ if succeed
6. Update R^1 's signature

3.5 Dynamic Data Operation with Integrity Assurance

Now we show how our scheme can explicitly and efficiently handle fully dynamic data operations including data modification (M), data insertion (I), and data deletion (D) for cloud data storage. Note that in the following descriptions, we assume that the file F and the signature ϕ have already been generated and properly stored at server. The root metadata R has been signed by the client and stored at the cloud server, so that anyone who has the client's public key can challenge the correctness of data storage. Data Modification: We start from data modification, which is one of the most frequently used operations in cloud data storage. A basic data modification operation refers to the replacement of specified blocks with new ones. Suppose the client wants to modify the i th block m_i to m_i^1 . The protocol procedures are described in Table 2. At start, based on the new m_i^1 , the client generates the corresponding signature $\sigma_i^1 = (H(m_i^1) \cdot u^{m_i^1})^\alpha$. Then, he constructs an update request message "update = $(m, i, m_i^1, \alpha_i^1)$ " and sends to the server, where M denotes the modification operation. Upon

receiving the request, the server runs $ExecUpdate(F, \Phi, update)$. Specifically, the server 1) replaces the block m_i with m_i^1 and outputs F^1 ; 2) replaces the α_i with σ_i^1 and outputs ϕ ; and 3) replaces $H(m_i)$ with $H(m_i^1)$ in the Merkle hash tree construction and generates the new root R^1 (see the example in Fig. 3). Finally, the server responses the client with a proof for this operation,

$P_{update} = (\Omega_i, H(m_i), sig_{sk}(H(R), R^1))$ where Ω_i is the AAI for authentication of m_i . After receiving the proof for

modification operation from server, the client first generates root R using $\{\Omega_i, H(m_i)\}$ and authenticates the AAI or R by checking $e(sig_{sk}(H(R)), g) \stackrel{?}{=} e(H(R), g^\alpha)$. If it is not true, output FALSE, otherwise the client can now check whether the server has performed the modification as required or not, by further computing the new root value using $\{\Omega_i, H(m_i^1)\}$ and comparing it with R0. If it is not true output FALSE, otherwise output TRUE. Then, the client signs the new root metadata R^1 by $sig_{sk}(H(R^1))$ and sends it to the server for update. Finally, the client executes them default integrity verification protocol. If the output is TRUE, delete $sig_{sk}(H(R^1))$; update and m_i^1 from its local storage.

Data Insertion: Compared to data modification, which does not change the logic structure of client's data file, another general form of data operation, data insertion, refers to inserting new blocks after some specified positions in the data file F. Suppose the client wants to insert block after the i^{th} block m_i . The protocol procedures are similar to the data modification case (see Table 2, now m_i^1 can be seen as m^*). At start, based on m_i the client generates the corresponding signature $\sigma^* = (H(m^*), u^{m^*})^\alpha$. Then, he constructs an update request message " $update = (I, i, m^*, \sigma^*)$ " and sends to the server, where I denotes the insertion operation. Upon receiving the request, the server runs $ExecUpdate(F, \Phi, update)$. Specifically, the server 1) stores m^* and adds a leaf $h(H(m^*))$ "after" leaf $h(H(m_i))$ in the Merkle hash tree and outputs F^1 ; 2) adds the σ^* into the signature set and outputs Φ^1 ; and 3) generates the new root R^1 based on the updated Merkle hash tree. Finally, the server responses the client with a proof for this operation, $P_{update} = (\Omega_i, H(m_i), sig_{sk}(H(R), R^1))$, where Ω_i is the AAI for authentication of m_i in the old tree. An example of

block insertion, to insert $h(H(m^*))$ after leaf node $h(H(m_2))$, only node $h(H(m^*))$ and an internal node C is added to the original tree, where $h_c = h(h(H(m_2)) || h(H(m^*)))$

. After receiving the proof for insert operation from server, the client first generates root R using $\{\Omega_i, H(m_i)\}$ and then authenticates the AAI or R by checking if $e(sig_{sk}(H(R)), g) \stackrel{?}{=} e(H(R), g^\alpha)$. If it is not true,

output FALSE, otherwise the client can now check whether the server has performed the insertion as required or not, by further computing the new root value using $\{\Omega_i, H(m_i), H(m^*)\}$ and comparing it with R^1 . If it is not true, output FALSE, otherwise output TRUE. Then, the client signs the new root metadata R^1 by $sig_{sk}(H(R^1))$ and sends it to the server for update. Finally, the client executes the default integrity verification protocol. If the output is TRUE, delete $sig_{sk}(H(R^1))$, P_{update} and m^* from its local storage.

Data Deletion: Data deletion is just the opposite operation of data insertion. For single block deletion, it refers to deleting the specified block and moving all the latter blocks one block forward. Suppose the server receives the update request for deleting block m_i , it will delete m_i from its storage space, delete the leaf node $h(H(m_i))$ in the MHT and generate the new root metadata R0 (see the example in Fig. 5). The details of the protocol procedures are similar to that of data modification and insertion, which are thus omitted here.

IV. SECURITY ANALYSIS

In this section, we evaluate the security of the proposed scheme under the security model defined in Section 2.2. we consider a file F after Reed-Solomon coding.

Definition 1 (CDH Problem). The Computational Diffie-Hellman problem is that, given $g, g^x, g^y \in G$ for unknown $x, y \in \mathbb{Z}_p$ to compute g^{xy} . We say that the (t, ρ) -CDH assumption holds in G if no t time algorithm has the non-negligible probability ϵ in solving the CDH problem. A proof-of-retrievability protocol is sound if any cheating prover that convinces the verification algorithm that it is storing a file F is actually storing that file, which we define in saying that it yields up the file F to an extractor algorithm which interacts with it using the proof-of-retrievability protocol. We say that the adversary (cheating server) is ϵ admissible if it convincingly answers an ϵ fraction of verification challenges. We formalize the notion of an extractor and then give a precise definition for soundness.

Theorem 1. Suppose a cheating prover on an n -block file F is well-behaved in the sense above, and that it is ρ admissible.

Let $w = 1/\#B + (\rho n)^l / (n-c+1)^e$. Then, provided that $\rho - w$ is positive and non-negligible, it is possible to recover a ρ -fraction of the encoded file blocks in $O(n/(e-\rho))$ interactions with cheating prover and in $O(n^2 + (1+en^2)(n)/(e-w))$ time overall.

Proof. The verification of the proof-of-retrievability is similar to [4], we omit the details of the proof here. The difference in our work is to replace $H(i)$ with $H(m_i)$ such that secure update can still be realized without including the index information. These two types of tags are used for the same purpose (i.e., to prevent potential attacks), so this change will not affect the extraction algorithm defined in the proof-of-retrievability. We can also prove that extraction always succeeds against a well-behaved cheating prover, with the same probability analysis given in .

Theorem 2. Given a fraction of the n blocks of an encoded file F , it is possible to recover the entire original file F with all but negligible probability.

Proof. Based on the rate ρ Reed-Solomon codes, this result can be easily derived, since any ρ fraction of encoded file blocks suffices for decoding. The security proof for the multi client batch auditing is similar to the single-client case, thus omitted here. variant of this relationship. $P = 1 - \rho^e$ Under this setting, we quantify the extra cost introduced by the support of dynamic data in our scheme into server computation, verifier computation as well as communication overhead.

V. CONCLUSION

To ensure cloud data storage security, it is critical to enable a TPA to evaluate the service quality from an objective and independent perspective. Public auditability also allows clients to delegate the integrity verification tasks to TPA while they themselves can be unreliable or not be able to commit necessary computation resources performing continuous verifications. Another major concern is how to construct verification protocols that can accommodate dynamic data files. In this paper, we explored the problem of providing simultaneous public auditability and data dynamics for remote data integrity check in Cloud Computing. Our construction is deliberately designed to meet these two important goals while efficiency being kept closely in mind. To achieve efficient data dynamics, we improve the existing proof of storage models by manipulating the classic Merkle Hash Tree construction for block tag authentication. To support efficient handling of multiple auditing tasks, we further explore the technique of bilinear aggregate signature to extend our main result into a multiuser setting, where TPA can perform multiple auditing tasks simultaneously. Extensive security and performance analysis show that the proposed scheme is highly efficient and provably secure.

REFERENCES

- [1]. Q. Wang, C. Wang, J. Li, K. Ren, and W. Lou, "Enabling Public Verifiability and Data Dynamics for Storage Security in Cloud Computing," Proc. 14th European Symp. Research in Computer Security (ESORICS '09), pp. 355-370, 2009.
- [2]. G. Ateniese, R. Burns, R. Curtmola, J. Herring, L. Kissner, Z. Peterson, and D. Song, "Provable Data Possession at Untrusted Stores," Proc. 14th ACM Conf. Computer and Comm. Security (CCS '07), pp. 598-609, 2007.
- [3]. A. Juels and B.S. Kaliski Jr., "Pors: Proofs of Retrieval for Large Files," Proc. 14th ACM Conf. Computer and Comm. Security (CCS '07), pp. 584-597, 2007.
- [4]. H. Shacham and B. Waters, "Compact Proofs of Retrieval," Proc. 14th Int'l Conf. Theory and Application of Cryptology and Information Security: Advances in Cryptology (ASIACRYPT '08), pp. 90-107, 2008.
- [5]. K.D. Bowers, A. Juels, and A. Oprea, "Proofs of Retrieval: Theory and Implementation," Report 2008/175, Cryptology ePrint Archive, 2008.
- [6]. M. Naor and G.N. Rothblum, "The Complexity of Online Memory Checking," Proc. 46th Ann. IEEE Symp. Foundations of Computer Science (FOCS '05), pp. 573-584, 2005.
- [7]. E.-C. Chang and J. Xu, "Remote Integrity Check with Dishonest Storage Server," Proc. 13th European Symp. Research in Computer Security (ESORICS '08), pp. 223-237, 2008.
- [8]. M.A. Shah, R. Swaminathan, and M. Baker, "Privacy-Preserving Audit and Extraction of Digital Contents," Report 2008/186, Cryptology ePrint Archive, 2008.
- [9]. A. Oprea, M.K. Reiter, and K. Yang, "Space-Efficient Block Storage Integrity," Proc. 12th Ann. Network and Distributed System Security Symp. (NDSS '05), 2005.
- [10]. T. Schwarz and E.L. Miller, "Store, Forget, and Check: Using Algebraic Signatures to Check Remotely Administered Storage," Proc. 26th IEEE Int'l Conf. Distributed Computing Systems (ICDCS '06), p. 12, 2006.
- [11]. Q. Wang, K. Ren, W. Lou, and Y. Zhang, "Dependable and Secure Sensor Data Storage with Dynamic Integrity Assurance," Proc. IEEE INFOCOM, pp. 954-962, Apr. 2009.
- [12]. G. Ateniese, R.D. Pietro, L.V. Mancini, and G. Tsudik, "Scalable and Efficient Provable Data Possession," Proc. Fourth Int'l Conf. Security and Privacy in Comm. Networks (SecureComm '08), pp. 1-10, 2008.
- [13]. C. Wang, Q. Wang, K. Ren, and W. Lou, "Ensuring Data Storage Security in Cloud Computing," Proc. 17th Int'l Workshop Quality of Service (IWQoS '09), 2009.
- [14]. C. Erway, A. Kupcu, C. Papamanthou, and R. Tamassia, "Dynamic Provable Data Possession," Proc. 16th ACM Conf. Computer and Comm. Security (CCS '09), 2009.
- [15]. K.D. Bowers, A. Juels, and A. Oprea, "Hail: A High-Availability and Integrity Layer for Cloud Storage," Proc. 16th ACM Conf. Computer and Comm. Security (CCS '09), pp. 187-198, 2009.
- [16]. D. Boneh, B. Lynn, and H. Shacham, "Short Signatures from the Weil Pairing," Proc. Seventh Int'l Conf. Theory and Application of Cryptology and Information Security: Advances in Cryptology (ASIACRYPT '01), pp. 514-532, 2001.
- [17]. R.C. Merkle, "Protocols for Public Key Cryptosystems," Proc. IEEE Symp. Security and Privacy, pp. 122-133, 1980.
- [18]. S. Lin and D.J. Costello, Error Control Coding, second ed., Prentice-Hall, 2004.

A Proposed REBA on Small Scale Forging Industry

Er. Surinder Singh, Er. Amanjot Singh, Er. Harvinder Lal,

Department of Mechanical engineering, CT group of institutions, Jalandhar, India, Department of Mechanical engineering,
Ramgharia polytechnic college, phagwara, India, 9914806868.
Department of Mechanical engineering, RIET, Phagwara, India,

Abstract: Musculoskeletal disorders (MSDs) are common health problem throughout the world. Work related musculoskeletal disorders are group of painful disorders of muscles, tendons and nerves. The low back or lumber area, serves a number of important functions for the men in working area many occupational tasks in industrial area still associated with strenuous working postures and movement. Assessment of exposure levels to MSD risk factors can be an appropriate base for planning and implementing interventional ergonomics programs in the workplace. Combined with a heavy physical workload, it results in a high frequency of work-related musculoskeletal disorders. The present study was aimed to evaluate the musculoskeletal disorder (MSD) of workers engaged in Small scale forging industries. Study was conducted on 102 workers of a forging industry using the posture analysis tool REBA Method. A video showing the different activities of the workers was shot and the snapshots were taken from it for the analysis. The results of REBA showed that about 7.63% of the workers were under very high risk levels and required immediate change. About 44.6% of the workers were at high risk levels which required changes soon and 45.03% of the workers were at medium risk levels. About 2.67% of the workers were at lower risk levels. The present Study recommended the awareness and proper ergonomics training to the workers.

Keywords: Musculoskeletal disorders, men, forging industry, REBA.

I. Introduction

There has been an increasing effort in recent years to investigate the causes of musculoskeletal disorders (MSDs) and to take action to prevent them. This has led to increasing recognition from workers, employers and government agencies that a strong relationship exists between factors within the working environment and the development of MSDs, and that these conditions result in significant sickness absence and reduced productivity. Musculoskeletal Disorders (MSD) are injuries affecting muscles, tendons, ligaments and nerves. They are sometimes called Repetitive Strain Injuries (RSI), Cumulative Trauma Disorders (CTD) and Repetitive Motion Injuries (RMI). MSD develop due to the effects of repetitive, forceful or awkward movements on injuries include Low Back Strain, Neck Strain, Tendonitis, Carpal Tunnel Syndrome (CTS) Rotator Cuff Joints, ligaments and other soft tissues. The objective of this study is to analyse the working postures of workers engaged in various processes of small scale forging industry. The study used assessment tool REBA (Rapid entire body Assessment), was developed by Hignett, S. and McAtamney, L. 2000, to provide a quick and easy observational postural analysis tool for whole body activities (static and dynamic giving musculoskeletal risk action level [1]. J.N.Saraji et al. (2004) were evaluation of WMSDs risk factors among the crew of the Iranian Ports and shipping organization's vessels. This paper clarify the WMSDs are major problem in almost all countries and are important causes of work incapacity and loss of work days. The aim of their studies is evaluation of WMSDs symptoms among the workers by using Nordic Musculoskeletal Questionnaire (NMQ) and determination of WMSDs risk factors by application of OWAS. After determination of risk factors, the OWAS methods can be used to identify any possible correction in working posture that leads to a better and less harmful posture [2]. Cleaning is associated with high physical and psychosocial workloads and musculoskeletal disorders related to it were studied. A few studies concern equipment design, working environments and factors affecting individual workers. A need to conduct research on cleaning tools and equipment, working environments and individual risk factors is apparent [3]. The study used assessment tool RULA (Rapid Upper Limb Assessment), REBA was developed by McAtamney, L. and Corlett, to provide a rapid objective measure of musculoskeletal risk caused by mainly sedentary tasks where upper body demands were high; where work related upper limb disorders are reported [4]. The relationship between the subjective ride comfort in a vehicle seat and whole-body vibration can be modeled using frequency weightings and rms averaging. From the results obtained in this study, it was clear that the alternative approach could give superior predictions of comfort than the method used in ISO 2631-1 [5]. Musculoskeletal disorders (MSDs) are common health problem throughout the world. Work related musculoskeletal disorders are group of painful disorders of muscles, tendons and nerves, recommended the awareness and proper ergonomics training to the workers [6]. A significant proportion of the works are working in very bad postures. The study recommended proposed that there is dire need of implementation of ergonomics intervention with proper awareness among worker[7].

II. Material And Methods

The study was done in small scale forging industries in Ludhiana and Jalandhar Region. A video of different sections like forging, punching, Trimming Furnace, broaching and grinding etc. showing different movements of the workers during an activity was recorded. Snapshots of 102 workers working in different sections were obtained. The snapshots were analyzed to fill the scores in REBA.

III. Reba Method

REBA Method is a quick and easy to use observational postural analysis tool for whole body activities and giving a musculoskeletal risk action level. The method is similar to RULA tool where the assessor assigns scores to postures and body alignment based on body part diagram. Load, Force and coupling scores are added to calculation for the body and then final score for both groups are summated to form the final action score .The REBA method evaluate the ergonomics risk factor by observation the posture of employees while they working at their workstation directly (Hignett, S. and McAtamney, L. 2000).Postural and biomechanical loading was assessed on the entire body by valid REBA method. We used several score in this method with the help of REBA score sheet, that the scores evaluate the posture of different body parts Neck, Trunk and Legs give posture score A with the help of standard Table and Upper Arm, Lower Arm, Wrist, and Wrist twist give the posture score B with the help of standard Table . The loading or coupling scores were added to posture scores A and posture score B to obtain scores A and B, respectively (McAtamney and Corlett 1993). Combination of scores A and score B give the Grand score with the use of standard Table and table score C is obtained. After this the activity score is added in the table score C the final REBA score is obtained. The range of Grand scores varies from 1 to 11 and reflects the musculoskeletal loading associated with the worker's posture. Whereas low scores of 1 indicate that the work posture is acceptable if not maintained or repeated for long time (action level 1), For low score of 2 to 3, further investigation is needed and changes may be necessary (action level 2). Investigation and changes are required for scores of 4 to 7 (action level 3). Further investigation and changes are required soon for score of 8 to 10 (action level 4). Further investigation and the changes required immediately for the score of 11 and onward. REBA action level is shown in Table -1. REBA score 1 show the negligible risk level, REBA score 2 to 3 shows the low level risk, REBA score 4 to 7 shows the medium level risk, REBA score 8 to 10 shows the high level risk. REAB score 11 to 12 shows very high level risk. Figure 2 to 5 shows the work of worker at different processes in awkward posture like shearing, furnace unloading, forging process, grinding process and picking or placing.

Table 1. Analysis of REBA

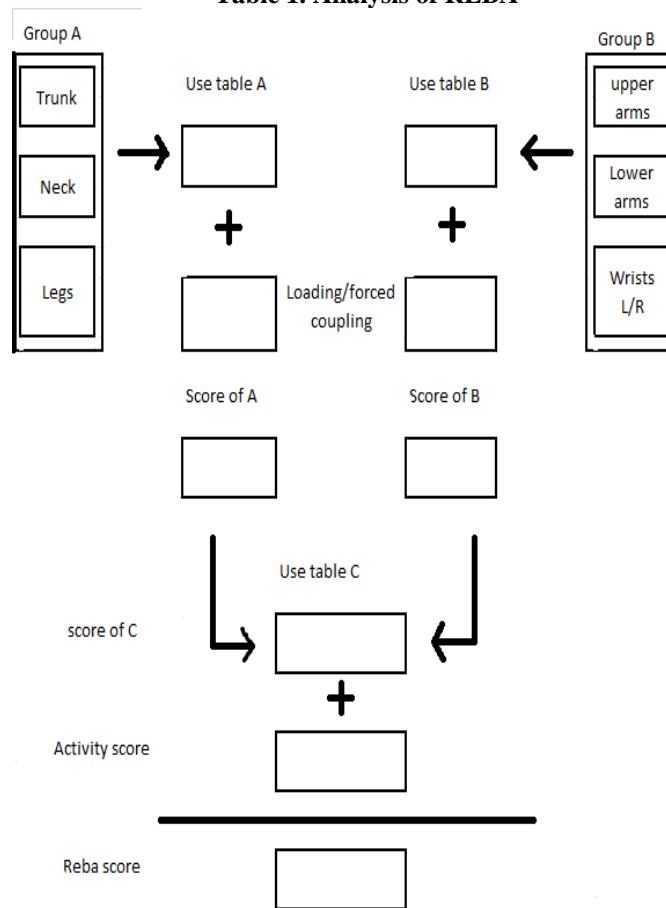


Figure-1 REBA Score Sheet

REBA SCORE	Risk level	ACTION LEVEL
1	Negligible	Corrective action including further assessment is not necessary
2 to 3	Low	Corrective action including further assessment may be necessary
4 to 7	medium	Corrective action including further assessment is necessary
8 to 10	High	Corrective action including further assessment is necessary soon
11 to 15	Very high	Corrective action including further assessment is necessary now



Figure 2: Odd posture in Picking and placing



Fig 3: Odd posture in Cutting



Fig: 4 : Odd posture in Furnance loading/ unloading



Fig: 5: Odd posture in Grinding

IV. RESULTS

The results of the REBA assessment of the Workers are shown in Table 2, 3. According to this technique of posture analysis 2.67 % of workers are working in Low Risk Level Posture and requires further investigation and changes may not be required. About 45.03 % workers were found be at medium level and require Investigation and changes are necessary. Around 44.6% workers are working in posture of high risk level and require corrective action required very soon. Around 7.63% workers are working in posture of very high risk level and require corrective action required immediately. These results reveal that all categories of the risk levels exist in jobs postures from left to right positions. In first category i.e. Blanking, Cutting and Shearing as shown in table 2. 47% of this category is of Medium level risk in which investigation is required and changes are necessary. 50% of this category is calculated to be as high level risk and rest 2.9% is of very high level risk, Investigations are to be done immediately and changes are needed as soon as possible. Next category in the table no.2 is of Furnace Loading in this category 16.9% of the postures fall under medium level risk, 64% comes under high risk and 18.8 % fall under High level risk. Investigations are required for all level of risks and changes are to be done according to the need.

Table.2 No. of posture with REBA score in each section and Abbreviations are L=Left, R=Right & T=Total

Process	REBA SCORE																		
	1			2 to 3			4 to 7			8 to 10			11 to 12						
	L	R	T	L	R	T	L	R	T	L	R	T	L	R	T				
Blanking, Cutting, Shearing	0	0	0	0	0	0	1	0	6	16	1	1	6	17	1	0	1		
Furnace loading	0	0	0	0	0	0	3	6	9	1	4	2	0	34	3	7	10		
Hammering	0	0	0	1	1	2	1	3	13	26	3	9	12	0	0	0			
Punching & Trimming	0	0	0	0	0	0	1	0	10	20	7	9	16	1	0	1			
Grinding & Drilling	0	0	0	0	0	0	7	7	14	4	8	12	2	0	2				
Broaching, Chamfering & Heat Treatment	0	0	0	1	1	2	4	1	5	0	0	0	0	0	0	0			
Inspection	0	0	0	0	0	0	0	6	6	2	0	2	0	0	0	0			
Picking & Placing	0	0	0	3	0	3	1	3	2	15	1	1	2	22	5	1	6		
Lathe & Welding	0	0	0	0	0	0	2	5	7	2	0	2	0	0	0	0			
TOTAL	0	0	0	4	2	7	6	2	56	118	5	6	11	3	4	7	12	8	20

Third category of the table is Hammering, Hammering is the main operation of the forging as the power hammer is dropped and the shape and size of the product is changed, so by the calculations 5 % of the postures are in the low level risks , 65% are in the medium level risks and rest 18.8% is under high risk. Investigations are required for all level of risks and changes are to be done according to the need. Further comes the process of the Punching and Trimming as from the table is that 52% is of medium level risks, 42% is of high level risks and remaining 2.6% is very high risk. Next is Grinding and Drilling 50% is medium level, 42.8% is high risks and 7% is very high risks, scope of improvement is always there so changes are to be made. Whereas in the next category broaching, chamfering and heat treatment there is only 28% of low level and 71% of medium risks as there is no high risks in these processes. Inspection is the most important aspect of any field which determines the quality of the product. but during there is always posture failures as no low level, 75% is of high level and 25% is of very high risks. Then comes the material handling or Picking and placing, in this category postures calculations are 6% of low level risks, 33% of medium and 48% of high risks and 13% is very high level risk. Investigations are to be made for better material handling methods. Last category of the table is Lathe and Welding. In this processes there is also scope of improvement as calculated as 77% of medium level risks and 22% of high risks are involved. As mentioned in the above processes examinations are to be made to check whether the methods can be improved to reduce the load on the worker and he could perform his duties with full efforts. Table-2 shows the No. of posture with REBA score in each section and. No. of posture left hand and right hand with percentage and risk level shown in Table-3.

Table.3 No. of posture left hand and right hand with percentage and risk level

REBA score	Risk level	No. of worker's posture		%age of worker's posture	
		Left	Right	Left	Right
1	Negligible	0	0	0	0
2 to 3	Low level	5	2	3.7	1.5
4 to 7	Medium level	62	56	46.9	43
8 to 10	High level	53	64	40.1	49.2
11 to 12	very high level	12	8	9	6.1
	Total	132	130		

V. DISCUSSIONS

After visiting various small scale industries, It was observed that in the small scale industries the ergonomics is hardly given preferences and the space provided to the workers is not appropriate. Workers are performing the operations under great difficulties and bear stress on their bodies. This is due to several reasons as justified by the photographs taken of the workers performing the operations. By using REBA method, it was observed that in every category of processes taken into consideration, each worker is under muscular stress. This has been shown by the percentage calculated from the REBA Score Sheet which is based on the posture analysis of photographs of the worker taken from different small scale industries. It is mandatory to make some urgent improvement in the industries for the betterment of the workers to perform their operations/tasks with minimum load and stress on their bodies. During the calculations of the postures, it was observed that the workers are subjected to different muscular disorders while performing different tasks. In the blanking, cutting and shearing operations the worker has to lift the heavy loads and to hold them for certain time while operation is to be performed. As in the furnace operation, the worker has to bend and the stress is observed on the back and neck. Hence the necessary and requisite improvement should be done in every operation. The owners of the industries must concentrate on the ergonomics to increase the productivity of the worker and to get the best results.

VI. CONCLUSION

REBA methods of postural analysis closely co-relate with the awkward postures adopted by the male workers. According to REBA Method the postures adopted by workers in these small scale forging industries have been categorized as having high to very high risk level. Blanking, Cutting, Shearing, Picking and placing or furnace loading workers are at very high risk of musculoskeletal disorders hence the ergonomically interventions are required in these sections. Proper training of workers and awareness may reduce the risk of musculoskeletal disorders. The results show that the operators are working in an inadequate working environment with awkward postures the results are supported by the subjective assessment of discomfort.

REFERENCES

- [1] Hignett, S. and McAtamney, L. 2000. Rapid Entire Body assessment (REBA). *Applied Ergonomics*, 31, 201 - 205
- [2] J.N.Saraji, M.A.hassanzadeh, M.Pourmahabadian & S.J.Shahtaheri. Evaluation of Musculoskeletal Disorders Risk Factors among the Crew of the Iranian Ports and Shipping Organization's Vessels. *Acta Medica Iranica*, 42(5): 350-354 (2004).
- [3] Christine Brulin, Karl-Axel Angquist, Margareta Barnekow-Bergkvist and Ulrika Aasa. Relationships between work-related factors and disorders in the neck-shoulder and low-back region among female and male Ambulance Personnel. (2003).
- [4] McAtamney, L. and Corlett. E. N., RULA: a survey method for the investigation of work related upper limb disorders. *Applied Ergonomics*, 24, 91-99(1993).
- [5] Dan Anton, John C Rosecrance, Linda A Merlino and Thomas M Cook. Method for quantitatively assessing physical risk factors during variable non cyclic work. (2003).
- [6] Jaspreet Singh et al., "Musculoskeletal Disorder risk Assessment in small scale forging Industry by using REBA Method," *International Journal of Engineering and Advanced Technology*, Volume-1, Issue-5, June 2012.
- [7] L P Singh. Work posture assessment in forging industry: an exploratory study in India *International Journal of Advanced Engineering Technology* Oct.-Dec.(2010).
- [8] S Sahu, M Sett, Ergonomic evaluation of tasks performed by female workers in the unorganized sectors of the manual brick manufacturing units in India *Ergonomics*. (2010)

- [9] Dan Anton, John C Rosecrance, Linda A Merlino and Thomas M Cook. Method for quantitatively assessing physical risk factors during variable non cyclic work. (2003)
- [10] M. Massaccesi, A. Pagnotta, A. Soccetti, M. Masali, C. Masiero, F. Greco Investigation of work-related disorders in truck drivers using REBA method Applied Ergonomics Received 1 January 2002; accepted 21 March 2003
- [11] www.dcmsme.gov
- [12] www.vassarstat.com
- [13] www.indianforging.com

Er. Surinder Singh



I have done my B-Tech in Mechanical Engineering from CT group of Institution, shahpur, jalandhar, under Punjab Technical University Jalandhar INDIA. Currently I am pursuing M.Tech from RIET Phagwara under Punjab Technical University Jalandhar INDIA. From three year I am lecturer in Department of Mechanical engineering, CT group of Institution, shahpur, jalandhar .

Er. Amanjot Singh



I have done my B-Tech in Mechanical Engineering from lovely institute of engineering and technology jalandhar, under Punjab Technical University Jalandhar INDIA. Currently I am pursuing M.Tech from RIET Phagwara under Punjab Technical University Jalandhar INDIA. From three year I am lecturer in Department of Mechanical engineering, Ramgharia polytechnic college, phagwara

Er. Harvinder Lal



I have done my B.E in Mechanical Engineering from G.Z.S.C.E.T. Bathinda, Punjab, INDIA. And I had completed my M.Tech in Industrial engineering from Dr. Ambedkar National Institute of Technology. Now I m HOD in RIET Phagwara. I have seven year experience in teaching field.
Qualification: B.E in Mechanical engineering, M.Tech in Industrial engineering

A Two Variable Experimental Study in Rectangular Open Channels of Smooth Boundaries

John Demetriou¹, Eugene Retsinis², Gerassimos Ballas³
^{1,2,3} Civil Engineer, National Technical University of Athens (NTUA), Greece

Abstract: In this experimental study a two variable investigation of pertinent velocity laboratory measurements is presented, analyzed and discussed. The research deals with the uniform-steady-turbulent water flows within an almost horizontal, smooth, rectangular open channel. The local (point) velocities were electronically measured in two long channels with low and medium-low aspect ratios (groups A, B), and a third channel with high aspect ratios (group C). The hydraulic centre's (H.C.) position on the vertical axis of symmetry is examined, after measuring a very large number of local velocities. A number of velocity diagrams in $Y=y/0.5 \cdot b$ and $Z=z/z_n$ (cross sections $b \cdot z_n$, y , z , axes) coordinates are also presented. A diagram of vertical strips within all water cross sections is created, and the internal distribution of partial discharges is examined in dimensionless terms. All dimensionless velocities \bar{U} are considered as two variable functions of Y and Z , $\bar{U}=f(Y, Z)$, and all data are elaborated with the aid of a computer program, giving a number of computer isovelocity lines, $\bar{U}=\text{const}$. A number of equations are also proposed in order to better examine the flows' structures, aiming on helping the hydraulic engineer when analyzing the mechanism of flow.

Keywords: Open Channels, Smooth Boundaries, Velocities' Two Variable Analysis.

I. Introduction

One of the basic uniform-steady-turbulent flows in open channel hydraulics is the smooth boundary case-within a rectangular cross section (Fig. 1). The structure of the velocity field of this water flow, although the extensive research in the past, still is of considerable interest.

At any point y, z , with $0 \leq y \leq 0.5 \cdot b$ and $0 \leq z \leq z_n \leq H$ of the semi-cross section ($0.5 \cdot b \cdot z_n$) the turbulent mean time x velocity is \bar{u} (or in dimensionless terms $\bar{U}=\bar{u}/V$), where with the water discharge (Q) the average cross sectional velocity is $V=Q/E$. On the flow axis (centre line plane) $y=0.5 \cdot b$, the maximum local velocity is \bar{U}_{max} (at a height $z=z_m$ -Hydraulic Centre), the longitudinal channel slope $J_0=\sin\phi$ -usually is very small (of the order of 0.001-0.0023), while the aspect ratio of the entire semi cross section is $\lambda=2 \cdot z_n/b$.

A very well known characteristic of this flow is that the flow stream lines are not exactly straight lines but helicoidal lines, since they are distorted from the secondary turbulent flow field, v', w' , where $v=\bar{v}+v'$ and $w=\bar{w}+w'$. Thus, the final result is that on any water cross section a number of weak closed vortices are formed. Sometimes it is useful to work with the depth-mean velocities along a vertical line (or strip)

$$\bar{u} = (1/z_n) \cdot \int_0^{z_n} \bar{u} dz, \text{ or, } \bar{U} = \bar{u}/V = (1/z_n) \cdot \int_0^{z_n} (\bar{u}/V) dz,$$

several results of which will be shown in this research.

In the present experimental investigation the local dimensionless velocities $\bar{U}=\bar{u}/V$ are mainly measured in a rectangular channel of smooth boundaries as two variable functions of both $y/0.5 \cdot b$ and z/z_n ,

$$\bar{U}=\bar{u}/V=f(y/0.5 \cdot b, z/z_n),$$

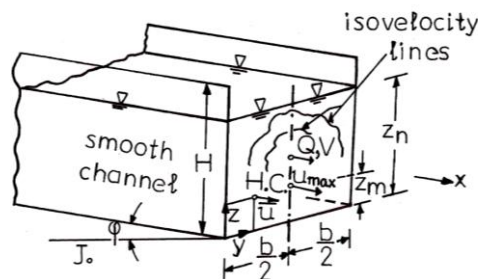


Figure 1. Geometry of flow.

and some of them are treated with the aid of computational methods. The final results are equations for various discharges and coordinates and a number of diagrams concerning the isovelocity lines $\bar{U}=\text{const}$., given by the computer.

From the older data, the pertinent issues by Chow (1959), [1], Goncharov (1964), [2] (who has investigated the H.C.) and Knight et al (1982), [3], are chosen as important here, while of some interest could be the paper by Demetriou, (1983), [4], and the book by the same author, (2008), [5]. Moreover, in the paper by

Knight et al (1983), [6], some interesting details on the experimental processes may be found.

It is to be noted that the concepts of smooth boundaries and hydraulically smooth channels are greatly differing between them.

II. Experiments

Three rigs were used in this investigation: (i) Groups' A data were undertaken in a long smooth (perspex) channel ($l \approx 15$ m), with $b=15.2$ cm. (ii) Groups' B measurements were performed in a long smooth (perspex) channel ($l \approx 12$ m), with $b=25$ cm, while, (iii) Groups' C measurements were undertaken in a shorter smooth channel with $b=10$ cm. The various laboratory elements are given in Table 1, where all discharges Q were measured by corresponding Venturi meters and suitable manometers, following proper electric pumps.

All A and C measurements' series were performed in the hydraulics laboratory of the Univ. of Birmingham (UK), while B series measurements were undertaken in the hydraulics laboratory of the Univ. of Athens (NTUA)-Greece.

In all laboratory series a number of about 1,000 local (point) velocities (\bar{u}) were measured, with the aid of a Pitot tube (external diameter 3.4 mm-B series), or an industrial miniature electronic propeller (A, C, series) supplied with revolving blades (of 4 mm size). This instrument could reliably measure velocities at minimum distances from any solid or water boundaries, at around 7.5 mm. In any turn of the blades the electric impedance was measured (in Hz) and corresponding velocity \bar{u} was determined through a pre-fabricated linear chart (Hz- \bar{u}). The flow's uniformity was succeeded through a suitable tail gate (Groups A, B), or another proper solid hydraulic construction within the downstream flow (Group C).

Table 1. Laboratory Elements

Group A						Group B					
N ^o	Q cm ³ /sec	z _n cm	V cm/sec	z _m /z _n	λ	N ^o	Q cm ³ /sec	z _n cm	V cm/sec	z _m /z _n	λ
A ₁	4,800	8.44	37.41	0.59	1.11	B ₁	7,400	7.44	37.98	0.85	0.59
A ₂	5,600	9.50	38.78	0.55	1.25	B ₂	7,440	8.62	34.52	0.81	0.69
A ₃	6,070	10.13	39.42	0.69	1.33	B ₃	9,010	9.27	38.88	0.85	0.74
A ₄	7,000	11.40	40.39	0.61	1.50	B ₄	9,600	11.05	34.75	0.73	0.88
A ₅	8,000	12.67	41.51	0.55	1.67	B ₅	10,170	11.65	34.01	0.86	0.93
A ₆	9,850	15.20	42.63	0.59	2.00	B ₆	17,610	15.21	46.31	0.77	1.22
A ₇	11,820	17.60	44.18	0.56	2.32	B ₇	10,150	15.94	50.73	0.76	1.28
Group C						B ₈	24,530	18.83	52.11	0.84	1.51
C ₁	3,627	21.3	17.03	0.65	4.26	B ₉	27,170	19.71	54.97	0.83	1.58
C ₂	5,510	23.45	23.50	0.63	4.69	B ₁₀	28,106	21.32	52.72	0.76	1.71
C ₃	7,792	25.91	30.07	0.61	5.18	B ₁₁	30,860	22.57	54.69	0.77	1.81
C ₄	10,288	28.55	36.04	0.62	5.71						

Following \bar{u} measurements, the $\bar{u}/V=\bar{U}$ ratios against $y/0.5 \cdot b=Y$ and $z/z_n=Z$ dimensionless coordinates were determined, and a large number of \bar{U} (against Y -at any $Z=\text{const.}$) graphical diagrams were constructed.

Finally, all water semi-cross sections of A₁ to A₆ groups of measurements were divided by suitable vertical lines in water strips of constant widths $\Delta(y/0.5 \cdot b)=0.05$, and the corresponding depth-mean velocities \bar{u} were determined in terms of $\bar{U}=\bar{u}/V$, giving-after a proper smoothing out-a unique \bar{U} value vs $Y=y/0.5 \cdot b$ diagram, holding for all present velocities' measurements. The last elaboration may give the experimental internal distribution of all particular discharges Q_i -especially in Q_i/Q terms, in those water strips, i.e. it may give the experimental composition of Q_i/Q within the entire semi-cross sections, for all present measurements.

III. Results/Analysis

Fig. 2 presents z_m/z_n ratios on the centerline flow axes vs λ , for all present Groups. On this Figure, from Group B (low λ , high z_m/z_n), a proper curve was traced through Group A (medium λ and z_m/z_n) to Group C (high λ , and medium z_m/z_n). In Group B z_m/z_n curve is abruptly falling, while through Group A the curve is slowly rising again (two Group C).

The above behavior is in general agreement with Goncharov's, (1964), [2], results and actually shows the end of the boundary layer on the central plain along the flow.

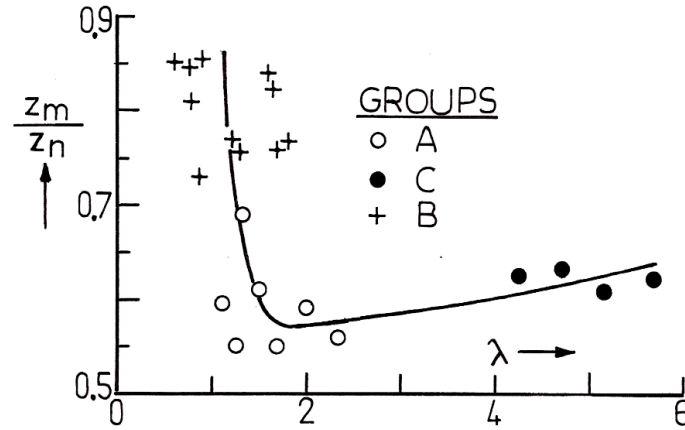


Figure 2. z_m/z_n vs λ for Groups.

Figs. 3 and 4 present some preliminary experimental results concerning \bar{U} vs $Y=y/0.5 \cdot b$ and $Z=z/z_n$, for two typical series A_1 and A_5 . As it may be seen all velocities are normally varying along Y , and thus these curves could be extrapolated to-corresponding free water surfaces and to zero values (on the beds).

Fig. 5 shows all $\bar{U}=\bar{u}/V$ distributions along Y , where \bar{u} are depth-mean velocities along a number of equal vertical strips with widths $\Delta(y/0.5 \cdot b)=0.05$. The discharge in each strip is the corresponding \bar{U} multiplied by 0.05 and expressed as a percentage. This result (%) on the i strip represents $0.5 \cdot Q_i / 0.5 \cdot Q$ where $0.5 \cdot Q_i$ is the water discharge in the i strip and $0.5 \cdot Q$ is the total discharge over the semi-cross section. This diagram holds for all present laboratory results of Group A, and shows the experimental internal distribution of all partial discharges of this study, i.e. 3.95%, 4.35%,... All these $0.5 \cdot Q_i$ percentages give a summation of $\approx 100\%$ in the semi-cross section. Perhaps this discharge has a wider interest for all smooth rectangular open channels of A Group.

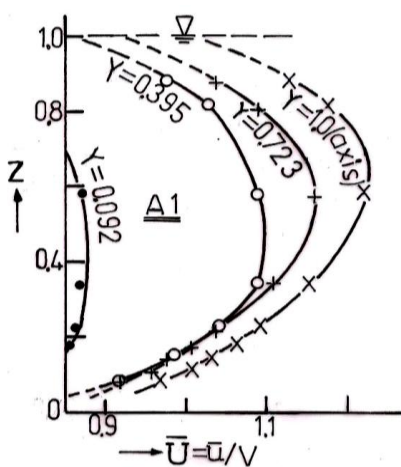


Figure 3. \bar{U} vs Y and Z for A_1 .

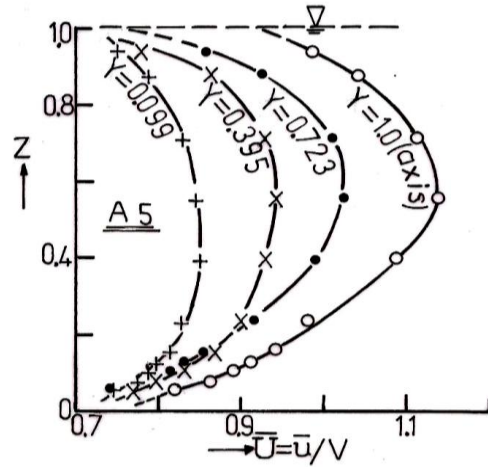


Figure 4. \bar{U} vs Y and Z for A_5 .

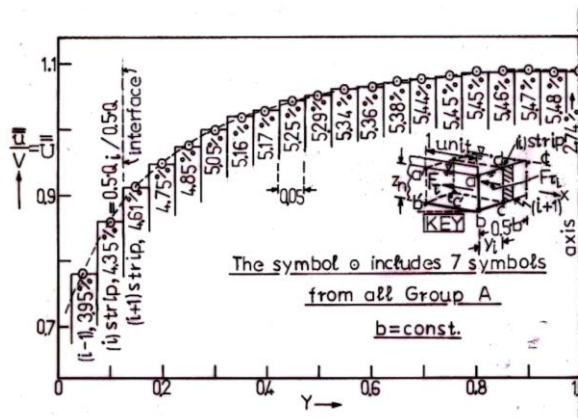


Figure 5. Discharge distribution in semi-cross section.

In Fig. 5 (KEY) suppose that the water control volume (c.v.) of unit length along x, (abcd) = z_n·y_i·1, where ab=cd=a'b'=z_n, while (z_n·1) is also the internal (imaginary) left side surface of the (i) vertical strip. Since the flow is uniform, in both (z_n·y_i) front and rear surfaces, the hydrostatic pressures are the same, i.e. F_px=0. Along the part of the solid boundary, (z_n+y_i)·1, the boundary shear force Fτ is opposing the flow, while on z_n·1-left surface of the strip (i), the corresponding shear force (apparent shear force) is Fτ_i. If, on the above c.v., the x momentum equation is applied, then Fτ+Fτ_i=(water weight component)=(z_n·y_i)·ρ·g·J_o·1=Fg, or Fτ_i=[Fg-Fτ]. Thus, the apparent shear force may be calculated if Fg and Fτ are known. It is easy to determine Fg, while Fτ may result either: (1). If the local (point) shear stresses are experimentally determined on surfaces (z_n+y_i)·1, followed by an integration of them along these surfaces, or, (2). If τ_{om} is the well known mean boundary shear stress (as in any open channel uniform flow), Fτ=τ_{om}·(z_n+y_i)·1. On the other hand it is well known that, τ_{om}=ρ·g·R·J_o, where R is the hydraulic radius R=(0.5·b·λ)·(1+λ)⁻¹, and thus

$$F\tau = 0.125 \cdot \rho \cdot g \cdot J_o \cdot b^2 \cdot (\lambda + Y_i) \cdot (\lambda + 1)^{-1},$$

becoming max when Y_i=1 and increasing with J_o, level of turbulence and wall's roughness. A similar analysis holds for horizontal layers.

The above mechanism explains the water momentum transfer from centre line vertical plane to the walls (and to free surface and channel bed). It is responsible for the \bar{U} variation perpendicularly to the flow, and consequently for the \bar{U} change along Y or Z (Fig. 5), Knight et al (1982), [3], (1983), [6], and Demetriou, (2008), [5].

Table 2 indicatively presents all measured values $\bar{u}/V = \bar{U}$ vs Y and Z dimensionless coordinates in the function $\bar{U} = f(Y, Z)$, for two characteristic flows (A₂ and A₃) in the channel, where all \bar{U} values on the solid boundaries ($\bar{U} = 0$) or on the free water surfaces were also taken into consideration.

Table 2. Measured and Predicted \bar{U} .

$\bar{U} = f(Y, Z)$									
A ₂ , r ² ≈0.92					A ₃ , r ² ≈0.92				
N ^o	Y Value	Z Value	\bar{U} Value	\bar{U} Predict	N ^o	Y Value	Z Value	\bar{U} Value	\bar{U} Predict
1	1	0	0	-	1	1	0	0	-
2	1	0.079	0.890	0.8250955	2	1	0.074	0.863	0.8006453
3	1	0.105	0.896	0.9170852	3	1	0.099	0.883	0.8954812
4	1	0.137	0.946	0.986896	4	1	0.128	0.921	0.9667821
5	1	0.168	0.962	1.0207285	5	1	0.158	0.939	1.007204
6	1	0.210	0.985	1.0317461	6	1	0.197	0.969	1.024685
7	1	0.263	1.021	1.0162621	7	1	0.247	1.005	1.0141294
8	1	0.316	1.047	0.9936951	8	1	0.296	1.035	0.9912943
9	1	0.526	1.135	1.0302155	9	1	0.494	1.116	0.9999867
10	1	0.734	1.106	1.0720519	10	1	0.691	1.126	1.0967345
11	1	0.916	1.037	0.9232934	11	1	0.888	1.055	0.9638362
12	1	1.000	1.037	-	12	1	0.947	0.994	0.9268352
13	0.724	0	0	-	13	1	1	0.994	-
14	0.724	0.079	0.879	0.8243455	14	0.724	0	0	-
15	0.724	0.105	0.921	0.9163352	15	0.724	0.074	0.877	0.8065683
16	0.724	0.137	0.949	0.986146	16	0.724	0.099	0.913	0.9014043
17	0.724	0.168	0.97	1.0199785	17	0.724	0.128	0.936	0.9727052
18	0.724	0.210	1.000	1.0309961	18	0.724	0.158	0.984	1.0131271
19	0.724	0.263	1.044	1.0155121	19	0.724	0.197	0.994	1.0306081
20	0.724	0.316	1.075	0.9929451	20	0.724	0.247	1.020	1.0200525
21	0.724	0.526	1.134	1.0294655	21	0.724	0.296	1.053	0.9972173
22	0.724	0.734	1.101	1.0713019	22	0.724	0.494	1.129	1.0059097
23	0.724	0.926	0.990	0.9225434	23	0.724	0.691	1.121	1.1026576
24	0.724	1.000	0.990	-	24	0.724	0.888	1.032	0.9697593
25	0.395	0	0	-	25	0.724	0.946	0.959	0.9327582
26	0.395	0.079	0.895	0.8079288	26	0.724	1	0.959	-
27	0.395	0.105	0.931	0.8999185	27	0.395	0	0	-
28	0.395	0.137	0.959	0.9697293	28	0.395	0.074	0.893	0.7863376
29	0.395	0.168	0.980	1.0035619	29	0.395	0.099	0.928	0.8811735

30	0.395	0.210	1.016	1.0145794	30	0.395	0.128	0.961	0.9524744
31	0.395	0.263	1.044	0.9990955	31	0.395	0.158	0.984	0.9928963
32	0.395	0.316	1.052	0.9765285	32	0.395	0.197	1.012	1.0103774
33	0.395	0.526	1.070	1.0130488	33	0.395	0.247	1.027	0.9998217
34	0.395	0.734	1.037	1.0548852	34	0.395	0.296	1.040	0.9769866
35	0.395	0.926	0.936	0.9061267	35	0.395	0.494	1.071	0.985679
36	0.395	1.000	0.936	-	36	0.395	0.691	1.045	1.0824268
37	0.092	0	0	-	37	0.395	0.888	0.967	0.9495285
38	0.092	0.079	0.786	0.6582621	38	0.395	0.946	0.893	0.9125275
39	0.092	0.105	0.905	0.7502519	39	0.395	1	0.893	-
40	0.092	0.137	0.817	0.8200626	40	0.092	0	0	-
41	0.092	0.168	0.830	0.8538952	41	0.092	0.074	0.781	0.6315683
42	0.092	0.210	0.841	0.8649128	42	0.092	0.099	0.789	0.7264043
43	0.092	0.263	0.851	0.8494288	43	0.092	0.128	0.807	0.7977052
44	0.092	0.316	0.854	0.8268618	44	0.092	0.158	0.819	0.8381271
45	0.092	0.526	0.848	0.8633822	45	0.092	0.197	0.835	0.8556081
46	0.092	0.734	0.812	0.9052185	46	0.092	0.247	0.845	0.8450525
47	0.092	0.943	0.758	0.75646	47	0.092	0.296	0.842	0.8222173
48	0.092	1.000	0.758	-	48	0.092	0.494	0.852	0.8309097
					49	0.092	0.691	0.835	0.9276576
					50	0.092	0.888	0.791	0.7947593
					51	0.092	0.946	0.753	0.7577582
					52	0.092	1	0.753	-

Based on the measured values of all six first flows (A) eqs. (1) to (6) were provided by the computer program, and the predicted, by those equations, \bar{U} values were also determined. For the two flows of Table 2 it is remarkable that measured and predicted \bar{U} values are very close among them (the majority of differences are of the order of $\approx \pm 10\%$). This happens for all the rest of the flows, being essential in order that the computer model predicted from all flows' equations is correct.

Based on all A measurements' results the following equations (1)-(6)-of the same type-are produced for all cross sections,

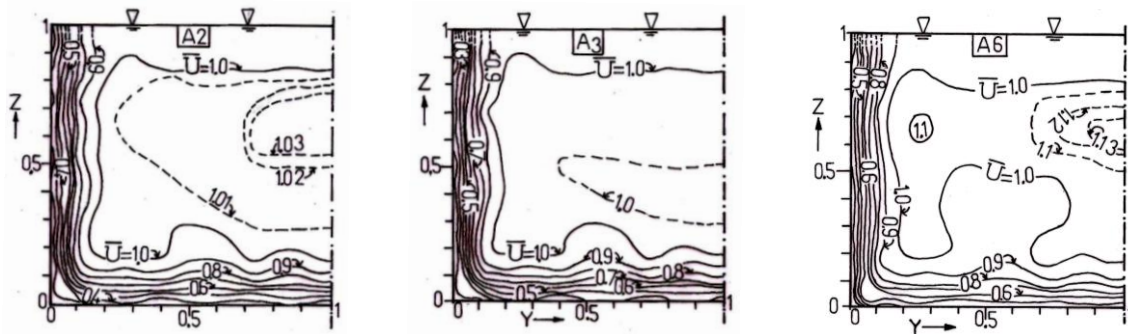
$$\bar{U}_i = (a_i) + (b_i) \cdot Y + (c_i) \cdot Y^2 + (d_i) \cdot Y^3 + (e_i) \cdot Y^4 + (f_i) \cdot Z + (g_i) \cdot Z^2 + (h_i) \cdot Z^3 + (k_i) \cdot Z^4 + (j_i) \cdot Z^5, \quad (1)-(6)$$

where $i=1, 2, 3, 4, 5, 6$. All pertinent arithmetic coefficients' values $a_i, b_i, c_i, d_i, e_i, f_i, g_i, h_i, k_i, j_i$ are shown in Table 3.

Table 3. Arithmetic Coefficients' Values for Eqs. (1) to (6).

	a_i	b_i	c_i	d_i	e_i	f_i	g_i	h_i	k_i	j_i	Remarks	
$i=1$	-0.680	12.010	-44.149	60.044	-26.985	9.945	-45.615	96.056	-92.890	33.251	For all cross sections (A ₁ -A ₆).	
$i=2$	-0.667	11.614	-42.031	56.650	-25.311	10.805	-54.228	120.296	-	119.780		43.641
$i=3$	-0.656	11.470	-41.420	55.831	-24.966	10.677	-53.429	117.290	-	114.896		41.052
$i=4$	-0.631	11.234	-40.634	54.862	-24.559	10.671	55.287	125.332	-	126.446		46.423
$i=5$	-0.622	10.719	-37.989	50.807	-22.628	10.727	-54.614	121.356	-	120.180		43.378
$i=6$	-0.578	11.162	-40.327	54.419	-24.343	10.138	-53.027	120.778	-	122.012		44.745

Fig. 6 shows diagrams of isovels $\bar{U}=f(Y, Z)=const.$ for all present measurements (A₂, A₃, A₆), given by the computer (continuous lines) and supplemented by secondary results (dashed lines).

Figure 6. $\bar{U}=\text{const.}$ (isovels) for A_2, A_3, A_6 flows.

As one can see from Fig. 6, the results cover almost all flow fields of the three A series. The dense isovels close to the solid walls and beds show the boundary layers created, while all curves terminate perpendicularly to corresponding flow axes.

The detailed velocity measurements for the C series of measurements are not shown here (although elaborated in the same way) two isovelocity lines' data are further presented, in order to show the results for high λ , C series-Fig. 7, where the dashed curves are the results of interpolations.

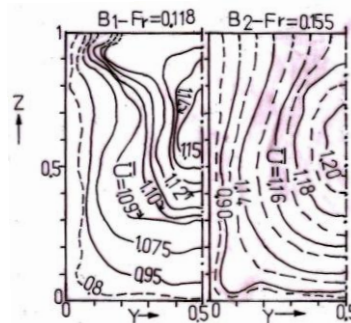


Figure 7. Isovels for Group B

IV. Conclusions

In this experimental and computational study a two variable investigation of the velocity field in uniform-steady-turbulent flows within a horizontal smooth boundaries' rectangular open channel is presented-analyzed and discussed. The main conclusions are: 1). The hydraulic centre (H.C.) depends on the form of water semi cross sections (low, medium or high), i.e. on the aspect ratio λ . 2). Fig. 2 shows that high λ values correspond to ascending positions of H.C., while low λ values correspond to dimensionless coordinates). 4). Fig. 5 presents all dimensionless velocity measurements (\bar{U}) as functions of Y. 5). In the previous Figure the internal distribution of the partial discharges within the general semi-cross section is investigated. 6). An explanation is provided on the role of the apparent shear forces within all cross sections. 7). In Table 2 a large number of local velocities (\bar{U}) are given for two typical groups of A flows. 8). A number of equations are given for the dimensionless velocities, \bar{U} , as two variable functions of Y and Z, which were also provided by a suitable computer program. 9). A number of isovelocity curves $\bar{U}=\text{const.}$ are given (by the computer) in order to better realise the flow structure. The present investigation is aiming at assisting the hydraulic engineer when analyzing the mechanism of such flows.descending positions of H.C. 3). Figs. 3 and 4 present a number of dimensionless velocities \bar{U} as functions of Y, Z (horizontal and vertical

References

- [1] V. T. Chow, *Open Channel Hydraulics* (Mc Graw-Hill Book Co., New York, pp. 24-25, 1959).
- [2] V. Goncharov, *Dynamics of Channel Flow* (Translated from Russian, Israel Program for Scientific Translations, Jerusalem, 1964).
- [3] D. W. Knight, H. S. Patel, J. D. Demetriou and M. E. Hame, Boundary Shear Stress Distributions in Open Channel and Closed Conduit Flows, *Enromech 156, Istanbul, Turkey, 1982, 6 pages.*
- [4] J. Demetriou, A Simple Method to Measure Shear Stresses in Open Channels, *Journal of Scientific Pages of the School of Civil Engineering, Nat. Tech. Univ. of Athens, Vol. 7, N° 2, 1983, pp. 17-31.*
- [5] J. Demetriou, Applied Hydraulics (Book Published by the National Technical University of Athens/Greece, 2008, pp. 184-187 and 229-241).
- [6] D. W. Knight and J. D. Demetriou, Flood Plain and Main Channel Flow Interaction, *Journal of Hydraulic Engineering, ASCE, Vol. 109, N° 8, 1983, pp. 1073-1092.*

Potentials Of and the Socio-Economic Benefits of Blacksmithing Production in Promoting Agricultural Development and Poverty Alleviation in Kwara State, Nigeria

Y. U. Oladimeji

Department of Agricultural Economics and Rural Sociology, Faculty of Agriculture, Ahmadu Bello University, P.M.B. 1044, Zaria, Kaduna State, Nigeria

Abstract: Agriculture and technological development including blacksmithing promotes agricultural tools production and offers an unexploited succor capable of salvaging the people from abject poverty. Blacksmithing and its products are frequently valuable in diverse ways and contribute to technological and agricultural development through agricultural tools production, income to artisans and technological recycling. The study examined the potentials and contribution of blacksmithing practices to household income and poverty alleviation in Kwara State, Nigeria. Eighty blacksmith artisans were randomly selected in the sixteen LGAs of Kwara State for the study. Primary data were obtained with the aid of structured questionnaire and personal interview schedule to elicit information relevant to the study. Descriptive statistics, net income and OLS models were employed in data analysis. The results revealed prospects of increased revenue generation to blacksmiths. The blacksmiths were at the edge of productive age with modal class of 48-57 years, low literacy rate and the bulk had subsidiary occupations to supplement their income. The average household size per smith was approximately 7 and mean daily income earned from production ranges from ₦500 to ₦950. The postulated explanatory variables explained 48.8% in the variations in income earned by blacksmiths. Given the opportunity and amazing potentials for widening agricultural tools production in Kwara State, it was recommended that the industry's private operators and government at all levels should provide social services particularly electricity, increased budgetary commitment to artisan sector and create enabling policies for the industry to thrive and shift from crude methods to mechanize system.

Keywords: Potentials, Blacksmith, Mechanize, Poverty alleviation, Nigeria.

I. Introduction

The current global economic meltdown has had its devastating turn on Nigeria as a nation, biting hard on organizations, businesses, families and homes. The frantic search for alternative resource of national revenue aside oil has become imperative for economic emancipation of the lots of Nigerians. Agriculture and technology including blacksmithing offers an unexploited succor capable of salvaging the people from abject poverty. Creating renewed awareness and practice of blacksmith in the rural setting would go a long way in eradicating global economic challenges and create a self-reliance enterprise that will help reduce the hardship, unemployment and other social vices associated with it. However, the blacksmith sector in Nigeria is rudimentary and not well explored due mainly to the high technical manpower requirement and neglect of artisans from successive government over the years. The industry is fading away like all other artisans and crafts as well as small and medium enterprises native to the country. However, blacksmith has direct, meandering and multiplier impacts on agricultural and technological development and its one of most crucial sectors that advanced technological development in the world.

For example, prior to the industrial revolution in develop countries; a village smithy was a staple of every town. However, factories and mass-production reduced the demand for blacksmith made tools and hardware. As demand for their products declined, many more blacksmiths augmented their incomes by working as shoeing horses. With the introduction of automobiles, the number of blacksmiths continued to decrease, many former blacksmiths becoming the initial generation of automobile mechanics. The nadir of blacksmithing in the United States was reached during the 1960s, when most of the former blacksmiths had left the trade and few if any new people were entering trade. By this time, most of the working blacksmiths were those performing farrier works, so the term blacksmith was effectively co-opted by the farrier trade.

Therefore, while developed nations saw a decline and re-awakening of interest in blacksmithing, many developing nations' particularly Nigerian blacksmiths have not advanced the frontier of technological development and continued doing what blacksmiths have been doing for 3500 years. These include making and repairing iron, steel and agricultural tools and hardware for people in their local area.

The word smith is from the Proto-German "smithaz" meaning skilled worker while the term "forging" means to shape metal by heating and hammering. A subset of smith is blacksmith which emanates from the activity of "forging" iron or the "black" metal and it was named due to the color of the metal after being heated, a key part of the blacksmithing process. Blacksmith is vocational sector that require competencies, strength and physical conceptualization. In other word, a blacksmith is a metal smith who creates objects from wrought iron or steel by forging the metal by using tools to hammer, bend, and cut (David and Bernhard, 1993). The "black" in "blacksmith" refers to the black fire scale, a layer of oxides that forms on the surface of the metal during heating. The word "smith" was also derives from an old word, "smite" (to hit). Thus, a blacksmith is a person who hits black metal (Bealer, 1996).

Therefore, blacksmith turns various reagents mostly metals, into agricultural implements, plate armor, local weapons, and some utility items. In addition, they produce objects such as gates, grilles, railings, light fixtures, furniture, sculpture, tools, decorative and religious items and cooking utensil. Suffice to note that blacksmith is recognize as one of the veritable weapons that can assist underdeveloped countries including Nigeria to achieve the 2015 anti poverty millennium

development goals (MDGs). For example, Kwara State has granted a loan of ₦100 million to artisans and expands an estimate of about 30 artisan trade in 2013, thus accounting for more than 20 per cent of sizeable employed artisans in Kwara State and subsidiary employment to a large number of farming households in the State. The bulk of artisans in the State include farming, artisanal fishery, blacksmith, tailoring, carpentry, weaving, dyeing, sculpture and ceramics; clay molding, hunting, mining, bead work, pottery, mud layer and other small scale enterprises native to State.

Furthermore, blacksmith in the State has advanced their service and production by going into repairing and maintaining mechanical devices and other related automobile industry. In addition, some youth who bag their certificate in city and guide in technical colleges and diploma in vocational and engineering in the State can venture into modern and mechanized blacksmithing that is powered by electricity, to design and manufacture agricultural implements, household utensils, mending and joining the machines and iron amongst other.

Essentially, blacksmith can have profound impact on the society particularly the youth, economy, agricultural and technological advancement. Socially, one of the most immediate benefits of blacksmith is its ability to create both skilled and unskilled employments. It is technological inclined trade and has the potential to create more jobs per unit of investment than any other artisan and can significantly cater for the employment of technical incline youth and adult alike. On technological and agricultural development, blacksmithing when properly developed and managed can advanced production of agricultural implements amongst other human utilities and stimulate local cultures and folklores (David and Bernhard, 1993, Francisco, 2005; Adedoyin et al., 2011). Economically, blacksmithing brings many benefits to both the government and private sector through the generation of foreign revenue, financial returns on investment as well as linkages to other local industries such as farming, carpentry, sculpture and ceramics; hunting, artisanal fishing, mining and fisheries.

Statement of Problem

Blacksmith is an ancient indigenous technology, which is the progenitor of various metal forging operation in used today and can be found virtually in all major cultures of the world (Oke and Aderoja, 2000). But, blacksmith processes still remain subsistence, primitive and rudimentary that it is hardly employed as the viable means of commercial production of metal wares in Nigeria (Thomas, 1980). For long particularly during the pre-colonial era and even now, some of Nigeria local blacksmith are traditional producer of simple tools such as cutlasses, knives, head pan, digger and machetes and many features and devices primary use for agricultural production. Other items produce through blacksmithing processes are domestic products, which include; kitchen ware, cooking utensils, basin, pails, which have found application in various homes. However, some blacksmith are involved in the production of industrial products, which include hammer head, key, chisel punch, bolt and nuts. The forge product of blacksmithing is also very important and highly demanded by those in the construction industry (RMRDC, 2000).

It is suffice to note that the major operations in local blacksmith shops consist of heating of work pieces, hard forging operation and heat treatment processes. There are several basic operations or techniques employed in forging: drawing down, shrinking, bending, upsetting, at a minimum, but smiths will also make use of other tools and techniques to accommodate odd-sized or repetitive jobs. The production facilities, consists of a forging facilities, which include anvil, hammer, chisels, fuller, drift punches. Open furnace with bellow is another blacksmith production facility for heating operation. This furnace makes use of palm kernel shell/waste to heat the metal, which is mostly iron and the heated metal is forged manually into desired tool. Occasionally, a primitive heat treatment process is achieved by quenching the forged metal in a container containing palm oil, water or some vegetable oil solution (Oke, 2007).

Blacksmith products have been recognized in the country from time immemorial and its importance, as an enterprise cannot be contested as one of the local skill necessary for sustainable development. The skill was extremely important to early Arkansan, to make and repairs tools, automobile spare parts, household implements and weapons (Oyeneye, 1984). The potential of blacksmiths for serious application sometimes demonstrated under unusual circumstances is beginning to find commercial application in satellite town of Nigeria urban centre where they serve as an adjunct to roadside mechanics (Eboh et al., 1995). Although the advent of the imported farm implements and machineries spare parts distorted the activities of local producers, but the increasing scarcity of foreign exchange is now necessitating a change of direction to abandon indigenous products (Obikwelu, 1999).

It is also suffice to note that the blacksmith skills is one of the basic skill required for producing innovative appropriate technological implements, but is unfortunate that, local blacksmith shop is about to be faced out due to the influence of western education and rural urban drift (Ezeadichie, 2002). The problem of flow of advance and improved western industrial products give blacksmiths little room to improve on their product in accordance with modern appropriate technology innovation (Atteh, 1992). The people are now neglecting the products of local blacksmith shops for the foreign products which suites the changing circumstances of time in term of quality and quantity. The situation has made the blacksmiths to be periodically engaged in the practice base on the demand of the product from individual customer. It was stressed that, development of indigenous technology for developing small-scale industry in which blacksmith shop is included is important for fast development of complex technology industries (Okopo and Ezeadichie, 2003). In addition, the development of this type of small-scale manufacturing industries is the cornerstone of sustainable economic self reliance (Oni and Lawal, 2006).

Despite these huge potentials of small scale enterprises including blacksmith, they have suffered neglect for long and have been less favoured by the different tiers of government and nongovernmental organisations in Nigeria to the oil, telecommunication and agriculture industries. This may be due to lack of know-how to develop and exploit the local resources and talents couple with our value of over dependence on the earlier traditional source of revenue. Small scale industry and artisans trade should be a source of income and revenue generation pivot for unemployed youth in the rural and

urban areas in the State, but the present revenue allocation structure which allows for allocation of nationally generated funds to the State may be a major factor for the State's reluctance to look inward and probably develop its resources and potentials. This has been a big concern for the State governments who again have shown little political will to create enabling environment and commit enough resources to develop the artisanal and local industry (Adedoyin et al., 2011).

From the foregoing considerations, it is very important to undertake in depth socioeconomic studies into artisanal blacksmith in the study area. This will enable us to accumulate adequate, sufficient and reliable data for analysis geared towards meaningful policy formulation for the artisans' sector especially artisanal blacksmith in the country. This study therefore investigated the potentials of and socioeconomic benefits of randomly selected blacksmiths in Kwara State, Nigeria.

Specifically, the study;

- (i) examine the structure and socioeconomic characteristics of blacksmiths;
- (ii) determined economic benefits derived by blacksmiths;
- (iii) determine the contribution of blacksmithing to household income;
- (iv) estimate factors that influence net income of the blacksmiths in the study area.

II. MATERIAL AND METHODS

Description of the Study Area

The study was conducted in 16 Local Government Areas (LGAs) of Kwara State (Figure 1). The State has a land mass covering about 32,500 square km and a total land size of 3,682,500 ha with majority living in rural areas. It has a population of about 2,365,353 people in 2006 according to the National Population Census (NPC, 2006). This is projected in 2013 to be 2,948,858 representing 3.2% annual growth rate in population and an average density of ninety one persons per km². It is bounded in the North by Niger State, in the South by Oyo, Osun and Ekiti states, in the East by Kogi state and in the west by Benin Republic (KWADP, 2011).

The State is divided into four agricultural zones by the Kwara State Agricultural Development Project (KWADP) in consonance with ecological characteristics, cultural practices and project administrative. The zones are: zone A; Baruten and Kaima LGAs; Zone B; Edu and Patigi LGAs; Zone C; Asa, Ilorin East, Ilorin South, Ilorin West and Moro LGAs and Zone D; Ekiti, Ifelodun, Irepodun, Offa, Oyun, Isin and Oke Ero LGAs. Blacksmith in the study area is contributing immensely to the socio-economic factors of the entire populace due to economic influx of people in search of agricultural tools, local weapons and kitchen utensils from the adjoining communities. The economic importance of blacksmith to the community includes provision of income, tools to rural development and source of raw materials to manufacturers.



Figure 1: Map of Kwara State Showing the 16 LGAs; Source: (KWADP, 2008)

Sampling Procedure and Data Collection

Primary data which was subjected to a pre-survey were used for this study. Blacksmith workshop survey provided the basic cross-sectional data from 80 blacksmiths in the study area. Data were collected from artisanal blacksmiths with the aid of structured questionnaire and interview schedule. A random sampling technique was used to select the representative of blacksmiths that were used for this study. Then, the lists of artisanal blacksmiths in all the 16 LGAs were compiled through blacksmith association for random selection. The stage involved random selection of twenty blacksmith workshops in each of the four ADP zone. In all, eighty respondents were sampled.

The questionnaire was administered to the blacksmith households randomly selected to generate information on socio-economic and demographic characteristics of households such as age, sex, marital status, family size, vocational and skill education, their smith experience, size of households as well as their major and subsidiary occupations. Other includes information on structure and production pattern, quantities and acquisition of inputs such iron and steel, wood handle, fuels such as palm oil/kernel, water or some vegetable oil solution as well as material inputs viz; anvil, hammer, chisels, fuller amongst other and their economic life span, products produced and their value in Naira.

III. ANALYTICAL TECHNIQUES

Profitability of Blacksmithing in the Study Area

Descriptive statistics such as frequency counts, mean, standard deviation, percentages, pie chart and tables were used to describe structure, socio-economic and demographic characteristics of artisanal blacksmith in the study area. Net income analysis provides the profit index and household income of the blacksmith in the study area. Profitability stimulates artisans to venture into risky business and also drives them to develop ways of cutting cost and adopting new technologies always in an effort to satisfy consumer interest. Profit maximization is the most important goal of artisan business. Profit is generally described as the difference between Total Revenue (*TR*) and the Total Costs (*TC*) as seen in equation 1 & 2. The total revenue is the blacksmith product or output sold and price while the total cost is divided into fixed and variable costs. Net income analysis forms an alternative basis for farm profitability analysis. It involves accurate collection of different costs of variable inputs and fixed assets and the gross income obtained from a particular enterprise in order to obtain the net returns.

Costs involved in blacksmithing operations are made up of total cost. Total cost consists of total variable cost (TVC) and total fixed cost (Equation 1 & 2). Total variable costs in blacksmithing depend essentially on the variable inputs. Unlike fixed costs, operating/variable costs depend on the volume of production, and they included cost of hired labour, imputed cost of family labour, fuel and lubricants expenses and maintenance charges while total fixed cost was made up of the depreciation costs or loss in value on fixed items as a result of their use in one production year. Items of fixed costs identified in the study included depreciation on open furnace with bellow, anvil, hammer, chisels, fuller, drift punches and interest charge on borrowed capital if any. Depreciation values were estimated using straight line method under the assumption that production facilities aforementioned were used for a period of 2 years before being scrapped without salvage values. Other fixed items such as simple open furnace with below and quenching bath are depreciated base on estimated life span suggested by blacksmiths. Blacksmith labour was standardized with adult male member of household having one labour day for working 6 hours while an adult female working for the same period was apportioned 0.75 labour day and grown up child, about 15 years was also assumed to have contributed 0.5 labour day for all kind of blacksmith operations (Oladimeji and Abdulsalam, 2013).

The Gross revenue (GR) consists of cash receipts from blacksmith products sold including the amount give away and used as household utensils or local weapons for hunting. The net income per blacksmith analysis was used to examine costs and returns in blacksmithing. The total variable and total fixed costs and total revenue were estimated. The difference between total revenue and total cost is the net income. The net income (NI) analysis was used with assumption that fixed costs though negligible in small scale farming (Olukosi and Erhabor, 2008), but play a prominent role in few artisan enterprise/trade including blacksmithing, and cannot be negligible. The net income per blacksmith analysis was expressed as:

$$NI = TR_{ij} - TVC_{ij} - TFC_{ij} \dots\dots\dots (1)$$

$$NFI (TN)^{-1} = (\sum_{i=1}^M TR_{ij}) (\sum_{i=1}^M TN_{ij})^{-1} (M_j)^{-1} - (\sum_{i=1}^M TC_{ij}) (\sum_{i=1}^M TN_{ij})^{-1} (M_j)^{-1} \dots\dots (2)$$

Where, NI (bt)⁻¹ = Annual net income per blacksmith in the jth ADP zone (□); TR_{ij} = Total sales revenue accruing to the ith blacksmith in the jth ADP zone (□); TVC_{ij} = Total variable cost incurred by the blacksmith in the jth ADP zone (□); TFC_{ij} = Total fixed cost incurred by the ith blacksmith in the jth ADP zone (□); TN_{ij} = Products produced by the ith blacksmith in the jth ADP zone (tons) and M_j = Total number of blacksmiths in the jth ADP zone.

Model Specification and Estimation

Estimation of the factors influencing net income of blacksmith involved the use of Ordinary Least Square (OLS) regression techniques and specified by equations:

$$\text{Log } NI_{ij} = \beta_0 + \beta_1 \text{LogFEX}_{1ij} + \beta_2 \text{LogNFF}_{2ij} - \beta_3 \text{LogCHL}_{3ij} - \beta_4 \text{LogCFL}_{4ij} - \beta_5 \text{LogDEP}_{5ij} + \mu_i \dots\dots\dots (3)$$

Where:

- NI_{ij} = Net income of the blacksmith in the jth ADP zone (□);
- FEX_{1ij} = Smith experience of the ith blacksmith in the jth ADP zone (years);
- NFF_{2ij} = Number of forge and furnace owned by the ith blacksmith in the jth ADP zone;
- CHL_{3ij} = Cost of hired labour by ith blacksmith in the jth ADP zone (□);
- CFL_{4ij} = Cost of family labour by the ith blacksmith in the jth ADP zone (□);
- DEP_{5i} = Depreciation of fixed inputs and cost of fuels used by ith blacksmith in the jth ADP zone (□);
- μ_i = error term associated with data collection from the ith blacksmith in the jth ADP zone which was assumed to be normally distributed with zero mean and constant variance.
- β₀ is a constant
- β₁- β₅ are regression parameters that were estimated.

IV. EMPIRICAL RESULTS AND DISCUSSION

Structure and socioeconomic characteristics of blacksmiths in Kwara State

The artisanal blacksmith is an important age long artisan in the areas of study. At the onset of the rain, the bulk of blacksmiths prefer to retire to farming which accounted for 65% of their major or subsidiary occupation (Table I). Farming as a subsidiary occupation was low in zone C comprising Asa, Ilorin east, west and south LGAs because the bulk of the blacksmiths were able to venture into menial and government jobs due to proximity to urban centres and State capital.

Majority of the pooled blacksmith (94%) had subsidiary occupations which served the dual purpose of alternative income and job opportunities. Engagement in subsidiary occupation in the rural community implies that rural areas have diversified enterprise oriented economy (Olayide *et al.*, 1982 and Oladimeji, 1999).

Artisanal blacksmith in the State rely heavily on the use family labour and the bulk was encouraged by their family antecedents to venture into blacksmithing. Blacksmithing like other artisans native to Nigeria rural areas, are family oriented business. The study was in line with Oke, 2011 and Oladimeji *et al.*, 2013. Further analysis showed that there is virtually no new entrance into the trade and most educated blacksmith family are shunning and shying away from the trade. This indicate that blacksmithing may soon fade out expect modern machines and inputs are injected into the trade to reduce the labour demand and improve the output to meet acceptable and international standard. Similar finding was documented by Oke, 2011.

Table I: Subsidiary Occupations of Artisanal Blacksmithing Kwara State, Nigeria.

Occupations	Frequency	Relative frequency (%)	Cumulative Frequency
Farming	52	65.2	-
Wood Carving/Carpentry	03	03.0	55
Govt. Employee	20	31.8	75
No subsidiary occupation	05	-	80
Total	80	100.0	-

Source: Field Survey, 2013

Results also showed the category of blacksmith products in Kwara State in figure 2. The bulk of blacksmiths output in the study area was agricultural products (55%) and domestic household utensils (30%) and others such as industrial products were estimated to be 15%. The finding was also in line with Oke, 2007. Therefore, it can be advisory that if blacksmithing is finance, developed and mechanized, its contribution will be felt by all area of human endeavours and this will improve the economy at large and increase rural household income and reduce poverty. In addition, the existence and development of blacksmith artisan will go a long way to employ the youth and adult and widening the industrial base of the State.

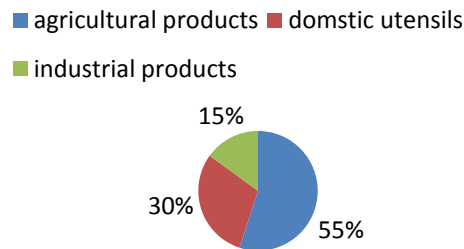


Fig. 2: category of blacksmith products in Kwara State.

The bulk of the blacksmith confirmed that given the opportunity and amazing potentials for sales of their products both locally and widening export base for their products in Kwara State. However, there are overwhelming constraints that retard and hampered their production in terms of quality and quantity and demand from customers. It was observed that the mode of manufacturing processes, workshops layout and the sources of raw materials, though were virtually the same in Nigerian blacksmith workshops, but such materials are sub standards and inappropriate compared to their counterpart in developed world. These production facilities include; open furnace without any temperature measuring instruments to help in reaching appropriate quenching birth and forging with the aid of hammer and anvil which absolutely stressful even below forging temperature.

The artisanal blacksmithing in the State are characterized by low capital investment and high labour intensive practices. For instance, the State investment in tools and facilities had a ranged of ₦10, 000.00 to ₦50, 000.00. The LGAs average for the workshop layout, furnace and forging materials are in the main unsophisticated comprising open furnace without any temperature measuring instruments to help in reaching appropriate quenching birth and forging with the aid of hammer and anvil which absolutely stressful even below forging temperature, fuels such as palm oil/kernel, water or some vegetable oil solution as well as other material inputs: chisels, fuller and drift punches. Both family and hired labours were used in blacksmithing operations in all the four zones of the State. Labour costs accounted for approximately 60% of average variable cost and 30% of Total cost. Hired labours were rewarded by cash and daily payment of ranged of ₦400 to ₦600 per labour day depending on volume of work done and output produced. However, hired labour was found to be scarce in zone C due to proximity to urban centre. Results also showed that sizeable blacksmiths received various amount of productive credit from their local blacksmith cooperative in their area and approximately 70% of sample blacksmith did not seek for any production credit. This result was in line with Oladimeji *et al.*, (2013), who affirmed that most artisans in Kwara State do not have access to production loan from formal credit institutions due largely to stringent and bureaucratic conditions offers by most formal lenders.

Socio-economic Characteristics

Analysis of socio-economic characteristics of the artisanal blacksmith is presented in Table II. The table indicates that males dominate the ownership of artisanal blacksmith venture in the State. Only 2 women (2.5%) of pooled blacksmiths owned and engaged in blacksmithing and the trade was inherited from their late husband. Therefore women do not usually engage in blacksmithing and other stressful rural artisans' operations, particularly when it involves actual production and manufacturing in the study area. Rather, women are engaged in sourcing for inputs and marketing of the output (Oladimeji, 1999 and Oladimeji et al., 2013). Further analysis revealed that bulk 75(94%) of the pooled blacksmith operate on a family unit bases that is, the blacksmith prefer sole proprietorship. This perhaps explained why most blacksmiths operate on a small scale basis in the study area. Table II also shows that the majority 84% of the pooled blacksmith had ages ranging from 38 to >57 years with the modal age interval being 48 to 57 years which accounts for 58% of the sample. Other things being equal, labour productivity is a function of age. It is believed that old people tend to adhere strictly to traditional methods of production while young people tend to be more willing to adopt new production methods in order to increase production. If old blacksmiths are defined as those who are above 48 years of age, 66% of blacksmith can be said to be old. In addition, if productive age group is defined as 18 - 57 years, the age distribution indicates that majority of blacksmiths (about 66%) fall the edge of unproductive age group and, therefore will not be able to imbibe new ideas and innovations to enhance increased productivity in the blacksmithing enterprise. Similar findings were documented by Oke, (2011).

The literacy rate was very low among the blacksmiths (Table II). The mean years of schooling of blacksmiths in the study area was 2.8 years. The estimated value fall below 2009–2012 UNDP mean education index of 5 years for Nigeria. In addition, more than Two-third (70%) of the pooled blacksmith did not have formal schooling while 21.3% attended primary school only. This implies that artisanal blacksmithing operations in the State were performed mostly by illiterate and semi-illiterate blacksmith. This could affect their chances of using improved and sophisticated machines which required skilled training and reading manuals to learn modern blacksmithing techniques. Low level of education can adversely affect success of small and medium scale enterprise and programmes because education and particularly training enhances adoption of technology and improved methods which are vital means of achieving higher productivity. Results are synonymous with Oladimeji et al., 2013 and Ajao and Oladimeji, 2013.

The marital status shows that majority 74 (92.5%) of the blacksmith are married while the residual 6 (7.5%) were single. Further analysis revealed that more than two-third of nuptial blacksmith (73%) had at least 2 wives while approximately 17.0% of had only one wife. Marrying more than one wife is common in rural setting either to ensure supply of additional family labour or to raise the status of the man in an illiterate setting. Findings were in line with Oladimeji et al., 2013. On the household size, the average number of persons per blacksmith was approximately 7 with 6-10 children as modal class. Table II shows that 7.5% of blacksmiths had no child, 45(56.3%) had household size of 6-10 children. The result shows that most of the population explosion occurs in rural areas. However, they are important in the supply of family labour after schooling hours particularly in blacksmithing and other households activities such as marketing of manufactured products.

Table II: Socio-Economic Characteristics of Artisanal Blacksmith in Kwara State

DISTRIBUTION	FREQUENCY	RELATIVE FREQUENCY (%)	CUMMULATIVE FREQUENCY
*Gender			
Male	78	97.5	-
Female	02	2.5	80
*Marital status			
Married	74	92.5	-
Single	06	7.5	80
*Age (years)			
18-27	3	04	-
28-37	8	10	11
38-47	16	20	27
48-57	46	58	73
Above 57	7	08	80
*Educational Level			
No Formal Schooling	56	70.00	-
Primary Education	17	21.25	73
Secondary Education	06	7.50	79
Tertiary Education	01	1.25	80
*Household Size(persons)			
None			-
1-5	20	25.0	20
6-10	45	56.3	65
11-15	10	12.5	75
>16	05	6.2	80

Source: Field Survey, 2013

Estimate Costs, Returns and Economic benefits from blacksmith

The net margin per blacksmith in the study area has shown that artisanal blacksmith is profitable. This is presented in Table III below. The AFC per blacksmith ranged between ₦5500.0 in zone A and ₦7800.0 in zone C giving an average of ₦6537.5 for the State. The table also shows that AVC per blacksmith had a range of ₦10500.0 in zone A to ₦13250.0 in zone D with a value of ₦11637.5 per blacksmith for the State. The standard deviations for AFC and AVC per blacksmith were ₦996.1 and ₦1255.2 respectively. The relatively high AFC/blacksmith in zone C was due to the fact that the blacksmiths operate in urban centres where the fixed and materials inputs are relatively costly. The fixed assets such as furnace, forging and heating equipments were acquired at relatively high price because of the prevailing high rate of inflation in the country. The standard deviation for the AVC per blacksmith was larger than that of the AFC because the former depended on the volume of production while the latter was invariant to the product produced. Table III also shows that the net return per blacksmith was highest, ₦27000.0 in zone C. Similarly, zone C blacksmith settlement recorded the highest NR/blacksmith because of their proximity to urban centre which enable them to have higher bargain for their product. The net return per blacksmith for the State was ₦24900.0 with a standard deviation of ₦1982.8. The revenue accrued to blacksmith was not only dependent on the product produced and price per product, but also dependent on the variable costs.

Table III: Estimated Average Costs and Returns (₦) Per Artisanal Blacksmith in Kwara State, Nigeria

Blacksmith settlements/Zones	Average Fixed Cost (AFC)	Average Variable Cost (AVC)	Average Total Cost (ATC)	Average Revenue (AR)	Monthly Return(NR) per smith*
A	5500	10500	16000	38350	22350
B	6050	10800	16850	41350	24500
C	7800	12000	19800	46800	27000
D	6800	13250	20050	45800	25750
Total	26150	46550	72700	172300	99600
Mean	6537.5	11637.5	18175	43075	24900
SD	996.1	1255.2	2052.8	3941.3	1982.8

SOURCE Data Analysis, 2013

Estimated Factors Influencing Net Incomes of Blacksmiths

Results showed that in study area, the postulated explanatory variables in equation 4 explained about 48.8% in the variations of net income of blacksmith. It also shows that the coefficients of all the variables included in the factors affecting blacksmith income carried *a priori* signs which supports the hypothesized that cost of family labour, hired labour, and depreciation of assets including fuels are expected to bear a negative sign with blacksmith income while years of experience and number of forging facilities and open furnace with bellow make positive contributions to the net income of blacksmith. Although, cost of hired labour carried the *a priori* sign, the variable was not statistically different from zero at the 5.0% level.

The F-test also revealed that the model was significant at 5.0%. However, the negative signs on the coefficients of Log CHL, CFL and DEP showed that an increase in the use of these inputs caused net income to declined, *ceteris paribus*. Small scale blacksmithing is labour intensive and every activity in the business, from forging and heating going to the molding and processing as well as marketing of the products required adequate amount of human effort. The F-test with a value of 11.50 revealed that the model was significant at the 5.0% level. Although all the estimated co-efficient carried the *a priori* signs, that of man-days of hired labour was not statistically different from zero at the 5.0% level (equation 4).

$$\text{Log } Y_i = 6.250^* + 0.0304 \text{LogFEX}_{1ij} + 0.006 \text{LogNFF}^*_{2ij} - 0.127 \text{LogCHL}_{3ij}$$

(0.155) (0.082) (0.018) (0.065)

$$- 0.0550 \text{LogCFL}_{5ij} - 0.164^{**} \text{LogDEP}_{6ij} \dots\dots\dots(4)$$

(0.220) (0.008)

$R^2 = 0.488; F=11.50^*$

* and ** Indicates that estimated co-efficients were significant at 1% and 5% level respectively. The standard errors of the co-efficient are in parenthesis.

Estimated Resource-use Efficiency of Blacksmith

The results of the estimated resource-use efficiency were derived with respect to number of traditional forging and heating materials, family and hired labours and as well as depreciation of fixed assets in table IV. The table shows that Marginal Value Product (MVP) of each production input was less than its acquisition cost implying that each of the input in blacksmithing were over utilized. The excessive uses of labour resource in rural areas tend to be a common occurrence due to rather low opportunity cost for the inputs (Oladimeji, 1999 and Oladimeji et al., 2013). Family labour cannot sensibly be 'laid off'. For instance, in blacksmithing and artisan activities even when family labour is making a negative contribution because it still has to be catered for whether it is employed or not. Besides, the existence of disguised unemployment and under-employment of labour in rural areas of the country necessarily promote excess labour in blacksmithing, agriculture and fishing enterprises (Oladimeji et al., 2013). In addition, small scale blacksmithing is a rising enterprise in that under the

prevailing technology in the country, blacksmith production depend more on chances of available inputs and product demand than on mandays of labour employed.

However the MVP of all resources used are positive, hence they all contribute positively to total output. To maximize profit the ratio must equal one. When the ratio is less than one, it is an indication of over-employment of the resources beyond the point of optimum profit. Profit can be increased by reducing the rate of use of the resources. When the ratio is greater than unity, it indicates that the rate of utilization of the resources is too small; increasing the rate of use would increase profit.

From the results obtained it was clear that the optimization condition was not attained for the given level of technology in the blacksmithing production. The MVPs obtained are less than unity. Results are consistent with findings by Oladimeji, 1999 and Oladimeji *et al.*, 2013.

Table IV: Estimated Resource-use Efficiency for Blacksmith in Kwara State

Resources	MVP (□)	Unit price of inputs(□)	Efficiency ratio MVP/Unit Cost
Number of forge and furnace	008	400.0	0.02
Family labour (imputed)	45.6	400.0	0.12
Hired labour	67.9	600.0	0.11
Depreciation of fixed assets	116.5	120.8	0.96

Source: field survey, 2013

V. CONCLUSION

The study examined the socio-economic characteristics and returns of rural blacksmithing in randomly selected four blacksmith areas of Kwara State, Nigeria. Although, the result showed that blacksmithing enterprise in the State is profitable. The estimated mean years of schooling of blacksmith in the study area was 2.8 years, fall below 2009–2012 UNDP mean education index of 5 years for Nigeria. This could have affected their chances of shifting from traditional blacksmithing to modern ones.

The result for access to credit shows that blacksmiths depend largely on personal saving and their cooperatives to procure inputs and adopt new technology and innovations because they lack the collateral demanded by financial institutions.

The marginal value product (MVP) of each production input was less than its acquisition cost implying that each of the input in blacksmithing were over utilized. This implies that the optimization conditions were not attained for the given level of technology in the blacksmithing production.

Recommendations

Based on the findings of this study, it is recommended, therefore;

1. That blacksmiths in the study area should be given adequate training using community based informal education, to enable them imbibe mechanized blacksmithing techniques and acquired materials inputs that will translate into reasonable quantity and quality products. This will ensure proper understanding of modern equipments and adopt technology capable of increasing not only the profitability of the blacksmith enterprise but also make efficient use of resources.
2. Establishment of blacksmiths' co-operative association for annexing financial aids, marketing information and inputs from government and non-government organizations through poverty alleviation Agencies.
3. Creating a market channel that will take care of commensurate price for products of blacksmith enterprise.
4. Government at all levels should endeavor to stimulate blacksmiths to produce quality products by providing and subsidize if need be, necessary infrastructures and enabling environment which provide impetus that will ease people transition from traditional to modern blacksmith easy.

References

- [1] S. F. Adedoyin, A. L. Kehinde, and A. F. Sodunke, Potentials of and socioeconomic benefits of selected ecotourim centres in Ijebu Zone of Ogun State, Nigeria. *Centre Point Journal* 17(1), 2011, Pp: 53-60.
- [2] D. O. Atteh, Indigenous local knowledge as a key to local development possibilities, constraints and planning issues, studies in technology and social changes, No 20. AMES: IOWA State University, Technology and Social Change Program. 1992.
- [3] W. Bealer, *The art of blacksmithing*. (Castle Books Revised edition ed. 1996).
- [4] H. Davd, and H. Bernhard, *Basic tools and equipment of the rural blacksmith*. (Intermediate Technology Publications. 1993).
- [5] E. C. Eboh, C. U. Okoye, and D. Ayichi, *Sustainable development: The theory and implication for rural development in Nigeria*. (Auto Century Publishing Company 1995).
- [6] U. E. Ezeadichie, External influence on nation building in Nigeria. A Critic. (Conference Paper, Montair State University, New Jersey, U. S. A 2002).
- [7] F. Francesco, Nigerian tourism development master plan <http://www.nacd.gov.ng> (2005).
- [8] Kwara Agricultural Development Project (KWADP), *House Journal and Bulletin*, July, 2008.
- [9] (NPC), Population Census of the Federal Republic of Nigeria. (*Analytical Report* at the National Population Commission, Abuja, Nigeria 2006).
- [10] Y. U. Oladimeji, An economic analysis of artisanal fisheries in kwara state, Nigeria. Unpublished MSc Thesis. Federal University of Technology, Akure, Nigeria. 1999.
- [11] K. C. Obikwelu, Development of auto component parts industry in Nigeria. (Magazine by National Automotive Council. 1 (9), 1999.

- [12] P. K. Oke, and A. A. Aderoba, Mechanization of heat treatment facilities in local blacksmithies. *Nigerian J. Eng. Mangt.*, 1, 20-26, 2000.
- [13] P. K. Oke, An evaluation of improved local blacksmith process. *Journal of Engineering and Applied Sciences*. 2(8), 2007, 1255-1261. I. Okopo, and U. E. Ezeadichie, Indigenous knowledge and sustainable development in Africa: The Nigeria Case. (The 5th World Archaeological Congress, Washington D. C. 2003).
- [14] Y. U. Oladimeji, and Z. Abdulsalam, Analysis of technical efficiency and its determinants among small scale rice farmers in Patigi L.G.A. of Kwara State, Nigeria. *IQSR Journal of Agriculture and Veterinary Science*. 3(3), 2013, 34-39.
- [15] Y. U. Oladimeji, Z. Abdulsalam, M. A. Damisa, and D. F. Omokore, Estimating the determinant of poverty among artisanal fishing households in Edu and Moro Local Government Area of Kwara State, Nigeria. *Agriculture and Biology Journal of North America*. 4(4), 2013, 422-429.
- [16] S. O. Olayide, S. M. Essang, O. Ogunfowora, and E. S. Idachaba, *Element of rural economics*. (Ibadan University Press. 1982).
- [17] J. O. Olukosi, and A. O. Ogunbile, *Introduction to agricultural production economics: principle and applications*. Agitab Publishers Limited Zaria, Nigeria. 2004, 97 – 111.
- [18] T. O. Oni, and K. O. Lawal, Development of small scale manufacturing industries. Cornerstone of Sustainable Economic Self Reliance. Proceeding of Nigeria Institution of Mechanical Engineers, Akure, 2003, 50-57.
- [19] O. Y. Oyenenye, *Indigenous Technologies*. A. J. West Africa Studies' University of Ife Press No 25M, 1984, 63-64.
- [20] RMRDC, *Cottase Level Investment Opportunities in State of Nigeria*. A publication of Raw Materials Research and Development Council, 2000, 111.
- [21] L. U. J. Thomas-Ogubuji, Blacksmithing: A Metallurgical Assessment. *Ife J. of Tech.*, 1, 1989, 41-50.

Study and Evaluation for the Double-Chambered Incinerator Using Biomass Gas-Derived From Gasification

Yaowateera Achawangkul¹, Naoki Maruyama¹, Chatchawan Chaichana²
 Masafumi Hirota¹, Pimpawat Teeratitayangkul²

¹graduate School of Engineering, Mie University, Japan

²department of Mechanical Engineering, Faculty of Engineering, Chiang Mai University, Thailand

Abstract: This research aims to study for the double-chambered incinerator using biomass producer gas derived from gasification process by adjust the optimal combustion characteristics that can efficiently prevent emissions from being released. 30 kilowatt-thermal of gasifier that can generate an average of 18 m³ per hour of producer gas at the maximum fuel input rate of 15 kg per hour. The incinerator prototype consists of 2 combustion chambers with 2 gas burners installed, one for sample meat combustion and one for pollution elimination. The calculated proper volume of the primary chamber and secondary chamber were 0.10 m³ and 0.03 m³, respectively, in order to maintain an adequate combustion residence time. The experiment shows the temperature of the primary and secondary rooms can achieve a maximum of 750°C and 500°C, respectively, when 100% of excess air condition was carried out. Meanwhile, a large input of excess air decreased the temperature inside the combustion chambers and also increased the flue gas opacity, which meant an increase of exhaust pollution in the atmosphere. In addition, an evaluated efficiency of the incinerator was 29-32 percent if only the primary chamber was operated. Accordingly, biomass producer gas is a feasible and appropriate renewable energy source to utilize as the main fuel for a double-chambered crematory in order to cremate the corpse and eliminate pollution simultaneously.

Keywords: Biomass, Cremation, Double-chambered incinerator, Energy balance, Gasification, Producer gas

I. INTRODUCTION

Cremation has been popular in many countries such as Thailand, Japan and India, including countries in Europe and North America, due to the local customs or land conservation point of views. The cremation process usually uses petroleum fuel such as diesel oil or LPG (Liquefied Petroleum Gas) because they contain a high calorific value, and can combust completely compared to traditional fuels. However, the operation cost per each cremation becomes higher due to the increasing price of global petroleum. For example, the average operation cost for cremation in Thailand is 2,000-3,000 Baht[1], or 70-100 USD equivalently. Furthermore, the issue of environmental impact by using petroleum fuel also needs to be considered. It is necessary, therefore, to research and develop an alternative energy utilization in the cremation process that contains a low operation cost and emits low pollution. Biomass gasification is a thermo-chemical conversion process that turns organic fuels into gaseous compounds (called producer gas or syngas) by supplying oxygen, of which less is needed, to complete fuel combustion. The main product of the syngas contains flammable gas such as carbon monoxide (CO), hydrogen (H₂) and some traces of methane (CH₄), which can be used as fuel in a gas engine for electricity generation or heat generation in a small or medium scale factory [2]. Owing to the biomass producer gas that can be combusted more easily than solid biomass can, it is possible to apply biomass gasification to the cremation process, especially in the modern crematory that contains multi-combustion chambers and in which the emission control system is included.

II. EXPERIMENTAL APPARATUSES PREPARATION

2.1 Biomass fuels

Macadamia shells and coffee bean pulp were selected as appropriate biomass fuels for this study, and proximate with ultimate analyses were also carried out. Table 1 shows the fuel properties from the analysis.

Table 1 Proximate and ultimate analysis of selected biomasses

Biomass	Proximate analysis (% by weight)				Ultimate analysis (% by weight)						Gross Calorific Value (MJ/kg)
	Moisture	Ash	Volatile matter	Fixed carbon	Ash	C	H	N	S	O	
Coffee bean pulp	11.29	0.38	73.94	14.39	0.43	50.28	5.46	0.15	0.05	43.62	17.91
Macadamia shell	10.14	0.40	69.86	19.59	0.45	53.11	6.15	0.35	0.05	39.89	21.10

2.2 Biomass gasifier

A fixed-bed downdraft gasifier was employed to generate the producer gas and was supplied to the double-chambered incinerator apparatus. The existing capacity of the gasifier is 30 kilowatts-thermal. The size of the biomass that

can be used in the gasifier should not be larger than 1 inch x 1 inch. Figure 1 shows a picture of the downdraft gasifier and its schematic diagram.

Biomass producer gas was drawn from the bottom of the gasifier using a 3-phase gas blower. Before utilization of biomasses as the main fuel source in the furnace, it is necessary to remove tar, dust particles and organic compounds in the fuel gas as much as possible. Consequently, a high-efficiency cyclone, tar extraction condensing unit and bag filters were used for efficient gas decontamination. The final temperature of producer gas reached 40-45°C before being sent to the incinerator.

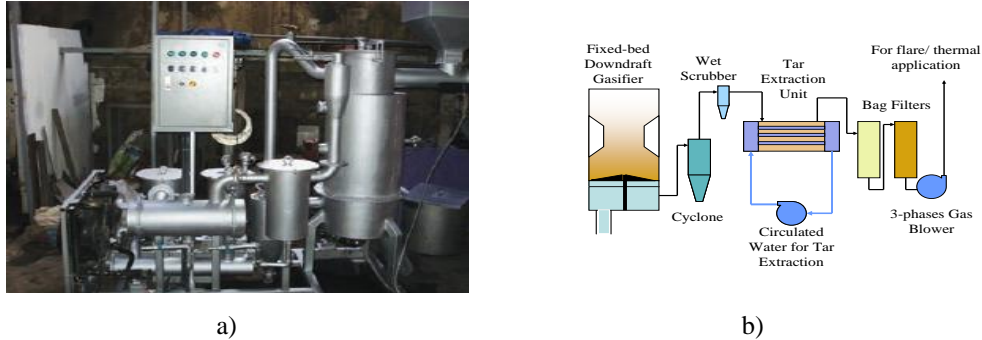


Fig.1 (a) Fixed-bed downdraft gasifier used in the experiment; (b) Diagram of the gasification and gas cleaning system

2.3 Double-chambered incinerator prototype

The prototype of the double-chambered incinerator was designed and constructed by scaling down the commercial double-chambered incinerator (Fig.2). The incinerator wall was made from refractory bricks, ceramic fibers and metal sheets in order to prevent most of the heat loss. Inside the primary combustion chamber, injected air holds were installed at both the left and right sides, with an angle of 330 degrees and 120 degrees, respectively [3]. The primary burner was located at a 25 degree downward angle at the backside of the chamber wall, in order to provide maximum impingement of the flame onto the sample material [4]. The total volume of the primary chamber was equal to 0.104 m³ in order to maintain the combustion retention time at longer than 5 seconds.

For the secondary chamber, combustion products from the primary chamber, including products from biomass producer gas combustion, are induced by a draft fan. In this chamber, the temperature must be maintained at a higher temperature than that of the primary chamber for the highest emission elimination [5], whereas the combustion retention time was appointed to be at least 1 second (neglecting the dead zone).



Fig.2 Prototype of double-chambered incinerator used in the experiment

2.4 Producer gas burner

There were two producer gas burners installed in the incinerator prototype (as shown in Fig.3). After producer gas was drawn by the gas blower, it passed through the burner that consisted of an injector to increase the velocity of the gas. Then, the gas was blended with the primary chamber's air in the mixing room before combusting in the burner's throat. The amount of air could be adjusted by the slide shutter.

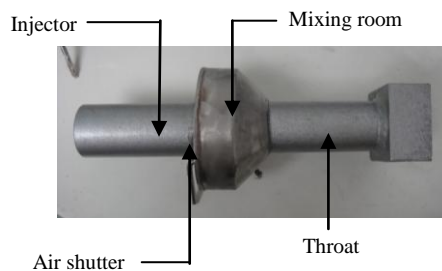


Fig.3 Producer gas burner

2.5 Sample material property

The main property of the sampling material is necessary to determine the stoichiometric air for complete combustion reaction. Consequently, the chemical composition of animal anatomical waste data was taken and referred to for the calculation and incinerator design. The dry combustible empirical formula of the whole dead animal is $C_3H_{10}O_3$.

Table 2 Ultimate analysis for whole dead body

Ultimate Analysis	Carbon	Hydrogen	Oxygen	Water	Nitrogen	Mineral (ash)
As charged (% by weight)	14.7	2.7	11.5	62.1	Trace	9.0
Ash and moisture free combustible (% by weight)	50.80	9.35	39.85	-	-	-

Source: Ministry of the Environment, Ontario, Canada [6]

It was found that the stoichiometric air to combust dry combustible material was 7.03 kg of dry air per kg of dry combustible material. However, actual air needs to be injected into the primary chamber due to the heterogeneous compositions with moisture content in the fuel. Therefore, the recommended actual air feed was 150% excess air [7].

III. METHODOLOGIES

After system design and construction, all experimental apparatuses were composed together. A steel tube was used to convey the producer gas from the gasifier to the incinerator via a gas cleaning system. Before obtaining proper producer gas for ignition in the incinerator, incombustible gas should be exhausted. Consequently, a steel ball valve was also installed to control the producer gas direction, including the flow rate of gas during the experiment. To control the amount of air injected into the incinerator, a centrifugal fan with an inverter was also set up in the same way as the induced draft fan that was installed at the flue gas stack to sustain both the gas flow and residence time in both the primary and secondary chamber. The schematic diagram of system installation is shown in Fig.4.

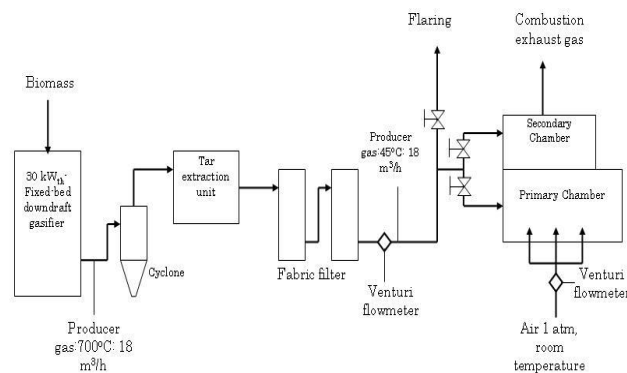


Fig.4 Schematic diagram of experimental apparatuses

According to the yield of CO production at the reduction zone, 90% of carbon dioxide (CO₂) will be transformed into CO if the temperature achieves 900°C [8]. Thus, the average temperature of the reduction zone was sustained at higher than 850°C throughout the experiment. Likewise, 5 kilograms of raw meat was selected instead of an actual corpse. An experiment of the incinerator side was started up after producer gas was already generated. The secondary burner was ignited first in order to conduct a high temperature inside the secondary chamber. The primary chamber was ignited as soon as the temperature of the secondary chamber was over 650°C. At the same time, auxiliary air was also injected for a combustion reaction. Significant parameters such as excess air, flue gas and the gas flow rate were measured by using a TESTO-320 gas analyzer. The investigated excess air can be employed for combustion equivalent ratio calculation (Eq.1)[9].

$$\% \text{ excess air} = \frac{(1-\Phi)}{\Phi} \times 100 \% \quad (1)$$

For an emission released measurement, the opacity of the flue gas measurement [10] using Ringelmann’s chart was selected as an adequate method (BS. 2742: 1969). Due to the regulation of the Pollution Control Department of Thailand [11] the opacity of exhaust gas released from cremation must be less than 10%.

In these experimental conduction, an observer has observed the opacity of flue gas released from the incinerator’s stack and compared it with the values shown in Ringelmann’s chart (Fig.5). The observation was conducted every minute until the experiment was finished.

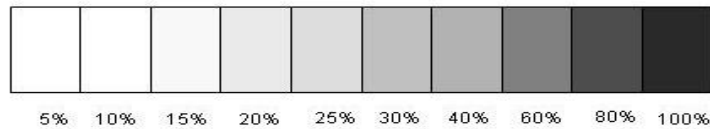


Fig.5 Ringelmann's chart

IV. RESULTS AND DISCUSSION

4.1 Producer gas properties

Biomass producer gas sampling was taken for component analysis using gas chromatography (GC). After the results were obtained, the gross calorific value of each producer gas sample was determined.

Table 3 Properties of the producer gas

Biomass	Gas content (% by volume)						Gross Calorific Value (MJ/m ³)
	H ₂	O ₂	N ₂	CO	CH ₄	CO ₂	
Macadamia shells	11.2	8.1	46.2	17.7	3.0	13.8	4.60
Coffee bean pulp	14.9	6.2	39.7	22.5	2.9	13.8	5.58

4.2 Temperature inside the incinerator at the adjusted excess air conditions

In each experiment, the producer gas volumetric flow rate was fixed at 0.15 m³/min for both the primary and secondary burner, and the percent of excess auxiliary air for the sample raw meat combustion was employed as 100%, 150% and 230%, respectively.

Both of the primary and secondary's temperature distribution are explained in Fig.6. When the primary burner was ignited and the primary chamber's excess air was set at 100%, it was found that the average temperature inside the primary chamber increased rapidly within a short time until it reached a maximum of 500°C. During the experimental conduction, the average temperature did not change drastically, and stayed around 450-500°C. For the temperature of the secondary chamber, the maximum temperature increased rapidly until it achieved 750°C, and also became steady throughout the experiment.

When the excess air fed to the primary chamber was changed to 150%, it was observed that it took a little bit of time for the primary chamber's temperature to achieve its maximum point, compared to the 100% excess air condition adjustment. Meanwhile, the temperature of the secondary chamber also presented a lower maximum point, which was 700°C on average.

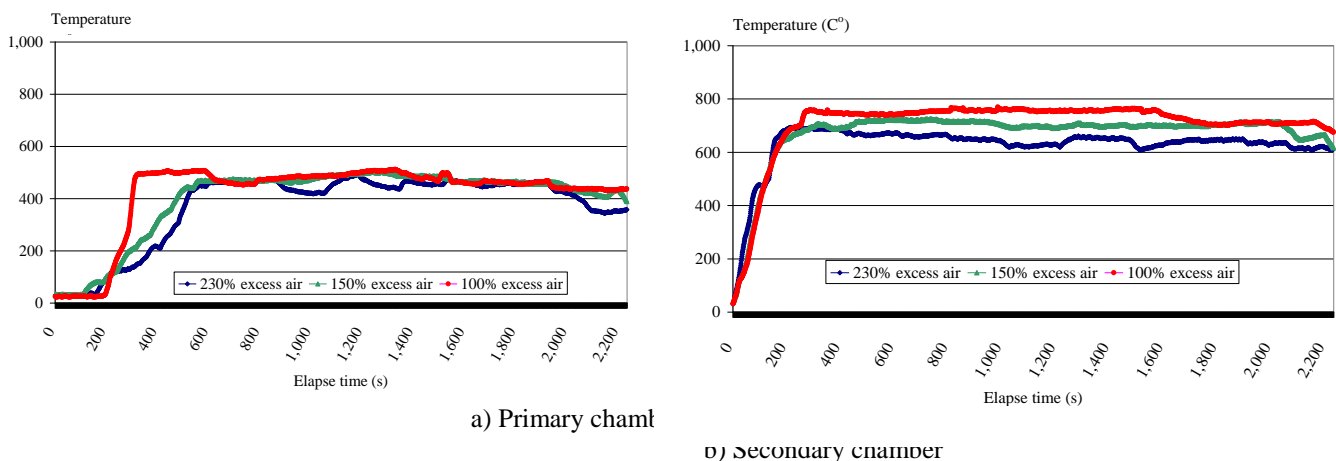


Fig.6 Temperature distribution inside the incinerator

The trend of temperature inside the primary chamber when adjusting the 230% excess air fed is presented in Fig. 6. It was found that the primary chamber's temperature needed a longer time for it to increase and to achieve its maximum point. In addition, the maximum temperature became lower than 500°C, and the temperature fluctuated throughout the experiment conduction time. Concerning the secondary chamber, the temperature achieved its maximum point at 650°C on average, which presented the lowest maximum temperature of those excess air conditions.

For the secondary chamber, the maximum temperature was reached when excess air was adjusted to be 100%. The increasing of the temperature profile in the secondary chamber was different from the primary chamber temperature profiles because there was no primary chamber's excess air that affected the temperature in this chamber. However, it can be

observed that the effect of excess air impacted the temperature in the secondary chamber after operating the primary chamber. The temperature became highest at 750°C when excess air was set at 100%, and became lower when adjusted for a new excess air condition by 150% and 230%, respectively. Concerning the flue gas opacity, which was employed for emission-released measurement, is the results are shown in Fig.7. It was found that the opacity observed was 10-15% on average when the primary chamber’s excess air conditions were set at 100% and 150%. However, the opacity of flue gas increased when the excess air condition was changed to 230%, which is found as approximately 20-25%.

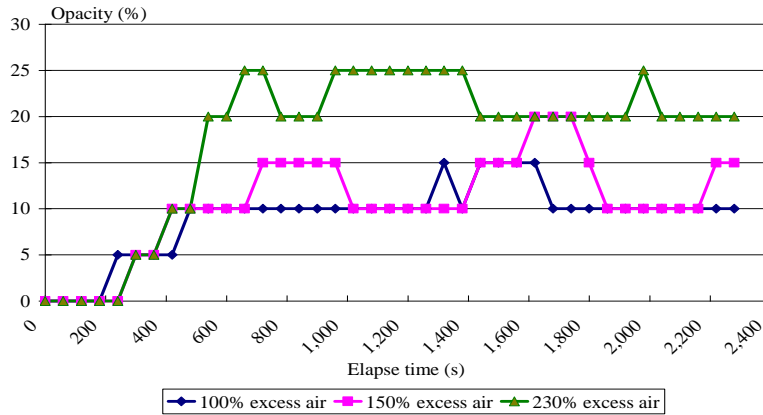


Fig.7 Opacity of exhaust gas

V. ENERGY BALANCE EVALUATION

An energy balance analysis of an incinerator prototype refers to the first law of thermodynamics and energy conservation.

$$\sum E_{input} = \sum E_{output} \tag{2}$$

where
$$\sum E_{input} = E_{i,producergas} + E_{i,fuel} + E_{i,elec} \tag{3}$$

and
$$\sum E_{output} = E_{used} + E_{o,exhaust} + E_{o,wall} + E_{o,unburnt} + E_{o,unaccountd} \tag{4}$$

In order to analyze the energy efficiency of the system, the incinerator was considered to be the control volume, in which the total energy input consisted of chemical energy from producer gas and sample material, and electrical energy was used. Whereas the energy outputs were energy from the combustion process (exhaust gas), energy loss through the incinerator wall, energy loss with unburnt matter and unaccounted losses.

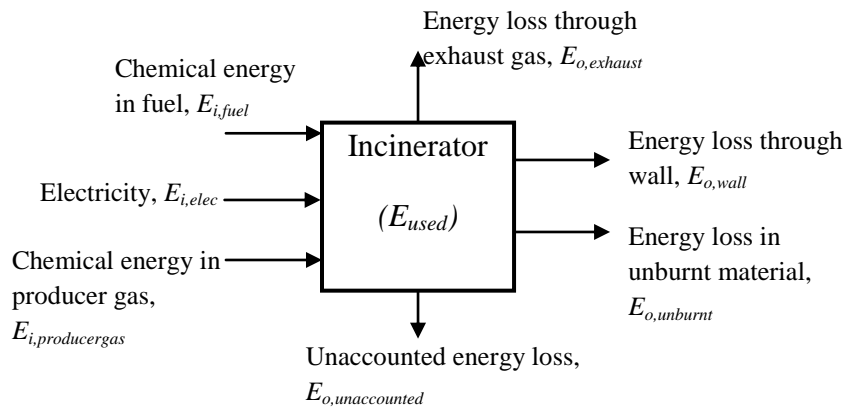


Fig.8 Incinerator’s energy balance diagram

5.1 Chemical energy from biomass producer gas combustion

A chemical energy input into the incinerator by the producer gas is determined by a lower heating value (LHV) of producer gas.

$$E_{i,producergas} = \dot{Q}_{producergas} \times LHV \tag{5}$$

5.2 Chemical energy from sample material

Chemical energy input from the sample material was derived from the LHV of the dry combustible substance of the sample material (raw meat).

$$E_{i,fuel} = m_{fuel} \times LHV \tag{6}$$

in which
$$LHV = HHV - 5.72(9H + M) \tag{7}$$

where H and M represent hydrogen and moisture content inside the sample material, respectively.

5.3 Electricity power consumption

The electricity used in the experimental rigs consisted of power used in the gas blower, power used for the air blower, and power used for the draft fan, which were measured by a digital power meter.

5.4 Energy loss in exhaust gas

Energy loss in exhaust gas can be determined from the composition of the measured exhaust gas and the gas mass flow rate.

$$E_{i,exhaust} = \dot{m}_{gas} C_{p,gas} (T_{gas} - T_a) \quad (8)$$

5.5 Energy loss through the incinerator wall

Fourier's law was used to calculate the total heat conduction through the incinerator's wall layers [12].

$$\dot{Q}_{conduct} = -kA \frac{dT}{dx} \quad (9)$$

5.6 Energy loss in unburnt material

Energy loss in unburnt material occurred due to some unburnt material contents lingering in the sample with the remaining material. Therefore, it was necessary to calculate unused energy in the conduction.

$$E_{o,unburnt} = m_{unburnt} \bar{C}_{p,unburnt} (T_h - T_c)_{unburnt} \quad (10)$$

where T_h and T_c are hot and cold temperatures of the unburnt material, respectively.

5.7 Unaccounted losses

Because of the complexity of determining unaccounted losses, such as radiation heat loss and heat contained in the incinerator after finishing experiment, these losses were computed by the difference between the heat input and determinable output. Furthermore, if the secondary chamber was ignited, the energy needed to maintain the maximum temperature for efficient combustion gas elimination was considered an unaccounted loss.

5.8 Energy used

Energy used in the incinerator consists of energy needed to evaporate moisture content in the raw meat and energy needed to burn the meat's dry combustible matter.

$$E_{used} = \{m_{water} C_{p,water} (T_{boil} - T_{initial})_{water}\} + \{m_{water} h_{fg}\} + \{m_{dry} C_{p,dry} (T_f - T_{initial})_{dry}\} \quad (11)$$

5.9 Incinerator efficiency

An efficiency (or the first law efficiency) of the incinerator is the ratio of the incinerator's energy utilization to the total energy input, which can be calculated by (12).

$$\eta_{incinerator} = (Energy\ used / Energy\ input) \times 100\% \quad (12)$$

5.10 Energy balance evaluation results

After completing the experiment, system energy balance was carried out using recorded parameters and equations (5)-(12), as exhibited earlier. The results of the energy balance are described in Table 4.

From the calculation results shown in Table 4, it was found that the major heat loss from the system was through exhaust gas, which accounted for approximately 40% of total heat loss. The others were loss through the incinerator wall, unaccounted losses and loss in ash and unburnt material, respectively.

Concerning the efficiency of incinerator, if only the primary chamber was operated, it was found that total efficiency was equal to 29-32%. The useful energy when using producer gas from coffee bean pulp as fuel was higher than when using macadamia shell gas due to the higher heating value (HHV) of producer gas, which can efficiently evaporate moisture and combust sample material.

When both the primary and secondary chambers were operated, it was found that the incinerator efficiency decreased by approximately 50% compared to when operating only the primary chamber, whereas unaccounted losses increased. This result can be explained by the fact that some producer gas was used in the secondary chamber in order to maintain a high temperature for pollution elimination. Therefore, the amount of producer gas required for sample material combustion was decreased, and also increased the amount of unburnt matter after the experiment was completed.

Table 4 Incinerator's energy balance calculation results

Parameters	Producer gas from macadamia shells		Producer gas from coffee bean pulp	
	Operated only 1 st chamber	Operated 1 st and 2 nd chamber	Operated only 1 st chamber	Operated 1 st and 2 nd chamber

Energy input				
Producer gas (MJ)	22.63	22.08	27.36	27.05
High moisture material	8.90	8.90	8.90	8.90
Power consumption (MJ)	0.78	0.38	0.74	0.33
Total energy input	32.31	31.36	37.00	36.28
Energy output				
Exhaust gas (MJ)	9.82	8.60	12.65	11.43
Heat loss through wall	7.23	7.06	7.45	7.31
Heat loss in ash and unburnt material (MJ)	1.43	2.81	1.06	2.63
Unaccounted loss (MJ)	4.37	8.29	4.01	9.67
Useful energy (MJ)	9.46	4.60	11.83	5.24
Incinerator efficiency ($\eta_{incinerator}$),	29.28 %	14.67 %	31.97 %	14.44 %

VI. CONCLUSION

According to the property of biomass producer gas generated from the gasification process that contains a lower and non-uniform heating value, it is important to follow significant parameters when the producer gas is used for thermal application, especially in cremation, which needs strict control of the combustion efficiency and emissions released. Firstly, the size of both the primary and secondary combustion chambers must be adequate in order to maintain the combustion residence time of both waste and flue gas. Second, due to the properties of the high-moisture material (raw meat), which was used instead of a corpse, and its high moisture content and complex chemical substances that are significantly different from liquid or gaseous fuel, it is, therefore, necessary to inject a large amount of excess air, to produce complete combustion and efficient emissions control to the extent possible. However, a large amount of excess air is not ostensibly beneficial to the combustion reaction, because unnecessary excess air usually affects the temperature distribution and efficiency of emissions control.

Concerning the results of the incinerator's energy balance evaluation, the efficiency reduces by approximately half when both primary and secondary chambers are operated, compare to when only the primary chamber is in operation. However, this results in efficient pollution elimination.

Acknowledgement

The authors would like to acknowledge the Dean of the Faculty of Engineering, Chiang Mai University, the faculty's lecturers and staff members for all their assistance.

REFERENCES

- [1] Wongschitwan P., Zero Pollution Cremation (online), available from <<http://gotoknow.org/blog/babyr2r/352380>>, (access on Feb.12, 2012).
- [2] A.K. Rajvanshi, Biomass Gasification, *Alternative Energy in Agriculture*, Vol. II, 1986, pp. 83-102.
- [3] W. Bubpamala, *Research and Development of Human Crematory for Energy Saving*, Master Degree Thesis: King Mongkutt's University of Technology North Bangkok, 2007.
- [4] S. Thavornun, *Study and research on crematory for energy saving*, Research's report, Energy Policy and Planning Office, Ministry of Energy of Thailand, 2007.
- [5] G. Tchobanoglous and F. Kreith, *Handbook of solid waste management*, 2nd edition, McGraw-hill, New York, 2002.
- [6] Ontario Ministry of the Environment, *Incinerator Design and Operating Criteria*, Volume II - Biomedical Waste Incinerators, 1986.
- [7] H. Floyd, *Practical Design of Waste Incineration*, Handbook of Environmental Engineering Calculations, 2007.
- [8] S. Gunther, Some Aspects on Producer Gas Operation of Internal Combustion Engine, *Biomass Gasification Workshop Proceedings*, Chulalongkorn University, Bangkok, 1984, pp.84-104.
- [9] S. R. Turns, *An Introduction to Combustion: Concepts and Applications*, 3rd Edition, McGraw-hill, Singapore, 2012.
- [10] Bureau of Mines, *Ringelmann Smoke Chart (Revision of IC 7718)*, United States Department of the Interior, 1967.
- [11] Pollution Control Department of Thailand, *Situation of air pollution from crematory*, Department's publishing document, 2005.
- [12] Y. A. Cengel and A. J. Ghajar, *Heat and Mass Transfer: Fundamentals and Applications*, 4th Edition, Mc Grawhill, Singapore, 2012.

Experimental Evaluation of a Chip Thickness Model Based on the Fracture Toughness of Abrasive and Work Material in Grinding of Alumina Ceramics

S. Somasundaram¹, C. Thiagarajan²

¹(Dept of Mechanical Engineering, National Institute of Technical Teachers Training & Research, Chennai, India)

²(Dept of Mechanical Engineering, Saveetha School of Engineering, Saveetha University, Chennai, India)

Abstract: Abrasive machining in general and grinding in particular are processes, which increase their importance with high demands on accuracy of surface finish. The chip thickness is an evaluating variable to describe the quality of ground surface as well as the performance of the overall grinding system. A significant characteristic that distinguishes ceramics from metals is their low fracture toughness, which also determines the material removal mechanism in the grinding of ceramics. An important prime requirement of an abrasive is its dynamic strength or fracture toughness which determines the fragmentation of the abrasive grain as it impacts the workpiece. In the present paper, a new chip thickness model has been formulated by incorporating the fracture toughness of abrasive and workpiece to assess the performance of super abrasive grinding of Alumina ceramics. The proposed model has been validated experimentally with the comparison of surface roughness obtained with the existing and proposed chip thickness models.

Keywords: Alumina ceramics, Alumina grinding, Chip thickness, Fracture toughness

I. INTRODUCTION

Grinding processes relies on the significant effectiveness of transferring the laboratory based research results and available models to industrial practice where grinding setups and parameters are different. Thus there is a necessity to integrate the various heterogeneous models and information. Models form the basis for simulation of grinding process and create a precondition for high product quality by increasing the efficiency of the process [1]. The present work envisages the need for developing a chip thickness model based on the fracture toughness of wheel and work material.

The grinding technology has improved considerably in terms of grinding wheels with wear resistant abrasives and improved bonding systems together with higher process reliability due to improved process monitoring and control [2]. However grinding is a complex manufacturing process with a large number of characteristic quantities influencing each other, making the reproducibility critical and selection of process parameters attains significance. Hence there is a need to develop analytical on empirical models for the reliable prediction of dimensional accuracy and surface finish in grinding.

A chip thickness model plays a pivotal role in determining the boundary conditions necessary to maintain a certain quality level of the ground surfaces. The chip thickness models proposed by various authors are based on the speed ratio, depth of cut and equivalent diameter of wheel [1]. In order to consider the deformation due to elasticity of wheel and work material, a model proposed by Anne et al incorporated the modules of elasticities of grinding wheel and work piece in the existing chip thickness model [3]. But none of the models took the fracture toughness of abrasive and work material for calculation of chip thickness. The fracture toughness of work material determines the chip formation mode by ductile or brittle fracture, while the fracture toughness of abrasive determines the friability or tendency to fracture when placed under pressure. In the present chapter a new chip thickness model based on fracture toughness of abrasive and work material has been developed. The new model has been compared with existing model by using experimental data from the grinding of Alumina ceramics using surface roughness as an evaluating parameter.

II. LITERATURE REVIEW

The sequential removal of chips lead to the generation of the machined surface and nature of chips produced with varying degrees of plastic deformation will depends on the structure of the grinding wheel, quantities of motion and the geometric parameters. The various chip thickness models proposed by different authors have been consolidated by Tonshoff et al and these models are based on the speed ratio, depth of cut and equivalent diameter of wheel [1]. Shaw[4] and Malkin[5] have considered the grinding wheel topography in two-dimensional form by determining the grain count. The chip thickness model given by Malkin elaborates the various aspects of grinding process and various parameters related to it. The topography of the wheel and its kinematic interaction with workpiece was also described. Nakayama et al. developed the interrelationship between force and elastic deflection of the wheel [6]. Experiments were conducted to measure the deflection associated with the individual grain. It was shown that the deflection of the individual grain to be of the same order of magnitude as that of the undeformed chip thickness. Kun Li et al developed a model for number of cutting points and grinding forces per grit during ceramic grinding.

The grinding forces were found to be a power function of average cross sectional area of cutting edges or grit depth of cut [7]. The chip thickness model by Snoeys and Peters for determining the equivalent chip thickness was based on the equation of continuity. This characteristic quantity represents the sum of all individual chip thicknesses in contact area between grinding wheel and workpiece [8]. This simple model offers advantages in practical application as the characteristic quantities of the grinding wheel topography do not have to be determined. Saini et al. described the need of contact deflection in grinding. The various components of local contact deflections including that due to grain rotation and their

combined influence on the ground surface from the point of view of industrial application was described [9]. As none of these models available in the literature take care of elastic deformation of grinding wheel and workpiece[1], a chip thickness model developed by Anne Venugopal[3] takes into account the modulus of elasticities of grinding wheel and work piece and the elastic modulus is incorporated in the existing basic chip thickness model to consider the elastic deformation. But one of the significant property of a work and an abrasive material (i.e) fracture toughness has not been considered into the above models and the incorporating the fracture toughness in the existing model would make a significant impact while estimating the chip thickness.

III. MODELING OF CHIP THICKNESS

The existing chip thickness model proposed by Malkin[5] is a well-known equation for estimating the maximum chip thickness. The equation is as follows

$$h_m = \left[\frac{4 V_w}{c.r V_s} \left(\frac{a_e}{d_e} \right)^{\frac{1}{2}} \right]^{\frac{1}{2}} \quad (1)$$

where r is the chip width to thickness ratio, c is the number of active grits per unit area, V_w is the work velocity V_s is the wheel velocity, a_e is the work engagement and d_e is the equivalent wheel diameter. The value of 'r' is difficult to determine and is assumed in the range of 10-20[10]. In this work 'r' was assumed to be equal to 10. The number of active grits per unit area 'c' derived by Xu et al [11] is as follows

$$c = \frac{4f}{\left[d_g^2 \left(\frac{4\pi}{3v} \right)^{\frac{2}{3}} \right]} \quad (2)$$

v = volume fraction of diamond in grinding wheel and f is the fraction of diamond particles involved in active grinding. As the grinding wheel used in this study has a density of 75, $v = 0.18$. For calculating the number of active grits per unit area, it is assumed that only one half of diamond particles are engaged in cutting [11] or $f = 0.5$. The equivalent spherical diameter of diamond grit (d_g) is given [5] as

$$d_g = 15.2.M^{-1} \quad (3)$$

where M is the mesh number used in the grading sieve.

A significant characteristic that distinguishes ceramics from metals is their low fracture toughness, which also determines the material removal mechanism in the grinding of ceramics. A chip formation model proposed by Subramanian suggests that materials of high strength and fracture toughness would exhibit greater plastic deformation during grinding [12]. On the other hand low fracture toughness materials would produce large degree of discontinuous brittle fractured chips. Thus the change in maximum chip thickness is directly proportional to the fracture toughness of the work material.

An important prime requirement of an abrasive is its dynamic strength or fracture toughness which determines the fragmentation of the abrasive grain as it impacts the workpiece. High toughness implies that an abrasive grain is less likely to fracture each time it engages the workpiece. On the other hand a more friable (less tough) abrasive would regenerate sharp cutting edges (self-sharpen) as the grain dulls by attrition. Hence more friable abrasive would promote significant undeformed chip thickness than the less friable abrasive, thus making an indirect proportionally with the maximum chip thickness.

Combining the above effects, the maximum chip thickness can be expressed as

$$h_m \propto \frac{F_1}{F_2} \quad (4)$$

Where F_1 is the fracture toughness of the work material and F_2 is the fracture toughness of abrasive. The fracture toughness of work material (Alumina) is $3.5 \mu\text{pam}^{1/2}$. The fracture toughness of the diamond abrasive is $9.5 \mu\text{pam}^{1/2}$. Thus the existing chip thickness model is modified by incorporating the fracture toughness of work and abrasive material and is expressed as

$$\bar{h}_m = \left[\frac{F_1}{F_2} \right]^n \left[\frac{4 V_w}{c.r V_s} \left(\frac{a_e}{d_e} \right)^{\frac{1}{2}} \right]^{\frac{1}{2}} \quad (5)$$

an is the exponent which accounts for the linear & non-linear deflections of the workpiece and grinding wheel. To validate the proposed model is surface roughness model written in terms of chip thickness [5] has been used and is given as

$$R_a = \frac{h_m^2}{a_e} \left[\frac{q}{q+1} \right]^2 \quad (6)$$

where R_a is centre line average value of surface roughness and q is the ratio of wheel speed to work speed = V_s / V_w .

IV. EXPERIMENTAL EVALUATION

The estimation of maximum chip thickness is done by carrying out the experiments according to the grinding conditions given in the table 1 and measuring the resulting tangential force. The exponent (n) is calculated with these tangential force values and the proposed model is validated using surface roughness as a parameter of evaluation.

Table 1 Grinding conditions

Factors	Values		
Mesh number	100		
Wheel Speed (m/s)	21.6		
Feed (m/min)	10	15	20
Depth of cut (μm)	10	20	30

IV.I Evaluation of the exponent (n)

The value of 'n' is calculated by solving the energy balance equation which is stating that energy given by the grinding wheel is equal to the amount of energy required to remove the material. It can be written as

$$F_t \cdot V_s = \text{specific energy} \times \text{volume of material removed} / \text{unit time} \quad (7)$$

where F_t is the tangential force on the grinding wheel.

$$\begin{aligned} \text{Volume of material removed} / \text{unit time} &= \text{No. of chips produced} / \text{unit time} \times \text{Volume of each chip} \\ &= (c \cdot b_s \cdot V_s) \cdot V_c \quad (8) \end{aligned}$$

where V_c is volume of each undeformed chip produced and b_s is the grinding wheel width. Assuming a chip with triangular cross section, V_c can be approximated, analogous to that of a triangular pyramid, as one third times the product of maximum cross sectional area ($r \cdot h_m^2 / 2$) and length l_c from the following formula (Malkin, S., 1989)

$$V_c = \frac{r \cdot \bar{h}_m^2}{6} \left(\sqrt{a_e \cdot d_e} \right) \left(\because l_c = \sqrt{a_e \cdot d_e} \right) \quad (9)$$

The value of specific energy is taken as 15 J/mm^3 for the present study which is carried out at faster material removal rate (Hwang et al., 1999) during which specific energy is minimum.

By substituting above equations (8) & (9) in (7), we get

$$F_t \cdot V_s = 25 \cdot c \cdot b_s \cdot V_s \cdot \bar{h}_m^2 \cdot \sqrt{a_e \cdot d_e} \quad (10)$$

$$F_t \cdot V_s = 25 \cdot c \cdot b_s \cdot V_s \cdot \left[\left(\frac{F_1}{F_2} \right)^n \bar{h}_m \right]^2 \cdot \sqrt{a_e \cdot d_e} \quad \left(\because \bar{h}_m = \left(\frac{F_1}{F_2} \right)^n h_m \right) \quad (11)$$

The tangential force is measured using a strain gauge dynamometer and value of n is calculated. During this study diamond wheel of D1A1 100/120 BNC 20 C75 has been used. The work material is Alumina ground at a speed of 21.59 m/sec without any lubricant. The values of 'n' were calculated for different values of feed and depth of cut and results are tabulated in Table 2. The new chip thickness model has been formulated by taking the average value of 'n' which was found to be 0.357.

Table 2 Values of exponent (n) at various grinding conditions

V_w (m/min)	a_e (μm)	F_t (N/mm)	n
10	10	7.95	0.276
15	10	10.33	0.32
20	10	11.72	0.333
10	20	10.65	0.344
15	20	15.54	0.351
20	20	16.2	0.383
10	30	14.4	0.39
15	30	17.5	0.404
20	30	19.3	0.41
Average			0.357

IV.II Validation of the proposed model

In order to validate the new chip thickness model, the surface roughness (R_a) of all ground specimens were measured and deviation of the measured roughness value (R_{a1}) with the surface roughness computed using existing model (R_{a2}) and surface roughness computed using new model (R_{a3}) has been shown in Figure 1.

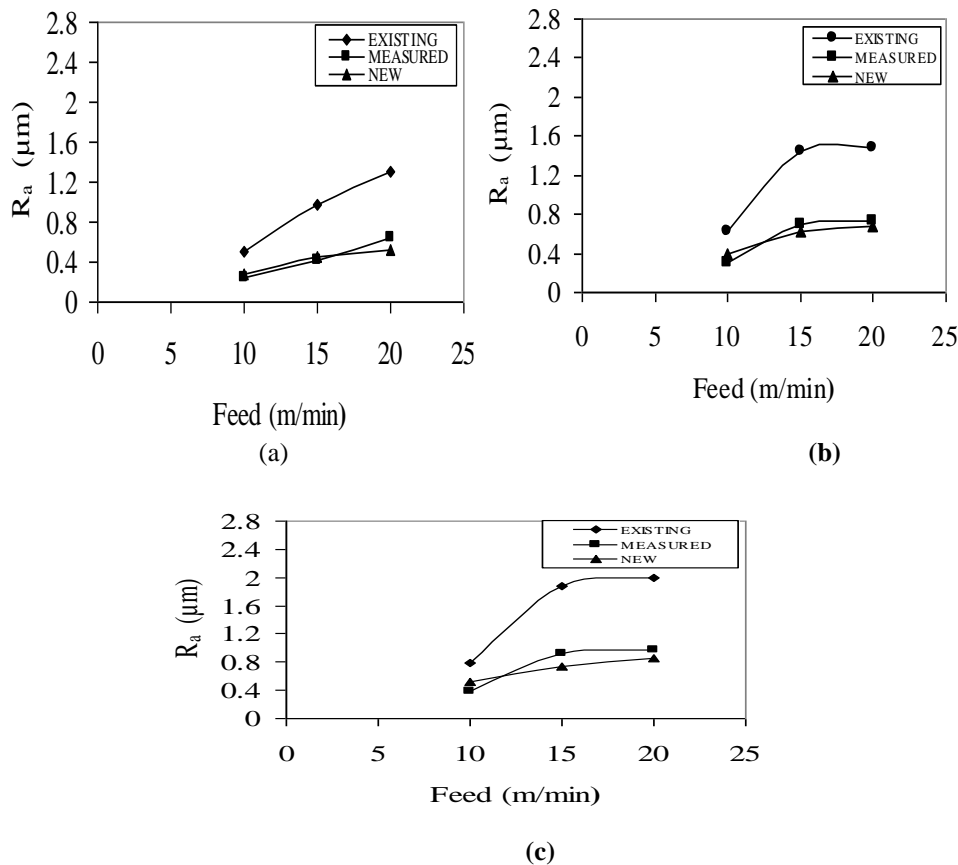


Figure 1. Variation of surface roughness with grinding variables at depth of grinding of (a) $a_e=10 \mu\text{m}$, (b) $a_e=20 \mu\text{m}$ and (c) $a_e=30 \mu\text{m}$

V. RESULTS AND DISCUSSION

The existing chip thickness models have taken the main influencing quantities into consideration and among these are speed ratio, working engagement and equivalent diameter. But none of these models considered one of the significant characteristics of the fracture toughness of work and abrasive material which determines the material removal mechanism in the grinding of brittle materials.

In the present work, the fracture toughness of work material and abrasive have been incorporated in the existing chip thickness model and deviation of the maximum chip thickness estimated by new model with the existing model is shown in Table 3. The surface roughness values measured experimentally were compared with the surface roughness values calculated using the existing and the proposed model.

Table 3. Values of Surface roughness by using the existing and newchip thickness models

Chip thickness using existing model (h_m) (□ m)	Chip thickness using modified model (\bar{h}_m) (□ m)	Surface roughness using existing model (R_{a_1}) (□ m)	Surface roughness using modified model (R_{a_2}) (□ m)	Surface roughness measured in experimental investigations (R_a) (□ m)	Deviation of R_a with respect to R_{a_1} (%)	Deviation of R_a with respect to R_{a_2} (%)
2.285	1.599	0.513	0.252	0.285	44.44	11.57
3.157	2.21	0.981	0.419	0.452	53.92	7.32
3.648	2.553	1.309	0.642	0.521	60.19	18.84
2.514	1.76	0.622	0.305	0.393	36.81	22.39
3.819	2.674	1.436	0.704	0.621	56.75	11.78
3.884	2.718	1.485	0.728	0.682	54.07	6.31
2.832	1.982	0.789	0.387	0.521	50.95	25.71
4.359	3.051	1.871	0.917	0.732	60.87	20.17
4.501	3.151	1.995	0.978	0.854	57.19	12.67

It can be observed from the Fig.1 that the surface roughness values computed by the new chip thickness model are closer to the actual values as compared with that of the existing model. The maximum percentage variation between the surface roughness predicted with existing model and measured value is 61% and the maximum percentage variation between the surface roughness predicted with the modified chip thickness model and measured value is 26%. Hence the proposed model shown in the following equation proves to provide an accurate estimation of the maximum chip thickness which is influenced by wheel, work, machine characteristics and operating conditions.

$$\bar{h}_m = \left[\frac{F_1}{F_2} \right]^{0.357} \left[\frac{4 V_w}{c.r V_s} \left(\frac{a_e}{d_e} \right)^{\frac{1}{2}} \right]^{\frac{1}{2}} \quad (12)$$

VI. CONCLUSIONS

The proposed chip thickness model lays an emphasis on incorporating a decisive material property of the fracture toughness of work piece and abrasive which were neglected in the basic model. The validation of the chip thickness model has been carried out by measuring the surface roughness experimentally and calculating the subsequent deviation of the surface roughness values computed from the existing and proposed model with the actual value. Hence the proposed model strengthens the representation of evaluating the competitiveness of the grinding system which is influenced by the surface quality of the specimen ground.

REFERENCES

- [1] H.K.Tonshoff, J.Peters, I.Inasaki, T.Paul, Modeling and simulation of grinding processes, *Annals CIRP*, 41,1992, 677-687.
- [2] J.Kopac, P.Krajnik, High-performance grinding- A review, *Journal of Materials Processing Technology*, 175,2005, 278-284.
- [3] Anne VenuGopal, P.Venkateshwararao, A new chip thickness model for performance assessment of silicon carbide grinding, *International Journal of Advanced Manufacturing Technology*, 24, 2004, 816-820.
- [4] M.C.Shaw, *Principles of Abrasive Processing*(Oxford University Press, New York, 1996)
- [5] S.Malkin, *Grinding Technology-Theory and Applications of Machining with Abrasives* (EllisHorwood, Chichester, UK, 1989)
- [6] K.Nakayama, J.Brecker, M.C.Shaw, Grinding wheel elasticity, *Journal of Engineering Industry*, 93, 1971, 609-614.
- [7] Kun Li,T.Warren Liao, Modeling of ceramic grinding processes - Number of cutting points and grinding forces per grit, *Journal of Material Processing Technology*, 65,1997, 1-10.
- [8] R.Snoeys, J.Peters, The significance of chip thickness in grinding, *Annals CIRP*, 23, 1974, 227-237.
- [9] D.P.Saini, J.G.Wager,R.H.Brown, Practical significance of contact deflections in grinding, *Annals CIRP*, 31,1982, 215-219.
- [10] J.E.Mayer,G.P.Fang, Effect of grit depth of cut on strength of ground ceramics, *Annals CIRP*, 43, 1994, 309-312.
- [11] Xu, Hockin, S.Jahanmir, L.K.Ives, Effect of grinding on strength of tetragonal zirconia and zirconia-toughened alumina', *Journal of Machining Science Technology*, 1, 1997, 49-66.
- [12] K.Subramanian, S.Ramanath, Principles of Abrasive Machining (Willis India, New Delhi, 1992)315-328.

Measurement of Total and Partial Mass Attenuation Coefficients of Oxide Glasses: A Radiation field

Sandeep Gupta¹, Gurdeep Singh Sidhu²

¹Department of Physics, Singhania University, Pachri Bari, Jhunjunu, Rajasthan-333515, India

²Government Sports school, Ghudda, Punjab-151001, India

Abstract : The variation in mass attenuation coefficient μ for total and partial photon interaction processes for three different oxide glasses (65CaO-35Al₂O₃(OG1), 20Na₂O-80SiO₂(OG2), and 20Na₂O-5Al₂O₃-75SiO₂ (OG3)), in the incident energy range from 10 keV to 100 GeV has been studied using software package XCOM and the effect of chemical composition on the values of μ is also interpreted graphically. Mass attenuation coefficient (μ) for the total photon interaction processes is initially high and decreases sharply with increase in incident photon energy up to 100 keV. Above 100 keV the rate of decrease of μ (total) with incident photon energy is less and above 4 MeV μ (total) increases slightly with further increase in incident photon energy. Significant variations due to chemical composition can be observed below 3 KeV and above 30 MeV incident energy.

Keywords: Gamma rays, mass attenuation coefficient and oxide glasses.

I. INTRODUCTION

The mass attenuation coefficient (μ) measures the probability of interaction (scattering / absorption) of photon with the interacting medium. It is helpful in deriving many types of other photon interaction parameters such as molecular cross-section, atomic cross-section, equivalent and effective atomic numbers, electron density, buildup factor. The mass attenuation coefficient values of partial photon interaction processes such as photoelectric effect, Compton scattering, pair production and total are available in the form of software package XCOM from Berger and Hubbell [2, 3] by substituting the chemical composition/weight fraction of compound/mixture, the mass attenuation coefficient of the shielding materials will be generated in the energy range 1 keV - 100 GeV [4]. Hubble are published tables of mass attenuation coefficients and the mass energy absorption coefficients for 40 elements and 45 mixtures and compounds for 1 keV to 20 MeV in 1982. Hubbell and Seltzer replaced these tables in form of tabulation for all elements having $1 \leq Z \leq 92$ and for 48 additional substances for dosimetric interest [5].

Glasses are transparent to the visible light and the fact that their physical and chemical properties can be modified by changing their chemical composition and taking various types of preparation techniques, these materials are one of the effective alternatives to concrete and used as gamma ray shielding materials [6], [7], [8]. Glasses containing heavy metal oxide such as PbO have many advantages due to their high density and high refractive index. These properties are making them important materials for development of advanced optical telecommunication and gamma-ray shielding materials [9], [10],[11].

In our previous work [12], the energy absorption buildup factors have been studied as functions of penetration depth, incident photon energy and effective atomic number (Z_{eff}) of chosen oxide glasses. Our present investigation of mass attenuation coefficients (μ) of different oxide glasses for both total and partial photon interaction processes (Photo-electric absorption, coherent scattering, incoherent scattering and pair production) should be useful to scientists and workers in related fields, filling a gap in the available information. In recent studies, attenuation coefficient for different energies for various samples in solid/ liquid/mixtures and alloys is reported by many workers [13-33].

In this paper, detailed calculations have been made to study the effect of chemical composition on μ for total and partial interaction processes in three different oxide glasses covering the energy range from 10 keV to 100 GeV.

II. THEORY

A narrow beam of mono-energetic photons having an initial intensity I_0 is attenuated to intensity 'I' after passing through a layer of material with mass-per-unit-area 'x', according to the exponential law:

$$I = I_0 e^{-\mu \rho \cdot x} \quad \text{---- (1)}$$

Where $\mu\rho$ is the mass attenuation coefficient, Eq. (1) can be rewritten as:

$$\frac{\mu}{\rho} = \frac{\ln\left(\frac{I_0}{I}\right)}{x} \quad \text{---- (2)}$$

Therefore, mass attenuation coefficient ($\mu_m = \mu/\rho$) can be calculated by substituting the measured values of I_0 , I and x in Eq. (2). The mass attenuation coefficient ($\mu_m = \mu/\rho$) is of more fundamental importance than linear attenuation coefficient (μ) because all mass attenuation coefficients are independent of the density and physical state (gas, liquid or solid) of the absorber.

The attenuation coefficient is interaction process dependent i.e. the attenuation coefficient is a measure of the average number of interactions between incident photon and matter that occur in a given mass-per-unit area thickness of the material encountered. It is distinguished sharply from the absorption coefficient which is always a smaller quantity and absorption coefficient measures the energy absorbed by the medium. Depending on its energy, gamma rays interact with

matter through different processes such as photoelectric effect, Compton scattering, pair-production, thomson scattering, nuclear photodisintegration and nuclear resonance scattering. Photons interact with matter and lose their energy because of the three main processes which are, photoelectric effect, Compton scattering and pair-production.

III. RESULT AND DISCUSSION

The results of the present investigation are shown graphically in figs. 1-9, where μ is given as a function of incident photon energy in all photon interaction processes. The chemical composition in grams for 100 grams of different types of oxide glasses are shown in table. 1 [1].

In fig. 1-3, μ values of OG1, OG2, and OG3 for total and partial interactions have been plotted against the incident photon energy. The graphs of mass attenuation coefficient for all the photon interactions are approximately similar to those of elements of low atomic number such as Na, Al, Si and Ca etc. because of the fact that effective atomic number values of the chosen samples lie in this range.

In the present work, the effect of chemical composition of oxide glasses on μ and the variations of μ with incident photon energy for all interactions are discussed in the following paragraphs.

Mass attenuation coefficient (μ) for the total photon interaction processes is initially high and decreases sharply with increase in incident photon energy up to 100 keV. Above 100 keV the rate of decrease of $\mu_{(total)}$ with incident photon energy is less and above 4 MeV $\mu_{(total)}$ increases slightly with further increase in incident photon energy. This behavior is due to dominance of different interaction processes in different incident photon energies i.e. below 100 keV photo electric process is dominant, from 100 keV to 4 MeV Compton scattering and above 4 MeV pair-production process is dominant.

It is also clear in fig. 4 that the oxide glass OG1, contains a higher percentage of heavy element such as calcium, has slightly lower values of $\mu_{(total)}$ in lower energy region whereas it has slightly higher values in the high energy region (after 10 MeV to 10^5 MeV) as compared to other oxide glasses.

The above observations of fig. 4 can also be extended to the other figures (5-9) in which the effect of oxide glasses chemical composition on μ is investigated for partial photon interactions (photo-effect (photo), coherent and incoherent scattering, pair production in the electric field, and pair production in the nuclear field) for same choosing samples.

From fig. 5, it is observed that the value of $\mu_{(photo)}$ decreases rapidly with increase in incident photon energy for all the selected materials. It may be due to reason that photo-electric cross-section varies inversely with incident photon energy as $E^{7/2}$. In the lower energy region values of $\mu_{(photo)}$ of OG1 slightly lower than other oxide glasses, but in the energy region of 0.3-100 MeV the values of OG1 are higher, which is due to chemical composition of oxide glasses as $\mu_{(photo)}$ is further strongly dependent on atomic number of interacting materials as Z^{4-5} . It implies that its shielding behavior is better in this energy region.

In figs. (6,7) it is observed that the values of $\mu_{(coh.)}$ decrease sharply with increase in incident photon energy for all chosen samples after the 10 keV and values of $\mu_{(incoh.)}$ rate of decrease is comparatively lower. This decrease in values with increase in incident photon energy may be due to the reason that $\mu_{(coh.)}$ and $\mu_{(incoh.)}$ is inversely proportional to incident photon energy E. The variations in the values of $\mu_{(incoh.)}$ due to chemical composition is low but it is almost same in case of coherent scattering.

From the above results it is interpreted that decreasing rate of values of $\mu_{(photo)}$ with incident photon energy is higher than $\mu_{(coh.)}$ decreasing rate. And the variation in $\mu_{(photo)}$ due to chemical composition can be seen clearly which is not significant in case of $\mu_{(coh.)}$. Above results clearly explain the variation of $\mu_{(total)}$ below 4 MeV in fig. 4.

The variation of μ for pair production in electric field and nuclear fields are shown in figs 8-9 respectively. In both cases, the values of $\mu_{(pp)}$ increases slightly with increase in incident photon energy up to 400 MeV but beyond this incident energy the values of $\mu_{(pp)}$ remains almost constant. It may be due $\mu_{(pp)}$ is directly proportional to $\log E$. For pair production in the nuclear field, the values of $\mu_{(pp)}$ of chosen samples show significant variation (fig. 9) but slight variation is observed for $\mu_{(pp)}$ in the electric field (fig. 8). It may be due to pair production in nuclear field is Z^2 dependent, whereas the Z dependence of pair production in the electric field is almost linear. In the high incident photon energy range, the variation is observed in $\mu_{(total)}$ (fig. 4) is because of Z^2 – dependence of the pair production in the nuclear field.

IV. FIGURES AND TABLES

Table 1: Chemical composition of oxide glasses (for 100 gm. of glass) [1].

Chosen Samples	CaO (gm.)	Al ₂ O ₃ (gm.)	Na ₂ O(gm.)	SiO ₂ (gm.)
65CaO-35Al ₂ O ₃ (OG1)	50.5	49.5	-----	-----
20Na ₂ O-80SiO ₂ (OG2)	-----	-----	20.5	79.5
20Na ₂ O-5Al ₂ O ₃ -75SiO ₂ (OG3)	-----	8.15	19.8	72.0

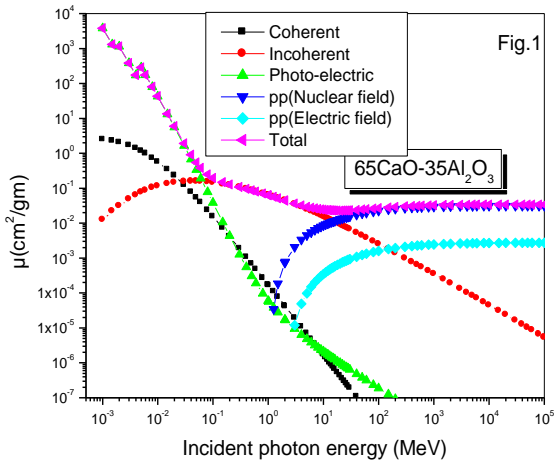


Fig.1: Variation of Mass attenuation coefficients of oxide glass (65 CaO-35 Al₂O₃) with incident photon energy (MeV) for different photon interaction processes.

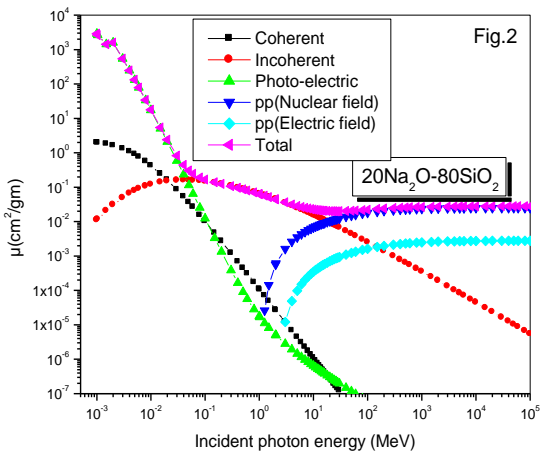


Fig.2: Variation of Mass attenuation coefficients of oxide glass (20 Na₂O-80SiO₂) with incident photon energy (MeV) for different photon interaction processes.

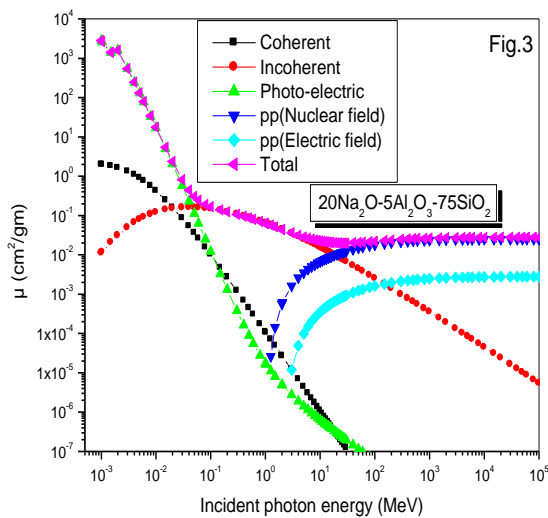


Fig.3: Variation of Mass attenuation coefficients of oxide glass (20 Na₂O-5Al₂O₃-75SiO₂) with incident photon energy (MeV) for different photon interaction processes.

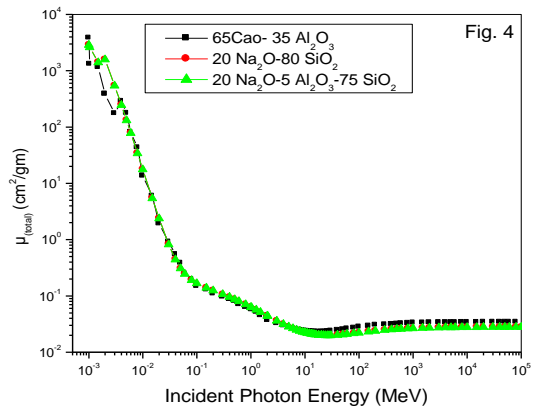


Fig.4: Variation of Total mass attenuation coefficients of all oxide glasses with incident photon energy (MeV).

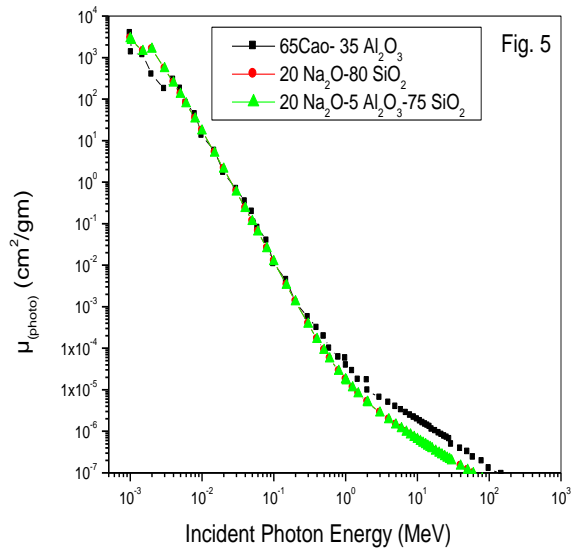


Fig.5: Variation of mass attenuation coefficients of all oxide glasses with incident photon energy (MeV) for photo electric absorption.

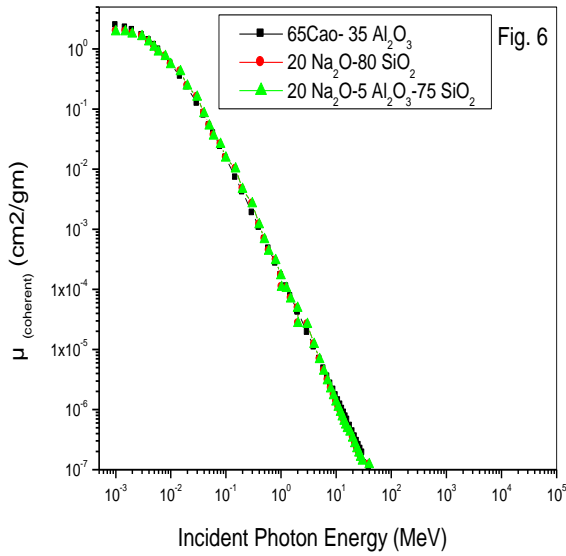


Fig.6: Variation of mass attenuation coefficients of all oxide glasses with incident photon energy (MeV) for coherent scattering.

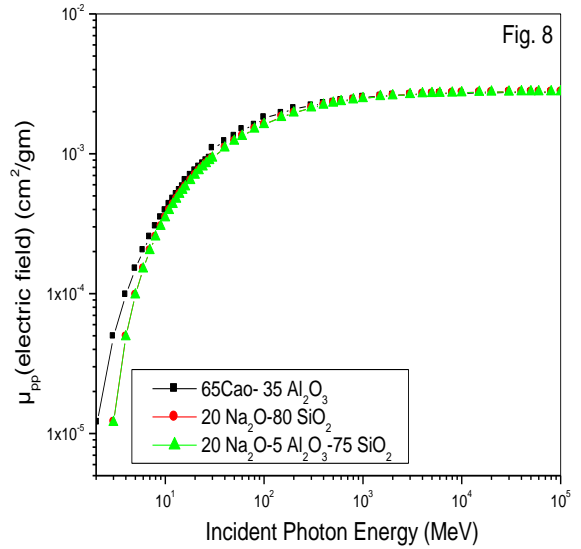


Fig.8: Variation of mass attenuation coefficients of all oxide glasses with incident photon energy (MeV) for pair production in the electric field.

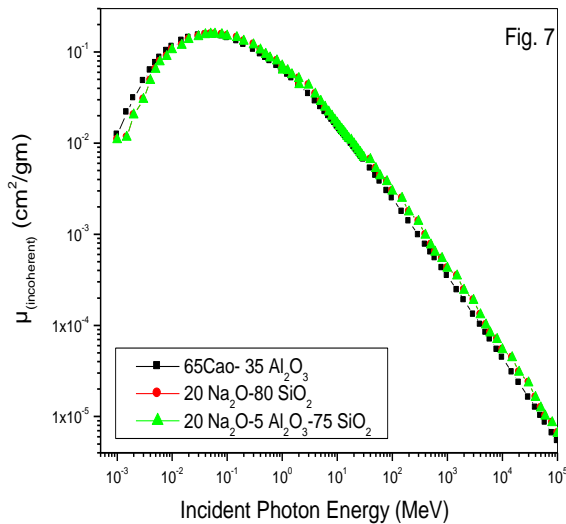


Fig.7: Variation of mass attenuation coefficients of all oxide glasses with incident photon energy (MeV) for incoherent scattering.

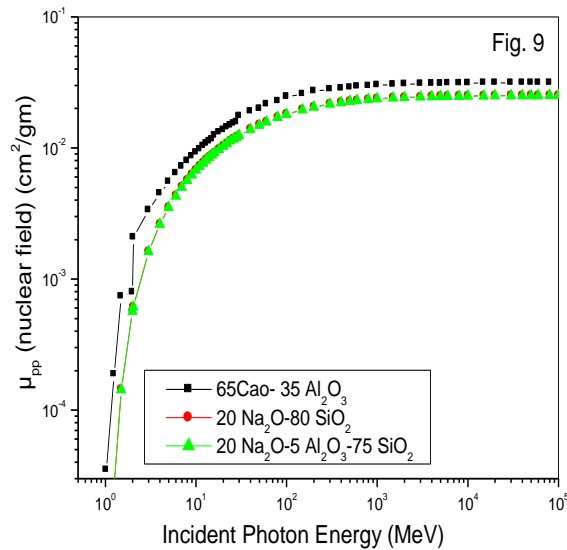


Fig.9: Variation of mass attenuation coefficients of all oxide glasses with incident photon energy (MeV) for pair production in the nuclear field.

V. CONCLUSION

- The mass attenuation coefficient (μ) is also deriving various other photon interaction parameters such equivalent and effective atomic numbers, electron density, buildup factor etc..
- Mass attenuation coefficient (μ) of chosen samples for the total photon interaction processes is high and decreases rapidly with increase in gamma photon energy up to 100 keV. After 100 keV the variation of μ with incident photon energy is less and above 4 MeV μ increases slightly with increase in photon energy. This behavior is due to dominance of different interaction processes in different incident photon energies i.e. below 100 keV photo electric process is dominant up to 100 keV after that Compton scattering up to 4 MeV and pair-production process is dominant above 4MeV. Mass attenuation coefficient helpful for detail study in shielding effectiveness of different types materials /mediums.
- In the three photon interaction processes, the value of μ also vary due to chemical composition. In the lower energy region values of $\mu_{(\text{photo})}$ of OG1 slightly lower than other oxide glasses, but in the energy region of 0.3-100 MeV the values of OG1 are higher. The variations in the values of $\mu_{(\text{incoh.})}$ due to chemical composition is low but it is almost same in case of coherent scattering. For pair production in the nuclear field, the values of $\mu_{(\text{pp})}$ of chosen samples show significant variation but slight variation is observed for $\mu_{(\text{pp})}$ in the electric field.

Acknowledgement

We are grateful to Berger and Hubbell for providing the convenient computer program XCOM with the help of National Institute of Standards and Technology (NIST), Gaithersburg. [34].

REFERENCES

- [1] J-E Shelby, *Introduction to glass science and technology*, 2nd edition (The royal society of chemistry, 2005, 33-34)
- [2] N Singh , K.J Singh, K Singh and H Singh, Comparative Study of Lead Borate and Bismuth Lead Borate Glass Systems as Gamma-Radiation Shielding Materials, *Nuclear Instruments and Methods in Physics Research, Section B*, 225,2004, 305-309.
- [3] S Singh, A Kumar, D Singh, K Singh and G.S. Mudahar, Barium-Borate-Flyash Glasses:As Radiation Shielding Materials, *Nuclear Instruments and Methods in Physics Research, Section B*, 226, 2008,140-146.
- [4] P. Limkitjaroenporn, J. Kaewkhao, W. Chewpraditkul and P. Limsuwan, Mass Attenuation Coefficient and Effective Atomic Number of Ag/Cu/Zn Alloy at Different Photon Energy by Compton Scattering Technique, *Procedia Engineering*, 32, 2012, 847 – 854.
- [5] K Singh ,H Singh ,V Sharma , R Nathuram ,A Khanna ,R Kumar , S.S Bhatti and H.S Sahota, Gamma-Ray Attenuation Coefficients in Bismuth Borate Glasses, *Nuclear Instruments and Methods in Physics Research, Section B*, 194, 2002, 1-6.
- [6] R.S. Kaundal, Sandeep Kaur, Narveer Singh and K.J. Singh, Investigation of structural properties of lead strontium borate glasses for gamma-ray shielding applications, *Journal of Physics and Chemistry of Solids*, 71, 2010, 1191-1195.
- [7] Chang-Min Lee, Yoon Hee Lee and Kun Jai Lee, Cracking effect on gamma-ray shielding performance in concrete structure, *Programme in Nuclear Energy*, 49, 2007, 303–312.
- [8] D. Rezaei, O chbelagh and S.Azimbhani, Investigation of gamma-ray shielding properties of concrete containing of different percentages of lead, *Applied Radiation and Isotopes*, 70, 2012, 2282-2286.
- [9] P. Limkitjaroenporn, J. Kaewkhao, P. Limsuwan and W. Chewpraditkul, Physical, Optical, Structural and gamma-ray shielding properties of lead sodium borate glasses, *Journal of Physics and Chemistry of Solids*, 72, 2011, 245–251.

- [10] M. Kurudirek, Y. Ozdemir, O. Simsekand and R. Durak, Comparison of some lead and non-lead based glass systems, standard shielding concretes and commercial window glasses in terms of shielding parameters in the energy region of 1 keV-100 GeV, *A comparative study. Journal of Nuclear Materials*, 407 (2), 2010, 110-115.
- [11] Sandeep kaur and K.J. Singh, comparative study of lead borate and lead silicate glass system doped with aluminium oxide as gamma ray shielding materials, *IJITEE*, 2, 2013, 172-175.
- [12] Sandeep Gupta and Gurdeep Singh Sidhu, Energy absorption buildup factor for some oxide glasses: Penetration depth, photon energy and effective atomic number dependence, *International journal of scientific and research publication*, 2, 12, 2012, 1-7.
- [13] L. Gerward L, On the attenuation of X-rays and gamma rays in dilute solutions, *Radiat. Phys. Chem.*, 48, 1996, 697.
- [14] Laxman Chaudhari and Dayanand raje, Attenuation coefficient of soil samples by gamma ray energy, *Research journal of recent sciences*, 1(9), 41-48, 2012.
- [15] G.S. Bhandal , Study of Photon attenuation coefficients of some multielement materials, *Nuclear Science and Engineering*, 116, 1994, 218-222.
- [16] A.H El-Kateb and Abdul Hamid, Photon attenuation study of some materials containing Hydrogen, Carbon and Oxyge., *Applied radiat.Isot.*, 42, 1991,303-307.
- [17] S. R. Mitkar and S. M. Dongarge, Measurement of linear and mass attenuation coefficient of alcohol soluble compound for gamma rays at energy 0.511 MeV, *Archives of Applied Science research*, 4 (4), 2012, 1748-1752.
- [18] Jarnail Singh, Karamjit Singh , S. Mudahar and S. Kulwant , Gamma ray attenuation studies in Telurite glasses, *National Symposia on radiation Physics*, 15, 2003, 36-39.
- [19] D. Demir, A. Ozgul, M. Un and Y. Sachin, Determination of Photon attenuation Coefficoent, Porocity and field capacity of soil by gamma ray transmission for 60, 356 and 662 keV gamma rays, *Applied Radiation and Isotopes*, 66, 2008, 1834- 1837.
- [20] C.R. Appoloni and E.A. Rios, Mass attenuation coefficients of Brazilian soils in the range10-1450 keV, *Applied Radiat. Isot*, 45, 2004, 287-291.
- [21] Pravina P. Pawar., Measurement of mass and linear attenuation coefficient of gamma rays of Al for 414, 662 and 1280 kev photons, *Journal of chemical and pharmaceutical research*, 3(4), 2011, 899-903.
- [22] M. T. Teli, L. M. Chaudhari and S.S. Malode, Attenuation coefficients of 123 keV gamma radiation by dilute solution of sodium chloride, *Appli. Radiat isot*, 45(10), 1994, 987.
- [23] M. T. Teli, L. M. Chaudhari and S.S. Malode, Study of absorption of 123 keV gamma radiation by dilute solution of zinc sulphate, *J. of Pure & applied Physics*, 32, 1994, 410.
- [24] N. Chanthima, Jakrapong Kaewkhao, Weerapong Chewpraditkul and Pichet Limsuwan., Gamma-rays absorption studies of PbO-SiO₂ glass system, *Advanced materials research*, 93-94, 2010, 71-74.
- [25] D.V. Raje and L.M. Chaudhari, Mass attenuation coefficients of soil samples in Maharashtra State (India) by using gamma energy at 0.662 MeV, *Bulg. J. Phys.*, 37, 2010, 158- 164.
- [26] L. M. Chaudhari and R. Nathuram, Absorption coefficient of polymers (Polyvinyl Alcohol) by using gamma energy of 0.39 MeV, *Bulg. J. Phys.*, 38, 2010.
- [27] Gurmel S. Mudahar, Sanjay Modi and Makhan Singh, Total and partial mass Attenuation Coefficient of Soil as a function of Chemical Composition, *Appl.Radiat.Isot.* 42 (1), 1991, 13-18.
- [28] Keerati Kirdsiri, Jakrapong Kaewkhao, Weerapong Chewpraditkul and Pichet Limsuwan, Photon interaction in Borate Glass System containing BiO₃, PbO and BaO at 60 keV, *Theoretical calculation Advanced materials research*, 93-94, 2010, 9-12.
- [29] Mustafa Recep Kacal, Ibrahim Han and Ferdi Akman, Measurement of Mass Attenuation Coefficient by Si (Li), NaI (TI) and Cd (TI) detectors, *Transworld Research Network Nuclear Science and Technology*, 2012, 59-69.
- [30] Samir Yousha El-Kameesy, Sahar Abd El-Ghany, Moenis Abd El-Hakam Azooz and Yaser Abd Allah El-Gammam, Shielding Properties of Lead Zinc Borate Glasses. *World Journal of Condensed Matter Physics*, 3, 2013, 198-202.
- [31] Firas M. Fathi., Mass Attenuation of Gamma photons in special lead glass that can be used in Radiation shielding, *Windows, Raf. Jour. Sci.*, 17(2) *Physics*, Special Issue, 2006, 6-12.
- [32] S.R. Manohara, S.M. Hanagodimath, L.Gerward and K.C. Mittal, Exposure buildup factors of heavy metal oxide glass:A radiation Shield, *Journal of the Korean Physical Society*, 59(2), 2011, 2039-2042.
- [33] M. Singh and G.S Mudahar, Energy dependence of total photon attenuation coefficients of composite materials, *Int. J. Appl. Radiat. Isot.* 43, 1992, 907.
- [34] M. J.Berger and J.H. Hubbell, XCOM: Photon Cross-Sections Database, Web Version 1.2, *National Institute of Standards and Technology, Gaithersburg, MD20899, USA*, 1987/1999, <http://physics.nist.gov/xcom> (Originally published as NBSIR 87-3597 "XCOM: Photon Cross Sections on a Personal Computer").

Development of Single wheel multi use manually operated weed remover

Sridhar.H .S

Asst. Professor Department of Mechanical Engineering, Sri Basaveshwara institute of technology,
Tiptur-572202, Tumkur (D), India.

ABSTRACT: Every year in INDIA, an average of 1980 Cr of rupees is wasted due to weeds. Our country faces the total loss of 33% of its economy from Weeds. The Losses are due to some of the following reasons, total loss of 26% from Crop Diseases, total loss of 20% from Insects and Worms, total loss of 6% from Rats. Has been Surveyed. Shrinking farm lands, acute labour shortage, decreasing income per acre of cultivation, and economic frustration are some of the key factors hurting a farmer's confidence in continuing farming. Weeding control is done by: mechanical weeding, thermal weeding: flaming, biological control, chemical control, and by farming pattern. It has always been a problem to successfully and completely remove weeds and other innocuous plants. Invariably, weeds always grow where they are not wanted. This work involved the design and construction of mechanical weeder, after discovering that tools such as cutlass and hoes require high drudgery, time consuming and high labour force. As a solution to these problems, mechanical weeder was designed and constructed. The mechanical weeder was made of two implements attachment i.e. the primary cutting edge which is in front to loose soil above and the secondary cutting edge which is behind to do cutting and lifting of weeds. The overall machine field efficiency was 98.67%. The Single Wheel Weeder being manufactured is the equipment, which is used for very special purpose when the weeding is required at narrow places or between rows. The blade is thin but very sturdy and tough besides, it is very safe to use and offers zero threat of hurting to the user, Other than the wheel, there is nothing mechanical in this single wheel weeder but, it works wonderfully under the condition where it is put into. This hassle free equipment requires no special maintenance. It is necessary to design the weeder which minimize the human effort and provide efficient work output. The tool which is designed is able to fulfill the present requirement for the weed control. The present design is directed to an improved manual tilling, mulching and weeding tool.

Keywords: Mechanical weeding, field performance, Drudgery.

I. Introduction

Manual weeding requires huge labour force and accounts for about 25 per cent of the total labour requirement which is usually 900 to 1200 man M hours/hectares [9]. This operation is mostly performed manually with cutlass or hoe that requires high labour input, very tedious and it is a time-consuming process. Moreover, the labour requirement for weeding depends on weed flora, weed intensity, time of weeding, and soil moisture at the time of weeding and efficiency of worker. Often several weeding operation are necessary to keep the crop weed free. Reduction in yield due to weed alone was estimated to be 16 to 42 % depending on crop and location which involves one third of the cost of cultivation [8]. Weeding and hoeing is generally done 15 to 20 days after sowing. The weed should be controlled and eliminated at their early stage. Depending upon the weed density, 20 to 30 percent loss in grain yield is quite usual which might increase up to 80 per cent if adequate crop management practice is not observed. Manual and mechanical techniques such as pulling, cutting, and otherwise damaging plants, may be used to control some invasive plants, particularly if the population is relatively small. These techniques can be extremely specific, minimizing damage to desirable plants and animals, but they are generally labor and time intensive. Treatments must typically be administered several times to prevent the weed from re-establishing, and in the process, laborers and machines may severely trample vegetation and disturb soil, providing prime conditions for re-invasion by the same or other invasive species. It is necessary to design the weeder which minimize the human effort and provide efficient work output. The tool we going to design is able to fulfill the present requirement for the weed control. Accordingly, the present invention is directed to an improved manual tilling, mulching and weeding tool.[1] Since weeds can be killed easily when they are at early stages of growth. This practice can also reduce labor and cost substantially Small holder farmers need low cost implements which can be purchased or made locally. Therefore the objective of this project was to develop a small hand weeder to be used for getting rid of young weeds growing between crop rows; and this implement must be relatively cheap and could be made locally. Before the existence of chemical weed control, mechanical weed control was the best option to solve issues related to manual weeding. In mechanized agriculture, there were times where weeding tools were pulled by draft animals such as buffaloes and horses, which now in the developed world have generally been replaced by tractors. There are various types of mechanical weeding implements in the market that use three main techniques: burying weeds, cutting weeds and uprooting weeds. The burial of weeds through the action of tillage tools, and is usually done during land preparation.[2].The earliest and the simplest weed control method is manual weed control. This method was and is accomplished by a person bending down and using their hands to pull weeds out of the soil. This method then advanced to hand tools, from using a stick to using a hand-hoe. The labor required for weeding is expensive, time consuming [4] To achieve a high yielding vegetable production, good agricultural practices are required. One of the most important practices is to properly manage weeds. Weeds affect crop yield due to competition to acquire plant nutrients and resources [4]. Weeds have very fast growth rates compared to crops, and if not treated and managed, they may dominate the field. There are various methods for controlling weed infestation in crop production. Some farmers adopt agronomic practices that improve crop competitiveness such as Planting vigorous crop seeds at relatively shallow depths and planting

right after a weed control operation. This method is used to prevent the weed seeds from germinating before the crop is planted and to ensure that crop plants emerge before the weed plants. This practice will not only ensure a maximized crop yield and reduce weed infestation, but also minimize any economic losses [3]. The above practice should be applied for controlling weeds if the canopy closes and does not allow much light onto the ground surface where weeds will germinate and grow. However, weed control is still required during the crop production cycle. Rice and groundnut are very sensitive to weed as Competition in the early stage of growth and failure to control weeds in the first three weeks after seeding, reduce the yield by 50 per cent [5]. In traditional method of rice cultivation, weeds are mostly removed from the field with manual process as they are seen more as a negative factor for crop growth. But in SRI (System of Rice Intensification), weeds are seen as growth promoters when they are appropriately managed. As the weeds are more in SRI due to intermittent wetting, it is important to manage the weeds regularly. Based on a model developed by International Rice Research Institute, the Acharya N G Ranga Agricultural University of Andhra Pradesh, developed 'cono weeder'. Few innovative farmers did several experiments for different soil situations and easy operation. Even multi-row weeders were developed by some farmers. At this point of time WWF Dialogue Project and WASSAN have organized an innovators workshop on SRI implements in July, 2005. After analyzing various issues the Workshop made the following recommendations regarding weeders human drudgery, risk and misery. The most common methods of weed control are mechanical, chemical, biological and traditional methods. Out of these four methods, mechanical weeding either by hand tools or mechanical weeders are most effective in both dry land and wet land [7]. Weeding and tilling that reduce the time spent on weeding (man hours), cost of weeding and drudgery involved in manual weeding. Weeds can cause several damages to the farming enterprise. These include: decrease in crop yield, impairment of crop quality, harboring of plant pests and diseases, increase in irrigation costs, injury to livestock and decrease in land Values [6] That 50 to 70 % of yield reduction is caused by poor weed control.

II. Aim of Project

The aim of the project is to design, construct and test manual weeder, to provide the best opportunity for the crop to establish itself after planting and to grow vigorously up to the time of harvesting.

2.1 Statement of Problem

Weeding with the use of tools like cutlass and hoe requires high labour force in a commercial farming system hence mechanical weeder is necessary to reduce the labour force. Environmental degradation and pollution caused by chemical is reduced by the use of Mechanical weeder. Low effective operation, low work effort and high time requirement for different types of hoe or cutlass, can be overcome with the use of mechanical weeder [9].

2.2 Justification

Presently in India, weeding with simple tools such as cutlass, hoe etc is labour intensive and intensive and time consuming. Thus, there is a need for the design of manually operated weeder for intensive and commercial farming system in India. One of the problems in crops and vegetables production is poor weed control; hence there is need of mechanical weeder to increase the production of these products. The cost for employing a Labour force when using simple tools is very high in commercial farming system. This can be reduced using mechanical weeder.

III. Materials and Methods

Part: Frame: The material used was metallic circular pipe of 1200mm and supported pipe of different Dimensions. Part: Secondary cutting edge: This part was made of a metallic flat bar of 170mm in length, and extra bar length 230mm sharpen at the one end. Part: Handle: The handle was made up of circular metallic pipe of different dimensions. Part: Primary cutting edge: There were 3 blades which are sharpen in front and at the bottom placed vertically on a flat bar of 108mm in length and teeth to teeth 6.5cm. Part: Funnel: The total height is 900mm and diameter 105 Φ [9].

3.1 methodologies

Weeding efficiency (Functional efficiency) was determined by removing manually the weeds in 1m x 1m area of the farm, the weeds was weighed and recorded. The process was repeated in five randomly selected locations on the farm. The average weight of the weeds in 1m x 1m area was calculated for the types of soil. The average weight of the weeds in 1m x 1m area after pass of the weeder through the farm was deducted from the actual weight of the weeds in 1m x 1m area. Thus, functional efficiency was determined from the relation:

$$\text{Functional Efficiency} = \frac{\text{Weight of weeds removed using weed remover}}{\text{Actual weight of weeds removed manually}} \times 100$$

The functional efficiency was carried out on different types of soil at the same average speed. The machine performance was evaluated using actual field capacity and design field capacity of the machine.

3.2 design requirements:

Physical and operational characteristics Safety: It provides safety to users, Life in service: The product will last approximately long duration, Ergonomics: Easy to operate by everyone, of all physique conveniently, Weight: The product must less in weight, Materials: The material used is mild steel.

IV. Concept

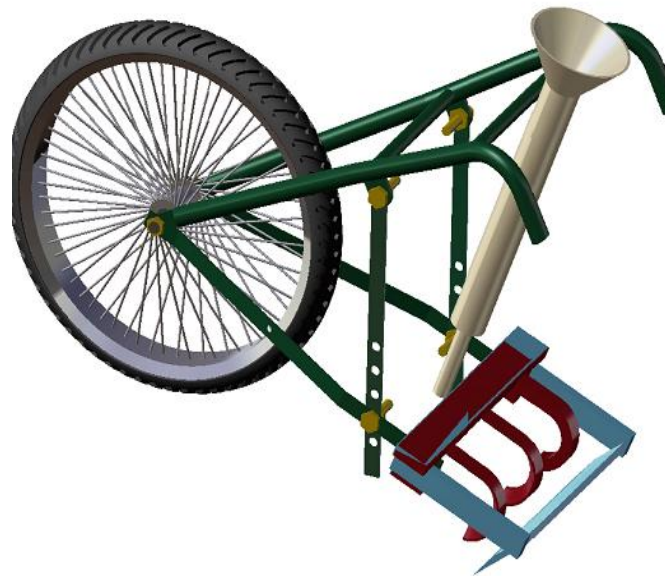


Figure 4.1 Concept idea

This Concept involved the development of mechanical weeder, after discovering that tools such as cutlass and hoes require high drudgery, time consuming and high labour requirement. As a solution to these problems, mechanical weeder was designed and developed. The mechanical weeder was made of two implements attachment i.e. the primary cutting edge which is in front to loose soil above and the secondary cutting edge which is behind to do cutting and lifting of weeds. An extra attachment of funnel and circular pipe for fertilizing and seeding of ragi after cultivation. The tool developed will be able to fulfill the present requirement for the weed control. Accordingly, the present development is directed to an improved manual tilling, mulching and weeding tool.

V. Compared With The Traditional Methods Of Weeding On 1m X 1m Area Of Land

Table 1: weeding test result on semi moisture land

AREA	WEIGHT OF REMOVER WEED USING HAND PULLING(Kg)	TOTAL WIGHT OF REMOVED WEED USING WEED REMOVER(Kg)
1	0.05	0.06
2	0.03	0.04
3	0.07	0.07
4	0.10	0.10
5	0.08	0.08
Total	0.33	0.35
Mean values	0.066	0.7

Functional efficiency for semi moisture land = 94.29%.

Table 2: weeding test result on dry land

AREA	WEIGHT OF REMOVER WEED USING HAND PULLING(Kg)	TOTAL WIGHT OF REMOVED WEED USING WEED REMOVER(Kg)
1	0.30	0.31
2	0.32	0.42
3	0.20	0.28
4	0.32	0.44
5	0.28	0.30
Total	1.42	1.75
Mean values	0.284	0.35

Functional efficiency for dry land = 81.14%.

Table 3: time spent when tested on semi moisture land

METHODS	LABOUR REQUIREMENT	TIME SPENT (Min)
Manually operated Weeder	1	1.0
Cutlass	1	4.49
Hoe	1	3.32

Hence by comparing weed remover and Cutlass it has been observed that weed remover is almost *4.5 times faster than Cutlass* and more than *3 times faster than Hoe* on semi moisture land.

Table 4: time spent when tested on dry land

METHODS	LABOUR REQUIREMENT	TIME SPENT (Min)
Manually operated Weeder	1	1.5
Cutlass	1	6.12
Hoe	1	5.1

Hence by comparing weed remover and Cutlass it has been observed that weed remover is more than *4 times faster than Cutlass* and more than *3 times faster than Hoe* on dry land.

VI. Conclusions

In conclusion, it was found during observations after the development and testing of this particular manually operated weeder that the overall benefits accruing and associated with the use of the equipment includes:

1. It was faster than the traditional method of removing weed.
2. It cannot work where there was stone or any obstacle.
3. Improvement could be brought in their postures, thereby facilitating them to walk comfortably along the rows while weeding with this manual weeder.
4. Less labor needed and it is more economical than hand weeding.
5. Here do not use any fuel and power, Hence maintenance cost is very less.

VII. Scope of Future Work

Through observation, this work was good for local farmers and small scales Agro-base industries that need a better treatment and operations carried out on farms.

1. The weight of the weeder can be reduced by using lightweight materials and by reducing the size of wheel.
2. Since the weeder was designed for low cost, the weeder was made manual but it can be made automatic by placing a motor.
3. By using some advanced attaching mechanisms, the time required for assembling can be reduced for additional attachments.
4. Fixing the extra attachment of leveler.

Acknowledgements

A dissertation work of this nature requires co-ordination and support from many, for its successful completion and I am fortunate enough in this direction. It gives me great pleasure to acknowledge and express my deep sense of gratitude to those who have helped me throughout this work.

I take this opportunity to express my heartfelt gratitude to my guide, **Mr. BHASKAR G**, M.Tech, MISTE, Assistant Professor, Department of Mechanical Engineering, SSIT, Tumkur, for his valuable, constructive, informative, detailed guidance, suggestions and encouragement at every step.

I am also thankful MR.SHARANAPPA JANGADI asst. agriculture engineer , national agriculture research Center ,bhabur Farm, heriur ,Karnataka.

References

Journal Papers:

- [1] Anonymous, 1985. RNAM test codes and procedure for farm machinery, Technical series No. 12, Economic and Social Commission for Asia and the Pacific, Regional Network for Agricultural Mechanization, Bangkok, Thailand.
- [2] Nag P.K. and P.Dutt. 1979. Effectives of some simple agricultural weeders with reference to physiological responses, *Journal of Human Ergonomics*, 13-21.
- [3] Tiwari, V.K., R. Ailavadi, K.N.Dewangan and S Sharangi. 2007. Rationalized database of Indian agricultural workers for equipment design. *Agricultural Engineering International: the CIGRE journal. Manuscript MES 05 004, Vol IX. August, 2007.*
- [4] Dryden, R.D. and C.H.Krishnamurthy. 1977. Year round tillage, *Indian Journal of Weed Science*, 9: 14-18.

Conference:

- [5] Gunasena, H.P.M. and L.M.Arceo. 1981. Weed control studies with bachelor in direct seeded rice in Shri Lawlea, *Proceedings of 8th Asian Pacific weed science society conference*, Bangalore, India, November 27-29.

Books:

- [7] Rangasamy, K., M. Balasubramaniam and K.R.Swaminathan. 1993. Evaluation of power weeder performance, Agricultural Mechanisation in Asia, Africa and Latin America, Vol. 24, No.4: 16-18.
- [8] Singh, G. and K.M.Sahay. 2001. Research Development and Technology Dissemination. A silver Jubilee Publication, CIAE, Bhopal, India.

Theses:

- [9] Quadri, Adegbeni wasiu matric number: 05/0204 OCTOBER, 2010., department of agricultural engineering college of engineering university of agriculture Abeokuta design, construction and testing of manually operated weeder.
- [10] Biswas, H.S. 1990. Soil tool interaction for mechanical control of weeds in black soils. Unpublished Ph.D. thesis, Indian Institute of Technology, Kharagpur.

An optimized evolutionary Multi-agent approach for Regulation of disrupted urban transport

Sondes Ben Cheikh¹, Slim Hammadi²

* École Centrale de Lille, LAGIS FRE CNRS 3303, BP 48, 59651 Villeneuve d'Ascq Cedex

** École Centrale de Lille LAGIS FRE CNRS 3303, BP 48, 59651 Villeneuve d'Ascq Cedex

ABSTRACT: For a sustainable people and goods mobility, CISIT (The International Campus on Safety and Intermodality in Transportation) has the objective to realize an optimal management of multimodal chains. In this context, this paper discusses the real-time regulation of traffic in a transportation system disruption.. In fact, the increase in the network size and the presence of multiple transportation modes had made the task of managing the transportation system more complex and more difficult for regulators especially during a disturbance. Hence, we propose a decision support system based on an evolutionary multi-agent approach. This system is able to detect perturbations, analyze, propose and evaluate solutions using Choquet integral.

Keywords: Choquet integral, Genetic algorithm, Multi-agent system, Regulation Support System.

I. Introduction

Seen an increase in the number of passengers and the development of various transportation modes, the great difficulty related to the traffic management is the respect of the planned departure and arrival times of the vehicles at the different stops in the network [1].

In fact, through an estimation of the demand, a travel time and traffic condition, a predictive scheduling was established [2]. This process consists in establishing different timetables describing the theoretical passage times of vehicles through the network stations. However, complex and random events can disrupt the network thus introducing considerable differences between the theory state and the real state, and subsequently causing deterioration in the quality of service provided. Hence the importance of a regulatory process that aims to generate fast and efficient solutions in real time. Therefore, to reduce the disturbances effects, the theoretical schedules have to be adapted to the real traffic conditions through regulation, or rescheduling tasks [3] [4] [5]. This process is then called reactive scheduling [3]. It results in the creation of new schedules that increase the level of service by undertaking operational decisions, such as, delay of one or several vehicles, injection of an extra vehicle in the network or routes deviation of some vehicles ...etc. Actually, it is a human operator, a regulator, who is responsible to manage and control the global network traffic. So, the regulator has to carry out difficult tasks that are often inaccessible at the human scale especially if many disturbances occur simultaneously, which involves the assistance of a RSS (Regulation Support System) [6].

Tools and regulatory approaches

Due to the imperfection of the data on which most mathematical models are based, fuzzy logic[7] has been introduced in various regulatory approaches[1][8]. Moreover, regulation is often seen as a real-time scheduling. Then it is a reordering of the following vehicles under real operating conditions [9].

Faced with the complexity of transportation problems, which requires the development of efficient and suitable solutions in a limited time, and noting the effectiveness of genetic algorithms for solving combinatorial optimization problems, several researchers have used these algorithms to optimize transportation networks [10][11]. Moreover, the problem of correspondence between different lines of a public transport network was also treated by approaches based on genetic algorithms [12], [13].

Due to the distributed nature of transportation systems, Laïchour in [14] proposed a decision support system to regulate a network of buses, based on Agent approach. Indeed, he proposed a multi-agent system capable of handling correspondence in real time.

Other researches had used hybrid approaches. In her doctoral thesis B.Fayech in [15] proposed an evolutionary multi-agents approach for the on-line regulation...

In this study, we propose a RSS which tries to assist the regulators to evaluate a pertinence of a disturbance and to choose the most efficient decision. We begin with a presentation of the mathematical formulation of the problem where the constraints and the regulation criteria are also stated. Then we propose decision support system that relies on cooperation between a multi-agent system [16][17],[18] and an evolutionary approach[3]. This system has to analyze disturbances, generate and evaluate solutions using Choquet integral. Some simulation results are finally shown in the last section.

II. Mathematical Formulation

A. Regulation horizon determination

In order to control the disturbances evolution, we have to search a set of network entities (vehicles and stations) involved in the detected disturbance $H = \{S^H \cup V^H\}$, where S^H is the set of the considered stops and V^H is the set of the vehicles. We note the k^{th} station of the line r by S_k^r . We also represent the i^{th} vehicle of the line l by V_i^l

To calculate the regulation horizon, MM.Ould Sidi [1] proposed a simple geometrical method which consists in a delay to be imposed on every vehicle during its passage in the terminus.

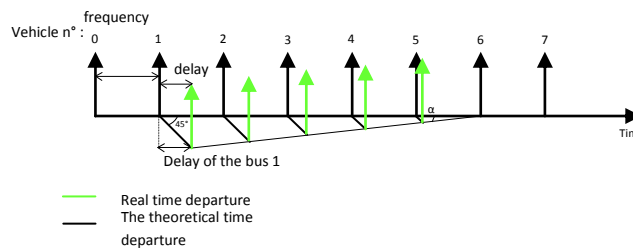


Figure 1. Principle of the regulation in terminus

The number of vehicles upstream expressed by the following formula:

$$N_{up} = (E(n_0) + 1) + 1 \tag{1}$$

The number of downstream vehicles expressed by using the following formula:

$$N_{down} = \begin{cases} N_{up} - 1, & \text{if } 0 < N_{up} \leq 3 \\ N_{up} - 2, & \text{if } N_{up} > 3 \end{cases} \tag{2}$$

Finally, the total vehicles number to consider is:

$$N_T = N_{up} + N_{down} + 1 \tag{3}$$

We note S_{up} the first station where a vehicle $(V_{distr} + N_{up})$ is going to serve after the moment of disturbance t_{distr} , and S_{down} the first station where the vehicle $(V_{distr} - N_{down})$ is going to serve after t_{distr} .

In the case of simultaneous disturbances, the determination of the horizon is even more complicated. To manage this complex incident, our proposed RSS must check whether these disturbances are overlapping or not.

- Separate disturbances: In this case, the RSS must identify the horizon associated with each disturbance and these will be treated separately.
- Overlapping disturbances: We note that H_1 is the horizon of the first disturbance and H_2 is the horizon of the second one. We assume that H_1 and H_2 are not disjoint. In this case more complex than the first, the RSS should determine the overall horizon H_{global} which is the union between H_1 and H_2 .
- Generalization to m overlapping disturbances: We consider m perturbations simultaneous and overlapping, we note H_i horizon associated with each disturbance. The global regulation horizon H_{global} is the union of different horizons H_i .

B. Decision variables

The passage variable, a_{ij}^m associated to the vehicle V_i^m and to the stop S_j^m is equal to 1 if the vehicle V_i^m passes by this stop and 0 otherwise. The destination variable, x_{ijk}^m is equal to 1 when V_i^m goes directly from S_j^m to S_k^m and to 0 otherwise. We note ta_{ij}^m the arrival time of the vehicle V_i^m at the stop S_j^m and td_{ij}^m its departure time. Considering the initial duration, t_{ijk}^m of the vehicle V_i^m direct route between the stations S_j^m and S_k^m , we represent the route time modification between these two stops by δ_{ij}^m . The variable ϵ_{ij}^m denotes the supplementary parking time of the vehicle V_i^m at the stop S_j^m .

C. Criteria

Through a comparison between the situation before regulation and that after the rescheduling, to conciliate the different aspects of the quality of service, we consider five criteria:

1. Regularity criterion:

The regularity criterion represents the time interval between the departure times of two successive vehicles at the same station. It concerns the waiting Time of the passengers at the different stops. The waiting time of all passengers in S_j^l is formulated as:

$$\text{attente}(S_j^l) = \sum_i (a_{ij}^l \times \sum_k \text{attente}(ta_{ij}^l - td_{ik}^l, S_j^l, S_k^l)) \tag{3}$$

The total passengers waiting time at the different stops of the spatial horizon is formulated as

$$WT = \sum_{S_j^l \in S^H} \text{attente}(S_j^l) \tag{4}$$

2. Transfer criterion:

The transfer criterion is related to the Transfer Time at the different nodes of the network. It is then to calculate the duration of correspondence in the horizon H. This criterion can be formulated as follows:

$$TT = \sum_{V_i^l \in V^H} \sum_{V_i^l \in V^H} \sum_{S_j^l \in S^H} y_{ii^l j}^l \times \omega_{ii^l j}^l \times (td_{ij}^l - ta_{ij}^l) \quad (5)$$

Where $y_{ii^l j}^l$ is equal to 1 if a connection is possible from V_i^l to V_i^l at S_j^l and equal to 0 otherwise, $\omega_{ii^l j}^l$ is the number of persons in transfer.

3. Route time criterion:

It consists in minimizing the total routes duration aboard the various vehicles according to their loads.

$$DT = \sum_{V_i^m \in V^H} \sum_{S_j^m \in S^H} a_{ij}^m \times C_{ij}^m \times (td_{ij}^m - td_{ij}^m) \quad (6)$$

where C_{ij}^m is the number of people who rise and fall of each vehicle at each station.

4. Commercial kilometers:

The commercial kilometers represent distance crossed in kilometers that the transport company has to assure.

$$KM = \sum_{V_i^m \in V^H} \sum_{S_j^m \in S^H} a_{ij}^m \times d_{ij}^m \times d_i^m(S_j^m, S_j^m) \quad (7)$$

With $d_i^m(S_j^m, S_j^m)$ the distance crossed by a vehicle V_i^m between these two stations.

5. Service quality:

The quality of service can be expressed differently from one operator to another. It can be based on the number of not served stations, the number of vehicles and drivers changes, and the number of transshipments (Not to confuse with correspondences), by minimizing the maximum of three terms:

$$SQ = \max_{V_i^m \in V^H} (n_change(V_i^m), n_trans(V_i^m), n_stat(V_i^m)) \quad (8)$$

D. Constraints

Several constraints should have to be considered during the real-time regulation of the traffic of a collective urban transport network. Therefore, we take into account the following constraints:

- Each vehicle V_i^m passing by a given point has a unique origin point and goes to a unique immediate destination point:

$$\sum_{S_j^m \in S^H} x_{ijk}^m = a_{ij}^m \quad (9)$$

-The minimal time interval between V_i^m and V_i^m its first successor at the stop S_j^m is stated as follow:

$$td_{ij}^m - ta_{ij}^m \geq Inter_{\min}^m \quad (10)$$

-The limit on the stop time of V_i^m at the station S_j^m is represented by the following constraint:

$$td_{ij}^m - ta_{ij}^m \geq ts_{ij}^m \quad (11)$$

-The time limits on the connection or transfer durations are presented by the following inequality:

$$Trans_{\min} \leq y_{ii^l j}^l \times (td_{ij}^l - ta_{ij}^l) \leq Trans_{\max} \quad (12)$$

- The vehicle load can not exceed the allowed maximum load:

$$C_{ij}^m \leq C \max_i^m \quad (13)$$

Our regulation problem can be formulated as a multi-objective optimization problem; it can be stated as follow:

$$\begin{cases} \min \{ \Delta(WT), \Delta(TT), \Delta(RT), \Delta(KM), \Delta(SQ) \} \\ \text{subject to: (15), (16), (17), (18) and (19)} \end{cases} \quad (14)$$

With $\Delta(x)$ the variation of the concerned criterion between the theoretical and the regulated states of the network. We present in the following paragraph, a proposed decisions generation and evaluation module.

III. Indentations and Equations Decisions Generation and Evaluation

A. Decisions generation:

1. Regulation in terminus:

It consists in making departures advanced or delayed from a terminus to restore on-line regularity by acting on one or two downstream and upstream vehicles of a disrupted one, according to the importance of the delay of this one.

2. On-line regulation

For the decisions generation, we choose the *On-line regulation* class. This decision class is used by the regulators for 90 % of the disturbances cases, it is reliable and easy to implement. It consists in delaying some upstream and downstream vehicles of a disrupted one in order to avoid an excess load on this last one, to help it to not increase its delay and to restore the intervals regularity [3]. However, the calculation of these delays in a way to obtain an optimal solution is very difficult. Then, this problem was shown NP-hard Multi objective Optimization Problem (MOP)[3].

B. A proposed approach for the on-line regulation

During the recent past, multi-objective evolutionary algorithms are subject to an increasing attention among researchers and practitioners mainly because of the fact that can be suitably applied find a set of Pareto-optimal solutions in one single simulation run [19][20][1]. In addition, the trade-off between obtaining this set as a well-converged and well-distributed as possible and obtaining that in a small computational time is an important issue in multi-objective evolutionary optimization [21][22]. However, the solutions depend on the decision maker preferences, and not only the search of solutions but also the decision making is important. To reach these objectives, we developed an aggregative approach based on an evolutionary algorithm [23][24] using the Choquet integral concept.

C. Decisions evaluation: Aggregative approach based on the Choquet integral

The classical weighted arithmetic mean method is the most commonly used operator to aggregate criteria in decision making problems without further considering the interactions among criteria. On the other side, the discrete Choquet integral has proven to be an adequate aggregation operator that extends the weighted arithmetic mean method by taking into consideration the interactions among criteria [24]. The philosophy of the Choquet integral was first introduced in capacity theory and used as a (fuzzy) integral with respect to a fuzzy measure proposed by Murofushi and Sugeno [25].

In the beginning, we define a few concepts necessary for understanding the Choquet integral and essential mathematical tools.

Definition 1: A fuzzy measure μ on N (the set of criteria) is a function $\mu: P(N) \rightarrow [0,1]$, satisfying the two following axioms:

$$1. \mu(\emptyset) = 0, \quad (15)$$

$$2. A \subset B \subset N \Rightarrow \mu(A) \leq \mu(B) \quad (16)$$

We will assume here $\mu(N) = 1$ as usual, although this is not necessary in general. $\mu(A)$ represents importance or power of the coalition A (group of criteria) for the aggregation problem in question. A fuzzy measure requires $2^n - 2$ coefficients to be defined, verifying the monotonicity conditions.

Definition 2: Let μ be a fuzzy measure on N . The Choquet integral of a function $f: N \rightarrow \mathbb{R}^+$ with respect to μ is defined by:

$$C_{\mu}(f) = \sum_{i=1}^n (f(x_{(i)}) - f(x_{(i-1)})) \mu(A_{(i)}), \quad (17)$$

Where $_{(i)}$ indicates that the indices have been permuted so that $0 \leq f(x_{(1)}) \leq \dots \leq f(x_{(n)})$ and $A_{(i)} = \{x_{(i)}, \dots, x_{(n)}\}$, and $f(x_{(0)}) = 0$.

Definition 3: Let μ an application (not necessarily a fuzzy measure) on C , the Möbius transform of μ is the set function defined by:

$$m(A) = \sum_{B \subset A} (-1)^{|A \setminus B|} \mu(B), \quad \forall A \subset N \quad (18)$$

Where $A \setminus B$ is the set of elements of A not belonging to B , that is the compliment of B in A .

Definition 4: The fuzzy measure μ is called k -additive if its Möbius transform satisfies the following conditions:

$$m(A) = 0, \quad (19)$$

$$\forall A \text{ such as } |A| > k \text{ and there is at least one subset of cardinality } k \text{ such that : } m(A) \neq 0. \quad (20)$$

The global importance of a criterion:

For reasons of simplification, let $\mu(c_i) = \mu_i = \mu(\{i\})$. By definition, $\mu(\{i\})$ reflects the importance of criterion i . The global importance of this criterion c_i is not determined only by the number μ_i but by all measures μ_k of all coalitions K where $c_i \in K$. For example, we can have a criterion c_i such that $\mu_i = 0$. The criterion c_i seems unimportant, but it is possible for several subsets K includes in $C \setminus \{c_i\}$, the number $\mu(K \setminus \{i\})$ is more important than $\mu(K)$ which proves the importance of this criterion c_i . In this context, we can define the global importance of a criterion by its Shapley index:

$$I_i = \sum_{K \subseteq N \setminus i} \frac{(n-|K|-1)!|K|!}{n!} (\mu(K \cup \{i\}) - \mu(K)) \quad (21)$$

Where n is the cardinality of N (set of criteria).

The Shapley index is interpreted as the average of marginal contributions of this criterion in all coalitions where he participates.

Interaction between two criteria:

There are three possible situations when we calculate the interaction between two criteria

- ✓ $\mu(\{i, j\}) > \mu(\{i\}) + \mu(\{j\})$: there is synergy of complementary between the two criteria.
- ✓ $\mu(\{i, j\}) < \mu(\{i\}) + \mu(\{j\})$: there is redundancy or negative synergy between these two criteria.
- ✓ $\mu(\{i, j\}) = \mu(\{i\}) + \mu(\{j\})$: the two criteria are independent.

Then, the interaction between two criteria can be defined by the following equation:

$$I_{ij} = \sum_{K \subseteq N \setminus \{i, j\}} \frac{(n-|K|-2)!|K|!}{(n-1)!} (\mu(K \cup \{i, j\}) - \mu(K \cup \{i\}) - \mu(K \cup \{j\}) + \mu(K)) \quad (22)$$

It is possible to express the Choquet integral in case of 2-additive measures by using only the interaction index, as follows. Let a_1, \dots, a_n be scores on criteria.

$$C_\mu(a) = \sum_{I_{ij} > 0} (a_i \wedge a_j) I_{ij} + \sum_{I_{ij} < 0} (a_i \vee a_j) |I_{ij}| + \sum_{i=1}^n a_i (I_i - \frac{1}{2} \sum_{j \neq i} |I_{ij}|) \quad (23)$$

where \wedge et \vee represent respectively the minimum and maximum.

It can be seen that the Choquet integral for 2-additive measures can be decomposed in a conjunctive, a disjunctive and a additive part, corresponding respectively to positive interaction indices, negative interaction and the Shapley value. This makes clear the meaning of I_{ij} the framework of the Choquet integral:

- A positive I_{ij} implies a conjunctive behavior between i and j . This means that the simultaneous satisfaction of criteria i and j is significant for the global score, but a unilateral satisfaction has no effect.
- A negative I_{ij} implies a disjunctive behavior, which means that the satisfaction of either i or j is sufficient to have a significant effect on the global score.

The Shapley value I_i acts as a weight vector in a weighted arithmetic mean. This represents the linear part of Choquet integral. It will be small if interaction indices are large.

Interaction index and Shapley values determination

To be able to calculate the global score of each decision, We have to determine the Shapley values and interaction index between criteria (coefficients of Choquet integral). For reasons of simplicity, we suppose that the regulator can express, quantitatively or qualitatively, his preferences and it can give the interactions index once for quite independently of the current situation.

Decision-making related to the regulation may be likened to solving an optimization problem whose objective function to maximize the number of passengers served and satisfaction while minimizing the waiting time and travel time under different constraints related to transmission and available resources. To achieve these objectives, we propose a Multi-agent approach based on an evolutionary algorithm using the Choquet integral. This approach will be more detailed later.

V. Multi-Agent System Description

As a result, the complexity of the problem addressed and the distributed nature and dynamics of the system, a newly developed multi-agent technique was introduced to solve multi-objective optimization, and is combined with genetic algorithm to form an evolutionary multi-agent system [25]. To resolve the problem described previously, we propose an optimized evolutionary multi-agent system based on the coordination of four kinds of reactive agents: AI, AH, AO and AE. Each agent must work and interact with other agents to achieve a common group goal.

The system allows interacting with the regulator by indicating the area of regulation, the list of operations it can perform and evaluate each action chosen for each criterion separately and taken by an aggregation of criteria by the Choquet integral whose coefficients represent preferences. To simplify, we can consider that the regulator detects the disturbance. But if we put the system in contact with the system operating assistance (SOA) used by the operator, we can improve our system since it can directly detect the presence of disturbances and even alert the regulator.

D. Agents' behaviours

To describe better the behaviour of our system, we use a modeling software called UML (Unified Modeling Language).

1. Interface Agents (AI): these agents interact with the controller who inputs data of the disturbance, so they manage requests and then display results.

Figures and Tables

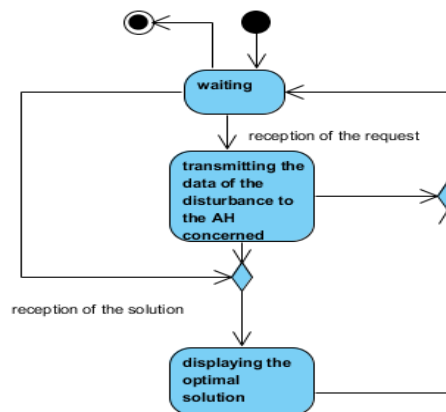
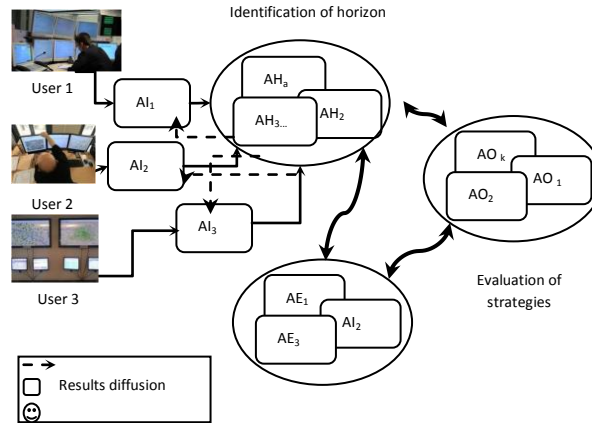


Figure 3. The AI's behaviour

- Horizon agents (AH): The Horizon agent checks the nature of the disturbance and identifies his horizon using the geometrical method detailed previously.

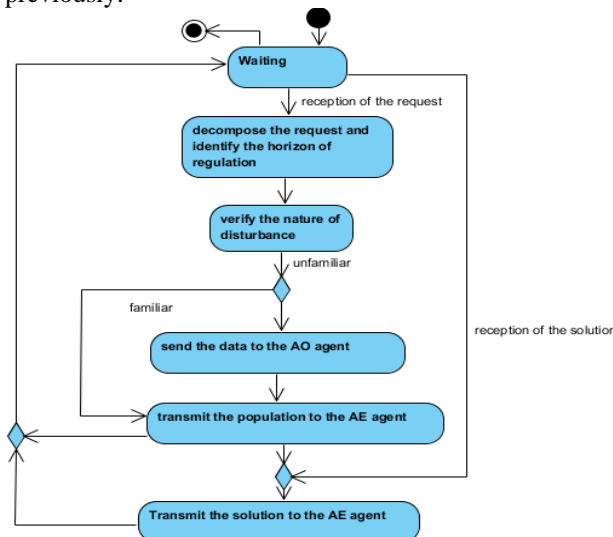


Figure 4. The AH's behaviour

- Optimizer Agents (AO): To generate optimized solutions, we propose an evolutionary approach. In our approach, the Optimizer agent is loaded by the application of the genetic algorithm.

- Evolutionary approach**

The genetic regulation algorithm starts by constructing an initial population of solutions. The genetic regulation algorithm starts by constructing an initial population of solutions. A part of this population is built through a first strategic decision level processed by the multi-agent decision support system which also defines the constraints, other part is constructed randomly.

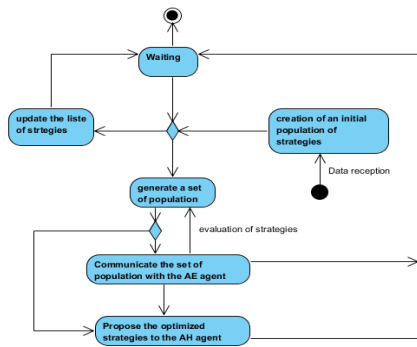


Figure 8. The AO's behaviour

4. Evaluator agents (AE): In other studies that have combined multi-agent systems and genetic algorithms, the procedure of evaluation of solution is integrated into the genetic algorithm [15]. But in our system, the multi-criteria evaluation is done by an independent agent. The AE agent evaluates the strategies by using an aggregative approach based on the Choquet integral. This design allows the regulator to evaluate strategies of regulation without going through the rest of the system.

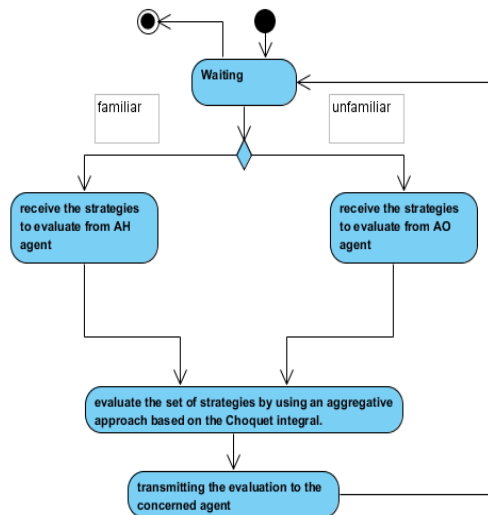


Figure 9. The AE's behaviour

E. The global behaviour of the system

After describing the individual behavior of different agents, we present a summary of the different interactions between entities of the system to better understand the regulatory process.

We illustrate the behaviour of system by a sequence diagram in UML. The sequence diagram expresses the dynamic structure modeling. It shows the communication and interaction between the different agents of the system.

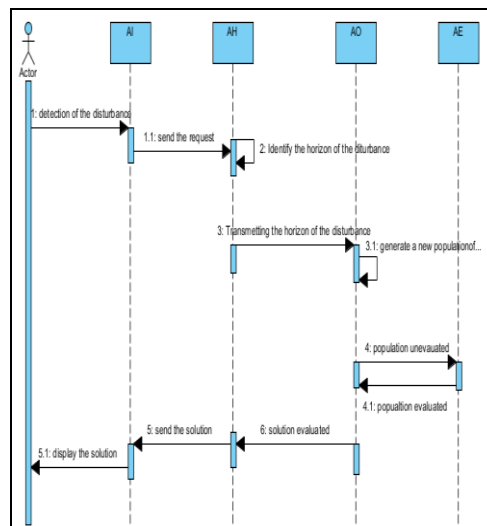


Figure 10. The global behaviour

VI. Simulation Results

Regulation is obtained thanks to communication, collaboration and negotiation between the agents; the programming is developed under the JADE platform (Java Agent Development Framework). This platform has several advantages. These benefits include:

- ✓ The distributed Processing
- ✓ The flexibility of Multi-Agent Systems communicating through effective transfer of messages ACL (Agent Communication Language).
- ✓ Write in JADE is like writing in JAVA

In order to evaluate the efficiency of the suggested approach, we present here a scenario of tow overlapping and simultaneous disturbances. Let's suppose that at 7:35am, a technical problem takes place on a section of the metro line with frequency of 1 metro / 2 minutes. This problem obliges the vehicle number 16, to stop during 4 minutes at the station number 12, and the vehicle number 20 to stop during 6 minutes at station number 8.

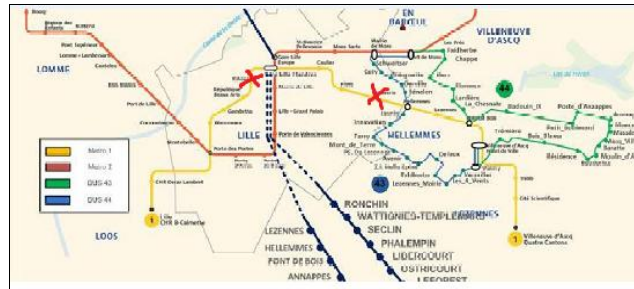


Figure 11. Tow overlapping and simultaneous disturbances.

F. Communication between different agents

The Sniffer agent visualizes the flow of communication between different agents in the system.

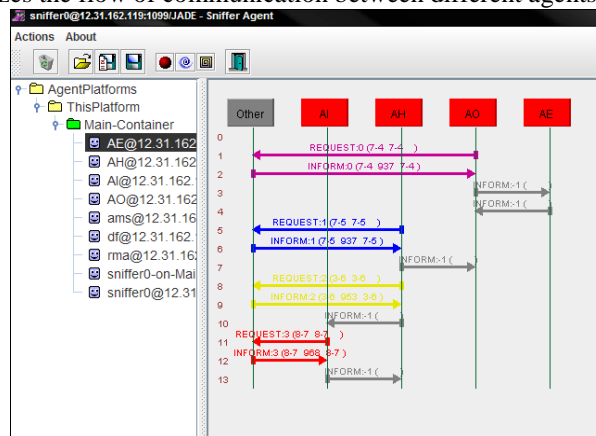


Figure 12. Communication between the system's agents

G. Determination of the regulation horizon

The first step of our regulation process consists of the determination of the regulation spatiotemporal horizon. So, the Horizon Agent uses the method explained in the paragraph II.A. Let us suppose that H1 is the horizon of the first disturbance, and H2 is the horizon of the second disturbance. So the global horizon HGlobal is the union between the two horizons. The following figure shows the solution presented by the Horizon agent.

```

Main (11) [Java Application] C:\Program Files (x86)\Java\jre7\bin\java
DB connection established..
request sent..
the horizon of the first disturbance
AH says : First pert: The vehicle downstream 28
AH says : First pert: The vehicle in front 6
First pert: The station downstream 1
AH says : First pert: The station in front 12
request launched..
the horizon of the second disturbance
AH says : Second pert: The vehicle downstream 33
AH says : Second pert: The vehicle in front 9
AH says : Second pert: The station downstream 1
AH says : Second pert: The station in front 8
two simultaneous and overlapping disturbances
The global horizon
AH says : The vehicle downstream 33
AH says : The vehicle in front 6
AH says : HA says : The station downstream 1
AH says : The station in front 12
disconnection..
    
```

Figure 13. The global Horizon

H. Decisions construction

When the regulation horizon created, the Optimizer agent uses the collected data to build the solutions coding and execute our evolutionary approach explained in the last section. The chromosomes of our problem are coded as follows: for the metro-line, we use an array with 28 lines corresponding to the vehicles included in the disturbance zone and 12 colons for the stations. The chromosome cells illustrate the decisions (delays to be imposed) to undertake for the vehicles of V^H at different stops of S^H . Our approach will try to find the best combination of delays to be applied to two concerned lines. The crossover operates on the lines of chromosome; it acts only on the decision variable ϵ_{ij}^{lm} in the chromosome cells. Two breakpoints are chosen randomly and the exchange of the genes between the individuals is made only between the same vehicles. The crossover probability is set at 0.8. The mutation operates by random changes on the stops variables. The mutation probability is set at 0.005.

I. Decisions evaluation

After the generation of decisions, the Evaluator agent calls the module of evaluation to determine the best feasible decision by taking into account the importance of every criterion and the interaction between criteria. Let's suppose that the regulation strategy adopted by the regulator was modeled with the following matrix representing the weights of criteria and their interactions (coefficients of Choquet integral).

$$\begin{matrix} & \begin{matrix} WT & TT & RT & KM & SQ \end{matrix} \\ \begin{matrix} WT \\ TT \\ RT \\ KM \\ SQ \end{matrix} & \begin{bmatrix} 0.1 & 0.15 & 0.2 & 0 & 0 \\ 0.15 & 0.5 & -0.2 & 0 & 0.1 \\ 0.2 & -0.2 & 0.1 & 0.1 & -0.1 \\ 0 & 0 & 0.1 & 0.1 & 0.05 \\ 0 & 0.1 & -0.1 & 0.05 & 0.2 \end{bmatrix} \end{matrix} = I_y$$

Figure 14. Coefficients of Choquet integral

Values on the diagonal of this matrix represent the criteria importance (Shapley values), whereas the others represent the interaction index between criteria [5]. Based on these coefficients, the Evaluator agent will calculate the score of each criterion then the global score of Choquet obtained for every solution. The optimized solution is the solution that corresponds to the highest score of Choquet.

The scores obtained by the optimized solution are shown in the following figure:

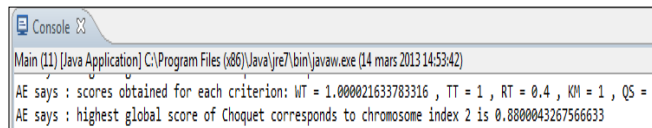


Figure 15. The Choquet scores

J. The optimized solution

For 10 generations and a population of 20 individuals, the optimized solution for the metro line is given in the following table, where columns represent the stations from 1 to 12 and the lines represent the vehicles from 6 to 33.

The values of the table correspond to the supplementary parking time of vehicles in each station.

Vehicle	St1	St2	St3	St4	St5	St6	St7	St8	St9	St10	St11	St12
6	0	0	0	0	0	0	0	0	0	0	0	0
7	0	0	0	0	0	0	0	0	0	0	0	0
8	0	0	0	0	0	0	0	0	0	0	0	0
9	0	0	0	0	0	0	0	0	0	0	0	0
10	0	0	0	0	0	0	0	0	0	0	0	0
11	0	0	0	0	0	0	0	0	0	0	0	0
12	0	0	0	0	0	0	0	0	0	0	0	0
13	0	0	0	0	0	0	0	0	0	0	0	0
14	0	0	0	0	0	0	0	0	0	0	0	0
15	0	0	0	0	0	0	0	0	0	0	0	0
16	0	0	0	0	0	0	0	0	0	0	0	0
17	0	0	0	0	0	0	0	0	0	0	0	0
18	0	0	0	0	0	0	0	0	0	0	0	0
19	0	0	0	0	0	0	0	0	0	0	0	0
20	0	0	0	0	0	0	0	0	0	0	0	0
21	0	0	0	0	0	0	0	0	0	0	0	0
22	0	0	0	0	0	0	0	0	0	0	0	0
23	0	0	0	0	0	0	0	0	0	0	0	0
24	0	0	0	0	0	0	0	0	0	0	0	0
25	0	0	0	0	0	0	0	0	0	0	0	0
26	0	0	0	0	0	0	0	0	0	0	0	0
27	0	0	0	0	0	0	0	0	0	0	0	0
28	0	0	0	0	0	0	0	0	0	0	0	0
29	0	0	0	0	0	0	0	0	0	0	0	0
30	0	0	0	0	0	0	0	0	0	0	0	0
31	0	0	0	0	0	0	0	0	0	0	0	0
32	0	0	0	0	0	0	0	0	0	0	0	0
33	0	0	0	0	0	0	0	0	0	0	0	0

Figure 16. Delays to impose on Metro

Finally, The distributed architecture, in conjunction with the Multi-Agent concept, helped to further reduce the initial problem's complexity thanks to the communication and the collaboration between the different agents of the system.

VII. Conclusion and Perspectives

The real-time regulation of an urban collective transport network is a very delicate problem, especially in the case of appearance of simultaneous disturbances (vehicle's breakdown, strike, demonstration.... etc). Our purpose in this paper, is to

assist the regulators (decision-makers) and to propose to them effective solutions by taking into account their preferences and uncertainties related to these preferences.

At the end, we will try to introduce personal transportation such as carpooling and car sharing as other regulation modes to provide more flexibility in the transport network...

References

- [1] MM. Ould Sid, S. Hammadi, P.Borne, (March 2008) "Urban transport networks regulation and evaluation: A fuzzy evolutionary approach": IEEE Trans Syst, Man, Cybern SMC Part A, vol 38, Issue:2, pp: 309 – 318.
- [2] M.T. Issai and N.P. Cassaigne, (Nov.2001) "Predictive and reactive approaches to the train-scheduling problem: A knowledge management perspective," IEEE SMC, Part C, special issue on knowledge management, vol 31, issue 4, pp. 476 - 484.
- [3] P. Borne, B. Fayech ; S. Hammadi ; S. Maouche, February 2003 "Decision support system for urban transportation networks". IEEE Trans Syst, Man, Cybern C, Vol 33, pp. 67-77.
- [4] Khoat, Nguyen-duc, (Oct. 2006) "Rescheduling In The Urban Transportation Networks", Service Systems and Service Management, International Conference, Vol 2, pp. 1501 – 1506, Troyes, 25-27.
- [5] MM. Ould Sidi, S. Hayat and S. Hammadi, (may 16-19, 2005). "Urban transport disrupted networks regulation strategies making and evaluation: A new approach". IESM'05, Marrakech, Morocco.
- [6] H.Ezzedine, C.Kolski, C.Tahon, (4-6 Oct. 2006) " Intermodal transportation system management,towards integration of traffic management system and users information system". Computational Engineering in Systems Applications, IMACS Multi-conference, Vol 1, p972 – 979.
- [7] B. Bouchon-Meunier, (octobre 1995) "Fuzzy logic and its applications", Addison-Wesley.
- [8] A. Soulhi, , (18 January 2000)"Contribution of artificial intelligence to decision support in the management of collective urban transport systems", Ph.D. degree in automatics and industrial computing, University of Sciences and Technologies of Lille.
- [9] H. Lourenço & al. Multiobjective, (August 2001) "Metaheuristics for the Bus-driver scheduling problem". Transportation science, 35(3): 331-343.
- [10] M. Bielli, M. Caramia, P. Carotenuto. (February 2002) "Genetic algorithms in bus network optimization". Transportation Research Part C: Emerging technologies, Volume 10, Issue 1, pages 19-34.
- [11] A.S.K. Kwan, R.S.K. Kwan, A. Wren, (1997) " Driver scheduling using genetic algorithms with embedded combinatorial traits", In preprints of the International Workshop on Computer Aided Scheduling of Public Transportation, Boston, USA.
- [12] K. Deb and P. Chakroborty, (1998) "Time scheduling of transit systems with transfer considerations using genetic algorithms", Evolutionary Computation 6(1), pages 1-24.
- [13] F.A. Kidwai, B.R. Marwah, K. Deb, M.R. Karim, (2005). "A genetic algorithms based bus scheduling model for transit network", Proceedings of the Eastern Asia Society for Transportation Studies, Vol 5, pages: 477-489.
- [14] H. Laïchour, S. Maouche, and R. Mandiau, (2001) "Traffic control in connection node," in Proc. IEEE Syst., Man, Cybern. Conf., Tucson, AZ, Oct.7–10, pp. 1355–1360.
- [15] B. Fayech ; S. Maouche, S. Hammadi ; P.Borne, (2002) "Multi-agent decision-support system for an urban transportation network," in Proc.World Automation Cong, Vol 14, pp27-32, Orlando, FL, June 9-13.
- [16] K. Bouamrane, C.Tahon, (2005) "Decision Making Systemm for Regulation of a Biomodal Urban Transportation Network, Associating a Classical and a Multi-agent Approaches" Journal Informatica, Vol 16, Number 4, pp. 473–502.
- [17] F. Balbo, S. Pinson, (February 2010) "Using intelligent agents for Transportation Regulation Support System Design", Transportation Research PartC: Emerging Technologies, Vol 18(1), Issue 1, pp 140-156.
- [18] P. Gruer, V. Hilaire, A. Koukam, (6-10 October 2001) "Multi-Agent Approach to Modelling and Simulation of Urban Transportation Systems", Proc. of the 2001 IEEE SMC Conference, Vol 4, pp.2499-2504, Tucson, Arizona, USA.
- [19] CA. Coello Coello, (2000) "A survey of GA-based multi-objective optimisation techniques". ACM Computing Surveys, Vol 32(2), pp 109-143.
- [20] B.Y. Qu, P.N. Suganthan, (1 September 2010) "Multi-objective evolutionary algorithms based on the summation of normalized objectives and diversified selection", Information Sciences, Vol 180, Issue 17, pp 3170–3181.
- [21] K. Sindhya, K. Deb, K. Miettinen. (September 13-17, 2008) "A Local Search Based Evolutionary Multi-objective Optimization Approach for Fast and Accurate Convergence", 10th International Conference Dortmund, Vol 5199, pp 815-824, Germany.
- [22] K. Takanori, T. Yasutaka and K. Eiji, (December 2003) "Unsatisfying functions and multi-objective fuzzy design using genetic algorithms". IEEE-SMC part B, Vol 33(6), pp 889-897.
- [23] Lin, Hou, (17-19 June 2009) "Public transport network optimization based on a Multi-objective Optimization Problems Evolutionary Algorithm". Control and Decision Conference CCDC '09, pp 4408 – 4412, China, Guilin.
- [24] M. Grabisch, M. Roubens, (2000) "Applications of the Choquet integral in multicriteria decision making. Fuzzy measures and integrals: theories and applications". Phisica Verlag, pp. 415-434.
- [25] T. Murofushi and M. Sugeno, (1991) "A theory of fuzzy mesures- representations, the Choquet integral, and null sets", Journal of Mathematical Analysis and Applications Vol. 159, No. 2, 532–549.
- [26] R.Sivaraj, T.Ravichandran, (May 2011) "A review of selection methods in genetic algorithm" International Journal of Engineering Science and Technology (IJEST), Vol. 3 No. 5.

Investigation of Barreling Radius and Top Surface Area for Cold Upsetting Ofaluminum Specimens

R. Raja¹, S. Lakshminarasimhan², P. Murugesan³

¹Associate Professor-Mechanical Engineering

²Principal, Bharath Niketan Engineering College, Aundipatti-625536, India

³Principal, Veerammal Engineering College, Batlagundu, India

Abstract: In this work cold upset forging experiments have been conducted on aluminum 6063 specimens without constraints and without use of lubricants. Strain behavior, barreling radius and top surface area characteristics have been studied and analyzed. The experimental data have been validated adopting finite element method and response surface methodology. The research fraternity has to their credit many such publications. Sensitivity analysis of behavior of key indices is a new innovation in this work. Intermittent work hardening, barreling radius and top surface area have been analyzed using sensitivity analysis and recorded. Stress, Strain distribution photographs have been placed in the appendix. The deduced observations will aid shopfloor forging manufacturing process and tools development.

Keywords: Aspect Ratio, Barreling Radius, Deformation behavior, Regression equation, Top surface Area, Upset Ratio.

I. INTRODUCTION

There has been a persistent endeavor by manufacturing industries to adopt metal moving in place of metal machining due to high yield of material, repetitive accuracy in quality and advantages in mechanical properties. Producing machine parts and structural parts for shock or sudden impact load applications by forging is a common practice. Upsetting and open die forging is one of the significant processes in the metal forming area. Ductile materials like Aluminum have been widely used for making rivets, fasteners and many other parts for a wide range of applications like consumer goods, automotive parts, structural, aeronautical and marine sectors. Taking cognizance of these developments the research fraternity has been focusing on studying physical and mechanical characteristics of upset forging of aluminum billets and blanks.

In this work the non-linear changes in top surface area dimensions, intermittent work hardening and the barreling radius behavior for cold upsetting of aluminum 6063 material without constraints and without lubrication has been detailed by conducting sensitivity analysis of the experimental observations. This paper is organized into several sections. The next section details the literature survey. The third section explains the problem background. Section four details the experimental study and results. The fifth section enunciates the sensitivity analysis for validating experimental data. The sixth part is the concluding part followed by the list of references. The appendices contain the illustrations, which showcase the stress, strain distribution.

II. LITERATURE SURVEY

Studying characteristics of cold upset forging of aluminum specimens have been a matter of considerable interest for the research fraternity. A number of publications have been made in this area of research interest. A few of them are enunciated here which bear some relevance to this work.

Banerjee [1] studied the axisymmetric loading of aluminum cylindrical work pieces for various aspect ratios and determined that the barreling profile approximates a circular arc and its radius follows a power law with true axial stress. He conducted the experiments with and without lubricant and proposed that forming energy is minimum with Teflon used as dry lubricant. Gupta and Shah [2] worked on deformation behavior of aluminum and low carbon steel short cylinders of various diameters and height to diameter ratios, loaded axially in a simple compression test without using any lubricant. The results of their work reveal that an arc of a circle can approximate the profile of a deforming specimen only after the onset of folding.

Narayanasamy and Pandey [3] conducted experiments to generate data on the upset forging of solid cylinders of annealed aluminum. The curvatures of the barreled aluminium cylinders measured physically were found to conform closely to the values calculated using the experimental data.

Malayappan and Narayanasamy [4] worked on cold upsetting of aluminum cylinders using die set with constraints. Malayappan and Narayanasamy [5] determined in their work that friction plays a major role in all bulk metalforming processes, except in a few isolated cases such as die-less wire drawing. Narayanasamy et al. [6] in their work generated data on cold upsetting of truncated cone billets of un lubricated and annealed commercial aluminum, copper and zinc alloys. Malayappan et.al [7] conducted experiments to generate data on the cold upset forging of solid cylinders of annealed aluminium using different lubricants with dies at both ends. Manisekar and Narayanasamy [8] conducted similar work on square and rectangular billets of aluminum.

Cetinarslan [9] studied the barreling phenomenon that occurs at the upsetting of a cylindrical specimen using aluminum 7075 and the effect of aspect ratio (h/d) on varying of a barrel contour were in this study. Progression of barreling contour and variation of total surface area according to the increase of barreling was investigated for different aspect ratios and friction value and surface roughness have been determined. Baskaran and Narayanasamy [10] carried out work to generate data on cold upset forging of commercially pure aluminum elliptical billets with white grease as lubricant applied on both sides in

order to evaluate the bulging characteristics. Baskaran and Narayanasmay[11] in their paper examined the effect of various stress ratio parameters on cold upset forging of commercially pure aluminium solid billets of irregular shapes using graphite mixed with oil as lubricant applied on both sides under plane and triaxial stress state conditions.

III. PROBLEM BACKGROUND

In this study deformation behavior of solid aluminium 6063 cylinders under axisymmetric compression over different aspect ratios without using any lubricants and without constraints are investigated. Data obtained in experimental work have been validated by conducting simulation using finite element method. Sensitivity analysis have been conducted to study barreling radius, load and strain, top surface area and the observations deduced will aid shop floor tooling and manufacturing in the area of upset forging. This is an important contribution of this work.

IV. EXPERIMENTAL STUDY

4.1 Blank Specification and Geometry

Aluminum 6063 is used in our study. This material is used for many applications in industry as it lends it self to cold formability. Cylindrical blanks of 25 mm diameter and six each of 25, 20 and 15 mm lengths were prepared for aspect ratios 1.0, 0.8 and 0.6 respectively. The undeformed blanks are shown in Fig.1. The chemical compositions of the specimen material is given in Table 1. The blank dimensions are detailed in Table 2.

Table 1

Chemical Composition of specimen material

Fe%	Si%	Cu%	Mn%	Mg%	Zn%	Tn%	Cr%
0.35	0.2-0.6	0.10	0.10	0.45	0.10	0.100.10	

Table 2

Specimen Details

Sl.n o.	Diameter (d)mm	Height (h)mm	Aspect ratio(h/d)	Blank number
1.	25	25	1.0	L1,L2,L3,L4,L5 and L6
2.	25	20	0.8	M1,M2,M3,M4,M5 and M6
3.	25	15	0.6	S1,S2,S3,S4,S5 and S6



Fig.1. Specimen of Aluminum 6063 for various aspect ratios- 1.0, 0.8 and 0.6

4.2 Experimental Set up

The experiments were carried out on a 10000 KN capacity Universal testing machine. The setup is shown in Fig.2.



Fig.2. Experimental Setup

4.3. Experiment Procedure

The upset forging tests were conducted at room temperature without lubrication. Blanks were cleaned before each trial. Extreme care is taken to place the blanks concentric with the axis of the machine ram. No lubricants were applied. Before

cold upsetting of the blanks, the initial dimensions such as original diameter (d_0) and original height (h_0) were measured. Listed hereunder was the experimental procedure carried out.

1. Place the blank in the machine table.
2. Apply load until desired upset ratio was obtained.
3. Load applied is noted down.
4. The following dimensions were measured before each experiment.
 - i. Original diameter
 - ii. Original height
5. The following dimensions were measured after each experiment
 - i. Upper diameter
 - ii. Major diameter of cylinder
 - iii. Height of the upset cylinder

Using Auto CAD 2007 software, barrel radius was measured. Fig.3a and 3b shows the front view of the billet before deformation and Fig.3c and 3d shows the shape after deformation.

Nomenclature

d_0 original diameter of a cylinder, mm

h_0 original height of a cylinder, mm

d_1 upper diameter of a cylinder, mm

h height of upset cylinder, mm

d_2 major diameter of a cylinder, mm R radius of barreling surface, mm

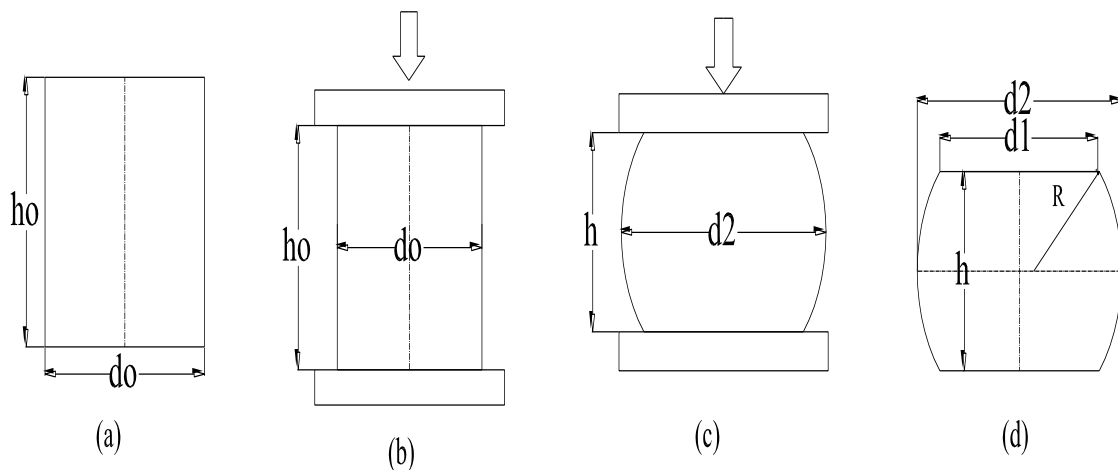


Fig.3. (a) Initial position, (b) Before deformation, (c) After deformation, (d) Final position

The blanks at different stages of upsetting for different aspect ratios and upset ratios are shown in fig.4.



Fig.4. Deformed specimen for various aspect ratios -1.0, 0.8 and 0.6

4.4. Results of Experiments

A comparison of the three aspect ratios, 1.0, 0.8 and 0.6 as illustrated in fig.5 led to the following observations.

Barrel Radius versus Upset Ratio

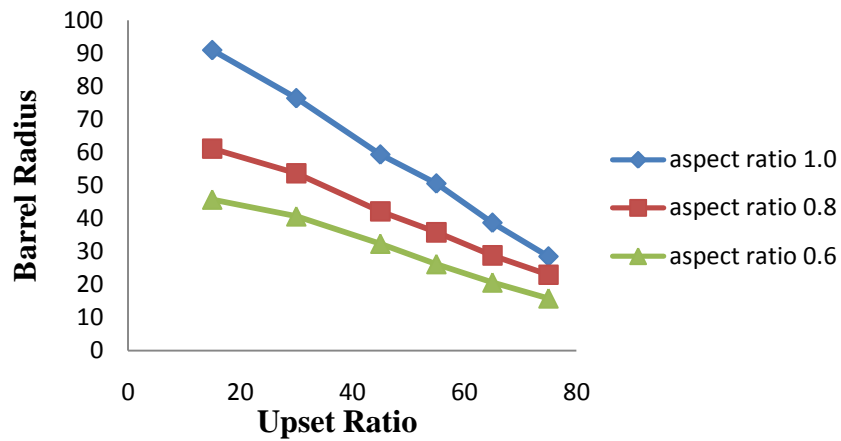


Fig.5. Variations of barreling radius vs. upsetting rate for aspect ratio - 1, 0.8 and 0.6.

Higher the aspect ratio higher upset ratios lead to lower barrel radius and at lower upset ratios results in higher barreling radius. For lower aspect ratios higher upset ratios lead to lower barrel radius and lower upset ratios results in relatively higher barrel radius. In general lower upset ratios results in higher barrel diameters for all aspect ratios. Fig.6 depicts the variation in top surface area for various upset ratios and aspect ratios.

Top Surface Area versus Upset Ratio

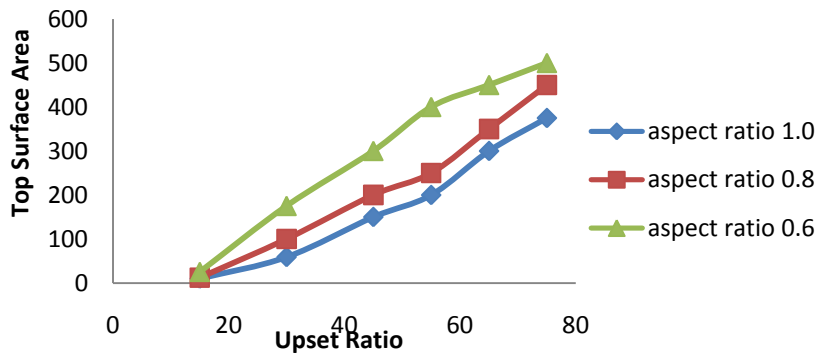


Fig.6. Variations of total surface area vsupsetting rate for the aspect ratio - 1.0, 0.8 and 0.6

Irrespective of aspect ratios the top surface area is higher for higher upset ratios and lower for lower upset ratios. Fig. 7 illustrates the relationship between load and strain. As it is common knowledge the strain is higher at higher loads and lower at lower loads irrespective of aspect ratios.

Load versus Strain

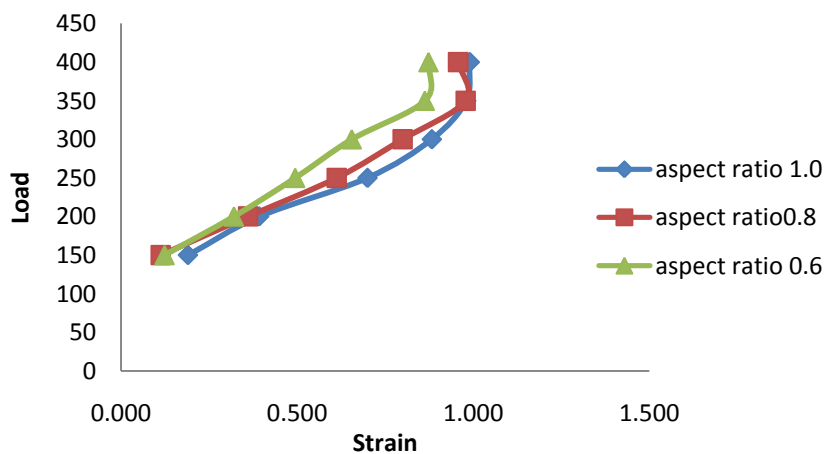


Fig.7. Variation of Load vs. Strain for aspect ratio-1.0, 0.8 and 0.6.

V. VALIDATION OF RESULTS

In order to validate the experimental results response surface method was employed to arrive at regression models and its coefficients employing the non-linear least squares (Full quadratic) method. Barreling radius was obtained as functions of upset ratio and aspect ratio and the barreling load was obtained as functions of aspect ratio and barreling radius. The regression analysis output is listed hereunder:

Estimated Regression Coefficients for barrel radius

Term	Coef	SECoef	T	P
Constant	41.655	26.7156	1.559	0.145
aspect	-94.044	66.2473	-1.420	0.181
upset	1.390	0.3543	3.923	0.002
aspect*aspect	152.849	41.7827	3.658	0.003
upset*upset	-0.017	0.0047	-3.585	0.004
aspect*upset	-1.726	0.3719	-4.642	0.001

Estimated Regression Coefficients for load

Term	Coef	SECoef	T	P
Constant	189.753	9.472	20.032	0.000
aspect	89.059	12.955	6.874	0.000
barrel	-206.872	18.629	-11.105	0.000
aspect*aspect	1.145	10.999	0.104	0.919
barrel*barrel	21.706	25.812	0.841	0.417
aspect*barrel	61.125	25.560	2.391	0.034

Fig.8 shows the variation of barreling radius as a function of aspect ratio and upset ratio.

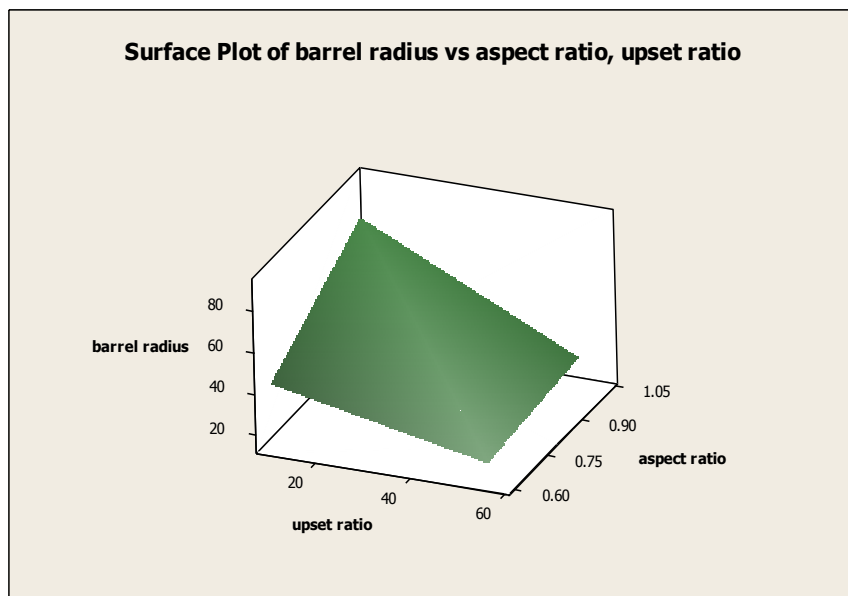


Fig.8. Barreling radius as a function of aspect ratio and upset ratio

The respective contour plot is shown in fig. 9.

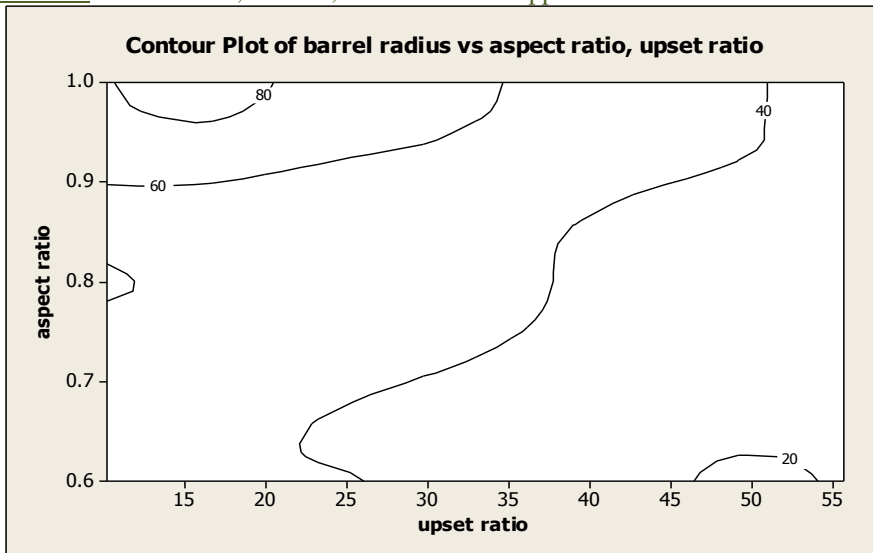


Fig.9. Contour plot for barreling radius as a function of aspect ratio and upset ratio.

Fig.10 shows the variation of load as a function of aspect ratio and barrel radius.

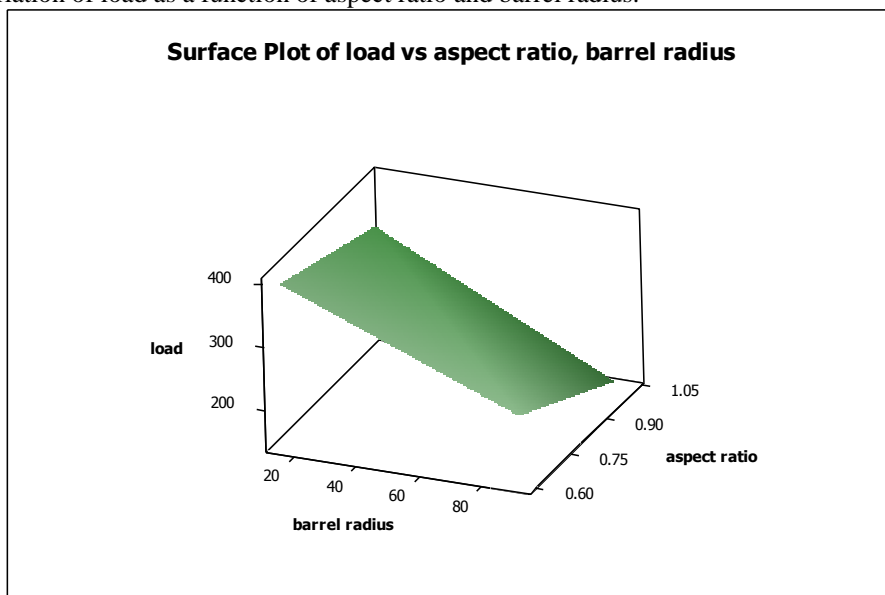


Fig.10. Load as a function of aspect ratio and barrel radius

The respective contour plot is shown in fig. 11.

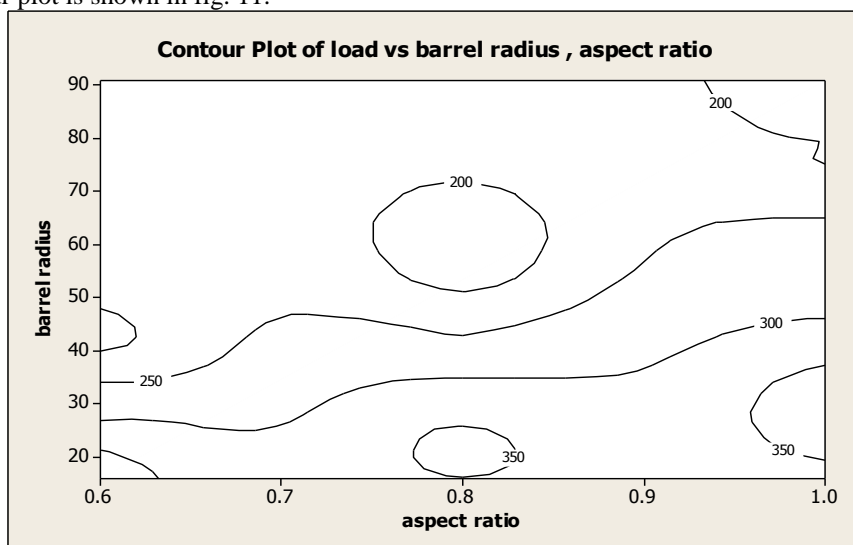


Fig.11. Contour plot for Load as a function aspect ratio and barrel radius

It can be seen that the increase in upset ratio is more pronounced compared to increase in aspect ratio resulting in increase in barrel radius as depicted in fig. 8. Likewise the increments of aspect ratio are more pronounced compared to load for increase in barrel radius.

Owing to Montgomery et al [12], the above contour plot suggests the regression equation,
 Barrel radius = $41.655 - 94.044 X \text{ aspect ratio} + 1.390 X \text{ upset ratio} + 152.849 (\text{aspect ratio})^2 - 0.017 (\text{upset ratio})^2 - 1.726 X \text{ aspect ratio} X \text{ upset ratio}$ and

Load = $189.753 + 89.059 X \text{ aspect ratio} - 206.873 X \text{ barrel radius} + 1.145 (\text{aspect ratio})^2 + 21.706 X (\text{barrel radius})^2 + 61.125 X \text{ aspect ratio} X \text{ barrel radius}$

$$R = 16.901 + 12.426 \times (h/d) + 0.406 \times e + 75.237 (h/d)^2 - 8.587 \times 10^{-4} \times e^2 - 1.35 \times (h/d) \times e \quad (1)$$

$$L = 577.131 - 129.902 \times (h/d) - 13.749 \times R + 72.585 \times (h/d)^2 + 0.013 \times (R)^2 + 8.550 \times (h/d) \times R \quad (2)$$

The comparison of experimental results is illustrated in fig.12.

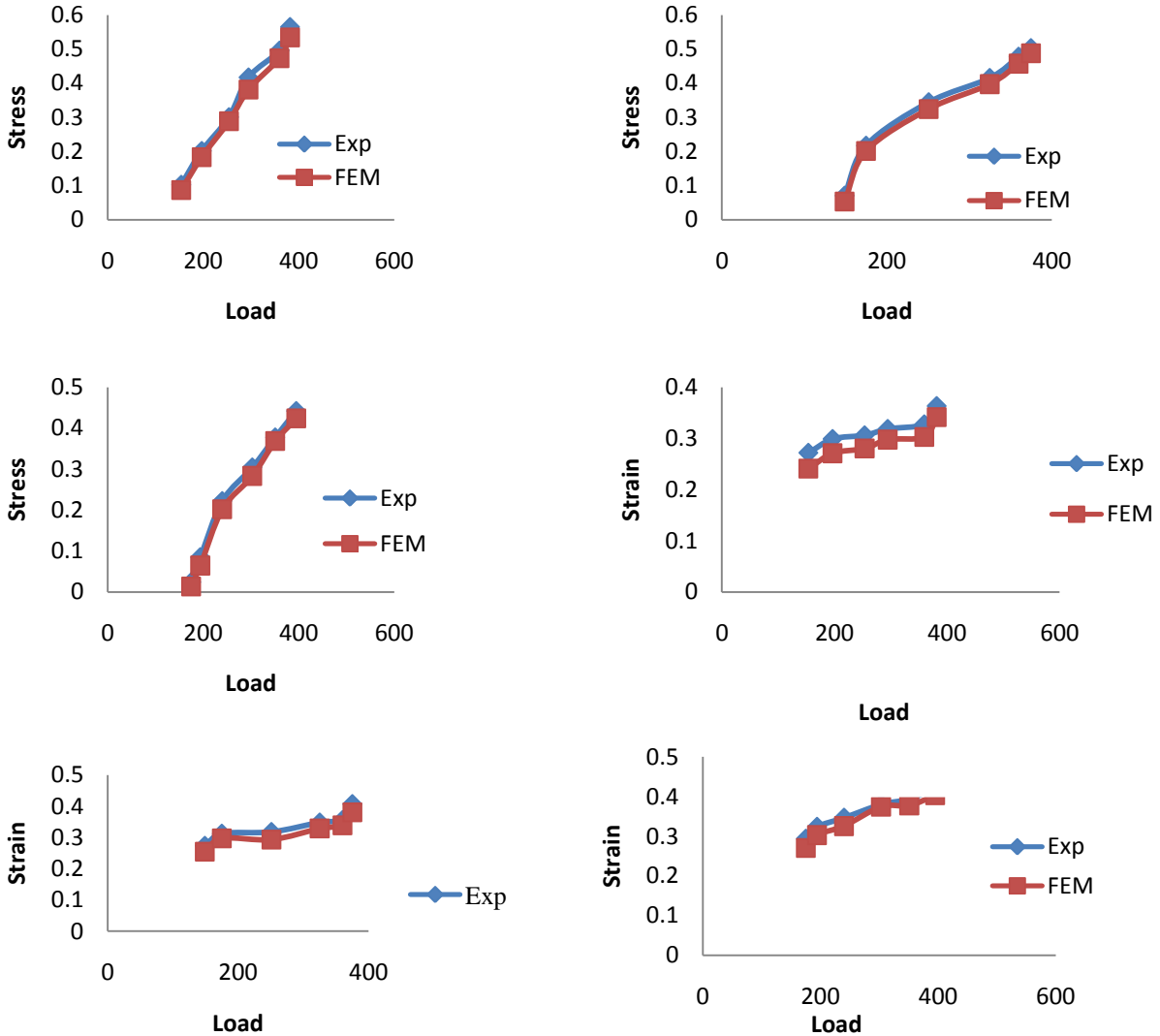


Fig.12. Comparison of experimental results and FEM values

It can also be seen from the illustration below that the experimental and simulated barrel radius are same.

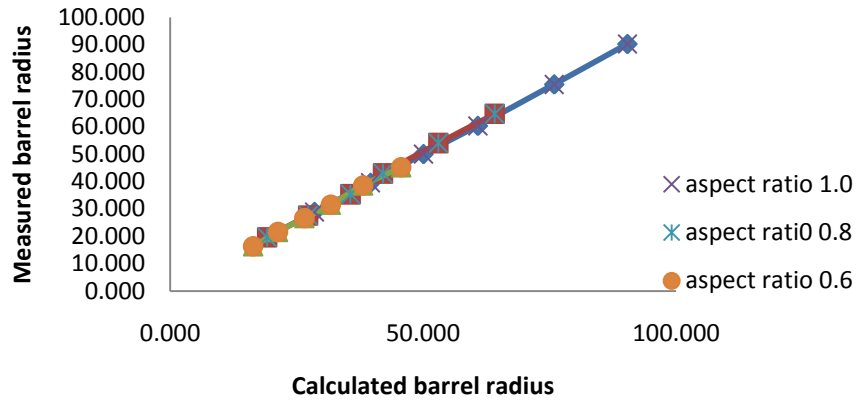


Fig.13. Graph of the measured barrel radius versus calculated barrel radius.

VI. SENSITIVITY ANALYSIS

Aluminum rivets and other fastening materials are widely used in industrial applications. The manufacturing process involves multistage production and progressive die operations. The top surface area is a critical dimension for the finished product, as it has to mate with the rivet hole. Many conclusions emanate from this study will facilitate tool design for rivets and fasteners. This study reveals that the surface area increases with increase in aspect ratio and upset ratio. There is no appreciable difference in characteristics between aspect ratio 0.6 and 0.8. There is a steep and linear increase in top surface area beyond upset ratio of 40 %. Relatively higher top surface area results for aspect ratio of 1.0 beyond upset ratio of 40 %. These are illustrated in Fig.14.

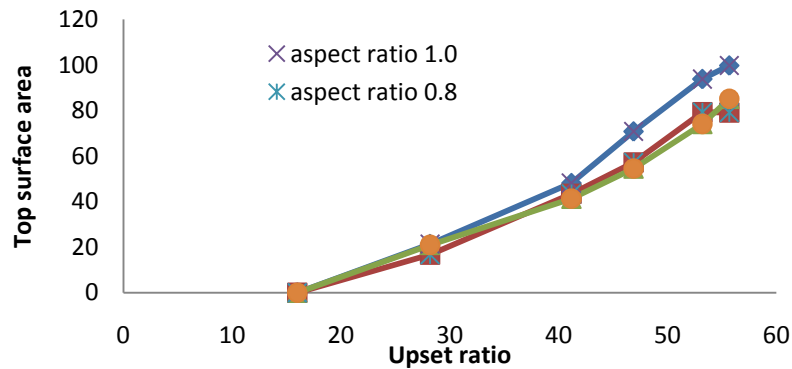


Fig. 14. Sensitivity graph of the Upset ratio versus Top surface area

The stress – strain characteristics by both experimental method and by simulation using finite element method shows that the increase in aspect ratios results in increase in strain. For upset ratios 20 % to 30 % there appears to be a characteristic plastic region. This is inferred as latent and sporadic work hardening. Similar phenomena are also observed in upset ratios 40 % to 50 %.

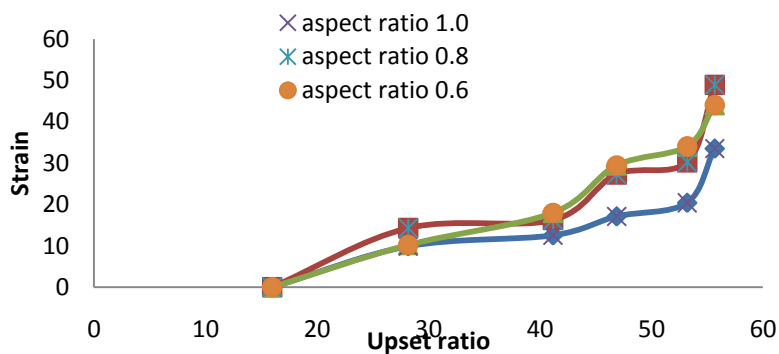


Fig.15. Sensitivity graph of the Upset ratio versus strain

A study of the sensitivity of barrel radius reveal that the barreling radius show a steep and linear decline until up to upset ratio of 40 % and further decline is observed to be non linear from 40 % to 50 %. Sudden drop in barrel radius is observed after upset ratios of 50 %.

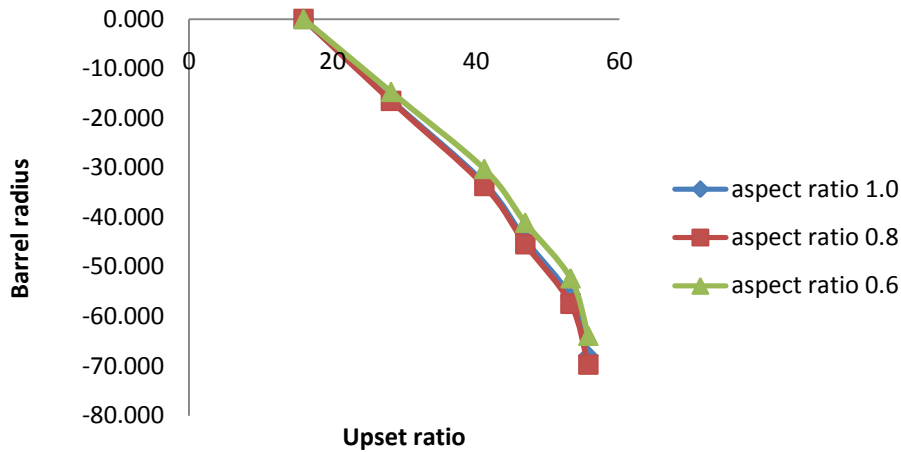


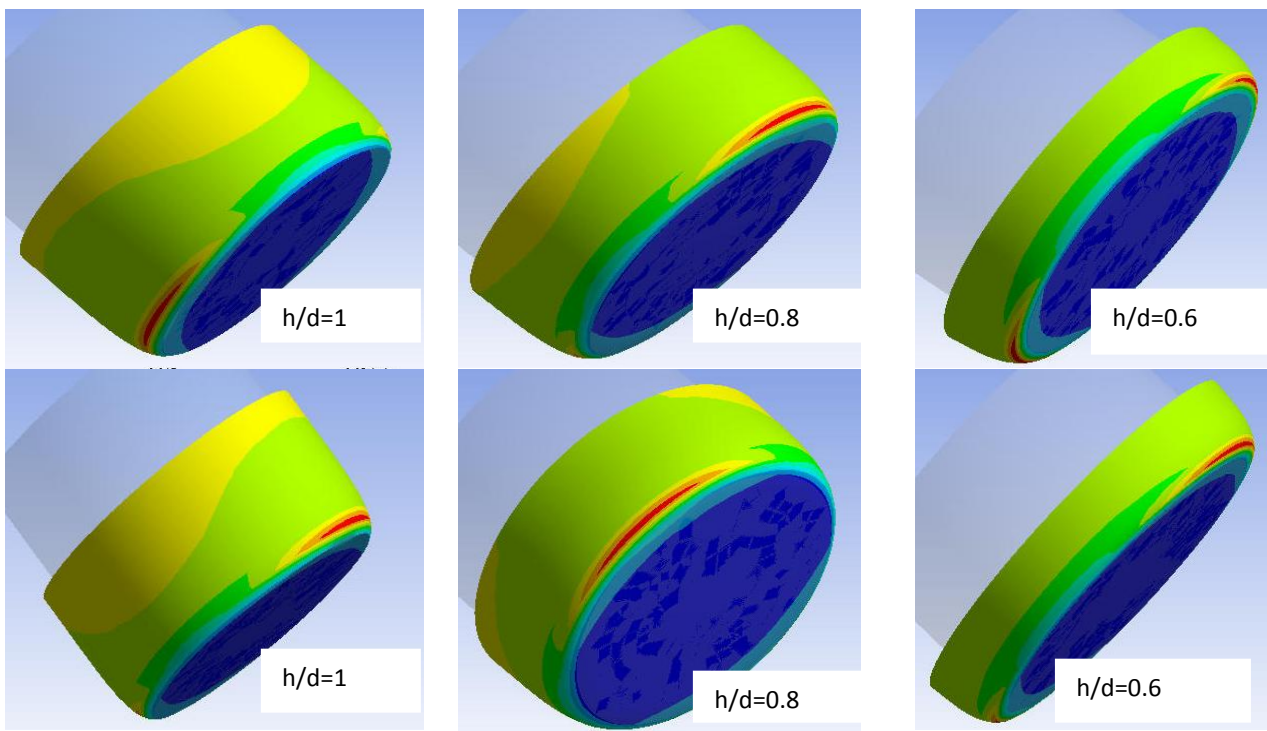
Fig.16. Sensitivity graph of the Upset ratio versus barrel radius
 Stress, strain distributions are illustrated in Appendix 1.

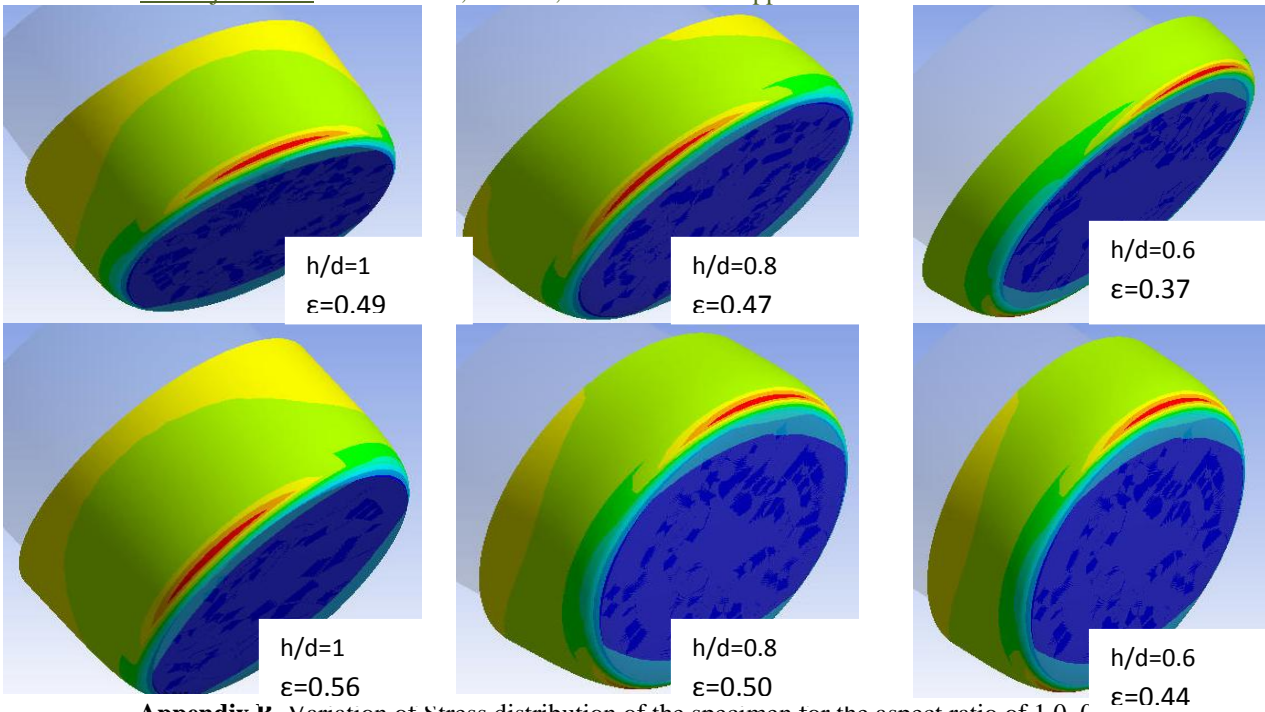
VII. CONCLUSIONS

In this work the characteristics of barreling radius, strain and top surface area have been studied for Aluminum 6063 material specimens. Some important inferences made will have direct application in shop floor production situations. The non linear changes in top surface area dimensions will form the basis in design of forging tools and design of statistical tolerance for the manufactured products. Intermittent work hardening inferred from no change in strain for increase in upset ratio will demand suitable increase in load requirements for forging process. The barreling radius behavior for various upset ratios will aid development of tooling and product design and development.

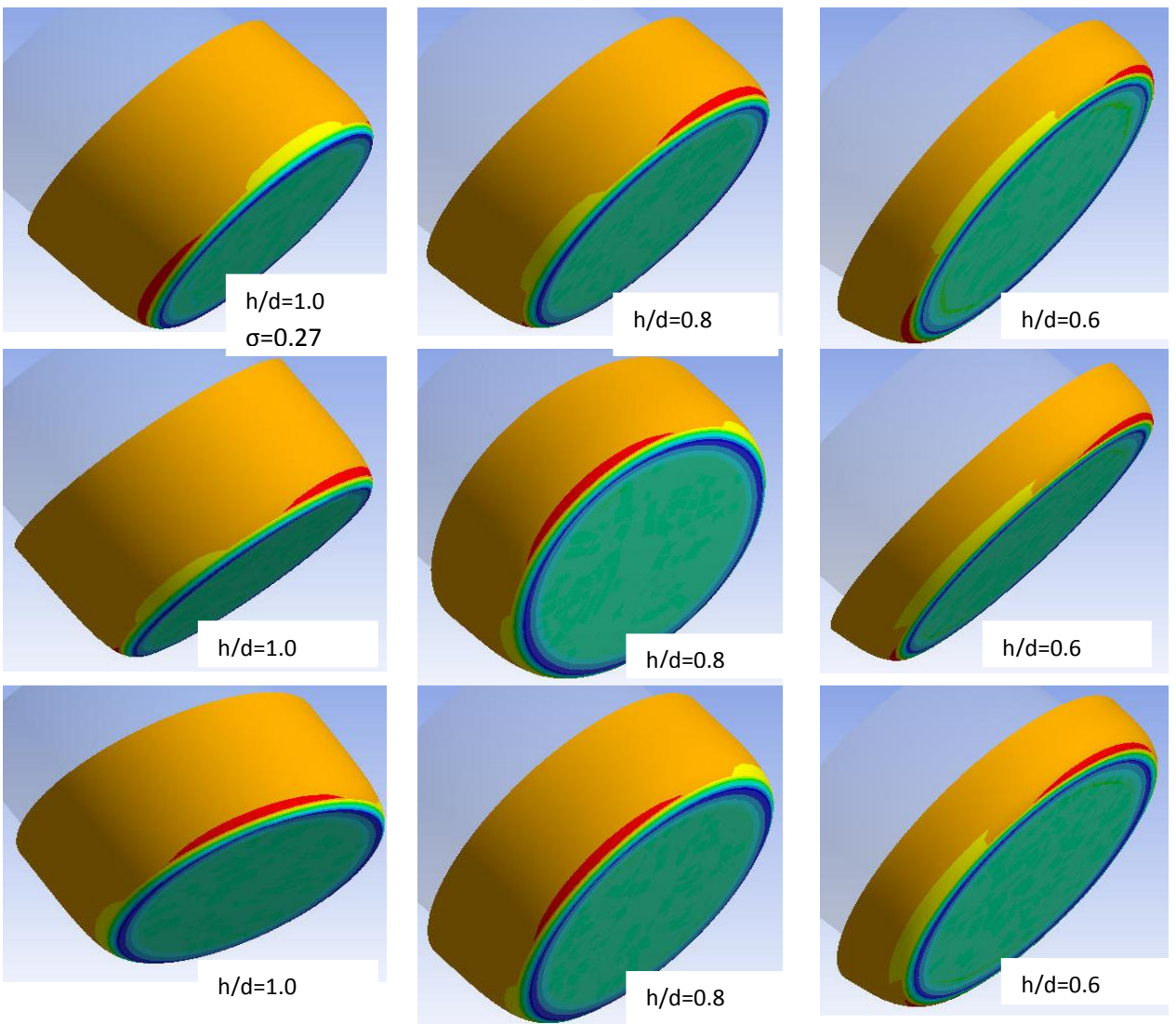
Further work exists in the areas of microscopic study of intermittent work hardening and study of parabolic behavior of changes in barreling radius and top surface area for aluminum 6063 material specimen

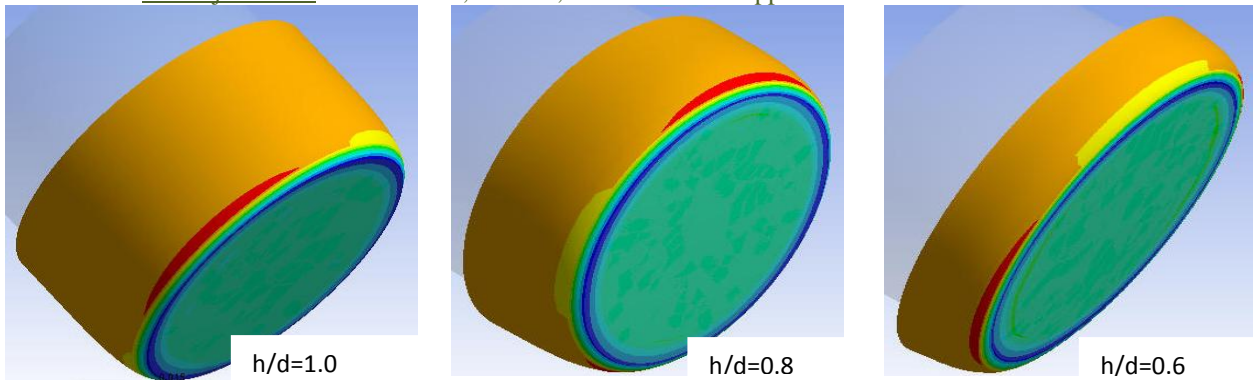
Appendix A Variation of Strain distribution of the specimen for the aspect ratio of 1.0, 0.8 and 0.6





Appendix B. Variation of Stress distribution of the specimen for the aspect ratio of 1.0, 0.8 and 0.6.





References

- [1] Banerjee JK. Barreling of solid cylinders under axial compression. *J Eng Mater Technology* 1985; 107:138-144.
- [2] Gupta NK, Shah CB. Barreling of a short cylinder in compression. *International Journal of Machine Tool Design Research* 1986; 26:137-146.
- [3] Narayanasamy R, Pandey KS. Phenomenon of barreling in aluminium solid cylinders during cold upset-forming. *J Mater Process Technol* 1997; 70:17-21.
- [4] Malayappan S, Narayanasamy R. Some aspects on barreling in aluminium solid cylinders during cold upset forging a die with constraints. *Journal of Materials processing technology* 2003; 135: 18-29.
- [5] Malayappan S, Narayanasamy R. An experimental analysis of upset forging of aluminium cylindrical billets considering the dissimilar frictional conditions at flat die surfaces. *Int J AdvManufTechnol*, 2004; 23: 636-643.
- [6] Narayanasamy R, Syed Abu Thaheer A, Baskaran K. Comparison of barreling in unlubricated truncated cone billets during cold upset forging of various metals. *Indian J of Engineering and Materials Sciences* 2006;13:202-208.
- [7] Malayappan S, Narayanasamy R, Esakkimuthu G. Barrelling of aluminium solid cylinders during cold upset forging with constraint at both ends. *Materials & Design* 2007;28:1404-1411.
- [8] Manisekar K, Narayanasamy R. Effect of friction on barreling in square and rectangular billets of aluminium during cold upset forging. *Materials& Design* 2007;28:592-598.
- [9] Cem S. Cetinarslan. Effect of aspect ratio on barreling contour and variation of total surface area during upsetting of cylindrical specimen. *Materials & Design* 2007; 28:1907-1913.
- [10] Baskaran K, Narayanasamy R. Some aspects of barreling in elliptical shaped billets of aluminum during cold upset forging with lubricant. *Materials& Design* 2008a; 29:638-661.
- [11] Baskaran K, Narayanasamy R. Effect of various stress ratio parameters on cold upset forging of irregular shaped billets using graphite as lubricant under plane and triaxial stress state conditions. *Materials& Design* 2008b;29:2089-2103
- [12] Montgomery DC, Peck EA, Vinin GC. *Introduction to Linear Regression Analysis*, 3rded. 2006 Wiley, India, New Delhi.

Mix Design of Fiber Reinforced Concrete (FRC) Using Slag & Steel Fiber

Mr. Nikhil A. Gadge¹, Prof. S. S. Vidhale²

¹Final Year Student (M.E. Structure) Prof. Ram Meghe Institute of Technology & Research Bandera, Amravati-444701, Maharashtra, India

²Professor Department Of Civil Engineering Prof. Ram Meghe Institute of Technology & Research Bandera, Amravati-444701, Maharashtra, India

Abstract: Concrete is probably the most extensively used construction material in the world. The main ingredient in the conventional concrete is Portland cement. The amount of cement production emits approximately equal amount of carbon dioxide into the atmosphere. Cement production is consuming significant amount of natural resources. That has brought pressures to reduce cement consumption by the use of supplementary materials. Availability of mineral admixtures marked opening of a new era for designing concrete mix of higher and higher strength. GROUND GRANULATED BLAST FURNACE SLAG (GGBS) is a new mineral admixture, whose potential is not fully utilized. Moreover only limited studies have been carried out in India on the use of slag for the development of high strength concrete with addition of steel fibers.

The study focuses on the compressive strength performance of the blended concrete containing different percentage of slag and steel fiber as a partial replacement of OPC. The cement in concrete is replaced accordingly with the percentage of 10 %, 20%, 30%, and 40% by weight of slag and 0.5%, 1%, 1.5%, 2% by weight of steel fiber. Concrete cubes are tested at the age of 3, 7, and 28 days of curing. Finally, the strength performance of slag blended fiber reinforced concrete is compared with the performance of conventional concrete. From the experimental investigations, it has been observed that, the optimum replacement of Ground Granulated Blast Furnace Slag Powder to cement and steel fiber without changing much the compressive strength is 20 % & 1.5 % respectively for M20, M30 & M40 grade resp.

Keywords: Concrete, GGBS, steel fibres, Compressive strength, UTM, CTM

I. INTRODUCTION

In the recent years, there is great development in the area of admixtures and now a day, the pozzolanic admixtures like fly ash, micro silica are commonly used to enhance performance characteristics of concrete. It is need of time to design and construct the structures which will have greater durability and strength and which have led to develop concept of high performance concrete. The major intension in developing high performance concrete is to have adequate resistance to aggressive environments and to make the structure impermeable. However, use of pozzolanic admixtures like micro silica adds to the cost of concrete which directly affects the cost of the project.

It is need to find out the substitute to micro silica without sacrificing the quality and performance of High performance concrete. One of the better alternatives to Micro silica is GGBS. Civil structures made of steel reinforced concrete normally suffer from corrosion of the steel by the salt, which results in the failure of those structures. Constant maintenance and repairing is needed to enhance the life cycle of those civil structures. There are many ways to minimize the failure of the concrete structures made of steel reinforce concrete. The custom approach is to adhesively bond fibre polymer composites onto the structure. This also helps to increase the toughness and tensile strength and improve the cracking and deformation characteristics of the resultant composite. But this method adds another layer, which is prone to degradation. These fibre polymer composites have been shown to suffer from degradation when exposed to marine environment due to surface blistering. As a result, the adhesive bond strength is reduced, which results in the de-lamination of the composite. The principal reason for incorporating fibres into a cement matrix is to increase the toughness and tensile strength, and improve the cracking deformation characteristics of the resultant composite. In order for fibre reinforced concrete (FRC) to be a viable construction material, it must be able to compete economically with existing reinforcing systems. As GGBS is good in resisting salt corrosion & chemical reactions it enhances the properties of FRC.

1.1 Ground Granulated Blast Furnace Slag (GGBS):

Ground granulated blast furnace slag or slag is the by-product of smelting ore to purify metals. They can be considered to be a mixture of metal oxides. However, they can contain metal sulphides and metal atoms in the elemental form. Slag is generally used as a waste removal mechanism in metal smelting but they can also serve other purposes such as assisting in smelt temperature control and to minimize re-oxidation of the final product before casting. Slag has a pozzolanic reaction which allows the increase of concrete strength. Slag has proven to produce very good and dense concrete allowing increased durability. it is observed from the studies, concrete made with GGBS continues to gain strength over time, and has been shown to double its 28-day strength over periods of 10 to 12 years.

1.2 Steel Fibres:

Plain concrete possesses a very low tensile strength, limited ductility and little resistance to cracking. Internal micro cracks are inherently present in the concrete and its poor tensile strength is due to the propagation of such micro cracks, eventually leading to brittle fracture of the concrete. It has been recognized that the addition of small, closely spaced and uniformly dispersed fibers to the concrete would act as crack arrester and would substantially improve its Compressive and

flexural strength properties. This type of concrete is known as fiber reinforced concrete. The crimped flat steel fibers were used in this study. The sizes (Length/aspect ratio) of the steel fibers are of 30mm/ 60.

II. Experimental study:

In order to achieve the stated objectives, this study was carried out in few stages. On the initial stage, all the materials and equipments needed must be gathered or checked for availability. Then, the concrete mixes according to the predefined proportions. Concrete samples were tested through concrete tests such as cube test. Finally, the results obtained were analyzed to draw out conclusion.

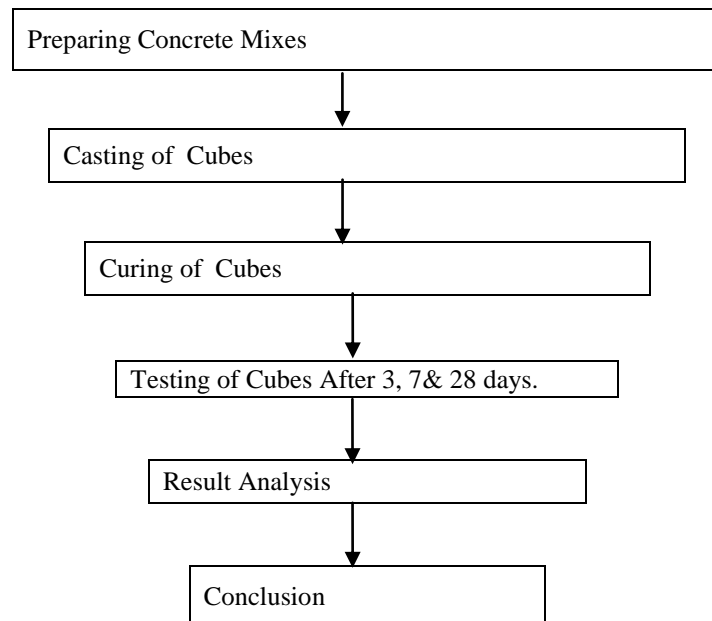


Figure3.1: Flow Chart of Experimental Program

High performance concrete was designed by using Indian Standard method. Trial control mixes for grades M20, M30, M40 grade concrete with replacement of cement by slag in concrete with different dosages i.e. 10%,20%,30%,40%. In addition of steel fibres with different dosages i.e. 0.5%, 1%, 1.5%, 2% respectively. The properties like compressive strength, flexural strength, split tensile strength of concrete using combinations of optimum values of slag and steel fibres are studied.

IS code method of mix design was used for mix design of M20, M30 &M40 grade of concrete. Concrete specimens with various percentages of slag & steel fiber were prepared. The details of various mix proportions for different replacement levels of cement by slag & steel fiber are shown in Table below.

Table 2.1: Details of concrete Mix Proportions for (M20) Grade of Concrete for slag

SN	Slag (%)	W/C Ratio	Mix Proportion (Kg/M ³)				
			Cement	slag	Sand	Agg.	Water
1	0	0.5	360	0	584	1224	180.42
2	10	0.5	324	36	584	1224	180.42
3	20	0.5	288	72	584	1224	180.42
4	30	0.5	252	108	584	1224	180.42
5	40	0.5	216	144	584	1224	180.42

Table 2.2: Mix Proportions for (M20) Grade for steel fiber

S N	S F (%)	W/C Ratio	Mix Proportion (Kg/M ³)				
			Cement	S f	Sand	Agg.	Water
1	0	0.5	360	0	584	1224	180.42
2	0.5	0.5	358.2	1.8	584	1224	180.42
3	1.0	0.5	356.4	3.6	584	1224	180.42
4	1.5	0.5	354.6	5.4	584	1224	180.42
5	2.0	0.5	352.8	7.2	584	1224	180.42

Table 2.3: Mix Proportions for (M20) Grade for optimum strength (slag & steel fiber)

S N	Slag+S F(%)	W/C Ratio	Mix Proportion (Kg/M ³)				
			Cement	Slag+S f	Sand	Agg.	Water
1	0	0.5	360	0	584	1224	180.42
2	20 + 1	0.5	284.40	72+3.6	584	1224	180.42

Table 2.4: Mix Proportions for (M30) Grade for slag

S N	Slag (%)	W/C Ratio	Mix Proportion (Kg/M ³)				
			Cement	slag	Sand	Agg.	Water
1	0	0.42	380	0	711	1283	160
2	10	0.42	342	38	711	1283	160
3	20	0.42	304	76	711	1283	160
4	30	0.42	266	114	711	1283	160
5	40	0.42	228	152	711	1283	160

Table 2.5: Mix Proportions for (M30) Grade for steel fiber

S N	S F (%)	W/C Ratio	Mix Proportion (Kg/M ³)				
			Cement	S f	Sand	Agg.	Water
1	0	0.42	380	0	711	1283	160
2	0.5	0.42	378.10	1.9	711	1283	160
3	1.0	0.42	376.20	3.8	711	1283	160
4	1.5	0.42	374.30	5.7	711	1283	160
5	2.0	0.42	372.40	7.6	711	1283	160

Table 2.6: Mix Proportions for (M30) Grade for optimum strength (slag & steel fiber)

S N	Slag+S F(%)	W/C Ratio	Mix Proportion (Kg/M ³)				
			Cement	Slag+S f	Sand	Agg.	Water
1	0	0.42	380	0	711	1283	160
2	20 + 1.5	0.42	298.30	76+5.7	711	1283	160

Table 2.7: Mix Proportions for (M40) Grade for slag

S N	Slag (%)	W/C Ratio	Mix Proportion (Kg/M ³)				
			Cement	slag	Sand	Agg.	Water
1	0	0.40	400	0	660	1168	160
2	10	0.40	360	40	660	1168	160
3	20	0.40	320	80	660	1168	160
4	30	0.40	280	120	660	1168	160
5	40	0.40	240	160	660	1168	160

Table 2.8: Mix Proportions for (M40) Grade for steel fiber

S N	S F (%)	W/C Ratio	Mix Proportion (Kg/M ³)				
			Cement	S f	Sand	Agg.	Water
1	0	0.40	400	0	660	1168	160
2	0.5	0.40	398	2	660	1168	160
3	1.0	0.40	396	4	660	1168	160
4	1.5	0.40	394	6	660	1168	160
5	2.0	0.40	392	8	660	1168	160

Table 2.9 Mix Proportions for (M40) Grade for optimum strength (slag & steel fiber)

S N	Slag+S F(%)	W/C Ratio	Mix Proportion (Kg/M ³)				
			Cement	Slag+Sf	Sand	Agg.	Water
1	0	0.40	400	0	660	1168	160
2	20 + 1.5	0.40	314	80+6	660	1168	160

Tests and Results Interpretation: A number of tests were carried out to ascertain the design mix properties of concrete in the laboratory.

These tests are based on strength as well as durability concern. The overall performance of any concrete is measured on the basis of mainly two criteria's viz strength and durability of hardened concrete. In case of HPC, strength is major governing attribute whereas durability is a measure of performance. In the present work, the strength of the hardened concrete is ascertained.

The strength criterion includes measurement of following parameters:

- Compressive Strength on cubes
- Flexural Strength
- Split Tensile Strength on Cylinders

Compressive Strength Test:

Compressive strength test is carried out on specimen cubes of concrete blended with various percent replacements to cement by GGBS & steel fiber (varying percentages) and conventional concrete at 3, 7 and 28 days of curing with compression testing machine. Optimized Results of Trial Mixes are as shown in tables from the results of trial mix, it is seen that the compressive strength of Concrete for all percentage remains nearly same with replacement of cement by GGBS and S F and found maximum for 20% and 1.5% slag & S F respectively replacement of cement.

After testing the concrete (compressive strength) for M20, M30 & M40 grade concrete separately for replacement of slag & steel fiber by cement respectively finally combined percentage of slag & steel fiber mix in which maximum strength is obtained was used to get optimized strength.

Optimized % of Slag & Steel Fiber for Compressive Strength of Concrete

Table 4.10:-compressive strength of cube for M-20 Grade (20 % SLAG & 1 % STEEL FIBER)

SN	% Of Slag & Steel Fiber		Compressive Strength (N/mm ²)		
			3 days	7 days	28days
1	0	0	9.35	17.12	26.33
2	20	1	7.15	15.39	25.25

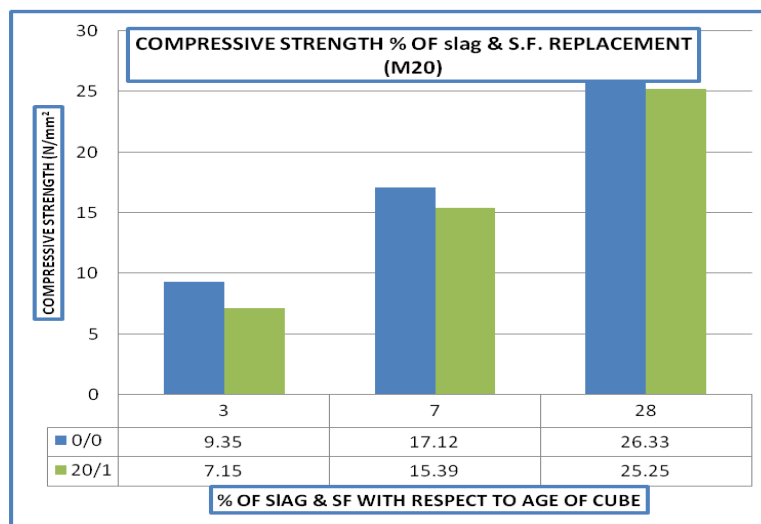


Figure 4.7: Optimized % of Slag & Steel Fiber for Compressive Strength (M20)

Table 4.11:-compressive strength of cube for M-30 Grade (20 % SLAG & 1.5 % STEEL FIBER)

SN	% Of Slag & Steel Fiber		Compressive Strength (N/mm ²)		
			3 days	7 days	28days
1	0	0	12.07	22.39	34.27
2	20	1.5	14.55	21.00	33.48

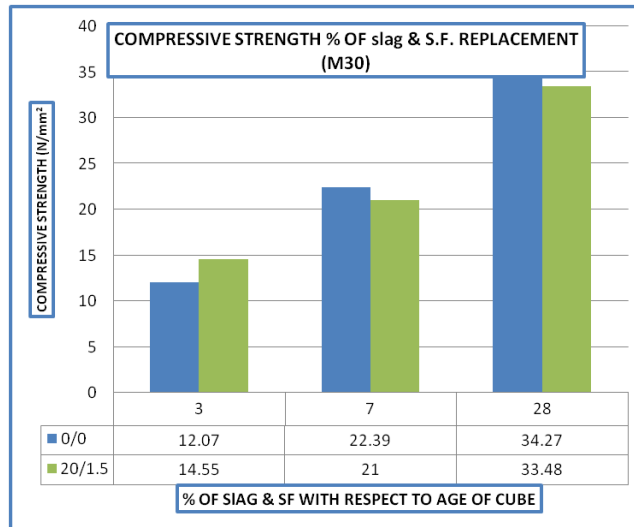


Figure 4.8: Optimized % of Slag & Steel Fiber for Compressive Strength (M30)

Table 4.12:-compressive strength of cube for M-40 Grade (20 % SLAG & 1.5 % STEEL FIBER)

SN	% Of Slag & Steel Fiber		Compressive Strength (N/mm ²)		
			3 days	7 days	28days
1	0	0	16.03	31.20	44.59
2	20	1.5	15.90	28.73	45.67

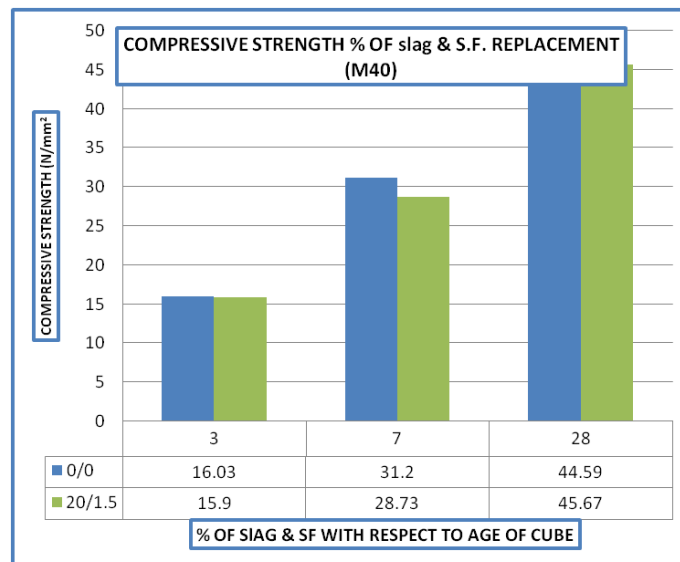


Figure 4.9: Optimized % of Slag & Steel Fiber for Compressive Strength (M40)

For partial replacement of cement with slag (20%) + Steel fiber (1.5%) fiber reinforced concrete got maximum compressive strength as compared to conventional concrete, the strength development of the concrete is increases slightly as its age increases. This can be clearly shown in above figures for all the three grades.

Flexural strength test on Beam

For finding flexural strength of concrete beam, load is applied uniformly on beam. The load was increased until the specimen fails, and maximum load applied to the specimen during the test, was recorded. Table below shows results of flexural strength test.

After testing the concrete (flexural strength) for M20, M30 & M40 grade concrete separately for replacement of slag & steel fiber by cement respectively finally combined percentage of slag & steel fiber mix in which maximum strength is obtained was used to get optimized strength.

OPTIMIZED % OF SLAG & STEEL FIBER FOR FLEXURAL STRENGTH OF CONCRETE

Table 4.19:- Flexural strength for M-20 Grade (20 % SLAG & 1.5 % STEEL FIBER)

SN	% Of Slag & Steel Fiber		Flexural Strength (N/mm ²) 28days
1	0	0	5.30
2	20	1.5	6.38

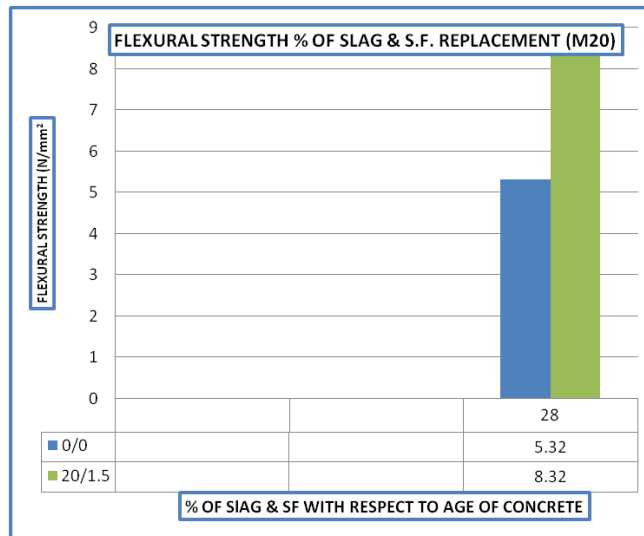


Figure 4.16: Optimized % of Slag & Steel Fiber for Flexural Strength (M20)

Table 4.20:- Flexural strength for M-30 Grade (20 % SLAG & 1.5 % STEEL FIBER)

SN	% Of Slag & Steel Fiber		Flexural Strength (N/mm ²) 28days
1	0	0	6.07
2	20	1.5	7.61

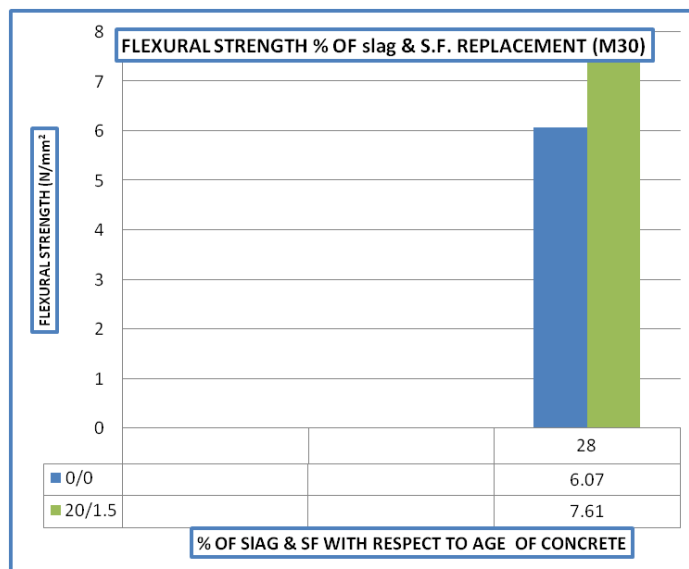


Figure 4.17: Optimized % of Slag & Steel Fiber for Flexural Strength (M30)

Table 4.21:- Flexural strength for M-40 Grade (30 % SLAG & 2 % STEEL FIBER)

SN	% Of Slag & Steel Fiber		Flexural Strength (N/mm ²) 28days
1	0	0	5.32
2	30	2	8.32

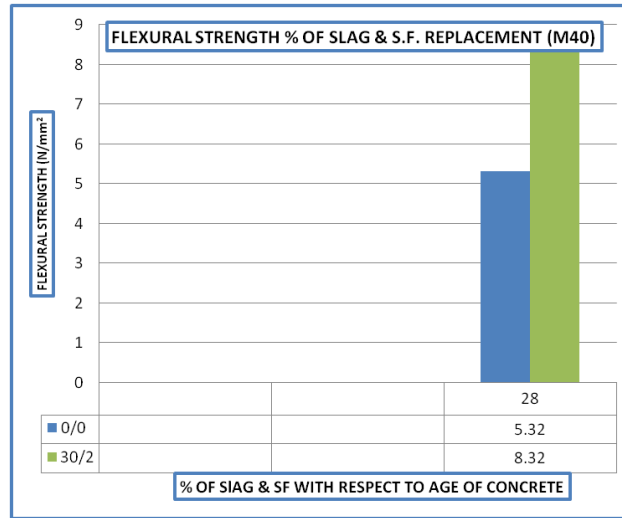


Figure 4.18: Optimized % of Slag & Steel Fiber for Flexural Strength (M40)

For partial replacement of cement with slag (20%) + Steel fiber (1.5%) fiber reinforced concrete got maximum flexural strength as compared to conventional concrete, the strength development of the concrete is increases slightly as its age increases. This can be clearly shown in above figures for all the three grades

4.2.3 Cylinder split tensile strength test

By conducting splitting tensile strength on cylinder following results were obtained which is given in table. After testing the concrete (split tensile strength) for M20, M30 & M40 grade concrete separately for replacement of slag & steel fiber by cement respectively finally combined percentage of slag & steel fiber mix in which maximum strength is obtained was used to get optimized strength.

OPTIMIZED % OF SLAG & STEEL FIBER FOR SPLIT TENSILE STRENGTH OF CONCRETE

Table 4.28:- Split tensile strength for M-20 Grade (20 % SLAG & 2 % STEEL FIBER)

SN	% Of Slag & Steel Fiber		Tensile Strength (N/mm ²) 28days
1	0	0	2.01
2	20	2	3.22

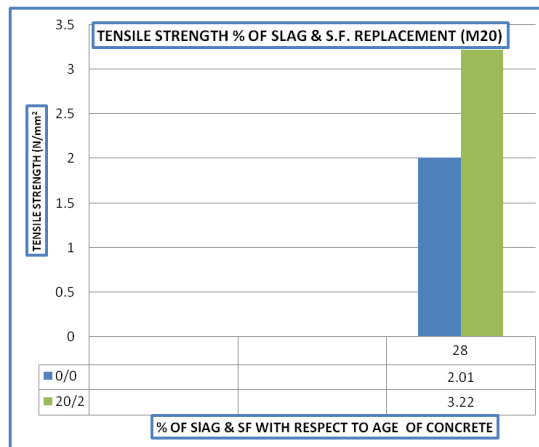


Figure 4.25: Optimized % of Slag & Steel Fiber for Tensile Strength (M20)

Table 4.29:- Split tensile strength for M-30 Grade (30 % SLAG & 1.5 % STEEL FIBER)

SN	% Of Slag & Steel Fiber		Tensile Strength (N/mm ²) 28days
1	0	0	3.32
2	30	1.5	5.27



Figure 4.26: Optimized % of Slag & Steel Fiber for Tensile Strength (M30)

Table 4.30:- Split tensile strength for M-40 Grade (20 % SLAG & 1.5 % STEEL FIBER)

SN	% Of Slag & Steel Fiber		Tensile Strength (N/mm ²) 28days
1	0	0	4.27
2	20	1.5	7.1

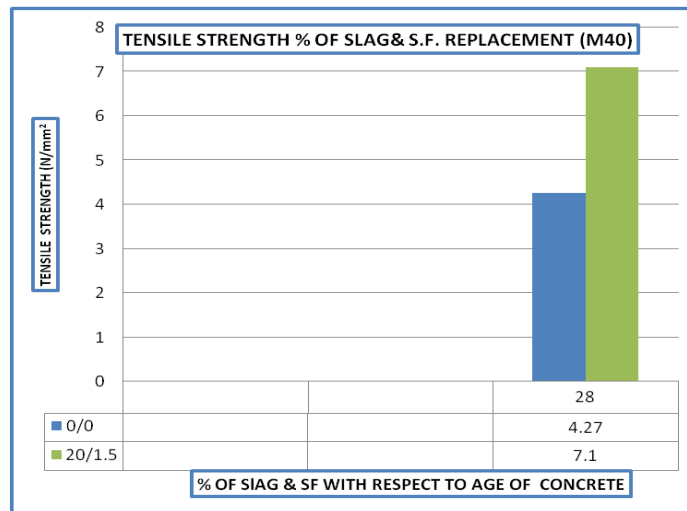


Figure 4.27: Optimized % of Slag & Steel Fiber for Tensile Strength (M40)

For partial replacement of cement with slag (20%) + Steel fiber (1.5%) fiber reinforced concrete got maximum split tensile strength as compared to conventional concrete, the strength development of the concrete is increases slightly as its age increases. This can be clearly shown in above figures for all the three grades

II. CONCLUSION

- 1) The optimum dosage for partial replacement of cement by ground granulated blast furnace slag is 20%
- 2) The optimum dosage for addition of steel fibred is 1.5%

- 3) The percentage of increase in compressive strength for M20, M30 & M40 grade for partial replacement of cement by GGBS (20%) + addition of steel fibred (1.5%) are nearly same for M20, M30 & 2.4% for M40 respectively for 28 days of curing.
- 4) The percentage of increase in flexural strength for M20, M30 & M40 grade for partial replacement of cement by GGBS (20%) + addition of steel fibred (1.5%) are 20.37%, 25.37% & 56.39% respectively for 28 days of curing.
- 5) The percentage of increase in split tensile strength for M20, M30 & M40 grade for partial replacement of cement by GGBS (20%) + addition of steel fibred (1.5%) are 60.19%, 58.73% & 66.27% respectively for 28 days of curing
- 6) The rate of gain of compressive strength of GGBS concrete is slow in the initial Stage i.e. up to 14 days & as the curing period increases strength also increases.
- 7) Test results reveal that higher fiber content has brought about increased compressive strength, flexural strength, abrasion resistance, and fiber crack-control effect. Hence the addition of steel fiber within FRC is more helpful for the flexural strength than the compressive strength.

References

- [1] SUSAN, BERNAL; RUBY, DE GUTIERREZ; SILVIO, DELVASTO; ERICH, RODRIGUEZ. Escuela de Ingeniería de Materiales, Grupo de Materiales Compuestos, CENM, Universidad Del Valle. Ciudad Universitaria Meléndez, AA 2188, Cali, Colombia
- [2] PAL, S.C, MUKHERJEE, A. and PATHAK, S.R,(2001) Development of high performance concrete composites using high volume cement replacement with supplementary pozzolanic and cementations solid waste, Proceeding ,Recent Developments in Structural Engineering, SERC, IIT Roorkee pp.215-229.
- [3] Collepardi M,(1994) “Super plasticizers and entraining Agents State of the art and future needs”, concerti Technology Past present and future, Proceedings of V. Mohar Malhotra symposium, 1994. ACI SP-144, pp.399-416.
- [4] C.D. Johnston (1982), “Definition and measurement of flexural toughness parameters for fiber reinforced concrete” Cem. Concr. Agg. 1982.
- [5] Vikrant S. Variegate, Kavita S. Kene (2012), “Introduction to Steel Fiber Reinforced Concrete on Engineering Performance of Concrete” International Journal of Scientific & Technology Research Volume 1, Issue 4, May 2012.
- [6] M.S Shetty Concrete Technology, Reprint (2003) S. Chand & Co. New Delhi.
- [7] Ramakrishna. V (1987), “Materials and Properties of Fiber Reinforced Concrete” – Proceedings of the international symposium on FRC, Madras.
- [8] Fibre Reinforced Concrete <http://www.latech.edu/~guice/ReinforcedCon/Papers/Perkins.htm>, January 29, 2001.
- [9] Ed. V .M. Malhotra and P.K Mehta,(1996) “ Pozzolanic and Cementations Materials”, Gordon publishers IS: 10262-1982: Recommended Guideline for concrete mix design

Cluster computing performance in the context of non extensive statistics

Paweł Dymora¹, Mirosław Mazurek¹, Rafał Gawron¹

¹(Department of Distributed Systems, Rzeszow University of Technology, Poland)

Abstract: This work presents the problem of clusters computing performance in the context of nonextensive statistics. Simulation studies have demonstrated that the cluster computing process is self-similar or long-range dependent and the Hurst coefficient estimation can be used to specify computing performance. The paper presents a comparison of several methods for estimating Hurst coefficient, characterized by simplicity of implementation and convergence results.

Keywords: long-memory effect, complex system, cluster, stationarity, Hurst coefficient, nonextensive statistics

I. INTRODUCTION

Nowadays, computers are an integral part of our lives. We are witnessing a significant technological progress and the creation of more and more new services. We have more and more efficient devices, and today mobile phones have the computing power comparable to that recently used servers. The demand for computing power continues to increase, and when individual servers are not able to provide us with the required level of service, are combined into groups called clusters. One group of clusters, providing high computing power are HPC clusters (*High Performance Computing*) [8, 10]. They represent an important part of business, economy, industry and science. The offered range of its possibilities is very wide but the demand for computing power continues to grow. Initially used for the calculation of individual servers, later mainframes and when they also were not sufficient it began to connect servers in a clusters. An important feature associated with the performance of the entire computing system is adequate assessment of its effectiveness and efficiency. It should be noted that not only the architecture and interrelationships of the various elements on the physical level is important, but the operating environment and the software is also important. Moreover, the input data used in the computation must be specially prepared to obtain maximal computation power of the cluster. Therefore, in addition to attempts of building and configuration of the efficient computing cluster a very important part is carrying out of various performance tests. However, we come to the point where adequate analysis of the obtained simulations results is a key element [7, 9, 10].

The computer or cluster systems consists of many interdependent subsystems. There are two possible approaches for their analysis. The first one is based on the idea of reductionism proposed by Descartes **Error! Reference source not found.** and can be considered as a still ruling paradigm in the case of computer science and engineering. The second one can be related to the still new idea of the complex systems approach, where in order to understand the behaviour of such systems one needs to have the knowledge about behaviour of system components and also, that is more important, how they act together [4, 5]. This specific paradigm change can be even shown in the case of the idea of Turing machines and new approach for considerations in the case of interactive processing – even the opinion that “*the computer engineering is not a mathematical science*” was presented. It should be noted that Turing machine is a mathematical idea while its implementations are the physical ones, but if the physical nature of computer systems was indicated, there is a need to have an appropriate physical (thermodynamical) basis for deliberations in such a case [2, 5]. In [11] it has been shown that the analysis of processes in computer systems can be based on non-extensive thermodynamics. However, this analysis considers only spatial correlations, meanwhile in this paper we will focus cluster computing performance in the context nonextensive statistics [6].

II. METHODOLOGY OF THE SYSTEM RESEARCH

The article presents results of the research on the analysis of the computational load on the cluster system in the context of nonextensive statistics. The obtained results allow to specify the characteristics of the system with regard not only to its hardware architecture or software, but also in relation to the processed input. In this context, we can say that the computing system presents the characteristics of a complex or simple system which has a direct impact on the understanding of the processes occurring in it. The result in knowledge can be used to optimize the entire computing system and its subsystems. The complex system is a theorem difficult to unambiguously explain. It is a system which consists of many diverse and autonomous, but mutually related and interdependent components joined together. It can be characterized by properties not directly arising from its basic components, making it difficult or even not possible to describe using the methods of classical physics or mathematics. Research on the analytical description methods of systems with very large amounts of data and properties led to the creation of statistical mechanics based on the self-similarity. Using these methods we are indeed able to accurately answer and calculate the specific properties, but with a certain probability and precision we can answer a series of questions related to our system. We have to agree with the statement of the Aristotle: “*The whole is more than the sum of the parts*” which, in relation to the subject of complex systems makes us aware that the systems are non-additive and non-linear. It is difficult to predict the effects of complex systems behaviour because the overall results are very sensitive to initial data and small noise [1, 3]. The system is constantly evolving and changing, and the number of interactions between the system elements causes that for the characteristics calculations in this type of systems we use probabilistic methods. In order to determine whether we are dealing with a complex or simple system we must consider three statistical properties of the system: stationarity, autocorrelation and self-similarity index [3].

The first examined property of the system is stationarity. In the simplest terms, the process can be called stationary if examining its properties at any time will have the same value. We can distinguish strict stationarity and stationarity in a wide range. Time series are strictly stationary if for any allowable data $\{t_1, \dots, t_k\}$ and any $h \in Z$ cumulative set $\{x_{t_1}, \dots, x_{t_k}\}$ distribution is identical to the set $\{x_{t_1+h}, \dots, x_{t_k+h}\}$ distribution. For the strict stationarity appears that the mean value and variance (also called variation measure) are constant in time. The time series with finite variance is weakly stationary or otherwise called stationary over a wide range if the average of its elements μ_t is constant in time and autocovariance $\gamma(s, t)$ depends only on the difference $h = |t - s|$. Stationarity condition in a wider sense of random process is that the first and second moment would not change in time. In other words, if successive values change in time [5, 11].

Another analysed parameter is the autocorrelation. Autocorrelation is a statistical tool for analysing the function describing the degree of a given time series elements depends on previous values in the same time series. In statistics, the autocorrelation of a random process describes the process correlation at different time points. When x_t the value of the process in time t is equal to μ and variation σ^2 then formula to determine the autocorrelation can be represented as:

$$R(t, s) = \frac{E[(X_t - \mu)(X_s - \mu)]}{\sigma^2}$$

Self-similarity index also known as Hurst coefficient is a real number taking values from 0 to 1. Describes the behaviour of the process in time and is associated with the autocorrelation and fractal dimension. However, it is problematic, to precisely calculate it so that we are talking about the coefficient estimation value. There are many computation methods which with different efficiencies allow to estimate the value of the index. Hurst exponent can be seen in three cases [3]:

1. $H = 0.5$ means that between the values of the tested time series, there is no correlation, the values are random.
2. $H > 0.5$ means that process has long-term relationships. Such a case is called persistent with positive autocorrelation and represents situations where there has been an increase in the value of the time series and there is a likelihood of its recurrence equal to H .
3. $H < 0.5$ analogous case of anti-persistent behaviour and the value increase is likely to be preceded by a decline.

Hurst exponent studies can be performed with four methods: absolute moments, aggregated variance, periodogram and method of residuals of regression. The method of absolute moments creates the aggregated time series of the original time series $X = \{X_i, i \geq 1\}$ by dividing into blocks of size m and averaging operation:

$$X^m(k) = \frac{1}{m} \sum_{i=(k-1)m+1}^{km} X(i)$$

where $X^m(k)$ denotes the aggregated time series and k is the index of the block. Then, for the prepared data the sum of absolute moments of the aggregated time series is calculated with the following formula:

$$\frac{1}{N/m} \sum_{k=1}^{N/m} |X^m(k)|$$

where N is the number of data in the tested series.

Method of aggregated variance unlike the previous implies that instead of calculating the sum of the absolute moments of aggregated series, calculate the variance of sampling rate according to the formula:

$$Var X^{(m)} = \frac{1}{N} \sum_{k=1}^N (X^{(m)}(k))^2 - \left(\frac{1}{N} \sum_{k=1}^N (X^{(m)}(k)) \right)^2$$

Calculations using the residuals of regression begin with data division on the blocks with size m , and within each block we calculate sum of partial data which will be marked as: $Y(i), i = 1, 2, \dots, m$. Then, the obtained results must match the trend line calculated by least square method. In this case the residual is calculated as the point of deviation from a given reference point in a created trend line. Residuals sampling variance is calculated with the following formula:

$$Var = \frac{1}{m} \sum_{i=1}^m (Y(i) - i * a - b)^2$$

where a and b are coefficients of the fit line. The obtained results should be averaged for large m , the calculation result is proportional to m^{2H} [5, 11].

Periodogram method has a different approach than presented in the previous examples. In this case, the Fourier transform is used for the obtained frequency dependence data. Statistics called periodogram generate the following formula:

$$I(\lambda) = \frac{1}{2\pi N} \left| \sum_{j=1}^N X_j e^{ij\lambda} \right|^2$$

III. HPC CLUSTER CONFIGURATION

The first task in order to examine the cluster computing performance with the use of nonextensive statistics was to

build the HPC cluster and perform a series of tests to gain data for further analysis. For the base cluster nodes we selected following machines: the Sun Fire X4270 and Sun Blade X6240. The cluster is based on the Beowulf architecture [9], combining servers with different processor architecture. This carries the risk associated with the uneven work of both servers and thus also lowers results in some performance tests. However, it permits building of universal cluster configuration which does not require the configuration of specialized and identical devices. Both servers are connected to a Gigabit Ethernet network with the use of the following device: Alcatel OmniSwitch 6850. The required network bandwidth for configuration and testing of designed cluster is 1 Gb/s. The less network bandwidth prevents from using the full CPU computing power, creating a bottleneck of the system. Figure 1 shows a logical diagram of the designed HPC cluster.

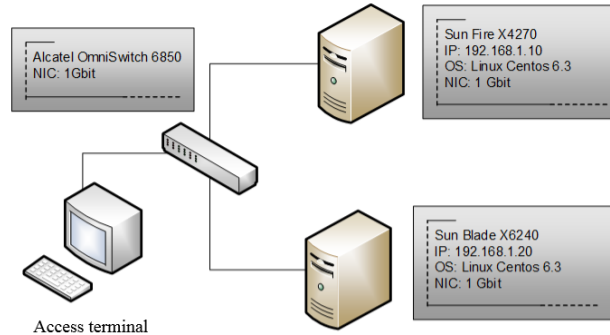


Fig. 1. The designed HPC cluster configuration schema.

IV. RESULTS OF INVESTIGATIONS

In this section we present the calculation of the statistical properties of the cluster computing system on the base of data collected during performance tests. We want to obtain the information whether the cluster computing system has the characteristic of the complex or the simple system. In order to do this we must determine few statistical features of the system on the base of its computation process characteristics. The first examined feature was to determine whether the process is a stationary or not. The study uses data in the form of system load time series. Analysing the stationarity chart presented in Fig. 2 the first visible thing is that characteristics of the graph is similar to the original load chart based on the performed computing system load analysis.

Graph presented in Fig. 2. shows that our tested process is not stationary. In addition to stationary graph also shows the variation characteristic of the tested process. The highest value increase can be observed during a drastic decrease in load due to the completion of the performed tests.

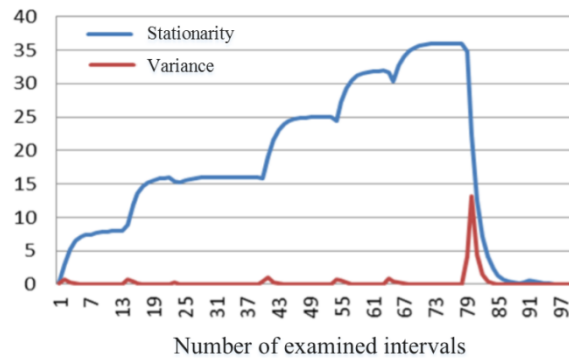


Fig. 2. Stationarity and the variance of the examined load time series.

The next studied parameter is the autocorrelation. Results are definitely different from zero which indicates the correlation of the tested process. The obtained data are shown in Fig. 3.

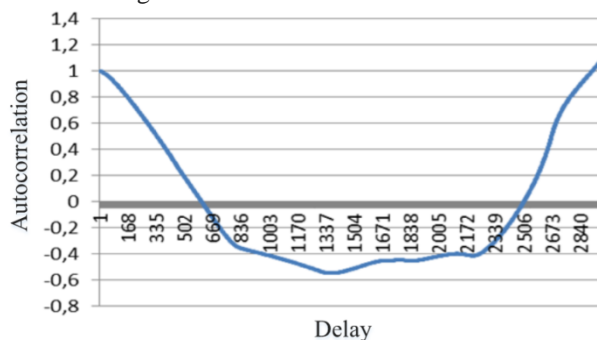


Fig. 3. Autocorrelation of the examined load time series.

Hurst parameter study was performed with the use of four methods: absolute moments, the aggregate variance, periodogram and residuals of regression methods. All analytical methods were implemented in a computer programs. When the studies

were performing on the original test data we did not get the expected results, because the obtained values did not fit into the expected ranges. Then, according to the fractional Brownian motion studies were carried out on modified data presented as increments calculated from the original test time series. Diagram in Fig. 4 shows the increases which were calculated and used for further analyses of the Hurst coefficient.

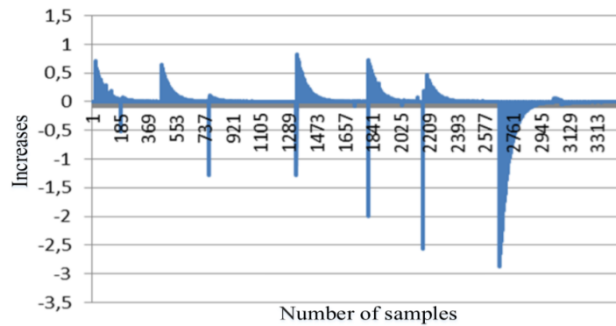


Fig. 4.Increases of the examined load time series.

The first method – the Hurst coefficient estimation with the absolute moments method was performed with the use of increases data (other methods also). The graph in the Fig. 5 shows the characteristic of the Hurst coefficient on the selected range of samples because in the whole samples range the graph would be illegible. Hurst coefficient estimation with the absolute moments method result: $H = 0.657836$.

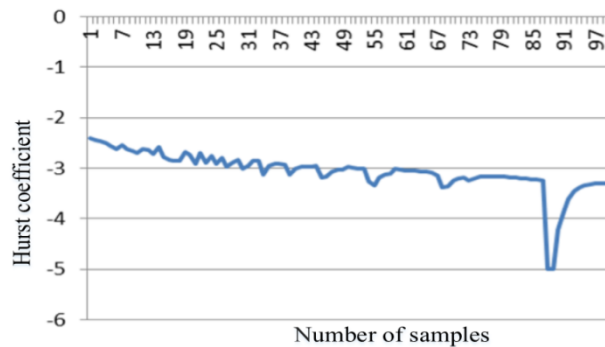


Fig. 5.Hurst coefficient estimation with the absolute moments method.

The second method – the Hurst coefficient estimation with the aggregate variance method was performed. The obtained results were presented in the Fig. 6, the graph shows only a selected samples range. The estimated Hurst coefficient for the whole data range is: $H=0.997984$.

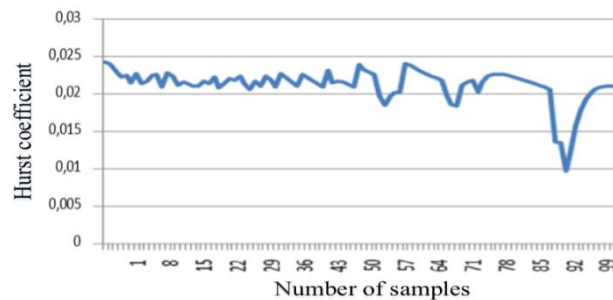


Fig. 6.Hurst coefficient estimation with the aggregate variance method.

The third method – the Hurst coefficient estimation with the residuals of regression method was performed and presented in the Fig. 7. The estimated Hurst coefficient for the whole data range is: $H = 0.932676$.

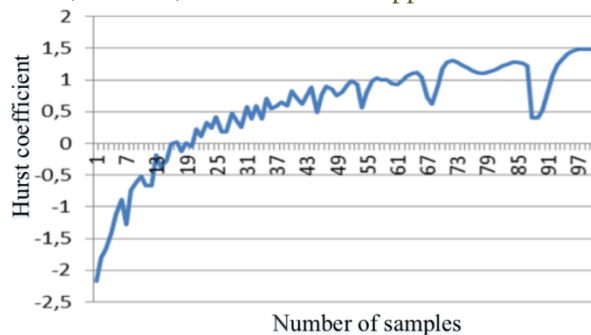


Fig. 7. Hurst coefficient estimation with the residuals of regression method.

The last method – the Hurst coefficient estimation with the periodogram method was performed and presented in the Fig. 8. The estimated Hurst coefficient for the whole data range is: $H = 0.969878$. During program execution we must additionally define the parameter which denotes the cutoff point.

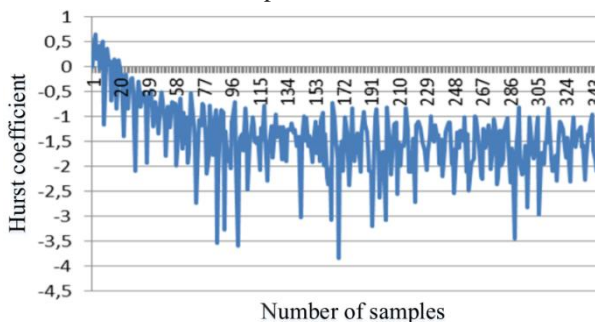


Fig. 8. Hurst coefficient estimation with the periodogram method.

V. CONCLUSION

In this paper we have presented a methods of nonextensive statistics used for performance analysis of a cluster computing system. The main purpose of these methods is classification of the systems as a complex or simple system category. The complex system is characterized by a lack of stationarity, autocorrelation and Hurst exponent belonging to $0 < H < 1$ and $H \neq 0.5$. The analysis of the stationarity in Fig. 2, shows a graph resembling the tested time series. Successive values don't still remain at the same level so that we can conclude that the test process is nonstationary. Another studied system feature was autocorrelation. The obtained values are different from zero, showing that the tested data are characterized by a correlation of data, such as in complex systems. The last studied property is self-similarity index, which was obtained using four methods. In most cases, the results were in the range of $0.5 < H < 1$ qualifying tested process as a process with a long memory. All presented properties and their estimation proves that created and tested HPC cluster system belongs to the group of complex systems. It can be concluded that the tested system is sensitive on the input data and the disruption caused by the other software operating in system or hardware limitations. Based on the obtained results and the knowledge that our system is classified as complex, the process of optimizing a computing cluster as also standalone servers should take into account the characteristics of long-term processes, in particular the effect of long memory. Therefore, in addition to the selection of appropriate physical elements as increased memory, cache or choosing the right processor also are important parameters of specific programs code or configuration parameters. The selection of the appropriate parameters were made by a number of test runs, configuration trials and appropriate modifications of testing algorithms. With this actions we have achieved a partial improvements of the next tests results, and thus the overall performance improvements of the of the cluster system.

The research presented in this work was done on the hardware that was supported by Grant POPW.01.03.00-18-012/09 The Operational Program Development of Eastern Poland.

REFERENCES

- [1] P. Dymora, M. Mazurek, *Delay analysis in wireless sensor network protocols*, PAK 2013 nr 10, s. 1054-1056, 2013.
- [2] Strzałka B., Mazurek M., Strzałka D., *Queue Performance in Presence of Long-Range Dependencies – an Empirical Study*, International Journal of Information Science, 2012, 2(4), pp. 47-53.
- [3] Yan R., Wang Y., *Hurst parameter for security evaluation of LAN traffic*, Information technology Journal 11(20), 2012, pp. 269-275.
- [4] Dymora P., Mazurek M., Strzałka D., *Long-range dependencies in memory pages reads during man-compute system interaction*, Annales UMCS Informatica XII (2) 2012, pp. 49-58.
- [5] Strzałka D., *Non-extensive statistical mechanics – a possible basis for modelling processes in computer memory system*, Acta Physica Polonica A 117(4), 2010, pp. 652–657
- [6] Dymora P., Mazurek M., Strzałka D., *Statistical mechanics of memory pages reads during man-computer system interaction*, Metody Informatyki Stosowanej, vol. 1/2011 (26), 2011, pp. 15-21.
- [7] Chuan-Lin Lai, Chao-Tung Yang, *Construct a Grid Computing Environment on Multiple Linux PC Clusters*, International

Conference on Open Source, 2003.

- [8] C. T. Yang, S. S. Tseng, M. C. Hsiao, *A Portable paralleling compiler with loop partitioning*, 1999.
- [9] *Beowulf Cluster Computing with Linux* Thomas Sterling, Massachusetts Institute of Technology, 2002.
- [10] Dymora P., Mazurek M., Strzałka D., Piękoś M., Influence of batch structure on cluster computing performance – complex systems approach, *Annales UMCS, Informatica*. Volume 12, Issue 1, Pages 57–66, 2013.
- [11] Strzałka D., Grabowski F., Non-Extensive Thermodynamics of Algorithmic Processing - the Case of Insertion Sort Algorithm, in *Thermodynamics*, ed. Tadashi Mizutani, InTech (2011)

Design, Control and Prototype Implementation of Maintenance Machine for Trenches

Mohamed H. Mabrouk¹, Mahmoud M. Ashry²

¹Head of Mechanical Equipment Department, M.T.C., Cairo, Egypt

²Automatic Control Department, M.T.C., Cairo, Egypt

Abstract: Trenches have a special importance in construction operations as they are widely used in both civil and military engineering. However, maintaining dozens kilometers of trenches that are located in an area of harsh weather condition can be difficult to be achieved manually. In this paper, the design and control of a new remotely controlled Trenches' Maintenance Machine (TMM) is presented. Elements like achieving machine stability and maneuverability, providing high performance while delivering the necessary traction in loose sand or mud, and using a powerful pneumatic system to overcome earth cutting resistance have been considered during the design procedures. A scaled prototype of the machine has been implemented and tested using an indoor soil-bin facility. The satisfying results assure the good functionality of the machine sub-systems as well as the reliability of the machine to accomplish the task successfully and within the required standards.

Keywords: Mobile robot control, Scaled prototypes, Soil-machine systems, Terramechanics.

I. INTRODUCTION

Soil-machine systems refer to systems in which the soil and machine tools interact to accomplish a specific task or purpose of production. These systems can perform many tasks such as tillage in agriculture, earth moving in civil engineering, and trench forming for installing long distant fuel pipelines and military fortifications.

A trench can be defined as a type of excavation whose depth is deeper than its width. Trenches have a special importance in construction operations as they are widely used to place underground easily damaged and obstructive infrastructure or utilities such as fuel and gas pipelines, electric cables, and sewage. Also, they are used as search trenches which are important to search for pipes and other infrastructures that are known to be underground, but whose exact location has been lost. Finally, trenches are used for transport purposes such as installing depressed motorways, open railway cuttings, or canals. On the other hand, in military engineering trenches and ditches are effectively used to shelter troops and firearms. They can extend for kilometers along a front without interruption. Some types of trenches and ditches can be up to 100 cm wide and 190 cm deep. While maintenance and repair operations are frequently needed to keep good state of the infrastructure of trenches, custom made machines are needed to apply any maintenance or repair requirements to such infrastructures [1].

The problem here can be defined in making a maintenance machine for ditches and utility trenches of width up to 100 cm especially those prepared for laying pipelines through long distances. This type of trenches and ditches is normally prepared for laying gas and petroleum pipelines through distant areas which are mostly deserts whose climate may backfill many parts of these trenches. The key point of this paper is to present the design and control of a new remotely controlled machine used for trenches' maintenance.

II. DESIGN OF THE TRENCHES' MAINTENANCE MACHINE AND ITS CONSTRUCTION

The design of a soil-system machinery include many factors that is related to required power, weight of the machine, spatial location of center of gravity, width and contact length of track, initial track belt tension, effective tractive effort, diameter of front idler and rear sprocket, number of road rollers, and suspension apparatus. In this paper, we focus on presenting the basic ideas of the sub-systems of the trenches' maintenance machine (TMM).

There are many detailed methods for engineering design process that can be used to devise a system to meet a desired need. Most of them have some common elements, such as brain-storming, analysis, and iterative decision making. In this paper, steps of the engineering design process from [2] are used. Elements such as recognition of need followed directly by problem definition with the idea based on components of the design have been accomplished. Before a system can be analyzed, it must at least be conceptualized. Therefore, synthesis must occur first and an initial concept to solve the problem is then determined. Once a concept is approved, schematics and layouts are created to visually depict the concept to other groups of people. Eventually, this will lead to detailed design and detailed drawings of each component along with assembly drawings. The maintenance machine consists of a tractor unit, a control unit, a sand disposal system and a blade attached to the front of the tractor unit as shown in Fig.(1). The tractor unit is a rectangular steel deck that carries the motors, the sand disposal system, the attachment and the controls. The control unit is responsible for enabling the operator to control the machine during all phases of operation.

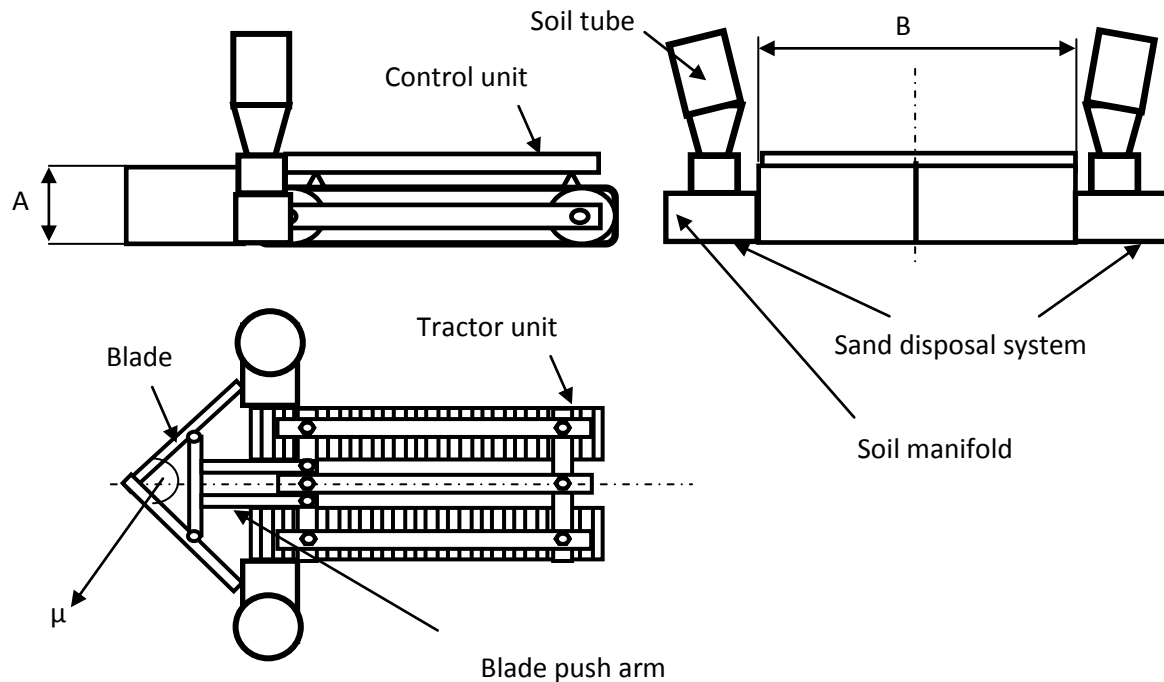


Fig. (1): An assembly drawing for the trenches maintenance machine (TMM).

2.1 The Blade

The blade specific parameters, shown in Fig. (1), are the blade angle (μ), the blade vertical height (A), blade width (B) that is the distance between both blade sides, and the maximum cutting depth (D) that is the maximum vertical distance that the center of the cutting edge can be lowered below ground with no blade tilt or angle.

The blade is used to shear, cut, and push or roll material ahead of the tractor. The blade consists of two 45° angled curved moldboards welded in the arrow-head shape with replaceable bolted teeth (cutting edges). In contrary to the design of the "U" shape blade used in some types of dozers, the arrow-head shape design of the blade assure cutting of earth and then rolling quantities of soil asides with fixed rate (as the machine's operation speed is kept constant) where they are collected in soil manifolds. The soil is then plowed outside the trench through soil tubes using the effect of the air generated by the blowers that are located directly behind the soil manifolds.

The design of the machine allows the blade to be raised or lowered in the vertical plane of the blade. A simple pneumatic system is used to control the cutting depth of the blade using a tilting pneumatic cylinder that is connected to the blade push arm, which is used to connect the blade to the tractor. The blade teeth cut the earth at the beginning of the operation phase and play a major role in how the machine performs. The hardened-steel cutting edges are bolted to the back of the moldboards which allows for their easy replacement as they receive most of the abrasion and therefore wear out rapidly. To keep a simple design of the machine, the blade can neither be pitched forward or backward (pitch angled) nor the mounted blades can be turned from the direction of travel as varying the angle of attack of the cutting edge is not needed to accomplish trenches' maintenance tasks. Former soil-machine system studies [3,4,5] provide us with the blade specific parameters convenient to work in gravelly sand such that (B/A) ratio was chosen to be 3, blade angle (μ) is chosen to be 80°, and the moldboard angle of curvature (θ) is chosen to be 45°.

2.2. The Tractor

The tractor consists of two main units, the power unit and the running gear unit. The power unit includes four DC motors that are used to independently drive the right sprocket, the left sprocket, the cutting depth pneumatic system, and the blowers of the sand disposal system. The running gear unit design assures the transform of the applied torque to the driving sprockets during the translatory motion of the equipment. It includes undercarriage, suspensions, and propeller. Generally in crawler machines, the steering is carried out by changing the relative velocities of the supporting tracks. As the relative velocity increases, the turning radius decreases and vice versa. This is called "skid steering" or "differential steering". The machine steering mechanism is designed to be skid steering which has the advantages of simple control along with its suitability for off road operation. The steering mechanism main idea depends on establishing a speed difference between the left and right motors used for the machine driving.

The undercarriage is a frame that supports all sub-systems of the machine. The track assembly consists of a continuous chain surrounding the track frame and drive sprockets. The links of the chain provide a flat surface for the track rollers to pass over, as they support the machine. Track shoes are bolted to the outside links of the chain and distribute the weight of the machine over a large surface area as shown in Fig. (2).

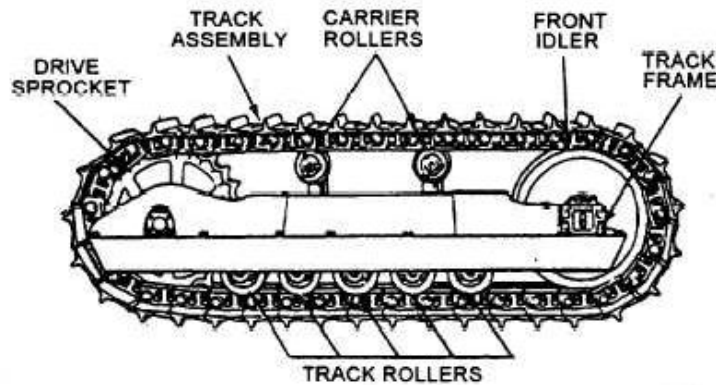


Fig. (2): Track assembly.

Track's low center of gravity and relatively large footprint increase stability of the machine during operation and provide smooth working pattern over rugged terrain. Also, track dimensions and design minimize the potential for trench collapse in loose soil conditions.

2.3. The Pneumatic System

The pneumatic circuit main task is to control the pneumatic cylinder which is responsible for giving the blade a specific cutting depth and to keep this cutting depth during the operation. The main advantages of the pneumatic system can be summarized in the small size and high actuating force, high power to weight ratio, high efficiency, easy to control, flexibility, low friction losses with a minimum possibility of leakage as the machine main job of maintenance of trenches acquires low pressure pneumatic circuit [6]. The main components that constitute the pneumatic circuit are the pneumatic storage and preparation unit, a compressor operated by a DC motor, a safety valve, a control valve, a cooling-filtering-drying integrated unit, pneumatic cylinder, and hoses. Figure (3) represents a typical pneumatic control system used for blade cutting depth control.

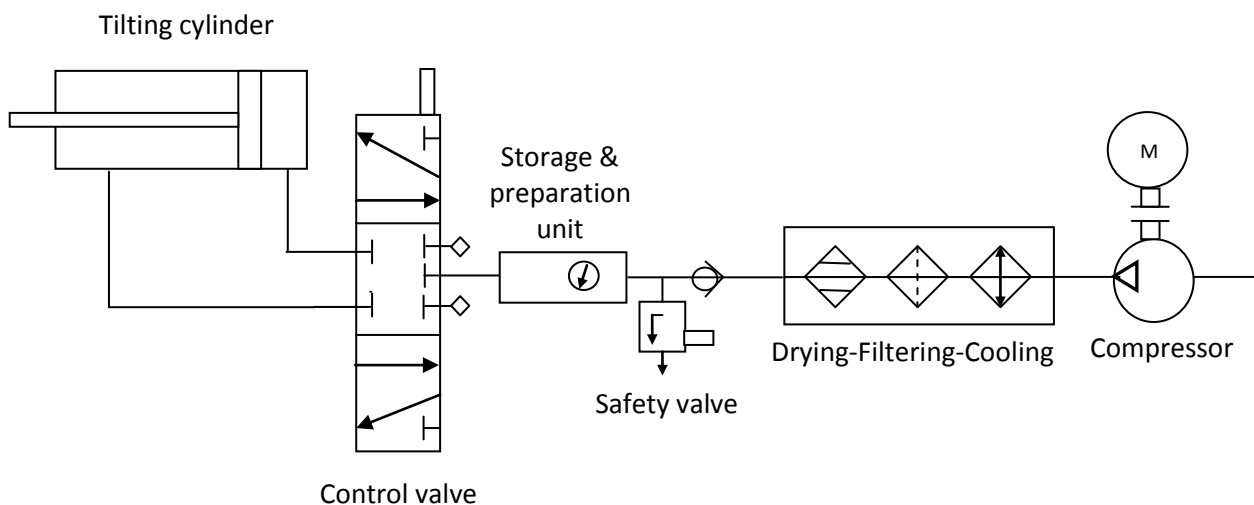


Fig. (3): Pneumatic circuit.

The pneumatic reservoir is attached to the rear of the machine to serve as counterbalance that increases the traction forces during operation. As the cutting depth should be kept constant, the cylinder is manually operated through the control valve at the beginning of the operation stroke. The positions of the control valve serve the different regimes of operation of the machine. The first position of the control valve is responsible for lowering the blade to reach a specific cutting depth while the machine is stationary. The second position of the control valve is engaged during the machine operation where the cutting depth is required to be maintained by the cylinder. Finally, the third position is responsible for raising the blade off the ground.

2.4. Sand Disposal System

The idea of sand disposing in our machine is similar to the disposing of waste in some mechanical equipment such as branches shredding machine [7]. The branch trimming process may generate waste in the form of dust, debris or wood where cleaning is completed at the job site, waste will often be left at the cleaning site (dust, grinded wood, and debris are blown from the machine using compressed air). This application depends mainly on the assumption that the loose sand-air mixture can be considered as a high density continuum fluid.

The main advantage of the design is that it allows the machine to drift large volume of sand efficiently over long distances. During operation, the center section of the moldboards drifts the soil with aside roll. The 45° angled curved moldboards assure rolling materials outward to keep the soil moved toward the soil manifolds at both sides of the blade with a minimum loss. The power train of the machine is shown in Fig. (4).

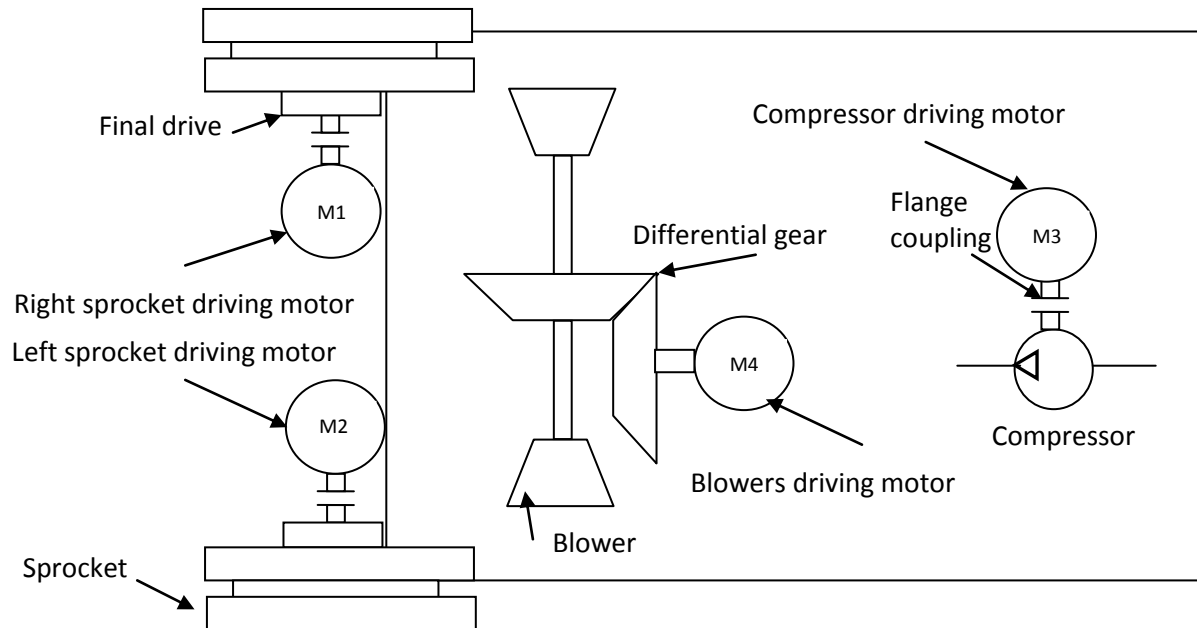


Fig. (4): Power train of the trenches maintenance machine (TMM).

III. POWER CALCULATIONS

From the machine construction explained in the previous section, it can be concluded that the system required total power can be defined as the sum of powers needed to drive each system of the machine taking the friction and losses waste in each system into consideration; such that:

$$P_t = P_p + P_d + P_b \quad (1)$$

Where P_t is the total power needed by the machine, P_p is the power needed to operate the compressor responsible for actuating the pneumatic cylinder which cuts the earth at the beginning of the operation. P_d is the total power needed to drive the machine that can be subdivided into two parts; the machine steering part P_s for skid steering system, which is small compared to the other major part; the earth cutting part P_c that is the power needed to drive the machine while overcoming the earth cutting resistance. P_b is the power required to operate the blowers. Also a small part of the total needed power should be dedicated to actuate the controls and the control unit. Since the machine main task is to exert a load on the blade during penetrating the earth to maintain the blade the required cutting depth, then it is expected that the main power needed to drive the machine comes from the calculations of the cutting forces exerted by the blade to overcome the earth resistance during the operation as will be explained in the following subsections.

3.1 Pneumatic Circuit Power (P_p) Calculations

The pneumatic circuit power P_p is the power required to overcome the soil resistance exerted on the blade during penetration the earth at the beginning of the operation to give the blade the required cutting depth. Considering soil-machine systems, good tool performance leads to considerable saving in energy and labor as well as improvement in working efficiency in the daily operations concerning earth cutting. Soil-machine systems studies can be dated back to early 1900s, but the real breakthrough has been achieved in the last three decades. Many investigations have been conducted using either an empirical or analytical approach, however because the complexity in soil mechanical behavior, empirical results are hardly extended to a general case. In this paper, we adopt the analytical approach where soil in front of the blade is broken up into several parts, each of which is considered as a rigid object. The limit equilibrium method is applied here to analyze the force balance in the entire system. When a single tooth of length (a_1) and width (b) is used for cutting the earth at a rake angle (α) and single tooth cutting depth (d) which will equals to ($a_1 \cdot \sin \alpha$), a set of resistance forces will be acting on the tooth. To determine these forces the soil shear wedge, shown in Fig. (5), should be studied [8] where:

- m_1 Weight of soil wedge being cut under the ground.
- W Normal force from effects above the surface.
- F_{f1} Friction force between soil and shank surface.
- F_{a1} Adhesion force between soil and shank surface.
- F_{sf} Friction force on the side of the soil wedge.
- F_{sc} ... Cohesion force on the side of the soil wedge.
- F_{rf} Friction force between soil wedge and ground at the rupture surface.
- F_{rc} Cohesion force between soil wedge and ground at the rupture surface.

Q Normal force on the rupture surface.

δ The angle of soil metal friction

ϕ Soil internal friction angle

β Angle of rupture plane with the X axis

μ Blade angle (angling)

θ Blade angle of curvature

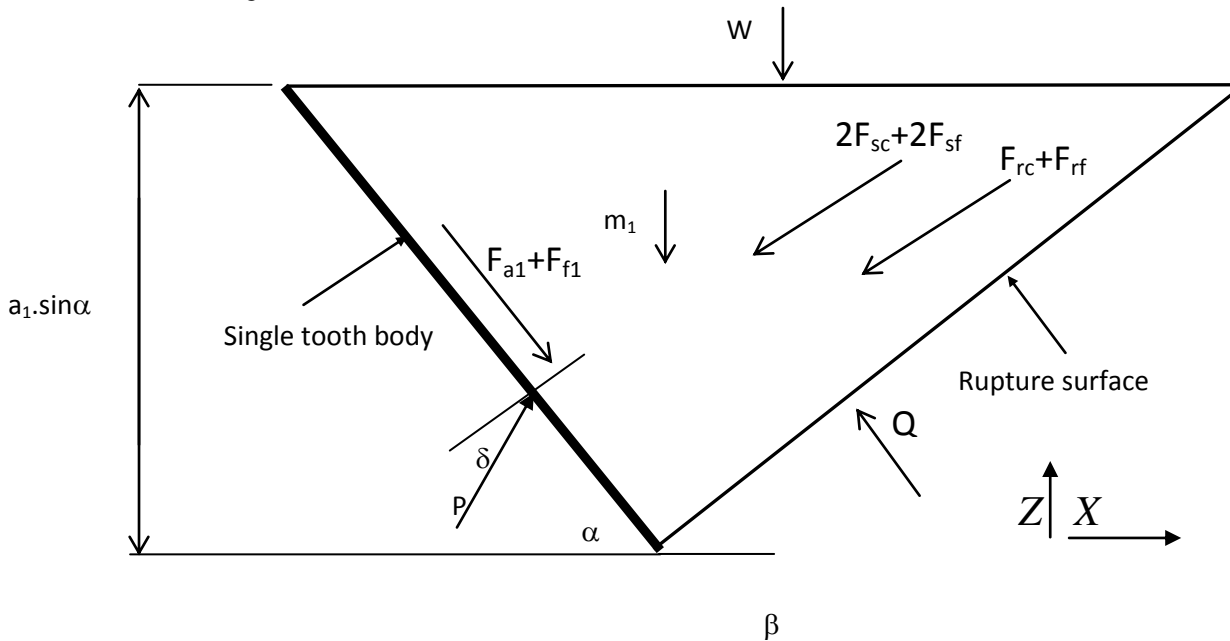


Fig. (5): Force analysis under the earth due to earth cutting by a single tooth

Studying the wedge as a free body diagram [8], it is noted that F_{sc} and F_{sf} are multiplied by two due to its generation from the two sides, it can be derived that:

$$P_x = Q \cdot \sin \beta + (2 \cdot F_{sc} + 2 \cdot F_{sf} + F_{rf} + F_{rc}) \cos \beta - (F_{a1} + F_{f1}) \cdot \cos \alpha \tag{2}$$

$$P_z = -Q \cdot \cos \beta + (2 \cdot F_{sc} + 2 \cdot F_{sf} + F_{rf} + F_{rc}) \sin \beta + (F_{a1} + F_{f1}) \cdot \sin \alpha + W + m_1 \tag{3}$$

$$\text{but, } P_x = P_p \cdot \sin(\alpha + \delta) \text{ and } P_z = P_p \cdot \cos(\alpha + \delta) \tag{4}$$

Therefore, P_p can be derived for unit linear velocity of the rod of pneumatic cylinder in the following form:

$$P_p = \frac{(2F_{sc} + 2F_{sf} + F_{rc}) \cos \phi - (F_{a1} + F_{f1}) \cos(\alpha + \beta + \phi) + (W + m_1) \sin(\phi + \beta)}{\sin(\alpha + \delta + \phi + \beta)} \tag{5}$$

3.2. Traction Power (P_d) Calculations

In the previous subsection the power needed to actuate the pneumatic cylinder during the whole operation regime to overcome the earth cutting resistance has been calculated. Considering that the machine is designed to accomplish only maintenance jobs for trenches and not building new ones, therefore it is safe to assume dealing with rather low soil cohesion forces, low soil-tool adhesion forces, and low cutting depths which means that the flat teeth, rather than the blade curved portion, are responsible for cutting the earth until reaching the cutting depth. Now the total earth resistance forces exerted on the blade calculated in [3-5,8] can be used to estimate the power needed for traction which is essential to design the track assembly through the empirical formulas included in [8]. The free body diagram of the blade during operation, shown in Fig. (6), illustrates that the (X,Z) reference axes are taken according to the blade such that the X axis is taken in the direction of movement of the blade which makes an angle equals to $(\mu/2)$ with the blade where (μ) is the blade angle. As a result of the side movement of the slice on the blades to the sides, friction and adhesion forces are generated and their direction will be aligned with the blades as shown in Fig.(6). Therefore, it can be concluded that:

$$F_{Xm} = P_x + 2 F_{bx} \cdot \sin(\mu/2) + 2(F_{fy} + F_{ay}) \cdot \cos(\mu/2) \tag{6}$$

$$F_{Zm} = P_z + 2 F_{bz} \tag{7}$$

where:

F_{Xm} the total draft resistance forces exerted on the blade.

F_{Zm} the total vertical resistance forces exerted on the blade.

F_{fy} soil-blade friction force that affect the curved portion of the blade.

F_{ay} soil-blade adhesion force that affect the curved portion of the blade.

F_b soil pile weight force that affect the curved portion of the blade.

Neglecting the soil adhesion and friction forces and assuming low cutting depth and therefore a small soil pile in front of the blade, it can be derived that total draft and vertical forces on the blade are:

$$F_{Xm} \approx P_x \text{ and } F_{Zm} \approx P_z$$

(8)

This means that the required traction power (P_d), for a unit linear velocity of the machine, is approximately equal to the power required by pneumatic system for unit linear velocity of the rod of pneumatic cylinder.

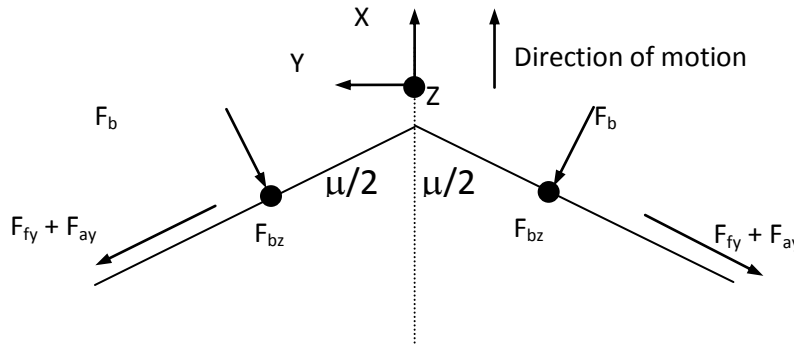


Fig. (6): Draft and vertical forces acting on the blade.

3.3 Sand Disposal System Power (P_b) Calculations

The total power needed to drive the two blowers can be calculated from the energy calculations which is subdivided into the kinetic energy (K) and the potential energy (H).

The kinetic energy can be derived from the equation

$$K=0.5mv^2 \tag{9}$$

Where:

m... The weight of the air-sand mixture flow

v... The air-sand mixture flow speed at a point on a streamline,

α ... The rake angle

D... The blade cutting depth

B... The blade cutting width

The flat part submerged in the soil and whose vertical projection equals (D), as shown in Fig.(7), is divided into two portions. The tooth portion of length a_1 , and another portion of the blade whose length equals $(D/\sin\alpha - a_1)$. The amount of soil cut per one meter travel accumulating to form a prism can be calculated as:

$$Q_s= B.\sin(\mu/2).(D - a_1\sin\alpha) \tag{10}$$

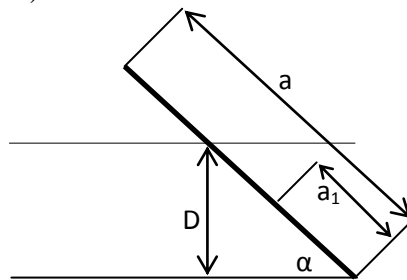


Fig. (7): The submerged part of the blade in earth.

The potential energy can be calculated assuming that loose sand-air mixture can be considered as a high density continuum fluid. Therefore, Bernoulli's principle from fluid dynamics can be used to derive a common approach in terms of total head or energy head H as follows:

$$H= (v^2 / 2g) + h = (v^2 / 2g) + (p/ \rho g) + z \tag{11}$$

where:

v... The fluid flow speed at a point on a streamline,

g ... The acceleration due to gravity,

z ... The elevation (head) of the point above a reference plane

p... The pressure at the chosen point, and

ρ ... The density of the sand-air mixture at all points.

h ... the pneumatic head which is the sum of the elevation z and the pressure head

Therefore, the power of motor needed to drive the two blowers (P_b) as a part of the overall power can be calculated for unit operating velocity of the machine.

IV. MACHINE CONTROL

Most of the used infrastructure maintenance machines are wire-based systems. The primary purpose of using the wires is to facilitate data communication and powering of motors and sensors. However, wire-based systems are practically difficult to use especially for a structure of complex design. Wireless monitoring systems, to a great extent, offers a solution for such problem. Being modular in nature, wireless systems has better maneuverability in a way that they can be moved easily to new locations as needed. The availability of low-powered cheap microcontrollers and DSP chips, radio frequency (RF) integrated circuits, and the development of new wireless standards are all advantages that favor the use of such systems. Although wireless technology is one of the promising technologies of the future, less active researches have been done in the use of wireless controlled systems for infrastructural and environmental monitoring and repair [9]. In this section, we discuss the proposed design of the machine wireless control system. Although commercial off-the-shelf (COTS) wireless systems [10] can be considered, most of them have limitations that made us to develop our own wireless control system. The proposed control system consists of a base station and a motor control unit, signal and power conditioning hardware, microcontroller, RF transmitter and RF receiver. The system is powered by four C-cell alkaline batteries. The sensing units were connected to the base station outside the trench. The complex design of the trench ruled out the possibility of using other existing technologies like laser-based controlled systems.

The Controlled vehicle works in ground conditions similar to that of tracked vehicles that use the skid steering mechanism. The skid steering depends on two different motors on each side of the vehicle. The required manoeuvre is achieved by the speed difference between the left and right motors of the vehicle. In our machine, it is preferable to control the motion of the vehicle wirelessly. The idea of sand disposing used in the TMM is based on blowing up the loose sand-air mixture using two blowers that are derived by a DC motor. The control of this DC motor is simply on-off control with maximum speed. Wireless control should be used in this case also. The designed easy-to-use control unit offers less jerking motions of the machine during operation. It allows the operator to steer the machine and adjust the cutting depth easily with minimum physical effort.

V. PROTOTYPE IMPLEMENTATION

Scaled prototypes are employed in many different areas of engineering to predict system performance under varying parameters on a relatively inexpensive scale. Scale model studies are based on the concept of similarity between the prototype and the real system, with the same physical laws governing both systems. Two systems will exhibit similar behavior if geometric, kinematic, and dynamic similarities are achieved. Although obtaining geometric similarity is a relatively simple matter, dynamic similarity requires that the ratios of all forces affecting the system must be the same [11].

The implemented prototype presented in this paper is a one-to-four scaled model of the real machine. The Rover 5[®] tracked robot chassis with settable ground clearance is used as the substructure of the TMM prototype to be controlled. Unlike conventional tracked chassis, the ground clearance can be adjusted by rotating the gearboxes in 5-degree increments. Stretchy rubber treads maintain tension as the clearance is changed. The standard chassis comes with two DC motors and gearboxes. Each gearbox, of 86.8:1 ratio, has an optical quadrature encoder with a resolution of 333.33 state changes per revolution [12]. The motor rated voltage is 7.2V and the TMM prototype speed is 1Km/hr. The TMM prototype is designed to allow Arduino development boards, power supply, and motor drivers to mount easily on the chassis [13]. The Rover 5 chassis with Arduino and motor driver unit mounted is shown in Fig. (8)

A four-channel motor driver unit designed originally for the Rover 5[®] chassis is used as shown in Fig.(8). Current sensing for each motor allows the processor to determine if a motor has stalled or is under excessive load. In the case studied, the motor control unit is connected to the front left and right motors of the TMM prototype as in two wheel drives, the DC motor that drives the compressor responsible for actuating the pneumatic cylinder, and the DC motor that drives the blowers.

The Arduino microcontroller is an easy to use and powerful single board computer that has gained considerable traction in the hobby and professional market. The Arduino is open-source, which means hardware is reasonably priced and development software is available. With the Arduino board, you can write programs and create interface circuits to read switches and other sensors, and to control motors and lights with very little energy consumption [14,15]. In the case studied, Arduino microcontroller is used to control the motion of the TMM prototype and the DC motor of the compressor, and the DC motor of the blowers. The control action is achieved using wireless network based on XBee. The Arduino is connected to the motor driver unit and the Rover 5[®] chassis as shown in Fig.(8).

The XBee radio frequency (RF) modem from Digi International[®] is a wireless transceiver. The XBee uses a fully implemented protocol for data communications that provides features needed for robust network communications in a wireless sensor network (WSN). Features such as addressing, acknowledgements and retries help to ensure safe delivery of data to the intended node. The XBee also has additional features beyond data communications for use in monitoring and control of remote devices [16]. A wireless network has to be formed using XBees. One XBee is updated with the “ZNet 2.5 Router[®]” firmware plugged into the XBee Shield on top of an arduino and the other XBee updated to the “ZNet 2.5 Coordinator” firmware and connected to the FT232 breakout which is plugged into the computer. The arduino should be connected to a power source so the wireless network is ready for transmission and reception, Fig.(9) shows the XBee plugged into the XBee shield on the top of Arduino as receiver and also shows the XBee connected to the FT232 breakout and plugged into the computer as transmitter.

The open loop control action is achieved using a personal computer (PC) as the base station. It controls the direction of the TMM prototype forward or backward and the speed of the left and right motors separately. The speed of each motor is controlled using pulse width modulation (PWM) technique through the motor driver unit. The control commands are sent

from the base station to the vehicle using the wireless network implemented by XBees. The base station controls the on-off action of the DC motor of the blowers used for sand disposing and the DC motor of the compressor that actuates the pneumatic cylinder. The power supply unit provide the required power for the arduino and the receiver XBee attached to it via the shield. It also provides the motor driver unit with the necessary power for the motors. The transmitter XBee connected to the PC consumes its necessary power from the PC itself via a USB cable.

The pneumatic system of the TMM prototype has been calibrated and tested, as shown in Fig (10). It is worth noted that the TMM prototype has been tested under normal operating conditions using an indoor soil-bin facility, as shown in Fig. (11). The satisfying results assured the good functionality of the machine sub-systems and therefore the reliability of the machine to accomplish the required tasks successfully and within the required standards.

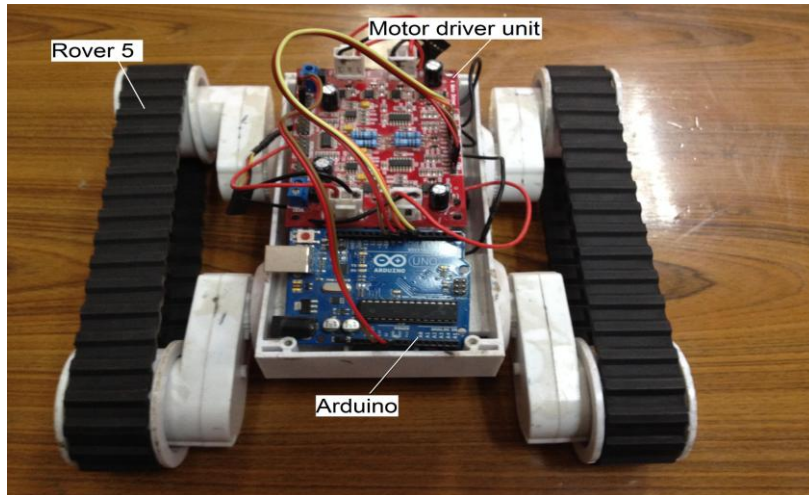


Fig.(8): The Rover 5[®] tracked robot chassis.



Fig. (9): Wireless connection between base station and the TMM prototype.

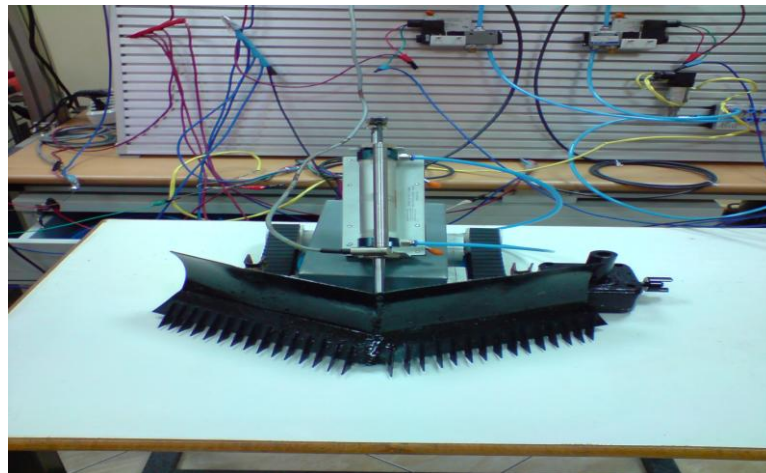


Fig. (10): Calibration and testing of the machine prototype pneumatic circuit.



Fig. (11): Testing the Prototype in an indoor soil-bin facility.

VI. CONCLUSIONS

This paper presents the design and control of a new remotely controlled machine used for trenches' maintenance (TMM). The machine is designed to meet the demanding conditions that trenches maintenance projects impose. The pneumatic system on the machine delivers the necessary power to overcome the soil cutting resistance. The designed easy-to-use control unit offers less jerking motions of the machine during operation. It allows the operator to steer the machine with one hand while adjusting cutting depth with the other in a way that helps in accomplishing the task with virtually no physical effort. Its compact design and easy to use control unit make our machine ideal for trenches' maintenance tasks especially for long distances. Although satisfactory results are obtained when testing the scaled prototype of the machine in normal operational conditions to ensure reliability, more extra-tough tests should be performed in the future for harsh service conditions.

REFERENCES

- [1] S. M. Cheekiralla. Development of a wireless sensing unit for tunnel monitoring. Master's thesis, Department of Civil and Environmental Engineering, Massachusetts Institute of Technology, <http://web.mit.edu/sivaram/www/> Sivaram-MS-thesis.pdf, February 2004.
- [2] Ertas, Atila and Jones, Jesse C., *The Engineering Design Process*, John Wiley and Sons, Incorporated, New York, 1996.
- [3] M.SPEKTOR, Principles of soil tool interaction. Journal of Terramechanics, Vol.18, No.1, pp.51 - 65, (1981) USA.
- [4] SUMINISTRADO, M.KOIKE, T.KONAKA, S.YUZAWA, and I.KUROISHI, Prediction of soil reaction forces on a moldboard plow surface. Journal of Terramechanics, Vol.27, No.4, pp.307 - 320, (1990) USA.
- [5] M.SPEKTOR and M.KATZ, Experimental study of frontal resistance forces in soil cutting. Journal of Terramechanics, Vol.22, No.3, pp.127 - 133, (1985) USA.
- [6] Rabie, M. G., " Fluid Power Engineering", McGraw-Hill, USA, (2009).
- [7] Russel, J. E., " Construction Equipment " , Prentice Hall, (1987).
- [8] Mootaz I. Abo-Elnor and Mohamed H. Mabrouk, "Terramechanics", *Lecture Notes*, Mech. Equip. Dept., M.T.C., Cairo, Egypt, 2013.
- [9] Technology Review. *10 Emerging Technologies That Will Change the World*, February 2003.
- [10] i-Bean brochure. http://www.millennial.net/pdf/MN_Brochure.pdf
- [11] R.K.KEPNER, ROY BAINER, AND E.L.BARGER."Principles of farm machinery", 2nd edition. AVI publishing company (1971) USA.
- [12] Dagu Rover 5 2WD Tracked Chassis W/Settable Ground Clearance, www.robotshop.com/dagu-rover-5-2wd-tracked-chassis.html, October 2012.
- [13] Rover 5 data sheet, www.pololu.com/file/0j467/Rover%205.pdf, December 2013.
- [14] W. Durfee, "Arduino Microcontroller Guide", University of Minnesota, www.me.umn.edu/courses/me2011/arduino/ , October 2011.
- [15] J. O. Lim, and T. Oppus, "Arduino Laboratory Manual: Using the Advanced Board", Bughaw Electronic Solutions and technologies, INC., 2011.
- [16] M. Hebel, G. Bricker, and D. Harris, "Getting Started with XBee RF Modules: A Tutorial for Basic Stamp and Propeller Microcontrollers", version1 (web release 2), Parallax INC., 2010.